Anthony J. Naldrett

**Magmatic Sulfide Deposits**

Geology, Geochemistry and Exploration

Anthony J. Naldrett

# Magmatic Sulfide Deposits

## Geology, Geochemistry and Exploration

With 325 Figures

Springer

**PROFESSOR ANTHONY J. NALDRETT**
DEPARTMENT OF GEOLOGY
UNIVERSITY OF TORONTO
22 RUSSELL ST.
TORONTO, ON M5S 3B1, CANADA

*E-mail: ajnaldrett@yahoo.com*

Library of Congress Control Number: 2004108879

ISBN 978-3-642-06099-1 ISBN 978-3-662-08444-1 (eBook)
DOI 10.1007/978-3-662-08444-1



springeronline.com

Originally published by Springer Berlin Heidelberg New York in 2004
Softcover reprint of the hardcover 1st edition 2004



Cover design: E. Kirchner, Heidelberg
Production: A. Oelschläger
Typesetting: Camera-ready by the Author

Printed on acid-free paper 32/2132/AO 5 4 3 2 1 0

# Author's Forward

As the time was approaching for me to graduate from the University of Cambridge with a B.A. degree in Geology, I started looking around the world for interesting places where I could put the degree to good use. In 1957, Canada stood out as an ideal environment for a young Anglophone, three of my co-students had a cabin booked on the Empress of Britain, which was scheduled to depart from Liverpool for Montreal in late July, and I took the fourth berth in the cabin. We arrived in Montreal on 28th July 1957, and after an entertaining weekend, I took leave of my friends to look for work in Toronto. I will always remember the Monday morning when I started my job search amongst the grey office buildings near King and Bay streets. My first stop was at the old Bank of Nova Scotia building where Falconbridge had their offices. Geof Mitchell, Falconbridge chief geologist, and Bill Taylor, his deputy, interviewed me and offered me a job in one of the company's mines at Sudbury. I was more interested in an exploration job, but they agreed to hold the position for me until the following evening. As I continued down my list of possible employers, I came to understand one of the maxims of the mining world, "employment depends on the price of metals". The then recent decline in the price of copper (to US$0.35/lb) meant that nobody was interested in offering an exploration job to an inexperienced young geologist from England. I was back that Monday evening accepting the job in the Sudbury mines, and two days later I was off on the train to Sudbury. It turns out that from that moment on my fate was welded to that of nickel in particular, and magmatic sulfides in general!

There are two principal types of magmatic sulfide deposit, those that are sulfide-rich, generally containing in excess of 30% sulfide, which are exploited primarily for their Ni, Cu and/or Co, with the PGE comprising a by-product, and those that contain less than 5% sulfide, which are of interest primarily because of their PGE with Ni and Cu as the by-products. For the first 20 years of my career, I worked, both as company geologist and then researcher, primarily on deposits of the first type. It came to be

appreciated that even though the PGE were only present in trace amounts, they could tell us much about the provenance of, and the processes that had operated in the formation of these deposits. This led me into studying PGE-rich deposits at a time when there was a growing commercial interest in them, driven by their increasing use in protecting the environment.

Looking back, I appreciate the tremendous benefit that an academic can gain from sabbatical leave. My first was granted in 1972, and I accepted Wilf Ewers invitation to work with the CSIRO in Perth, Western Australia as part of their research on the developing komatiite-related Ni sulfide camp in the Eastern Goldfields. This year gave me a grounding in this style of deposit and showed me that not all magmatic sulfides ores were the same as those at Sudbury! My second sabbatical in 1980 allowed me to accept Gero von Gruenewaldt's invitation to join the Bushveld Research Institute of the University of Pretoria, and coincided with my then developing interest in PGE deposits. This was the start of a 10-year long close association with South Africa and the ores of the southern part of that continent, and without this start, Chap. 9 would never have been written.

By the late 1980's, another factor was about to influence the direction of my science. A freer flow of information was sweeping behind the iron curtain and soon this curtain, in the shape of the Berlin wall, came tumbling down. As a result of an association with Vilen Zharikov, I had already developed a productive relationship with scientists of the Institute of Experimental Mineralogy of the Russian Academy of Sciences. The events of the late 80's gradually allowed increasing collaboration on scientific topics that previously had been closed to foreigners. In 1990 I received an invitation from Anatoly Vasily Filatov, General Director of the Noril'sk Kombinat, to visit the mines at Noril'sk. My first visit took place in January 1991, and was followed by four subsequent visits. These have resulted in my coming to know and make friends with many Noril'sk geologists to whom I owe a huge debt of gratitude for showing me their outstanding work and increasing my understanding of the geology of magmatic sulfides so much. In particular, I would like to acknowledge Valeri Andrew Fedorenko of TsNIGRI and formerly of the Noril'sk Expedition. His intelligence and encyclopedic knowledge of Noril'sk geology has remained of incalculable value to me and many other western scientists during our research on the Noril'sk area. Chap. 4 of this book is based on research stimulated by my visits to Noril'sk.

As research on the Noril'sk deposits moved into top gear, another "distraction" appeared on the horizon! A small company, Diamond Fields Resources Inc., had encountered a deposit of nickel sulfide in the course of their search for diamond indicator minerals in central Labrador. They asked me to augment their knowledge on the subject of nickel by acting as their consultant. I agreed, and this led to a research programme that was collaboratively funded by Canada's Natural Sciences and Engineering Research Council and initially Diamond Fields and then their successor company, the Voisey's Bay Nickel Company. The world-wide interest that was stimulated by the Voisey's Bay discovery meant that many distinguished researchers were eager to collaborate in the programme, and I've done my best to summarise the results in Chap. 6.

Despite the opportunities that have presented themselves to wander far from home, and the distractions that these wanderings have brought, home has always been Sudbury. It's where I started in 1957, and where I have always returned intellectually. The evolution in geological understanding about Sudbury over the last 40–50 years has been extraordinarily exciting, and it has been a privilege to watch it and make some small contributions myself. The evolution came about because of the lateral thinking of one man, Robert Dietz, who developed the impact hypothesis. This was what was needed to bring many workers, with backgrounds that would never have drawn them to take an interest in a layered intrusion and its nickel deposits, to come to Sudbury and apply their special knowledge. Sudbury is an object lesson as to the importance of a multi-faceted approach in research, and, again, I have tried to capture salient features of this lesson in Chap. 8.

I cannot conclude without paying especial thanks to certain individuals who have helped me so much during my scientific career. Professor Edward Hawley, Professor and Chair at Queen's University, was the reigning authority on Sudbury mineral deposits when I had decided to attend graduate school, and he taught me how to ask the right questions without which research is pointless. Gunnar Kullerud passed through Queen's on a lecture tour in 1963, and invited me to work with him as a Post-Doctoral Fellow at the Geophysical Laboratory from 1964 to 1967. Working with Gunnar and others at "The Lab" exposed me to the use of experimental data in the solution of geological problems. It also allowed me to mix and make friends with the very vital group of young experimental and theoretical petrologists who were working in

Washington DC in the mid 60's. These were undoubtedly the halcyon days of the US Geological Survey's interest in theoretical, as opposed to empirical, approaches to the solution of geological problems. Professor Les Nuffield invited me to return to Canada from Washington and take up a position at the University of Toronto in 1967. I can never thank him enough for giving me the time and resources to develop my research interests during my early years, years when it is so easy for a young professor to be "ground down" by the daily preparation of courses and departmental administration. Above all, I thank my students, Post-doctoral Fellows and Research Associates, to whom this book is dedicated, and whose ideas and hard work have contributed so much to the University of Toronto's research output on magmatic sulfides.

Tony Naldrett
University Professor Emeritus,
University of Toronto,
April 2004

# Dedication

To my Students, Post-doctoral Fellows and Research Associates in the Department of Geology, University of Toronto

Their's was the greater part

Nick Arndt
Mohammed Asif
Steve Barnes
Sarah-Jane Barnes
Tucker Barrie
Alistair Borthwick
Gerhard Brugmann
Greg Cameron
Ian Campbell
Gang Chai
Tom Clark
Paul Coad
Debbie Conrod
Chris Doyle
Murray Duke
Denton Ebel
Valeri Fedorenko
Cesar Ferreira Filho
Derek Fisher
David Good
Megally Graterol
Tony Green
Larry Greenman
Roger Hewins
Eric Hoffman
Craig Jowett
Dorota Kiersnowski
Ross Large
Chusi Li
Peter Lightfoot
Heather MacDonald
Paul Mainwaring
Dave Moore
Ted Muir
Walter Peredery
Reza Pessaren
Don Rae
"Raja" Rajamani
B.V. Rao
Eva Schandl
Randy Scott
Brian Scribbins
Tim Searcy
Hiromi Shima
Jagomohan Singh
John Thompson
Oleg Valeyev

# Acknowledgments

This book would never have been written without the enormous amount of help provided by Valeri Fedorenko. Valeri was the translator of the Russian version, published in 2003. He not only drafted all of the figures, but gave encouragement and helpful advice at all stages while I was writing it and it was being prepared for publication.

I am grateful for the copyright holders of the originals of many of the figures reproduced in this book for permission to use them. In particular, I would like to acknowledge:

The Canadian Institute of Mining, Metallurgy and Petroleum for their permission to reprint Figures 3.11 and 3.14, previously published in the Transactions of the Canadian Institute of Mining and Metallurgy, vol. 76; Figures 10.6 and 10.7, previously published in the Bulletin of the Canadian Institute of Mining and Metallurgy, vol. 77; Figure 6.7, previously published in Exploration and Mining Geology, vol. 5; and Figures 9.3, 9.4, 9.8, 9.9, 9.14, 9.20, 9.26, 9.27, 9.35, 9.36, 9.38, 9.40, 9.41, 9.42, 9.43, 9.44, 9.45, 9.46 and 10.19, previously published in "The geology, geochemistry, mineralogy and mineral beneficiation of platinum-group elements" Special Publication No. 54.

The Oxford University Press for their permission to reprint Figures 2.10, 2.11, 3.3, 5.13, 7.1, 7.2, 7.3, 7.4, 7.5, 7.6 and 9.48 previously published in the Journal of Petrology; and Figures 2.2, 2.16, 9.5, 9.7, 9.13 and 9.49 previously published in MAGMATIC SULFIDE DEPOSITS by Anthony J. Naldrett, Copyright – 1989 by Oxford University Press Inc. and used by permission of the Oxford University Press Inc.

The American Journal of Science for their permission to reprint Figures 6.32, 6.33, and 6.34 from the paper by A. Kerr appearing in the American Journal of Science, vol. 303.

# Contents

# List of abbreviations

An – Anorthite
Ap – Apatite
Aug – Augite
bn – Bornite
bnss – Bornite solid solution
Br – Bronzite
cc – Chalcocite
ccss – Chalcocite solid solution
Chr – Chromite
cp – Chalcopyrite
Cpx – Clinopyroxenite
cub – Cubanite
cv – Covellite
D – Nernst partition coefficient
dg – Digenite
Di – Diopside
En – Enstatite
Fa – Fayalite
FeOT – Total Fe calculated as FeO
Fo – Forsterite
$fO_2$ –Oxygen fugacity
$fS_2$ –Sulfur fugacity
god – Godlevskite
hz – Heazlewoodite
Ilm – Ilmenite
iss – Intermediate solid solution
$K_D$ – Exchange partition coefficient
L – Liquid in phase diagrams
Liq –Liquid in text
M/S – Metal/sulfur ratio, e.g. Ni/S, Pt/S
mh – Mooihoekite
mill – Millerite
mod% – Modal percent
MORB – Mid Ocean Ridge Basalt
mss – Monosulfide solid solution
OIB – Oceanic Island Basalt
Ol – Olivine
Opx – Orthopyroxene
Pl – Plagioclase
pn – Pentlandite
pn(h) – High-temperature pentlandite in phase diagrams
pn(l) – Low-temperature pentlandite in phase diagrams
po – Pyrrhotite
po(h) – Pyrrhotite (hexagonal)
po(m) – Pyrrhotite (monoclinic)
poss – Pyrrhotite solid solution
ppb = mg/t
ppm = g/t
put – Puteronite
py – Pyrite
Q – Quartz
R = R Factor – Mass ratio of silicate magma to sulfide liquid (involved in equilibration)
SCSS – Sulfur content at sulfide saturation
Sil.m –Silicate magma
sp – Sphalerite
Sul – Sulfide
Sul.l – Sulfide liquid
Sul.m –Sulfide melt
tal – Talnakhite
TiMt – Titaniferous magnetite
tr – Troilite
Vap –Vapour
viol – Violarite
vs – Vaesite

# 1 Introduction

Magmatic Nickel-Copper-Platinum-group element sulfide deposits form as the result of the segregation and concentration of droplets of liquid sulfide from mafic or ultramafic magma, and the partitioning of chalcophile elements into these from the silicate magma.

The size of the deposits, their grades and ratios of economic metals are very variable. This is illustrated in Table 1.1, which summarizes data on tonnes of resources + production, grades of Ni, Cu, Co and PGE, tonnes of contained metal, and value of the ore and of the individual metals. It is also illustrated in Fig. 1.1, which shows the percentages that Ni+Co, Cu and the PGE contribute to the value of many magmatic sulfide deposits/camps.

## 1.1 Classification of Magmatic Sulfide Deposits

The deposits fall naturally into two major groupings, those that are of value primarily because of their Ni and Cu, and which tend to be rich in sulfide with the ore containing 20 to 90 percent sulfide, and those of value primarily because of their PGE, which tend to be sulfide poor with the ore containing 0.5 to 5 percent sulfide (see Fig. 1.1). With certain exceptions, sulfide-rich types cluster at the nickel apex of the diagram; many of the smaller deposits and camps, which are not included in this compilation, also fall in this area. Sulfide-poor PGE-rich deposits cluster near the PGE apex. Exceptions to this grouping are the Platreef, which consists of a cloud of stratigraphically controlled, weakly disseminated sulfides, and the deposits of the Noril'sk and Duluth regions. The Cu-rich footwall ores at Sudbury also plot in the intervening area, but these have been derived from the contact ores (see Chap. 8) and do not constitute a separate camp, merely a sub-type of mineralization that occurs within the Sudbury camp.

In this book, the primary division of magmatic sulfide deposits is between the sulfide-poor type that cluster close to the PGE apex of Fig. 1.1 and those much richer in sulfide for which Ni and Cu together constitute the metals of major economic interest. Because of their origin, magmatic

**Table 1.1.** Estimated resources (including that already mined) and values of main deposits of Ni-Cu and PGE sulfide ores

1. Ore resources (including that already mined) and average metal concentrations in the ores[1]

| Deposit/camp | Ore resource [$10^6$ t] | Ni wt% | Cu wt% | Co wt% | Pt g/t | Pd g/t | Rh g/t | Ru g/t | Ir g/t | Os g/t | Total PGE g/t |
|---|---|---|---|---|---|---|---|---|---|---|---|
| Noril'sk region[2] | 1309.3 | 1.77 | 3.57 | 0.061 | 1.84 | 7.31 | 0.191 | 0.093 | 0.026 | 0.036 | 9.50 |
| Sudbury[3] | 1648.0 | 1.20 | 1.08 | 0.038 | 0.46 | 0.58 | 0.056 | 0.044 | 0.019 | 0.008 | 1.17 |
| Duluth[4] | 4000.0 | 0.20 | 0.60 | 0.019 | 0.15 | 0.49 | 0.007 | 0.007 | 0.003 | 0.003 | 0.66 |
| Jinchuan[5] | 515.0 | 1.06 | 0.75 | 0.019 | 0.13 | 0.10 | 0.005 | 0.010 | 0.010 | 0.011 | 0.26 |
| Pechenga[6] | 339.0 | 1.18 | 0.63 | 0.045 | 0.12 | 0.17 | 0.005 | 0.007 | 0.004 | 0.006 | 0.32 |
| Thompson[7] | 150.3 | 2.32 | 0.16 | 0.046 | 0.10 | 0.54 | 0.046 | 0.072 | 0.033 | 0.041 | 0.83 |
| Mt Keith[8] | 478.0 | 0.60 | 0.01 | 0.014 | | | | | | | 0.00 |
| Voisey's Bay[9] | 136.7 | 1.59 | 0.85 | 0.090 | 0.07 | 0.10 | 0.005 | 0.007 | 0.002 | 0.002 | 0.19 |
| Kambalda[10] | 67.0 | 2.90 | 0.21 | 0.207 | 0.30 | 0.42 | 0.065 | 0.197 | 0.047 | 0.097 | 1.13 |
| Perseverance (Agnew)[11] | 52.0 | 1.90 | 0.10 | | | | | | | | 0.00 |
| Raglan[12] | 24.7 | 2.72 | 0.70 | 0.054 | 0.82 | 2.27 | 0.150 | 0.374 | 0.065 | 0.080 | 3.76 |
| Total Bushveld | 11549.9 | 0.13 | 0.06 | | 2.87 | 1.80 | 0.307 | 0.539 | 0.100 | 0.054 | 5.67 |
| – UG-2[13] | 5742.6 | 0.04 | 0.02 | | 2.66 | 1.71 | 0.428 | 0.710 | 0.131 | 0.062 | 5.70 |
| – Merensky[13] | 4210.0 | 0.15 | 0.06 | | 3.57 | 1.85 | 0.216 | 0.449 | 0.082 | 0.051 | 6.21 |
| – Platreef[14] | 1597.3 | 0.41 | 0.20 | | 1.77 | 2.01 | 0.114 | 0.165 | 0.038 | 0.033 | 4.12 |
| Great Dyke[15] | 2574.0 | 0.21 | 0.14 | | 2.77 | 2.13 | 0.130 | 0.289 | 0.052 | 0.047 | 5.42 |
| Stillwater[16] | 32.3 | 0.05 | 0.02 | | 5.30 | 19.11 | 0.270 | 0.100 | 0.096 | 0.043 | 24.91 |
| Portimo Area[17] | 218.6 | 0.08 | 0.18 | | 0.38 | 1.54 | | | | | 1.92 |
| Lac des Iles[18] | 94.1 | 0.05 | 0.06 | | 0.18 | 1.66 | 0.008 | | 0.000 | | 1.85 |

**Table 1.1** (cont.)

2. Metal resources (including that already mined out)

| Deposit/camp | Ni [$10^3$ t] | Cu [$10^3$ t] | Co [$10^3$ t] | Pt [t] | Pd [t] | Rh [t] | Ru [t] | Ir [t] | Os [t] | Total PGE, [t] |
|---|---|---|---|---|---|---|---|---|---|---|
| Noril'sk region[2] | 23201 | 46728 | 801 | 2412 | 9573 | 250 | 122 | 34 | 47 | 12438 |
| Sudbury[3] | 19776 | 17798 | 621 | 763 | 961 | 92 | 73 | 31 | 13 | 1933 |
| Duluth[4] | 8000 | 24000 | 757 | 585 | 1959 | 27 | 27 | 11 | 12 | 2621 |
| Jinchuan[5] | 5459 | 3888 | 99 | 65 | 51 | 3 | 5 | 5 | 6 | 135 |
| Pechenga[6] | 4000 | 2150 | 152 | 41 | 59 | 2 | 2 | 1 | 2 | 107 |
| Thompson[7] | 3486 | 243 | 69 | 15 | 80 | 7 | 11 | 5 | 6 | 124 |
| Mt Keith[8] | 2868 | 57 | 67 | | | | | | | |
| Voisey's Bay[9] | 2174 | 1162 | 123 | 10 | 13 | 1 | 1 | 0 | 0 | 26 |
| Kambalda[10] | 1943 | 144 | 139 | 20 | 28 | 4 | 13 | 3 | 7 | 75 |
| Perseverance (Agnew)[11] | 988 | 49 | | | | | | | | |
| Raglan[12] | 672 | 173 | 13 | 20 | 56 | 4 | 9 | 2 | 2 | 93 |
| Total Bushveld | 15276 | 6881 | | 33111 | 20803 | 3548 | 6231 | 1157 | 623 | 65473 |
| – UG-2[13] | 2412 | 1034 | | 15279 | 9809 | 2457 | 4077 | 752 | 356 | 32730 |
| – Merensky[13] | 6315 | 2652 | | 15012 | 7790 | 909 | 1891 | 345 | 214 | 26161 |
| – Platreef[14] | 6549 | 3195 | | 2820 | 3204 | 182 | 263 | 60 | 53 | 6582 |
| Great Dyke[15] | 5405 | 3604 | | 7130 | 5483 | 335 | 744 | 135 | 120 | 13946 |
| Stillwater[16] | 15 | 7 | | 171 | 616 | 9 | 3 | 3 | 1 | 804 |
| Portimo Area[17] | 175 | 393 | | 83 | 337 | | | | | 420 |
| Lac des Iles[18] | 50 | 58 | | 17 | 156 | 1 | | | | 174 |

**Table 1.1** (cont.)

3. Value of ore resources (millions US$), value of ore (US$ per tonne) and proportion (%) that PGE contribute to total value[19]

| Deposit/camp | Ni | Cu | Co | Pt | Pd | Rh | Ru | Ir | Os | Total | Ore (US$/t) | PGE (%) |
|---|---|---|---|---|---|---|---|---|---|---|---|---|
| Noril'sk region[2] | 191870 | 77101 | 18029 | 49864 | 59734 | 4591 | 352 | 98 | 135 | 401774 | 307 | 29 |
| Sudbury[3] | 163548 | 29367 | 13972 | 15765 | 5998 | 1682 | 210 | 91 | 38 | 230670 | 140 | 10 |
| Duluth[4] | 66160 | 39600 | 17033 | 12093 | 12224 | 500 | 78 | 31 | 34 | 147753 | 37 | 17 |
| Jinchuan[5] | 45146 | 6415 | 2238 | 1354 | 316 | 46 | 15 | 15 | 17 | 55562 | 108 | 3 |
| Pechenga[6] | 33080 | 3548 | 3420 | 847 | 366 | 34 | 7 | 4 | 6 | 41312 | 122 | 3 |
| Thompson[7] | 28828 | 402 | 1555 | 310 | 502 | 126 | 31 | 14 | 18 | 31786 | 212 | 3 |
| Mt Keith[8] | 23718 | 95 | 1506 | | | | | | | 25319 | 53 | |
| Voisey's Bay[9] | 17975 | 1917 | 2768 | 212 | 82 | 12 | 3 | 1 | 1 | 22971 | 168 | 1 |
| Kambalda[10] | 16069 | 237 | 3123 | 417 | 175 | 79 | 38 | 9 | 19 | 20166 | 301 | 4 |
| Perseverance (Agnew)[11] | 8171 | 82 | | | | | | | | 8252 | 159 | 0 |
| Raglan[12] | 5556 | 286 | 298 | 421 | 349 | 68 | 27 | 5 | 6 | 7015 | 284 | 12 |
| Total Bushveld | 126332 | 11353 | | 684404 | 129811 | 65035 | 18008 | 3344 | 1800 | 1040086 | 90 | 87 |
| – UG-2[13] | 19946 | 1706 | | 315817 | 61208 | 45037 | 11783 | 2173 | 1029 | 458698 | 80 | 95 |
| – Merensky[13] | 52225 | 4376 | | 310298 | 48610 | 16662 | 5465 | 997 | 618 | 439251 | 104 | 87 |
| – Platreef[14] | 54161 | 5271 | | 58289 | 19993 | 3336 | 760 | 173 | 153 | 142137 | 89 | 58 |
| Great Dyke[15] | 44703 | 5946 | | 147377 | 34212 | 6146 | 2149 | 390 | 346 | 241269 | 94 | 79 |
| Stillwater[16] | 124 | 12 | | 3533 | 3846 | 160 | 9 | 9 | 4 | 7698 | 239 | 98 |
| Portimo Area[17] | 1446 | 649 | | 1717 | 2101 | | | | | 5913 | 27 | 65 |
| Lac des Iles[18] | 412 | 96 | | 350 | 975 | 14 | | | | 1848 | 20 | 72 |

**Table 1.1** (cont.)

[1]Metal contents are in situ, with no allowances made for dilution or loss on beneficiation.

[2]estimate, Naldrett and Searcy (unpublished data), based on analytical data of Naldrett et al. (1996), Distler and Kunilov (1994).

[3]reserves and Ni grade after Naldrett et al. (1989); Cu/Ni, Co/Ni and PGE/Ni ratios after data of Naldrett et al. (1999) (~350 analyses Co, and ~1500 analyses PGE in typical Sudbury ores).

[4]tonnage, Ni and Cu grade from Listerud and Meinecke (1977); Co/Ni and PGE/Ni ratios from Naldrett (1989).

[5]tonnage and Ni grade from Chai and Naldrett (1992); Cu/Ni, Co/Ni, PGE/Ni ratios from Tang (1993), his Table IV.

[6]Ni data from Green (personal communication 1999); Cu/Ni and PGE/Ni ratios from Brugmann et al. (2000).

[7]reserves of Ni from INCO Ltd, Cu/Ni ratio from Theyer (1980), Co/Ni and PGE/Ni ratios from data of Bleeker (1990).

[8]Ni data from poster at AGSO meeting, Canberra, 1996.

[9]tonnage and Ni, Cu and Co grades, Lightfoot and Naldrett (1999); PGE data obtained from PGE/Ni ratios of 190 samples with >20% sulfide from Naldrett et al. (2000a).

[10]tonnage and Ni grade from Stone and Masterton (1998); Cu/Ni and PGE/Ni ratios from Naldrett (1989); Co/Ni ratio is an average value from Lesher (1989), his Table 5.1.

[11]Ni data from poster at AGSO meeting, Canberra, 1996; Ni/Cu from Keays and Davidson (1976).

[12]Data from Lesher, ed (1999).

[13]tonnes of PGE from Vermaak (1995), his Table 2.7; grade of total PGE from Vermaak (1995) his Table 2.1; Ni and Cu grades using Ni/(Pt+Pd) and Cu/Ni ratios of Naldrett (1989).

[14]tonnes of PGE from Vermaak (1995), his Table 2.7; grade of total PGE from Vermaak (1995, p. 17); Ni and Cu grades from Naldrett (1989).

[15]PGE data from Vermaak (1995); Ni/(Pt+Pd) and Cu/(Pt+Pd) ratios from study of Naldrett and Wilson (1990).

[16]tonnes and grade of (Pt+Pd) of proven and probable reserves for Stillwater and East Boulder mines from Zientek et al. (2002); Pt/Pd ratio from Vermaak (1995); Ni and Cu calculated using Zientek et al.'s Pt and Pd data and Naldrett's (1989) ratios for Ni/(Pt+Pd) and Cu/(Pt+Pd).

[17]information from release on Internet by Arctic Platinum Partnership (Goldfields and Outokompu), July 2002.

[18]data for tonnage and Pt and Pd grades as given at Cordilleran Round-up, Vancouver, January 2000; metal:Pd ratios from Naldrett (private data).

[19]Prices used for April 2003: Ni = 8.27 US$/kg (3.75 US$/lb); Cu = 1.65 US$/kg (0.75 US$/lb); Co = 22.05 US$/kg (10.00 US$/lb); Pt = 20.67 US$/g (643 US$/troy oz); Pd = 6.24 US$/g (194 US$/troy oz); Rh =18.33 US$/g (570 US$/troy oz); Ru = 2.89 US$/g (90 US$/troy oz); Ir = 2.89 US$/g (90 US$/troy oz); Os = 2.89 US$/g (90 US$/troy oz).

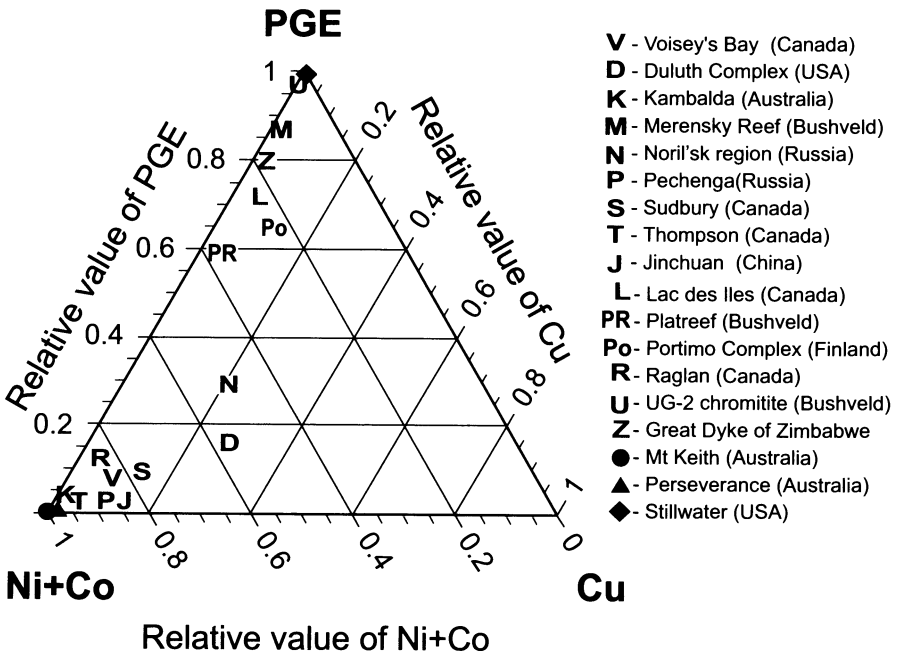


**Fig. 1.1.** Relative value of the contributions of Ni+Co, Cu and PGE to the magmatic sulfide deposits listed in Table 1.1

sulfide deposits are closely related to bodies of mafic or ultramafic rock, and the most convenient way in which to consider them is in terms of the type of magma responsible for the rocks with which they are associated. Typically the type of magma involved bears a close relationship to the tectonic setting within which it was emplaced.

The locations of important deposits, both Ni-Cu dominant and PGE dominant, are shown in Fig.1.2.

Considering first Ni-Cu deposits, these are further divided into six classes (Table 1.2) on the basis of their associated magma type. Class NC-1 (Chap. 3) comprises those related to komatiitic magmatism. Currently known deposits fall into two sub-classes, those related to Archean komatiites (e.g. the deposits of Western Australia, Zimbabwe and the Abitibi belt of Canada) and those related to Proterozoic komatiites (e.g. those of the Raglan and Thompson belts which are both in Canada)[1]. The

[1] References for the literature related to individual deposits or camps are given in this section only in cases in which the deposits are not mentioned in subsequent chapters of this book.

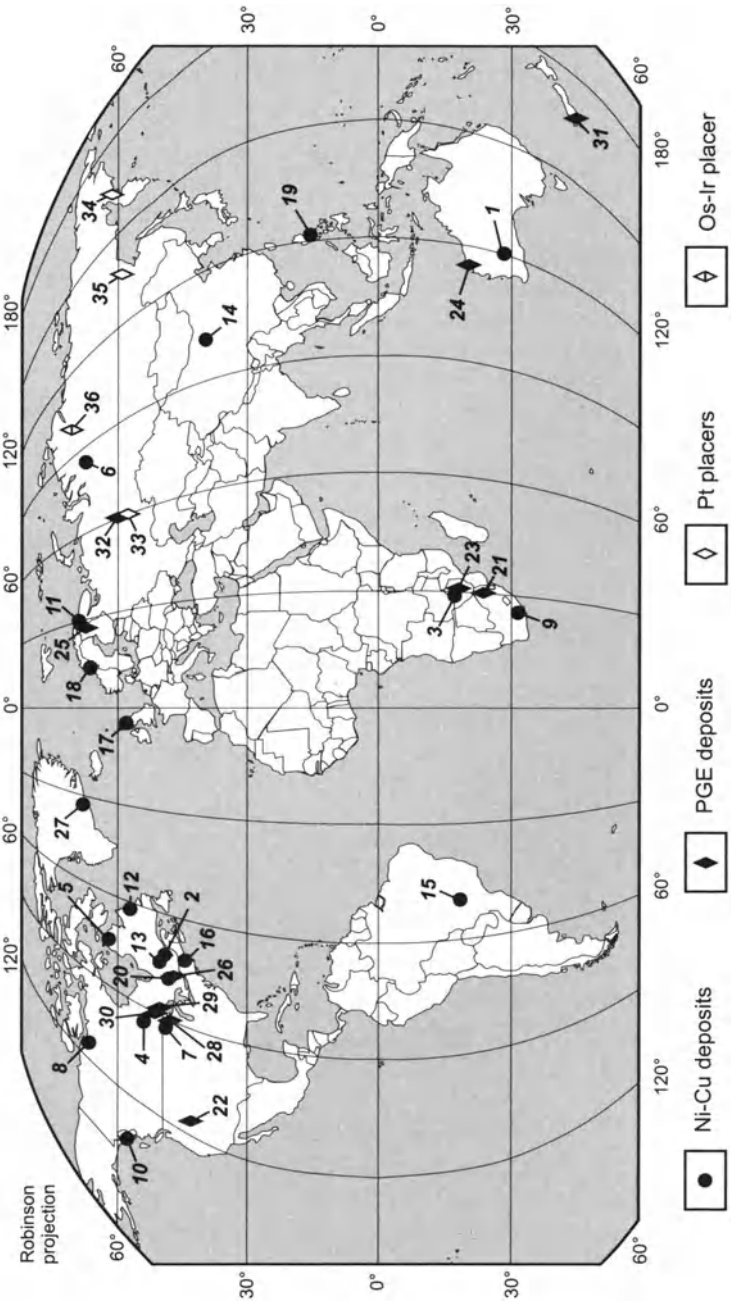


**Fig. 1.2.** Geographic distribution of the world's most important magmatic sulfide Ni-Cu and PGE deposits. Numbers of the deposits correspond to those used in Tables 1.2 and 1.3

**Table 1.2.** Classification of sulfide nickel-copper deposits based on "petro-tectonic setting"

| Class | Related Magmatism | Camps and deposits (No on Figure 1.2, name and age) | Tectonic Setting of magmatism |
|---|---|---|---|
| NC-1 | Komatiite | 1 = Wiluna-Norseman greenstone belt (Kambalda, Mt Keith, Perseverance and others) (A)<br>2 = Abitibi (A)<br>3 = Zimbabwe (A) | Greenstone belts (rift?) |
| | | 4 = Thompson (PPR)<br>5 = Raglan (PPR) | Rifted Continental Margin |
| NC-2 | Flood Basalt | 6 = Noril'sk (Ph)<br>7 = Duluth (NPR)<br>8 = Muskox (NPR) | Rift (Triple junction) |
| | | 9 = Insizwa (Ph) | Rifted Continental Margin |
| | | 10 = Wrangelia (Ph) | Rifted Island Arc |
| NC-3 | Ferropicrite | 11 = Pechenga (MPR) | Rifted Continental Margin |
| NC-4 | Anorthosite-Granite-Troctolite | 12 = Voisey's Bay (NPR) | Rift |
| NC-5 | Miscellaneous Picrite-Tholeiite | 13 = Montcalm (A) | Greenstone belts (rift?) |
| | | 14 = Jinchuan (MPR) | Rifted Continental Margin |
| | | 15 = Niquelandia (MPR) | Continental rift |
| | | 16 = Moxie (Ph)<br>17 = Aberdeenshire Gabbros (Ph)<br>18 = Rona (Ph) | Orogenic (Compressive) |
| | | 19 = Acoje (Ph) | Ophiolite Belt (ocean) |
| NC-6 | Impact Melt | 20 = Sudbury (MPR) | Meteorite Impact |

Age: A = Archean (>2500 MA); PPR = Paleoproterozoic (2500-2000 MA); MPR = Mesoproterozoic (2000-1400 MA); NPR = Neoproterozoic (1400-600 MA); Ph = Phanerozoic (<600 MA)

tectonic setting of Archean komatiites is debatable, but certainly is related to rifting, while the Proterozoic examples are the result of magmatism that developed at rifted continental margins. With certain exceptions, komatiitic magmatism has become less magnesian and lower in temperature on progressing from the Archean to the Proterozoic, and this accounts for some of the differences between the two sub-classes.

Class NC-2 (Chap. 4) comprises deposits that have developed within the feeders to Flood basaltic magmatism. They can be further subdivided in terms of their tectonic setting: i.e. those related to an intra-continental rift or triple junction (e.g. Noril'sk, Duluth and Muskox); those related to a rifted continental margin (e.g. Insizwa) and those related to flood basalts that have developed in an oceanic environment (e.g. Wrangelia see Chap. 10). The most important deposits belong to the first sub-class, and there are insufficient examples of the other sub-classes to allow one to determine whether there are significant differences within these sub-classes.

Class NC-3 comprises a relatively uncommon magmatic association, that of ferropicrites, for which the only significant example is the Pechenga camp of the Kola peninsular. The tectonic setting is debated (see Chap. 5), but is most likely that of a rifted continental margin.

Class NC-4 covers those deposits that are related to Anorthosite-Granite-Troctolite complexes such as the Nain Plutonic Complex of Labrador, Canada. For many years this association was not thought to be important as a source of magmatic sulfide deposits, but the 1995 discovery of Voisey's Bay deposit (Chap. 6) changed this prevailing viewpoint. Thus far Voisey's Bay is the only significant deposit of this association, although the uneconomic mineralization at Pants Lake (80 km south of Voisey's Bay and also associated with the Nain Plutonic Suite) constitutes another example of sulfides that have developed with this association. As discussed in Chap. 10, the Voisey's Bay deposit appears to be closely related to faulting that may be incipient rifting.

Class NC-5 comprises a miscellaneous grouping of deposits that are all associated with magmas ranging from picritic to tholeiitic in composition. Their tectonic settings are very varied. Montcalm (Barrie and Naldrett 1988) occurs in an Archean greenstone belt and the tectonic setting is undetermined at present. Jinchuan, described in Chap. 7, is associated with a fault system that is interpreted as a rifted continental margin (see Chap. 10). The Niquelandia deposit occurs in one of a series of mafic/ultramafic intrusions which form a belt in the central part of Brazil. The intrusions occur in a mixed psammitic-pelitic sequence of sediments with interlayered volcanic horizons, and are thought to have been intruded into a Mesoproterozoic continental rift that became metamorphosed during Neoproterozoic continental collision (Ferreira-Filho et al. 1995). The Moxie intrusion of Northern Main (Thompson and Naldrett 1984), the Caledonian intrusions of north-eastern Scotland (Fletcher 1987), and the Rona intrusion near Narvik, Norway (Boyd and Mathiesen 1979) were emplaced in a compressive orogenic environment. The Acoje Ni sulfide deposit in the Zambales ophiolite of the Phillipines (Bacuta et al. 1987,

**Table 1.3.** Classification of PGE deposits based on "petro-tectonic setting"

| Class | Related Magmas | Intrusive Complex (No on Figure 1.2, name and age) | Tectonic condition of magmatism | Example of deposits (name and type) |
|---|---|---|---|---|
| PGE-1 | High Proportion of U-type magma*, Lesser amount of Tholeiite | 21 – Bushveld (PPR) | Intra-Cratonic | Merensky Reef (1); UG-2 Chromitite (3); Platreef (5); Dunite Pipes (8) |
| | | 22 – Stillwater (A) | Not determined | J-M Reef (1) |
| | | 23 – Great Dyke (A) | Intra-Cratonic Rift | Main Sulfide Zone (2) |
| PGE-2 | U-type and Tholeiite | 24 – Munni-Munni i (A) | Intra-Cratonic? | Layer of Porphyritic Websterite (2) |
| | | 25 – Penikat (PPR) | Rifted Continental Margin | SJ Reef (1) |
| | | 25 – Portimo (PPR) | | SK and RK Reefs (1); Marginal Ore (5) |
| PGE-3 | Tholeiite | 26 – East Bull Lake (PPR) | | Marginal Ore (5) |
| | | 26 – River Valley (PPR) | | Marginal Ore (5) |
| | | 27 – Skaergaard (Ph) | | Platinova (2) |
| | | 27 – Cap Edvard Holm (Ph) | | Willow Ridge Reef (1) |
| | | 28 – Sonju Lake (NPR) | Rift (Triple junction) | Sonju Lake "Reef" (2) |
| | | 29 – Coldwell (NPR) | | Marathon (5); Bermuda (4) |
| | | 30 – Lac des Iles (A) | Not determined | Robie Zone (7) |
| PGE-4 | Calc-alkaline mafic | 31 – Longwoods (Ph) | Orogenic (Island Arc) | Longwoods area (10) |
| | | 32 – Volkovsky (Ph) | | Volkovsky (6); Baron (?) |
| PGE-5 | Ural-Alaskan Ultramafic/Mafic of Alkaline Affinity | 33 – Nizhny Tagil and others of Urals Platinum Belt (Ph) | | Soloviev Hills (9); Urals placers (10) |
| | | 34 – Koryakia Region (Ph) | | Seynav-Galmoznav (10) |
| | | 35 – Kondyor (Ph) | Craton, at boundary with VPB** | Kondyor (10) |
| PGE-6 | Alkaline Mafic/Ultramafic | 36 – Guli (Ph) | Rift | Ingarinda (10) |

Table 1.3. (cont.)

*U-type magma is high-magnesian basaltic andesite with approx. 52-55wt% $SiO_2$, 12-14 wt% $Al_2O_3$, 1000-2000 ppm Cr (Irvine and Sharpe, 1986). **VPB = Volcano-plutonic Belt.

Deposit types: 1-4 = Stratiform deposits: 1 = Sulfide-bearing reef; 2 = Sulfide association, no reef; 3 = Chromitite association; 4 = Magnetite association; 5-6 = Stratabound deposits: 5 = Sulfide association; 6 = Magnetite association; 7-9 = Discordant deposits: 7 = Sulfide association; 8 = Dunite pipes; 9 = Chromitite veinlets and schlieren; 10 = Placers.

Age symbols are explained in Table 1.2

Rossman et al. 1989) is the only known example of a deposit occurring within an ophiolite complex. Sudbury (NC-6) is unique (Chap. 8) and comprises a class on its own, i.e. mineralization that has developed from the melt produced by extra-terrestrial impact (see recent summary by Naldrett 2003).

Considering now sulfide-poor, PGE-rich deposits, the initial division of these deposits is on the basis of petro-tectonic setting, as has been done above for Ni-Cu deposits (Table 1.3). In Chap. 9, where these deposits are discussed in detail, they are further sub-divided on the basis of morphology and predominant mineralogical association of the ore bodies, including whether they are stratiform, stratabound or discordant; and whether the PGE show a sulfide, chromite or magnetite association. As discussed in Chap. 9, it has become apparent (Iligna 1994; Miller and Andersen 2002; Alapieti and Lahtinen 2002), that the largest PGE deposits of the world occur in intrusions (Bushveld Igneous; Stillwater Igneous Complex; Great Dyke of Zimbabwe) that are characterized by a high proportion of an early magma with a distinctive $Al_2O_3$-poor and MgO-, Cr- and yet $SiO_2$-rich (U-type) composition, which was followed in the same intrusion by one with a more typical tholeiitic composition. Many of the PGE concentrations occur at levels in the intrusions at which there is trace element evidence of variable degrees of mixing of these two magma types. This association is grouped as a distinctive class, PGE-1, in Fig. 1.2.

Deposits in intrusions that also show evidence of U-type and tholeiitic magmas, but in which the tholeiitic component is dominant are grouped as class PGE-2. These deposits include the Pennikat and Portimo complexes in Finland, and the Munni Munni intrusion in the Pilbarra Archean block of Western Australia.

Class PGE-3 comprises intrusions for which there is no evidence of an early U-type magma, but for which the magma is clearly tholeiitic. Examples include the East Bull Lake and River Valley intrusions respectively west and east of Sudbury, Keweenawan intrusions of the Lake

Superior area including the Sonju Lake intrusion within the Duluth Complex and the Coldwell intrusion (Barrie et al. 2002), the Kap Edvard Holm and Skaergaard intrusions of East Greenland, and the Lac des Iles deposit in Canada.

Calc-alkaline magmatism (Class PGE-4) is known to host PGE concentrations, although none of these have proved to be economic. Examples include intrusions of the Platinum Belt in the Ural mountains of Russia, where at both the Volkovsky deposit and the Baron prospect PGE are concentrated in zones rich in titaniferous magnetite, apatite and Cu sulfides (see Chap. 9 for details). The Longwoods Intrusive Complex (Cowden et al. 1990) is clearly calc-alkaline and forms part of an accreted volcanic terrain at the southern tip of the southern end of the South Island of New Zealand. PGE-bearing gold placers have been derived from the intrusion, but the nature and origin of the primary PGE mineralization is not understood at the present time.

Class PGE-5 deposits are associated with a distinctive style of dominantly ultramafic intrusion that is commonly referred to as the Ural-Alaskan type (Johan 2002). The nature of the magma to which they are related is still not clearly defined, but the primary melt had an alkaline affinity (see Chap. 9). These intrusions are the source of the most important of the world's Pt placers: Soleviev Hills, Urals; Kondyor massif, Eastern Siberia (Malich 1999); and the Seynav-Galmoznav massif, Koryakia, Russia (Batanova and Astrakhantzev 1992; Vidik at al. 1999). Bedrock platinum is associated primarily with veinlets and segregations of remobilized chromite in recyrstallised dunite in the Nizhniy Tagil massif of the Urals Platinum Belt (Soloviev Hills deposit) where some mining has taken place. Van Treeck and Newberry (in press) reported hydrothermal remobilized Pt associated with magnetite in the Union bay intrusion of SE Alaska.

Class PGE-6 covers mineralization associated with carbonatite-bearing mafic/ultramafic intrusions that are clearly alkaline in composition. An example is the Early Triassic Guli intrusion in the northern part of the Siberian platform that is the source of Os-Ir placers (Malich 1999). The placers are not economic, but they are important because they constitute the only significant concentration of Os-Ir minerals in placers, and are exploited on a small scale by local prospectors.

It should be noted that the foregoing classification of deposits that is based primarily on the petrology and to a lesser extent on the tectonic setting of the host magmatic formations is not the only way in which to consider the deposits. A somewhat different scheme for grouping deposits, which is more useful when the objective is exploring for them, is discussed in Chap. 10. Here they are viewed in terms of how they fit into a very

simple scheme of rifting. Discussion of this different scheme has been confined to the end of this book, and it has not been used to guide its layout, because our understanding of the environments of ore formation are constantly changing, and it was thought unwise to use a framework for the book which might itself require modification in a few years. It has been decided, therefore, to use the more firmly established petrogenetic framework that has been outlined above.

## 1.2 Size and Composition of Deposits

The relative importance of a selected group of the world's largest deposits/camps as a source of Ni is illustrated in Fig. 1.3. The Noril'sk and Sudbury camps dominate in terms of contained Ni, although the Ni/Cu ratio at Noril'sk is approximately 0.5 while at Sudbury it is about 1.1. Duluth represents a major Ni resource, but the low grade (0.2 wt% Ni, 0.66wt% Cu), coupled with environmental constraints on operating large, low grade deposits means that as yet it has not been mined. Excluding Duluth, Jinchuan

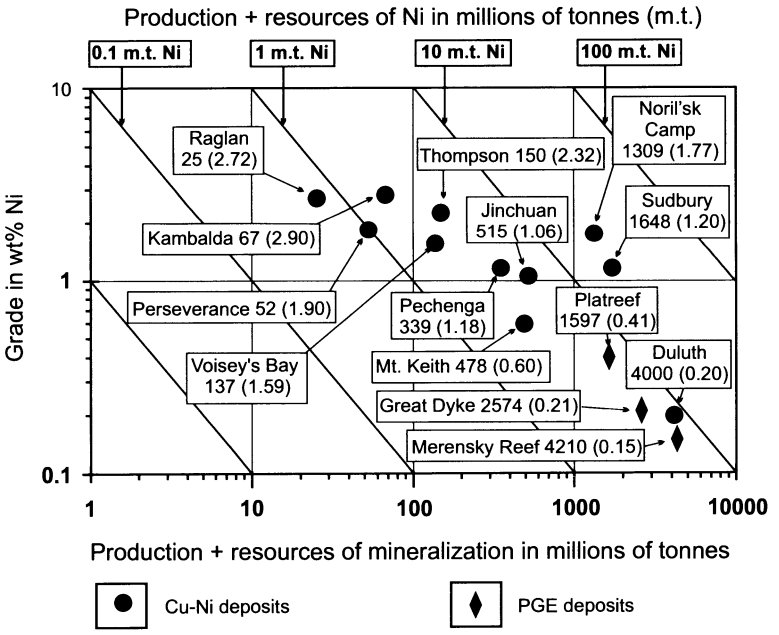


**Fig. 1.3.** Plot of grade in wt% Ni versus production + resources of mineralization in millions of tonnes for major Ni and PGE sulfide deposits of the world. Data are from Table 1.1

ranks third in the world in terms of contained Ni, with Pechenga, Thompson, Mt Keith, Voisey's Bay, Kambalda, Perseverance and Raglan in 4th to 10th places respectively. Important reserves of Ni are associated with some PGE deposits (in the reefs of the Bushveld Complex and sulfide zones of the Great Dyke Zimbabwe) but Ni grades are very low (0.04 to 0.41 wt% – Table 1.1) and Ni only constitutes a byproduct.

The importance of deposits in terms of their PGE is illustrated in Fig. 1.4. The sources of these data are explained in Table 1.1. The deposits of the Bushveld complex (Merensky Reef, UG-2 chromitite and Platreef) dominate, although the Noril'sk ores and the Main Sulfide zone in the Great Dyke constitute important resources. It should be noted that despite their near equivalence with regard to total contained Ni, the data indicate that the deposits at Noril'sk contain 6 to 7 times as much PGE as those at Sudbury.

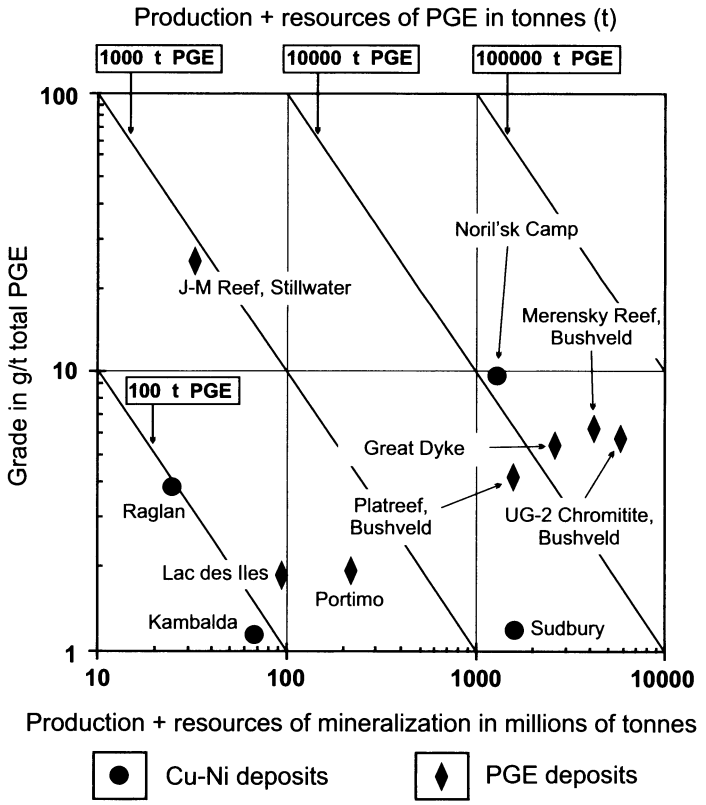


**Fig.1.4.** Plot of grade in g/t total PGE versus production + resources of mineralization in millions of tonnes for major PGE-containing deposits. Data are from Table 1.1

Some important compositional differences exist between Ni-Cu deposits that have formed in association with different magma types. These are illustrated in Table 1.4 and in the Appendix. Most Archean Komatiite-related deposits are characterized by high Ni tenors (=Ni content in 100% sulfide)[2] and high Ni/Cu ratios, which reflect the compositions of their source magmas. The Mt Keith (50) and Epoch (58) deposits have particularly high Ni/Cu ratios, but these deposits have been affected strongly by talc-carbonate alteration, and their compositions have likely been changed by the transfer of Ni from silicates to sulfides during this alteration (Eckstrand 1975).

The Pd/Ir ratio is a measure of the steepness of the PGE profile on a chondrite- or mantle-normalized PGE plot. As pointed out by Naldrett and Duke (1980), Archean komatiite-related deposits have relatively low ratios, while those related to progressively less mafic magmas have progressively higher ratios. This is shown in Table 1.4 in the progressive increase of this ratio from Archean komatiite deposits (typical MgO contents of magma = 30wt%), through Proterozoic komatiite deposits (typical MgO contents = 20wt%), the ferro-picrite related deposits of Pechenga (typical MgO contents = 15wt%), the magnesian basalt-related deposit at Jinchuan (MgO content of magma = 12 wt%) to the deposits at Sudbury and Voisey's Bay. The flood basalt-related deposits, with the exception of Insizwa, have the highest Pd/Ir ratios of all deposits. The Alexo deposit is exceptional with regard to other Archean komatiite-related deposits in terms of its high Pd/Ir and Pd/Pt ratios and low Ni content in 100% sulfides – in many respects it resembles those deposits that are associated with much less mafic magmas, although the environment at Alexo is one of typical Archean komatiitic lavas.

---

[2] In calculating the metal content in 100% sulfide, the whole-rock Ni content is assumed to be all in sulfide, and is then calculated as though it were all in pentlandite containing 36 wt% Ni (a typical value for Sudbury pentlandite). The sulfur required for the pentlandite is then subtracted from the whole rock sulfur content. The same calculation is made for Cu, assuming that it is all present as chalcopyrite, and the sulfur subtracted as was done for Ni. The remaining sulfur is then calculated as though it were present in monoclinic pyrrhotite. The percentages of pentlandite, chalcopyrite and pyrrhotite are combined to give a total percent sulfide in the sample. This gives a conversion factor to recalculate the metals as though they were present in 100% sulfide. Errors will occur in this recalculation if the sulfide content is low, and significant Ni is present in olivine (a correction for this effect is discussed in Chap. 6), or if other minerals, such as pyrite, bornite or chalcocite are present in significant amounts. The errors introduced by assuming fixed compositions for pentlandite and pyrrhotite (both solid solutions) are minor in comparison with other potential errors.

**Table 1.4.** Average Sulfide Compositions of Different Classes of Nickel Deposits (based on data presented in Table 1.1 and in the Appendix)

| | Wt% Ni in 100% Sulfide | | Ni/Cu | Ni/Co | Pd/Pt | Pd/Ir |
|---|---|---|---|---|---|---|
| | Range | Average | | | | |
| **Archean komatiite-related deposits** | | | | | | |
| ***Western Australia*** | | | | | | |
| Kambalda | 9–19 | 14.20 | 13.50 | 0.07 | 1.39 | 8.87 |
| ***Zimbabwe (massive ore)*** | | | | | | |
| Trojan | | 10.80 | 7.71 | | 0.49 | 7.14 |
| Epoch | | 23.60 | 58.00 | | 0.49 | 0.95 |
| Shangani | | 13.33 | 13.50 | | 0.30 | 8.58 |
| ***Canada*** | | | | | | |
| Langmuir | | 12.33 | 25.08 | | 1.88 | 5.88 |
| Alexo | | 6.42 | 15.07 | | 2.62 | 77.27 |
| **Proterozoic komatiite-related deposits** | | | | | | |
| ***Cape Smith Belt*** | | | | | | |
| Raglan | 10.4–15.3 | 12.8 | 3.88 | 0.02 | 2.84 | 38.06 |
| ***Thompson Nickel Belt*** | | | | | | |
| Pipe-2 | | 3.95 | 24.68 | 22.00 | 2.26 | 2.15 |
| Thompson | | 8.46 | 14.32 | 50.00 | 4.46 | 13.40 |
| Bucko Lake | | 20.85 | 3.88 | | 2.87 | 21.19 |
| **Flood basalt-related deposits** | | | | | | |
| Noril'sk | | 6.25 | 0.58 | 58.00 | 3.43 | 217.34 |
| Duluth | | 4.09 | 0.33 | 10.50 | 3.35 | 184.17 |
| Great Lakes Nickel | | 5.19 | 0.52 | | 4.02 | 303.56 |
| Insizwa | | 5.88 | 0.91 | | 2.40 | 18.12 |
| **Anorthosite-related deposits** | | | | | | |
| Voisey's Bay | 3.64–4.61 | 4.07 | 1.87 | 18.00 | 1.29 | 59.98 |
| **Other deposits** | | | | | | |
| Pechenga | 2.7–13.7 | 10.49 | 1.86 | 26.00 | 1.33 | 9.74 |
| Jinchuan | 9.4–11.0 | 10.69 | 1.76 | 56.00 | 1.00 | 14.37 |
| Sudbury | 2.5–8.0 | 5.5 | 1.11 | 32.00 | 1.26 | 30.65 |

A more detailed break-down of these deposits appears in the Appendix

It can be seen from the Appendix that different classes of deposit have characteristic proportions of the PGE, expressed in terms of the ratio of (Pt+Pd)/(Ni+Cu) with PGE expressed in g/t and Ni and Cu expressed in wt%. Essentially all of the komatiite deposits have ratios between 0.1 and 0.5, with the exception of the Raglan deposits, which have ratios of about 0.7 to 0.9. The Sudbury deposits show a variation, depending on location. Typical ore from those on the South Range (see Chap. 8) have ratios from 0.3 to 1, while those on the North and East Ranges have ratios between 0.05 and 0.3. Marked exceptions to this generalization are the Cu-rich

footwall ores of the North and East Ranges which have ratios from 0.5 to 1. The ores at Voisey's Bay, Pechenga and Jinchuan have similar ratios to those at Sudbury, respectively ranging from 0.05 to 0.1, 0.05 to 0.3 and 0.04 to 0.5. Deposits related to Flood basalts are generally characterized by higher proportions of PGE to other metals, with ratios between 0.5 and 5.

As would be expected, deposits that are mined primarily for PGE have (Pt+Pd)/(Ni+Cu) (PGE in g/t, Ni and Cu in wt%) that are much higher than in Ni- and Cu-rich ores. PGE-enriched horizons such as the Merensky and UG-2 Reefs of the Bushveld, the J-M Reef of the Stillwater, the SK Reef of the Portimo area, Finland and the Main Sulfide Zone of the Great Dyke vary between 9 and 350. PGE-rich mineralization in the marginal zones of the East Bull Lake and River Valley intrusions near Sudbury and the Portimo intrusion(s) in Finland is also characterized by high ratios from 11 to18.

In summary, one can say that most sulfide-rich Ni-Cu deposits have (Pt+Pd)/(Ni+Cu) (PGE in g/t, Ni and Cu in wt%) ratios of less than 0.5, except those related to flood basalts, which have ratios between 0.5 and 5. Most sulfide-poor, PGE-rich deposits have ratios of 10–30, with some exceptional deposits with ratios >100.

The compositional characteristics discussed above are the consequence of the genesis of the sulfides constituting the mineralization, and are unlikely to vary widely within mineralization of the same style within a given area. It is thus important to establish these characteristics at an early stage of exploration, because it will provide a guide as to the kind of deposit that one should be exploring for.

## 1.3 General Considerations for the Genesis of the Deposits

Key aspects in the genesis of a magmatic sulfide ore deposit are (i) that the host magma becomes saturated in sulfide and segregates immiscible sulfide, (ii) that the sulfides are themselves concentrated in a restricted locality where their abundance is sufficient to constitute ore, and (iii) that these sulfides react with a sufficient amount of magma to concentrate chalcophile elements to an economic level. It is the objective of this section to examine some of the world's major magmatic sulfide camps with a view to determining how these aspects have been fulfilled.

Early segregation of liquid sulfide is not part of the normal cooling and crystallization of mafic magma. The world's important deposits of Ni-Cu sulfides (as opposed to sulfide deposits of interest primarily because of

their PGE content) occur almost exclusively at the base of their associated igneous bodies, which implies that the magmas involved were saturated in sulfide, and carrying excess sulfide at the time of their final emplacement. The high PGE content (1–10 ppb Pt, Pd) of most basaltic magma other than MORB implies that these magmas are not sulfide saturated as they leave the mantle, or during their ascent into the crust. Something has to happen to specific batches of magma prior to emplacement to cause sulfide saturation, if a significant magmatic deposit is to form.

The principal factors controlling the solubility of iron sulfide in a silicate melt are discussed in Chap. 2, in which it is concluded that these are: 1) Pressure; 2) Temperature; 3) FeO+$TiO_2$ content of the melt; 4) Oxidation state of the melt; 5) Mafic versus felsic components in the melt.

With regard to factor 1, Mavrogenes and O'Neill (1999) have shown that pressure has a negative effect on the ability of a silicate melt to dissolve sulfide, that is, as a melt ascends in the crust, its ability to dissolve iron sulfide increases. Since most melts leave the mantle unsaturated in sulfide, they will not achieve saturation as they ascend to shallower depths (lower pressures). This effect can be offset to some extent by decrease in temperature, which has a negative effect on sulfur solubility (Buchanan and Nolan 1979). Most melts are intruded or extruded close to their liquidus temperatures, indicating that they have cooled during ascent, however the data of Mavrogenes and O'Neill (1999) indicate that the effect of cooling is likely to be less than the effect of decreasing pressure, so that, apart from the influence of changing composition, melts are likely to reach the surface unsaturated in sulfide. Silicates will start crystallizing before sulfides segregate, and any sulfides that develop subsequently will therefore be intermixed with cumulus silicates. Ni-Cu-dominant (as opposed to PGE-dominant) magmatic sulfide deposits need to be much richer in sulfide than will be produced by the co-precipitation of solid silicate and sulfide liquid under cotectic conditions. What is required is for some external factor to bring about the segregation of considerable sulfide in a magma without causing significant silicate crystallization.

Variation in the FeO or $TiO_2$ content (factor 3), while occurring as a magma crystallizes and fractionates, is also not something which is readily imposed on a magma externally, and, in general, these elements either remain constant (FeO), or increase ($TiO_2$) during the early stages of fractional crystallization, thus adding to the ability of the melt to dissolve sulfide. Oxidation (factor 4) is capable of causing sulfide precipitation without necessarily causing silicates to form; to this author's knowledge, the only situation where this might have played a role is that of the Platreef of the Bushveld Complex, where the Bushveld magma has ingested a large amount of limestone from adjacent country rocks (Buchanan and Rouse

1984). This is however a deposit of rather weakly disseminated sulfide, important primarily for its PGE content. As will be seen in Chap. 2, felsification of a mafic magma, and the addition of sulfur from an external source, are the most important causes of sulfide segregation. PGE deposits in layered intrusions, such as the Merensky Reef of the Bushveld Complex and the J-M Reef of the Stillwater Complex have different characteristics, and are the result of different genetic processes, as is brought out in Chap. 9.

The composition of the sulfide liquid responsible for a deposit of magmatic sulfide depends on (a) the composition of the silicate magma with which the sulfide liquid reacted, (b) the value of the coefficients governing the partitioning of elements between silicate magma and sulfide liquid, (c) the ratio of silicate magma to sulfide liquid involved in the reaction. The effect of magma composition on the resulting magmatic sulfide deposit is considered for individual deposit types in many of the following chapters. Factors (b) and (c) are discussed in Chap. 2.

As with silicate liquids, sulfide liquids do not normally freeze in situ, but cool slowly, depositing cumulates of early forming nickeliferous pyrrhotite (monosulfide solid solution or mss) with the remaining liquid becoming steadily depleted in Fe and enriched in Cu. Commonly, this liquid escapes from early-forming cumulates, so that some parts of a deposit are enriched in cumulates, and others are enriched in the crystallization products of the fractionated liquid (Ebel and Naldrett 1997; Naldrett et al. 1997). This is also discussed below. Sulfide systems react much more rapidly at a given temperature than silicate systems, so that the mineralogy of a magmatic sulfide deposit is the result of the equilibration of the initially-formed minerals over a range of subsolidus temperatures, down to below 150°C. Sulfide phase equilibria governing these reactions are also discussed in Chap. 2.

The order of chapters subsequent to Chap. 2 requires some comment. In general it follows the classification scheme proposed above. Class NC-1, komatiite-related deposits, are discussed first in Chap. 3. Class NC-2, deposits related to flood basalt magmatism are the focus of Chap. 4. Class NC-3, deposits related to ferropicritic magmatism form the focus of chapter 5, while Class NC-4 (anorthosite-granite-troctolite-related deposits) is discussed in Chap. 6. Jinchuan is by far the most important deposit belonging to Class NC-5 and this is described in Chap. 7. Sudbury (Class NC-6) is the oldest of the major magmatic sulfide districts, and, from a historical perspective, has received the greatest amount of attention from researchers over the longest time and is the subject of Chap. 8. As discussed above, PGE deposits occur associated with many different magma types. Descriptions of many of these, and a discussion of the genesis of the different

styles of mineralization involved are found in Chap. 9. This book concludes with a chapter (Chap. 10) summarizing key factors that have arisen from consideration of individual districts, and outlining guidelines for using these factors in exploration.

# 2 Theoretical considerations

Magmatic sulfide ores form as the result of droplets of an immiscible sulfide-oxide liquid developing within silicate magma and then becoming concentrated in a particular location. Certain elements, notably the Group VIII transition metals Fe, Co, Ni, Pd, Pt, Rh, Ru, Ir and Os together with Cu and Au, partition strongly into the sulfide-oxide liquid, and thus become concentrated with it. An understanding of deposits of this type requires an understanding of the chemical and physical processes that are involved. To help in this, we first discuss (section 2.1) factors governing the solubility of sulfide in mafic and ultramafic melts. This is followed by a discussion of the partitioning of elements between sulfide-oxide liquid and silicate magma or olivine, and the influence of mass ratios between sulfide liquid and silicate melts ("R" and "N" factors) on the composition of sulfides. Some relevant phase equilibria are discussed in section 2.3. Section 2.4 is devoted to fractional crystallization of sulfide melts which is particularly relevant to the formation of valuable PGE-rich zones within deposits such as are known at Noril'sk and Sudbury and elsewhere. In a final section, 2.5, the poorly understood problem of how sulfur enters a magma from an external source is briefly discussed.

## 2.1 The solubility of sulfur in silicate melts

Knowledge of the solubility of sulfur in mafic and ultramafic silicate melts is important in understanding how magmatic sulfide deposits form and also in evaluating the potential of igneous bodies as hosts for ore deposits of this type. Early work on sulfur solubility was undertaken by metallurgists, notably Richardson and his co-workers (Fincham and Richardson 1954; Abraham et al. 1960). Although the melt compositions studied by these workers were those of smelter slags rather than natural magmas, Fincham and Richardson's (1954) study provided valuable insight into the mechanism of sulfur solution and its important implications in nature. They showed that at oxygen fugacities above $10^{-6}$ in melts studied at 1400 and 1500°C, sulfur dissolves primarily as $SO_4^{2-}$, but at oxygen fugacities

less than $10^{-6}$ atm it dissolves primarily as sulfide. They introduced a function termed the "sulfur capacity"[3] of the melt, $C_S$, and showed that it is constant for melts of the same composition and obeys the relationship:

$$C_S = (wt\%S * pO_2^{1/2})/pS_2^{1/2}, \quad (2.i)$$

where $pO_2$ and $pS_2$ are the partial pressure of oxygen and sulfur respectively.

$C_S$ increases with rise in temperature and changes with composition, generally increasing with increasing FeO, MgO, and CaO contents and decreasing with increasing $SiO_2$ and $Al_2O_3$.

MacLean (1969), in his study of the system Fe-S-O-$SiO_2$, found that the sulfur content of a silicate melt in equilibrium with sulfide-rich liquid decreases with increasing oxygen content (this sulfur content is henceforth referred to as the "sulfur content at sulfide saturation" or "SCSS"). He attributed this observation to the fact that sulfur dissolves by displacing oxygen bonded to $Fe^{2+}$ and that increasing oxygen results in an increase in $Fe^{3+}$ at the expense of $Fe^{2+}$ in the melt. Connolly and Haughton (1972) confirmed this point.

Shima and Naldrett (1975) studied a komatiitic melt and obtained strong evidence supporting MacLean's contention as to the mechanism of sulfur solution.

Considering the reaction:

$$FeO^{(in\ melt)} + 1/2S_2 = FeS^{(in\ melt)} + 1/2O_2 \quad (2.1)$$

the activities of the reactants ($a$) are related by the expression:

$$a_{FeS} = \gamma_{FeS} * N_{FeS} = K * a_{FeO} * (fS_2^{1/2}/fO_2^{1/2}) \quad (2.ii)$$

thus,

$$\log N_{FeS} = 0.5 * \log fS_2 + (\log K + \log a_{FeO} - 0.5 * \log fO_2 - \log \gamma_{FeS}), \quad (2.iii)$$

where $\gamma_{FeS}$ is the rational activity coefficient for FeS in the melt, $N_{FeS}$ is the mole fraction of FeS, K is the equilibrium constant, and $fS_2$ and $fO_2$ are the fugacities of sulfur and oxygen respectively. If, for small changes in $N_{FeS}$, $a_{FeS}$ is assumed to remain constant and also if the amount of FeO consumed or formed in a reaction such as (2.1) is sufficiently small that its

[3] It should be noted that the function "sulfur capacity" is somewhat misleading. It does not represent the overall capacity of a melt to dissolve sulfur, but is somewhat akin to the equilibrium constant for reaction (2.1). It merely relates the amount of sulfur that will dissolve in a given melt in response to imposed sulfur and oxygen fugacities.

formation has no appreciable effect on $a_{FeO}$[4], it follows from expression (2.i) that a plot of $\log N_{FeS}$ against $\log fS_2$ ($fO_2$ and T kept constant) should produce a straight line relationship with a slope of 1/2, provided that sulfur is dissolving according to reaction (2.1). Fig. 2.1, a plot of Shima and Naldrett's (1975) data, indicates that this relationship is obeyed. Furthermore, Fig. 2.1 shows that as $\log fO_2$ increases, $\log N_{FeS}$ decreases. This is also in accordance with expression (2.ii) above.

It should be appreciated that the preceding discussion and data apply to the solution of S in a silicate melt from a superjacent gas phase in response to changes in the fugacity of sulfur in the gas. In the case of Shima and Naldrett's study, it was only in their experiment at $\log fO_2 = -10.4$ and $\log fS_2 = -2$, that saturation in iron sulfide liquid was achieved.

Haughton et al. (1974) were the first to provide extensive data on the solubility of S in a silicate melt of naturally occurring composition in equilibrium with a sulfide liquid (sulfur content at sulfide saturation = SCSS). They found a strong correlation of SCSS with FeO and, to a lesser extent, with $TiO_2$ contents, but no systematic change with the varying $fO_2$ of their experiments. Buchanan and Nolan (1979) performed a similar series of experiments and were able to demonstrate that increasing $fO_2$ decreased solubility (Fig. 2.2). The data at high FeO contents in this figure are not directly applicable to natural basalts, since FeO increased in their experiments at the expense of **all** other elements, and as a result, at high FeO contents, $SiO_2$ fell well below the level to be expected in even the most Fe-rich natural basalts.

Mathez (1976) studied the S content of the glassy margins of submarine basalt pillows from the Atlantic and Pacific that had been quenched at depths >1000 m. He concluded that these were saturated or nearly saturated when they were quenched. Their S content increases markedly and linearly with increasing FeO content from about 0.105 wt% S at 9.0 wt% FeO to 0.18 wt% at 12.9 wt%. These S concentrations are substantially higher than the experimental results illustrated in Fig. 2.2, an observation that Mathez attributed to the high pressure at which the submarine basalts were quenched, but which, in the light of Buchanan and Nolan's (1979) data, could be due to $fO_2$.

[4] This is a reasonable assumption, since the amount of Fe interacting with sulfur amounts to 0.2 to 0.6 wt% in most melts containing 8 to 12 wt percent FeO.

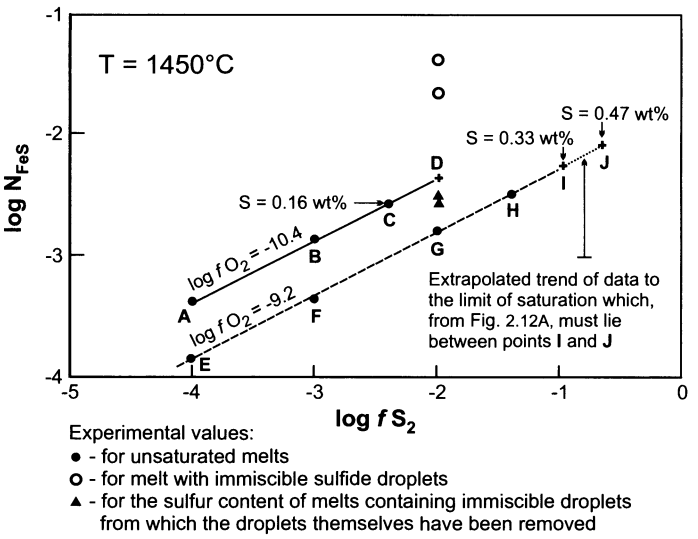


**Fig. 2.1.** Relationship between $N_{FeS}$ and $fS_2$ in a given silicate melt at 1450°C and two values of $fO_2$. Solid line = trend of the data at $fO_2 = 10^{-10.4}$; dashed line = trend of data at $fO_2 = 10^{-9.2}$. From Shima and Naldrett (1975)

### 2.1.1 Effect of Temperature

Buchanan et al, (1983) determined the solubility of sulfur as a function of $fS_2$ in a basaltic melt containing 17 wt% FeO at 1200, 1300 and 1400°C. Data were obtained in the field of undersaturation which indicated that at constant $fO_2$ and $fS_2$, the dissolved sulfur content increases by a factor of 8.5 times per 100°C at 1000°C but that at 1400°C this factor is only 3 times per 100°C. Buchanan et al. also attempted to predict the saturation values of the sulfur content (i.e. SCSS) but their inability to achieve saturation in most of their samples indicates that their predicted values should be treated with caution.

Relatively few data exist on the variation of SCSS with temperature. There seems to be little doubt that SCSS increases with temperature. Haughton et al. (1974) found that tholeiitic melts containing 10 wt% FeO dissolve about 0.04 wt% S when saturated with iron sulfide at 1200°C and $fO_2 = 10^{-10.5}$, whereas Shima and Naldrett (1975) found that a komatiitic melt containing the same FeO content dissolves between 0.16 and 0.27 wt% S at an $fO_2$ of $10^{-10.4}$ at 1450°C. This comparison is rendered inaccurate by differences in melt composition, but indicates an increase of between 0.05 and 0.09 wt% S per 100°C. Wendlandt (1982) found that the

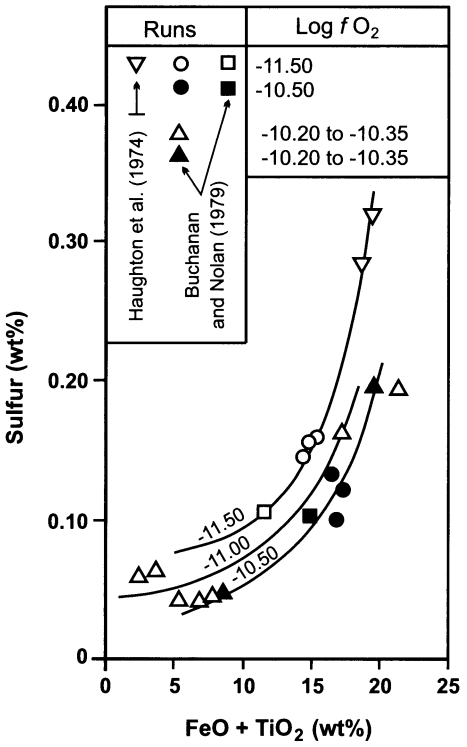


**Fig. 2.2.** Sulfur content of silicate glass in equilibrium with an immiscible sulfide melt, illustrating the effect of varying $fO_2$ and FeO content of the melt. From Buchanan and Nolan (1979), and Haughton et al. (1974)

increase in temperature of a basaltic melt containing close to 8 wt% FeO from 1300 to 1460°C at 20 kb total pressure and an $fO_2$ close to the C-$CO_2$-CO buffer (about one log unit above the quartz-fayalite-magnetite [QFM] buffer according to Wendlandt) caused an increase in SCSS of from 0.09 to 0.16 wt%, corresponding to an increase of 0.04 wt% per 100°C. Wendlandt's experiments on silicate melts of differing FeO contents produced similar results, given the errors inherent in his data. Possibly an increase in SCSS of 3 to 5 times from 1200 to 1450°C is of the order of that to be expected in nature.

### 2.1.2 Effect of Pressure

Huang and Williams (1980) investigated portions of the system Fe-Si-S-O at 32 kb and found that the miscibility gap between sulfide and silicate liquids expands with increasing pressure. Wendlandt (1982) studied the

variation in SCSS in two basalts and an andesite at pressures between 12.5 and 30 kb. He found that SCSS increases with FeO and temperature and decreases with increasing pressure. Comparison with other studies was difficult because he relied on the C-$CO_2$-CO buffer which varies in $fO_2$ with changing pressure, and yet the extent of these variations were uncalibrated between his experiments. However, his studies also indicate that under natural conditions increasing pressure has a depressing effect on SCSS. Mavrogenes and O'Neill (1999) have studied the solubility of sulfur at sulfide saturation (SCSS) in basaltic melts containing 6–14 wt% FeO using Fe and Fe-Ir capsules at pressures ranging from 5 to 90 kb and temperatures of 1400 and1800°C. Their data indicated that SCSS increases exponentially with increase in pressure and increases only slightly with temperature (Fig. 2.3). They also found that $fO_2$ has relatively little influence on SCSS, except in so far as it influences $a_{FeS}$ in the sulfide liquid forming in their experiments. All recent studies therefore imply that as a magma rises to surface, its ability to dissolve sulfur increases and therefore it is not likely to approach saturation with sulfide. Mavrogenes and O'Neill (1999) predict that most basaltic magmas will **never** achieve saturation under near surface conditions unless they have undergone at least 60% fractional crystallization, or have acquired crustal sulfur [Author's comment: or have undergone felsification as a result of interacting with crustal rocks – see below].

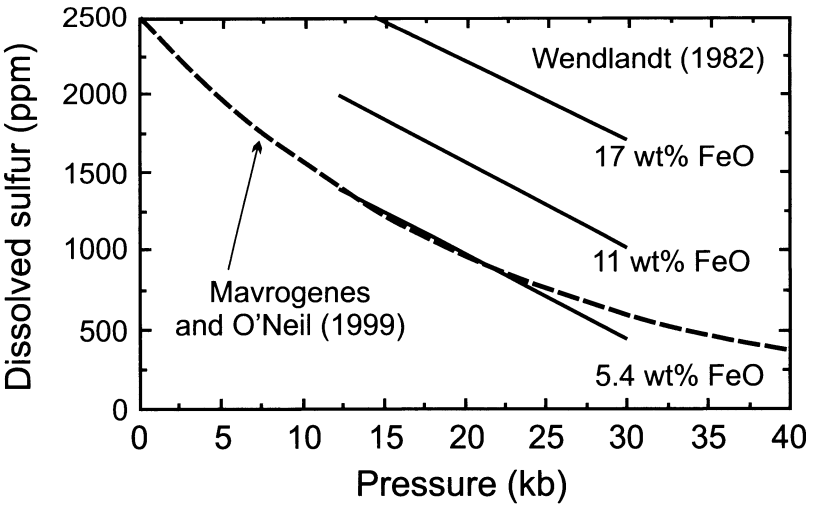


**Fig. 2.3.** Experimental determination of solubility of sulfur in basaltic melts of different FeO content estimated as a function of pressure at 1400°C. Based on the data of Wendlandt (1982) and Mavrogenes and O'Neill (1999)

### 2.1.3 Influence of felsification of mafic/ultramafic magma

Irvine (1975) investigated the effect of the addition of felsic magma to a mafic magma and showed that, when the mafic magma had an adequately high Cr content, this could cause the bulk composition of the resulting hybrid to move into a phase volume in which chromite was the sole liquidus phase. He suggested that convective overturn and intermixing of a felsic melt rock that had developed at the roof of the chamber with the crystallizing magma in the chamber could cause the formation of a chromitite horizon. He also suggested that sulfide immiscibility could result from the mixing.

Li and Naldrett (1993) developed a function for calculating the solubility of FeS in a mafic magma as a function of the prevailing $a_{FeO}$ in the magma. They used this to model changes in the solubility of FeS during the mixing of a basaltic magma with one of granodioritic composition, They used a Keweenawan basalt as the mafic end member and a mixture of tonalite and granitic gneiss from the Sudbury area in a proportion of 1:2 as the felsic end member. Modeling was performed for melts at 1 atm total pressure and the liquidus temperatures of the resulting mixtures, with values of $\log f O_2$ between -9.76 and -9.53 and $\log f S_2$ between -1.90 and 0.80. Their calculations (Fig. 2.4) indicated that a mixture of flood basalt magma that contains sulfur at about 2/3 of its saturation level and a sulfur-free variant of the felsic contaminant will segregate immiscible sulfides for mixing proportions of between 20 and 80 wt% of the contaminant.

### 2.1.4 Variation of Solubility of Sulfide During Fractional Crystallization of a Layered Intrusion

The data on sulfide solubility discussed above has been used (Naldrett and von Gruenewaldt 1989) to construct a curve depicting approximately how sulfide solubility will vary during the fractional crystallization of the magma of a layered intrusion. It has been shown above that, at constant pressure, three factors are extremely important to the solubility of sulfide in a silicate magma, temperature, the FeO content of the magma and oxygen fugacity. Mathez (1990) argued that under closed conditions, and when not crystallizing large amounts of spinel, magmas follow buffer curves when cooling and crystallizing, which would tend to eliminate oxygen fugacity as a major control on sulfide solubility. Decreases in both temperature and FeO content of the magma decrease the solubility of sulfide.

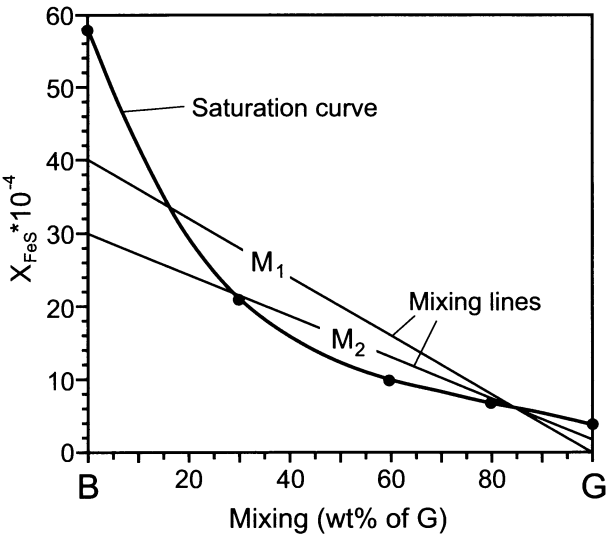


**Fig. 2.4.** Calculated curve showing variation in sulfur solubility with the mixing of Continental Flood Basalt (B; $SiO_2$ = 49.10, FeO = 11.20, MgO = 6.61 wt %; T = 1250°C) and a felsic melt (G; $SiO_2$ = 66.70, FeO = 3.30, MgO = 1.86 wt%; T = 1180°C). $X_{FeS}$ - mole fraction of FeS. The saturation curve is concave upward, so that within wide limits any mixture of the two magmas which are unsaturated in sulfide will itself contain more than the saturation limit. $M_1$ and $M_2$ are two hypothetical mixing lines; in the case of $M_1$, mixtures of between 17 and 84 wt% of component B with G will be saturated, in the case of $M_2$, mixtures of between 30 and 84 wt% of component B with G will be saturated. From Li and Naldrett (1993)

During olivine crystallization, both temperature and the FeO content of the magma decrease[5] so that sulfide solubility decreases. During bronzite crystallization, temperature continues to decrease sharply, but FeO content is relatively constant and then increases as the increase in the FeO/MgO becomes more pronounced. Once plagioclase joins either mafic mineral, the FeO content of the magma will start to increase, and this will inevitably moderate the rate at which the solubility of sulfide declines with continuing crystallization.

Mathez (1976) and Czamanske and Moore (1977) have discussed these general principles with respect to the differentiation of submarine basalts. Mathez pointed out that the crystallization of olivine alone drives submarine basalt magmas towards the sulfide saturation field, of plagioclase

[5] Note that we are speaking of the FeO content of the magma here, not its FeO/MgO ratio. The latter will, of course, increase with olivine crystallization.

alone drives these magmas away from the field, while removal of plagioclase and olivine in the commonly observed proportions of 3 to 1 drives the magmas approximately parallel to the sulfide saturation surface.

Li et al. (2001a) derived an empirical regression equation based on the FeO content of a magma and its temperature, calibrated against sulfide-saturated oceanic basalts, to calculate the solubility of sulfur at sulfide saturation in a mafic magma. They used the programme MELTS (Ghiorso and Sack 1995) to calculate the intrinsic variables of a basaltic magma represented by the chilled margin composition of the Bushveld Complex (B1 magma of Harmer and Sharpe, 1985) during fractional crystallization. They then used the regression equation for sulfide solubility to calculate the variation in sulfur solubility in this magma during fractional crystallization. Their results are shown in Fig. 2.5.

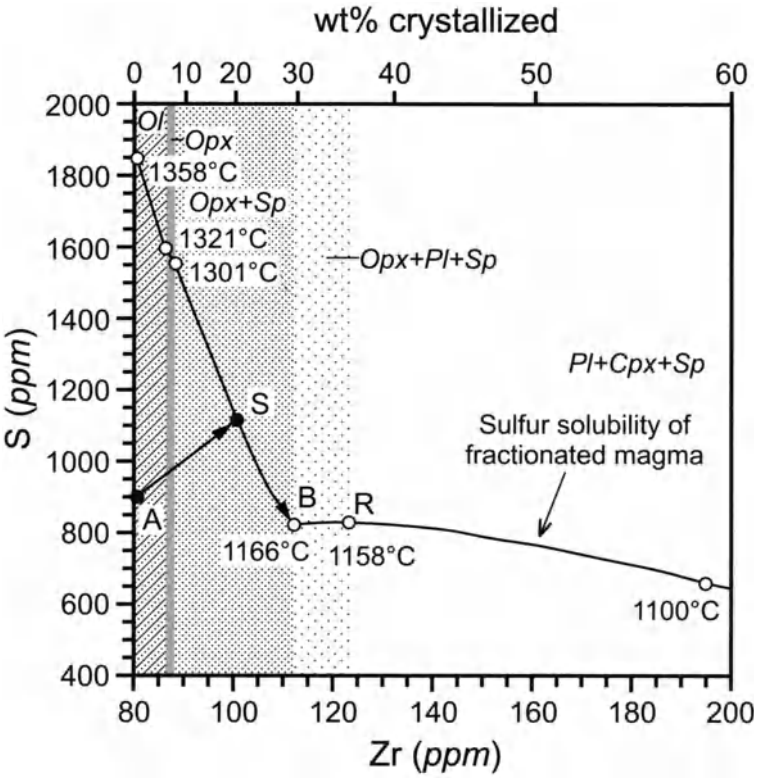


**Fig. 2.5.** Diagram illustrating the variation in the solubility of sulfur in Harmer and Sharpe's (1985) best representative (a sample of chilled marginal material) for the magma responsible for the Lower zone of the Bushveld Complex - B1 magma). After Li et al. (2001a). The concentration of the incompatible element Zr is used as an index of magma crystallization

Initially crystallization is marked by a sharp fall in sulfur solubility, because of the steep decrease in temperature and the sensitivity of sulfur solubility to temperature. Once plagioclase appears on the liquidus, the decrease in temperature for amount of magma crystallized is significantly lower than during the crystallization of olivine and/or pyroxene, the FeO content of the residual magma increases slightly, so that the slope of the sulfur saturation curve is much shallower. These results of Li et al. (2001) are very similar to those of Naldrett and von Gruenewaldt (1989), which were based solely on qualitative considerations of the controls on sulfur solubility. Looking at an initial magma containing about 900 ppm S (the average for samples of B1 magma), the sulfur content of the residual magma will rise along the path A-S until it reaches the saturation curve after about 20% crystallization. Further crystallization will cause sulfides to segregate and the sulfur content to move along path S-B.

Naldrett and von Gruenewaldt (1989) argued that mixing of a fresh input of original magma with fractionated magma such as that shown by point R in Fig. 2.5 will cause the hybrid to lie above the saturation curve and thus immiscible sulfide to segregate, and the new data of Li et al. (2001a) seemed to confirm this. However, using the empirical equation of Li et al. (2001a) to compute the ability of the resultant hybrids to dissolve sulfide, Cawthorn (2002) showed that they would be capable of dissolving more sulfide than they would contain, so that magma mixing of this type, i.e. fractionated with unfractionated magma, would not cause sulfide saturation. Advised in advance of his conclusions, Li et al. (2001b) revisited this problem and agreed with Cawthorn (2002).

## 2.2 Partitioning of Chalcophile Metals between Sulfides and Silicate Melts

It is common to discuss the partitioning of a trace or minor element between two phases, A and B, in terms of a partition coefficient. Referring to equilibria between sulfide melts and silicate magmas, the Nernst partition coefficient $D_i$ for a metal i is defined as:

$$D_i^{(Sul.m/Sil.m)} = (wt\%\ i)^{Sul.m}/(wt\%\ i)^{Sil.m.} \qquad (2.iv)$$

In many cases, one is considering a situation in which metals with a relatively low concentration, such as Ni, Cu and Co, are exchanging with one that has a substantially higher concentration, such as Fe. In these cases, an exchange partition coefficient is commonly defined as in (2.v) below:

$$K_D^{i\text{-}j} = (\text{wt\% i})^{\text{Sul.m.}}*(\text{wt\% j})^{\text{Sil.m.}}/ (\text{wt\% j})^{\text{Sul.m.}}*(\text{wt\% i})^{\text{Sil.m.}} \quad (2.v)$$

where the metal j is Fe.

### 2.2.1 Partitioning of nickel between sulfide and silicate liquids

In the case of metals such as Fe, Ni, Cu, and Co, it is believed (see Shimazaki and MacLean, 1976; Rajamani and Naldrett, 1978) that they are bonded to oxygen in the silicate magma and to sulfur in the sulfide melts[6]. Thus the reaction considered is (for example, in the case of Ni):

$$NiO^{(Sil.m)} + 1/2S_2 = NiS^{(Sul.m)} + 1/2O_2 \quad (2.2)$$

The equilibria involved in reaction (2.2) are related to the thermodynamic equilibrium constant $K_2$ by the expression:

$$K_2 = (a_{NiS}/a_{NiO})*(fO_2^{1/2}/fS_2^{1/2}) = \quad (2.vi)$$

$$(\gamma_{NiS}/\gamma_{NiO})*(N_{NiS}/N_{NiO})*(fO_2^{1/2}/fS_2^{1/2}) \quad (2.vii)$$

Similarly, for reaction (2.3) involving Fe:

$$FeO^{(Sil.m)} + 1/2S_2 = FeS^{(Sul.m)} + 1/2O_2, \quad (2.3)$$

the expression would be:

$$K_{Fe} = (\gamma_{FeS}/\gamma_{FeO})*(N_{FeS}/N_{FeO})*(fO_2^{1/2}/fS_2^{1/2}), \quad (2.viii)$$

where $a$ refers to the respective activities, $\gamma$ to the activity coefficients, N to the mole fractions and $fO_2$ and $fS_2$ are the fugacities of the gases.

From comparison of expressions (2.iv) and (2.vi), one would expect $D_{i\text{-}Sul.\ melt/Sil.magma}$ for all of the metals Ni, Fe, Cu, and Co to be a function of $fO_2$ and $fS_2$ in addition to being a function of the temperature and pressure and the compositions of the two phases in question. However, reactions for

---

[6] This footnote has been added in the final preparation stages of the manuscript. It now appears that this assumption is not strictly true. Chusi Li (personal communication 2004) has informed the author that he has experimental data involving the partitioning of Ni between olivine and silicate melts (a) which are free of sulfur and (b) which contain sulfur. The partition coefficients from melt into olivine are lower in the case of the S-bearing melts than in the case of the S free melts, which suggests that some Ni is bonded to sulfur when it is present in a silicate melt. No data are available to be quoted at this stage (February 2004) and the author suggests that those interested in the problem should research the latest literature.

each of Ni and Fe such as (2.2) and (2.3) may be combined to give exchange reactions of the type:

$$NiO^{(Sil.m)} + FeS^{(Sul.m)} = NiS^{(Sul.m)} + FeO^{(Sil.m)}. \quad (2.4)$$

The equilibrium constant for this reaction ($K_4$) can be expressed by:

$$K_4 = (a_{NiS} * a_{FeO})/(a_{NiO} * a_{FeS}) = \quad (2.ix)$$
$$[(\gamma_{NiS} * \gamma_{FeO})/(\gamma_{NiO} * \gamma_{FeS})] * [(N_{NiS} * N_{FeO})/(N_{NiO} * N_{FeS})].$$

The equilibrium constant of this reaction is independent of the fugacities of sulfur and oxygen except in so far as these affect the activities of components in the reaction. For example, $fS_2$ will affect the activity coefficients of NiS and FeS. Citing the work of Scott et al. (1974) on the $Fe_{(1-x)}S$-$Ni_{(1-x)}S$ solid solution, Rajamani and Naldrett (1978) suggested that in liquids of similar composition to monosulfide solid solution, $\gamma_{NiS}$ and $\gamma_{FeS}$ have similar values despite the fact that both would decrease with increasing $fS_2$, and therefore that the ratio of these two functions will remain close to 1, despite variations in $fS_2$. Variations in $fO2$ can affect $N_{FeO}$ by changing the $Fe^{3+}/Fe^{2+}$ ratio of the magma, but so long as the value of $fO_2$ remains below about $10^{-8}$ atm (cf. Fudali 1965), the effect on the $Fe^{3+}/Fe^{2+}$ ratio of basaltic magmas is small. Doyle and Naldrett (1986) emphasize that variations in $fO_2$ also affect the oxygen content of sulfide-oxide liquids, and hence activity-composition relationships within them.

From the point of view experimental and natural observations, as discussed above, one must define an exchange partition coefficient $K_D$ (e.g. $K_D^{Ni\text{-}Fe}$, $K_D^{Co\text{-}Fe}$, $K_D^{Cu\text{-}Fe}$) which expresses the observed partitioning of chalcophile elements between sulfide and silicate melts. The values of $K_D$ will then be related to the thermodynamic equilibrium constant (e.g. $K_4^{Ni\text{-}Fe}$ etc.) by functions involving the activity coefficients of the elements involved and the molecular weights of the species involved.

It is customary to express the exchange as one of Ni, Co, Cu etc. exchanging with Fe, which is the principal metal in the sulfide melt. $K_D$ values that are discussed below always involve an exchange with Fe.

Rajamani and Naldrett (1978) obtained values for $K_D$ for Ni, Cu, and Co using liquids with compositions of natural basalts, picrites and andesites (Table 2.1). Subsequently, Boctor and Yoder (1983) obtained similar values. The latter also demonstrated a dependence of $K_D$ on $fO_2$.

Rajamani and Naldrett's (1978) data on sulfide-oxide liquid-silicate magma partitioning (with $K_D$ values for Ni of about 40) are compatible with the magmatic hypothesis, leading, as they showed, to reasonable predictions of the actual compositions of specific Ni-sulfide ores. The oxygen fugacity in their experiments was not buffered, but they predicted from the starting compositions of their materials that it was close to the quartz-

**Table 2.1.** Exchange distribution coefficients ($K_D$) and Nernst partition coefficient (D) for Ni, Cu between sulfide melt and silicate magma (after experimental studies and observations on sulfide-bearing MORB)

| Metal | $K_D$ | D | T°C | Pressure | $\log fO_2$ | Magma composition | Data source |
|---|---|---|---|---|---|---|---|
| Nickel | 42 | | 1255 | Very low | Unknown* | Basalt | Rajamani and Naldrett (1978) |
| | 38 | | 1305 | Very low | Unknown* | Basalt | Rajamani and Naldrett (1978) |
| | 34 | | 1325 | Very low | Unknown* | Olivine basalt | Rajamani and Naldrett (1978) |
| | 59 | | 1255 | Very low | Unknown* | Andesite | Rajamani and Naldrett (1978) |
| | 49.4±3 | | 1300 | 1 bar | -9.0 | Basalt | Boctor and Yoder (1983) |
| | 50.9±2.6 | | 1300 | 1 bar | -9.0 | Basalt | Boctor and Yoder (1983) |
| | 43.1±3.2 | | 1400 | 1 bar | -8.0 | Basalt | Boctor and Yoder (1983) |
| | 35.9±2.5 | | 1460 | 1 bar | -8.0 | Basalt | Boctor and Yoder (1983) |
| | 22.4 | | 1250 | 1 bar | -8.55 | 21 wt% MgO | Boctor and Yoder (1983) |
| | 10 to 219 | 1031 to 8857 | 1450 | 8 kb | -8.4 to -9.1 | 8.3 to 18.1 wt% MgO | Peach and Mathez (1993) |
| | | 800 | 1200 | Observations on quenched MORB pillow rims | | | Peach et al. (1990) |
| Copper | 35 | | 1255 | Very low | Unknown* | Basalt | Rajamani and Naldrett (1978) |
| | 24 | | 1305 | Very low | Unknown* | Basalt | Rajamani and Naldrett (1978) |
| | 48 | | 1325 | Very low | Unknown* | Olivine basalt | Rajamani and Naldrett (1978) |
| | 34 | | 1255 | Very low | Unknown* | Andesite | Rajamani and Naldrett (1978) |
| | | 1400 | 1200 | Observations on quenched MORB pillow rims | | | Peach et al. (1990) |
| Cobalt | 15 | | 1255 | Very low | Unknown* | Basalt | Rajamani and Naldrett (1978) |
| | 9 | | 1305 | Very low | Unknown* | Basalt | Rajamani and Naldrett (1978) |
| | | 40 | 1200 | Observations on quenched MORB pillow rims | | | Peach et al. (1990) |

*The oxygen fugacity was not buffered, but it was predicted from the starting compositions of the materials that it was close to the quartz-fayalite-magnetite buffer, i.e., within the range of natural magmas

fayalite-magnetite buffer, i.e., within the range of natural magmas. Boctor and Yoder's (1983) data also indicate $K_D$ values of around 40 to 50 at temperatures of 1250 to 1300°C and $fO_2$ values of $10^{-8}$ to $10^{-9}$ atm. Boctor and Yoder's data also demonstrate that $K_D$ decreases with increasing temperature of equilibration and increasing maficity of the silicate magma, as predicted by the calculations of Rajamani and Naldrett (1978) and Duke and Naldrett (1978), and the experimental studies of Campbell et al. (1979a).

Peach and Mathez's (1993) experiments, which were performed at 8 kb total pressure and at or close to saturation with a C-O-S vapour phase, showed that $D_{Ni}$ and $D_{Fe}$ between sulfide and silicate melts vary strongly with $fO_2/fS_2$ ratio. In the case of Ni, their data indicated that logD for Ni, expressed on a mol% basis, varies linearly with $\log fO_2/fS_2$, from near 3.75 at $\log fO_2/fS_2 = -8$ to 3.15 at -6. In comparing their data with other experimental data and with observations on natural material, they found that $\log D_{Ni\ wt\%}$ was a function of the FeO content of the magma (Fig. 2.6). They comment that Rajamani and Naldrett's (1978) data are lower than the line through the other data, because these were performed at higher $fO_2/fS_2$ ratios than the other experiments. On the other hand it is possible to show (for example see Figure 2.12 below), that isopleths of $fO_2/fS_2$ ratio are more or less parallel to isopleths of $a_{FeO}$ in Fe-S-O melts in the temperature range 1200-1450°C. Thus the FeO content of the melt essentially controls the $fO_2/fS_2$ ratio prevailing when the melt is saturated with a sulfide-oxide

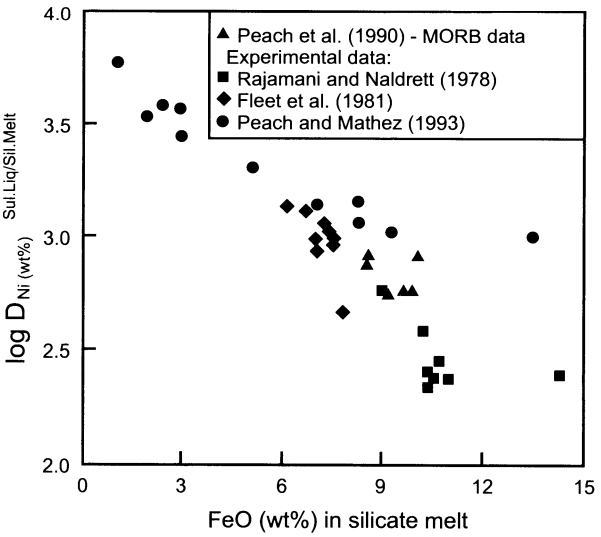


**Fig. 2.6.** Plot of the logarithm of the Nernst distribution coefficients for Ni against the wt% FeO in the silicate melt from the studies of Peach and Mathez (1994), natural MORB data, Rajamani and Naldrett (1978), and Fleet et al. (1981)

liquid. At this stage, the reader is referred to the subsequent section of this chapter, particularly Brenan and Caciagli's discussion of the value of $K_D$ for Ni distribution between olivine and sulfide. These author's found that at constant $fO_2$, $K_D$ is a function of the Ni content of the sulfide melt. It is thus very likely that the Ni content of the sulfide melt also exerts and influence on Ni partitioning between sulfide melt and silicate melt.

Celmer (1987) studied the distribution of Ni between Ni-Cu-Fe matte and fayalite-rich slags. He found that the Nerns't distribution coefficient for Ni was about 160 in $SiO_2$ saturated slags at 1250°C, $fO_2$'s of about $4x10^{-9}$ and $fS_2$'s of about $5x10^{-3}$. The coefficient decreased with decreasing Fe/Ni ratio in the matte and with increasing $fS_2$ and $fO_2$, and increased by a factor of 1.5 to 2 with the addition of up to 15 wt% $Al_2O_3$ and 10 wt% CaO to the slag. The slag compositions are far from those of basaltic melts, so that a comparison of absolute values is not relevant.

In conclusion, the available data suggest that Rajamani and Naldrett's (1978) assumption that $\gamma_{NiS}/\gamma_{FeS} = 1$ is not justifiable in the light of new data, that $D_{Ni}^{(Sul.l/Sil.m)}$ varies with $fO_2/fS_2$ ratio, but tends to be constant for melts with the same FeO content, is of the order of 250-800 for silicate melts with about 10 wt% MgO, and increases sharply for melts with less MgO than this. Values for $D_{Cu}$ of the order of 1000-1400 appear to be reasonable in most natural situations, and have been adopted by a number of authors in recent work (c.f. Brugmann et al. 1993; Peach and Mathez 1993).

### 2.2.2 Partitioning of Ni between Olivine and sulfide liquid

The partitioning of Nickel between olivine and sulfide melt has been the object of numerous studies (Fleet and MacRae 1983, 1987; Fleet and Stone 1990; Gaetani and Grove 1997; and, most recently, Brennan and Caciagli 2000), following on Clark and Naldrett's (1970) study of partitioning between olivine and solid mss. The reaction in question:

$$FeS_{(Sul.m)} + NiSi_{0.5}O_{2\,(Ol)} = NiS_{(Sul.m)} + FeSi_{0.5}O_{2\,(Ol)}, \qquad (2.5)$$

where FeS and FeO are hypothetical species in the sulfide melt and $NiSi_{0.5}O_{2(Olivine)}$ and $FeSi_{0.5}O_{2(Olivine)}$ are components in the olivine solid solution.

In the presence of oxygen, components in the liquid can react to form oxide species:

$$FeS_{(Liq)} + 1/2O_{2(Vap)} = FeO_{(Liq)} + 1/2S_{2(Vap)}; \qquad (2.6)$$

$$NiS_{(Liq)} + 1/2O_{2(Vap)} = NiO_{(Liq)} + 1/2S_{2(Vap)}. \quad (2.7)$$

and thus the relative proportions of the reactants and products in equations (2.6) and (2.7), and consequently the value of $K_D$ for this reaction, will be expected to vary with both $fO_2$ and $fS_2$.

Brennan and Caciagli (2000) have measured values of $K_D$ for olivine in equilibrium with sulfide liquids of different compositions and have found that at constant $fO_2$, these vary linearly with the Ni content of the sulfide liquid, and are independent of temperature and $fS_2$. At constant Ni in the sulfide liquid, they found $K_D$ to vary with $fO_2$ according to the empirical equation:

$$\log fO_2 = -8.43*[(K_D/Ni, wt\%)^{0.177}] \quad (2.x)$$

Thus, knowing the Ni content of the sulfide liquid, determination of $K_D$ will indicate the value of $fO_2$ at the temperature at which the exchange reaction became blocked. Brennan and Caciagli (2000) note that in situations in which olivine and sulfide are in close proximity, but in which olivine grains are of the order of 1 mm or more in diameter, the blocking temperature is likely to be above 1000°C. Since the $fO_2$ of most natural magmas cooling through their liquidus-solidus interval tends to follow the path of the appropriate buffer curve, extrapolation up-temperature to the liquidus temperature along the buffer curve will give the $fO_2$ of the initial crystallization of the olivine and segregation of the sulfide. Fig. 2.7 is a plot of their curves relating $K_D$, wt% Ni in sulfide liquid and $fO_2$, along with determinations for several plutonic suites, illustrating the values of $fO_2$ relevant to the crystallization of these suites.

### 2.2.3 Partitioning of PGE between Sulfide and Silicate Melts

Studies of naturally occurring concentrations of PGE and Au indicate that the sulfides are very enriched in these metals in comparison with their concentrations in most mafic magmas (Naldrett and Cabri 1976; Naldrett and Duke 1980; Sharpe 1982, Peach et al. 1990). If the concentrations are due to the segregation of immiscible sulfides from magma, and if these sulfides have not been significantly upgraded in their PGE contents subsequent to their segregation, the coefficients governing the partition of the PGE and Au between liquid sulfide and liquid silicate must be very high. Estimates have ranged from the order of $10^3$ (Naldrett et al. 1979) to $10^5$ (Campbell and Barnes 1984). A number of authors (see discussion below) have sought to explain the difference between Pt and Pd tenors typical of

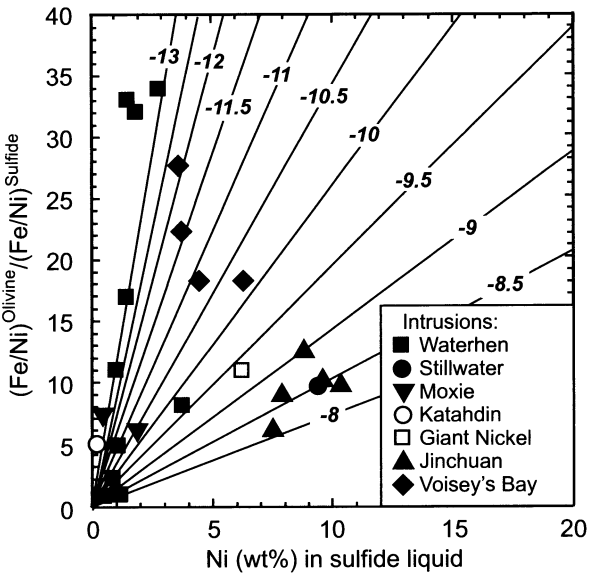


**Fig. 2.7.** Variation of $K_D^{Ni}$ with wt% Ni in the sulfide melt, contoured with respect to $fO_2$ (after Brenan and Caciagli, 2000)

sulfides of Ni- and Cu-sulfide-rich ores, such as those at Sudbury or Kambalda (1000-3000 ppb) and of sulfide-poor ores, such as those in the Merensky Reef (approx. 250-600 ppm) and the J-M Reef (approx. 5000 ppm) as the consequence of the amount of silicate magma that a given mass of sulfide (R value) has achieved effective equilibrium with. High ratios of silicate magma to sulfide will lead to high PGE tenors (see for example Campbell and Naldrett 1979; Campbell et al. 1983; Naldrett et al. 1987). Explanations of this type require the partition coefficients of the noble metals to be two orders of magnitude greater than those of Cu and Ni, that is about $10^4$-$10^5$. This hypothesis has been part of the stimulus for several attempts to determine partition coefficients experimentally. Since 1986, seven separate experimental studies of the partitioning of noble metals between sulfide and silicate melts have been made (Jones and Drake 1986; Stone et al. 1990; Fleet et al. 1991; Crocket et al. 1992; Bezmen et al. 1994; Peach et al. 1994).

The main experimental problems are those of analyzing the noble metal-poor phase without invalidating the analysis by the accidental inclusion of some of the noble metal-rich phase, of containing molten silicate and sulfide melts without their reacting with the container, and of controlling intensive parameters such as the oxygen and sulfur fugacities and total pressure. Containers have included $Al_2O_3$, graphite or carbon-glass crucibles, or Pt capsules for the sulfide and silicate melts enclosed in fused silica

tubes or suspended in controlled atmosphere furnaces. Oxygen fugacity has been controlled (i) by pre-conditioning the silicate portion of the charge in a controlled atmosphere furnace, (ii) by using solid buffers, (iii) by conducting the experiments in an atmosphere of $CO$-$CO_2$-$SO_2$ or (iv) by placing the charge in a graphite crucible, and enclosing this together with water in a Pt-capsule immersed in an atmosphere composed of $H_2$ and Ar in known proportions. The noble metal content of the bulk silicate charge has been determined in all cases by instrumental or radiochemical neutron activation analysis and that of the sulfide charge by broad-beam microprobe analysis or calculated.

The values obtained for Pt, Pd, Rh and Au are illustrated in Fig. 2.8.

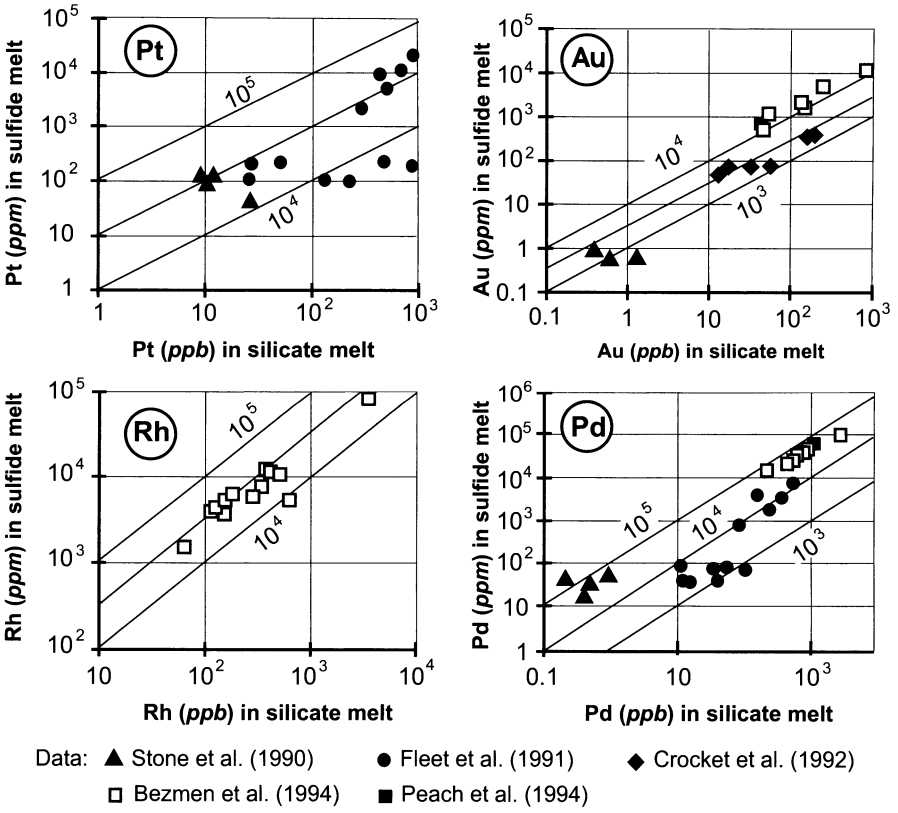


**Fig. 2.8.** Plots of concentrations of different PGE in sulfide melts against their concentration in the co-existing silicate melt, illustrating the values of the Nernst distribution coefficients that have been obtained in different experimental studies (see text). Sloping straight lines are values of the Nernst distribution coefficients

Average results obtained from the different studies have been very variable, the range for $D_{Au}$ is $1.24x10^3$–$2x10^4$; for $D_{Pd}$ is $7.05x10^3$–$8.78x10^4$; for $D_{Pt}$ is 8.59–$9.3x10^3$, and for $D_{Rh}$ (one study only) the value is $2.74x10^4$. Values obtained for $D_{Ir}$ vary to an even greater extent $2.79x10^3$–$3.16x10^5$; those for $D_{Os}$ vary from $6.25x10^2$ to $3.34x10^3$ while the value for $D_{Ru}$ (one study only) is $1.36x10^3$. Experimental problems, particularly the development of a colloidal suspension of Ir metal in the silicate melt, may account for the spread in Ir values, and invalidate results obtained so far. The lower result for Os and the result for Ru may be unreliable for analytical reasons. For the remainder, the higher results are usually those determined under wet conditions at high pressure.

In none of the studies except for one was it possible to hold all parameters constant, and study the effect of variations in this on partitioning independently of variations in the others. Nevertheless, a review of the results of all of the studies together indicates that variations in the following parameters produce these effects on D: (i) temperature (no effect observed on Ir, Au and Pt), (ii) oxygen fugacity (no significant effect observed on Ir, Au, Pd, Pt, Os and Rh), (iii) increasing concentration of the noble metal under study in the sulfide melt (no significant effect observed except for Pt for which a slight increase may exist); (iv) increasing Ni content of the sulfide melt (no significant effect observed for Ir, Au, Pd, Pt, Os and Rh); (v) increasing Cu content of the sulfide melt (decrease for Pd and Rh, possible decrease for Ir and increase for Au), and increasing MgO content of the silicate melt (no effect observed for Ir and Au).

The highly variable results mean that is impossible to choose with certainty any values for a particular geological situation. However some values have more credibility than others. Peach et al. (1994) report the results of experiments for Ir and Pd ($D_{ir} = 3.0x10^4$ and $D_{Pd} = 4*10^4$) which compare closely with those obtained from the analysis of sulfide globules in MORB basalt ($D_{Ir} = 1*10^4$, $D_{Pd} > 2.3x10^4$). The Pd value is close to that obtained by Bezmen et al. (1994) ($D_{Pd} = 5*10^4$) although Bezmen et al.'s value for Ir is much higher ($D_{Ir} = 3*10^5$).

Recent experimental work has focussed on the solubility of Pt and Pd in sulfur-free silicate melts (Borisov et al. 1994; Borisov and Palme 1997; Bezmen, 1997). In these studies, it has been found that $fO_2$ has a profound effect on the solubility of both metals. For example, Bezmen (1997, and personal communication 1999) finds that under water saturated conditions the solubility of Pt in a diopside-anorthite-albite melt at 1200°C and 2 kb pressure decreases from 75 to 22 ppm, and the solubility of Pd from 50 to 20 ppm as the $fO_2$ decreases from $10^{-2.5}$ to $10^{-9.5}$. Bezmen also reports that the presence of S in the melt appears to have no effect on the solubility of Pt. In the light of these findings, one would expect the distribution coeffi-

cient between sulfide and silicate liquids also to be affected in a systematic way by $fO_2$, although, as reported above, this is not apparent in the experimental determinations made to-date.

### 2.2.4 Effect of ratio of magma to sulfide

Expression (2.iv) above relates the composition of a sulfide liquid to the composition of the silicate magma with which it is in equilibrium. When modeling the composition of natural sulfide ores, it is often useful to be able to model the composition of the sulfide melt in terms of the initial composition of the silicate magma (i.e., before the segregation of, or reaction with, sulfide occurs – for example if one is interested in the tenor of a deposit that could result from a magma as represented by any particular basalt). Where the ratio of silicate magma to sulfide melt is very large, expression (iv) provides a satisfactory answer. However, as this ratio decreases, a stage is reached at which the sulfide has concentrated so much of the metal present in the whole system that it causes a significant drop in the concentration of this metal in the silicate magma with which it is equilibrating. This effect becomes more pronounced as the proportion of silicate magma equilibrating with a given amount of sulfide decreases. Under these circumstances, it is necessary to make allowances for differing proportions of magma and sulfide.

Three approaches have been taken to this question in the recent literature. The first is based on the assumption that sulfide liquid equilibrated in bulk with the magma and was then removed (Campbell and Naldrett 1979). The magma/sulfide ratio in this type of equilibration has become known in the literature as "R" and the effect that it has on sulfide composition as the "R factor". The second is based on the assumption that the mass of sulfide is continuously exposed to fresh magma, which flows by the sulfide and reacts with it and is then replaced by fresh magma. Brugmann et al. (1993) and Naldrett et al. (1995, 1996) discussed this type of equilibration, noting that the process is analogous to zone refining; they designated the ratio of the mass of sulfide to the total mass of magma involved as "N". The third approach is that of the fractional segregation of sulfide liquid, possibly along with the fractional crystallization of silicate minerals such as olivine. This last approach is developed further in Chap. 10. This chapter is restricted to consideration of "R factor" and "N factor" modeling.

### *The "R factor" Approach*

When bulk equilibration of sulfide and magma occurs:

$$Y_i = [D_i * C_{oi} * (R+1)]/(R+D_i), \quad \text{(2.xi)}$$

where $Y_i$; is the final concentration of metal i in the sulfide melt; R is the ratio of the mass of silicate magma to the mass of sulfide, and $C_{oi}$ refers to the original concentration of metal i in the silicate magma before reaction with sulfide commenced. Fig. 2.9 illustrates schematically the effect that variations in R and D have on the Cu and Pt contents of sulfides segregating from a magma such as that responsible for the Bushveld Complex. Where R is low, in the range of 100 to 2000, the Cu content of the sulfides will be typical of most Ni sulfide ores, and the Pt concentrations will be relatively low, corresponding to those observed in ores such as those at Sudbury. Where R is in the range of 10,000 to 100,000 the Cu content will not be much higher than at lower R values, but the Pt concentration will be much higher and in the range of that characterizing the Merensky Reef.

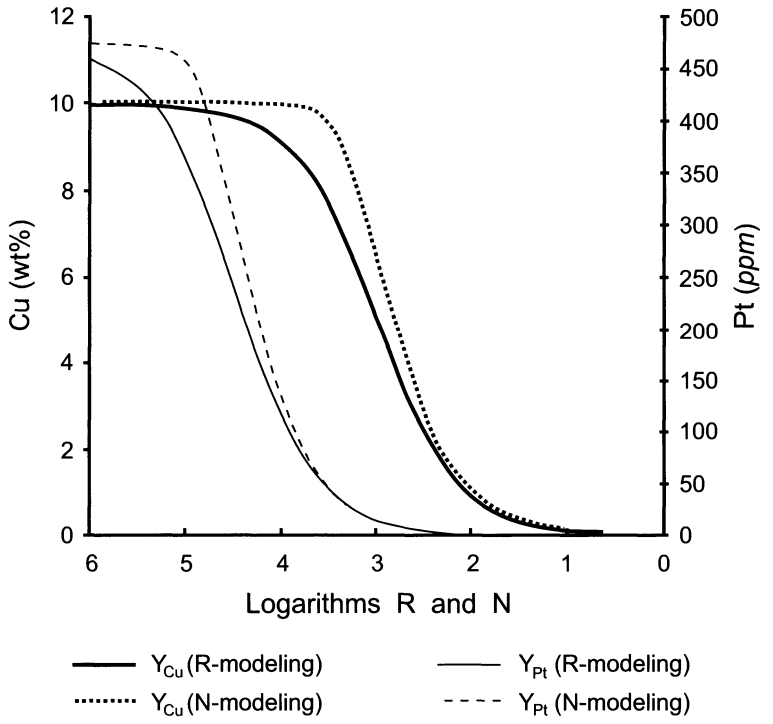


**Fig. 2.9.** The effect of variations in silicate magma/sulfide liquid mass ratio on the concentrations of Cu and Pt of sulfides in equilibrium with basaltic magma containing typical concentrations of these elements (R- and N-modeling)

### *The "N factor" Approach*

Situations in which sulfide droplets are introduced at the top of a magma chamber and slowly settle through it (Brugmann et al. 1993), or, alternatively, in which sulfides are located in a hydrodynamic trap within a magma conduit along which fresh magma continues to flow and interact with the sulfides (Naldrett et al. 1995, 1996), are analogous to the industrial process of zone refining. For example, the zone refining of a steel bar involves introducing one end of the bar into a furnace so that the bar starts to melt, and then moving it continuously through the furnace so that the zone of melting moves along the length of the bar, with the metal of the bar recrystallising as it emerges from the furnace. Impurities that are present throughout the bar partition into the melt in accord with their (crystalline metal)/(liquid metal) partition coefficients, and are retained within the zone of melting as it moves along the length of the bar. The "contaminated" melt is then discarded by cutting off one end of the bar, leaving a purified metal within the remainder of the bar. Sulfides interacting with a continuous stream of magma are analogous to the melt zone within the metal bar, and will concentrate the "impurities" within the magma (= chalcophile metals), leaving the magma depleted in these. The equation governing this process is (Cox et al. 1979):

$$Y_i = X_i * \{D-[(D-1)*e^{-(1/D*N)}]\}, \qquad (2.xii)$$

where $Y_i$ is the metal concentration in the sulfide, $X_i$ is the initial concentration of the metal in the silicate magma, D is the partition coefficient and N is the ratio of the amount of magma passing through the system and reacting with the sulfide to the amount of sulfide in the system. The effect that variation in N has on Y is compared with that resulting from variation in R in Fig. 2.9. The two effects are similar, but Y varies more rapidly with change in N than it does with change in R.

## 2.3 Relevant Phase Equilibria

Students of magmatic sulfide ores are particularly fortunate in comparison with those of most other types in that five elements (Fe, S, Ni, Cu and O) account for well over 99 percent of the total composition of the ore. Furthermore, in most cases the ores have been introduced as melts with essentially their present compositions, so that considerations of solubility in a transporting fluid do not arise.

Despite the simple composition, five components still require a considerable stretch of one's powers of visualization if their mutual phase rela-

tions are to be considered simultaneously. It is possible, however, to simplify the discussion by considering melting relations firstly in the two component Fe-S system, and then the three component Fe-S-O system, and then by considering the effect on the melting relations of introducing small amounts of the two other components, Ni and Cu. Once the ore has crystallized, essentially all of the oxygen is present as magnetite, which partakes in no major reactions with the rest of the ore during cooling. Thus at sub-solidus temperatures the ore can be treated as the four-component system, Fe-Ni-Cu-S. Furthermore, once the bulk of the Cu has exsolved as chalcopyrite above 500-600$^0$C, it is believed not to react with the rest of the ore to any major extent, and a great deal can be learned simply by analogy with the system Fe-Ni-S.

For these reasons high-temperature phase relations in the systems Fe-S and Fe-S-O are discussed, followed by phase relations in the system Fe-Ni-S and pertinent portions of the systems Cu-Fe-S and Cu-Fe-Ni-S.

### 2.3.1 The System Fe-S-O and its application to natural ore magmas

For reasons given later in this section, natural magmas fall within a limited range of Fe/S and Fe/O ratios. Within this range, the important features of the system Fe-S are the congruent melting of pyrrhotite at 1190°C, and the two bounding phase regions, pyrrhotite + liquid + vapor on either side. The three-phase region terminates on the metal-rich side at the eutectic at 988$^0$C and on the sulfur-rich side at 1083°C. Of the Fe oxides, magnetite is the dominant oxide mineral crystallizing from high temperature magmas. More rarely wustite forms, but because of its lower stability limit of 560°C, it is rarely preserved in the natural environment. Above 900°C, magnetite shows considerable solid solution toward hematite.

Condensed phase relations at 900°C (15°C below the temperature of the first appearance of a liquid in the Fe-rich portion of the system Fe-S-O) are shown in Fig. 2.10, which outlines the compositional field occupied by almost all natural ore magmas. Phase relations on the (O + S)-rich side of the magnetite – pyrrhotite tie-lines drawn in the figure have not been determined experimentally because of the high vapor pressures associated with these compositions. It is very likely, however, that these compositions involve the four-phase field of magnetite + hematite + pyrrhotite + vapor (in which the pyrrhotite is somewhat richer in sulfur than that shown in equilibrium with magnetite in the figure) followed by the three-phase field of hematite + pyrrhotite + vapor.

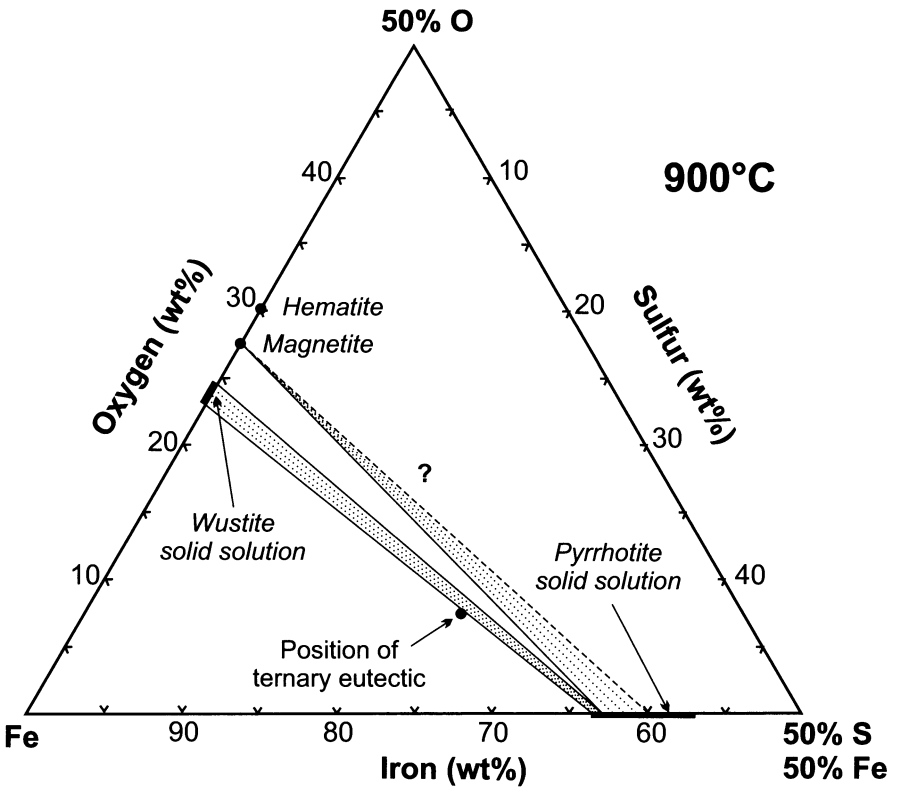


**Fig. 2.10.** Phase relations at 900°C (15°C below the temperature of the first appearance of a liquid in the Fe-rich portion of the system Fe-S-O). From Naldrett (1969)

Liquidus relations in the system Fe-S-O (in the presence of vapour) are shown in Fig. 2.11a and b. The dashed lines in Fig. 2.11a are based on Hilty and Craft's (1952) data, the dashed-dotted lines are interpretative, and the solid lines are from the data of Naldrett (1969). Fig. 2.11a is characterised by fields of iron, wustite, pyrrhotite and magnetite. The iron, wustite, and pyrrhotite fields meet at a ternary eutectic where these three phases plus liquid and vapour are all stable. The wustite, pyrrhotite and magnetite fields meet at a ternary reaction point at which magnetite plus liquid react in the presence of vapour to form pyrrhotite (containing 62.8±0.2 wt percent Fe) and wustite. Fig. 2.11b is an enlargement of a portion of Fig. 2.11a. Tie-lines in Fig. 2.11b illustrate the composition of pyrrhotite in equilibrium with iron oxide and liquid at different temperatures along the wustite-pyrrhotite and magnetite-pyrrhotite cotectic lines.

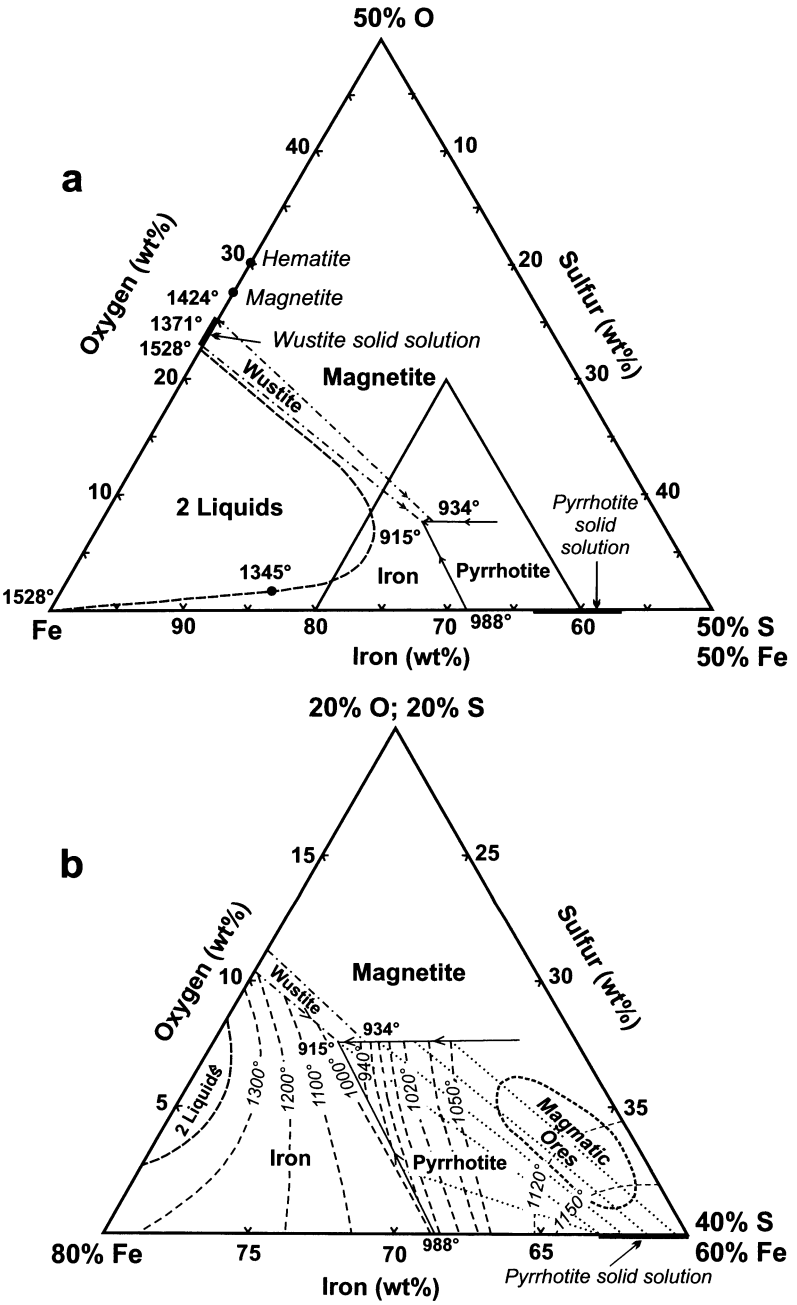


**Fig. 2.11.** Liquidus relations in the Fe-rich portion of the system Fe-S-O in the presence of vapor (a), and an enlargement of the portion covering the compositions of natural magmatic ores (b). From Naldrett (1969)

The ternary eutectic, iron-wustite-troilite, was reported by Naldrett (1969) to occur at 915±2°C in the "condensed" system and to have the composition 68.2 wt% Fe, 24.3 wt% S and 7.5 wt% O. The ternary reaction point occurs at 934±2°C. Wendlandt and Huebner (1979) investigated the effect of pressure on the position and temperature of the ternary eutectic in the Fe-S-O system. At 30 kb pressure, this has a temperature of 1000±10°C and a composition containing 72–73 wt% Fe and less than 0.75 wt% O. This is very close to the binary Fe-FeS eutectic at this pressure in terms of both temperature and composition.

Brett and Bell (1969), Ryzhenko and Kennedy (1973) and Usselman (1975) studied the effect of pressure on the Fe-FeS eutectic in the Fe-S system up to 60 kb. All workers found that pressure had either no or just a slight effect on the temperature of the eutectic, although the composition became more Fe-rich with increase in pressure (Ryzhenko and Kennedy report it to contain 22 wt% S at 60 kb). Sharp (1969) and Ryzhenko and Kennedy (op cit) investigated the effect of pressure on the congruent melting of pyrrhotite and have found the melting point to increase at the rate of 13°C/kb up to 65 kb.

Mungall (personal communication, February 2004) has drawn the author's attention to an investigation (see reference to Mungall et al., submitted) of the effect of Ni and Cu on the position of the magnetite-mss cotectic. This involved a starting sulfide composition of $Fe_{49}S_{35}Ni_{5.3}Cu_{7.6}$ to which 0.5 wt% of each of Pt, Pd, Rh, Ru, Os, Ir and Au had been added. It was found that the cotectic remained parallel to the Fe-S join, but, rather than containing about 8 wt% $O_2$ as it does in the Ni- and Cu-free system, it is much closer to the join, containing less than 2 wt% $O_2$.

### *Effect of other components on solidus temperatures*

Naldrett (1969) pointed out that at temperatures immediately below the solidus, a pyrrhotite-pentlandite-chalcopyrite-magnetite ore in which the sulfides contained less than 15 wt% Ni and 4 wt% Cu would consist of two phases, a nickeliferous cupriferous pyrrhotite solid solution and magnetite. Craig and Naldrett (1967) investigated the effect of the substitution of Ni and Cu for Fe in the pyrrhotite on the solidus temperatures of pyrrhotite-magnetite mixtures. They found that the substitution of up to 20 wt% Ni for Fe on an atom for atom basis did not lower melting temperatures measurably below those established for the pure system Fe-S-O. The substitution of 2 wt% Cu on a similar basis lowered solidus temperatures 15 to 20°C.

Naldrett and Richardson (1967) investigated the extent to which water lowered the melting temperature of pyrrhotite-magnetite mixtures. Within

the accuracy of their experiments (±10°C), they concluded that water did not act as a flux for sulfide ores, nor could it dissolve appreciably in a sulfide-oxide melt.

The above data indicate that, ignoring the pressure effect, melting temperatures in the Fe-S-O system are probably within 20°C of the solidus temperatures of natural low-Cu (<2 wt%) sulfide-oxide magmas.

### *Variation in $fO_2$, $fS_2$ and aFeO*

The composition of an iron-sulfide-oxide liquid at any given temperature is a function of its oxygen and sulfur fugacities (Naldrett, 1969; Kress 1997). This point is illustrated in Fig. 2.12 in which isobars of sulfur and oxygen fugacity are shown at 1200 and 1450°C over the same portion of the Fe-S-O system as is shown in Fig. 2.12b. The isobars are drawn on the basis of the data of Rosenqvist (1954), Bog and Rosenqvist (1958), and Nagamori and Kameda (1965). In all of these studies, the investigators equilibrated an Fe-S-O liquid with three $O_2$ and $S_2$-bearing gases (for example CO, $CO_2$ and $SO_2$) in proportions defining a series of different values of $fO_2$ and $fS_2$ at the temperatures in question. The composition of the liquids corresponding to the specific values of $fO_2$ and $fS_2$ were then determined at equilibration.

Knowing the chemical potentials (or activities) as a function of composition for two of the components in a three-component system, the Gibbs-Duhem relation allows calculation of the chemical potential of the third component. This calculation has been done for the data given above on the system Fe-S-O (Shima and Naldrett 1975) to obtain the activity of Fe. In turn, since the standard free energy for the reaction

$$Fe + 1/2O_2 = FeO_{(Liq)} \qquad (2.8)$$

is known, it is possible to combine activity data for Fe and fugacity data for $O_2$ to calculate the activity of FeO. These data then serve as the basis for the *a*FeO contours in Fig. 2.12a–b, for which the standard state of FeO is taken to be a supercooled liquid of stoichiometric FeO composition at 1200°C and a liquid of the same composition at 1450°C.

### *Controls on the S and O content of ore magmas*

Consider a basaltic magma at 1200°C, devoid of Ni, Cu, and Co but just saturated in sulfide, so that a small number of sulfide droplets are segregating from it and are in equilibrium with it. Since the droplets are small and widely dispersed throughout a large body of magma, their compositions are controlled by the composition of the host magma. This magma

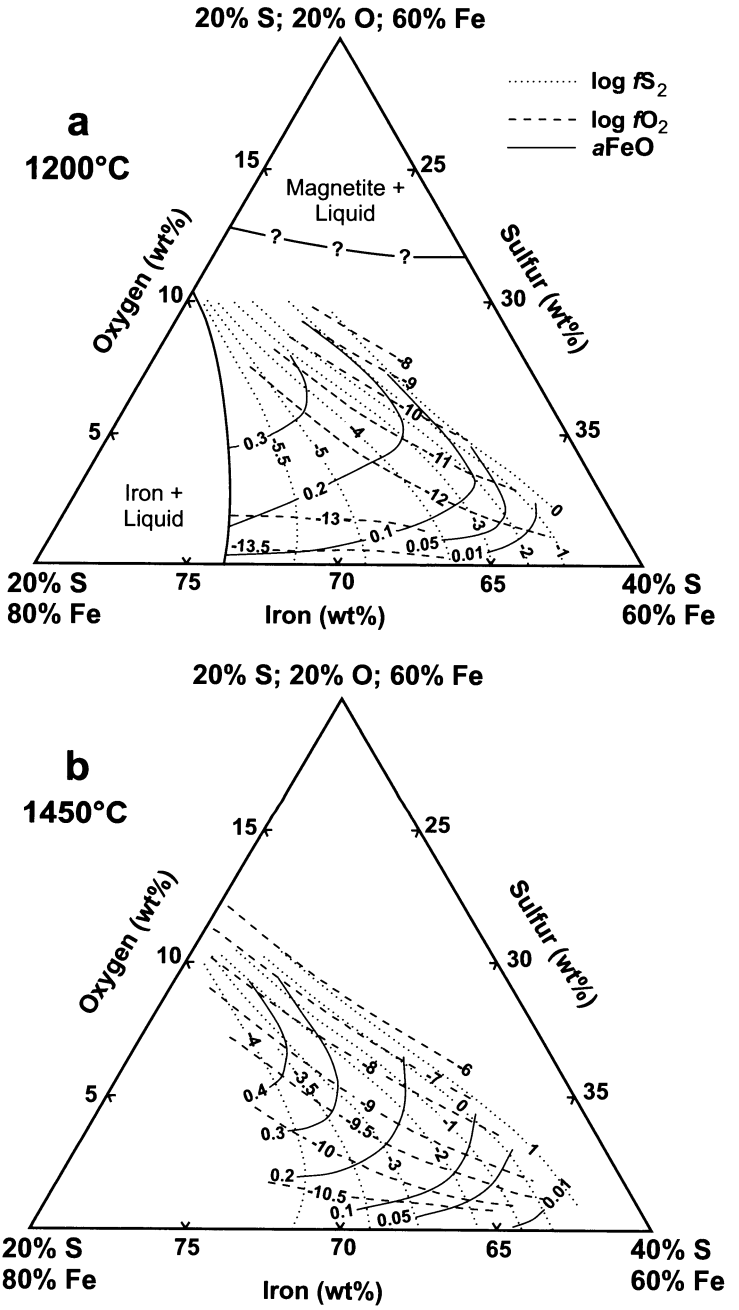


**Fig. 2.12.** Contours of $fO_2$, $fS_2$,and $a$FeO in the part of system Fe-S-O, shown in Fig. 2.11b, at 1200°C (a) and 1450°C (b). References for data sources are given in text

has a certain FeO content and a certain $Fe^{3+}/Fe^{2+}$ ratio, which, together with other major elements, define the values of $a$FeO (see Roeder 1974; Holzheid et al. 1997) and $fO_2$ in the magma. Since at equilibrium, the same values of $\mu$FeO that control $a$FeO and $fO_2$ must apply to the sulfide droplets, the composition of the droplets must correspond to the values in Fig. 2.12a; i.e. in the hypothetical case under consideration, the composition of the basalt magma, in particular its FeO content and $Fe^{3+}/Fe^{2+}$ ratio, define the composition of the segregating sulfide ore and the $fS_2$ prevailing at the time of segregation. Since most natural magmas have relatively restricted ranges of FeO content and oxidation state, the compositions of magmatic ores are similarly restricted in their S and O contents.

In nature, Ni, Cu, and Co are also present in the basaltic magma and partition into the sulfide droplets, as discussed above. This tendency complicates the simple relationship presented in this section, but only does so to a limited extent. The composition of the sulfide liquid is still controlled by the $a$FeO and $fO_2$ of the host magma.

### *Temperatures of crystallization of natural sulfide ores*

The temperatures of the beginning of crystallization and final solidification of a sulfide ore are important when considering how far the sulfides can move away from their host intrusion as an ore magma, and whether they are likely to be mobilized as a liquid during high grade metamorphism.

The region representing the compositions of most magmatic ores is superimposed on the Fe-S-O system in Fig. 2.11b. It is seen that most ores will start to crystallize between 1160 and 1120°C. Since ores, like silicate magmas, can probably move as a mixture of crystals and liquid, the solidus temperature of an ore provides a minimum temperature for its intrusion in a partly liquid state. Naldrett (1969) showed that the solidus temperature varies with the Fe content of the pyrrhotite forming the deposit. Almost all ores are made up of pyrrhotite containing between 62.5 and 60.5 wt% Fe (due to the controls on their composition discussed above) so that, on the basis of the system Fe-S-O, one would predict that their solidus temperatures would be between 1010 and 1050°C. As reported above, the substitution of up to 20 wt% Ni for Fe has no measurable effect on the solidus temperature. The substitution of 2 wt% Cu lowers the solidus temperature by 20°C. The substitution of more than 2 wt% Cu has a much greater effect, so that temperatures are distinctly lower than those estimated above for Cu-poor ores; exactly how much lower is not known, although this author is of the opinion that liquids close to chalcopyrite in composition can probably occur in nature below 850°C. Since the upper stability of pentlandite has now been shown to be 865°C (see below), this means that pent-

landite can crystallize as a liquidus phase from very Cu-rich (probably >25 wt% Cu) sulfide liquids.

### 2.3.2 Relevant Sulfide Systems

#### *The System Fe-Ni-S*

The bounding binary systems, Fe-S and Ni-S to the ternary Fe-Ni-S system have been described by Kullerud and Yoder (1959), Kullerud (1967) and Chuang et al. (1985); and Kullerud and Yund (1962) and Sharma and Chang (1980) respectively. The most comprehensive study of the ternary is that of Kullerud et al. (1969). More detailed studies include those of Hsieh et al. (1982) and Karup-Moller and Makovicky (1995) on high temperature phase relations, those of Kullerud (1963), Bell et al. (1964), Fedorova and Sinyakova (1993) and Sugaki and Kitakaze (1998) on pentlandite stability, those of Naldrett et al. (1967), Misra & Fleet (1973) and Barker (1983) on the limits of the $Fe_{(1-x)}S$ - $Ni_{(1-x)}S$ or monosulfide solid solution (mss), those of Craig (1971) and Misra and Fleet (1973) on violarite stability, those of Craig (1973) and Misra and Fleet (1974) on pentlandite-pyrite equilibria, and that of Lenz et al. (1978) on liquidus relations. The isothermal sections of the condensed Fe-Ni-S system shown in Figs. 2.13–15 have been selected to illustrate many of the more important aspects of the system that have a bearing on the crystallization of Ni sulfide ores.

Apart from alloys along the Fe-Ni join, the system is composed entirely of liquids at 1200°C, a metal-rich liquid spanning the centre of the system and a S-rich liquid containing probably less than 2 wt% metal at the sulfur apex. $Fe_{(1-x)}S$ appears on the Fe-S join at 1190°C and spreads farther into the Fe-Ni-S system at lower temperatures (as shown at 1100°C in Fig. 2.13a), forming the mss. The early crystallizing phase in the system is Fe-rich and Ni-poor with respect to the liquid with which it is in equilibrium; thus continued fractional crystallization of mss results in Ni-enrichment in the later fractionated sulfide liquid (Ebel and Naldrett 1996, 1997). The metal-rich liquid draws completely away from the Fe-S join at 1083°C on the S-rich side and at 988°C on the S-poor side of $Fe_{(1-x)}S$. The mss reaches the Ni-S join at 999°C, dividing the system in two. This barrier remains in effect, isolating S-rich from metal-rich phases to below 250°C.

The 850°C isotherm (Fig. 2.13b) illustrates the appearance of the high-temperature polymorph of pentlandite, which forms as the result of reaction between *mss* and liquid at 865°C (Sugaki and Kitakaze 1998). Previously, Kullerud (1963) had argued that pentlandite appeared in the system at 610°C as the result of a reaction between $(NiFe)_{(3+/-x)}S_2$ and mss. Fedorova and Sinyakova (1993) recognized the presence of a phase of

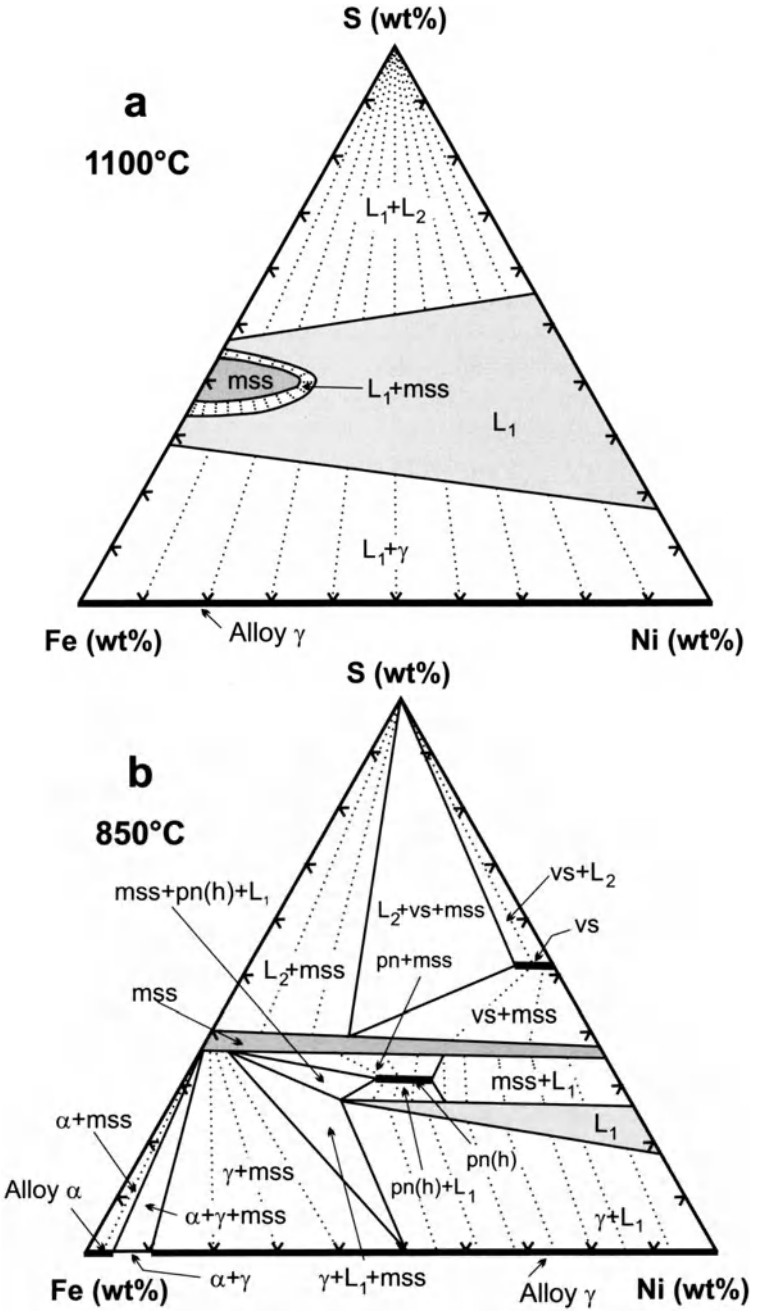


**Fig. 2.13.** Isothermal sections of the condensed system Fe-Ni-S at temperatures 1100°C (a), and 850°C (b). References for sources of data are given in the text. α and γ – structural varieties of Fe-Ni alloys

approximately pentlandite composition, which they believed to be heazlewoodite solid solution that had formed as a result of a peritectic reaction between liquid and *mss* at 876°C. However, Sugaki and Kitakaze (op. Cit.) have demonstrated that this phase has a high temperature pentlandite structure and that the 610°C DTA anomaly attributed by Kullerud to his reaction is, in fact, the unquenchable inversion of high to low pentlandite. Pentlandite rapidly increases in Ni content below 865°C, to form a continuous solid solution with $Ni_{3\pm x}S_2$ below 806°C (Sugaki and Kitakaze 1998; Fedorova and Sinyakova 1993; Karup-Moller and Makovicky 1995).

Vaesite ($NiS_2$) appears on the Ni-S join at 1022°C and pyrite on the Fe-S join at 743°C; both phases take a few percent of the other into solid solution at these temperatures. An important development in the system is the formation of a pyrite-vaesite tie-line at 728°C (Fig. 2.14a) Above this temperature, mss is in equilibrium with liquid S. Liquid sulfur at these high temperatures (~728°C) is extremely reactive and would extract Fe from most Fe-bearing silicates to form Fe sulfide (cf Naldrett and Gasparrini 1971). Since magmatic ores are intimately related to their host magmas and subsequently to their host rocks, which usually contain substantial amounts of FeO, this reaction essentially precludes the existence of liquid sulfur, and hence these bulk compositions, at these high temperatures; i.e. magmas which subsequently crystallize to form large proportions of pyrite and/or vaesite cannot exist in nature. Deposits with this mineralogy cannot have formed with their present bulk compositions from a sulfide magma, and are likely to have formed through the alteration of an original, normal high temperature assemblage of minerals, or to have been deposited hydrothermally.

Most Ni sulfide ores have bulk compositions which, when projected into the Fe-Ni-S system, lie within but towards the S-rich side of the mss at 600°C. Thus, ignoring the effect of Cu, one would not expect pentlandite to occur as a phase in these ores at this temperature. With falling temperature, the mss narrows, drawing back from both its S-rich and metal-rich sides but, since most ores lie towards the S-rich side, it is the S-rich phases pyrite, vaesite or violarite which exsolve first from the mss, not pentlandite. Violarite first appears as a phase within the Fe-Ni-S system at 461°C, whence its Ni/Fe ratio extends to reach the Ni-S join at 356°C where it has the mineral name polydymite.

Craig (1973) concluded that the mss breaks away from the Ni-S join between 300 and 250°C but that tie-lines still connect it to NiS (millerite). He found that by 250°C (Fig. 2.15a), mss has separated into 2 phases plus millerite; however, all phases are connected by tie-lines, so that pentlandite is still isolated from bulk compositions on the S-rich side of the mss. Craig concluded that it is only between 250 and 200°C that these tie-lines

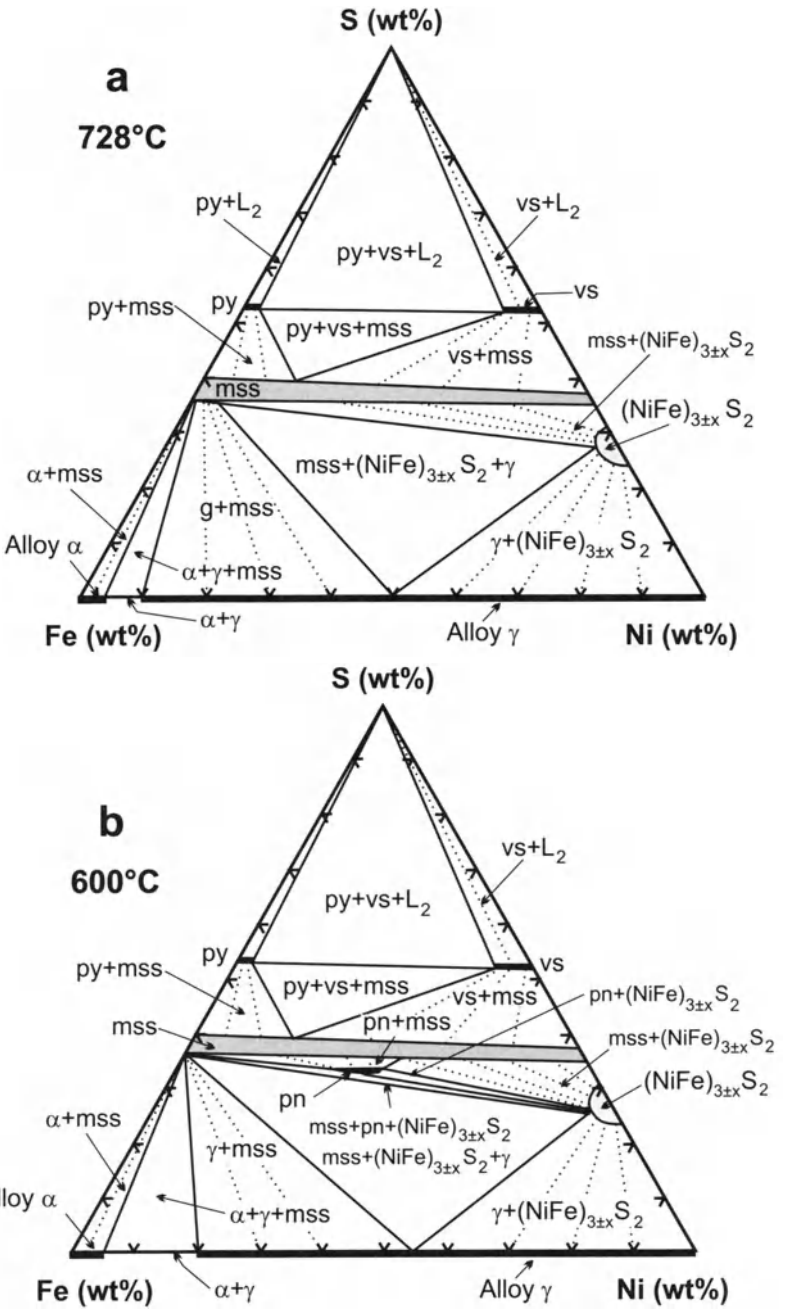


**Fig. 2.14.** Isothermal sections of the condensed system Fe-Ni-S at temperatures 728°C (a), and 600°C (b). References for sources of data are given in the text. α and γ – structural varieties of Fe-Ni alloys

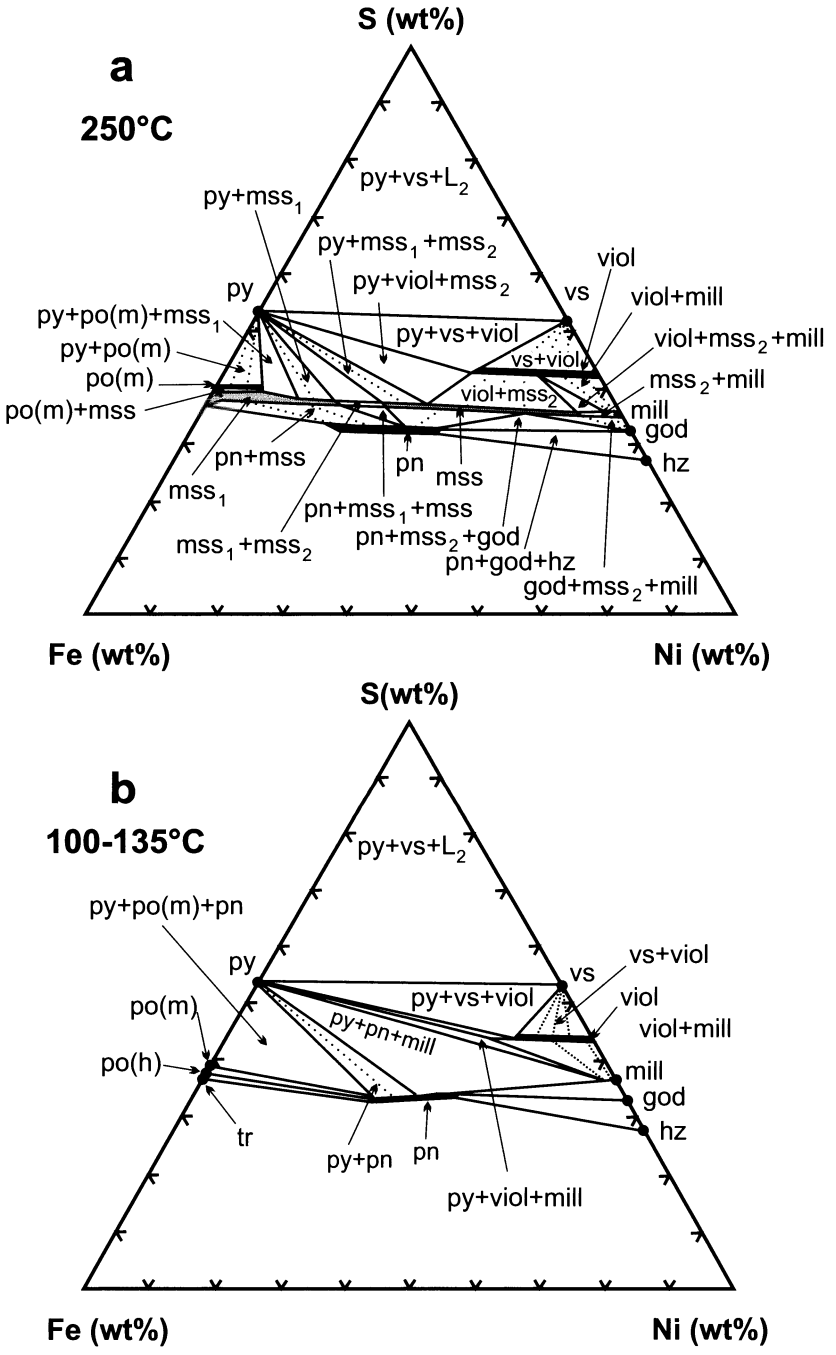


**Fig. 2.15.** Isothermal sections of the condensed system Fe-Ni-S at temperatures 250°C (a), and 100–135°C (b). References for sources of data are given in the text.

break down and new tie-lines are established between pyrite and pentlandite. By this stage, a S-rich monoclinic and S-poor hexagonal variant of the Fe-rich mss have separated from one another. Presumably these phases both contain Ni, but draw back rapidly with decreasing temperature to the Fe-S join, exsolving pentlandite and pyrite. In contrast to Craig, Misra and Fleet (1973) found that the mss starts to break down by 300°C. Barker (1983) also interpreted his results to imply that mss was not continuous at this temperature.

The slow reaction rates in the system at low temperature have precluded experimental investigations so far. Fig. 2.15b is based on the studies of Graterol and Naldrett (1971), Misra and Fleet (1973) and Craig (1973) and is a reconstruction of possible phase relations in the system at about 140°C. Misra and Fleet's low temperature reconstruction differs from Fig. 2.15b in that they concluded that godlevskite is not a stable phase at low temperature and that millerite and heazlewoodite co-exist stably.

### *The systems Cu-Fe-S and Fe-Cu-Ni-S*

Phase relations in the Cu-Fe-S system have been studied amongst others by Merwin and Lombard (1937), Schlegel and Schiller (1952), Hiller and Probsthain (1956), Yund and Kullerud (1966), Kullerud et al. (1969), Mukaiyama and Isawa (1970), Cabri (1973), Barton (1973), Ueno (personal communication, 1981), Li et al. (1996) and Ebel and Naldrett (1996, 1997). The nature of the phase relations at 600°C are well established and are illustrated in Fig. 2.16a. The system is dominated by 3 solid solutions, the bornite, the intermediate (iss) and the pyrrhotite (= mss) solid solutions. Although mss is capable of dissolving several percent Cu, the Cu content of the mss is always less than that of the coexisting sulfide liquid. Thus the sulfide liquid in equilibrium with mss is enriched in Cu with respect to mss. It is pointed out above that the liquid is also enriched in Ni with respect to mss, therefore fractional crystallization of mss from this liquid leads to a Ni and Cu-rich residual liquid. Ebel and Naldrett (1996, 1997) showed that in the Fe-Cu-Ni-S system, as the Cu content increases due to the fractionation of mss, Ni becomes eventually more compatible in mss than in the sulfide liquid. This is in agreement with Craig and Kullerud (1969) who showed that the liquid in equilibrium with mss at 850°C is enriched in Cu but depleted in Ni with respect to mss. Thus fractional crystallization of Cu-rich Fe-Cu-Ni-S liquids is likely to reverse the trend of increasing Ni and lead to residual liquids richer in Cu, but poorer in Ni than their predecessors in the fractionation process.

Based on their observations of natural assemblages at Noril'sk-Talnakh, Distler and Genkin (personal communication, 1984) believe that liquid

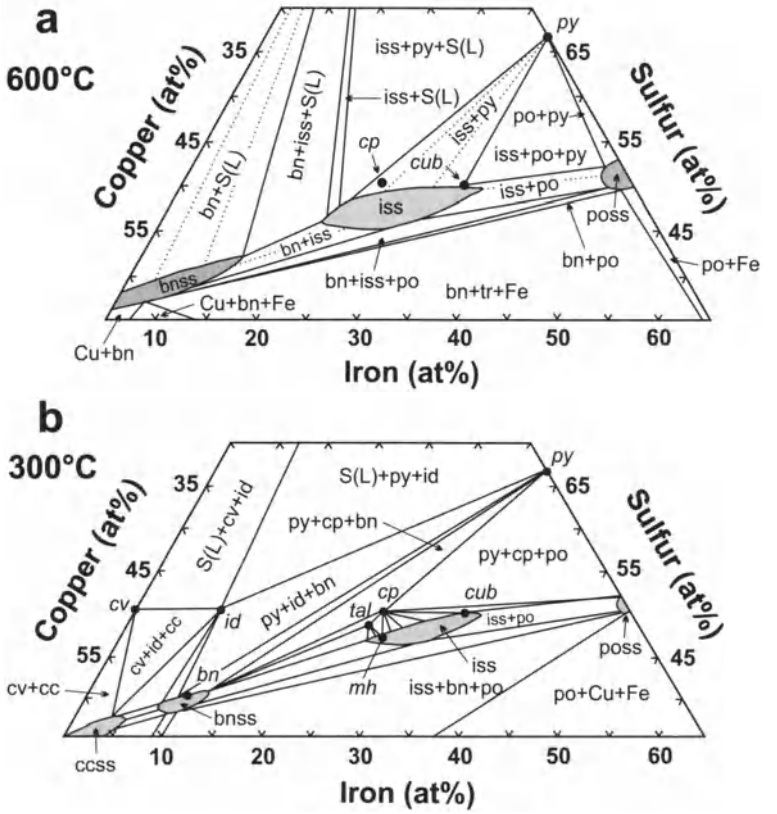


**Fig. 2.16.** Isothermal sections of central part of system Fe-Cu-S: a – at 600°C (from Cabri 1973); b – at 300°C (after compilation by Craig and Scott 1974)

immiscibility occurs within Fe-Cu-Ni-S liquids in nature, leading to co-existing Cu-rich and mss-rich liquids. Ballhaus (1999) suggested that he may have experimental substantiation of this miscibility gap, but this remains to be confirmed.

Below 600°C, phase relations in the Cu-Fe-S system are less well established, except for the unpublished study of Ueno (personal communication, 1981). Fig. 2.16b is a reconstruction of possible phase relations at 300°C by Craig and Scott (1974) based "on data and discussions of several workers". The data of Ueno (personal communication, 1981) are in general agreement with this, although the bounds of the intermediate solid solution (iss) and the compositions of the solid solution participating in adjacent 3-phase assemblages are somewhat different. The crystallization of most of the Cu-bearing mineral phases in Ni-Cu ores is therefore not well understood. Judging from the Cu-Fe-S system, it would seem that iss exsolves from a cupriferous mss and that in the more sulfur-rich (pyrite-bearing) as-

semblages, the major part of this exsolution occurs between 700 and 400°C, depending on Cu content. Iss presumably breaks down with falling temperature to chalcopyrite and pyrrhotite; to chalcopyrite, pyrrhotite and cubanite; or to pyrrhotite, cubanite and one of the sulfur-deficient intermediate phases talnakhite, mooihoekite or haycockite. The effect of Ni on low temperature phase relations in the Cu-Fe-S system is not known.

Hill (1984) and Peregoedova et al. (1995) have studied the effect of Cu on phase relations in the Fe-Ni-S system at 600°C. Mss in equilibrium with iss can contain up to 1 wt% Cu at this temperature. Both pyrite (on the S-rich side) and pentlandite (on the metal-rich side) can co-exist with Cu-bearing mss in equilibrium with chalcopyrite at temperatures higher (150°C in the case of pyrite, 300°C in the case of pentlandite) than would be predicted from the pure Fe-Ni-S system. The pentlandite co-existing with mss and chalcopyrite can contain significant amounts of Cu (up to 10 wt% and commonly 2 wt%).

## 2.4 Fractional crystallization of sulfide liquids

The concept of the fractional crystallization of sulfide liquids has been extensively discussed in the recent literature, although the parameters used or modeling the process are still a matter of debate. Arguments for and against fractional crystallization per se are not the objective of this book, and the idea is used at many stages in the developments of our arguments. What do need discussion are the partition coefficients used to quantify the modeling, which is the purpose of this section.

It has long been appreciated (Hawley 1965; Keays and Crocket 1970; Naldrett et al. 1982) that PGE-bearing Fe-Ni-Cu sulfide melts differentiate as they cool, initially crystallizing mss with the fractionated liquid becoming enriched in Cu, Pt, and Pd. The early studies of liquidus relations in the Fe-Ni-S and Cu-Fe-S systems (see above) paid relatively little attention to the exact positions of tie-lines connecting crystalline mss and the liquid with which it is in equilibrium. Chang and Hsieh (1986) used an associated-solution model for Fe-Ni-S liquid, coupled with a subregular solution model for mss to quantify the thermodynamics of the Fe-Ni-S ternary system. Fleet and Pan (1994) and Li et al. (1996) focused particularly on mss-liquid tie-line relationships with a view to modeling fractional crystallization of sulfide liquids in the quaternary system. Ebel and Naldrett (1996, 1997) approached the same problem as Fleet and Pan and Li et al., extending their work to higher temperatures, and over a larger range of composi-

tions; in addition Ebel and Naldrett refined early work in the bounding ternary systems, for which quantitative tie-line data were sparse.

The partition of both Ni and Cu between mss and coexisting liquid is clearly a function of the path that the liquid takes across the relevant system. This cannot be determined for any particular deposit by using the phase diagrams themselves, since to do so requires (1) assuming that the sulfide ore magma crystallized as a closed system and (2) a very precise knowledge of the initial metal:sulfur ratio of the sulfide liquid. With regard to point (1), nature exerts a control on the sulfur content of a magmatic sulfide liquid, and if this rises too much, iron in the adjacent silicates reacts with the liquid to form additional iron sulfide, thus controlling the metal:sulfur ratio (see Naldrett and Gasparrini, 1971, for a discussion of this phenomenon). With regard to point (2), the dominant mineral in most magmatic deposits, pyrrhotite, is very susceptible to oxidation by ground water, changing from the sulfur-poor hexagonal form to the sulfur-rich monoclinic form. Thus determination of the present metal:sulfur ratio may indicate little about the original ratio. A second complication affecting point (2) is that the simple high-temperature mineralogy of magmatic ores undergoes many changes on cooling, with the appearance of some phases either through exsolution or reaction, and also the disappearance of other phases through reaction. Thus, a calculation of the actual metal:sulfur ratio of an ore from the composition of constituent phases requires a very accurate knowledge of their relative proportions.

Perhaps the best guide to the path that liquids takes across the relevant system is the succession of mineral assemblages that are observed in ore bodies within which a wide range of assemblages representative of different stages of fractionation have been described. The most systematic work on this aspect is that of Genkin et al. (1981) and Duzhikov et al. (1988, 1992). They identified a number of mineral assemblages from the Noril'sk ores which they recognized as being members of two types of zoning. Their type I zoning, which they recognized as "high sulfur", ranged from [po(m>h) + cp + pn(Fe<Ni)] to [cp + po(m+h) + pn(Fe<Ni)]; type II zoning, identified as "intermediate sulfur", ranged from [po(h) + cp + pn(Fe=Ni)] through [po(h>tr) + cp + pn(Fe>Ni)] and [po(h>tr) + cp + cub + pn(Fe>Ni)] to [cub ± cp + pn(Fe>Ni) ± tr]. A "low sulfur" variant of type II zoning ended with the assemblage [tal(mh, put) + cub + pn][7].

Mungall (personal communication, February 2004) has informed the author of a submitted manuscript (see Mungall et al., submitted) in which the

[7] po = pyrrhotite (h = hexagonal, m = monoclinic, tr = troilite), cp = tetragonal chalcopyrite, pn = pentlandite, cub = cubanite, tal = talnahkite, mh = mooihoekite, put = putoranite.

concept of fractional crystallization of mss from a sulfide liquid as the origin of Cu-, Pt-, Pd- and Au-rich segregations associated with massive Ni-Cu sulfide ores is criticized in the light of new partition coefficients that have been determined under conditions of controlled $fO_2$ and $fS_2$. These data indicate that under conditions likely to occur in nature, Ni is significantly incompatible in mss. Their hypothesis is that the evolution of a sulfide liquid progresses by equilibrium crystallization to an advanced stage before any separation of solid and liquid sulfide takes place. These data and ideas have arrived too late for them to be evaluated in subsequent chapters of this book, but the reader is advised to research the submitted paper before reaching his/her own conclusions.

### 2.4.1 Partition coefficient of Ni and Cu between mss and coexisting sulfide liquid

With what has been written above in mind, partition coefficients have been calculated from the data of both Fleet and Pan (1974) and Ebel and Naldrett (1996, 1997) and are shown for both Ni and Cu as a function of increasing Cu content in Fig. 2.17. $D_{Ni}$ increases with increasing Cu content, from a value of about 0.6 at < 2 wt% Cu to 1.1 at about 25 wt% Cu, which is consistent with the observations of Li et al. (1996). The scatter in the data in Fig. 2.17a is largely due to the fact that sulfur content also affects $D_{Ni}$, lower sulfur contents favoring lower values of $D_{Ni}$. The scatter in $D_{Cu}$ also reflects non-linear composition dependencies. A $D_{Cu}$ of 0.28 at low Cu decreases to about 0.19 at 15 wt% Cu, which is consistent with the findings of Li et al. (1996). Although the data become more ambiguous at higher Cu contents than 15 wt%, the data can be extrapolated to give $D_{Cu}$ = 0.1 at 30 wt% Cu.

### 2.4.2 Partition of noble metals

The first attempt to model variation of PGE with fractionation of a sulfide liquid was that of Li et al. (1992). They used $D_{PGE}$ values obtained by comparing concentrations (obtained by Accelerator Mass-Spectrometry) in natural pyrrhotite from early crystallizing cumulates, with the estimated bulk composition of the entire Strathcona ore deposit, and also by comparing the bulk composition of the early-forming cumulates with the estimated bulk composition of the deposit. Theoretically, the two methods would bracket the D value for Pt (an element incompatible in mss) and provide reasonable estimates for Rh and Ir (elements compatible in mss). Their results are shown in Table 2.2. Makovicky et al. (1986) studied the

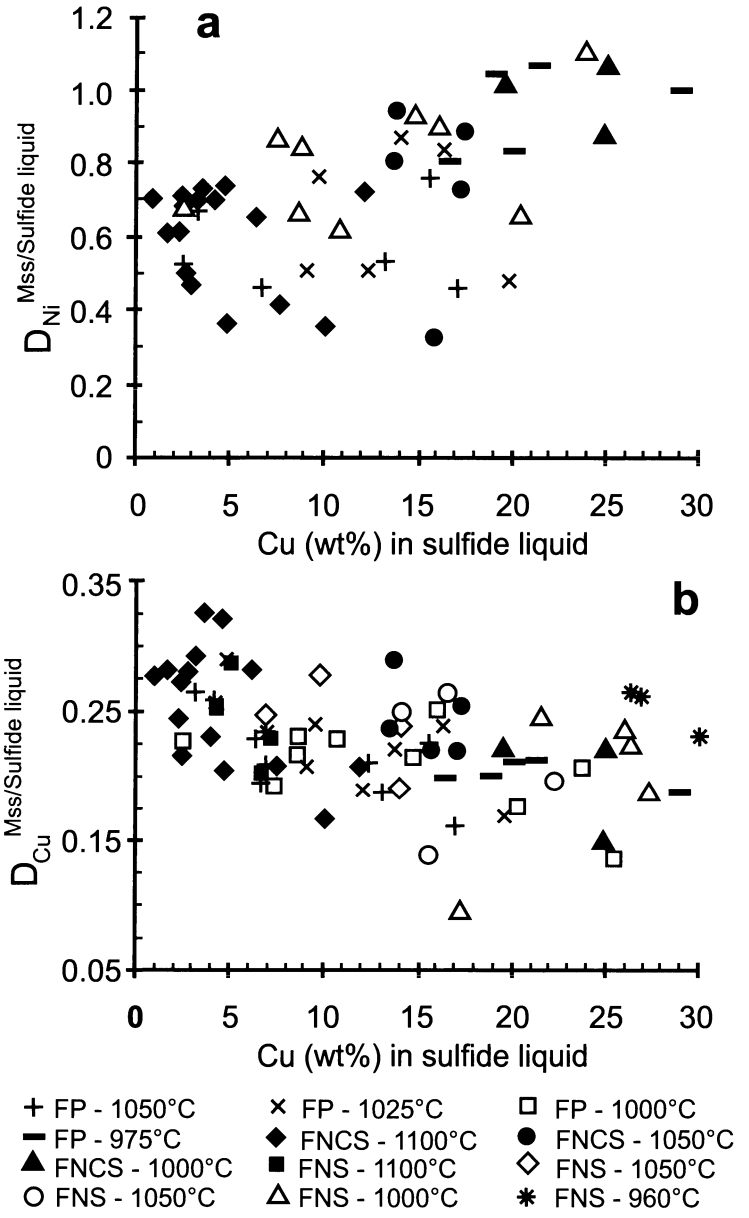


**Fig. 2.17.** Variations in $D_{Ni}$ (a) and $D_{Cu}$ (b) between mss and coexisting sulfide liquid with variations of Cu content in sulfide liquid (from Ebel and Naldrett 1997). FP – data of Fleet and Pan (1994) at temperatures from 105 to 975°C; FNCS – data of Ebel and Naldrett (1996) for system Fe-Ni-Cu-S at temperatures from 1100 to 1000°C; FCS - data of Ebel and Naldrett (1996) for system Fe-Cu-S at temperatures from 1050 to 960°C

**Table 2.2.** Nernst partition coefficients for noble metals between *mss* and sulfide liquid

| Study | $D_{Pt}$ | $D_{Pd}$ | $D_{Au}$ | $D_{Rh}$ | $D_{Ir}$ | $D_{Os}$ | $D_{Ru}$ |
|---|---|---|---|---|---|---|---|
| Li et al. (1992) | | | | | | | |
| (1) Pyrrhotite and bulk ore | 0.008 | | | 3.2 | 5.9 | | |
| (2) Early cumulus pyrrhotite and bulk ore | 0.10 | | | 4.1 | 4.4 | | |
| Mackovicky et al. (1986)* | 0.08–0.2 | | | | | | |
| Fleet et al. (1993)* | 0.2 | 0.2 | 0.09 | 3.0 | 3.6 | | |
| Li et al. (1996a)* | 0.07–0.16 | | | 1.5–5.0 | 2.0–5.0 | | |
| Barnes et al. (1997)* | 0.14–0.24 | 0.13–0.24 | | 3.9–11.0 | 5–17 | | |
| Mungall** at 1050°C* | 0.04 | 0.08 | 0.01 | 5.7 | 7 | | 16 |
| at 950°C* | 0.05 | 0.12 | 0.01 | 3.3 | 4.6 | | 9 |
| Naldrett et al. (1999) | | | | 4.0 | 4.4–4.8 | 4.2 | |
| Used in this book | | | 0.001 | 4.0 | | | |

*Experimental study, other figures are based on analyses of natural materials
**Personal communication 2004, see text

partitioning of Pt between mss and a Cu-rich residual liquid in the Cu-Fe-Pt-S system at wt% levels, and his result is also shown in Table 2. 2. The most comprehensive experimental studies are those of Fleet et al. (1993), Li et al. (1996) and Barnes et al. (1997) whose data are compared with earlier data in Table 2.2. The very recent data of Mungall et al. (Mungall, personal communication February 2004) are also shown there. Fleet et al.'s value for $D_{Au}$ is based on a single experiment in which the concentration in the mss was below their stated detection limit for their

analytical method (SIMS). It must therefore be regarded as a maximum limit; Au is clearly highly incompatible in mss and a value of 0.001 has been found to better quantify the behavious of Au in nature, which is much more incompatible than that of either Pt or Pd (c.f. Naldrett et al. 1994), and has been adopted for the modeling conducted here. Li et al. (1996) investigated the effect of sulfur fugacity on PGE partitioning, and showed that this had a major effect, with partition coefficients increasing with sulfur fugacity (i.e. into more sulfur-rich mss). The effect for Rh was particularly remarkable, with Rh being incompatible in mss in equilibrium with Fe-Ni alloy, and strongly compatible in S-rich mss. Naldrett et al. (1999) found that $D_{Rh} = 4$ provided the best fit to their data on the Sudbury deposits. Given this value, plots of Rh versus Ir and Os indicated strongly that $D_{Os} = 4.2$ and $D_{Ir} = 4.4$ in most deposits, and 4.8 in two (see Naldrett et al., 1996). These observations are consistent with experimental data.

### 2.4.3 Modeling of fractional crystallization of sulfide melts

Li et al., (1992) and Naldrett et al. (1994a,c; 1996a) have shown that much can be learned about the fractional crystallization of mss from sulfide liquids by plotting an element that is compatible in mss, such as Rh or Ir, against one that is incompatible, such as Cu or Au. The compatible element decreases in abundance exponentially as fractionation proceeds and the incompatible element increases in concentration. Model curves showing the covariation between Rh ($D^{mss/sulfide\ melt} = 4$) and Cu ($D^{mss/sulfide\ melt} = 0.2$) in liquid, mss and a 50:50 mixture of liquid+mss for perfect Rayleigh fractionation are plotted in Fig. 2.18. Ebel and Naldrett (1996) noted that knowing the Rh and Cu content of a sample, the initial composition of the sulfide liquid, and the appropriate partition coefficients, it is possible to calculate both the percentage of trapped liquid in the sample (they defined this as the function phi [$\phi$]) and the percentage of fractionation. Alternatively, of course, these variables can be read off Fig. 2.18.

It is seen that for samples that are rich in cumulus mss and that are relatively unfractionated, the Rh/Cu ratio is high, but that this decreases to a very low number in highly fractionated sulfide liquids.

As a result of their studies at Noril'sk and Sudbury, Naldrett and Pesseran (1992) and Naldrett et al. (1994a, b) pointed out that the fractionation proceeds by leaving a residue of cumulus mss mixed with varying proportions of fractionated liquid; where the residue is an mss adcumulate, they termed the ore 'dry' and where the cumulate has retained a high proportion of the liquid they termed it 'wet'. They made the case that Cu-,

PGE- and Au-rich ore bodies can form from the fractionated liquid, and that these are more likely where nearby cumulus ores are dry than where they are wet.

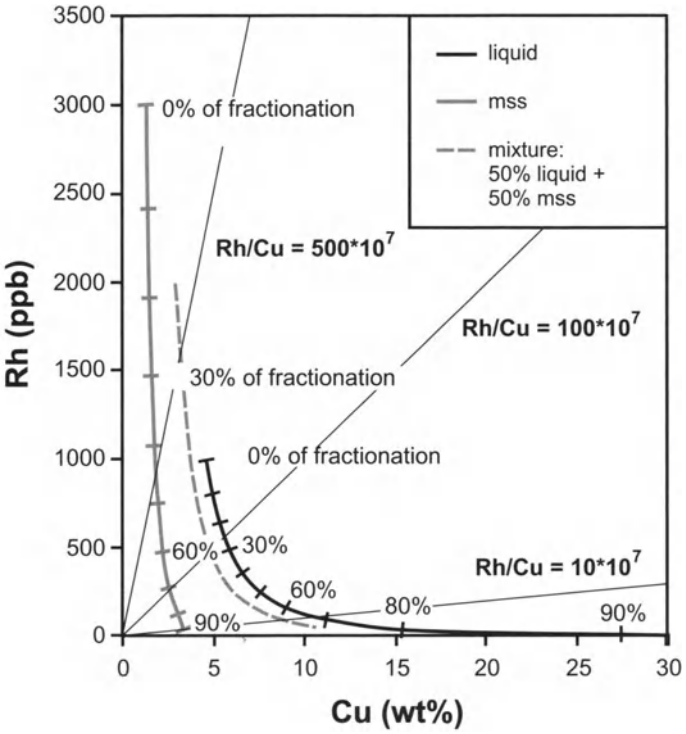


**Fig. 2.18.** Model curves showing the covariation between Rh ($D^{Mss/Sul.Liq} = 4$) and Cu ($D^{Mss/Sul.Liq} = 0.2$) in liquid, mss and a 50:50 mixture of liquid + mss for perfect Rayleigh fractionation

## 2.5 External sources of sulfur

As the reader continues through this book, it will become apparent that the majority of Ni-Cu sulfide deposits (low sulfur PGE-rich deposits are not so dependent on external sulfur) require the addition of sulfur from an external source close to the final emplacement point. There are many lines of evidence for this. These include:

1. The non-mantle isotopic composition of sulfur as at Duluth, Noril'sk.

2. The association of magmatic sulfides with inclusions of country rock, as at Voisey's Bay, Noril'sk, Duluth.
3. The very common association of Ni-Cu sulfide deposits with sulfur-rich country rocks as at Duluth, Noril'sk, Pechenga, Kambalda, Raglan.
4. A further strong line of evidence is the experimental data which indicates that magmas are likely to be able to dissolve more sulfur as they rise up towards surface, which, unless they gain sulfur from the rocks through which they pass, means that they will move farther and farther from saturation with sulfide as the pressure decreases.

The method by which sulfur enters a magma is less clear. In some cases, as at Duluth and Voisey's Bay, there is clear evidence of the incorporation and reaction with inclusions, but the adjacent igneous rock is not highly enriched in the trace elements that characterize the source rocks of the inclusions, nor does it reflect the oxygen isotopic composition of the crustal rocks. This is also the case at Kambalda. Further more, it is difficult to envisage a magma having sufficient superheat to assimilate the large amount of country rock that would be necessary to give rise to the amounts of sulfide present at Noril'sk or Voisey's Bay. Ripley (1981, 1986) has investigated this problem closely at Duluth, and has suggested that the heat of the magma metamorphoses the country rocks and liberates a volatile phase rich in sulfur, which then enters the magma and causes the precipitation of magmatic sulfide. Pyrite rich country rocks are especially important to this hypothesis, since pyrite breaks down in the upper crust at around 800°C, releasing sulfur and giving rise to pyrrhotite. It also seems likely that, as is clearly the case at Kambalda, Voisey's Bay and Noril'sk, much more magma has passed through the system than is observed in contact with the sulfides. This magma has carried away evidence of reaction, such as key trace elements and isotopic information, leaving in its place less contaminated igneous rock. The sulfides and their contained chalcophile metals remain behind, probably because of the different physical properties of the sulfide.

The deposits at Noril'sk present a unique problem. The only obvious sulfur source is the local sulfate evaporite. Obtaining sulfur from this requires the evaporite to be reduced. Most magmas have very limited buffering capacity, and can only bring about significant reduction if they precipitate large amounts of magnetite. The Noril'sk magmas are chromite-bearing, and there is no evidence that they have precipitated magnetite before flowing through the ore-bearing conduits. The problem with respect to their buffering capacity is illustrated in Fig. 2.19. The current hypothesis (Chap. 4) is that the initial sulfides were deposited from the Nadezhdinsky magma. If, as the current hypothesis would maintain, this magma has

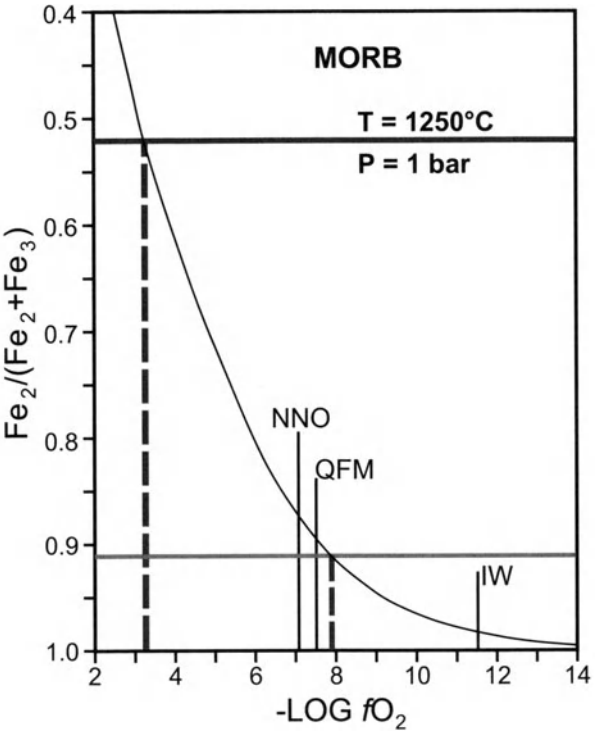


**Fig. 2.19.** Plot showing variation in the $Fe^{2+}/(Fe^{2+}+Fe^{3+})$ ratio with $fO_2$ for a typical MORB along with the increase in $fO_2$ (shown by the position of the two vertical, dashed lines) that would accompany the increase in $Fe^{2+}/(Fe^{2+}+Fe^{3+})$ ratio if sulfide were produced within the basalt at a magma/sulfide ratio of 130 as a result of the reduction of $CaSO_4$, and if the released oxygen were taken up by the oxidation of $Fe^{2+}$ to $Fe^{3+}$. Data for MORB from Mathez (1990)

formed as a result of contamination of and reaction of sulfide with Tuklonsky magma, the average Ni content of the Nadezhdinsky would require the Tuklonsky to have reacted with the sulfide at a magma/sulfide ratio of 130. If all of this sulfide were to have been derived from evaporite, the resulting oxygen would have been released from $CaSO_4$ as it was reduced and would have had to have been taken up by oxidizing a significant amount of the $Fe^{2+}$ in the Tuklonsky/Nadezhdinsky magma to $Fe^{3+}$. Given the Fe content of the Tk magma, this would have changed its $Fe^{2+}/(Fe^{2+}+Fe^{3+})$ ratio from the normal value of about 0.91 (QFM buffer) to 0.52. Precise data on the variation of $fO_2$ with $Fe^{2+}/(Fe^{2+}+Fe^{3+})$ ratio for the Tuklonsky/Nadezhdinsky magmas are not available, but Mathez (1990) presented data for typical MORB. The Tuklonsky/Nadezhdinsky magma can be expected to show a similar relationship to that shown by MORB. It can be

seen in Fig. 2.19 that a change of $Fe^{2+}/(Fe^{2+}+Fe^{3+})$ ratio of the magnitude required to reduce sufficient evaporite to account for the ores would require an increase in $fO_2$ from $10^{-8}$ to $10^{-3.3}$. An increase of this magnitude carries two problems with it. The first is that compositions of the minerals and mineralogy of the Tuklonsky and Nadezhdinsky basalts are totally inconsistent with their being as oxidized as this. The second is that if the magma truly had been oxidized to this extent, the sulfur would be dissolved in it as $SO_4^{2-}$ [see discussion of Fincham and Richardson (1954) in section 2.1 of this chapter] not $H_2S$, S or $S^{2-}$, and would not be capable of giving rise to sulfide.

The presence of inclusions of anhydrite floating in gabbro-dolerite (e.g. as seen at the Taymyrsky mine) with no evidence of reaction or the precipitation of sulfide around them is a graphic illustration of the apparent unreactivity of the evaporite. It is possible that in the intrusions of which the ore-bearing conduits may be exit channels, both evaporite and coal from the Tunguskaya series have reacted in the equivalent of a natural smelter, that sulfate was reduced, and Fe sulfide produced, with the release of the oxygen as $CO_2$. There is, however, no evidence to support this hypothesis. Grinenko (1985) has expressed the view that sour gas, rather than evaporite, was the sulfur source at Noril'sk. This would seem to offer a possible alternative to sulfate reduction, but raises the problem of how the $H_2S$ of the sour gas was able to enter and react with the hot intrusion.

# 3 Komatiite-Related Deposits

Komatiites are rocks that have been the subject of intensive investigation since they were first recognized as a separate class during the 1960's (Viljoen and Viljoen 1969; Naldrett and Mason 1968; Nesbitt 1971). Initially they were only recognized in sequences of Archean rocks, where they constitute as much as 10% of the total volcanic succession. However, soon they were identified as important components of Proterozoic and Phanerozoic successions (Arndt and Nisbett 1982). In general the younger the komatiites, the lower the MgO content of the magma responsible for them, although the Paleocene komatiites on Gorgona Island (off the coast of Ecuador) developed from magma containing up to 24 wt% MgO (Ganser et al. 1979). It is also clear that komattiites constitute a progressively lower proportion of the volcanic succession in progressively younger successions. This has been attributed to the cooling of the earth's mantle with time.

The most ancient komatiite complexes, Archean and Early Proterozoic, host important Cu-Ni sulfide deposits. Five of the ten foremost ore deposits (or ore camps) listed in Table 1.1(excluding those mined primarily for their PGE) are related to komatiites (Thompson, Mt Keith, Kambalda, Perseverance, Raglan), although they are not amongst the "big four" economic deposits (Noril'sk, Sudbury, Jinchuan and Pechenga). As discussed in Chapter 1 (see Table 1.2), Archean komatiite-related deposits have the highest Ni contents in 100% sulfides, highest Ni/Cu ratios and lowest Pd/Ir ratios of all deposit types. Proterozoic komatiite deposits tend to be intermediate in their chemical characteristics between Archean deposits and those related to less magnesian magmas.

## 3.1 Archean Komatiite-Related Deposits

### 3.2.1 General information about Archean komatiites and associated mineralization

Recent studies in the Wiluna-Norseman greenstone belt (Hill et al. 1989, 1990, 1995; Lesher and Arndt 1995) have shown that the komatiitic lavas

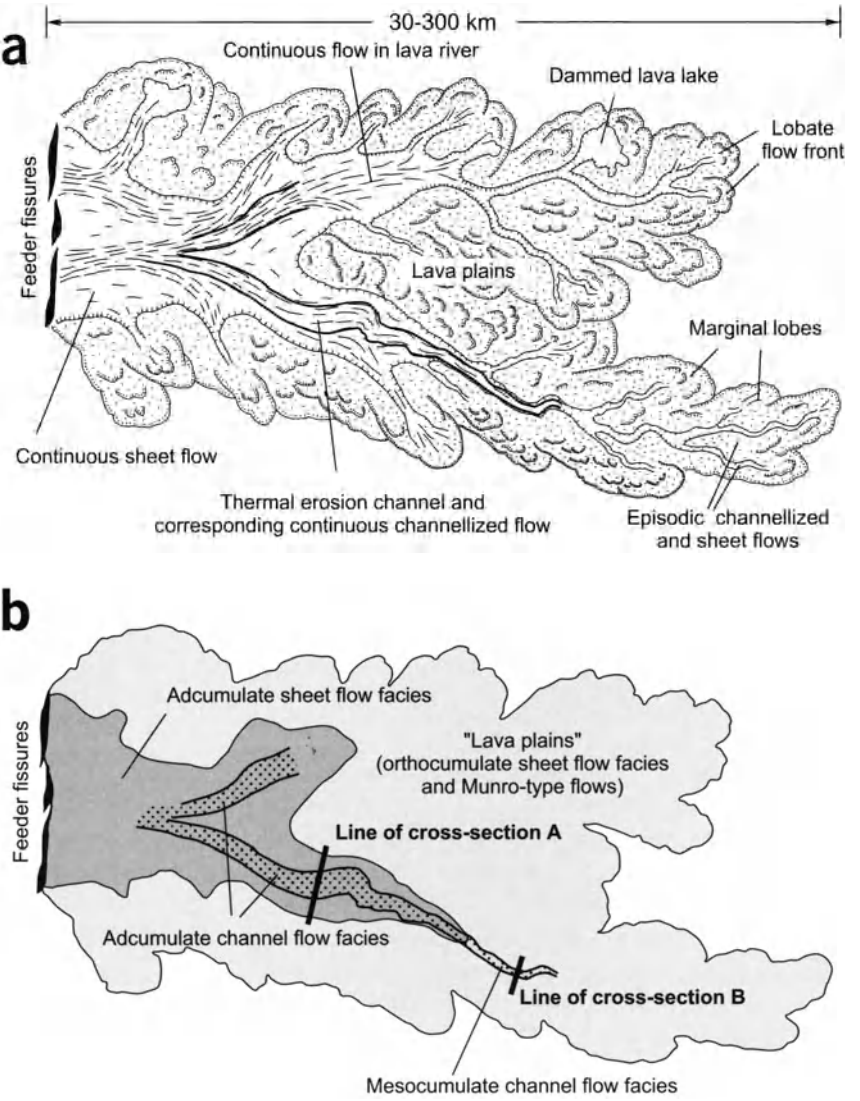


**Fig. 3.1.** Schematic illustration of construction (a) and facies b) of a regional komatiite volcanic complex, formed by cataclysmic sustained eruption. Note that adcumulate (dunite) sheet flow facies (ASF) develops close to the vent, and becomes channelized to adcumulate channel flow facies (ACF) farther from the vent. Downstream, cooling lava gives rise to orthocumulate sheet flow facies (OSF) within which a facies composed of mesocumulate dunite channel flows (MCF) may be present. The margins and farthest extremities of the volcanic complex consist of lava plains comprising flows of OSF intermixed with or capped by thin "Munro-type" flows (MunF). Modified after Hill et al. (1990). Cross-sections are shown in Fig. 3.2

can be subdivided into a number of distinctive facies, which relate to their distance from the eruptive source and the rate of eruption (Fig. 3.1). Flows that are close to their source (probably a series of fissures as shown schematically in Fig. 3.1), and which therefore are hottest, tend to develop as very extensive sheets (in some cases in excess of 35x150 km by several 100s of m thick) of adcumulate dunite (adcumulate sheet flow facies or ***ASF***). The adcumulate texture is believed to be due to the direct growth of olivine from overlying, turbulently flowing hot magma, which has only a very low degree of supercooling. When this facies develops over a substrate with low melting temperature, such as felsic volcanic rocks, the flow may become channelized with the principal flow restricted to a number of channels (several km wide by several 100s m thick) (adcumulate channel facies or ***ACF***). These channels have been cut into the underlying substrate by thermal erosion of the flowing komatiitic magma. The channels can be recognised by lenses of adcumulate dunite which have formed for the same reasons as the adcumulate sheet flows. Dunites which have developed within the channels may contain sulfides and thus comprise olivine-sulfide adcumulates (Fig. 3.2a).

Farther downstream, where flow is less rapid and probably lamina, "lava plains" composed of sheet flows with orthocumulate rather than adcumulate dunite (orthocumulate sheet flow facies or ***OSF***) develop. Channelization under these circumstances can give rise to lenses of mesocumulus olivine (several 100s m wide and up to 100 m thick), which represent the main flow channels (mesocumulate channel flow facies or ***MCF***). Such units have the appearance of meandering streams in plan view that are separated by ***OSF*** lava plains in which the upper parts of the flows have well-developed spinifex texture. Sometimes, if sulfide-bearing rocks are present in the substrate, either in place or upstream, sulfide mineralization can develop in ***MCF*** (Fig. 3.2b).

Even greater degrees of cooling and supercooling of komatiitic magma can give rise to sequences of "Munro-type" finely laminated flows,10 cm-10 m thick (***MunF***), which commonly cap or are intermixed with those composed of orthocumulate dunite. Lava plains comprising this facies are believed to mark the margins and distal extremities of komatiite volcanic complexes. "Munro-type" flows are those originally described by Pyke et al. (1973) from the type locality in Munro Township, Ontario, Canada; amongst other variants in this locality, flows in which spinifex-textured material (A zone) overlies cumulate-textured peridotite (B zone) are very common and well developed (see Fig. 3.3).

Hill et al. (1995) emphasized that the waning of an eruptive event usually results in a regressive sequence in which dunitic sheets or lenses pass up into orthocumulate dunite (as the amount and rate of magma eruption

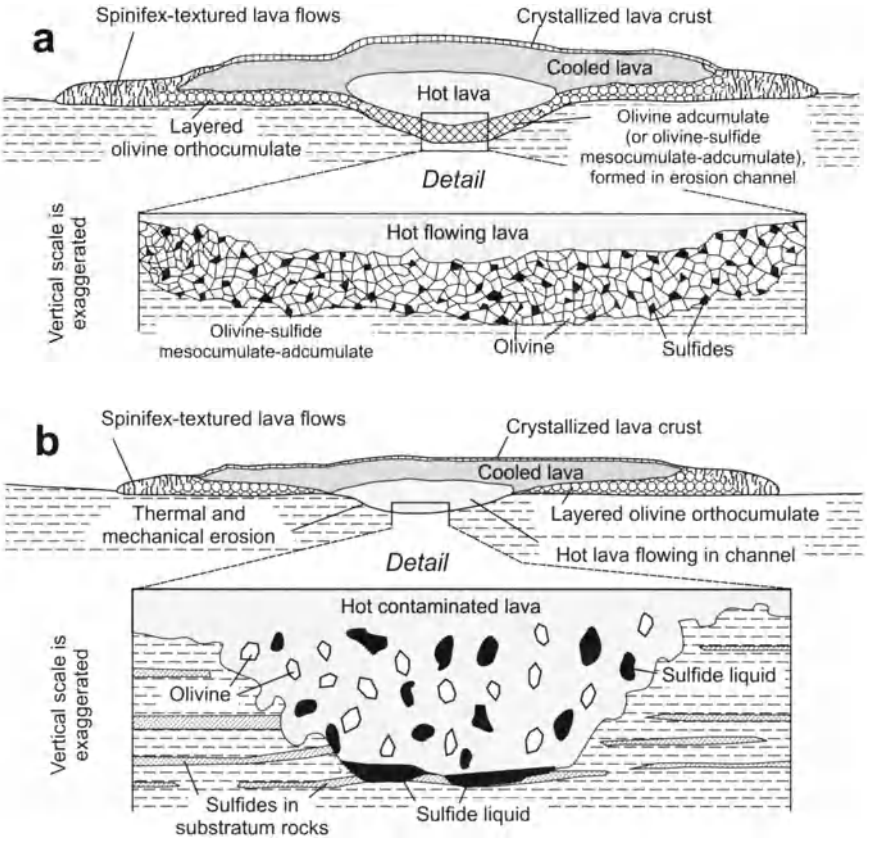


**Fig. 3.2.** Cross-sections illustrating formation of adcumulate (a) and mesocumulate (b) facies of lava channels. Locations of the section lines are shown in Fig. 3.1

decreases, and therefore the super-cooling becomes more pronounced) followed by sequences of Munro-type flows.

Intrusive komatiitic bodies occur in many areas (for example the Eldorado dome south of Timmins, Naldrett 1964) but in general have been less well studied than the extrusive facies. They tend to consist of irregular lenses of cumulus dunite (mesocumulate or adcumulate) enclosed within a marginal facies of orthocumulus peridotite. The Dumont sill, near Amos, Quebec is a mineralized example of an intrusive komatiite (Duke 1986; Brugman et al. 1990).

Sulfide deposits are associated with many areas of Archean komatiites throughout the world, including Ontario, Canada; Zimbabwe; Tanzania; and Western Australia. They all have many features in common. The deposits of the Eastern Goldfields of Western Australia, particularly of the Wiluna-Norseman greenstone belt (Fig. 3.4), have proved to be the most

important economically, and are thus the best studied. They are described here as the type example.

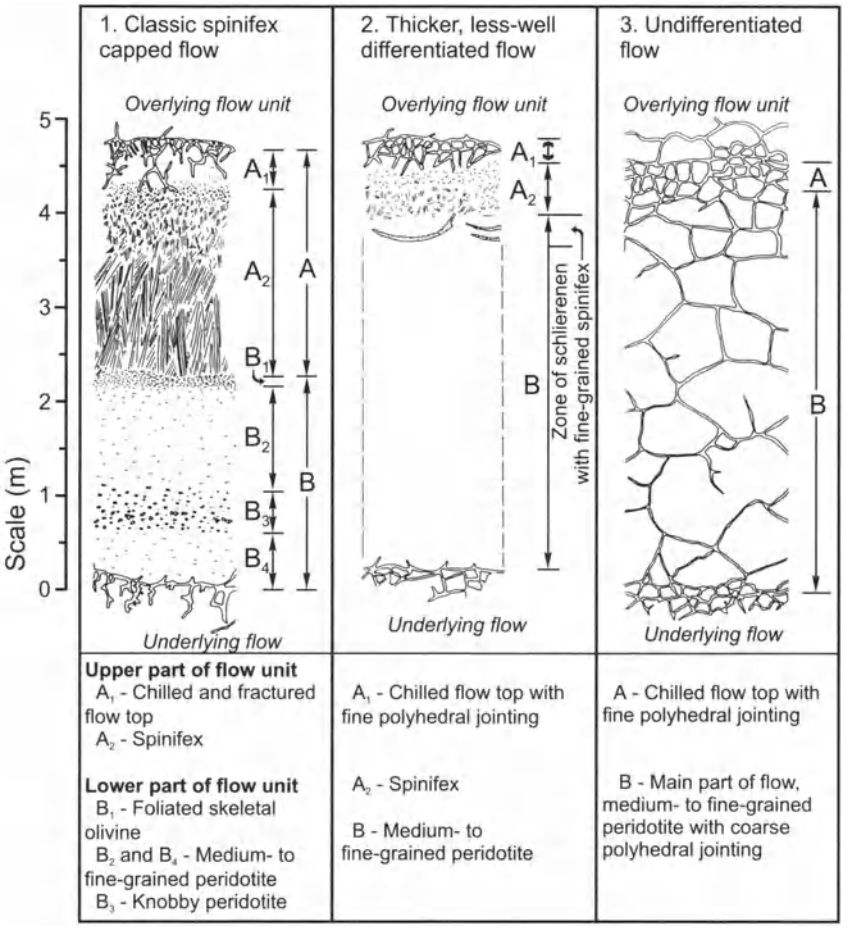


**Fig. 3.3.** Sections through three variants of Munro-type flows, showing a classic spinifex capped flow (1), a thicker, less-well differentiated flow (2) and an undifferentiated flow (3). After Arndt et al. (1977)

### 3.1.2 Deposits of the Wiluna-Norseman greenstone belt (Eastern Goldfields, Western Australia)

Komatiitic ore deposits of the Wiluna-Norseman belt can be considered, as can all other komatiite-related deposits, as falling into one of two groups:

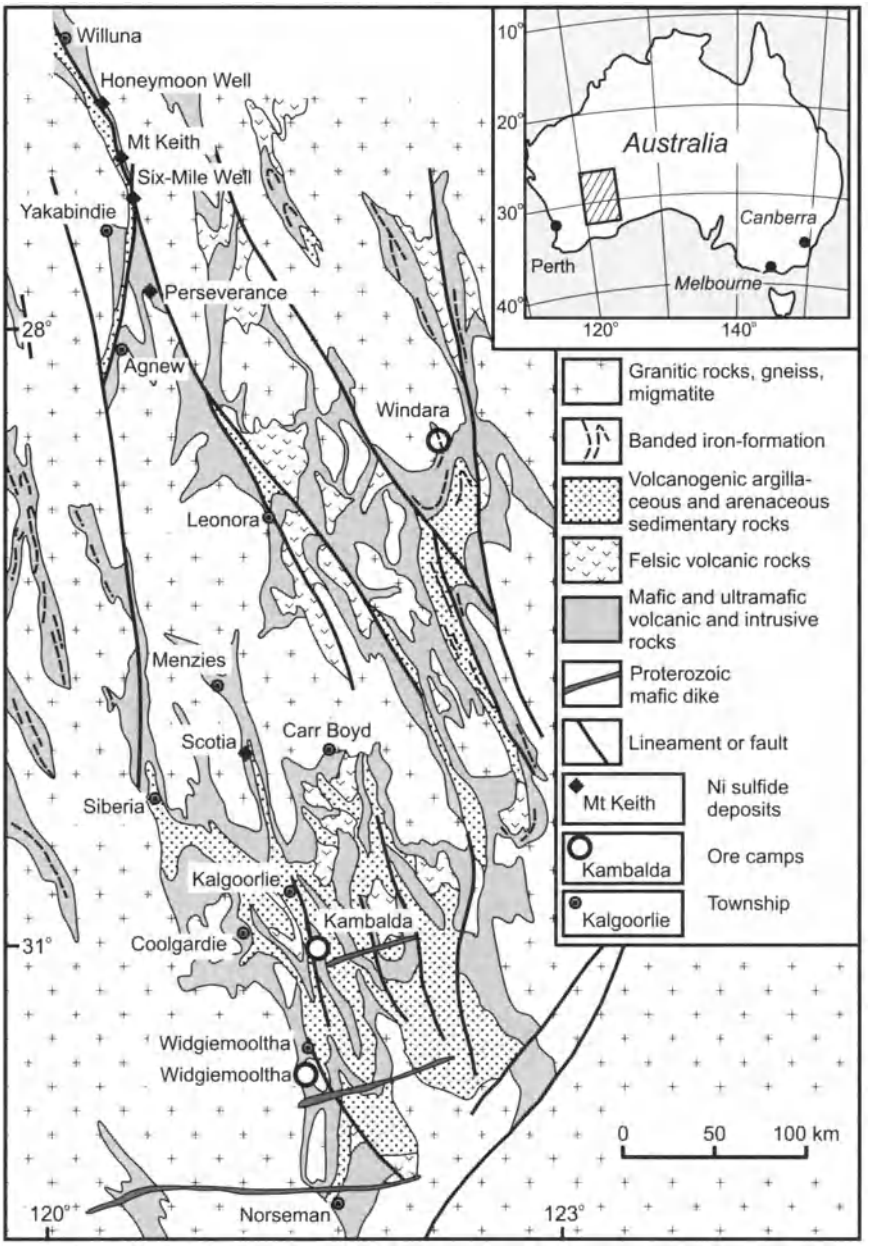


**Fig. 3.4.** Geological map of the Wiluna-Norseman area (Yilgarn Block, western Australia)

Group 1: Orebodies occurring at the base of mesocumulate dunitic flows (see above), generally small (1 to $5x10^6$ tonnes) and of high grade (1.5-3.5% Ni). Examples include the deposits of the Kambalda district (Ross and Hopkins 1975; Gresham and Loftus-Hills 1981; Gresham 1986) and the Widgiemooltha dome (Fisher 1979; McQueen, 1981).

Group 2: Very large ($100\text{-}250x10^6$ tonnes), low-grade (0.6% Ni) deposits of finely disseminated sulfide in channel-like lenses of adcumulate dunite. Examples include the Six-Mile and Mt. Keith deposits near Yakabindie, Western Australia (Burt and Sheppy 1975; Naldrett and Turner 1977; Hill et al. 1989; Hill et al. 1995).

The Perseverance deposit, which is located near the village of Agnew is unique. It contains more then $40x10^6$ tonnes of ore grading 2.0% Ni. It is thought now (Hill et al. 1985; Barnes et al. 1988a, b) that the deposit belongs to group 1. However because it is much larger than other group 1 deposits and its ores are not as rich on average, it is described separately.

### *Group 1: generally small deposits of rich ores at the base of lava flows (example of Kambalda camp)*

**Geology of the Kambalda district**. The extrusive association of komatiite-related deposits was first recognized and described (Woodall and Travis 1969) in the Kambalda-St Ives mining camp of Western Australia (referred to hereafter as the Kambalda mining camp). In the summer of 2000 reserves plus past production stood at $67x10^6$ tonnes at 2.90 wt% Ni, 0.21 wt% Cu. Individual ore shoots range in size from very small to over $5x10^6$ tonnes. Of the eighteen shoots described by Gresham and Loftus-Hills, five appear to be over $2.8x10^6$ tonnes, four between 1.4 and $2.8x10^6$ and seven less than $500x10^3$ tonnes.

The Kambalda district lies within the Eastern Goldfields, which comprises the eastern half of the Yilgarn Archean block of Western Australia. As stated above, it forms part of the Wiluna-Norseman greenstone belt, which Groves et al. (1984) interpret as a fault-bounded rift zone. The earliest folding in the belt is thought to have been a stage of recumbent folding and nappe development (Archibald et al. 1978; Platt et al. 1978), but the most pronounced folding is about north-northwest axes which have been refolded about east-west axes, so that the stratigraphy is delineated in a series of north-northwest trending basins and domes.

The Kambalda deposits are located around one of these domes, the Kambalda dome (Fig. 3.5). The volcanic and sedimentary rocks have been intruded by Archean granites, felsic and intermediate porphyries, mafic dykes and sills, and Proterozoic dykes. Metamorphic studies indicate peak

temperatures slightly in excess of 500°C and pressures of around 2.5 kb (Barrett et al. 1977; Bavington 1979).

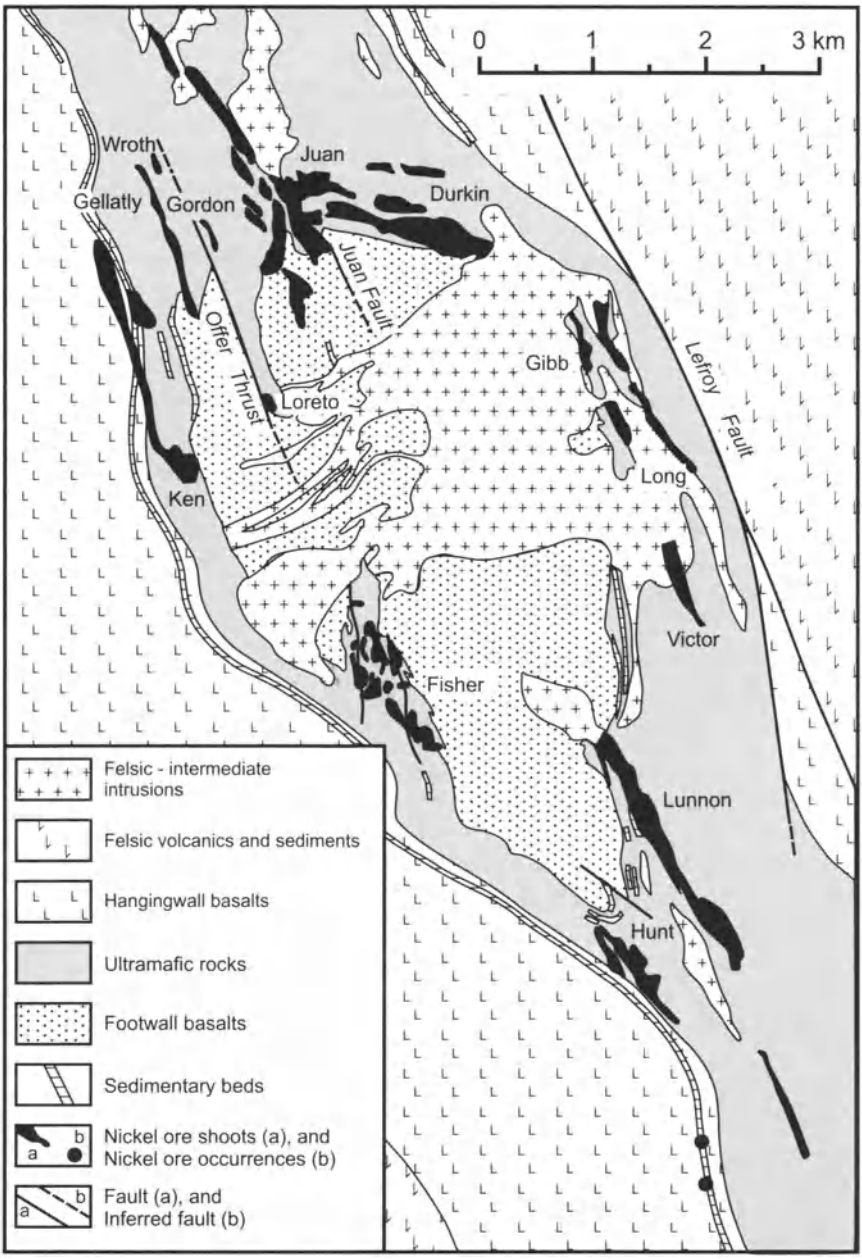


**Fig. 3.5.** Geology of the Kambalda dome, showing the plan-projection of the principal nickel ore shoots (after Gresham and Loftus-Hills 1981)

At Kambalda, the ore-bearing mafic-ultramafic sequence consists of a lower (>200 m) unit of pillowed basalt, the Lunnon Basalts, overlain by an ultramafic unit, the Kambalda formation, which is up to 1000 m in thickness. This formation consists of two members, the Silver Lake member, which is overlain by the Tripod Hill member. Chauvel et al. (1985) have dated the sequence as 2.7 Ga. Gresham and Loftus-Hills (1981) emphasized the difference between the general succession at Kambalda and the succession developed immediately above the ore deposits. Although they did not have the understanding of komatiite facies that is available to day, their desciptions indicate that their "ore environment" is one of ***MSF*** (see above); the elongate channels forming this facies are separated by a lava plain environment in which orthocumulate sheet flows ***(OSF)*** pass upwards into Munro-type flows (***MunF***). Gresham and Loftus-Hills (1981) pointed out that the lower flows of the lava plain environment are commonly separated by thin-bedded, 'exhalite-type' sediments, consisting of a mixture of clastic, tuffaceous and chemically precipitated components (Bavington 1981), but that sediments are commonly lacking in the ore environment.

The Kambalda formation is overlain by komatiitic basalts, the Devon Consuls formation (consisting of pillowed basalts, some with felsic ocelli), and an upper massive, more magnesian member (the Paringa basalt formation).

**Geochemistry of the Lavas.** The major element compositions of the komatiitic and related basaltic rocks of the Kambalda dome, with some data for the Scotia and Wannaway areas, are given in Table 3.1. The same data are the basis for the $CaO - MgO - Al_2O_3$ plot appearing as Fig. 3.6. The highly magnesian composition of the B zone mesocumulate dunite of the ore-bearing channel facies at Lunnon and at other Kambalda ore shoots stands out in contrast to the lower MgO content of the orthocumulate peridotite forming the B zones of the thinner komatiitic flows that constitute the sheet facies flanking the ore environments. Even higher MgO contents characterize the ore-bearing units at Scotia (45.4 wt%) and Wannaway (44.6 wt%).

Recent work on the geochemistry of the Kambalda formation includes that of Lesher and Arndt (1995), Arndt and Lesher (1992), Lesher (1989) and Lesher and Groves (1984). Some geochemical criteria for A and B zones in the different flow facies of the Siver Lake and Tripod Hill members of the Kambalda formation are shown in Table 3.2.

Lesher and Arndt (1995) noted that the ore-bearing, channelized flows of the Silver Lake member have crystallized from the most magnesian magma, and one which shows the least evidence of contamination by

**Table 3.1.** Major element analyses (wt%) of komatiite and associated basalt lavas from the Kambalda area of the Eastern Goldfields of Western Australia with some data for the Scotia and Wannaway areas

| No | 1* | 2* | 3* | 4* | 5* | 6* | 7* | 8** | 9** | 10* | 11* | 12* | 13* | 14* | 15** |
|---|---|---|---|---|---|---|---|---|---|---|---|---|---|---|---|
| Rock | B | B | B | B | SK | SK | SK | SK | SK | KTF | CK | CK | CK | CK | CK |
| Area | K | K | S | S | K | K | K | S | W | K | K | K | K | S | W |
| $SiO_2$ | 52.10 | 53.12 | 49.70 | 49.10 | 47.70 | 45.70 | 49.20 | 44.10 | 46.90 | 49.30 | 45.10 | 44.30 | 42.80 | 42.20 | 43.60 |
| $TiO_2$ | 0.68 | 0.62 | 0.65 | 1.07 | 0.34 | 0.33 | 0.40 | 0.43 | 0.27 | 0.20 | 0.14 | 0.14 | 0.17 | 0.09 | 0.11 |
| $Al_2O_3$ | 14.70 | 12.23 | 12.48 | 14.99 | 7.87 | 8.01 | 9.40 | 8.34 | 6.04 | 4.92 | 3.23 | 2.81 | 4.02 | 1.63 | 2.53 |
| $Fe_2O_3$ | | 1.43 | 12.05 | 13.37 | | 2.64 | 2.15 | 12.81 | 1.79 | 2.06 | | | 3.76 | 9.32 | 4.61 |
| FeO | 10.70 | 9.23 | | | 11.50 | 8.59 | 10.11 | | 9.86 | 6.65 | 8.80 | 9.20 | 5.93 | | 4.14 |
| MnO | 0.07 | 0.20 | 0.20 | 0.23 | 0.20 | 0.14 | 0.15 | 0.16 | 0.18 | 0.15 | 0.12 | | | 0.14 | 0.11 |
| MgO | 8.20 | 11.37 | 12.92 | 7.03 | 23.90 | 26.90 | 26.50 | 28.20 | 26.5 | 31.80 | 41.10 | 41.70 | 37.90 | 45.40 | 44.6 |
| CaO | 11.00 | 9.53 | 9.39 | 11.68 | 7.79 | 5.95 | 6.81 | 5.92 | 6.33 | 3.89 | 1.41 | 1.69 | 2.68 | 0.51 | 0.51 |
| $Na_2O$ | 2.10 | 1.53 | 2.22 | 2.21 | 0.15 | 0.12 | 0.22 | | 0.11 | 0.11 | 0.06 | 0.03 | 0.06 | | <0.01 |
| $K_2O$ | 0.36 | 0.45 | 0.40 | 0.30 | 0.06 | 0.06 | | 0.05 | 0.03 | 0.07 | 0.02 | <0.01 | | 0.02 | 0.02 |
| $P_2O_5$ | | 0.07 | 0.08 | 0.10 | 0.08 | 0.02 | 0.03 | 0.43 | 0.03 | 0.02 | 0.05 | <0.01 | 0.01 | 0.09 | 0.01 |
| S | | 0.02 | | | 0.39 | 0.08 | 0.72 | | | 0.65 | 0.30 | | 0.55 | | |

* = average ** = single sample

1 = Average footwall basalt, Lunnon. (Gresham and Loftus-Hills 1981, Table 2, No. 1.). 2 = Upper average hanging-wall komatiitic basalt, Lunnon. (Gresham and Loftus-Hills 1981, Table 2, No. 8). 3 = Average basalt, Scotia. (Stolz and Nesbitt 1981, Table 2, No. 3). 4 = Average tholeiitic basalt, Scotia (Stolz and Nesbitt 1981, Table 2, No. 4). 5 = Average spinifex-textured or equivalent flow top material from basal unit at Lunnon shoot (Gresham and Loftus-Hills 1981, Table 3, No. L). 6 = Average spinifex-textured or equivalent flow top material from second unit above base at Lunnon shoot (Gresham and Loftus-Hills 1981, Table 3, No. 5). 7= Average spinifex textured or equivalent flow top material from the upper flows at Lunnon shoot (Gresham and Loftus-Hills 1981, Table 3, No. 8). 8 = Spinifex-textured peridotite, from Scotia. (Stolz and Nesbitt, 1981 Table 3, No. 5). 9 = Spinifex-textured rock from same unit as No. 10. (McQueen 198 1, Table 5, No. 84517). 10 = Average peridotite from thin upper flows at Lunnon shoot. (Gresham and Loftus-Hills 1981, Table 3, No. 9). 11 = Average olivine peridotite from basal unit at Lunnon shoot (Gresham and Loftus-Hills 1981, Table 3, No. 3). 12 = Average olivine peridotite from basal units at Hunt, Fisher, Gibb, Long, Otter, Juan and Durkin shoots (Gresham and Loftus-Hills 1981, Table 3, No. 4). 13 = Average olivine peridotite from same unit as 4. (Gresham and Loftus-Hills 1981, Table 3, No. 7). 14 = Average ore-bearing dunite, Scotia. (Stolz and Nesbitt 1981, Table 2, No. 7). 15 = Ore-bearing dunite, Wannaway. (McQueen 1981, Table 5, No. 84520)

**Table 3.2.** Some geochemical data for the Kambalda Formation (after Lesher and Arndt 1995)

| Unit | Flow Facies | Flow Zone * | MgO (wt%) | $TiO_2$ (wt%) | Fo in olivine | Cr (ppm) | Zr (ppm) | Zr/Y | La/Sm | εNd |
|---|---|---|---|---|---|---|---|---|---|---|
| Silver Lake | Mesocumulate channel flow facies or ***MCF*** (ore environment) | A | 20–32 | 0.3–0.53 | | 1280–3670 | 15–27 | 1.8–2.2 | 0.4–0.7 | +1.8 to +5.4 |
| | | B | 40–45 (maximum 50) | | 90–94 | | | | | |
| | Orthocumulate sheet flow facies or ***OSF*** | A | 12–21 | 0.4–0.5 | | 424–1810 | 24–34 | 2.6–3.9 | 0.6–1.0 | |
| | | B | 35–40 (maximum 45) | | 89–91 | | | | | |
| Tripod Hill | ***OSF*** and Munro-facies | A | 15–32 (normally <26) | 0.4–0.5 | | 2500–4020 | 14–31 | 2–3 | 0.6–0.8 | +2.7 to +4.7 |

*Flow zone: A = spinifex-textured or quenched flow top; B = cumulate zone

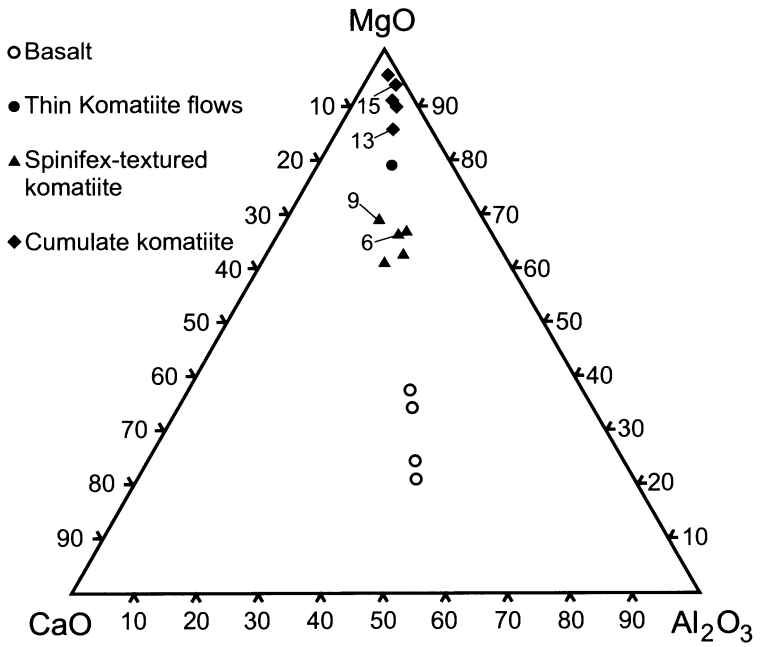


**Fig. 3.6.** Variation in the relative proportions of MgO, CaO and Al2O3 (wt%) in volcanic rocks of the Kambalda area with some data from the Scotia and Wannaway areas of the Eastern Goldfields of Western Australia. Figures (according Table 3.1) mark compositions of komatiitic rocks that represent different zones of the same lava flows

crustal rocks. On the other hand lavas forming the sheet facies that flanks the channel facies include some very contaminated magma, including zones of identifyable melted footwall sediments. The overlying Tripod Hill member is even more crustally contaminated. They note that when the underlying Lunnon basalts, and overlying Devon Consuls and Paringa basalts are considered together with the Kambalda formation rocks, a picture of progressively increasing crustal contamination with time emerges. They attribute this to progressive warming of the magma conduits with time. Referring to the contrast between the low degree of crustal contamination of the Silver Lake channel facies and more crustally contaminated, stratigraphically equivalent, sheet facies, they conclude that the sheet flows represent early eruptions of magma that had become contaminated through contact with the conduit walls and the substrate on which the eruption occurred. The channel flows continued flowing after the sheet facies crystallized, flushing out early contaminated magma, and replacing it with fresh, less-contaminated magma.

**Ore Deposits.** Ore occurs in three environments at Kambalda:

i) *contact ore* at the base of the lowermost unit, in contact with the underlying footwall basalt;

ii) *hanging wall ore,* either at the base of the overlying units (in most cases the second or third unit up from the base of the ultramafic sequence) or, much more rarely, as zones of blebby sulfide within the basal unit;

iii)*offset ore* which has been structurally displaced from either an original contact or hangingwall position.

**Ore Control.** *Contact ores* account for 77 percent, hanging wall ores for 18 and offset ores for 5 percent of the total reserves plus past production at Kambalda (calculated from data of Gresham 1986). The contact ores are localized by basinal depressions in the ultramafic-underlying basalt contact or, more commonly, by north-northwest trending troughs. These are narrow elongate depressions with length to width ratios of about 10:1 and depths below the basalt flanks ranging from a few metres to as much as 100 m. A typical example is shown in Fig. 3.7. The boundaries of the troughs are commonly steeply dipping reverse or normal faults.

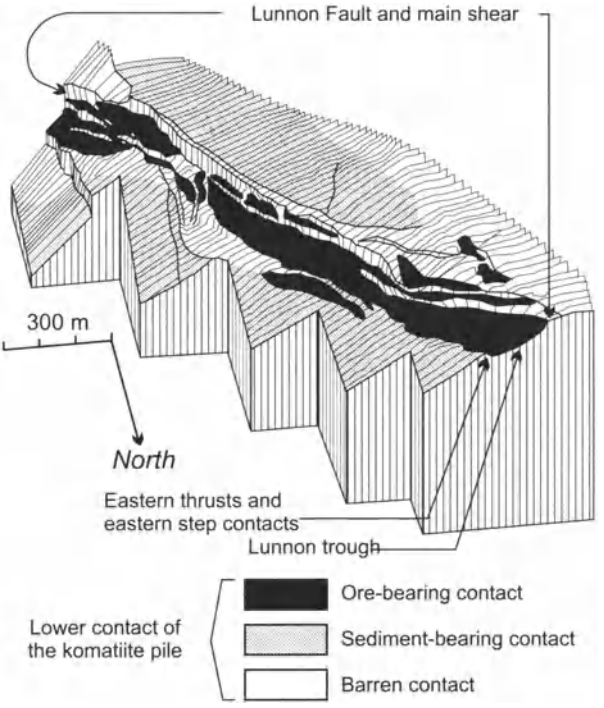


**Fig. 3.7.** An isometric view of the Lunnon ore structure (after Gresham and Loftus-Hills 1981)

Ross and Hopkins (1975) pointed out that the faults may have been active during deposition, because they appear to offset the basal contact of the lowermost flow unit more than its upper contact. On the other hand, Gresham and Loftus-Hills (1981) concluded from drilling at the northwestern end of Foster shoot that the trough structure may be underlain by an unfaulted sedimentary layer within the basalt, indicating that the deep trough here was a feature of the pre-ultramafic topography, unrelated to faulting. Lesher (1983) has shown that (i) the fabric of ultramafic rock immediately adjacent to the basalt walls of the troughs is different from material within the centres of the troughs (Figs. 3.8 and 3.9); (ii) that the rocks themselves are less magnesian than that in the centre; and (iii) that chromite has crystallized in the sulfides adjacent to basalt where the komatiite has become chilled (Fig. 3.10); all of these observations indicate that the troughs predated the extrusion of the komatiite. He has also (Fig. 3.8) documented stratiform features such as horizons of breccia and contacts between pillowed and unpillowed basalt at the base of troughs (Fig. 3.9) which have not been offset by faulting, but which should have been if such faulting was responsible for the troughs.

The *hangingwall ores* occur in the lower three flows, generally where contact ores are also developed, and grade laterally into sediments which themselves carry nickeliferous sulfides in some cases. In general they are characterized by lower grades, but by sulfides with higher nickel tenor than the more massive contact ores (Gresham 1986).

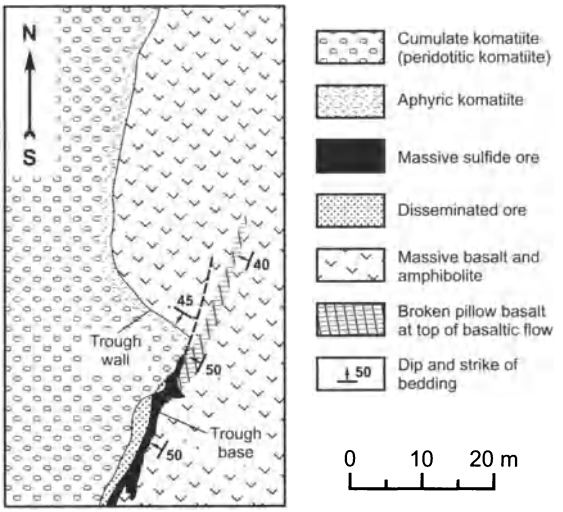


**Fig. 3.8.** Plan showing stratigraphic relationships in the footwall basalt adjacent to the ore pinch-out at Juab B 1118 W, Kambalda. From Lesher (1990). Note correlation between the ore horizon and the broken pillow flow-top breccia

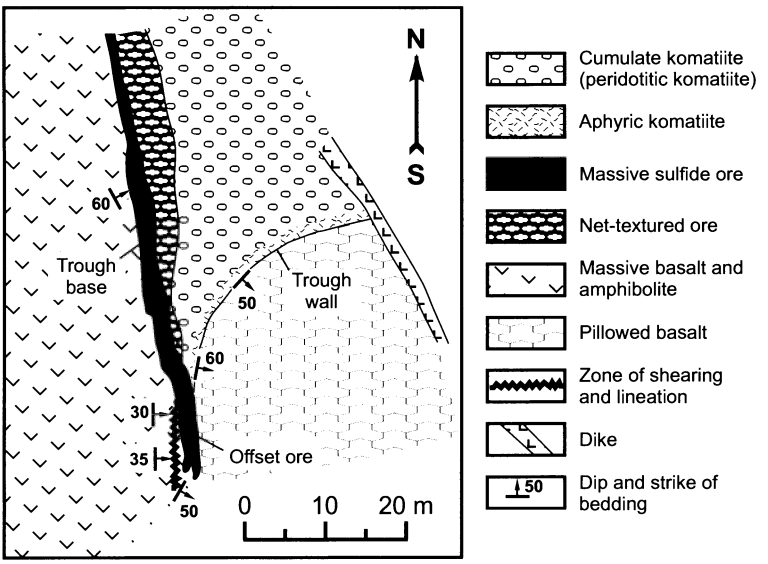


**Fig. 3.9.** Map showing stratigraphic relationships in the footwall basalt adjacent to the ore pinch-out on 4 level, Lunnon Upper Roll, Kambalda. Note that the basalt above the ore horizon is pillowed whereas that below is massive; they are not structurally equivalent. From Lesher (1990)

The *offset ores* occur along shears and comprise sulfides that have been sheared off from their original basal or interflow contact positions, so that they now lie in atypical intra-flow or intra-basalt positions. One such example is shown in Fig. 3.9.

**Ore Types.** Fig. 3.11 illustrates a typical section through the ore at the Lunnon shoot, compared with the profile at the Alexo deposit (Timmins area, Ontario). Minor, generally Cu-enriched stringers penetrate between pillows of the footwall basalts and are overlain by massive ore. This ore commonly has a banded appearance due to the presence of thin (1 cm thick) lenses (10 cm long) of pentlandite which is thought to have exsolved at low temperature from pyrrhotite and to have nucleated in response to the prevailing stress field. Bands of pyrite up to 30 cm thick may occur in this ore. Massive ore commonly shows deformation textures and swells and thins over short distances, giving the appearance of having been remobilized over short distances in response to stress.

The massive ore is overlain in sharp contact by net-textured ore (referred to locally as matrix ore) in which a network of sulfides encloses olivine grains. This ore, in turn, grades abruptly upwards into low-grade ore. Contacts between these ore types tend to be parallel to what is

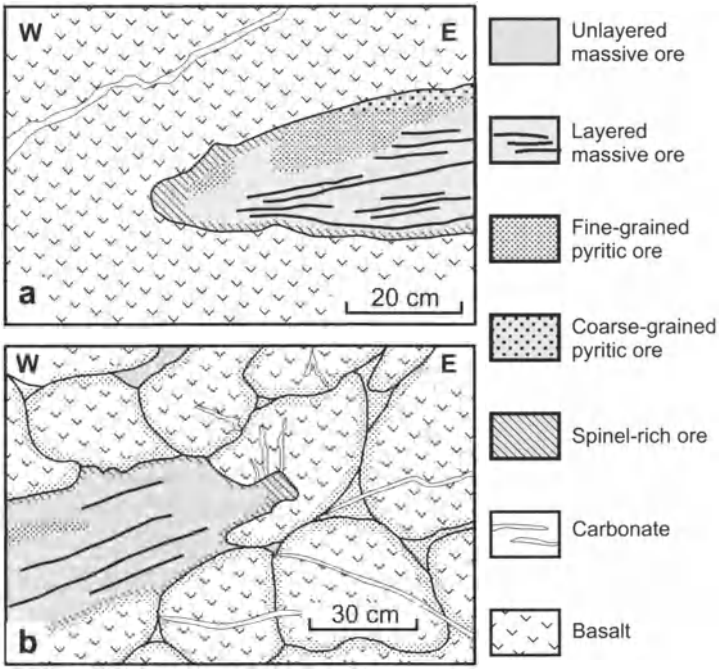


**Fig. 3.10.** Sketches from underground faces showing possible magmatic intrusive ore pinch-outs into (a) unfoliated basalt at Juan B 1118W and into (b) pillow basalt at Juan B 1218 NNW. Both pinch-outs are bordered by skeletal ferrochromite. From Lesher (1990)

interpreted as the original horizontal. Concentrations of a Cr-rich, Mg- and Al-poor, spinel occur at the base of the massive and net-textured ore, or, in some cases, within the massive ore.

Most of the hangingwall ores consist of net-textured and disseminated sulfides, although zones of massive sulfide are present in some deposits. An unusual type of ore found in the hangingwall is spinifex ore; in this ore sulfides appear to have replaced or displaced the matrix between blades of olivine in the spinifex-textured zone of the underlying flow.

As mentioned above, a clear antithetic relationship generally exists between sediments and nickel sulfide ore. This relationship is well illustrated in Fig. 3.7, and is also apparent from Marston and Kay's (1980) reconstruction of the Juan area (Fig. 3.12). However, ore and sediments are intermixed in some localities. One such area is the Jan shoot (its location is shown in Fig. 3.13) where some of the sediments are mined as ore. Here the sulfides appear to have replaced the sediments, penetrating them along fractures and along their planes of fissility. Field observation suggests that this replacement might have been due to impregnation of the cherty

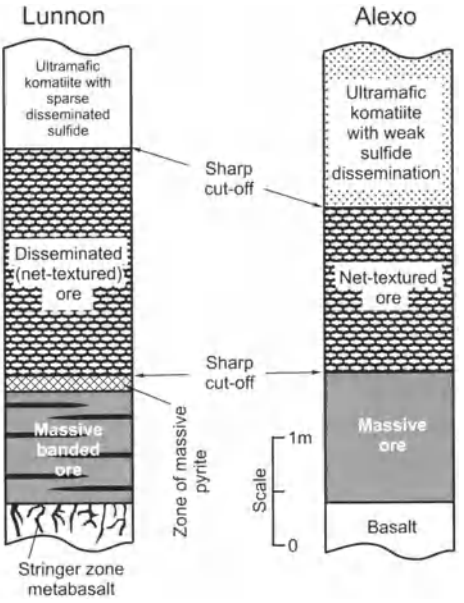


**Fig. 3.11.** Typical vertical profile through the Lunnon shoot (Kambalda area of Western Australia) and its comparison with a profile of the Alexo shoot (Ontario, Canada). From Naldrett (1973)

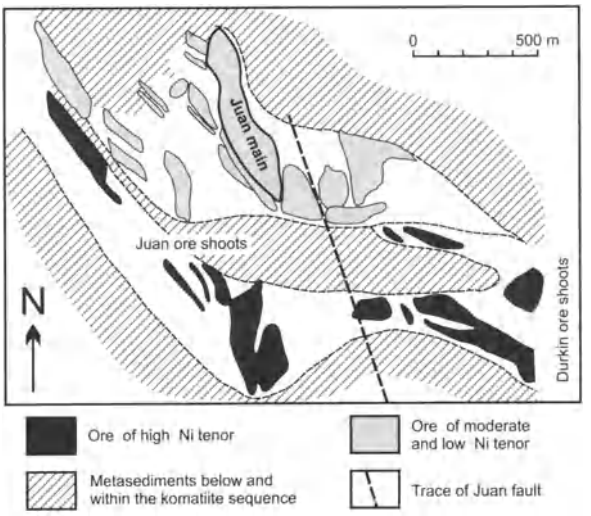


**Fig. 3.12.** Reconstruction, showing ore shoots at the base of the komatiite sequence at Juan and Durkin, the extent of sedimentary rocks within and at the contact between the komatiites and underlying basalt, and illustrating how the shoots define different lava streams that carried sulfides of different Ni tenor (from Marston and Kay 1980)

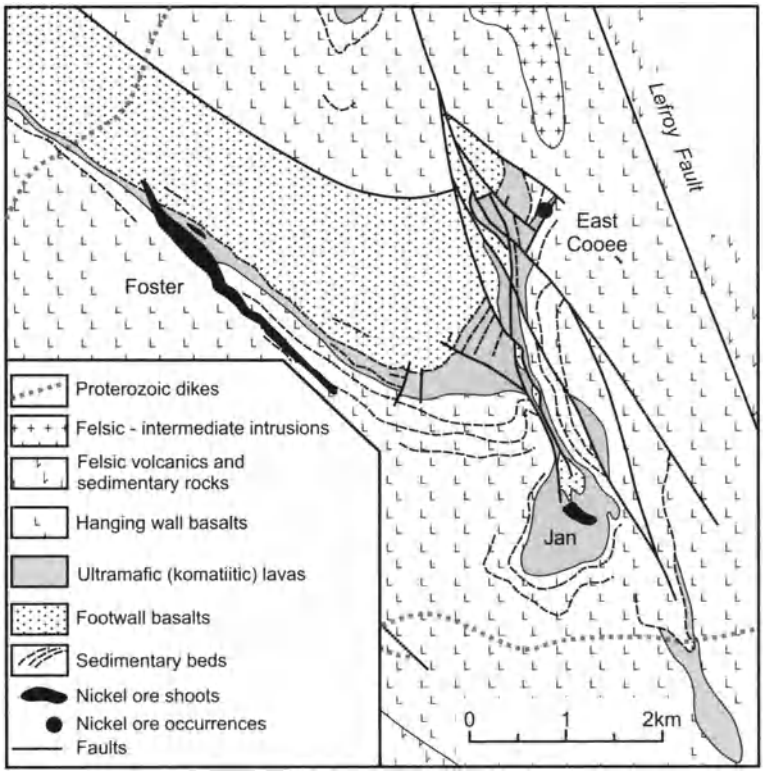


**Fig. 3.13.** Geology of the southern part of Kambalda Camp in the vicinity of Jan Shoot (from Groves and Lesher 1982)

sediments by sulfide magma-wetting (it is known from experiments that sulfide liquids have a great wetting ability when they come into contact with silica glass); however, the extremely high Pd/Ir ratios of the sediment-hosted ore in comparison with normal massive ore indicates that the process is more complex than simple impregnation by the original ore magma. Paterson et al. (1984) ascribe the Ni, Pd and other economic elements in the sulfides of the sediments to diffusion and hydrothermal remobilization out of the magmatic ore during metamorphism. In the light of recent observations concerning the fractional crystallization of sulfide melts (Naldrett and Pessaran 1992; Naldrett et al. 1994; Stekhin 1994), the high Pd/Ir ratios can equally well be attributed to fractionated magma, devoid of mss cumulate crystals, penetrating the sediments.

The Windarra deposits (270 km north-northeast of Kalgoorlie) are another area where sedimentary rocks are mineralized with Ni-sulfide ore. Much massive ore is associated with pods of highly magnesian komatiite and is interpreted as having settled from this (Schmulian 1984). However,

Schmulian points out that several ore shoots are "unbrecciated equivalents of nickel-free sulfide-facies BIF (banded iron formation) with no evidence of sulfide enrichment within the ore zone." The sulfur isotope data of Seccombe et al. (1977) are consistent with a sedimentary origin for the sulfur in these zones, and the S/Se ratios demand a significant contribution of sedimentary sulfur. Schmulian (1984) proposes that the ore is due to the diffusion of Ni and Cu from adjacent ultramafic-hosted ore into nickel-poor sulfide-facies BIF.

The principle ore minerals at Kambalda are, in order of decreasing abundance, pyrrhotite, pentlandite, pyrite, oxides (magnetite and chromite), chalcopyrite, millerite and violarite. Pyrrhotite and millerite are mutually exclusive, as would be predicted from stability relations in the Fe-Ni-S system (see Chapter 2, Figure 2.15). The mineralogical variations reflect chemical variations. Chemical analyses are compiled in Table 3.3, from which it is seen that the average Ni content of the various Kambalda shoots varies from 1.9 to 4.2 wt%, Cu – from 0.12 to 0.26 wt%, Co – from 0.024 to 0.068 wt%. Ni/Cu ratios vary from 11.4 to 16.4. Pd dominates among PGE; Pd/Pt ratios are 1.2-2.2 in the majority of deposits. The (Pt+Pd)/(Ni+Cu) ratio (PGE in g/t, Ni and Cu in wt%) ranges from 0.19 to 0.27, which is similar to other known Archean komatiite deposits.

**Models of Ore Emplacement.** Three relationships between ore and komatiite are common to nearly every deposit: (i) the ore is very commonly found at the bases of the flows; (ii) there is a close spatial relationship between massive and net-textured ore, and, when they are found together (as they are in the less structurally deformed areas), the net-textured ore overlies the massive ore; and (iii) the contacts between different ore types is sharp and, where shearing is minor, can be seen to parallel the apparent original horizontal.

These simple relationships suggest strongly that the sulfides formed as an immiscible liquid and thus, that the ore had a primary magmatic origin. Naldrett (1973) suggested that the gross features of the ore could be explained by analogy with billiard balls in a cylinder of mercury and water. As illustrated in Fig. 3.14, the billiard balls are denser than the water but float on the mercury. Some of the balls are forced down by the weight of the overlying balls, to become enclosed in a continuous network of mercury. Naldrett equated the massive ore to the massive mercury, the net-textured ore to the net-textured mercury, and the overlying low grade and barren peridotite to the billiard balls in the water.

The narrow, elongate nature of the ore-bearing flows has been emphasized by Lesher et al. (1984), who proposed that flow in the Kambalda district was in the direction of the long axis, comparable to a

**Table 3.3.** Average chemical compositions of ores, related to komatiite magmatism

| Area; Deposit | n | S | Ni | Cu | Co | Pd | Pt | Rh | Ru | Ir | Os | Au | Ni/Cu | Pd/Pt | Ref. |
|---|---|---|---|---|---|---|---|---|---|---|---|---|---|---|---|
| **Archean komatiites** | | | | | | | | | | | | | | | |
| **Western Ausrralia, Kambalda Camp** | | | | | | | | | | | | | | | |
| Fisher | * | 4.67 | 1.89 | 0.12 | 0.033 | 246 | 204 | 38 | 109 | 27 | 61 | 694 | 16.2 | 1.21 | 3 |
| Juan | * | 10.75 | 3.82 | 0.26 | 0.066 | 513 | 488 | 87 | 282 | 66 | 150 | 155 | 15.0 | 1.05 | 3 |
| Durkin | * | 5.50 | 2.74 | 0.20 | 0.044 | 461 | 312 | 75 | 229 | 51 | 119 | 104 | 13.4 | 1.48 | 3 |
| Lunnon | * | 7.05 | 2.44 | 0.19 | 0.049 | 362 | 298 | 47 | 130 | 37 | 80 | 855 | 12.7 | 1.21 | 3 |
| Ken | * | 5.50 | 2.05 | 0.18 | 0.041 | 312 | 181 | 45 | 132 | 32 | 72 | 66 | 11.4 | 1.73 | 3 |
| Jan | * | 5.00 | 2.44 | 0.18 | 0.037 | 488 | 223 | 59 | 156 | 34 | 76 | 71 | 13.5 | 2.19 | 3 |
| Hunt | * | 10.70 | 3.01 | 0.23 | 0.068 | 364 | 374 | 57 | 221 | 52 | 95 | 1 285 | 13.1 | 0.97 | 3 |
| McMahon | * | 8.10 | 2.49 | 0.19 | 0.049 | 333 | 166 | 56 | 186 | 46 | 85 | 74 | 12.9 | 2.01 | 3 |
| Carnelia Hill | * | 7.90 | 4.17 | 0.25 | 0.024 | 699 | 325 | 97 | 306 | 91 | 167 | 68 | 16.4 | 2.15 | 3 |
| **Canada, Ontario** | | | | | | | | | | | | | | | |
| Alexo | 33 | 14.42 | 2.45 | 0.16 | 0.059 | 1 108 | 423 | 60 | 118 | 14 | 22 | 108 | 15.0 | 2.62 | 4 |
| Dundonald prospect | 20 | 1.65 | 1.56 | 0.02 | 0.041 | 243 | 227 | 34 | 108 | 23 | 25 | 60 | 65.1 | 1.07 | 8 |
| Hart prospect | 8 | 9.55 | 0.89 | 0.03 | 0.026 | 141 | 58 | 19 | 42 | 11 | 13 | 18 | 32.3 | 2.44 | 5 |
| Texmont Mine | 17 | 2.65 | 1.93 | 0.08 | 0.051 | 243 | 140 | 31 | 148 | 26 | 43 | 68 | 24.1 | 1.74 | 5 |
| Langmuir Mines #'s 1&2 | 42 | 19.50 | 6.52 | 0.26 | 0.130 | 606 | 322 | 100 | 321 | 103 | 172 | 48 | 25.1 | 1.88 | 5 |
| **Zimbabwe** | | | | | | | | | | | | | | | |
| Epoch Mine | | | | | | | | | | | | | | | |
| *Disseminated ores* | 5 | 1.48 | 1.32 | 0.07 | 0.021 | 404 | 183 | 51 | 137 | 20 | 22 | 31 | 17.9 | 2.20 | 8 |
| *Massive and rich-disseminated ores* | 14 | 22.49 | 13.15 | 0.20 | 0.170 | 786 | 357 | 926 | 3 115 | 369 | 404 | 93 | 64.8 | 2.20 | 8 |
| Shangani Mine | | | | | | | | | | | | | | | |
| *Disseminated ores* | 5 | 1.42 | 0.79 | 0.06 | 0.020 | 244 | 102 | 25 | 60 | 8 | 10 | 14 | 14.1 | 2.39 | 8 |
| *Massive ores* | 15 | 31.60 | 11.36 | 0.65 | 0.137 | 2 104 | 613 | 602 | 929 | 88 | 84 | 29 | 17.4 | 3.43 | 8 |
| Trojan Mine | | | | | | | | | | | | | | | |
| *Disseminated ores* | 18 | 1.72 | 0.78 | 0.07 | 0.020 | 128 | 77 | 18 | 55 | 11 | 12 | 8 | 11.4 | 1.66 | 8 |
| *Massive ores* | 11 | 26.10 | 7.58 | 0.75 | 0.154 | 1 593 | 621 | 252 | 769 | 105 | 113 | 128 | 10.1 | 2.57 | 8 |
| Perseverance | 18 | 18.66 | 1.44 | 0.36 | 0.064 | 545 | 289 | 97 | 51 | 12 | 7 | 34 | 4.0 | 21.88 | 8 |

Table 3.3 (cont.)

| Area; Deposit | n | S | Ni | Cu | Co | Pd | Pt | Rh | Ru | Ir | Os | Au | Ni/Cu | Pd/Pt | Ref. |
|---|---|---|---|---|---|---|---|---|---|---|---|---|---|---|---|
| **Proterozoic Komatiites** | | | | | | | | | | | | | | | |
| **Cape Smith Belt, Canada** | | | | | | | | | | | | | | | |
| ***Raglan Camp*** | | | | | | | | | | | | | | | |
| Donaldson West | 23 | 14.49 | 6.01 | 1.34 | 0.094 | 4 626 | 1 327 | 360 | 967 | 154 | 175 | 152 | 4.5 | 3.49 | 2 |
| Katinniq | 23 | 16.07 | 4.49 | 1.23 | 0.087 | 2 895 | 1 409 | 253 | 518 | 91 | 137 | 92 | 3.6 | 2.05 | 2 |
| ***Expo-Mesamax Camp*** | | | | | | | | | | | | | | | |
| Expo | | | 0.6 | 0.8 | | | | | | | | | 0.75 | | 9 |
| Mesamax | | | 2.1 | 2.7 | | 4 200 | 1000 | | | | | 300 | 0.77 | 4.20 | 9 |
| **Thompson Nickel Belt, Canada** | | | | | | | | | | | | | | | |
| Pipe-2 | 25 | 32.20 | 3.32 | 0.13 | 0.151 | 99 | 44 | 28 | 180 | 46 | 88 | 49 | 24.7 | 2.26 | 1 |
| Bucko | 23 | 2.01 | 1.51 | 0.20 | | 407 | 138 | 29 | 75 | 25 | 48 | 16 | 7.6 | 2.94 | 7 |
| Thompson | 28 | 27.45 | 6.34 | 0.29 | 0.094 | 1 357 | 253 | 116 | 182 | 82 | 105 | 108 | 21.6 | 5.35 | 6 |

*n* number of samples. Contents of S, Ni, Cu, Co in wt%; Pd, Pt, Rh, Ru, Os, Ir, Au in mg/t (ppb). References: 1 – Hoffman et al. (1979); 2 – Naldrett and Duke (1980); 3 – These data are the original data that Cowden et al. (1986) presented recalculated to 100% sulfide. The PGE analyses were performed by the University of Toronto PGE laboratory on samples that were mine composites. The composites were the result of the collection of a grab sample from each car of ore leaving the mine during 2 six month periods over the years 1980, 1981, 1982; 4 – Barnes and Naldrett (1986); 5 – Barnes and Naldrett (1987); 6 – Bleeker (1990); 7 – Good and Naldrett (1993); 8 – Unpublished materials by author; 9 – Mungall and Keast (2003)

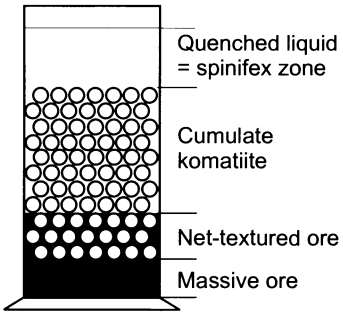


**Fig. 3.14.** The "billiard ball" model (modified from Naldrett, 1973)

volcano such as Mauna Loa. They argued that the presence of horizons of crescumulate olivine within the thick, MgO-rich, ore-bearing flows indicates that these flows are not the result of the accumulation of phenocrysts, but that crystallization occurred in situ from an overlying, moving body of magma.

Huppert and Sparks (1985) showed that the flow of komatiite is likely to have been turbulent. Given this, the transfer of heat to the underlying basalt would have been approximately an order of magnitude more rapid than would have been the case if the flow were laminar. Heat transfer at this speed would inevitably cause severe thermal erosion of the basalt, at a rate varying from several metres per day for a 1600°C flow within a few km of its source, to several 10's of cm per day some 10's of km away. They proposed that the troughs are almost entirely due to thermal erosion beneath flows travelling many 10's of kilometers parallel to the pitch line of the regional slope. Sparks et al. also suggested that assimilation and incorporation of sulfide from the underlying sediments may have contributed to the sulfide content of the ores.

Frost and Groves (1989) have pointed out that ocellie of mafic-poor, $SiO_2$, $Al_2O_3$, $Na_2O$ and $K_2O$-rich material occur in komatiites near the top of spinifex-capped flows, vertically above the edges of troughs. They have argued that these are due to the melting of interflow sediments. The Pb isotope studies of McNaughton et al. (1988) support this interpretation of the ocelli. Lesher and Groves (1986) argued in favour of a sedimentary source for a large proportion of the sulfur on the grounds that (1) the komatiites would have been unlikely to have reached the surface saturated in sulfide, and (2) variations in ore tenor between different deposits and within individual deposits are best explained by variations in the mass ratio of sulfide to magma with which they equilibrated (Campbell and Naldrett, 1982), which are, in turn, best explained by varying degrees of sulfide assimilation.

The assimilation of significant amounts of country rocks, both during ascent through underlying crust and while flowing across the surface, is supported by the data of Arndt and Jenner (1986). They found that the REE and Sm-Nd characteristics of the komatiitic flows could best be explained if komatiitic magma had assimilated up to about 8 wt% of underlying sediment. On the other hand, basalts belonging to the komatiitic suite, and immediately overlying the komatiites, appeared to have been contaminated primarily by granites of the upper crust.

It would seem that the origin of the Kambalda troughs is very probably the consequence of thermal erosion. If so, there is likely to have been some contribution of sedimentary sulfide to that in the ore zones. What is less clear is whether this was a major contribution, which, in essence, accounts for the presence of the ores, or whether they would have accumulated in economic amounts without this contribution.

The points discussed above have been incorporated, together with other information given by Lesher et al. (1984) and ideas of the present author, into the following model, which is designed in particular to explain the differences between the ore-bearing and ore-free environments described by Gresham and Loftus-Hills (1981). The model is illustrated in Fig. 3.15. The seven cartoons in this figure show a cross-section through a lava river which was channelled along a trough in the basalt surface across which it was flowing and into which it has eroded to some extent. The steep walls of the trough are consistent with experiments of Sparks and Huppert (Sparks, personal communication 1984) involving the flow of hot water across wax. In some of these experiments, the steady-state flow of water resulted in the erosion of channels with re-entrant walls, very similar in configuration to some of those observed at Kambalda. It is likely that the orientation of the troughs (so pronounced at Kambalda) reflects the regional slope.

The first eruption eroded the trough (Fig. 3.15, cartoon 1) and, during brief periods of very rapid flow overflowed the banks to a limited extent, to form levees composed of congealed (in part pahoehoe-like) lava. Sulfides settled rapidly and became trapped by irregularities in the base of the flowing river. As eruption ceased and the magma level fell (cartoon 2), levees of congealed lava were left on each bank and a zone of congealed peridotite formed above the now largely solid basal accumulation of sulfide. The peridotite was itself overlain by a zone of fluid peridotite beneath a crust.

Resurgence of the eruption (cartoon 3) caused renewed flow along the river, guided by the pre-existing levees; continued thermal erosion of the

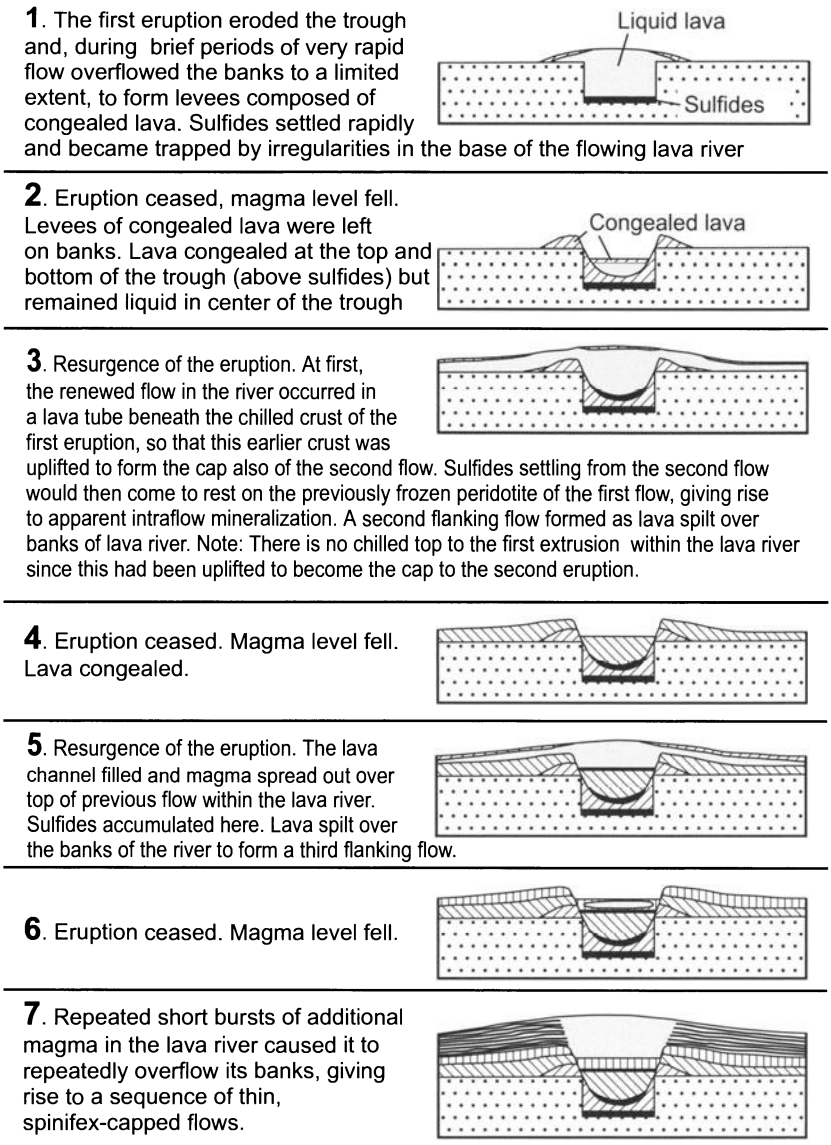


**Fig. 3.15.** Model for the development of a typical mineralized sequence of komatiites of the Kambalda area

underlying basalt was prevented by the refractory peridotite at the base of the river. Renewed flooding resulted in additions to the levees; in places, breaching of the banks produced extensive flanking flows which moved away at an angle to the main flow direction of the river to form lava plains (see Fig. 3.1). Ponding of these flows between levees of adjacent lava riv-

ers and dams composed of their own congealed material, allowed them to crystallize under static conditions. Turner et al. (1986) argued that the turbulent flow of komatiitic lava will prevent all but a thin crust forming to a flow while it is in motion, and that well-developed spinifex texture will only form once it has become stationary. It is suggested that the ponding of the flows flanking the main conduits provided the necessary static environment for spinifex development, in contrast to the active environment of the conduit, leading to the best development of spinifex texture on the flanks rather than within the conduit komatiite itself.

It is possible, in some cases, that the renewed flow in the river occurred in a lava tube beneath the chilled crust of the first eruption (see Fig. 3.15-2), so that this earlier crust was uplifted to form the cap also of the second flow. Sulfides settling from the second flow would then come to rest on the previously frozen peridotite of the first flow, giving rise to apparent intra-flow mineralization as is seen in cartoon 3. A second cessation in eruption, accompanied by a second fall in the magma level in the river may have been followed by a longer interval of quiescence, giving more time for cooling so that the whole of the second flow solidified (cartoon 4).

Further magmatic activity was also guided by the river and its levees, this time flowing above the top of the preceding flow. Sulfides settling from this third eruption gave rise to an ore zone located clearly at an inter-flow contact (cartoon 5). The eruption, while broadly following the river, also overflowed its banks to give rise to further lateral flows.

It is likely that away from the hotter zone overlying the lava river itself, chemical and clastic sedimentation could occur, giving rise to the intra-flow sediments that characterize the non-ore bearing environments. Turbulent motion in the sea overlying the hotter environment of the lava rivers, coupled with thermal erosion by the lavas themselves, probably accounts for the sparsity of sediments in this environment.

A cessation of activity and an accompanying drop in the magma level in the river (cartoon 6) was followed by a new phase of activity. In this case, a series of lava floods along the river resulted in repeated overflowing of the banks and gave rise to the thin picritic flows which characterize the upper parts of the non-ore environment at Kambalda (cartoon 7).

### *Group 2: large, low-grade deposits*

Deposits of this type are known principally from northern part of the Wiluna-Norseman greenstone belt (Fig. 3.16). They are not known elsewhere, although the Epoch deposit in Zimbabwe, and the Proterozoic Mystery Lake and Moak Lake deposits (as yet not mined) of the Thompson belt have some similarities with this style of deposit.

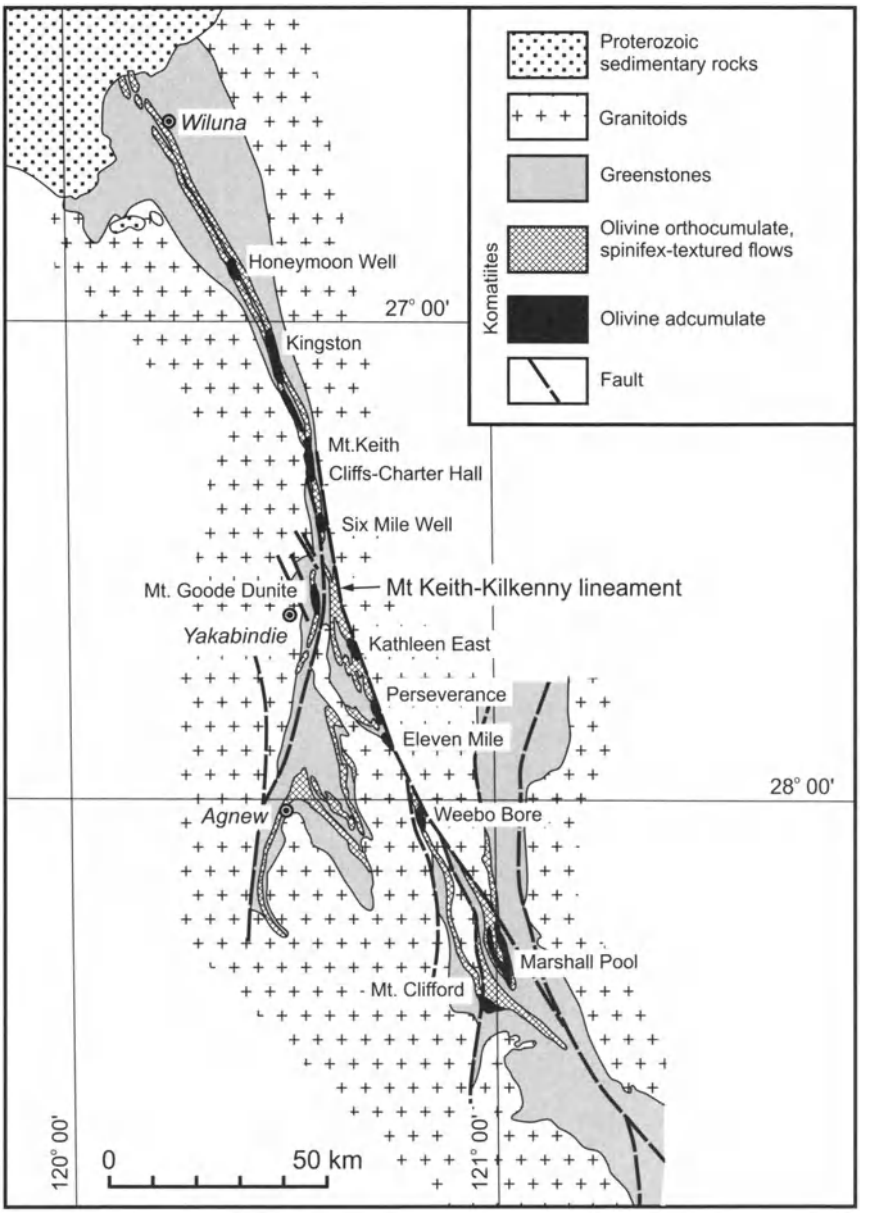


**Fig. 3.16.** Schematic geological map of northern part of the Wiluna-Norseman greenstone belt showing the location of olivine adcumulate bodies with disseminated sulfide mineralization (from Hill et al. 1989)

Two greenstone sequences, an upper and lower sequence, have been recognised at the northern end of the Wiluna-Norseman belt (Naldrett and Turner 1977), The upper sequence is composed of a lower basaltic unit overlain by a thin chert, a thick series of volcaniclastic and minor pelitic sediments, black shales, and then by komatiitic volcanic rocks. The komatiite sequence consists of spinifex textured flows (***MunF***) and large (>5 km x 1 km), concordant, lenticular bodies of olivine adcumulate (***ASF***). These are shown in Fig. 3.16 and include Honeymoon Well, Kingston, Mt Keith, Six Mile Well, Kathleen East, Perseverance, Weebo, and others. Many host huge tonnages of low-grade disseminated Ni sulfides.

The Six-Mile deposit at Yakabindie, Western Australia, is a typical example of the low-grade mineralization. The deposit is one of a series of lenses emplaced within sediments and felsic volcanics which underlie a sequence of tholeiitic and komatiitic lavas and shallow gabbroic intrusions. Hill et al. (1989) have shown that the lens consists of a series of layered olivine and olivine-sulfide adcumulates, overlain by olivine adcumulate, olivine-sulfide adcumulate, olivine and olivine sulfide orthocumulate and capped by cyclic layers of olivine mesocumulate to orthocumulate (Fig. 3.17). The bulk of the nickel sulfide mineralization occurs within the olivine-sulfide adcumulate (layer 3A in Figure 3.17). The olivine meso- to adcumulate cyclic units lie at the stratigraphic top of the lens and exhibit cyclical variations in MgO, CaO and $Al_2O_3$ which Naldrett and Turner (1977) ascribed to fractional crystallization. Hill et al. (1990) attribute this to fluctuations in eruption rate leading to stagnation, ponding and fractionation in the flow channels, followed by more rapid flow.

Hill et al. (1989) pointed out that the alternation of adcumulate with orthocumulate layers ruled out compaction as a cause of adcumulate texture. They concluded that the olivine adcumulates could only have developed in a komatiite in contact with flowing magma which would sweep away fractionated liquid from top of the growing pile of cumulates, allowing fresh magma to be in constant contact with the growing crystals. They noted that flow of komatiitic liquid is likely to be turbulent (see above), so that the magma in contact with the cumulates would be at high temperature, accounting for the adcumulate nature of the growth. They noted (Fig. 3.18) that bodies with adcumulate texture tend to be lens-like when they overlie felsic volcanic rocks, and to be sheet-like when they overlie mafic volcanics. They ascribed this to thermal erosion causing a greater degree of down-cutting into a felsic than mafic footwall, resulting in the lava flow being more "channelised" in the former than in the latter situation. It will be recalled that this has been documented at Perseverance, where more than 100m of felsic material was eroded before the erosion was halted by a

komatiite flow. Fig. 3.19 summarizes their model and illustrates the progressive development of a large lava river flowing across a substrate of largely felsic volcanic rocks.

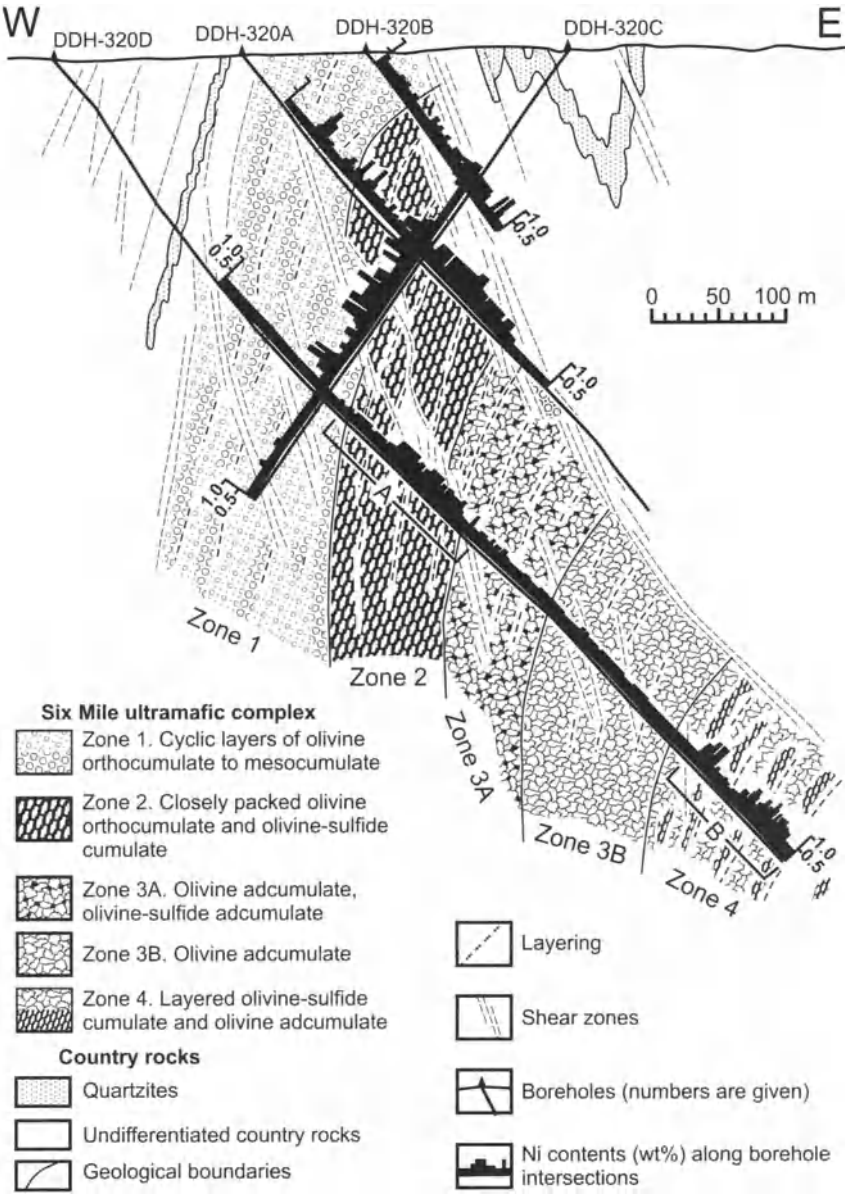


**Fig. 3.17.** Geological cross-section on line 320 N, Six Mile Well area. Intervals "A" and "B" show the upper and lower zones of mineralization (from Hill et al. 1989)

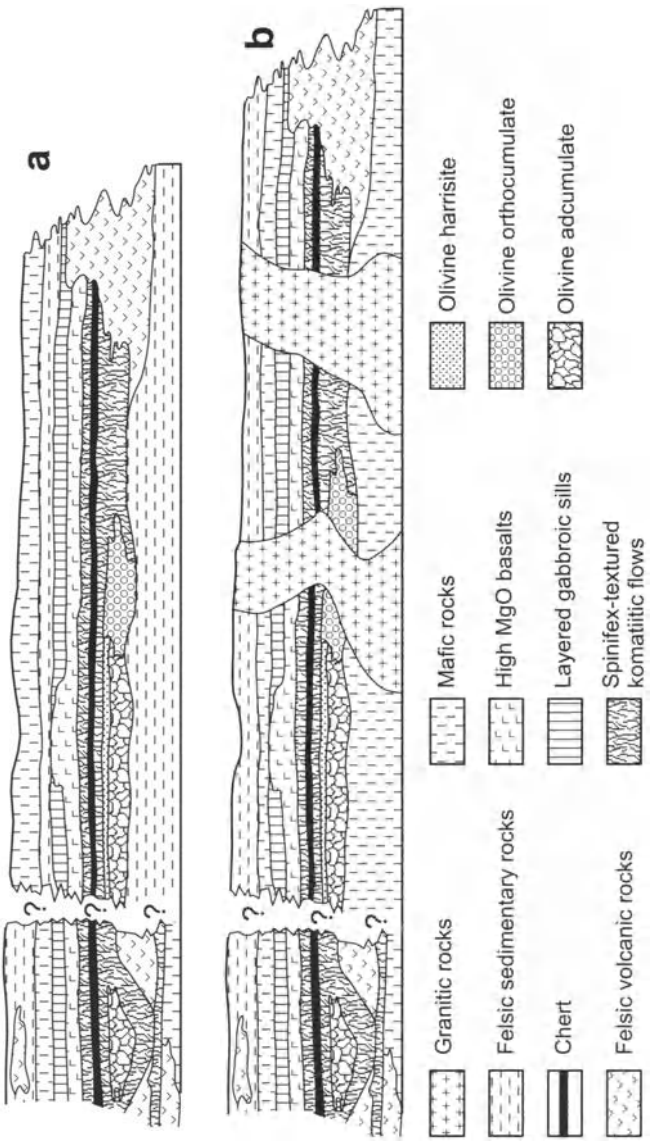


**Fig. 3.18.** Schematic cross section of an Archean greenstone sequence: a – before deformation and granitoidal magmatism; b – after emplacement of large granitoidal intrusions. After Hill et al. (1989). Harrisite: Official definition = olivine plagioclase rock (70% olivine, 30% plagioclase) consiting of branching, elongate olivine crystals in a matrix of plagioclase (type location, Rhum, Scotland). In this case, the branching olivine crystals are contained within a matrix of skeletal pyroxene that is itself contained within a matrix of serpentine, chlorite and other alteration products

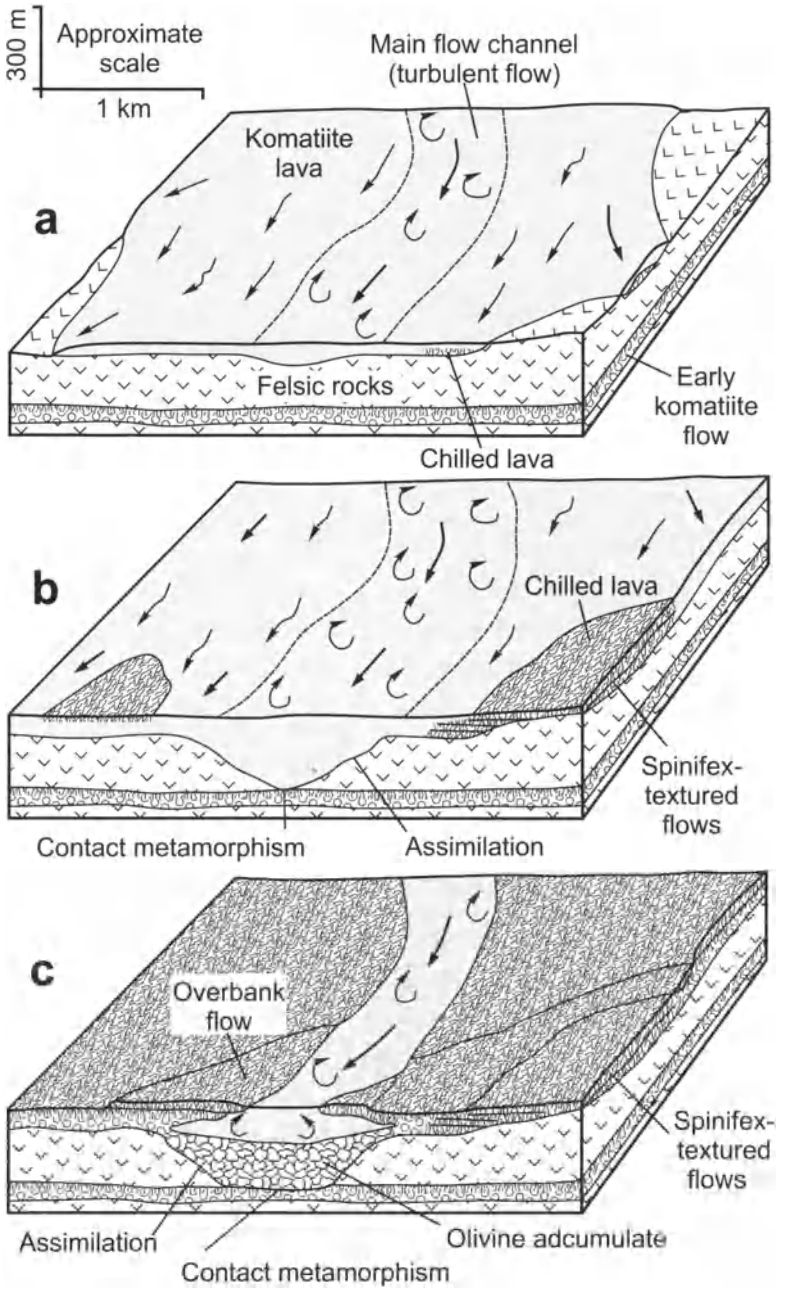


**Fig. 3.19.** Model for developing a body of adcumulate dunite and associated rocks accompanying the formation of a large thermal erosion channel (after Hill et al. 1989)

### *The Perseverance (formerly Agnew) deposit*

This deposit also occurs in the Wiluna-Agnew greenstone belt (see Fig. 3.16), which differs from the environment of Kambalda in having a much higher proportion of felsic volcanic rocks and their sedimentary derivatives. As described above, the areas within the belt that are characterized by mafic and ultramafic volcanism contain a high proportion of lenses of adcumulate dunite, some of which contain the Group 2 low-grade disseminated sulfide deposits that are described above. Originally the Perseverance deposit was regarded as a special case of this of group (Billington 1984). More recently, evidence has accumulated that it belongs with those of Group 1 (Barnes et al. 1988a,b; Hill et al. 1989), although its large size ($52x10^6$ tons – see Table 1.1) and lower grade (1.90 wt% Ni, 0.1 wt% Cu) make it an exception within this group also, which is the reason that it is described separately.

The ore of the deposit (Figs. 3.20 and 3.21) occurs within an ultramafic flow which is in contact with and has been deformed by a large mass of adcumulate dunite similar to those found elsewhere in the belt. Disseminated sulfides also occur within the dunite. Barnes et al. (1988a) showed that the dunite cuts down through several hundred meters of felsic volcanics to bottom out at the horizon of the mineralized flow. They pointed to metamorphic temperatures of in excess of 1000°C which were produced in a komatiite flow beneath another dunitic mass 50 km to the north. In the light of these extremely high temperatures beneath a body of this type, they suggested (see discussion below on thermal erosion by komatiites) that the Perseverance body represents a very large lava river which has thermally eroded its base, and that this thermal erosion was arrested by the higher melting temperature of the underlying komatiitic flow.

## 3.2 Early Proterozoic Komatiite-Related Deposits

Two areas are known which contain major economic Ni-Cu-PGE mineralization related to Proterozoic komatiites. Both occur in Canada within a structure that has been referred to as the "Circum-Superior Belt" (Barragar and Scoates 1981) (see Fig. 3.22). The areas are the Cape Smith tectonic belt, and the Thompson Nickel Belt. Both are described below. Despite the similarities in their gross tectonic settings, major differences exist between the two areas. Mineralization is associated with extrusive komatiitic rocks at the Raglan camp within the Cape Smith belt and with komatiitic

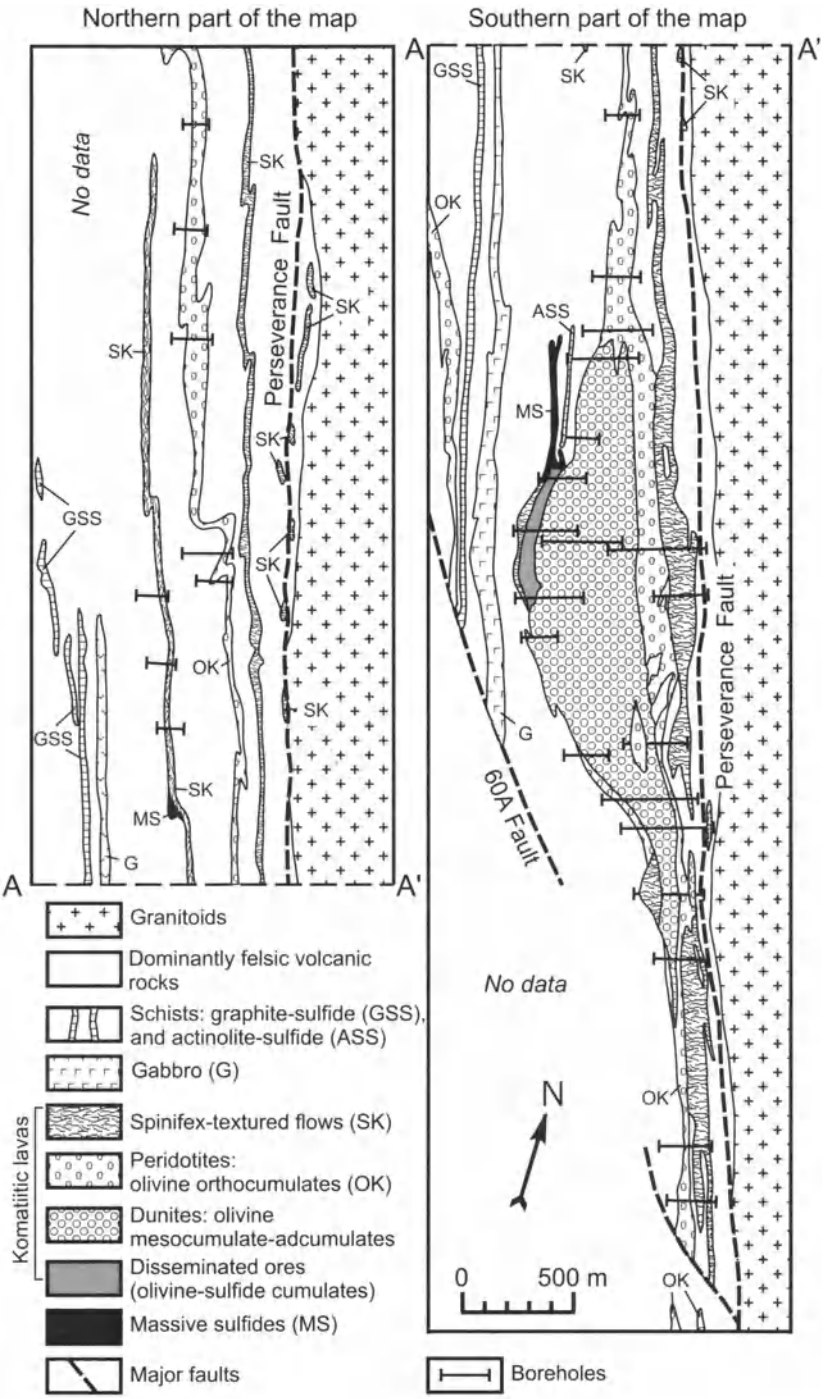
Northern part of the map
Southern part of the map
A
A'
No data
Perseverance Fault
SK
GSS
OK
MS
G
ASS
60A Fault
N
0
500 m
Granitoids
Dominantly felsic volcanic rocks
Schists: graphite-sulfide (GSS), and actinolite-sulfide (ASS)
Gabbro (G)
Komatiitic lavas
Spinifex-textured flows (SK)
Peridotites: olivine orthocumulates (OK)
Dunites: olivine mesocumulate-adcumulates
Disseminated ores (olivine-sulfide cumulates)
Massive sulfides (MS)
Major faults
Boreholes

**Fig. 3.20.** Geological map of the Perseverance mine area showing the olivine adcumulate lens and its spatial relationship to other rocks. The plunge of the body is subvertical and the map approximates a true cross-section through the stratigraphy of the sequence between the 60A and Perseverance faults. (After Hill et al. 1989)

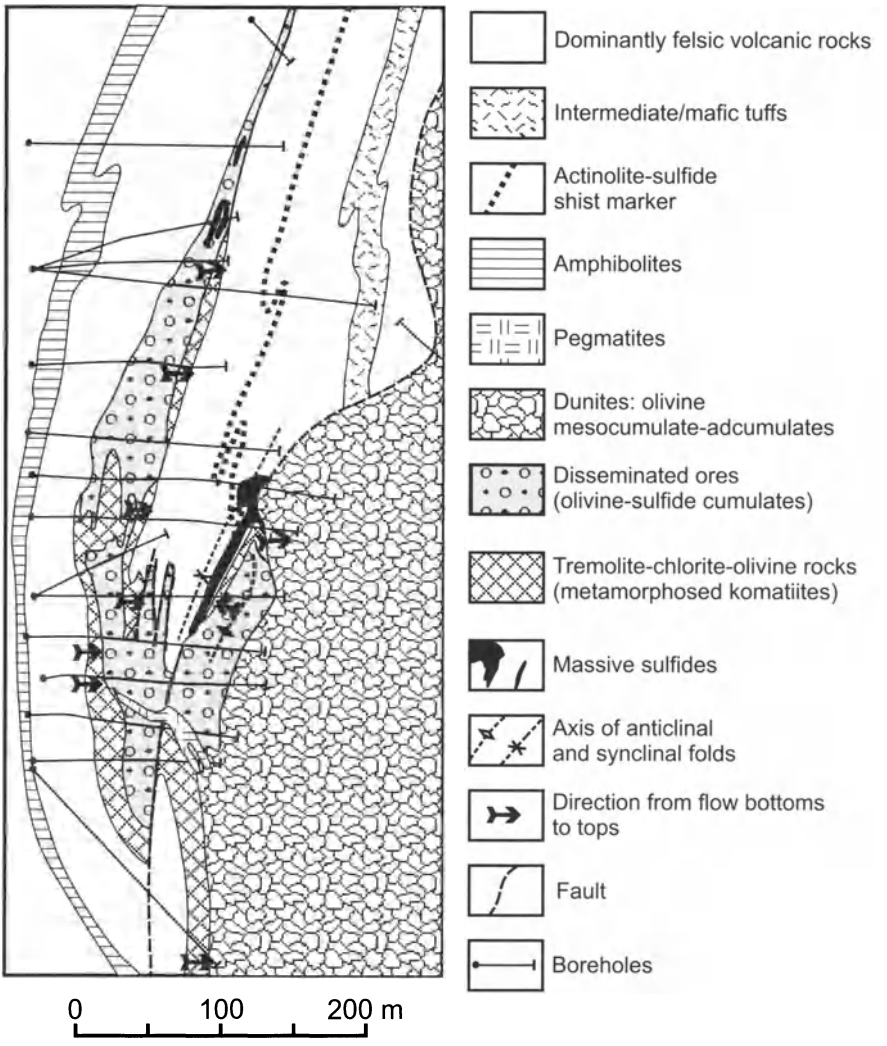


**Fig. 3.21.** Plan of the Perseverance deposit at level 760 m (after Goles et al. 1987)

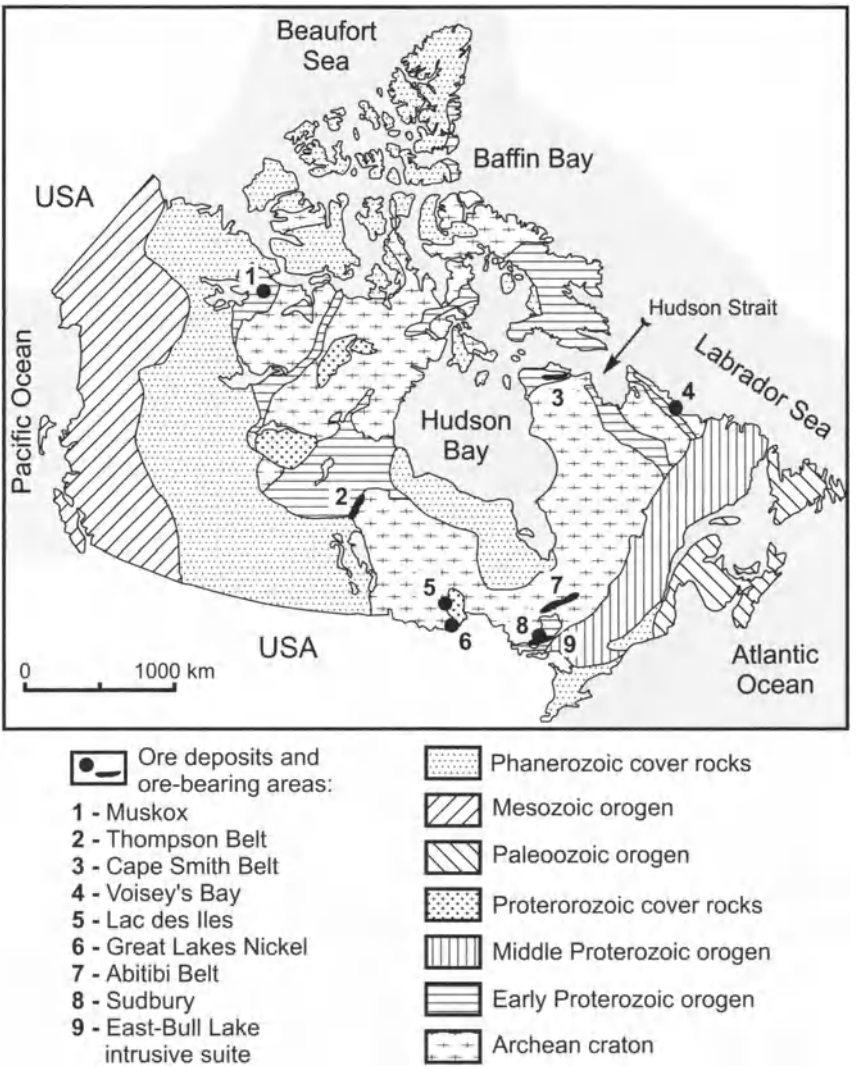


**Fig. 3.22.** Tectonic map of Canada showing the locations of the most important Ni-Cu and PGE deposits and mining camps

intrusions at Thompson. Both areas have suffered deformation but this largely comprises thrusting in the Cape Smith belt, while the Thompson belt has undergone major compression with the development of tight isoclinal folding and is much more complex tectonically. Both of these areas are described here as examples of Proterozoic komatiite-related mineralization.

Exploration is currently underway (2002) at the Kingash camp in Russia. This camp is part of the Proterozoic Kingash greenstone belt. It lies NW of the Eastern Sayan fold belt, which defines the southwestern limit of the Siberian platform. The ore-bearing sequence at Kingash consists mainly of mafic-ultramafic metavolcanic rocks after basalts, picrobasalts, komatiites and their tuffs. The zircon U-Pb isochron age of the rocks is 2.0–2.2 Ga. The Kingash Cu-Ni deposit and several other occurrences have been discovered in the area. The ores are disseminated, containing 5-50 % sulfides; the ore-bodies vary from 1 to 60 m in thickness, and from several tens of m to 1 km in length. Grades vary from 0.3–1.4 wt% Ni, 0.1–0.7 wt% of Cu, and 0.1–3.0 g/t of PGE+Au (Kornev and Ekhanin 1997, and reports referenced in their publication).

### 3.2.1 Deposits of the Cape Smith belt, Quebec, Canada

Sulfide-bearing outcrops were first noted in coastal exposures of a greenstone belt by A.P. Low of the Geological Survey of Canada in 1899. In 1931 these sulfides were traced inland along the belt which was found to extend 375 km across the northern tip of the Ungava peninsula from Wakeham Bay in the east to Cape Smith in the west. Subsequent exploration, including drilling, focused on the eastern end of the belt and continued through the 1950's. In 1961 Falconbridge Nickel Mines Ltd. (later to become Falconbridge Ltd.) obtained control of the permitted areas covering the Raglan mineralization and continued exploration intermittently. Production commenced in December 1997. Mineralization has also been discovered in the area occupied by (but probably not within – see below) Povungnituk rocks 15–20 km south of the Raglan belt at Mesamax, Expo Ungava, Mequillon and farther west (see Fig. 3.24). Exploration is currently very active in the southern area, details of the geological setting are still emerging, and the deposits and their relationships to the enclosing rocks are mentioned only briefly below.

#### *Regional geology*

The Raglan deposits occur within a series of ultramafic bodies, which were originally regarded as intrusive (see Barnes et al. 1982). Subsequently (see Lesher et al. 1999), these have been re-interpreted as channels that carried ultramafic magma comprising a suspension of olivine crystals in a liquid containing 18–19 wt% MgO.

The deposits lie within the early Proterozoic Cape Smith Belt. This belt extends across the Ungava Peninsula, between the Archean Superior Prov-

ince to the south and Proterozoic "suspect" terranes to the north (Fig. 3.22). The eastern half of the belt is illustrated in Fig. 3.23 with enlargement in Fig. 3.24. High-grade gneisses and plutonic rocks of the Superior

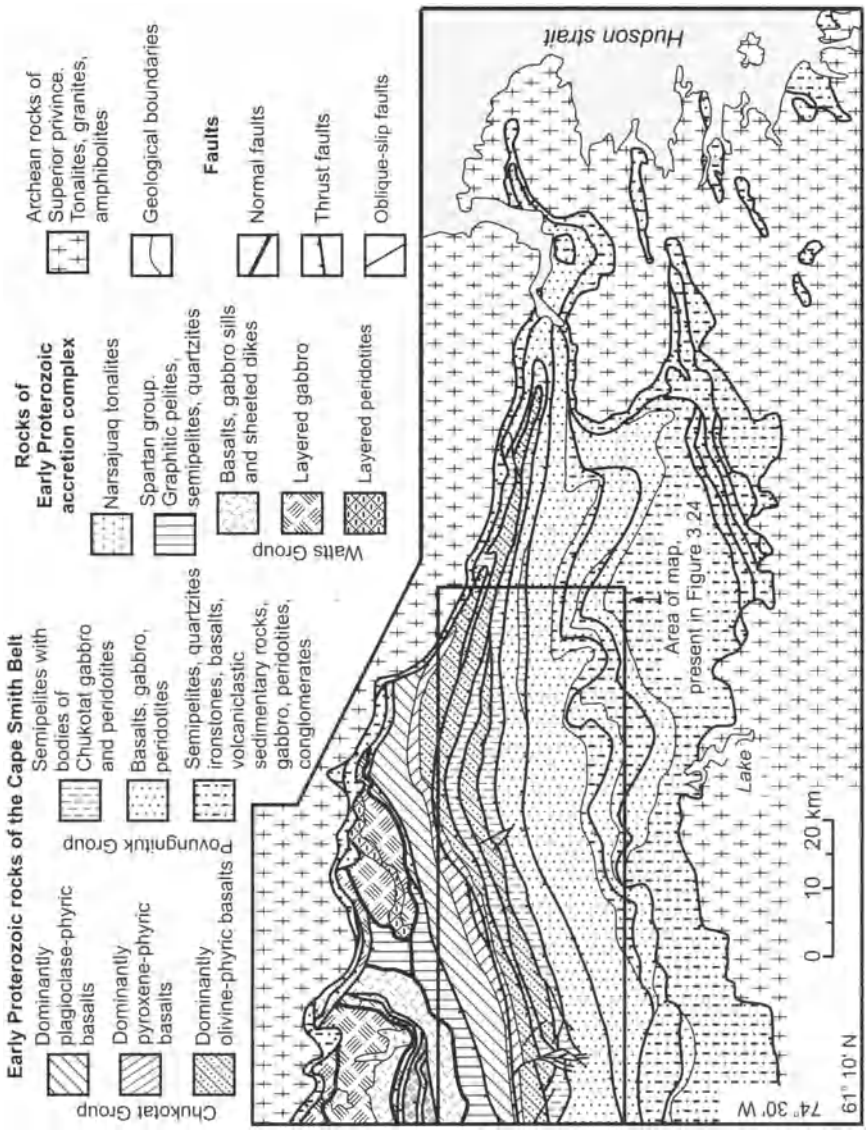


**Fig. 3.23.** Geological map of eastern part of the Cape Smith tectonic belt (after Lesher, 1999)

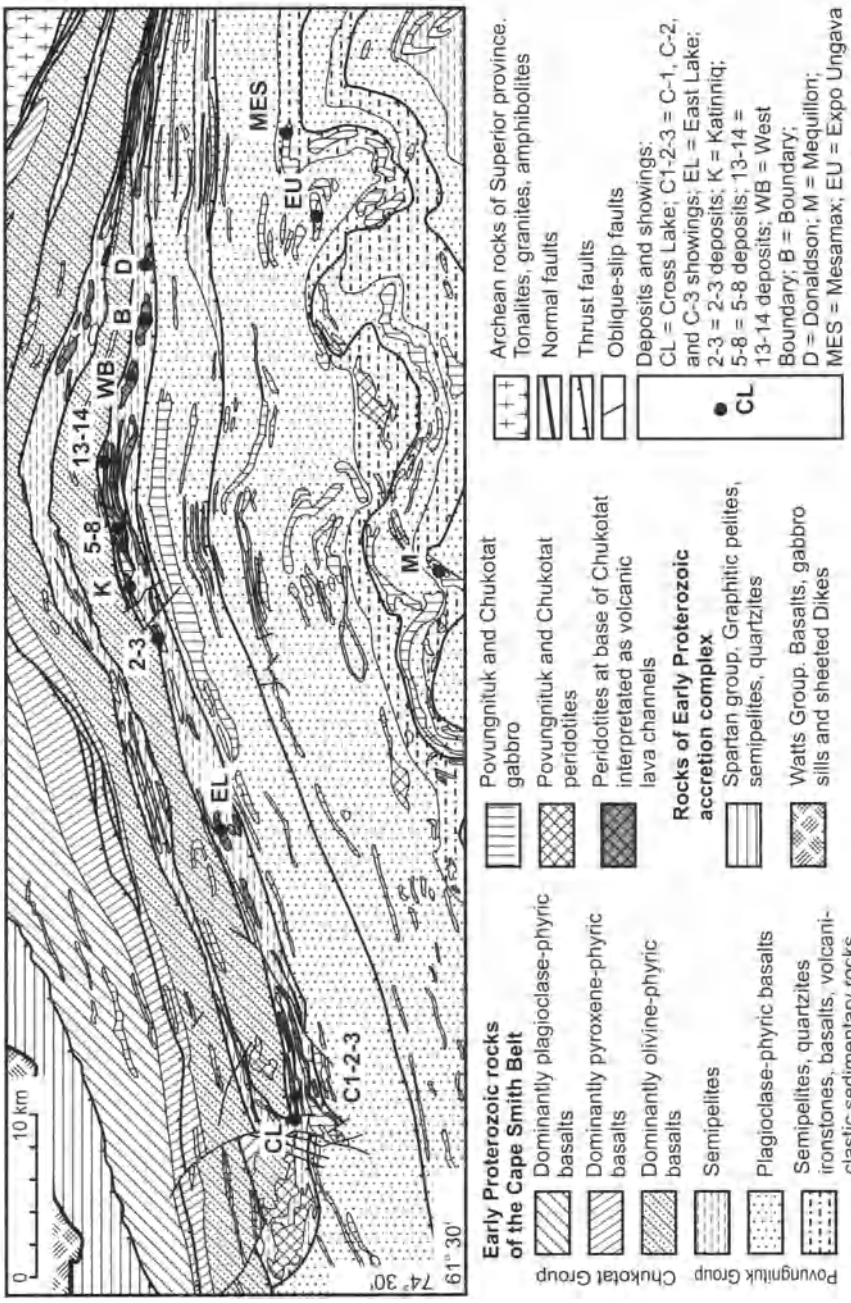


**Fig. 3.24.** Geological map of the Raglan ore camp and adjacent area (after Lesher, 1999)

Province define the south, east, and northeast boundaries of the belt, while, to the northwest, metavolcanic rocks of the Parent Group (interpreted as a volcanic island arc; Picard et al. 1990), fine-grained clastic rocks of the Spartan Group (interpreted as fore-arc basinal deposits; St-Onge and Lucas 1993), and mafic-ultramafic metavolcanic and intrusive rocks of the Watts Group (interpreted as an ophiolite complex; Scott et al. 1989) occur. Hofmann (1985) has interpreted the belt as a thin-skinned thrust belt preserved as a stack of klippen in a doubly-plunging synclinorium. St-Onge and Lucas (1993) regard it as an arc-continental collisional zone. They proposed that a continental rift started to develop prior to 1960 Ma and that continental margin sediments were deposited within it (the Lower Povungnituk). Rifting gave rise to mantle melting and basalts and associated intrusions developed at 1960 Ma (volcanic and intrusive rocks of the Upper Povungnituk). Continued rifting resulted in crustal thinning to the extent that starting at 1922 Ma, deep water sediments and the mafic-ultramafic volcanism of the Chukotat group formed in an oceanic environment. Rifting terminated as convergence from the north (St Onge et al. 1992) along a north dipping subduction zone gave rise to the Narsajuaq island arc at 1870 Ma. The Watts group, which comprises an ophiolite succession dated at 1999 Ma, was obducted to overlie the Chukotat at this time. St Onge et al. (1991) argue that the polarity of subduction changed to south dipping prior to final collision and accretion. The collision resulted in a series of south verging thrusts which characterise the Povungnituk and Chukotat groups today. Lithologies comprising different units of the Cape Smith belt are summarised in Table 3.4 (from Lesher et al. 1999). The thrusting prevents an estimate of the original thicknesses of the Povungnituk and Chukotat groups, although 7 km is thought to be the minimum thickness of the Povungnituk group (Lucas 1989)

Relatively few age determinations have been made on rocks of the eastern Cape Smith Belt. Zircon from a rhyolite in the upper part of the Povungnituk Group has been dated at 1.9586 +0.0031/-0.0027 Ga and badellyite and zircon from ferrogabbro within a sill intruding the uppermost part of the Povungnituk Group give a U-Pb age of 1.918 +0.009/-0.007 Ga. Lesher et al. (1999) noted that sills of this type are petrogenetically similar to the olivine and pyroxene-phyric basalts in the lower part of the Chukotat Group, and they surmise that they are probably of similar age, thus placing an age on the mineralized ultramafic complexes in the Raglan Formation of 1.959 to 1.918 Ga.

**Table 3.4.** Lithologies of the Cape Smith Belt (from Lesher, ed. 1999, adapted from St-Onge and Lucas 1993)

| Era | Group/Suite | Lithologies |
|---|---|---|
| Late Proterozoic | | Diabase dikes |
| Early Proterozoic | Narsajuaq | Tonalite |
| | Spartan | Semipelite, pelite, quartzite, gabbro |
| | Watts | Basalt, gabbro sills, sheeted gabbroic dikes |
| | | Pyroxenite |
| | | Layered gabbro |
| | | Layered peridotite |
| | Chukotat | Dominantly plagioclase-phyric basalt, gabbro |
| | | Dominantly pyroxene-phyric basalt, gabbro |
| | | Dominantly olivine-phyric basalt, gabbro; thick differentiated peridotite-gabbro flows, peridotite ± gabbro lava channel complexes, differentiated peridotite-gabbro sheet flows |
| | Upper Povungnituk | Semipelite, layered gabbro-peridotite sills |
| | | Basalt, volcaniclastic sedimentary rock, rhyolite; minor semipelite and quartzite, gabbro, peridotite, layered gabbro-peridotite sills |
| | Lower Povungnituk | Micaceous quartzite |
| | | Basalt, volcaniclastic sedimentary rock, rhyolite; minor quartzite, dolomite, calc-silicate rock, gabbro, peridotite, layered peridotite gabbro sills |
| | | Semipelite, pelite, micaceous quartzite, quartzite, conglomerate, ironstone, dolomite, calc-silicate rock; minor basalt and volcaniclastic rocks, gabbro, peridotite, layered peridotite-gabbro sills |
| | | Ironstone, minor quartzite and semipelite |
| | | Quartzite, ironstone, conglomerate, semipelite |
| Archean | | Tonalite, granite, amphibolite |

### Volcanic Setting

Excluding thermal erosional features, the mineralized peridotite-pyroxenite ± gabbro units in the Raglan Block conformably overlie metapelites in the upper part of the Povungnituk Group and are conformably overlain by and are petrogenetically-related to Chukotat Group basalts. As such, they are interpreted to represent the initial phase of komatiitic volcanism of the Chukotat Group.

Lesher et al. (1999) concluded that the first phase of Chukotat volcanism appears to have formed *channelized sheet flows* in areas ranging from Cross Lake in the west to the Donaldson area in the east (Fig. 3.24). Where present, mineralization appears to be restricted to the thickest and most magnesian parts of the units, which represent a *channel-flow facies*. The channel-flow facies are flanked by thinner, less magnesian zones of differentiated peridotite-gabbro, representing a *sheet-flow facies*.

Lesher et al. (1999) reported that the initial phase of high-Mg eruption appears to have been followed by a hiatus, during which graphitic, sulfidic sediments and basalts were deposited. While they are preserved in some areas, these rocks appear to have been extensively thermally eroded by a second phase of high-Mg eruption. This second phase also formed *lava channels* along much of the zone from Cross Lake to the Donalson area.

The peridotite zones in both phases of volcanism are composed of multiple, overlapping lava channels (see below) that grade laterally and upwards into komatiitic basalts and are capped by basaltic breccias.

Subsequent volcanic episodes became progressively less voluminous, grading from relatively massive peridotite-pyroxenite units through thick olivine pyroxenite-gabbro flows, thin pyroxenite-basalt flows, and thick medium-grained ("gabbroic") komatiitic basalt flows to thin massive and pillowed komatiitic basalt lava lobes.

Lesher et al. argue that the presence of fine-grained graphitic, sulfidic clastic metasedimentary rocks underlying the mineralized peridotite units, the presence of pillow basalts overlying the mineralized peridotites, and the virtual absence of vesicles in any of the volcanic rocks, indicates that the volcanic sequence was erupted into relatively deep water (greater than the sulphide compensation depth and the carbonate compensation depth), probably on a continental margin.

### Mineralization

Ni-Cu mineralization occurs in two distinct settings: 1) within the ultramafic lavas of the lower part of the Chukotat group and 2) in ultramafic rocks that are part of the basaltic/magnesian basaltic magmatism at the top of the

Povungnituk group. Thus far setting 1 has proved by far the most important and constitutes the mineralization normally referred to when the Raglan camp is referenced. Some brief comments with respect to setting 2 follow the discussion of setting 1.

In the Raglan camp per se mineralization occurs intermittently all along the belt between Cross Lake and Donaldson (Fig. 3.24) The tenor of the mineralization, and the degree to which the sulfides are concentrated varies from locality to locality, and within individual localities. Some of the more significant localities which are of economic interest include East Lake, 2-3, Katinniq, Bounday and Donaldson. The Katinniq locality is one of the best understood, appears to be representative of much of the belt, and is described here as a typical example of the style of mineralization found within the belt.

**The Katinniq deposit.** Slates belonging to the Upper Povungnituk group form the footwall to the volcanic sequence in the Katinniq area. A long gabbroic body, contiguous with gabbro in the 2-3 locality to the west and the 5-8 area to the east, overlies the slate, except in areas where the gabbro has apparently been thermally eroded by the overlying extrusive ultramafic rocks (Fig. 3.25). The ore-bearing Katinniq ultramafic complex is composed primarily of mesocumulate peridotite with lesser olivine pyroxenite, internal horizons of basalt, gabbro, pyroxenite, and metasediment; its upper and lower margins consist of olivine pyroxenite and pyroxenite. Two major internal units have been distinguished, the lower of which consists of massive mesocumulate peridotite, capped by gabbro. The upper unit consists of two sub-units. The lower sub-unit is composed of massive and columnar-jointed peridotite, capped locally by pyroxenite ± basalt ± metasediment. The upper sub-unit consists of three parts: (1) massive mesocumulate peridotite and oikocrystic olivine pyroxenite lie at the base; this is overlain (2) by massive microspinifex-textured pyroxenite and/or (3) basaltic flow-top breccia. The lower sub-unit is thicker (up to 65m) and laterally more extensive than the upper sub-unit. The sequence of volcanic rocks overlying the Katinniq Complex includes massive, pillowed, and brecciated komatiitic basalts (primarily olivine- and pyroxene-phyric) and differentiated peridotite-gabbro and pyroxenite-basalt flows.

The Katinniq ultramafic complex has been interpreted by Lesher et al. (1999) to represent a series of overlapping lava channels that mark a period of voluminous eruption of relatively primitive komatiitic basaltic lavas at high effusion rates. It grades laterally into komatiitic basalts and sedimentary breccias, which appear to represent a levee facies. The presence of hornfelsed fragments of metasediment and basalt in a slightly metamorphosed sedimentary matrix indicates that the breccias formed

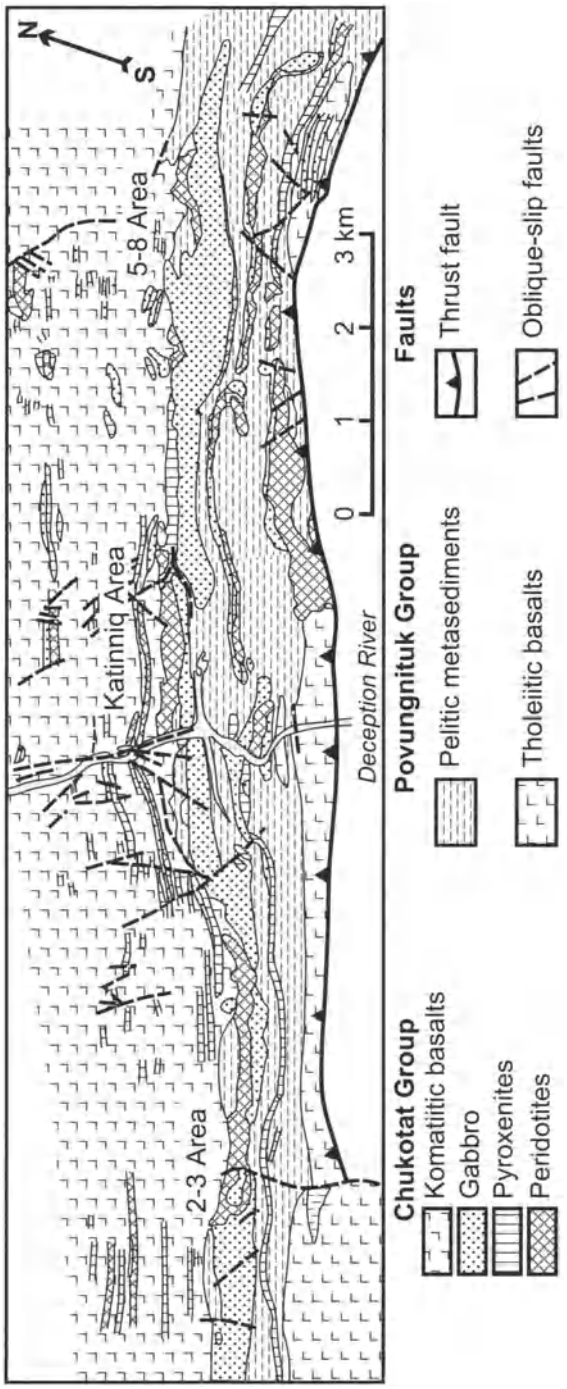


**Fig. 3.25.** Geological map of the Zone 2-3 – Katinniq – Zone 5-8 area of the Raglan Camp (after Lesher et al. 1999b)

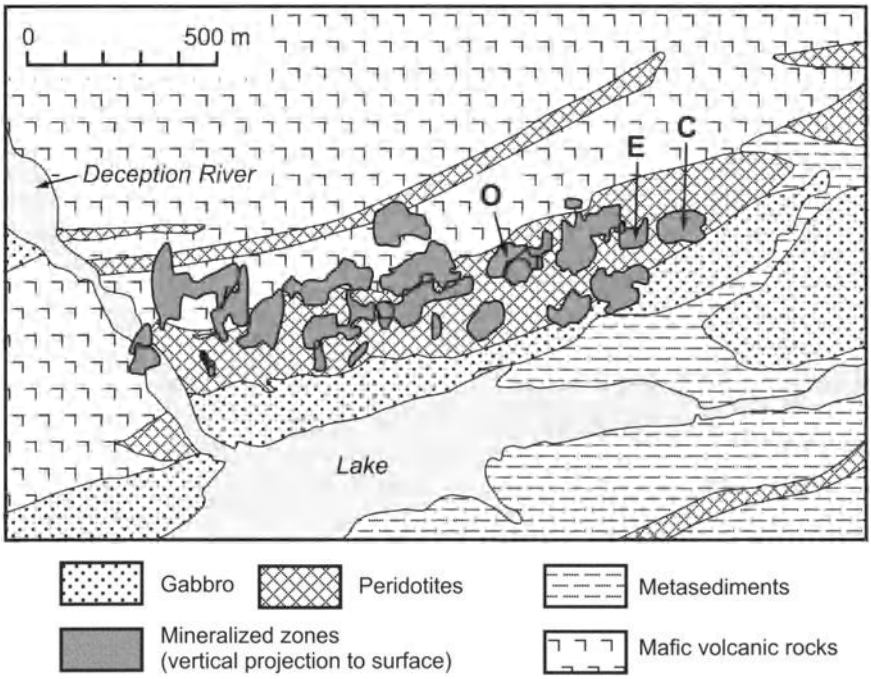


**Fig. 3.26.** Geological map of the Katinniq deposit (after Chisholm et al. 1999). C, E and O are refered to in the text

concurrently with the emplacement of the ultramafic complex; i.e. that sediments were accumulating adjacent to the channel during its development.

The Katinniq deposit has mineable reserves of 7.63 Mt grading 2.72% Ni and 0.75% Cu. The distribution of the mineralization is complex and comprises nineteen distinct ore lenses (Fig. 3.26). Mineralization is typically localized within second-order footwall embayments in the footwall rocks (Fig. 3.27) and within interpreted transgressive units in the complex (Gillies 1993). It occurs as blebby, disseminated, net-textured, and massive sulfides. The main ore minerals are pyrrhotite and pentlandite with accessory chalcopyrite, similar to other Raglan ores.

The Katinniq Gabbro forms the footwall in most areas (see Figs. 3.28a, b, c). Contacts are irregular and generally are thought to reflect the effect of thermal erosion (see Figs. 3.28a, b). The ores zones exhibit a typical magmatic segregation profile consisting of massive sulfides (8–15 % Ni) overlain by net-textured sulphides (5 to 7 % Ni) grading upwards into disseminated (1.5–4.5 % Ni) and then blebby sulfides (1 % Ni) (Figs. 3.28b, c). The ore zones are typically 15-40 m thick, have a strike length of 35–150 m, and dip NNE at 30 to 45°. Zones vary from less than 50,000 to

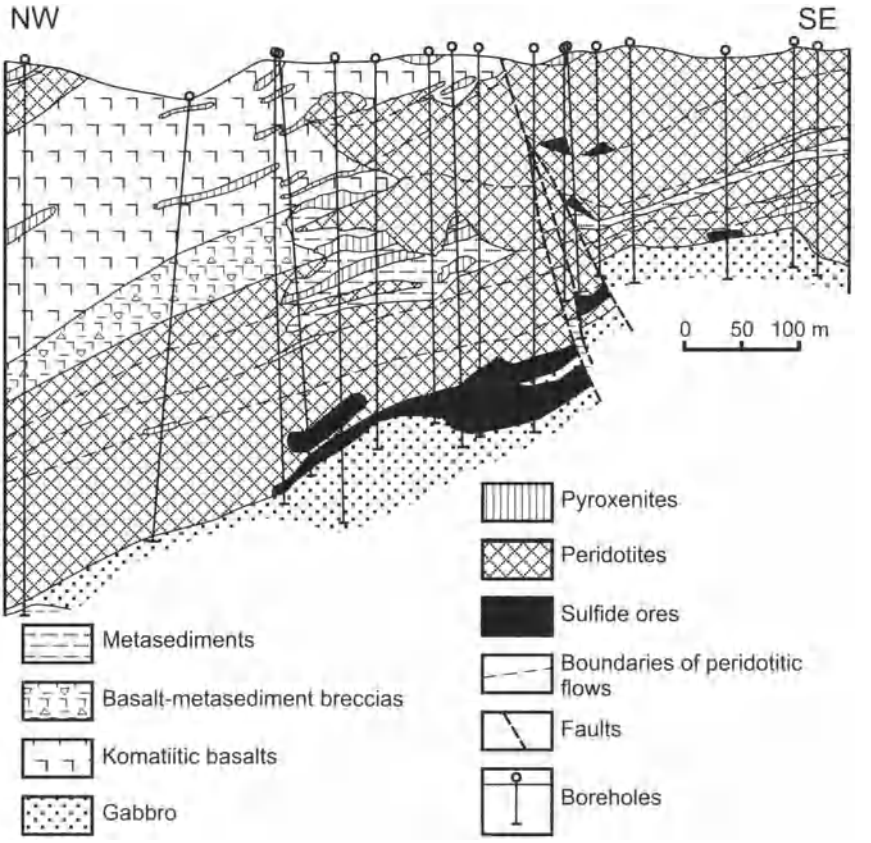


**Fig. 3.27.** NW – SE vertical section through the central part of the Katinniq ultramafic complex (after Lesher and Charland 1999)

1,200,000 Mt. To date the mineralization has been encountered at depths of 250–300 m. Of the 19 discrete ore lenses found up to 1999, 16 occur at or near the footwall contact (contact ore zones) of the basal flow unit. This is principally the lower sub-unit of the upper unit described above, although correlation of units throughout the body is not perfectly understood, and the precise association of some ore lenses remains open to interpretation.

The C, E, and O ore zones at Katinniq are stratigraphically complex (e.g., Fig. 3.28d), comprising two or more "cycles" of massive, net-textured, and disseminated mineralization. The interlayering of ore types in this manner at Katinniq has been interpreted as evidence for multiple episodes of sulfide emplacement (Gillies 1993).

Three of the 19 ore lenses (internal ore zones) occur within overlying flow units (lowest part of the upper sub-unit of the upper unit described

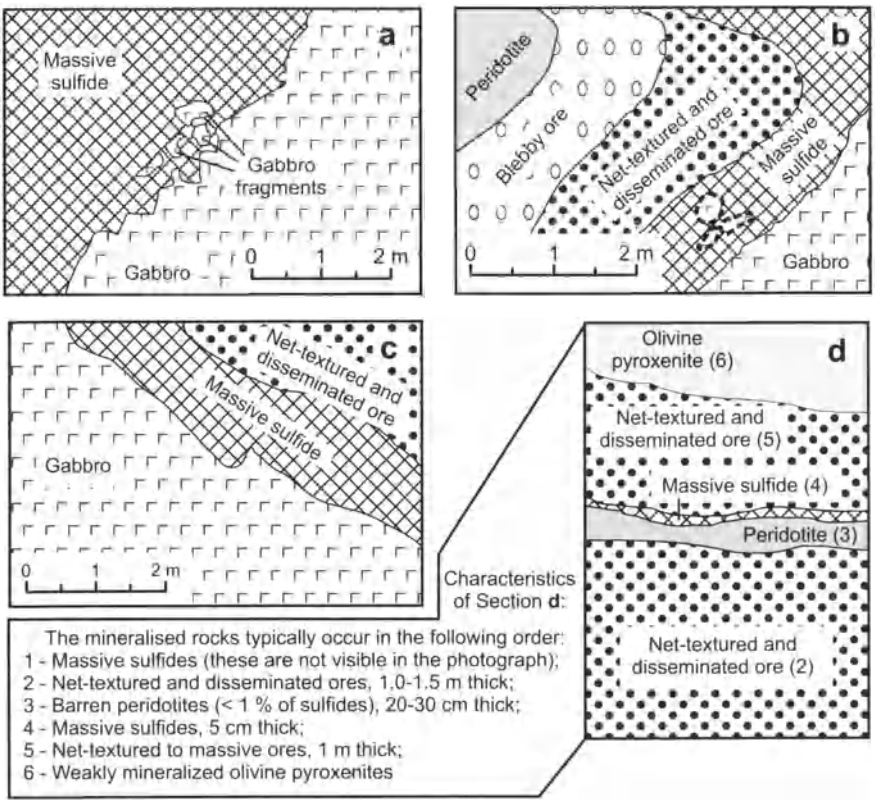


**Fig. 3.28.** Sketches made from photographs of underground faces, presented in Lesher. ed., 1999). a – Irregular (thermal-erosion) contact of massive sulfides with Katinniq gabbro (orebody O); b – Sequence of massive, net-textured to disseminated, and blebby ores. Gabbro fragments in massive ores are rimmed by chalcopyrite (ore body O); c – Lower contact of the ore body C; d – Cyclic change of ore types in the ore body C. from Lesher et al. (1999)

above) and comprise strata-bound lenses of massive (less abundant than in the contact ores), net-textured, and disseminated mineralization along internal stratigraphic horizons (see Fig.3.28). In some of these cases disseminated and massive sulfides occur on interpreted flow contacts and overlie net-textured sulfides, which appear to have percolated down and filled the spaces between olivine grains in the underlying flow (Gillies 1993).

**Composition of Sulfide Ores**. Average compositions for different types of ore from different deposits are shown in Table 3.5 (note concentrations are recalculated to metal content in 100% sulfide).

**Table 3.5.** Average compositions of various Ni-Cu-(PGE) ore types in the Raglan Ore Camp recalculated to 100% sulfide (see footnote in Chapter 1 for details of recalculation)

| Locality | Ore Type | | n | S, wt % | Ni, wt % | Cu, wt% | Pd, ppb | Pt, ppb | Rh, ppb | Ru, ppb | Ir, ppb | Os, ppb | Au, ppb | Ref. |
|---|---|---|---|---|---|---|---|---|---|---|---|---|---|---|
| Zone 2-3 | Disseminated | | 33 | 37.7 | 12.20 | 2.64 | 7 782 | 3 125 | 505 | 1 133 | 167 | 225 | 326 | 1 |
| Donaldson | Disseminated | | 6 | 37.1 | 17.10 | 4.16 | 25 261 | 6 606 | 695 | 1 943 | 362 | 459 | 246 | 3 |
| | Massive and semimassive | Cu-rich | 5 | 36.0 | 17.70 | 9.08 | 15 408 | 2 040 | 73 | 77 | 11 | 16 | 3 766 | 3 |
| | | Cu-poor | 9 | 40.0 | 10.10 | 1.06 | 3 153 | 2 791 | 704 | 1 575 | 286 | 337 | 43 | 3 |
| Katinniq | Disseminated | | 21 | 38.3 | 11.40 | 3.45 | 11 878 | 4 032 | 796 | 2 109 | 396 | 467 | 525 | 4 |
| | Massive and semimassive | Cu-rich | 16 | 38.6 | 10.00 | 4.57 | 7 290 | 3 427 | 481 | 988 | 178 | 249 | 272 | 4 |
| | | Cu-poor | 14 | 38.9 | 12.50 | 1.34 | 5 122 | 2 190 | 722 | 1 881 | 301 | 445 | 135 | 4 |
| Cross Lake | Massive and semimassive | Cu-rich | 5 | 39.5 | 6.31 | 3.26 | 8 997 | 2 548 | 320 | 227 | 41 | 45 | 627 | 2 |
| | | Cu-poor | 3 | 40.4 | 4.25 | 1.31 | 2 971 | 850 | 603 | 950 | 183 | 139 | 108 | 2 |

*n* number of samples. References: 1 = averages compiled from unpublished data of S.-J. Barnes; 2 = averages compiled from Giovenazzo (1991); 3 = average compiled from Giovenazzo (1991) and Dillon Leitch (1986); 4 = average compiled from Barnes et al. (1982), Giovenazzo (1991), and Gillies (1993)

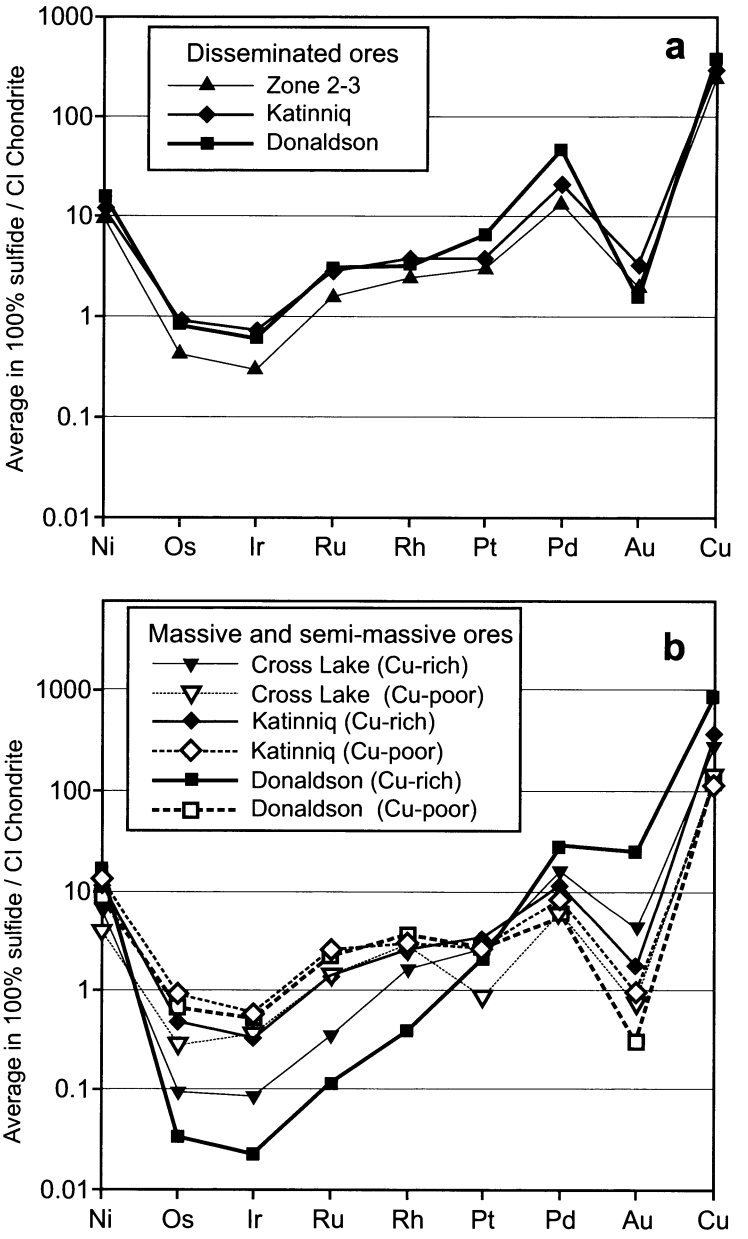


**Fig. 3.29.** Average contents of PGE, Au, Ni, and Cu (normalized to CI Chondrite) in ores of some deposits of the Raglan Camp. Ore compositions are recalculated to 100% sulfide. References for data sources are given in Table 3.5. a – disseminated ores of the Zone 2-3, Katinniq, and Donaldson deposits; b – massive and semi-massive ores of the Cross Lake, Katinniq, and Donaldson deposits: Cu-rich and Cu-poor ores are compared

attributable to variations in R Factor. The answer to this probably lies in Fig. 3.29b in which it is seen that there is a major difference between Cu-rich and Cu-poor ore at Donaldson. This difference is much more pronounced than at the other two deposits. It would seem that the Donaldson ore has suffered a much higher degree of sulfide fractionation than ore from the other two deposits, and it is likely that some fractionated samples have been included amongst the samples of disseminated ore that have been averaged for Donaldson. The behaviour of Au is somewhat out-of-step with that of the other noble metals. Au is the most mobile of all of the noble metals and it is possible that it has been re-distributed during the low-grade metamorphism that has affected the area.

### *Genetic Aspects*

Watts and Osmund (1999) report on the results of the application of 3D potential field inversion techniques that had been developed at the University of British Columbia's Geophysical Inversion Facility to magnetic susceptibility and gravity data. They used the latest version of the MAG3D (v.3) susceptibility inversion program and 1988 airborne total field magnetic data to develop a 3D magnetic susceptibility plot for the entire Raglan block covering an area of more than a 500 square km and extending to a depth of 1.1 km (Fig. 3.30).

This pattern was originally postulated to represent a secondary fold structure. However, in the light of the successful application of a lava channel model to Kambalda (Lesher et al. 1984) and the recognition that some of the Raglan deposits might be extrusive, not intrusive (Albino 1984; Barnes and Barnes 1999), the pattern is now considered to be a primary flow structure that is characteristic of a meandering flow type environment, similar to that illustrated for Archean komatiite-related deposits in Fig. 3.19. This is consistent with the work of Lesher and collaborators (see above) who had already developed a model in which most of the mineralized ultramafic bodies at Raglan were interpreted as flow channels. The lava channel model had been applied at Katinniq between 1990-1993 by Falconbridge geologists and had successfully predicted continuations and extensions of known mineralization.

Green and Dupras (1999) noted that the regional 3D magnetic model confirms some of the plunges of ore zones that had been inferred from earlier studies, but indicates that the channels at Zone 3, Zone 2, Katinniq, and Zone 5-8 are part of a single meandering or intensely folded lava channel system with an overall E-W trend, not a system of multiple subparallel lava channels with an overall NE trend. Subsequent stratigraphic drilling between Katinniq and 5-8 provided overwhelming support for a

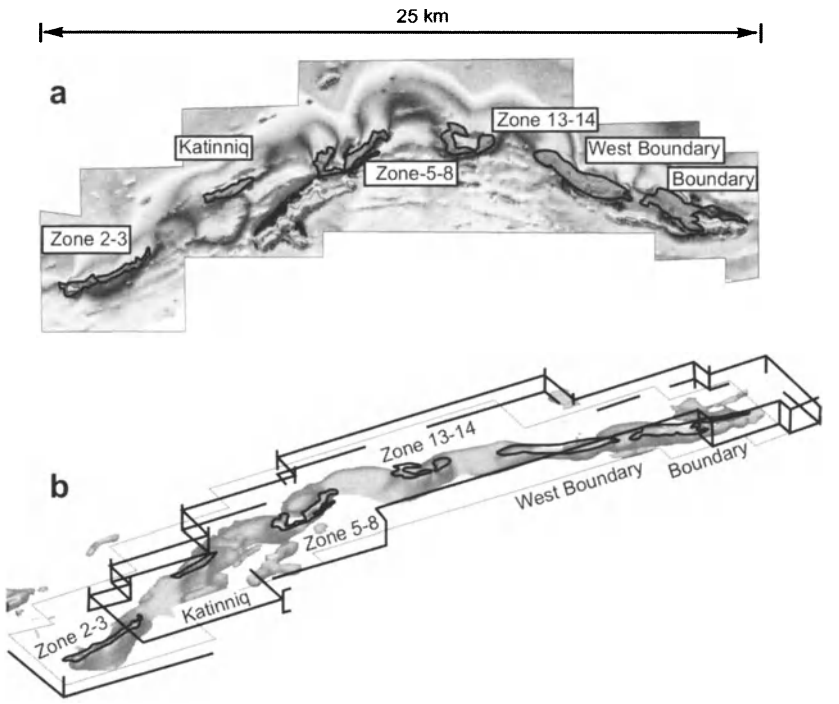


**Fig. 3.30.** Air magnetic map (a) and 3-dimensional magnetic model (b) for the eastern part of the Raglan ore camp between the 2-3 zones and the Boundary deposit (after Watts and Osmund 1999)

meandering lava channel model with a broadly east to west or west to east flow direction. The thick total field magnetic anomaly (Fig. 3.30) that is interpreted to be the lava channel, winds in and out of the current erosion surface. It has been accurately traced in the subsurface in four areas – between Zone 2 and Katinniq, between Katinniq and Zone 5-8, between Zone 5-8 and Zone 13-14, and between Zone 13-14 and West Boundary. It is interpreted to have been partly or wholly eroded away between Zones 3 and 2, in the middle of Katinniq, in the middle of Zone 5-8, and in the middle of Zone13-14.

Green and Dupras (1999) reported that the latest drilling and underground mining has shown that there are two main trends of ore lenses at Katinniq, the northerly one having a nickel tenor of ca. 10 wt% and the southerly one having a nickel tenor of ca. 15 wt% (Gillies 1993). The lenses rise gradually in elevation to the east and disappear near the eastern outcrop limit of Katinniq, where some of the orebodies are partly eroded. It is interpreted from the magnetic model that the Katinniq ultramafic body

(including both channels) bends northward at its eastern end, plunges again to approximately 1000 metres depth, bends southward, and rises gradually again to reappear at surface as Zone 5-8. A number of deep exploration holes drilled at the ends of the known zones or between them have confirmed this interpretation.

The work of Burnham et al. (1999) on the trace element composition of lavas, intrusions and country rocks of the Raglan Belt has shown that whereas the trace element compositions of the enriched Povungnituk Group basalts appear to closely resemble those of crustally contaminated modern ocean-island basalts, the compositions of the Chukotat Group basalts and ultramafic bodies of the Raglan Horizon coincide with those expected for depleted mantle melts that have assimilated the local Upper Povungnituk Group sedimentary rocks. This has led them to propose that as the Chukotat magmas rose through the thick sedimentary substrate of the Upper Povungnituk Group assimilation occurred, giving rise to the contamination signature. The hottest parts of the extrusive sequence were the channels within which most flow was concentrated. This led to flow remaining turbulent in these areas, with the result that a lower boundary layer did not develop, and assimilation was thus maximized. Sulfides caught up in this assimilation interacted with the magma, concentrating Ni, Cu, PGE and Au, and were then trapped in structures at the base of the flow channels.

The S isotopic compositions of several Raglan ores and metasedimentary rocks have been determined by Lesher and Ripley (1992). They found that $\delta^{34}S$ values of 31 whole rocks and 14 mineral separates (Po and Cp) representing a variety of ore types (disseminated, net-textured, and semi-massive) from 8 deposits across the belt range from 3–6 ‰. Furthermore, $\delta^{34}S$ values of disseminated and massive sulfide layers in metasedimentary rocks from 3 localities across the belt are similar to the ores, ranging between 4-5‰. Sulfur isotope data are thus consistent with the above model of country rock assimilation.

The Re-Os isotope systematics of the ores and host rocks have been studied by Luck and Allegre (1982) and Shirey and Barnes (1994, 1995). Re concentrations in the ores range from 0.184 to 25.6 ppb, Os concentrations range from 0.108 to 23.9 ppb, $^{187}Re/^{188}Os$ ratios range from 1.63 to 9.97, and $^{187}Os/^{188}Os$ ratios range 0.168–0.441. The underlying S-rich Povungnituk slates contain 17 ppb Re, 0.39 ppb Os, $^{187}Re/^{188}Os$ ratios range from 216 to 278, and $^{187}Os/^{188}Os$ ratios from 7.8 to 9.2. Shirey and Barnes (1994, 1995) used the near-chondritic Os isotopic compositions of the ores and host rocks and the highly radiogenic compositions of the slates to suggest that the ore deposits could not have formed by assimilation of sulfidic sediments. However, Lesher et al. (1995), Lesher and Stone

(1996), and Lesher and Burnham (1999) have shown that Os isotopic signatures are more rapidly changed than S isotopic signatures in dynamic magmatic systems, and that, given the R factors in the range of 300–1100 that have been determined by Barnes et al. (1993) and Gillies (1993), the predicted $^{187}Os/^{188}Os$ ratios are consistent with those that have been recorded (see Lesher, Barnes, Gillies and Ripley 1999).

### *Brief notes on mineralisation in the Povungnituk Group*

As discussed above, the Povungnituk Group developed along the southern margin of a rift zone that formed the northern margin of the Superior craton across what is now the Ungava peninsula. The Lower Povungnituk group comprises sediments that are thought to have accumulated during the initial stages of rifting. The Upper Povungnituk consists of slates and basalts, both of which are intruded by gabbro-peridotite sills and interleaved with zones of olivine-rich ultramafic rocks. The Povungnituk basalts consist of simple and compound massive and pillowed flows of tholeiitic basalt. Slates of the Upper Povungnituk occur as a 1-2 km thick sequence of metapelites at the top of the Povungnituk. They are dominated by semi-pelitic, fine-grained graphitic sulfidic slate and argillite with minor quartzite.

The Povungnituk basalts and slates are interleaved with mafic-ultramafic bodies up to several hundred metres in thickness. These vary in composition from massive gabbro or pyroxenite, or less commonly peridotite, while others differentiated with relatively thin lower zones of columnar-jointed peridotite or oikocrystic olivine pyroxenite, and thick upper zones of layered gabbro. A number of the differentiated mafic-ultramafic bodies (e.g., Delta, Romeo I) contain narrow PGE-rich zones associated with thin pyroxene-rich pegmatoidal gabbro (e.g., Giovenazzo et al. 1989; Thibert 1993). Some of the undifferentiated ultramafic bodies have a U-shaped cross section and contain accumulations of Ni-Cu-(PGE) sulfides at the base of the "U" (e.g., Expo Ungava).

Recent mapping in the vicinity of Expo Ungava has shown that the sulfide ores of this and a recent discovery (Mesamax NW) a few km to the east are related to a >30 km-long mafic/ultramafic dike that intruded after the volcanic and sedimentary strata had been affected by 2 phases of folding ( Jim Mungall, personal communication at University of Toronto workshop, March 5$^{th}$ 2004). It is tempting to suggest that this dike is a feeder to the stratigraphically higher Raglan mineralization, but Ni and Cu tenors and the Ni/Cu ratio of the Povungnituk mineralization is much lower than that at Raglan [Ni/Cu = 0.76 at Expo, 0.78 at Mesamax NW as compared to 3.6 at Raglan (see Table 3.4)]. The PGE contents at Mesamax

NW are high with (Pt+Pd)/(Ni+Cu) ratios (Ni+Cu in wt%, PGE in g/t) of 1.1 compared with values of 0.75–0.81 at Raglan.

### 3.2.2 Deposits of the Thompson Nickel Belt, Manitoba, Canada

After 10 years of intense exploration in the Thompson Nickel Belt (TNB), during which the low grade Moak and Mystery deposits were outlined, INCO discovered the Thompson ore body in 1956. A shaft had been sunk at Moak the previous year, for underground exploration and to prepare this deposit for production, but these operations were discontinued as soon as the Thompson discovery proved to be of sufficient tonnage (Fraser 1985). At Thompson, production commenced in 1961 at which time 25 million tons of ore with 2.97% combined Ni+Cu had been intersected (Zurbrigg 1963). In this volume (Table 1.1) a figure for the present day total reserves for the district is reported as 150.3 million tones at 2.32 wt% Ni, 0.16 wt% Cu and 0.046 wt% Co.

#### *Regional geology*

The TNB and its deposits have been described by Zurbrigg, (1963); Bell (1971); Coats and Brummer (1971); Coats et al. (1972); Cranstone and Turek (1976); Peredery et al. (1982); Green et al. (1985) and Bleeker, (1989b, 1990). It forms a 10 to 35 kilometer wide belt of variably reworked Archean basement gneisses and Early Proterozoic cover rocks along the northwestern margin of the Superior craton (Fig. 3.31). Strong gravity and magnetic expressions (Gibb 1968; Kornik and MacLaren 1966; Kornik 1969) permit delineation of the TNB and its extension below platformal cover, as far south as South Dakota (Green et al. 1979). To the NNE, the TNB appears structurally coextensive with the Owl River shear zone (Bell 1966), the aeromagnetic expression of which indicates a minimum sinistral displacement of the order of 100 km (Fig. 3.31). Lithotectonically, however, the TNB as part of the "Churchill -Superior Boundary Zone" (Weber and Scoates 1978), swings to the east and has its extension in the Split Lake Block and the Fox River Belt (Fig. 3.31). Like the TNB, the Split Lake Block is dominated by variably reactivated basement gneisses, whereas the Fox River Belt consists of a homoclinal, steeply north-dipping sequence of Aphebian supracrustal rocks and related intrusions (Baragar and Scoates 1981).

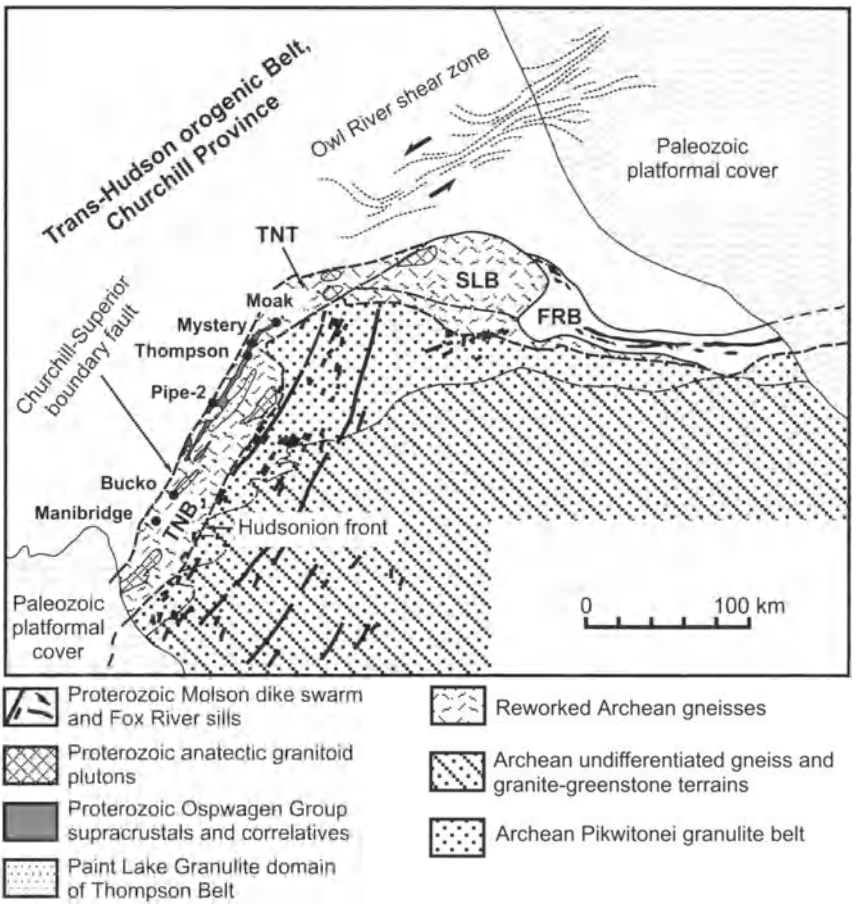


**Fig. 3.31.** Simplified geological map of the northwest part of the Superior craton, "Churchill Superior Boundary Zone" and adjacent internal zone of Trans-Hudson Orogen (Churchill Province). Modified after Bleeker (1990). The "Churchill - Superior Boundary Zone" comprises the Thompson Nickel Belt (TNB), Split Lake Block (SLB) and Fox River Belt (FRB)

### *Geology and history of tectonic evolution of the Thompson Nickel Belt*

Variably reworked Archean basement gneisses are volumetrically the dominant rock type in the TNB. These have been derived, at least partially, from Pikwitonei granulite facies protoliths which parallel the belt to the southeast. Along the eastern boundary of the Thompson Nickel Belt, referred to as the Hudsonian front, Pikwitonei granulites can be mapped into the TNB where they show progressive overprinting by Hudsonian ductile

deformation and amphibolite facies metamorphism. Various gneisses along the western margin of the belt have been dated. Rb-Sr whole rock data (Cranstone and Turek 1976) indicate an Archean origin, which has been confirmed .by U-Pb zircon dating (Machado et al. 1987).

Remnants of the thin Early Proterozoic cover sequence that may have accumulated in a rift structure, and which is referred to as the Ospwagan Group (Scoates et al. 1977; Bleeker and Macek 1988a), occur along the western margin of the TNB, in deeply dissected fold interference patterns of regional scale. Recent detailed mapping (Bleeker 1989a, Bleeker and Macek 1988a) has revealed a detailed lithostratigraphy which can be correlated throughout the TNB (Fig. 3.32). A lower clastic sequence (Manasan Formation) is overlain by rocks dominated by chemical and pelitic sediments (Thompson and Pipe Formations), after which there is a return to a coarse clastic facies (Setting Formation) , which is finally overlain by mafic to ultramafic volcanics (Ospwagan Formation). The volcanics are probably cosanguinous with ultramafic sills which intruded the supracrustal sequence at various levels, most commonly near the base, and which generated the Ni sulfide deposits.

The strong tectonism that has affected the area, coupled with the poor exposure, make it difficult to obtain thicknesses for the rocks sequences. Bleeker (1990) did not comment on the thickness of individual sedimentary and volcanic formations. He wrote only that the thickness of the ultramafic sill at the Pipe II deposit is 150 m. It can be concluded from cross-sections of the Thompson deposit that are given in Bleeker (1990) that, at the Thompson deposit the maximum thickness of the Manasan Formation is 60 m, Thomson Formation – 90 m and at the Pipe-2 deposit, Manasan – 20 m, Thompson – 90 m, Pipe – more than 160 m.

The autochtonous nature and detailed lithostratigraphy of the Ospwagan Group cover sequence have allowed Bleeker (1990) to make inferences about the early tectonic evolution of the TNB (Fig. 3.33). He concluded that the TNB represents a domain on the down-dropped margin of the Superior Craton (as shown by the Manasan Formation). Subsidence likely accompanied rifting that occurred farther to the west, but evidence for a rift zone, apart from the subsidence required to explain the Manasan Formation, is not preserved. Remnants of the Ospwagan Group are truncated by the fault-bounded western margin of the TNB, a relatively late structure known as the "Churchill -Superior boundary fault". Thus the original extent of the Ospwagan Group and consequently the Superior plate likely reached much farther west. The TNB domain developed on a stable platform as shown by the rocks of the Thompson and Pipe formations. The platform then evolved into an active tectonic environment – possibly a foredeep – as shown by the Setting Formation. Clastic sediments of this

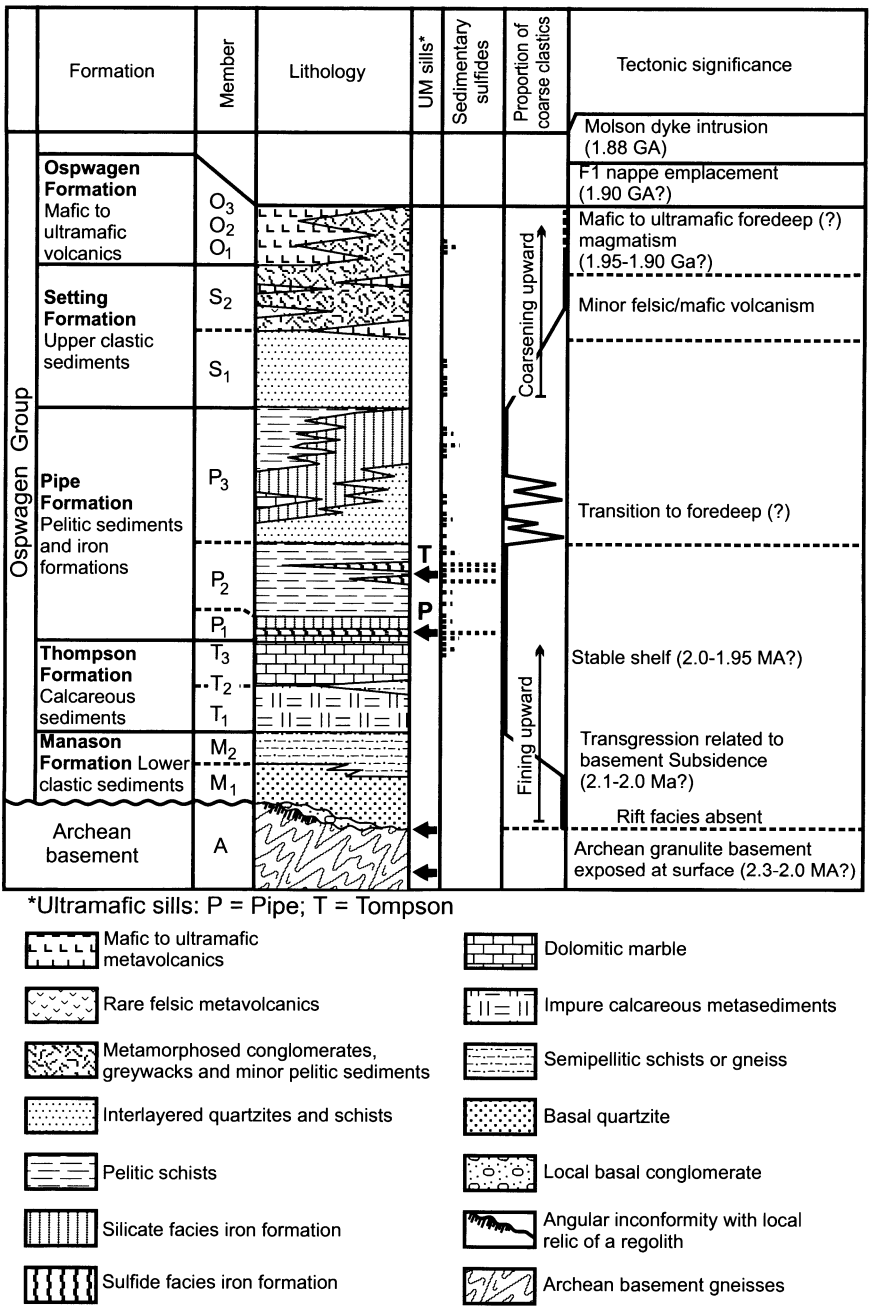


**Fig. 3.32.** Stratigraphy of the Ospwagan Group and its tectonic significance for the early development of the Thompson Nickel Belt. After Bleeker (1990)

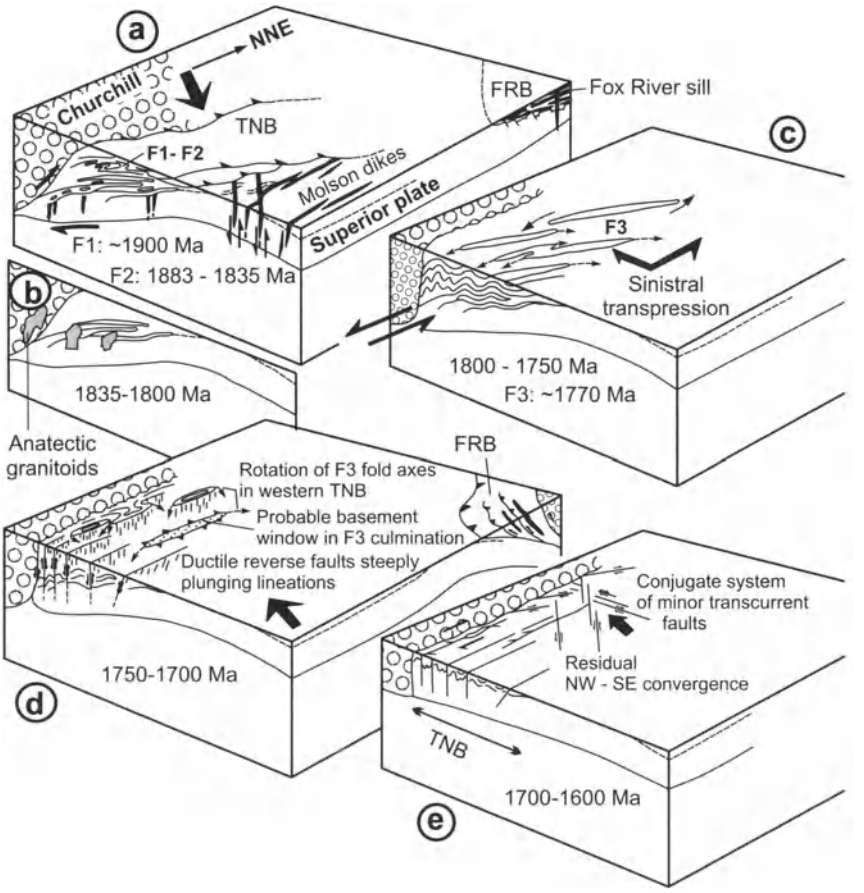


**Fig. 3.33.** Time-sequential block diagrams, illustrating the tectonic evolution of the Thompson Nickel Belt during the Hudsonian orogeny. After Bleeker (1990) TNB = Thompson Nickel Belt; FRB = Fox River Belt; F1, F2, and F3 – fold systems

possible foredeep are associated with minor mafic and felsic volcanics and are overlain by the main sequence of mafic to ultramafic volcanics (Ospwagan Formation) at the top of the Ospwagan Group.

The earliest folding (Hudsonian orogeny) to effect the rocks of the TNB was thrusting that gave rise to a series of nappe-like folds (F1) (Fig. 3.33) associated with lower amphibolite facies metamorphic conditions (Bleeker 1989b). The exact timing is uncertain but certainly predated 1.833 Ga. Bleeker noted that this initial folding was followed by a stage of higher temperature isoclinal, recumbent folding (F2) accompanied by ductile thrusting. The thermal peak of regional metamorphism overprinted the second phase of folding and probably occurred at about 1.82 Ga. Bleeker

concluded that at least 30 Ma later and at much lower temperatures, intense sinistral transpression of the nappe/thrust pile produced high amplitude, nearly upright, doubly-plunging F3 folds which are the most obvious structures throughout the TNB. A main phase of mylonitization occurred late during or after the F3 folding and is confined to shear zones that tend to be parallel to steeply dipping limbs of the upright F3 folds.

### *Geology of the Moak Lake - Pipe Lake area*

Although many deposits are known from the southern part of the belt, some of which were mined for some time, such as the Falconbridge-owned Manibridge deposit (Coats and Brummer 1971), the Moak Lake - Pipe Lake area in the northern part of the belt has been more productive. All deposits in this area occur within the Early Proterozoic cover sequence which is preserved in the deeply dissected remnant of a complex fold interference pattern involving an Fl nappe refolded by tight, upright, doubly plunging F3 folds. This is illustrated in Fig. 3.34a that is a schematic longitudinal cross-section of the F1 nappe from which the effects of F3 folding have been removed. The majority of the ore deposits occur in the recumbent limb of the fold, the "Pipe limb". Only the Thompson deposit occurs within the upper limb ("Thompson limb"). The Archean gneiss of the Thompson limb is highly metasomatised, including enrichment in K-spar and the development of pegmatoidal schlieren. Ultramafic sills are much more highly strained on the Thompson than on the Pipe limb. Metavolcanics of the Ospwagan Formation are preserved only in the Pipe limb.

Following his structural interpretation, Bleeker (1990) noted that the ore-related ultramafic sills intruded the cover sequence at various levels (Fig. 3.35). Sill- or dike-like bodies occur also within the underlying basement. The Pipe II sill intruded low in the cover sequence, below the pelitic schists, along a graphitic sulfide facies iron formation (Fig. 3.34a). Other ultramafic bodies on the lower limb of the nappe occur in a similar lithostratigraphic position, e.g. those at Birchtree Mine. The Thompson sill intruded higher in the sequence, near the top of the pelitic schist unit (Fig. 3.34b). This horizon is also characterized by large concentrations of sedimentary sulfides in the form of disseminated, banded or massive pyrrhotite in a host of extremely graphitic schist or interlayered with chert. This second level of sulfide facies iron formation can also be identified at the Pipe II, where it forms a 10 to 50 centimetre thick band of pyrrhotite with inclusions of graphitic schist and chert.

All known deposits in the Moak Lake - Pipe Lake area are thus associated with major sedimentary sulfide concentrations. As a result of their work on the Pipe I deposit, Naldrett et al. (1979) proposed that the ul-

tramafic bodies had assimilated sedimentary sulfide to give rise to the ores. The PGE tenor of the sulfides varies greatly between the Pipe II, Birchtree and Thompson deposits, which, they suggested, is likely the result of varying proportions of sulfide being assimilated locally by the intrusions related to the deposits.

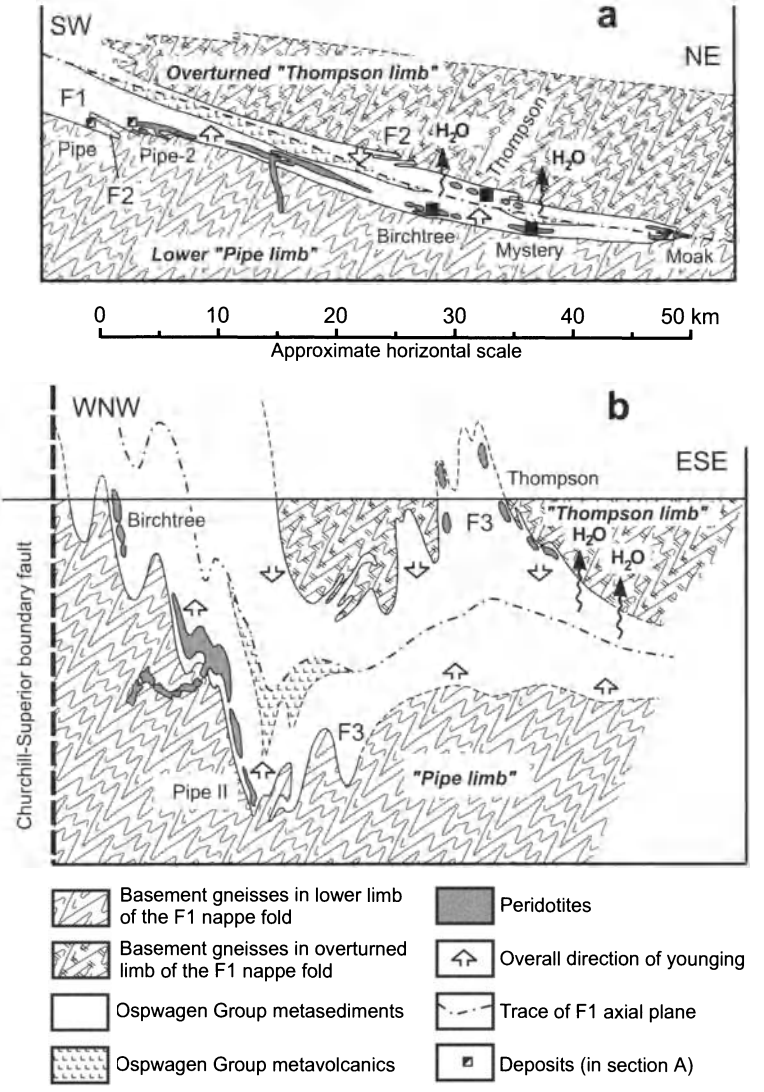


**Fig. 3.34.** Schematic cross sections (a – longitudinal; b – transverse) through the refolded nappe structure F1, to which all ore deposits of the Moak-Pipe area are related. After Bleeker (1990)

### *The Thompson deposit*

**Geology.** The Thompson ore zone extends six km on surface and has been shown to extend to a depth of more than 1200 m. The ore body is stratabound and occurs within and generally near the top of a pelitic schist unit (Figs. 3.36, 3.37). Despite the complex and protracted structural - metamorphic history of the ore body, involving several phases of folding and sillimanite- garnet- K feldspar grade metamorphism, no significant remobilization of sulfides beyond the original host unit (pelitic schist horizon) has been observed, except along late faults and as an infilling of late stage tension gashes. Bleeker (1990) noted that important remobilization occurred within the original host horizon, but described this as "passive" in response to folding and extension (see Fig. 3.41b below). Consequently, magmatic Ni sulfides do not extend beyond the range of ultramafic boudins that are the remnants of the original parent sill.

**Sulfide Mineralization.** Bleeker (1990) has argued that the sulfides of the Thompson belt can be divided into three categories, Ni-poor sedimentary sulfides, Ni-enriched sedimentary sulfides and Ni-bearing magmatic sulfides. The Ni-poor sedimentary sulfides consist of pyrrhotite, chalcopyrite, late pyrite and accessory phases and show a millimeter to decimeter scale interlayering with graphitic schist, chert or silicate facies iron formation. The compositions of samples of Ni-enriched sedimentary sulfide and magmatic sulfide are compared in Table 3.6. The Ni-enriched sedimentary sulfides are indistinguishable from barren sedimentary sulfides, except for elevated levels of Ni and Co. All occurrences of this sulfide type occur in close proximity to the main magmatic Ni sulfide ore zones. Ni concentrations vary from slightly enriched (> 1000 ppm) up to 10 wt% and decrease with distance from the main Ni ore zones. Only the more Ni-rich examples, for which PGE data are also available, are shown in Table 3.6.

Magmatic nickel sulfides consist of pyrrhotite, pentlandite, chalcopyrite, gersdorffite, chrome spinel and various accessory and secondary phases. Bleeker (1990) classifies them as "endogenic" or "exogenic", depending on whether they occur within or external to the ultramafic parent rocks: Exogenic magmatic sulfides comprise the typical massive Ni sulfide ore at Thompson; they occur as pods and lenses of variable size within the pelitic schist host rock generally adjacent to ultramafic boudins. They are usually coarse grained, “clean” with little or no graphite, with few other inclusions except for biotite flakes. They are chemically rather homogeneous with high Cr levels (500 to 1500 ppm) and with Ni/Cu, Ni/Co and Ni/S ratios that are characteristic for a given deposit. Endogenic magmatic sulfides occur within their ultramafic parent rocks as minor disseminations,

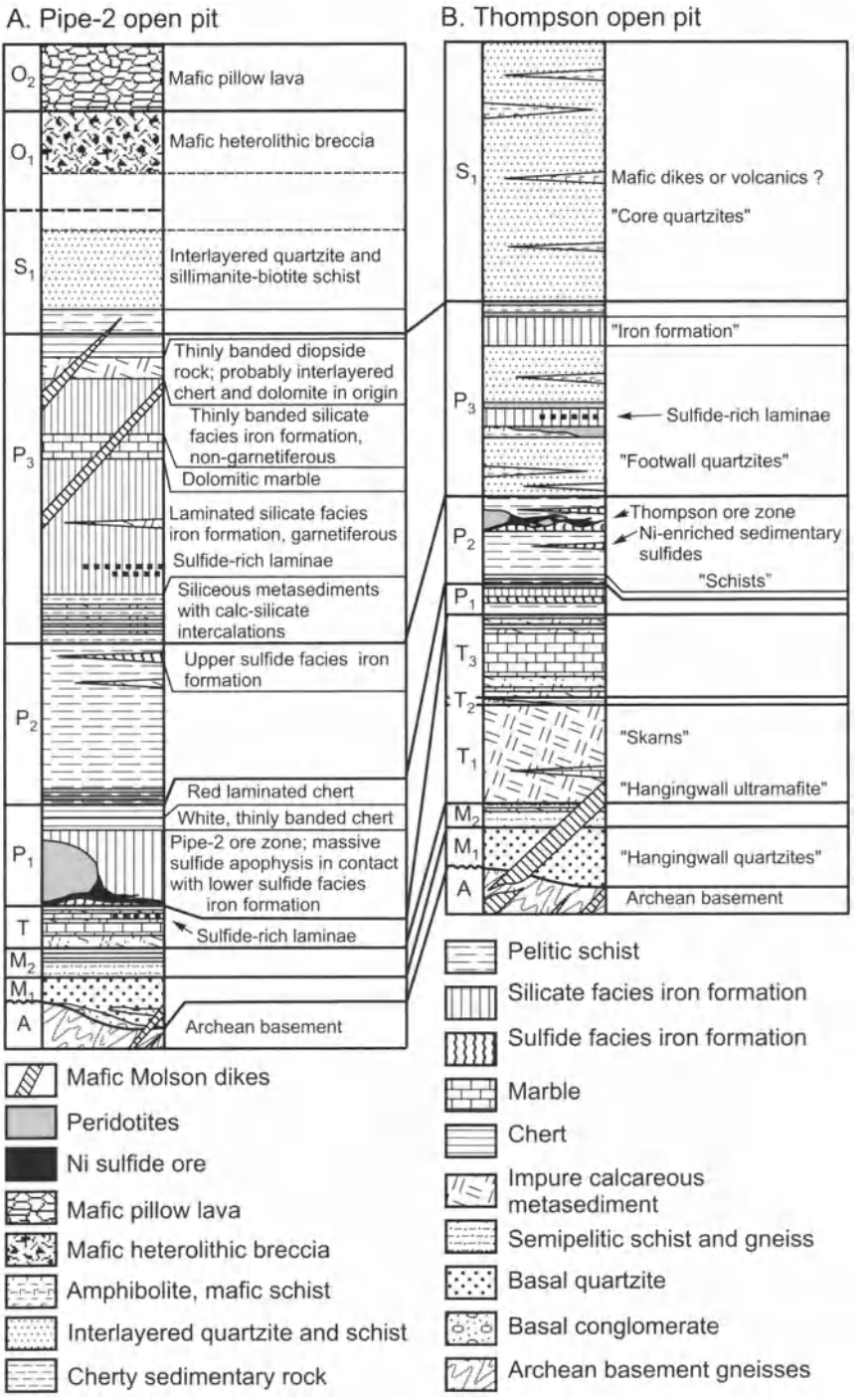
A. Pipe-2 open pit
O2
Mafic pillow lava
O1
Mafic heterolithic breccia
S1
Interlayered quartzite and sillimanite-biotite schist
P3
Thinly banded diopside rock; probably interlayered chert and dolomite in origin
Thinly banded silicate facies iron formation, non-garnetiferous
Dolomitic marble
Laminated silicate facies iron formation, garnetiferous
Sulfide-rich laminae
Siliceous metasediments with calc-silicate intercalations
P2
Upper sulfide facies iron formation
Red laminated chert
White, thinly banded chert
P1
Pipe-2 ore zone; massive sulfide apophysis in contact with lower sulfide facies iron formation
T
Sulfide-rich laminae
M2
M1
A
Archean basement
Mafic Molson dikes
Peridotites
Ni sulfide ore
Mafic pillow lava
Mafic heterolithic breccia
Amphibolite, mafic schist
Interlayered quartzite and schist
Cherty sedimentary rock
B. Thompson open pit
S1
Mafic dikes or volcanics ?
"Core quartzites"
P3
"Iron formation"
Sulfide-rich laminae
"Footwall quartzites"
P2
Thompson ore zone
Ni-enriched sedimentary sulfides
"Schists"
P1
T3
T2
T1
"Skarns"
"Hangingwall ultramafite"
M2
M1
"Hangingwall quartzites"
A
Archean basement
Pelitic schist
Silicate facies iron formation
Sulfide facies iron formation
Marble
Chert
Impure calcareous metasediment
Semipelitic schist and gneiss
Basal quartzite
Basal conglomerate
Archean basement gneisses

**Fig. 3.35.** Reconstructed Ospwagan Group lithostratigraphy for the Pipe II Open Pit (a) and Thompson Open Pit (b). Note the different levels of the Pipe II and Thompson ore zones. Both occur along thin sulfide facies iron formations. After Bleeker (1990). Indices of the stratigraphic units are shown to the left of the columns that are explained in Fig. 3.32. The local terminology is written in quotes against the Thompson column

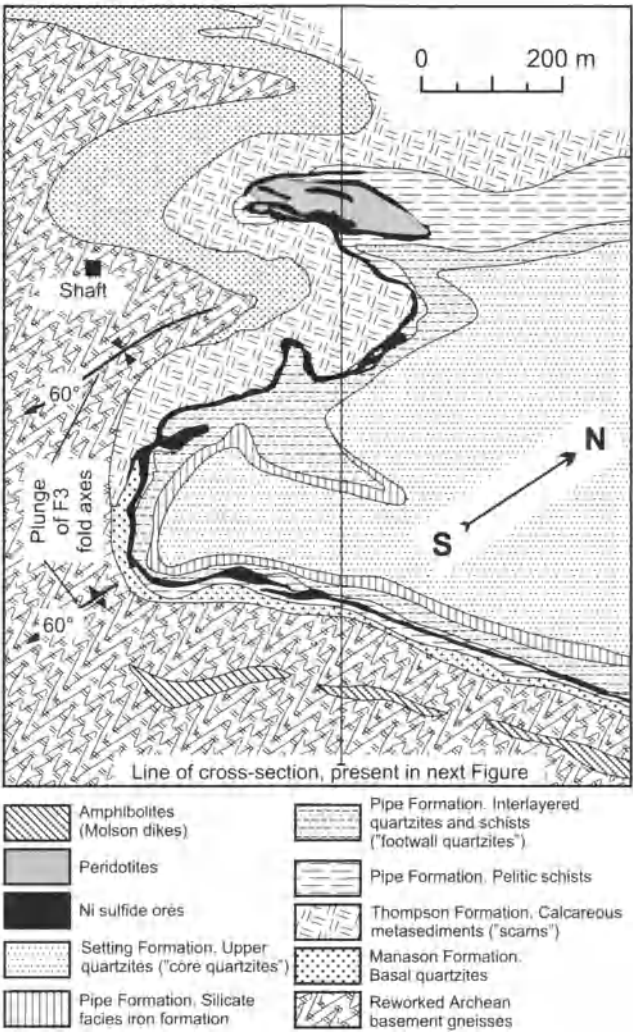


**Fig. 3.36.** Plan showing map the geology of 1000 ft level of the Thompson Mine. After Bleeker (1990), modified after Zurbrigg, (1963). The local terminology is written in quotes in the legend

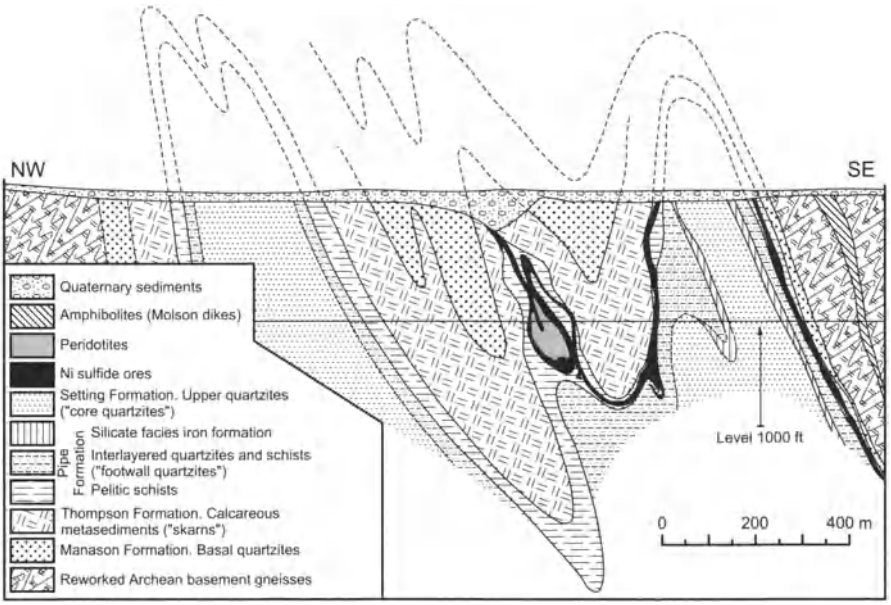


**Fig. 3.37.** Cross section through the Thompson deposit (after Bleeker 1990). Location of the cross section is shown in Fig. 3.37. The local terminology is written in quotes in the legend

net-textured interstitial sulfides, irregular interstitial sulfide specks or "nests" of specks, and as semi-massive to massive concentrations in veins and breccias.

Data for both exogenic magmatic sulfides and Ni-enriched sedimentary sulfide are shown in Table 3.6. Both have somewhat similar Ni, Cu and Co contents, but Pt, Rh, Ru, Ir and Os are distinctly less concentrated in the Ni-enriched sedimentary sulfide, as are Cr, Se and As.

### *The Pipe II deposit*

**Geology.** The Pipe II deposit differs from the Thompson deposit in that it has undergone less deformation. The ore zone extends for approximately one kilometer along strike at surface. It is located for much of its length along the stratigraphic base of a more than two kilometer long, up to 150 meter thick, serpentinized ultramafic body. The ultramafic body, which is thought to be the boudinaged remnant of a larger sill, occurs on the western limb of the main mine structure (Fig. 3.34b) – a tight, steeply NE plunging F3 synform. The ultramafic boudin dips 75° to the SE and is conformable with the enveloping metasediments. The facing of the sill, based on its sulfide to dunite to peridotite to orthopyroxenite differentiation pro-

file, is towards the southeast. This facing conforms with the overall younging direction of the enclosing metasediments on the western limb.

On a regional scale, the Pipe II ultramafic boudin is the southernmost member of a discontinuous array of ultramafic bodies which stretches from the Pipe II Open Pit, along the west shore of Ospwagan Lake, to Birchtree Mine (see Fig. 3.34a). Where the lithostratigraphic position of these bodies could be checked, they occur at exactly the same horizon within the Ospwagan Group cover sequence, i.e. above the carbonates and lower sulfide facies iron formation; and below the first silicate facies iron formation. This level is well below the lithostratigraphic horizon of the Thompson ore zone (see Fig. 3.35).

**Sulfide Mineralization.** The spectrum of sulfide mineralizations at Pipe II is essentially similar to Thompson with endogenic disseminated, net-textured interstitial, and massive magmatic sulfides, exogenic massive magmatic sulfides, Ni-enriched sedimentary sulfides and barren sedimentary sulfides. However, whereas at Thompson exogenic magmatic sulfides predominate, the bulk of the Pipe II ore occurs within and at the base of the parent ultramafic sill. The sulfides at Pipe contain significantly lower concentrations of metals (calculated as metal content in 100% sulfides) as is discussed below.

### *Comparison of the Composition of Different Ores from the Thompson belt*

Bleeker's (1990) data on the composition of ore types from the Thompson mine are given in Table 3.6. As described above he argued that some exocontact ores are magmatic and others are sedimentary sulfides into which metals have diffused from the magmatic ores during subsequent metamorphism. As remarked above, there are significant compositional differences between these two types. This is brought out particularly in the chondrite-normalized plot shown as Fig. 3.38. The Ni, Pd, Au and Cu contents of magmatic and sediment-enriched ores are relatively similar, but the sedimentary ores are much poorer in Pt, Rh, and particularly in Ru, Ir, and Os. In general, the slope of the PGE profile for the sedimentary ores is much steeper than that for the magmatic ores. The smoothness of the slope for the sedimentary ores is interrupted by a pronounced negative Pt anomaly. This negative anomaly is also present to a less pronounced extent in the magmatic ores and also in the ores from the Pipe II deposit. It is likely a characteristic of the belt.

Data for the Pipe and Bucko deposits are also shown in Fig. 3.39. The Pipe ores are much lower in all metals than the magmatic ores at Thomp-

**Table 3.6.** Chemical compositions of the magmatic sulfides and enriched sedimentary sulfides from the Thompson deposit (after Bleeker 1990)

| Sample No | S wt% | Ni wt % | Cu wt % | Co wt % | Pt ppb | Pd ppb | Rh ppb | Ru ppb | Ir ppb | Os ppb | Re ppb | Au ppb | Cr ppm | Zn ppm | Se ppm | As ppm | Mo ppm | C wt % |
|---|---|---|---|---|---|---|---|---|---|---|---|---|---|---|---|---|---|---|
| ***Magmatic sulfides*** | | | | | | | | | | | | | | | | | | |
| T.372.1 | 4.70 | 1.30 | 0.03 | 0.03 | 150 | 330 | 27 | 60 | 27 | 26 | 2 | 54 | 590 | 280 | 4 | 19 | 1 | 0.60 |
| T.527C | 9.30 | 1.70 | 0.21 | 0.03 | 110 | 420 | 25 | 33 | 17 | 22 | 6 | 21 | 230 | 190 | 6 | 55 | 4 | 0.70 |
| T.533 | 20.20 | 3.60 | 0.12 | 0.06 | 48 | 430 | 55 | 120 | 44 | 69 | 24 | 21 | 290 | 180 | 9 | 40 | 10 | 1.40 |
| T.527B | 23.30 | 4.10 | 0.15 | 0.08 | 100 | 850 | 110 | 180 | 70 | 97 | 35 | 110 | 410 | 280 | 14 | 63 | 9 | 1.10 |
| T.239 | 25.00 | 7.00 | 0.17 | 0.12 | 450 | 1 260 | 150 | 240 | 110 | 130 | 2 | 55 | 530 | 330 | 8 | 1 661 | 8 | 0.30 |
| T.353A | 26.00 | 5.90 | 0.12 | 0.09 | 200 | 1 200 | 113 | 190 | 77 | 110 | 45 | 29 | 460 | 260 | 16 | 69 | 7 | 0.20 |
| T.251 | 26.70 | 4.40 | 0.05 | 0.07 | 320 | 1 160 | 129 | 250 | 95 | 140 | 32 | 65 | 610 | 430 | 20 | 47 | 8 | 0.40 |
| T.188C | 28.70 | 7.10 | 0.38 | 0.11 | 1 175 | 900 | 161 | 280 | 170 | 180 | 74 | 100 | 530 | 360 | 20 | 86 | 6 | 0.20 |
| T.271 | 29.90 | 5.70 | 0.22 | 0.13 | 100 | 950 | 137 | 230 | 94 | 140 | 2 | 120 | 620 | 320 | 19 | 71 | 10 | 1.00 |
| T.527A | 29.90 | 7.10 | 0.10 | 0.09 | 580 | 940 | 127 | 210 | 91 | 130 | 12 | 84 | 600 | 420 | 18 | 75 | 8 | 0.70 |
| T.188A | 30.20 | 7.10 | 0.35 | 0.13 | 180 | 540 | 130 | 250 | 110 | 140 | 72 | 50 | 580 | 340 | 21 | 96 | 7 | 0.10 |
| T.545 | 30.90 | 8.00 | 0.13 | 0.08 | 230 | 450 | 210 | 270 | 130 | 160 | 100 | 49 | 520 | 470 | 19 | 153 | 7 | 0.10 |
| T.346A | 31.10 | 3.50 | 0.25 | 0.10 | 500 | 1 230 | 156 | 250 | 100 | 140 | 2 | 100 | 560 | 450 | 22 | 73 | 8 | 0.40 |
| T.15A | 33.30 | 6.90 | 0.21 | 0.11 | 110 | 600 | 161 | 300 | 110 | 180 | 94 | 55 | 570 | 380 | 22 | 63 | 10 | 0.40 |
| T.534 | 35.70 | 9.80 | 0.37 | 0.13 | 66 | 4 770 | 218 | 300 | 160 | 220 | 120 | 42 | 930 | 560 | 17 | 94 | 11 | 0.10 |
| T.296 | 35.90 | 9.30 | 0.50 | 0.15 | 100 | 2 900 | 210 | 360 | 160 | 240 | 130 | 220 | 1 200 | 700 | 24 | 92 | 8 | 0.00 |
| T.188B | 36.80 | 10.10 | 0.38 | 0.15 | 1 700 | 4 200 | 286 | 400 | 200 | 200 | 88 | 240 | 500 | 500 | 42 | 166 | 9 | 0.10 |
| T.512B | 38.00 | 10.50 | 0.53 | 0.15 | 100 | 2 520 | 238 | 330 | 170 | 210 | 79 | 99 | 560 | 550 | 33 | 93 | 5 | 0.00 |
| T.512A | 38.50 | 10.20 | 0.39 | 0.14 | 190 | 3 000 | 183 | 420 | 200 | 220 | 76 | 340 | 610 | 580 | 34 | 95 | 5 | 0.10 |
| Average | 28.11 | 6.49 | 0.25 | 0.10 | 337 | 1 508 | 149 | 246 | 112 | 145 | 52 | 98 | 574 | 399 | 19 | 164 | 7 | 0.42 |

**Table 3.6** (cont.)

| Sample | S | Ni | Cu | Co | Pt | Pd | Rh | Ru | Ir | Os | Re | Au | Cr | Zn | Se | As | Mo | C |
|---|---|---|---|---|---|---|---|---|---|---|---|---|---|---|---|---|---|---|
| No | wt% | wt % | wt % | wt % | ppb | ppb | ppb | ppb | ppb | ppb | ppb | ppb | ppm | ppm | ppm | ppm | ppm | wt % |
| ***Enriched sedimentary sulfides*** | | | | | | | | | | | | | | | | | | |
| T.273 | 19.50 | 5.80 | 0.50 | 0.08 | 54 | 760 | 39 | 31 | 11 | 5 | 2 | 61 | 160 | 310 | 3 | 64 | 9 | 2.20 |
| T.436 | 19.90 | 1.80 | 0.07 | 0.02 | 13 | 450 | 7 | 11 | 3 | 4 | 14 | 30 | 29 | 190 | 8 | 6 | 19 | 4.00 |
| T.522 | 21.60 | 3.50 | 0.21 | 0.06 | 24 | 760 | 69 | 19 | 14 | 17 | 29 | 26 | 160 | 220 | 9 | 85 | 19 | 3.10 |
| T.212A | 21.80 | 3.50 | 0.04 | 0.06 | 34 | 600 | 30 | 30 | 8 | 7 | 9 | 60 | 66 | 190 | 8 | 46 | 14 | 1.90 |
| T.512C | 27.60 | 6.60 | 0.60 | 0.12 | 150 | 600 | 91 | 70 | 28 | 30 | 2 | 635 | 140 | 310 | 10 | 56 | 25 | 5.60 |
| T.426 | 31.60 | 10.90 | 0.56 | 0.09 | 40 | 1 750 | 6 | 6 | 3 | 5 | 12 | 15 | 5 | 470 | 7 | 122 | 19 | 3.10 |
| T.549 | 32.20 | 10.50 | 0.88 | 0.11 | 100 | 2 070 | 60 | 38 | 19 | 11 | 33 | 210 | 44 | 420 | 7 | 122 | 17 | 3.50 |
| T.425A | 32.90 | 5.20 | 0.40 | 0.07 | 18 | 990 | 14 | 23 | 5 | 6 | 57 | 13 | 0 | 280 | 17 | 64 | 34 | 1.90 |
| Average | 25.89 | 5.98 | 0.41 | 0.08 | 54 | 998 | 40 | 29 | 11 | 11 | 20 | 131 | 76 | 299 | 9 | 71 | 20 | 3.16 |

son or Bucko Lake. This feature was first pointed out by Naldrett et al. (1979). Except for Au, the Bucko Lake ores are significantly richer in all metals when compared with the other deposits. Bucko Lake is located in the southern part of the belt within high grade gneisses. It is interpreted as part of a feeder system (Good and Naldrett 1993) for ultramafic rocks which originally occurred in Proterozoic supracrustal rocks analogous to those farther north at Thompson. Sulfides are very sparse in the enclosing gneisses and this may be the reason that a higher R factor, and thus higher tenor sulfides were developed at Bucko than elsewhere.

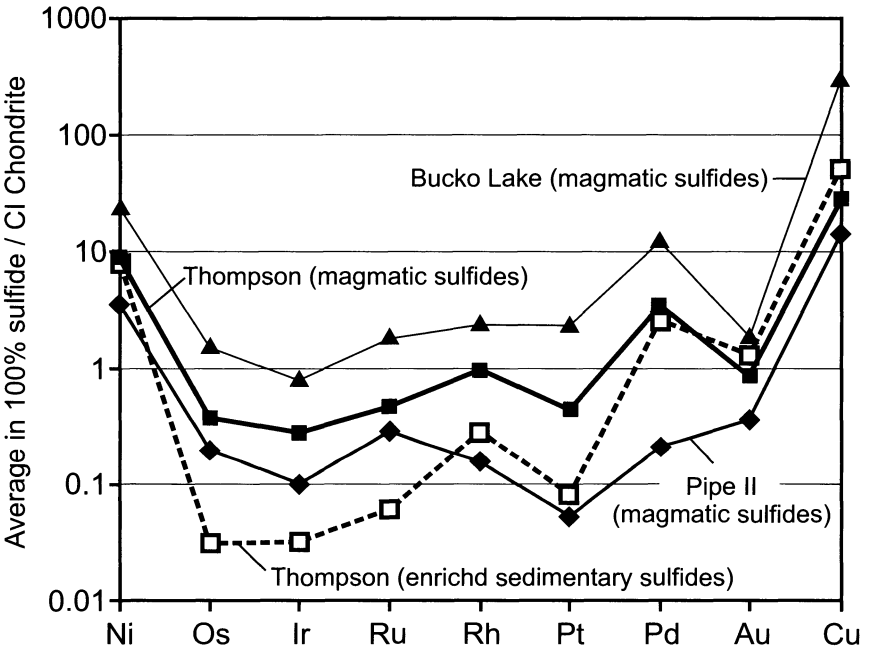


**Fig. 3.38**. Average contents of PGE, Au, Ni, and Cu (normalized to CI Chondrite) in ores of some deposits of the Thompson Nickel Belt. Ore compositions are recalculated to 100% sulfide. Data on Thompson after Bleeker (1989), on Pipe II from Naldrett et al. (1979) and on Bucko Lake from Goode and Naldrett (1993)

### *Genesis of Ni Sulfide Mineralization in the Thompson Nickel Belt*

Chemical, textural and field observations indicate a magmatic origin for the bulk of Ni sulfides ores. Nevertheless the presence of an external sulfur source, such as the two horizons of sulfide facies iron formation that have

been referred to above, appears to have been a controlling factor in the generation of the voluminous magmatic sulfides.

A clear link between sedimentary sulfides and the nickeliferous magmatic sulfides is provided by Se/S ratios of the various sulfides (Eckstrand et al. 1989). In terms of this ratio, Ni sulfide ores of the Thompson Nickel Belt show a mixing trend between mantle ratios and the Se-depleted ratios of the sedimentary sulfides (Fig. 3.39), suggesting that on average as much as 80 % of the ore sulfide was derived from the sedimentary sulfide source. Addition of sedimentary sulfide may also have caused a slight positive shift in $\delta^{34}S$ values.

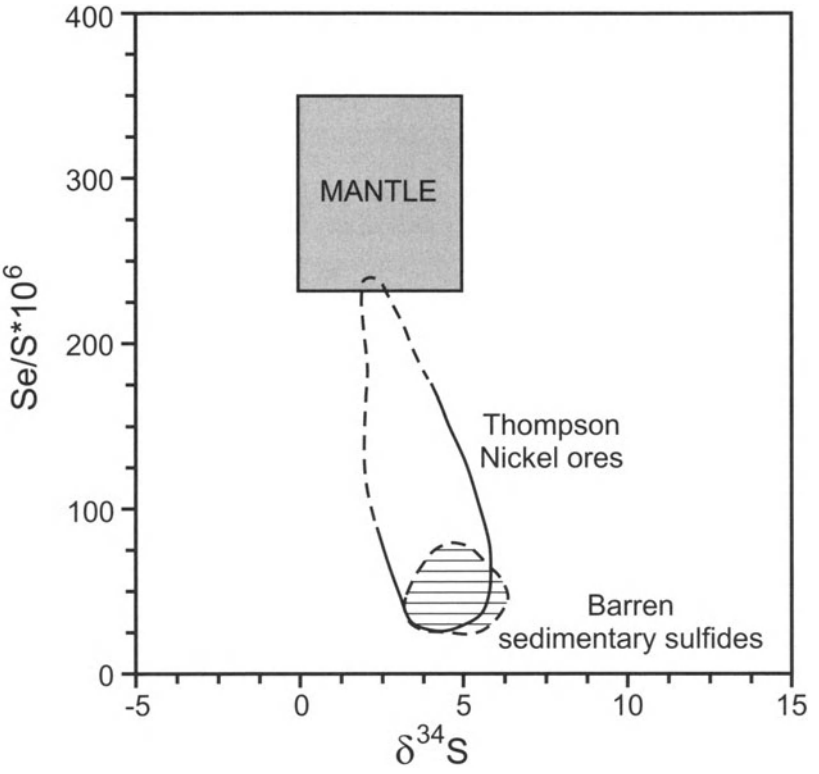


**Fig. 3.39.** Se/S and $\delta^{34}S$ data for Ni sulfide ore and barren sedimentary sulfides from the Thompson Nickel Belt (after Eckstrand et al. 1989)

Bleeker (1990) studied the nature of the igneous bodies that host the ores and concluded that the available evidence favors a sill rather than a volcanic origin. He proposed that the ultramafic sills may have acted as magma chambers to some of the overlying volcanics (Fig. 3.40).

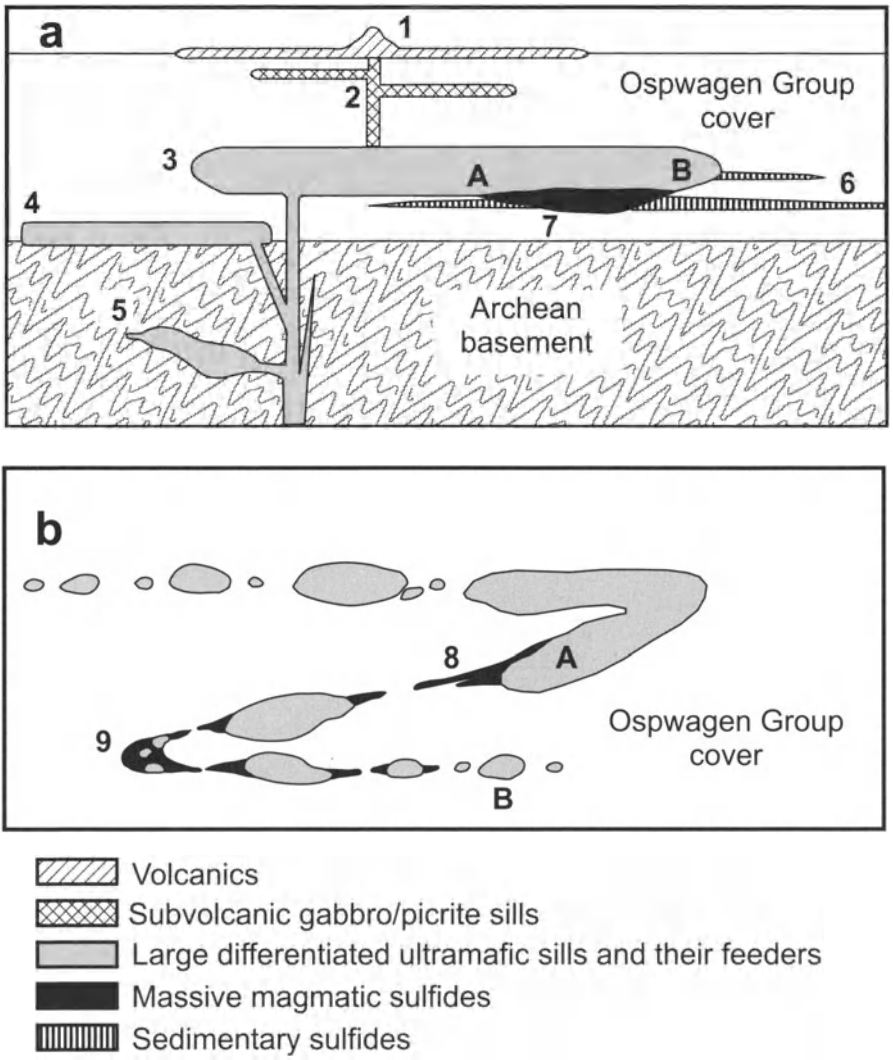


**Fig. 3.40.** Model for the formation of the sulfide Ni deposits of the Thompson Nickel Belt, (a) at the magmatic stage of the development and (b) after folding and deformation. After Bleeker (1990). Numbers and letters, written in the Figure are explained in text

Bleeker (1990) argued that a second important process that has contributed to the mineralization is the redistribution of Ni and to a lesser extent of other metals such as Co and Cu during medium to high grade metamorphism. Graphitic sedimentary sulfides, barren at relatively large distances from known Ni ore bodies (< 1000 ppm Ni), show elevated Ni concentrations in proximity to Ni ore bodies. Ni enrichment varies from slightly

over 1000 ppm to 10 wt% and shows an inverse correlation with distance from the main ore zone. Sedimentary sulfides in close proximity to magmatic sulfides are characterized by Ni and Ni/Co values which have completely equilibrated with the respective values in these magmatic sulfides. Cr concentrations have remained distinct. On approaching magmatic sulfide ore zones, Ni/Co increases from typical "barren" sedimentary values (2.5 to 7.0) to the magmatic ratios (e.g. Pipe II = 22; Thompson = 50) of adjacent magmatic sulfides. Bleeker noted that Ni redistribution is much more extensive at Thompson than at Pipe II, and thus correlates with metamorphic grade. He suggested that the redistribution occurred during metamorphism.

Note, as described in Chapter 6, this author has studied core from the Pants Lake mineralization 80 km south of Voisey's Bay, where olivine gabbro magma has come into contact with underlying pyrrhotite-rich sediment. The regional metamorphic grade is very low (zeolite facies) so that extensive diffusion during metamorphism is unlikely. The sulfides contain many flakes of graphite, and looks "dirty" in hand specimen or polished section. The sulfide can be seen becoming melted and incorporated in the troctolite, whereupon its pentlandite content increases and it loses the graphite which gives it its "dirty" appearance. However, as described in Chapter 6, the appearance of pentlandite is not restricted to the fresh-looking sulfides, but can be seen developing several feet below the base of the fresh, melted sulfide. Thus it is this author's opinion that Ni, and likely other metals, can diffuse into and react with sedimentary sulfide at the time of intrusion, and that it is not necessary for a high grade metamorphic event for this process to occur.

Bleeker 's (1990) model for the genesis of the deposits of the TNB is shown in Fig. 3.40. He suggested that ore-forming ultramafic magmatism occurred near the end of Ospwagan Group deposition, associated with the emplacement of mafic to ultramafic volcanics (1) and the intrusion of subvolcanic gabbro/picrite sills (2). Large ultramafic sills deeper in the cover sequence and more irregular bodies within the basement (3, 4 and 5) are thought to be related to the volcanics. He proposed that some of the sills acted as magma conduits to some of the volcanics. Locally, sills intruded along sulfide facies iron formation (6), reacting with the sulfide between points A an B in Fig. 3.40a, and giving rise to large concentrations of magmatic sulfides (7). Stretching and folding of the parent sills occurred during orogenesis, leading to "passive" remobilization of sulfides along the host horizon (Fig. 3.40b). He noted that massive sulfide tends to be concentrated at the necks between boudins ( e.g. Pipe II, 8) and as completely separated lenses between larger boudins; (9; such as

some of the ore lenses at Thompson), but do not occur beyond the original boundaries, A and B, of the ultramafic body.

# 4 Ore deposits associated with flood basalt volcanism

Flood basalt volcanism is a feature of the later stages of the Earth's evolution, beginning in the mid to late Proterozoic. Specific episodes are characterized by the immense areas that they cover (commonly hundreds of thousands $km^2$) and the short duration of the magmatic activity (up to 15 My in the Proterozoic and, typically, 1-2 My in the Phanerozoic). Lava facies dominate over explosive and intrusive facies and uniform tholeiitic basalts predominate among the rock types. The flood basalt provinces are typically, but not universally, equant in shape. These eruptions represent the most catastrophic igneous events in the Phanerozoic history of the earth. The magmatism occurred both in oceanic and continental environments. Oceanic flood-basalt provinces can be much more extensive than continental provinces. The largest oceanic province (the Outang-Java plateau) comprises over 60 millions $km^3$ (Mahoney and Coffin, eds 1997) while the largest continental province (the Siberian trap) comprises about 4 millions $km^3$ (Masaitis 1983) (see Fig. 4.1). However continental flood-basalt events had the greater effect on geological history because they resulted in ecological catastrophes that brought with them major mass extinctions. The Siberian trap define the biostratigraphic boundary between the Paleozoic and Mesozoic (Czamanske et al. 1998 and their references), the Karoo-Ferrar between the Lower and Middle Jurassic (Duncan et al. 1997), and the Deccan – between the Mesozoic and Cenozoic (e.g. Courtillot et al., 1986, 1988).

In recent years, it has been proposed that flood-basalt volcanism is the result of mantle plumes (e.g. Richards et al., 1989; Campbell and Griffiths, 1990; Griffiths and Campbell, 1991). However numerical modeling by Farnetani and Richards. (1994) have demonstrated that a plume fitted for a flood-basalt province such as the Siberian trap would have had a "head" radius of 400 km and have been superheated as much as 350° C. This would have caused an uplift of 2-4 km height, that would have been developing for tens of millions of years prior to the advent of volcanism. There is no reliable evidence available as to whether such uplifts developed in the majority of flood-basalt provinces. However, Czamanske et al. (1998)

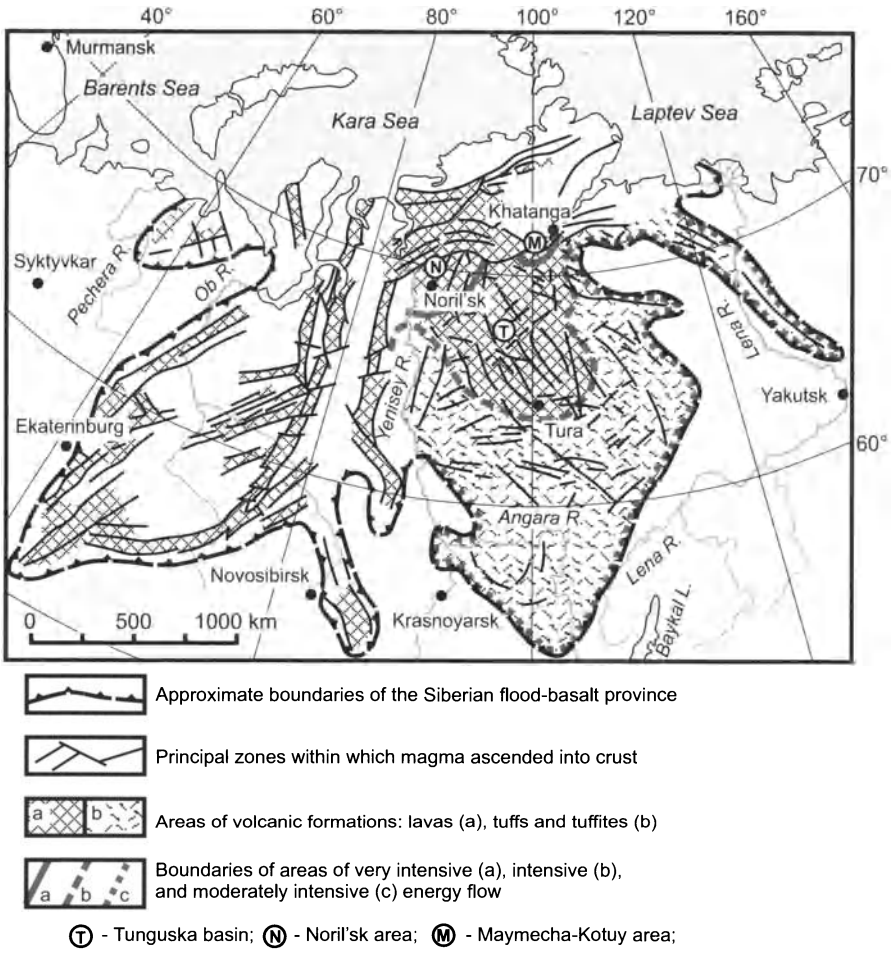


**Fig. 4.1.** Plan of the reconstruction of the Siberian flood-basalt province (simplified after Masaitis, 1983)

have demonstrated that the Siberian platform was a low plain (close to sea level in elevation) for tens of My before volcanism (at Tungusskaya time) and at the time of the lava eruptions. They concluded that, since uplift did not develop, the plume could not have existed. They adopted the model of Anderson (1994) and King and Andersen (1995) that attributes flood basalt provinces to lithospheric pull apart at Precambrian craton boundaries. The split that caused the Siberian volcanism passed, most likely, along the western boundary of the Siberian platform, and was most active in the region of Noril'sk. In answering the question as to how this split could have caused extension and volcanism over an area of many hundreds of km$^2$, Czamanske et al. cite the paleodynamic reconstruction of Segnor et al.

(1993), who suggested that the flood-basalt volcanism may have been related to the reversal from right-lateral shear to left-lateral shear between the Baltic and Siberian cratons that took place at the end of the Paleozoic. Such a major structural reversal could have caused extension far from the craton boundary.

Farnetani and Richards (1994) calculations do not take into account a continental-type lithosphere above the plume head, and its presence at Noril'sk would modify their estimates as to the amount of uplift to be expected. It would seem that the question as to whether a plume was, or was not the cause of the Siberian trap remains unresolved at this juncture.

Intrusions related to flood basalts in the Noril'sk region of Siberia and to the Keewanawan magmatism of the Lake Superior area contain two out the three largest accumulations of magmatic sulfide discovered so far. Intrusions of this type therefore constitute a very important exploration target. As explained below, this author considers that the mineralized intrusions fed volcanic eruptions at both of these localities. Information as to how the magmas developed immiscible sulfides, and how these sulfides came to be localized where they are, is critical to the development of exploration strategies.

## 4.1 Ni-Cu-PGE deposits of the Noril'sk region, Siberia

The Ni-Cu deposits of the Noril'sk region comprise, along with those at Sudbury, Canada, the two largest economic concentration of Ni in the world and far exceed all other deposits in size (see Fig. 1.3). The Noril'sk deposits also rank with the deposits of the Bushveld complex and Great Dyke in terms of their content of PGE (see Fig. 1.4). This places them in the almost unique situation of being important both for their Ni and PGE, rather than one or the other (Fig. 1.1, Table 1.1). This aspect is also brought out by their high (Pt+Pd)/(Ni+Cu) ratios (PGE in g/t, Ni and Cu in wt%) of between 1 and 5 , in comparison with ratios of between 0.05 and 0.5 which characterize most gabbro-related deposits (Appendix). It is also notable that the Noril'sk deposits exceed all other deposits (both Ni-Cu and PGE deposits) in the value of in situ metals per tonne of ore (Table 1.1). The huge resources of Noril'sk are concentrated principally in the Talnakh ore junction, which is an area only 8x18 km in extent, in comparison with the 30x60 km of extent of the Sudbury structure and 280x450 km area underlain by rocks of the Bushveld complex.

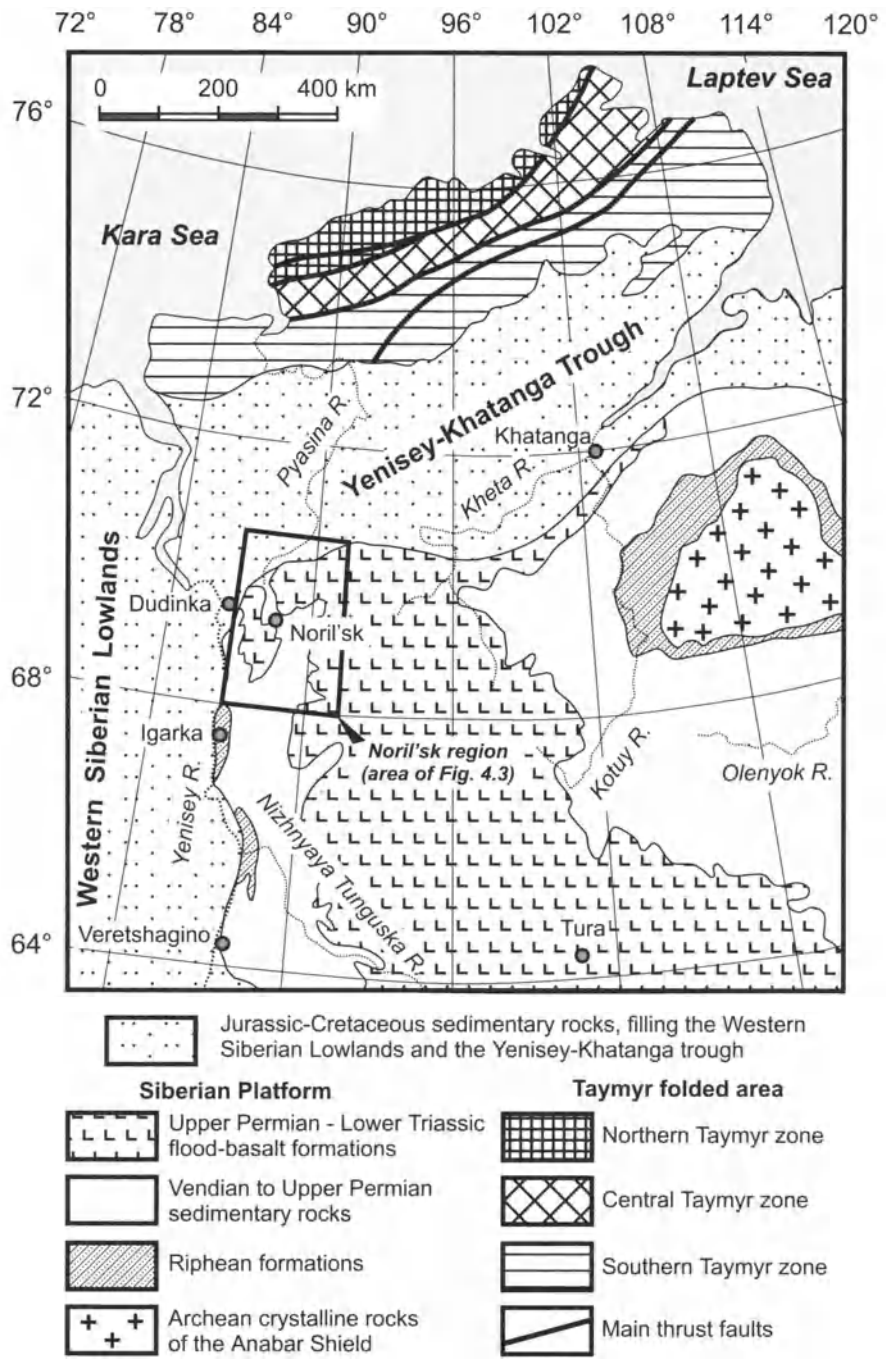


**Fig. 4.2.** Regional map of North-Central Siberia showing the position of the Noril'sk region.

### 4.1.1 Geological Setting

The deposits occur at the extreme northwestern corner of the Siberian platform at the boundary with the Yenisey-Khatanga trough to the north and the Western Siberian lowland to the west (Fig. 4.2). The tectonics of this region (the Noril'sk region) is dominated by a series of positive and negative structures and major fault zones (Fig. 4.3). Most faults trend either in a northeasterly direction or east northeast, with a few faults trending north northwest.

Important from the point of view of mineralization are the Noril'sk-Kharaelakh and Imangda faults, which are both north northeast-trending, and the North Kharaelakh fault which forms the southern boundary of the Yenisey-Khatanga trough. Seismic evidence indicates that these major faults extend to the base of the crust (Rempel 1994).

Both Rempel (1994) and Simonov et al. (1994) emphasized the difference between the structure of the Precambrian basement underlying the Noril'sk region and the remainder of the Siberian platform. Outside the Noril'sk region, the basement is Archean and is overlain by thin, relatively undisturbed Proterozoic and Paleozoic sediments. A north-south trending trough occupied the Noril'sk area during the Riphean (Late Proterozoic), and the thick strata that accumulated within it were deformed during an orogeny that was preceded by volcanism. Subsidence continued in the region during the Vendian and Paleozoic. The latter is marked by three cycles of marine transgression and regression, each involving the deposition of dolomite, limestone and argillite of marine origin overlain by calcareous and dolomitic marl, dolomite and sulfate-rich evaporite in each cycle. Devonian- and Lower Carboniferous-aged evaporites of the last cycle were succeeded after structural deformation by the terrigenous, coal-bearing, Tungusskaya series (up to 600 m thick) and up to 3500 m of Upper Permian – Lower Triassic flood basalt. The stratigraphy of the upper part of the Paleozoic sedimentary rocks at the Noril'sk and Talnakh ore junctions is shown in Fig. 4.4.

A surprising result has been obtained from the study (Czamanske et al., 2000) of xenoliths brought up by a diatreme, Maslov's diatreme, situated 25 km south of the city of Noril'sk and just east of the Noril'sk-Kharaelakh fault. The diatreme is thought, on the basis of stratigraphy, to be very close in age to the 251Ma flood basalt activity at Noril'sk. Of the fragments obtained from it, one rhyodacite sample contained zircons that gave a SHRIMP U-Pb age of 270 Ma. This sample is unlike any of the Siberian trap volcanic rocks and is interpreted to indicate that subduction/underthrusting occurred to the east, from the West Siberian Lowlands beneath the northwest edge of the Siberian craton in late Permian time.

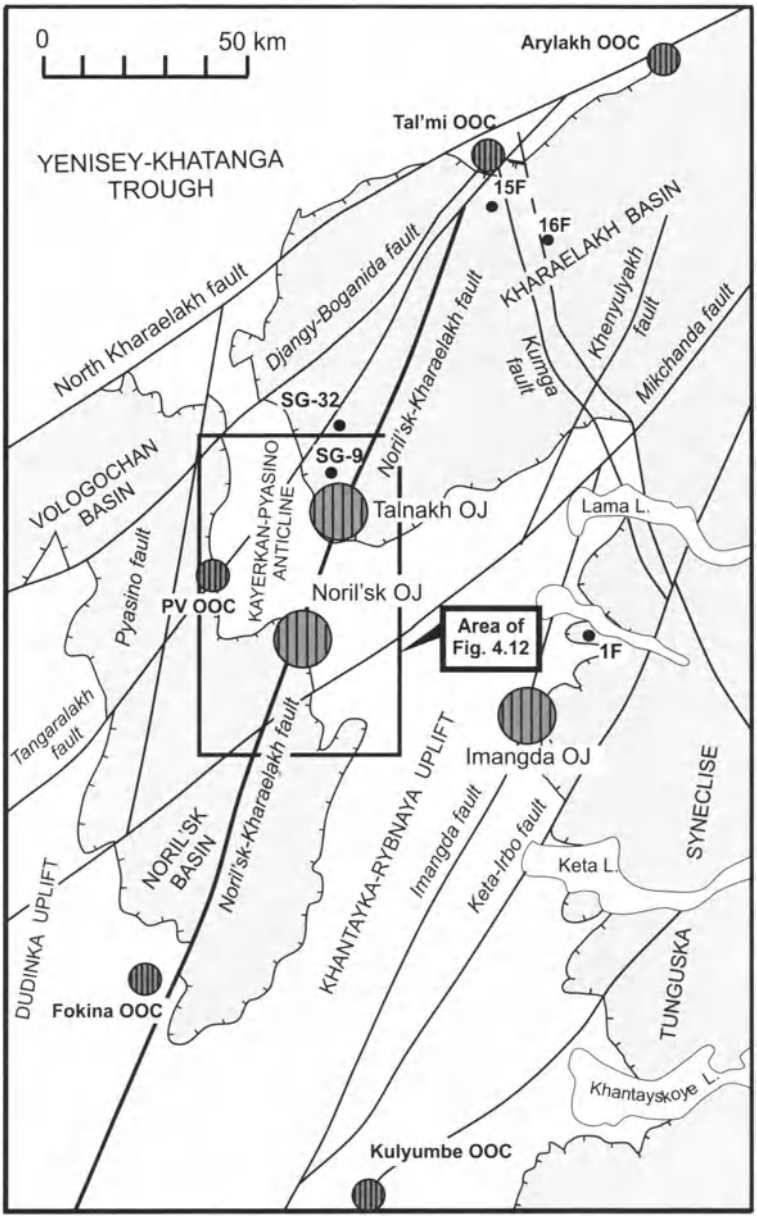


**Fig. 4.3.** Main structural elements of the Noril'sk region where locations of Ore Junctions (OJ), Ore-Occurrence Clusters (OOC), and sampled sections of the volcanic formations (boreholes SG-9, SG-32, exposures 1F, 15F, 16F) are shown. Modified after Naldrett et al. (1992)

PV OOC = Pyasino-Vologochan Ore-Occurrence Cluster

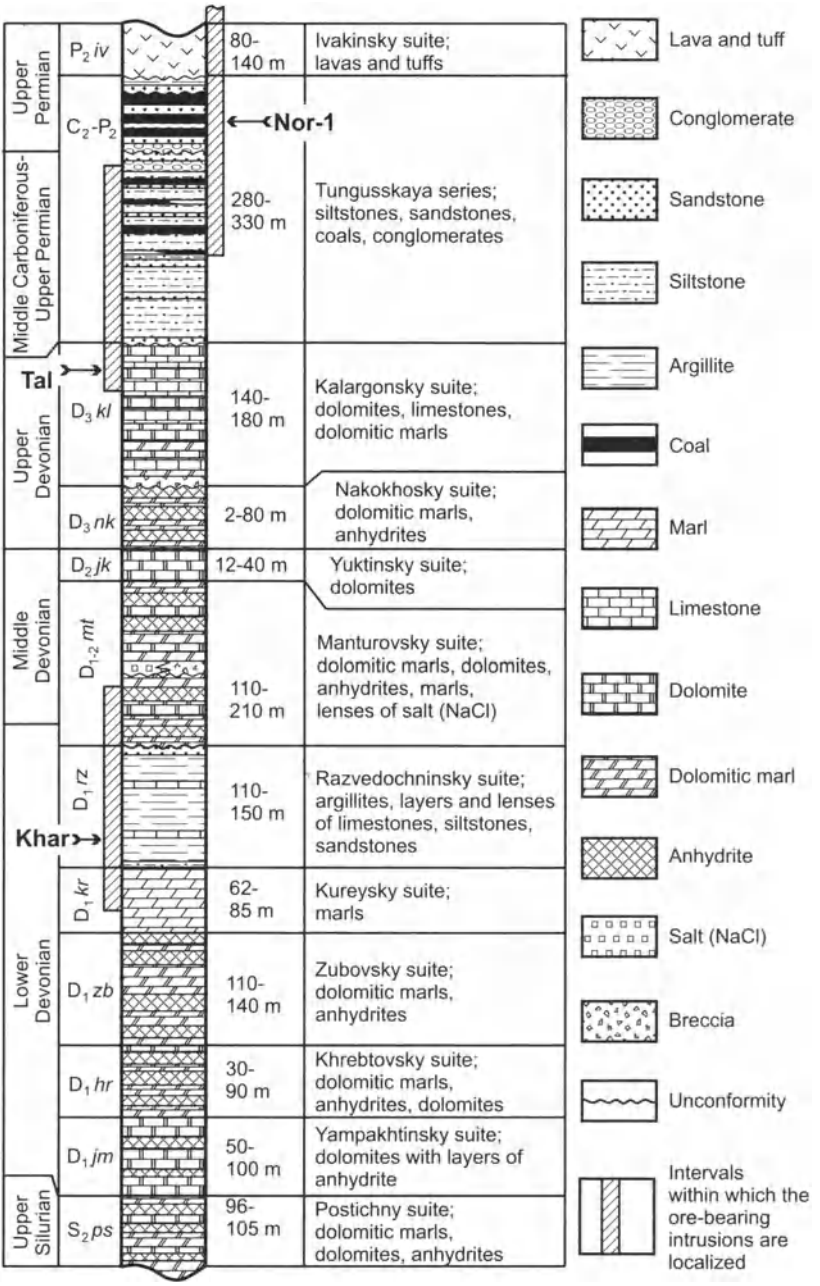


Ore-bearing intrusions: **Nor-1** - Noril'sk-1; **Tal** - Talnakh; **Khar** - Kharaelakh

**Fig. 4.4.** Stratigraphy of upper part of Paleozoic sedimentary rocks at Noril'sk and Talnakh ore junctions showing the positions of the ore-bearing intrusions. After Czamanske et al. (1995)

### 4.1.2 Permo-Triassic Volcanism

The Noril'sk Cu-Ni sulfide deposits are associated with a group of ultramafic-mafic intrusions that are part of the Permo-Triassic basalt volcanism.

The largest basin occupied by the Siberian Trap is the Tunguska basin in which the thickness of the volcanic succession is 2000-3000 m and in which lavas predominate over tuffs. Two areas of more intense magmatism are located to the north: the Noril'sk and Maymecha-Kotuy basins. These are distinguished by greater thicknesses of volcanic rocks (3500 m at Noril'sk and 4000 m at Maymecha-Kotuy) and a greater variability in the composition of the lavas and intrusions. While the Tunguska basin consists almost entirely of tholeiitic basalt; picritic, alkalic and sub-alkalic basalts are present, along with tholeiites in the lower part of the succession in the Noril'sk area (see Fig. 4.5 below) together with differentiated mafic-ultramafic intrusions, some of which host Cu-Ni mineralization. The Maymecha-Kotuy area is unique in that alkaline-ultramafic lavas and intrusions (with carbonatites) are widely developed. U-Pb dating by Kamo et al. (2000) has shown that all of the highly divergent basalt compositions of these two areas were formed during 1.5 My from 251.7±0.5 to 250.2±0.3 Ma. The peak of the magmatism coincides with the biostratigraphic boundary between the Permian and Triassic that, in the China stratotype, has been dated at 251.2±0.3Ma (Bowring et al 1998). It was at precisely this time (251.2±0.3) that the ore-bearing intrusions of the Noril'sk region were formed (Kamo et al. 1996).

On a regional scale, the magmatic activity in Siberia appears to have been focussed along discrete lineaments (Fig. 4.1). The principal magma-controlling structures in the Noril'sk area were the North Kharaelakh, Noril'sk-Kharaelakh, and Imangda faults shown in Fig. 4.3. Isopach maps of the thicknesses of different lava units (Fedorenko 1979; Naldrett et al. 1992) indicate that the center of magmatism moved with time being located within the Noril'sk area during eruption of the lower formations, and then, at the close of the Morongovsky, migrating to the northeast.

#### *Stratigraphy of the volcanic sequence*

Volcanic rocks overly the terrigenous coal-bearing Tungusskaya Series (Middle Carboniferous –Upper Permian) without an angular disconformity. In some areas, erosion of the uppermost Tungusskaya amounts to several tens to 300 m, although erosion is absent in other areas. In the central part of Noril'sk area, a locality has been described where sedimentary rocks and tuffs are interlayered at the boundary between the Tungusskaya

and the lowermost suite of the volcanic sequence (Distler and Kunilov 1994).

Eleven suites are recognized in the 3500 m vertical thickness of extrusive rocks at Noril'sk, which, from the base to the top, are (Distler and Kunilov 1994):

1. The Ivakinsky (***Iv***) suite comprising 1 to 25 flows of alkaline and subalkaline lavas, which amount to up to a total stratigraphic thickness of 475 m. Alkaline trachybasalts (***Iv$_1$***) occur at the base of the suite, and are overlain by subalkaline, titanium-augite, labradorite, and two-plagioclase basalts (***Iv$_{2-3}$***).
2. The Syverminsky (***Sv***) suite comprising up to 20 flows (maximum stratigraphic thickness ~195 m) of tholeiitic basalt.
3. The Gudchikhinsky (***Gd***) suite of which the lower part (***Gd$_1$***) comprises 1 to 10 flows of glomeroporphyritic to porphyritic tholeiitic basalt (maximum total thickness ~120 m) and the upper part (***Gd$_2$***) 1–27 flows of picritic and olivinephyric basalt with a total thickness of 190 m.
4. The Khakanchansky (***Hk***) suite that comprises 18–25 m of tuffite with rare intercalated flows. In general, the Khakanchansky tuffite is of andesitic composition, while the intercalated flows resemble the overlying Tuklonsky or Lower Nadezhdinsky basalts in composition.
5. The Tuklonsky (***Tk***) suite only occurs in the eastern part of the Noril'sk region, and consists of 8–10 flows of poikilophitic tholeiitic basalt, in many places intercalated with Khakanchansky tuffite. The total thickness amounts to 220 m, including 1 to 3 flows (60–65 m) of picritic basalt.
6. The Nadezhdinsky (***Nd***) suite of tholeiitic basalts, that is sub-divided into: (a) The Lower Nadezhdinsky (***Nd$_1$***) subsuite, that consists of 10 to 14 flows (50-260 m) of porphyritic and aphyric basalt; (b) The Middle Nadezhdinsky (***Nd$_2$***) subsuite comprising 5 to 12 flows (75-260 m) of porphyritic basalt; (c) The Upper Nadezhdinsky (***Nd$_3$***) subsuite that consists of 1 to 8 flows (25–150 m) of glomeroporphyritic basalt (the lowermost flow commonly has porphyritic texture) with a layer of tuff at the base.
7. The Morongovsky (***Mr***) suite of tholeiitic basalts, that is subdivided into: (a) The Lower Morongovsky (***Mr$_1$***) subsuite that comprises several flows of generally aphyric basalt (45–150 m); (b) The Upper Morongovsky (***Mr$_2$***) subsuite of generally poikilophitic and aphyric basalt (175–320 m).
8. The Mokulaevsky (***Mk***) suite – tholeiitic basalts of porphyritic, glomeroporphyritic, and poikilophitic texture. Thickness 400–670 m.

9. The Kharaelakhsky (***Hr***) suite – tholeiitic basalts with poikilophitic, aphyric, and, very occasionally, porphyritic and glomeroporphyritic texture. Thickness 475–600 m.
10. The Kumginsky (***Km***) suite – tholeiitic basalts with glomeroporphyritic texture. Thickness 475–600 m.
11. The Samoedsky (***Sm***) suite – tholeiitic basalts of porphyritic, poikilophitic and aphyric texture. Thickness up to 600 m.

Variations in the lower part of the volcanic sequence from the base to the bottom of the Kharaelakhsky suite, based on borehole SG-9 at the Talnakh ore junction and exposure 1F in the eastern part of the Noril'sk region are illustrated in Fig. 4.5.

During the 1990's the entire sequence of the volcanic formations was characterized in detail in terms of major, trace element and isotope geochemistry (Lightfoot et al. 1990, 1993, 1994; Naldrett et al. 1992; Wooden et al. 1993; Fedorenko 1994; Hawkesworth et al., 1995; Fedorenko et al. 1996; Lightfoot and Hawkesworth 1997). Average compositions of the different lavas, subdivided stratigraphically and on the basis of their geochemistry, are shown in Table 4.1.

Naldrett et al. (1992) reviewed the major, trace element and isotopic data and suggested that 5 major magma types had been involved in the formation of the traps of the Noril'sk region. From earliest to latest, these are: (1) the Ivakinsky and Syverminsky magma type of alkalic to subalkalic affinity; (2) the Gudchikhinsky type, which gave rise to picritic basalts, and in general has high concentrations of Ni; (3) the primitive, but slightly Ni-depleted Tuklonsky magma type; (4) the very chalcophile-depleted Lower (and Middle) Nadezhdinsky magma type, which is LREE-enriched and has low Nd and high Sr isotopic ratios; and (5) the Mokulaevsky type, which is primitive, with some similarities to and some major differences from the Tuklonsky (see Wooden et al. 1993; Fedorenko et al. 1996; Lightfoot and Naldrett 1999). All lavas from the Upper Morongovsky subsuite to the Samoedsky suite belong to the last, Mokulaevsky magma-type. The Upper Nadezhdinsky and the Lower Morongovsky consist of flows that are geochemically transitional between the Lower-Middle Nadezhdinsky (type 4) and the Upper Morongovsky that resembles type 5, the Mokulaevsky magma-type. The above magma types, and the 11 formations within which they are represented, have been grouped into 2 principal extrusive associations, the second of which is sub-divided into two (Lightfoot at al., 1993; Naldrett et al., 1995). These are: Association I comprising the Ivakinsky (***Iv***), Syverminsky (***Sv***) and Gudchikhinsky (***Gd***); Association IIA comprising the Tuklonsky (***Tk***) and Lower-Middle Nadezhdinsky ($Nd_{1\text{-}2}$); and Association IIB comprising the Upper Moron-

govsky to Samoedsky (***$Mr_2$-Sm***). The Upper Nadezhdinsky and Lower Morongovsky (***$Nd_3$-$Mr_1$***) are transitional in composition between Associations IIA and IIB.

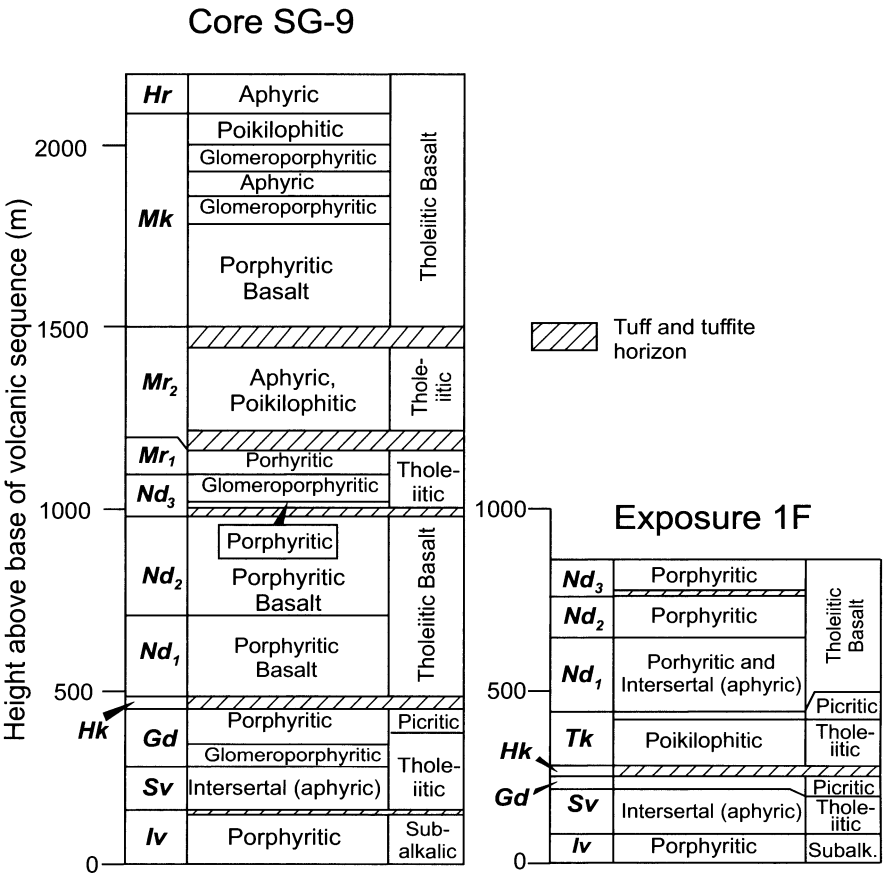


**Fig. 4.5.** Volcanic formations comprising the succession in the Noril'sk region, showing variation in texture and rock type in drill core SG-9 (from the base up to the lower part of the Kharaelakhsky suite) and exposure 1F (from the base up to the upper part of the Nadezhdinsky suite). Abbreviations: ***Iv*** = Ivakinsky, ***Sv*** = Syverminsky, ***Gd*** = Gudchichinsky, ***Hk*** = Khakanchansky, ***Tk*** = Tuklonsky, ***$Nd_1$*** = Lower Nadezhdinsky ***$Nd_2$*** = Middle Nadezhdinsky ***$Nd_3$*** = Upper Nadezhdinsky, , ***$Mr_1$*** = Lower Morongovsky, ***$Mr_2$*** = Upper Morongovsky, ***Mk*** = Mokulaevsky. Modified after Naldrett et al. (1995)

**Table 4.1.** Average chemical compositions of main volcanic rock types from the Noril'sk region (after published data by Lightfoot, Wooden, Naldrett, Czamanske, Hawkesworth, Brugmann, and Horan, compiled by Fedorenko et al., 1996)

| Unit | *Iv*$_1$ | *Iv*$_2$ | *Iv*$_3$ | *Sv* | *Gd*$_1$ | *Gd*$_2$ |
|---|---|---|---|---|---|---|
| n* | 3(3) | 4(3) | 9(5) | 23(8) | 7(4) | 28(9) |
| $SiO_2$ | 47.35 | 50.74 | 53.29 | 53.17 | 50.86 | 48.58 |
| $TiO_2$ | 3.79 | 2.35 | 2.33 | 1.67 | 1.76 | 1.54 |
| $Al_2O_3$ | 15.48 | 15.62 | 15.25 | 15.79 | 17.05 | 10.26 |
| FeOT | 14.72 | 13.65 | 12.23 | 10.14 | 10.07 | 13.37 |
| MnO | 0.19 | 0.24 | 0.20 | 0.15 | 0.15 | 0.18 |
| MgO | 4.67 | 4.67 | 3.33 | 6.18 | 6.53 | 15.85 |
| CaO | 7.03 | 6.47 | 6.82 | 7.98 | 9.36 | 8.37 |
| $Na_2O$ | 3.77 | 4.05 | 3.32 | 3.30 | 3.19 | 1.50 |
| $K_2O$ | 1.68 | 1.51 | 2.43 | 1.36 | 0.82 | 0.22 |
| $P_2O_5$ | 1.33 | 0.70 | 0.80 | 0.25 | 0.20 | 0.13 |
| LOI | 5.14 | 3.77 | 2.31 | 3.85 | 3.16 | 6.64 |
| V | n.d. | 114 | 123 | 177 | 189 | 232 |
| Sc | 21 | 21 | 23 | 23 | 25 | 22 |
| Cr | 13 | 23 | 45 | 209 | 221 | 819 |
| Y | 53 | 40 | 47 | 26 | 23 | 16 |
| Ni | 43 | 36 | 19 | 59 | 74 | 696 |
| Co | 39 | 31 | 25 | 35 | 37 | 70 |
| Cu | 37 | 24 | 26 | 34 | 58 | 107 |
| Pd (ppb) | <0.5 | <0.5 | <0.5-4.9 | <0.5-<2 | <0.5-2.7 | 6.9 |
| Pt (ppb) | <0.5-<0.7 | <0.5-<1 | <0.5-<1 | <0.5-3 | <0.5-5.8 | 8.8 |
| Ru (ppb) | <0.5 | <0.5 | <0.5 | <0.5 | <0.5 | 2.5 |
| Rb | 31.33 | 33.03 | 46.51 | 35.16 | 18.93 | 5.31 |
| Sr | 315 | 545 | 425 | 432 | 453 | 156 |
| Ba | 807 | 869 | 941 | 592 | 344 | 120 |
| Th | 5.683 | 3.592 | 5.748 | 3.303 | 1.381 | 0.904 |
| U | 2.427 | 0.916 | 1.446 | 0.852 | 0.325 | 0.336 |
| Ta | 2.223 | 1.239 | 1.526 | 0.855 | 0.580 | 0.398 |
| Zr | 367 | 264 | 351 | 193 | 141 | 85 |
| Hf | 7.083 | 6.046 | 8.348 | 4.885 | 3.35 | 2.271 |
| La | 48.37 | 37.48 | 49.24 | 23.20 | 14.4 | 6.61 |
| Ce | 108.00 | 84.77 | 108.66 | 50.85 | 32.8 | 17.37 |
| Nd | 51.77 | 43.91 | 54.58 | 25.59 | 18.5 | 11.61 |
| Sm | 10.41 | 9.47 | 11.36 | 5.70 | 4.54 | 3.22 |
| Eu | 2.677 | 2.659 | 3.112 | 1.793 | 1.61 | 1.105 |
| Gd | 9.453 | 9.175 | 10.232 | 5.375 | 4.68 | 3.458 |
| Tb | 1.420 | 1.364 | 1.567 | 0.832 | 0.739 | 0.548 |
| Yb | 4.370 | 3.557 | 4.136 | 2.338 | 1.85 | 1.304 |
| Lu | 0.636 | 0.521 | 0.594 | 0.347 | 0.270 | 0.181 |
| Gd/Yb | 2.16 | 2.58 | 2.47 | 2.30 | 2.53 | 2.65 |
| La/Sm | 4.65 | 3.96 | 4.33 | 4.07 | 3.17 | 2.05 |
| Th/U | 2.34 | 3.92 | 3.97 | 3.87 | 4.26 | 2.69 |
| $^{87}Sr/^{86}Sr$** | 0.7060(3) | 0.7063(3) | 0.7065(4) | 0.7059(8) | 0.7058(4) | 0.7063(8) |
| $^{206}Pb/^{204}Pb$** | 17.951(3) | 17.463(2) | 17.596(2) | 17.548(3) | 17.885(2) | 17.832(5) |
| εNd** | -0.20(1) | -4.46(1) | -3.01(3) | -2.03(6) | 0.30 | 4.05(5) |
| γOs** | n.d. | n.d. | n.d. | n.d. | n.d. | 5.85(2) |

**Table 4.1** (cont.)

| Unit | *Hk* (Tuff) | *Tk* (Bas) | *Tk* (Picr) | $Nd_1$ | $Nd_2$ | $Nd_3$ |
|---|---|---|---|---|---|---|
| n* | 1(1) | 12(7) | 6(5) | 41(18) | 22(9) | 8(5) |
| $SiO_2$ | 52.72 | 50.07 | 48.23 | 52.87 | 52.87 | 50.71 |
| $TiO_2$ | 0.90 | 0.90 | 0.77 | 0.96 | 1.06 | 1.06 |
| $Al_2O_3$ | 15.09 | 15.91 | 12.82 | 15.76 | 15.69 | 16.21 |
| FeOT | 9.34 | 9.97 | 11.21 | 9.40 | 10.13 | 10.62 |
| MnO | 0.21 | 0.17 | 0.18 | 0.17 | 0.17 | 0.18 |
| MgO | 7.08 | 8.98 | 15.69 | 6.73 | 6.34 | 6.63 |
| CaO | 10.35 | 11.46 | 9.44 | 9.94 | 9.81 | 11.51 |
| $Na_2O$ | 2.26 | 2.09 | 1.23 | 2.67 | 2.53 | 2.21 |
| $K_2O$ | 1.92 | 0.30 | 0.35 | 1.39 | 1.26 | 0.70 |
| $P_2O_5$ | 0.13 | 0.09 | 0.07 | 0.12 | 0.13 | 0.16 |
| LOI | 11.00 | 3.90 | 5.00 | 2.94 | 1.92 | 2.33 |
| V | n.d. | 226 | 186 | 207 | 214 | 228 |
| Sc | 22 | 31 | 28 | 29 | 30 | 33 |
| Cr | 320 | 364 | 707 | 136 | 79 | 124 |
| Y | 25 | 17 | 12 | 22 | 24 | 26 |
| Ni | 118 | 118 | 288 | 28 | 44 | 86 |
| Co | 35 | 48 | 72 | 35 | 39 | 40 |
| Cu | 110 | 103 | 69 | 33 | 78 | 92 |
| Pd (ppb) | 6.9 | 10.99 | 8.24 | <0.5-2.9 | <2 | <2-8.2 |
| Pt (ppb) | 5.7 | 9.30 | 11.20 | <0.5-5 | <0.7-2.5 | <1-7.8 |
| Ru (ppb) | <0.5 | <0.5-0.9 | 2.35 | <0.5 | <0.5 | <0.5 |
| Rb | 50.00 | 5.61 | 8.75 | 40.97 | 37.33 | 13.95 |
| Sr | 188 | 254 | 157 | 284 | 328 | 269 |
| Ba | 285 | 178 | 141 | 459 | 387 | 372 |
| Th | 2.470 | 0.644 | 0.512 | 3.132 | 3.271 | 2.086 |
| U | 0.865 | 0.159 | 0.129 | 0.830 | 0.908 | 0.904 |
| Ta | 0.369 | 0.178 | 0.136 | 0.485 | 0.526 | 0.404 |
| Zr | 100 | 63 | 56 | 123 | 137 | 114 |
| Hf | 2.110 | 1.676 | 1.426 | 3.069 | 3.466 | 2.76 |
| La | 16.50 | 5.58 | 4.72 | 16.95 | 17.92 | 13.4 |
| Ce | 31.50 | 13.05 | 10.91 | 36.57 | 39.11 | 29.2 |
| Nd | 15.30 | 7.80 | 6.44 | 17.26 | 18.49 | 14.9 |
| Sm | 3.36 | 2.23 | 1.82 | 3.84 | 4.16 | 3.62 |
| Eu | 0.877 | 0.864 | 0.709 | 1.083 | 1.161 | 1.10 |
| Gd | 3.480 | 2.677 | 2.210 | 3.860 | 4.158 | 4.03 |
| Tb | 0.529 | 0.437 | 0.345 | 0.626 | 0.686 | 0.683 |
| Yb | 1.750 | 1.624 | 1.279 | 2.136 | 2.364 | 2.68 |
| Lu | 0.262 | 0.242 | 0.199 | 0.320 | 0.352 | 0.407 |
| Gd/Yb | 1.99 | 1.65 | 1.73 | 1.81 | 1.76 | 1.50 |
| La/Sm | 4.91 | 2.50 | 2.60 | 4.41 | 4.30 | 3.70 |
| Th/U | 2.86 | 4.05 | 3.98 | 3.77 | 3.60 | 2.31 |
| $^{87}Sr/^{86}Sr$** | 0.7072(1) | 0.7058(6) | 0.7057(3) | 0.7082(11) | 0.7086(5) | 0.7065(5) |
| $^{206}Pb/^{204}Pb$** | 18.130(1) | 17.351(2) | 16.912(2) | 17.621(5) | 17.590(2) | 17.967(2) |
| εNd** | n.d. | -4.17(2) | -2.03(3) | -8.45(9) | -7.90(4) | -2.49(4) |
| γOs** | n.d. | n.d. | 4.68(2) | n.d. | n.d. | n.d. |

**Table 4.1** (cont.)

| Unit | *$Mr_1$* | *$Mr_2$* | *Mk* | *Hr* | *Km* | *Sm* |
|---|---|---|---|---|---|---|
| n* | 11(7) | 16(11) | 43(22) | 26(10) | 10(3) | 26(6) |
| $SiO_2$ | 50.16 | 49.61 | 49.47 | 49.28 | 49.65 | 49.32 |
| $TiO_2$ | 1.15 | 1.16 | 1.27 | 1.41 | 1.52 | 1.44 |
| $Al_2O_3$ | 15.70 | 16.16 | 15.93 | 15.59 | 15.52 | 15.46 |
| FeOT | 11.31 | 11.36 | 11.76 | 12.32 | 12.32 | 12.25 |
| MnO | 0.20 | 0.20 | 0.20 | 0.20 | 0.20 | 0.20 |
| MgO | 7.14 | 7.44 | 7.25 | 7.30 | 6.62 | 7.24 |
| CaO | 11.65 | 11.56 | 11.52 | 11.09 | 11.19 | 11.33 |
| $Na_2O$ | 2.18 | 2.04 | 2.19 | 2.30 | 2.42 | 2.30 |
| $K_2O$ | 0.37 | 0.34 | 0.31 | 0.35 | 0.37 | 0.31 |
| $P_2O_5$ | 0.13 | 0.13 | 0.14 | 0.16 | 0.20 | 0.17 |
| LOI | 2.37 | 2.03 | 1.99 | 2.04 | 2.24 | 2.10 |
| V | 269 | 262 | 266 | 291 | 295 | 284 |
| Sc | 36 | 35 | 36 | 39 | 38 | 37 |
| Cr | 119 | 136 | 144 | 142 | 110 | 156 |
| Y | 24 | 24 | 24 | 27 | 31 | 27 |
| Ni | 86 | 116 | 111 | 123 | 94 | 118 |
| Co | 43 | 46 | 45 | 47 | 44 | 46 |
| Cu | 103 | 117 | 135 | 160 | 152 | 165 |
| Pd (ppb) | 4.91 | 7.74 | 8.92 | 15.0 | 14.00 | 12.50 |
| Pt (ppb) | 6.23 | 9.11 | 9.46 | 11.0 | 11.00 | 11.83 |
| Ru (ppb) | <0.5 | <0.5-0.7 | <0.5-0.6 | <0.5-0.6 | <0.5 | <0.5-0.7 |
| Rb | 6.79 | 6.11 | 6.46 | 6.89 | 8.26 | 6.71 |
| Sr | 228 | 193 | 211 | 181 | 193 | 184 |
| Ba | 271 | 202 | 167 | 133 | 161 | 132 |
| Th | 1.651 | 1.114 | 0.993 | 0.945 | 1.373 | 1.002 |
| U | 0.617 | 0.445 | 0.378 | 0.383 | 0.658 | 0.411 |
| Ta | 0.341 | 0.283 | 0.265 | 0.284 | 0.352 | 0.277 |
| Zr | 106 | 93 | 95 | 106 | 127 | 107 |
| Hf | 2.622 | 2.371 | 2.391 | 2.56 | 3.010 | 2.662 |
| La | 10.32 | 7.66 | 7.30 | 7.0 | 9.44 | 7.72 |
| Ce | 23.56 | 18.01 | 17.84 | 17.2 | 22.58 | 18.91 |
| Nd | 13.49 | 11.03 | 11.56 | 11.4 | 14.03 | 12.22 |
| Sm | 3.47 | 3.10 | 3.30 | 3.48 | 3.94 | 3.54 |
| Eu | 1.096 | 1.048 | 1.138 | 1.19 | 1.307 | 1.241 |
| Gd | 3.893 | 3.736 | 3.873 | 4.24 | 4.598 | 4.300 |
| Tb | 0.651 | 0.626 | 0.662 | 0.737 | 0.814 | 0.745 |
| Yb | 2.334 | 2.364 | 2.449 | 2.75 | 2.996 | 2.692 |
| Lu | 0.360 | 0.360 | 0.367 | 0.411 | 0.448 | 0.403 |
| Gd/Yb | 1.67 | 1.58 | 1.58 | 1.54 | 1.53 | 1.60 |
| La/Sm | 2.98 | 2.47 | 2.21 | 2.01 | 2.40 | 2.18 |
| Th/U | 2.68 | 2.50 | 2.62 | 2.47 | 2.09 | 2.44 |
| $^{87}Sr/^{86}Sr$** | 0.7063(3) | 0.7051(5) | 0.7055(10) | 0.7046(9) | 0.7047(4) | 0.7047(7) |
| $^{206}Pb/^{204}Pb$** | 17.851(1) | 18.144(3) | 17.945(5) | 17.901(5) | 17.991(2) | 17.771(3) |
| εNd** | -0.24(3) | 1.99(3) | 1.23(6) | 2.32(5) | 2.38(2) | 1.69(4) |
| γOs** | n.d. | n.d. | n.d. | n.d. | n.d. | n.d. |

**Table 4.1** (cont.)

Major elements in wt%; PGE in ppb; other trace elements in ppm; *n.d.* = no data. Major elements are recalculated to 100%, anhydrous. Initial isotopic ratios are recalculated to 250 Ma.

*$n$ number of analyzed samples (number of PGE analyses is given in brackets).

**Number of isotopic analyses is given in brackets.

### *Intrusive facies of the trap*

Fedorenko (1994) estimated that intrusions account for 6.5% of the magmatic rocks in the Noril'sk region. They outcrop predominantly around the present margins of the trap (which is not the original margin of the volcanic basin), where the substrate has been exposed by structural uplift. However, drilling has shown that there is a close relationship of the intrusive rocks to major faults (Noril'sk-Kharaelakh, North Kharaelakh and Imangda). The intrusions vary from a few m to at least 300 m in thickness in the Noril'sk region, and up to 500 m in the south of the Tunguska basin.

The intrusions of the Noril'sk region have been subdivided in detail on the basis of their field relationships, petrography, geochemistry and isotope geochemistry. It was shown that the majority of the intrusions, excepting specific mica lamprophyres and granitoids, are comagmatic with the lavas or were formed immediately after eruption ceased (see Distler and Kunilov 1994; Fedorenko 1994; Hawkesworth et al. 1995). Naldrett et al. (1992) identified 5 main groups: (1) those of alkaline and sub-alkaline affinity; (2) Ti-rich dolerite dykes that are restricted to the northeastern part of the Noril'sk region; (3) dolerite sills and dykes that are found throughout the Noril'sk region (4) differentiated intrusions that are not related to ore junctions; and (5) differentiated mafic/ultramafic intrusions that occur in the vicinity of ore junctions. The Ni-Cu-PGE deposits are associated with intrusions of the last group. Naldrett et al. (1992) showed that the mineralized intrusions greatly resemble the association II lavas. Fedorenko (1994) proposed that intrusions formed during the interval between accumulation of the Lower and Upper Morongovsky lavas. Naldrett et al. (1992, 1995) pointed out that the stratigraphic succession of the lavas provides periodic samples of the changes that were taking place within the magma that was present in the system of chambers and conduits beneath the Noril'sk region. These changes resulted in the development of the sulfide mineralization, which is the reason why the geochemistry of the basalts is considered in some detail here.

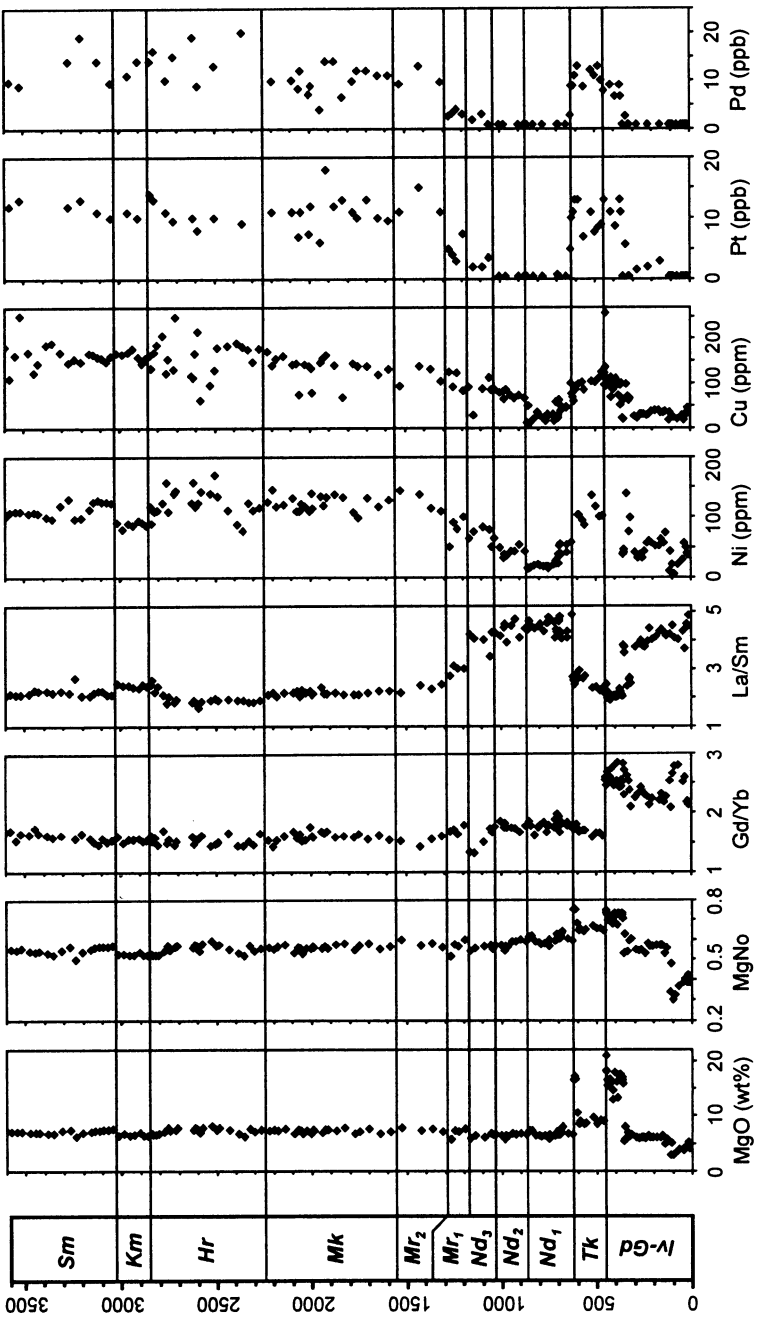
Height above base of volcanic sequence (m)
0
500
1000
1500
2000
2500
3000
3500
Iv-Gd
Tk
Nd1
Nd2
Nd3
Mr1
Mr2
Mk
Hr
Km
Sm
MgO (wt%)
0
10
20
MgNo
0.2
0.5
0.8
Gd/Yb
1
2
3
La/Sm
1
3
5
Ni (ppm)
0
100
200
Cu (ppm)
0
100
200
Pt (ppb)
0
10
20
Pd (ppb)
0
10
20

**Fig. 4.6.** Variations of magnesium No, trace-element ratios and chalcophile element contents across a generalized section of the volcanic strata, based on samples from cores SG-9, SG-32 and exposures 1F, 15F, and 16F (their locations are shown in Figure 4.3). The samples were collected by Valeri Fedorenko. Analyses were made by the Ontario Geological Survey (Lightfoot et al., 1990, 1993, 1994; Hawkesworth et al., 1995), University of Toronto (Brugmann et al., 1993), and US Geological Survey (Wooden et al, 1993). High Ni contents, characteristic of the picritic basalts (509-1034 ppm in the Gudchikhinsky suite and 605-623 ppm in the Tuklonsky suite) are not shown.

### *Geochemistry of the Volcanic Formations*

Fig. 4.6 shows the variation of some chemical parameters with stratigraphic height throughout entire volcanic sequence. It illustrates that the MgNo of the volcanics from the Nadezhdinsky suite (***Nd***) upward is relatively constant[8], except for a slight decrease across the $Nd_1$ and $Nd_2$, which implies in turn that fractionation of mafic minerals had no significant effect on the geochemical variations as the lavas were erupting.

Naldrett et al. (1992) have shown (see below) that the Gd/Yb ratios of the mineralized intrusions are less than 2, which means that they are part of the Association II magmatism. For this reason, more emphasis is placed in this discussion and those following it on geochemical variations within the lavas of Association II than on those of Association I. Furthermore, lavas belonging to the *Hr-Sm* suites are similar those belonging to the $Mr_2$ and *Mk* suites, and are very uniform in composition throughout (e.g. Fedorenko et al., 1996); the composition of these lavas is also not discussed here.

**Gd/Yb vs La/Sm.** A plot of Gd/Yb versus La/Sm (Fig. 4.7) is an effective discriminator of the different volcanic formations (Lightfoot et al. 1990; Naldrett et al. 1992). The ***Iv*** and ***Sv*** are characterized by Gd/Yb >2 and La/Sm >3. The ***Gd*** has Gd/Yb >2 and La/Sm <3. All formations stratigraphically above the ***Gd***, that is all formations belonging to association II have Gd/Yb <2. Amongst these, the $Nd_1$ and $Nd_2$ define a grouping with the highest La/Sm (>4) and the ***Tk***, $Mr_2$ and ***Mk*** a grouping with the lowest (<3); ratios for the $Nd_3$ and $Mr_1$ are transitional between these.

[8] MgNo was calculated as MgO/[(MgO+(0.85*FeOT)], where FeOT is total iron as FeO; MgO and FeO in mol%.

The distinctions made on the basis of Gd/Yb ratio between volcanic associations I and II is also reflected in $TiO_2$ [association I has higher values (Fedorenko 1981; Lightfoot et al. 1990)].

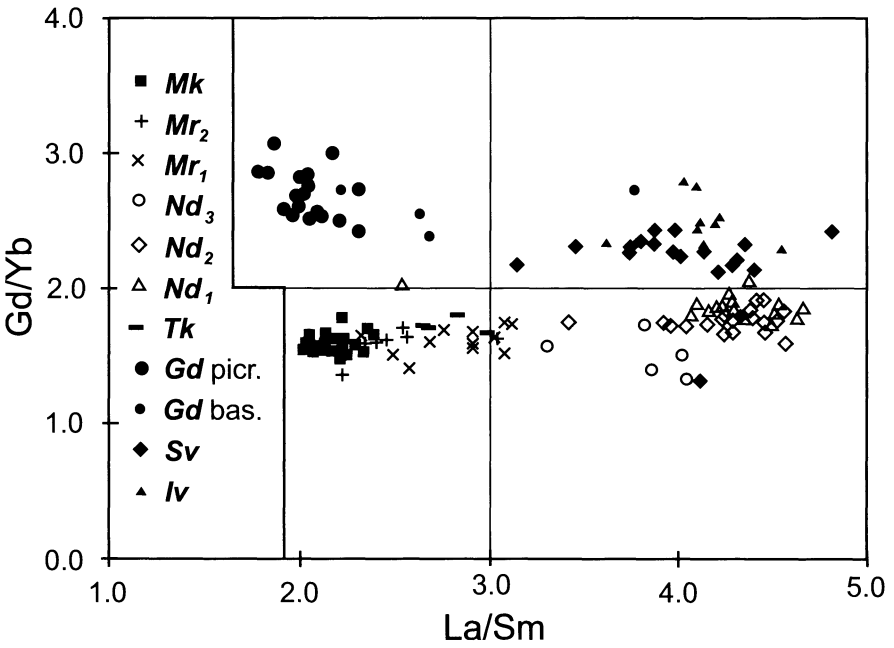


**Fig. 4.7.** Plot of Gd/Yb versus La/Sm for volcanic formations from the ***Iv*** to the ***Mk*** (after Naldrett et al., 1995)

**Th/U vs La/Sm.** While the La/Sm and Gd/Yb ratios of the ***Tk***, ***Mr*$_2$** and ***Mk*** to the **Sm** are similar; the variation in Th/U shown in Fig. 4.8 indicates a decoupling of their chemical compositions. The ***Tk*** has a Th/U ratio of 4-4.5 in comparison with a ratio of 2.0-3.0 that is characteristic of the ***Mk***, ***Km,*** and ***Sm***. The ***Hr*** has slightly higher Th/U and slightly lower La/Sm ratios than the other volcanic rocks. The ***Nd*$_1$** and ***Nd*$_2$** have similar high ratios to the ***Tk***; the ***Mr*$_2$** resembles the ***Mk*** to ***Sm***, particularly the ***Km***; and the ***Mr*$_1$** and ***Nd*$_3$** are transitional between the ***Nd*$_1$-*Nd*$_2$** grouping and the ***Mr*$_2$-*Sm***.

**Chromium**. A complete record for this part of stratigraphic sequence is present in Fig. 4.9, for which data from boreholes SG-9 and SG-32, and exposure 1F are used. Variations of Cr and chalcophile elements are shown, together with variations of La/Sm ratio and MgNo. It will be recalled, as shown in Fig. 4.6, that fractionation of mafic minerals had no

significant effect on the geochemical variations from ***Nd*$_1$** to ***Mr*$_2$** and above.

The Cr content of the ***Tk*** basalts is relatively high (average of 391 ppm). There is an abrupt decrease across the ***Tk-Nd*$_1$** contact to 230 ppm in the latter (see Fig. 4.9). Cr then decreases progressively upward through this unit to reach 70 ppm at the top; it jumps sharply at the base of the ***Nd*$_2$** to 100-140 ppm and then again decreases progressively throughout this unit to reach 30-40 ppm at the top. Another sharp increase in Cr occurs at the base of the ***Nd*$_3$** to 100-150 ppm, and thereafter Cr increases slowly upsection to average 180 ppm in the ***Mr*$_2$**.

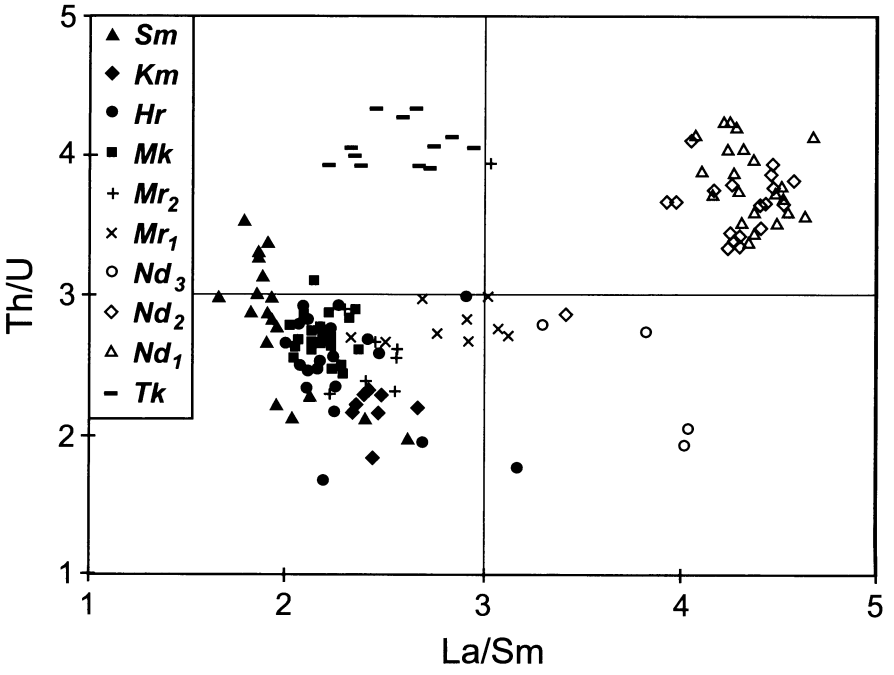


**Fig. 4.8.** Plot of Th/U versus La/Sm for volcanic formations from the ***Tk*** to the ***Sm*** (data from Naldrett et al. 1995 and Hawkesworth et al. 1995)

**Nickel**. The ***Nd*$_1$** (average 25 ppm Ni) and ***Nd*$_2$** (average 41 ppm Ni) are very depleted when compared with other formations on the basis of MgO content (Fig. 4.6, 4.9). This is due to two factors: (1) Ni decreases sharply from the ***Tk*** to the base of the ***Nd*$_1$**; (2) it also decreases progressively upward throughout the ***Nd*$_1$**, shows a slight but abrupt rise at the base of the ***Nd*$_2$** and then remains relatively constant to the base of the ***Nd*$_3$**, before increasing upward across this and the overlying ***Mr*$_1$**.

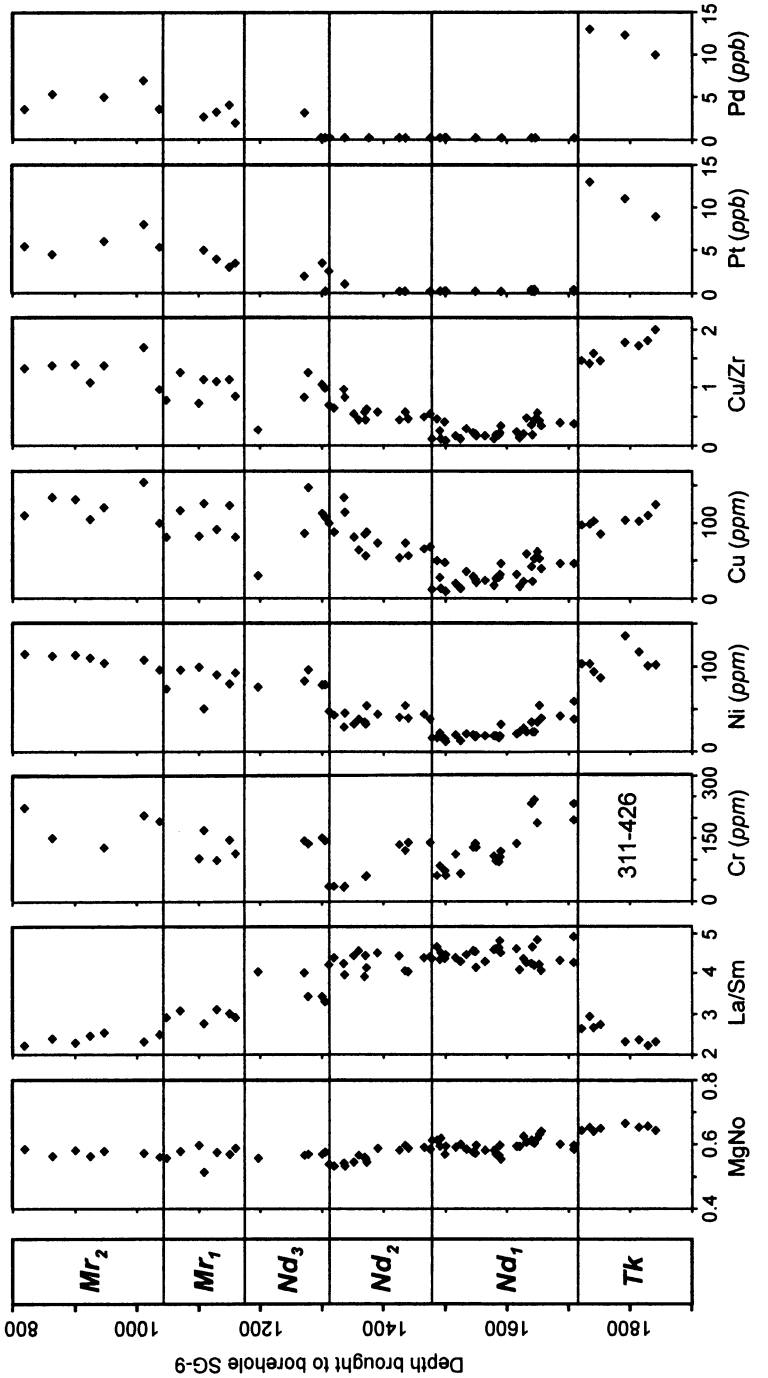
Depth brought to borehole SG-9
800
1000
1200
1400
1600
1800
Mr2
Mr1
Nd3
Nd2
Nd1
Tk
MgNo
0.4
0.6
0.8
La/Sm
2
3
4
5
Cr (ppm)
0
150
300
311-426
Ni (ppm)
0
100
Cu (ppm)
0
100
Cu/Zr
0
1
2
Pt (ppb)
0
5
10
15
Pd (ppb)
0
5
10
15

**Fig. 4.9.** Stratigraphic variation of some critical geochemical parameters across a generalized section through the Tuklonsky basalts (the Tuklonsky picrites are omitted) and the Nadezhdinsky-Morongovsky lavas, based on samples from cores SG-9, SG-32 and exposure 1F. The positioning of the samples from SG-32 and 1F have been extrapolated to the level at which they would occur in borehole SG-9. Analytical data are from the Ontario Geological Survey and the University of Toronto (Lightfoot et al., 1990, 1993, 1994; Brugmann et al., 1993). Data for the Tuklonsky picrites can be seen Fig. 4.6

**Copper.** As with Ni (Fig. 4.6, 4.9), there is a very sharp decrease in Cu from the ***Tk*** tholeiites to the base of the ***Nd$_1$*** (Cu decreases by about 50 ppm). Cu continues to decrease upward in the ***Nd$_1$*** to reach 10-30 ppm at the top. It also shows an abrupt increase to 40-80 ppm at the base of the ***Nd$_2$*** but then, unlike Ni, rises across this unit to approach 100 ppm at the top. It continues to rise to reach 155 ppm in the ***Mk***.

**Platinum group elements.** Data on Pt and Pd through the entire volcanic sequence are present in Fig.4.6, which is based on the analytical results of two laboratories (University of Toronto and US Geological Survey). Fig. 4.9 shows variations of these elements from the ***Tk*** up to the ***Mr$_2$*** using University of Toronto data alone. The ***Tk*** is characterized by the highest PGE contents. The ***Nd$_1$***, except for the lowermost flow, contains less than the detection limit of both Pt and Pd (this is also true for Ir, and Rh – see Brugmann et al., 1993). Samples from the lower and middle parts of the ***Nd$_2$*** also have less than the detection limit of Pt and Pd, but above this Pt and Pd concentrations increase systematically upward in the stratigraphy.

**Sr and Nd isotopes**. Fig. 4.10 is a plot of average εNd versus average $^{87}Sr/^{86}Sr$, recalculated for 250Ma, for the suites of Associations IIA and IIB after the summary by Fedorenko et al. (1996) of data from Hawkesworth et al. (1994); Lightfoot et al. (1993, 1994); Walker et al. (1994) and Wooden et al. (1993). The ***Tk***, ***Mr$_2$*** and the average of 120 samples covering all suites from the ***Mr$_2$*** to ***Sm*** are characterized by $^{87}Sr/^{86}Sr$ ratios of 0.705-0.706. In contrast the ***Nd$_1$*** and ***Nd$_2$*** have values of 0.708 to 0.709, with the ***Nd$_3$*** and ***Mr$_1$***. suites being transitional between the ***Nd$_{1-2}$*** and the average of the ***Mr$_2$*** to ***Sm***. A similar relationship is exhibited by εNd with the ***Tk*** picrites and tholeiites having values of -2 to -4.2, the ***Nd$_1$*** and ***Nd$_2$*** about -7.5, the ***Mr$_2$*** and the average of the ***Mr$_2$*** to ***Sm*** samples about +2, with the ***Nd$_3$ and Mr$_1$***. suites again being transitional between them.

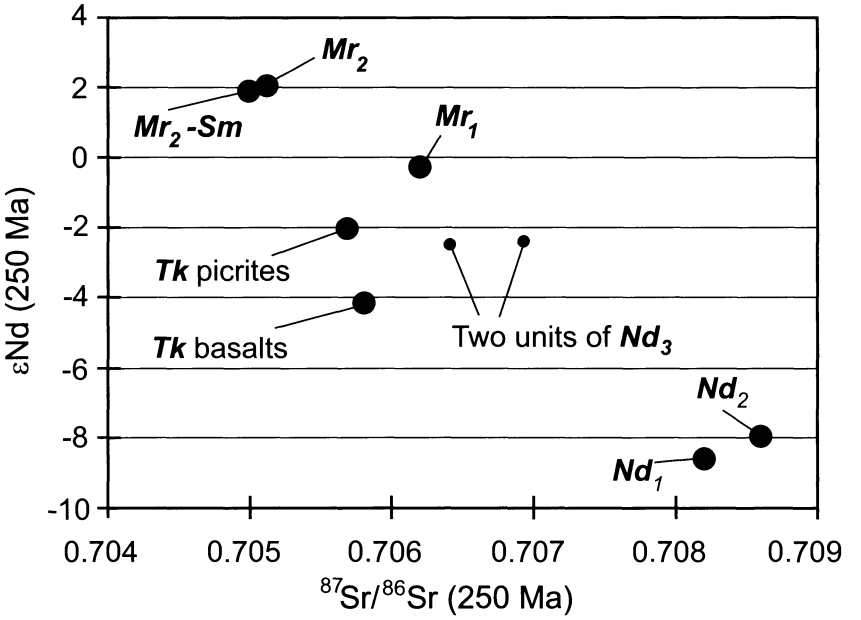


**Fig. 4.10.** Plot of average εNd versus average $^{87}Sr/^{86}Sr$ for Association IIA and B lavas. Initial isotopic ratios are for 250 MA. Data are averages compiled by Fedorenko et al. (1996) from the data of Lightfoot et al. (1993, 1994), Wooden et al. (1993), Walker et al. (1994), and Hawkesworth et al. (1995)

**Discussion of the Geochemistry of the Volcanic Rocks**. Reasons for the geochemical trends shown by the association II basalts have been discussed by Fedorenko (1981, 1994), Naldrett et al. (1992, 1994a, 1995), Lightfoot et al. (1993,1994), Wooden et al. (1993), and Fedorenko et al. (1996). The general consensus is that an initial Tuklonsky picritic magma erupted in the eastern part of the Noril'sk region (possibly along fissures related to the Imangda fault), but failed to reach the surface in the vicinity of the Noril'sk-Kharaelakh fault. Following this, highly contaminated ***Nd*$_1$** lavas erupted from both the Imangda and the Noril'sk-Kharaelakh faults. All of the above authors are in agreement that the ***Tk*** picritic magma was parental to the ***Nd*$_1$** magma; it fractionated olivine followed by a gabbroic cumulate (transforming to the ***Tk*** basalt) and, while this was happening, became contaminated with upper crustal material to give rise to the ***Nd*$_1$** magma. Replenishment and mixing of this with fractionated residual magma gave rise to the ***Nd*$_2$** lavas that closely resemble the ***Nd*$_1$** in composition. After eruption of the ***Nd*$_2$**, ***Mr*$_2$*-Mk***-type magma entered and mixed with that in both the Imangda and Noril'sk-Kharaelakh plumbing systems.

Successive flows of the ***Nd₃ - Mr₁*** suites reflect the progressive nature of this mixing with time.

The relatively comprehensive set of new isotopic and trace element data that is now available for the lavas allows one to re-examine the viability of the model outlined above. The model accounts for all aspects of the Gd/Yb versus La/Sm plot (Fig. 4.7). The sharp increase from the low La/Sm ratios of the ***Tk*** to the high values of the ***Nd₁*** and ***Nd₂*** can be accounted for by crustal contamination. Indeed this abrupt increase, accompanied by an increase in the $SiO_2$ content of the rocks from an average for most of the ***Tk*** basalts of about 49.5 wt% to 52.3 wt% in the ***Nd₁***, led initially to the suggestion of contamination (Lightfoot et al., 1990). The intermediate ratios of the ***Nd₃*** and ***Mr₁*** formations are explicable as either a lower degree of crustal contamination of ***Tk*** magma, or intermixing with fresh magma (Lightfoot et al. 1993, 1994). However the plot of Th/U versus La/Sm (Fig. 4.8) shows that the ***Tk*** has a much higher Th/U ratio than the ***Mr₂-Sm***, and that the ***Nd₃-Mr₁*** lie on a mixing line with the latter, not the former. This indicates, as Wooden et al. (1993) and Fedorenko (1994) have shown, that these units must be a result of mixing of a contaminated ***Nd₁-₂*** magma with less contaminated, low Th/U, ***Mr₂-Mk*** -type magma.

The overall conclusion from the trace element data, that crustal contamination of the ***Tk*** to produce the ***Nd₁*** and ***Nd₂*** formations was followed by mixing with ***Mr₂-Sm***-type magma to produce the ***Nd₃ - Mr₁*** formations, is confirmed by the εNd – $^{87}Sr/^{86}Sr$ plot of Fig. 4.10. Estimates of the amount of required contaminant range from 6.5 (Fedorenko 1994), to 8 (Lightfoot et al. 1994), up to 15 wt% (Wooden et al. 1993).

Figure 4.11 illustrates, as Wooden et al. (1993) have shown, that contamination increased the Th/Ta ratio in the ***Nd₁*** and ***Nd₂*** from the value of 3.75 characteristic of the ***Tk*** to 6.25. The spread in Th and Ta along the line of slope 6.25 is due to fractional crystallization that has increased the concentrations of incompatible elements; the fact that all ***Nd₁-₂*** samples scatter along the same line is evidence that this fractionation affected a previously contaminated magma, and that further change in Th/Ta did not occur during the fractionation. Fig. 4.11 also supports the conclusion that the ***Nd₃*** and ***Mr₁*** are transitional formations, since the Th/Ta ratio changes systematically across them back to the former ratio of 3.75, which is also characteristic of the ***Mr₂-Mk***. As Wooden et al. (1993) point out, this is most readily explained by the influx of a ***Mr₂-Mk***-type magma into the system feeding the Noril'sk-Kharaelakh eruptive center.

The progressive decrease in Cr upward across both the ***Nd₁*** and ***Nd₂*** (Fig. 4.9) is possibly due to the contamination having caused chromite to appear on the liquidus of the contaminated magma (Irvine 1975, 1977) followed by fractional crystallization accompanied by chromite precipitation;

the increase in Cr at the base of the $Nd_2$ indicates an influx of fresh magma into the zone of chromite crystallization.

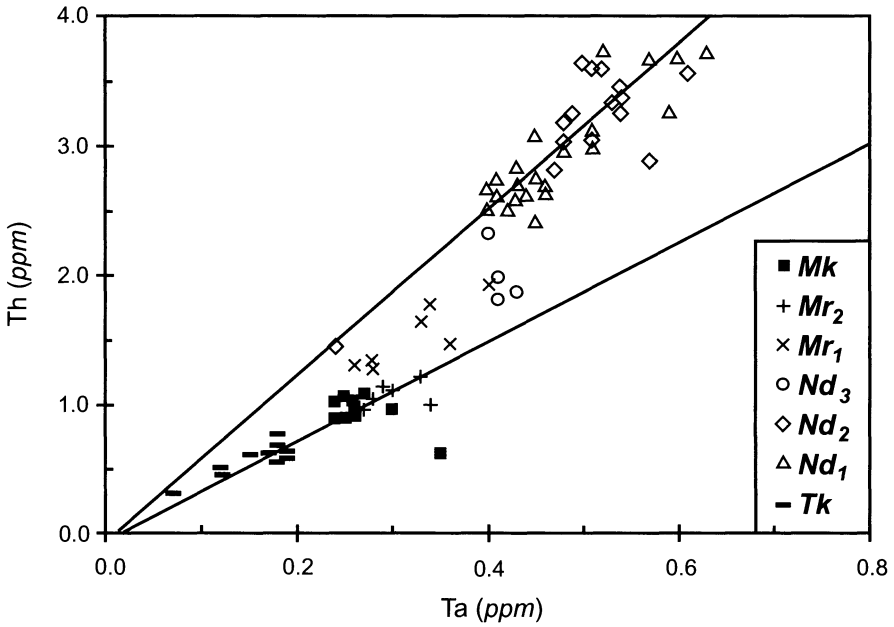


**Fig. 4.11.** Plot of Th vs. Ta for the Tuklonsky – Mokulaevsky lavas. Lines show trends of the ***Tk*** lavas (Th/U = 3.75) and $Nd_{1\text{-}2}$ basalts (Th/U = 6.25). From Naldrett et al. (1995)

The trace element geochemistry of the association IIA lavas therefore indicates that large amounts of crustal contamination occurred, accompanied by some fractional crystallization (e.g. the MgNo of the ***Tk*** lavas is not that of a primary, mantle-derived melt), but that the contaminated melt continued to differentiate without undergoing further contamination of the same type. Naldrett et al. (1995) suggested that the first fractional crystallization and contamination occurred at mid-upper crustal levels, and that the magmas then underwent a further stage of differentiation at a very shallow level.

### *Onset of sulfide immiscibility*

The behavior of the chalcophile elements (Ni, Cu and the PGE) is not explicable in terms of crustal contamination per se. The 50 percent depletion in Ni and Cu and the even more drastic depletion of the PGE (about 90%; see Table 4.2) from the ***Tk*** to the $Nd_1$ can only be explained in terms of

equilibration with sulfide, as Lightfoot et al. (1990), Naldrett et al. (1992), Brugmann et al., (1993), and Fedorenko (1994) have pointed out.

**Table 4.2.** Average contents of Cr and chalcophile elements in lavas from Tuklonsky to Mokulaevsky suite. After Naldrett et al. (1995)

| Suite | n Cr, Ni, Cu | n PGE | Cr (*ppm*) | Ni (*ppm*) | Cu (*ppm*) | Pd (*ppb*) | Pt (*ppb*) | Rh (*ppb*) | Ir (*ppb*) |
|---|---|---|---|---|---|---|---|---|---|
| ***Tk**** | 8 | 6 | 391 | 109 | 107 | 10.7 | 11.17 | 0.36 | 0.137 |
| ***Nd*$_1$** | 38 | 9 | 124 | 25 | 33 | <2.0 | <1.0 | <0.10 | <0.02 |
| ***Nd*$_2$** | 16 | 4 | 74 | 41 | 82 | <2.0 | 0.9 | <0.10 | 0.016 |
| ***Nd*$_3$** | 12 | 3 | 147 | 84 | 98 | 1.7 | 2.80 | 0.14 | 0.028 |
| ***Mr*$_1$** | 9 | 4 | 134 | 84 | 110 | 3.0 | 3.88 | 0.20 | 0.043 |
| ***Mr*$_2$** | 8 | 5 | 184 | 112 | 126 | 4.9 | 5.88 | 0.27 | 0.100 |
| ***Mk*** | 17 | 9 | 160 | 101 | 155 | 6.2 | 6.30 | 0.32 | 0.094 |

*n* number of samples

*For the Tuklonsky suite data for Cr, Ni and Cu are given for basalts only; data for PGE are given for basalts and picrites

The initiation of sulfide immiscibility might have been brought about by one or both of two mechanisms. The mixing of mafic magma with a felsic contaminant can so lower the ability of the resulting hybrid to dissolve sulfides that immiscibility can result, even if the two magmas involved in the mixing are sulfide unsaturated [see discussion in Chapter 2 and the references therein to Irvine (1975) and Li and Naldrett (1993)]. Assimilation of this kind can also cause chromite to appear as a liquidus phase in a magma (Irvine, 1975). Alternatively, with respect to sulfide segregation, the heavy isotopic signature of the ores (see Fig. 4.25 below and related discussion in the text) suggests that contamination may have involved the ingestion of crustal sulfur.

The question remains as to the stage at which the bulk of the sulfide was removed. Fig. 4.9 provides some insight into this. While average Ni, Cu and Cr concentrations decrease sharply from the ***Tk*** to the ***Nd*$_1$**, a detailed examination of their behavior shows that up to 50 percent of the decrease occurs across the ***Nd*$_1$** itself (one must discount the behavior of Ni, Cr and Cu in the ***Tk*** picrites, since these contain intratelluric olivine phenocrysts and thus are enriched in Ni and Cr and depleted in Cu). These progressive changes occurred in magma that had already acquired its high La/Sm signature. Thus it is not the initial crustal contamination which was responsible for much of the depletion in the chalcophile metals, but it was something that occurred within the magma after this. The progressive decrease in Cr in successively later flows of the ***Nd*$_1$** (Fig. 4.9) is likely the result of

these flows having been derived from a body of magma that was fractionating chromite in addition to silicates; the behavior of Ni and Cu indicates that sulfides were also being removed at this (***Nd$_1$***) stage. In contrast, Cu increases upwards throughout the ***Nd$_2$*** and Ni, after an initial sharp increase from the top of the ***Nd$_1$***, remains relatively constant through this subsuite. The increase in Cu is not consistent with continued sulfide removal, and indicates that sulfides were no longer segregating from this magma during eruption of the ***Nd$_2$*** lavas, despite the fact that it continued to fractionate chromite, as shown by the continued decrease in Cr. The contrast in the behavior of Ni and Cu, Ni remaining constant and Cu increasing during fractionation in the ***Nd$_2$***, is explicable if Ni was being removed from the magma due to the crystallization of mafic silicates. A slight decrease in MgNo is present across the ***Nd$_2$*** (Naldrett et al. 1995), which is consistent with limited fractionation of mafic minerals.

In summary, three stages may be identified in the behavior of chalcophile metals in the ***Nd*** magma. The first involved bulk contamination, probably at the mid- to upper-crustal level – Ni, Cu and Cr were reduced to about 50% of their concentrations in ***Tk*** magma at this time. The second stage was the evolution across the ***Nd$_1$***, with all three metals being reduced to about 10% of their levels in the ***Tk***. The third stage is represented by the ***Nd$_2$*** in which Cr continued to decrease, but sulfide removal had ceased.

Considering now the volcanic sequence above the ***Nd$_2$***, the data reviewed above, particularly the Th/U and Th/Ta ratios and the isotopic data, indicate that the formations from the ***Nd$_3$*** to the ***Mr$_1$*** are the result of the mixing of ***Nd$_{1-2}$*** type with ***Mr$_2$-Sm***-type magma, probably as a result of the new magma entering reservoirs in the ***Nd$_1$-$_2$*** plumbing system. The mixing of fresh, chalcophile element-undepleted magma with depleted magma that had remained in the system, accounts in part for the progressive increase in Ni, Cu and particularly the PGE from the ***Nd$_2$*** through the ***Nd$_3$*** and ***Mr$_1$*** to the ***Mr$_2$***. This is discussed in more detail below.

### *Summary of Development of the Association IIA (Tuklonsky – Early Morongovsky) Volcanism*

In summary, the major and trace element, and isotopic variations in lavas extending from the *Tk* up to the *Mr$_2$* suggest that *Tk* magma, which erupted in the eastern part of the Noril'sk region, became impounded beneath the center of the volcanic basin centered on the Noril'sk and Talnakh ore junctions, and underwent contamination by 6.5-15 percent of mid-upper crustal granodioritic melt. Following contamination, the magma fractionated, precipitating chromite and sulfide liquid, giving rise to the sequence of lavas grouped as the *Nd$_1$*. Rejuvenation of the Cr- and chalcophile element-

depleted magma was followed by further chromite fractionation (to give rise to the $Nd_2$ lavas), but segregation of sulfide had ceased. With the onset of the $Nd_3$, a new magma type, characterized by slightly higher Th and much higher U than the *Tk*, entered the Noril'sk high level magma system of feeders, mixing with old magma and giving rise to the transitional $Nd_3$ and $Mr_1$ formations.

### 4.1.3 Ore-Bearing and Related Intrusions

The purpose of this section is to investigate how the ore-bearing and other closely related intrusions fit into the model summarized above.

#### *General information*

Naldrett et al. (1992) and Czamanske et al. (1995) showed that the intrusive bodies with which the ores are associated are one of a wide range of types that occur in the Noril'sk region ranging from alkalic sills and undifferentiated dolerite dykes and sills to differentiated bodies. Mineralization is associated with specific differentiated bodies that, on the basis of their field relationships, appear to be post-***Nd*$_2$** and pre-***Mk*** in age [Naldrett et al.'s (1992) Group 5 intrusions]. A second group of intrusions, that are very close in age to the mineralized bodies, also occur close to the Talnakh and Noril'sk ore junctions. These tend to have a higher proportion of ultramafic rock, but are much less well mineralized. Naldrett et al. (1992) grouped the ore-bearing intrusions as Group 5A and the less well mineralized bodies as Group 5B. They are referred to locally as Noril'sk-type and Lower Talnakh type respectively. Observations on core from the Noril'sk area (see compilations in Naldrett et al. 1992; Czamanske et al. 1995) indicate that Lower Talnakh type intrusions were emplaced somewhat earlier than the Noril'sk type, although the emplacement of both was very close in time. When they are in direct contact, quenched zones at boundaries are absent. As is discussed below, field and geochemical data support that both types of intrusion formed during the interval between eruption of the ***Nd*$_2$** and the ***Mk*** (Fedorenko 1994; Naldrett et al. 1995 and their references).

Zen'ko and Czamanske (1994a) showed that the Lower Talnakh intrusion forms a flat sheet, <40 m in thickness, that cuts through the stratigraphy. It is at the highest stratigraphic level in the northeast of the Talnakh area, and is at progressively lower levels to the southwest. The intrusion shows a marked thickening to 80 m or more along a series of curvelinear

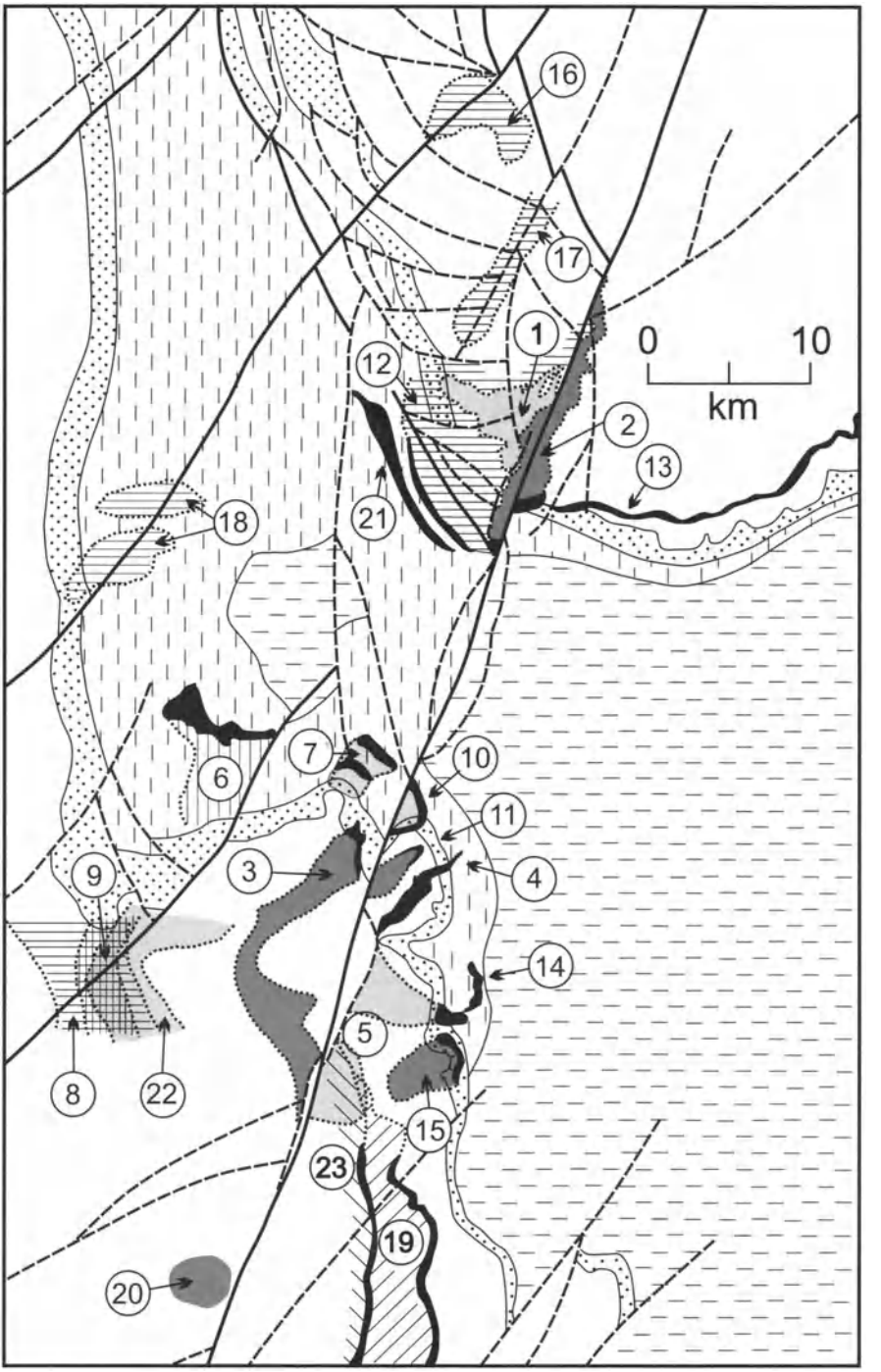
16
17
1
0
10
km
12
2
13
18
21
7
10
6
11
9
3
4
14
5
8
22
15
23
19
20

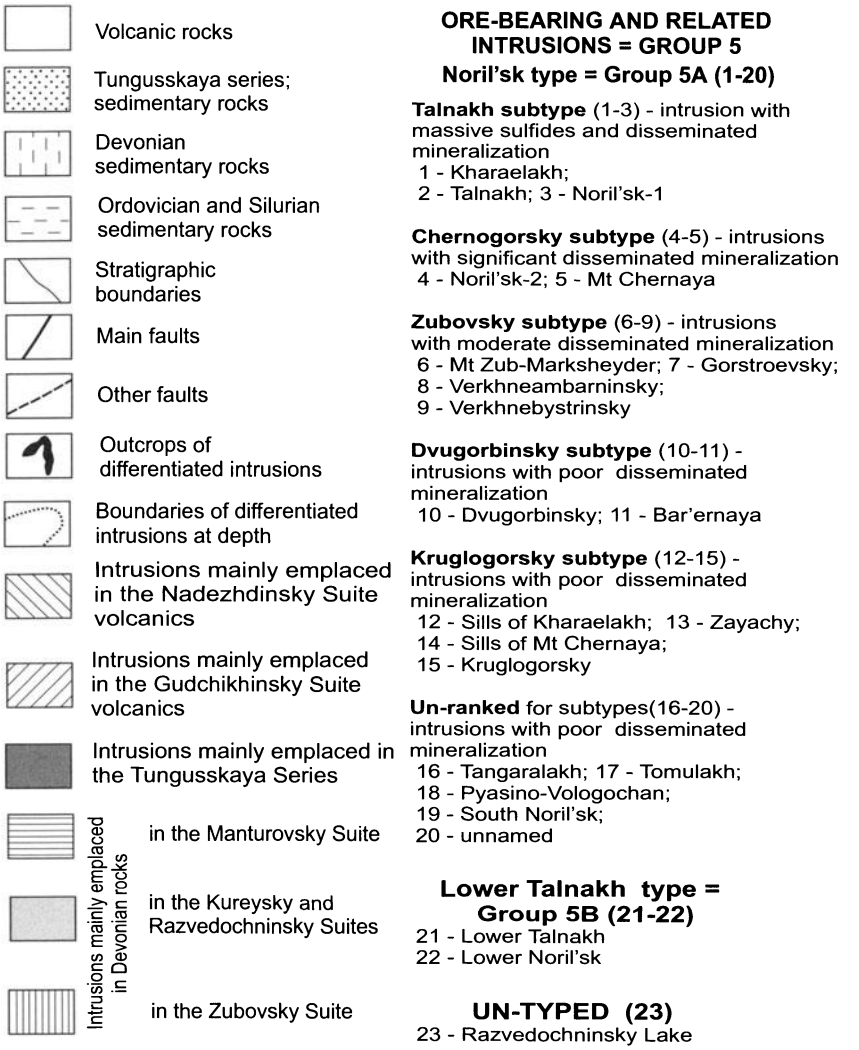


**Fig. 4.12.** Geological plan showing locations of differentiated intrusions in the vicinity of the Talnakh and Noril'sk ore junctions. For all intrusions (except the Lower Talnakh type) their sub-surface outline, in so far as it is known, is projected to surface. In the case of the Lower Talnakh intrusions only their outlines at the bedrock subsurface, beneath the Quaternary cover are shown; at depth these intrusions occupy all of the Kharaelakh basin that is covered by this figure, along and to the west of the Noril'sk-Kharaelakh fault. Depending on the location, the Lower Talnakh-type intrusions occur at stratigraphic levels ranging from the Lower Devonian Zubovsky suite up to the Tungusskaya series. Modified after Naldrett et al., (1992); map compiled on the basis of data collected by NKGRE and TsNIGRI

faults that extend in a northwest to west direction from the Noril'sk Kharaelakh fault, before curving to strike southwest. The thickening of the Lower Talnakh intrusion is particularly pronounced along the most northerly of these faults, and Zen'ko and Czamanske (1994a) suggested that the fault could be part of the feeder system to the intrusion. The Noril'sk-type intrusions at Talnakh, the Kharaelakh and Talnakh intrusions, appear to be controlled by different structures. The Talnakh intrusion is a linear body that extends 22 km along the length of the Noril'sk-Kharaelakh fault, mainly east of the fault, but also within the central graben of the fault in the south. The Kharaelakh intrusion lies entirely to the west of the fault, and has a triangular shape in plan, with the base of the triangle paralleling the fault and the apex projecting 7 km away from it in a west northwest direction (Fig. 4.12).

Both Lower Talnakh and Noril'sk type intrusions contain olivine with similar Fo contents, and include rocks of both mafic and picritic composition. However, there are some significant differences. Apart from the generally higher proportion of ultramafic rock associated with the Lower Talnakh type, these are much lower in Cr than the Noril'sk type. The amount of sulfide, and the Ni, Cu and PGE tenor of these sulfides are also much lower in the former than in the latter (see Table 4.5 below).

The well-mineralized intrusions of the Noril'sk-type are not known to extend more than 7 km from the Noril'sk-Kharaelakh fault (Fig. 4.12). Deposits that are or have been actively mined occur in three intrusions: The Talnakh and Kharaelakh[9] intrusions of the Talnakh ore junction, and the Noril'sk-1 intrusion of the Noril'sk ore junction. The Kharaelakh and Noril'sk-1 intrusions are situated to the west of the Noril'sk-Kharaelakh fault. As discussed above, the major part of the Talnakh intrusion (its North-Eastern branch) lies to the east of the fault, and the South-Western branch occurs in the Central graben of the fault zone (Fig. 4.12). The Kharaelakh intrusion is emplaced in Devonian argillites, marls and evaporites; the Talnakh intrusion in the Tungusskaya Series (Coal-bearing rocks of Middle Carboniferous – Upper Permian); and the Noril'sk-1 intrusion in the Tungusskaya and lower part of the overlying volcanic sequence (see Fig. 4.4).

The Lower Talnakh-type intrusions include, amongst others, the Lower Talnakh and Lower Noril'sk bodies that are present at the Talnakh and Noril'sk ore junctions correspondingly. The Lower Talnakh intrusion

[9] In Naldrett et al. (1992) these intrusions were referred to as the Main Talnakh and North-West Talnakh intrusions respectively. In this book the names that are used in the majority of Russian studies and in the paper by Czamanske et al. (1995) have been adopted.

mostly lies a few tens of m directly below the Talnakh intrusion (Fig. 4.13), while the Lower Noril'sk intrusion lies a similar distance stratigraphically below and 5-10 km to the west of the Noril'sk-1 body.

The internal structure of the mineralized intrusions is divisible into two distinctive zones, a relatively restricted "Main Body" (MB) and peripheral sills (Zen'ko and Czamanske 1994b). A schematic generalized section of a typical intrusion appears as Fig. 4.14. A generalized representation of the stratigraphy along with brief descriptions of the characteristics of the dominant rock types is given in Fig. 4.15. The MB are subdivisible into a lower contact gabbrodolerite marginal zone, which is overlain by a zone of plagioclase- and sulfide-rich taxitic (vari-textured) gabbrodolerite. This is followed by picritic gabbrodolerite containing 40-80 modal percent olivine (18-29 wt% of MgO), chromite and abundant disseminated sulfide. Olivine gabbrodolerite overlies the picritic zone. The contact is sharp and is marked by an abrupt decrease in sulfide. In some locations a thin (3 to 50 cm thick) picrite-like gabbrodolerite, containing 15-17 wt% of MgO and an unusually high content of chromium is present at the contact (note that the chromium content of the picritic layer increases systematically upward and then falls sharply in the olivine gabbrodolerite). There is a continuous upward decrease in the olivine content of the olivine gabbrodolerite as it grades into gabbrodolerite.

Rocks formed from magma that was the final residuum to the fractional crystallization of the intrusions overly the olivine gabbro. These include interlayered gabbro-diorite (prismatic gabbro), magnetite gabbro and quartz gabbro-diorite (Czamanske et al. 1995). The last rock type is found only in the Talnakh intrusion. According to Czamanske et al. (1995), it represents a hybrid rock formed at the contact of the intrusion with terrigenous sediments of the Tungusskaya Series. Leucogabbro, composed mainly (~80 mod%) of large tabular and xenomorphic, anorthite-rich plagioclase crystals occurs in the upper parts of the intrusions. Several hypotheses exist for the origin of the leucogabbro. Likhachev (1965) suggested that it corresponds to an early phase of the ore-bearing intrusion that had crystallized before injection of later batches of magma; Zolotukhin et al. (1975) attribute a major role to autometasomatism in its formation; Ryabov et al. (2000) related the appearance of the leucogabbro to liquid interlayering as a result of relatively "dry" and fluid-saturated leucocratic magmas separating from each other. An intrusive breccia is present in some localities at the roofs of intrusions, particularly in the Noril'sk-1 body where it may reach a thickness of 25 m. Fragments in the breccia comprise hornfelsed and metasomatised (skarn type alteration) sandstones, argillites, basalts and coal altered to graphite. The breccia matrix is composed of olivine-free and olivine-bearing gabbrodolerite, leucocratic and

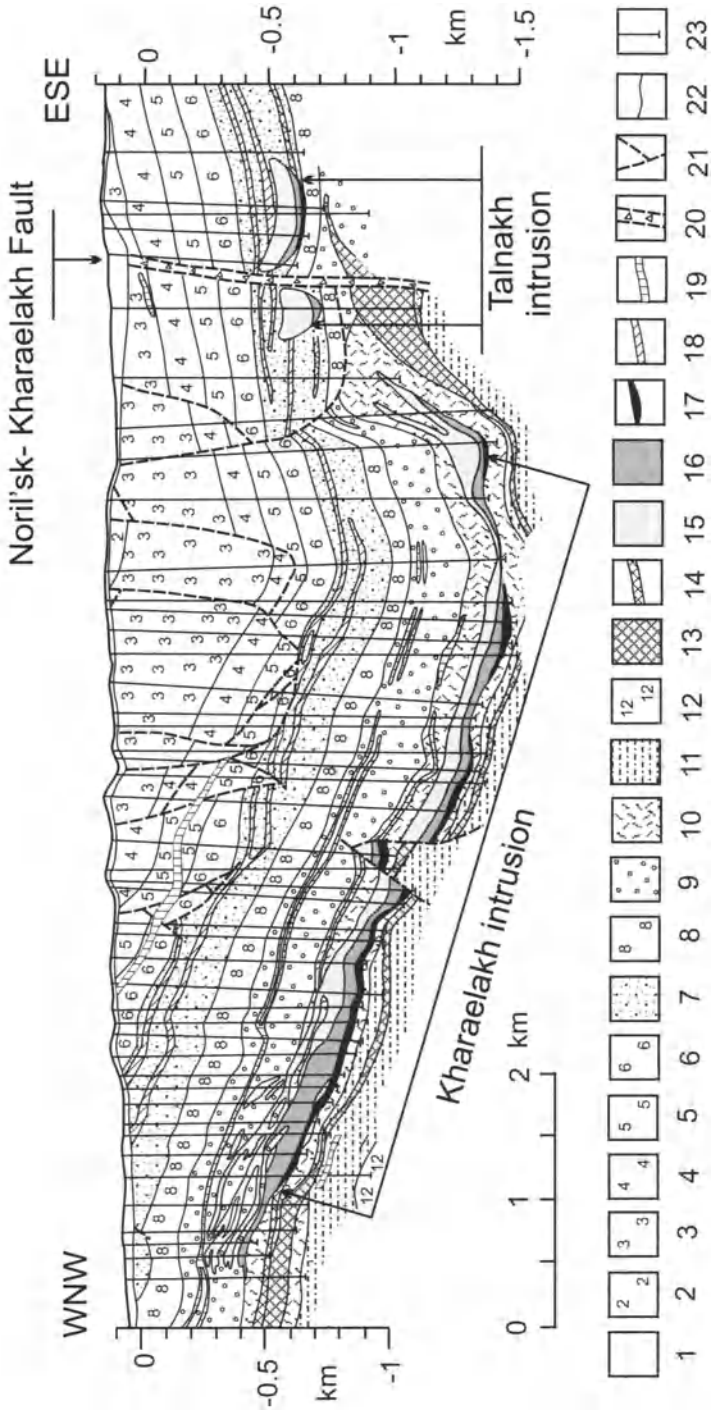
WNW
ESE
Noril'sk- Kharaelakh Fault
Talnakh intrusion
Kharaelakh intrusion
0
-0.5
-1
-1.5
km
0
1
2 km
1 2 3 4 5 6 7 8 9 10 11 12 13 14 15 16 17 18 19 20 21 22 23

**Figure 4.13.** East-West geologic cross section showing the relationship between the Kharaelakh, Talnakh and Lower Talnakh intrusions. Section compiled by Zen'ko on the basis of data collected by NKGRE and TsNIGRI. Patterns: 1 = Quaternary cover; 2-6 = basalts, 2 = ***Mr***, 3 = ***Nd***, 4 = ***Gd***, 5 = ***Sv***, 6 = ***Iv***; 7 = Tungusskaya series (terrigenous coal-bearing sediments); 8 = Kalargonsky, Nakokhzsky, Yuktinsky suites (Upper - Middle Devonian dolomites, limestones, marls, anhydrites); 9 = Manturovsky Suite (Middle Devonian marls, anhydrites, argillites); 10 = Kureysky and Razvedochninsky suites (Lower Devonian argillites, marls); 11 = Yampakhtinsky, Khrebtovsky and Zubovsky suites (Lower Devonian marls, anhydrites and dolomites); 12 = Silurian dolomites; 13 = Lower Talnakh intrusion; 14 = sills of Kharaelakh and Talnakh intrusions; 15-17 = Kharaelakh and Talnakh intrusions (15 = gabbrodolerites, 16 = picritic and taxitic gabbrodolerites with disseminated sulfides, 17 = massive sulfides) 18 = trachydolerite sills; 19 = dolerite sills; 20 = Noril'sk-Kharaelakh fault; 21 = other faults; 22 = formation boundaries; 23 = boreholes. From Naldrett et al. (1992)

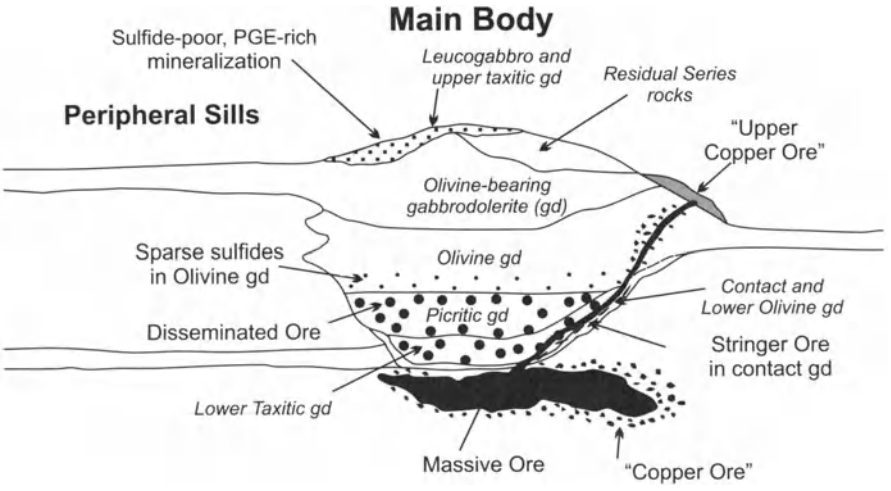


**Figure 4.14.** Schematic cross-section of a typical Noril'sk-type ore-bearing intrusion showing internal structure and associated ore-types. Modified after Naldrett et al. (1995)

taxitic gabbro, and hybrid-metasomatic rocks (Sluzhenikin et al., 1994; Sluzhenikin, 2000).

Not infrequently, taxitic gabbrodolerite near the roof of the intrusions is associated with a leucogabbro that is host to a sparse, PGE-rich sulfide mineralization. The sulfide-bearing rocks occur as layers and lenses; the most uniform and PGE-rich of these zones occur near the base of the leucogabbro (Fig. 4.16). Sluzhenikin (2000) observed that the upper taxitic gabbrodolerites are composed of large (up to 2 cm) zoned crystals of early

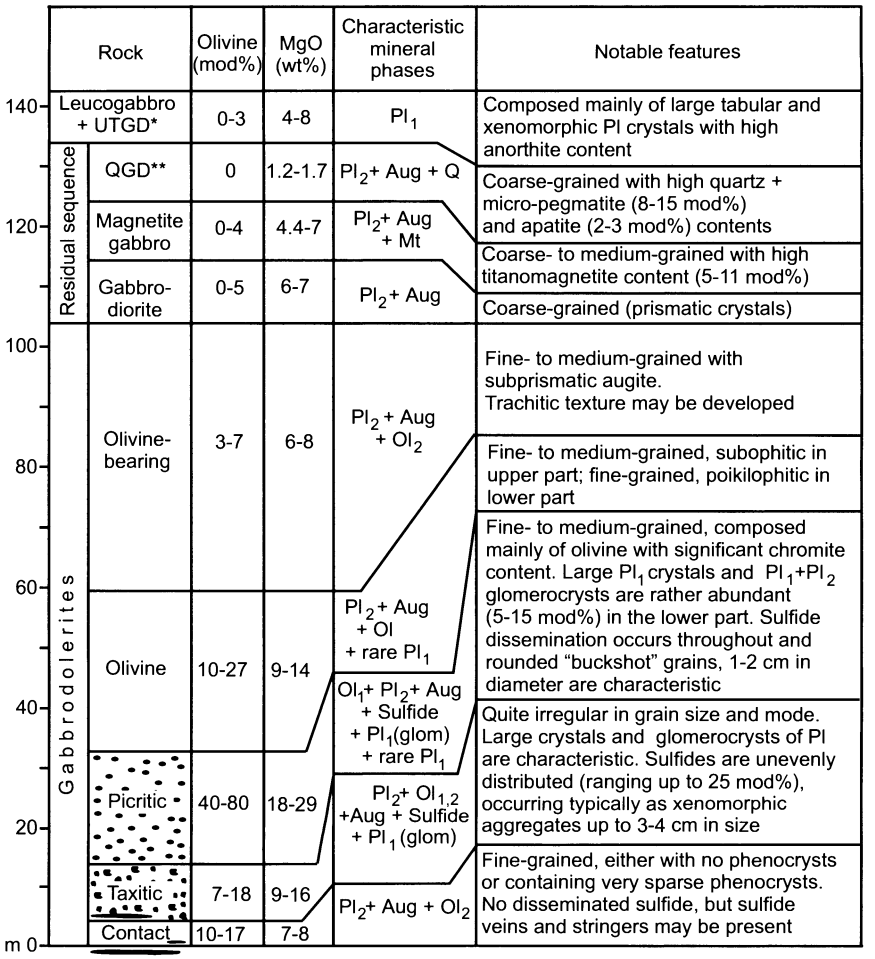


**Figure 4.15.** Generalized lithological section for the main bodies of the ore-bearing intrusions along with brief characteristics of the dominant rock types. Sulfide mineralization is shown: disseminated [predominately globular in picritic gabbrodolerite and xenomorphic (interstitial) in taxitic gabbrodolerite], and massive sulfide veins in taxitic and contact gabbrodolerites, and in the country rocks below the intrusion. The weak sulfide mineralization in the upper taxitic gabbrodolerite is not shown. Mineral phases: Pl1 – prismatic, tabular and xenomorphic grains without inclusions and with few twins; Ol1 – large (up to 3-4 mm) euhedral and resorbed grains; Ol2 - large (up to 7 mm) paw-shaped grains, oikocrysts containing Pl chadacrysts, small (up to 0.4-0.5 mm) xenomorphic and rounded grains. After Czamanske et al. (1995)

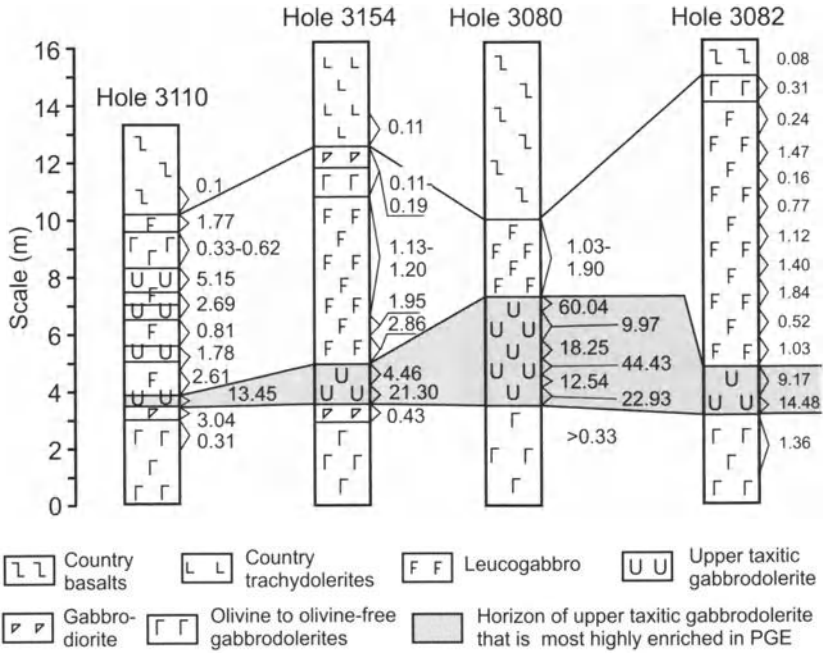


**Figure 4.16**. Position of the upper taxitic gabbrodolerite with PGE-rich low-sulfide mineralization in the stratigraphic section of the Noril'sk-1 intrusion. Total PGE contents (g/t) are given to right of the columns. After Sluzhenikin (2000)

cumulate plagioclase ($An_{75-85}$) with prismatic and lath-like plagioclase ($An_{54-61}$)[10], clinopyroxene and magnesian phlogopite interstitial to them. The fabric of these rocks is ataxitic, with variable grain size and uneven distribution of the clinopyroxene, phlogopite, chromite, and secondary silicates. A characteristic feature of these upper taxitic rocks and associated leucogabbros is the presence of amygdules (up to 3 cm in diameter) that can constitute as much as 25 percent of the rock volume. They are filled by prehnite, actinolite, saponite, chlorite, angidrite and carbonates. Their compositions are marked by elevated concentrations of Cr and Cl (the Cl content can reach 2 wt%). The whole-rock Cr content in the upper taxitic gabbrodolerite is unusually high, reaching 1.5-6 wt%, in comparison with a maximum of 0.5 wt% Cr in the lower parts of the intrusions. The Cr oc-

[10] These data relate to the Noril'sk-1 intrusion. In the underlying part of the intrusion, the percentage of anorthite in plagioclase (rim – center) varies from 27-47 in olivine-free gabbrodolerite, increases from 41-62 to 66-84 through the olivine-bearing and olivine gabbrodolerites, and reaches a maximum of 55-88 in the picritic gabbrodolerite before decreasing to 65-69 in the lower part of the taxitic gabbrodolerite (Sluzhenikin, 2000).

curs principally in Cr-spinel that forms segregations a few mm to a few cm in diameter. Sulfides constitute only about 1-2 mod% of the rock and occur commonly in the inner parts of amygdules along with $H_2O$-, Cl-, and F-bearing minerals. The sulfides (dominantly pyrrhotite) are extensively replaced by silicate minerals, principally actinolite, biotite, chlorite, and prehnite. Sluzhenikin (2000) attributed an important role to volatiles during postmagmatic cooling in the formation not only of the $H_2O$-, Cl-, and F-bearing minerals but also of the Cr-spinels and minerals of the noble metals.

Compositions of the principal rocks of the ore-bearing intrusions are given in Table 4.3. Variations in the proportions and compositions of the main constituent minerals over a vertical sequence through the Talnakh intrusion are illustrated in Figs. 4.17 and 4.18.

The thickness of the complete sequence through the main body of an ore bearing intrusion varies from several 10's of m to 300-350 m, but most commonly is between 70 and 180 m. In many locations, the intrusions diverge from the "type" sections shown in Fig. 4.15, 4.17 and 4.18. Systematic differences exist between specific intrusions. The Kharaelakh intrusion is characterized by a higher proportion of taxitic than picritic gabbrodolerite, an unusually thick sequence of leucogabbro and associated taxitic gabbrodolerite at the upper contact, and a lower proportion of "residual dioritic" rocks than is found in other intrusions. The Kharaelakh intrusion also shows major differences between its center, "flanks" (northern and southern margins) and the frontal zone (western limit). In the frontal zone, the intrusion fingers out (as seen in vertical section) with taxitic gabbrodolerite increasing at the expense of picritic gabbrodolerite to an even greater degree than in the rest of the intrusion, to the extent that the frontal zone consists almost entirely of mineralized, olivine-bearing taxitic gabbrodolerite (Torgashin, 1994). Lateral variations of this kind are not present in the elongated Talnakh and Noril'sk I intrusions. The southwestern branch of the Talnakh intrusion (west of the Noril'sk-Kharaelakh fault) has a higher than usual proportion of picritic gabbrodolerite, while the northeastern branch (east of the fault) has a higher than usual proportion of "residual diorites" (Fig. 4.19).

The peripheral sills of the ore-bearing intrusion extend up to 10 km from the main bodies (Zen'ko, 1986). Some of them are up to 20 m thick close

**Table 4.3.** Chemical compositions of principal rock types of the ore-bearing intrusions of the Talnakh ore junction (range of element contents). After data of Czamanske et al. (1995)

| | LG | QGDi | MG | GDi | OBGD | OGD |
|---|---|---|---|---|---|---|
| n | 2 | 4 | 7 | 3 | 11 | 9 |
| $SiO_2$ | 45.1-46.1 | 53.3-56.9 | 41.0-49.7 | 49.3-50.1 | 48.5-49.6 | 44.5-47.0 |
| $TiO_2$ | 0.33-0.56 | 1.27-2.09 | 2.12-3.00 | 1.12-1.30 | 0.72-1.14 | 0.60-0.88 |
| $Al_2O_3$ | 23.0 | 11.5-12.1 | 11.2-12.2 | 15.1-13.8 | 14.1-17.8 | 12.5-18.8 |
| FeOT | 5.7-7.0 | 12.3-14.5 | 16.5-22.1 | 10.7-11.6 | 7.4-10.9 | 7.7-13.3 |
| MnO | 0.15-0.16 | 0.14-0.25 | 0.21-0.41 | 0.22-0.27 | 0.14-0.22 | 0.13-0.22 |
| MgO | 3.7-7-6.1 | 1.16-2.35 | 3.6-6.9 | 6.0-6.4 | 6.0-8.2 | 8.9-14.6 |
| CaO | 10.3-11.6 | 4.8-6.8 | 7.2-10.6 | 10.5-11.9 | 11.1-13.8 | 9.1-11.5 |
| $Na_2O$ | 1.9-2.0 | 4.1-6.0 | 1.8-3.3 | 2.4-2.5 | 1.6-2.4 | 1.2-1.9 |
| $K_2O$ | 1.2-2.8 | 0.25-2.1 | 0.6-1.3 | 0.6-0.9 | 0.40-0.86 | 0.32-0.49 |
| $P_2O_5$ | 0.06-0.08 | 0.44-0.48 | 0.10-0.36 | 0.13-0.18 | 0.09-0.14 | 0.07-0.11 |
| LOI | 3.9 | 0.9-1.5 | 0.8-2.0 | 1.2-1.5 | 0.9-2.3 | 1.0-1.7 |
| $CO_2$ | 0.13-019 | 0.06-1.15 | 0.01-0.06 | 0.04-0.04 | 0.01-0.05 | 0.03-0.14 |
| S | 0.23-0.29 | 0.46-0.94 | 0.16-0.79 | 0.09-0.21 | 0.03-0.20 | 0.04-0.69 |
| Sc | 11-15 | 17-26 | 33-43 | 37-44 | 35-46 | 20-28 |
| Cr | 172-270 | 2.6-2.7 | 4-116 | 12-35 | 18-740 | 300-2750 |
| Y | 7-20 | 68-114 | 22-47 | 28-31 | 14-36 | 11-20 |
| Ni | 200-570 | 17-21 | 34-154 | 59-71 | 60-114 | 210-860 |
| Co | 28-36 | 11-31 | 39-83 | 37-46 | 35-47 | 47-94 |
| Cu | 450-700 | 25-124 | 13-870 | 134-235 | 55-192 | 65-1050 |
| Au | 10-30 | <2.5 | <8.3 | <2.7-7.1 | <0.3-16.3 | 2-19 |
| Pd | 270-840 | <1 | <0.5 -4.6 | <0.5-0.6 | <2-85 | 3-410 |
| Pt | 130-370 | <0.6 | <0.5 -2.0 | <0.5-4.2 | 0.8-180 | 5-130 |
| Rh | 20-38 | <0.5 | <1 | <0.5 | <0.5-2.1 | 0.6-21.0 |
| Ru | 6-13 | <0.5 | <1 | <0.5 | <0.8 | 0.7-10.0 |
| Ir | 2-5 | <0.5 | <1 | <0.5 | <0.5-1 | 0.6-3.8 |
| Rb | 36-85 | 11-42 | 17-46 | 23-37 | 15-30 | 10-21 |
| Sr | 325-350 | 158-254 | 180-275 | 260-290 | 215-290 | 190-280 |
| Ba | 178-400 | 170-370 | 126-350 | 192-230 | 97-250 | 82-184 |
| Th | 0.5-0.64 | 4.2-6.4 | 0.6-2.8 | 0.9-1.4 | 0.57-1.09 | 0.46-0.90 |
| U | 0.27-0.39 | 1.3-2.0 | 0.30-1.10 | 0.37-0.65 | 0.22-0.50 | 0.21-0.37 |
| Ta | 0.12-0.15 | 0.9-1.8 | 0.17-0.73 | 0.23-0.38 | 0.13-0.26 | 0.12-018 |
| Zr | 41-48 | 260-370 | 66-166 | 81-122 | 51-87 | 45-68 |
| Hf | 0.98-1.14 | 7.3-9.4 | 1.5-4.7 | 1.9-2.8 | 1.1-2.2 | 1.0-1.6 |
| La | 3.1-6.7 | 23-39 | 6-23 | 8-12 | 4.2-8.4 | 3.7-5.3 |
| Ce | 7.8-5.1 | 64-111 | 12-49 | 18-23 | 9-19 | 8.9-12.6 |
| Nd | 4.9-8.5 | 39-66 | 7-25 | 10-14 | 6.0-10.6 | 5.4-8.0 |
| Sm | 1.4-2.1 | 10-17 | 2.2-6.6 | 3.0-3.7 | 1.8-3.1 | 1.5-2.3 |
| Eu | 0.6-0.7 | 2.8-3.4 | 0.8-2.3 | 1.1-1.2 | 0.7-1.1 | 0.59-0.84 |
| Gd | 1.7-2.2 | 12-19 | 2.8-7.9 | 3.6-4.0 | 2.2-3.5 | 1.7-2.7 |
| Tb | 0.27-0.33 | 1.9-3.5 | 0.5-1.3 | 0.58-0.68 | 0.38-0.59 | 0.28-0.45 |
| Ho | 0.35-0.46 | 2.7-5.0 | 0.7-1.8 | 0.85-0.96 | 0.56-0.88 | 0.42-0.66 |
| Tm | 0.14 | 1.1-2.0 | 0.28-0.82 | 0.36-0.43 | 0.24-0.40 | 0.19-0.29 |
| Yb | 1.2-0.9 | 7-10 | 1.8-5.1 | 2.3-2.7 | 1.5-2.5 | 1.2-1.8 |
| Lu | 0.14-0.18 | 1.0-1.4 | 0.25-0.73 | 0.33-0.41 | 0.22-0.35 | 0.17-0.28 |

**Table 4.3** (cont.)

| | PLGD | PGD | TGD | TLGD | CGD |
|---|---|---|---|---|---|
| n | 1 | 9 | 4 | 4 | 1 |
| $SiO_2$ | 45.1 | 34.8-42.6 | 34.9-42.0 | 38.4-48.4 | 48.1 |
| $TiO_2$ | 0.70 | 0.41-0.66 | 0.23-0.71 | 0.61-1.02 | 1.20 |
| $Al_2O_3$ | 13.9 | 5.7-10.1 | 7.8-14.6 | 14.0-16.5 | 15.2 |
| FeOT | 11.34 | 13.2-20.6 | 12.1-19.9 | 10.7-16.9 | 12.5 |
| MnO | 0.19 | 0.20-0.22 | 0.17-0.21 | 0.15-0.21 | 0.22 |
| MgO | 15.5 | 19.8-25.1 | 9.7-16.8 | 7.1-8.9 | 7.2 |
| CaO | 9.3 | 4.4-7.2 | 6.0-10.0 | 8.7-10.4 | 10.3 |
| $Na_2O$ | 1.53 | 0.69-1.01 | 0.88-1.12 | 1.05-2.05 | 1.91 |
| $K_2O$ | 0.33 | 0.09-0.29 | 0.22-0.61 | 0.54-0.85 | 0.89 |
| $P_2O_5$ | 0.08 | 0.05-0.10 | 0.03-0.09 | 0.08-0.13 | 0.15 |
| LOI | 1.0 | 2.4-6.8 | 4.7-6.1 | 1.3-4.9 | 1.2 |
| $CO_2$ | 0.15 | 0.06-0.60 | 0.06-0.45 | 0.08-0.53 | 0.05 |
| S | 0.12 | 0.14-5.60 | 2.3-6.5 | 1.14-4.66 | 0.32 |
| Sc | 25 | 16-23 | 14-28 | 20-33 | 34 |
| Cr | 2750 | 520-4550 | 225-590 | 170-280 | 170 |
| Y | 13 | 5-14 | 7-19 | 9-20 | 27 |
| Ni | 430 | 740-8700 | 2350-7500 | 1250-6800 | 225 |
| Co | 77 | 103-316 | 135-316 | 84-250 | 54 |
| Cu | 122 | 270-13800 | 8600-21000 | 2700-16900 | 640 |
| Au | 3.12 | 10-175 | 87-491 | 38-361 | 7 |
| Pd | 46 | 420-3500 | 2800-8500 | 810-5200 | 66 |
| Pt | 59 | 220-1100 | 750-3200 | 260-750 | 28 |
| Rh | 8.1 | 34-190 | 83-270 | 24-120 | 1.5 |
| Ru | 5.5 | 12-63 | 26-81 | 5-36 | 0.6 |
| Ir | 1.8 | 4.8-140 | 9-29 | 2-11 | <0.5 |
| Rb | 11 | 4-12 | 7-27 | 13-38 | 31 |
| Sr | 200 | 88-146 | 120-215 | 182-270 | 250 |
| Ba | 91 | 48-94 | 71-136 | 164-295 | 330 |
| Th | 0.47 | 0.71-0.20 | 0.36-0.41 | 0.41-1.07 | 1.13 |
| U | 0.233 | 0.09-0.28 | 0.09-0.23 | 0.21-0.63 | 0.53 |
| Ta | 0.12. | 0.08-0.15 | 0.05-0.14 | 0.12-0.24 | 0.30 |
| Zr | 46 | 24-56 | 27-49 | 40-76 | 98 |
| Hf | 1.1 | 0.66-1.36 | 0.55-1.13 | 1.05-1.87 | 2.39 |
| La | 4.0 | 2.3-4.6 | 2.0-4.0 | 3.6-6.8 | 10.1 |
| Ce | 9.3 | 6.0-10.3 | 3.8-9.7 | 9.8-15.9 | 23.7 |
| Nd | 5.2 | 3.3-6.6 | 2.6-6.6 | 5.3-10.3 | 13.1 |
| Sm | 1.6 | 1.1-1.9 | 0.78-1.80 | 1.60-2.75 | 3.71 |
| Eu | 0.60 | 0.36-0.58 | 0.40-0.59 | 0.61-0.99 | 1.17 |
| Gd | 1.9 | 1.2-2.3 | 1.0-2.0 | 2.0-3.0 | 4.09 |
| Tb | 0.31 | 0.19-0.35 | 0.16-0.34 | 0.32-0.52 | 0.66 |
| Ho | 0.45 | 0.30-0.54 | | 0.47-0.77 | 0.93 |
| Tm | | 0.17-0.23 | | 0.23 | 0.39 |
| Yb | 1.28 | 0.82-1.48 | 0.64-1.31 | 1.2-2.1 | 2.56 |
| Lu | 0.20 | 0.13-0.21 | 0.09-0.19 | 0.17-0.30 | 0.38 |

**Table 4.3** (cont.)
*LG* leucogabbro; *QGDi* quartz gabbro-diorite; *MG* magnetite gabbro; *GDi* gabbro-diorite; *OBGD* olivine-bearing gabbrodolerite; *OGD* olivine gabbrodolerite; PLGD picritic-like gabbrodolerite; *PGD* picritic gabbrodolerite; *TGD* taxitic gabbrodolerite; *TLGD* Taxitic-like gabbrodolerite; *CGD* contact gabbrodolerite.

*n* quantity of samples. Leucogabbro is from the Kharaelakh intrusion (hole KZ-1879), other rocks from the Talnakh intrusion (holes KZ-1713 and KZ-1799). Major elements in wt%, PGE in ppb, other elements in ppm

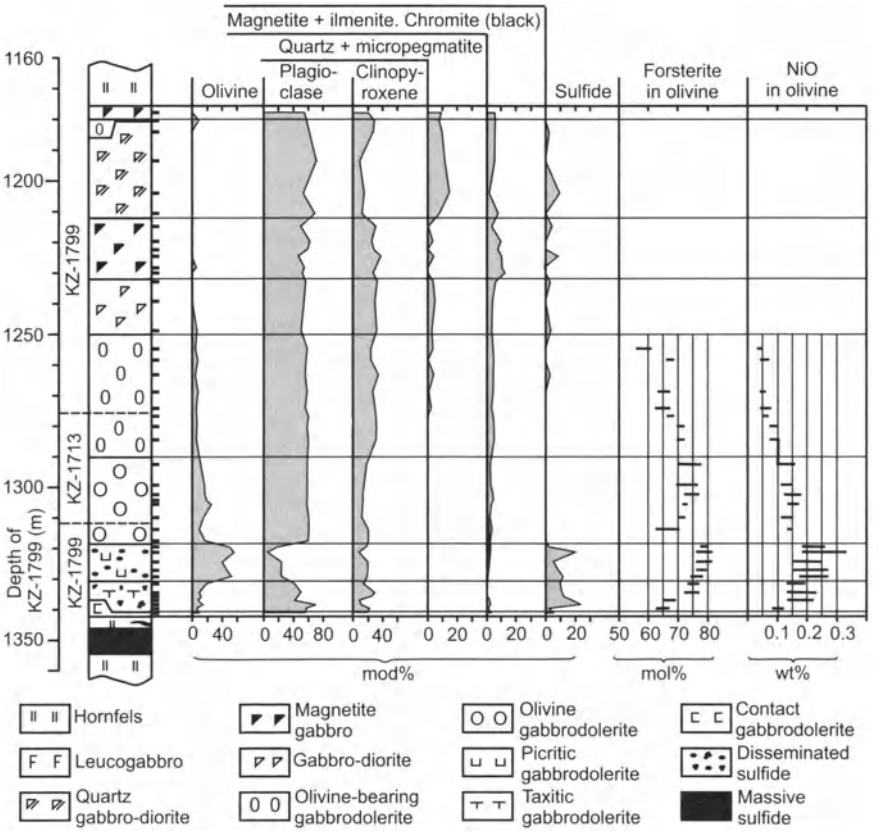


**Fig. 4.17.** Variation in the proportions and compositions of the principal minerals in the Talnakh ore-bearing intrusion. Data are from core KZ- 1799, supplemented by data from KZ-1713 over the interval 1276-1312 m, for which data for KZ-1799 are not available. Borehole locations are shown in Fig. 4.28 below. After Czamanske et al. (1995)

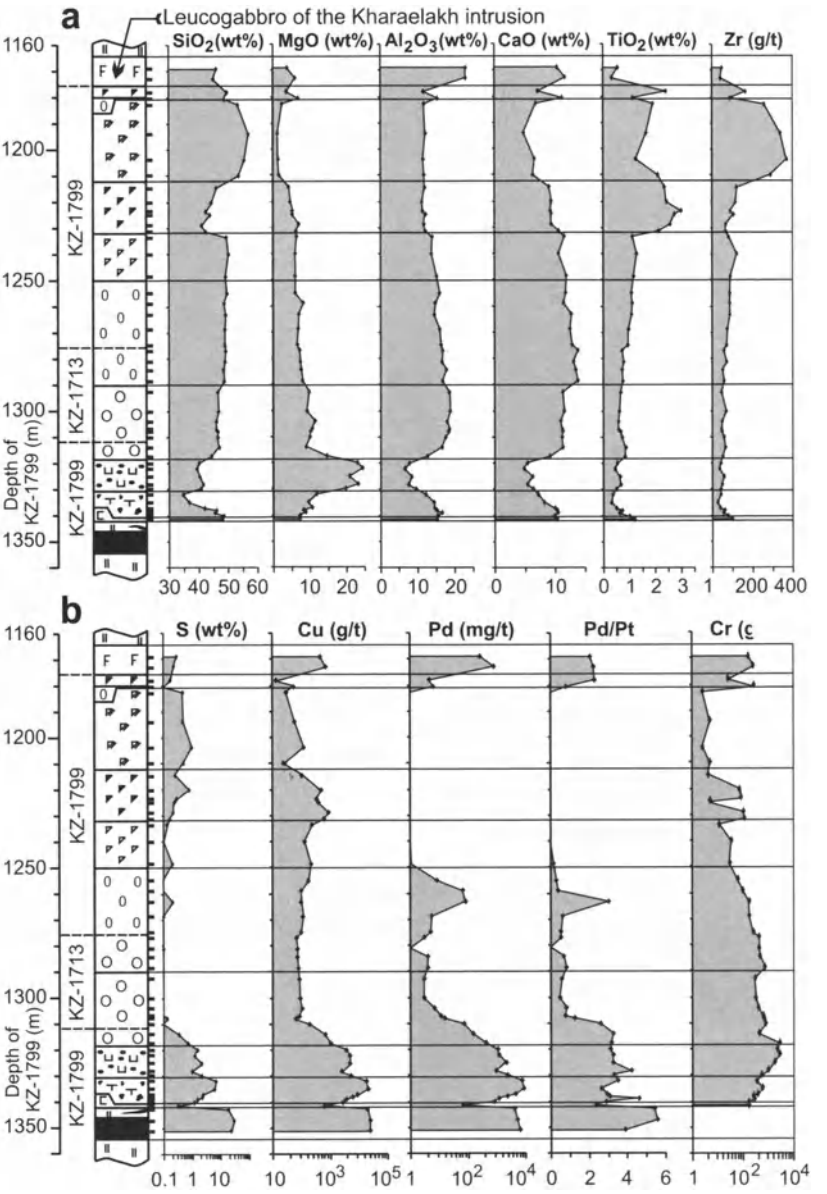


**Fig. 4.18.** Variation in the concentrations of: rock forming elements (a) and ore elements (b) through a section of a typical Noril'sk-type ore-bearing intrusion. Section of the Talnakh intrusion from Fig. 4.17 is present supplemented by data for leucogabbro from hole KZ-1879 (interval 1698-1705 m). Legend is as in Fig. 4.17; borehole locations are in Fig, 4.28. After data of Czamanske et al. (1995)

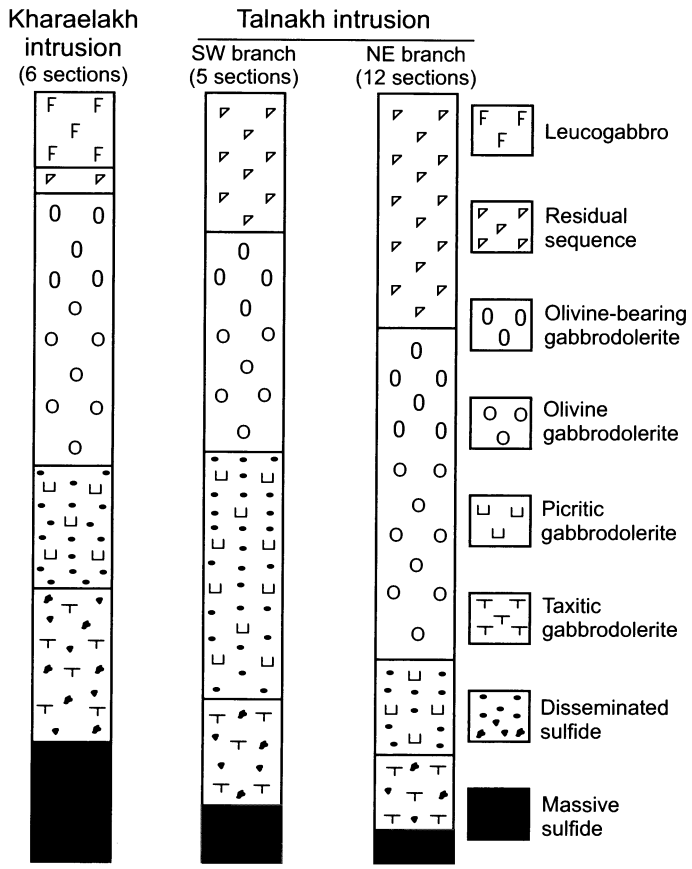


**Fig. 4.19.** Lithologic columns showing the variation in average thickness of principal rock units in main bodies of the Kharaelakh and SW and NE branches of the Talnakh intrusion. The columns have been normalized to equal thickness for comparative purpose. Actual thicknesses for the Kharaelakh intrusion and the SW and NE branches of the Talnakh intrusion range from 49 to 173 m, 83 to 126 m, and 88 to 187 m, respectively. Irregular black blobs represent the occurrence of globular disseminated ore in picritic gabbrodolerite and interstitial disseminated ore in taxitic gabbrodolerite. The number of sections given at the head of each column is the number of individually measured sections from which the columns have been generalized. After Czamanske et al. (1995)

to main bodies. These relatively thick sills are composed mainly of olivine gabbrodolerite, that commonly shows a taxitic-like fabric. They are enriched in plagioclase near the roof and may contain lenses of picritic gabbrodolerite near the base (Zen'ko and Czamanske, 1994). Sulfides sometimes occur in the lower parts of those sills that show the greatest variability in composition. For example, disseminated mineralization close

to economic grade (2 m thick) was intersected in hole VH-4 the sill, that was drilled north of the Talnakh intrusion on the east side of the Noril'sk-Kharaelakh fault (Lev Shadrin, personal communication, 1994). However, many of the sills, both close to and at a distance from the main bodies consist of uniform, sulfide-free dolerite and gabbrodolerite with or without olivine. They correspond to normal tholeiitic basalt in their chemical composition (see below).

A number of explanations have been proposed for the origin of the main bodies and their peripheral sills. The classical view is that both formed as the result of a single injection of magma containing 10-12 wt% MgO, charged with phenocrysts of olivine and plagioclase along with droplets of immiscible sulfide, that then differentiated within the chambers currently occupied by the bodies (Korovyakov et al. 1963; Zen'ko 1983, 1994). Zen'ko (1994) proposed that the peripheral sills are apophyses to the main body magma chambers that developed after the main chambers had differentiated, although she calculated that the volume of the apophyses of the Talnakh ore junction is twice that of the main bodies themselves. Likhachev (1965) regarded the sills as being formed by an early injection of magma, prior to formation of the main bodies. In a later paper (Likhachev 1994) he suggested that the main bodies developed from convecting magma that circulated through them, cooling, and then sank back to deeper levels than the bodies themselves, so that the bodies acted as a natural radiator. Fedorenko (in Czamanske et al., 1995) suggested that the material in the main bodies was injected as a series of pulses from a deeper magma chamber where the magma was differentiating. He proposed that an early basaltic pulse (which also produced the peripheral sills) was followed by picrite charged with sulfide droplets, and that finally a nearly pure sulfide liquid was emplaced.

This author's model, is described below, and holds that the ore-bearing intrusions (both main bodies and peripheral sills), along with the associated Lower Talnakh type intrusions, were feeder conduits for the overlying $Nd_1$ to $Mr_2$ volcanic formations, through which periodic pulses of magma flowed.

## *Geochemistry of the Noril'sk- and Lower Talnakh-type Intrusions and their relation to the volcanic formations*

**Trace-element geochemistry**. The succession of lavas discussed above gives an indication of the sequence of changes that were occurring in the main magma system. It is important to review how the ore-bearing intrusions fit into this evolutionary scheme.

Figure 4.20 is a plot of Gd/Yb versus La/Sm, with samples of the group 5 intrusions (Noril'sk and Lower Talnakh types) superimposed on the field for the volcanics. As was shown by Naldrett et al. (1992), the Gd/Yb ratios (and $TiO_2$ content) indicate that these intrusions are part of the association II magmatism (***Tk-Sm***). The bulk of the Noril'sk-type intrusions coincide in this diagram with the ***Tk*** and ***$Mr_2$-Mk*** formations. Most of the samples

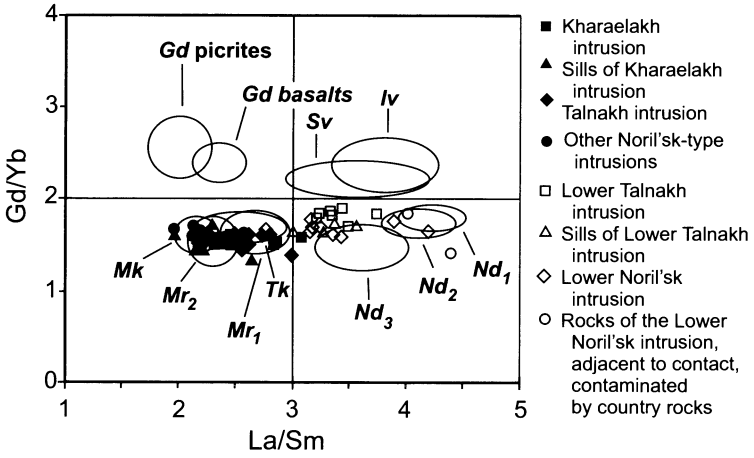


**Fig. 4.20.** Plot of Gd/Yb versus La/Sm showing the Noril'sk-type and Lower Talnakh-type intrusions superimposed on the fields for the volcanic formations from the ***Iv*** to the ***Mk***. From Naldrett et al. (1995)

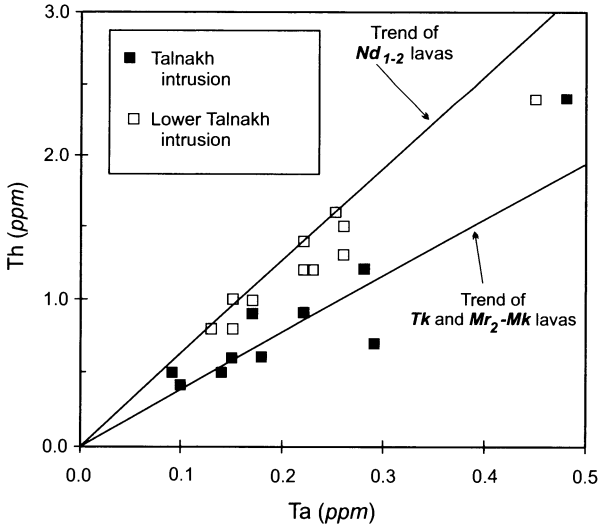


**Fig. 4.21.** Plot of Th vs. Ta for rocks from the Noril'sk- and Lower Talnakh-type intrusions (from Naldrett et al., 1995)

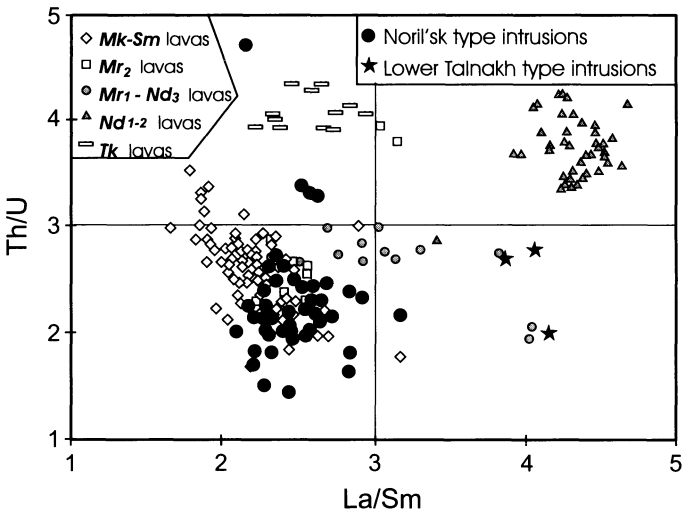


**Fig. 4.22.** Plot of Th/U versus La/Sm in which data for the Noril'sk- and Lower Talnakh-type intrusions are superimposed on that for the volcanic suites from the ***Tk*** to the ***Mr*$_2$**. The figure provides strong support for the correlation between the Noril'sk-type intrusions and ***Mr*$_1$-*Mr*$_2$** magma and between the Lower Talnakh-type intrusions and ***Nd*$_2$-*Nd*$_3$** type magma. Data from Lightfoot at al. (1994, 1995)

of Lower Talnakh-type intrusions plot between the ***Nd*$_2$** and ***Mr*$_1$**, essentially coincident with the ***Nd*$_3$** formation.

In the plot of Th versus Ta (Fig. 4.21), the Lower Talnakh-type intrusions clearly scatter along and slightly below the trend for the ***Nd*$_1$-*Nd*$_2$** (a ratio of 6.25) while the Noril'sk-type follow the trend of the ***Tk***, ***Mr*$_2$** and ***Mk*** (ratio = 3.75).

The Ni contents of unmineralized rocks from the Lower Talnakh intrusions are about 50% of the Ni contents characteristic of unmineralized rocks from the Noril'sk-type intrusions with the same MgO content (Naldrett et al. 1992).

It was shown above, that a major argument that a new type of magma from a different source (the ***Mk-Sm*** magma type) had entered the plumbing system at Noril'sk was the difference in Th/U ratios between the ***Tk*** and ***Nd*$_{1-2}$** and the ***Mk-Sm*** magmas, and that, coincident with this change in geochemistry, the thickness of individual units increased to the northeast, rather than toward the Noril'sk-Kharaelakh fault. Fig. 4.22 is a plot of Th/U versus La/Sm for the intrusions superimposed on the similar data from Fig. 4.8. The figure reinforces the correlations made on the basis of other geochemical data between the Lower Talnakh intrusions and the ***Nd*$_2$-*Nd*$_3$** transitional magmas and the Noril'sk type intrusions and the ***Mr*$_1$-*Mr*$_2$** magmas.

**Radiogenic Isotopes.** Fig. 4.23 shows $^{87}Sr/^{86}Sr$ plotted against La/Sm ratio for the volcanic formations from the ***Tk*** to the ***Sm*** and for the Noril'sk- and Lower Talnakh-type intrusions. $^{87}Sr/^{86}Sr$ increases regularly with increase in La/Sm ratio; this is to be expected (see section 4.1.2) if the magmas are the result of contamination of an initial ***Tk***-type magma by a crustal component with high La/Sm and $^{87}Sr/^{86}Sr$, followed by mixing with increasing amounts of $Mr_2$-***Sm*** magma that had similar concentrations of REE and Sr and similar $^{87}Sr/^{86}Sr$ and La/Sm ratios to the ***Tk*** (averages of La and Sr are, respectively, 7.7 and 207 ppm in the $Mr_2$, and 5.8 and 267 ppm in the ***Tk***).

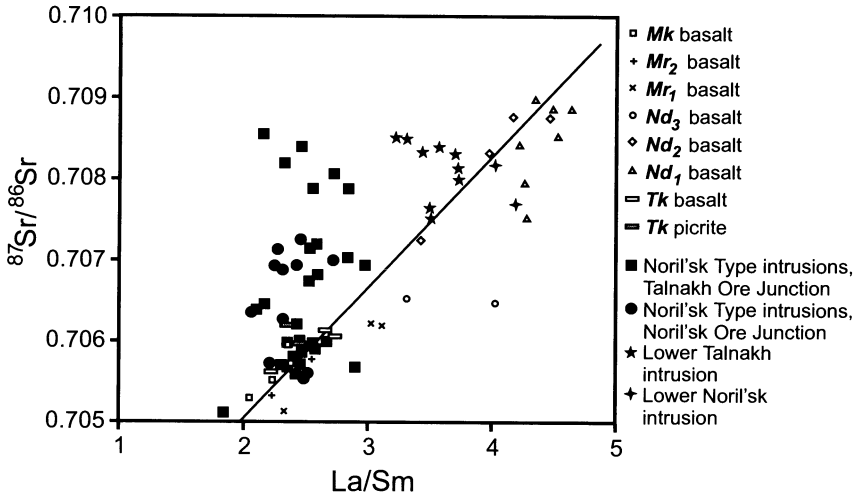


**Fig. 4.23.** Plot of $^{87}Sr/^{86}Sr$ versus La/Sm for the volcanic rocks and Noril'sk- and Lower Talnakh-type intrusions of the Noril'sk region. Data from Lightfoot et al. (1993), Hawkesworth et al. (1995), Arndt et al. (2003)

Some samples of intrusions (data of Hawkesworth et al. 1995, Arndt et al. 2003) are displaced to higher $^{87}Sr/^{86}Sr$ values than volcanic rocks with the same La/Sm ratio. Czamanske et al. (1995) noted that the intrusions replace evaporite beds; these contain of the order of 2500 ppm Sr, so that presumably contamination by radiogenic Sr would have occurred during their emplacement. However, Sr is particularly radiogenic in the plagioclase-rich marginal parts of the intrusions; for example Czamanske et al. (1995) show that $^{87}Sr/^{86}Sr_{250Ma}$ varies from 0.7051 in olivine-rich rocks at the center of one profile through the Kharaelakh intrusion to 0.7081 at the upper margin and 0.7088 at the lower margin. The isotopic composition of Sr in these samples is decoupled from all other geochemical parameters and Naldrett et al. (1995) suggested that radiogenic Sr had been added to

the intrusions subsequent to their crystallization, as a result of hydrothermal activity transferring radiogenic Sr from the enclosing adjacent evaporite. If this is the case, the conclusion from Fig. 4.23 is that the $^{87}Sr/^{86}Sr$ of the Noril'sk- and Lower Talnakh-type intrusions may have been increased subsequent to their emplacement. Arndt et al. (2003) argued against this interpretation for two reasons; (i) that in places high ratios occur near the center of intrusions and lower ratios at the margins and (ii) that there are abrupt changes in ratio at the contacts between different units in the intrusions that they (and this author) attribute to different pulses of magma flowing through them, citing their Fig.5. This author is not impressed with the clarity of the changes cited in their figure, and leaves it to the reader to draw his/her conclusions on this matter. The reason that we have considered this point in some detail is that it is a very important one. If the radiogenic Sr in the intrusions is original, and characteristic of the magma of the intrusions, it rules out this magma being correlated with any of the magma represented by the volcanic stratigraphy, i.e. that the mineralized intrusions were not flow-through channels for the overlying volcanic rocks.

Arndt et al.'s (2003) Nd and Sr isotopic data for the Lower Talnakh and Noril'sk, Talnakh, Kharaelakh, Noril'sk-1 and Noril'sk-2 intrusions are superimposed on averages for the volcanic suites (see Fig. 4.10) in Fig 4.24. On the basis of their εNd values, the Lower Talnakh intrusions fall between the $Nd_{1-2}$ and $Nd_3$ volcanic suites while the Talnakh, Kharaelakh and Noril'sk-1I and -2 data fall between the $Mr_1$ and $Mr_2$ volcanic suites, which is consistent with conclusions based on trace element data. The intrusions show a much wider spread in $^{87}Sr/^{86}Sr$ ratio than in εNd, which is attributed to the enrichment discussed above.

**Sulfur Isotopes.** The sulfur isotopic composition of intrusions and ores of the Noril'sk region have been investigated by Godlevsky and Grinenko (1963), Gorbachev and Grinenko (1973), Grinenko (1985a,b) and Li et al. (2003). Results of these studies for the Noril'sk I, Talnakh and Kharaelakh intrusions and related ores are shown in Fig. 4.25. Sulfur isotope ratios are heavy with values ranging from +5 to +15 $\delta^{34}S$. The average of 43 determinations of $\delta^{34}S$ for Noril'sk-1 is 8.5, in comparison with averages of 10.9 for the Talnakh ores and 10.5 for the Kharaelakh ores. Li et al. (2003) noted that there is little difference between different ore types (massive sulfide, disseminated sulfide in taxitic gabbrodolerite and disseminated sulfide in picritic gabbrodolerite) in a given deposit. Two of their samples of sulfide-poor olivine gabbrodolerite from the center of the Kharaelakh

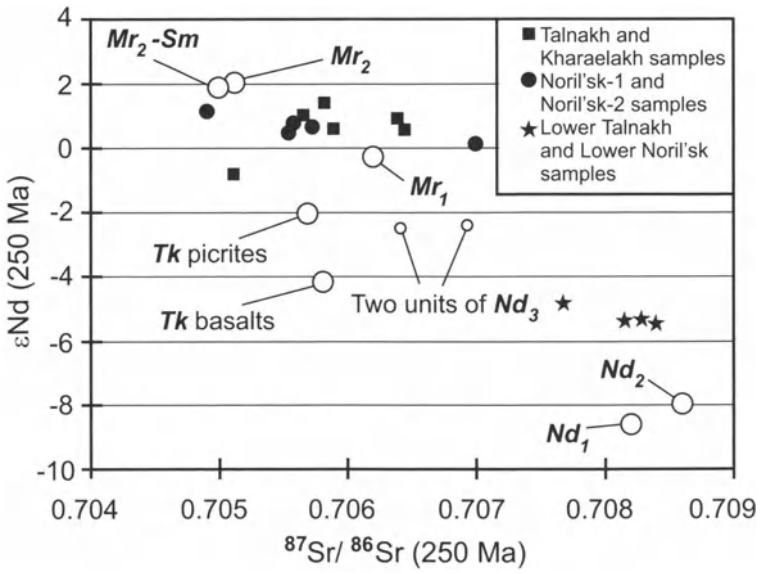


**Fig. 4.24.** Plot of εNd versus $^{87}Sr/^{86}Sr$ comparing data for the Main Talnakh and Lower Talnakh-type intrusions with averages for the volcanic formations. Data from Wooden et al, (1993); Czamanske et al., 1995; Hawkesworth et al. 1995

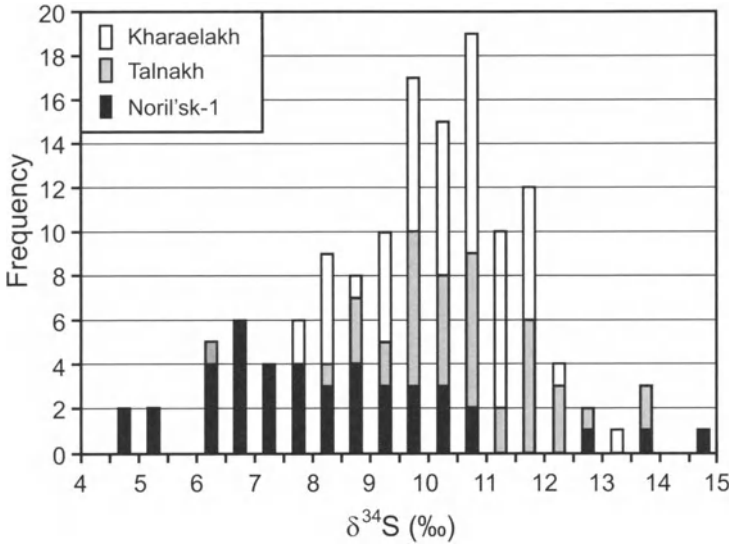


**Fig. 4.25.** Histogram showing the $\delta^{34}S$ values for samples from the Noril'sk-1, Talnakh and Kharaelakh intrusions and related ore bodies. Data from Grinenko (1985a) and Li et al. (2003)

intrusion gave $\delta^{34}S$ values of 1.3 and 3.6 permil. They remarked that these were similar to Grinenko's (1985) values for unmineralized intrusions from the Noril'sk area. It would seem that the high $\delta^{34}S$ values are associated with sulfide-rich, generally ore-bearing intrusions, but are not characteristic of all intrusions, nor, indeed of all magma pulses through an ore-bearing intrusion. This casts doubt on the hypothesis advanced by Likhachev, (1994) and Wooden et al. (1992) that the heavy sulfur of the ores at Noril'sk is due to a reservoir of $^{34}S$-, PGE-enriched sulfide in the mantle beneath the area. As Li et al. (2003) remark, it is unlikely that a magma derived from, and receiving its sulfur from a deep source such as this would show a range of $\delta^{34}S$ values, with only sulfide-rich rocks enriched in the $^{34}S$ isotope. It is much more logical to suppose that the heavy sulfur was ingested from some source en route and caused the deposition of sulfides in sufficient quantity that they resulted in ore bodies, and that some later pulses of magma through the same intrusion were less affected by this. Grinenko's (1985) data for the Lower Talnakh intrusion vary between +5 and +13 $\delta^{34}S$, which indicates that weakly mineralized intrusions of this type also had access to the source of heavy sulfur.

The nature of this source (of heavy sulfur) and how the sulfur entered and reacted with the intrusions remains debatable. In many ways, the obvious source is the surrounding evaporites. Problems associated with calling upon this as the source are discussed in Chapter 2, section 2.5, and will not be repeated here. Grinenko (1985) called upon sour gas, associated with the Tunguska coal measures, as the source. Li et al. (2003) have suggested that the sulfur was introduced by hydrothermal fluids that leached sulfur from the evaporites, were reduced by the coal measures, and then entered the intrusion to react with it and give rise to sulfides. The favored model of this author (discussed in more detail below) is that a near surface intrusion developed that assimilated both evaporite and coal measures, and that reduction occurred in the environment of a natural smelter. The intrusions are exit channels from this smelter. Notwithstanding the foregoing hypotheses, the question of the sulfur source remains an open one.

**Olivine Compositions**. In their study of olivine compositions in the Kharaelakh, Talnakh and Noril'sk-1 intrusions, Li et al. (2003) noted that they fall into three groups, some of which have different compositional characteristics. These are: Group (i) that comprises those olivines that occur as small (< 100 micron) inclusions in pyroxene and plagioclase; Group (ii) that consists of discrete grains with granular or subophitic pyroxene and plagioclase and interstitial sulfide and Group (iii) comprising large (5-10 mm) irregular olivines enclosing other minerals poikilitically. They de-

scribed a fourth type of olivine, which occurs in inclusions of 'olivinite', that are common in picric gabbrodolerite, less common in taxitic gabbrodolerite and uncommon in olivine gabbrodolerite. Olivines belonging to Group (i) and those in the olivinite inclusions are the most primitive, with the highest Fo and Ni contents, and appear to have been insulated from reaction with interstitial liquid subsequent to their crystallization. Those in Group (ii) are less primitive than those of Group (i) and exhibit what is interpreted as a 'trapped liquid shift' (see discussion in Chapter 6). Some olivines of this group also show an inverse relationship between Ni and Fo, which is due to exchange of Ni and Fe with adjacent sulfide (see also discussion in Chapter 10, section 10.1.4 and Figure 10.9b). Group (iii) olivines are zoned and appear to have grown from a localized volume of liquid that became depleted in Ni and MgO as they grew. Li et al. (2003) focussed their attention on the Group (i) olivines, which they believed to be most representative of the magma from which they grew. They modeled variation in Ni and Fo of olivine using the MELTS program of Ghiorso and Sack (1995; JAVA version 1.1.1, 2001, provided on-line by M.S. Ghiorso) and appropriate partition coefficients and concluded that Group (i) olivines in the Talnakh intrusion had crystallized from their assumed starting liquid after 2 percent fractionation, those in the Kharaelakh intrusion as sampled at the Komsomolsky mine had crystallized from the same liquid after 5 percent fractionation, as had those in the Noril'sk-1 intrusion. The olivines in the Oktyabrsky area of the Kharaelakh intrusion had crystallized from a liquid with much lower Ni content (180 ppm Ni as contrasted with 300 ppm Ni in the liquid required for the other olivines). They noted abrupt shifts in olivine composition at the contacts between different units of the intrusions (taxitic and picritic gabbrodolerite, picritic and olivine gabbrodolerite) and concluded that although the olivines were related by fractional crystallization from the same magma, this fractionation had occurred elsewhere, and that pulses of progressively fractionated magma were responsible for the different units of the intrusions. Arndt et al. (2003) reached the same conclusion from their study of olivine compositions.

Latypov (2002) pointed out that none of the Associations IIA and B volcanic suites, with the exception of the ***Tk***, could have been in equilibrium with olivine, and concluded that the intrusions were not related directly to the lavas. Li et al.'s (2003) modeling using the MELTS program substantiated the view that these could not have been in equilibrium with olivine.

Using estimates of the compositions of the magmas responsible for the intrusions gained from weighted averages of the different layers, Latypov (2002) also concluded that fractional crystallization of these magmas would not give rise to the lavas of Associations IIA and B. The demonstra-

tion that the intrusions are the result of several pulses of variably fractionated magma invalidates taking weighted averages of their compositions as indicative of the magmas responsible for them, and this author therefore disagrees with Latypov's conclusion that the lavas cannot be the result of further differentiation of the magma responsible for the intrusions, although he accepts the conclusion that the lavas above the level of the ***Tk*** could not have crystallized olivine.

**Summary of correlations based on geochemistry**. In summary, the geochemical work undertaken to date has shown that the Noril'sk-type intrusions correspond in their εNd, Th/Ta and La/Sm ratios to values intermediate between $Mr_1$ and $Mr_2$ magma. Their $^{87}Sr/^{86}Sr$ ratios show a wide range from values intermediate between those of the $Mr_1$ and $Mr_2$ suites to much higher values of more than 0.707 in some samples. It appears that a contaminant with a high concentration of very radiogenic Sr, but low concentrations of REE, Nd and Pb, has affected these marginal rocks[11].

The Lower Talnakh-type intrusions are distinguished from the Noril'sk-type by their lower Ni and Cr contents, their lower εNd and higher La/Sm and Th/Ta ratios. Conflicting correlations arise from this geochemical data; they correspond closely with the $Nd_3$ in their La/Sm ratios and with the $Nd_2$ in their εNd, Th/Ta and $^{87}Sr/^{86}Sr$ ratios.

A major problem remains in that the lower parts of the intrusions are olivine-bearing, but the volcanic rocks to which they appear to be so closely related geochemically could not have crystallized olivine. This problem is addressed below.

### *Model Of The Intrusions As Lava Conduits*

**Unusual Aspects of the Noril'sk-type Intrusions**. The Noril'sk-type (mineralized) intrusions are unusual in a number of ways.

---

[11] Since the intrusions are sitting within, or have passed up through evaporite-bearing sediments, it is logical to look to incorporation of Sr from the evaporite as the source of the contamination; Walker et al. (1994) have made a similar suggestion. Walker has also remarked (personal communication, 1994) that no good Sr isotopic analysis of Noril'sk anhydrite is available, but it is likely to be similar to that of Devonian sea water, that is have ($^{UR}S$ r ~ +45-+60). One cannot call upon wholesale assimilation of anhydrite of this composition to modify the magmas involved, since so much would be required. As mentioned above, it is possible that hydrothermal processes have changed the isotopic composition of the Sr. The solution to this question may come as individual minerals in the rocks in question are studied.

1. In the Talnakh ore junction they contain or are associated with a very high proportion of sulfide, ranging from 2 and 10 wt% of their total mass (Naldrett et al. 1992).
2. These sulfides contain a very large concentration of PGE, which, according to Naldrett et al. 1992, must have come from at least 200 times more magma than that represented by the mass of the intrusions.
3. The intrusions have not pushed the country rocks apart, but have replaced them (see Fig. 4.31 below).
4. It has been emphasized repeatedly in the Russian literature on Noril'sk that the mineralized intrusions are surrounded by an intense metamorphic and metasomatic aureole (e.g. Genkin et al., 1981; Likhachev, 1994). In many cases this extends farther into the country rocks than the thickness of the intrusions themselves, in some cases 400 m (Genkin et al. 1981).
5. The sulfur isotopic composition of the sulfides is very heavy for mantle-derived sulfur, ranging from +8 to +12 $\delta^{34}S$ (Godlevsky and Grinenko 1963; Grinenko 1985).

**Concept of Intrusions as feeders to Volcanism.** These aspects are explicable if the Noril'sk- and Lower Talnakh-type intrusions have acted as feeders to the 5000-10,000 $km^3$ of volcanic magma represented by the ***$Nd_1$-$Mr_2$*** formations (this estimate of the volume of lava involved is after Fedorenko 1981), and if much of the sulfide has formed at a shallow level in the crust, essentially in situ. Such an interpretation is not a new idea. Godlevsky (1959b) concluded that the intrusions had formed close to the surface, and referred to them as chonoliths. Ivanov et al. (1971) proposed that the Noril'sk I intrusion was a feeder pipe to overlying volcanism particularly to picritic basalts. Rad'ko (1991) proposed a similar origin for the intrusions of the Talnakh ore junction. It was only when extensive drilling of the Kharaelakh intrusion showed that the main body within this did not break though the sedimentary strata to reach the level of the volcanics (and thus that the intrusion appeared to be blind), that the concept of volcanic feeders fell into disfavor.

In response to the apparent contradiction of the need for flow-though of magma but the blind nature of the intrusions, Likhachev (1994) suggested (as discussed above) that magma ascended from a deep reservoir, circulated through each individual intrusion, and then descended back to the reservoir, behaving as water does in a system of convectively driven radiators. He proposed that the ascent and descent of magma occurred along one and the same conduit.

As noted above, Zen'ko and Czamanske (1994b) suggested that the peripheral sills are an integral part of the mineralized intrusions. If this is so,

the Kharaelakh intrusion is not blind. This led Naldrett et al. (1995) to study the composition of the Lower Talnakh and Kharaelakh peripheral sills and compare their average compositions with averages of the ***Mk***, ***Mr*$_2$**, ***Mr*$_1$**, ***Nd*$_3$** and ***Nd*$_2$** volcanic formations. The average bulk composition for the Kharaelakh sills, both major and trace elements (no isotopic data are available on the sills), is essentially indistinguishable from the average for the ***Mr*$_2$** volcanic formation, with which the Kharaelakh intrusion as a whole has been equated on the basis of ratios of incompatible trace elements (Fig. 4.26, Table 4.4). The average composition of the Lower Talnakh sill is intermediate between that of the ***Nd*$_2$** and ***Nd*$_3$** suites. The data therefore provide support for the flow of magma through the mineralized intrusions, with magma moving out of the thicker parts of both the Lower Talnakh-type and Noril'sk-type intrusions and through the peripheral sills. The composition of the peripheral sills is representative of the last magma to flow through the ore-bearing system. In most cases all evidence of earlier magma, which could have been in equilibrium with olivine, has been

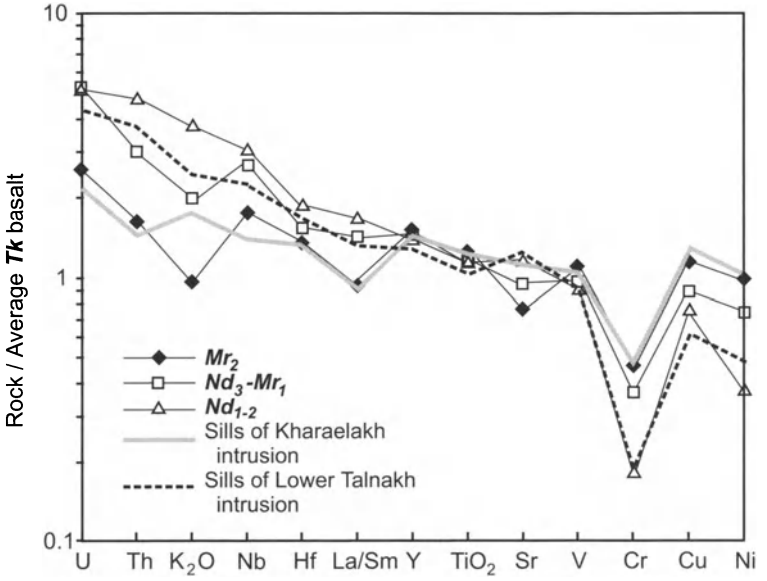


**Fig. 4.26.** Comparison of the values of some geochemical parameters between the sills peripheral to the Lower Talnakh and Kharaelakh intrusions and the ***Nd*$_2$**, ***Nd*$_3$**-***Mr*$_1$**, and ***Mr*$_2$** volcanic formations. All data are normalized to average ***Tk*** basalt. From Naldrett et al. (1995)

**Table 4.4.** Comparison of average chemical compositions of the sills peripheral to the Lower Talnakh and Kharaelakh intrusions and basaltic lavas of the Tuklonsky, Nadezhdinsky, and Morongovsky suites

| | n | $SiO_2$ | $TiO_2$ | $Al_2O_3$ | FeOT | MgO | $K_2O$ | Sr | Y | Zr | Nb | Rb | Ba | Cr | V | Ni | Cu | La | Sm | Hf | Th | U | La/Sm |
|---|---|---|---|---|---|---|---|---|---|---|---|---|---|---|---|---|---|---|---|---|---|---|---|
| SLTI | 5 | 51.81 | 0.96 | 15.50 | 10.47 | 7.45 | 0.82 | 322 | 20 | 107 | 6.25 | 15 | 254 | 69 | 221 | 53 | 66 | 11.8 | 3.44 | 2.99 | 2.40 | 0.70 | 3.43 |
| SKh | 6 | 49.22 | 1.20 | 16.00 | 11.61 | 6.94 | 0.67 | 266 | 23 | 85 | 4.22 | 15 | 224 | 156 | 256 | 103 | 121 | 7.0 | 3.17 | 2.51 | 0.95 | 0.35 | 2.20 |
| ***Tk*** | 8 | 50.22 | 0.89 | 15.99 | 9.94 | 8.91 | 0.34 | 257 | 15 | 63 | 2.75 | 5 | 198 | 379 | 226 | 106 | 103 | 5.6 | 2.19 | 1.77 | 0.65 | 0.16 | 2.54 |
| ***Nd$_1$*** | 31 | 52.87 | 0.96 | 15.91 | 9.38 | 6.67 | 1.32 | 267 | 21 | 122 | 8.17 | 38 | 423 | 132 | 207 | 25 | 32 | 17.0 | 3.82 | 3.13 | 3.16 | 0.83 | 4.46 |
| ***Nd$_2$*** | 17 | 52.81 | 1.07 | 15.85 | 10.18 | 6.27 | 1.24 | 331 | 23 | 136 | 9.03 | 35 | 397 | 82 | 214 | 43 | 81 | 17.9 | 4.14 | 3.53 | 3.25 | 0.88 | 4.33 |
| ***Nd$_3$*** | 6 | 50.72 | 1.05 | 16.41 | 10.62 | 6.59 | 0.74 | 267 | 24 | 111 | 7.05 | 15 | 416 | 134 | 228 | 80 | 96 | 13.4 | 3.58 | 2.81 | 2.10 | 0.89 | 3.74 |
| ***Mr$_1$*** | 8 | 50.19 | 1.15 | 15.85 | 11.32 | 7.06 | 0.40 | 222 | 23 | 104 | 5.66 | 6 | 319 | 131 | 269 | 81 | 104 | 10.3 | 3.42 | 2.67 | 1.65 | 0.60 | 3.01 |
| ***Mr$_2$*** | 10 | 49.49 | 1.16 | 16.52 | 11.37 | 7.30 | 0.32 | 188 | 22 | 91 | 4.77 | 4 | 245 | 150 | 262 | 109 | 124 | 7.5 | 3.07 | 2.47 | 1.10 | 0.42 | 2.45 |

*SLTI* sills of the Lower Talnakh intrusion.
*SKh* sills of the Kharaelakh intrusion.
*n* number of samples/
Major elements (wt%) are recalculated to 100% anhydrous. Trace-element contents in ppm

washed away. There is one location known to this author at which olivine cumulate, along with sulfide, is preserved. This is the Gabbrovy body (hole VH-4) which is a peripheral sill extending north from the Talnakh intrusion (see discussion below).

Naldrett et al.'s original model was that both sets of intrusions, Lower Talnakh-type and Noril'sk-type had acted as conduits for all of the ***Nd*$_1$** to ***Mk*** magma. However, Arndt et al. (2003) have suggested a modification to the flow-through model, in which the Nadezhdinsky suite is the result of mid-crustal contamination causing sulfides to segregate at depth, without having reacted with the evaporates, while the later suites did not precipitate sulfide at depth, but achieved sulfide saturation at the level of the evaporites and ore bearing intrusions. The Arndt et al. modification carries with it the implication that the chalcophile depletion shown by the ***Nd*$_1$** and ***Nd*$_2$** in no way contributes to the metals of the ores, and that this depletion is not a guide to the presence of ore. Their principal argument is that the sulfides of the Lower Talnakh-type intrusions, with their very high values of $\gamma$Os, could not be the predecessor of the ore-bearing sulfides with their much lower $\gamma$Os. They regard these intrusions as passageways for the ***Nd*$_{1-2}$** magma en route to surface, and that the ore-bearing intrusions acted as passageways for a different magma. This author accepts that the Noril'sk-type intrusions may well not have been conduits for ***Nd*** magma, but he is impressed with the transition between the ***Nd*$_{1-2}$** lavas and the ***Mr*$_2$** magma as displayed by the ***Nd*$_3$** and ***Mr*$_1$** lavas, and believes that part of the high-level system of intrusions and conduits remained open to both the Nd and later ***Mr*$_2$*-Mk*** magma and it is only the exits to this system which changed, with the Lower Talnakh-type intrusions becoming closed, and the Noril'sk type intrusions opening up. As discussed earlier, in the Talnakh area the Lower Talnakh intrusion appears to have been fed from a series of curvilinear faults extending west of the Noril'sk-Kharaelakh fault. The Talnakh and Kharaelakh intrusions are much more closely related to the Noril'sk-Kharaelakh fault. A change in the regional stress during eruption could well have pinched the curvilinear faults shut and led to an opening of fractures related to the Noril'sk-Kharaelakh fault. The early-formed sulfides remained behind in the high level magma chamber (pictured schematically in Fig. 4.27), along with olivine. The magma in this chamber slowly changed as more and more ***Mr*$_2$*-Mk*** type magma mixed with it, exiting through the new conduits. Sulfides in the chamber became upgraded, and their $\gamma$Os became reduced. When the magma in the chamber had become diluted to the extent that its composition was close to that of the ***Mr*$_1$** suite, an extra violent influx of new magma swept much of the trapped

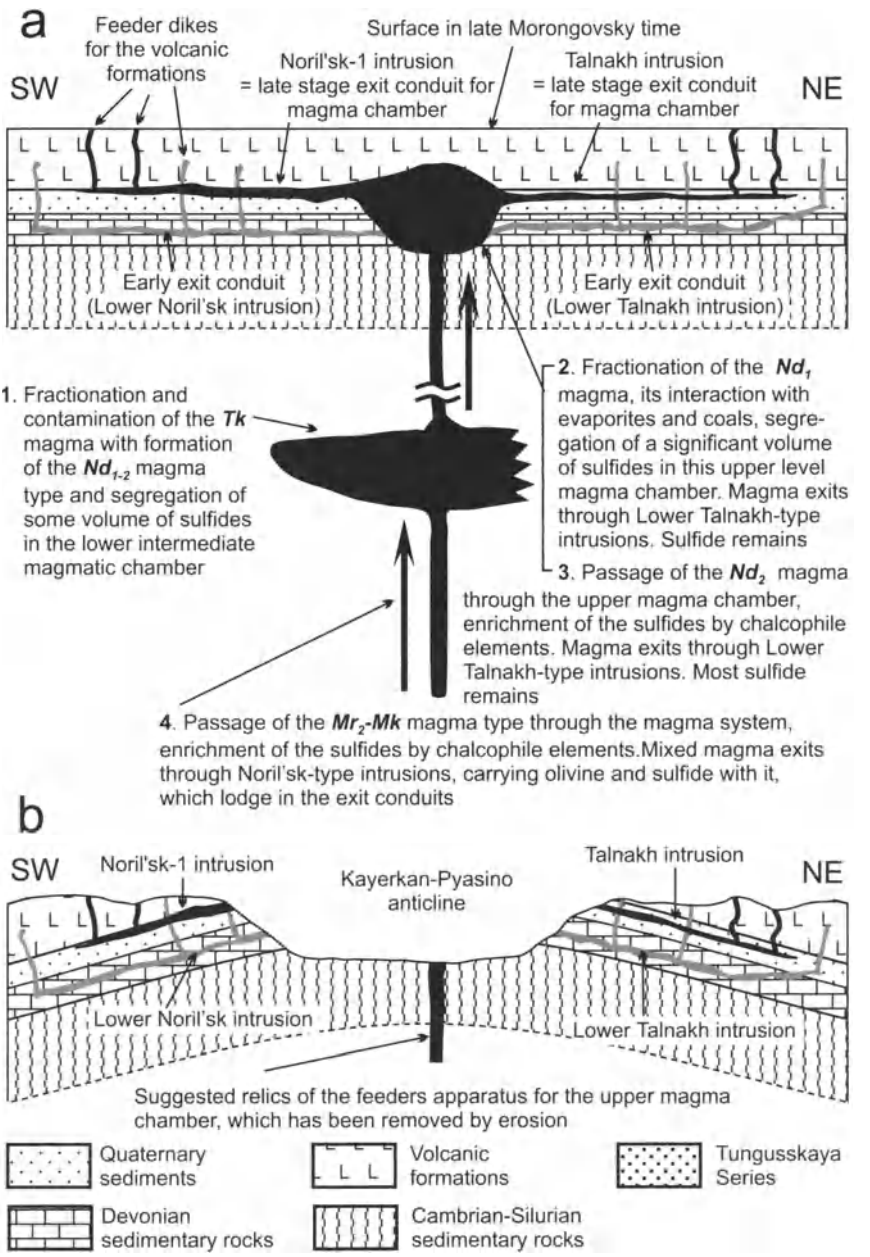


**Fig. 4.27.** A model for development of the magmatic system of the central part of the Noril'sk region in Nadezhdinsky and Morongovsky time, shown as a cross-section (a), and present day schematic geological cross-section (after folding) and erosion (b). Vertical scale of the cross-sections is strongly exaggerated relative to the horizontal scale

sulfide and olivine out of the chamber where it had been accumulating and into the exit conduits where it became lodged. Some of this sulfide affected at this time probably became separated from the main pulse of magma, to intrude by itself and give rise to the massive sulfide ores (see below). The magma responsible for this extra violent pulse may well not have been in equilibrium with olivine, although that coming into direct contact with the olivine would have equilibrated with it and would have formed the intercumulus liquid of the taxitic, picritic and olivine gabbrodolerite layers. The olivinite inclusions found in these rocks are likely remnants of the olivine in the high level magma chamber that resisted disaggregation. The alternative to this interpretation is that the occurrence of massive depletion in Ni, Cu and PGE within a 600 m-thick sequence of volcanic rock that extends over an area extending at least 200 by 150 km in close proximity to the world's richest magmatic sulfide deposits is nothing but coincidence.

**Sequence of events.** The following sequence of events is therefore proposed (Fig. 4.27):

1. ***Tk*** magma erupted in the eastern part of the region, probably along conduits related to the Imangda fault, but did not extrude directly at surface in the central part of the Noril'sk region; in this area (possibly because the east-west horizontal tectonic stress was more intense and prevented easy ascent). In the vicinity of the Talnakh and Noril'sk ore junctions a magma, similar to the ***Tk*** picritic lavas, became trapped and underwent contamination and fractionation to produce the $Nd_{1\text{-}2}$ magma type. As discussed above on the basis of the variation of Cr, Ni, Cu and PGE, this contaminated magma lost some of these elements, probably through precipitation of chromite and sulfide liquid at this stage in a deep level chamber.
2. $Nd_1$ magma then underwent further fractionation, coupled with additional removal of chromite and sulfide to give rise to the chemical variations noted in successive the $Nd_1$ lava flows (Fig. 4.9). This stage of fractionation and chromite and sulfide removal occurred very close to surface in a high level magma chamber, and the sulfides remained trapped in this chamber, while the overlying magma was "decanted off" to erupt as lava, following exit channels which included the Lower Talnakh-type intrusions. The formation of the sulfides at this stage presumably involved assimilation of evaporite-laden sedimentary rocks and further sulfide saturation.
3. Judging from the increase in Cu from the base to the top of the $Nd_2$ subsuite, sulfide segregation had ceased in the upper level chamber

during $Nd_2$ time. However, overall the $Nd_2$ basalts are depleted in Ni, Cu, and, especially, in PGE in comparison with the *Tk* and $Nd_3$-$Mr_1$ lavas (Fig. 4.9). It is likely that fresh inputs of less depleted *Nd* magma (magma that had only suffered the mid-crustal level of depletion and was therefore equivalent to the first pulse of $Nd_1$ magma, i.e. the lowest $Nd_1$ flow) mixed with the highly depleted $Nd_1$ magma (magma equivalent to the uppermost $Nd_1$ flow) to produce the $Nd_2$ magma.

4. Following eruption of the $Nd_2$, new magma of $Mr_2$-*Mk* type entered the high level magma chamber as a series of influxes, which mixed with silicate magma already resident there. The incoming magma already bore the imprint of fractionation and crustal interaction (Wooden et al. 1993). The new hybrid magmas ($Nd_3$, $Mr_1$) produced by the intermixing of $Mr_2$-*Mk* type magma with the *Nd* type magma still remaining in the chamber were characterized by progressively higher εNd and lower $^{87}Sr/^{86}Sr$, higher Cr, and lower La/Sm ratio, features that distinguish the $Mr_2$-*Mk* magma.
5. At about $Mr_1$ time the Lower Talnakh-type intrusions ceased to act as exits to the high level chamber, and their place was taken by the Noril'sk-type intrusions (the contact olivine gabbrodolerite of the Talnakh intrusion has a composition close to that of average $Mr_1$ magma). A violent influx of fresh magma during this time disrupted sulfides and olivine layers within the chamber, sweeping these out to lodge in the Main Bodies of the Noril'sk type intrusions.

**Further aspects of the model.** The flow of a large amount of magma through a plumbing system of which the mineralized intrusions are part accounts for the very extensive metamorphism associated with them. It also demolishes the argument used previously (for example Naldrett et al. 1992; see below) that the sulfides **must** have segregated from the magma at depth because of the high proportion of PGE and sulfide present in the mineralization. But the model presented here requires granodiorite contamination to be linked to S saturation, so some significant sulfide removal at depth appears inescapable. Further contamination occurred and further sulfides segregated at the present stratigraphic level of the intrusions during the differentiation (and associated chalcophile element depletion) that is reflected in successive $Nd_1$ lava flows. It is likely that the magma was progressively eroding the walls of its chamber at this time, ingesting Devonian evaporite and C-bearing Tungusskaya formation, and reducing the evaporite to produce sulfide. An interruption in the input of magma into the high-level chamber at the close of $Nd_1$ time allowed magma there to cool and line the walls of the chamber. This insulated the walls from further erosion when new magma entered the chamber to differentiate and

**Table 4.5.** Average composition of disseminated ores from different intrusions (recalculated to metal in 100% sulfide)

| | NL | NS | Ni (wt%) | Cu (wt%) | Au (ppm) | Pd (ppm) | Pt (ppm) | Rh (ppm) | Ru (ppm) | Ir (ppm) | Os (ppm) |
|---|---|---|---|---|---|---|---|---|---|---|---|
| **Ore-bearing intrusions of the Noril'sk ore junction** | 4 | | | | | | | | | | |
| Picritic gd | | 31 | 15.20 | 11.15 | 3.30 | 78.99 | 35.32 | 5.80 | 1.307 | 0.693 | 0.510 |
| Taxitic gd | | 8 | 8.59 | 14.98 | 9.56 | 74.41 | 36.77 | 4.25 | 0.955 | 0.505 | 0.324 |
| **Talnakh intrusion** | 4 | | | | | | | | | | |
| Picritic gd | | 55 | 7.50 | 11.03 | 2.14 | 39.42 | 13.96 | 1.73 | 0.387 | 0.207 | 0.166 |
| Taxitic gd | | 32 | 5.28 | 9.41 | 1.31 | 24.49 | 7.60 | 0.98 | 0.218 | 0.093 | 0.068 |
| **Kharaelakh intrusion (Central and Eastern parts)** | 2 | | | | | | | | | | |
| Picritic gd | | 9 | 7.42 | 14.03 | 1.94 | 36.38 | 9.48 | 1.24 | 0.238 | 0.113 | 0.098 |
| Taxitic gd | | 27 | 6.31 | 11.20 | 1.52 | 29.86 | 7.34 | 1.16 | 0.220 | 0.078 | 0.068 |
| **Kharaelakh intrusion (Western part)** | 1 | | | | | | | | | | |
| Taxitic gd | | 11 | 4.24 | 7.15 | 0.79 | 14.98 | 3.57 | 0.29 | 0.018 | 0.037 | 0.047 |
| **Lower Talnakh intrusion** | 1 | 10 | 2.26 | 1.78 | 0.03 | 0.17 | 0.21 | 0.01 | 0.004 | 0.004 | 0.002 |

*NL* Number of Localities; *NS* Number of Samples

form the $Nd_2$ lavas; sulfide segregation therefore ceased, and chalcophile metals started to increase in concentration.

Since the Lower Talnakh-type intrusions represent exit conduits which became closed at the end of $Nd_2$ or at the very start of $Nd_3$ magmatism, they reflect the chalcophile-poor composition of this magma, and the sulfides that they contain are much less enriched in chalcophile metals than those of the Noril'sk-type bodies (Table 4.5).

## 4.1.4. Ore Deposits

### *Introduction*

The northern end of the Noril'sk-1 deposit was exposed at surface (this portion, which turned out to contain some of the richest ore, has long been removed by mining operations) and was the reason that attention became focused on the area as a potential source of nickel, that was located safely within the borders of the USSR; this aspect was thought important in the politically turbulent years that followed the Bolshevik revolution. Kunilov (1994) reported that the deposits may have been worked by ancient man, and that archeological evidence has been obtained that an active smelting industry, based on the Noril'sk ores, existed at the Mangasei settlement on the Taz river during the 16th and 17th centuries.

Systematic geological study began in 1919 after an expedition by Nikolai Urvantsev had shown the possibility for large deposits of coal and base metals in this part of Siberia. He likened the Noril'sk ores to those at Sudbury. Exploration resulted in the discovery of the Noril'sk-1 deposit in 1926, and in 1935 the Soviet government passed a resolution with respect to the development of the Noril'sk Copper-Nickel Mining and Metallurgical Kombinat. Construction started on a railway linking the Noril'sk area with the port of Dudinka on the Yenisey river, 100 km to the west. The first mine was established in 1936, the first massive sulfide ore was mined in 1938, the first cathode nickel obtained in 1942 and the first copper plant opened in 1949. The Talnakh deposit was discovered 30 km north of Noril'sk in 1960. In 1965 the Oktyabrsky deposit was discovered. Drilling on 50x50, or 100x50 m grids down to depths as much as 3000 m was undertaken to outline the main zones of massive ore and a reasonable estimate of the size and richness of the Talnakh area ores had been obtained by the late 1960's. Regional exploration was undertaken concurrent with the detailed study of the deposits over the area shown in Fig. 4.28, accompanied by drilling to 1000m depth, together with deep holes in some areas up to 2500 m in depth.

Six deposits, associated with 3 ore junctions, have been discovered so far. These are the Oktyabrsky and Talnakh deposits of the Talnakh ore junction, the Noril'sk-1, Noril'sk-2 and Mt Chernaya deposits of the Noril'sk ore junction and the Imangda deposit of the Imangda ore junction (Fig. 4.28). The Oktyabrsky and Talnakh deposits are much richer than those of the Noril'sk ore junction, which are in turn much richer than that at Imangda. The result is that only the Oktyabrsky, Talnakh and Noril'sk-1 deposits have been mined to-date. Several independent mines are operating

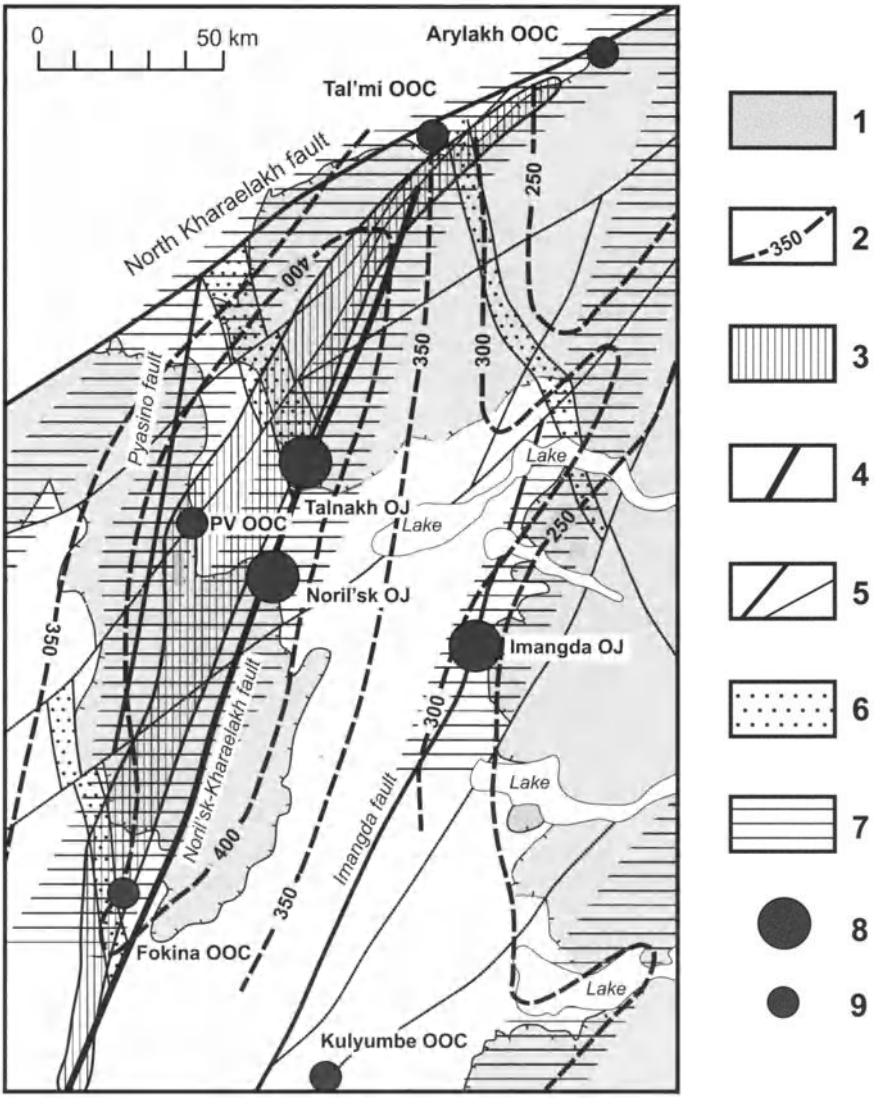


**Fig. 4.28.** Map of the mineralized areas of the Noril'sk region and of factors thought to control their localization (from data V.A. Fedorenko). 1 = Area presently occupied by volcanic formations; 2 = Paleoisopachs of the Lower–Middle Nadezhdinsky lavas; 3 = Area underlain by Lower Talnakh type intrusions; 4 = Noril'sk-Kharaelakh fault; 5 = Other main faults; 6 = Zones of transverse faulting (Kraevoy, Vodorazdelny, and Kumga from SW to NE); 7 = Likely feeder zones for the volcanic formations (after Fedorenko, 1979); 8 = Ore junctions; 9 = Ore-occurrence clusters (PV OOC = Pyasino-Vologochan ore-occurrence cluster)

at each deposit; the Oktyabrsky, Taymyrsky and Komsomolsky mines at the Oktyabrsky deposit, the Komsomolsky and Skalisty mines at the Talnakh deposit (the Komsomolsky mine covers parts of both the Oktyabrsky and Talnakh deposits), and the Bear's Brook open pit and Zapolyarny mine at the Noril'sk-1 deposit. In addition to the above named ore junctions, several "ore occurrence clusters" are recognized in the region, the Arylakh, Talmi, Fokina, Pyasino-Vologochan and Kulyumbe clusters (Fig. 4.28).

Maslov (1963) showed that the intrusions with economic mineralization were controlled by the Noril'sk-Kharaelakh fault. Observations from subsequent exploration of the intrusions of the Talnakh ore junction provided strong support for this interpretation (Fig. 4.13, 4.29, 4.30). Five of the six deposits in the region are related to the Noril'sk-Kharaelakh fault. The Imangda deposit, which occurs within the similarly named ore-junction is the only exception.

The mineralized intrusions of the Talnakh ore junction are shown in plan view, along with their related ore massive and disseminated ore deposits, in Fig. 4.29. The Kharaelakh intrusion lies west of the Noril'sk-Kharaelakh fault within Devonian strata; it is triangular in plan view, extending 8 km along the fault and up to 7 km west of it. The main body of the Talnakh intrusion occurs in the Tungusskaya series and consists of two branches. The largest of these, the Northeastern branch, is an elongate lens that extends for 14 km along the east side of the Noril'sk-Kharaelakh fault with a width of 0.8-1.5 km. The smaller, Southwestern branch is also elongate extending for 8 km with a width of 0.5-1 km along the west side of the fault within a structure that is referred to as the "central graben". The total length of the Talnakh intrusion is 18 km.

The intrusions of the Noril'sk ore junction are shown in Fig. 4.30. The Noril'sk-1 intrusion has the form of an elongate (15 km), flattened tube (1-2.5 km wide, 50-320 m thick). It intrudes the lower part of the lava sequence and sediments of the Tungusskaya series and plunges gently to the southwest at 8-15°. The intrusion is highly discordant with respect to the layering of the country rocks (Fig. 4.31); this relationship is attributed to thermal erosion of the enclosing rocks due to the heat derived from the passage of large volumes of magma through the body.

The Mt. Chernaya (or Chernogorka) intrusion consists of two branches (Fig. 4.30), both of which have been intruded along the contact between Devonian and overlying Tungusskaya sediments. The northern branch is thicker and better mineralized than the southern branch. It is an elongate, sill-like body, oriented almost at right angle to the Noril'sk-Kharaelakh fault. It is about half as long (7 as opposed to 15 km) as the Noril'sk-1

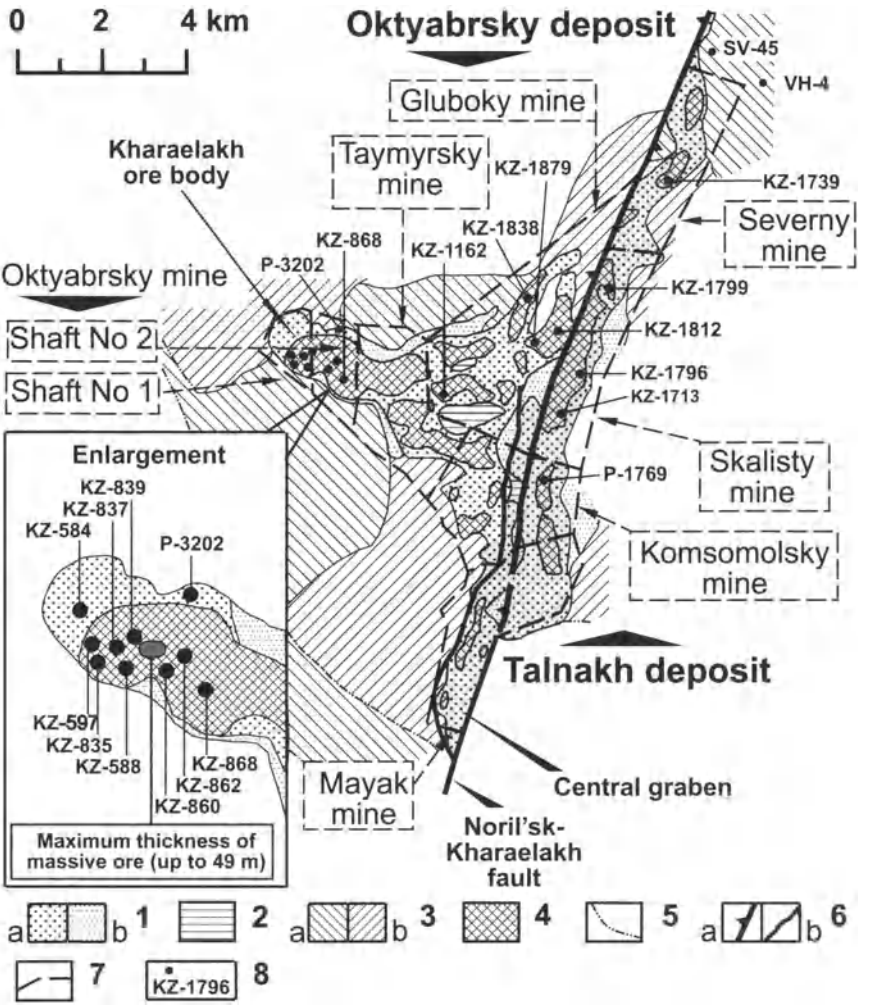


**Fig. 4.29.** Plan view of the Talnakh ore-junction, showing the outline of the Kharaelakh (west of Noril'sk-Kharaelakh fault) and Main Talnakh (east of fault) intrusions, along with the distribution of disseminated and massive ore, the approximate boundaries of the individual mines, and the location of boreholes sampled for this study (and referred to in the text). Modified after Zen'ko (1986) and von Gruenewald (1991).

1 = Main bodies of ore-bearing intrusions (a) where they contain picritic and/or taxitic gabbrodolerite (gd) and disseminated mineralisation, (b) flank areas without picritic and taxitic gd and disseminated mineralisation; 2 = "Windows" into main bodies where picritic and taxitic gd and disseminated mineralisation are absent; 3 = Peripheral sills of the ore-bearing intrusions (a) lower in the stratigraphy (for the Kharaelakh intrusion this is at the horizon of the low to middle Razvedochnisnky suite, in the Talnakh intrusion it is at the level of the Zubovsky and

Kureysky suites), (b) higher in the stratigraphy (for the Kharaelakh intrusion this at the level of the Upper Razvedochnisnky and Manturovsky suites, for the Talnakh intrusion it is near the contact between the Devonian strata and the Tungusskaya Series); 4 = Massive sulfides underlying the intrusions; 5 = Erosional boundaries of intrusions and their peripheral sills; 6 = Faults, (a) the Noril'sk-Kharaelakh fault, (b) other faults; 7 = Boundaries of individual mines; 8 = Boreholes.
Note. Where both ore-bearing intrusions are superimposed, the uppermost is shown; the same is true of the sills. The main body of the Talnakh intrusion is shown in light-gray, with the exception of its less well studied eastern flank

intrusion, but is otherwise very similar in thickness, composition of its constituent rocks, and in the disposition of these in vertical section. The Noril'sk-2 intrusion is trumpet-shaped in cross section, narrowing downward into a dyke (see Distler and Kunilov, 1994, Fig. 19). All rock types characterizing the other Noril'sk-type intrusions occur within the Noril'sk-2 body, but their spatial relationships to each other are complex. Sulfides in both the Noril'sk-2 and Mt Chernaya intrusions are primarily of disseminated type and are sub-economic at the present time (October 2003) (Table 4.6).

The genesis of the sulfide ores at Noril'sk has been debated since the earliest discoveries. Godlevsky (1959a) considered that they had segregated from silicate magma as a sulfide liquid. He suggested that the reason this occurred was that the host magma had assimilated material rich in $Al_2O_3$ and $SiO_2$ at depth. The primary magma was so rich in sulfur that sulfide immiscibility occurred at an early stage and continued as olivine started crystallizing and the magmas rose rapidly to their present, high-level chambers.

Godlevsky and Grinenko (1963) and Gorbachev and Grinenko (1973) drew attention to the heavy isotopic composition of sulfur in the Noril'sk ores (from +8 to +12 ‰ $\delta^{34}S$, see discussion above) and proposed that the sulfides had formed as the intruding magma reacted with local sulfur derived either from the surrounding evaporites or from $H_2S$ that had migrated from hydrocarbon deposits. Zotov (1980) argued that sulfide-bearing rocks in the basement were the source of the sulfur. He accepted that the disseminated ores developed through sulfide segregation in the final intrusive chambers; but thought that the massive ores had formed as a result of sulfur metasomatism of the intruding magma, at an intermediate depth, and were then intruded into their final positions after the disseminated ores had formed. Zolotukhin (1991) and others have suggested that the sulfides formed in situ from fluids that had scavenged sulfur from crustal rocks and metals from the intruding magma. In contrast to these ideas, all which at-

tribute an intra-crustal origin to the sulfides, Likhachev (1978,1994) argued that the sulfides were present in the magmas from the moment the latter developed as a result of partial melting of particularly sulfide-rich mantle, and were transported within the magma into the supracrustal rocks.

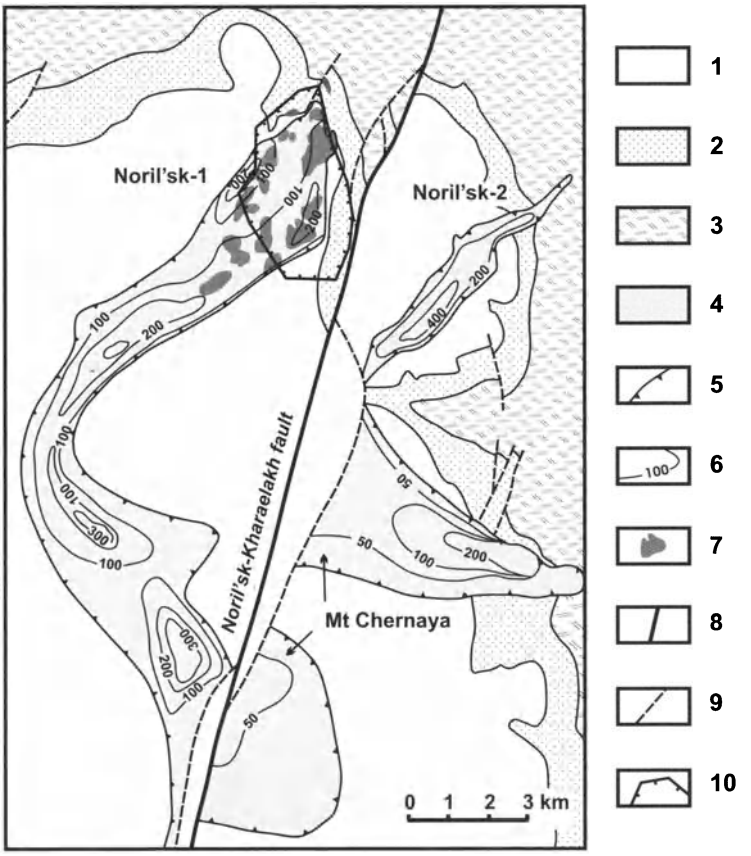


**Fig. 4.30.** Plan view showing distribution of the most important ore-bearing intrusions of the Noril'sk ore junction (Noril'sk-1, Noril'sk-2, and Mt Chernaya). After Distler and Kunilov (1994) and other information made available by the Noril'sk Kombinat to participants in the 7th International Platinum Symposium (Moscow – Noril'sk, 1994).
1 = Volcanic formations; 2 = Tungusskaya series (Middle Carboniferous – Upper Permian Coal-bearing sedimentary rocks); 3 = Devonian sedimentary rocks; 4 = Most important ore-bearing intrusions (distribution at surface and at depth); 5 = Borders of the ore-bearing intrusions; 6 = Thickness of the ore-bearing intrusions (m); 7 = Massive sulfides; 8 = Noril'sk-Kharaelakh fault; 9 = Some other important faults; 10 = Boundaries of the Medvezhy (Bear's) Brook open pit. Note: many faults are not shown in the plan view

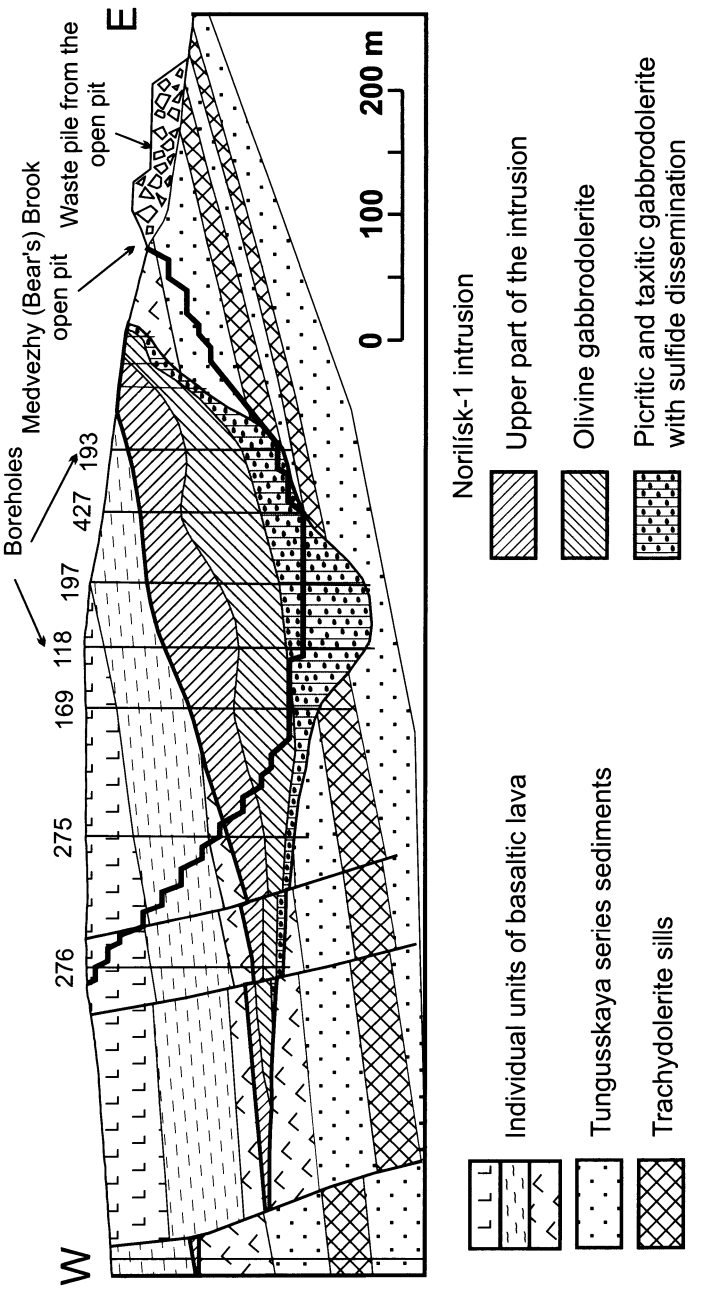


**Fig. 4.31.** Vertical section through the northern part of the Noril'sk-1 intrusion, showing the discordance between layering in the country rocks and the margins of the intrusion (after material provided by the Noril'sk Kombinat to participants at the 7th International Platinum Symposium, Moscow – Noril'sk, 1994)

**Table 4.6.** Average chemical composition of Ni-Cu-PGE ores associated with Flood Basalt Magmatism

| Area<br>Deposit | T | n | S<br>wt% | Ni<br>wt% | Cu<br>wt% | Pd<br>ppb | Pt<br>ppb | Rh<br>ppb | Ru<br>ppb | Ir<br>ppb | Os<br>ppb | Au<br>ppb | Pd/Pt | R |
|---|---|---|---|---|---|---|---|---|---|---|---|---|---|---|
| **Noril'sk region** | | | | | | | | | | | | | | |
| **Talnakh ore junction** | | | | | | | | | | | | | | |
| **Oktyabrsky deposit** | | | | | | | | | | | | | | |
| ***Western part*** | | | | | | | | | | | | | | |
| «Upper Copper ore» | | | | | | | | | | | | | | |
| *Hole P-3202, upper zone* | 18 | 8 | 8.07 | 0.73 | 5.07 | 9 275 | 1 132 | 49 | 5 | 4 | 10 | 4 945 | 8.20 | 1 |
| *Hole P-3202, lower zone* | 42 | 23 | 14.49 | 1.47 | 5.77 | 13 102 | 1 076 | 44 | 4 | 2 | 6 | 3 182 | 12.18 | 1 |
| Disseminated ore[1] | | | | | | | | | | | | | | |
| *Hole KZ-868* | 18 | 10 | 4.62 | 0.54 | 1.25 | 2 391 | 649 | 38 | 8 | 5 | 5 | 242 | 2.68 | 1 |
| Massive ores | | | | | | | | | | | | | | |
| *Hole KZ-868* | 30 | 24 | 28.06 | 2.89 | 3.83 | 6 415 | 1 469 | 195 | 24 | 14 | 9 | 107 | 4.37 | 1 |
| *Taymyrsky mine* | | 15 | 35.76 | 3.57 | 4.05 | 5 854 | 1 438 | 743 | 75 | 63 | 37 | 91 | 4.77 | 1 |
| Cu-rich massive ore | | | | | | | | | | | | | | |
| *Oktyabrsky mine* | | 11 | 35.13 | 2.76 | 21.56 | 43 503 | 9 011 | 146 | 4 | 16 | 11 | 2 992 | 4.83 | 1 |
| ***Central and eastern part*** | | | | | | | | | | | | | | |
| «Low-sulfide mineralization» | | | | | | | | | | | | | | |
| *Hole KZ-1838* | 13 | 4 | 1.55 | 0.80 | 1.10 | 6 085 | 2 015 | 285 | 41 | 24 | 11 | 252 | 3.02 | 1 |
| Disseminated ores[1] | | | | | | | | | | | | | | |
| *Hole KZ-1162* | 48 | 23 | 2.79 | 0.44 | 0.91 | 2 384 | 611 | 77 | 14 | 6 | 5 | 138 | 3.90 | 1 |
| *Hole KZ-1812* | 8 | 6 | 3.11 | 0.53 | 0.95 | 2 633 | 508 | 125 | 18 | 8 | 7 | 121 | 5.19 | 1 |
| Massive ores | | | | | | | | | | | | | | |
| *Hole KZ-1162* | 5 | 7 | 31.51 | 3.84 | 12.87 | 15 344 | 2 400 | 187 | 10 | 7 | 9 | 787 | 6.39 | 1 |
| *Hole KZ-1812* | 3 | 4 | 30.75 | 4.63 | 3.90 | 7 454 | 1 390 | 1155 | 64 | 54 | 27 | 81 | 5.36 | 1 |
| «Copper ore» | | | | | | | | | | | | | | |
| *Hole KZ-1812* | 4 | 4 | 8.63 | 1.34 | 1.29 | 2 954 | 876 | 573 | 118 | 54 | 30 | 72 | 3.37 | 1 |
| *Komsomolsky mine* | | 5 | 7.54 | 1.02 | 4.04 | 50 791 | 15.367 | 595 | 155 | 75 | 109 | 622 | 3.31 | 1 |

**Table 4.6** (cont.)

| Area<br>Deposit | T | n | S<br>wt% | Ni<br>wt% | Cu<br>wt% | Pd<br>ppb | Pt<br>ppb | Rh<br>ppb | Ru<br>ppb | Ir<br>ppb | Os<br>ppb | Au<br>ppb | Pd/Pt | R |
|---|---|---|---|---|---|---|---|---|---|---|---|---|---|---|
| **Talnakh deposit** | | | | | | | | | | | | | | |
| Disseminated ore[1] | | | | | | | | | | | | | | |
| *Hole KZ-1739* | 59 | 35 | 3.95 | 0.57 | 0.89 | 2 271 | 604 | 123 | 26 | 12 | 8 | 94 | 3.76 | 1 |
| *Hole KZ-1796* | 24 | 16 | 4.66 | 0.65 | 0.92 | 2 260 | 779 | 215 | 45 | 23 | 15 | 141 | 2.90 | 1 |
| *Hole P-1769* | 46 | 26 | 4.14 | 0.69 | 1.14 | 3 335 | 1 142 | 133 | 32 | 15 | 10 | 188 | 2.92 | 1 |
| *Mayak mine* | | 5 | 4.02 | 0.79 | 1.16 | 5 875 | 2 312 | 278 | 70 | 37 | 30 | 299 | 2.54 | 1 |
| Massive ore | | | | | | | | | | | | | | |
| *Hole KZ-1739* | 5 | 6 | 33.60 | 4.58 | 4.82 | 7 747 | 1 837 | 1 168 | 246 | 108 | 68 | 133 | 4.22 | 1 |
| *Hole KZ-1796* | 3 | 3 | 28.56 | 4.77 | 2.95 | 5 897 | 1 844 | 1 863 | 424 | 236 | 115 | 49 | 3.20 | 1 |
| *Hole P-1769* | 2 | 3 | 34.13 | 5.18 | 3.86 | 12 223 | 2 756 | 803 | 111 | 56 | 27 | 129 | 4.44 | 1 |
| **Noril'sk ore junction** | | | | | | | | | | | | | | |
| **Noril'sk-1 deposit** | | | | | | | | | | | | | | |
| Disseminated ore[1] | | | | | | | | | | | | | | |
| *Hole P-3010* | 12 | 8 | 1.78 | 0.41 | 0.70 | 3 335 | 1 979 | 14 | 53 | 26 | 15 | 274 | 1.69 | 1 |
| Massive ore | | | | | | | | | | | | | | |
| *Hole P-3010* | | 2 | 35.60 | 6.55 | 4.56 | 23 518 | 8 995 | 6 072 | 1 105 | 713 | 270 | 661 | 2.61 | 1 |
| Cu-rich massive ore | | | | | | | | | | | | | | |
| *Medvezhy (Bear's) Brook pit* | | 4 | 33.18 | 7.08 | 25.59 | 348 750 | 108 725 | 267 | 15 | 14 | 1 | 7 175 | 3.21 | 2 |
| **Noril'sk-2 deposit** | | | | | | | | | | | | | | |
| Disseminated ore[1] | | 7 | 1.27 | 0.20 | 0.26 | 1 548 | 521 | 165 | 25 | 25 | 12 | 41 | 2.97 | 1 |
| **Mt Chernaya deposit** | | | | | | | | | | | | | | |
| Disseminated ore[1] | | 8 | 0.68 | 0.19 | 0.25 | 1 357 | 566 | 94 | 16 | 9 | 6 | 221 | 2.39 | 1 |

**Table 4.6** (cont.)

| Area<br>Deposit | T | n | S<br>wt% | Ni<br>wt% | Cu<br>wt% | Pd<br>ppb | Pt<br>ppb | Rh<br>ppb | Ru<br>ppb | Ir<br>ppb | Os<br>ppb | Au<br>ppb | Pd/Pt | R |
|---|---|---|---|---|---|---|---|---|---|---|---|---|---|---|
| **Keweenawan magmatism (Lake Superior Area)** | | | | | | | | | | | | | | |
| **Duluth Complex** | | | | | | | | | | | | | | |
| **Babbit deposit** | | | | | | | | | | | | | | |
| Disseminated ore | | 15 | 2.00 | 0.22 | 0.98 | 208 | 283 | 7 | 7 | 3 | 3 | 58 | 0.73 | 1 |
| Rich ore of Local Boy | | 7 | 18.46 | 1.36 | 5.08 | 155 | 226 | 34 | 37 | 13 | 8 | 213 | 0.68 | 1 |
| **Dunka Road deposit** | | | | | | | | | | | | | | |
| Disseminated ore | | 52 | 0.83 | 0.18 | 0.49 | 706 | 438 | | | 9 | 5 | 71 | 1.61 | 1 |
| **Birch Lake deposit** | | | | | | | | | | | | | | |
| PGE-rich, low-sulfide mineralization | | 9 | 0.16 | 0.13 | 0.08 | 2 510 | 2 762 | | | 84 | 57 | 81 | 0.91 | 1 |
| **Crystal Lake intrusion** | | | | | | | | | | | | | | |
| **Great Lakes Nickel deposit** | | | | | | | | | | | | | | |
| Disseminated ore | | 29 | 3.19 | 0.36 | 0.69 | 1 422 | 361 | 39 | 24 | 5 | 8 | 167 | 3.92 | 1 |
| **Karoo magmatism** | | | | | | | | | | | | | | |
| **Insizwa intrusion** | | | | | | | | | | | | | | |
| **Waterfall Gorge deposit** | | | | | | | | | | | | | | |
| Disseminated ore | | 13 | 2.66 | 0.42 | 0.46 | 453 | 189 | 19 | 30 | 25 | 13 | 157 | 2.40 | 1 |
| Cu-poor massive ore | | 7 | 31.60 | 4.13 | 1.45 | 3 311 | 530 | 347 | 1 100 | 549 | 374 | 65 | 6.25 | 1 |
| Moderately Cu-rich massive ore | | 9 | 28.67 | 18.50 | 7.41 | 3 504 | 1 793 | 290 | 387 | 219 | 67 | 216 | 1.95 | 1 |
| Cu-rich massive ore | | 8 | 25.39 | 6.35 | 14.71 | 2 287 | 1 302 | 245 | 496 | 81 | 55 | 226 | 1.76 | 1 |

*T* Thickness of the ores [m]; *n* Number of samples; *R* References: 1 – Unpublished materials by Naldrett and his coworkers, 2 = Czamanske et al. (1992);

[1]Ores, disseminated in picritic and taxitic gabbrodolerite of the ore-bearing intrusions of the Noril'sk region

### *General information about the mineralization*

Older work summarized by Genkin et al. (1981), Duzhikov et al. (1988) and the subsequent papers of Distler and Kunilov (1994), Kunilov (1994), Stekhin (1994), Torgashin (1994), Sluzhenikin et al. (1994), and Sluzhenikin (2000), have shown that mineralization in the Noril'sk deposits can be subdivided into the following types:

1. Disseminated sulfides in picritic gabbrodolerite (gd)
2. Disseminated sulfides in lower taxitic gd
3. Disseminated and stringer sulfides in contact and lower olivine gd
4. Massive ore. This is very variable in composition from pyrrhotite-rich variants containing 2-3 wt% of Cu to Cu-rich variants (27-32 wt% of Cu) "Copper ore" – disseminated and veinlet-disseminated ores, usually rich in Cu forming a halo in the country rocks around massive sulfides and permeating hornfels inclusions in the massive ore.
5. "Upper copper ore" which occurs in the western part of the Kharaelakh intrusion and occupies the matrix of breccia zones at the top of and along the frontal portions of the intrusion (Fig. 4.32).
6. Sparse sulfides that are sometimes developed in olivine-bearing gd.
7. Sulfide-poor, PGE-rich disseminated mineralization in upper taxitic gd.

The position of the above ore types in a schematic section of an ore-bearing intrusion is shown in Fig. 4.14. Almost all of the ore types are mined in one location or another, except for type 7, the PGE-rich sulfide-poor ores, that are in preparation for mining at the present time, and the sparsely disseminated sulfides in olivine gabbrodolerite (type 6) that are too low in grade to be economic.

In the Talnakh ore junction all of the above ore types are developed. At present, the massive ore, whose thickness is typically 10-20 m, is the principal target of mining operations, although copper, upper copper, and disseminated ore are being mined to a lesser extent.

The principal ore that is mined in the Noril'sk-1 deposit is disseminated mineralization in picritic and taxitic gabbrodolerite. Massive ore, which was originally present as small lenses, 2-5 meters in thickness, has largely been mined out. The massive (Fig, 4.30) and related copper ore was located mainly in northern part of the deposit. Upper copper ore is unknown in this deposit, although the type 7 PGE-rich, low-sulfide mineralization is well developed (Sluzhenikin 2000), and is currently being developed for mining.

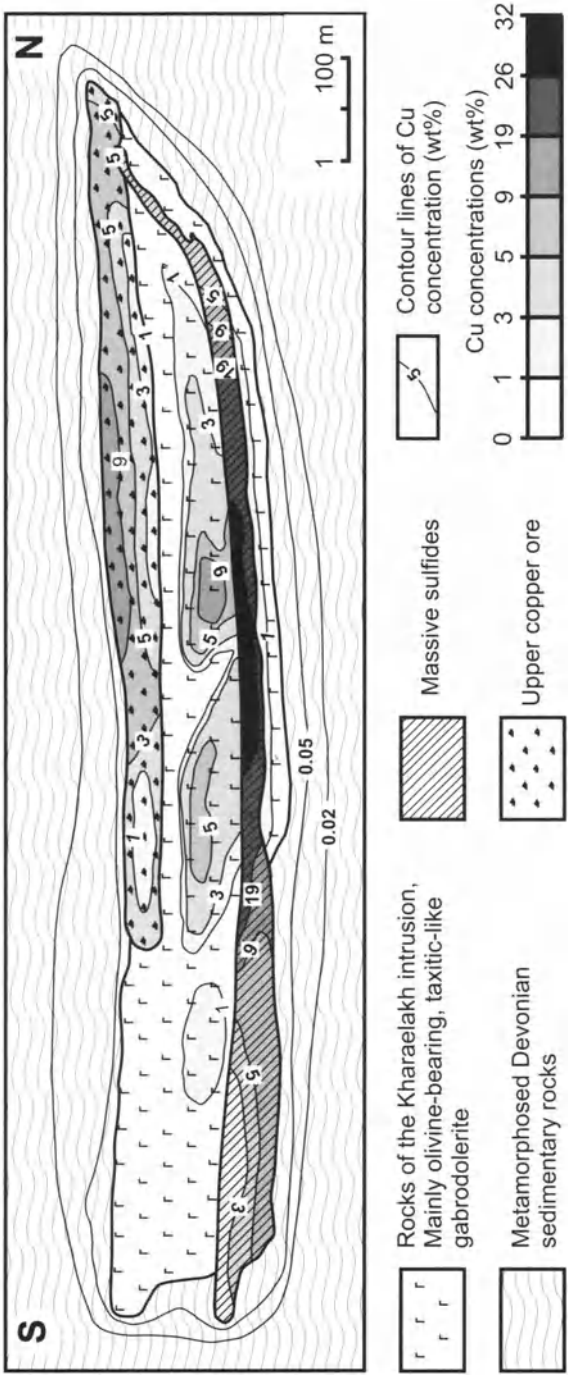


**Fig. 4.32.** Geological section showing the connection between massive and "upper copper" ores in the western part of the Oktyabrsky deposit (Oktyabrsky mine). After Torgashin (1994)

In all deposits, the massive sulfide ore generally occurs in the country rocks directly beneath the main bodies of the ore-bearing intrusions, although in places it is present in the lowermost parts of the intrusions. It is not gradational upwards into disseminated ore – there is almost always an intervening selvage of chilled contact gabbrodolerite with relatively little disseminated sulfide, and frequently a few centimeters to a few meters of unmineralized country rock separating the two ore types. Sulfides are integral parts of the picritic and taxitic gabbrodolerite. Field relations do not support the massive ore as having settled in situ from the overlying intrusions. It is not unusual to observe veins of massive ore cutting across the contact between the intrusions and country rocks (Fig. 4.33). Many Russian geologists regard the massive sulfide as the result of a separate intrusion of sulfide magma (e.g. Urvantzev 1972; Zotov 1979; Stekhin 1994). Zotov (1979) described the melting of terrigenous rocks to form a granophyric melt (T ~940°C) at the contact with massive sulfide. The reason why massive sulfides are developed exclusively beneath the main bodies of the intrusions, and did not intrude away from them is therefore something of an enigma.

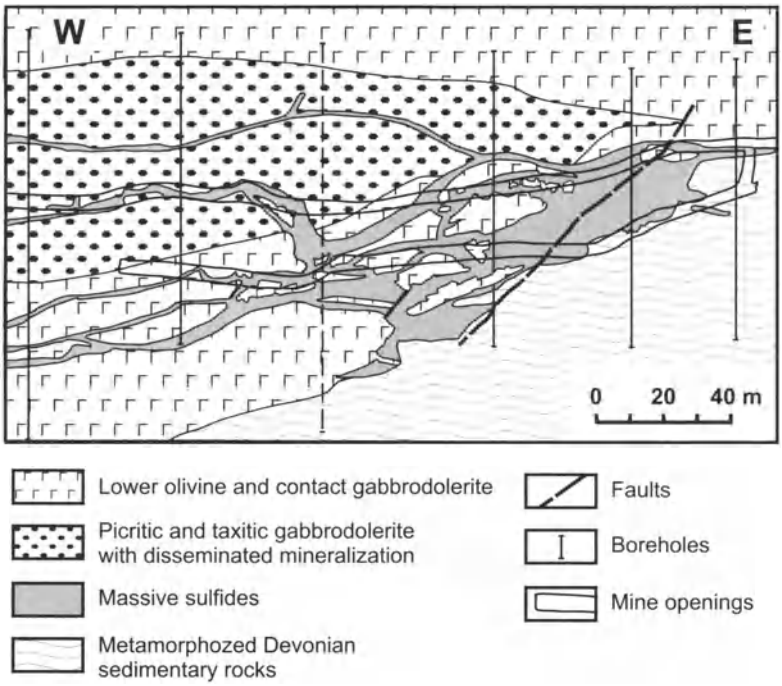


**Fig. 4.33.** Geological section showing relation between massive sulfide and rocks of the ore-bearing intrusion in the southern part of the Oktyabrsky deposit (Komsomolsky mine). After Kunilov (1994)

Genkin et al. (1981) gave a comprehensive description of the mineralogy and mineral associations of the Noril'sk ores. They reported that more then 100 hypogene minerals have been found in the ores, 26 of which were new minerals and mineral varieties. Almost all of the main classes of hypogene ore minerals are present, ranging from native elements to sulfides and hydroxides. More then 30 elements are present in the ore minerals as major components (with contents >1 wt%). The major ore minerals comprise those of the pyrrhotite group (hexagonal and monoclinic pyrrhotite and troilite), pentlandite, chalcopyrite, cubanite and magnetite. The ores are characterized by an unusually varied minor and trace mineralogy in addition to the major constituents. These include minerals of the chalcopyrite group (tetragonal chalcopyrite, talnakhite, mooihoekite, putoranite, nickeliferous putoranite, ferriferous chalcopyrite), and those of the noble metals including atokite, rustenburgite, isoferroplatinum, tetraferroplatinum, paolovite, stannopalladinite, plumbopalladinite, sobolevskite, kotulskite, moncheite, insizwaite, mayakite, cooperite, braggite, vysotskite, sperrylite, and hollingworthite (Distler et al., 1999).

Overall, 97-99 wt% of the Pt occurs in discrete minerals of the platinum group (PGM), but the major part of the Pd (67-98 wt% depending on locality) is present in solid solution in pentlandite where its concentration may reach 200-1600 g/t (Sluzhenikin and Distler 1998; Distler et al. 1999; Sluzhenikin 2000). Exceptions to this generalization with respect to Pd include the talnakhite-mooihoekite ores of the Oktyabrsky mine (where Pd is distributed roughly equally between pentlandite and discrete PGM), and the low-sulfide ores of the Noril'sk-1 deposit (where 95 wt% of the Pd occurs in PGM). Rh, Ru, Ir, and probably Os only occur in solid solution in pyrrhotite and pentlandite.

### *Ores of the Talnakh Ore Junction*

All 7 of the ore types itemized in the preceding section are present at the Talnakh ore junction. Average chemical compositions of the major types (massive, disseminated in picritic and in taxitic gabbrodolerite, copper ore, upper copper ore, and low-sulfide ore) are given in Table 4.6. Additional data for other types of mineralization (disseminated and veinlet-disseminated sulfides in olivine and contact gabbrodolerites) appear in figures and are discussed below.

It became clear at beginning of 1990s that disseminated ores within the Kharaelakh intrusion differ significantly in composition between the western and the central to eastern parts of the intrusion, and therefore the two areas are treated separately below. Much of the following discussion is

based on the results of a systematic study that is reported in Naldrett et al. (1996).

**Western Part of the Kharaelakh intrusion.** The western part of the Kharaelakh intrusion contains the Kharaelakh massive sulfide ore body (Fig. 4.34), which is the largest, and richest concentration of massive ore discovered anywhere so far. Naldrett et al. (1996) obtained their samples from the Oktyabrsky mine (Shafts No. 1 and 2), Bore hole 868, and samples collected underground at the Taymyrsky mine (Fig. 4.29). Noril'sk Kombinat data (comprising Ni, Cu, Pt, Pd and Au, but not Rh, Ir, Ru or Os) was provided to Naldrett et al. (1996) for both massive and disseminated ore for holes 597, 588, 835, 837, 839, 860 and 862 (see Fig. 4.29 for the locations of these holes). Overall, the samples showed a wide range in composition with Cu ranging from 2 to 18 wt% and Rh varying inversely with Cu (Fig. 4.35).

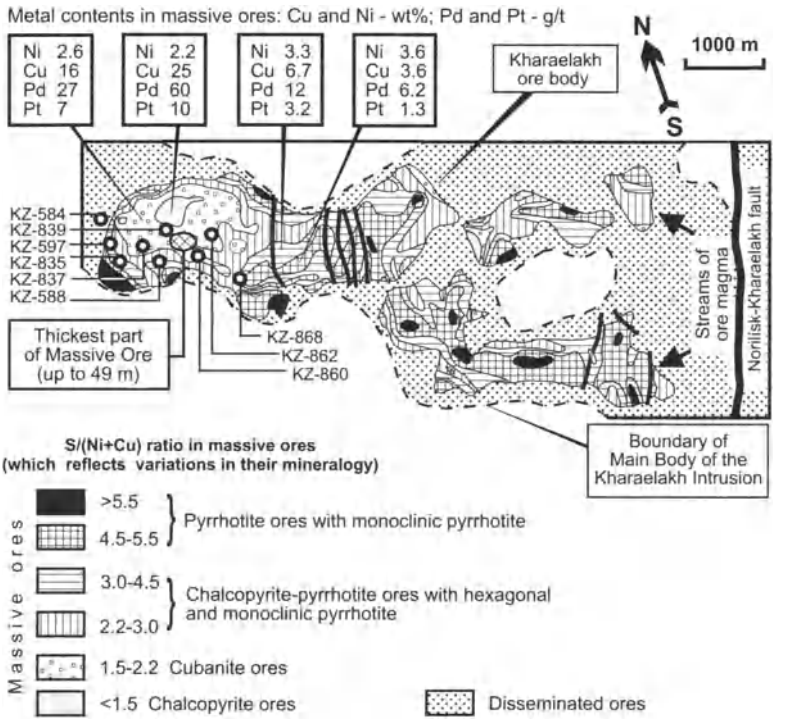


**Fig. 4.34.** Plan of the Kharaelakh ore body and adjacent parts of the Oktyabrsky deposit showing variation in S/(Ni+Cu) ratios (which reflect the ore mineralogy). The locations of drill holes for which the Kombinat's analytical data were obtained (KZ 584-862) are shown, together with that of hole KZ 868, from which samples were analyzed by this author and his coworkers. Modified after Stekhin (1994)

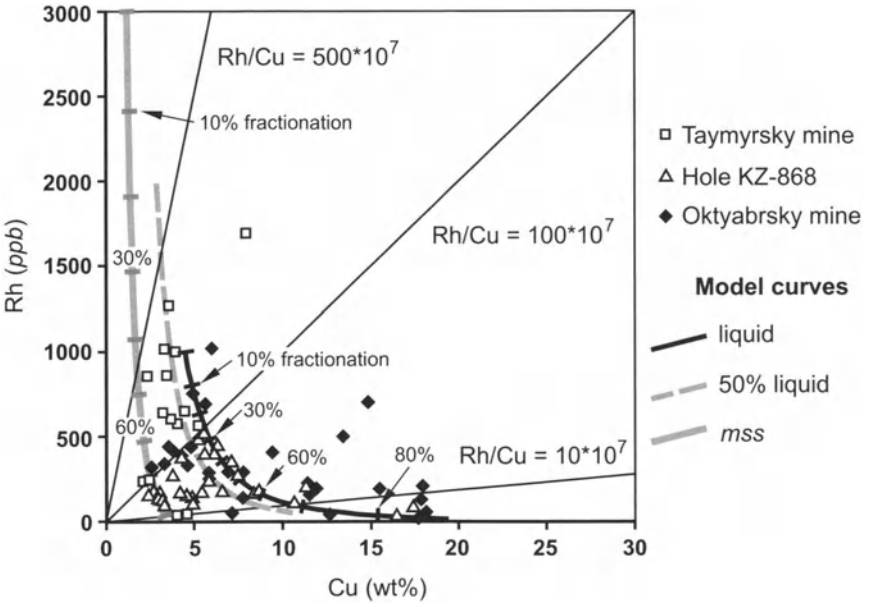


**Fig. 4.35.** Plot of Rh versus Cu, in massive ore from the Kharaelakh ore body together with model curves for the Rayleigh fractionation of mss from a sulfide liquid

Samples from typical Upper Copper ore (Table 4.6) were obtained from core from underground borehole P-3202 that is located in the northern part of the Oktyabrsky mine that is serviced by No. 2 shaft.

The problem with discussing the genesis of any ore type at Noril'sk is that the sulfides of many samples have not retained their initial compositions, but have had these changed at an early, post emplacement but still magmatic stage. Evidence to support this is best shown in the western part of the Kharaelakh intrusion, which overlies the Kharaelakh ore body.

The Rh and Au contents of sulfides (recalculated to 100% sulfide) are about 300 ppb in the disseminated ore in the upper part (above 865 m) of the taxitic and taxite-like gabbrodolerites in hole KZ 868 (Fig. 4.36). Below this, the Au content of the sulfides increases markedly (1000 to 3000 ppb), but the increase in Rh and Ir (Ir is not shown) is not so marked, so that the Rh/Au and Ir/Au ratio decrease significantly. The sulfides from the massive ore contain distinctly less Au, and approximately the same amount of Rh as those in the disseminated ores. However, inclusions of hornfelsed argillite within the massive ore contain sulfides with very much lower Rh and higher Au. The consequence of these metal variations is that the Rh/Au and Ir/Au ratios of sulfides are close to 1 and 0.1 respectively in the disseminated ore above 865 m, that is about 5 times lower than these ratios

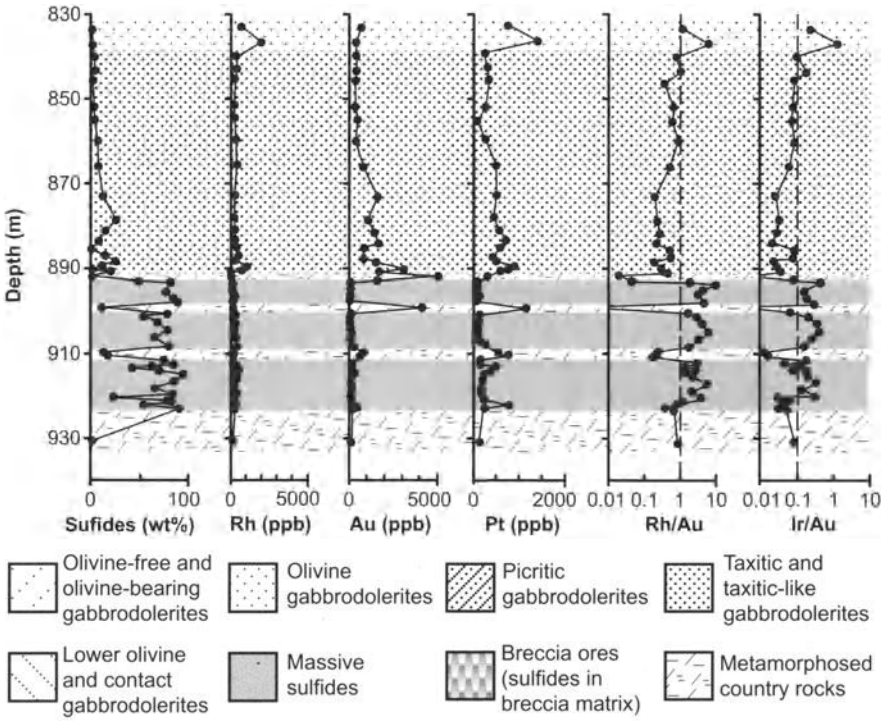


**Fig. 4.36.** Profile through the ore zone of hole KZ 868 showing variation in rock types and metal contents of 100% sulfides with elevation in the hole

in the massive ore. The inclusions have values of 0.1 and 0.01 for Rh/Au and Ir/Au respectively, 10 times lower then in the disseminated ore above 865 m. In the disseminated ores below 865 m, the ratios are intermediate between ratios above this and those of the sulfides in the inclusions. As can be seen from the figure, the behavior of Pt (and Pd and Cu although they are not shown) is essentially identical to that of Au.

Turning to the data provided by the Noril'sk Kombinat, these show characteristic metal contents in disseminated ore both in picritic and taxitic gabbrodolerites (Fig. 4.37). In the picritic gabbrodolerites the Au content of 100% sulfides is, on average, between 1000 and 1600 ppb and Pt content between 2000 and 3000 ppb. In the taxitic gabbrodolerites Au and Pt are very variable, sulfides in this unit are characterized by 400-1000 ppb Au and 2000-4000 ppb Pt. Sulfides in massive ore generally contain lower Au (200-600 ppb) and lower Pt (1500-2000 ppb) than those in taxitic and picritic gabbrodolerites (Table 4.7).

It is apparent that in all of the holes for which the Noril'sk Kombinat provided data, except KZ-860 (which is atypical because of the breccia

**Table 4.7.** Average metal contents in 100% sulfide of disseminated and massive ores of the Noril'sk region

| Rock | Intrusion | Hole | n | Ni | Cu | Au | Pd | Pt | Rh | Ir | Rh/Au | Ir/Au |
|---|---|---|---|---|---|---|---|---|---|---|---|---|
| OGD | Talnakh | KZ-1739 | 14 | | 3.35 | 642 | 4 738 | 5 161 | 293 | 39 | 0.5 | 0.06 |
| Picritic gabbro-dolerite | Noril'sk-1 | P-3010 | 13 | 11.82 | 11.85 | 3 986 | 72 961 | 37 933 | 4 376 | 634 | 1.1 | 0.16 |
| | Noril'sk-2 | | 7 | 7.66 | 7.72 | 1 271 | 52 494 | 19 978 | 5 663 | 540 | 4.4 | 0.42 |
| | Mt. Chernaya | | 7 | 14.26 | 11.78 | 2 728 | 70 705 | 24 630 | 6 622 | 657 | 2.4 | 0.24 |
| | Talnakh | P-1769 | 16 | 7.02 | 10.41 | 1 782 | 31 433 | 10 790 | 1 466 | 185 | 0.8 | 0.10 |
| | | KZ-1796 | 9 | 6.60 | 10.44 | 2 360 | 40 114 | 16 090 | 1 931 | 301 | 0.8 | 0.13 |
| | | KZ-1739 | 23 | 6.95 | 10.40 | 1 517 | 34 574 | 10 201 | 1 752 | 169 | 1.2 | 0.11 |
| | | KZ-1162 | 8 | 7.25 | 12.66 | 1 662 | 31 489 | 7 672 | 1 266 | 118 | 0.8 | 0.07 |
| | Kharaelakh (Center) | KZ-1162 | 8 | 7.25 | 12.66 | 1 662 | 31 489 | 7 672 | 1 266 | 118 | 0.8 | 0.07 |
| | Kharaelakh (West) | KZ-835 | 3 | 1.97 | 8.33 | 1 019 | 8 059 | 2 975 | | | | |
| | | KZ-588 | 2 | 2.88 | 5.96 | 933 | 12 268 | 2 740 | | | | |
| | | KZ-839 | 2 | 2.52 | 5.85 | 758 | 10 625 | 2 605 | | | | |
| | | KZ-862 | 4 | 3.59 | 9.37 | 1 205 | 18 643 | 5 140 | | | | |
| Taxitic gabbro-dolerite | Talnakh | P-1769 | 12 | 5.96 | 9.25 | 1 402 | 28 964 | 10 496 | 1 200 | 122 | 0.9 | 0.09 |
| | | KZ-1796 | 6 | 5.83 | 10.62 | 1 631 | 25 105 | 8 822 | 1 035 | 118 | 0.6 | 0.07 |
| | | KZ-1739 | 14 | 4.60 | 10.73 | 1 084 | 26 348 | 6 009 | 1 055 | 771 | 1.0 | 0.07 |
| | Kharaelakh (Center) | KZ-1162 | 16 | 5.23 | 10.45 | 1 700 | 28 620 | 8 068 | 778 | 65 | 0.5 | 0.04 |
| | Kharaelakh (East) | KZ-1812 | 8 | 6.15 | 11.45 | 1 455 | 32 809 | 6 117 | 1 522 | 96 | 1.0 | 0.07 |
| | Kharaelakh (West) | KZ-868 | 16 | 3.74 | 6.29 | 369 | 11 365 | 2 272 | 313 | 31 | 0.8 | 0.08 |
| | | KZ-597 | 6 | 2.18 | 7.73 | 1 251 | 16 200 | 4 157 | | | | |
| | | KZ-835 | 6 | 3.34 | 6.69 | 1 017 | 13 417 | 2 675 | | | | |
| | | KZ-588 | 4 | 2.49 | 5.63 | 1 054 | 13 618 | 2 994 | | | | |
| | | KZ-839 | 12 | 2.34 | 6.09 | 1 064 | 14 820 | 3 348 | | | | |
| | | KZ-862 | 5 | 2.45 | 5.78 | 688 | 12 432 | 2 464 | | | | |

**Table 4.7** (cont.)

| Rock | Intrusion | Hole | n | Ni | Cu | Au | Pd | Pt | Rh | Ir | Rh/Au | Ir/Au |
|---|---|---|---|---|---|---|---|---|---|---|---|---|
| Massive ore | Talnakh | P-1769 | 3 | 5.81 | 4.33 | 144 | 13 705 | 3 091 | 900 | 62 | 6.2 | 0.43 |
| | | KZ-1796 | 2 | 6.39 | 3.97 | 66 | 7 925 | 2 464 | 2 467 | 309 | 37.4 | 4.69 |
| | | KZ-1739 | 2 | 5.24 | 5.48 | 100 | 7 415 | 1 720 | 2 027 | 272 | 20.3 | 2.72 |
| | | KZ-1739 | 3 | 5.07 | 6.02 | 223 | 9 664 | 2 397 | 1 068 | 45 | 4.8 | 0.20 |
| | | KZ-1739 | 1 | 5.46 | 4.04 | 51 | 9 364 | 1 958 | 448 | 7 | 8.7 | 0.14 |
| | Kharaelakh (Center) | KZ-1162 | 7 | 4.48 | 15.05 | 951 | 18 161 | 2 897 | 216 | 9 | 0.2 | 0.01 |
| | Kharaelakh (East) | KZ-1812 | 3 | 5.81 | 4.33 | 144 | 13 705 | 3 091 | 900 | 62 | 6.2 | 0.43 |
| | Kharaelakh (West) | Taym | 15 | 3.99 | 4.39 | 100 | 7 347 | 1 568 | 780 | 65 | 7.8 | 0.65 |
| | | KZ-868 | 24 | 3.92 | 5.32 | 152 | 8 805 | 2 126 | 264 | 19 | 1.7 | 0.13 |
| | | KZ-835 | 2 | 3.37 | 3.68 | 172 | 7 110 | 1 414 | | | | |
| | | KZ-837 | 6 | 3.40 | 5.77 | 637 | 9 982 | 2 772 | | | | |
| | | KZ-588 | 7 | 3.41 | 5.43 | 367 | 10 687 | 3 214 | | | | |
| | | KZ-839 | 16 | 3.43 | 6.79 | 495 | 13 321 | 2 791 | | | | |
| | | KZ-860 | 4 | 3.42 | 4.19 | 316 | 5 063 | 2 156 | | | | |
| | | KZ-862 | 6 | 3.45 | 6.58 | 525 | 9 685 | 2 603 | | | | |
| | | Okt-Cu | 18 | 3.38 | 19.53 | 2 428 | 37 919 | 8 449 | 215 | 21 | 0.1 | 0.01 |

For hole KZ-1739, where three horizons of massive sulfides are present (see Fig. 4.39), data of each of them are given separately (from top to bottom). *Taym* Taymyrsky mine; *Okt-Cu* Cu-rich massive ores of the Oktyabrsky mine

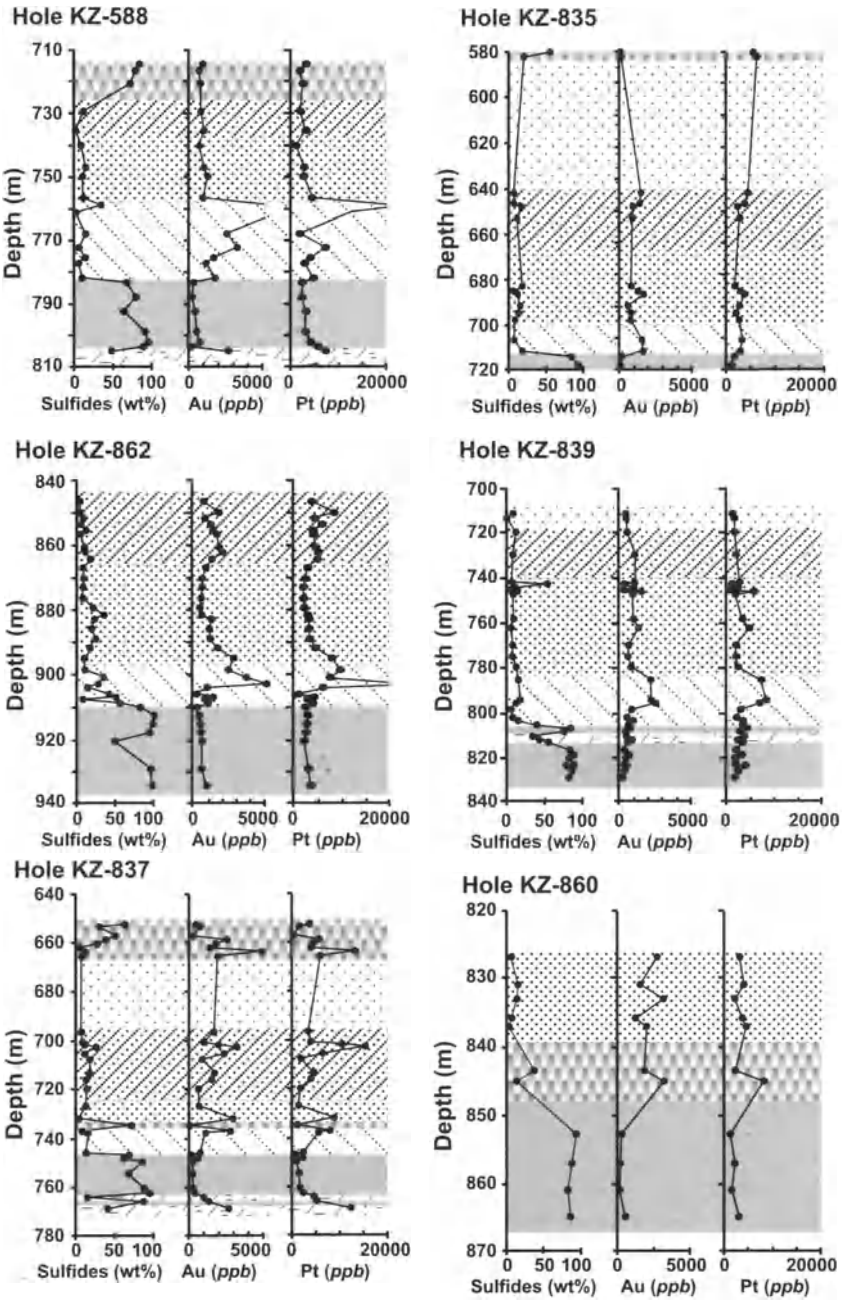


**Fig. 4.37.** Profiles through holes at the western end of the Kharaelakh ore body (see Fig. 4.29 for their location) showing variation in rock types and metal contents with depth. Data made available by the Noril'sk Kombinat. Rh and Ir concentrations were not available for these holes. See Fig. 4.36 for the legend

zone overlying the massive sulfide zone), sulfides in the rocks immediately above the massive sulfides show a pronounced upward increase in Au and Pt, which peaks 10-20 m above the top of the massive zone, and then decreases progressively upward to assume the values typical of the taxitic or picritic gabbrodolerites. The position at which this peak occurs appears to be independent of rock type, since it is observed in the lower part of the contact olivine gabbrodolerites in hole KZ-835, in the middle of this unit in holes KZ-862 and KZ-839, and at the contact between the contact olivine gabbrodolerites and taxitic gabbrodolerites in hole KZ-588 and within the lower part of the taxitic gabbrodolerite in hole KZ-837. As seen in Fig. 4.37 the enrichment in Au is accompanied by an enrichment in Pt; data not plotted in the figure indicate that it is also associated with enrichments in Pd and Cu. As noted above, the peak in Au in hole KZ-868 occurs at the immediate upper contact of the massive ore with contact olivine gabbrodolerites (Fig. 4.36), and then decreases through this unit and the overlying taxitic gabbrodolerites. Rh and Ir data are also available for hole KZ-868 and show that the enrichment in Au is associated with a marked decrease in the Rh/Au and Ir/Au ratios; it is believed that this behavior is characteristic of all zones enriched in Cu, Pt, Pd and Au above massive ore; if Rh and Ir data had also been available in the Noril'sk Kombinat data base provided to Naldrett et al. (1996), it is thought very likely that the same variation in Au/Rh and Au/Ir ratios would have been observed in these holes as in hole KZ-868.

Naldrett et al. (1982, 1992, 1994a,c) showed that, on cooling, natural sulfide ore magmas crystallize mss and become enriched in Cu, Pt, Pd and Au and depleted in Co, Rh, Ru, Ir and Os (see Chapter 2 and also Fig. 4.35). Because the enrichment described above for the western part of the Kharaelakh ore body is independent of rock type, it appears that it is the result of a Cu-, Pd-, Pt- and Au-rich, fractionated sulfide liquid escaping from the massive ore as this cooled. Sulfide liquids have long been known to have a very strong wetting ability against silicates (c.f. Naldrett 1969). Ebel and Naldrett (1996) noted that this increases with increasing Cu and decreasing S content of the liquid. This physical characteristic would have assisted the fractionated liquid that developed during crystallization of the Kharaelakh ore body to permeate the hornfels, both within and adjacent to the massive ore zone, to form a halo. The liquid has also penetrated the overlying igneous rocks, along fractures to produce small, massive stringers, and along grain boundaries to form disseminated sulfides. The liquid crystallized and became progressively more fractionated as it progressed, thus accounting for the increase in sulfide tenor away from the massive ore. What the samples of the intrusive rocks show today is the sum of any original primary sulfide, plus the component added by this permeating liq-

uid. The downward increase in Au, Pt, Pd and Cu which is so commonly observed in the taxitic and contact olivine gabbrodolerite is not, therefore, a characteristic of the primary disseminated ore; it was imposed on this ore at a later, but still high temperature, stage as the underlying massive ore crystallized and fractionated.

**Central and Eastern Part of the Kharaelakh intrusion.** Systematic sets of samples were only available from holes KZ-1162 and KZ-1812 holes (Fig. 4.38) in the central and eastern parts of the Kharaelakh intrusion. Hole KZ-1162 intersected the entire zone of mineralization, and thus provided information about the disseminated ores in both the picritic and taxitic gabbrodolerite, but massive sulfides were only intersected in thin veinlets in hornfels. Hole KZ-1812 provided no opportunity to sample disseminated sulfide in the picritic gabbrodolerite, but samples of taxitic and contact gabbrodolerite, the underlying mineralized hornfels, and also the massive sulfide were available.

The picritic gabbrodolerite in hole KZ-1162 is marked by sulfides with relatively constant values of PGE and Au (averages for metal content in 100% sulfide are Cu = 12.7 wt%, Rh = 1266 ppb, Pd = 31489 ppb, Au = 1662 ppb, Pt = 7672 ppb, and Ir = 118 ppb), which gives Rh/Au and Ir/Au ratios close to 1 and 0.1 respectively (Table 4.7).

Sulfides in the taxitic gabbrodolerite in hole KZ-1812 contain constant values of Rh (~1500 ppb) and Au (~1500 ppb) and the Rh/Au and Ir/Au ratios are also constant, again close to 1 and 0.1 respectively. There is a slight decrease in both Rh and Au in sulfides across the taxites in hole KZ-1162 and the Rh concentration (778 ppb) is lower and Au concentration (1700 ppb) higher than in hole KZ-1812.

In both holes KZ-1162 and KZ-1812, the massive ore lies outside the intrusion within the underlying hornfelsed sediment. In general, the massive ore is characterized by sulfides with lower Rh and similar Au concentrations to the ore in the overlying taxitic gabbrodolerites. Average metal values in 100% sulfide in holes KZ-1812 and KZ-1162 respectively are Cu = 4.33 and 15.05 wt%, Rh = 900 and 216 ppb, Pd = 13705 and 18161 ppb, Au = 144 and 951 ppb, Pt = 3091 and 2897 ppb, and Ir = 62 and 9 ppb. The massive ore in hole KZ-1812, with Rh/Au = 6.2 and Ir/Au = 0.43 is very different to that in hole KZ-1162 in which Rh/Au = 0.23 and Ir/Au =0.01 (Table 4.7) (the reason for the very different compositions of the massive ore in these two holes is discussed below). A zone of Au+Pt+Pd+Cu enrichment occurs above the massive ore in both holes, in hornfels in KZ-1812 and in contact gabbrodolerite in KZ-1162, again pointing to the lack of dependence of this enrichment on host rock.

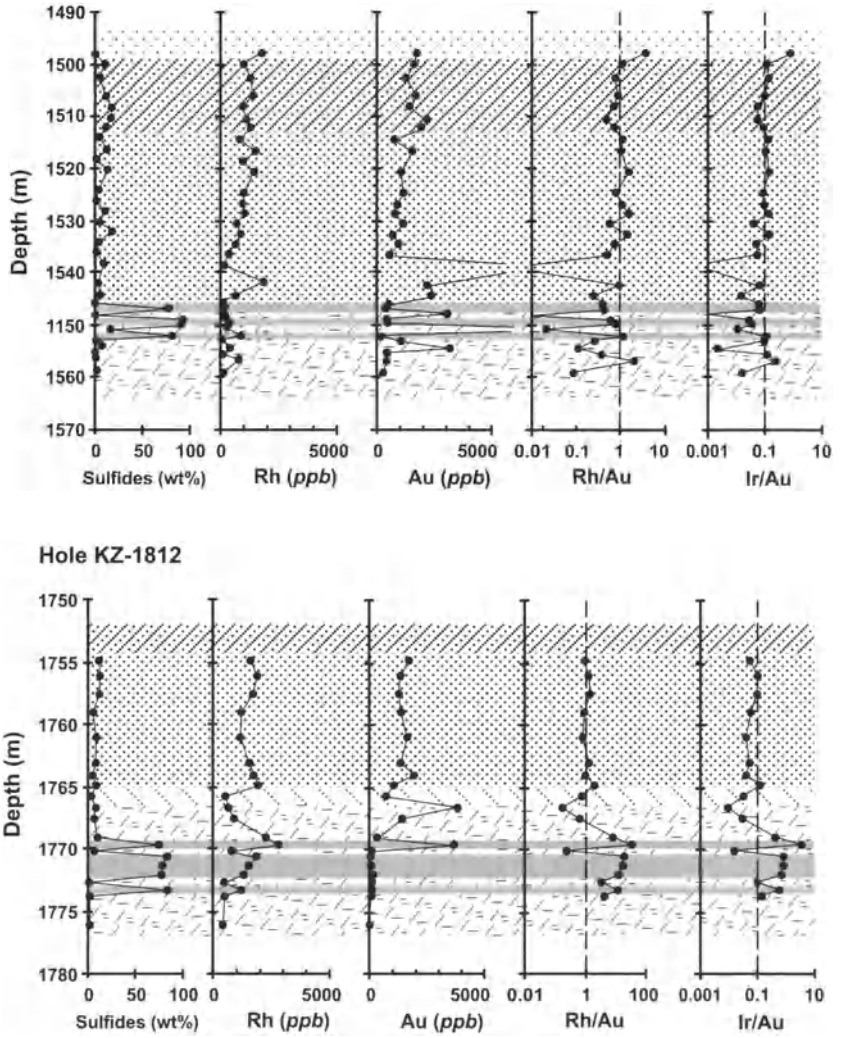


**Fig. 4.38.** Profiles through holes KZ-1162 and KZ-1812 in the central and eastern parts of the Kharaelakh intrusion, showing variation in rock types and some metal contents and ratios with depth in the holes. See Figure 4.36 for the legend

Accepting the evidence that Cu-, Au-, Pt- and Pd-rich sulfide liquid escaping from the massive ore as it cooled has affected the lower parts of the disseminated ore in some areas, both in the western and central and eastern parts of the Kharaelakh intrusion, one must exclude these parts if one wants to obtain the original composition of the sulfides. If one does this, one obtains the following values: hole KZ-868, 836-865 m (representative

of the western part of the Kharaelakh intrusion), Ni = 6.2 wt%, Cu = 5.8 wt%, Pd = 14582 ppb, Pt = 3898 ppb, Rh = 493 ppb, Au = 431 ppb; hole KZ-1162, 1500-1530 m (representative of the central part of the intrusion), Ni = 6.1 wt%, Cu = 10.8 wt%, Pd = 25728 ppb, Pt = 6339 ppb, Rh = 1068 ppb, Au = 1273 ppb; hole KZ-1812, 1755-1765 m (representative of the eastern part of the intrusion), Ni = 6.1 wt%, Cu = 11.4 Wt%, Pd = 32808 ppb, Pt = 6117 ppb, Rh = 1522 ppb, Au = 1455 ppb. Clearly there are major differences in the metal content of the sulfides carried in different parts of the intrusion, with most metals except for Ni being twice to three times as rich in the central and eastern parts of the Kharaelakh intrusion than in the western part. Reasons for this are discussed below.

**Talnakh Intrusion**. Drill core from three holes were sampled along the length of the Main Talnakh intrusion; P-1769, KZ-1796 and KZ-1739 spaced along the intrusion progressively farther to the north (Fig. 4.39). Massive sulfide ore occurs in hornfelsed Tungusskaya sediment in P-1769 and KZ-1796, but in KZ-1739, the massive sulfide forms three veins within taxitic gabbrodolerite, with only a small amount of sulfide in the underlying hornfels. In addition, samples of disseminated ore were obtained from the Gabbrovy intrusion (hole VH-4)[12], which is a peripheral sill that extends north from the Talnakh intrusion (Zen'ko and Czamanske, 1994).

The picritic gabbrodolerite is characterized in all holes by sulfides with fairly high levels of PGE, showing relatively little variation, except for one or two higher values in each hole (averages for 100% sulfides in holes P-1769, KZ-1796 and KZ-1739 are Cu = 10.4 wt %; Rh = 1500–2000 ppb; Pd = 30–40,000 ppb; Au = 1500–2400 ppb; Pt = 10–16,000 ppb, Ir = 170–300 ppb). The tenor in the sulfides tends to decrease downward through the picrite in each hole.

The taxitic gabbrodolerite is more variable in the tenor of its contained sulfides (Fig. 4.39) and on average the tenor is lower than that characterizing sulfides in the picritic gabbrodolerite (averages for 100% sulfides in holes P-1769, KZ-1796 and KZ-1739 are about, Cu = 10 wt%; Rh = 1100 ppb; Pd =25–29,000 ppb; Au = 1000–1600 ppb; Pt = 6000–10,000 ppb; Ir = 120–770 ppb). The downward decrease in Rh characterizing the picritic gabbrodolerite continues through the taxitic gabbrodolerite in hole P-1769 and KZ-1796. Au decreases downward through the taxitic gabbrodolerite in hole P-1796, and the Rh/Au ratio remains close to 1 and the Ir/Au close to 0.1. In P-1769 sulfide compositions from the lower half of the taxitic

[12] Composition of these ores is discussed below

gabbrodolerite indicate that this mineralisation has been affected by fractionated sulfide liquid from the underlying massive ore, as has been discussed above. Massive sulfide occurs within the intrusion near the base of P-1739, and the Au-enrichment appears to have affected rocks below the level of the sulfide but not above.

The sparse sulfide dissemination in olivine gabbrodolerite, studied in hole KZ-1739, is distinctly poorer in metal tenor by a factor of about 3, than in the underlying picritic gabbrodolerite (average Cu = 3.35 wt%; Rh = 293 ppb; Pd = 4738 ppb; Au = 642 ppb; Pt = 5161 ppb; Ir = 39 ppb).

Sulfides comprising massive ore contain about 50% of the Cu (4–6 wt%), generally higher Rh (900–2500 ppb) and Ir (50-300 ppb), and much lower Pd (8000–14000 ppb), Au (50–250 ppb) and Pt (2000–3000) than those in the overlying taxitic- and picritic-hosted ore.

**Rh/Au and Ir/Au ratios.** It is clear from the above discussion that Rh/Au and Ir/Au ratios are powerful discriminants of ore types. Sulfides from the picritic gabbrodolerite and the upper part of the taxitic gabbrodolerite have Rh/Au ~1 and Ir/Au ~0.1. Values in the olivine-bearing and olivine gabbrodolerites are more scattered (due to their concentrations approaching the detection limits) but are about 1/2 of these values. Massive ore is generally characterized by Rh/Au ratios >5 and Ir/Au ratios >0.5. Sulfides in both the hornfels and contact and taxitic gabbrodolerites close to intersections of massive ore tend to have higher Cu, Pd, Au and Pt and distinctly lower Rh/Au and Ir/Au ratios.

**Comparison of Ore Intersections in different parts of the Talnakh ore junction.** Average analytical data for the metal contents of 100% sulfides in picritic gabbrodolerite, taxitic gabbrodolerite and massive sulfide are given in Table 4.7 and compared in Fig. 4.40. In computing these averages, allowance has been made for the Cu, Pt, Pd and Au enrichment caused by fractionating sulfide liquid escaping from the underlying massive ore. Thus it is only those portions of these intersections that lie above the zone of enrichment, and have Rh/Au and Ir/Au ratios close to 1 and 0.1 which have been included in the averages. The reason for this is to obtain the composition of the original sulfide liquid, before Cu and Au-enriched liquid migrating out of the underlying massive ore affected the bulk composition of this material.

It is seen in Fig. 4.40a that sulfides in picritic gabbrodolerite from the Talnakh and central-eastern parts of the Kharaelakh intrusions contain about the same concentrations of Ni, Cu, PGE and Au but that sulfides from the western part of the Kharaelakh intrusion contain very much lower

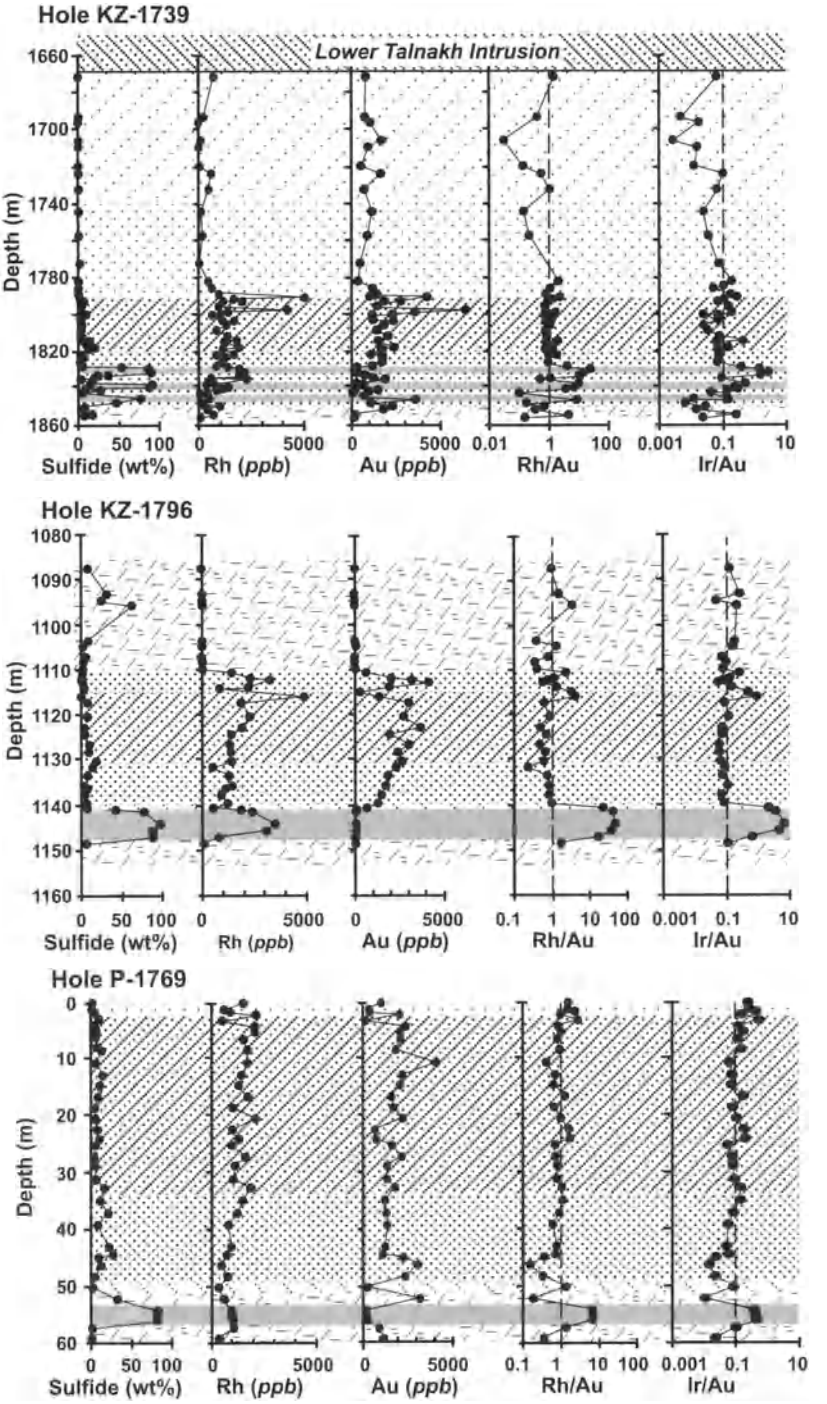
Hole KZ-1739
Lower Talnakh Intrusion
Depth (m)
1660
1700
1740
1780
1820
1860
0 50 100
Sulfide (wt%)
0 5000
Rh (ppb)
0 5000
Au (ppb)
0.01 1 100
Rh/Au
0.001 0.1 10
Ir/Au
Hole KZ-1796
Depth (m)
1080
1090
1100
1110
1120
1130
1140
1150
1160
0 50 100
Sulfide (wt%)
0 5000
Rh (ppb)
0 5000
Au (ppb)
0.1 1 10 100
Rh/Au
0.001 0.1 10
Ir/Au
Hole P-1769
Depth (m)
0
10
20
30
40
50
60
0 50 100
Sulfide (wt%)
0 5000
Rh (ppb)
0 5000
Au (ppb)
0.1 1 10 100
Rh/Au
0.001 0.1 10
Ir/Au

**Fig. 4.39.** Profiles through holes KZ-1739, KZ-1796 and P-1769 through the Talnakh intrusion, showing variations in rock type and metal content with depth in the hole. See Figure 4.36 for Legend.
Notes: (1) In borehole KZ-1796 the rocks above the intrusion, shown by shading corresponding to hornfels are in fact metasomatic pyritized rocks belonging to the Tungusskaya Series; (2) Borehole P-1769 is an underground hole, drilled upwards; the depths shown in the profile are therefore the inverse of those appearing in the corebox

concentrations. This difference is also apparent in sulfides in taxitic gabbrodolerite (Fig. 4.40b), although the averaged data present in Table 4.5 brings out the generally lower metal concentrations in sulfides in the taxitic as compared to the picritic gabbrodolerite. These observations do not apply to the massive ore (Fig. 4.40c). Unlike those of the taxitic and picritic ores, sulfides in the massive ores of the western part of the Kharaelakh intrusion contain similar amounts of Pd, rather higher Pt and Cu, much higher Au, somewhat lower Ni and distinctly lower Rh than those from the Talnakh and central-eastern parts of the Kharaelakh intrusion.

In Fig. 4.40c, the data for the western part of the Kharaelakh intrusion are arranged from left to right in the order of the increasing proximity of the holes that they represent to the extremely Cu-rich massive ore (see Fig. 4.34). Looking at Fig, 4.40c, data on samples collected underground at the Taymyrsky mine, near the eastern end of the Kharaelakhsky ore lens, mark the start and that on the Cu-rich ore itself (Okt-Cu) the end of this progression (note that holes KZ-837, KZ-588, KZ-839, KZ-860 and KZ-862 are approximately equidistant from the center of the Cu-rich zone). It is seen that there is a tendency for metal concentrations in massive sulfide to increase from left to right, that is on approaching the Cu-rich ore; this is especially noticeable for Au. This is interpreted (see below) as being due to the progressive fractionation of the liquid giving rise to the massive ore within this lens, as it moved from east to west. The fractionation reaches its apogee in the Cu-rich zone itself.

The question arises as to whether the massive ore in the western part of the Kharaelakh intrusion was derived from a source which, like that giving rise to the picritic and taxitic ore, was less rich than the sources responsible for the central-eastern part of the Kharaelakh and Talnakh intrusions or was similar to the source of these. This is a difficult question to resolve, because the massive ore is both fractionating from east to west and retaining what is probably a variable proportion of the sulfide liquid (i.e. the adcumulus nature of the ore is variable). This point is addressed again in the discussion of the variation diagrams (see below).

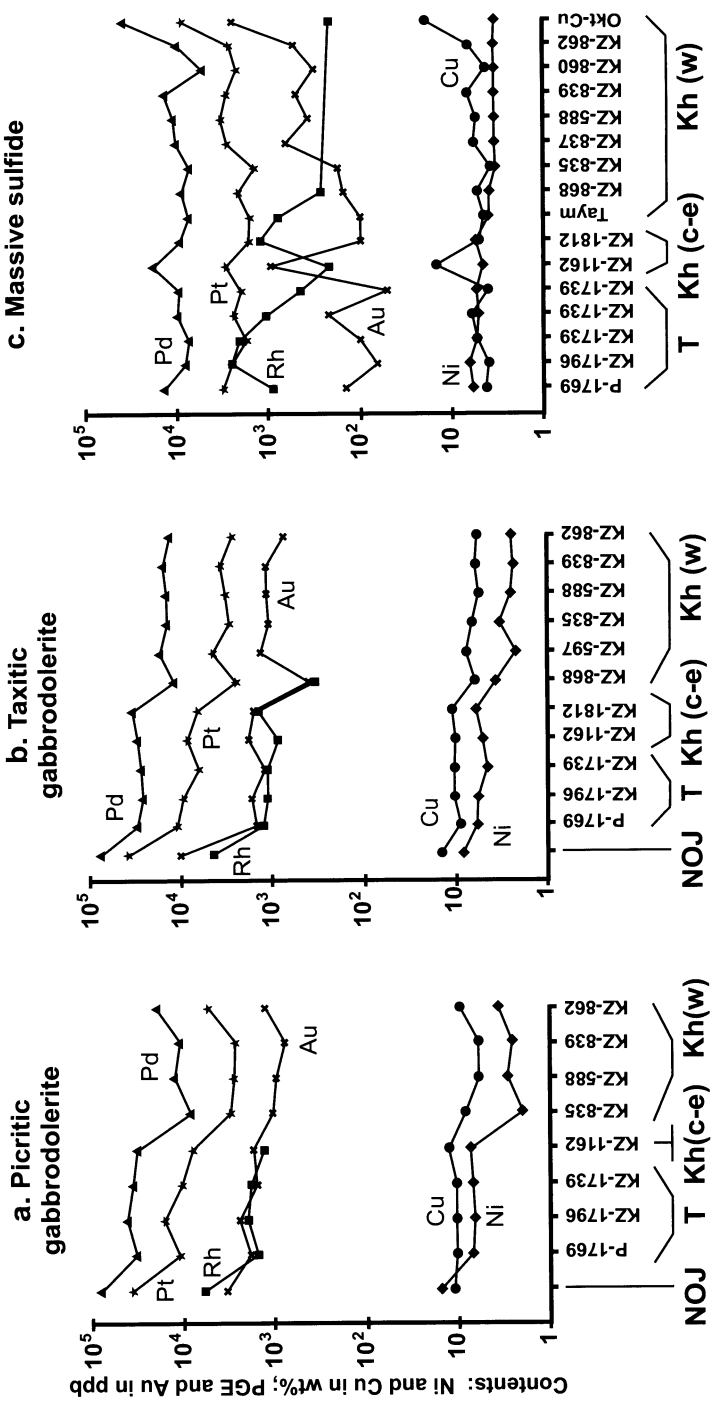
a. Picritic gabbrodolerite
b. Taxitic gabbrodolerite
c. Massive sulfide
Contents: Ni and Cu in wt%; PGE and Au in ppb
Pt
Pd
Rh
Au
Cu
Ni
NOJ T Kh(c-e) Kh(w)
P-1769
KZ-1796
KZ-1739
KZ-1162
KZ-835
KZ-588
KZ-839
KZ-862
KZ-597
KZ-868
KZ-1812
KZ-1739
T Kh (c-e) Kh (w)
Okt-Cu

**Fig. 4.40.** Average metal contents (excluding samples that have been enriched subsequently – see text) in disseminated ore in Picritic (a) and Taxitic (b) gabbrodolerite and Massive sulfide (c) from intrusions of the Talnakh ore junction and (where available) intrusions of the Noril'sk ore junction. Data for the Talnakh ore junction are taken from Table 4.7. For hole KZ-1739 where three veins of massive sulfide are present, the data are given separately for each of them (the upper vein at the left, lower vein at the right). *NOJ* Noril'sk ore junction (intrusions Noril'sk-1, Noril'sk-2, and Mt Chernaya); *T* Talnakh intrusion; *Kh(c-e)* central and eastern parts of the Kharaelakh intrusion; *Kh(w)* western part of the Kharaelakh intrusion; *Taym* Taymyrsky mine; *Okt-Cu* Cu rich ores of the Oktyabrsky mine

**Composition of massive ore of the Kharaelakh Ore Body and comparison with other massive ore of the Talnakh Ore Junction.** The Kharaelakh Ore body lies beneath, and partly within the western part of the Kharaelakh intrusion. It extends 3.5 km east-west by 1-1.3 km north-south, reaching a maximum thickness of 49 m and averaging 20 m in thickness (Fig. 4.34). All previous studies of the Kharaelakh ore body have drawn attention to the development of a concentrically zoned Cu-rich ore zone, characterized by sulfur-deficient minerals including mooihoekite, talnakhite and putoranite at the western end of the Kharaelakh ore lens. Stekhin (1994) drew attention to the variation in S/(Ni+Cu) ratios in massive ore underlying both the Kharaelakh and Talnakh intrusions. He suggested that this was due to a decrease in the Fe content of the ore magma as intrusion proceeded; on this basis he defined 4 main 'streams' which represented the flow direction of ore magma responsible for the pools of massive sulfide. His data for the Kharaelakh ore body and adjacent areas are shown in Fig. 4.34.

As noted above, the massive sulfide lenses at Talnakh, are thought to have fractionated as they intruded, thus giving rise to the asymmetric zoning present in the ores. The data allow investigation of this concept in greater detail for the Kharaelakh ore body.

In Fig. 4.41 data for the different sample locations are compared on a series of plots of noble metals vs Cu, in which Cu is used as an index of fractional crystallization, much as $SiO_2$ is used in Harker variation diagrams in petrology. Data for the Taymyrsky mine, hole KZ-868, and samples collected from the Cu-rich ore zone toward the western end of the Kharaelakh lens are plotted together with evolution lines for the liquid, mss and a 50:50 mixture of liquid and mss in Fig. 4.41a (an enlarged version of this illustration appears above as Fig. 4.35). The model lines represent Rayleigh curves for perfect fractionation, using the coefficients for the partitioning of metals between mss and sulfide liquid discussed in Chapter 2 ($D_{Rh} = 3$; $D_{Pd} = 0.2$; $D_{Pt} = 0.1$; $D_{Au} = 0.01$; $D_{Cu}$, has been assumed to vary from 0.28 to 0.088, decreasing with increase of Cu content – see Fig. 2.17).

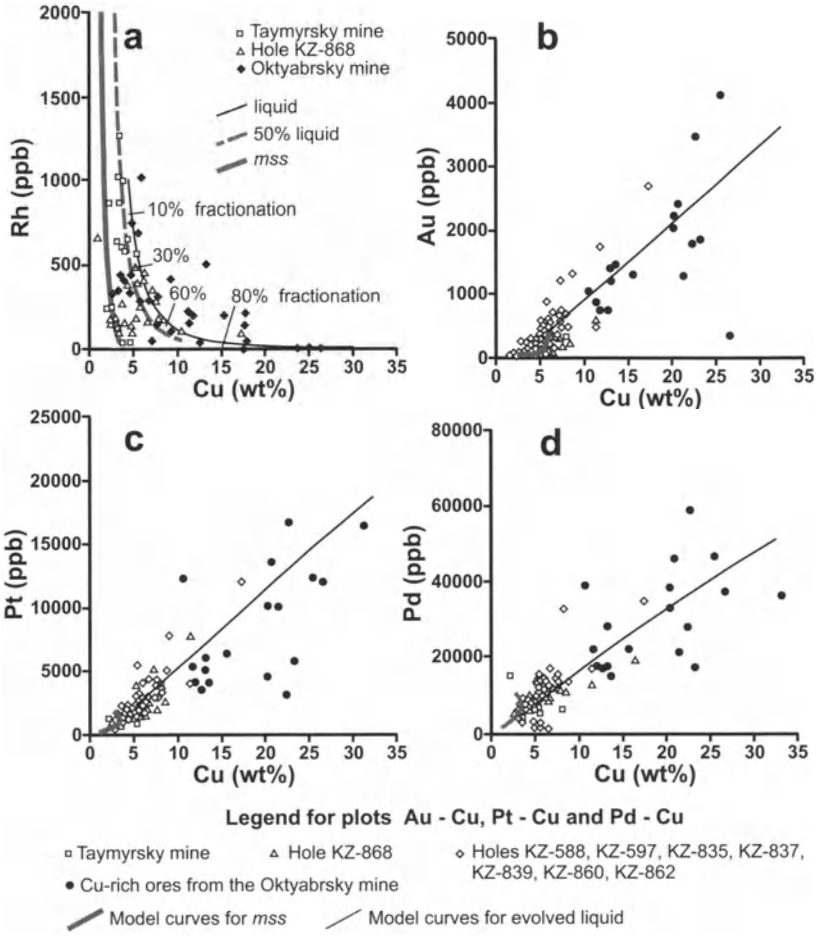


**Fig. 4.41**. Variation of (a) Rh, (b) Pt, (c) Pd and (d) Au with Cu in massive ore from the Kharaelakh ore body, together with model curves for the Rayleigh fractionation of mss from a sulfide liquid. Note that the legend for the plot of Rh vs. Cu differs from that for the other plots and is shown separately

The data indicate that, as suggested above, on progressing from Taymyrsky in the east to the Cu-rich zone at the western end of the Kharaelakh ore lens, there is a progressive increase in degree of fractionation. Most samples from Taymyrsky exhibit 30-50 % fractionation, those from hole KZ-868 50-80% and many of those from the Cu-rich zone show greater than 80%. Some samples, in particular those from the Cu-rich zone, lie above the model liquid line. These are interpreted as mixtures of less fractionated, mss-bearing ore with highly fractionated liquid. Some samples from hole KZ-868 are of particular interest; these lie on the line of

100% mss at about 80% fractionation. They form a cohesive grouping, coming from the interval 892-906 m in hole KZ-868. Two interpretations can be made of their chemical compositions, one that they represent very fractionated, very "dry" mineralization, as indicated in Fig. 4.41a, or that they have crystallized from an early pulse of sulfide liquid which had formed at a lower "N" value than that responsible for the remainder of the ore. The concept of variable "N" is discussed below.

Fig. 4.41b shows Au plotted against Cu for massive sulfide intersections from the Kharaelakh ore body, together with model curves drawn using the coefficients given above. A choice of a starting liquid composition with 400 ppb Au, 5 wt% Cu generates a liquid evolution line that provides an approximation to the compositional spread of the massive Cu ore[13]. The evolution line for pure mss lies extremely close to the x-axis, since Au is assumed to be essentially incompatible in mss. Modeling indicates that many samples contain 10% or less of the liquid component. Samples collected from holes that occur closer to the center of the Cu-rich zone have higher Au contents for a given Cu content, and lie closer to the modeled liquid evolution line, than those farther away (Taymyrsky and hole KZ-868). Plots of Pt and Pd versus Cu (Fig. 4.41c–d) do not show the same offset between the trend of many of the samples of massive sulfide and that calculated for the liquid. Naldrett et al (1994a) showed that this is to be expected as a result of the similarity between the partition coefficient of Pt, Pd and Cu.

### *Noril'sk Ore Junction*

Data from the Noril'sk ore junction are much more limited than those from Talnakh. Samples from the base of the Noril'sk-1 intrusion up to the top of the picritic gabbrodolerite were collected from hole P-3010 from the Zapolyarny mine (13 samples), from the Medvezhy (Bear's) Brook open pit (3 samples), and from surface traverses across the Noril'sk-2 (7 samples) and Mt Chernaya (8 samples) intrusions. Samples of massive ore are too few in number to have statistical significance and have not been included in the analysis presented here. A more comprehensive data set for massive ores from the Noril'sk-1 intrusion is given by Zientek et al (1994).

---

[13] It might be thought that, given the scatter of the data, a choice of 400 ppb Au as a starting composition is fairly arbitrary. However, given the partition coefficients that we have chosen on the basis of experimental data, if, for example, 450 ppb Au had been chosen, the evolution line would rise much more steeply than the spread of the Cu-rich data and similarly, if 350 ppb had been chosen, the line would rise less steeply than the majority of the data.

Average compositions of disseminated ores, all from picritic gabbrodolerite are given in Table 4.7. These samples, which are from all of the 4 localities in the 3 intrusions mentioned above, have very similar compositions and have been treated as a single population (Noril'sk ore junction picritic gabbrodolerite) in the analysis included in the following discussion. Sulfides of these ores differ greatly from disseminated ores of the Talnakh ore junction in having much higher contents of all PGE (see below).

### *Typical metal contents in bulk ore compositions*

In Fig. 4.42, average values of the analytical data have been plotted through zones of different styles of mineralisation at both the Talnakh and Noril'sk ore junctions. Similar information augmented by data for Rh, Ru, Ir, Os, and Au is present also in Table 4.6. The resulting values are a function of both the amount of sulfide within the ore zones, and the metal contents of the sulfides. It should also be recognized that the averages are for single, widely spaced intersections, and thus do not constitute realistic grades over these intervals, but only provide an indication of the magnitude of the grades to be expected.

It is seen that despite the differences in the compositions of their constituent sulfides, the disseminated ores throughout the Kharaelakh and Talnakh intrusions, except for those of the Mayak mine, have similar metal contents, containing 2.3–3.3 g/t Pd, 0.5–1.1 g/t Pt, 0.4–0.7 wt% Ni, 0.9–1.2 wt% Cu. Those from the Mayak mine are notably richer in PGE (5.9 g/t Pd and 2.3 g/t Pt). Massive ores in all studied boreholes (except KZ-1162) contain 4.6–5.2 wt% Ni, 2.9–4.8 wt% Cu, 5.9–12.2 g/t Pd and 1.4–2.8 g/t Pt. Concentrations of metals in both disseminated and massive ores of the Talnakh intrusion, in general, increase from north to south. Massive ore in KZ-1162 is very much richer in Cu, Pt and Pd than other zones of massive ore, presumably because this hole intersected a zone that was enriched in fractionated sulfide liquid (see below).

The Cu-rich massive ores of the Oktyabrsky mine display very high Cu (21.6 wt% and low Ni (2.8 wt%) contents; they are very rich in Pd (43.5 g/t) and Pt (9 g/t).

Disseminated and veinlet-disseminated ores in country rocks (so-called "Cu-ores") studied in borehole KZ-1812 are relatively rich in S (8.6 wt%) but are low in Ni and Cu (both about 1.3 wt%), and relatively low in Pd (3 g/t) and Pt (0.9 g/t) (Table 4.6). In contrast, the "Cu-ores" of the Komsomolsky mine, with around 7.5 wt% S and 1 wt% Ni, are much richer in Cu (4 wt%) and exceptionally rich in Pd (51 g/t) and Pt (15 g/t). These ores contain the highest PGE contents of all those studied from the Talnakh ore

junction, even higher than the Cu-rich massive ores of the Oktyabrsky mine. When calculated on the basis of metal content in 100% sulfide, the sulfides of the Komsomolsky Cu-ores contain 4.9 wt% Ni, 19 wt% Cu, 238 g/t Pd and 71 g/t Pt.

Samples of the "Upper copper ores" that overly the main body of the Kharaelakh intrusion came from borehole P-3202. The sulfides occur as two zones, one above the other, both characterized by high Cu and Pd and low Ni and Pt. The lower zone (42 m thick) is richer (1.5 wt% Ni, 5.8 wt% Cu, 13.1 g/t Pd, 1.1 g/t Pt) than the upper zone (18 m thick, 0.7 wt% Ni, 5.1 wt% Cu, 9.3 g/t Pd and 1.1 g/t Pt) (see Table 4.6).

Low-sulfide mineralisation was studied in hole KZ-1838 in the NE part of the Kharaelakh intrusion. In comparison with the disseminated ores in picritic and taxitic gabbrodolerites intersected in the nearby hole KZ-1812, the S content is half as much (1.5 in comparison with 3.1 wt%), but the base metal contents are higher (Ni = 0.8 in comparison with 0.5; Cu = 1.1 in comparison with 0.9 wt%) and the PGE much higher (Pd = 6.1 as compared to 2.6; Pt = 2.0 as compared to 0.5 g/t).

Despite the limited data base for the Noril'sk ore junction, it is clear that the ores, although poorer in sulfides in comparison with Talnakh ore junction, contain sulfides of much higher metal tenor. For example, the disseminated ores of the Noril'sk-1 deposit, have on average only half as much sulfide as those at Talnakh (6 wt% as compared 12–15 wt% sulfide) but are richer than majority of Talnakh disseminated ores in their bulk contents of Pd (3.3 as compared to 2.3–3.3 g/t) and, especially Pt (2.0 as compared to 0.6–1.1 g/t).

At present massive ore is not mined separately at Noril'sk-1. It occurs as thin veins (from several cm to 0.5 m in thickness) within zones of disseminated mineralization in picritic and taxitic gabbrodolerite, where it adds considerably to the value of this mineralization. Pyrrhotite-bearing massive ore at the Noril'sk-1, contains an average of 4.6 wt% Cu but is much richer in Pd and Pt than Talnakh massive ore with a similar Cu content (Pd = 24 g/t in comparison with 6–12 g/t at Talnakh; Pt = 9 g/ in comparison with 1.4–2.8 g/t at Talnakh). Czamanske et al. (1992) reported that small Cu-rich veinlets in the disseminated ore of the Bear's Brook pit contain about 25 wt% Cu, 7 wt% Ni, and almost 500 g/t total PGE (Table 4.6, Fig 4.42).

The low-sulfide mineralisation related to the upper taxitic gabbrodolerite of the Noril'sk-1 deposit has been known since the 1950's, but has only attracted attention since the early 1980's (e.g. Ryabov, 1982), and its economic significance has only been appreciated since 1990 (Slyzhenikin et al., 1994; Slyzhenikin, 2000). The sulfur contents of the low-sulfide ores

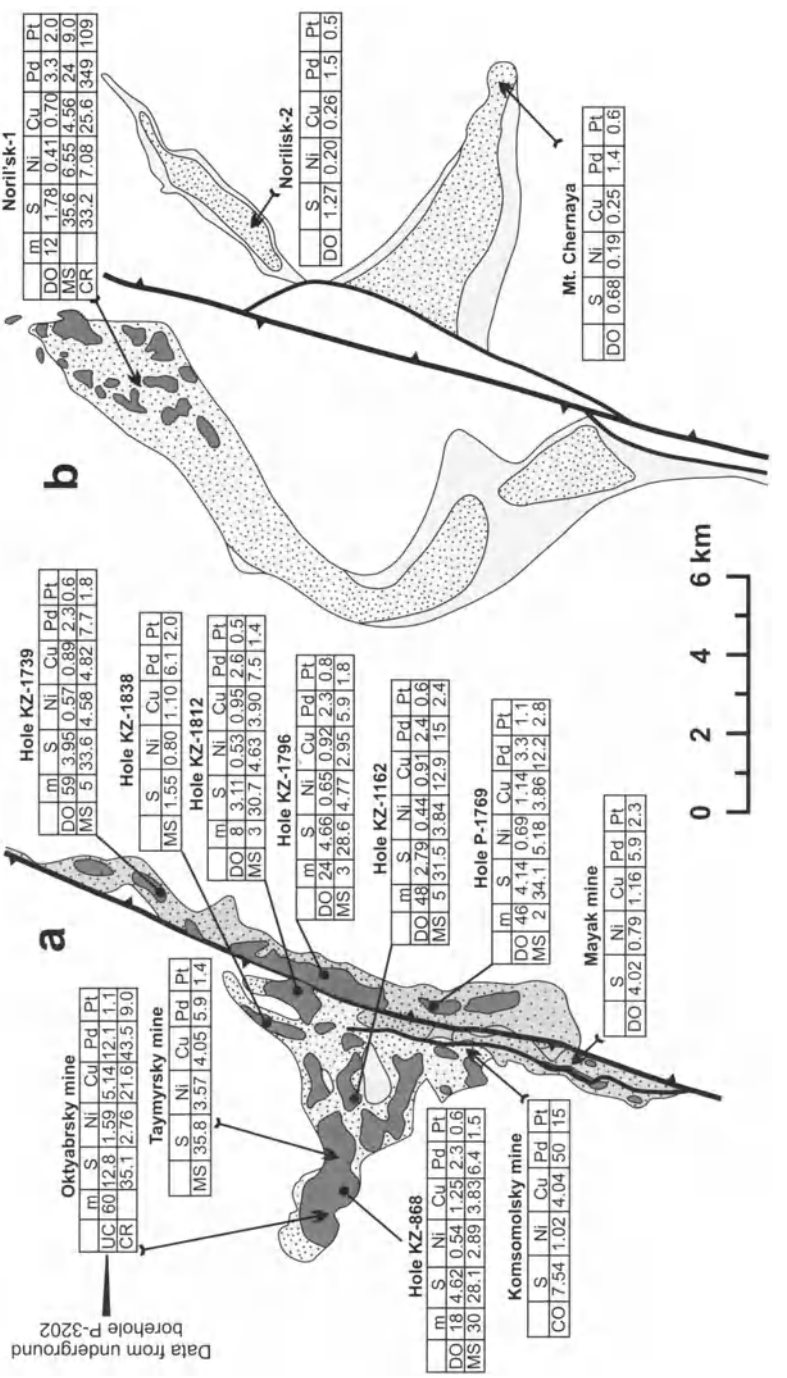
a
b
Data from underground borehole P-3202
Oktyabrsky mine
Taymyrsky mine
Hole KZ-868
Komsomolsky mine
Hole KZ-1739
Hole KZ-1838
Hole KZ-1812
Hole KZ-1796
Hole KZ-1162
Hole P-1769
Mayak mine
Noril'sk-1
Norilisk-2
Mt. Chernaya
0 2 4 6 km

**Fig. 4.42**. Plan view of deposits of the Talnakh (a) and Noril'sk (b) ore junctions where average contents of S, Ni, Cu (wt%) and Pd, Pt (g/t) in different ore types around areas of the deposits are shown. In the Talnakh ore junction the Oktyabrsky deposit (Kharaelakh intrusion) is shown by lighter filling, the Talnakh deposit – by darker filling. Distribution of disseminated ores is shown by gray speckled pattern, massive ores – by dark-gray. For ores, studied from borehole cores thickness (m) is given. Abbreviations for ore types: CO = "Copper ores"; CR = Cu-rich massive ores; DO = Disseminated ores in picritic and taxitic gabbrodolerite; LS = Low-sulfide mineralisation; MS = Massive sulfides; UC = "Upper copper ores". Data for Cu-rich massive ores of the Noril'sk-1 deposit are from Czamanske et al. (1992), Naldrett et al. (1996a) with additions from unpublished materials of the author

do not exceed 1.5–2.0 wt% and the Cu+Ni contents are no more than 1 wt%, but the total PGE content are commonly of the order of tens g/t, reaching 60 g/t (see Fig. 4.16). According Slyzhenikin (2000) the bulk of the PGE occur as discrete mineral phases and only 1% of the Pt and 5% of the Pd are present in solid solution in sulfides. About 30 PGM are known from this ore type; $Pt_2Fe$, atokite, vysotskite, and sperrylite are predominant. In a plot ΣPGE vs. Cu+Ni (Fig. 4.43) low-sulfide ores form their own trend; their compositions do not overlap compositions of ores disseminated in the lower units of the ore-bearing intrusions.

The present author has only studied ores that are disseminated in picritic gabbrodolerite for the Noril'sk-2 and Mt Chernaya deposits. The samples that were available contain about half as much sulfide as the disseminated ore in the Noril'sk-1 deposit and correspondingly less metals (Table 4.6, Fig. 4.42). However, according to the more comprehensive data set of Slyzhenikin (2000), the ores of the Mt Chernaya deposit are close in their bulk composition to those of Noril'sk-1 (Fig. 4.43). Low-sulfide mineralization is also present in the Mt Chernaya deposit, but so far it has not been studied in detail (Slyzhenikin, 2000). As mentioned above, massive sulfides have not been observed in the Noril'sk-2 and Mt Chernaya deposits.

Disseminated and low-sulfide mineralization is present at the Imangda ore junction, but it has not been studied by this author. According to Slyzhenikin (2000), the Imangda disseminated mineralization is close to that of the Noril'sk area in the ratio ΣPGE/(Cu+Ni). Bulk metal contents are similar to those at Noril'sk-2 and Mt Zub-Marksheyder, but are significantly less than at Noril'sk-1 and Mt Chernaya (Fig. 4.43).

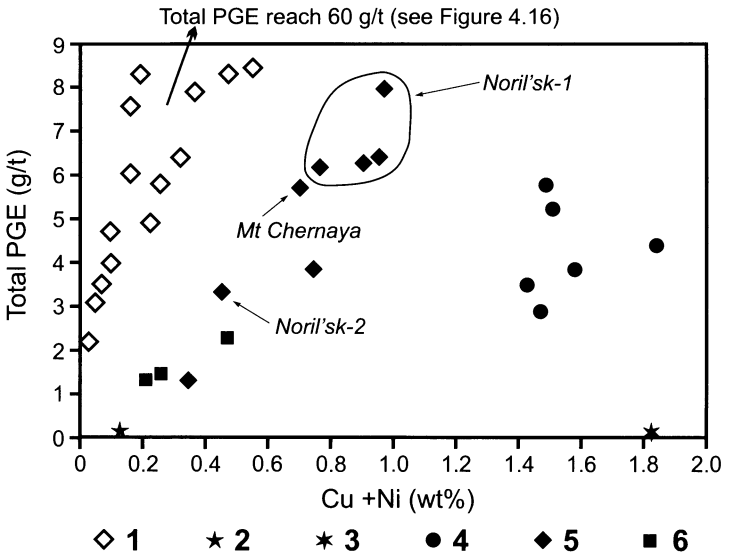


**Fig. 4.43.** Plot of Total PGE vs. Cu+Ni showing compositions of low-sulfide ores of the Noril'sk-1 deposit (single analyses of individual and channel samples) compared with ores disseminated in picritic and lower taxitic gabbrodolerites of different intrusions (average compositions for representative sample selections). 1 = Low-sulfide ores of northern part of the Noril'sk-1 deposit; 2 = Mineralization of the Lower Talnakh intrusion; 3 = Mineralization of the Lower Noril'sk intrusion; 4 = Ores of the Talnakh ore junction (data for the Oktyabrsky, Taymyrsky, Skalisty, and Mayak mines, for Oktyabrsky and Talnakh sections of the Komsomolsky mine); 5 = Ores of the Noril'sk ore junction (data for the Medvezhy (Bear's) Brook, Zapolyarny, Coal Creek mines and southern part of the Noril'sk-1 deposit; Noril'sk-2, Mt Chernaya, Mt Zub-Marksheyder deposits and Verkhneambarnaya ore occurrence); 6 = Ores of the Imangda ore junction (data for northern and southern parts of the Imangda deposit and Nakokhoz ore occurrence)

## *Discussion*

**Variation in Disseminated Ore and the Concept of Variable "N".** Fig. 4.44 shows plots of Rh, Pd, Pt and Au versus Cu for the composition of sulfides in disseminated ore in picritic and taxitic gabbrodolerites for both the Talnakh and Noril'sk ore junctions. In constructing these figures, samples of ore that have been affected by the Cu-, Pt-, Pd- and Au-enrichment discussed above have been excluded. It is seen in Fig. 4.44a that the trend is one of increasing Rh with Cu, which is perpendicular to that expected to result from the fractional crystallization of a sulfide liquid (compare with Fig. 4.41a). The trends for Pd, Pt and Au (Fig. 4.44b–d) also do not correspond with those expected from fractional crystallization.

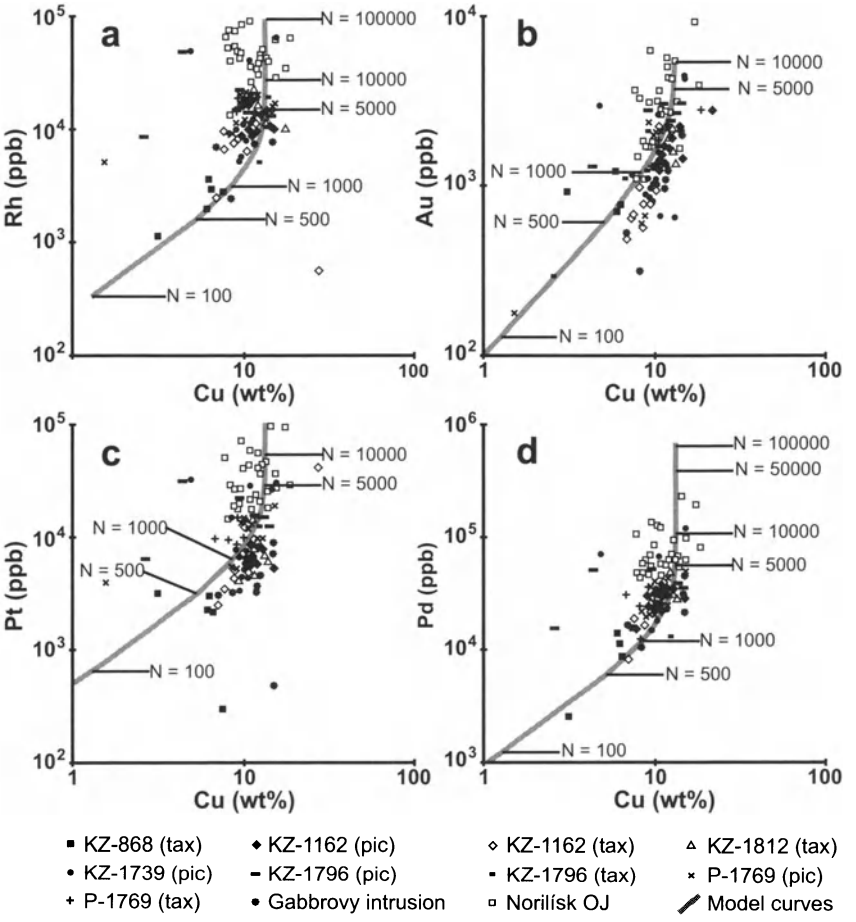


**Fig. 4.44** Variation of (a) Rh, (b) Pt, (c) Pd and (d) Au with Cu in disseminated ore of picritic (pic) and taxitic (tax) gabbrodolerite from the western part of the Kharaelakh intrusion (hole KZ-868), central and eastern parts of the Kharaelakh intrusion (holes KZ-1162 and KZ-1812), Talnakh intrusion (holes KZ-11739, KZ-1796 and P-1769), from taxitic-like olivine gabbrodolerite of the Gabbrovy intrusion and picritic gabbrodolerite of the Noril'sk ore junction (OJ), together with model curves showing the results of "N" modeling. Samples of ores that had been enriched subsequently are excluded. Note that sulfides which have equilibrated with infinite amounts of magma have the composition corresponding closely to that labeled N = 100,000

In seeking an explanation for these trends, it should be recalled that Naldrett et al. (1995) have proposed that the mineralized intrusions at Noril'sk are feeders for the overlying volcanic rocks, some of which have lost over

lost over 90% of their PGE and up to 75% of their Ni and Cu. As outlined above (Fig, 4.6 and 4.9), the decrease in chalcophile element concentrations starts abruptly at a specific level in the lavas (the base of the Lower Nadezhdinsky) and is followed initially by a decrease and then by a progressive upward increase from flow to flow which flattens out at plateau values in the Upper Morongovsky and Mokulaevsky lavas. As demonstrated above, the Upper Morongovsky – Mokulaevsky lavas are comagmatic with the last magma to flow through the Talnakh intrusions. It is suggested (Fig. 4.27) that the Lower Nadezhdinsky magma is the Tuklonsky magma that became contaminated in a holding chamber at mid-crustal levels. It started to fractionate, assimilate walls rock and as a result of this silicification (c.f. Li and Naldrett's, 1994 study of Sudbury) became saturated in sulfide. Sulfides thus segregated from it first at this stage, accounting for some of the chalcophile element depletion; the magma then rose to intrude and ingest Devonian evaporites and coal measures, where sulfides again segregated, causing further chalcophile element depletion. Naldrett et al. (1995) proposed that, following this, successive pulses of magma, first of Nadezhdinsky (***Nd)*** and then of Upper Morongovsky-Mokulaevsky (***$Mr_2$-Mk***) magma, passed through the same chamber. The Lower Talnakh-type intrusions served as exit conduits to this chamber up to about ***$Nd_3$*** time, and after which, magma exited through Noril'sk-type intrusions. Sulfides that first formed at the ***Nd*** stage came into contact with and were upgraded by later magma pulses (a very similar process is believed to have operated at Voisey's Bay, see Chapter 6). As the sulfides in the chamber became progressively more chalcophile-rich with time, successive magma influxes lost progressively less metals to them, which accounts for the progressive upward increase in chalcophile elements in successively higher lava flows at the top of the sequence.

As discussed in Chapter 2, the compositional change in sulfides undergoing enrichment in this way can be modeled using the zone refining equation:

$$Y = X_i * \{D-[(D-1)*e^{-(1/D.N)}]\} \quad \text{.....(4.1)}$$

where Y is the metal concentration in the sulfide, $X_i$ is the initial concentration of the metal in the silicate magma, D is the partition coefficient and N is the ratio of the amount of magma passing through the system and reacting with the sulfide to the amount of sulfide in the system.

In their paper discussed above, Brugmann et al. (1993) used equation (4.1) to model the compositional change of a layer of sulfides, settling through and interacting with magma in a chamber, and scavenging chalcophile metals from the magma as they settled. The composition of the sul-

fides then becomes a function of the initial composition of the magma, the sulfide-silicate partition coefficient for each metal in question, and the function "N". Naldrett et al. (1995) pointed out that the situation envisaged by Brugmann et al. is the same as that of pulses of magma moving along a magma conduit in which trapped sulfides were stirred up by each pulse. They applied this concept to explain the variation in the composition of ores of the Noril'sk region.

The question may be asked as to why the parameter "N" is used in this analysis, rather than the long established (c.f. Campbell and Naldrett, 1979) parameter "R". R refers to bulk equilibration between a mass of silicate magma and sulfide liquid, in which all of the magma is in equilibrium with the final composition of the sulfide liquid (see Chapter 10). This situation is not that which is thought to have occurred in the system of high level magma chamber and conduits at Noril'sk. The progressive increase in chalcophile elements in the lavas overlying the mineralized intrusions at Noril'sk indicates that the magma exiting the conduits became progressively less depleted in chalcophile elements. Thus, the sulfides trapped within the system were continuously exposed to fresh, undepleted magma. They reacted with this, extracting chalcophile metals from it. As the sulfides themselves became richer in chalcophile metals, they extracted progressively less of these metals from the magma passing through the system, so that, on exiting the environment of the sulfides, this magma became progressively richer in chalcophile metals with time.

**Modeling of the sulfide compositions.** Use of equation (4.1) requires a knowledge of the initial content of chalcophile metals in the magma equilibrating with the sulfides, and also the appropriate sulfide liquid – silicate magma partition coefficients. Since Naldrett et al. (1995) conclude that the last magma to flow through the ore-bearing intrusions was the Late Morongovsky – Mokulaevsky magma type, in most cases the average concentration of Cu, PGE and Au in the Mokulaevsky (Table 4.2) have been used as the initial values of PGE in the magma. This is not strictly correct, because Naldrett et al. (1995) proposed that the sulfides first segregated from Early Nadezhdinsky magma, and that it was only subsequent to this that Late Morongovsky – Mokulaevsky magma entered the plumbing system, mixed with the Nadezhdinsky magma resident there, and flushed part of it out. The assumption that has been made is that in reacting with and enriching the sulfides, the Late Morongovsky – Mokulaevsky magma swamped out any signature remaining from the Nadezhdinsky stage, as appears to have been the case with Osmium isotopes.

Recent experimental data on the partitioning of PGE between sulfide and silicate melts are discussed in Chapter 2. The different sets of

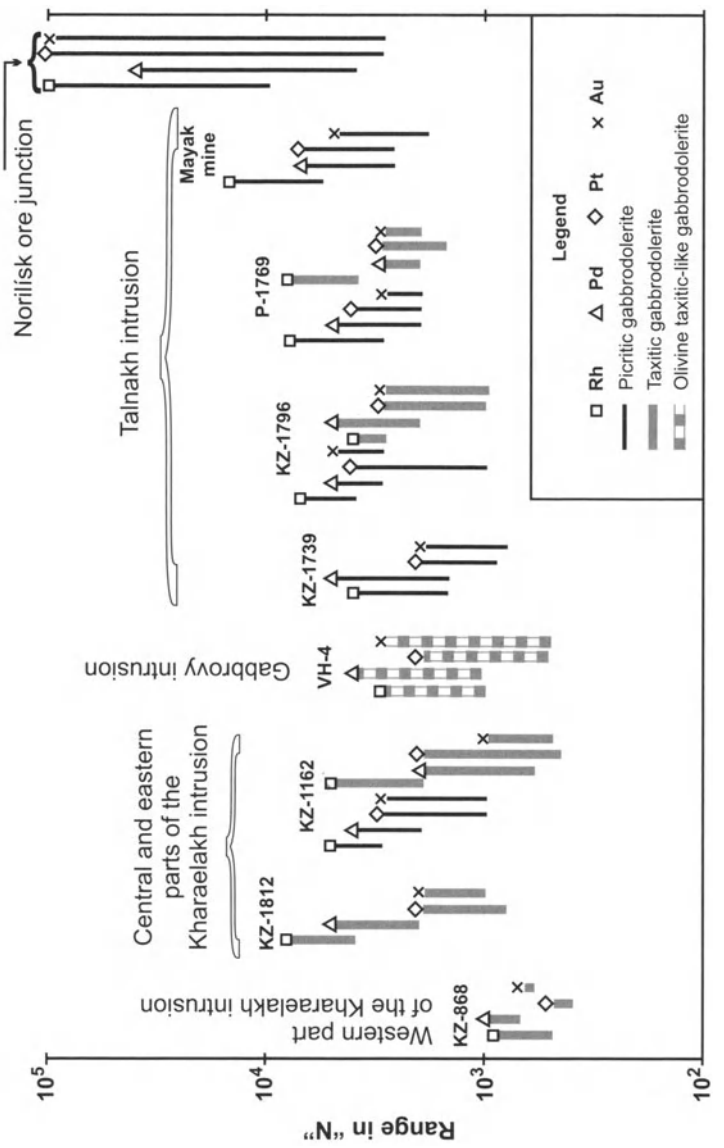


**Fig. 4.45.** Comparison of ranges of "N" obtained with Rh, Pd, Pt and Au in picritic, taxitic and olivine taxitic-like gabbrodolerites from different ore-bearing intrusions of the Noril'sk region. Ore compositions are recalculated for 100% sulfide

experimental determinations vary for some elements by several orders of magnitude. However, a value of $3x10^4$ for Rh is consistent with the results of Bezmen et al. (1994) and this value has been used. Bezmen et al.'s (1994) value of $5.5x10^4$ for Pd is close to the value of $3.4x10^4$ given by Peach et al. (1994) and this has also been used this. In addition, $4x10^3$ is fairly close to the results of most workers for Au, and this has been used. Lastly, $3x10^4$ approximates some of the data for Pt (although other data are

significantly lower) and this value has been adopted. Experimental data for Ir (not shown) are too variable and modeling of this element has not been attempted. A D value for Cu of 1000, which is Peach et al.'s (1994) preferred value, has been chosen; this was also adopted by Brugmann et al. (1993).

Results of the modeling of sulfide compositions are shown by the curves superimposed on the plots of Rh, Pd, Pt and Au against Cu in Fig. 4.44. Values of N corresponding to given positions on the curves are also shown. In order to bring the model curves into correspondence with the data it was necessary to use a value of 12 ppb for the Pd content of the initial magma instead of the average value for the Mokulaevsky of 6.2, and 1.3 ppb for Au instead of the ***Mk*** average of 1.75 ppb (These are data from Brugmann et al. (1993) for 9 samples; it should be noted that Wooden et al. (1993), studied 13 samples of Mokulaevsky lava which averaged content 11.0 ppb Pd; Au was not studied by them[14]).

Modeling of this kind should not only reproduce the trends of the data in Fig. 4.44 but should also give similar values of N for each element pair. The range of N that includes the majority of samples of each ore-type in each drill hole or sample location has been estimated from the plots of Fig. 4.44; only those samples that clearly lie outside the trend of the data have been omitted. The estimates are compared in Fig. 4.45. Rh and Pd when plotted against Cu tend to give higher values for "N" than Pt and Au. This is attributed both to imperfections in the modeling (incorrect values of D and element concentrations in the silicate magma) and failure to achieve equilibrium. Nevertheless, bearing in mind that errors caused by uncertainties in the partition coefficients and initial magma composition that were selected apply to all data, certain generalizations are apparent:

1. "N" for sulfides in the taxitic gabbrodolerite of the western part of the Kharaelakh intrusion is much lower (of the order of 500-1000) than that for taxitic gabbrodolerite from the eastern part of the same intrusion (500-8000). This is consistent with the comparison made in Fig. 4.40b.
2. "N" for sulfides in picritic gabbrodolerite from the Talnakh intrusion decreases from south to north [from Mayak to hole KZ-1739 (see Fig. 4.45)]. This can be interpreted in two ways: (i) as due to a decreasing

[14] It might be asked why we did not use slightly different partition coefficients instead of selecting different values for the Pd and Au contents of ***Mk*** magma. The answer is that the partition coefficients have relatively little effect on the position of the curves at low values of N (which was where the discrepancies arose). The only variable which has an effect is the assumed initial composition of the magma.

value of "N" in this direction, and (ii) as the result the magma becoming progressively depleted in PGE+Au in this direction (i.e. supporting the suggestion that the flow direction of the magma was from south to north as proposed by Naldrett et al. 1995).

3. Sulfides in olivine taxitic-like gabbrodolerite in the Gabbrovy intrusion [one of the peripheral sills (4 km to the north of hole KZ-1739) which is close to the northern extremity of the of the Talnakh intrusion] have "N" values which are similar to, but slightly lower than those in the picritic gabbrodolerite of hole KZ-1739. This is consistent with these sulfides having been swept out by magma flowing through from the Main Body into the peripheral sill, and subsequently having interacted with slightly less magma than is the case with the sulfides retained within the Main Body of the intrusion.
4. "N" for picritic gabbrodolerite from hole KZ-1162 in the central part of the Kharaelakh intrusion is similar to that from hole KZ-1739 in the Talnakh intrusion, again as to be expected from Fig. 4.40.
5. Where data for sulfides from picritic and taxitic gabbrodolerites are available from the same hole, "N" for the taxitic gabbrodolerite is generally less than for the picritic. It appears that, as time progressed, sulfides settled into the taxitic gabbrodolerite from the picritic gabbrodolerite, and that these became isolated from the main stream of magma at an earlier stage than those sulfides that are present in the overlying picritic gabbrodolerite. The downward decrease in sulfide tenor that is commonly observed across horizons of taxitic gabbrodolerite is also explicable in this way.
6. Picritic gabbrodolerite from bodies in the Noril'sk ore junction contain sulfides with very much higher "N" values (10,000–100,000) than those characterizing sulfides in the Talnakh intrusions, indicating that the ratio of magma to sulfide in the dynamic system at this location was several times greater than that at Talnakh.
7. It is possibly not coincidental that the part of the mineralization of the Noril'sk region that has the most sulfide (the western part of the Kharaelakh intrusion) has the lowest "N" value, and that the part with the least sulfide (the Noril'sk ore junction) has the highest "N" value.

### *Conclusions with regard to Ores*

1. Massive ore of the Kharaelakh ore body is fractionated laterally over a distance of more than of 2 km, with Cu, Pt, Pd and Au increasing progressively toward the Cu-rich zone at the Oktyabrsky No 1 mine.
2. A Cu-, Pt-, Pd- and Au-rich sulfide liquid has left massive ore as this crystallized, enriching sulfides in both adjacent intrusive and country

rock, causing these to have a low Rh/Au ratio, and leaving the massive ore with a high Rh/Au ratio.

3. Once this enrichment from massive ore is corrected for, the sulfides of disseminated ore from the western part of the Kharaelakh intrusion are found to be distinctly poorer in chalcophile elements than those associated with the central and eastern part of the same intrusion, or with the Talnakh intrusion.
4. The trends of Rh, Pt, Pd and Au versus Cu can be modeled closely using the concept of variable "N" along with sulfide-silicate partition coefficients extant in the literature, and the chalcophile metal concentrations equal to or only slightly different to those of Upper Morongovsky – Mokulaevsky magma. "N" is the ratio of the mass of magma exchanging chalcophile metals with sulfide to the mass of sulfide. The parameter is given by the "zone refining" equation, which models silicate magma-sulfide liquid interaction assuming that the silicate magma is constantly being removed from contact with the sulfide and being replaced by fresh magma.
5. Using this concept, differences between the composition of the sulfides of the disseminated ore in the Noril'sk, Talnakh, and central-eastern and western parts of the Kharaelakh intrusions are explicable if they had reacted with progressively lower proportions of magma flowing through the plumbing system (i.e. are the result of progressively lower values of "N").
6. Sulfides in the taxitic gabbrodolerite generally have lower metal contents than those in the picritic gabbrodolerite, which suggests that they interacted with a lower proportion of magma, perhaps due to their lower and thus more isolated (from the flowing magma) position in the intrusive body.
7. The marked decrease in metal contents from south to north along the Talnakh intrusion is difficult to explain if the flow of magma was from north to south, but is explicable if it was from south to north, either as a result of magma escaping along lateral sills as it flowed, so that the effective value of "N" was decreasing in this direction, or as a result of the magma becoming progressively depleted in chalcophile elements as it flowed northward as a result of interacting with sulfide. This trend extends into the Gabbrovy peripheral sill, supporting the interpretation that this is part of the flow system. The second of the two alternative explanations is the one preferred by this author.

### 4.1.5 Summary of the model for the Noril'sk Ore Camp

At this stage it is perhaps helpful to summarize the key points of the model proposed above for the Noril'sk ores.

1. The geological setting is that of thick deposits of $CaSO_4$ overlain by coal measures (see Fig. 4.4), i.e. a source of sulfur (oxidized) and a reductant. Evaporites by themselves are probably not a suitable source of sulfur, since mafic magmas have a very limited ability to absorb large amounts of oxygen. This author has seen inclusions of anhydrite within gabbrodolerite at the Taymyrsky mine with no evidence of assimilation, or sulfides developing in the igneous host rock in the vicinity of the inclusions.
2. The flood basalts include horizons with relatively primitive compositions (MgNo ~0.55, some of the flows are picritic). This means that much of the magma was relatively hot, with the potential to erode and assimilate country rocks. Thermal erosion explains why the ore-bearing intrusions take the place of the country rocks, cutting across contacts between units, rather than intruding along the contacts and forcing the units apart.
3. The taxitic gabbrodolerite is evidence of the partial assimilation of country rocks by some of the intruding magma. This rock type only occurs within the type of intrusion that also hosts the mineralization.
4. Much of the magma flow during the interval from the Early Nadezhdinsky to the Late Morongovsky appears to have been channelised in parts of the intrusions referred to as the Main Bodies. The Main Bodies themselves resemble "arteries", i.e. principal conduits for magma flow, within the much more widespread peripheral sills. They have developed as the magma feeding the sills became concentrated along certain zones, and the concentration of this flow resulted in thermal erosion enlarging the channel ways by cutting into the strata adjacent to these zones.
5. It is very likely that much of the magma feeding the lavas from the Early to Late Nadezhdinsky or Early Morongovsky flowed through Lower Talnakh-type intrusions and that later pulses of magma flowed through the Noril'sk-type intrusions. Both types of intrusion exhibit thickened zones which indicates that the magma flow, and related thermal erosion was channelized. The result is that any sulfides that had developed within the magma would have flowed through these structures and would have become concentrated in hydrodynamic traps within them.
6. A large thickness (500 m) of volcanic lava has suffered chalcophile depletion. The Ni, Cu and PGE removed from this portion of the volcanic

stratigraphy, which has a volume of at least 200x100x0.5 km, is enough to account for more than 200 times the amount of these metals that is present in the Noril'sk-Talnakh ore.

7. Mineralization is found throughout the Noril'sk region from Khantayka lake in the south to the southern boundary of the Yenisey-Khatanga trough in the north, and from the Western Siberian lowlands in the west to Arylakh and Imangda in the east (see Fig. 4.28). However, the best ore is found in the vicinity of the Kayerkan-Pyasino uplift, in intrusions that originally lay beneath the deepest part of the initial volcanic basin. If uplift had not brought this "keel" of the basin to surface, the mineralisation would still be buried by 3.5 km of basalt. It would seem that, in general, the intrusions that underlie the centers of volcanic basins are more prospective than those that are peripheral to the basins, perhaps because more magma has flowed through them.
8. The Main Bodies have unusually well-developed metamorphic aureoles. This is probably a pointer to intrusions through which large masses of magma have flowed.

Noril'sk provides a model for exploration in other areas, but, like so many other "Giant" ore deposits, the size of the deposits depends on a particularly fortuitous combination of factors. One or two of these factors in another area would not be sufficient to guarantee the presence of similar mineralization. It is the combination of many of the above factors that is necessary.

## 4.2 Mineralization of the Lake Superior Region (North America)

Major rifting affected central North America in the Neoproterozoic (1.1Ga) with the formation of a structure known as the Mid-continent Gravity High that is the result of mafic volcanic and intrusive activity associated with the rifting. The Lake Superior region lies at what is believed to be a triple junction, where the mid- continent structure turns from a northeast to a southwest trend. The structure is marked by a series of aeromagnetic anomalies supporting the interpretation that the gravity feature is due to the presence of mafic igneous rocks. The interpretation has been confirmed by boreholes that have penetrated the Pa- leozoic cover to reach the Precambrian (Fig. 4.46) and have intersected red-bed sandstones and Keweenawan-aged (1.1 Ga) mafic volcanics and intrusions along the trend of the gravity structure.

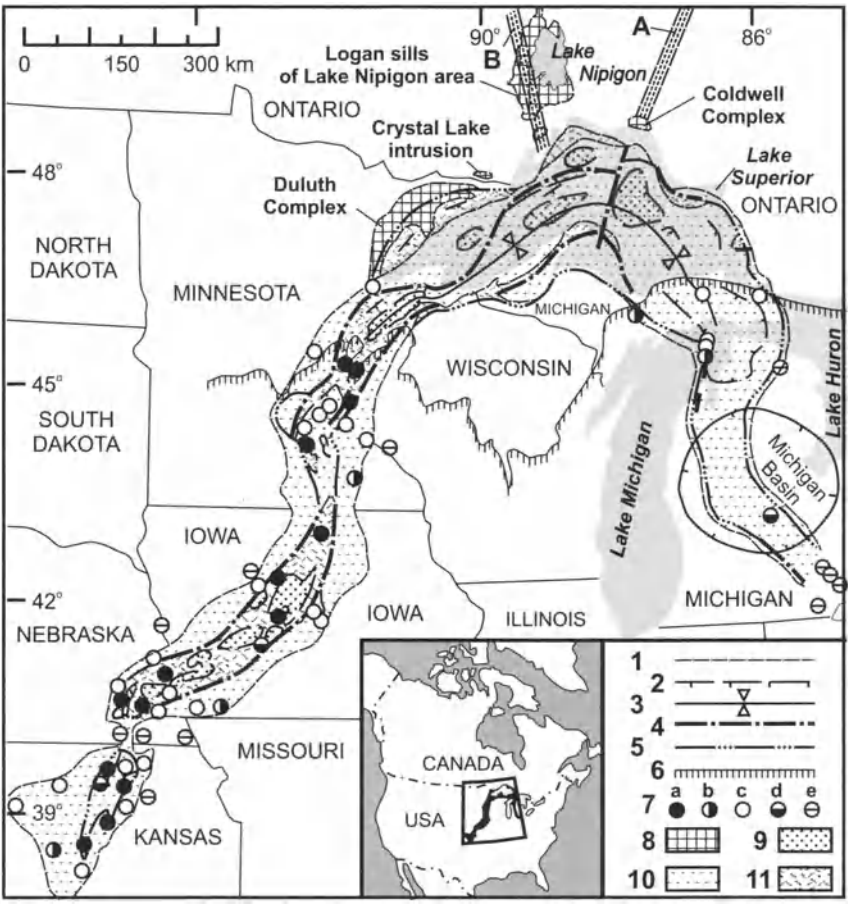


**Fig. 4.46.** Distribution of rock types within the North American Midcontinent rift structure (Drafted using data from Halls, 1978). 1 = geological contact; 2 = structural form lines; 3 = synclinal axes; 4 = faults; 5 = boundary of Keweenawan volcanic rocks; 6 = northern limit of Paleozoic cover; 7 = rocks intersected by bore holes penetrating to Keweenawan rocks, (a) Keweenawan mafic igneous rocks, (b) = Keweenawan red clastic and underlying mafic volcanic rocks, (c) = Keweenawan red clastic rocks, (d) Keweenawan red clastics lying directly on pre-Keweenawan basement, (e) = pre-Keweenawan basement only; 8 = Keweenawan intrusive rocks; 9 = outline of major zones of subsidence; 10 = area overlain by Keweenawan red clastic rocks; 11 = area overlain by Keweenawan volcanic rocks

The geology of the Lake Superior region is shown in Figs. 4.46 and 4.47. Basement rocks include Archean gneisses, greenstones and granites,

overlain to the northwest and south of Lake Superior by iron formation (known as the Gunflint in Canada and the Biwabic in the United States) and a sequence of sulfidic and carbonaceous pelites (the Rove in Ontario, the Virginia in Minnesota and the Michigamme in Northern Michigan) which belong to the Animikie Supergroup (approx. 1.9 Ga). Archean and Animikie rocks are overlain to the north of Lake Superior by the Sibley (approx. 1.3 Ga) sediments. These are thought to have been laid down in a north-south basin, and to be of "playa-lake" type. They are composed of fine-grained dolomites and silicate-carbonate rocks (sometimes with stromatolitic structure) and include one thin horizon of gypsum evaporite. The Sibley is overlain in the Nipigon area by the Osler group volcanics, which dip gently and young to the south into Lake Superior. At the western end of Lake Superior, the North Shore volcanics dip southeast into Lake Superior. South of the lake, the Portage Lake volcanics, that are in part equivalent and in part younger than the Osler, dip to the north; they are overlain by red-bed sandstones of the Bayfield and Oronto groups, that are overlain in turn by the Jacobsville sandstone (Figs. 4.47 and 4.48). As illustrated in Fig. 4.48, Lake Superior itself consists of a central graben, defined by major faults and hinge lines, within which Archean crust has been thinned to less than 1/4 of its previous thickness, and over 26 km of volcanics and sediments have accumulated. It represents, therefore, the focus of the Keweenawan-aged volcanic activity. This activity comprised an enormous outpouring of lava and intrusion of related magma that developed in response to a plume and associated "triple junction" located beneath the present position of Lake Superior. The Oronto, Bayfield and Jacobsville red bed sediments have developed within the rift and cover the Keweenawan lavas in many locatities, particularly south of Lake Superior.

The southwestern and southeastern arms of the Mid-continent structure are taken to represent the two active arms of the triple junction. The location of the third "failed" arm of the triple junction is not certain. It has been suggested that it extends northward from the vicinity of the town of Nipigon to Lake Nipigon. Alternatively, Mitchell and Platt (1994) noted that the Coldwell Complex, dated at 1108 Ma, represents some of the earliest magmatism associated with the Keweenawan event. The combination of tholeiitic and alkalic magmatism within this complex, coupled with the Killalla Lake and Prairie Lake alkalic complexes, 60 km to the north, is similar to magmatism characterizing many failed arms. The Thiel fault is an important structure within the rift. In general, the rift has developed as a series of half grabens, some with the downslip occurring to the north, some with it occurring to the south (Figs. 4.46, 4.47). West of the Thiel fault, the bounding fault of the half graben is on the northern side of the rift,

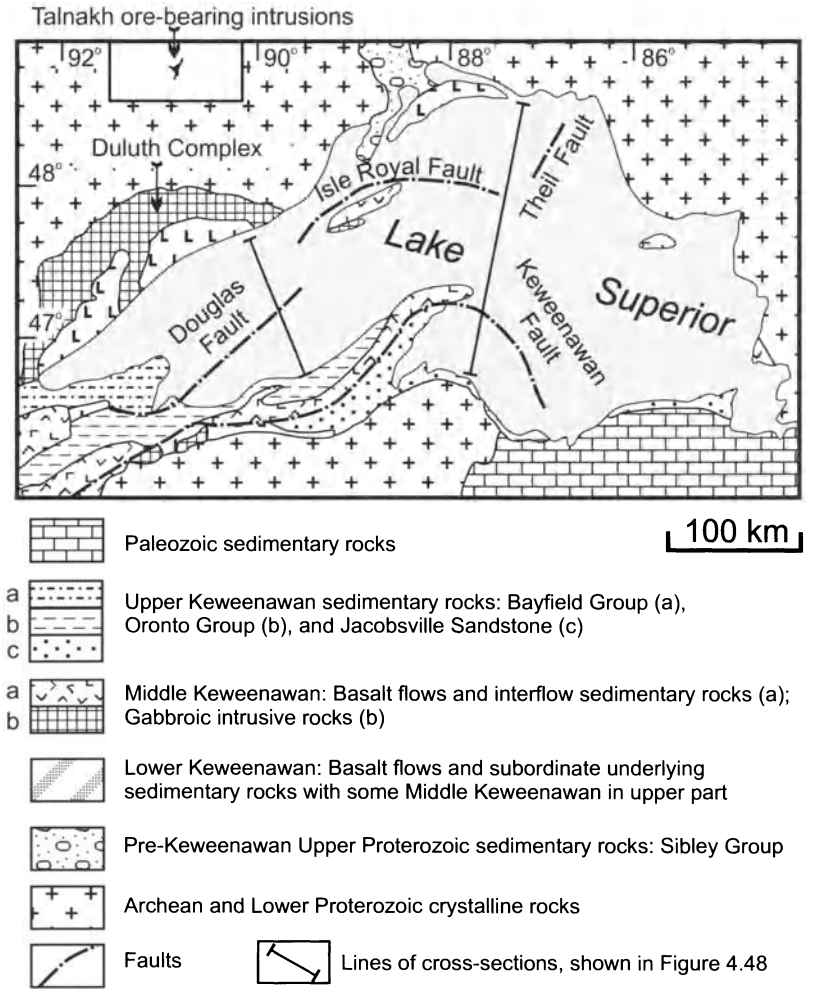


**Fig. 4.47.** Geological map of the Lake Superior region (modified after Naldrett, 1992). Hyperbyssal Keweenawan-aged intrusions are not shown here, their position is given in Figure 4.50. An outline of the ore-bearing intrusions of the Talnakh ore junction (Noril'sk region) are shown at the upper left of the Figure for the purpose of comparison

coincident with the Isle Royal fault. East of the Thiel fault, the bounding fault is to the south (the Keweenawan fault). The Coldwell complex lies directly on the extension of the Thiel fault. Sage (1991) joins the Thiel

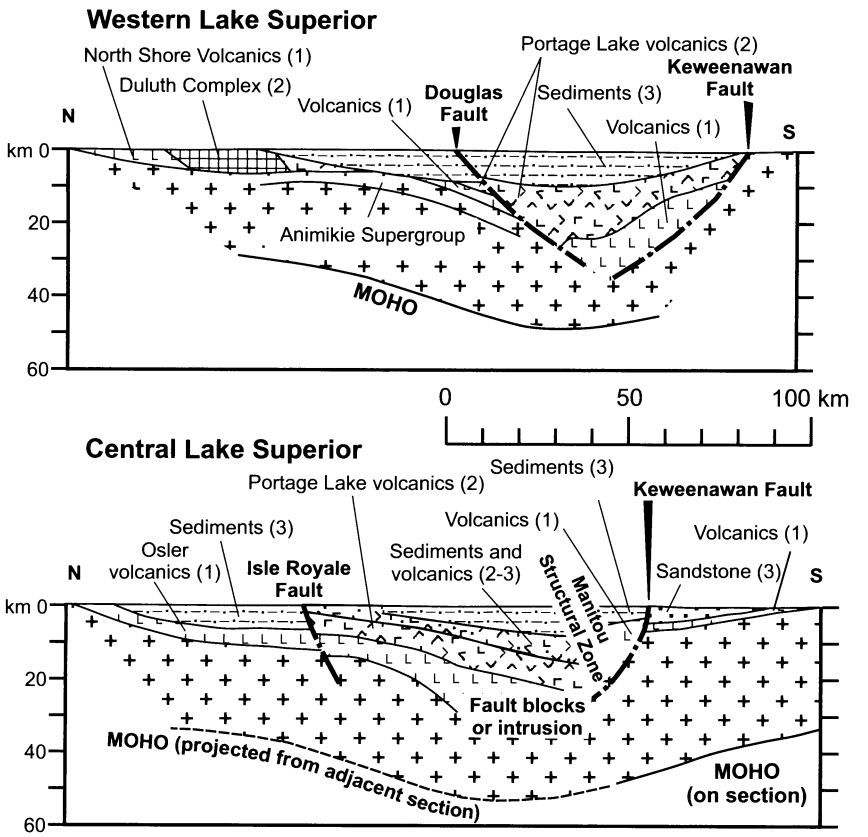


**Fig. 4.48.** Cross-sections through the Lake Superior Rift zone (after Naldrett, 1992). Positions of the sections and Legend are shown in Figure 4.47. 1 = Lower Keweenawan; 2 = Middle Keweenawan; 1 = Upper Keweenawan

fault with the Big Bay-Ashburton Bay fault and extrapolates this 130 km north of the complex, close to the Killala complex to the series of carbonatite dykes and fenites known as the Chipman complex. It is possible that the initial triple junction developed near the Coldwell Complex and then shifted westward, so that both the Coldwell and Nipigon intrusions represent locations of the failed arm.

The oldest Keweenawan magmatism has been dated at 1108Ma (Fig. 4.49). This comprises the Coldwell complex, and a series of sills, the Logan sills, which outcrop in the western half of the Lake Superior (Figs. 4.46, 4.50). A magnetic reversal, from reversely to normally polarized, has been dated at 1102 Ma. The Powder Mill volcanics of Northern Michigan and Wisconsin, a limited portion of the North Shore volcanic group in Minnesota, and the lower part of the Osler volcanic group in Ontario also

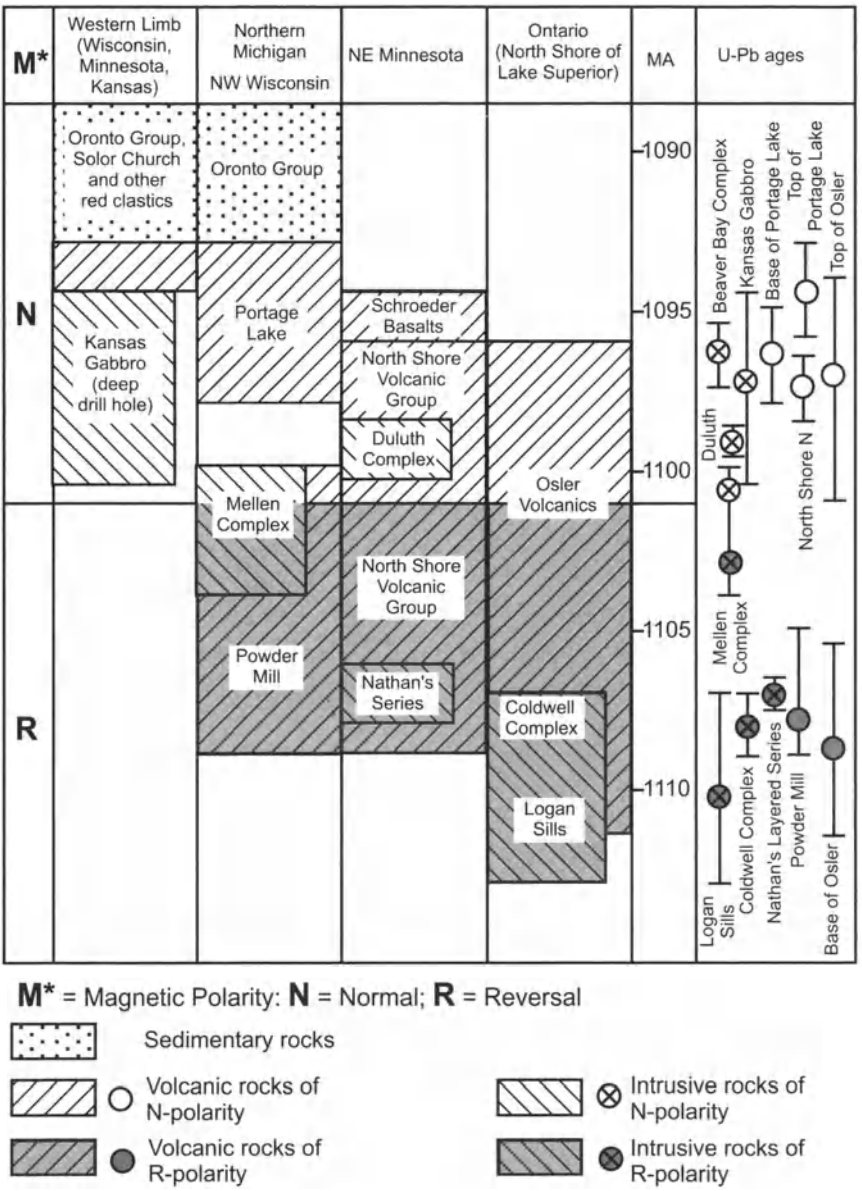


**Fig. 4.49.** Corellation of Keweenawan-age stratigraphy throughout the Lake Superior region, showing rocks that are reversely and normally polarized, along with available U-Pb ages

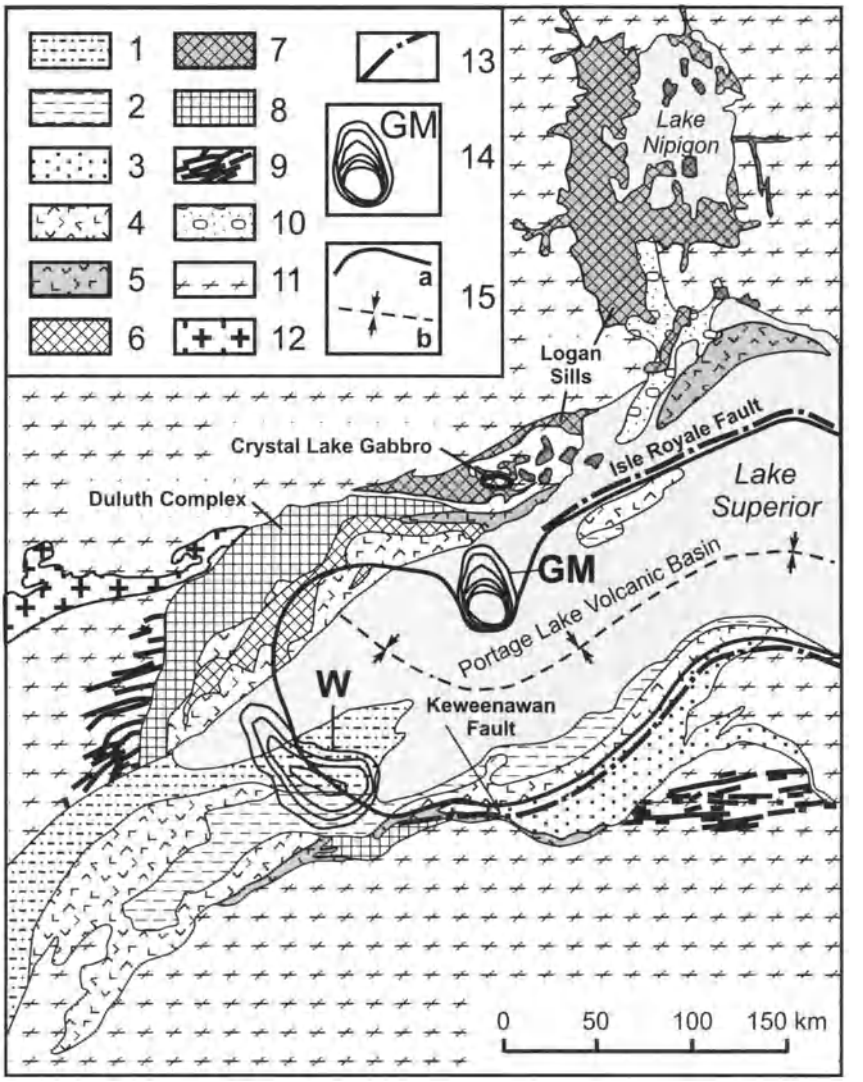


**Fig. 4.50.** Map of the western half of Lake Superior rift showing distribution of volcanic, hyperbyssal and plutonic igneous rocks with respect to major structures within the rift. 1-3 = Sediments (1 = Bayfield Group; 2 = Oronto Group; 3 = Jacobsville Sandstone); 4-5 = Volcanic Rocks (4 = Normal Polarity; 5 = Reversed Polarity); 6-7 = Hypabyssal Rocks (6 = Normal Polarity; 7 = Reversed Polarity); 8 = Plutonic Rocks (all of Normal Polarity; 9 = Diabase Dikes; 10 = Sibley Group; 11 = Archean and Early Proterozoic crystalline rocks, excluding Giants Range Granite; 12 = Archean granitic Batholith Giants Range; 13 = Faults; 14 = Ridges of Basement in the Lake Superior Rift (GM = Grand Marais; W = Whites); 15 = Boundary (a) and axis (b) of the Portage Lake Volcanic Basin

show reverse polarity and ages consistent with this polarity. The Portage Lake volcanic group, the greater part of the North Shore volcanic group and the upper part of the Osler volcanic group show normal polarity, and ages younger that 1102Ma. A series of igneous complexes, of which the Duluth complex is the largest, but also including the Mellen complex, the Echo Lake complex (hidden beneath Bayfield group sediments in Northern Michigan) and the Crystal Lake gabbro in Ontario have normal polarity and ages younger than 1102 Ma. In the western Lake Superior area, the volcanism has been active in localized areas at any one time, areas which appear to be controlled in part by structures in the underlying Archean basement. The principal development of the last volcanic episode within the Lake Superior rift is outlined in Fig. 4.50, where its distribution is related to the Isle Royale and Keweenawan faults, both of which are part of the rifting, and the Grand Marais and White's ridges, which are thought to overlie to Archean granite batholiths. Important, if as yet uneconomic mineralization is present in the Duluth complex and Crystal Lake Gabbro.

### 4.2.2 Duluth Complex

#### *Geology*

The Duluth complex is a large body of troctolite-gabbroic anorthosite, that crops out as an arcuate body that extends about 240 km northeast from Duluth, Minnesota, to the Canadian border. Along its western margin, the complex dips 50° E and is strongly discordant with respect to the Animikie sediments, cutting progressively lower strata on proceeding from south to north (Fig. 4.51). The northwestern margin of the complex dips 20-30° SE, and is relatively conformable with respect to the Animike strata, cutting down gently on proceeding from southwest to notheast until it is in contact with the Archean "Giants Range Granite". Despite poor outcrop, a number of intrusions have been recognized along the western-northwest margin of the complex including the "Western Margin Intrusion", the "Partridge River Intrusion" and the "South Kawishiwi Intrusion" (Grout 1918; Green et al. 1966; Bonnichsen 1970, 1972; Phinney 1970, 1972; Weiblen and Morey 1975, 1980; Martineau 1989; Severson 1988, 1991; and Severson and Hauck 1990). Outcrop is even poorer of the centre of the Complex. Nevertheless, Miller and Chandler (1999), using aeromagnetic data, coupled with information from the few available outcrops and boreholes, have proposed that the area is underlain by a series of troctolitic/gabbroic plutonic intrusions, including the Greenwood Lake, Cloquet Lake and Sonju Lake bodies (Fig. 4.52). Rocks of the North Shore volcanic form a semi-continuous, northeast-striking zone that lies to the southeast of these bod-

ies. These rocks have been intruded by a series of hyperbyssal intrusions known jointly as the Beaver Bay complex (Fig. 4.51).

The most important mineralization is related to the South Kawishiwi Intrusions. This body lies northeast of the Partridge River Intrusion (Fig. 4.51) and is thus in contact with a lower part of the stratigraphic succession (Fig. 4.53). Foose and Weiblen (1986) report that the South Kawishiwi intrusion consists of an upper portion, 1000-1200 m thick, in which troctolite and minor anorthosite are interlayered. In the lower part of the intrusion, repetitive sequences of layers are present in which

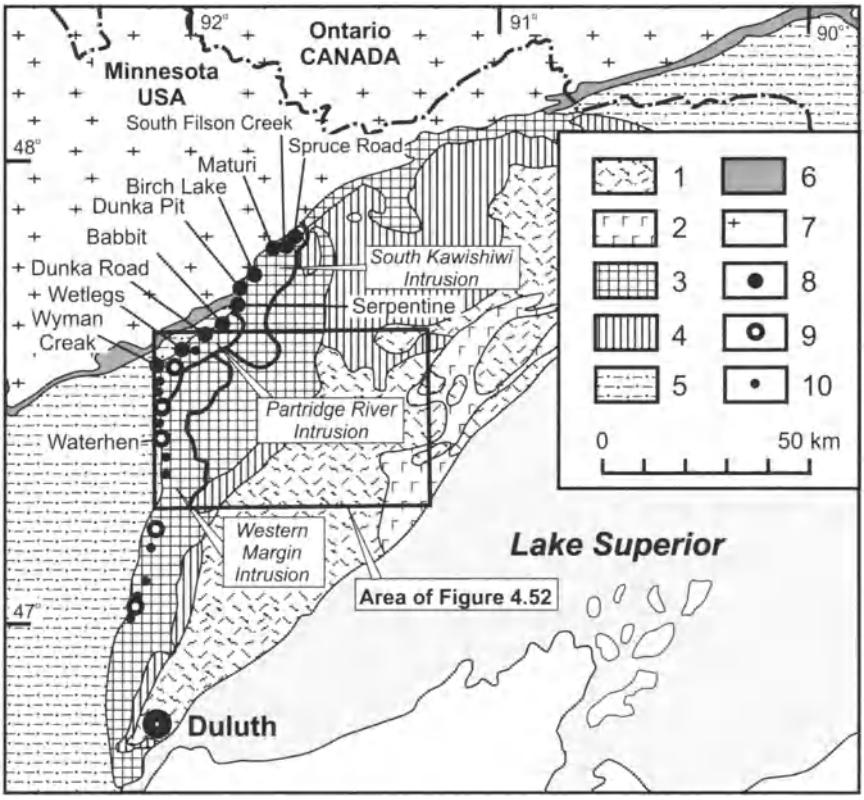


**Fig. 4.51.** Map showing principal mineralized zones of the Duluth complex. 1 = North Shore volcanics, subvolcanic intrusion, and felsic series at roofs of mafic intrusions; 2-4 = Duluth Complex (2 = Beaver Bay Complex; 3 = young troctolitic and gabbroic series; 4 = Older anorthositic and gabbroic series); 5 = Proterozoic sediments; 6 = Proterozoic Iron Formation; 7 = Archean granites and greenstones; 8 = sulfide Cu-Ni deposits; 9 = Oxide-bearing ultramafic intrusions (OUI) with sulfide mineralization; 10 = Exploration areas (April 2000)

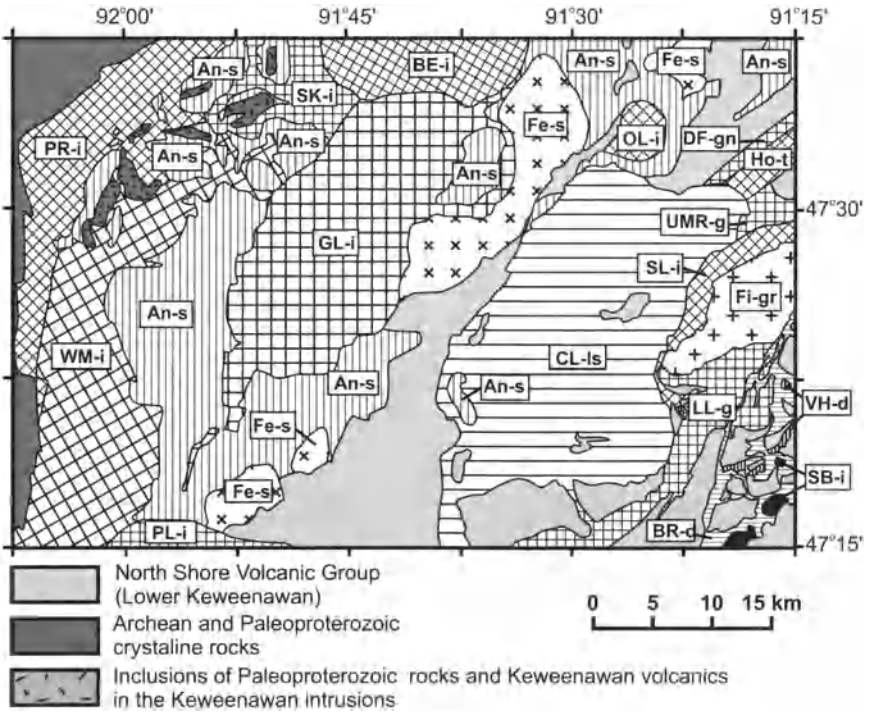


**Fig. 4.52.** Interpreted distribution of intrusions within the central part of the Duluth complex, based on aeromagnetic data and available information from outcrops and boreholes (after Miller and Chandler, 1999). An-s = Anorthositic Series; BE-i = Bold Eagle Intrusion; BR-d= Beaver River Diabase; CL-ls = Cloquet Lake Layered Series; DF-gn = Dam Five Gabbronorite; Fe-s = Felsic Series; Fi-gr = Finland Granite; GL-i = Greenwood Lake Intrusion; Ho-t = Houghtaling Troctolite; LL-g = Lax Lake Gabbro; OL-i = Osler Lake Intrusion; PL-i = Poquayan Lake Intrusion; PR-i Partridge River Intrusion ;SB-i = Silver Bay Intrusions; SK-i = South Kawishiwi Intrusion; SL-i = Sonju Lake Intrusion; UMR-g = Upper Manitou River Gabbro; VH-d = Victor Head Diabase; WM-i Western Margin Intrusion. Note: granites and felsic rocks are the product of the melting of country rocks at the roofs of the mafic intrusions

pegmatoidal layers of plagioclase are commonly in sharp contact with underlying troctolite, and form the bottoms of the sequences which grade upwards into medium grained plagioclase cumulates and then plagioclase-olivine cumulates. Constituent minerals show normal and reverse cryptic variation within individual rock sequences, but there is no systematic overall vector to the compositional variation, leading Foose and Weiblen (1986) to suggest that the chamber was repetitively recharged with new magma, possibly some of it from adjacent intrusions. Severson and Hauck

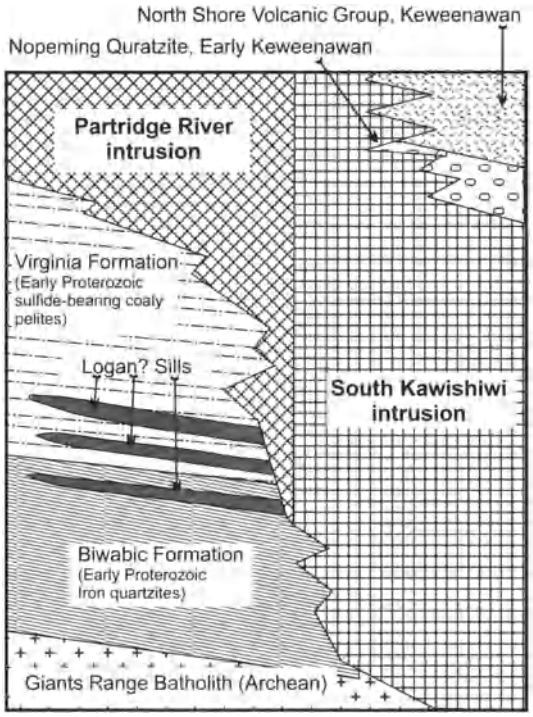


**Fig. 4.53.** Regional stratigraphic setting of the South Kawishiwi and Partridge River Intrusions relative to their country rocks. After Severson and Hauck (1990)

(1990) and Miller and Ripley (1996) compared the South Kawishiwi and Partridge River Intrusions and showed that they have unique differences in their layering, which enable one to clearly define the contact between them (Fig. 4.54).

### *Sulfide Mineralization*

The Duluth complex is the host to more than $4x10^9$ tonnes of mineralisation averaging 0.66 wt% Cu and 0.2 wt% Ni (Listerud and Meineke, 1977), the greater part of which occurs as a series of mineralized zones close to the base (northwestern margin) of the Partridge River and South Kawishiwi intrusions (Fig. 4.51). Overall, the PGE content of the sulfides is relatively high for a mafic intrusion with (Pt+Pd)/(Ni+Cu) (PGE in g/t, Ni and Cu in wt%) between 0.4 and 1.7. Local zones of sulfide containing high PGE concentrations occur in the South Kawishiwi intrusion at a higher stratigraphic level than the main Cu-Ni mineralization (see below).

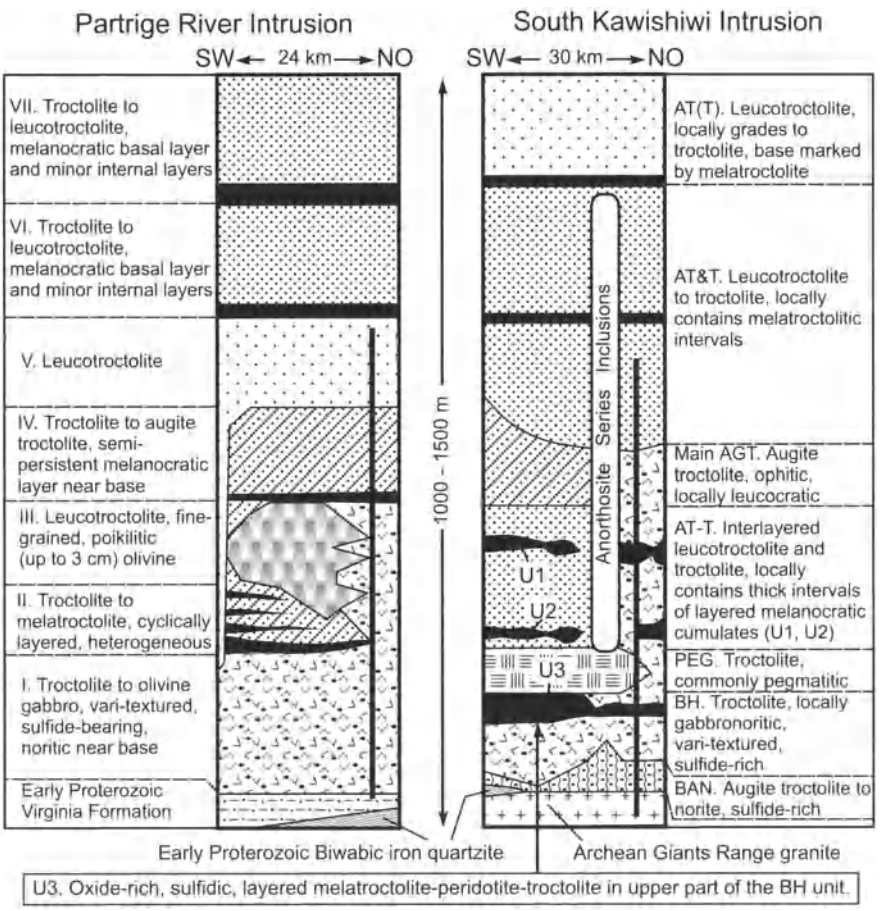


**Fig. 4.54.** Generalized igneous stratigraphy of the lower parts of the Partridge River and South Kawishiwi intrusions. After Miller and Ripley (1996). Unit labels and descriptions after Severson (1994). Heavy vertical lines denote sections intersected by boreholes: DDH-189 and DDH-221 for the Partridge River intrusion, and DDH-24870-A for the South Kawishiwi intrusion

**Cu-Ni Mineralization.** Wager et al. (1969) described the geology of the Spruce and Maturi deposits of INCO Metals Ltd; Matlock and Watowich (1980) described the geology of AMAX Exploration Ltd's Babbit deposit; Rao and Ripley (1983) and Ripley (1981) described the petrology and geochemistry of U.S. Steel Corporation's Dunka Road deposit; and Martineau (1989) described the mineralization throughout the region. The locations of these deposits are shown in Fig. 4.51 and grades and tonnages are summarized in Table 4.8. Average compositions of ores from the Babbit and Dunka Road deposits are given in Table 4.6.

**Table 4.8.** Resources and grades of Cu-Ni ores for deposits of the Duluth Complex (as of April 2000)

| Deposit | Known Resources of Ore [$10^6$ t] | Average grade (wt%) | | Cu cutoff (wt%) | Ownership |
|---|---|---|---|---|---|
| | | Ni | Cu | | |
| Spruce Road | 261 | 0.17 | 0.46 | | "INCO" and "Wallbridge" joint venture |
| South Filson Creek | ? | ? | ? | | ? |
| Maturi | 224 | 0.19 | 0.50 | | "INCO" and "Wallbridge" joint venture |
| | including: 50 | 1.00% Ni+Cu | | | |
| Birch Lake | ? | ? | ? | | "Ernie Lehman" |
| Dunka Pit | ? | ? | ? | | ? |
| Serpentine | 7 | 0.30 | 0.88 | 0.60 | ? |
| Babbit-Minnamax | 3300 | 0.19 | 0.65 | 0.38 | Reported to be under negotiation by "COMINCO" (03/04/00) |
| | including: 4.5 | 0.60 | 1.90 | | |
| Dunka Road | 197 | 0.09 | 0.42 | | "Polymet" |
| Wetlegs | ? | ? | ? | | Open? |
| Wyman Creek | ? | ? | ? | | Open? |
| Total Northwestern Margin of the Duluth Complex | 4400 | 0.20 | 0.66 | | |

The mineralization consists of pyrrhotite, chalcopyrite, pentlandite, and cubanite weakly disseminated (referred to as "cloud sulfide") in troctolite and norite within 300 m of the base of the intrusions. The mineralized zones are characterized by numerous inclusions of country rocks consisting of hornfelsed Virginia and Biwabik Formations, together with barren gabbro and peridotite. Inclusions of Virginia and Biwabic rocks occur even at the Spruce deposit, where granite forms the footwall and the Virginia and Biwabik do not appear to be present in situ at surface within several kilometers of the deposit (Fig. 4.51). At both the Babbit and Dunka Road deposits, norite is more common and troctolite less common in the vicinity of the sulfide horizons, attesting to reactions between the troctolite and country-rock inclusions.

The "Local Boy" section of the Babbit deposit is an exception to the generally sparsely disseminated nature of the sulfides. Here the basal con-

tact of the complex is more irregular than is usually the case and defines a series of east-trending synclines and anticlines. A thin (10-20 m) veneer of Virginia formation, that overlies Biwabic iron formation, has been intensively hornfelsed and, in part, ripped up to form inclusions in the overlying intrusive rocks. The basal Virginia and related inclusions are enveloped in a cloud of norite (= contaminated troctolite) and form the host to schlieren of massive, generally Cu- and PGE-enriched sulfide (Table 4.6).

A number of smaller, very different deposits occur close to the north-south-striking, western edge of the Duluth complex. These are located within small (0.5-2 km-diameter) intrusions composed predominantly of olivine and ilmenite and/or magnetite that form pipe- or blob-like masses cutting the host troctolite. The intrusions are referred to as OUI-type (oxide-ultramafic) intrusions. Mainwaring and Naldrett (1977) described the mineralisation in one of these, the Waterhen Complex. The sulfides comprise pyrrhotite, chalcopyrite/cubanite and pentlandite, along with considerable graphite. Other unusual features of the sulfide environment include the presence of green (Mg-Al.) spinel in some of the troctolites, and the local occurrence of cordierite. As in other deposits, numerous partially resorbed remnants of what appear to be hornfelsed Virginia slate occur in the mineralized zones.

Mainwaring and Naldrett (1977) found that barren sulfides from the Virginia Formation average about 18 $\delta^{34}S$ per mil whereas the Waterhen sulfides range from 11 to 16 $\delta^{34}S$ per mil. Ripley's (1981) sulfur isotope data for the ore of the Dunka Road deposit (Fig. 4.55) ranged from 0.2-15.3 per mil with a mean of 7.5 $\delta^{34}S$ per mil. Pyrrhotite in the underlying Virginia Formation shows a similar range in isotopic composition, also supporting a country rock source for much of the sulfur. The heterogeneous distribution of the sulfur isotope values throughout the deposit, coupled with a wide range in the nickel contents of olivine in the mineralized zone led Ripley (1986) to suggest that sulfur introduction had occurred essentially in situ, and that widespread equilibration between the sulfides and their enclosing silicates had not occurred. In contrast, his sulfur isotope data for the Babbit deposit (Fig. 4.55) show a narrower spread in values, and he suggested that sulfide saturation here had been achieved somewhat farther from the site of the deposit than was the case for Dunka Road, and the isotopic composition of the sulfur had become homogenized during flow.

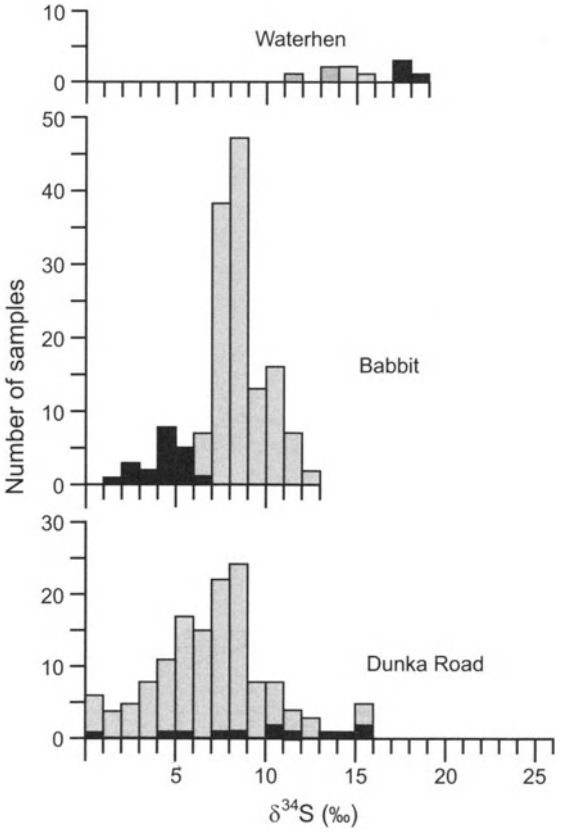


**Fig. 4.55.** Isotopic compositions of sulfur in magmatic Ni-Cu ores (light filling) and sedimentary sulfides (dark filling) for deposits of the Duluth complex. Data for Waterhen from Mainwaring and Naldrett (1977), for Babbit from Ripley (1986), and for Dunka Road from Ripley (1981)

Ripley (1986) found that the $\delta^{18}O$ values at Dunka Road ranged from 5.8-9.6, but that anomalous values (>8 per mil) only occurred near (within 3 m) of the margins of country rock xenoliths (which themselves have a range of 8.6–11.1 per mil). The olivine of the troctolite gives way to orthopyroxene in these zones, suggesting that the change in $\delta^{18}O$ was related to $SiO_2$ contamination. The localized nature of the oxygen isotope contamination led Ripley to suggest that whole-rock assimilation was not a major cause of sulfur contamination. He proposed that the sulfur had been introduced in a volatile phase that was released from the footwall rocks as they were metamorphosed by the intrusion. This is supported by the common association of hydrous minerals such as biotite and amphibole and patches of pegmatite with the mineralization.

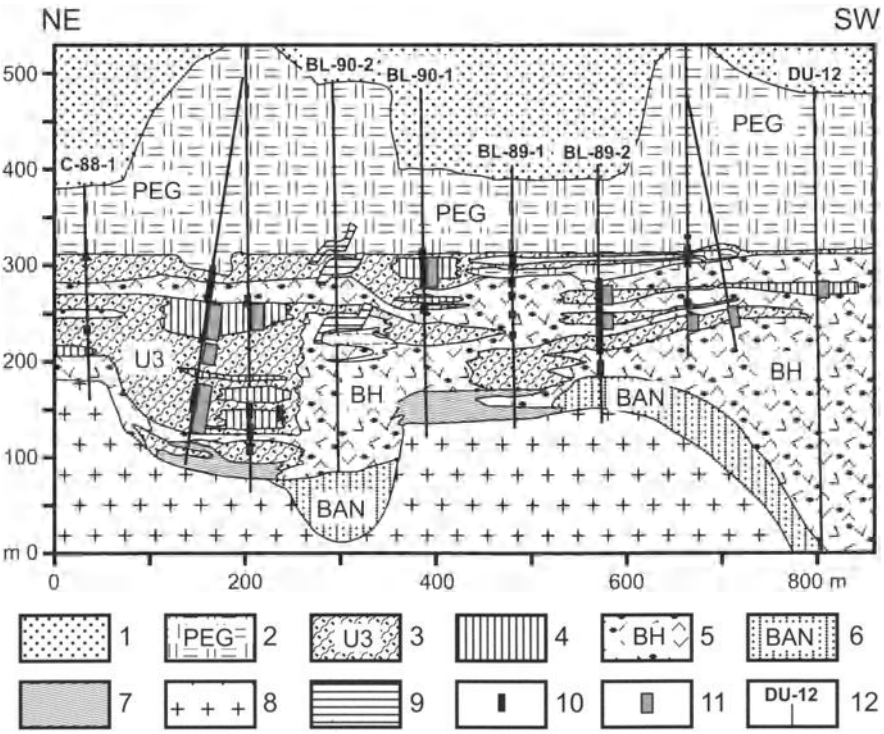


**Fig. 4.56.** Longitudinal projection illustrating relationship of PGE-rich zones to igneous stratigraphy in the Birch Lake region of the South Kawishiwi intrusion (after Severson, 1994). 1 = Troctolite; 2 = Pegmatoidal troctolite; 3 = Picrite with sulfide dissemination in the U3 unit; 4 = Oxide-rich zones; 5 = Vari-textured troctolite with sulfide dissemination; 6 = Augite troctolite with sulfide dissemination; 7 = Early Proterozoic banded Fe-formation; 8 = Archean Giants Range Granite; 9 = Uralitized zones; 10 = Zones of PGE mineralization with Pt+Pd >1 g/t; 11 = Zones with the appearance of Cl-rich drops on core; 12 = Boreholes and their numbers. BAN, BH, PEG, U3 = Units according Fig. 4.54

**PGE-rich mineralization.** Fig. 4.56 shows a longitudinal cross section, adopted from Severson (1994) (vertical scale has been exaggerated) along a portion of the South Kawishiwi intrusion. Giants Range Granite forms the footwall to the intrusion in this area. The granite is overlain by an augite troctolite that is the contact phase of the intrusion. This is overlain in turn by a heterogeneous troctolite, that contains many inclusions of Biwabic Iron Formation (a component of the footwall succession to the west of the area illustrated in Fig. 4.51) and is interleaved with a complex series

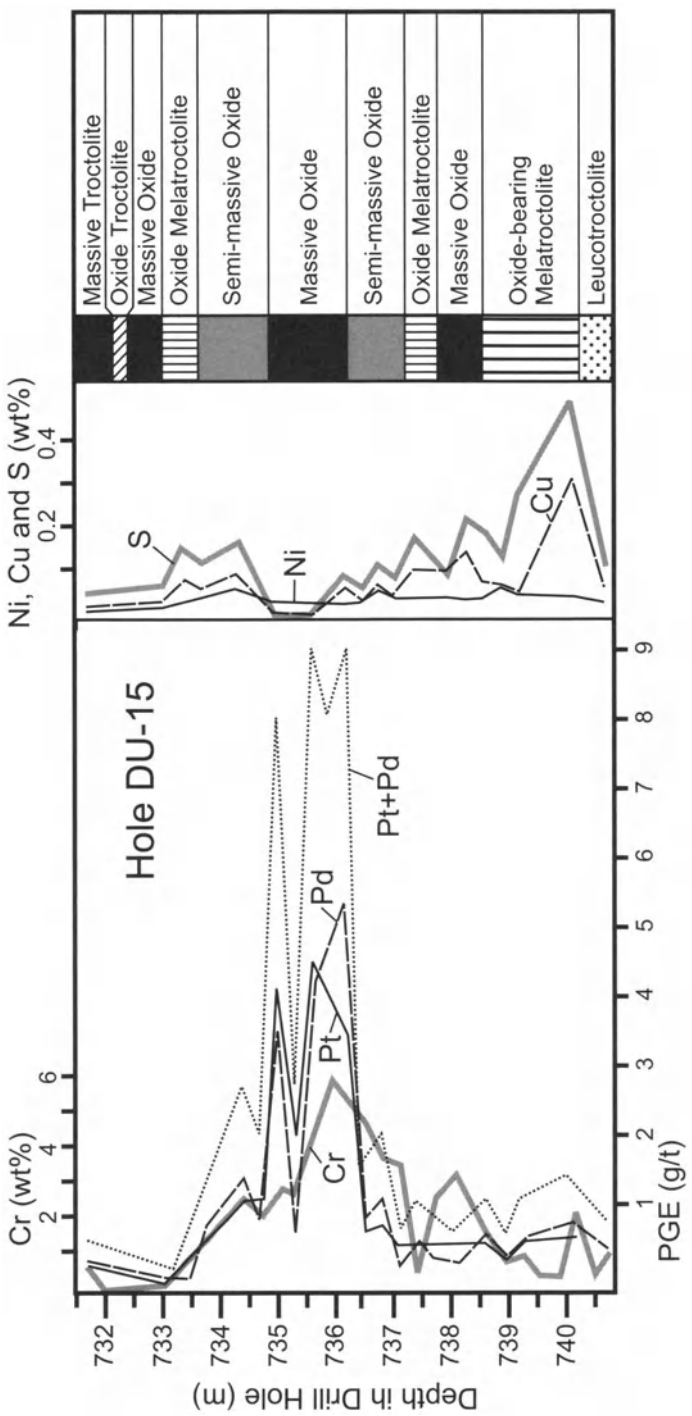


**Fig. 4.57.** Distribution of Pt and Pd within an oxide-rich interval in Drill Hole DU-15 (Birch Lake deposit of the South Kawishiwi intrusion). After Hauck et al. (1997)

of picritic layers which together are referred to as the U3 unit (Ultramafic 3 unit; i.e. the third ultramafic unit down from the top of the intrusion). The U3 picrite is capped by a layer of pegmatitic troctolite/gabbro. Drilling has revealed the presence of pod-like masses rich in titaniferous magnetite. The origin of these is uncertain but it is thought that they might be the residue from the partial melting and reaction of large inclusions of Biwabic Iron Formation with troctolitic magma.

Some intervals of picritic and oxide-rich rocks are enriched in PGE and show Pt+Pd contents >1 g/t (Figs. 4.56 and 4.57) and (Pt+Pd)/(Ni+Cu) (PGE in g/t, Ni and Cu in wt%) of 25 (Appendix 1). Average PGE contents significantly exceed contents in usual disseminated ores of the Duluth (Table 4.9). Pt and Pd show a tendency to be correlated with Cr within oxide-rich zones, but show no correlation with Cu, Ni and S (Fig. 4.57).

**Table 4.9.** Comparison of average compositions of PGE-rich low-sulfide ores and typical disseminated ores of the Duluth Complex (after Hauck et al., 1997)

| Ore Type | Deposit | n | S | Ni | Cu | Pd | Pt | Ir | Os | Au |
|---|---|---|---|---|---|---|---|---|---|---|
| PGE-rich low-sulfide ores | Birch Lake | 9 | 0.16 | 0.13 | 0.08 | 2 510 | 2 762 | 84 | 57 | 81 |
| Undepleted disseminated ore (Pd/Cu = $10^3$–$10^4$) | Dunka Road and Birch Lake | 52 | 0.83 | 0.18 | 0.49 | 706 | 438 | 9 | 5 | 71 |

*n* number of samples. Sulfur, Ni and Cu in wt%; PGE and Au in ppb (mg/t)

Very commonly, lengths of core that carry high PGE concentrations develop droplets of chloride-rich fluid or a brown encrustation of a hydrated iron chloride when they have remained in the core box for some time. While the correlation between high PGE and chloride is not perfect, it is thought that it is significant. Severson (1994) has proposed that chloride-rich solutions have entered the base of the hot intrusion from the underlying footwall rocks, have leached PGE from zones of sulfide near the base, and have then re-deposited the PGE higher in the stratigraphy. Several areas of the intrusion that are characterized by a high degree of uralitic alteration (see Fig. 4.56) may mark the passage of these solutions. Thus far, the PGE-rich zones are discontinuous, and have not proved to be of economic importance.

### 4.2.3 Crystal Lake Gabbro

The Crystal Lake Gabbro (Mainwaring 1968; Reeve 1969; McRae and Reeve 1968; Eckstrand and Cogulu 1989; Cogulu 1990) forms an elongate, Y-shaped body, at least 6 km long, 800 m thick and 3 km wide. The individual limbs of the Y are about 1 km wide and occupy troughs, in which the sides dip inward at 45° and plunge east at 15-20° (Fig. 4.58).

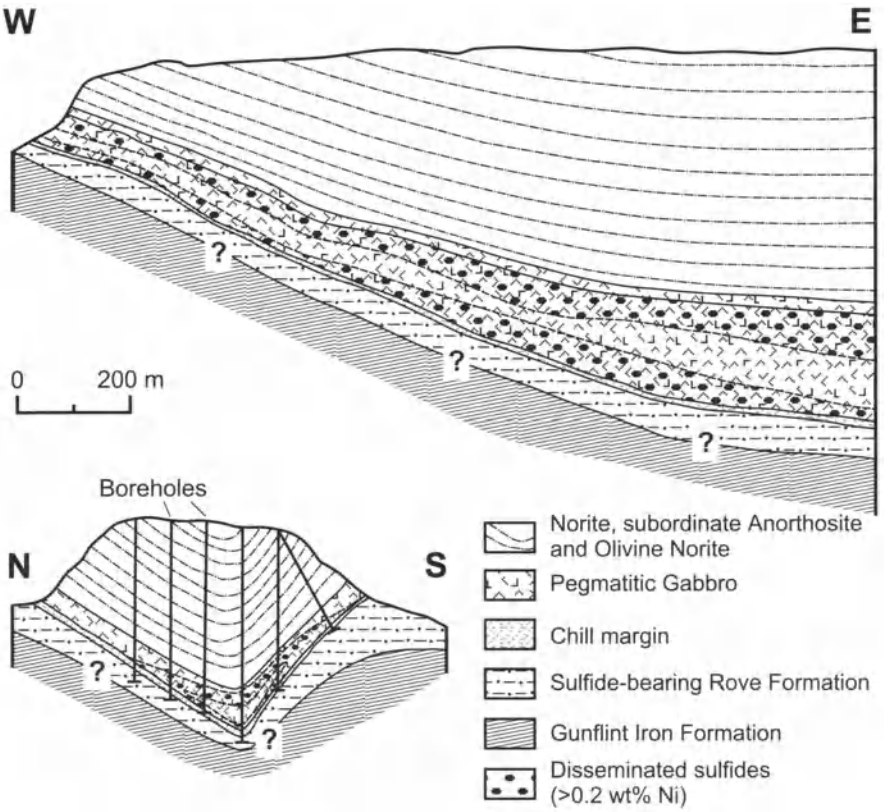


**Fig. 4.58.** Longitudinal and cross-sections of the Great Lakes Nickel deposit in the Crystal Lake Gabbro. From Martineau (1989), after Mainwaring (1968) and Reeve (1969)

Pegmatitic gabbro occurs at the base of the intrusion, immediately above the chilled margin. They are overlain by two cycles of layered olivine-orthopyroxene-plagioclase cumulates, olivine-rich at the base and grading upwards into norites. The upper part of the upper cycle consists of a 400-600 m sequence of norites. The pegmatitic zone varies from 50 to 200m in thickness (Fig. 4.58), has a highly variable crystal size and tex-

ture, and is closely associated with a chromitite seam. It contains a stratiform sheet of disseminated chalcopyrite-cubanite-pentlandite-pyrrhotite mineralization. The sulfide content within this sheet is relatively low, leading to an overall low grade (see Table 4.6), but the sulfides themselves are enriched in Ni, Cu and PGE, and have the relatively high (Pt+Pd)/(Ni+Cu) ratio (PGE in g/t, Ni and Cu in wt%) of 1.76, indicating that they have achieved a high "R" or "N" factor (Fig. 4.59). The sheet merges to the east with a picritic dyke (the Mt Mollie dyke), and dyke and sill together were very likely a magma conduit, similar to the mineralized conduits at Noril'sk, which probably accounts for the high "R" or "N" factor.

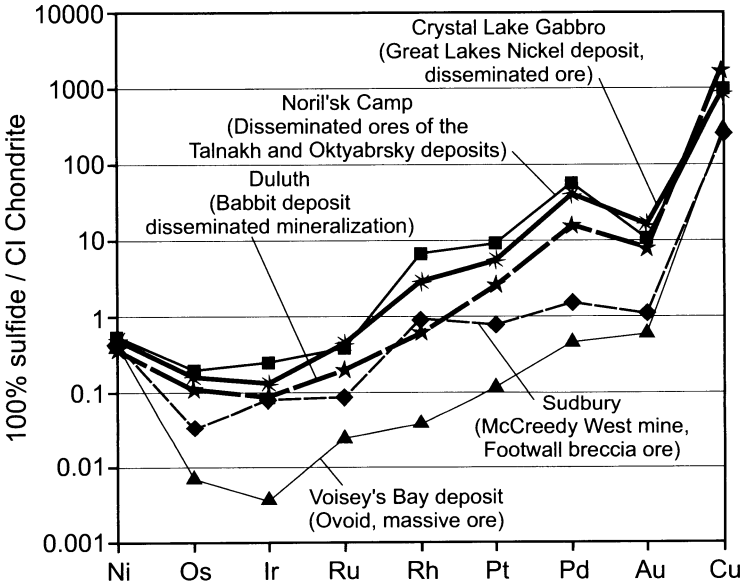


**Fig. 4.59.** Average contents of PGE, Ni and Cu (normalized to CI Chondrite) in ore of the Crystal Lake intrusion in comparison with ores of some other deposits. Ore compositions are recalculated to 100% sulfide

### 4.2.4 Conclusions arising from Keweenawan Mineralization

The case for addition of external sulfur is clear with respect to the formation of the principal deposits of cloud sulfide at Duluth, with the bulk of the sulfur coming from the underlying or adjacent Virginia slates and Biwabic Iron Formation. It is likely that the deposits occur too close to the source of sulfur for subsequent flow of magma to have concentrated the prevailing economic conditions. Duluth may in fact be an example of the

type of reaction chamber from which sulfide-bearing magma rises to a higher level. During this subsequent ascent, the sulfides become concentrated within the magma conduits, giving rise to concentrations that are rich enough to be mineable. It is not certain that such flow channels exist in the Lake Superior region, although the Crystal Lake gabbro has many of the characteristics (shape, size, contaminated lower zone) of the Noril'sk mineralized intrusions, except for necessary high sulfide content.

## 4.3 Deposits Associated with the Karoo Flood Basalt of Southern Africa

### 4.3.1 General information

Karoo magmatism coincided with the break-up of Gondwanaland and occurred between the Early and Middle Jurassic at 183± 1 Ma (Duncan et al. 1997). In addition to the Karoo igneous province of Southern Africa, flood basalts and intrusive rocks of this age are preserved in Mozambique, Antarctica, New Zealand and Australia. However, the only significant Ni-Cu mineralisation discovered thus far is that at Waterfall Gorge in the Insizwa Complex (Fig. 4.60). The deposit consists of 600,000 tonnes of mineralisation grading 0.5 wt percent Ni+Cu (Scholz 1952).

The Karoo-age volcanic formations of Southern Africa are underlain by a thick (about 10 km) series of terrigenous sedimentary rocks that fill the Karoo basin. Accumulation of these rocks continued from the Early Carboniferous to end of the Early Jurassic. Accumulation started with the tillites of the Dwyka Formation (1100 m thick) and was followed by a sequence of alternating sandstones and shales that comprise the Ecca, Beauford, Molteno, Elliot and Clarens Formations (Stratten 1986). Discrete lava flows occur in upper part of the Clarens Formation which is followed by volcanic rocks of the Drakensberg Formation and localized occurrences forming the Lebombo and Bumbeni Groups. The Drakensberg Formation (1400 m thick) consists of low-Ti tholeiitic basalts, which are referred to here as Lesoto type (Marsh and Eales 1985). Andesites, dacites and rhyolites, along with basalts comprise the Lebombo Group. The Bumbeni Group consists of basaltic, andesitic, trachytic and rhyolitic lavas and tuffs. The volcanic rocks have an $^{40}Ar$-$^{39}Ar$ age of 184-179 My (Duncan et al. 1997).

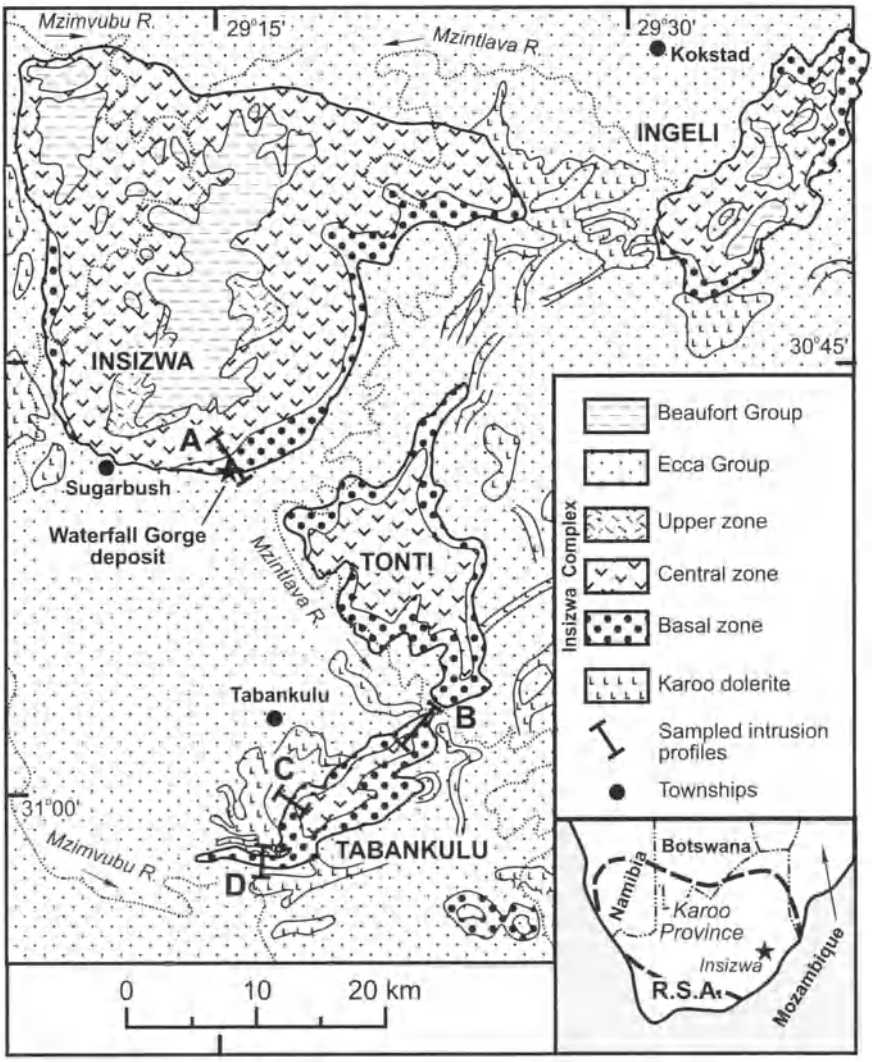


**Fig. 4.60.** Regional geology of the Insizwa Complex compiled from regional mapping by Dowsett and Reid (1974), and mapping by Maske (1966) and Lightfoot (1982). From Lightfoot et al. (1984)

Intrusions of the Karoo province comprise the Karoo dolerite sills (equivalent of the Lesoto basalts) and thicker intrusive complexes composed of gabbroic and picritic cumulates (Table 4.10).

### 4.3.2 Geology of the Insizwa Complex

The Insizwa Complex (Fig. 4.60) is one of the largest of the Karoo age intrusions within the Central Flood Basalt Province of southern Africa. The four components of the complex – Insizwa, Ingeli, Tonti, and Tabankulu – each occupy basinal depressions close to the contact of the Beaufort and Ecca Group sediments. The sequence of rock types exposed through each component has been described by Scholtz (1936), Bruynzeel (1957) and Lightfoot et al. (1984) at Insizwa, Maske (1966) at Ingeli, and Lightfoot (1982) and Lightfoot and Naldrett (1984a) at Tabankulu. Scholtz (1936) subdivided each component of the complex into three zones:

1. The Basal zone, or lower basic phase, is composed predominantly of an olivine cumulate with intercumulus augite, bronzite, and plagioclase (the picrite unit) and a plagioclase-olivine cumulate with intercumulus bronzite and augite (the troctolite unit). At the base of the intrusion there is a narrow but ubiquitous olivine gabbro unit which consists of cumulus olivine set in a chilled groundmass of augite, bronzite, and plagioclase.
2. The Central zone is composed of an olivine-plagioclase cumulate with variable proportions of intercumulus augite and bronzite, with intercumulus olivine in some horizons (olivine, augite, and bronzite gabbros).
3. The Roof zone, or upper acid phase, is composed of cumulus plagioclase and intercumulus quartz, K-feldspar, hornblende, and biotite (quartz diorites and monzonites).

Early work by Du Toit (1920) suggested that the four components were once linked together as part of a single continuous and undulating intrusive sheet. Structural mapping at Ingeli by Maske (1966) has shown that this component occupies a basinal depression in the Ecca Group sediments, but Maske found no evidence to suggest that the magma was intruded from directly below the basin through a subintrusive feeder dike. Consequently, he postulated that the main influx of magma was injected laterally from the direction of the Insizwa intrusion.

Significantly deeper levels of erosion have occurred at Tabankulu compared with Insizwa and Ingeli. Lightfoot and Naldrett (1984a) have suggested that at Tabankulu the magma entered the chamber from below,

**Table 4.10.** Average chemical compositions of the Lesoto Basalt and Karoo Dolerite (after Marsh and Eales, 1985); and compositions of contact rocks and rocks from the Basal Zone of the Insizwa Intrusion at Waterfall Gorge section (after Lightfoot and Naldrett, 1984b)

| Rock | Basalt | Dolerite | Hornfels | Chill | Basal gabbro | Basal gabbro | Basal gabbro |
|---|---|---|---|---|---|---|---|
| (n) No | (48) | (22) | INS301 | INS302 | INS303 | INS304 | INS305 |
| $SiO_2$ | 51.51 | 51.76 | 68.46 | 53.72 | 49.16 | 48.15 | 48.14 |
| $TiO_2$ | 0.95 | 1.00 | 0.47 | 0.96 | 0.68 | 0.68 | 0.62 |
| $Al_2O_3$ | 15.69 | 15.23 | 12.23 | 13.36 | 14.07 | 14.01 | 13.15 |
| FeOT | 10.95 | 10.90 | 7.91 | 11.77 | 13.21 | 13.21 | 13.27 |
| MnO | 0.16 | 0.20 | 0.10 | 0.18 | 0.17 | 0.17 | 0.17 |
| MgO | 7.02 | 6.86 | 1.46 | 7.07 | 11.88 | 13.02 | 14.90 |
| CaO | 10.69 | 10.57 | 2.47 | 9.01 | 8.42 | 8.09 | 7.49 |
| $Na_2O$ | 2.17 | 2.28 | 2.72 | 1.88 | 1.61 | 1.78 | 1.75 |
| $K_2O$ | 0.70 | 0.56 | 3.60 | 0.75 | 0.46 | 0.47 | 0.40 |
| $P_2O_5$ | 0.16 | 0.17 | 0.00 | 0.18 | 0.17 | 0.16 | 0.16 |
| LOI | | | 1.78 | 1.17 | 0.42 | 0.49 | 0.50 |
| Total | | | 101.20 | 100.05 | 100.25 | 100.23 | 100.55 |
| Ba | 175 | 213 | | | | | |
| Rb | 12.0 | 12.5 | 153.0 | 29.5 | 21.5 | 18.0 | 17.0 |
| Sr | 191 | 208 | 266 | 188 | 153 | 140 | 131 |
| Y | 24.4 | 25.7 | 21.5 | 24.6 | 20.9 | 19.4 | 18.1 |
| Zr | 94 | 97 | 201 | 90 | 78 | 70 | 65 |
| Nb | 4.8 | 6.3 | 10 | 8 | 6 | 5 | 6 |
| V | 241 | 246 | | | | | |
| Zn | 86 | 87 | | | | | |
| Cu | | | 3703 | 597 | 1525 | 1108 | 1081 |
| Ni | 94 | 87 | 2640 | 705 | 1972 | 1439 | 1551 |
| Co | 48 | 46 | | | | | |
| La | | | 27.3 | 14.4 | 10.8 | 10.1 | 9.0 |
| Ce | | | | 28.9 | 22.0 | 21.2 | 19.2 |
| Nd | | | | 13.5 | 12.3 | 10.7 | 9.8 |
| Sm | | | 5.2 | 3.7 | 2.9 | 2.8 | 2.5 |
| Eu | | | | 1.2 | 1.1 | 0.8 | 0.9 |
| Tb | | | | 0.2 | 0.5 | 0.5 | 0.4 |
| Ho | | | 1.6 | 1.0 | | | |
| Yb | | | 2.0 | 2.5 | 2.0 | 2.0 | 1.8 |
| Lu | | | 0.3 | 0.4 | 0.3 | 0.3 | 0.3 |

**Table 4.10** (cont.)

| Rock | Basal gabbro | Basal gabbro | Basal gabbro | Basal gabbro | Basal gabbro | Basal gabbro | Picrite |
|---|---|---|---|---|---|---|---|
| (n) No | INS306 | INS307 | INS308 | INS309 | INS310 | INS311 | ES20 |
| $SiO_2$ | 47.52 | 47.12 | 48.97 | 47.45 | 46.31 | 45.36 | 43.91 |
| $TiO_2$ | 0.65 | 0.63 | 0.66 | 0.59 | 0.55 | 0.46 | 0.34 |
| $Al_2O_3$ | 12.68 | 12.47 | 13.73 | 11.66 | 10.85 | 10.73 | 8.39 |
| FeOT | 13.30 | 13.67 | 13.11 | 13.08 | 13.83 | 13.94 | 15.45 |
| MnO | 0.17 | 0.17 | 0.17 | 0.18 | 0.18 | 0.18 | 0.19 |
| MgO | 16.43 | 16.73 | 12.94 | 18.58 | 20.86 | 21.74 | 26.98 |
| CaO | 7.38 | 6.98 | 7.89 | 6.74 | 6.15 | 5.83 | 4.09 |
| $Na_2O$ | 1.43 | 1.15 | 1.58 | 1.42 | 1.05 | 1.54 | 0.72 |
| $K_2O$ | 0.41 | 0.39 | 0.49 | 0.29 | 0.25 | 0.16 | 0.01 |
| $P_2O_5$ | 0.16 | 0.16 | 0.16 | 0.13 | 0.11 | 0.08 | 0.07 |
| LOI | 0.46 | 0.43 | 0.89 | 0.72 | 0.89 | 0.60 | 0.29 |
| Total | 100.59 | 99.90 | 100.59 | 100.78 | 101.03 | 100.62 | 100.44 |
| Ba | | | | | | | |
| Rb | 16.0 | 17.5 | 21.5 | 13.5 | 12.5 | 11.0 | 9.0 |
| Sr | 131 | 136 | 147 | 118 | 101 | 96 | 76 |
| Y | 17.5 | 18.1 | 19.6 | 15.7 | 14.6 | 13.2 | 9.3 |
| Zr | 64 | 66 | 72 | 57 | 51 | 46 | 33 |
| Nb | 6 | 5 | 6 | 5 | 5 | 5 | 4 |
| V | | | | | | | |
| Zn | | | | | | | |
| Cu | 602 | 1063 | 1300 | 243 | 360 | 602 | 301 |
| Ni | 1034 | 1566 | 1798 | 882 | 1093 | 1367 | 1010 |
| Co | | | | | | | |
| La | 9.2 | 9.3 | 10.8 | 8.3 | 6.8 | 7.2 | |
| Ce | 19.9 | 19.1 | 32.1 | 17.4 | 13.9 | 13.9 | |
| Nd | 9.9 | 10.5 | 11.9 | 8.4 | 8.0 | 6.5 | |
| Sm | 2.5 | 2.5 | 2.9 | 2.2 | 1.9 | 1.9 | |
| Eu | 0.8 | 0.8 | 0.9 | 0.8 | | | |
| Tb | 0.4 | 0.5 | 0.5 | 0.5 | 0.1 | 0.4 | |
| Ho | 0.6 | 0.7 | 0.8 | 0.8 | | | |
| Yb | 1.8 | 1.7 | 2.0 | 1.7 | 1.2 | 1.3 | |
| Lu | 0.2 | 0.3 | 0.3 | 0.2 | 0.2 | 0.2 | |

*(n)* Number of analyses; *No* Sample number. Major elements in wt%; Trace elements in ppm

along a subvertical feeder dike which forms the southern extremity of the body (see Figs. 4.60 and 4.61).

Nickel sulfide mineralization occurs disseminated throughout the Basal and Upper zones of all four intrusions, and subeconomic concentrations have been observed along the southeastern slopes of the Insizwa massif at Waterfall Gorge section.

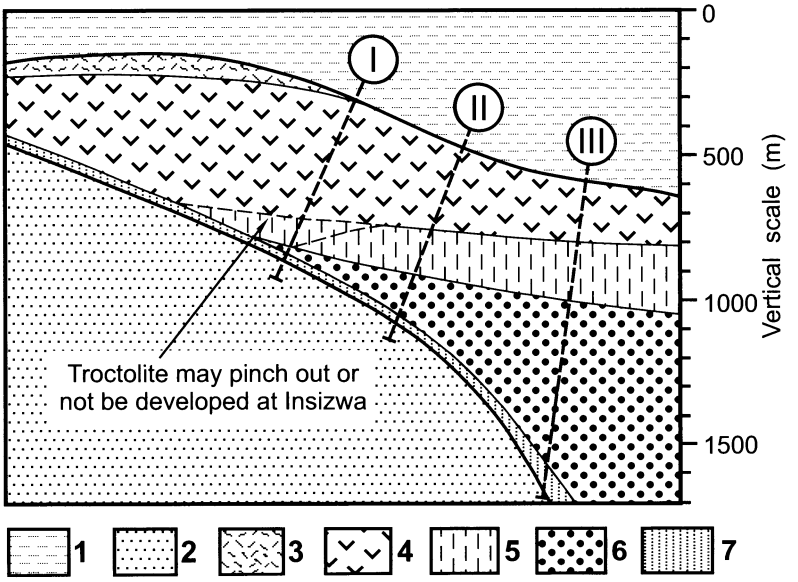


**Fig. 4.61.** Simplified sketch showing a possible scenario for the relationship between the Tabankulu and Insizwa intrusions before deformation and erosion (lateral scale is not defined). I = southern part of the Insizwa intrusion; II = Northwestern part of the Tabankulu intrusion; III = Axial part of the Tabankulu intrusion at the supposed feeder dike. 1-2 = Country rocks (1 = Beaufort Group; 2 = Ecca Group); 3 = Upper zone of the Insizwa Complex; 4 = Central zone of the Insizwa Complex; 5-7 = Rocks of Basal zone of the Insizwa Complex (5 = Troctolite; 6 = Picrite; 7 = Basal gabbro). After Lightfoot et al. (1984)

### 4.3.3 The Insizwa intrusion at Waterfall Gorge

The Waterfall Gorge section of the Insizwa complex intrusion is located at the southern margin of the Insizwa intrusion where a river has cut a deep gorge into the massif. The geology of the complete sequence has been outlined by Bruynzeel (1957), but most work has been focused on the basal olivine gabbro where a nickel sulfide deposit is located (Scholtz 1936).

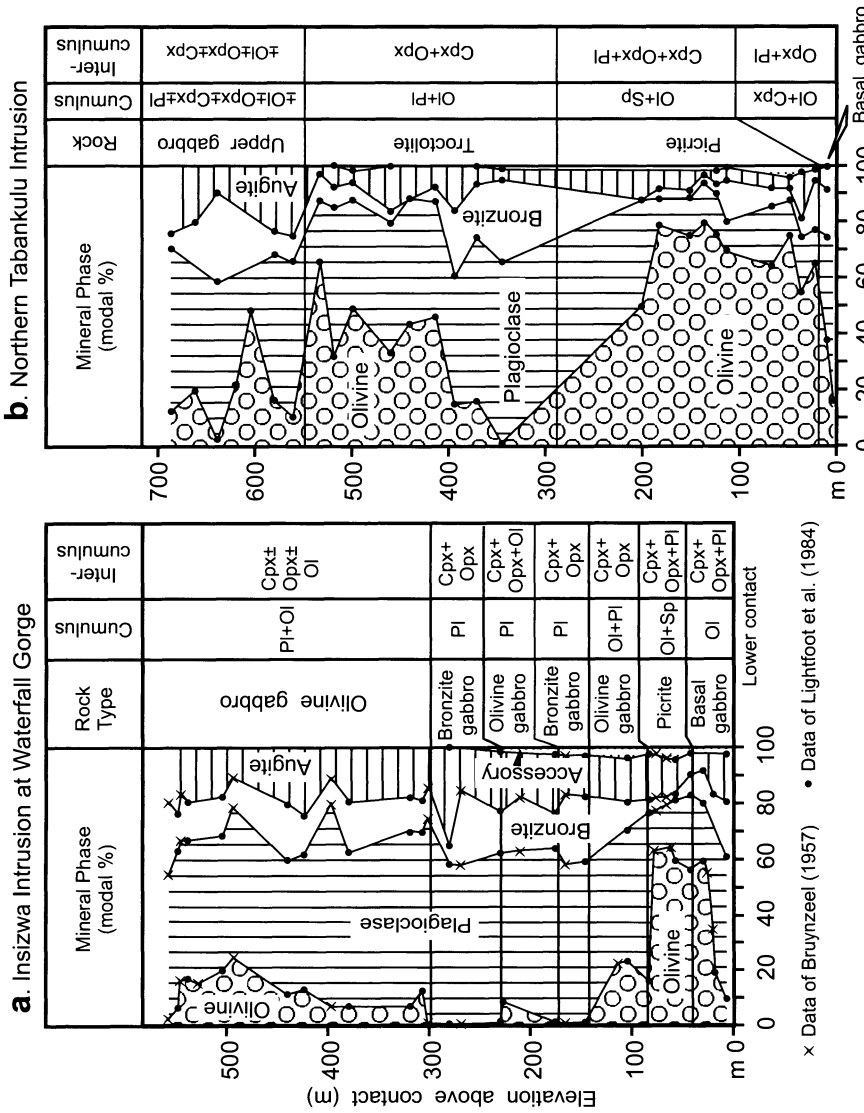


**Fig. 4.62.** Petrographic variations and variations in modal mineralogy through the Waterfall Gorge section of the Insizwa intrusion, compiled from Bruynzeel (1957) and the data of Lightfoot et al. (1984) along with a section through the Tabankulu intrusion for comparison. (After Lightfoot et al., 1984)

The Waterfall Gorge section (Fig. 4.62a) consists of a sequence of Basal and Central zone rock types which dip at 5° to 30° in a northerly direction. The Basal zone consists of a basal gabbro and picrite unit, which together are 70 m thick where exposed at surface but which have been found to

have a thickness of 320 m (largely composed of picrite) in drill core taken about 300 m north of the intrusive contact (Bruynzeel 1957). The Central zone consists of a sequence of gabbros. The gabbros belong to two units, a lower unit composed of rocks with moderate MgO contents (decreasing upward) and an upper unit with more MgO-rich rocks (MgO also decreasing upward). Roof zone rocks are absent from the intrusion at the southern margin, but 5 km to the northwest the intrusion is capped by monzonites. The sequence of rock types shows little local variation laterally except at the base of the intrusion, where granophyric veins, calcareous nodules, veins of massive sulfide ore, and zones of disseminated ore are developed.

### *Geology of the contact and basal zones at Waterfall Gorge*

Lightfoot et al. (1984) have described geological relations exposed in the old mine workings at the Waterfall Gorge deposit at Insizwa (Fig. 4.63). Their account of generalized contact relations is illustrated in Fig. 4.64.

The Ecca Group footwall sediments at Waterfall Gorge consist of black, poorly bedded, fissile shales which contain bands of ovate calcareous nodules at 10- to 15-m intervals through the sedimentary stratigraphy. Close to the contact, the shales have been metamorphosed to form a strongly cleaved, dense, black, fine-grained hornfels which contains deformed calcareous nodules. The contact zone between the hornfels and the basal olivine gabbro (referred to as the chill) is 0.5 m wide; the exact location of the contact is difficult to determine in the field due to the intense recrystallization of the hornfels and the fine-grained nature of the chill. The chill is a dense, black rock which contains less than 1 percent olivine but large amounts of fine-grained quartz, K-feldspar, apatite, and ilmenite set in a groundmass of small plagioclase laths and granular bronzite and augite. Away from the contact, the chill changes into a fine-grained olivine gabbro over a distance of 1 m and shows supercooling textures, including occasional skeletal olivines, many small intercumulus plagioclase laths, and granular pyroxenes. The gabbro contains between 1 and 60 modal percent olivine, the proportion increasing fairly regularly away from the contact. At a distance of 20 m from the contact, the olivine gabbro changes into a picrite with over 60 modal percent olivine set in large poikilitic plates of pyroxene and plagioclase. The footwall hornfels, hanging-wall gabbro, and picrite are cut by veins and segregations of granophyre (Fig. 4. 64). The olivine gabbro hosts much of the massive ore, with the remainder being hosted by hornfels proximal to the contact.

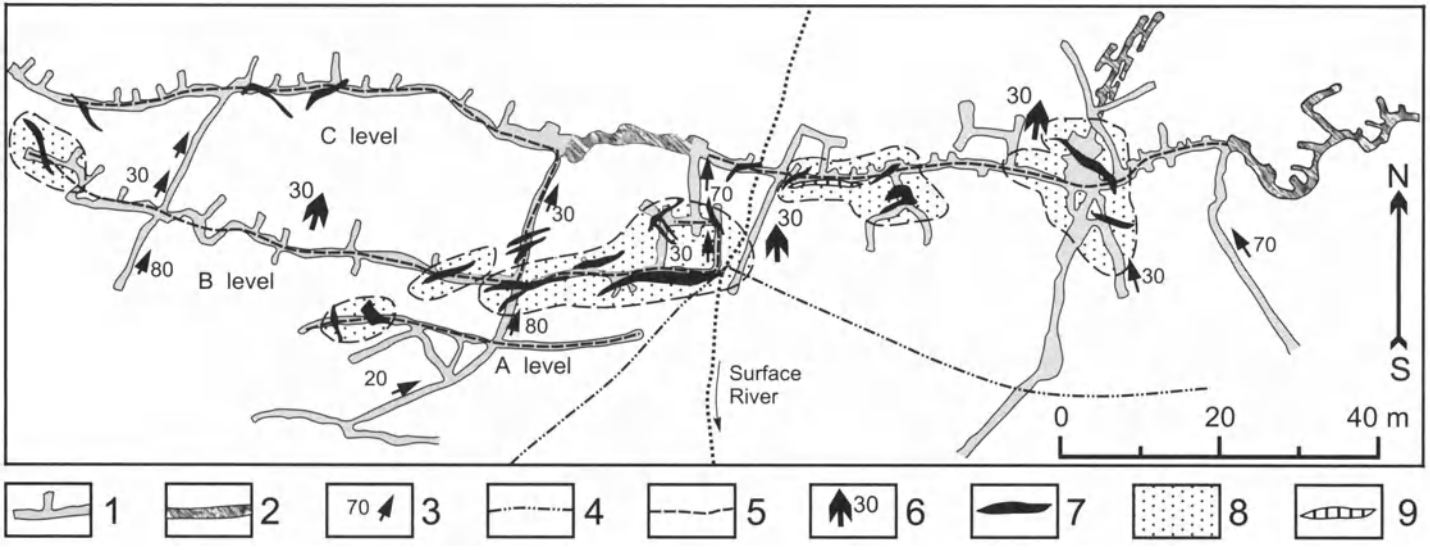


**Fig. 4.63.** Plan of the abandoned mine workings at Insizwa, Waterfall Gorge, documented by Lightfoot, showing the location of the contact in the three adits, and the zones of massive and disseminated ore. After Lightfoot et al. (1984). 1 = Adits and winzes; 2 = Flooded adit and winze sections; 3 = Dip of winze; 4 = Lower contact of the intrusion at surface; 5 = Contact underground; 6 = Dip of contact; 7 = Sulfide veins; 8 = Zones of extensive country rock assimilation and disseminated ore; 9 = Large granophyric vein

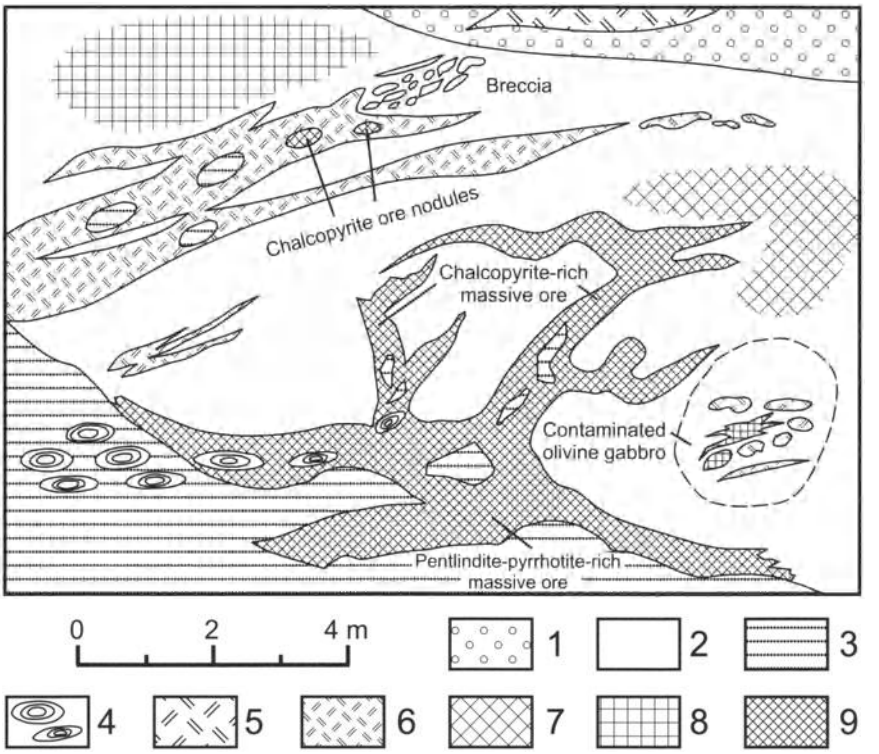


**Fig. 4.64.** Sketch showing contact zone relations in the mine workings at Waterfall Gorge (after Lightfoot at al., 1984). 1 = Picrite; 2 = Olivine gabbro; 3 = Hornfels; 4 = Calcareous nodules; 5 = Coarse granophyre; 6 = Fine granophyre; 7 = Disseminated sulfide; 8 = Disseminated, net-textured and globular sulfide; 9 = Massive sulfide

### *Sulfide mineralization*

The bulk of the ore at Waterfall Gorge consists of globular, net-textured, and disseminated nickel sulfide that is confined to the basal olivine gabbro and is associated with regions of massive ore and granophyre. Typical average analyses of different ore types are given in Table 4.6.

The globular ore consists of small, vertically oriented, elliptical globules of nickel sulfide varying between 0.5 and 3 cm in length. The globules consistently have a lower pyrrhotite pentlandite-rich section and an upper chalcopyrite-rich section[15]. The net-textured ore occurs as pyrrhotite-

[15] Globular ore of the Insizwa intrusion resembles visually the ovoidal dissemination in picritic gabbrodolerite of the Noril'sk region ore-bearing intrusions.

pentlandite-chalcopyrite ore enclosing olivine phenocrysts and grains of plagioclase, bronzite, augite, and ilmenite.

The remaining ore consists of two types: sheets of massive pyrrhotite-pentlandite-rich ore which follow the contact, and veins of chalcopyrite-rich ore which cut up through the hanging-wall gabbros away from the contact (Fig. 4.64). The pyrrhotite-pentlandite sheets extend parallel to the contact, for up to 15 m along strike and 4 m down dip and vary in width between 10 cm and 1 m. Large, vertical (approximately 1 m wide) and subvertical veins are visible in crosscuts in the underground workings. Gangue constitutes between O and 10 percent of the veins, most of which is in the form of sheared out nodules and xenoliths of hornfels. At a distance of 2 to 3 m from the basal contact of the intrusion, the veins narrow substantially and either disappear or split into several smaller veins, which may travel for a further 3 or 4 m.

### *Granophyre*

The granophyres of the Basal zone occur as: (1) large, coarse-grained veins of variable orientation cutting through the picrite – they have dimensions of 20 m in length, 1 m in width, and a third dimension of at least 2 m; (2) fine-grained veins cutting the basal gabbro and running subparallel to the contact before abruptly terminating in the overlying gabbro—these veins reach 4 m in width; (3) clusters of subrounded bodies of granophyre – each body varying in size from 5 to 30 cm and occurring in large groups, or in smaller numbers associated spatially with granophyric veins; and (4) breccia zones consisting of sheared-out relict calcareous nodules surrounded by granophyre, olivine gabbro, and irregular bodies of massive ore.

## 4.3.4 Petrography

**Basal zone.** Lightfoot et al. (1984) describe the Basal zone as consisting of a contact chill, a basal olivine gabbro and a picrite unit (Fig. 4.62a). The contact chill is a fine-grained rock with granular aggregates of augite and bronzite, small (1 mm) radiating laths of plagioclase, and occasional grains of resorbed and hollow cumulus olivine rimmed by bronzite. Accessory phases include quartz, K-feldspar, apatite, biotite, and sulfide. The basal chill grades into an olivine-plagioclase cumulate (the basal olivine gabbro) with an increase in the modal proportion and grain size of the olivine and plagioclase. The olivines retain a resorbed appearance and some have hollow cores. The basal olivine gabbro grades upward into the overlying pic-

rite as the plagioclase changes from a cumulus to an intercumulus phase and as the modal proportion of olivine peaks at 60 to 65 modal percent. The picrite consists of large intercumulus grains of plagioclase, bronzite, and augite hosting equant to subequant grains of olivine and small crystals of spinel. The intercumulus plagioclase shows oscillatory zoning from core to rim.

**Central zone.** The Central zone consists of a sequence of gabbros which are subdivided on the basis of the nature and proportion of the cumulus and intercumulus mineral phases. Lightfoot et al. (1984) distinguish the following units (Fig 4.62a):

1. The lower olivine gabbro, which consists predominantly of cumulus olivine, plagioclase, and spinel with intercumulus bronzite, augite, biotite, and sulfide. Olivines occur as phenocrysts which are resorbed when enclosed in bronzite. The unit has a remarkably low olivine content when compared to the underlying picrite. Exposure of the relationship between the picrite and this unit was not observed in the field. Bruynzyl (1957) was able to show, with the aid of drill core, that the transition from the Basal zone into the Central zone is quite rapid and occurs over a distance of a few meters.
2. The lower olivine-free gabbro consists predominantly of cumulus plagioclase. Bronzite is the dominant pyroxene and occurs as large intercumulus plates enclosing laths of plagioclase and subrounded augite grains.
3. The central olivine gabbro consists of cumulus plagioclase with intercumulus bronzite, augite, and olivine. Large (1.5–5 mm) ophitic plates of olivine and pyroxene enclose small (0.5–1 mm) subrounded laths of plagioclase.
4. The upper olivine-free gabbro is similar to the lower olivine-free gabbro.
5. The upper olivine gabbro consists of a lower olivine-plagioclase cumulate with intercumulus augite and bronzite. The olivine is resorbed and surrounded by wide rims of bronzite.

### 4.3.5 Mineralogy and Mineral Chemistry

The mineralogies of the Waterfall Gorge have been described by Bruynzyl (1957) and Lightfoot et al. (1984). Maske (1966) performed a detailed mineralogical study at Ingeli. Eales (1980) presented the first microprobe data for olivines, from the picrite unit, in the Waterfall Gorge section. Both

mineralogical and mineral chemical data are presented for the Tabankulu intrusion by Lightfoot and Naldrett (1984a) where analytical techniques are described.

**Olivine.** The main compositional features exhibited by the olivines include (Fig. 4.65):

1. A rapid increase in the forsterite content of the olivine from $Fo_{76}$ to $Fo_{83}$, and in the nickel content from 1,400 to 1,700 ppm, from the chill to the base of the picrite unit. These trends correlate with an increase in the modal proportion of olivine.
2. In the picrite, the olivines reach a maximum forsterite content of between $Fo_{8O}$ and $Fo_{84}$ but contain only 1,100 to 1,200 ppm nickel, distinctly lower than those from the basal olivine gabbro unit.
3. There is a rapid decrease in the forsterite content from $Fo_{8O}$ to $Fo_{65}$ and in the nickel content from 1,000 to 400 ppm from the picrite to the lower Central zone gabbro unit. The nickel content then increases to 1,450 ppm in the gabbro before olivine disappears, while the forsterite content increases from 65 to 68 mole percent.
4. Olivine from the middle of the Central zone contains 72 mole percent forsterite, varying upward between this value and 65 mole percent. The nickel content varies between 1,000 and 1,200 ppm upward to the top of the section.

Following the approach of Li and Naldrett (1999), the olivine data from Insizwa are shown on plots of Ni versus Fo in olivine in Fig. 4.66 along with curves modeling the variations to be expected as a result of perfect fractional crystallization. Li and Naldrett noted that in developing the curves and at the same time maintaining a reasonable FeO content of 9 wt%, the composition of the more primitive olivines required the assumption that the initial magma contained 14 wt% MgO and 450 ppm Ni. It is seen from Fig.4.66 that the fractionation of olivine alone rapidly depletes the magma (and thus olivines) in Ni and that all of the Insizwa rocks plot above this line. The Insizwa gabbros describe a trend which can be modeled by fractionating 3.5 wt% olivine (this reduces the Fo content from 90 to 89.3 mole percent and the Ni in the liquid from 450 to 367 ppm), followed by fractionation of olivine+clinopyroxene (ratio 1:1) plus plagioclase (ratio 0.425(Ol+Cpx):0.575 Pl). These ratios correspond to the average cumulus mineralogy of the rocks of the intrusion.

Much of the Tabankulu basal gabbro and picrite falls below the olivine fractionation line, but is reasonably well modeled on the basis of the fractionation of olivine + sulfide in a ratio of 133:1. The segregation of a

slightly higher proportion of sulfide, or the bulk equilibration with sulfide as was suggested at Voisey's Bay (see Chapter 6), would produce an even closer match for the data.

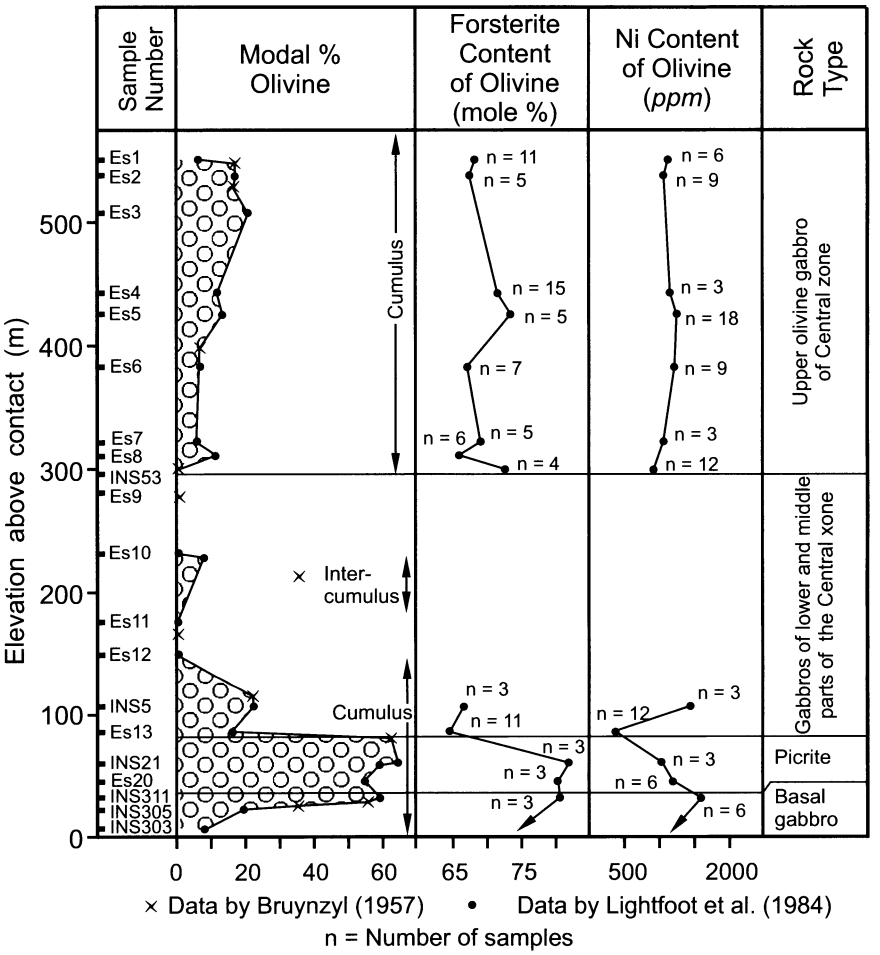


**Fig. 4.65.** Section through the Waterfall Gorge locality showing the variation in modal olivine and the forsterite and nickel contents of the olivines (after Lightfoot et al., 1984)

**Plagioclase and pyroxenes.** Compositional data for plagioclases and pyroxenes are illustrated in Figs. 4.67 and 4.68, respectively. The trends in compositional variation parallel the variation in olivine composition, although possible trends tend to be obscured by zoning (Lightfoot 1982). Given the evidence from other deposits that local assimilation of country

rocks is important in causing sulfide immiscibility, it is interesting to examine the Waterfall Gorge deposit from this viewpoint.

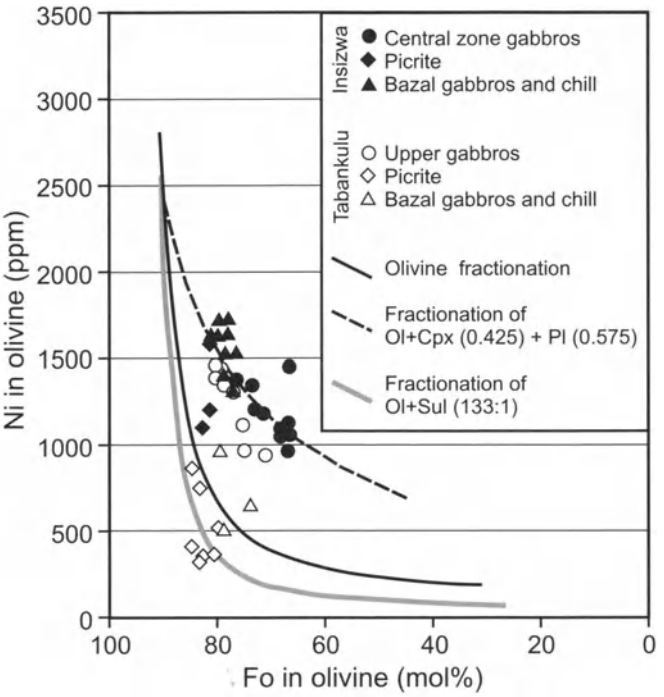


**Fig. 4.66.** Plot of Ni versus Fo content of olivines from the Insizwa and Tabankulu intrusions, along with model curves as discussed in the text

### 4.3.6 Evidence relating to contamination and ore genesis at Waterfall Gorge

**Field and petrographic data.** Examination of the contact relations at the old Insizwa mine workings provide evidence for (Lightfoot et al. 1984): (1) melting of footwall hornfels to form a granophyre melt, which was intruded into the basal olivine gabbro and now forms veins and segregations of granophyre which have sharp contacts with the surrounding gabbro; and (2) addition of $CO_2$ to the magma as a result of the metamorphism of footwall carbonate concretions. The latter is supported by the presence of wollastonite in the nodules, which would form by the reaction of $CaCO_3$ with $SiO_2$, releasing $CO_2$ into the magma. Petrographically, it can be seen that the contact phase of the olivine gabbro is enriched in quartz and K-feldspar within 50 cm of contact with masses of granophyre. However, direct field observation indicates that visible contamination is only detect-

able very close to the granophyre which is insufficient to account for most of the sulfide. Thus, should contamination be significant in stimulating sulfide segregation, it is more likely to have occurred prior to intrusion at depth and is unlikely to be due to localized incorporation of $CO_2$ or granophyre.

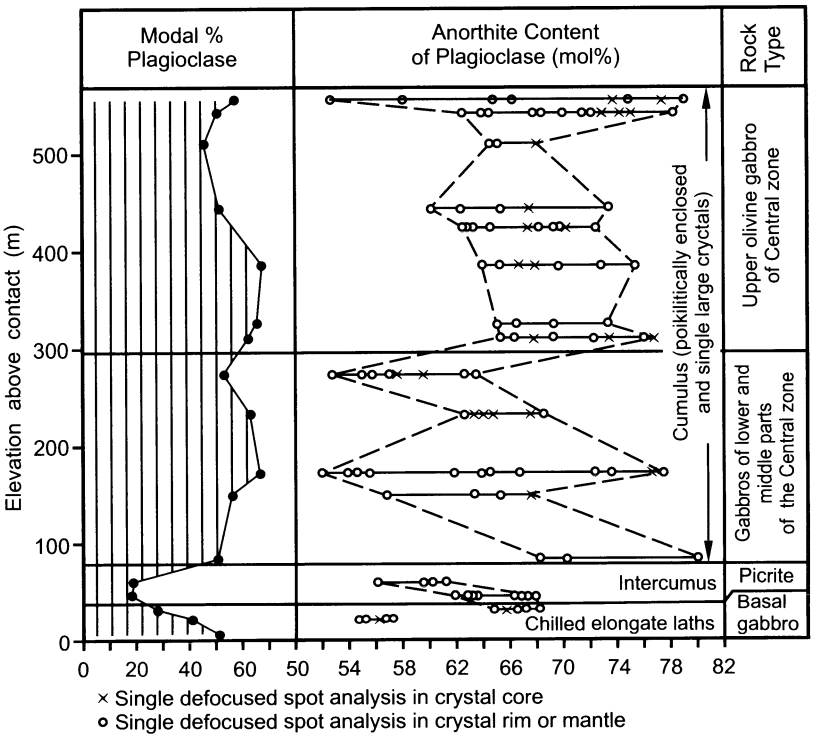


**Fig. 4.67.** Variation in the modal % plagioclase and anorthite content of plagioclase at the Waterfall Gorge locality. After Lightfoot at al. (1984)

**Geochemical evidence.** Whole-rock major, trace, and rare earth element data (Table 4.10) demonstrate that, with the exception of the sample collected within 50 cm of the contact, there is very little support for local contamination by wholesale or selective incorporation of elements into the magma. Sr and Nd isotope ratios were determined by Lightfoot et al. (1984) (Fig. 4.69) who noted that the high $^{87}Sr/^{86}Sr$ ratios of the granophyre, and the similarity between both the Sr and Nd isotopic compositions of the granophyre and adjacent hornfels are consistent with local melting of the latter as the origin of the former. They drew attention to the restricted Sr isotopic range of the basal gabbros, which characterize rocks with MgO contents ranging from 7 to 20 wt% MgO, and concluded that

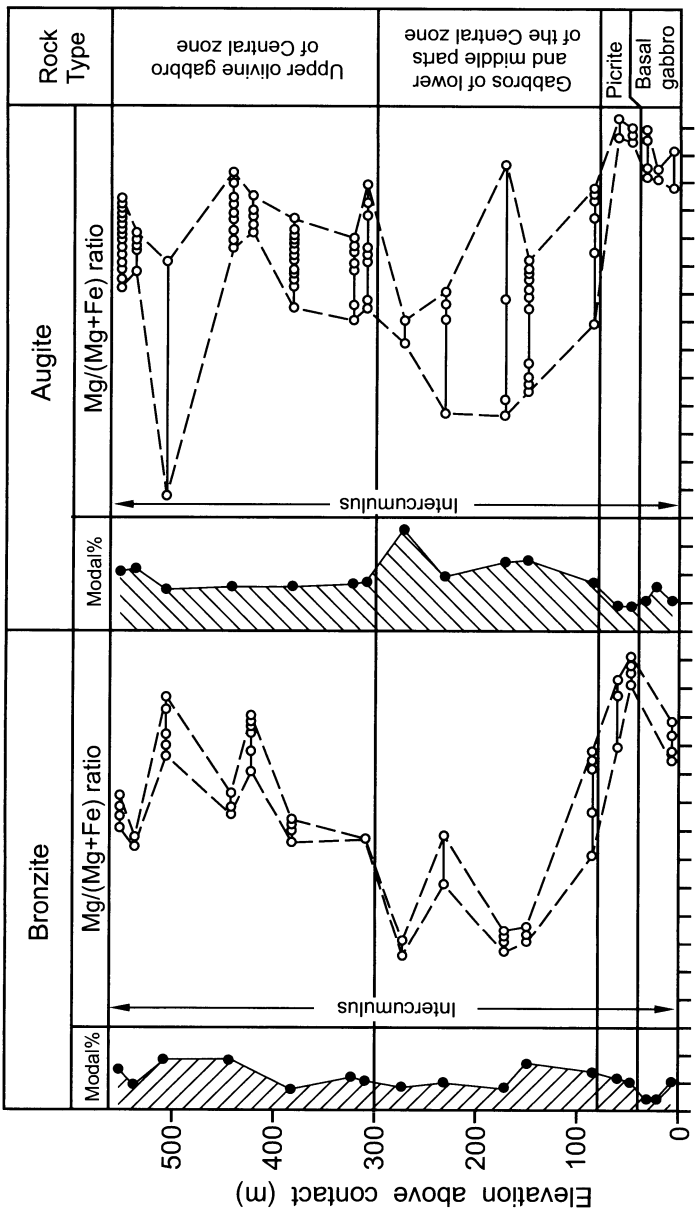


**Fig. 4.68.** Variation in modal percent and Mg/(Mg+Fe) ratio of ortho- and clinopyroxene at the Waterfall Gorge locality. After Lightfoot et al. (1984)

this is consistent with the variations in bulk composition being the result of accumulation of olivine in a low MgO magma without systematic changes in the Sr isotopic composition. Nevertheless, they emphasized that both the Insizwa and Tabankulu bodies are the result of repetitive influxes of magma that cannot be directly related by low pressure crystal fractiona-

tion. The different batches of magma appear to have had different evolutions prior to emplacement. These evolutions have involved different amounts of interaction with country rocks, which accounts for the spread in the $^{87}Sr/^{86}Sr$ ratios within a single intrusion.

Sulfur isotope ratios reported for the Waterfall Gorge occurrence by Jensen (1970) and Lightfoot et al. (1984) range from +4 to -4 $\delta^{34}S$, and thus provide no conclusive evidence as to the incorporation of country rock sulfur into the intrusion.

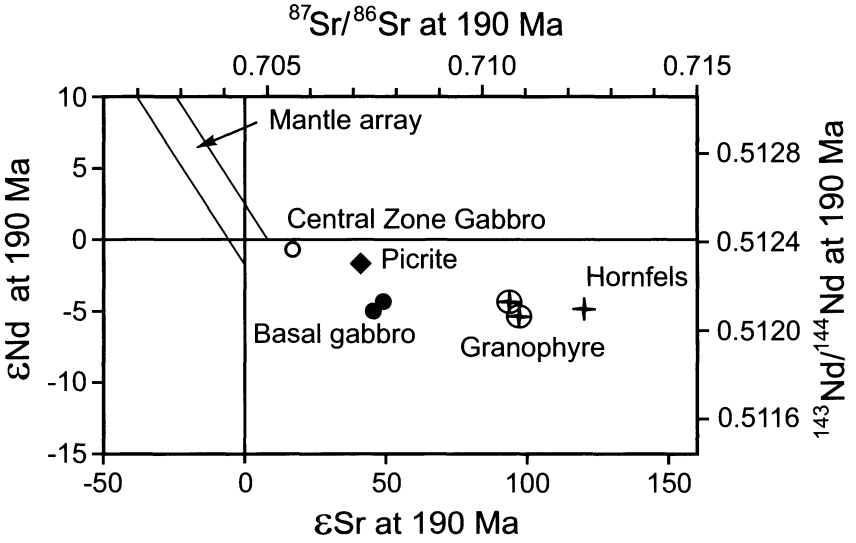


**Fig. 4.69.** Plot of variation in Sr and Nd isotope compositions in samples from Insizwa. Initial isotope ratios recalculated for 190 Ma. Modified after Lightfoot et al. (1984)

### 4.3.7 Conclusions for the Insizwa Complex

In conclusion, interaction with country rocks has clearly affected the Insizwa magmas, but this interaction has occurred before final emplacement. The Ni-depleted olivines that characterize some units of the Tabankulu body indicate that this interaction has resulted in sulfide immiscibility, and the removal of chalcophile metals. This occurred before final emplacement of the magma at Tabankulu. Thus emplacement would have involved the flow of sulfide-bearing magma along the Tabankulu magma conduit, which, by analogy with Noril'sk and Voisey's Bay (see Chapter 6), would make this a prospective environment for sulfide concentration.

## 4.4 Flood Basalt Provinces as Environments for Mineralization

Over the 1990's, flood basalt provinces (including the Keweenawan Province of Lake Superior, the Karoo of Southern Africa, the Parana of South America, the Coppermine River area of northern Canada) have come to be favorably regarded as prospective environments for Ni-sulfide mineralization, largely as a result of an appreciation of the size and richness of the Noril'sk ores. In the view of this author, the Noril'sk model includes some key components which are:

1. A large volume of relatively primitive (MgNo ~0.55) magma including olivine-phyric magma.
2. Evidence of chalcophile depletion in some of the magma.
3. A source of sulfur in the country rocks. If the sulfur source is oxidized (i.e. evaporitic), a reductant in the country rocks is also required.
4. A structural setting which exposes intrusions feeding the lavas. Deposits will not be found in the lavas themselves (any sulfides will burn off as $SO_2$ once the magma approaches the surface).
5. An intrusive environment in which the magma has had the opportunity to thermally erode and react with the country rocks (see Fig. 4.31 above).
6. Flow of magma that has already developed immiscible sulfides. This will enable hydrodynamic traps within the flow channel to cause the concentration of the sulfides.
7. Flow will also expose the sulfides to subsequent batches of magma using the same conduit as the batch from which the sulfides segregated initially. These later batches will be less depleted in chalcophile metals and, if brought into contact with sulfides trapped within the conduit system, will enrich them in chalcophile metals.

Referring to the Keweenawan Rift system, the intrusions of the Duluth complex have derived their sulfur from the Virginia formation, a sulfide-bearing graphitic slate that forms the footwall to much of the mineralized part of the complex. This formation is widespread, being present south of Lake Superior, where it is known as the Michigammi formation, and along the Canadian part of the north shore of Lake Superior, where it is referred to as the Rove slate. The Rove slate thins out northward in Canada, and is missing beneath much of the Keweenawan intrusive rocks of the Lake Nipigon area. The chances of finding a Noril'sk-type deposit where the Rove slate is absent are thought by this author to be significantly less than

where it is present. The deposits of the Duluth Complex are typically composed of weakly disseminated sulfides, and are thus non-economic. It is possible that much of the magma hosting these sulfides has not undergone a great deal of flow subsequent to the development of sulfide immiscibility. The key to finding rich concentrations in this environment would seem to be the identification of conduits where such flow has occurred.

The deposits of the Noril'sk region appear to this author to be due to a particularly fortunate sequence of events, not the least of which is the Kayerkan-Pyasino uplift, which has brought the keel forming the deepest part of the original volcanic basin to surface. It is along this keel that the Noril'sk and Talnakh intrusions occur. If it were not for this uplift, the deposits would still be buried by 3500 m of basalt.

# 5 Deposits of the Pechenga area, Russia

## 5.1 Regional geology

The deposits of the Pechenga area are associated with a major Early Proterozoic rift system that is referred to in Russia as the Pechenga-Varzuga sedimentary-volcanic belt (e.g. Smolkin et al. 1995a), and referenced as the Polmak – Opukasjarvi – Pasvik – Pechenga - Imandra/Varzuga - Ust'Ponoy greenstone belt in some of the Western literature (e.g. Melezhik et al. 1995). This belt traverses the northeastern part of the Fennoscandian shield for a distance of about 700 km (Fig. 5.1). It includes a series of depressions filled by Early Proterozoic sedimentary and volcanic rocks (the Polmak, Pasvik, Pechenga, Imandra-Varzuga and Ust'Ponoy Structures) that occur within a reactivated Archean basement, that is cut by dikes and granitoid intrusions in intervening areas. The belt developed at about 2.3 Ga, after the emplacement and partial erosion of a series of peridotite-gabbronoritic layered intrusions, (Mt. Generalskaya, Monchegorsk, Pana and Fedorova Tundra which are the equivalents of the 2.5-2.4Ga intrusions of Northern Finland – see Chapter 9). Rifting started in the eastern and central parts of the Imandra-Varzuga structure and propagated to the west. The greatest amount of spreading along the rift occurred in the Pechenga area (Smolkin 1992, 1993, 1997). Northwest-oriented compression took place from 1.75–1.70 Ga and the belt, especially the southern part, suffered intense deformation and greenschist to amphibolite metamorphism (Smolkin at al. 1995a).

Several Ni sulfide deposits and/or prospects occur within and adjacent to the Pechenga-Varzuga belt. They are concentrated primarily in and around the Pechenga and Imandra-Varzuga structures. Gorbunov et al. (1985a) subdivided them in two groups, according age and type of host intrusion.The first group (deposits of the Allarechka, NE Pechenga and Monchegorsk area – see Yakolev et al. 1981; Gorbunov et al. 1985b) are related to the Early Karelian (~2.5 Ga) layered intrusions of Mt Generalskaya type, that consist of peridotite, pyroxenite and gabbronorite.

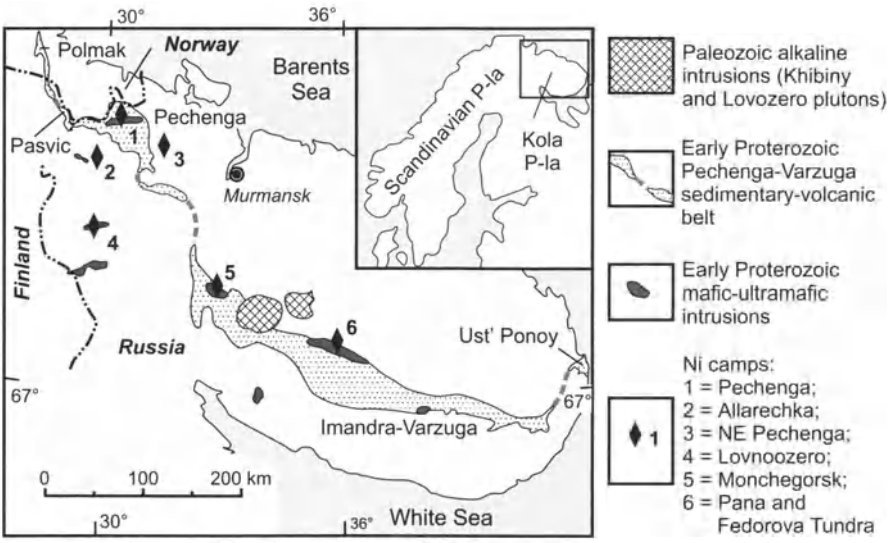


**Fig. 5.1.** Schematic geological map of the Pechenga Structure. Simplified after Papunen and Gorbunov (1985) with modified legend

The intrusions hosting these deposits occur within faults, either at the margins of greenstone belts (Monchegorsk) or in gneisses forming the basement to the belt (Allarechka and NE Pechenga). The second group comprises the Late Karelian (about 2.0 Ga) deposits that are associated with wehrlite-pyroxenite-gabbro intrusive rocks and the related ferropicritic volcanic suite. The second group, particularly those at Pechenga, are the more important and are described below.

## 5.2 Geology of the Pechenga Structure

The Pechenga Structure is subdivided into two zones on the basis of structural type: the North Pechenga (or Northern) zone is a monocline, complicated by steep reverse faults and low angle thrusts, while the South Pechenga (Southern) zone is very highly deformed (Fig. 5.2). The Northern zone is composed of earlier and the Southern zone of later sedimentary-volcanic rocks (Smolkin et al. 1995a). The Poritash fault forms the boundary between the zones. It trends NW, concordant with the regional strike of this part of the rift belt. Vibroseismic surveys have shown that the fault dips steeply SW at surface and has shallower dips at depth (Pozhilenko et al., 1997). In the Northern zone the majority of the large faults are sub-perpendicular or diagonal to the regional strike, but are mainly

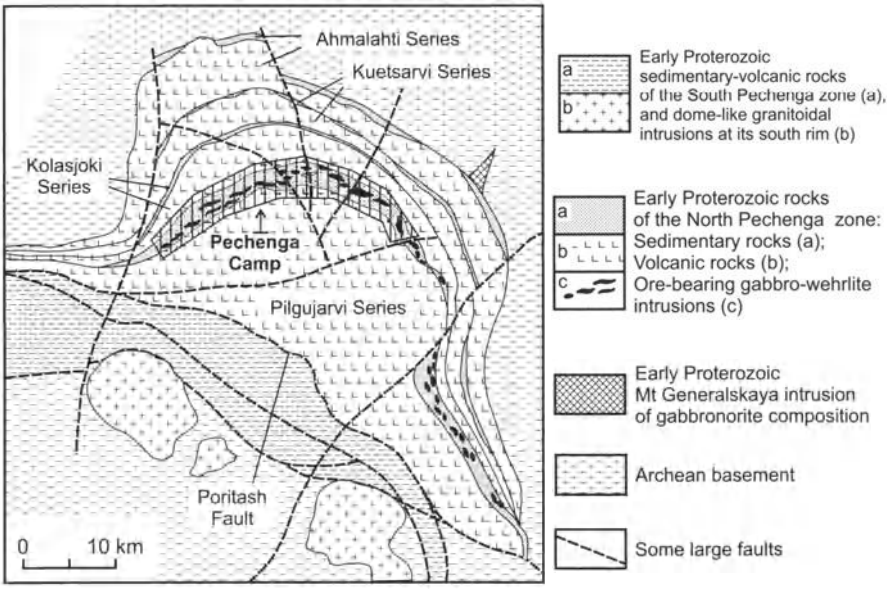


**Fig. 5.2.** Subdivision of sedimentary-volcanic and intrusive formations of the Pechenga and Pasvic Structures with indication of ages for magmatic rocks in Ga. After Papunen and Gorbunov (1985)

sub-parallel to strike in the Southern zone. Large dome-like granitoid bodies have intruded along the southern margin of the structure.

In the early Russian stratigraphic scheme (Geology of USSR 1958), the sedimentary-volcanic rocks of the Pechenga Structure were mistakenly regarded as Paleozoic in age and were subdivided into five groups. Four of these groups were recognized as constituting the Northern zone and each comprised a sedimentary-volcanic cycle, ranging from sediments at the base upward into volcanic rocks. All of the rocks of the Southern zone were included in the 5th group. Once the early Proterozoic age of the rocks was recognized, the stratigraphic succession underwent many stages of revision (see the overview in Smolkin et al. 1995a, b). In the mid-1990s, at the time of the preparation of the International Geological Map of Fennoscandia, the Norwegian working group (Melezhik et al. 1995) developed a legend for the Pasvic and Pechenga areas that is shown in Fig. 5.3. All Early Proterozoic rocks were combined as the Petsamo Supergroup. This was divided into two groups: the North Pechenga (which included all formations of the Northern Zone) and the South Pechenga (which included all rocks of the Southern Zone). Russian geologists (e.g. Smolkin et al. 1995a,b) did not accept this stratigraphy and developed an alternative

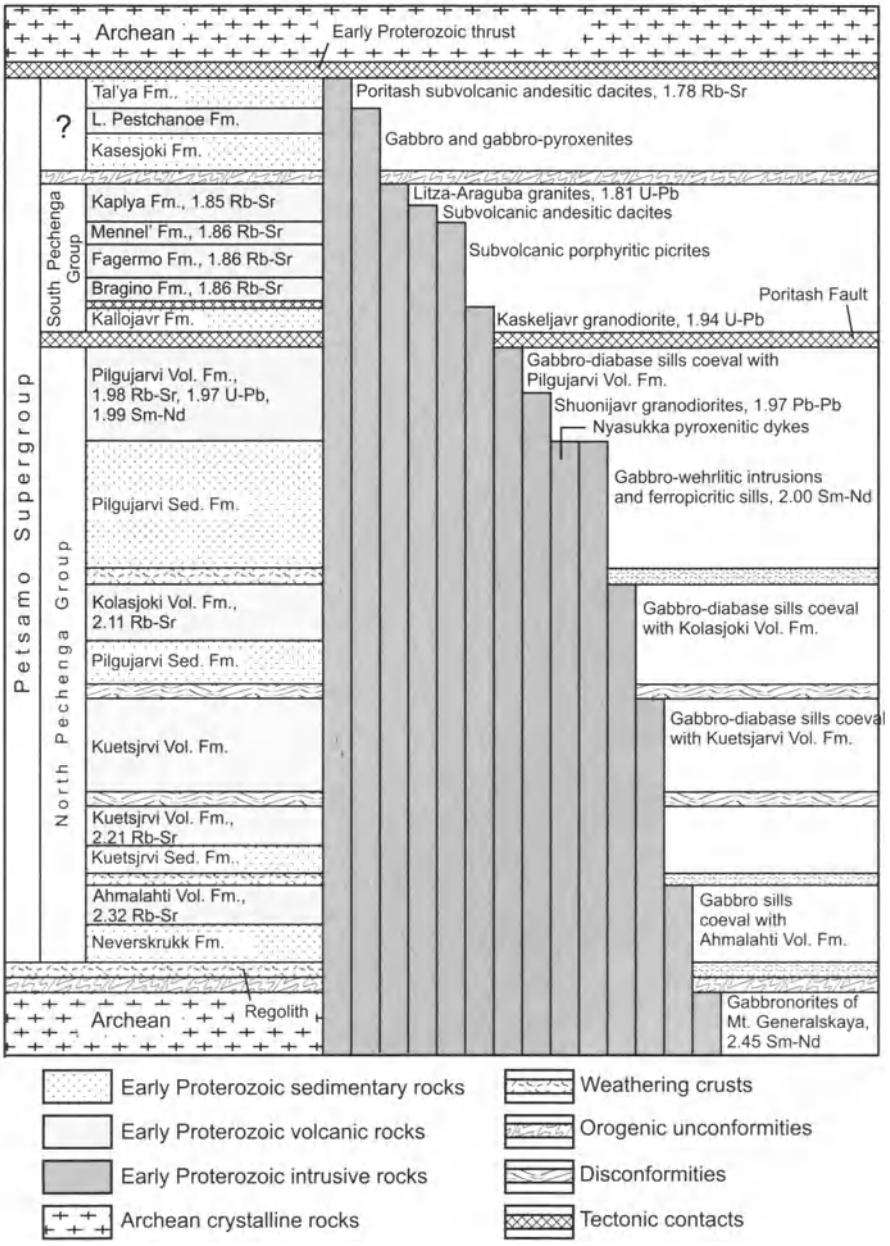


**Fig. 5.3.** Vertical stratigraphic sections showing the interval intruded by gabbro-wehrlitic intrusions both at Pasvic and Pechenga. After Melezhik at al. (1995)

**Table 5.1.** Correlation of some stratigraphic schemes of the North Pechenga structure-facial zone

| Kuryleva (Geology of USSR, 1958) | Melezhik et al. (1995) | Smolkin et al. (1995) | |
|---|---|---|---|
| 4-th sedimentary-volcanic group | Pilgujarvi Volcanic Formation* | Pilgujarvi Series | Suppvaara Suite. Basalts (lavas and tuffs). Up to 1700 m. |
| | | | Matert Suite. Basalts, subordinate ferropicrites (lavas, tuffs and lava breccia); Felsic strata. Up to 3000 m. |
| | Pilgujarvi Sedimentary Formation* | | Lammas Suite. Tuffs and lava breccia of ferropicrites and infrequent basalts. 10-600 m. |
| | | | Zhdanov Suite. Aleuro-psammitic carbonaceous sulfide-bearing shales, tuffs, tuffites and lava breccia of basalts and ferropicrites. 800-1100 m. |
| 3-rd sed.-volc. group | Kolasjoki Volcanic Formation* | Kolosjoki Series | Zapolyarny Suite. Basalts (lavas, tuffs and hyaloclastics), tuff agglomerates, with schistose ferropicrite at base of the Suite. 1500-2000 m. |
| | Kolasjoki Sedimentary Formation* | | Luchlompolo Suite. Red terrigenous sedimentary rocks, schists. 80-150, seldom up to 400 m. |
| 2-nd sed.-volc. group | Kuetsarvi Volcanic Formation* | Kuetsarvi Series | Orshoaivi Suite. Basalts (lavas, tuffs), subordinate trachyandesibasalts and dacites. 400-600 m |
| | | | Pirttijarvi Suite. Trachyandesibasalts and trachybasalts, rare picrobasalts. 150-1000 m. |
| | Kuetsjarvi Sedimentary Formation* | | Kuvernerinjoki Suite. Carbonate rocks, quartzites. 0-400 m. |
| 1-st sed.-volc. group | Ahmalahti Volcanic Formation* | Ahmalahti S. | Majarvi Suite. Andesibasalts, subordinate picrobasalts, dacites and rhyolites. 100-1600 m. |
| | Neverskrukk Formation** | | Televi Suite. Conglomerates, greywacke gritstones and metapsammites. 0-250 m. |

*In earlier work by Zagorodny et al. (1964) these Formations are described as Sub-suites
**This Formation is subdivided by Melezhik et al. (1995) in the Pasvic Depression

scheme for the Northern Zone of the Pechenga Structure which is given in Table 5.1. The Russian scheme for the Southern Zone is similar to that given in Fig. 5.3, except that units that western geologists term formations are referred to as suites in the Russian scheme. In this volume the Russian stratigraphic scheme has been adopted (Smolkin et al.1995a).

The combined thickness of the sedimentary-volcanic rocks of the North Pechenga Zone exceeds 10,000 m. The Televi conglomerate and sand-

stones lie at base of the sequence. They are overlain by the Majarvi volcanics of andesibasaltic to dacitic composition in which pillow lavas dominate. These are overlain in turn by quartzites, dolomites, red terrigenous rocks and lavas of subalkaline basaltic and andesibasaltic, rarely of normal basaltic compositions, belonging to the Kuvernerinjoki, Pirtijarvi, Orshoaiviand and Luchlompolo Suites. Rocks of the lower part of the sequence, up to the sedimentary Luchlompolo Suite, accumulated under shallow marine or continental conditions. The overlying Zapolyarny Suite is composed of massive and pillowed lavas, tuffs and hyaloclastics of basaltic composition that probably formed either under deep marine conditions or in a deep depression such as the Red Sea rift. A schistose rock of ferropicritic composition (likely former lava) occurs at the base of the Zapolyarny Suite.

The Zhdanov Suite overlies the Zapolyarny and consists of metamorphosed aleurolites, sandstones and shales, and tuffs and tuffites of basaltic, rarely ferropicritic composition. This Suite is not uniform, but consists of several packets of rocks that show different compositions and interrelationships between the sedimentary and tuffaceous components. Characteristic features of these rocks include their enrichment in sulfide and carbonaceous material, and locally in carbonate and phosphate. Some geologists have suggested that the sediments of the Zhdanov Suite accumulated under shallow, near-shore conditions (e.g. Predovsky et al. 1974); whilst others regard them as deep marine in origin. The overlying Lammas Suite is composed mainly of ferropicritic tuffs and tuffites with subordinate strongly schistose lava flows that contain 8–11 wt% MgO, 650-1600 ppm Cr, 279-850 ppm Ni. Granitoidal boulders occur in the tuffs, supposedly deposited from floating ice.

Tholeiitic basalts predominate in the overlying Matert Suite. They are close to MORB in REE compositions (see Fig. 5.7 below). However they, as well as the Zapolyarny basalts, differ from MORB in their contents (and ratios) of other incompatible elements (Smolkin 1992; Hanski and Smolkin 1989, 1995). Mints et al. (1996) regard them as being close to T- and E-MORB in composition. Ferropicrites and tufogenic-sedimentary rocks (carbonaceous, sulfide-bearing) are present in the Matert Suite in small amounts. The basalts and ferropicrites occur mainly as lavas with massive, pillowed and variolitic morphologies. Ferropicritic lavas are developed in the Matert at five stratigraphic levels. They form rather thick layered flows with caps of olivine- and pyroxene spinifex (Smolkin 1992); the spinifex textures are similar to those described by Arndt et al. (1977) in Archean komatiites. A marker horizon comprising felsic rocks occurs 700-800 m above base of the Matert Suite. These rocks are very rich in $SiO_2$ (up to 80–87 wt%), Zr (up to 740 ppm), and LREE and show very variable

$Na_2O/K_2O$ ratios (0.01–7). Their origin is not clear. Zagorodny et al. (1964) and Predovsky et al. (1974) considered them as tuffs and lavas of quartz porphyry. Smolkin (1992) described them as rocks, formed as a result of the underwater weathering of ferropicritic volcanics. The Suppvaara Suite that crowns sequence of the North Pechenga Zone, is composed of basaltic lavas and tuffs.

The thickness of the sedimentary-volcanic rocks in the South Pechenga Zone is 2500–3000 m. The most northern Kallojavr Formation is composed of metamorphosed tuffaceous rocks, carbonaceous and carbonaceous-carbonate shales, and metabasalts. Farther south metabasalts with subordinate andesibasalts and picrobasalts belonging to the Bragino, Fagermo and Mennel formations are developed. They are followed by the Kaplya Formation, composed of andesite-dacite-rhyolite volcanics. Sericite shales (primary volcanoclastic rocks) and metatuffaceous rocks of the Kasesjoki Formation occur along the southern boundary of the Pechenga Structure. Mints et al. (1996) regard the rocks of the Bragino, Fagermo and Mennel formations as being close to T-MORB tholeiite in composition, while the rocks of the Kaplya Formation could have formed in an island-arc environment.

Numerous intrusions that are comagmatic with the volcanic formations occur in the Pechenga Structure (see Fig. 5.3). Gabbro and gabbro-diabase sills coeval with mafic lavas of all four sedimentary-volcanic cycles are predominant amongst them. Intrusions comagmatic with the Matert ferropicritic lavas are also widely developed. They form ferropicritic sills and olivine ferrodolerite, peridotite and olivine gabbro dykes (Smolkin 1992; Smolkin et al. 1995a), as well as layered gabbro-wehrlitic intrusions that host the Ni-Cu mineralization. Ferropicritic sills and ferrodoleritic dykes cut shales of the Zhdanov Suite. Dykes of peridotite and olivine gabbro form a system of sub-parallel, thick bodies at the northern rim of the Pechenga Structure. The majority of the ore-bearing gabbro-wehrlitic intrusions occur in the sedimentary rocks of the Zhdanov Suite. Only few (containing insignificant amounts of mineralization) occur in the upper part of the volcanic Zapolyarny Suite.

The Zhdanov Suite that controls localization of the ore bearing intrusions, was often referred to as the "Productive Formation" in earlier literature. This suite is present in both the Pechenga and nearby Pasvic Structures, but it is much thicker at Pechenga. The Lammas Suite occurs in places between the Zhdanov and Matert Suites at Pechenga but is absent at Pasvic (Fig. 5.4).

The gabbro-wehrlitic intrusions occur throughout the Zhdanov Suite in the Pechenga Structure (Fig. 5.2) and are also found also at Pasvic (Fig. 5.4). However, intrusions hosting significant mineralization are

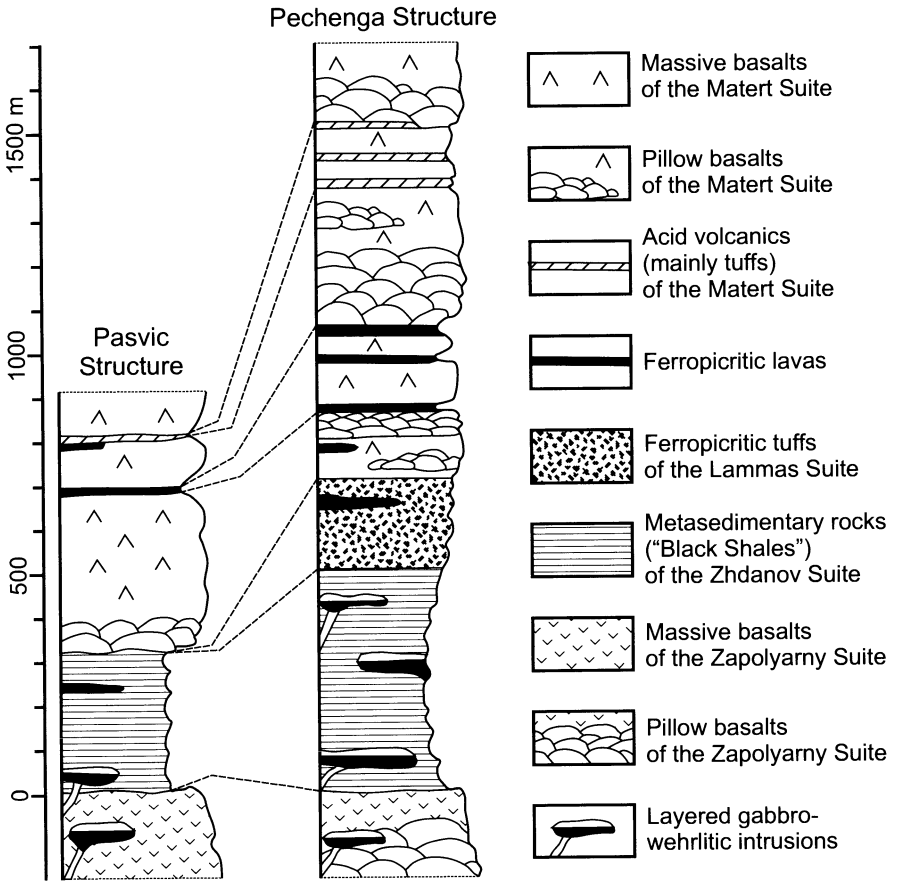


**Fig. 5.4.** Vertical stratigraphic sections showing the interval intruded by gabbro-wehrlitic intrusions both at Pasvic and Pechenga. After Melezhik at al. (1994) with modified legend

known only in the central part of the Pechenga Structure, where the Zhdanov Suite reaches its maximal thickness and is particularly rich in sedimentary sulfide. This area corresponds to the Pechenga Ni-Cu Camp (Fig. 5.2), that is referred to as the "Pechenga Ore Field" in the Russian literature.

Two centers of ferropicritic eruption, the Kaula and Pilgujarvi centers have been defined, one in the western and the other in the eastern part of the Pechenga Camp (Fig. 5.5). They developed after accumulation of the Zhdanov Suite and before deposition of the Lammas Suite (Skuf'in and Fedotov 1989; Melezhik and Sturt 1994). In the Kaula center the thickness of the rocks interpreted as eruptive is about 100 m. Ferropicritic agglomerates lie at the base. They contain angular fragments of underlying

rocks including black shales and diagenetic carbonate concretions of the Zhdanov Suite, and basalts, phosphorous-bearing limestones and partially melted and recrystallized cherts that are chemically similar to units throughout the underlying sequence. A volcanic breccia with a matrix of ferropicritic lapilli tuff that grades upward into black shales of ferropicritic composition overlies the centre. The Pilgujarvi center is composed of a 600 m-thick pile of ferropicritic lavas and tuffs.

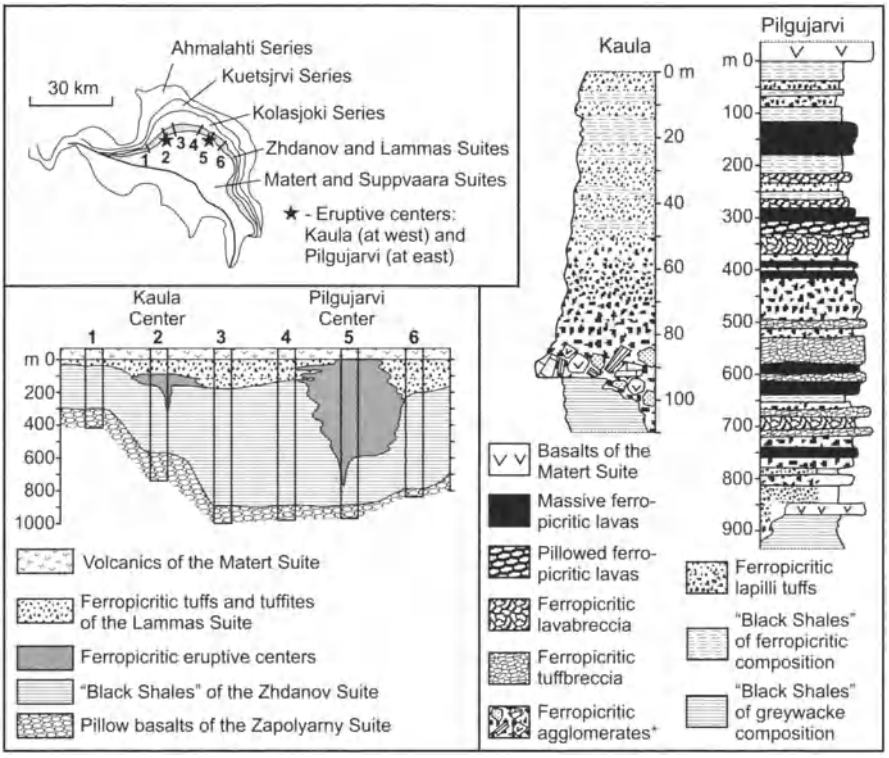


**Fig. 5.5.** Locations and lithological sections of the Kaula and Pilgujarvi centers of ferropicritic volcanism. After Melezhik et al. (1994) with modified legend

## 5.3 Geochemistry of Ferropicritic Rocks

Predovosky et al. (1971) showed on the basis of bulk composition, that although the ferropicritic lavas alternated in sequence with tholeiitic basalts, they were independent genetically and related to a different mantle source.

Hanski and Smolkin (1989) were the first to use the term "ferropicrite" in referring to the magnesian volcanic rocks, pointing out that they contained 15-16 wt% of FeOT. They are characterized by high $TiO_2$ and low $Al_2O_3$ (Table 5.2), resulting in low $Al_2O_3/TiO_2$ and $Al_2O_3$/(FeO/FeO+MgO) ratios (Fig. 5.6). The ferropicrites are enriched in incompatible elements and have strongly fractionated REE patterns: $La/Yb_N$ ratios of about 10 (Fig. 5.7), which distinguishes them from komatiites, and also from the basalts with which they are spatially associated.

Besides the Pechenga and Pasvic regions, ferropicritic rocks and comagmatic intrusions have been found in the western part of the Imandra-Varzuga Structure (Smolkin and Dayn 1985), which attests to a large, Fe-enriched source underlying the Kola Peninsula at that time.

## 5.4 Comagmatic Relationship between the Ferropicritic Volcanic rocks and the Ore-bearing Gabbro-wehrlite Intrusions

The conclusion that the ferropicritic volcanics and ore-bearing gabbro-wehrlite intrusions are comagmatic is based on mineralogical, geochemical and geochronological data.

The ferropicritic volcanic rocks, sills and dykes, as well as the differentiated gabbro-wehrlite intrusions have a very similar and distinctive mineralogy which includes fayalitic olivine; titaniferous augite, amphibole (kaersutite), and biotite; anorthitic plagioclase; and titanium-rich chromite and ulvospinel (found in ferropicrites only) along with titanomagnetite and ilmenite (Smolkin 1977, 1992; Smolkin et al. 1995a).

Similarities between the major element contents of the lavas and intrusions are illustrated by Table 5.2. In addition, both lavas and intrusions are enriched in incompatible elements and have similar isotopic characteristics with εNd of about +1.5 and $^{87}Sr/^{86}Sr$ ratios of about 0.7032 (Smolkin et al. 1995a).

Hanski et al. (1990) showed that the ferropicrites and gabbro-wehrlites have similar ages of about 2.0 Ga on the basis of Pb-Pb, Sm-Nd, Rb-Sr and

**Table 5.2.** Bulk composition of ferropicrites and of differentiated gabbro-wehrlite intrusions, Pechenga and Pasvik (after Melezhik et al. 1994)

| | Ferropicrites | | | | | | | Intrusions | | | |
|---|---|---|---|---|---|---|---|---|---|---|---|
| | 1 | 2 | 3 | 4 | 5 | 6 | 7 | 8 | 9 | 10 | 11 |
| $SiO_2$ | 43.86 | 43.71 | 45.97 | 44.96 | 46.29 | 43.11 | 41.88 | 41.14 | 43.03 | 45.13 | 38.53 |
| $TiO_2$ | 1.99 | 1.83 | 2.57 | 2.31 | 1.99 | 2.01 | 2.99 | 1.81 | 2.07 | 2.07 | 1.76 |
| $Al_2O_3$ | 6.97 | 8.12 | 7.68 | 6.39 | 7.18 | 7.73 | 6.81 | 6.22 | 6.37 | 7.21 | 3.61 |
| $Fe_2O_3$ | 3.09 | 3.02 | n.d. | n.d. | n.d. | 17.63 | 3.33 | 7.33 | n.d. | n.d. | 18.26 |
| FeO | 11.83 | 12.24 | 14.99 | 15.73 | 15.23 | n.d. | 12.83 | 9.96 | 17.85 | 16.77 | n.d. |
| MnO | 0.17 | 0.18 | 0.21 | 0.21 | 0.23 | 0.21 | 0.18 | 0.21 | 0.219 | 0.22 | 0.21 |
| MgO | 14.79 | 15.28 | 17.39 | 19.92 | 18.67 | 15.04 | 15.61 | 19.33 | 22.61 | 18.66 | 23.07 |
| CaO | 11.35 | 9.06 | 10.51 | 9.47 | 9.16 | 6.17 | 10.68 | 6.53 | 5.95 | 8.96 | 4.09 |
| $Na_2O$ | 0.29 | 0.39 | 0.17 | 0.41 | 0.32 | 0.72 | 0.77 | 0.93 | 0.91 | 0.27 | 0.02 |
| $K_2O$ | 0.11 | 0.19 | 0.07 | 0.07 | 0.18 | 0.19 | 0.65 | 0.43 | 0.33 | 0.09 | 0.03 |
| $H_2O+$ | 4.69 | 4.76 | n.d. | n.d. | n.d. | n.d. | n.d. | 5.09 | n.d. | n.d. | n.d. |
| $P_2O_5$ | n.d. | 0.31 | 0.24 | 0.22 | 0.32 | 0.17 | n.d. | n.d. | 0.11 | 0.19 | 0.16 |
| $S_{total}$ | 0.04 | 0.11 | n.d. | n.d. | n.d. | 0.11 | 0.37 | 0.31 | n.d. | n.d. | 0.04 |
| $CO_2$ | 0.52 | 0.39 | n.d. | n.d. | n.d. | n.d. | n.d. | 0.36 | n.d. | n.d. | n.d. |
| Cr ($Cr_2O_3$) | n.d. | 0.094 | (0.10) | (0.20) | (0.15) | (0.36) | n.d. | n.d. | (0.36) | (0.28) | (0.22) |
| Ni (NiO) | 0.11 | 0.064 | (0.1) | (0.11) | (0.27) | 0.11 | (0.06) | 0.15 | (0.21) | (0.15) | 0.16 |
| Cu | 0.02 | n.d. | n.d. | n.d. | n.d. | 0.02 | n.d. | 0.03 | n.d. | n.d. | 0.01 |
| Co | 0.01 | n.d. | n.d. | n.d. | n.d. | 0.01 | n.d. | 0.01 | n.d. | n.d. | 0.01 |
| LOI | n.d. | n.d. | n.d. | n.d. | 6.31 | 5.68 | 4.02 | n.d. | n.d. | n.d. | 9.24 |

1 = average of picrites, Pechenga, n = 7 (Predovosky et al., 1971); 2 = average of picrites, Pechenga, n = 10 (Predovosky et al., 1987); 3 = average lower chilled margin of picritic flow, Pechenga, n = 4 (Brugmann et al, 1991); 4 = weighted average of picritic flow, Pechenga, n = 16 (Brugmann et al, 1991); 5 = average of picrites Pechenga, n = 68 (Brugmann et al, 1991); 6 = average of ferropicrites, Pasvik, n = 3 (Melezhik and Sturt, 1994); 7 = average of Ni-bearing intrusions, Pechenga (Papushis, 1952); 8 = weighted average of Ni-bearing intrusions, Pechenga, n = 88 (Predovosky et al., 1971); 9 = weighted average of Ni-bearing intrusions, Pechenga, n = 163 (Brugmann et al, 1991); 10 = average of lower chilled margins of Ni-bearing intrusions, Pechenga (Brugmann et al., 1991); 11 = average of differentiated intrusions, Pasvik, n = 33 (Melezhik and Sturt, 1994)
*n.d.* not determined

Re-Os isotopic measurements. Recently, an U-Pb age of 1.980±0.010 Ga has been obtained for the intrusive gabbroic rocks (Smolkin and Bayanova 1999), a Sm-Nd age of 1.980±0.040 Ga for the ferropicritic volcanic rocks (Smolkin et al. 1995a), and a Sm-Nd age of 1.956±0.020 Ga for the peridotite and olivine gabbro dykes (Huhma et al. 1996).

## 5.5 Gabbro-wehrlite intrusions

Zak et al. (1982) reported that 226 discrete gabbro-wehrlite intrusions were known in the Pechenga Ore Field at beginning of 1980, and that 25 of these contained magmatic sulfide deposits and ore occurrences.
As discussed above, the majority of the intrusions occur in the tuffites and sediments of the Zhdanov Suite. Some bodies occur in volcanic rocks of the Zapolyarny Suite where their position is controlled by the Kolasjoki Fault (Fig. 5.8). The intrusions were emplaced over an interval of time, the earliest are being those that cut the Zapolyarny Suite (Smolkin et al. 1995a). Smolkin (personal communication to the author, 2002) believes that the richest mineralization is related to the bodies that formed during the final stages of ferropicritic volcanism.

The gabbro-wehrlite intrusions outcrop over an area of 19.1 $km^2$ in the Pechenga Camp that amounts to 25 % of the area underlain by the host tuffites and sediments of the Zhdanov suite. The intrusions vary from 10 to 600 m in thickness and from 100 to more than 3000 m along strike. Some have been shown to exceed 1000 m down-dip . Bodies with thicknesses of 10–50 m and strike lengths of 100–500 m predominate (Smolkin et al. 1995a). The intrusions are lens-like in form and dip steeply SW in conformity with the country rocks (see cross-section in Fig. 5.8). The outlines of many bodies are complicated by thrusts and transverse steeply-dipping reverse faults.

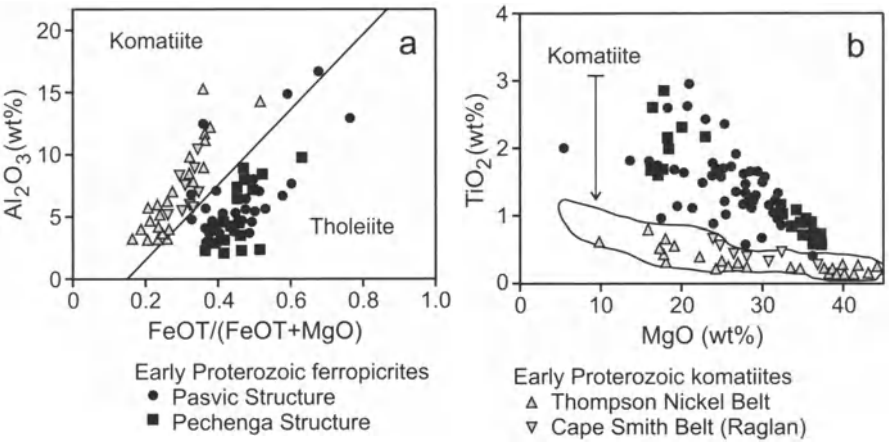


**Fig. 5.6.** Ferropicritic rocks from Pasvic and Pechenga and Early Proterozoic komatiites from Canada plotted on diagrams of (a) $Al_2O_3$ versus FeOT/(FeOT+MgO) and (b) $TiO_2$ versus MgO. Melezhik et al. (1994)

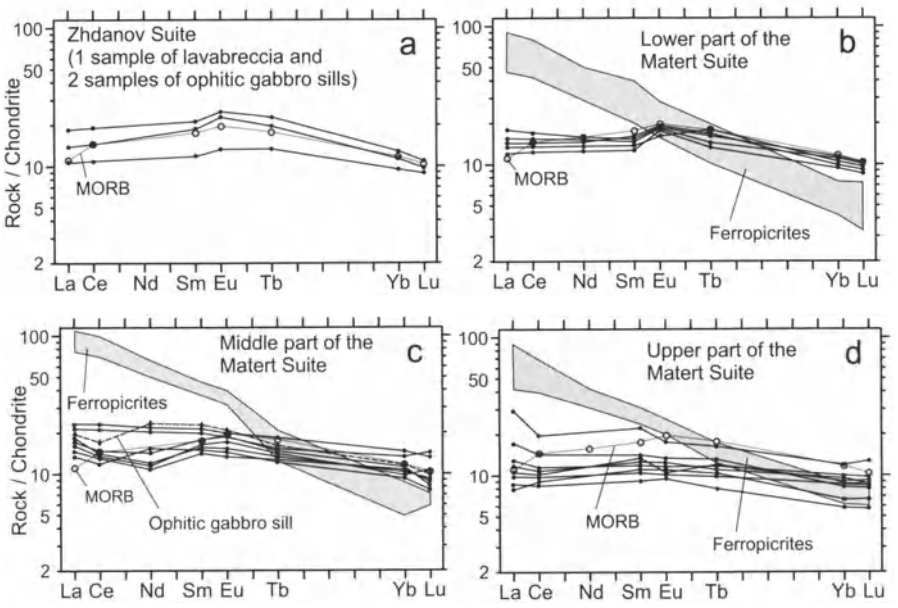


**Fig. 5,7.** REE profiles normalized to Chondrite for basaltic and ferropicritic rocks of the Zhdanov and Matert Suites in comparison with MORB basalts. Dots in plots b, c and d correspond to Pechenga basalts. After Smolkin et al. (1995)

In vertical profile, the intrusions are characterized by a basal chill zone, composed of metamorphosed fine-grained clinopyroxenite and olivine clinopyroxenite. Olivine cumulates overlie this and are overlain in turn by a thin clinopyroxenite layer, that in places contains layers of titanomagnetite. Massive, vari-textured and banded gabbros overlie the clinopyroxenite, and, in some of the thickest intrusions are overlain by orthoclase gabbro. The upper endocontact zone is heterogeneous, consisting of quartz diorite, diorite and gabbro cut by clinopyroxenite veins (Smolkin et al. 1995a). The average chemical compositions of the principal rock types and average weighted compositions of the intrusions are given in Table 5.3. Many of the intrusions consist only of ultramafic rocks.

The principal primary minerals of the intrusions, in the order of their crystallization, are chromium spinel, olivine, clinopyroxene, titanomagnetite and plagioclase. Orthopyroxene is never present. In many places the intrusive rocks are strongly altered with peridotite replaced by serpentinite and talc-chlorite-carbonate-serpentine and pyroxenite by chlorite-actinolite, while the gabbros are strongly saussuritised.

The largest of the gabbro-wehrlite intrusions is the Pilgujarvi body (Fig 5.9) in the eastern part of the Pechenga Camp, close to the eruptive center

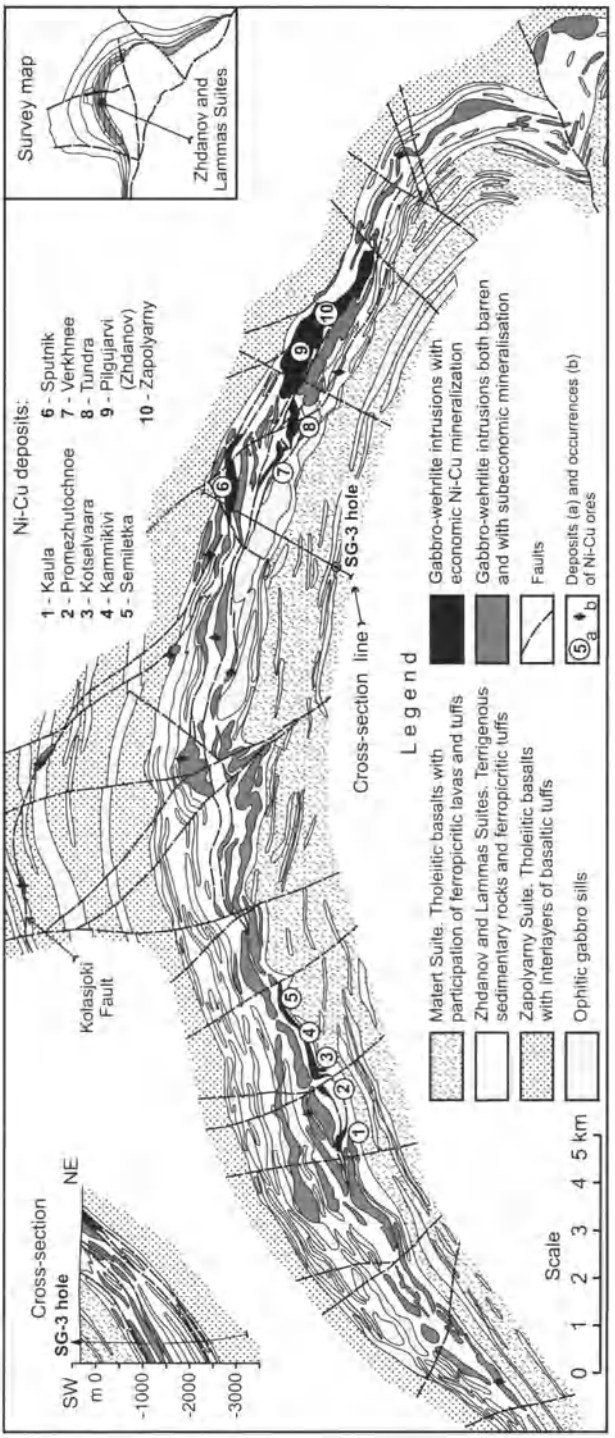


**Fig. 5.8.** Schematic geological map of the Pechenga Camp (Ore Field). Simplified after Gorbunov et al. (1999) with modified legend. Hole SG-3 is the Kola deep drill hole (12 km)

**Table 5.3.** Average chemical compositions of main rock types and average weighted compositions of the gabbro-wehrlite intrusions (after Smolkin 1992)

| | 1 | 2 | 3 | 4 | 5 | 6 | 7 | 8 | 9 | 10 |
|---|---|---|---|---|---|---|---|---|---|---|
| n | 51 | 42 | 19 | 25 | 12 | 21 | 12 | 23 | 163 | 290 |
| $SiO_2$ | 36.40 | 37.13 | 39.53 | 46.25 | 40.31 | 44.56 | 49.65 | 44.70 | 42.70 | 42.85 |
| $TiO_2$ | 0.72 | 0.95 | 1.35 | 1.49 | 4.45 | 3.66 | 2.58 | 2.05 | 2.05 | 1.42 |
| $Al_2O_3$ | 2.46 | 3.16 | 4.58 | 4.59 | 6.52 | 11.90 | 13.49 | 7.13 | 6.32 | 6.66 |
| $Fe_2O_3$ | 9.16 | 8.42 | 6.66 | 2.60 | 5.91 | 4.20 | 3.01 | 3.46 | 3.85 | 4.81 |
| FeO | 7.41 | 8.58 | 10.74 | 10.31 | 14.61 | 11.65 | 10.68 | 13.51 | 14.25 | 11.45 |
| MnO | 0.20 | 0.20 | 0.19 | 0.17 | 0.19 | 0.18 | 0.19 | 0.22 | 0.20 | 0.15 |
| MgO | 32.09 | 28.20 | 23.02 | 15.73 | 10.18 | 6.66 | 3.30 | 18.48 | 22.44 | 22.76 |
| CaO | 1.22 | 2.65 | 5.13 | 14.90 | 13.44 | 9.93 | 6.85 | 8.87 | 5.91 | 7.44 |
| $Na_2O$ | 0.77 | 0.10 | 0.13 | 0.46 | 0.63 | 2.37 | 4.05 | 0.27 | 0,89 | 1.33 |
| $K_2O$ | 0.11 | 0.11 | 0.09 | 0.24 | 0.50 | 0.60 | 1.90 | 0.09 | 0.34 | 0.23 |
| $P_2O_5$ | 0.04 | 0.07 | 0.11 | 0.10 | 0.11 | 0.15 | 0.43 | 0.19 | 0.11 | 0.03 |
| $H_2O+$ | 8.00 | 9.00 | 6.24 | 2.40 | 2.50 | 3.37 | 2.94 | | | |
| $CO_2$ | | 0.29 | 0.65 | 0.27 | 0.11 | 0.22 | 0.31 | | | |
| S | | 0.33 | 0.40 | 0.27 | 0.48 | 0.40 | 0.13 | 0.55 | 0.37 | 0.40 |
| Cr | 3490 | 3420 | 2670 | 1370 | 410 | 70 | 70 | 1915 | 2460 | 1985 |
| V | 120 | 170 | 170 | 170 | 810 | 230 | 60 | 220 | 220 | 220 |
| Ni | 2820 | 2200 | 2800 | 500 | 800 | 200 | 200 | 1140 | 1650 | 1650 |
| Co | 190 | 200 | 200 | 100 | 70 | 90 | 50 | 120 | 190 | 190 |
| Cu | 320 | 200 | 1200 | 200 | 80 | 100 | 40 | 340 | 190 | 190 |

*n* number of samples. Concentrations of major elements and S are in wt%, ore elements in ppm. Compositions 8–10 are recalculated water free.
1 = serpentinized wehrlite, rich in original olivine; 2 = serpentinized wehrlite; 3 = carbonate-talc-chlorite serpentinite; 4 = amphibolitic olivine clinopyroxenite; 5 = amphibolitic plagioclinopyroxenite; 6 = saussuritic gabbro; 7 = orthoclase gabbro; 8 = quenched zones; 9 = average weighted compositions of the intrusions on the basis of the chemical compositions of the rock types (contents of FeO and $Fe_2O_3$ have been estimated on the basis of the primary compositions of minerals); 10 = average weighted compositions of the intrusions on basis of reconstructed mineralogical compositions of rock types.
Composition are calculated for intrusions for which complete sections were intersected in boreholes (mainly in the Pechenga Ore Field, partly in the eastern part of the Pasvic structure)

of the same name. Smolkin (1977) subdivided the vertical profile of the intrusion into seven zones (Fig. 5.10). The lowermost, Zone I, is a quenched zone, composed by fine-grained metaclinopyroxenite. Zone II is an olivine-chromite-sulfide cumulate with interstitial clinopyroxene, amphibole, plagioclase and ilmenite; rocks of this zone contain 27–35 wt% of MgO. The primary minerals are usually strongly replaced by serpentine or chlorite, talc and carbonate. The lower part of Zone II hosts disseminated

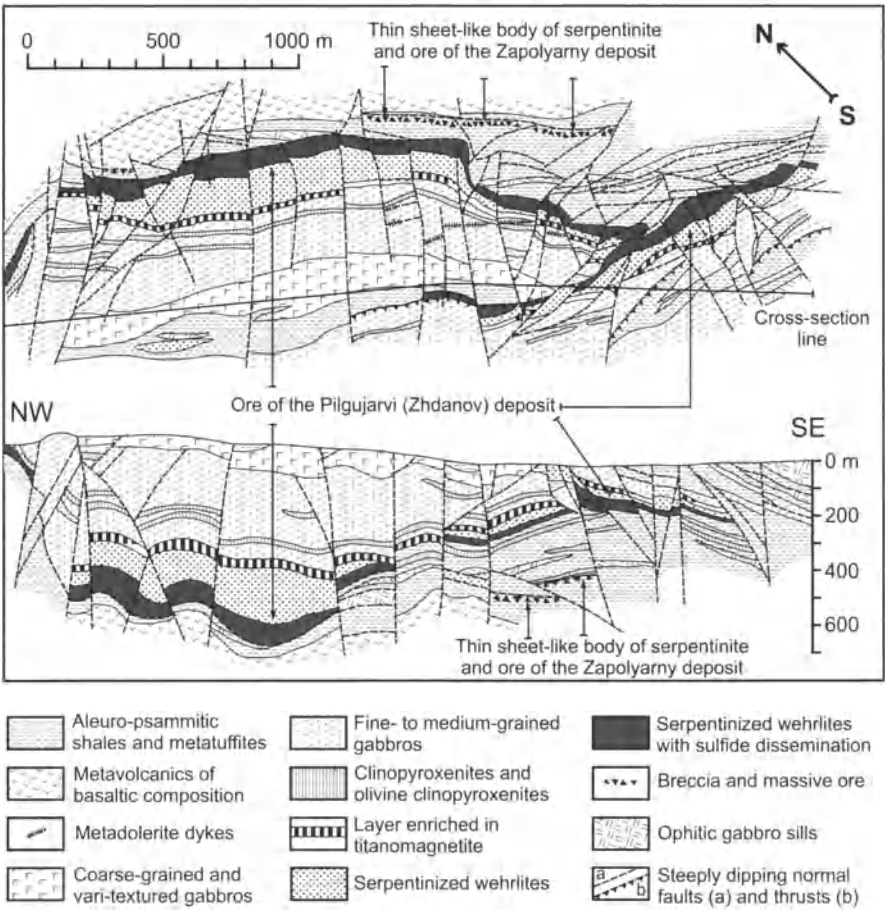


**Fig. 5.9.** Schematic geological map and longitudinal cross-section of the Pilgujarvi intrusion (simplified after Smolkin 1977)

sulfide mineralization. Zone III is transitional from fine-grained clinopyroxenite and olivine clinopyroxenite cumulates at the base upward to olivine-titanomagnetite cumulate and then titanomagnetite-clinopyroxenite cumulate (the titanomagnetite contains 12-16 wt% $TiO_2$). Hornfelsed country-rock xenoliths occur in the upper part of Zone III. Zone IV is composed of melanocratic olivine-bearing gabbro with lenses of clinopyroxenite. Zones V and VI consist of vari-textured gabbroic rocks. Orthoclase gabbro is present in the upper part of the Zone VI. The uppermost (endocontact) zone, Zone VII, contains, from base to top, pyroxenite, gabbro, diorite and quartz diorite. The Pilgujarvi intrusion is cut by dolerite and some ferropicritic dykes, as well as by numerous diopside-antigorite, diopside-garnet-vesuvianite, serpentine-asbestos and antigorite veins.

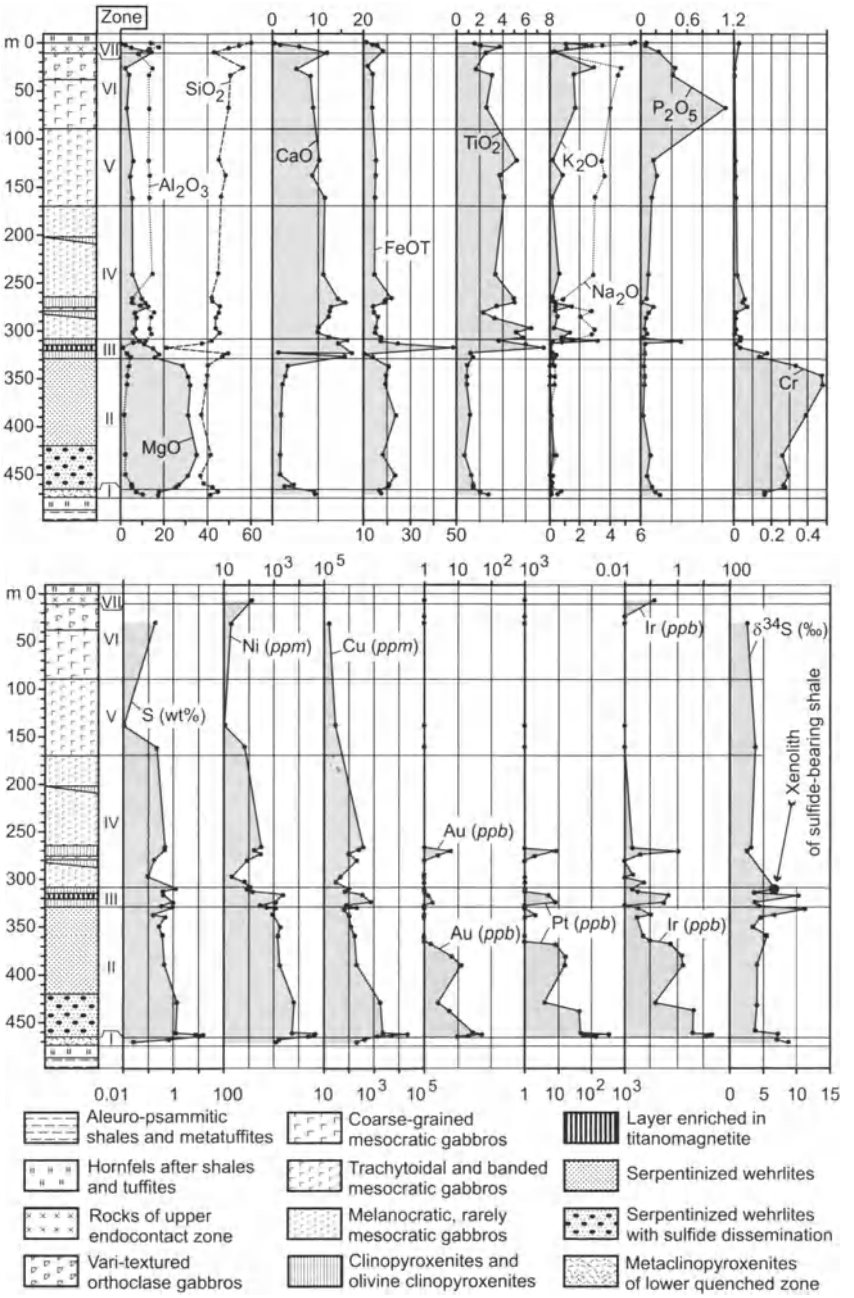


**Fig. 5.10.** Igneous stratigraphy (with geochemical characteristics) of the Pilgujarvi intrusion. Major elements and Cr in wt%. Major elements are recalculated for water free compositions. From data of Smolkin (1977, 1992) and Smolkin et al. (1995)

The ferropicritic sills that occur in the Pechenga Camp more closely resemble lava flows in their degree of crystallization and differentiation than the layered intrusions. Clearly distinguishable zones of quenching and hornfels are absent, as are extreme differentiates such as olivine-rich wehrlite and orthoclase gabbro. The sills can easily be confused with lava flows. Some sills contain sulfide ores. One such sill, located in the upper part of the Zhdanov Suite, was found in the eastern part of the Camp, at Kierdzhipori (close to the Verkhnee Deposit, shown in Fig. 5.8). Gorbunov et al. (1989) described this as a lava flow, but subsequently Smolkin (1992) observed apophyses of the body cutting overlying shales that were slightly hornfelsed, and concluded that the body is intrusive. The Kierdzhipori sill is interesting in that it is 3.2 m thick and contains 0.45 m of massive sulfide at its base, overlain by 1 m of disseminated sulfide. Another sill containing disseminated sulfide, also located in the upper part of the Zhdanov Suite, was found in western part of the Camp, close to the Kammikivi Deposit (Hanski 1992; Hanski and Smolkin 1995). A vertical section through this sill appears in Fig. 5.13.

## 5.6 Magmatic Sulfide Deposits

### 5.6.1 General information

Gorbunov et al. (1999) subdivided the Pechenga camp into two ore junctions within which all of the economic Ni-Cu deposits occur; these are the Western (Kaula) and Eastern (Pilgujarvi) ore junctions (Fig. 5.8). Their data, based largely on records of past production, led them to group the deposits into "giant" (>$7x10^6$ tonnes of Ni+Cu, "large" (250,000 to $1x10^6$ tonnes) and "medium" (200,000-25,000 tonnes of Ni+Cu). Of those shown in Fig. 5.8, the Pilgujarvi is the only "giant" deposit, with the majority of the others falling into the "large" class.

Deposits belonging to the Western Ore Junction were richer than those of the Eastern Ore Junction, but are mined out with no current activity. The only deposits currently (2003) in production are the Pilgujarvi, comprising 97 % disseminated ore, and the Zapolyarny, in which rich breccia and massive ores predominate.

The ore bodies are principally located at the bases of intrusions, usually with tectonic contacts against the underlying tuffaceous and sedimentary rocks. The ore bodies range from 0.2 m to 100 m in thickness and from 5–10 to 1500 m in strike length, depending on the size of the associated intrusion. The ores are classified into massive, breccia, rich-disseminated and disseminated types. So-called "grey" ores occur in close association

with rich-disseminated ores. These are rocks in which olivine is completely and clinopyroxene partially replaced by sulfides, with the preservation of their original crystalline outlines. Silicate minerals in the "grey" ores include talc, chlorite, carbonate, antigorite and tremolite. "Grey" ores were mainly present in the Western Ore Junction, but also occur in the Pilgujarvi deposit.

Gorbunov (1968) noted that the Pechenga ores generally display an asymmetric pattern that is characteristic for magmatic Ni-Cu sulfide deposits. The lower part of a mineralized zone is composed typically of sulfide with a massive, spotted or banded texture and a thickness from 1 to 10 meters. Where the lower contact is tectonic, variable thicknesses of breccia ore, containing up to 80% sulfide, may be present.A zone of veinlet-disseminated and disseminated mineralization typically overlies the massive sulfides with a thickness from several to 100 m. The boundary between the massive and disseminate ores is sharp in most places but is gradational between disseminated ore and barren peridotite. In places Ni-Cu sulfides occur interbanded with the country-rock shales up to 400 m along strike beyond the limit of the intrusions. These zones are contiguous with zones of massive and/or breccia ore and are chalcopyrite dominant with a Ni/Cu ratio of about 1:5. Such ores are often connected to large faults. The Zapolyarny deposit, related to a thin sheet-like serpentinite body, is unusual. It consists of rich ore (breccia and massive), with the volume of the mineralization exceeding the volume of the intrusive rocks. The ore zone is controlled by a fault, oriented parallel to base of the Pilgujarvi intrusion (Fig. 5.9).

The Pechenga ores, like most other magmatic Ni-Cu deposits, consist primarily of pyrrhotite, pentlandite, and chalcopyrite along with minor pyrite, magnetite, violarite, sphalerite, bornite, cubanite, mackinawite, valleriite and platinum-group minerals. Typical ore compositions are given in Table 5.4.

Some of the ore bodies have been affected by metasomatism in which sulfides have been replaced in part by magnetite, and in part redeposited in hydrothermal veins of diopside-vesuvianite-garnet and serpentinite composition. Co-bearing pyrrhotite and pentlandite predominate in such veins (Smolkin and Abzalov 1990).

### 5.6.2 Sulfur isotopic composition of ores and country rocks

Sulfur isotope ratios in the ores, ore-bearing intrusions and ferropicritic lavas of the Pechenga Camp have been studied by Grinenko et al. (1967) and Grinenko and Smolkin (1991). Melezhik et al. (1994) have studied the

**Table 5.4.** Chemical compositions of ores of the Pechenga Camp, after Brugmann et al. (2000)

| Deposit | Sample | Ore Type | S | Ni | Cu | Pd | Pt | Rh | Ru | Ir | Os | Au | (Pt+Pd)/ (Ru+Ir+Os) |
|---|---|---|---|---|---|---|---|---|---|---|---|---|---|
| Kaula (W.O.J.) | 26 | Massive | 26.00 | 7.07 | 3.99 | 304 | 148 | 30 | 72 | 23 | 51 | 95 | 3.1 |
| | 28 | Breccia | 17.20 | 5.00 | 4.28 | 268 | 233 | 22 | 48 | 17 | 17 | 216 | 6.1 |
| Kotselvaara (W.O.J.) | Kotsel-2 | Dissem. | 14.30 | 3.77 | 4.21 | 960 | 717 | 14 | 2 | 6 | 2 | 26 | 167.7 |
| | Kotsel-1 | Dissem. | 10.40 | 5.28 | 2.51 | 560 | 417 | 12 | 3 | 9 | 4 | 10 | 61.1 |
| Ortoajvi (W.O.J.) | Ortoaivi 2 | Dissem. | 16.30 | 3.80 | 1.53 | 366 | 288 | 13 | | 6 | 4 | 100 | 65.4 |
| | Ortoaivi 1 | Dissem. | 10.50 | 5.53 | 2.05 | 1 248 | 1 198 | 21 | 2 | 11 | 4 | 31 | 143.9 |
| Kammikivi ore-bearing sill, Pet/1 borehole (W.O.J.) | Kam 45.1 | Dissem. | 16.42 | 3.69 | 4.09 | 659 | 380 | 16 | | 9 | 6 | 50 | 69.3 |
| | Kam 44 | Dissem. | 13.46 | 5.07 | 2.03 | 1 116 | 678 | 15 | 6 | 9 | 5 | 162 | 89.7 |
| | Kam 42.8 | Dissem. | 12.36 | 4.66 | 1.55 | 699 | 525 | 17 | | 9 | 6 | 59 | 81.6 |
| | Kam 40.6 | Dissem. | 11.86 | 3.11 | 0.39 | 331 | 301 | 15 | 13 | 10 | 7 | 38 | 21.1 |
| | Kam 41.5 | Dissem. | 10.94 | 3.73 | 1.20 | 750 | 373 | 11 | | 9 | 4 | 59 | 86.4 |
| Pilgujarvi (Zhdanov) (E.O.J.) | 236-1 | Breccia | 8.50 | 3.81 | 0.81 | 197 | 74 | 13 | 32 | 19 | 29 | 394 | 3.4 |
| | 256-1 | Dissem. | 11.20 | 2.20 | 0.14 | 297 | 124 | 17 | 49 | 16 | 37 | 10 | 4.1 |
| | 37/3 | Dissem. | 8.20 | 3.93 | 2.10 | 437 | 323 | 22 | 26 | 20 | 44 | 49 | 8.4 |
| | 65 | "Grey" | 14.30 | 3.77 | 0.50 | 57 | 55 | 17 | 24 | 16 | 22 | 20 | 1.8 |
| Kierjipori ore-bearing sill (E.O.J.) | C-2904/542 | Massive | 32.40 | 2.27 | 1.23 | 1 182 | 732 | 18 | 6 | 5 | 4 | 10 | 127.6 |
| Xenolith of sulfide-bearing shale from middle part of sequence of the Pilgujarvi intrusion (sample 116-2) | | | 13.50 | 0.15 | 0.05 | 8 | 15 | | | 1 | 2 | 1 | |

S, Ni, Cu in wt%; PGE and Au in ppb.
*W.O.J.* Western Ore Junction; *E.O.J.* Eastern Ore Junction

sulfur isotope ratios of the tuffaceous and sedimentary rocks. Melezhik et al.'s (1994) compilation of these data is shown in Fig. 5.11.

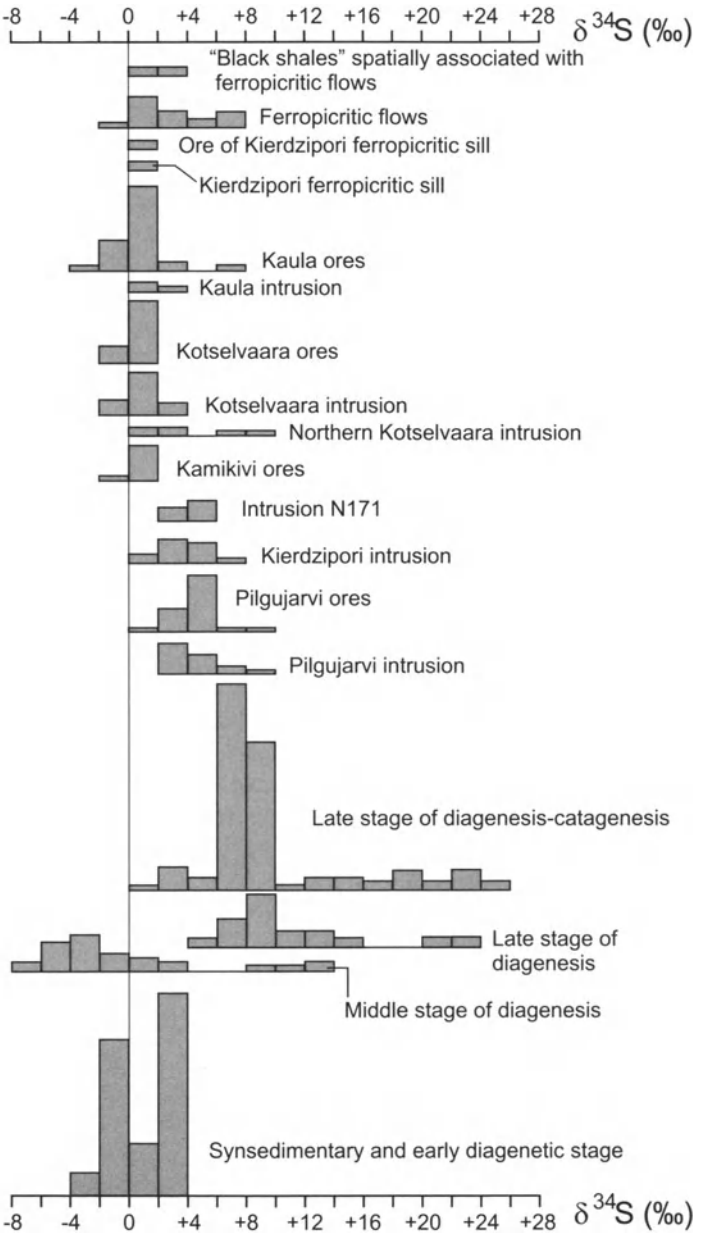


**Fig. 5.11.** Sulfur isotopic composition in ores, intrusions and country rocks of the Pechenga Camp. After Melezhik et al. (1994)

Deposits and their host intrusions in the Western Ore Junction (Kaula, Kotselvaara and Kammikivi) are characterized by near chondritic values of $\delta^{34}S$ (-3 to +6 ‰), while those in the Eastern Ore Junction have heavier sulfur (+1 to +8.5 ‰ with maxima between +2 and +6‰). The data of Abzalov et al. (1995) and Abzalov and Both (1997) are essentially the same as those shown in Fig. 5.11.

Grinenko and Smolkin (1991) suggested that the sulfur isotopic composition of the ores and host intrusions was the result of different degree of contamination by either Archean (mainly acid) rocks or the tuffaceous and sedimentary country rocks that are rich in pyrite and pyrhotite. They observed that the highest degree of contamination occurred at contacts of the intrusions with country rocks and xenoliths.

As seen in Fig. 5.11, Melezhik et al. (1994) distinguished between sedimentary and early diagenetic sulfides which have $\delta^{34}S$ values from -4 to +4 ‰, middle stage diagentic sulfides with scattered values but maxima less than 0 ‰, and late stage diagenetic sulfides which have much heavier sulfur ranging from 0 to >20 ‰. In their opinion, intrusions of the Western Ore Junction assimilated sulfur from country rocks containing early diagenetic sulfides; with the result that the sulfur isotopic composition in the intrusions and ores is close to chondritic. In the Eastern Ore Junction, the intrusions were emplaced into consolidated sedimentary rocks and assimilated late diagentic sulfides, rich in heavy sulfur.

Abzalov et al. (1995) and Abzalov and Both (1997) presented another interpretation. They considered that sulfides of wide-ranging $\delta^{34}S$ values from -1 to +20 ‰, broadly dispersed in shales of the Zhdanov Suite of the Eastern Ore Junction, are the result of the biogenic reduction of seawater $SO_4^{2-}$. In contrast, massive sulfide beds and sulfide concretions in the more sulfide-rich rocks of the Western Ore Junction show a strong association with Ni- and Cr-rich exhalative sediments close to the Kaula picritic eruptive center, and contain juvenile sulfur with $\delta^{34}S$ values between -1 and -4. Citing lack of evidence for significant crustal contamination in the host intrusions, Abzalov et al. (1995) and Abzalov and Both (1997) proposed that the sulfur in the western deposits is juvenile also. They suggest that the larger intrusions found in the Eastern Ore Junction, such as Pilgujarvi, had enough thermal energy to mobilize sulfides disseminated within the enclosing sediments, thus accounting for the heavier sulfur found within these intrusions. It should be noted, however, that the opinion of Absalov and his co-authors concerning the absence of evidence of significant contamination in the Western intrusions is not supported by Os isotopic data (see discussion below).

### 5.6.3 Ni, Cu and PGE variations and Re-Os isotopic systematics of the Ores and Ore-bearing Intrusions

Papunen and Gorbunov (1985) report that massive and breccia ores of the Pechenga ore camp contain up to 10–12 wt% of Ni, rich-disseminated ores contain less than 6 wt% Ni, and low-grade disseminated ores no more than 1.5 wt%. Cu contents range from 0.1 to 13 wt% in rich ores, and to 4–6 wt% in breccia and rich-disseminated ores. Co contents range up to 0.25 wt% in massive ores.

Detailed information on ore compositions are given by Brugmann et al. (2000). They are reproduced here in Table 5.4 and are shown in chondrite-normalised plots in Fig. 5.12. It should be noted that relatively few samples are represented in Table 5.4, which means that their interpretation should be treated with caution. However, it is clear that the Ni contents in Table 5.4 are much lower than the values reported by Papunen and Gorbunov (1985). In terms of their (Pt+Pd)/(Ni+Cu) ratios, deposits of the Pechenga camp have ratios between 0.05 and 0.26 (Appendix), which is comparable with other sulfide-rich deposits associated with mafic/ultramafic intrusions.

As discussed in Chapter 2, the composition of sulfide ores is governed by three main factors: the initial composition of the source magma, the R-factor involved and the extent to which the sulfide liquid has fractionated during crystallization. Looking at data for disseminated ores, shown in Fig. 5.12a, it is seen that the ores of the Western Ore Junction have similar patterns marked by low Ru, Ir and Os and elevated Pt and Pd. (Pt+Pd)/(Ru+Ir+Os) = 102 for Kotselvaara, 107 for Ortoaivi[16], and 48 for Kammikivi. All three have a negative Au anomaly, which is likely due to hydrothermal leaching of the gold during alteration of the host ultramafic rocks. Ores of the Eastern ore junction (the Pilgujarvi samples) have a much flatter PGE profile: (Pt+Pd)/(Ru+Ir+Os) = 6.2.

Turning to the samples of massive and breccia ores (Fig. 5.12b), one of these (from the Kierdzhipori ferropicritic sill) shows a profile marked by low Ru, Ir and Os, and higher Pt and Pd with (Pt+Pd)/(Ru+Ir+Os) = 128, while the remainder have much flatter profiles: (Pt+Pd)/(Ru+Ir+Os) = 4.2 for rich ore from Kaula, 3.4 for Pilgujarvi breccia ore, and 1.8 for Pilgujarvi "grey" ore. Abzalov and Both (1997) reported that this ratio is 2.0 for

[16] The uneconomic Ortoaivi deposit is situated between the Kammikivi and Semiletka deposits, as seen in Fig. 5.8.

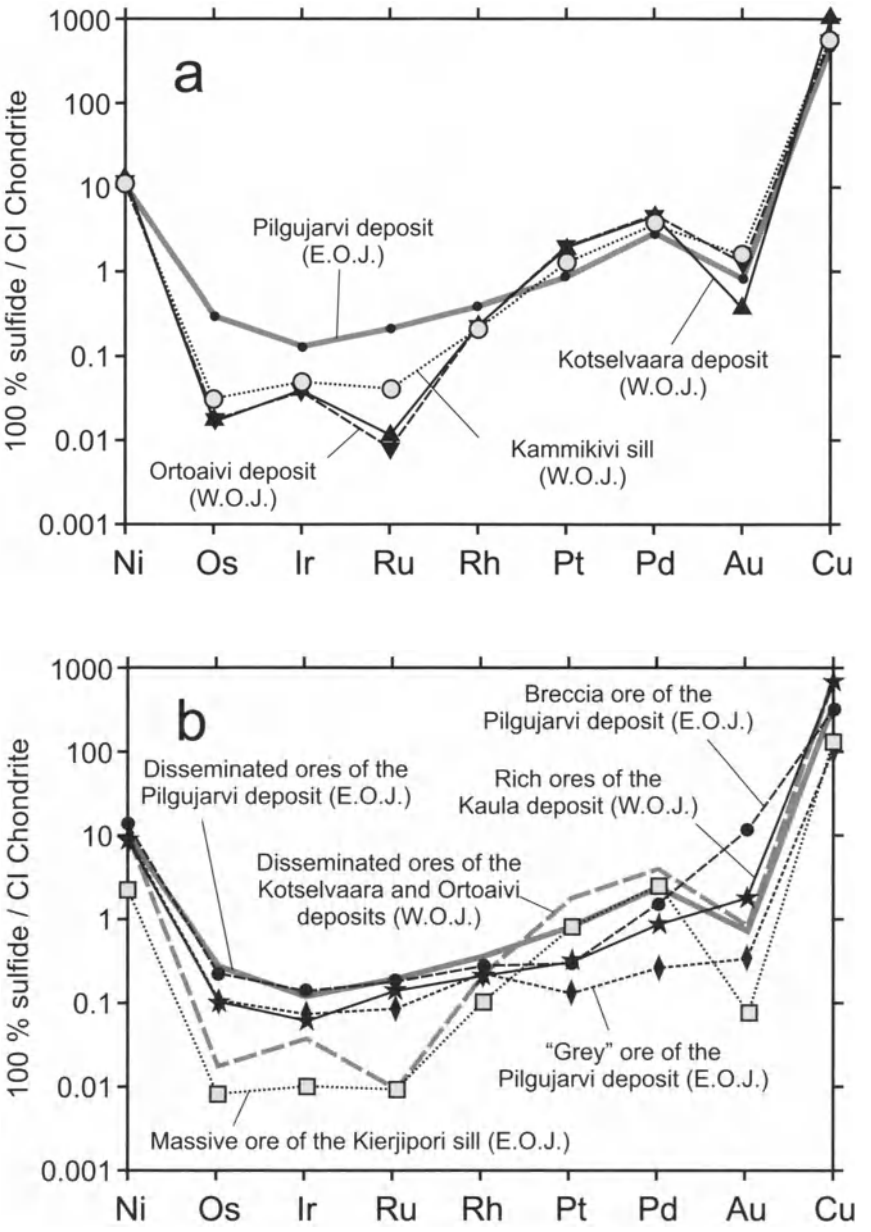


**Fig. 5.12.** Contents of chalcophile elements (normalized to CI Chondrite) in disseminated ores (a) and compared with other types of mineralization (b) in deposits and ore occurrences of the Pechenga Camp. Data are from Brugmann et al. (2000) and are given in Table 5.4

the Kotselvaara (Western Ore Junction) and 2.6 for the Sputnik and Verkhnee (Eastern Ore Junction) massive ore. Brugmann et al. (2000) showed that these differences not only characterize the ores but also the less sulfide-rich samples from the respective intrusions. They noted that Walker et al. (1997) showed that the Pilgujarvi intrusion has $\gamma$Os values of <50, whereas those bodies that have high (Pt+Pd)/(Ru+Ir+Os) values (Kammikivi sill, Ortoaivi and Kotselvaara intrusions of the Western Ore Junction) have $\gamma$Os >100.The large variation in $\gamma$Os has been explained as being due to the assimilation of significant amounts of radiogenic pelitic sediment which has $\gamma$Os >300. Brugmann et al. (2000) argue that fractionation of an ultramafic magma tends to lower Ru, Ir and Os and raise Pt and Pd. They suggested that this is the explanation for the differences observed in the Pechenga Camp. A magma with a lower initial Os content would be more affected in terms of its $\gamma$Os by the assimilation of the same amount of high $\gamma$Os sediment than one with a higher Os content.

While fractionation of the host silicate magma can account for some of the variability shown by the PGE profiles, another factor has also likely influenced the composition. This is particularly true at the Kammikivi sill (its igneous stratigraphy is shown in Fig.5.13), in which the unmineralized rocks have $\gamma$Os of about 20, while the basal sulfides have values of about 250 (Walker et al. 1997). This is evidence that the rocks of the sill formed from a magma that had incorporated less radiogenic (crustal) Os than the initial magma responsible for the mineralization, in other words that the initial magma has been "flushed out" by an influx of magma that contained sulfide with a lesser crustal component. Furthermore, the overlying rocks have (Pt+Pd)/(Ru+Ir+OS) values of about 7 in comparison with the underlying disseminated sulfides which average about 48. In the ore zone (Pt+Pd)/(Ru+Ir+Os) ratios increase from 69 at the top of the disseminated ore to 86 close to base then decrease to 21 just at the base (Table 5.4). As discussed in Chapter 2, much of the fractionation of a sulfide liquid involves the crystallization of mss. Ru, Ir and Os are compatible in mss, and are removed from the liquid, while Pt and Pd, along with Au and Cu, are incompatible and build up in the residual liquid. Thus fractionation of the sulfide liquid can cause variations in the (Pt+Pd)/(Ru+Ir+Os) ratio. In the case of the Kammikivi sill, it would seem that the residual liquid has been expelled downward during fractional crystallization. The failure of Au to increase along with Pt and Pd in the Pechenga ores is probably the consequence of hydrothermal leaching of Au from the magmatic sulfides and its re-deposition elsewhere.

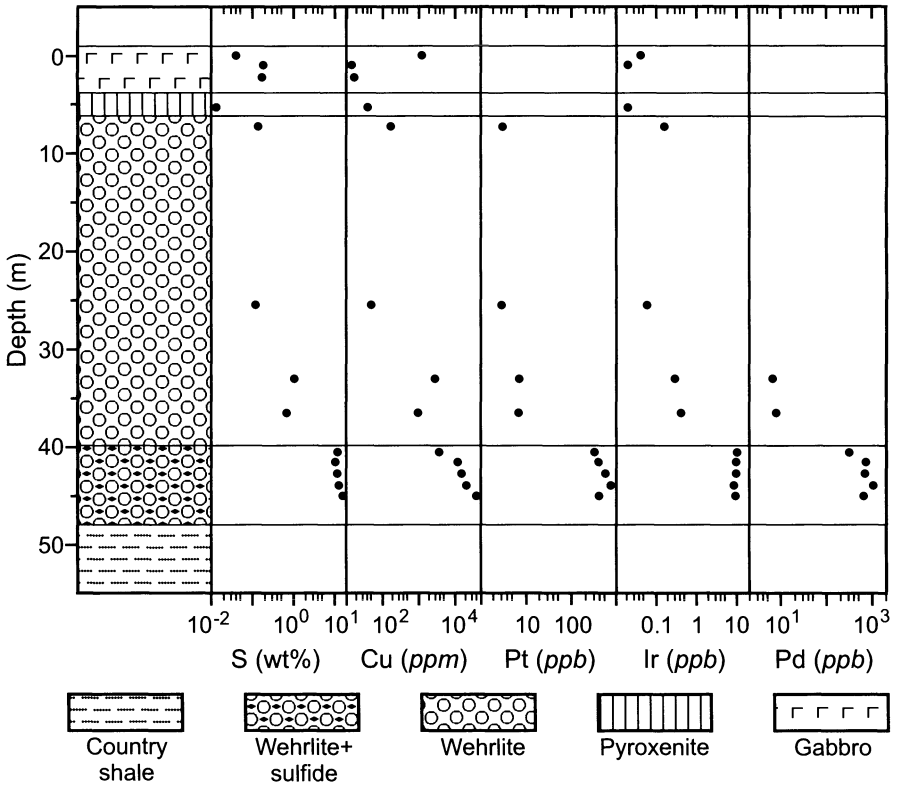


**Fig. 5.13.** Variations of sulfur, Cu, Pt, Ir and Pd across a vertical section through the Kammikivi ore-bearing sill (borehole Pet/1). After Brugmann et al. (2000)

## 5.7 A Genetic Model for the Pechenga Ores

Critical factors bearing on the genesis of the Pechenga ores are:

1. Major, trace element and isotopic data indicate the ores are associated with intrusions that formed from the same magma which gave rise to the ferropicrtic flows that occur within the tholeiitic basalts overlying the sedimentary formation hosting the intrusions.
2. Two ferropicritic eruption centers have been recognized in the Pechenga area. All intrusions with economic mineralization are associated with one or other of these centers, which, using terminology developed at Noril'sk, can be described as ore junctions: the Western and the Eastern Ore Junctions.

3. The intrusions occur within the Productive Formation (the Zhdanov Suite), which is thickest and most sulfide-rich sedimentary formation of the four inter-volcanic horizons that are present within the North Pechenga Structural Zone.
4. Inclusions of local country rocks occur at the center and towards the top of some ore-bearing intrusions, which attests to the close association that was achieved between the intruding magma and the rocks it was intruding.
5. Re-Os isotopic systematics indicate that much of the Os in the ores had undergone a residence time in an environment with a high, non-mantle Re/Os ratio (i.e. was derived from a crustal source).
6. Differences in the $\gamma$Os values of sulfides from different deposits indicates that certain intrusions incorporated more "crustal" Os than others.
7. Some ferropicritic sills, such as that the ore-bearing sill at Kammikivi, host economic-grade mineralization that has a higher value of $\gamma$Os than the value characterizing the main body of the sill. This attests to fresher magma flowing through the sill and flushing out that responsible for the bulk of the magmatic sulfide formation.
8. The S isotopic compositions indicate that a component of non-juvenile sulfur has definitely been added to intrusions in the Eastern Ore Junction (the Pilgujarvi area), although the data from the Western Ore Junction (the Kaula area) is permissive but provides no proof of an addition of this kind. However, Os isotope compositions provide evidence that the western intrusions assimilated as much and possibly more crustal material than the eastern ones.

The above observations are best explained by a model in which ferropicritic magma from a unique source in the mantle beneath the western portion of the Pechenga-Varzuga rift ascended into the Pechenga Structure during the deposition of the Pilgujarvi Volcanic Formation (the Matert Suite). The magma formed differentiated gabbro-wehrlitic intrusions and ferropicritic sills within the underlying Pilgujarvi Sedimentary Formation (the Zhdanov Suite or Productive Formation) when it had reached its hydrostatic level. During this process the magma interacted with sulfur in the enclosing sediments, acquiring sulfide, also gaining a component of radiogenic Os. Immiscible sulfides formed, concentrating chalcophile metals and settling towards the base of the intrusive bodies, in some places giving rise to pools of massive sulfide, in others concentrations of disseminated sulfide. In some, perhaps most of the cases, fresh magma continued flowing so that the old magma was flushed out and continued to surface to give rise to ferropicritic flows.

An oceanic basin was formed during the development of the rift, giving rise to the island arc rocks preserved in the South Pechenga Structural Zone that lie south of the Poritash fault. Deformation along the north shore of the ocean during its closure resulted in crumpling of rocks, including the Productive Formation (the Zhdanov Suite) that hosted the ore-bearing intrusions. This deformation caused a remobilization of the ores at the base of the intrusions, giving rise to the breccia and banded ores that extend laterally away from massive sulfide at the base of some intrusions.

# 6 Voisey's Bay and other deposits , Labrador, Canada

## 6.1 History of discovery and exploration

In the summer of 1993, two prospectors, Albert Chislett and Chris Verbiski, who had been sent to Labrador by Diamond Fields Resources Ltd. to conduct stream sampling for diamond indicator minerals, discovered a gossan with the blue staining characteristic of copper on a hill-top, 45 km southwest of the village of Nain. An initial 5-hole drill programme was conducted to investigate the occurrence in October 1994 and one of the holes intersected a 41.2 m zone of semi-massive to massive sulfide grading 2.96% Ni, 1.89% Cu and 0.16% Co within a wider 71.0 m zone which graded 2.23% Ni, 1.47% Cu and 0.12% Co. A major drilling program was started by Diamond Fields Resources Ltd in January 1995 and by July 1995, 31.7 million tonnes of ore grading 2.83% Ni, 1.68% Cu and 0.12% Co had been outlined at surface in the area known as the "Ovoid" and "Mini-Ovoid". In October 1995 a second major discovery, known as the "Eastern Deeps", was made during a stratigraphic drilling program. The deposit was acquired by INCO Ltd in August 1996. Current reserves plus inferred and indicated resources stand at $136.7 \times 10^6$ tonnes grading 1.59 wt% Ni, 0.85 wt% Cu, 0.06 wt% Co. The success at Voisey's Bay led to a huge surge in exploration in this part of Labrador in 1995, 1996 and to a lesser extent in 1997. Many Ni-bearing occurrences were located and explored, and some of these are discussed in the closing sections of this chapter.

## 6.2 General geology

The geology of the Nain area has been described by Ryan (1990, 1996, 2000), Ryan et al. (1995), and Kerr et al. (2000). The deposit has been described by Naldrett et al. (1996, 1997), Ryan (1996), Li and Naldrett (1999), Lightfoot and Naldrett (1999) and Evans-Lamswood et al. (2000); aspects of the geochemistry have been addressed by Lambert et al. (1999,

2000), Ripley et al. (1999, 2000), Li et al. (2000), Li and Naldrett (2000), Naldrett et al. (2000a) and Amelin at al. (2000); Naldrett et al. (2000b) described the sulfide mineralogy. The deposit is associated with the 1.334 Ga (Amelin et al. 1999) Voisey's Bay intrusion which belongs to the Nain Plutonic suite and transects the east-dipping 1.85 Ga collisional boundary between the Proterozoic Churchill Province to the west and the Archean

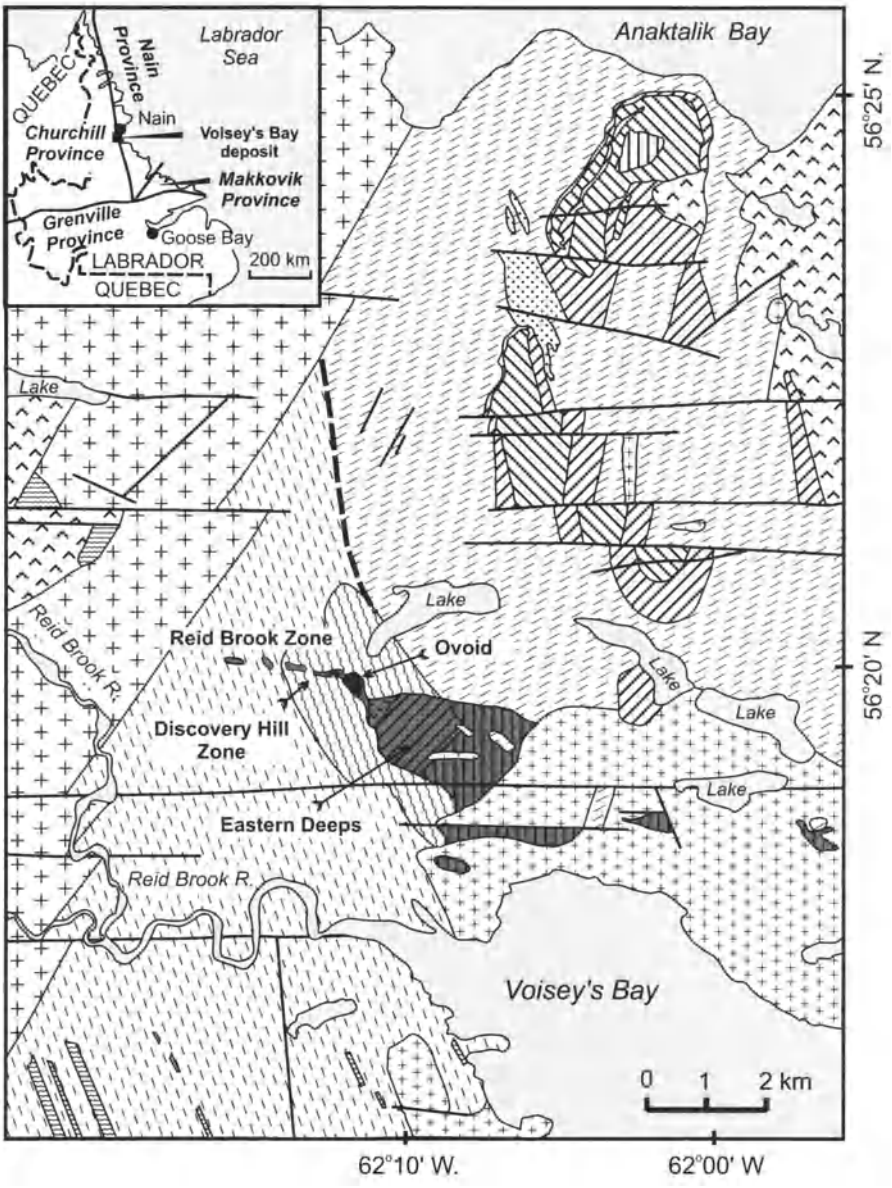

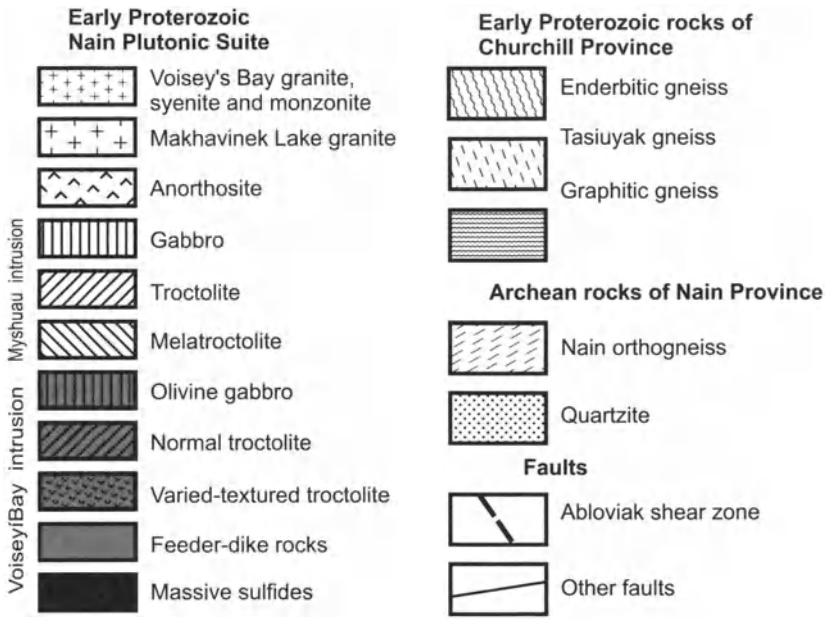


**Fig. 6.1.** Geology of the Voisey's Bay area. Drafted using data from Ryan (1990) and Evans-Lamswood et al. (2000)

Nain Province to the east (Ryan et al. 1995) (Fig. 6.1). The Churchill Province comprises re-worked Archean rocks and Proterozoic-aged interbanded garnet-sillimanite and sulfide- and graphite-bearing quartzo-feldspathic paragneisses collectively known as "Tasiuyak gneiss", and minor massive to lineated enderbitic gneiss. The Nain Province comprises interbanded granitic, intermediate and mafic orthogneisses that exhibit retrogressed granulite- and amphibolite-facies mineral assemblages. The latest movement along the collisional zone is marked by the Abloviak shear zone, for which the last movement has been dated at 1.73-1.75 Ga (Van Kranendonk 1996).

Two troctolitic intrusions are present in the Voisey's Bay area (Fig. 6.1), the Voisey's Bay Intrusion and the Mushuau intrusion. Both are members of the Nain Plutonic Suite, which comprises a suite of anorthosite, granite, ferrodiorite (in the area, shown in Fig. 6.1, ferrodiorite bodies are not developed) and troctolite bodies that were emplaced in the interval 1.350-1.290 Ga (Ryan 2000) (Fig. 6.2). The Voisey's Bay and Mushuau intrusions were originally regarded as a single complex (Ryan et al. 1995) but Amelin et al. (1999) dated the Voisey's Bay Intrusion at 1.334 Ga and Li et al. (2000) report the age of the Mushuau Intrusion as 1.317-1.313 Ga (Fig. 6.2). The two intrusions also have distinctly different trace element and isotopic signatures (see below).

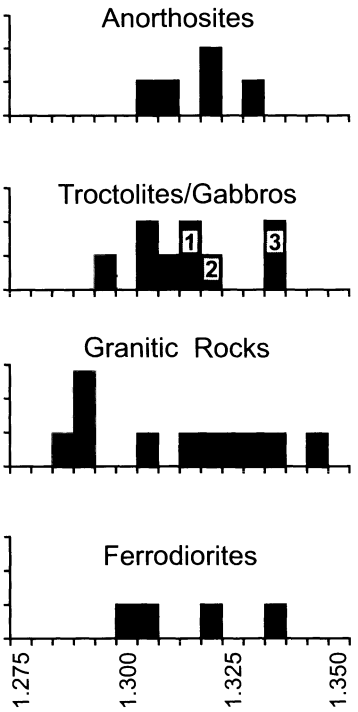


**Fig. 6.2.** Histogram of ages of Nain Plutonic suite. Ages from: Hamilton 1994; Amelin et al 1999; Ryan 2000; Smith et al 1999, 2001. 1 = Mushuau Intrusion; 2 = Pants Lake North Intrusion ; 3 = Voisey's Bay, Pants Lake South Intrusions

## 6.3 Geology of the Voisey's Bay intrusion

At the present level of understanding (Fig. 6.3), the Voisey's Bay intrusion comprises five components: (1) an upper chamber (the "Eastern Deeps"), which comprises an olivine gabbro (OG) sequence, a normal troctolite (NT) sequence and a varied-textured troctolite (VT) sequence; (2) this is fed from below by a gabbroic/troctolitic feeder sheet, which is exposed at surface farther west (the Discovery Hill Zone); (3) the "Ovoid", which is situated between the Eastern Deeps and the Discovery Hill Zone, appears to be the base of the Eastern Deeps exposed at surface; (4) the "Minio-void" lies directly west of the Ovoid but is separate from it; (5) the feeder sheet has been traced 2.5 km west of the Ovoid, and in its western part, the Reid Brook Zone, it dips steeply south and appears to widen out into a lower chamber. These are described in turn below.

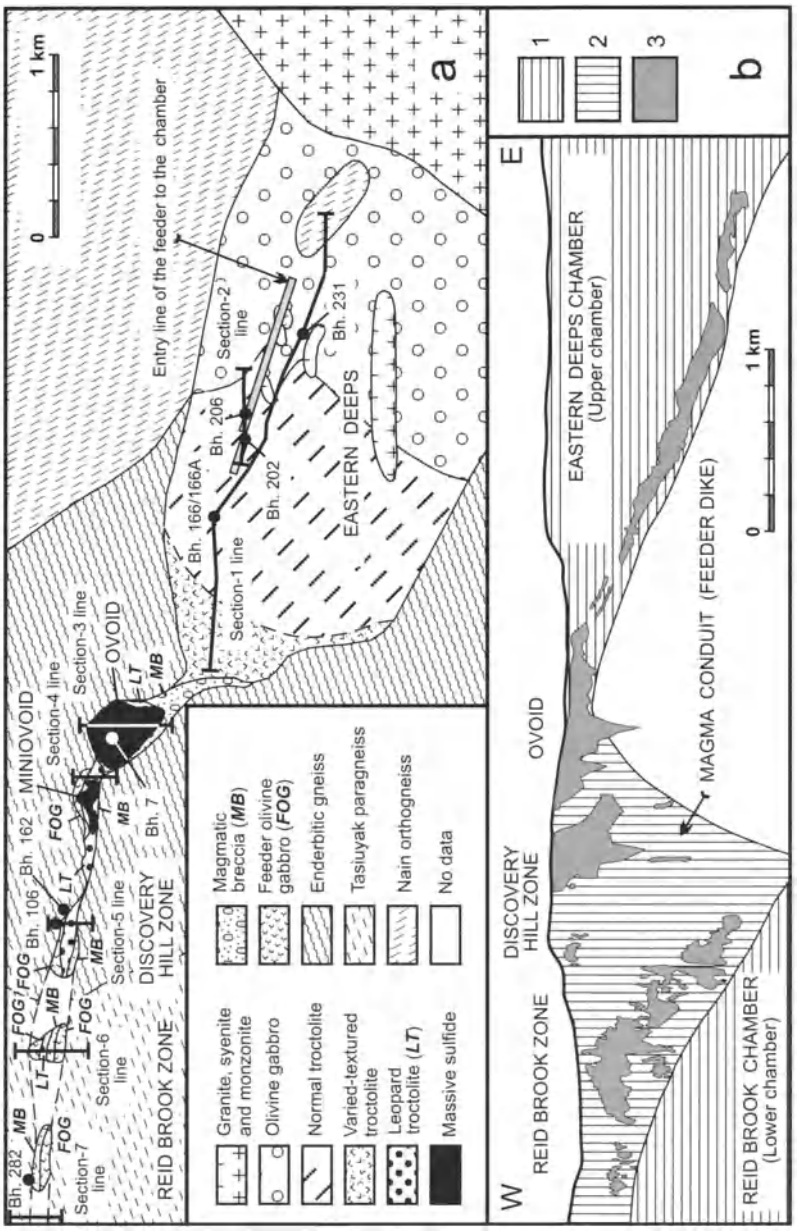


**Fig. 6.3. a** – Geological map of the Voisey's Bay intrusion (modified after Li and Naldrett, 1999); **b** – Generalized longitudinal cross-section – the igneous rocks have been projected onto a vertical plane (modified after Lightfoot and Naldrett 1999). Legend for cross-section: 1 = Gabbro-troctolite bodies (magmatic chambers); 2 = Rocks comprising the magma-conduit assemblage; 3 = Sulfide mineralization

**The Eastern Deeps.** The Eastern Deeps chamber (Fig. 6.3) is exposed at surface as a troctolite-olivine gabbro body intruded by syenite and monzonite. The basal contact of the troctolite dips uniformly at 25° southeast from the vicinity of the Ovoid (Figs. 6.3b, 6.4). In this area, the Basal (= Magmatic) Breccia Sequence (BBS), which is composed of a few ultramafic rock inclusions of mela-troctolite, wehrlite and dunite, and abundant gneissic inclusions, lies at or close to the basal contact of the chamber and is overlain by troctolite with a texture ranging from pegmatitic to medium grained (Varied-textured Troctolite or VT, see description below). A feeder sheet enters the Eastern Deeps from the north; although the sheet appears to enter horizontally when viewed on a north-south cross section (Fig. 6.5), the entry line rakes southeast, following the plunge of the base of the Eastern Deeps. Several hundred metres north of the entry line, the sheet assumes a steep dip, similar to that of the feeder to the west (Fig. 6.6). Large blocks of ultramafic rock appear to choke the feeder sheet in a few places. Pegmatite usually occurs as irregular masses, some 10 cm across, commonly associated with sulfide. The Varied-textured Troctolite is overlain by a medium grained, uniformly-textured troctolite (Normal Troctolite or NT, see description below).

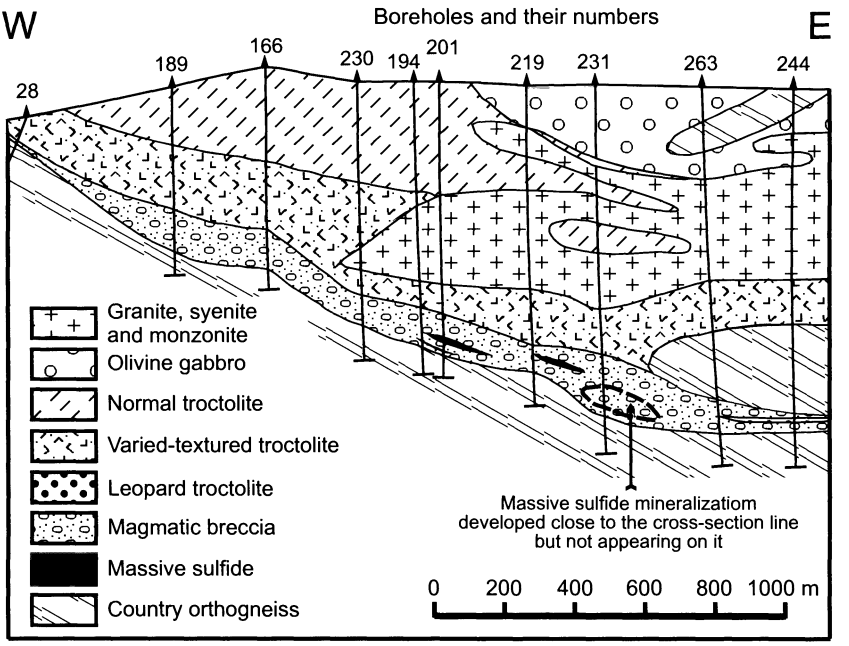


**Fig. 6.4.** Cross section through Eastern Deeps at line 1 (modified after Li and Naldrett 1999). The line of the cross-section is shown in Fig. 6.3a

Sulfide, which is present in trace amounts throughout most of the Varied-textured Troctolite, increases to 10-15 modal percent (in places up to 25%) over the lower 40-60 m. At this point, the Varied-textured Troctolite is in contact with the Basal Breccia Sequence which contains both disseminated and blotchy sulfide and also lenses of massive sulfide.

Naldrett et al. (1996) have shown that massive sulfide occurs at the base of the Eastern Deeps both within the feeder sheet (i.e. north of the stippled line representing its line of entry into the chamber in Fig. 6.3a) and up to 100 m south into the chamber. The Basal Breccia Sequence is absent or thin near the line of entry of the feeder, and thickens away from this in a southwesterly direction, before thinning out again farther southwest. The Basal Breccia Sequence seems to form a "bar" just off the entry line of the sheet, with the best development of massive sulfide lying between this bar and the entry line (Fig. 6.7).

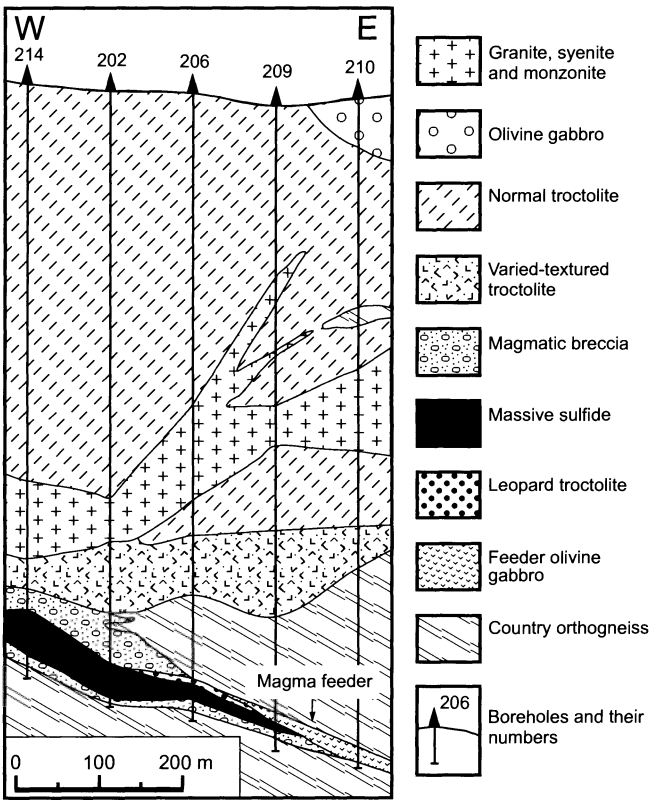


**Fig. 6.5.** Cross section along line 2 illustrating the merging of the feeder with the Eastern Deeps chamber (modified after Li and Naldrett 1999). The line of the cross-section is shown in Fig. 6.3a

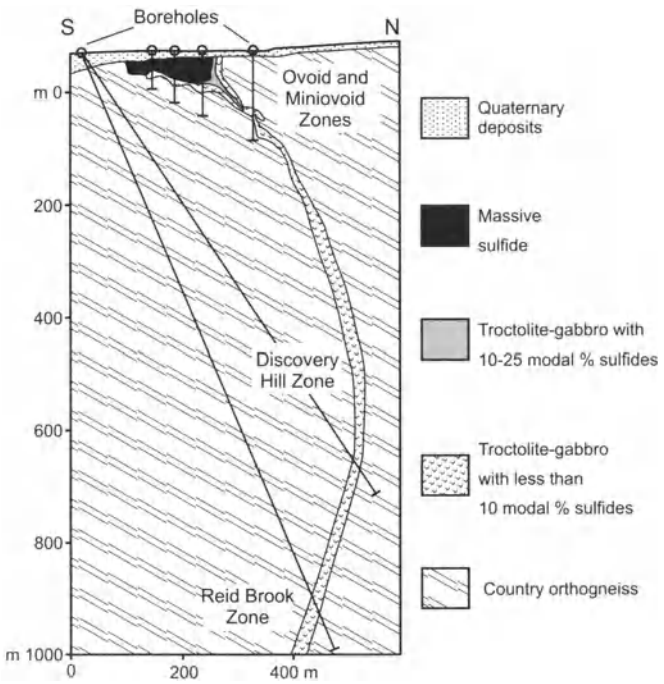


**Fig. 6.6.** Generalized cross section showing morphology of the feeder with respect to the Ovoid, Miniovoid, Discovery Hill, and Reid Brook Zones (modified after Evans-Lamswood et al. 2000)

The stratigraphy of the feeder sheet extending north of the chamber is a close match to that observed in the Discovery Hill Zone (see below), although it tends to be less thick where it has been studied so far. The upper part of the sheet consists of unmineralised Olivine Gabbro (Feeder Olivine Gabbro or FOG), either in chilled contact with the overlying gneiss, or as a mixed zone of troctolite and gneissic fragments. Sulfides increase downward and much of the disseminated sulfide shows "leopard texture" (Leopard Troctolite or LT)[17] which consists of a troctolite containing interstitial sulfides, and oikocrysts of augite. The latter have grown and pushed the interstitial sulfide aside, so that the rock has the appearance of black spots in a yellowish background. Sulfide content may increase to about 50%, below which there is an abrupt change in some holes to massive sulfide, which is underlain by mineralized Basal Breccia Sequence. The Basal Breccia Sequence is separated from the gneiss in most places by a thin zone of sulfide-poor, fine-grained Ferrogabbro.

[17] Leopard texture has not been observed so far within the main intrusion, only within the sheet-like body of troctolite

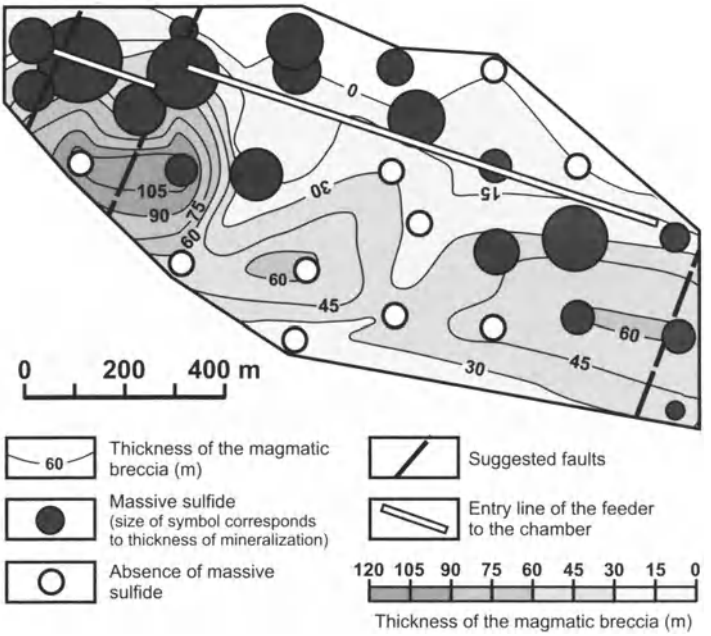


**Fig. 6.7.** Plan of the northern part of the Eastern Deeps chamber with contours showing thickness of the magmatic breccia sequence , relative proportions of massive sulfide and the entry line of the feeder to the chamber. The entry line of the feeder is shown in Fig. 6.3a. Modified after Naldrett et al. (1996)

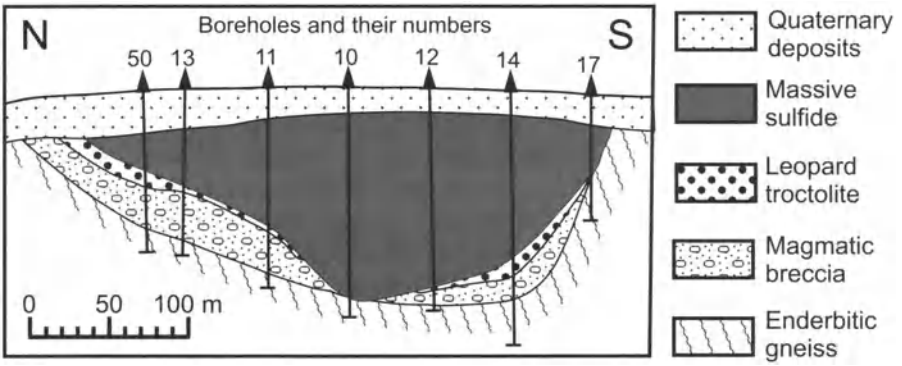


**Fig. 6.8.** North-south cross section of the Ovoid for line 3. Position of the section line is shown in Fig. 6.3a. Modified after Li and Naldrett (1999) Fig. 8

**The Ovoid and Miniovoid.** The Ovoid consists of up to 110 m of massive sulfide overlying a variable thickness of Basal Breccia Sequence and minor Leopard Troctolite, all located within a bowl-shaped structure and

overlain by 10–20 m of gravel (Fig. 6.8). A thin (10-20 m thick) feeder sheet joins it from below. Westward, the Ovoid merges with the Miniovoid, which is essentially a thickened variant of the Discovery Hill Zone, dipping 40° N and displaying the stratigraphic succession typical of this zone together with a thick zone of massive sulfide between the Leopard Troctolite and Basal Breccia Sequence (Fig. 6.9).

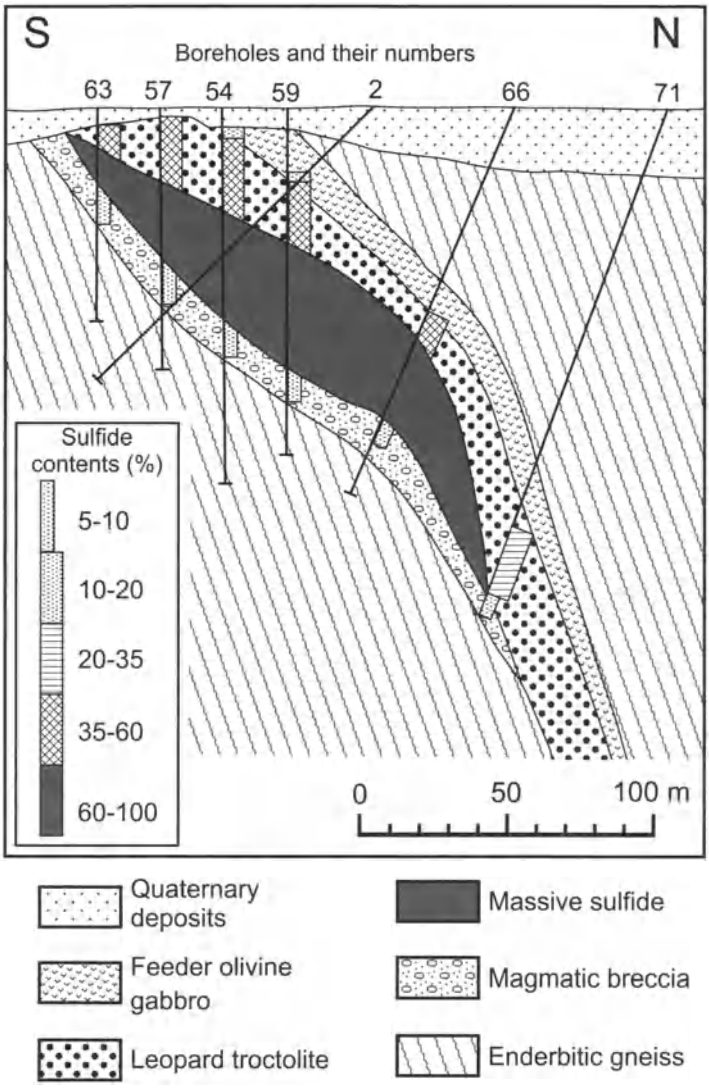


**Fig. 6.9.** North-south cross section through the Miniovoid along line 4. Position of the section line is shown in Fig. 6.3a. Modified after Li and Naldrett (1999)

**The Discovery Hill Zone.** In this zone the thickness of the feeder sheet varies from 10-100 m; the dip changes from 40°N close to surface and close to the Ovoid to a steep southerly orientation at depth. Where the dip is less than 70° the same stratigraphy is developed (Fig. 6.10) as in the vicinity of the Eastern Deeps. Mineralization is restricted to the wider parts of the feeder, which occur as a series of elongate lenses, within the plane of the sheet, all raking to the east.

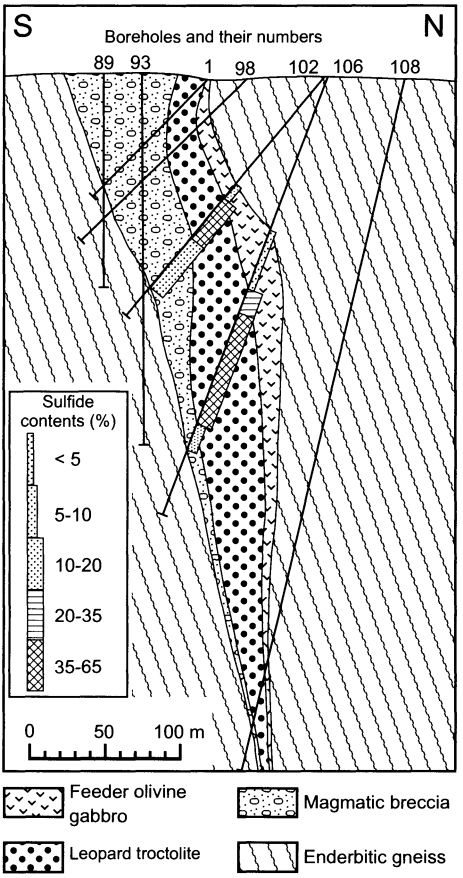


**Fig. 6.10.** North-south cross section through the Discovery Hill Zone along line 5. Position of the section line is shown in Fig. 6.3a. Modified after Li and Naldrett (1999)

**The Reid Brook Zone.** In the Reid Brook Zone, the dip of the feeder sheet is in excess of 70° to the south. The sub-vertical stratigraphic succession that characterises the Discovery Hill Zone is not well developed here. The breccia sequence that occurs at the basal contacts of both the Eastern

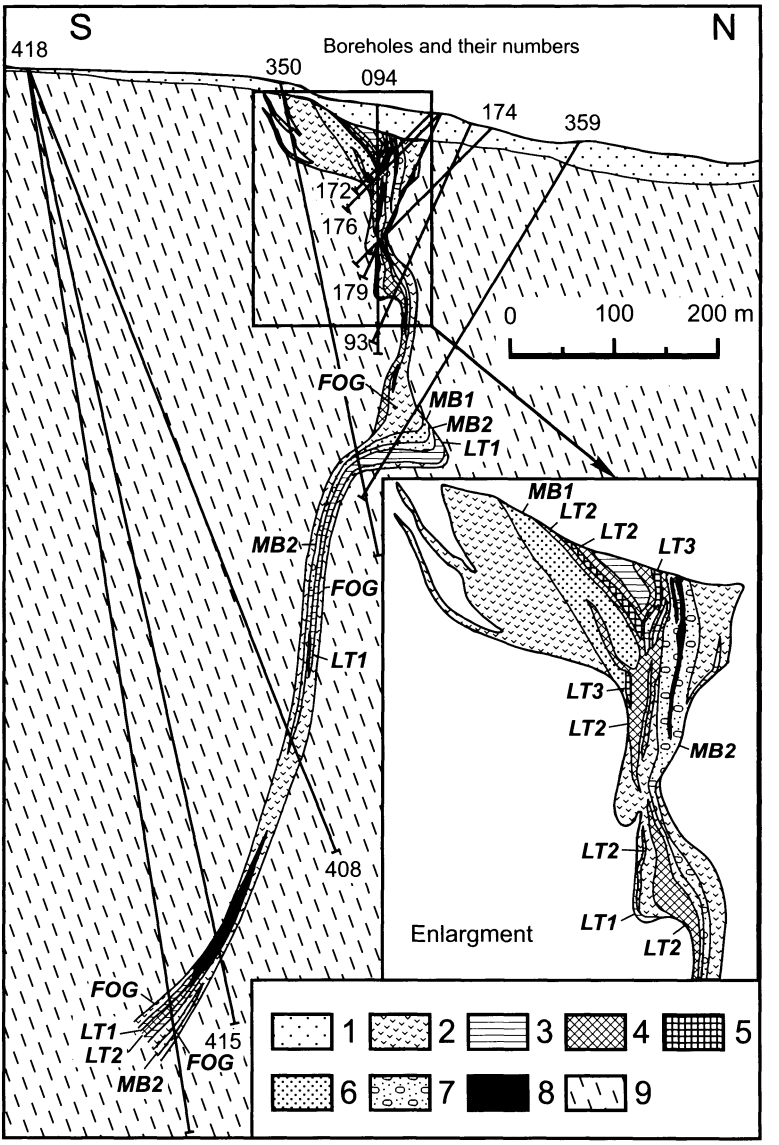


**Fig. 6.11.** North-south cross section through the Reid Brook Zone along line 6. Position of the section line is shown in Fig. 6.3a. Modified after Li and Naldrett (1999). 1 = Quaternary deposits; 2 = Feeder olivine gabbro (FOG); 3–5 = Leopard troctolites: 3 = with 10-25 modal % sulfide (LT1), 4 = with 25-50 modal % sulfide (LT2), 5 = with 50-75 modal % sulfide (LT3); 6–7 = Magmatic breccias: 6 = with less than 10 modal % sulfide (MB1), 7 = with 10-25 modal % sulfide (MB2); 8 = Massive sulfide; 9 = Tasiuyak paragneiss

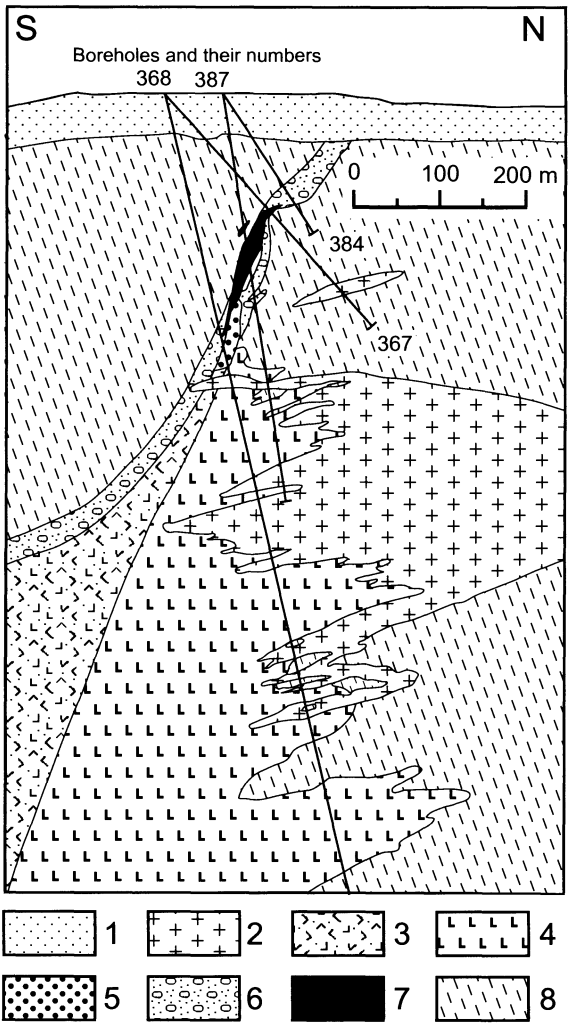


**Fig. 6.12.** North-south cross section of the Reid Brook Zone along line 7. Position of the section line is shown in Fig. 6.3a. Modified after Li and Naldrett (1999). 1 = Quaternary deposits; 2 = Granite, syenite and monzonite; 3 = Varied-textured troctolite with less than 10 modal % sulfide; 4 = Leucotroctolite with less than 10 modal % sulfide; 5 = Leopard troctolite with 10-25 modal % sulfide; 6 = Magmatic breccia with less than 10 modal % sulfide; 7 = Massive sulfide; 8 = Tasiuyak paragneiss

Deeps and Discovery Hill Zone (i.e. Basal Breccia Sequence) is referred to as "Feeder Breccia" in the Reid Brook Zone, because the inclusions are more closely packed. The Feeder Breccia is not restricted to the footwall of

the steeply dipping sheet, but can occur anywhere within it. The Feeder Olivine Gabbro and Leopard Troctolite envelop massive sulfides within the feeder in some places (Fig. 6.11); in addition, in this zone, massive sulfides occur as lenses in the gneiss up to 20 m from the feeder itself. At depth in the Reid Brook Zone, as mentioned above, the feeder merges with a second chamber (Fig. 6.12) that is characterised by large thickness of a more plagioclase-rich troctolite (Leucotroctolite or LUT).

## 6.4 Petrography of Rock Types

The rock classification used below follows the convention recommended by the IUGS Subcommission on the Systematics of Igneous Rocks as summarised by Streckeisen (1976). The cumulus terminology is that presented by Irvine (1982).

**Olivine Gabbro and Leucotroctolite.** Olivine gabbro is a common rock-type that occurs, together with several thin (10-30 m) layers of gabbro in the Olivine Gabbro sequence of the Eastern Deeps. It is an olivine-plagioclase cumulate with 50-70 modal percent (mod%) plagioclase and 15-30 mod% olivine. Plagioclase normally occurs as euhedral to subeuhedral tabular crystals ranging from 5 to 20 mm in length. Olivine occurs as elliptical grains, 5-10 mm in diameter. Interstitial minerals comprise hornblende, biotite, ilmenite and trace sulfide. Collectively, these interstitial minerals amount to less than 20 mod%. Augite varies from 10 to 20 mod% and occurs mainly as large oikocrysts enclosing grains of olivine and plagioclase. Reaction rims of orthopyroxene surrounding olivine are not common in the Olivine Gabbro. Serpentinization of olivine is rare and, where found, is restricted to the contact of the host rock with the younger Voisey's Bay granite.

The Leucotroctolite (LUT) in the Reid Brook lower chamber has a ratio of olivine to plagioclase similar to that in the Olivine Gabbro of the Eastern Deeps. Oikocryst augite however is less abundant in the Leucotroctolite (usually less than 5 mod%) than in the Olivine Gabbro. Reaction rims of orthopyroxene on olivine are more common in the Leucotroctolite than in the Olivine Gabbro.

**Feeder Olivine Gabbro.** Feeder Olivine Gabbro (FOG) is a plagioclase±olivine cumulate containing much more intercumulus minerals (between 30-50 modal percent) than either the Leucotroctolite or Olivine Gabbro. Euhedral to subeuhedral plagioclase crystals constitute 40-50

mod%. They vary in size from 2-10 mm in length and are randomly oriented to form a framework for intercumulus minerals. Small amounts of olivine and augite (less than10 mod% each) often occur as oikocysts enclosing grains of plagioclase. Intercumulus minerals include hypersthene (5–10 mod%), hornblende (8–15 mod%), biotite (up to 15 mod%), ilmenite (around 5 mod%) and small (less than 1 mm) subhedral plagioclase laths (up to 15 mod%). Granular hypersthene crystals appear to have intergrown with intercumulus plagioclases to form a centre for aggregates of hornblende and biotite. The hornblende has a distinct brownish green colour in contrast to its typical greenish brown colour observed in other types of rock. Most of the olivine grains have been serpentinised along their cleavages while some cumulus plagioclase laths are cut by micro veinlets of sericite.

**Normal Troctolite.** Normal Troctolite (NT) is a medium grained troctolite of uniform texture. It consists of 20-40 mod% cumulus olivine and 40-65 mod% cumulus plagioclase laths 5-10 mm in length. The plagioclase laths are randomly oriented and are often partially enclosed by olivine, in some places to the extent that olivine oikocrysts surround plagioclase grains. Oikocryst augite is rare in the Normal Troctolite, instead small amounts of orthopyroxene (less than 5 mod%) occur as reaction rims on some olivine grains. Greenish brown hornblende comprises less than 5 mod% and often occurs as epitaxial overgrowths on orthopyroxene and olivine. Biotite constitutes up to 8 percent and occurs as an interstitial mineral in many places closely associated with oxides and sulfides. Ilmenite is the only common oxide mineral and generally constitutes 2-5 mod% in the Normal Troctolite. Rare titanomagnetite occurs as an intercumulus mineral associated with ilmenite. Several bands of ilmenite, 0.5-1.5 m thick, occur in the upper part of the Normal Troctolite. Small amounts of augite are present in a myrmekitic intergrowth with the ilmenite in these bands.

**Varied-textured Troctolite.**Varied-textured Troctolite (VT) differs from the Normal Troctolite in that it contains up to 25 volume percent gneiss inclusions and some blotchy sulfide. Plagioclase varies in size from several millimetres to several centimetres in length. Larger plagioclase crystals occasionally enclose grains of euhedral olivine. Pegmatitic plagioclase laths, more than 15 mm in length, are often observed projecting into patches of sulfide. Mantling of olivine by orthopyroxene is more common and interstitial hornblende, biotite and apatite are more abundant in the Varied-textured Troctolite than in the Normal Troctolite. On the other hand, augite oikocrysts are less abundant and have more often been altered to tremolite, particularly in areas where they are in direct contact with sul-

fide. A few olivine crystals with orthopyroxene overgrowths have been replaced by iddingsite; many others have experienced partial serpentinization along fractures. Biotite most typically occurs as bands around gneiss inclusions and to a lesser extent around sulfide patches. Interstitial ilmenite is less abundant in the Varied-textured Troctolite than in the Normal Troctolite. Magnetite, which is rare in the Normal Troctolite, is more common in the Varied-textured Troctolite in which it is often associated with gneissic inclusions and patches of sulfide.

**Leopard Troctolite.** Leopard Troctolite (LT) contains up to 50 volume percent interstitial sulfide and about 10 mod% oikocrysts of augite. So far Leopard Troctolite has only been observed within the feeder and in the Ovoid. Cumulus plagioclase ranges from 40 to 60 and cumulus olivine from 20 to 30 mod%. Augite oikocrysts generally constitute less than 5 modal percent but locally may reach a maximum of 15 mod%. Reaction rims of orthopyroxene on olivine are rare in the Leopard Troctolite. Other interstitial minerals such as hornblende and biotite are much less abundant than in the Feeder Olivine Gabbro. With increasing amounts of sulfide, oikocrysts disappear from Leopard Troctolite and the mineralisation grades into interstitial sulfide ore.

**Magmatic breccias.** As described above, Basal Breccia (BBS) and Feeder Breccia (FB) are similar in mineral composition but are recognized by different names because of their generally different inclusion content and different distribution within the feeder. Both contain more than 25 volume percent of inclusions and variable amounts of sulfide. Three types of inclusions are present: (i) fragments of gneisses (i.e. Tasiuyak gneiss); (ii) ultramafic rocks (in a few places); and (iii) sulfide-poor troctolite (rare). The troctolite fragments are irregular, several centimetres in diameter, and often have sharp margins; they have experienced only minor alteration including serpentinization of olivine and sericitization of plagioclase. The ultramafic fragments, mainly mela-troctolite, wehrlite and dunite, are irregular in shape with diameters of up to tens of centimetres. Olivines in the ultramafic rock inclusions are often highly serpentinized. The inclusions of gneiss are smaller, ranging from a few millimetres to several centimetres in diameters. They have resorbed margins and sometimes show a preferred orientation, particularly in areas where sulfide is dominant in the matrix. Evidence that chemical reaction occurred between the gneiss inclusions and the enclosing troctolite magma is well preserved. The degree of reaction generally increases from the Reid Brook Zone through the Discovery Hill Zone to the Eastern Deeps. The series of reactions, starting with a typical garnet-corderite-hypersthene hornfels with a matrix of two

feldspars and biotite, have been described by Li and Naldrett (2000) and are discussed below.

Sulfides occur in three principal forms in Basal Breccia Sequence/Feeder Breccia, (i) as zones or stringers of interstital sulfide enclosing inclusions and cross-cutting sulfide-poor breccia ore; (ii) as irregular blotches and (iii) as stringers of massive sulfide that cross-cut other variants of this environment.

**Ferrogabbro.** This is a fine grained, non-cumulate rock comprising granular pyroxene (less than 10 mod%, mainly clinopyroxene), greenish brown hornblende (25-40 mod%), small plagioclase laths (30-40 mod%), biotite (10-15 mod%) and ilmenite (5-10 mod%). Ferrogabbro is generally massive but occasionally exhibits flow banding particularly in areas where sulfide is present.

## 6.5 Olivine and Plagioclase Compositions

Li and Naldrett (1999) have determined the compositions of plagioclase and olivine using wavelength dispersive microprobe analysis. The variation of mineral compositions is discussed below.

### 6.5.1 Stratigraphic Variation in Olivine and Plagioclase Composition

**The Eastern Deeps.** The variation in olivine and plagioclase composition with depth in the Olivine Gabbro, Normal Troctolite, Varied-textured Troctolite and Basal Breccia Sequence in the Eastern Deeps is illustrated in Figs. 6.13a&b (see Fig. 6.3a for drill hole locations). The forsterite content (Fo) of olivine and the anorthite (An) content of plagioclase are positively correlated, both increasing upward. There is a pronounced decrease in the Ni content of olivine in the Olivine Gabbro as compared to the underlying Normal Troctolite (less than 530 vs. 900–1700 ppm) for olivines with similar Fo content.

**The Discovery Hill Zone.** Fig. 6.13c illustrates the stratigraphic variation of Fo in olivine and An in plagioclase along drill hole 106 within the Discovery Hill Zone. The Fo content of olivine increases upward from 48 to 62 mole percent within the Leopard Troctolite and varies between 42 and 48 in the Feeder Olivine Gabbro. The Ni content of olivine in the Feeder Olivine Gabbro is much lower than in the underlying Leopard Troctolite

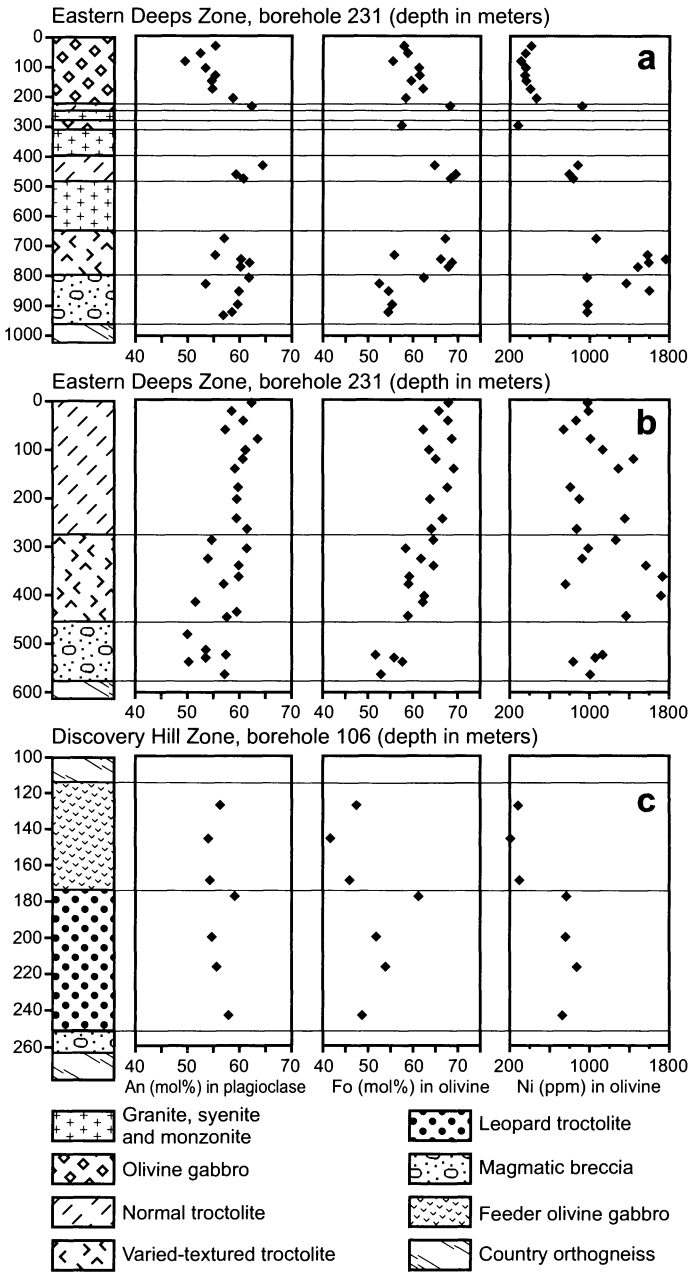


**Fig. 6.13.** Stratigraphic variations of plagioclase and olivine composition in boreholes 231 and 166 in the Eastern Deeps chamber (a, b), and borehole 106 in the Discovery Hill Zone (c). Position of the boreholes is shown in Fig. 6.3a. Modified after Li and Naldrett (1999)

(150-300 ppm in Feeder Olivine Gabbro vs 500-900 in Leopard Troctolite).

**The Reid Brook Zone.** In the Reid Brook Zone olivine in Feeder Olivine Gabbro is similarly depleted in Ni (less than 250 ppm in Feeder Olivine Gabbro as compared to 600-700 ppm in the adjacent Feeder Breccia). The Fo contents of olivine in the Leucotroctolite show little variation with depth, being relatively constant at around 60 mole percent while the Ni content of olivine generally decreases upward from 800 to 500 ppm. Two populations of olivine with significantly different Ni contents are retained in the Varied-textured Troctolite close to where it merges with the feeder. The Ni-depleted type of olivine is similar to that in the underlying Leucotroctolite while the Ni-undepleted type of olivine is similar to that in the Varied-textured Troctolite of the Eastern Deeps chamber.

### 6.5.2 Ni and Fo content of Olivine in Different Rock Sequences

A plot of Ni in olivine versus Fo content in olivine is shown in Fig. 6.14. Olivines in the ultramafic rock inclusions show a steep trend of decreasing Ni content, with Ni decreasing from 2600 ppm at about $Fo_{80}$ to 1300 ppm at $Fo_{73}$. Olivines in the Leucotroctolite, Olivine Gabbro and Feeder Olivine Gabbro show a more gentle trend with Ni decreasing from <900 ppm at $Fo_{65}$ to as low as 100 ppm at $Fo_{41}$. Olivines in the Normal Troctolite, Varied-textured Troctolite and Basal Breccia Sequence show no systematic trend but form a "cloud" with Fo varying between 72 and 52 and Ni between 1800 and 700 ppm. In these rocks the Fo content of olivine decreases systematically from the Normal Troctolite ($Fo_{73-62}$ in most samples), through the Varied-textured Troctolite ($Fo_{68-58}$ in most samples) to the Basal Breccia Sequence ($Fo_{60}$ to $Fo_{53}$ in most samples). Olivines in the Leopard Troctolite, most of which contain 30% or more sulfide, describe a trend of increasing Ni with decreasing Fo content, in which Ni increases from about 500 ppm at $Fo_{69}$ to 800 ppm at $Fo_{41}$.

A model trend for the co-variation of the Ni and Fo contents of olivine crystallising from a magma that initially gives rise to olivine with 2600 ppm Ni and Fo80 is shown in Fig. 6.14. In calculating this trend it has been assumed that the magma is crystallising olivine and plagioclase together (ratio of olivine to plagioclase = 1), that the olivine-magma partition coefficient for Ni is 9 and that the ratio (weight or mole) of $(FeO/MgO)_{olivine}/(FeO/MgO)_{liquid}$ = 0.3 (Roeder and Emslie 1970). This trend is superimposed on that for the ultramafic rock inclusions; it is seen that 20% crystallization in accordance with the above parameters accounts

well for the trend of the natural observations. As shown, extension of the model trend to 40% crystallization skirts the upper side of the data for the Leucotroctolite, Olivine Gabbro, Feeder Olivine Gabbro and Normal Troctolite, and the lower side of the cloud of data from the Varied-textured Troctolite.

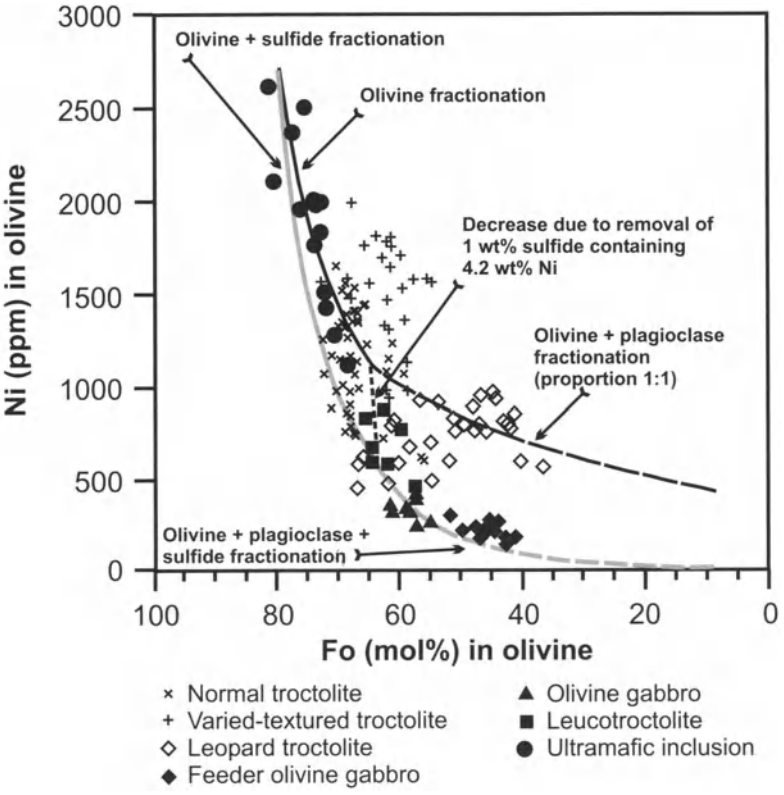


**Fig. 6.14.** Plot of olivine nickel content versus its forsterite content (Fo) in rocks of the Voisey's Bay intrusion and model curves. See text for discussion of modeling. After Li and Naldrett (1999)

Li and Naldrett (1999) have shown that the data for the Leucotroctolite, Olivine Gabbro and Feeder Olivine Gabbro are explicable if the fractionating magma became saturated with sulfide, possible as a result of interaction with the surrounding Tasiuyak gneiss after 20% of sulfide-free crystallisation, and then separated olivine, plagioclase and sulfide in a ratio of (olivine+plagioclase)/sulfide = 50/1 (dashed curve in Fig. 6.14). Scatter to the right of this line is explicable as a result of the olivine interacting with trapped intercumulus liquid (see Chap. 10).

Turning now to the Leopard Troctolite, Varied-textured Troctolite and Normal Troctolite, many samples of these rocks contain appreciable amounts of sulfide. Li and Naldrett (1999) have shown re-equilibration of olivine with sulfide accounts for much of the dispersion shown by these samples. This is discussed in Chap. 10, section 10.1.4 and Fig. 10.9b. The higher Fo contents of the Normal Troctolite and Varied-textured Troctolite, which are present in rocks that are younger than the Leucotroctolite, Olivine Gabbro, Feeder Olivine Gabbro and some of the ultramafic inclusions, is strong evidence that one or more influxes of fresh magma passed through the Voisey's Bay system of magma conduits (see section 6.8).

## 6.6 Geochemistry of Voisey's Bay Rocks

### 6.6.1 Major Elements

Average chemical compositions of main rock types of the Voisey's Bay intrusion and country gneisses are shown in Table 1.1. Li et al. (2000) have shown that major element compositions of the intrusive rocks are controlled essentially by the proportion of cumulus plagioclase, olivine and trapped silicate liquid. Most samples of Normal Troctolite and Varied-textured Troctolite in the Eastern Deeps subchamber fall within or close to the olivine-plagioclase composition array (Fig. 6.15). A few Varied-textured Troctolite samples show abnormally high $Al_2O_3$ contents, which is attributed to the presence of high-Al residual gneiss inclusions in the samples (see above discussion). Due to their high hornblende and biotite contents, the Ferrogabbros are displaced to the right in the plot of CaO versus MgO. The Olivine Gabbro in the Eastern Deeps and the Feeder Olivine Gabbro in the conduit are displaced toward the right close to the field of the chilled margin rocks of the conduit. The samples of Leucotroctolite in the Reid Brook subchamber plot close to the olivine-plagioclase arrays. The Basal Breccia Sequence samples contain abundant $Al_2O_3$-rich residual gneiss inclusions and plot, as would be expected, to the left of olivine-plagioclase array. Due to their high pyroxene contents, many of the ultramafic rock fragments in the Basal Breccia Sequence, are significantly displaced to the right of the arrays in both plots CaO – MgO and $Al_2O_3$ – $SiO_2$ (Fig. 6.15).

**Table 6.1.** Average chemical composition of the Igneous and Country Rocks at Voisey's Bay

| Rock | NT | VT | LT | MB | FOG | UM | TG | NG |
|---|---|---|---|---|---|---|---|---|
| n | 7 | 57 | 2 | 4 | 6 | 8 | 7 | 6 |
| $SiO_2$ | 46.45 | 45.88 | 30.58 | 41.71 | 44.73 | 43.67 | 59.23 | 53.99 |
| $TiO_2$ | 0.57 | 1.10 | 1.79 | 2.62 | 3.92 | 0.87 | 0.84 | 0.75 |
| $Al_2O_3$ | 21.18 | 18.97 | 12.18 | 19.90 | 16.72 | 6.52 | 14.43 | 16.58 |
| $Fe_2O_3T$ | 7.04 | 9.56 | 40.90 | 16.82 | 13.39 | 14.56 | 11.11 | 11.31 |
| MgO | 10.05 | 10.54 | 4.77 | 5.89 | 6.04 | 24.88 | 3.95 | 2.82 |
| MnO | 0.07 | 0.09 | 0.12 | 0.13 | 0.15 | 0.18 | 0.08 | 0.10 |
| CaO | 9.27 | 8.51 | 5.54 | 6.92 | 7.41 | 6.17 | 4.29 | 5.90 |
| $Na_2O$ | 2.74 | 2.86 | 2.03 | 3.12 | 3.66 | 1.15 | 2.55 | 4.72 |
| $K_2O$ | 0.24 | 0.31 | 0.34 | 1.00 | 0.94 | 0.28 | 2.84 | 1.60 |
| $P_2O5$ | 0.13 | 0.17 | 0.26 | 0.50 | 0.70 | 0.13 | 0.09 | 0.31 |
| Total | 97.73 | 97.99 | 98.50 | 98.61 | 97.66 | 98.41 | 99.42 | 98.08 |
| LOI | 0.31 | 0.43 | 5.98 | 1.28 | 0.29 | 3.19 | 3.46 | 1.17 |
| S | 0.03 | 0.43 | 13.85 | 2.71 | 0.12 | 0.16 | 2.43 | 1.40 |
| Ni | 308 | 939 | 6011 | 2543 | 74 | 1261 | 192 | 1124 |
| Cu | 12 | 329 | 2657 | 1266 | 56 | 133 | 186 | 484 |
| Co | 48 | 75 | 608 | 176 | 50 | 101 | 36 | 88 |
| Cr | 67 | 152 | 101 | 154 | 64 | 1872 | 211 | 59 |
| Sc | 6 | 11 | 7 | 14 | 16 | 25 | 15 | 12 |
| V | 37 | 74 | 86 | 165 | 149 | 134 | 198 | 105 |
| Zn | 45 | 69 | 118 | 185 | 141 | 92 | 157 | 85 |
| Ga | 12 | 14 | 10 | 27 | 19 | 8 | 19 | 22 |
| Cs | 0.04 | 0.05 | 0.08 | 0.61 | 0.14 | 0.13 | 0.58 | 0.14 |
| Rb | 2 | 3 | 4 | 24 | 10 | 7 | 85 | 24 |
| Sr | 565 | 501 | 323 | 456 | 474 | 108 | 223 | 1006 |
| Ba | 139 | 158 | 176 | 362 | 427 | 85 | 622 | 924 |
| Y | 5 | 7 | 8 | 17 | 23 | 11 | 13 | 14 |
| Zr | 12 | 18 | 26 | 43 | 39 | 34 | 144 | 56 |
| Hf | 0.47 | 0.69 | 1.11 | 1.64 | 1.80 | 1.21 | 4.89 | 1.83 |
| Nb | 1.62 | 2.42 | 3.52 | 9.04 | 9.99 | 2.15 | 6.60 | 7.00 |
| Ta | 0.11 | 0.50 | 0.24 | 0.61 | 0.68 | 0.15 | 0.29 | 0.33 |
| Pb | 1.05 | 11.69 | 68.16 | 18.82 | 8.45 | 6.03 | 12.84 | 13.93 |
| Th | 0.12 | 0.18 | 0.21 | 3.33 | 0.54 | 0.29 | 20.73 | 0.70 |
| U | 0.03 | 0.04 | 0.08 | 0.33 | 0.12 | 0.09 | 0.76 | 0.24 |
| La | 4.70 | 5.55 | 7.38 | 20.86 | 20.57 | 4.73 | 47.83 | 31.64 |
| Ce | 10.76 | 13.01 | 18.13 | 47.82 | 49.93 | 12.32 | 98.50 | 65.90 |
| Pr | 1.43 | 1.75 | 2.48 | 6.23 | 6.83 | 1.81 | 11.75 | 8.13 |
| Nd | 6.31 | 7.87 | 10.85 | 26.56 | 30.20 | 8.78 | 43.22 | 32.41 |
| Sm | 1.31 | 1.69 | 2.30 | 5.31 | 6.43 | 2.18 | 6.17 | 5.66 |
| Eu | 0.82 | 0.90 | 0.98 | 1.64 | 2.20 | 0.69 | 1.34 | 1.82 |
| Gd | 1.19 | 1.61 | 2.04 | 4.50 | 5.76 | 2.13 | 3.96 | 4.24 |
| Tb | 0.17 | 0.23 | 0.30 | 0.63 | 0.82 | 0.32 | 0.50 | 0.56 |
| Dy | 0.95 | 1.32 | 1.59 | 3.28 | 4.45 | 1.94 | 2.30 | 2.72 |
| Ho | 0.18 | 0.26 | 0.31 | 0.63 | 0.85 | 0.40 | 0.47 | 0.52 |
| Er | 0.47 | 0.67 | 0.79 | 1.56 | 2.17 | 1.02 | 1.31 | 1.33 |
| Tm | 0.07 | 0.10 | 0.11 | 0.23 | 0.31 | 0.15 | 0.22 | 0.20 |
| Yb | 0.40 | 0.56 | 0.62 | 1.28 | 1.72 | 0.86 | 1.37 | 1.13 |
| Lu | 0.06 | 0.08 | 0.09 | 0.18 | 0.26 | 0.13 | 0.22 | 0.17 |

**Table 6.1.** (cont.)
*n* number of samples. Major elements and S in wt%; trace elements in ppm. Rock types: *NT* Normal Troctolite; *VT* Varied-textured Troctolite; *LT* Leopard Troctolite; *MB* Magmatic breccia; *FOG* Feeder Olivine Gabbro; *UM* Ultramafic inclusions; *TG* Tasiuyak gneiss; *NG* Nain gneiss

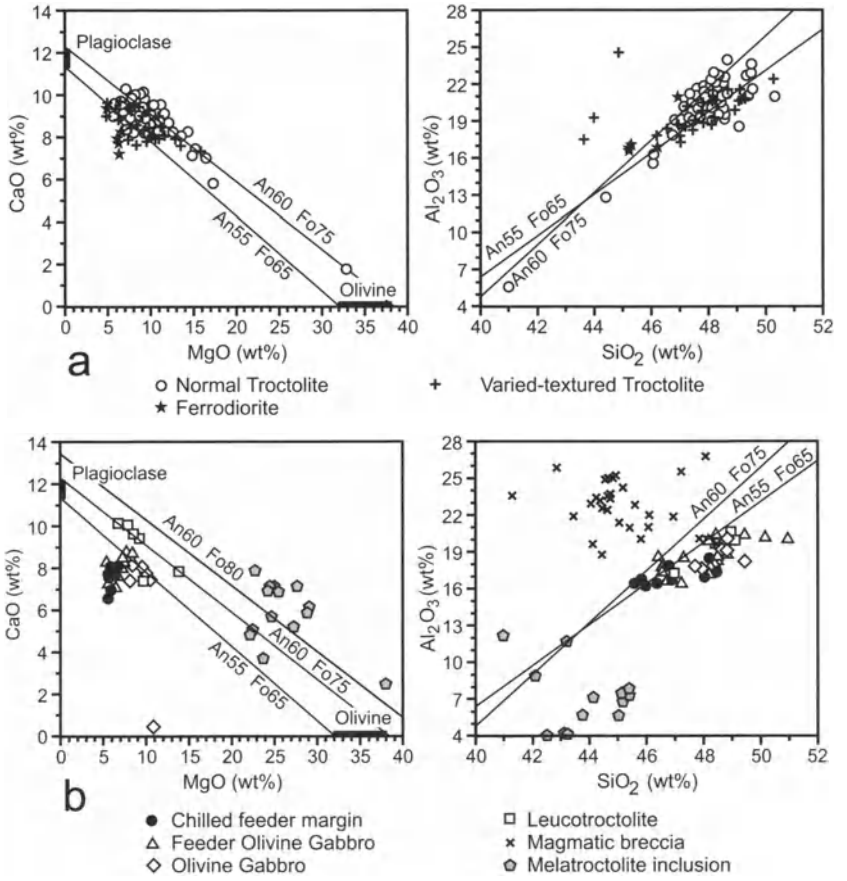


**Fig. 6.15.** Plots of CaO vs. MgO and Al2O3 vs, SiO2 for rocks of the Voisey's Bay intrusion: **a** = Normal Troctolites, Varied-textural Troctolites, and Ferrogabbronorites; **b** = Olivine Gabbro, Leucotroctolite, feeder rocks, Magmatic breccias, and melatroctolite inclusions. After Li et al. (2000)

## 6.6.2 Trace Elements

**General Information.** Samples from the conduit and marginal zones of the Eastern Deeps, Ovoid and Mini-ovoid, Discovery Hill Zone, and Reid

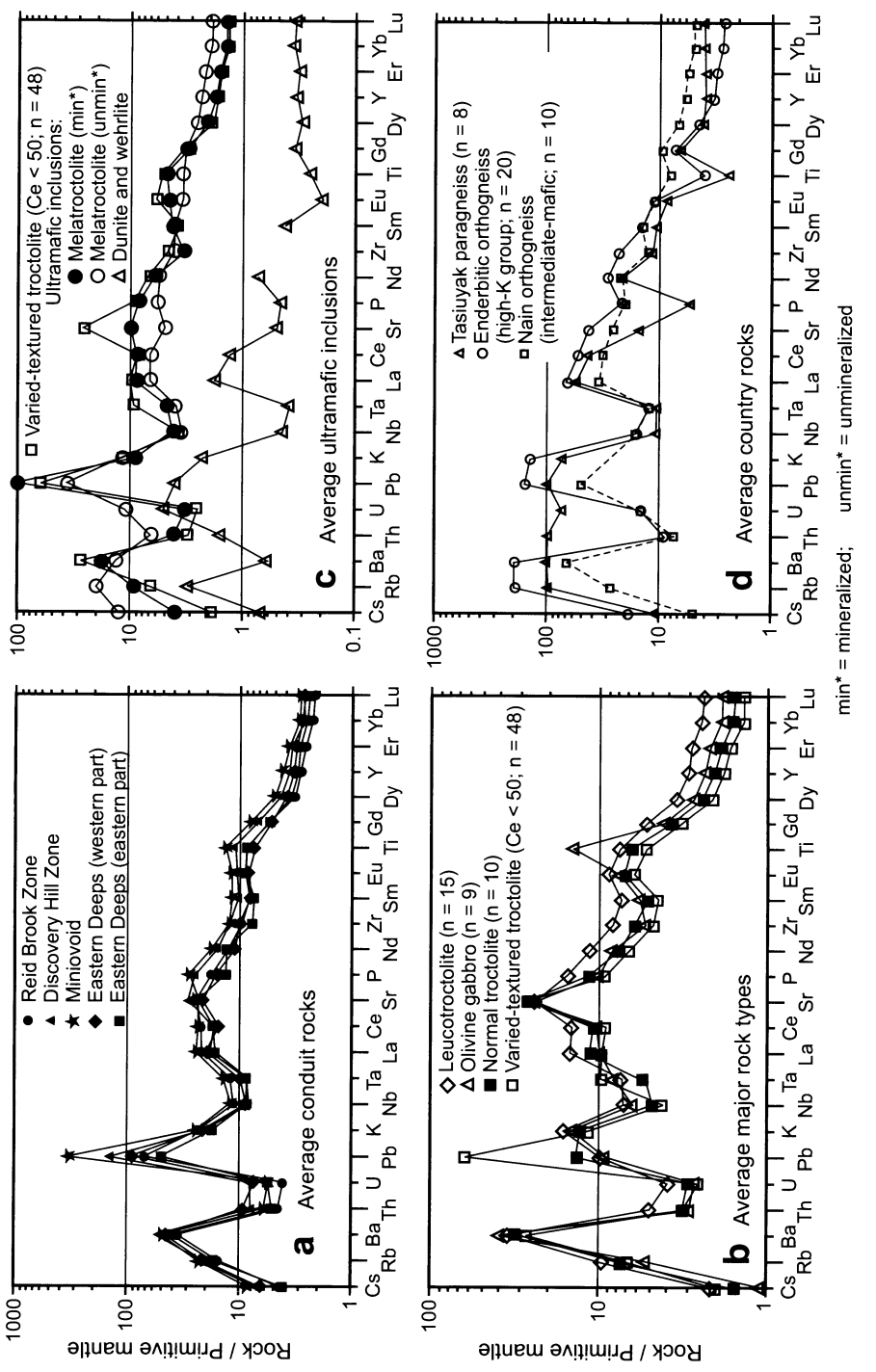
Rock / Primitive mantle
1000
100
10
1
Cs Rb Ba Th U Pb K Nb Ta La Ce Sr P Nd Zr Sm Eu Ti Gd Dy Y Er Yb Lu
● Reid Brook Zone
▲ Discovery Hill Zone
★ Miniovoid
◆ Eastern Deeps (western part)
■ Eastern Deeps (eastern part)
a Average conduit rocks
◇ Leucotroctolite (n = 15)
△ Olivine gabbro (n = 9)
■ Normal troctolite (n = 10)
□ Varied-textured troctolite (Ce < 50; n = 48)
b Average major rock types
□ Varied-textured troctolite (Ce < 50; n = 48)
Ultramafic inclusions:
● Melatroctolite (min*)
○ Melatroctolite (unmin*)
△ Dunite and wehrlite
c Average ultramafic inclusions
0.1
▲ Tasiuyak paragneiss (n = 8)
○ Enderbitic orthogneiss (high-K group; n = 20)
□ Nain orthogneiss (intermediate-mafic; n = 10)
d Average country rocks
min* = mineralized; unmin* = unmineralized

**Fig. 6.16.** Primitive mantle normalized (Sun and McDonouugh, 1989) spidergrams for rocks of the Voisey's Bay intrusion. After Li et al. (2000)

Brook Zone are shown in Fig. 6.16a as a primitive mantle-normalized spidergram plot (Sun and McDonough, 1989). The samples show strong enrichment in the LREE, enrichment in some of the large ion lithophile elements (Rb, Ba and K), low Th and U contents, and a slightly negative Ta+Nb anomaly. The elevated Sr and Eu concentrations reflect the modal plagioclase content; likewise Ti is present in oxide minerals (ilmenite and titanomagnetite), and P is present in apatite; both the oxide and apatite contents of the conduit and marginal rocks tend to be high but variable. Apart from these elements, the spidergram profiles are very similar, and show no relationship to the nature of the immediate host rocks. The data presented in Fig. 6.16a indicate that the marginal ferrogabbro and olivine gabbro are enriched in trapped liquid relative to the troctolites, and that the compositions of the finer-grained (chilled) marginal rocks are not influenced by chemical contributions from the immediate country rocks. The presence throughout the deposit of inclusions that have originated from paragneiss indicates that equilibration of the melt with country rock occurred at depth, and not in-situ within the conduit. Indeed, there is every indication that the Voisey's Bay Intrusion magma did not react extensively with the wall rocks, although projections of orthogneiss within the Eastern Deeps do show extensive local evidence of assimilation as evidenced by the presence of troctolite-gneiss melange along the contact. White feldspathic clots within the Varied-textured Troctolite, 0.5-5cm in diameter may also be the result of such assimilation.

Average primitive mantle-normalized spidergram patterns of troctolitic rocks and olivine gabbro of the Eastern Deeps and Reid Brook chambers are shown in Fig. 6.16b. With the exception of Pb and Ta, the normalized patterns of the Varied-textured Troctolite and Normal Troctolite are essentially indistinguishable. The absolute abundances of trace elements are controlled by the amount of trapped liquid, which is higher in the Olivine Gabbro than the Varied-textured Troctolite and Normal Troctolite. The profiles have a similar shape to the conduit assemblage rocks, with moderate LREE enrichment, and steep negative Th+U and lesser Ta+Nb anomalies.

Figure 6.16c shows the spidergram patterns of different groups of ultramafic inclusions. The mineralized melatroctolite inclusions have similar spidergram patterns to the Varied-textured Troctolite; as would be expected if they are ultramafic cumulates that were formed at an early stage with the sulfide saturated magma, and were subsequently broken up and incorporated as cognate xenoliths. A second group of unmineralized mela-

troctolite inclusions have spidergram patterns slightly flatter than the first group. These rocks may have crystallized from a less fractionated, less contaminated and sulfide-undersaturated magma. The third group of ultramafic inclusions are essentially highly altered rocks that have compositions between dunite and wehrlite, and are characterized by no disseminated sulfide and very different sipdergram patterns when compared to the Voisey's Bay Intrusion and other ultramafic inclusions (Figure 6.16c). The gabbroic fragments in the breccia sequence are geochemically like the fine-grained ferrogabbroic rocks developed at the walls of the conduit (both have Ce/Yb=27–33 and MgO=5–8 wt%).

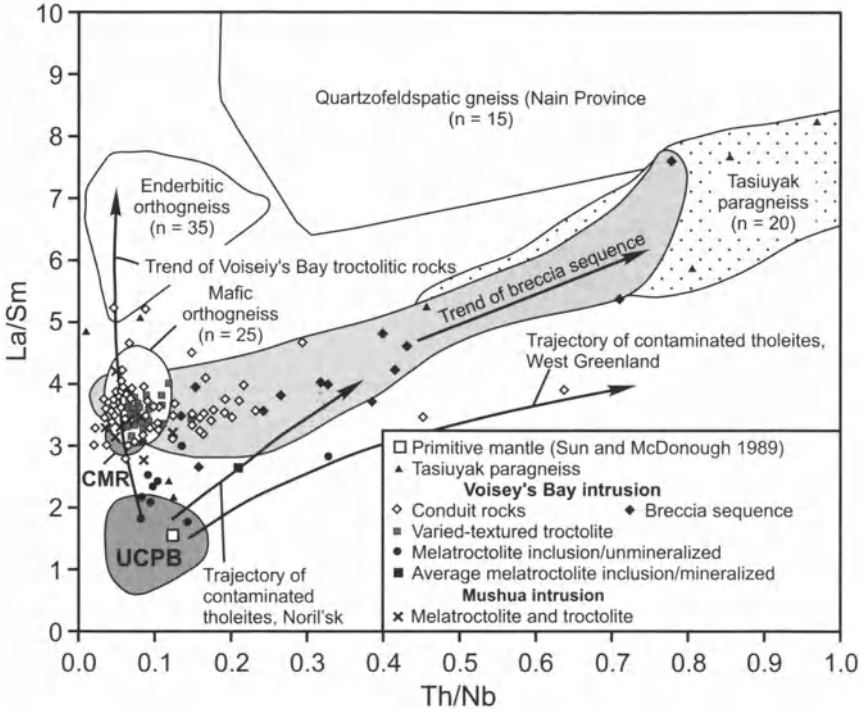


**CMR** = chilled margin of the Voisey's Bay intrusion (n = 8)

**UCPB** = Uncontaminated picritic basalts from Noril'sk and West Greenland (after Lightfoot and Hawkesworth 1997)

**Fig. 6.17.** Plot of La/Sm versus Th/Nb for rocks of the Voisey's Bay and Mushua intrusions, and country gneisses. After Li et al. (2000)

Figure 6.17 shows samples of different phases of the Voisey's Bay Intrusion, the nearby Mushuau Intrusion and the Tasiuyak paragneiss on a plot of La/Sm versus Th/Nb. Most Varied-textured Troctolite and conduit

samples from the Voisey's Bay Intrusion have La/Sm ratios between 3.0 and 4.0 and Th/Nb ratios of less than 0.1. The Normal Troctolite samples, which are not shown in the plot, have the ratios of La/Sm and Th/Nb similar to the Varied-textured Troctolite samples. The Tasiuyak paragneiss is characterized by La/Sm between 4.0 and 7.0 and Th/Nb between 0.4 and 1.0. The Basal Breccia Sequence samples, which contain high proportions of inclusions of what are interpreted to be reacted Tasiuyak paragneiss extend in array from the field of the Varied-textured Troctolite of the Voisey's Bay Intrusion and conduit rocks towards that of the Tasiuyak paragneiss, lending support to the interpretation that the inclusions are indeed of Tasiuyak paragneiss. Some conduit and Varied-textured Troctolite samples also extend toward the field of the Tasiuyak paragneiss, in part due to their content of inclusions. Li et al. (2000) conclude that all rocks of the Voisey's Bay Intrusion are consistent with derivation from mantle derived picritic magma that underwent an early phase of contamination in which the La/Sm ratio was increased, but the Th/Nb ratio was unaffected, before rising to the present stratigraphic level of the Voisey's Bay Intrusion. Support for their supposition that the initial magma at Voisey's Bay had been derived from a primitive mantle comes from the trend of the Voisey's Bay Intrusion unmineralized melatroctolite inclusions which provide a link between primitive mantle and that of the Voisey's Bay Intrusion conduit rocks (Fig. 6.17).

**Reaction between Troctolitic Magma and Inclusions of Tasiuyak gneiss.** Li and Naldrett (2000) have shown that inclusions of gneiss in the Basal Breccia Sequence and Feeder Breccia have reacted extensively with the enclosing magma. In general, the degree of reaction of the inclusions increases from the Reid Brook Zone through the Discovery Hill Zone to the Eastern Deeps. In the course of this reaction, garnet in the gneiss has been oxidised to form hercynite and magnetite with the release of $SiO_2$ to the magma; cordierite has been dehydrated to form hercynite with the release of $SiO_2$; hypersthene and K-feldspar have reacted together to produce hercynite with the release of $SiO_2$ and $K_2O$; plagioclase has broken down to produce corundum, losing $SiO_2$ and $Na_2O$ to the magma and itself becoming enriched in anorthite; and the corundum has subsequently reacted with FeO and MgO from the enclosing magma to form hercynite. The colour of the hercynite changes progressively from beige in the Reid Brook Zone, through green in the Discovery Hill Zone to black in the Eastern Deeps; this colour change reflects an increase in $FeAl_2O_4$ at the expense of the $MgAl_2O_4$ in the hercynite. The inclusions of the Eastern Deeps characteristically show a series of reaction rims ranging from labradorite through biotite to orthopyroxene, which is thought to be the consequence of diffu-

sion controlled activity gradients of the principal oxide components. It is seen that interaction with the gneiss results in the addition of $SiO_2$, $K_2O$ and $Na_2O$ to the magma. This felsification of magma would have resulted in a decrease in its ability to dissolve sulfide and therefore would have promoted sulfide immiscibility.

**Cu/Zr Ratios.** Both Cu and Zr are incompatible elements during the early stages in the fractional crystallization of sulfide-unsaturated mafic/ultramafic magams, and thus both increase in concentration as fractionation proceeds, with the Cu/Zr ratio remaining constant. Since in cumulate rocks incompatible elements are contributed by the magma that has become trapped interstially between cumulus grains, the Cu/Zr ratio of any sample of cumulate will reflect the ratio in the magma that gave rise to the cumulate. Once sulfide immiscibility develops in a magma, Cu is no longer incompatible, and the Cu/Zr ratio will decrease as sulfides are removed. In the same way, if the magma or cumulates acquire additional sulfides from elsewhere, the Cu/Zr ratio will be higher than that of the initial, sulfide-unsaturated magma. Lightfoot et al. (1994) pointed out that Noril'sk basalts that were known **not** to have reacted with sulfide (Tuklonsky, Upper Morongovsky, Mokulaevsky) had Cu/Zr ratios between 1 and

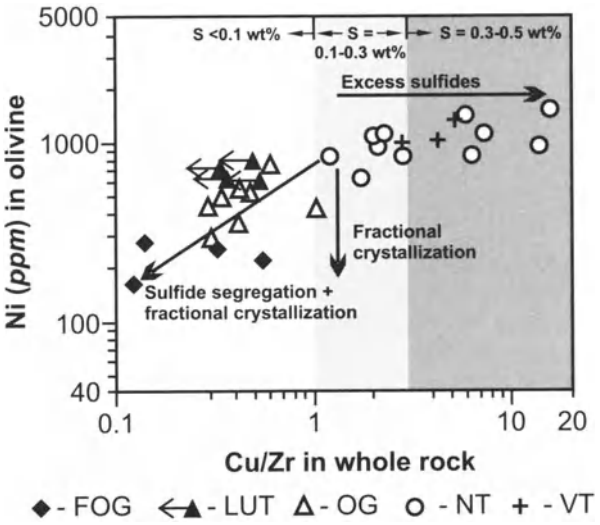


**Fig. 6.18.** Plot of olivine Ni content versus whole rock Cu/Zr ratio (after Li and Naldrett, 1999). FOG = Feeder olivine gabbro; LUT = Leucotroctolite; OG = Olivine gabbro; BBS = Basal breccia; NT = Normal troctolite; VT = Varied-textured troctolite. Small arrows indicate that Cu contents in these rocks are lower than the detection limit of 20 ppm that is used in calculating the Cu/Zr ratios for these samples

3, while those that were know to have reacted with sulfide had ratios <1. Li et al. (1999) showed that there is a correlation between Ni-depletion shown by olivine and the Cu/Zr ratios of the rocks hosting the olivine. Their data are reproduced in Fig. 6.18 in which it is seen that those rocks with Cu/Zr ratios <1 contain less S and also contain olivines with generally low Ni contents. Thus, at Voisey's Bay, Cu/Zr ratios are a useful indication of rocks that have formed from magma that has interacted with sulfide liquid and has thus become chalcophile-depleted.

### 6.6.3 Isotope Geochemistry

**Nd-Pb-Sr Isotopic Data.** Amelin et al. (2000) have studied the Nd-Pb-Sr isotopic systematics of the Voisey's Bay and nearby Mushuau (1.317-1.313 Ga) intrusions. They found that the Voisey's Bay intrusion has the most mantle-like, least contaminated initial isotopic compositions among the mafic intrusions of the Nain Plutonic Suite: εNd = -1 to -2; $^{87}Sr/^{86}Sr$ = 0.7034–0.7038; $^{206}Pb/^{204}Pb$ = 15.34–15.54; $^{207}Pb/^{204}Pb$ = 15.10–15.18; $^{208}Pb/^{204}Pb$ = 35.24–35.56. These ratios were found to be uniform in troctolites and gabbros from throughout the intrusion. Isotopic ratios for the Mushuau intrusion are quite distinct from the Voisey's Bay intrusion and are typical for the rest of the Nain Plutonic Suite: εNd = -3 to -10, $^{87}Sr/^{86}Sr$ = 0.7034–0.7052; $^{206}Pb/^{204}Pb$ = 14.21–14.55; $^{207}Pb/^{204}Pb$ = 14.63–14.77; $^{208}Pb/^{204}Pb$ = 34.36–34.65. Amelin et al. concluded that the primary magmas of the Voisey's Bay intrusion were either derived from an enriched continental mantle, or contaminated by a small amount of crustal material during ascent through lower-middle crust, and then by a volumetrically minor (probably 8–13%) amount of Tasiuyak gneiss. They attribute the observed variations in the Mushuau Intrusion, and the reported variations in other mafic intrusions of the Nain Plutonic suite to assimilation of 15–35% of a U-depleted Archean crust. They suggest that the larger amount of contamination experienced by intrusions other than the Voisey's Bay body is due to the magmas giving rise to these having passed through the crust 15 or more million years later than the Voisey's Bay magma, by which time the crust had become much hotter due to the passage of preceding magma.

**Re-Os Isotopic Data.** Lambert et al. (2000) have found that massive sulfide samples from the Voisey's Bay ores have high Re concentrations (148 to 288 ppb) for their Os concentrations (4.8 to 28 ppb), yielding high Re/Os ratios (2.9 to 38) that are similar to those for massive sulfides from Sudbury and the Duluth Complex. Whole rock Re-Os isotopic data exhibit

a large spread in $^{187}Re/^{188}Os$ (14 to 157) but do not define a precise isochron, which they attribute to the result of R-factor variations. However, large whole rock sulfide samples from the Ovoid yield an imprecise 1320 Ma isochron age that is consistent with baddeleyite U-Pb ages from the magmatic system (Amelin et al. 1999).

Lambert et al. (2000) argue that the high initial $\gamma_{Os}$ values (+200 to +1100 = percent deviation in calculated initial $^{187}Os/^{188}Os$ from mantle of the same age) for sulfide-rich samples from the Voisey's Bay intrusion document significant magma interactions with older Nain-Churchill Province crust. They consider the hypothesis that their Re-Os isotopic data is the result of contamination of basaltic magma similar to fine-grained feeder zone olivine gabbros and troctolites with sulfidic/graphitic Proterozoic Tasiuyak paragneiss ($\gamma_{Os}$ = +1900), followed by an R-factor process (300 to >5,000) that improved the tenor (metal concentration in 100% sulfide) of the sulfide liquid during transport in the active Voisey's Bay magma conduit[18]. However, they point out that R-factors of this magnitude are inconsistent with Naldrett et al.'s (2000) Cu, Ni and PGE data for the mineralization (see below). Their preferred model (see Fig. 6.19 and associated legend) is that the initial immiscible sulfide liquid interacted with a second, chalcophile-element undepleted (> 150 ppt Os) magma. This model gives R-factors (50–500) that are consistent with those of Naldrett et al. (2000), and conforms with that proposed by Li et al. (2000) on the basis of their geochemical data.

**Oxygen isotope data.** Ripley et al. (2000) have shown that the $\delta^{18}O$ values of Tasiuyak gneiss range from 8.3 to 16.1 per mil, and the enderbitic and mafic orthogneiss from 5.7 to 8.5 with most values less than 7.5 ‰. Reacted inclusions of Tasiuyak gneiss in Basal Breccia Sequence are depleted in $^{18}O$ relative to Tasiuyak gneiss outside the intrusion, ranging from 4.7 to 10.6 ‰. Elevated $\delta\ ^{18}O$ values (up to 9.3 ‰) are found in the troctolitic and noritic matrix to the breccias, but are restricted to less than 2 cm from the edges of inclusions. These isotopic exchange profiles have been produced during subsolidus cooling, and do not record the major $^{18}O$ depletion that has been experienced by the gneiss inclusions. It is thought that major contamination has been diluted by large volumes of later

[18] Strickly speaking in a dynamic environment such as Voisey's Bay, Lambert et al. should have modeled their data using the "N-factor" (see Chap. 2). However they did not do this and since I quote their work, I must continue their error. As shown in Chap. 2 the numerical difference between R and N is relatively small.

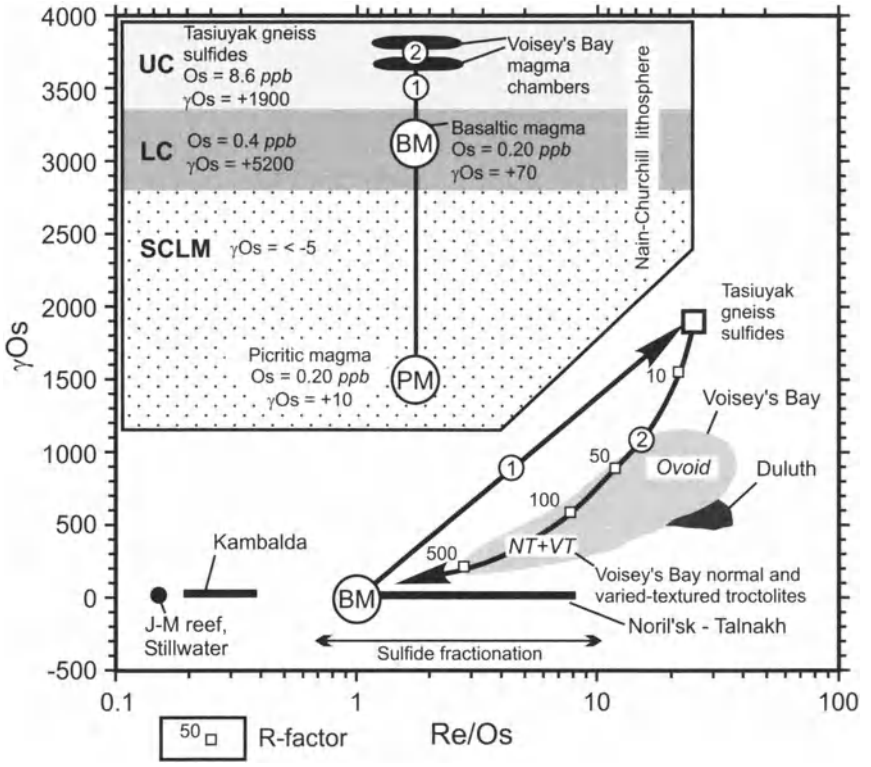


**Fig. 6.19.** Plot of initial γOs vs. Re/Os, showing data for Cu-Ni-Co mineralization from the Voisey's Bay deposit (after Lambert et al. 2000), J-M reef of Stillwater complex (after Lambert et al. 1994), Duluth complex (after Ripley et al. 1999), Noril'sk-Talnakh area (after Walker et al. 1994), and Kambalda camp (after Foster et al. 1996). Modified after Lambert et al. (2000).
The inset shows a model in which the picritic magma (PM), derived from a mantle plume, passes through Subcontinental lithospheric mantle (SCLM). In the lower crust (LC) it fractionates and forms basaltic magma (BM). Owing to interaction with surrounding rocks, its γOs increases to +70. The basaltic magma (BM) then ascends into the upper crust (UC) where it develops a magmatic chamber in the Tasiuyak gneiss (Reid Brook chamber) and assimilates sulfides from the gneiss (line 1 in inset and main plot). Tasiuyak sulfides contain 8.6 ppb Os with γOs = +1900. The assimilated sulfides saturate the basaltic magma, immiscible Fe-sulfide liquid develops and absorbs Ni, Cu, Co and PGE, causing the the magma to become strongly depleted in these elements. Fresh, undepleted magma subsequently enters the magmatic system and forces the previously depleted magma up a vertical dyke, to form the Eastern Deeps magmatic chamber. The fresh magma interacts with the early formed sulfides enriching them in chalcophile metals, decreases their Re/Os ratio and γOs value (line 2 in the plot). Sulfide compositions of the Voisey's Bay deposit correspond to an R-factor = 50–500

magma that have passed through the system, disrupting and moving breccia, sulfides and early magma up to a higher level.

## 6.7 Mineralization within the Voisey's Bay Intrusion

### 6.7.1 Types of Mineralization

There are 4 principal types of mineralization at Voisey's Bay; representatives of each are found in most of the mineralized environments. These are (i) massive sulfides, (ii) leopard textured sulfides, (iii) sulfides in Basal Breccia Sequence and (iv) disseminated sulfides in Varied-textured Troctolite. In addition, chalcopyrite- and bornite-bearing Cu-rich veins within the adjacent gneiss constitute what is yet an insignificant mineralization type – time will show whether substantial reserves of this material will be discovered, as has been the case at Sudbury and Noril'sk.

The mineralogy of each of the types of mineralization is described in detail by Naldrett et al. (2000b). Brief descriptions of their sulfide morphologies are given below. Average chemical compositions of the ores are present in Table 6.2.

**Massive Sulfide.** This consists of massive (>85% sulfides) accumulations of pyrrhotite (varying proportions of troilte and hexagonal pyrrhotite), pentlandite, chalcopyrite, cubanite and magnetite. Pyrrhotite occurs as coarse crystals, exceeding 10 cm in diameter in some samples. Naldrett et al. (2000b) pointed out that troilite is missing from the Eastern Deeps and most abundant within the Ovoid. Where present, troilite occurs as fine exsolution lamellae in hexagonal pyrrhotite. Cubanite occurs as discrete grains and exsolution lamellae in chalcopyrite and shows a similar distribution to troilite, being present where troilite is present and absent where it is absent. Massive sulfide of the Ovoid, Mini-ovoid and Reid Brook Zone is characterised by very coarse grains (1-2 cm) of pentlandite, with little or no pentlandite occurring as rims to pyrrhotite or as lamellae within pyrrhotite. Coarse pentlandite grains are rare in the massive sulfide of the Eastern Deeps and most pentlandite forms rims around crystals of pyrrhotite or occurs as lamellae within pyrrhotite. Magnetite is present in amounts of about 5% by volume in sulfides at the periphery of the Ovoid, 1% at the centre; it is rare in the massive sulfide of the Eastern Deeps.

**Leopard textured Sulfide.** As discussed above, the term "leopard texture" is derived from the principal characteristic of this sulfide which is that of

**Table 6.2.** Average composition of mineralization from different environments at Voisey's Bay

| Mineralization type<br>Deposit Zone | n | S | Ni | Cu | Co | Pd | Pt | Rh | Ru | Ir | Os | Au | Pd/Pt |
|---|---|---|---|---|---|---|---|---|---|---|---|---|---|
| **Massive Mineralization** | | | | | | | | | | | | | |
| Eastern Deeps | 5 | 37.66 | 3.19 | 0.85 | 0.18 | 145 | 51 | 19 | 34 | 7.4 | 16 | 22 | 2.82 |
| Ovoid | 52 | 33.76 | 4.12 | 2.53 | 0.18 | 226 | 88 | 7 | 13 | 1.8 | 2 | 82 | 2.57 |
| Mini-Ovoid | 11 | 35.65 | 3.72 | 2.16 | 0.18 | 208 | 166 | 8 | 16 | 2.3 | 4 | 109 | 1.25 |
| Discovery Hill | 1 | 36.60 | 2.50 | 1.02 | | 73 | 25 | 9 | | 1.9 | | 36 | 2.98 |
| Reid Brook | 15 | 37.01 | 2.84 | 1.11 | | 97 | 28 | 10 | 11 | 2.8 | 4 | 40 | 3.42 |
| **Leopard Textured Mineralization** | | | | | | | | | | | | | |
| Eastern Deeps | 8 | 15.90 | 1.45 | 0.75 | | 89 | 50 | 7 | 13 | 2.6 | 6 | 35 | 1.79 |
| Mini-Ovoid | 7 | 13.64 | 1.42 | 0.90 | 0.07 | 78 | 70 | 4 | 5 | 1.0 | 2 | 73 | 1.11 |
| Discovery Hill | 18 | 13.09 | 1.16 | 1.28 | 0.06 | 77 | 76 | 3 | 9 | 0.7 | 1 | 77 | 1.01 |
| Reid Brook | 9 | 12.32 | 1.04 | 0.69 | | 41 | 45 | 3 | 7 | 0.8 | 1 | 55 | 0.92 |
| **Mineralization in Magmatic Breccia** | | | | | | | | | | | | | |
| Eastern Deeps | 42 | 8.86 | 1.00 | 0.47 | 0.06 | 69 | 38 | 4 | 10 | 1.3 | 3 | 41 | 1.81 |
| Ovoid | 3 | 7.43 | 0.83 | 0.72 | 0.04 | 96 | 41 | 5 | 13 | 2.2 | 3 | 46 | 2.37 |
| Mini-Ovoid | 1 | 15.30 | 1.24 | 1.12 | 0.06 | 25 | 112 | 4 | 4 | 1.1 | 2 | 31 | 0.22 |
| Discovery Hill | 34 | 7.16 | 0.75 | 0.39 | 0.06 | 63 | 40 | 2 | 6 | 0.6 | 1 | 47 | 1.56 |
| Reid Brook | 23 | 5.86 | 0.59 | 0.30 | | 40 | 25 | 2 | 6 | 0.5 | 1 | 29 | 1.58 |
| **Mineralization in Varied textured troctolite** | | | | | | | | | | | | | |
| Eastern Deeps<br>(> 10% sulfide) | 21 | 10.64 | 1.21 | 0.75 | | 73 | 71 | 6 | 11 | 1.9 | 3 | 68 | 1.02 |

*n* number of samples. Contents: S, Ni, Cu, Co – wt%; Pd, Pt, Rh, Ru, Os, Ir, Au – mg/t (ppb)

black spots (augite and olivine oikocrysts ≈0.5 cm diameter) in a yellow matrix. The matrix consists of sulfides (primarily pyrrhotite, pentlandite and chalcopyrite) which occur interstitial to the principal cumulus silicates (plagioclase and olivine). The proportion of sulfide varies from 20 to 50 percent. In samples with more than 50 % sulfide, the sulfides have separated from the silicate host to form small schlieren of massive material. As has been remarked previously, the black spots are due to the development of oikocrysts of augite and olivine, which appear to have grown interstitial to the other silicates, when the sulfides were still liquid, and to have pushed the latter aside. The mineralogy of the leopard textured sulfide is similar to that of adjacent massive sulfide (Naldrett et al. 2000). The rock showing this texture is referred to in this chapter as "Leopard Troctolite".

**Sulfides in Magmatic breccias.** Mineralization in the Basal Breccia Sequence is much more variable than that of the two preceding mineralization types. In part it consists of small lenses of massive sulfide, in part of veins of Leopard Troctolite. Much of the mineralization comprises "blotches" of sulfide interstitial to the inclusions of gneiss, troctolite, melatroctolite and ultramafic rocks which are common in this rock unit (Li and Naldrett 1999; Li et al. 2000). Again, the mineralogy tends to reflect that of adjacent massive sulfide.

**Disseminated Sulfides in Varied-textured Troctolite.** Sulfides are abundant (approx. 25%) in the lower part of the Varied-textured Troctolite, and decrease in amount upward. They occur in two forms; the most common is as irregular "blotches", 10-30 cm in diameter, of sulfide intergrown with coarse silicates. The silicate minerals in these blotches comprise plagioclase and olivine which are very much coarser than those in the enclosing rock. In addition, coarse rods of plagioclase penetrate the sulfide blotches, growing away from plagioclase in the enclosing Varied-textured Troctolite. The second form of sulfide comprises irregular patches of disseminated sulfide, generally less than 20% in amount, which are present within Varied-textured Troctolite that displays a normal, medium-grained, igneous fabric.

### 6.7.2 The Ni and Cu content of Sulfide Mineralization from Different Mineralized Environments

Note that all Ni and Cu concentrations quoted in this section refer to metal content in 100% sulfide and have been taken from Naldrett et al. (2000a)[19].

[19] Note on calculating metal content in 100% sulfide. In calculating the metal content in 100% sulfide, the whole-rock Ni content is taken, on the assumption that it is all in sulfide, and then Ni is calculated as though it were all in pentlandite containing 36 wt% Ni (a typical value for Sudbury pentlandite). The sulfur required for the pentlandite is then subtracted from the whole rock sulfur content. The same calculation is made for Cu, assuming that it is all present as chalcopyrite. The remaining sulfur is then calculated as pyrrhotite, so that one can obtain the total sulfide content of the rock by summing the amounts of pentlandite, chalcopyrite and pyrrhotite. Because the amounts of sulfide in many of the samples in hole 166 and some samples from other holes are relatively low, Ni contained in olivine constitutes a significant proportion of the total Ni content of the rock, and has to be corrected for. This has been done by performing the calculation at first with no allowance made for Ni in olivine, and obtaining the composition of the resulting sulfide. The Ni content of the olivine is then calculated using this value and assuming (1) that the $Ni/Fe_{olivine} = (Ni/Fe_{sulfide})/25$, where 25 is the observed exchange partition coefficient between co-existing sulfide and olivine at Voisey's Bay (see Li and Naldrett 1999) and (2) that $Ni/Fe_{sulfide}$ excludes Fe tied up as chalcopyrite. In making this calculation it is assumed that the composition of the olivine is Fo65 (an average value for olivine of the Varied-textured Troctolite). Again, assuming that the non-sulfide portion of the sample contains 25 wt% olivine (the observed average content for the Varied-textured Troctolite), this amount of Ni is then subtracted from the whole rock Ni content, and the calculation repeated for Ni in 100% sulfide. The whole calculation is iterated until the calculated Ni content in sulfides varies by no more than 0.05 wt% between the last and penultimate iteration. In the case of many samples with less than about 2% sulfide, the calculation never converges, and these samples have been omitted. Several assumptions are required in making this correction (e.g. the Fo content of the olivine and the amount of olivine in the rock) that are not constant in all of the samples. However, one is using thousands of analyses performed in the course of routine exploration analysis, and it is not practical to measure the olivine composition and modal proportion of olivine for every sample. The reader can assure himself/herself that the error introduced in this way is relatively small, by repeating the correction procedure assuming, for example, that the Fo content is 60 instead of 65, or that the modal percent olivine is 30 instead of 25.

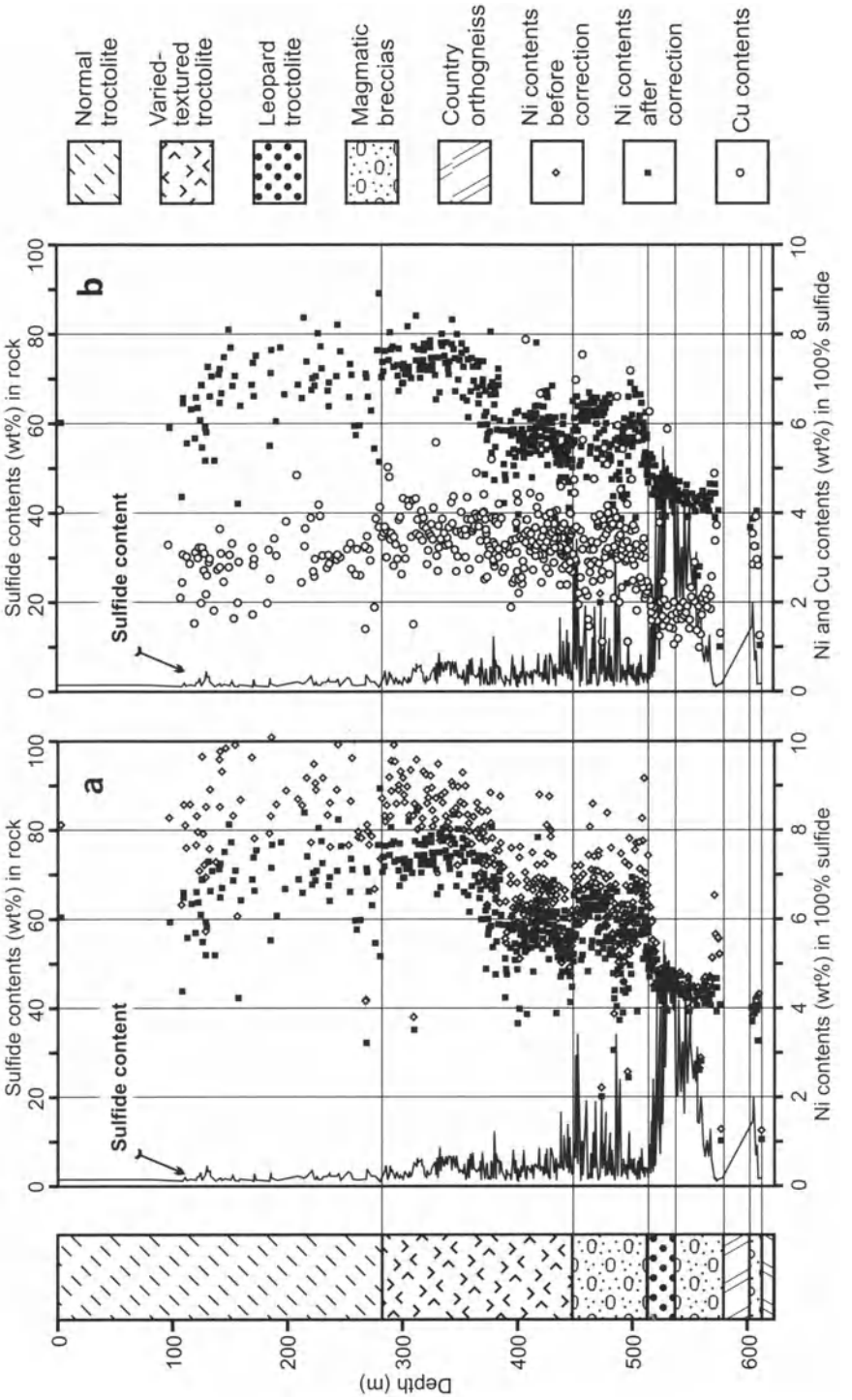
Normal troctolite
Varied-textured troctolite
Leopard troctolite
Magmatic breccias
Country orthogneiss
Ni contents before correction
Ni contents after correction
Cu contents
a
b
Sulfide content
Sulfide contents (wt%) in rock
Ni contents (wt%) in 100% sulfide
Ni and Cu contents (wt%) in 100% sulfide
Depth (m)
0
100
200
300
400
500
600
0
20
40
60
80
100
0
2
4
6
8
10

**Fig. 6.20.** Sulfide content in rock and Ni and Cu concentrations in 100% sulfide in borehole 166 at Eastern Deeps (borehole location is shown in Fig. 6.3a). Plot a shows the Ni concentration in sulfide before and after correction for Ni contained in olivine (the method used for the correction is described in text). Plot b shows the Ni concentration after correction along with Cu concentration in 100% sulfide. After Naldrett et al. (2000a)

**Eastern Deeps.** Variation in the Ni and Cu content of sulfides across typical profiles through the Eastern Deeps are illustrated in Figs. 6.20 - 6.22 (holes 166, 202, and 205). The location of these holes are shown in Fig. 6.3. Hole 166 was drilled very close to the mouth of the feeder with the Eastern Deeps intrusion (see Fig. 6.3a), but at a location at which massive sulfide is not developed.

The calculated amount of Ni in 100% sulfides is shown both before and after making the above correction in Fig. 20a. As would be expected, there is no significant difference in samples containing more than 10% sulfide, but in samples with less than this, the difference between corrected and uncorrected Ni is appreciable. Corrected values for Ni and Cu are shown in Fig. 20b (the correction for Ni in olivine has very little effect on Cu in 100% sulfide, except in so far as the total sulfide content changes very slightly). It is seen that sulfides in Basal Breccia Sequence and in which the sulfide content is relatively high (20-40%) contain about 4.5 wt% Ni and 1.75 wt% Cu. Sulfides in Troctolite Gneiss Melange and Varied-textured Troctolite immediately overlying this zone contain about 5.5 wt% Ni and 3.5 wt% Cu. The Ni content of sulfide then rises again upward in the Varied-textured Troctolite to about 7.5 wt% Ni (Cu does not show a similar increase). In the upper part of the Varied-textured Troctolite there is a suggestion that both Ni and Cu decrease upward.

Hole 202 was drilled east of hole 166, again just at the mouth of the feeder but in a location where a 40 m-thick lens of massive sulfide occurs in a slight depression in the base of the intrusion adjoining the feeder mouth. It is seen from the profile of Fig. 6.21 that Ni in the massive sulfide is relatively constant, averaging 3-3.5 wt%. Cu is scattered and low, averaging about 1 wt%. Both Ni and Cu rise in sulfides in the Basal Breccia Sequence that overlies the massive zone, Ni to 4.5–5 wt%, Cu to 1–2 wt%. Hole 206, which was drilled due east of hole 202, passed downward through Varied-textured Troctolite lining the base of the main body of the Eastern Deeps, 100 m of underlying gneiss, and. below this, Leopard Troctolite, massive sulfide and Basal Breccia Sequence within the feeder. As in Hole 202, the massive sulfide contains 3–3.5 wt% Ni (Fig. 6.22) and scattered Cu values averaging about 1 wt%. The Varied-textured Troctolite

above the screen of gneiss contains 5–15 wt% sulfides which contain upward of 5 wt% Ni and 2–3 wt% Cu.

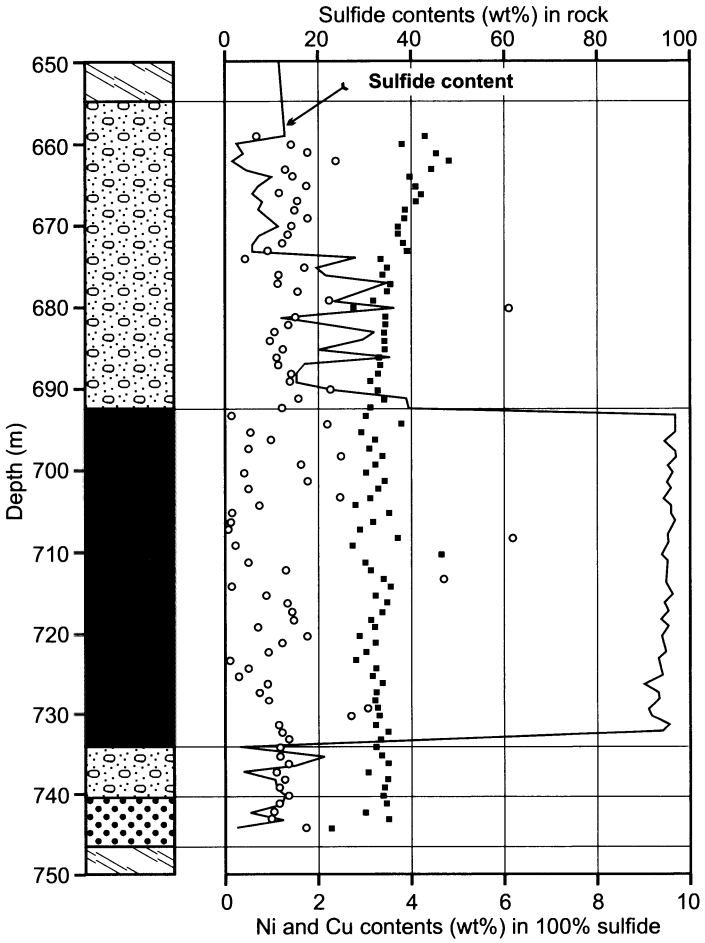


**Fig. 6.21.** Sulfide content of rock and Ni and Cu concentrations in 100% sulfide in borehole 202, Eastern Deeps (borehole location is shown in Fig. 6.3a). Black fill in borehole log marks massive sulfides; the remaining patterns are those used in Fig. 6.20. After Naldrett et al. (2000a)

**Ovoid.** Hole 7 penetrates through the massive sulfide occupying the centre of the Ovoid. It is seen from Fig. 6.23 that Ni increases upward from an average of 3.90 wt% over the lowermost 20 m of massive sulfide to an average of 4.66 wt% over the uppermost 20 m. Cu increases even more markedly from an average of 2.06 wt% over the lowermost 20 m to 4.66 wt% over the uppermost. In contrast, Co shows a slight decrease from an

average of 0.16 wt% over the lowermost 20 m to 0.15 wt% over the uppermost. These variations are attributed to fractional crystallisation as is discussed below.

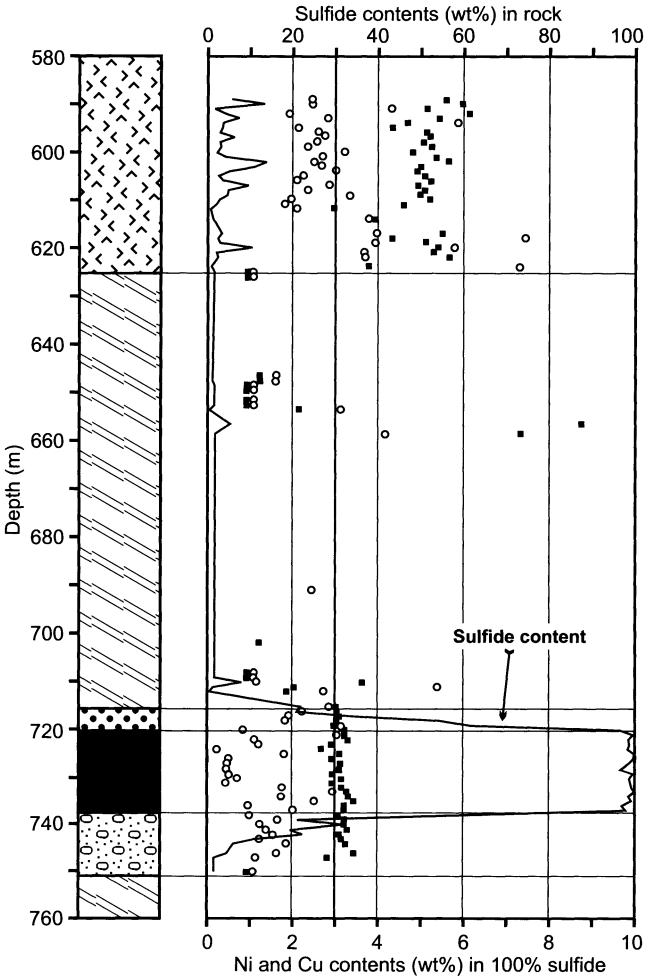


**Fig. 6.22.** Sulfide content of rock and Ni and Cu concentrations in 100% sulfide in borehole 206, Eastern Deeps (borehole location is shown in Fig. 6.3a). Black fill in borehole log marks massive sulfides; the remaining patterns are those used in Fig. 6.20. After Naldrett et al. (2000a)

**Discovery Hill Zone.** Hole 162 (see Fig, 6.3a for location) was selected for study as typical of the mineralization of the Discovery Hill Zone. It intersected 55 m (true thickness) of Leopard Troctolite containing 15 m of Basal Breccia Sequence (Fig. 6.24). The sulfide distribution is variable, generally between 20 and 40 wt%, rising to 50–60 wt% in many samples

near the base of the zone. The Ni content is very consistent averaging 4.04 wt% Ni in 100% sulfide. Cu is more variable but shows no consistent variation with either rock type or position and averages 3.15 wt% over the mineralized intersection.

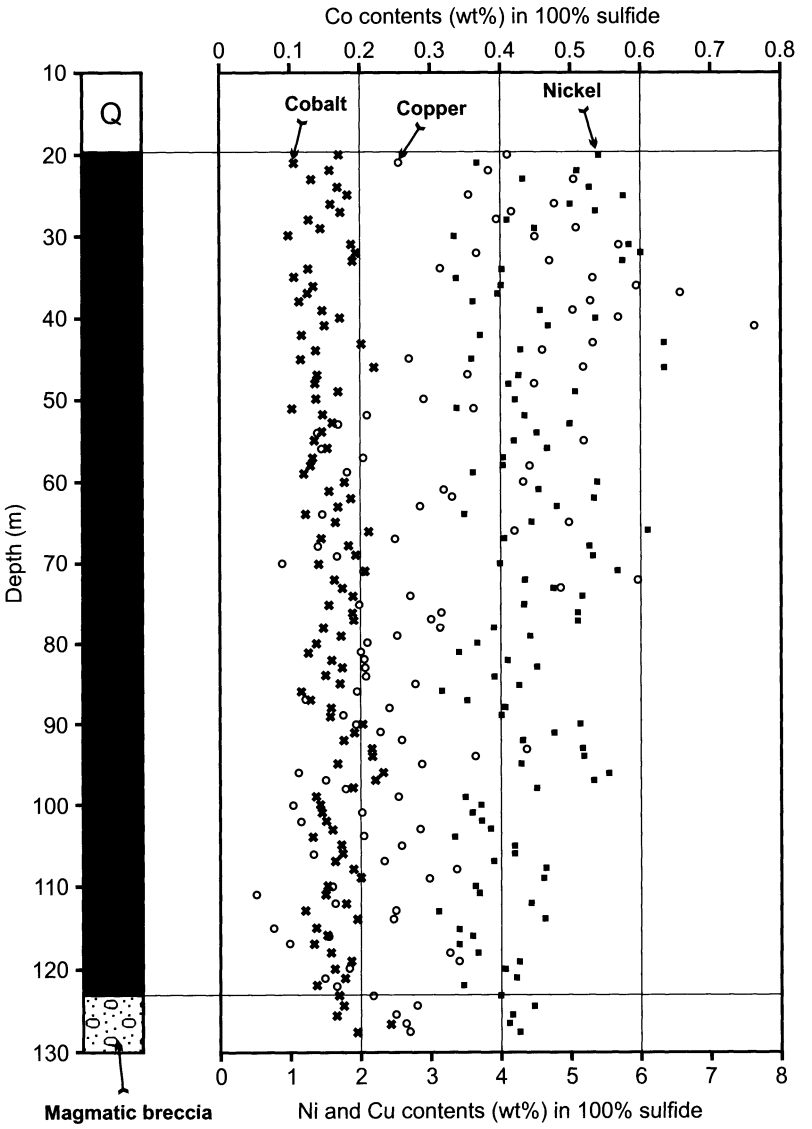


**Fig. 6.23.** Ni, Co and Cu concentrations in 100% sulfide in massive ore (black fill) and mineralization of magmatic breccia of Ovoid in borehole 7 (borehole location is shown in Figure 6.3a). After Naldrett et al. (2000a)

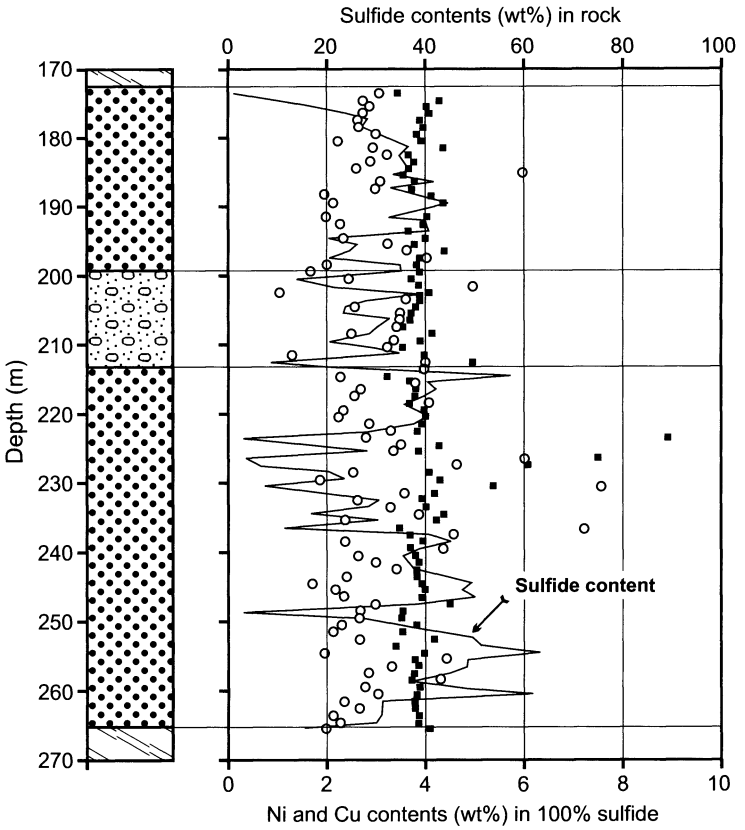


**Fig. 6.24.** Sulfide content in rock and Ni and Cu concentrations in 100% sulfide in borehole 162, Discovery Hill Zone (borehole location is shown in Fig. 6.3a). Explanation of shading is as for Fig. 6.20. After Naldrett et al. (2000a)

**Reid Brook Zone.** Hole 282 (see Fig. 6.3a for location) is typical of those cutting the Reid Brook mineralized zone which plunges east a short distance above the Reid Brook Subchamber. The hole cut a 25 m-thick (true thickness) zone of Feeder Breccia containing a weak dissemination of sulfide interspersed with stringers of massive sulfide, and then a thin stringer of massive sulfide in the Tasiuyak gneiss 20 m below the zone of Feeder Breccia (Fig. 6.25). The values of Ni and Cu in 100% sulfides are more scattered than elsewhere, but average respectively 3.13 wt% and 1.91 wt% over the zone of Feeder Breccia and 3.20 wt% and 0.86 wt% for the massive stringer in the gneiss.

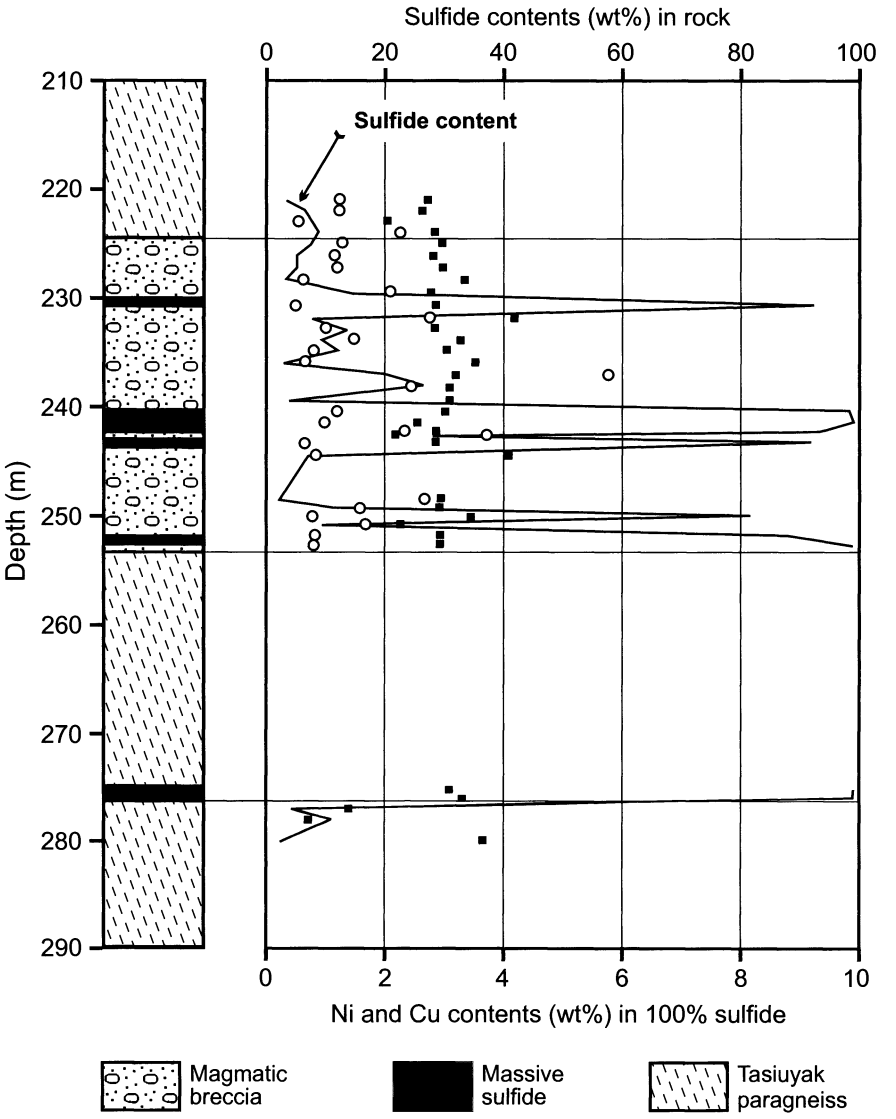


**Fig. 6.25.** Sulfide content of rock and Ni and Cu concentrations in 100% sulfide in magma conduit in borehole 282 at Reid Brook Zone (borehole location is shown in Fig. 6.3a). Legend is present in Fig. 6.20. After Naldrett et al. (2000a)

**Summary.** Averages of Ni and Cu for specific zones within the mineralized system are given in Table 6.3. The Ni content in 100% sulfides varies greatly from a low of 3–3.5 wt% in much of the mineralization from the Eastern Deeps and Reid Brook Zone, through values of 4–4.5 wt% in the Ovoid and Discovery Hill Zone to 5–7 wt% in sulfides in the Varied- tex-

tured Troctolite. Cu contents are even more variable. In general massive sulfide is characterized by low Cu and thus high Ni/Cu ratios in excess of 2.0 (the Ovoid is a marked exception to this generalization), and disseminated sulfides have values less than 2, typically about 1.6. These differences are discussed in the light of variation in PGE+Au concentrations below.

**Table 6.3.** Average Ni and Cu contents in 100% sulfide in different mineralized environments at Voisey's Bay (method of recalculation is explained in text)

| Environment, Ore type, Borehole | True Thickness in m | No of samples | Ni wt% | Cu wt% | Ni/Cu |
|---|---|---|---|---|---|
| **Eastern Deeps** | | | | | |
| Massive sulfide at mouth of feeder (Hole 202) | 40 | 39 | 3.38 | 1.43 | 2.4 |
| Massive sulfide in feeder (Hole 206) | 37 | 16 | 3.13 | 1.31 | 2.4 |
| Leopard troctolite in feeder | | | | | |
| Hole 202 | 15 | 6 | 3.48 | 1.80 | 1.9 |
| Hole 206 | 7 | 8 | 3.04 | 2.43 | 1.2 |
| Hole 166 | 37 | 62 | 4.48 | 2.01 | 2.2 |
| Varied textured troctolite | | | | | |
| Hole 206 | 35 | 33 | 5.01 | 3.30 | 1.5 |
| Hole 166 (upper 360 m) | 360 | 219 | 6.98 | 3.34 | 2.1 |
| Hole 166 (lower 35 m) | 35 | 67 | 5.64 | 3.50 | 1.6 |
| **Ovoid** | | | | | |
| Uppermost 20 m of massive sulfide (Hole 7) | 20 | 20 | 4.66 | 4.66 | 1.0 |
| Lowermost 20 m of massive sulfide (Hole 7) | 20 | 20 | 3.90 | 2.06 | 1.9 |
| **Discovery Hill Zone** | | | | | |
| Leopard troctolite | 30 | 14 | 4.04 | 3.15 | 1.3 |
| **Reid Brook Zone** | | | | | |
| Magmatic breccia (Hole 282) | 25 | 22 | 3.13 | 1.91 | 1.6 |
| Massive sulfide in gneiss (Hole 282) | 2 | 2 | 3.20 | 0.86 | 3.7 |

### 6.7.3 Noble metal content of Sulfides from Different Mineralized Environments

Naldrett et al. (2000a) report the results of the analysis of a total of 315 samples from the Voisey's Bay deposit. Data on these samples are summarised in Table 6.4.

.

**Variation in Ni, Cu and Noble Metals within the Ovoid.** Naldrett et al. (2000a) showed a marked co-variation in Cu, Au, Pd and Pt within the Ovoid mineralisation which they argue is consistent with that to be expected as a result of the fractional crystallisation of monosulfide solid solution (mss) from a sulfide melt (see variation in Ni, Cu and Co with height in hole 7 in Fig. 6.23). They conclude that this body of sulfide has cooled upward (and possibly inward from the sides), with the crystallisation of mss first occurring adjacent to the margins. The residual liquid became concentrated toward the top of the body, enriched in those elements that are incompatible in mss, i.e. Cu, Au, Pd and Pt.

**Use of Rh/Cu vs Rh diagrams in Interpreting Compositions of Mineralization.** The importance of examining the co-variation of an element that is compatible in mss with one that is incompatible during the fractional crystallisation of a sulfide liquid has been emphasised in a number of papers, (Naldrett and Pessaren 1992; Li et al. 1993; Naldrett et al. 1994; Zientek et al 1994; Naldrett et al. 1996b; Li et al., 1996). Naldrett et al. (1999) have shown that a plot of Rh/Cu versus Rh can assist in understanding compositional variations within a magmatic sulfide deposit in terms of fractional crystallisation and the effect of "R" or "N" factor[20] (The reader is reminded that a discussion of "R" and "N" appears in Chap. 2). Naldrett et al. (2000a) used this approach (Figs. 6.26 and 6.27) to examine their data with respect to model curves representing perfect Rayleigh fractionation of mss from sulfide liquid.

---

[20] The reader is reminded that a discussion of "R" and "N" modeling is given in Chap. 2. Following Naldrett et al. (2000a) compositional variations at Voisey's Bay are discussed in terms of "R" modeling (i.e bulk equilibration between different relative proportions of silicate magma and sulfide liquid). In reality, in the genetic picture presented at the end of the chapter, whereby a continuous flow of new magma is responsible for upgrading the sulfides in chalcophile elements, a case could be made that "N" modeling is more appropriate, or possibly a combination of both mechanisms. I have chosen to refer to values of "R", not "N" because "R" was used in the original paper, and others, e.g. Lambert et al. (2000) have also used it. As is shown in Chap. 2, the end results of the two approaches are not so very different

**Table 6.4.** Average metal contents in 100% sulfide of ores of the Voisey's Bay deposit (standard deviations in parenthesis). Data from Naldrett et al. (2000)

| Mineralization type, Location and No. of samples | Ni, wt% | Cu, wt% | Pt, ppb | Pd, ppb | Rh, ppb | Ru, ppb | Ir, ppb | Os, ppb | Au ppb |
|---|---|---|---|---|---|---|---|---|---|
| **Varied textural troctolite** | | | | | | | | | |
| Eastern Deeps, >10% sulfide (21) | 4.72 (1.03) | 2.91 (1.38) | 360 (309) | 354 (264) | 19 (9) | 31 (34) | 6.4 (3.8) | 10 (8) | 355 (349) |
| Eastern Deeps, <10% sulfide (25) | 6.08 (1.04) | 3.22 (0.93) | 447 (251) | 354 (347) | 19 (10) | 60 (88) | 5.1 (2.7) | 4 (7) | 546 (387) |
| **Leopard troctolite** | | | | | | | | | |
| Eastern Deeps (9) | 3.41 (0.23) | 1.87 (0.50) | 107 (75) | 154 (126) | 16 (3) | 23 (20) | 6 (1.4) | 13 (4) | 93 (49) |
| Miniovoid (7) | 3.94 (0.24) | 2.77 (0.94) | 145 (71) | 228 (60) | 12 (6) | 25 (16) | 2.9 | 7 (2) | 224 (80) |
| Discovery Hill Zone (12) | 3.79 (0.27) | 2.23 (0.47) | 377 (197) | 345 (129) | 9 (1) | 35 (24) | (0.91) | 3 (1) | 337 (73) |
| Reid Brook Zone (20) | 3.29 (0.58) | 1.98 (1.32) | 162 (119) | 143 (76) | 10 (1) | 30 (12) | 2.0 (0.8) | 4 (2) | 189 (119) |
| | | | | | | | 2.5 (0.5) | | |
| **Magmatic breccia** | | | | | | | | | |
| Eastern Deeps (44) | 4.40 (0.88) | 2.47 (1.09) | 242 (220) | 264 (180) | 13 (6) | 37 (26) | 4.6 (2.5) | 9 (6) | 245 (176) |
| Ovoid (4) | 4.14 (1.10) | 3.44 (1.31) | 430 (159) | 521 (136) | 23 (5) | 70 (16) | 9.1 (1.9) | 13 (4) | 469 (178) |
| Miniovoid (6) | 4.11 (0.85) | 3.83 (1.68) | 489 (255) | 307 (181) | 10 (2) | 56 (43) | 3.6 (2.3) | 11 (8) | 360 (452) |
| Discovery Hill Zone (18) | 4.06 (0.41) | 2.20 (0.78) | 266 (154) | 346 (163) | 11 (4) | 31 (17) | 2.7 (1.7) | 5 (3) | 278 (168) |
| Reid Brook Zone (26) | 3.75 (0.72) | 1.69 (0.72) | 203 (136) | 258 (171) | 14 (10) | 82 (60) | 4.1 (4.2) | 7 (5) | 200 (143) |
| **Massive sulfide** | | | | | | | | | |
| Eastern Deeps (12) | 3.32 (0.99) | 1.15 (1.55) | 34 (30) | 144 (106) | 18 (6) | 26 (17) | 6.6 (2.4) | 15 (6) | 18 (17) |
| Ovoid (52) | 4.61 (1.08) | 2.84 (1.40) | 123 (111) | 252 (115) | 8 (3) | 17 (10) | 2.0 (1.1) | 4 (1.5) | 93 (130) |
| Miniovoid (11) | 3.96 (1.23) | 2.30 (2.41) | 178 (85) | 221 (127) | 9 (3) | 17 (5) | 2.5 (0.6) | 5 (2) | 116 (48) |
| Reid Brook Zone (16) | 2.95 (0.43) | 1.17 (0.86) | 42 (33) | 102 (36) | 10 (1) | 19 (6) | 2.8 (0.8) | 4 (3) | 60 (67) |

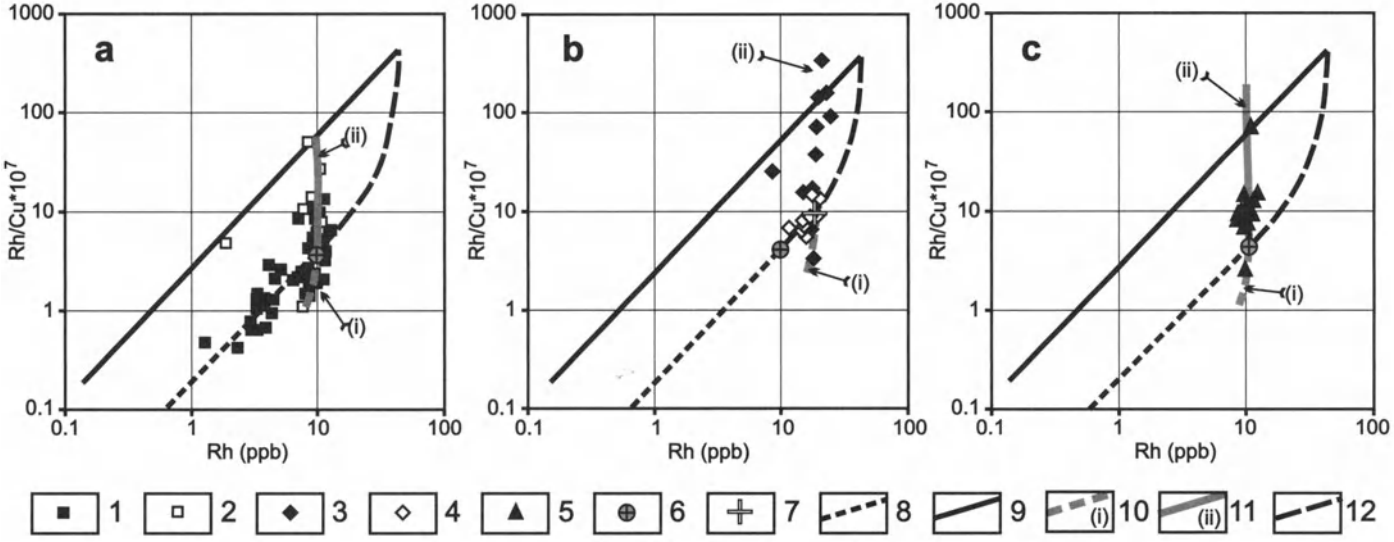


**Fig. 6.26.** Plots Rh/Cu*$10^7$ vs. Rh, showing compositions of massive ores from the Voisey's Bay deposit (recalculated to 100% sulfide) and model curves for perfect Rayleigh mss fractionation from sulfide liquid (a = ores of Ovoid and Miniovoid; b = ores of the Eastern Deeps; c = ores of Reid Brook Zone).
1–5 = ore compositions (1 = Ovoid; 2 = Miniovoid; 3 = Eastern Deeps, massive sulfides; 4 = Eastern Deeps leopard troctolite of the feeder; 5 = Reid Brook Zone); 6 = primitive sulfide liquid of Ovoid; 7 = primitive composition of Eastern Deeps sulfide (shown in plot b); 8–12 = model curves (8 = evolution of sulfide liquid; 9 = evolution of mss; 10 = addition of Cu-rich sulfide liquid to primitive ore; 11 = removal of Cu-rich sulfide liquid from primitive ore; 12 = mixing of non-fractionated sulfide liquid and coexisting mss). After Naldrett et al. (2000a)

**Massive Mineralisation.** Samples of massive sulfide from the Ovoid, Mini-ovoid, Reid Brook Zone and Eastern Deeps are plotted in Fig. 6.26. It is seen that the sulfides show contrasting behavior. Samples from the Ovoid occur within the envelope defined by model curves for mss and liquid, and also scatter along the line of liquid fractionation. In contrast, the samples from the Mini-ovoid, Reid Brook Zone and Eastern Deeps define nearly straight vertical trends; the trends for the Mini-ovoid and Reid Brook zones pass through a point corresponding to the initial liquid for the Ovoid, the trend for the Eastern Deeps lies to the right of the Ovoid initial liquid.

Naldrett et al. (2000a) point out that the behavior of the Ovoid samples is what is to be expected in the light of the suggestion made above that the body crystallized from the base upward, with fractionated liquid becoming concentrated within a lens near the present top of the body. The near vertical trends shown by the Eastern Deeps, Mini-ovoid and Reid Brook zones fit neither the trend of a fractionating liquid, nor the composition of cumulates to be expected as a result of fractional crystallization. However, they do fit with the concept of bodies of massive sulfide within which the composition has been modified subsequent to the original crystallization by the re-distribution of Cu. This could have occurred possibly as the result of the re-mobilisation of a very small percentage of low melting-point (eutectic), Cu-rich liquid within an initial body of unfractionated mineralisation (a Cu-rich eutectic composition exists in the Cu-Fe-S system at low temperature [Merwin and Lombard 1937]). Two trend lines (i and ii) have been plotted in Figs 6.26a and c, one above and one below the composition of the Ovoid initial liquid; line (i) corresponds to the progressive addition of Cu-rich, Rh-poor liquid to this composition, line (ii) to its progressive removal. It is seen that the lines duplicate the trends of the Mini-ovoid and Reid Brook Zone massive sulfide mineralization.

Considering the massive mineralization of the Eastern Deeps, Naldrett et al. (2000a) note that the composition of the cross in Fig. 6.26b (18 ppb Rh, 1.8 wt% Cu) corresponds to a mixture of 75% of the initial liquid of the Ovoid mineralization with 25% of the cumulus mss in equilibrium with this liquid. As in Figs. 6.26a&c, trend lines (i) and (ii) have been plotted in the figure, one above and one below this composition; again they model the variation in composition of the massive mineralization, in this case that of the Eastern Deeps.

Naldrett et al. (2000a) suggest that the vertical trends on plots of Rh/Cu vs Rh are the consequence of sulfide bodies composed of crystalline sulfide, with the composition of the Ovoid initial liquid in the case of the Miniovoid and Reid Brook Zone, and, in the case of the Eastern Deeps, the same liquid plus 25% of co-existing cumulus mss, initially becoming

lodged in the respective conduits or in fractures in the surrounding gneiss. These bodies were subsequently re-heated by the passage of fresh hot magma along the conduits and a low temperature eutectic liquid formed and was re-distributed. Areas from which it was removed changed in composition along the lines marked (ii) in Figures 6.26a&b, and those to which it was added changed along the lines marked (i) in the same figures.

To conclude this section, the variation of Rh/Cu with Rh supports the earlier contention that the Ovoid started as a body of sulfide liquid which crystallized from the base upward, with the accumulation of fractionated liquid towards the top of the body. Samples of Miniovoid mineralization have the same average composition as those of the Ovoid, which suggests that this composition may be close to that of the original unfractionated liquid. Rh shows very little variation throughout the massive sulfide of the Mini-ovoid and the large variations in Rh/Cu ratio that are observed are due to the re-distribution of Cu, either as favored here by disequilibrium melting, or by hydrothermal activity. Massive sulfide from the Reid Brook Zone appears to have been affected similarly. In contrast, the massive sulfide of the Eastern Deeps has the composition of the same liquid as that of the Ovoid mixed with 25% of cumulus mss; however it also shows the re-distribution of Cu that has affected the Mini-ovoid and Reid Brook zones.

**Sulfides in Varied-textured Troctolite.** Data on sulfides from the Varied-textured Troctolite are plotted in Fig. 6.27. Only those samples for which the original analysis (before recalculation to 100% sulfide) indicated >0.5 ppb Rh have been included. This has been done in an attempt to avoid the magnification of error that occurs when analytical data for a sample with a low sulfide content, which are close to the detection limit, are multiplied by a large factor in the conversion of the data to values in 100% sulfide. The data in Fig. 6.27 show a wide spread, which Naldrett et al. (2000a) attribute to the small size of the samples (< 500g) that were available for analysis. The sulfides in much of the Varied-textured Troctolite occur as coarse "blotches", 10-20 cm in diameter, and it is likely that some of the samples included a high proportion of original cumulus mss, which is Rh-rich and Cu-poor, and others a high proportion of fractionated, Rh-poor, Cu-rich liquid.

Naldrett et al. (1999) showed that, when the sulfide content in disseminated ore at Sudbury is less than 10-15%, fractionated Cu-rich liquid appears to have difficulty in migrating away from crystalline mss, while in more sulfide-rich samples, the fractionated liquid escapes, leaving a Rh-rich mss cumulate behind. They observed that on the scale of a sample comprising 20-30 cm of drill core, the bulk compositions of sulfide-poor samples corresponded to that of unfractionated liquid, while the composi-

tion of sulfide-rich samples either corresponded to that of *mss* cumulate or Cu-rich liquid. This observation led Naldrett et al. (2000a) to separate their Varied-textured Troctolite samples into those with more and those with less than 10 percent sulfide; these are shown by the crosses and solid dots respectively in Fig. 6.27.

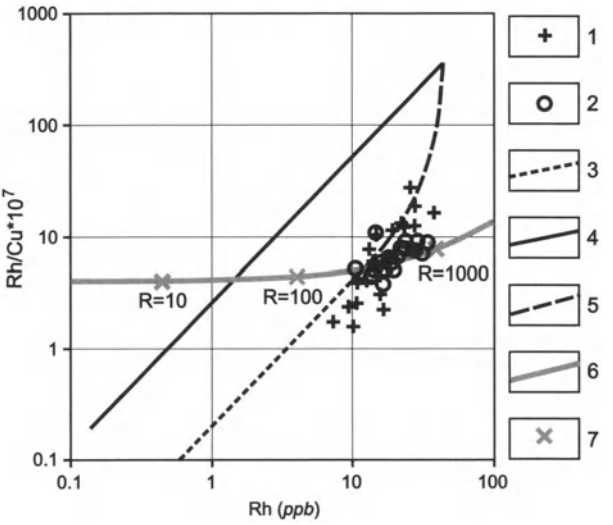


**Fig. 6.27.** Plot Rh/Cu*$10^7$ vs. Rh, showing compositions of ores disseminated in Varied-textured Troctolite from the Eastern Deeps (recalculated to 100% sulfide) and model curves for perfect Rayleigh mss fractionation.
1 = ore with > 10% of sulfide (>5 ppb Rh); 2 = ore with < 10% of sulfide (>5 ppb Rh); 3–6 model curves (3 = evolution of sulfide liquid with mss fractionation; 4 = evolution of mss with mss fractionation; 5 = mixing of non-fractionated sulfide liquid and coexisting mss; 6 = changing of sulfide liquid composition as function of "R" value); 7 = "R" values. After Naldrett et al. (2000a)

It is seen that the Varied-textured Troctolite samples containing more than 10% sulfide spread out along a line that is consistent with mss fractionation. The low sulfide samples still show a spread, but spread out close to a line representing the variation in composition to be expected from reaction of sulfides with magma at different R values, ranging from 280-1000. To test this hypothesis further, Fig. 6.28 shows the variation of Ni and Cu with Rh in this low-sulfide subset of samples. It is seen that both Ni and Cu increase with Rh. This is what would be expected if variable R was indeed the cause of the variability in the subset; if the variability had been due instead to fractional crystallization, Cu, and possibly Ni, would have decreased with increasing Rh, as they do in mineralization from the

Ovoid. The Rh/Cu data therefore indicate that the variability in Ni and Cu contents in 100% sulfides that was documented in holes 166, 202 and 206 through the Eastern Deeps is the consequence of the sulfides having interacted with different proportions of magma. Higher R values are associated with those from the Varied-textured Troctolite than with those from Leopard Troctolite, Basal Breccia Sequence or massive sulfide; the upward increase in the Ni and Cu contents within the Varied-textured Troctolite of hole 166 (Fig. 6.20) is also likely an R factor effect.

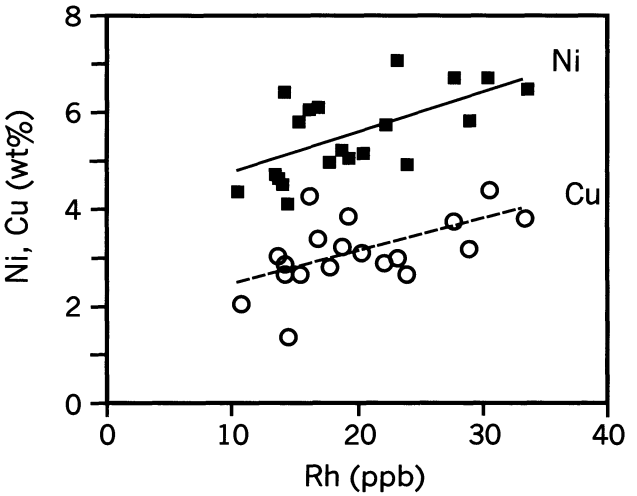


**Fig. 6.28.** Plot of Ni and Cu vs. Rh contents in disseminated ores of varied-textured troctolites of Eastern Deeps. The samples shown are those with sulfide contents <10% and Rh contents >0.5 ppb. Ore compositions are recalculated for 100% sulfide; Ni contents are corrected for Ni in olivine. After Naldrett et al. (2000a)

### 6.7.4 Sulfur Isotopes

Ripley et al. (1999) have shown that $\delta^{34}S$ for the different mineralized environments within the Voisey's Bay Intrusion are as follows: Disseminated ore from Eastern Deeps, -2.0 to 2.7 per mil (‰); Massive ore from the Ovoid and Mini-ovoid, -2.1 to 0 ‰; and disseminated mineralization from the Reid Brook Zone, -4.1 to 1.4 ‰. Pyrrhotite from the Tasiuyak gneiss ranges from –0.9 to – 17.0, while that from the Nain gneiss ranges from 0.2 to 3.3. The westward trend to lower $\delta^{34}S$ values in the mineralization is consistent with a higher proportion of the sulfur being derived from Ta-

siuyak gneiss in the west, where the gneiss forms the country rock, than in the east, where the Nain gneiss forms the country rock.

## 6.8 Geological Model

The overall plunge of all components of the Voisey's Bay deposit is about 25° east, with the result that different levels of the system are exposed at different localities (see Fig. 6.3a). The deepest level is exposed to the west so that the feeder occurs at surface and the exit of the feeder from the lower chamber has been intersected in the drilling. The Discovery Hill Zone represents an intermediate level comprising the feeder between the lower and upper chamber, while the upper chamber is preserved as the Eastern Deeps. It is thought (Naldrett et al. 1996a) that the Ovoid represents the base of the upper chamber exposed at surface, although others (cf Lightfoot 1997) believe it to be a swelling in the feeder conduit.

As discussed above, the systematic relationship between the Ni and Fo content of olivines from the ultramafic rock inclusions, Feeder Olivine Gabbro at all localities, Olivine Gabbro of the Eastern Deeps chamber and Leucotroctolite of the Reid Brook chamber that is illustrated in Fig. 6.14 suggests that these rocks are related to each other by fractionation of a single magma. The rapid decline in Ni with decreasing Fo content in the olivines, taken in conjunction with low whole rock Cu/Zr (see Fig. 6.18) ratios for the same samples, suggests that the magma from which they crystallized was sulfide saturated. The appreciably higher Ni content of olivine in the Varied-textured Troctolite and Normal Troctolite of the Eastern Deeps, coupled with the high whole rock Cu/Zr ratios, indicates that their parental magma was less fractionated and less chalcophile depleted than other sequences. Li and Naldrett (1999) concluded, therefore, that at least two waves of magma were involved at Voisey's Bay. The first crystallized in a lower chamber to form the ultramafic/mafic layers from which the inclusions were derived, (Fig. 6.29a), before fractionating further as it progressed up the feeder to form the Feeder Olivine Gabbro lining the walls of the feeder and ultimately the Olivine Gabbro of the Eastern Deeps (Fig. 6.29b). While in the lower chamber, this magma reacted with gneiss fragments derived from the walls and roof. The reaction resulted in sulfide immiscibility developing as fractionation was proceeding, either as a result of felsification of the magma (c.f. Li and Naldrett, 1993) and/or due to the addition of sulfur from the gneiss.

The trace element data of Li et al. (2000) indicate that an early magma, most probably of picritic composition, fractionated and interacted with

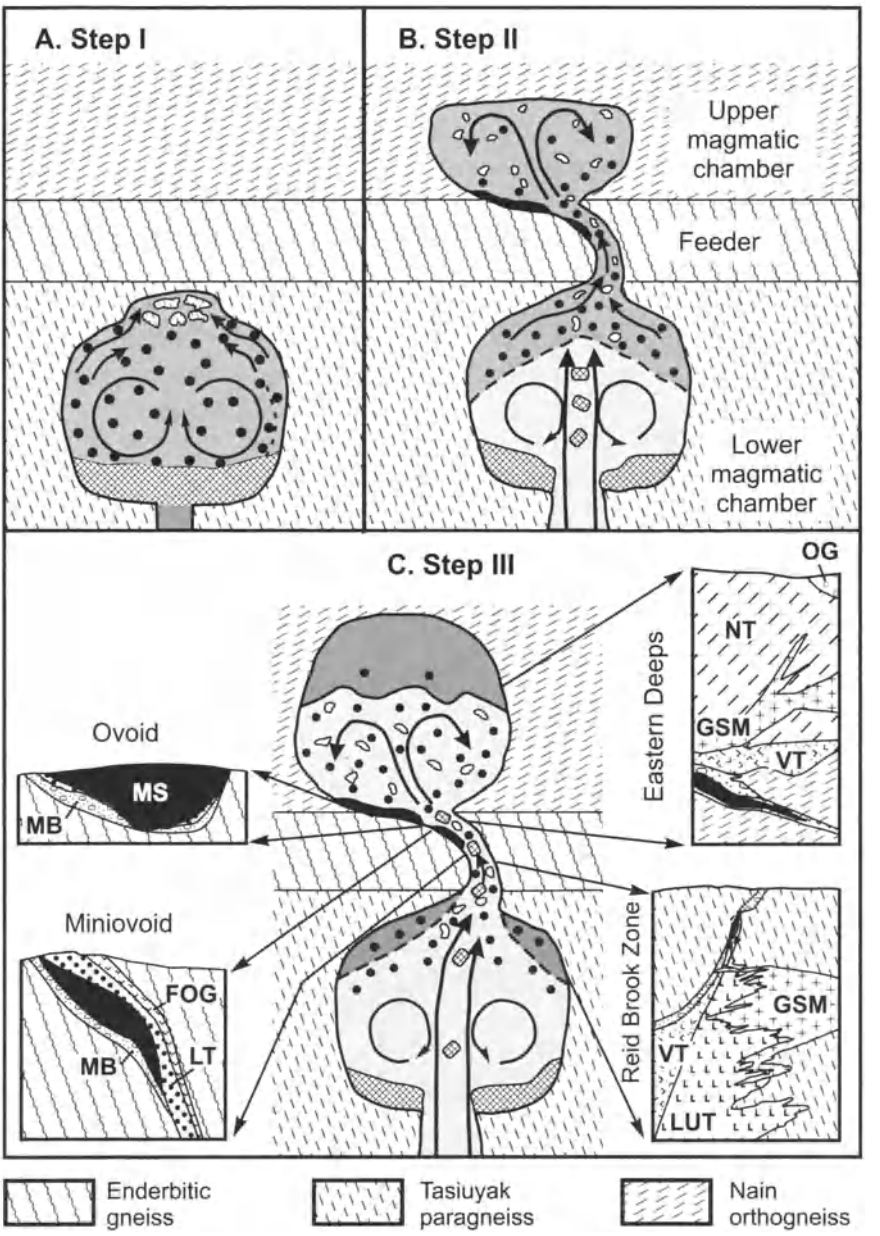


**Fig. 6.29.** Genetic model for the Voisey's Bay deposit. A. Step I: Magma rose to a lower chamber within Tasiuyak gneiss, olivine crystallization occurred with the formation of ultramafic cumulates. The magma reacted with gneiss fragments from the collapsed roof, and became sulfide saturated. B. Step II: New, Ni-undepleted magma entered the lower chamber, disrupting early cumulates, and

pushing up the early magma to an upper chamber in Nain Gneiss. During transportation some sulfide became lodged in and near the feeder as the magma rose. C. Step III: The later magma continued to flow through the system, picking up sulfides and partially reacted gneiss inclusions and transporting them up the feeder system to spread out over the lower part of the upper chamber. The fresh, undepleted magma enriched the sulfides in chalcophile metals. The insets show the types of sulfide accumulation that developed as illustrated in Figs. 6.5, 6.8, 6.9, and 6.12. Modified after Li and Naldrett (1999).
FOG = Feeder Olivine Gabbro; GSM = Granite, syenite and monzonite; LT = Leopard Troctolite; LUT = Leucotroctolite; MB = Magmatic breccia; MS = Massive sulfide; NT = Normal Troctolite; OG = Olivine Gabbro; VT = Varied-textured Troctolite.

mid-crustal rocks, and acquired an elevated, non-mantle, La/Sm ratio. The magma then ascended into rocks with a high Th/Nb ratio (Tasiuyak gneiss) where further reaction and incorporation of gneissic inclusions resulted in this signature also being imposed on the magma. Amelin et al.'s (2000) Nd, Pb and Sr data support this concept of a 2-stage interaction at different crustal levels. The Re-Os data of Lambert et al. (2000) also provide strong support for reaction between an early picritic predecessor of the troctolitic magma and enclosing Tasiuyak gneiss. Ripley et al.'s (1999) S-isotope data are consistent with the derivation of at least part of the sulfur from the gneiss; the oxygen isotope data (Ripley et al. 2000) again support interaction between troctolite and wall rocks.

Li and Naldrett (1999) proposed that the sulfides that segregated from the first wave of magma remained within the lower chamber but were then picked up by the second pulse of magma and carried up along the overlying conduit. Calculations based on recently determined partition coefficients for the distribution of Ni between olivine and sulfide melt (Caciagli and Brennan 1999) indicate that sulfide liquid in equilibrium with magma giving rise to the olivines found in rocks that formed from the first magma pulse would have contained less than 3.0 wt% Ni. As Naldrett et al. (2000a) have shown, the Ni content of the sulfide liquid responsible for the ores was between 3.5 and 4.5 wt%, which argues strongly that this liquid has re-equilibrated with a magma of higher Ni content than that first passing through the feeder into the upper chamber. Varying degrees of re-equilibration can account for the variable metal contents documented by Naldrett et al. (2000a) in the different mineralised environments of the deposit. As the second wave of magma advanced up the conduit into the upper chamber (the Eastern Deeps), sulfides became concentrated in hydrodynamic traps within the conduit (Evans-Lamswood et al. 2000) and at the point where the conduit broadened out (Fig. 6.29c) as it entered the upper chamber (Naldrett et al. 1996).

## 6.9 Conclusions as to the genesis of the Voisey's Bay Deposit

At this stage in studies of the Voisey's Bay deposit, certain key aspects of its genesis have emerged:

1. The deposit is related to two magma chambers, one 1.5 km stratigraphically above the other, connected by a feeder dyke (Fig. 6.3b).
2. Magma, most likely of picritic composition, rose into the crust where it started to crystallise and interact with mid-crustal gneisses, acquiring a crustal trace element and isotopic signature.
3. The magma continued its ascent and swelled out to form the lower (Reid Brook) chamber. Here it reacted with the enclosing Tasiuyak gneiss and eventually became saturated in sulfide. Various degrees of this reaction are preserved in the inclusions of the Basal Breccia Sequence, Feeder Breccia and Varied-textured Troctolite.
4. The initial magma lost much of its Ni as a consequence of olivine fractionation and separation of immiscible sulfide liquid; this liquid also removed other chalcophile elements including Cu, causing a decrease in the Cu/Zr ratio.
5. The initial magma was forced out of the lower chamber, along with some of the sulfide that had segregated from it, and rose up the feeder sheet to develop an upper chamber about 1–5 km vertically above the lower chamber. Sulfides became lodged in and near the feeder as the magma rose up it.
6. Fresh, chalcophile element-undepleted magma entered the lower chamber and was probably responsible for the early magma being forced upward. The new magma continued through the system, disrupting early cumulates, and picking up sulfides and partially reacted inclusions and transporting all of these up the feeder system to spread out in the lower part of the upper chamber.
7. As it progressed through the system, the new magma interacted with sulfides that were lodged there, upgrading them in chalcophile elements.

## 6.10 Other deposits associated with the Nain Plutonic Suite

The exploration activity that was stimulated by the discovery of the Voisey's Bay deposit lead to the discovery of many other Ni-Cu sulfide showings associated with rocks of the Nain Plutonic Suite, none of which

thus far have proved to be of economic interest. The combined knowledge resulting from this work does, however, present an object lesson as to the essential components of an economic deposit in this setting. The locations of the principal discoveries are shown in Fig. 6.30. Kerr and Ryan (2000) have subdivided the deposits and prospects into:

1. Troctolite/gabbro related
2. Pyroxenite-related
3. Anorthosite-related
   a) In norites-gabbros within or close to anorthosites
   b) Within the anorthosites themselves
4. Ferrodiorite-related

The Ni and Cu tenor of the sulfides of a number of these deposits are shown in Fig. 6.31. As discussed above, the Ni tenor of the Voisey's Bay sulfides ranges from 3.4 to 4.7 wt% Ni, with a Ni/Cu ratio of about 1.75:1. All other deposits are marked by much lower Ni and Cu tenors, and most have a Ni/Cu ratio of around 1.

Examples of these will be discussed briefly in turn, along with reasons as to why they are both lower in tenor, and lower in grade and size than Voisey's Bay.

### 6.10.1 Troctolite/gabbro related

#### *The Pants Lake Deposits*

This series of deposits (also referred to as the Voisey's Bay South deposits) have been described by MacDonald (1999), Kerr and Ryan (2000), Kerr et al. (2001) and Kerr (2003). The area lies 80 km south of Voisey's Bay, 10 km to 30 west of the Nain-Churchill boundary (Fig. 6.30). The oldest rocks are the orthogneisses of the Nain Province, which are developed in the eastern part of the area and are bounded to the west by a major 1.85–1.82 Ga shear zone, corresponding to the Abloviak shear zone farther north. Archean to Paleoproterozoic quartzo-feldspathic gneisses, that were extensively reworked in the 1.85 Ga Torngat orogen, lie west of the shear zone (Fig. 6.32). These are associated with a belt of granulite facies, pelitic paragneiss (the Tasiuyak gneiss that is also found at Voisey's Bay). The area is bounded to the south by the 1.44 Ga Harp Lake anorthosite complex. Components of the 1.35–1.29 Ga Nain Plutonic suite within the area include granitoid rocks, anorthosites, olivine gabbros/troctolites and ferrodiorite/ferromonzonites.

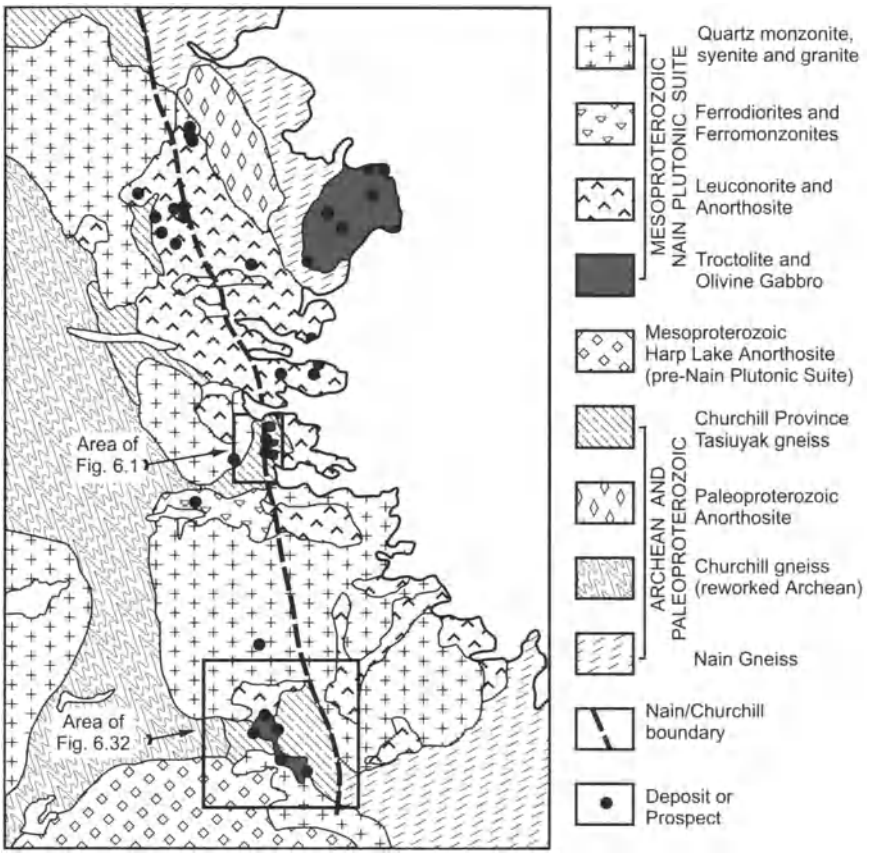


**Fig. 6.30.** Regional map of the Nain Plutonic Suite showing locations of sulfide mineralization (after Kerr and Ryan, 2000)

**Geology of Deposits.** The mafic rocks occur in two intrusions, the 1.337 Ga South Intrusion and the 1.322 Ga North intrusion (Smith et al. 1999, 2001). The South Intrusion is geochemically distinct from the younger North Intrusion, and more closely resembles that at Voisey's Bay both in its age and geochemical composition (MacDonald 1999; Kerr et al. 2001; Kerr 2003). It comprises a gently west-dipping slab-like body, 600 m thick, with a basal zone of mafic-rich cumulates, and consists predominantly of fine-grained olivine gabbro (Fig. 6.33). In drill holes 97-79 and 97-94 two zones of olivine gabbro are present, an upper zone 250 m thick that is separated from a lower zone by a thin layer of sulfide-bearing gabbro and a screen of gneiss. The North Intrusion consists of three interconnected lobes, the Happy Face, NDT and Taheke Lake lobes. The Happy Face lobe is dominantly massive leucogabbro overlying a thin sequence of sulfide-bearing layered gabbro, the NDT lobe is marked by 400 m of lay-

ered gabbro, underlain by sulfide mineralization and capped by leucogabbro, and the Taheke Lake lobe comprises leucogabbro overlying layered gabbro which is underlain by black gabbro (Fig. 6.32). A series of sill like bodies occur in the Mineral Hill area to the south, and are related to the North Intrusion.

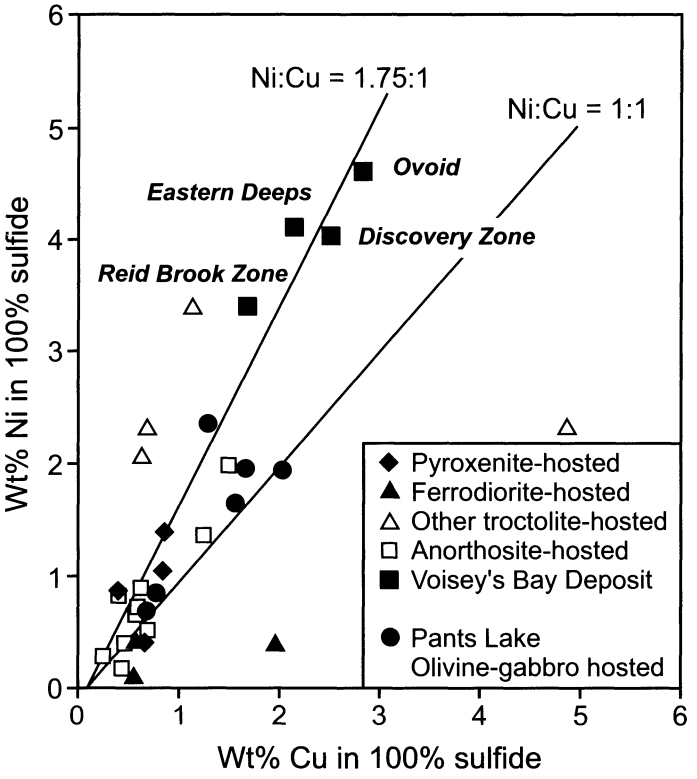


**Fig. 6.31.** Average Ni and Cu concentrations in 100% sulfide for various deposits hosted by igneous rocks belonging to the Nain Plutonic suite. Data from Kerr and Ryan (2000)

**Mineralization.** In the South Intrusion, disseminated (<10 wt%) pyrrhotite (with exsolved pentlandite) and chalcopyrite form interstitial patches within a discontinuous zone of basal melagabbro The host rocks to the mineralization contain dark grey to white gneissic inclusions which show dark, spinel-rich reaction rims very similar to those in the magmatic breccias at Voisey's Bay. Grades of the mineralization are low (0.1-0.55 wt% Ni, 0.1-0.32 wt% Cu) with some of the Ni contained within olivine (Kerr, 2003).

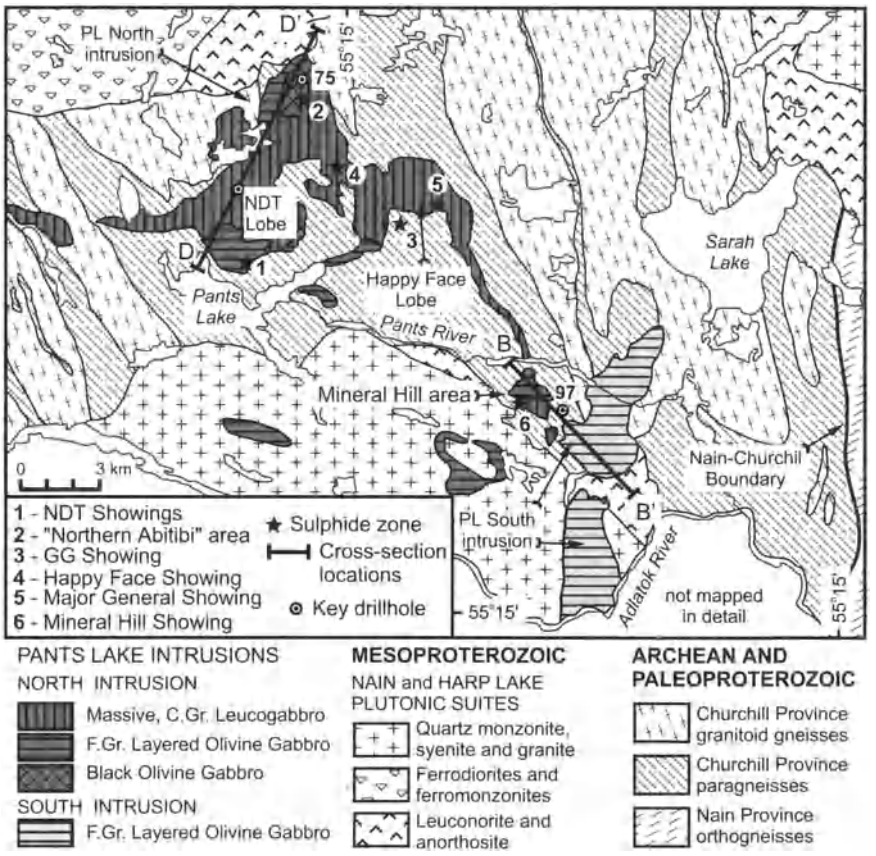


**Fig. 6.32.** Geology of Pants Lake area (after Kerr, 2003)

In the North Intrusion, mineralization occurs within a 5 to 60 m zone just above the basal contact. It comprises two distinct facies (Fig. 6.34). An upper facies consists of fine-grained olivine gabbro grading down with increase in sulfide content into a composite gabbro containing numerous reacted fragments of gneiss. The proportion of both fragments and sulfide generally increases downward in the composite gabbro. Zones of leopard gabbro (analogous to the leopard troctolite at Voisey's Bay) occur within this facies. The composite gabbro of the upper facies is underlain by a more homogeneous lower facies, similar to the layered gabbro of the main bodies of the intrusive lobes, but also containing rounded masses of sulfide (Kerr 2003 suggests that these are frozen droplets), interstitial sulfide and fragments of reacted gneiss. Leopard gabbro is also common in the lower facies. There is evidence of gravitational settling of sulfide towards the base of the lower mineralized facies with the sulfides accumulating above

a barren, fine-grained gabbro that in places is chilled against the underlying country rocks. Sulfides consist of pyrrhotite/troilite with exsolution pentlandite, chalcopyrite and minor cubanite. Grades of this mineralization vary from 0.2 to 2 wt% Ni with Ni/Cu ratios of about 1. A spectacular 1.1 m zone was intersected some 10's of m within the footwall gneiss, across which Ni = 11.7, Cu = 9.7 and Co = 0.4 wt%, with 0.8 g/t Pd (Kerr, 2003).

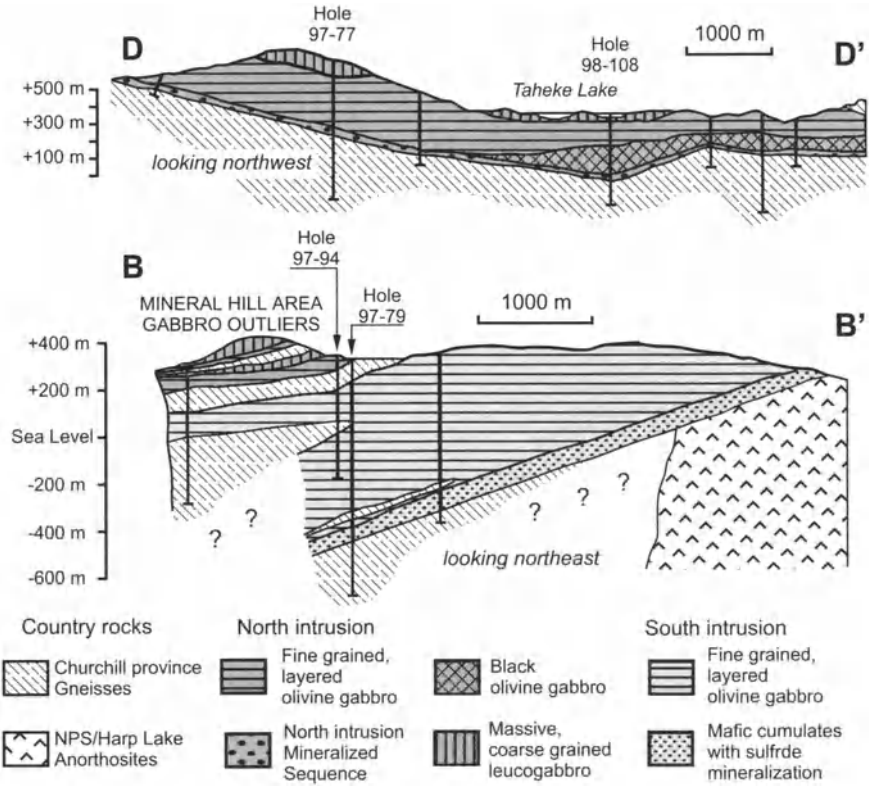


**Fig. 6.33.** Cross-sections through the Pants Lake area (after Kerr, 2003). Section locations are shown in Fig. 6.32

This author has made a detailed examination of the contact between gabbro and a large (3 m thick) inclusion of sulfide- and graphite-bearing pelitic gneiss very close to the base of the intrusion. Within the gneiss, pyrrhotite+troilite is present with no pentlandite or chalcopyrite but containing finely dispersed flakes of graphite, that give the sulfide a dull appearance to the eye. Closer to the contact with the overlying gabbro, chalcopyrite and minor pentlandite occur within the sulfide, which still retains its dull

appearance. Within both the gabbro and gneiss, at distances of less than 0.5 m from the contact, sulfide blebs occur, comprising pyrrhotite+troilite with exsolution pentlandite and also chalcopyrite; these blebs are devoid of graphite flakes and the sulfides look bright to the naked eye. Graphite is present as larger flakes within the rock, but is not finely dispersed within the sulfide. The impression given is one of small amounts of Ni and Cu diffusing into the barren sulfides within the gneiss, and close to the contact between gabbro and gneiss, of the sulfides being melted out of the gneiss to enter the gabbro, leaving the graphite behind and acquiring a higher proportion of Ni and Cu.

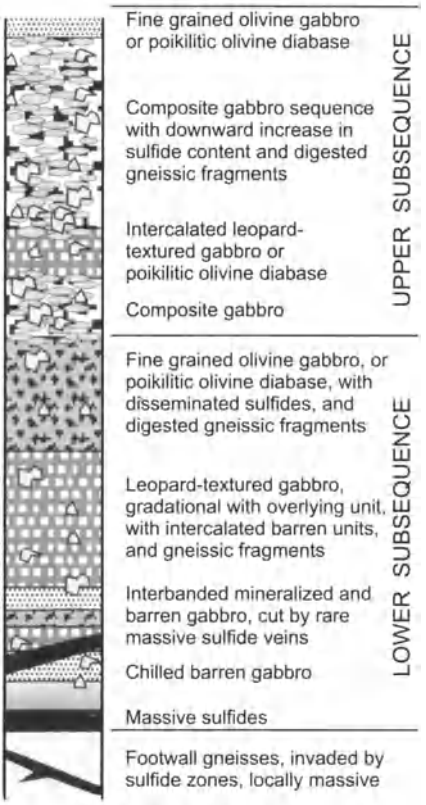


**Fig. 6.34.** Idealized stratigraphy of the North intrusion mineralized sequence, showing its persistent subdivision into an upper and a lower sequence. Individual intersections of the mineralized sequence may lack some of the components, but the basic pattern is almost always present. After Kerr (2003)

**Geochemistry of Intrusions.** It was shown above that strong evidence of contamination at Voisey's Bay comes from consideration of variations of

La/Sm versus Th/Nb ratio. The evidence supported early contamination in the middle to lower crust, as shown by a rise in the La/Sm ratio from that characteristic of primitive, mantle-derived rocks, followed by contamination by the Tasiuyak gneiss, which caused a marked increase in Th/Nb ratio accompanied by only a modest rise in the La/Sm ratio. In Fig. 6.35, cumulus rocks from both the North and South Pants Lake intrusions are plotted on a similar diagram. These both show a marked increase in Th/Nb ratio with essentially no change in La/Sm ratio. The trend is highly indicative of contamination by a contaminant with a high Th/Nb ratio, although the contaminant has a La/Sm ratio of 2 to 3, in comparison with the ratio of 5 to 7 shown by the Tasiuyak gneiss at Voisey's Bay (no analyses are available of the pelitic, Tasiuyak-like gneiss at Pants Lake). It should stressed that the wide range in Th/Nb ratio that has been documented for the North and South Intrusions occurs in cumulus rocks that are essentially devoid of gneissic inclusions.

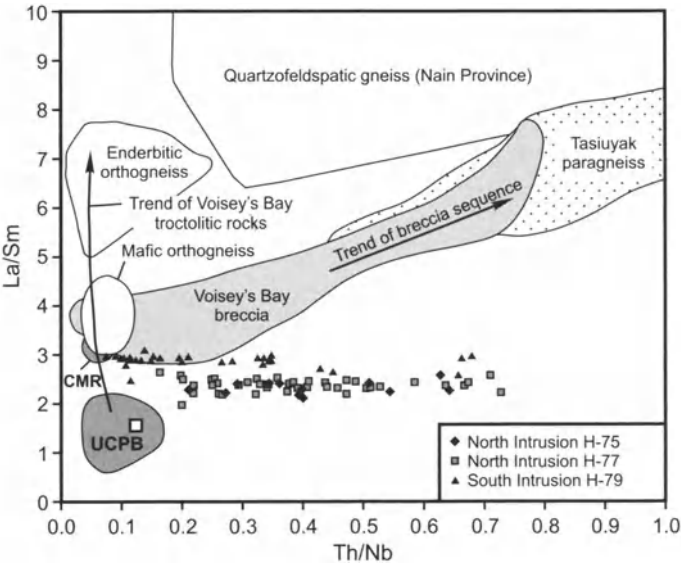


□ = Primitive mantle (Sun and McDonough, 1989)

**CMR** = chilled margin of the Voiseyís Bay intrusion (n = 8)

**UCPB** = Uncontaminated picritic basalts from Norilísk and West Greenland (after Lightfoot and Hawkesworth, 1997)

**Fig. 6.35.** Plot of La/Sm versus Th/Nb showing data for the Pants Lake North and South Intrusions superimposed on that for the Voisey's Bay intrusion (see Figure 6.17). Data from MacDonald (1999)

In Chap. 10, the importance of Cu/Zr ratios as an indication of chalcophile depletion is discussed, and in Fig. 10.15 it is shown that essentially

all of the Pants Lake intrusive rocks have Cu/Zr ratios <1, which is a strong indication that they have interacted with sulfide. Also in Chap. 10, the Ni content of the olivines in the Pants Lake intrusions is compared with their Fo content (Fig. 10.10). It is apparent that the olivines fall on the fractionation trend of a sulfide-saturated magma. Unlike that at Voisey's Bay, the trend at Pants Lake does not indicate sulfide-unsaturated fractionation followed by saturation, but demonstrates that the magma was sulfide saturated from the stage at which the most primitive olivines observed at Pants Lake started to crystallize.

**Conclusions as to genesis of the sulfides.** The trace element data indicate that both the earlier Southern and younger North Intrusions at Pants Lake underwent contamination with a contaminant that had a high Th/Nb ratio, not unlike the Tasiuyak gneiss at Voisey's Bay. All of the magma appears to have been depleted as result of having become sulfide saturated at an early stage, very likely when it became crustally contaminated, and before it intruded into its present positions. The location of the sulfides discovered to-date in a basal, inclusion rich zone, suggests that the first wave of magma that was the forerunner of both intrusions carried with it an inclusion-rich "sludge" that was a product of this initial contamination, along with some of the resulting sulfide. Subsequent inputs of magma appear to have been relatively free of this sludge, but were derived from a reservoir that had interacted with sulfide and had thus become depleted in chalcophile elements. The amount of sulfide present in the showings discovered so far is insufficient to account for the major chalcophile depletion shown by the olivine compositions and Cu/Zr ratios. Presumably at depth, but likely at or above the level at which the magma first came into contact with the pelitic gneiss, there is a large reservoir of Ni-bearing sulfide that accounts for the depletion that has been documented. There is no indication of a second wave of undepleted magma such as that which occurred and upgraded the sulfides at Voisey's Bay. This accounts for the low Ni and Cu tenors that characterize the Pants Lake sulfides in comparison with those at Voisey's Bay (Fig. 6.31).

### *Other troctolite bodies belonging to the Nain Plutonic Suite*

**Kiglapait Intrusion.** The Kiglapait (1.308 Ga) is the largest and most intensively studied of the troctolite bodies of the Nain Plutonic Suite; indeed, along with the Bushveld, Stillwater and Skaergaard complexes, it constitutes one of the "classics" in the study mafic/ultramafic igneous complexes (Morse 1969, 1979a, b, 1980, 1981a, b, 1982). The intrusion developed as an essentially "closed" system, i.e as the result of a single injection of

magma that then cooled and crystallized (DePaolo 1985; Weis and Morse 1993). For much of the crystallization, the magma was unsaturated in sulfide and saturation appears only to have been achieved after 91% of the magma had crystallized. This gave rise to a zone of blebby pyrrhotite and chalcopyrite in the upper part of the body. Geochemical studies indicate that very little crustal contamination of the magma has occurred. The majority of the sulfide mineralization found at Kiglapait occurs at the margin of the intrusion in association with pyroxenites which are thought to be hybrids that have developed through reaction of the troctolitic magma with country rocks. These hybrids appear to have remained liquid longer than the main body of the intrusion and cross cut it around the margins. Their sulfides consist of pyrrhotite and chalcopyrite, rarely exceeding 5 wt% of the rock. The tenor of the sulfides is mostly below 1 wt% Ni and Cu with Ni/Cu ratios of about 1. Because of their occurrence in marginal pyroxenites, the sulfides are shown as pyroxenite-hosted in Fig. 6.31.

**Hettasch and Newark Island Intrusions.** Sporadic sulfides of no economic value were intersected near the base of the Hettasch Intrusion, which lies adjacent to and just south of Kiglapait, and minor sulfide mineralization, with low Ni and Cu tenors, occurs near the top of the Newrak Island intrusion. Other troctolitic bodies have not been found to contain significant amounts of sulfide.

### 6.10.2 Mineralization associated with Anorthosites

Kerr and Ryan (2000) summarized the results of sulfide prospects that were discovered in anorthosites. These accounted for the bulk of the exploration activity during the 1995–1997 exploration boom in Labrador apart from that at Voisey's Bay. The anorthosite complexes themselves have been introduced as diapers of plagioclase-rich magmatic "mush", injections of relatively fluid magma, or intermediaries between these two end members (Kerr and Ryan 2000; Emslie et al. 1994; Ryan et al. 1998).

Kerr and Ryan (2000) pointed out that within anorthosite complexes, in many localities there is a close association between sulfides and mafic rocks (leuconorites, gabbro-norites and ferrogabbros), and they characterize these as forming subgroup 1 of the anorthosite class. Disseminated sulfides occur interstitially within the mafic rocks themselves, as veinlets and interstital zones within the anorthosites (these sulfides often appear to be thermally corroding the host anorthosite), and as semi-massive to massive accumulations at the contacts between rock types. Sulfides within anorthosites alone (Kerr and Ryan's subgroup 2) are less common. In general,

there appears to be a spectrum between sulfides within mafic rocks alone to sulfides within anorthosite alone as is illustrated in Fig. 6.36. Kerr and Ryan (2000) suggested that the mafic rocks within the anorthosite plutons represent residual liquid that has coalesced as the anorthosite crystallized and has then back-veined the pluton. Continued crystallization of the mafic magma resulted in sulfide separation. The low Ni tenor and low Ni/Cu ratio of these sulfides (Fig. 6.31) is consistent with their derivation from fractionated magma.

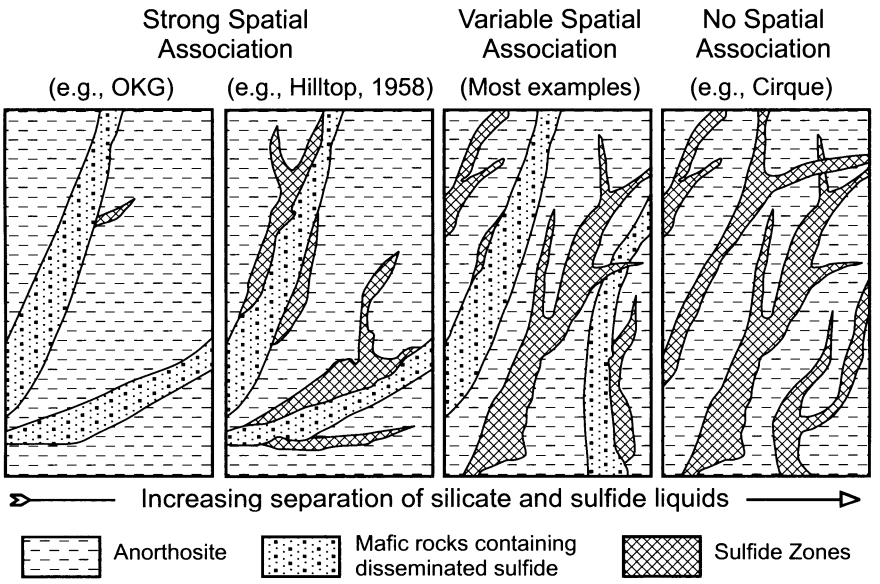


**Fig. 6.36.** Illustration of the range of associations of sulfides in anorthosites (after Kerr and Ryan 2000)

### 6.10.3 Mineralization associated with Ferrodiorites

This mineralization occurs in a spectrum of rock types ranging from iron-rich gabbro to diorite that are grouped collectively as "ferrodiorite". Ferrodiorites are regarded by Emslie et al. (1994) as the consequence of the separation of a fractionated, mafic-rich magma at depth from anorthosite plutons before the latter rose diapirically to higher levels in the crust. In some areas the ferrodiorite magma has ascended into the upper crust, but in general the relatively high density of the Fe-rich magma means that intrusions resulting from it are more abundant in areas where uplift had exposed deeper crustal levels. The sulfides that have developed within fer-

rodiorite intrusions are associated with zones of titaniferrous magnetite and apatite (Kerr and Ryan, 2000). Grades are low (0.2 wt% Cu and 0.05 wt% Ni in the Umiakovic Lake area, and < 0.2 wt% Cu+Ni in the Puttuaalu Lake area and Cabot Lake intrusion). Ni tenors are less than 0.5 wt% with Cu tenors ranging up to 2 wt% (Fig. 6.31). The low Ni tenors and high Ni/Cu ratios are consistent with derivation from fractionated mafic magma.

### 6.10.4 Lessons to be learned from the Mineralization associated with the Nain Plutonic Suite

The intense exploration undertaken on intrusions that form the Nain Plutonic Suite in the aftermath to the Voisey's Bay discovery, coupled with the careful documentation of the results of this exploration that was undertaken by members of the Newfoundland Geological Survey (Ryan et al. 1995; Kerr 1999, 2003; Kerr and Ryan 2000) means that we have an almost unique overview of the different types of deposit, their genesis and relative importance, associated with a single igneous province.

It has become clear that sulfide mineralization in hybrid pyroxenites at the margins of large intrusion has not had the access to sufficient quantities of magma to concentrate Ni and Cu to any great degree, and that the pyroxenitic magmas themselves have not experienced the dynamic flow regimes that are necessary to concentrate the sulfides that they carried. Sulfides within the anorthosites are the end products of the cooling of small batches of mafic magma that originated during the crystallization of the anorthosites; again, these magmas have not experienced the dynamic environment necessary to concentrate sulfides, or, indeed, to expose the sulfides to large volumes of magma. The ferrodiorites are extreme differentiates within which sulfides developed at a late stage when most of the Ni present in the original magma had been removed in mafic silicates. This is illustrated in Fig. 6.37 which is taken from Scoates and Mitchell (2000) and is based on the magmatic evolution of the Kiglapait intrusion. It shows how the sulfide concentration in the magma will vary with fractional crystallization in comparison with the calculated variation of the sulfide saturation level in the magma. Sulfide saturation occurs at such a late stage in the crystallization that the magma will have become essentially depleted in Ni, due to this having been removed in early forming mafic silicates, by the time saturation is achieved.

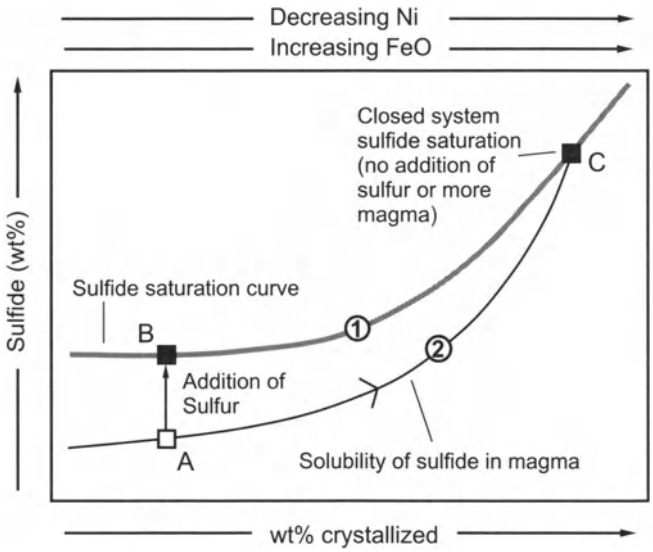


**Fig. 6.37.** Schematic diagram showing the variation in the sulfide content of a magma that is saturated in sulfide (curve 1) and initially unsaturated in sulfide (curve 2). The latter magma ultimately becomes saturated as a result of crystallizing silicate minerals, due to the original sulfur content becoming concentrated in less and less magma. After Scoates and Mitchell (2000)

The majority of the troctolite/gabbro bodies lie east of the Nain-Churchill suture; they do not seem to have achieved sulfide saturation at an early stage, probably for the reason illustrated in Fig. 6.37. If one looks at Fig. 6.30, it is clear that the only troctolites/gabbros that have developed significant amounts of sulfide are those that have intruded the sulfide-bearing Tasiuyak gneiss, namely those at Voisey's Bay and Pants Lake. These magmas have had their sulfide content increased (path A-B in figure 6.37) through reaction with the Tasiuyak gneiss. However, at Pants Lake, so much sulfide appears to have entered the magmas responsible for both the intrusions, that these became very chalcophile depleted. This accounts for the fact that any sulfides that have been found associated with them are low in tenor. Additionally at Pants Lake, the sulfides have also not been in the right dynamic environment to have been concentrated. Voisey's Bay would also have been characterized by sulfides of low tenor if it had not been the site of a feeder system, and had not experienced the influx of new, fresh magma which upgraded the sulfides. The feeder system was a very dynamic environment, which also led to the concentration of the sulfides from large amounts of flowing magma into specific hydraulic traps which now constitute the ore zones.

# 7 The Jinchuan deposit, China

The Jinchuan Ni-Cu deposit in Northwest China, with ore reserves of 500 million tons at Ni and Cu grades of 1.2 wt% and 0.7 wt%, respectively, is ranked as the third largest economic Ni-Cu deposit in the world after Noril'sk and Sudbury (see Table 1.1, Chap. 1). Ores of the deposit are relatively rich in Cu with an average ratio Ni/Cu = 1.76 (see Table 1.1) and have moderately high PGE concentrations with a total PGE and Au content of around 1 ppm in the sulfide ores (Sun 1986; Yang 1989) and (Pt+Pd)/(Ni+Cu) ratios (PGE in g/t, Ni and Cu in wt%) in the three different ore bodies of 0.04 to 0.45. However, the intrusive rocks that host the sulfide ores are all ultramafic, ranging from dunite to olivine pyroxenite, and, previously, had been thought to have formed from an ultramafic magma with an MgO content of >30 wt% (S.G.U. 1984); this is quite different to the general features of other Cu and PGE rich Ni sulfide deposits.

As was noted in Chap. 1, the nature of the parental magma is generally accepted as critical to the formation of different types of Ni-Cu sulfide mineralization (Naldrett 1981; Ross and Travis 1981). Ultramafic magmas usually give rise to Ni dominated sulfide deposits with Ni/Cu ratios higher than 7 (Marston et al. 1981), such as the volcanic peridotite associated Ni deposits of Kambalda, Western Australia (Ni/Cu=13.5) (Lesher et al. 1984), of the Abitbi greenstone belt, Canada (Ni/Cu = 25) (Green and Naldrett 1981), and of Perseverance, Western Australia (Ni/Cu = 40) (Bames et al. 1988) and the intrusive peridotite associated deposit at Dumont, Canada (Ni/Cu >20) (Duke 1986). Mafic magmas commonly produce Ni-Cu-PGE dominated deposits with Ni/Cu usually less than 2. Examples of these include those of the Sudbury camp Canada (Ni/Cu =1.1), Noril'sk, Russia (Ni/Cu = 0.5–1.06), and Duluth Minnesota, USA (Ni/Cu = 0.3).

The peculiar features of the Jinchuan sulfide ores and their host rocks have posed several questions: 1) can ultramafic magma truly give rise to a sulfide deposit with a relatively high Cu/Ni ratio? 2) or has some post magmatic process upgraded the ore in Cu? 3) or are the ultramafic rocks hosting the Jinchuan deposit really part of an intrusion with an overall mafic mafic composition? These questions have been addressed by Chai and Naldrett (1992a,b) from whose work much of this section is taken.

## 7.1 Geology of the deposit

The Jinchuan intrusion occurs at the southwest margin of the Sino-Korea platform and intrudes into the Early-Proterozoic marbles and gneisses of the Baijiazhuzhi formation (Fig. 7.1). It has a dyke-like form with a general northwest strike, which is about the same direction as the regional structural lineation. The intrusion is about 6 km long, has an average width of 300 m and is more than 1000 m deep in its central part. Most of the intrusion outcrops, except at its eastern and western extremities, but the rocks are heavily oxidized and have a rubbly surface expression. Different aspects of the deposit have been described by Tang (1990, 1993), Tang and Li (1995), Tang et al. (1992, 2002), De Waal et al. (2003) and Zhou et al. (2002).

Mapping and exploration of the Jinchuan area was carried out in the late 1950s to early 1970s by the Geological Survey of Gansu province (S.G.U. 1984). Based on fault-block relationships, they divided the Jinchuan intrusion, together with its sulfide ores, into four mining areas (S.G.U. 1984). However, this division does not have any petrological significance since the faults are all post-magmatic. For example, the two extremities of the intrusion, that lying west of Fault 8 (F8) and that east of F23 should obviously be parts of their neighboring sections (Fig. 7.1-2), but were treated as two separate areas by the S.G.U.

Based on the geometry of the intrusion and the distribution of rock types, Chai and Naldrett (1992a) divided the Jinchuan intrusion into two parts: a laterally zoned western part (Figs. 7.1-4 and 7.1-5) and a vertically layered eastern part (Fig. 7.1-6).

The western part consists of two subchambers: the West and West-central subchambers (Fig. 7.1). The two subchambers have a similar tabular shape and lateral variations including a dunite core, lherzolite wings and olivine pyroxenite margins. The dunite has a lens-like shape that parallels the walls of the intrusive body. It is usually about 50-150 m thick, extends vertically for more than 500 m and is enveloped by lherzolite in most locations. The lower part of the intrusion consists almost entirely of sulfide-bearing dunite and either lacks, or has only thin marginal zone of lherzolite. Lherzolite predominates in the upper part, reaching a width of nearly 300 m at the surface. Locally, on the surface, small amounts of plagioclase lherzolite are encountered. The plagioclase lherzolite forms narrow, discontinuous bands, usually less than 10 m thick. Towards the east, zones of plagioclase lherzolite are more numerous and coalesce to form a plagioclase lherzolite layer (Fig. 7.1-5) which characterizes the eastern part of the intrusion. Olivine pyroxenite always occurs on the margins of the in-

trusion. It is usually less than 40 m thick and is discontinuous in some areas. Olivine pyroxenite is slightly thicker on the north side of the intrusion (the present hangingwall side) than the south side, but the reverse is also true at some localities (Figs. 7.1-4 and 7.1-5). At the contact between the intrusion and the country rock, the intrusive rocks are often sheared, forming a 0-5 m thick chlorite-serpentine schist zone. Vertically, the rocks change from dunite at the base to lherzolite upwards with an irregular transition.

The eastern part of the intrusion is a boat-like body with a "V-shaped cross section (Fig. 7.1-6). The intrusive rocks show quite different features. Generally, there is a very thin olivine pyroxenite zone of less than 20 m on the margin, but other rock types show a horizontal layering. Dunite is mainly located near the base of the intrusive body and is closely related to the sulfide mineralization; it disappears rapidly upwards, changing to lherzolite, then plagioclase lherzolite and back to lherzolite again at the top.

The age of the Jinchuan intrusion is not well defined. A lamprophyre dyke which cross-cuts the intrusion was dated by the Rb-Sr method on biotite and gave an age of 1339 Ma (S.G.U. 1984) which provides minimum age for the intrusion. K-Ar isotopic dating was also performed on biotite from the intrusion itself, giving two ages, 1505 and 1529 Ma, respectively (Jia 1986). Since biotite is not a primary mineral phase of the intrusive rocks and intense alteration possibly has had some effect on the isotopic systems, these results must be regarded with caution. However, based on the relationships of the intrusion to the Precambrian stratigraphy and with the lamprophyre dyke, the Jinchuan intrusion may have been emplaced between 1719-1339 Ma.

## 7.2 Petrography

Chai and Naldrett (1992a) reported that the Jinchuan intrusion comprises four main rock types: dunite, lherzolite, plagioclase lherzolite and olivine pyroxenite.

**Dunite** is usually sulfide-bearing, with 8–30% Ni-Cu sulfide. The modal abundance of olivine ranges from 70–90%, pyroxenes (mostly orthopyroxene) 1–8%, plagioclase commonly less than 1% and chromite 1–2%. There is also 1–3% magnetite which is mainly associated with the sulfides. Olivine occurs as medium grained (0.5–6 mm) euhedral to subhedral crystals. It is always intensely altered to serpentine and magnetite. Orthopyroxene occurs as reaction rings around olivine and is sometimes replaced by clino-

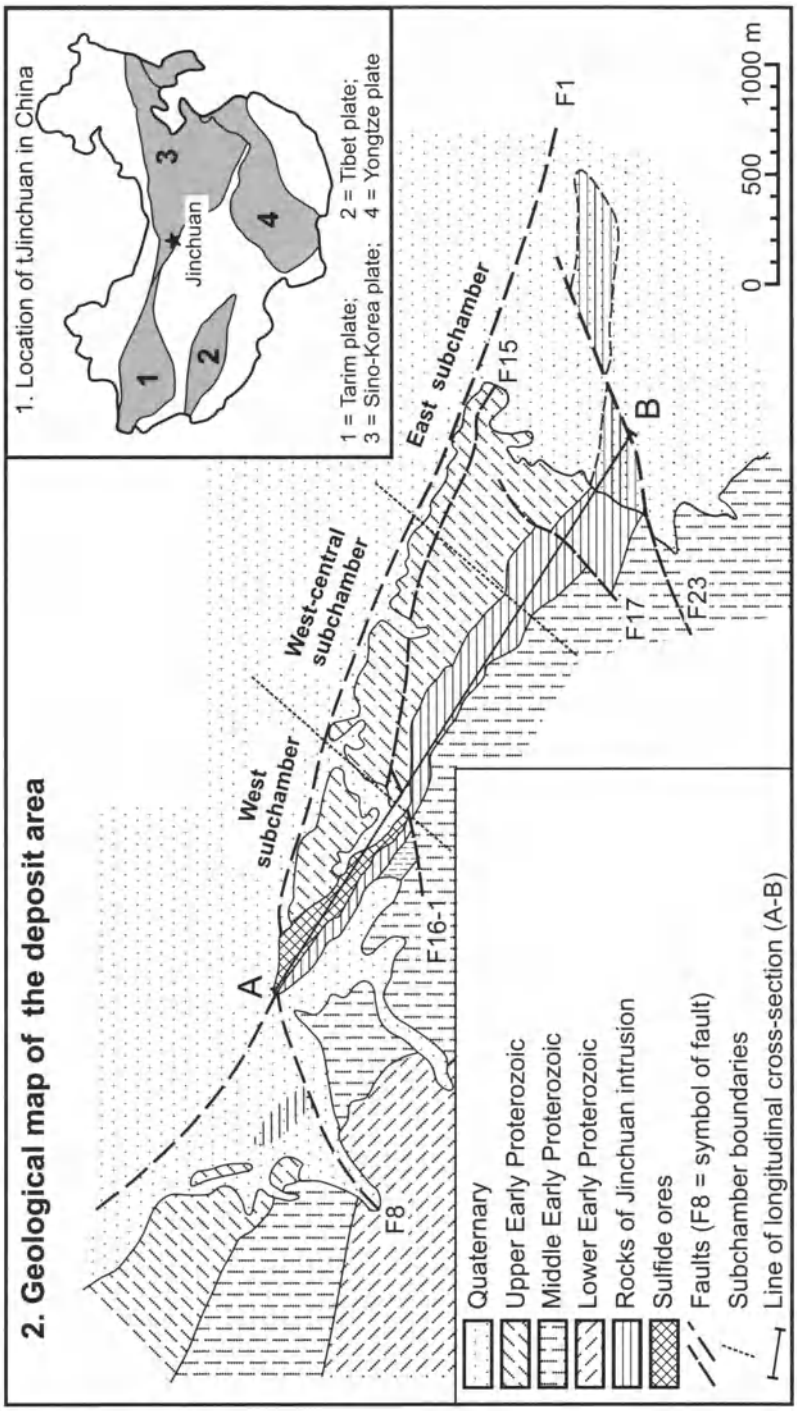
2. Geological map of the deposit area
1. Location of tJinchuan in China
Jinchuan
1 = Tarim plate; 2 = Tibet plate;
3 = Sino-Korea plate; 4 = Yongtze plate
West subchamber
West-central subchamber
East subchamber
A
B
F1
F8
F15
F16-1
F17
F23
0 500 1000 m
Quaternary
Upper Early Proterozoic
Middle Early Proterozoic
Lower Early Proterozoic
Rocks of Jinchuan intrusion
Sulfide ores
Faults (F8 = symbol of fault)
Subchamber boundaries
Line of longitudinal cross-section (A-B)

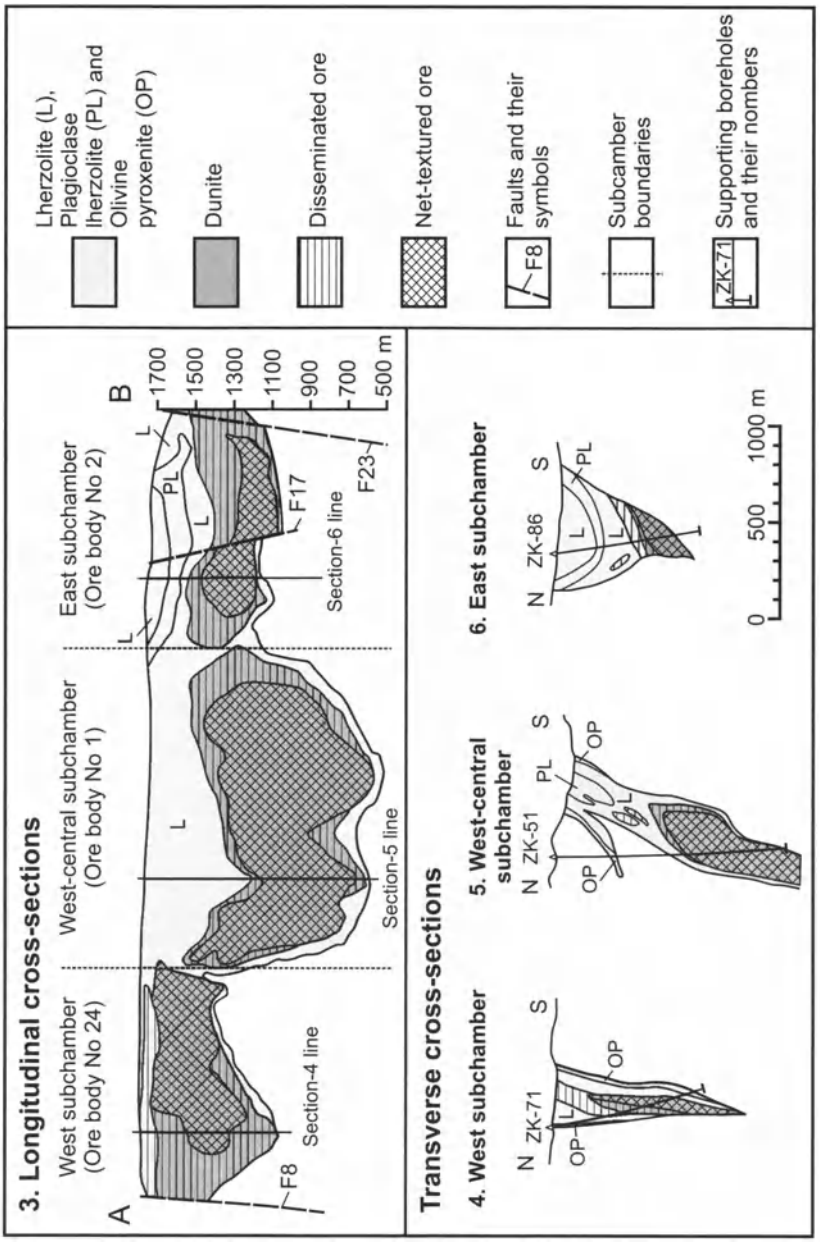


**Fig. 7.1.** Geology of the Jinchuan deposit. 1. Location of Jinchuan in China. 2. Geological map of the deposit area (modified from Jia 1986). 3. Longitudinal cross-section of the deposit (after Chai and Naldrett 1992a). 4 – 6. Transverse cross-sections (after Chai and Naldrett 1992a)

pyroxene. Chromites are always fine grained (0.01-0.02 mm) and euhedral; most grains occur as inclusions within olivine, but some are interstitial. Sulfides are also interstitial along with pyroxene and plagioclase. Where there is a pyroxene corona developed around olivine, sulfides commonly occur between the silicate aggregates. In extreme cases, dunite consists entirely of olivine and interstitial sulfides in a proportion of roughly 4:1.

**Lherzolite** is by far the dominant rock type of the Jinchuan intrusion, making up about 80% of the total volume of the intrusive rocks. It is usually massive without visible layering, although it is not clear whether the lack of layering is a primary feature of the rocks or the result of intense alteration. Lherzolite is essentially an olivine-chromite mesocumulate, containing interstitial pyroxenes, sulfides and a small amount of plagioclase. The modal percent of olivine varies from 40–85%. Pyroxene accounts for 10–50% of the rock, with orthopyroxene predominant in the olivine-rich parts and clinopyroxene in the less olivine-rich parts. Plagioclase is usually present in amounts of less than 2%. Cumulus chromite ranges from 0.5–2%. The grain size of olivine in this rock varies greatly in different localities, ranging from 0.2–8mm. Generally, in the western part of the intrusion, coarse-grained olivine occurs in the core and the lower part of the intrusion ranging from 2–8 mm, whereas olivines in the marginal olivine pyroxenite are usually very fine-grained, ranging from 0.3–3 mm, and in the eastern part the grain size of the olivine ranges from 0.5–4 mm. The coarse-grained olivine usually has irregular margins due to replacement by pyroxene and amphibole, and is sometimes cross-cut by serpentine and talc in altered rocks. Medium grained olivine commonly has rounded comers and is often enclosed by pyroxene oikocrysts, giving rise to a typical poikilitic texture. Fresh olivine is commonly seen in this rock type, especially where it occurs within pyroxene oikocrysts. Pyroxenes are always interstitial to cumulus olivine and are often replaced by amphibole and chlorite. When seriously altered, it is difficult to distinguish orthopyroxene and clinopyroxene, but in other less intensely altered rocks, clinopyroxene can be seen either enclosing orthopyroxene or as an independent interstitial phase. There is usually less than eight volume percent of sulfide in this rock type with the amount decreasing upwards.

**Plagioclase lherzolite** is distinguished separately because of its importance as a visible marker layer in the eastern part of the intrusion. In this rock type, between 3–10% plagioclase is present, occurring as an interstitial phase along with pyroxene. Plagioclase is often sausseritized or chloritized. The average modal composition of plagioclase lherzolite is olivine

74%, pyroxene 17% and plagioclase 6%. Small amounts of biotite and magnetite are also present. Sulfides are either absent or present in trace amounts.

**Olivine pyroxenite** accounts for less than 10% volume percent of the intrusive rocks. The amount of olivine varies from 10–40% and the rest consists of pyroxene, mostly clinopyroxene. Olivine pyroxenite is much fresher than the other rock types and olivine is almost always unaltered. Pyroxene is sometimes altered to chlorite and amphibole. Pyroxenes are usually clinopyroxene dominant. The rock is mesocumulus to orthocumulus in texture. Mostly, oikocrysts of pyroxene enclose olivine; the olivine grain size (0.2 to 2 mm) is much finer than that in the rest of the intrusion. Trace amounts of sulfides are present in some samples of this rock.

## 7.3 Geochemistry Of The Intrusive Rocks

### 7.3.1 Major elements

Representative major element analyses for the Jinchuan intrusion are presented in Table 7.1 (from Chai and Naldrett 1992a), in which all the oxides are calculated on an anhydrous basis and sulfide contents are subtracted. All the intrusive rocks, including those for which analyses are not given in the Table, are very high in MgO (24–42 wt%). Dunite has the highest MgO content (39–42 wt%) with very low $A1_2O_3$, CaO, $TiO_2$, $Na_2O$ and $K_2O$. Lherzolite has an MgO content of from 26–39 wt% with most samples between 30–35 wt%. Olivine pyroxenite commonly has an MgO content of around 25 wt%. $SiO_2$, $Al_2O_3$, CaO and $TiO_2$ increase gradually from dunite to olivine pyroxenite.

In Fig. 7.2 the major elements are plotted versus MgO content. Chai and Naldrett (1992a) pointed out that systematic variation trends are present for most of the elements. $SiO_2$, $Al_2O_3$, CaO and $TiO_2$ decrease with increasing MgO. When the least square regression lines are drawn for the plots of these elements, $SiO_2$, $Al_2O_3$ and CaO have correlation coefficients ($r^2$) of more than 0.9 and $TiO_2$ has an $r^2$ of 0.86, indicating that these elements are incompatible with MgO. The latter three oxides intercept the MgO axis at about 42–46 wt% which is about the MgO content of olivine in the Jinchuan rocks. Thus the rocks can be considered as mixtures of olivine with the original silicate magma. Generally, FeO increases with increasing MgO, varying from 18 wt% in the most MgO-rich rocks to 12 wt% in the less MgO-rich rocks; this indicates its compatible nature with MgO, but the trend of FeO with MgO is not as good as those of $SiO_2$,

**Table 7.1.** Compositions of representative rocks from the Jinchuan intrusion (after Chai and Naldrett 1992a)

| Sample | I-13 | I-17 | I-18 | II-26 | I-4 | I-6 | I-8 | II-7 |
|---|---|---|---|---|---|---|---|---|
| Rock | Dunite | Dunite | Dunite | Dunite | L | L | L | L |
| $SiO_2$ | 39.76 | 39.70 | 41.35 | 38.86 | 41.00 | 41.22 | 41.03 | 42.50 |
| $Al_2O_3$ | 1.34 | 1.08 | 1.79 | 1.48 | 2.75 | 2.29 | 2.25 | 2.79 |
| CaO | 0.46 | 0.20 | 1.19 | 1.33 | 1.64 | 1.42 | 1.40 | 2.05 |
| MgO | 41.17 | 42.52 | 39.66 | 39.99 | 38.15 | 38.73 | 38.97 | 35.95 |
| $Na_2O$ | 0.06 | 0.07 | 0.10 | 0.06 | 0.23 | 0.25 | 0.23 | 0.13 |
| $K_2O$ | 0.32 | 0.06 | 0.09 | 0.03 | 0.27 | 0.16 | 0.16 | 0.15 |
| FeOT | 15.56 | 15.08 | 14.64 | 17.34 | 14.58 | 14.50 | 14.60 | 15.05 |
| MnO | 0.21 | 0.22 | 0.18 | 0.27 | 0.21 | 0.22 | 0.22 | 0.20 |
| $TiO_2$ | 0.16 | 0.12 | 0.19 | 0.13 | 0.29 | 0.31 | 0.28 | 0.38 |
| $P_2O_5$ | 0.04 | 0.04 | 0.03 | 0.03 | 0.04 | 0.06 | 0.05 | 0.05 |
| $Cr_2O_3$ | 0.67 | 0.74 | 0.71 | 0.44 | 0.76 | 0.70 | 0.75 | 0.68 |
| Total | 99.08 | 99.09 | 99.22 | 99.51 | 99.17 | 99.14 | 99.18 | 99.26 |
| MgNo | 0.83 | 0.83 | 0.83 | 0.80 | 0.82 | 0.83 | 0.83 | 0.81 |
| Ni | 2653 | 4716 | 4269 | 5227 | 2143 | 1638 | 2005 | 1572 |
| Co | 197 | | 213 | 243 | 176 | 154 | 139 | 146 |
| Cr | 4580 | 5041 | 4843 | 3009 | 5172 | 4807 | 5129 | 4640 |
| V | 44.70 | 44.45 | 52.58 | 49.43 | 75.25 | 69.71 | 73.49 | 91.72 |
| Nb | 2.30 | 1.63 | 2.94 | 2.11 | 3.54 | 3.17 | 2.48 | 3.55 |
| Zr | 11.08 | 7.53 | 16.80 | 5.07 | 24.02 | 23.75 | 19.76 | 36.69 |
| Y | 1.58 | 0.14 | 2.27 | 0.50 | 4.12 | 3.31 | 3.94 | 6.74 |
| Sr | 1.17 | 3.67 | 12.27 | 28.69 | 21.71 | 39.08 | 31.26 | 76.75 |
| Rb | 17.92 | 3.02 | 4.73 | 0.93 | 9.64 | 6.59 | 6.22 | 7.80 |
| Th | 0.42 | | 1.21 | 0.00 | 0.57 | 0.34 | 0.25 | 0.38 |
| Sc | 7.10 | | 5.41 | 7.06 | 8.86 | 8.96 | 7.79 | 13.67 |
| Hf | 0.32 | | 0.40 | 0.00 | 0.61 | 0.57 | 0.43 | 0.74 |
| La | 0.78 | | 0.64 | 0.88 | 3.08 | 2.66 | 2.71 | 5.10 |
| Ce | 2.06 | | 2.62 | 1.80 | 7.46 | 5.54 | 5.63 | 10.79 |
| Nd | 1.19 | | 2.08 | 0.88 | 3.32 | 2.80 | 2.16 | 5.10 |
| Sm | 0.45 | | 0.56 | 0.20 | 0.88 | 0.86 | 0.68 | 1.18 |
| Eu | 0.06 | | 0.09 | 0.06 | 0.29 | 0.24 | 0.19 | 0.36 |
| Tb | 0.06 | | 0.08 | 0.03 | 0.11 | 0.13 | 0.10 | 0.19 |
| Yb | 0.22 | | 0.21 | 0.06 | 0.40 | 0.36 | 0.35 | 0.55 |

**Table 7.1.** (cont.)

| Sample | II-7 | II-10 | II-12 | II-15 | II-w-16 | I-25 | II-w-7 | II-w-10 |
|---|---|---|---|---|---|---|---|---|
| Rock | L | L | L | L | L | OP | OP | OP |
| $SiO_2$ | 42.50 | 41.70 | 42.07 | 40.42 | 42.56 | 46.21 | 45.71 | 45.62 |
| $Al_2O_3$ | 2.79 | 2.74 | 2.76 | 2.16 | 4.00 | 4.93 | 6.81 | 6.72 |
| CaO | 2.05 | 1.75 | 1.86 | 1.81 | 2.31 | 7.69 | 5.93 | 5.95 |
| MgO | 35.95 | 37.16 | 36.76 | 36.33 | 33.75 | 25.73 | 25.70 | 25.81 |
| $Na_2O$ | 0.13 | 0.09 | 0.15 | 0.26 | 0.29 | 0.11 | 0.87 | 0.91 |
| $K_2O$ | 0.15 | 0.03 | 0.22 | 0.13 | 0.51 | 0.04 | 0.50 | 0.49 |
| FeOT | 15.05 | 15.11 | 14.79 | 16.49 | 15.45 | 13.67 | 13.21 | 13.21 |
| MnO | 0.20 | 0.23 | 0.22 | 0.22 | 0.21 | 0.26 | 0.18 | 0.18 |
| $TiO_2$ | 0.38 | 0.33 | 0.40 | 0.41 | 0.21 | 0.30 | 0.52 | 0.52 |
| $P_2O_5$ | 0.05 | 0.06 | 0.07 | 0.08 | 0.03 | 0.04 | 0.06 | 0.06 |
| $Cr_2O_3$ | 0.68 | 0.78 | 0.64 | 0.67 | 0.57 | 0.60 | 0.50 | 0.50 |
| Total | 99.26 | 99.20 | 99.29 | 98.30 | 99.33 | 98.97 | 99.49 | 99.46 |
| MgNo | 0.81 | 0.81 | 0.82 | 0.80 | 0.80 | 0.77 | 0.78 | 0.78 |
| Ni | 1572 | 1613 | 1604 | 3920 | 5268 | 4641 | 877 | 922 |
| Co | 146 | 168 | 165 | 286 | 251 | 301 | 88 | 96 |
| Cr | 4640 | 5323 | 4408 | 4605 | 3866 | 4118 | 3452 | 3410 |
| V | 91.72 | 86.58 | 90.56 | 86.86 | 74.77 | 136.55 | 140.39 | 136.06 |
| Nb | 3.55 | 2.34 | 3.48 | 4.61 | 2.67 | 2.60 | 4.42 | 4.63 |
| Zr | 36.69 | 27.39 | 37.61 | 45.92 | 19.11 | 17.27 | 48.31 | 47.27 |
| Y | 6.74 | 4.23 | 5.06 | 6.28 | 4.66 | 3.92 | 10.49 | 10.31 |
| Sr | 76.75 | 53.23 | 49.73 | 40.95 | 56.35 | 76.02 | 90.72 | 92.40 |
| Rb | 7.80 | 3.28 | 10.34 | 5.72 | 22.45 | 2.43 | 20.57 | 20.29 |
| Th | 0.38 | 0.35 | 0.51 | 0.49 | 0.33 | 0.51 | 0.75 | 0.78 |
| Sc | 13.67 | 12.72 | 12.70 | 11.16 | 12.18 | 21.02 | 20.22 | 17.36 |
| Hf | 0.74 | 0.69 | 0.95 | 0.99 | 0.40 | 0.52 | 1.43 | 1.27 |
| La | 5.10 | 4.02 | 4.96 | 3.66 | 2.15 | 1.29 | 3.72 | 3.94 |
| Ce | 10.79 | 9.09 | 10.20 | 8.06 | 5.57 | 3.21 | 12.84 | 12.58 |
| Nd | 5.10 | 4.34 | 4.91 | 5.40 | 3.36 | 2.40 | 5.86 | 7.28 |
| Sm | 1.18 | 1.13 | 1.20 | 1.26 | 0.68 | 0.66 | 1.68 | 1.67 |
| Eu | 0.36 | 0.38 | 0.38 | 0.35 | 0.28 | 0.21 | 0.49 | 0.57 |
| Tb | 0.19 | 0.19 | 0.15 | 0.19 | 0.16 | 0.13 | 0.28 | 0.24 |
| Yb | 0.55 | 0.55 | 0.61 | 0.59 | 0.41 | 0.55 | 0.79 | 0.86 |

*L* Lherzolite; *OP* Olivine pyroxenite. Major elements in wt%, trace elements in ppm. Major elements are recalculated for water-free and sulfide-free compositions; Fe total as FeOT. MgNo = Molecular ratio of MgO/(MgO+FeO)

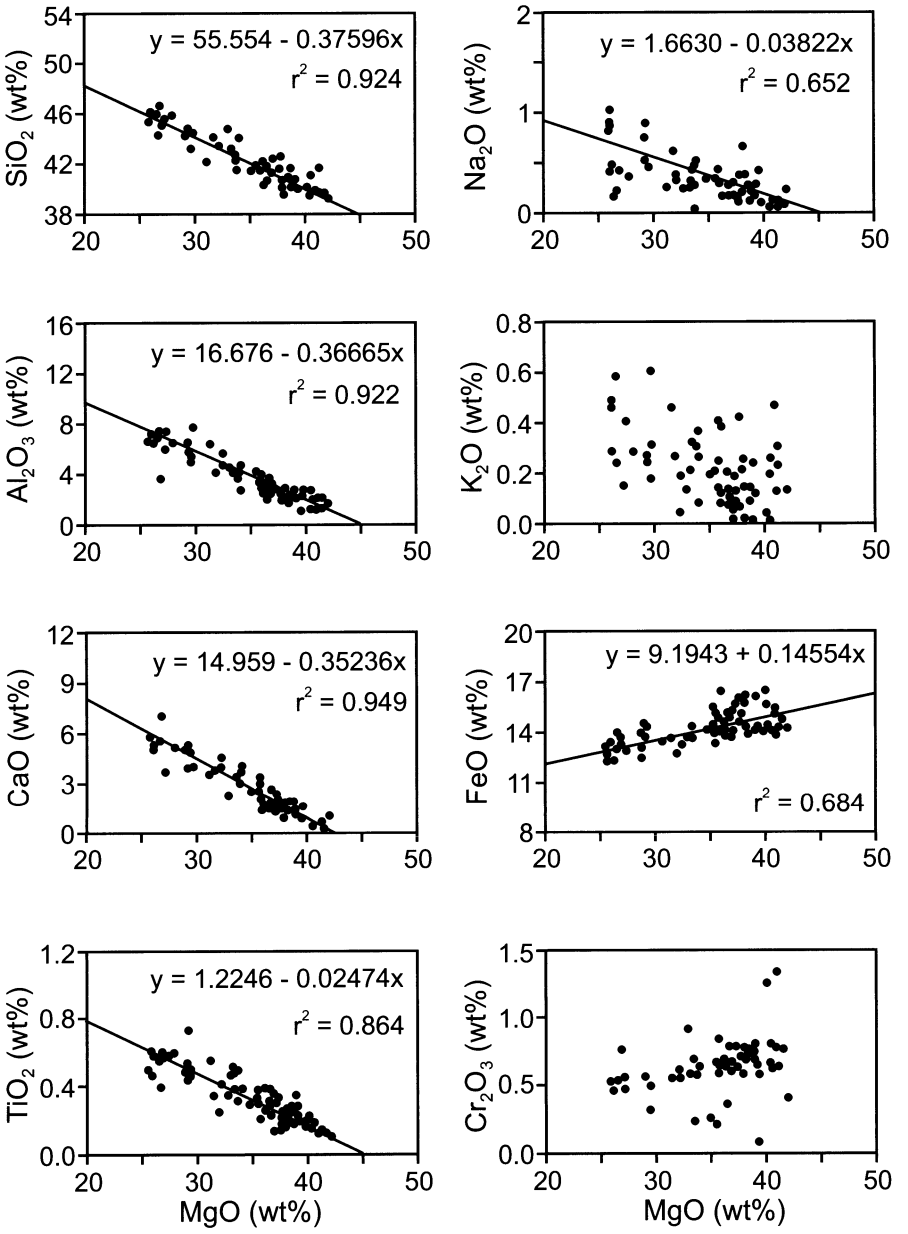


**Fig. 7.2.** Harker diagram showing variation of major elements with MgO. $SiO_2$, $Al_2O_3$, CaO and $TiO_2$ show a strong negative linear correlation with MgO, while FeO increases with MgO (after Chai and Naldrett 1992a)

$Al_2O_3$, CaO and $TiO_2$. The scatter on the FeO versus MgO plot is most likely due to the presence of magnetite and chromite. There is a very rough trend of decreasing $Na_2O$ with MgO but $K_2O$ does not show any discernable trend. The scattering of $Na_2O$ and $K_2O$ on the plot is likely due to the mobility of these elements after consolidation of the intrusion, most possibly as a result of the hydrothermal alteration that is ubiquitous in the intrusive rocks. $Cr_2O_3$ contents are between 0.5- and 0.8 wt% for most Jinchuan rocks.

The olivine mixing line can be best demonstrated on the molecular $(MgO+FeO)/TiO_2$ versus $SiO_2/TiO_2$ and $(MgO+FeO)/Al_2O_3$ versus $SiO_2/Al_2O_3$ ratio diagrams (Fig. 7.3). All the samples fall on to a regression line with $r^2$ of more than 0.93, reflecting a perfect fit by a simple straight regression line. The slopes of the lines in both the diagrams are within the range of 2±0.05, which is the molecular $(MgO+FeO)/SiO_2$ ratio of the olivine. This indicates clearly that the compositional trend of the Jinchuan intrusive rocks is controlled only by olivine.

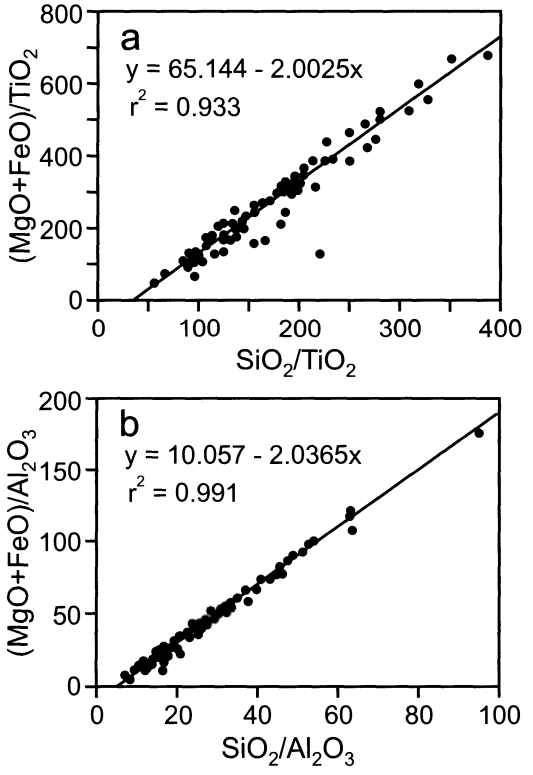


**Fig. 7.3.** Molecular ratio diagrams of $(MgO+FeO)/TiO_2$ vs $SiO_2/TiO_2$ and $(MgO+FeO)/Al_2O_3$ vs $SiO_2/Al_2O_3$ (after Chai and Naldrett 1992a)

### 7.3.2 Trace elements

Selected trace elements analyses of the intrusive rocks (after Chai and Naldrett, 1992a) are also listed in Table 7.1. All the trace elements except Ni, Co, Cr and V are very low in dunite (almost zero in the most Mg-rich parts) and increase systematically through lherzolite to olivine pyroxenite. Ni and Co contents of the rocks are affected by the presence of sulfides, so that caution has to be taken in interpreting these data.

The most impressive correlations are shown by the variation of the trace elements with $TiO_2$ (Fig 7.4). Most of the trace elements are positively correlated with $TiO_2$, in particular, the immobile elements such as Hf, Zr, V and Y.

Chai and Naldrett's (1992a) REE data, listed in Table 7.1, are shown in Fig. 7.5 as chondrite normalized REE patterns. In the case of the West subchamber (hole ZK-71) REE in both barren and sulfide-bearing rocks were analyzed, but only sulfide-free rocks or those with small amounts of sulfide were analyzed from the West-central and East subchambers. In the West subchamber REE contents in sulfide-bearing rocks are several times lower than in barren, although the shape of the profiles are similar (Fig. 7.5a), indicating that that interstitial sulfides displaced the interstitial silicate liquid that contributed the bulk of the REE in the rocks.

Chai and Naldrett (1992a) point out that the main features of the Jinchuan rocks are their LREE-enriched patterns with LREE for the sulfide free rocks around 8–20 times the chondritic value and HREE around 2–6 times. Variation of the REE patterns from La to Lu is quite smooth without obvious Eu anomalies. The chondrite normalized La/Lu ratios are between 4 and 10. The REE profiles therefore point to the original magma having had a basaltic rather than an ultramafic composition. The LREE enrichment and HREE depletion for samples of the East subchamber of the intrusion, is slightly greater than those of the other two, with La usually more than 10 times and Lu around 2 times the chondritic value. Chai and Naldrett suggest that this feature may indicate a more evolved interstitial liquid in the East subchamber.

## 7.4 Olivine Compositions

Li et al. (2003b) have made an exhaustive study of the Fo and Ni content of olivines from the No.1 and No. 2 orebodies at Jinchuan. They

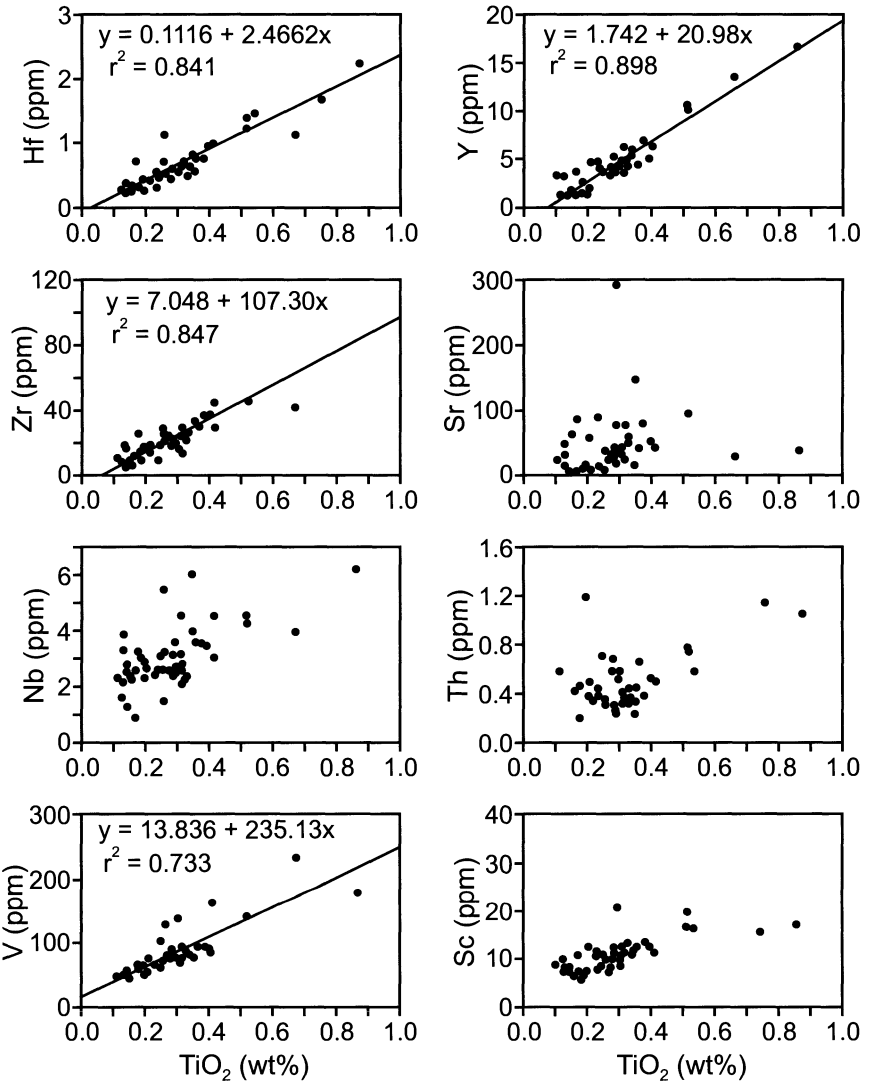


**Fig. 7.4.** Correlations of selected trace elements with $TiO_2$. Hf, V, Zr and Y show clear positive linear correlations with $TiO_2$ (after Chai and Naldrett 1992a)

observed that in grains of olivine that had been subjected to amphibole alteration (Mg-hornblende and actinolite) the margins of the olivine grains recrystallised to a more Fa-rich component (in general 8 mole % more fayalite than in the original olivine). In each of the two holes that they studied through the western part of the Jinchuan intrusion, the intersection could be divided into three zones, marginal zones on each side in which Fo contents were in the region of 82 to 83 mole percent, and a central zone in

which the Fo contents ranged from 83 to 86 mole percent. These values agree closely with Chai and Naldrett's (1992a) microprobe analysis of olivine in different rock types which indicated that forsterite contents range from 84–85 mole % in dunite, 82–85% in lherzolite and 79–82% in olivine pyroxenite. Chai and Naldrett noted that the majority of olivine has MgO contents between 43–44.5 wt% which agrees with the values of 42–44 wt% MgO extrapolated from the whole rock data. NiO contents of olivine range from 0.15–0.3 wt%.

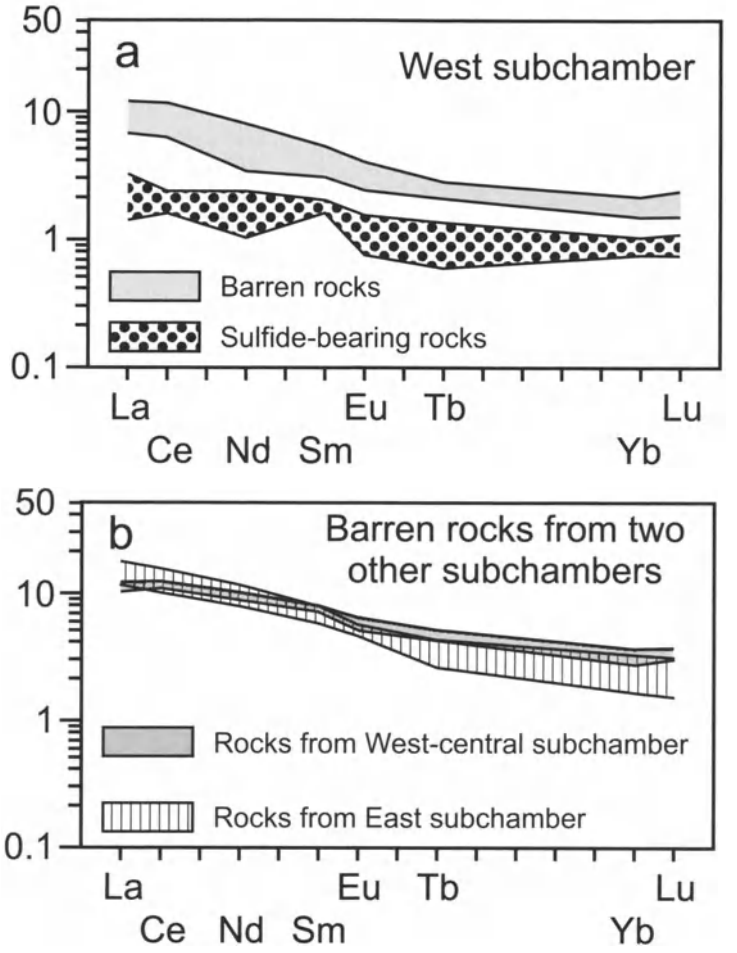


**Fig. 7.5.** Chondrite normalized REE patterns for samples from the three subchambers of the Jinchuan intrusion. The barren rocks of all of them show similar features. Sulfide-bearing rocks have lower REE concentrations due to the dilution of the REE by the sulfides. After Chai and Naldrett (1992a)

## 7.5 Petrogenesis

### 7.5.1 MgO/(MgO+FeO) ratio of the parental magma

Chai and Naldrett (1992a) noted that the MgO/(MgO+FeO) ratio of a parental magma can be easily calculated by using the composition of olivine, since the Mg and Fe distribution coefficient between olivine and coexisting silicate liquid has been well established as:

$$K_D = (FeO/MgO)_{olivine}/(FeO/MgO)_{liquid} = 0.3 \quad (7.1)$$

This coefficient is relatively insensitive to temperature, pressure and composition of the liquid which is in equilibrium with olivine (Roeder and Emslie 1970). One problem with this method of estimation is that the composition of cumulus olivine is usually less Mg-rich than that which crystallized originally, due to overgrowth from and re-equilibrium with the interstitial liquid (Bames 1985; Chalokwu and Grant 1987; see also discussion in Chaps. 6 and 10). However, two features of the Jinchuan olivine indicate that the present olivine composition may not have changed very much. Firstly, cumulus olivine in the Jinchuan intrusion does not appear to have developed much overgrowth from the interstitial liquid. On the contrary, it is often resorbed by pyroxene. Secondly, olivines immersed in sulfides may not always have been in contact with interstitial silicate liquid. The sulfides may have protected olivine from overgrowth as the interstitial liquid fractionated. Therefore, olivine with the highest forsterite content may be very close to the initial composition. The highest forsterite content of olivine in the Jinchuan intrusion is 85.5 %. The calculated MgO/(MgO+FeO) ratio of the parental magma is thus calculated to be 0.64 if it is assumed that distribution coefficient is 0.3. This is much lower than the MgO/(MgO+FeO) ratios of any of the Jinchuan intrusive rocks (Table 7.1). Therefore, Chai and Naldrett (1992a) concluded that the bulk composition of all of the Jinchuan rocks has been enriched in MgO by addition of cumulus olivine.

### 7.5.2 Composition of the parental magma

In order to estimate the composition of the parental magma, more information is needed than just the MgO/(MgO+FeO) ratio. A method commonly used to infer parental magma composition is to take the calculated MgO/(MgO+FeO) ratio and look for a chilled zone of the intrusion or a komatiite with a similar ratio (Bames 1985; Duke 1986).

Chai and Naldrett (1992a) pointed out that the composition of the Jinchuan intrusion is more difficult to estimate since there are no equivalent spinifex-textures or chilled contact zones. The previous researchers (S. G. U. 1984) had suggested that the Jinchuan igneous body represented a composite intrusion formed by several influxes of magmas with compositions equivalent to the corresponding rock types. Therefore, they estimated the composition of the parental magma by calculating a weighted average of the constituent rocks, which gave an anhydrous composition of 33.90 wt% MgO and 14.53 wt% FeO (assuming the total content of FeO was proportioned as 10 % $Fe^{3+}$ and 90 % $Fe^{2+}$). This result is clearly fallacious since it gives an MgO/(MgO+FeO) ratio of 0.81, much higher than the calculated value of 0.64.

However, Chai and Naldrett (1992a) argued that if one ignores the small amount of uniformly distributed chromite, the Jinchuan intrusive rocks can be taken as a mixture of the parent magma and cumulus olivine. As discussed, olivine from most parts of the intrusion shows a narrow range of forsterite contents from 83–85 mole percent. If a regression line is drawn through the rock compositions on a plot of FeO versus MgO (Fig. 7.6), the liquid and the average olivine composition will lie at the two ends of this mixing line. The interception of this line with a line having a slope equal to the MgO/(MgO+FeO) ratio of the liquid will give the MgO and FeO contents of the parent magma.

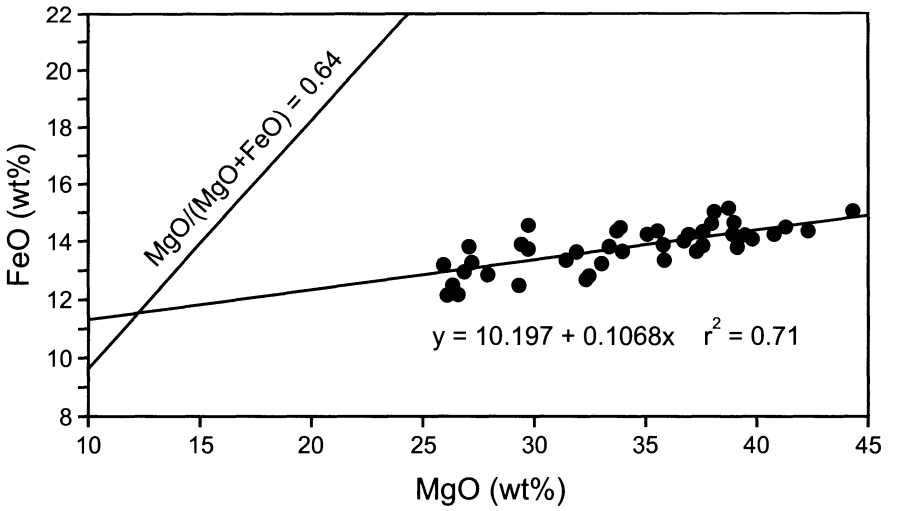


**Fig. 7.6.** Extrapolation of the variation diagram of FeO versus MgO to the estimated the composition of the Jinchuan parental magma. The interception of the two line gives an MgO content of about 12 wt%. After Chai and Naldrett (1992a)

Several conditions are needed to justify this approach: 1) the whole-rock samples must be sulfide free since even small amounts of sulfide can add significant amount of iron to the bulk rock composition ; 2) all of the iron in the bulk rock must be present as FeO. With regard to the first condition, only samples with less than 0.2% sulfur were plotted in Fig. 7.6. With regard to the second, the Jinchuan rocks are dominated by olivine which contains almost no $Fe_2O_3$, and the small amount of $Fe_2O_3$ present in chromite and the interstitial liquid will not materially affect the calculation. The plot shows that FeO decreases slightly with decreasing MgO with a regression line having an $r^2$ value of 0.71. Furthermore, since the trend of the regression line through the rock compositions is quite flat, and the MgO/(MgO+Fe0) trend is quite steep, a slight variation in the slope or position of the trend line for the rock compositions does not significantly change the MgO content at the point of intersection. This point corresponds to 11.2 wt % FeO and 11.5 wt% MgO which are therefore the concentrations of these elements in the parent magma. The result indicates that the magma was a high-MgO basalt, which is consistent with the Ni/Cu ratio and PGE profiles (see Fig. 7.10 below) of the ores, and REE profiles of the rocks (Fig. 7.5).

Li et al. (2003b) modeled the variation in the Fo and Ni contents of olivine fractionating from an initial magma with 11.5 wt% MgO, 11.2 wt% FeO and 330 ppm Ni, assuming that $D_{Ni}^{ol.-sil.} = 7$ and $(FeO/MgO)^{olivine}/(FeO/MgO)^{magma} = 0.3$. Their modeling involving 5% fractional crystallization reproduced their observed variations in Ni and Fo content of olivine, but indicated that a lowering of Ni content of up to 100 ppm and up to 2 mole % Fo had been caused by interaction of the olivine with trapped interstitial liquid.

### 7.5.3 Constraints on Magma Emplacement and Differentiation

Chai and Naldrett (1992a) argue that the lateral zonation in the west and horizontal layering in the east of the Jinchuan intrusion indicate that the two parts of the intrusion formed as the result of different processes. In the western part, the lateral variation is due to variations in the grain size and proportions of constituent minerals, with the rocks ranging from dunite at the core, through lherzolite to olivine pyroxenite at the margin. They argued that this zonation was due to the transverse movement of olivine crystals towards the axis within the liquid. This cannot be explained by gravitational settling, and they proposed that a flow differentiation process (Barker 1983), caused crystal grains and other more dense phases to migrate towards the center of the magma conduit (Fig. 7.7).

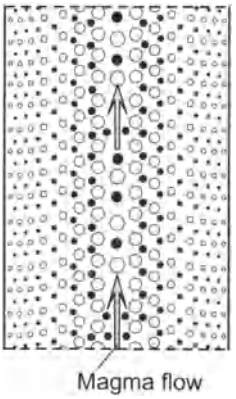


**Fig. 7.7.** Model of flow differentiation (after Barker, 1983)

In the case of the eastern part of the intrusion, the cumulus texture and macro scale phase layering, in addition to the greater width of the intrusion chamber, are compatible with this part of the intrusion developing as a layered sequence through the normal process of gravitationally controlled crystallization. The thinning of the lithological layers from the center towards the margin implies that the interface between magma and cumulates in the chamber was not flat, but was inclined towards the axis, similar to Wilson and Prendergast's (1989) model for the Great Dyke (see Chap. 9).

Plagioclase lherzolite occurs only locally at surface in the western part of the intrusion, but is much more prevalent in the east. At the western end of the eastern part, plagioclase lherzolite is observed to pinch out westwards. These observations are consistent with the interpretation that the eastern part represents a higher level in the original magma chamber than the western part. The slightly lower MgO content of the lherzolite in the eastern part (35–38 wt%) and slightly greater degree of LREE enrichment compared with that in the western part (37–39 wt%) also implies that the magma in the eastern part was more fractionated than that responsible for the rocks that are now exposed in the west. Since the Jinchuan intrusion is open to the surface and becomes wider upwards, the greater part of the original magma chamber was very likely above the level of the present surface. Chai and Naldrett (1992a) suggest that the overall shape of the magma chamber was originally trumpet-like in cross section, somewhat similar to the Great Dyke of Zimbabwe (see Chap. 9). The present Jinchuan intrusion can thus be compared with the ultramafic portion of the Great Dyke. This model calls for a sequence of layered mafic rocks to have existed above the level of present exposure at Jinchuan.

Li et al. (2003b) reached a similar conclusion on the basis of their olivine compositional data. As discussed above, the results of their calculations indicated that a maximum of 5 % olivine had crystallized from the parental magma. They noted that the magma/olivine ratio in such a system is thus more than 19. Their mass balance calculations using these constraints indicated that the current Jinchuan body accounts for less than 2% of the total parental magma involved in the intrusion.

## 7.6 Sulfide Mineralization

### 7.6.1 Geology of the Ore Bodies

Three ore bodies, No.24, No.1 and No.2, have been outlined at Jinchuan (S.G.U. 1984), corresponding to the three magmatic subchambers described above (Fig. 7.1).

No. 24 Ore Body is a tabular-shaped mass in the West subchamber, subparallel to the walls of the chamber. The ore body extends along the length of the chamber with a width of about 100–200 m. The mineralization occurs within dunite and lherzolite, and lies closer to the footwall side (Fig. 7.1-4) of the chamber. Two main ore types, disseminated and net-textured ores (Ni = l-4 wt%), account for more than 95 percent of the sulfides. Disseminated ore dominates in the western part of the ore body with a width of more than 200 m at its widest point. The width decreases towards the east and in the deeper portions of the ore body, bifurcating in places. Net-textured ore occurs below 50 m in the eastern portion of the ore body (Fig. 7.1-3). It appears as a small lens close to the footwall of the ore body and widens eastwards and with depth. The net-textured ore is enveloped by disseminated ore in the east, and the zone is usually thicker on the hanging wall side than on the footwall side. The PGE content in the net-textured ore is about 2-3 times that of the disseminated ore with an average Pt concentration of about 0.4 ppm, increasing with depth (S.G.U. 1984). The PGE are distributed irregularly and thus far 13 zones have been defined that are particularly PGE-rich.

The West-central subchamber hosts the largest ore body (No. 1) of the deposit which accounts for more than 50 % of the total reserves of both Ni and Cu. The ore body is tabular shaped about 1600 m long (Fig. 7.1-3) and 200 m wide (Fig. 7.1-4). Sulfide mineralization occurs from about 200 m to more than 1000 m below surface, for a strike length of 1500 m, and is dominated by net-textured sulfide ore. Low grade disseminated ore dominates at both ends and in the upper part of the ore body and envelopes net-textured ore. The ore body also has very high PGE and Au concentrations.

The greatest PGE enrichment occurs within a lens in the lower part of the ore body. The lens sub parallels the margins of the Ni-Cu ore body and has a length of more than 500 m and a maximum width of 47 m. The Pt grade averages 2.4 ppm but ranges to more than 9 ppm. Several other PGE enriched sections are also present in this ore body, but these are smaller in size and lower in grade.

Ore body No. 2 is at the base of the East subchamber. It is 1300 m long with a width of 118 m. Herein the body of net-textured ore is 900 m long, 40 m wide and occurs spatially below the disseminated ore (Fig. 7.1-6). Towards the east, the net-textured ore decreases gradually and sulfide mineralization becomes dominated by disseminated ore which forms about 59% of the nickel reserve in the No. 2 ore body. Massive ore, which contains 4–9 wt% Ni, is only present in Ore body No. 2. This ore type commonly occurs as small "segregations" or irregular veins with the same strike as the main ore body. The segregations are usually located at the base of the ore body and grade upward into net-textured and disseminated ore. Massive ore veins commonly occur in the net-textured ore and have a width of about 1–5 m. Some small massive ore veins (~1 m) cut sulfide ores and extend into the country rocks, although they do not extend very far. Xenoliths of intrusive rocks, gneiss, marbles and other types of sulfide ores commonly occur in the massive sulfides.

Ore minerals include pyrrhotite, pentlandite (violarite), chalcopyrite, cubanite, mackinawite and pyrite. Pyrrhotite is the dominant sulfide mineral in all the sulfide ores. It occurs mainly as anhedral or subhedral crystals (0.1–3 mm). Pentlandite occurs with pyrrhotite and commonly forms subhedral to euhedral crystals (0.1–2 mm) enclosed by anhedral pyrrhotite. Rarely, exsolution flames of pentlandite occur at boundaries or fractures of pyrrhotite crystals. In the oxidized ore, pentlandite is replaced by violarite that occurs as very fine grains along grain margins or cleavages and forms a regular framework in the pentlandite crystals. This replacement of pentlandite by violarite increases in intensity upwards in the deposit. Chalcopyrite occurs predominantly as anhedral crystal assemblages disseminated within other sulfides or as very fine veinlets which cross-cut either sulfide or olivine grains. In some massive ore, fragments of pyrrhotite and pentlandite are included within a chalcopyrite-dominant groundmass. It is not uncommon to see small sulfide droplets, less than 0.05mm in diameter, in olivine and chromite. One chromite crystal contains about four sulfide inclusions which show perfect rectangular outlines which are negative to the chromite morphology. All of the sulfide inclusions comprise pyrrhotite, pentlandite and chalcopyrite in the proportion of roughly about 7:2:1. Cubanite usually occurs as small bands intercalated with chalcopyrite bands perpendicular to the boundaries or fractures of the chalcopyrite. In places,

it replaces pentlandite along the cleavages or fractures of the latter. Mackinawite occurs predominantly in pyrrhotite and pentlandite as various irregular replacements.

More than ten PGE minerals are observed in association with the sulfide minerals (S.G.U. 1984). Sperrylite ($PtAs_2$) is the most common, and occurs as euhedral crystals (0.005–0.2 mm) at the margins of pentlandite, chalcopyrite and pyrite grains, or within chalcopyrite and cubanite. Other PGE minerals include native platinum, moncheite ($PtTe_2$), (Pd, Au), (AuPtPd), palladian melonite (Ni,Pd,Pt)(Te, $Bi)_2$, michenerite (PdBiTe), and sudburite (Pt,Pd)Sb (S.G.U. 1984).

### 7.6.2 Geochemistry of Sulfide Ores

Analytical results for Ni, Cu, Co, S and the PGE from selected samples are given in Table 7.2.

#### *West subchamber (ore body No 24)*

Drill hole ZK-71 transverses the complete lateral extent of the intrusive rocks and ore body No 24 (Fig. 7.1-4). As stated above, the ore body is within dunite and lherzolite which are located at the core of the intrusion. Ni, Cu, S and PGE profiles, as well as the metal elements in sulfides, are plotted in Fig. 7.8a.

Ni content is usually below 1 wt% along the section sampled by this drill hole, only exceeding 1 wt% in the central part of the mineralization between 350–430 m in depth. There are three sulfide-rich zones that were intersected in the drill hole: 1) a 20 m wide zone (2 wt% S) at the bottom; 2) a central zone, in which S increases upwards from about 520 m to 420 m before it declines slightly, before reaching a maximum of 4 wt% S at 365 m; 3) an upper zone, at about 270 m depth. Within these intervals, Ni and Cu correlate positively with S; the profile of Os+Ir+Ru also shows three highs although the central peak is much more obvious than the other two. Pt, Pd and Au show only two main peaks although the central peak is divided into two where Pt content reaches values of more than 1 ppm. When normalized to S content, the noble metals, in particular Pt and Au, increase inwards and, although maxima correlate with S maxima, it is clear that PGE and Au increase more rapidly than total sulfide (as indicated by S). The profiles Ni/S and Cu/S are smooth, increasing slightly down the drill hole.

**Table 7.2.** Representative analyses of sulfide ores of Jinchuan deposit (after Chai and Naldrett 1992b)

| Sample | Loc | D | Sul | S | Ni | Cu | Co | Pd | Pt | Rh | Ru | Ir | Os | Au |
|---|---|---|---|---|---|---|---|---|---|---|---|---|---|---|
| **West subchamber (ore body No 24)** | | | | | | | | | | | | | | |
| L-16 | Shaft | | 25.02 | 9.32 | 2.24 | 1.58 | 0.07 | 194.1 | 108.3 | 20.5 | 76.0 | 87.3 | 70.2 | 120.3 |
| L-20 | Shaft | | 13.39 | 4.96 | 0.99 | 2.08 | 0.02 | 185.4 | 446.4 | 9.8 | 29.3 | 24.8 | 23.1 | 368.7 |
| L-25 | Shaft | | 5.64 | 2.07 | 0.42 | 0.83 | 0.02 | 299.8 | 730.5 | 15.0 | 16.8 | 8.2 | 12.5 | 513.3 |
| I-13 | ZK-71 | 185 | 1.52 | 0.57 | 0.23 | 0.07 | 0.02 | 73.7 | 129.1 | 4.7 | 9.0 | 8.5 | 6.5 | 38.5 |
| I-17 | ZK-71 | 270 | 7.85 | 3.00 | 0.56 | 0.20 | 0.03 | 299.5 | 659.6 | 6.8 | 14.1 | 6.0 | 8.5 | 55.8 |
| I-18 | ZK-71 | 305 | 6.00 | 2.23 | 0.59 | 0.30 | 0.03 | 154.1 | 256.7 | 3.3 | 6.7 | 7.4 | 6.4 | 114.6 |
| I-20 | ZK-71 | 340 | 3.38 | 1.26 | 0.41 | 0.19 | 0.02 | 93.9 | 195.7 | 4.7 | 11.7 | 9.8 | 7.5 | 32.7 |
| I-21 | ZK-71 | 360 | 17.97 | 6.70 | 1.73 | 0.93 | 0.06 | 78.7 | 55.5 | 4.2 | 4.0 | 3.4 | 4.2 | 112.4 |
| I-22 | ZK-71 | 394 | 7.02 | 2.60 | 0.70 | 0.36 | 0.02 | 271.4 | 591.5 | 8.0 | 11.3 | 13.6 | 14.6 | 192.8 |
| I-23 | ZK-71 | 420 | 7.06 | 2.55 | 0.89 | 0.82 | 0.02 | 302.7 | 877.0 | 9.5 | 20.2 | 17.0 | 17.5 | 417.3 |
| I-25 | ZK-71 | 465 | 4.39 | 1.65 | 0.49 | 0.14 | 0.03 | 59.7 | 129.6 | 1.7 | 5.8 | 4.2 | 4.4 | 28.8 |
| I-26 | ZK-71 | 527 | 0.70 | 0.26 | 0.18 | 0.01 | 0.02 | 33.1 | 32.0 | 0.9 | 2.4 | 2.1 | 1.9 | 1.5 |
| I-27 | ZK-71 | 540 | 7.73 | 2.92 | 0.73 | 0.20 | 0.03 | 115.0 | 54.1 | 10.6 | 27.4 | 21.6 | 19.7 | 48.8 |
| I-29 | ZK-71 | 580 | 5.63 | 2.10 | 0.62 | 0.16 | 0.02 | 169.3 | 127.5 | 0.8 | 1.2 | 0.9 | 1.4 | 33.3 |
| ***Average OB No24 (n = 14)*** | | | 8.09 | 3.01 | 0.77 | 0.56 | 0.03 | 166.3 | 313.8 | 7.2 | 16.9 | 15.3 | 14.2 | 148.5 |
| **West-central subchamber (ore body No 1)** | | | | | | | | | | | | | | |
| A2-35 | Shaft | | 18.43 | 6.94 | 1.96 | 0.15 | 0.06 | 103.0 | 1514.0 | 35.6 | 70.6 | 61.3 | 62.8 | 33.4 |
| 2-W-18 | Shaft | | 17.47 | 6.53 | 1.56 | 0.10 | 0.07 | 510.2 | 3 046.6 | 20.9 | 11.4 | 19.6 | 26.7 | 48.7 |
| 2-W-6 | Shaft | | 5.71 | 2.12 | 0.40 | 0.69 | 0.02 | 105.5 | 76.1 | 2.1 | 7.4 | 3.6 | 3.9 | 63.6 |
| 2W12 | Shaft | | 3.94 | 1.49 | 0.38 | 0.07 | 0.08 | 132.0 | 65.1 | 6.3 | 6.7 | 6.2 | 6.7 | 20.5 |
| S89-1 | Shaft | | 19.78 | 7.41 | 2.24 | 0.28 | 0.07 | 126.6 | 371.3 | 112.9 | 224.8 | 208.3 | 179.4 | 224.5 |
| S89-2 | Shaft | | 19.05 | 7.08 | 2.06 | 0.84 | 0.06 | 184.4 | 467.8 | 32.2 | 65.6 | 87.8 | 71.2 | 56.6 |
| S89-3 | Shaft | | 18.24 | 6.74 | 1.98 | 1.14 | 0.06 | 110.8 | 128.2 | 36.1 | 77.3 | 63.8 | 70.2 | 98.2 |
| S89-4 | Shaft | | 18.32 | 6.77 | 1.46 | 1.88 | 0.05 | 271.6 | 325.3 | 30.0 | 51.1 | 49.1 | 38.1 | 206.5 |

**Table 7.2.** (cont.)

| Sample | Loc | D | Sul | S | Ni | Cu | Co | Pd | Pt | Rh | Ru | Ir | Os | Au |
|---|---|---|---|---|---|---|---|---|---|---|---|---|---|---|
| S89-5 | Shaft | | 20.56 | 7.40 | 2.30 | 2.71 | 0.07 | 320.7 | 161.5 | 26.6 | 53.0 | 31.7 | 37.0 | 96.3 |
| S89-6 | Shaft | | 18.64 | 6.91 | 2.03 | 0.97 | 0.06 | 161.6 | 134.2 | 26.9 | 57.8 | 41.9 | 49.6 | 134.5 |
| S89-7 | Shaft | | 18.84 | 7.02 | 2.09 | 0.63 | 0.07 | 199.7 | 128.6 | 39.0 | 82.4 | 70.2 | 66.4 | 93.0 |
| S89-8 | Shaft | | 20.76 | 7.72 | 2.57 | 0.41 | 0.07 | 153.2 | 193.0 | 62.1 | 84.9 | 66.5 | 70.7 | 94.2 |
| II-89-1 | ZK-51 | 614 | 14.45 | 5.34 | 1.49 | 1.03 | 0.04 | 168.2 | 179.1 | 13.0 | 15.6 | 19.9 | 19.4 | 103.6 |
| II-89-2 | ZK-51 | 640 | 14.58 | 5.36 | 1.34 | 1.50 | 0.04 | 180.4 | 997.4 | 8.1 | 13.0 | 12.8 | 12.5 | 162.8 |
| II-89-3 | ZK-51 | 664 | 18.40 | 6.62 | 2.38 | 2.01 | 0.05 | 810.0 | 9 217.1 | 0.0 | 0.5 | 3.6 | 14.9 | 200.0 |
| II-89-4 | ZK-51 | 700 | 20.62 | 7.57 | 2.33 | 1.50 | 0.06 | 216.9 | 303.1 | 5.2 | 12.8 | 7.8 | 10.0 | 461.1 |
| II-89-5 | ZK-51 | 750 | 18.37 | 6.88 | 2.14 | 0.21 | 0.04 | 319.1 | 1 921.3 | 2.7 | 1.8 | 6.4 | 3.9 | 46.7 |
| II-89-6 | ZK-51 | | 8.36 | 3.06 | 0.65 | 1.20 | 0.03 | 95.7 | 158.5 | 5.5 | 16.0 | 13.4 | 14.7 | 81.3 |
| II-89-7 | ZK-51 | 780 | 19.80 | 7.14 | 1.14 | 4.07 | 0.03 | 499.4 | 3 113.9 | 0.0 | 0.3 | 4.8 | 5.2 | 474.2 |
| II-89-8 | ZK-51 | 815 | 17.05 | 6.15 | 0.76 | 3.80 | 0.03 | 179.0 | 1 985.0 | 0.0 | 0.2 | 18.9 | 7.4 | 880.8 |
| II-89-9 | ZK-51 | 857 | 15.44 | 5.44 | 2.05 | 2.54 | 0.05 | 671.9 | 3 815.7 | 0.6 | 1.0 | 10.8 | 2.1 | 547.1 |
| II-89-11 | ZK-51 | 760 | 21.05 | 7.65 | 3.00 | 1.27 | 0.06 | 85.5 | 1 396.9 | 0.0 | 0.4 | 4.6 | 2.5 | 142.3 |
| II-89-12 | ZK-51 | 800 | 18.96 | 6.95 | 1.77 | 2.04 | 0.05 | 321.0 | 2 212.8 | 6.7 | 3.9 | 8.8 | 8.4 | 96.4 |
| II-89-13 | ZK-51 | 870 | 20.13 | 7.40 | 2.53 | 1.04 | 0.06 | 499.1 | 500.3 | 6.5 | 2.2 | 5.5 | 3.3 | 139.6 |
| II-89-14 | ZK-51 | 920 | 27.46 | 10.50 | 1.84 | 0.46 | 0.06 | 125.3 | 514.7 | 14.7 | 16.7 | 4.2 | 14.0 | 79.2 |
| II-89-15 | ZK-51 | 975 | 23.63 | 8.78 | 2.92 | 0.52 | 0.09 | 246.0 | 251.7 | 7.9 | 3.1 | 4.4 | 2.8 | 51.3 |
| II-W-9 | ZK-81 | 490 | 27.51 | 10.10 | 2.99 | 2.13 | 0.09 | 723.6 | 147.3 | 46.5 | 89.6 | 77.0 | 75.6 | 185.5 |
| II-W-11 | ZK-81 | 565 | 18.37 | 6.88 | 1.88 | 0.58 | 0.05 | 186.1 | 87.0 | 3.5 | 66.5 | 60.7 | 51.6 | 117.2 |
| II-W-13 | ZK-81 | 610 | 19.50 | 7.24 | 2.13 | 0.90 | 0.06 | 198.4 | 135.5 | 17.7 | 11.8 | 26.3 | 17.8 | 263.3 |
| II-W-15 | ZK-81 | 650 | 19.84 | 7.33 | 2.00 | 1.45 | 0.06 | 140.9 | 1074.0 | 10.5 | 11.1 | 12.2 | 8.3 | 258.8 |
| II-W-16 | ZK-81 | 670 | 6.77 | 2.59 | 0.54 | 0.09 | 0.03 | 62.7 | 54.0 | 7.8 | 15.0 | 12.2 | 11.9 | 48.9 |
| II-W-17 | ZK-81 | 685 | 20.08 | 7.32 | 1.74 | 2.64 | 0.06 | 565.5 | 3 520.1 | 5.7 | 13.5 | 6.5 | 12.6 | 295.3 |
| II-W-19 | ZK-81 | 720 | 16.07 | 5.88 | 1.58 | 2.19 | 0.05 | 230.1 | 522.9 | 5.4 | 10.5 | 4.8 | 4.6 | 680.9 |
| II-W-21 | ZK-81 | 755 | 13.51 | 5.10 | 1.26 | 0.30 | 0.05 | 164.3 | 303.1 | 10.3 | 11.4 | 10.5 | 8.4 | 324 |

**Table 7.2.** (cont.)

| Sample | Loc | D | Sul | S | Ni | Cu | Co | Pd | Pt | Rh | Ru | Ir | Os | Au |
|---|---|---|---|---|---|---|---|---|---|---|---|---|---|---|
| II-W-22 | ZK-81 | 780 | 26.68 | 10.20 | 1.82 | 0.43 | 0.06 | 273.8 | 2 457.8 | 51.5 | 161.4 | 105.9 | 137.4 | 140.8 |
| ***Average OB No 1 (n = 35)*** | | | 17.90 | 6.62 | 1.81 | 1.25 | 0.06 | 266.9 | 1 185.2 | 18.9 | 36.3 | 32.9 | 32.3 | 198.6 |
| **East subchamber (ore body No 2)** | | | | | | | | | | | | | | |
| A2-32 | Shaft | | 25.13 | 9.52 | 2.00 | 0.68 | 0.07 | 19.5 | 38.6 | 2.4 | 5.7 | 3.7 | 4.7 | 73.1 |
| A2-41 | Shaft | | 94.59 | 35.60 | 8.26 | 3.22 | 0.08 | 169.3 | 35.6 | 11.7 | 2.6 | 2.6 | 1.9 | 28.5 |
| 2-E-3 | Shaft | | 20.10 | 7.44 | 1.92 | 1.46 | 0.07 | 49.3 | 21.7 | 2.3 | 5.7 | 3.2 | 3.5 | 30.9 |
| 2-E-4 | Shaft | | 38.64 | 14.50 | 3.97 | 0.83 | 0.08 | 322.6 | 246.3 | 9.8 | 10.1 | 10.2 | 12.4 | 30.8 |
| 2.E-5 | Shaft | | 74.26 | 27.00 | 9.00 | 6.36 | 0.14 | 266.7 | 142.3 | 33.1 | 26.3 | 11.8 | 14.8 | 197.8 |
| 2-E-7 | Shaft | | 20.49 | 7.65 | 1.37 | 1.83 | 0.06 | 48.0 | 18.3 | 1.9 | 2.6 | 2.5 | 2.8 | 41.9 |
| 2-E-8 | Shaft | | 16.34 | 6.21 | 1.30 | 0.34 | 0.04 | 11.1 | 55.1 | 5.2 | 7.1 | 9.7 | 7.4 | 10.1 |
| 2-E-9 | Shaft | | 5.86 | 2.24 | 0.49 | 0.06 | 0.03 | 52.4 | 41.0 | 13.5 | 5.1 | 3.0 | 3.6 | 21.1 |
| 2-E-11 | Shaft | | 81.28 | 31.20 | 4.90 | 1.07 | 0.07 | 101.0 | 21.4 | 4.2 | 6.2 | 3.6 | 3.9 | 29.6 |
| II-89-16 | Shaft | | 92.83 | 34.20 | 4.73 | 13.50 | 0.24 | 128.7 | 330.4 | 52.3 | 131.6 | 157.2 | 144.9 | 36.7 |
| II-7 | ZK-86 | 102 | 0.95 | 0.37 | 0.11 | 0.01 | 0.02 | 37.1 | 0.8 | 0.0 | 2.6 | 0.1 | 0.5 | 1.8 |
| II-12 | ZK-86 | 237 | 0.66 | 0.25 | 0.17 | 0.00 | 0.01 | 19.0 | 0.5 | 0.0 | 1.6 | 0.0 | 0.4 | 0.8 |
| II-16 | ZK-86 | 306 | 5.29 | 1.96 | 0.45 | 0.55 | 0.02 | 18.1 | 20.4 | 1.0 | 1.2 | 3.2 | 0.8 | 21.7 |
| II-17 | ZK-86 | 320 | 5.83 | 2.20 | 0.58 | 0.18 | 0.02 | 35.3 | 49.0 | 1.3 | 2.4 | 1.5 | 1.9 | 9.9 |
| II-19 | ZK-86 | 355 | 18.66 | 7.06 | 1.70 | 0.30 | 0.06 | 309.3 | 106.6 | 7.8 | 11.6 | 8.3 | 8.0 | 103.7 |
| II-21 | ZK-86 | 385 | 17.34 | 6.48 | 1.72 | 0.71 | 0.05 | 34.6 | 71.0 | 5.6 | 3.8 | 10.0 | 1.8 | 54.7 |
| II-22 | ZK-86 | 408 | 26.66 | 10.10 | 2.10 | 0.75 | 0.07 | 98.2 | 30.9 | 6.4 | 13.5 | 8.8 | 8.3 | 20.4 |
| II-23 | ZK-86 | 425 | 27.26 | 10.20 | 2.82 | 0.84 | 0.06 | 28.4 | 145.2 | 6.9 | 3.5 | 5.3 | 4.1 | 12.4 |
| II-24 | ZK-86 | 440 | 19.25 | 7.23 | 1.69 | 0.83 | 0.05 | 63.9 | 24.7 | 2.0 | 3.5 | 1.8 | 2.3 | 20.0 |
| II-26 | ZK-86 | 474 | 18.90 | 6.94 | 1.56 | 1.80 | 0.03 | 32.6 | 50.6 | 4.1 | 6.7 | 5.7 | 4.5 | 23.4 |
| ***Average OB No 2 (n = 20)*** | | | 30.52 | 11.42 | 2.54 | 1.77 | 0.06 | 92.3 | 72.5 | 8.6 | 12.7 | 12.6 | 11.6 | 38.4 |

*D* Depth in m; *Loc* Location; *Sul* Sulfides; *OB* Ore Body. Contents: Sulfides, S, Ni, Cu, Co – wt%; Pd, Pt, Rh, Ru, Os, Ir, Au – mg/t (ppb)

### *West-central subchamber (ore body No 1)*

Drill hole ZK-51 cuts the major ore body (No 1) which is almost totally within dunite on this section (Figs. 7.1-3 and 7.1-5). The variation of the metal elements with depth of the drill hole is shown in Fig. 7.8b. Overall, S increases slightly down the drill hole. Ni is generally between 1 and 2 wt% and shows little systematic variation. Cu is usually lower than 1 wt% except for the interval 750 to 870 m within which it increases to more than 2 wt% and around 660 m where it also reaches 2 wt%. The highest Pt value (9 ppm) is encountered in this section at a depth of 670 m, while Pt in both marginal zones is very low (0.2 ppm). When the elements are normalized to S, Ni is uniform over the whole profile, but Cu varies irregularly with depth and is very low at the footwall margin. Pt+Pd show the same positive central anomaly with a large peak at 670 m; this is mainly due to the contribution of Pt.

### *East subchamber (ore body No 2)*

Drill hole ZK-86 cuts the intrusive rocks of the east subchamber and the ore body in which the layering of the intrusion (Fig.7.1-6) is horizontal. Variation from layer to layer is reflected in the element variation diagram along the drill hole appearing as Fig. 7.8c.

Sulfur concentrations are generally very low in the unmineralized rocks intersected in the upper part of the drill hole to a depth of 320 m. Below this, in disseminated ore, sulfur increases rapidly from 320 m down the drill hole to reach 7 wt% at 350 m, at the boundary with the net-textured ore. In the net-textured ore (from 350 m to the base of the ore body at 480 m) sulfur contents are 7–10 wt%. PGE are extremely low in this ore body (total PGE < 0.3 ppm) which is very different to the PGE concentrations in the other two ore bodies in which Pt alone may exceed 1 ppm. The PGE correlate positively with S and peak in the upper part of the net-textured ore. In general, Pd decreases towards the base of the sulfide zone, Pt concentration fluctuates irregularly down the sulfide ore zone and Os, Ru and Rh behave more or less similarly to Pd. When normalized to the S content of the samples, Pt+Pd are lowest at the base of the intrusion and increase gradually upwards, reaching a high in the upper part of the net-textured ore and fluctuating in the upper unmineralized rocks. The reverse trend of PGE in sulfide to the absolute concentrations indicates that sulfide increases more rapidly downwards than the PGE. Ni+Cu increases slightly down the drill hole to the level of the ore body, within which they remain more or less constant.

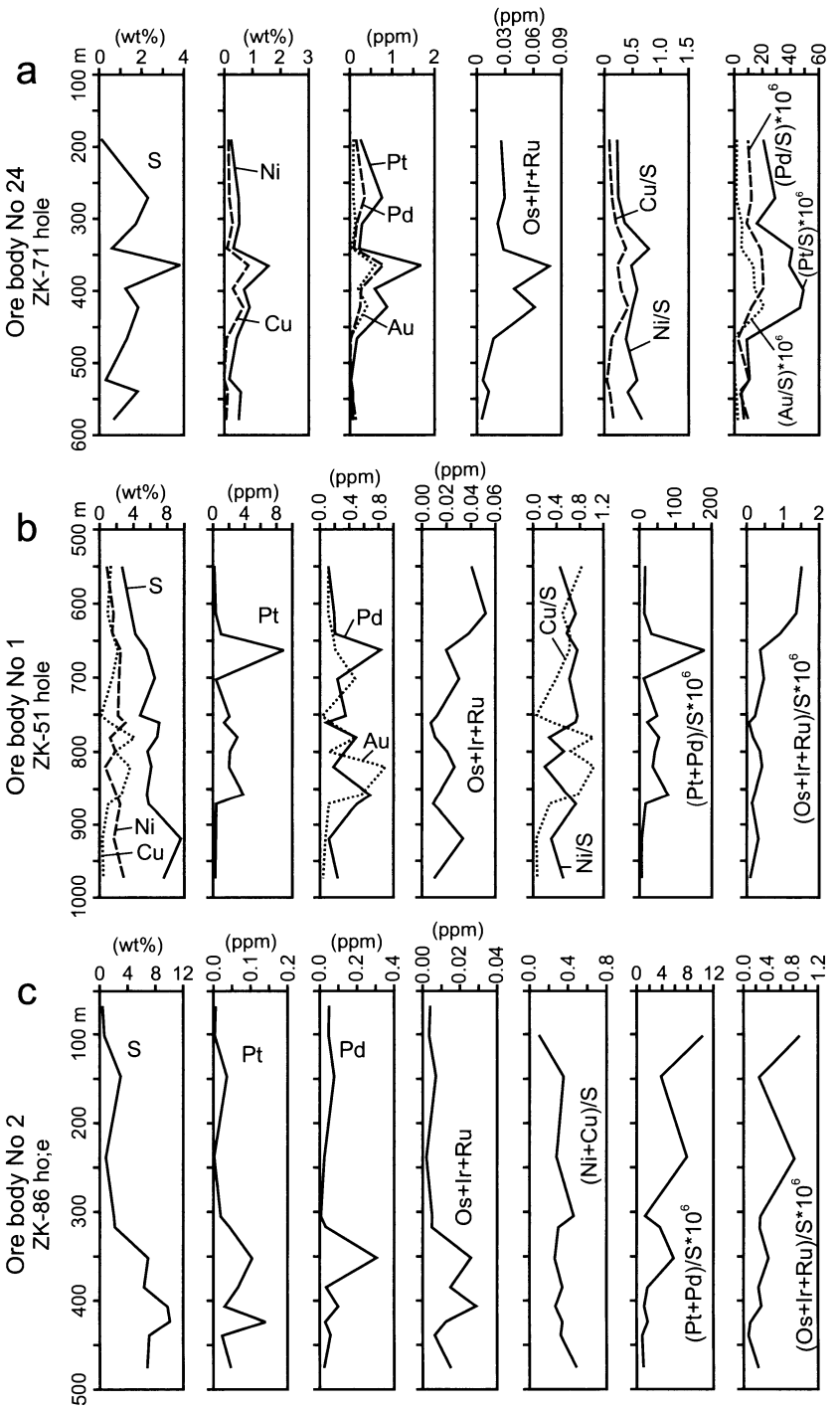
a
Ore body No 24
ZK-71 hole
(wt%)
(wt%)
(ppm)
(ppm)
100 m
200
300
400
500
600
S
Ni
Cu
Pt
Pd
Au
Os+Ir+Ru
Cu/S
Ni/S
(Au/S)*10^6
(Pt/S)*10^6
(Pd/S)*10^6
b
Ore body No 1
ZK-51 hole
500 m
600
700
800
900
1000
(Ni+Cu)/S
(Pt+Pd)/S*10^6
(Os+Ir+Ru)/S*10^6
c
Ore body No 2
ZK-86 ho;e

**Fig. 7.8.** Metal elements profiles through the Jinchuan deposit: a) drill hole ZK 71 which represents a transverse section of ore body No 24; b) drill hole ZK 51 which represents a transverse section of ore body No 1; c) drill hole ZK 86 which represents a vertical section through the layered sequence and ore body No 2. After Chai and Naldrett (1992b)

### *Inter-element relationships*

In this section, all analyzed samples from different parts of the deposit are considered as a whole in order to compare and contrast the variation in characteristics of ore throughout the Jinchuan intrusion.

Covariation diagrams of Ni and Cu with S are shown in Fig. 7.9. Ni correlates positively with S, although the correlation between Cu and S is not so clear. Samples from Ore body No 2 have slightly lower Ni values than those from the other two ore bodies.

When shown on a plot of PGE and Au concentrations versus S, the PGE data form two groups (Fig. 7.9): Group 1, which has higher PGE concentrations, consists of samples from the western two ore bodies (No1 and No 24). Group 2, which comprises samples from No 2 ore body, along with some samples from No. 1 has lower PGE concentrations. This division into groups is also reflected in the (Pt+Pd)/(Ni+Cu) ratio (PGE in g/t, Ni and Cu in wt%); the ratios for ore bodies No. 24 and No 1 are 0.36 and 0.45 respectively, while that for No. 2 is 0.04 (see the Appendix). Within each group, noble metals generally correlate with S, although the correlation between Au and S tends to be more scattered than those of the PGE, probably due to the ease with which Au is mobilized hydrothermally.

Fig. 7.10 shows PGE data from Jinchuan compared with data from other bodies on a chondrite-normalized chalcophile-element plot. Naldrett and Duke (1980) pointed out that deposits that are associated with igneous bodies resulting from ultramafic magma (e.g. those related to komatiites) have relatively flat PGE profiles on this type of diagram, while those associated with igneous bodies formed from basaltic or magnesian basaltic magma have much steeper slopes. The Jinchuan data resemble the latter type, providing yet more evidence that the Jinchuan magma was not ultramafic. Steepnesses of PGE profiles are usually expressed in terms of the (Pt+Pd)/(Ru+Ir+Os) ratio. Values of this ratio for the ores depicted in Fig. 7.10, are given in Table 7.3. Both from the profiles in Fig. 7.10 and the ratios in Table 7.3, it is seen that the Jinchuan ores are intermediate between ores of Proterozoic komatiites (Thompson and Katinniq deposits) and ores of mafic intrusions (Voisey's Bay and Talnakh deposits), which is consis-

tent with the estimate, discussed above, of 12 wt% MgO in the Jinchuan parental magma.

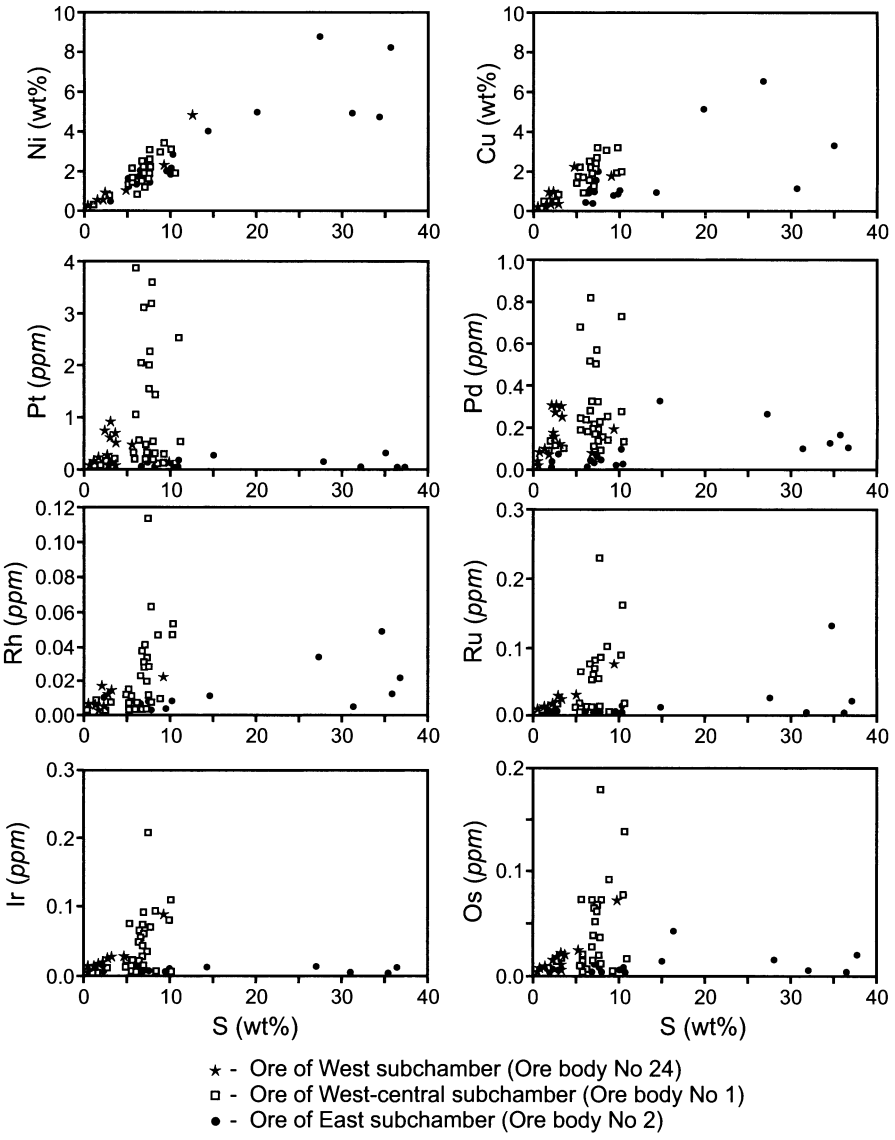


**Fig. 7.9.** Ni, Cu and PGE versus S contents of the Jinchuan ores. After Chai and Naldrett (1992b)

**Table 7.3.** Ratios (Pt+Pd)/(Ru+Ir+Os) in average compositions of Jinchuan ores in comparison with ores of some another well known deposits

| Deposit | Approximate MgO content (wt%) in parental magma | (Pt+Pd)/(Ru+Ir+Os) |
|---|---|---|
| Jinchuan (Ore body No 24) | 12 | 13.05 |
| Jinchuan (Ore body No 1) | 12 | 14.78 |
| Jinchuan (Ore body No 2) | 12 | 7.70 |
| Kambalda (generalized data for the Camp) | 30 | 2.06 |
| Langmuir (mines No 1 and No 2) | 30 | 1.56 |
| Thompson | ? | 4.36 |
| Katinniq | 19 | 5.77 |
| Voisey's Bay (Ovoid) | <8 | 18.69 |
| Talnakh (disseminated ores) | <8 | 60.24 |

Data for the Jinchuan deposit are from Chai and Naldrett (1992b). Average compositions of ores from Kambalda Camp, Langmuir, Thompson and Katinniq deposits are calculated using data from Table 3.3. Data for the Voisey's Bay deposit are from Table 6.2, for the Talnakh deposit from Table 4.6

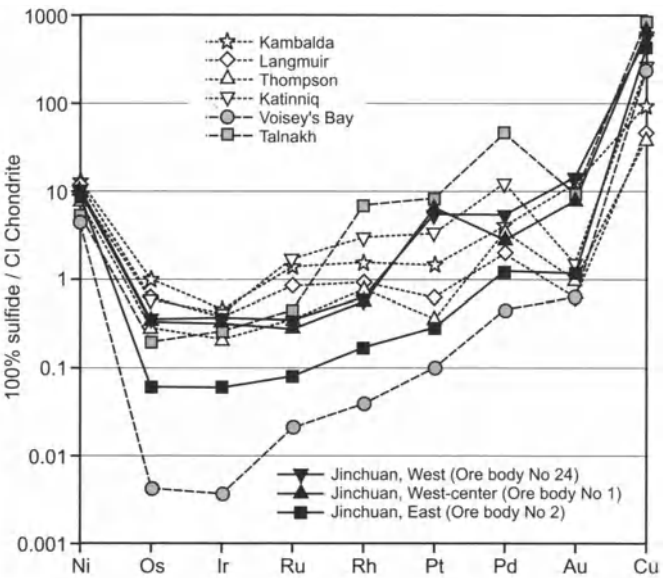


**Fig. 7.10.** Chondrite normalized chalcophile-element distribution patterns for the Jinchuan ores in comparison with ores of some other deposits related to ultramafic igneous bodies (Kambalda, Langmuir, Thompson, Katinniq) and mafic intrusions (Voisey's Bay, Talnakh). All compositions are recalculated for 100% sulfide. References for the data used are given in Table 7.3

## 7.7 Metallogenesis

The Jinchuan deposit lies completely within the Jinchuan intrusive rocks, sulfide ore bodies occur mainly in the lower parts of the intrusion and the Ni contents of the ores shows a good linear correlation with S. These features indicate that the deposit is magmatic in origin.

Sulfur isotopic measurements on sulfide minerals from different ore types of the deposit indicates that the $\delta^{34}S$ of sulfide minerals lies between -2 and +4 ‰ with most values being slightly positive (S.G.U. 1984; Ripley et al. 2003). This suggests that the sulfur may have been derived from the mantle, or, alternatively from an unfractionated crustal source.

Texturally the sulfides are mostly interstitial to cumulus olivine. When olivine shows a corona texture, sulfides commonly occur between the silicate aggregates. With the increase of sulfides, interstitial silicates decrease, and in the extreme situation, the net-textured ore consists only of cumulus olivine and interstitial sulfide. A small amount of sulfide occurs as blebs and inclusions in cumulus olivine and chromite; in chromite sulfide may occupy voids with the shape of negative chromite crystals. These features suggest: 1) much but not all of the sulfide liquid was moved into its present positions somewhat later than olivine cumulates; 2) pyroxene and plagioclase did not crystallize until after the sulfide liquid had settled down into the cumulus pile, partially or completely displacing the interstitial silicate liquid, although not before some of this liquid had reacted with olivine in some areas to form corona structures. Such an interpretation is supported also by the REE data, present in Fig. 7.5a, and discussed above; 3) sulfide immiscibility clearly occurred early during crystallization of the magma as evidenced by the sulfide inclusions in olivine and chromite, which would have been in existence as droplets at the time of crystallization of their host minerals. The data therefore indicate that the magma was sulfide saturated and carrying immiscible sulfide at the time of its emplacement.

Li et al. (2003) remarked that the average sulfide content in the Jinchuan body is about 5 wt%. Using the magma compositions of Chai and Naldrett (1992a), a liquidus temperature and $FeO/Fe_2O_3$ ratio that they calculated using the silicate liquid model MELTS of Ghiorso and Sack (1995), and the sulfur solubility equation of Li et al. (2001), they estimated the solubility of sulfur in the Jinchuan magma to be ~1,150 ppm (~0.3 wt% FeS) under an assumed total pressure of 3 Kb and an oxidation state equivalent to the quartz-fayalite-magnetite buffer. Assuming that the amount of the trapped magma in the Jinchuan rocks is 50 wt%, which is at the higher end of the values determined by De Waal et al. (2003), their mass balance cal-

culations indicated that the magma now represented by the Jinchuan body only accounts for about 3 % of the total magma in which the total sulfide in the body could have been dissolved. Another 97 % of the total mass of the parental magma is not accounted for by the current Jinchuan body, which agreed with their conclusion based on the average content of cumulus olivine in the rocks discussed above.

## 7.8 Genetic model for the Jinchuan deposit

A hypothetical model for the genesis of the Jinchuan deposit that is consistent with the geology and geochemistry is shown schematically in Fig. 7.11.

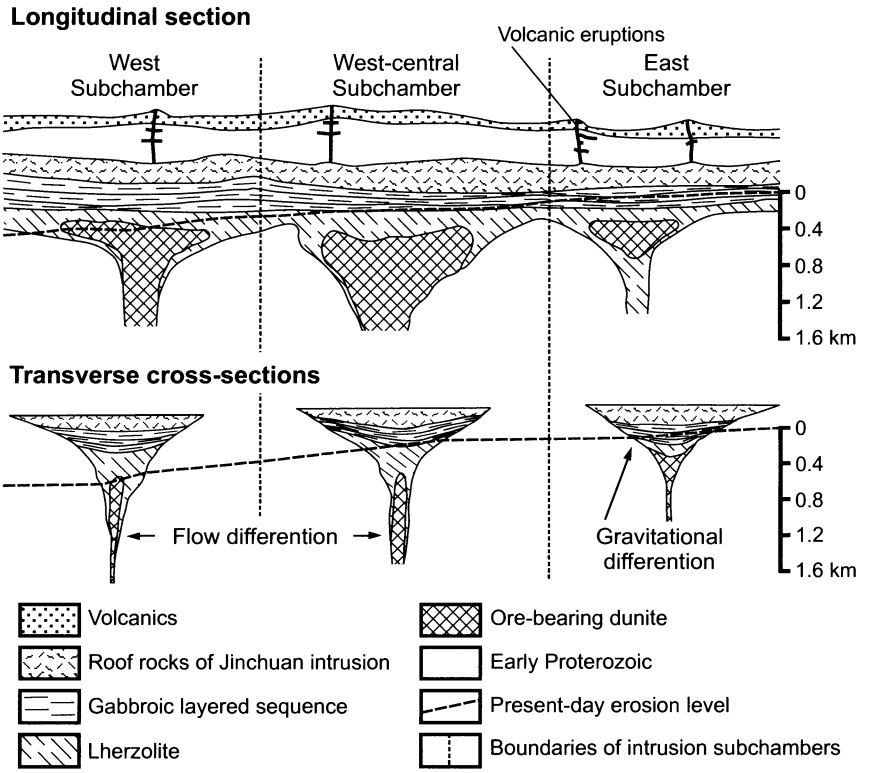


**Fig. 7.11.** Genetic model for the formation of the Jinchuan Ni-Cu deposit

Tectonic rifting accompanying the opening of an ocean to the south resulted in the intrusion of a high Mg basaltic magma along one of the rift-related faults. It is proposed that magma, carrying olivine, chromite and

droplets of immiscible sulfide, rose up through a series of funnel-shaped structures such as those preserved in the western part of the intrusion. As the funnels widened upwards, the velocity of the intruding magma decreased and suspended, higher density material became trapped there, much as sand carried along with water flowing through a hose will collect if the hose is connected to a vertical funnel. The distribution of the suspended material was controlled by flow differentiation in the magma and became concentrated in the central part of the conduit (Barker 1983; see Fig. 7.7), which likely remained open while material near the periphery cooled and adhered to the walls of the funnel. Magma intruded along the fault away from the main funnels, and gave rise to a sequence of layered rocks, similar to those preserved at the eastern end of the Jinchuan intrusion. Some sulfide left the feeder funnels and was deposited as stratabound zones of disseminated mineralization within the layered rocks.

With continued flow up the funnels, fresh magma was constantly brought into contact with the sulfides suspended there, enriching them in chalcophile metals and giving rise to the lateral zonation of the PGE contents in 100% sulfide that are illustrated in Fig. 7.8a, b. The sulfides in the central parts of the ore bodies (and in the central part of the deposit on the whole) were upgraded to the greatest extent. The sulfides that became trapped in the early cooling, marginal parts of the funnel were exposed to less magma and therefore became less enriched in sulfide. This process is akin to that thought to have operated at Noril'sk and Voisey's Bay, where flow of fresh magma along conduits containing sulfide is thought to have upgraded this sulfide.

# 8 Deposits of the Sudbury Camp, Ontario, Canada

## 8.1 Some History

The first recorded mention of mineralization in the vicinity of what subsequently became the town of Sudbury occurs in a report by Alexander Murray of the Geological Survey of Canada. As Dr Murray wrote:

"Previous to my visit to Whitefish lake, I had been informed by Mr. Salter that local attraction of magnet had been observed by himself, while he was engaged in running the meridian line, and he expressed it to be his opinion that the presence of a large body of iron ore was the immediate cause. When, therefore, I came to the part indicated by Mr. Salter, I made a very careful examination not only in the direction of the meridian line, but for a considerable distance on each side of it, and the result of my examination was that the local attraction, which I found exactly as described by Mr. Salter, was owing to an immense mass of magnetic trap... Specimens of this trap given to Mr. Hunt for analysis, and the result of his investigations shows that it contains magnetic iron ore and magnetic iron pyrites generally disseminated through the rock, the former in very small grains; titaniferous iron was found associated with the magnetic ore, and a small quantity of nickel and copper with the pyrites."

(From: Report of Alexander Murray, Geol. Surv. Can, 1853-56, 180, 181)

The location of the "meridian line" referred to by Murray is documented by C.W. Knight in the 1917 report to the Royal Ontario Nickel Commission:

"The location of this nickeliferous material is easily found. Salter's meridian line was retraced in 1883, and was made to form the west boundary of the townships of Waters and Snider ... This locality is only 200 yards west of the great open pit of Creighton Mines. Unquestionably then, Murray walked over and examined the long gossan-stained ridge, at the foot of which in later years the greatest nickel mine in the world was discovered."

(From: Report of the Royal Ontario Nickel Commission, 1917, p 29.)

Despite Murray's early report, the discovery of the Sudbury Ni-Cu ores is generally attributed to construction of the Canadian Pacific transcontinental railway, which had reached Sudbury by 1883. Limited produc-

tion started in 1886, and the subsequent growth of the mining camp, and the companies involved in this growth, are documented by the Ni production figures appearing as Fig. 8.1.

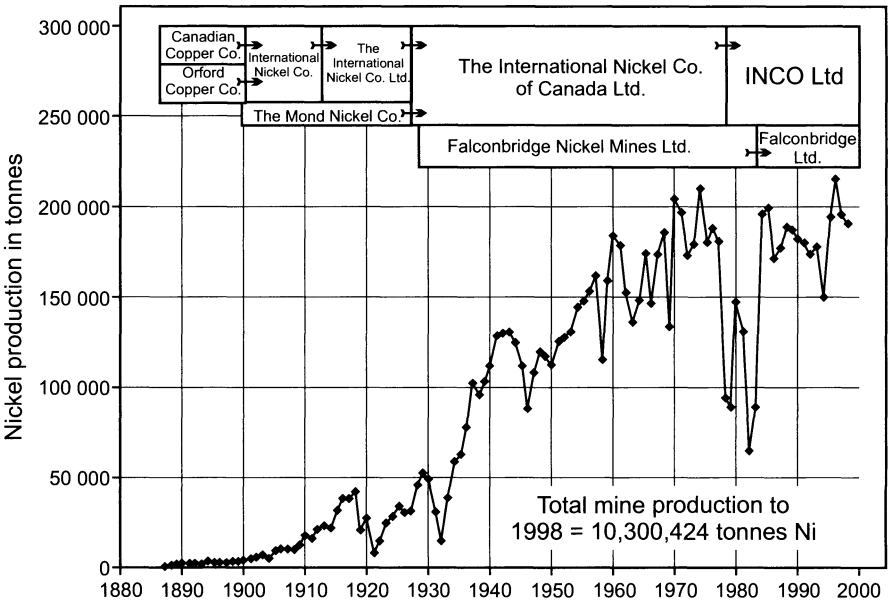


**Fig. 8.1.** Production of Ni metal from the Sudbury district, together with the companies responsible for the production. Arrows show the results of re-structuring and mergers

## 8.2 Geology

### 8.2.1 Regional Setting

The ores are associated with the Sudbury Igneous Complex (SIC), a layered intrusion (1.85 Ga) ranging from quartz norite at the base, through quartz gabbro to a granophyric cap. The SIC is located at the contact between tonalitic gneisses and intrusive quartz monzonites, all of Archean (>2.5 Ga) age to the north, and rocks of the Proterozoic Southern Province, which overlie the Archean basement unconformably and thicken to the south (Fig. 8.2). The Levack gneisses around much of the northern and western margins of the Complex (Fig. 8.3) exhibit granulitic metamorphism (James and Dressler 1992). The Proterozoic rocks belong to the

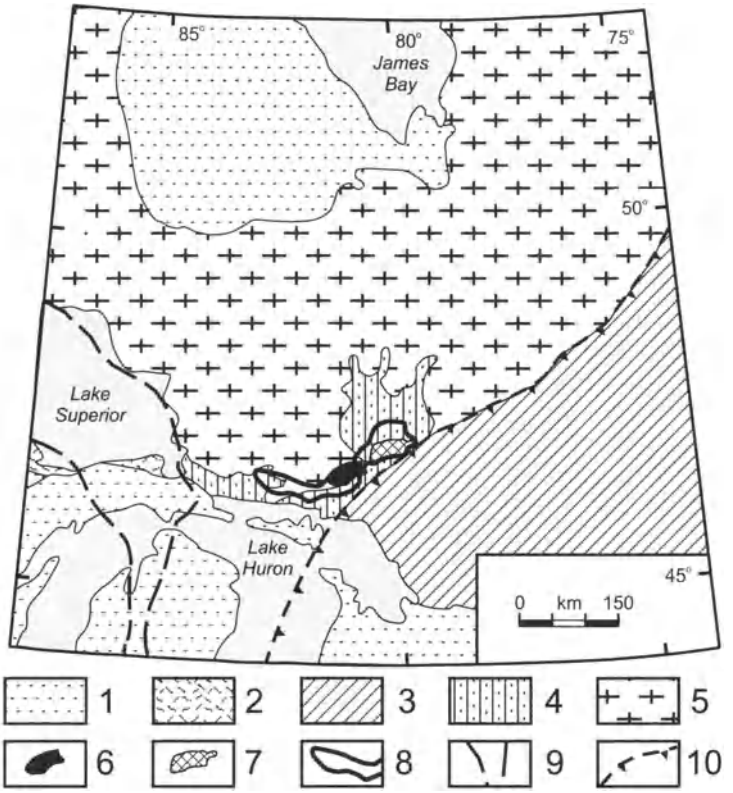


**Fig. 8.2.** Position of the Sudbury Igneous Complex within the regional geological setting (modified after Boerner et al. 1994). 1 = Paleozoic sedimentary cover; 2 = Late Proterozoic Keweenawan Supergroup, related to the Midcontinent rift system; 3 = Late Proterozoic rocks of the Grenville Province; 4 = Early Proterozoic Huronian Supergroup of the Southern Province; 5 = Archean rocks of the Superior Province; 6 = Sudbury Igneous Complex; 7 = Temagami magnetic anomaly (after Card et al. 1984), see our Fig. 8.8; 8 = Elliot-Sudbury-Englehart Bouguer gravity anomaly (after Card et al. 1984); 9 = Faults of the Midcontinent rift system; 10 = Frontal fault of the Grenville Province

Huronian Supergroup; in the Sudbury area they consist of local accumulations of mafic and felsic volcanics and related mafic/ultramafic intrusions (e.g. the East-Bull Lake intrusion, Peck et al. 1993, 2001) which are associated with the 2.4 Ga rifting that gave rise to the Penokean ocean along what is now the southern margin of the Superior Province. The volcanic and associated intrusive rocks are overlain by greywackes and siltstones, and then by arenites, all of which constitute a marginal facies to the oceanic trough. All of these rock units thicken abruptly a few km south of the southern margin of the SIC as the inferred continental shelf merges into a

continental slope. The rocks were folded in the Penokean orogeny, dated at 1.85 Ga, which developed as the Penokean ocean closed. The major part of the folding preceded the formation of the SIC.

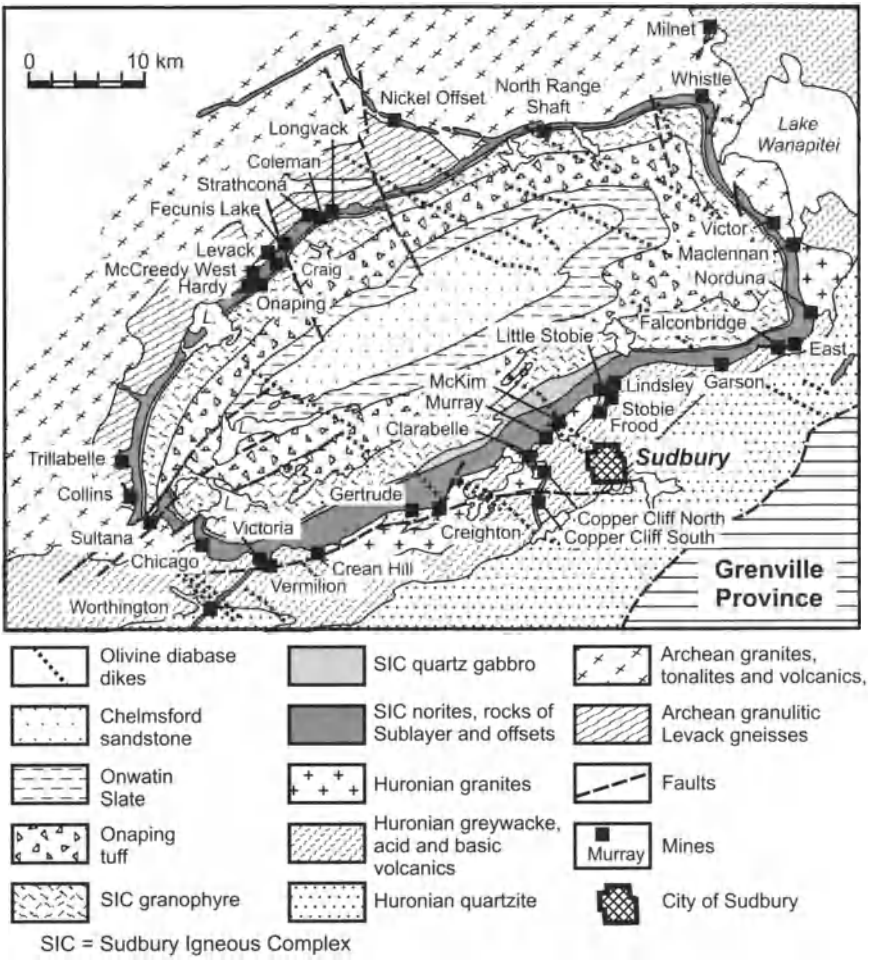


**Fig. 8.3.** Geological Map of the Sudbury district

## 8.2.2 Geology of the Sudbury Structure

Geological rock units directly related to the Sudbury event are summarized in Fig. 8.4. They include (in the order of their appearance): Sudbury Breccia, Footwall Breccia, Onaping Formation and the Sudbury Igneous Complex itself.

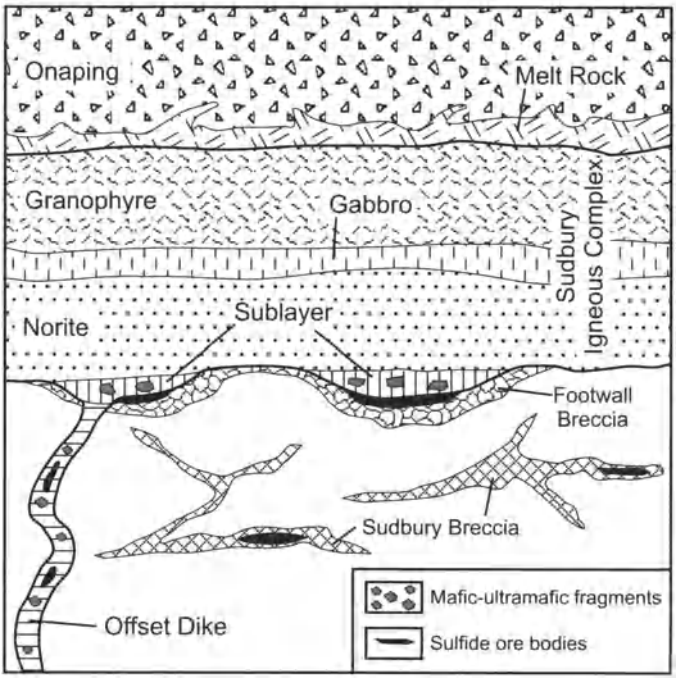


**Fig. 8.4.** Schematic vertical section showing interrelation of the geological units related to formation of the Sudbury Igneous Complex

Sudbury Breccia is a breccia composed of fragments of country rock ranging from microscopic to more than 10 m in diameter, occurring as dykes and irregular masses which cut all pre-SIC rock-types outside the Sudbury structure. In places the matrix of the breccia shows signs of incipient melting. It has never been observed to cut rocks comprising the SIC or rocks younger than the SIC. The breccia is most abundant close to the SIC but has been observed up to 20 km outside the outer margin of the SIC (Fig. 8.5). The thickness of the breccia bodies is very variable: from 1 cm to 100 m and more.

Footwall Breccia is a breccia composed of shattered and crushed country rocks along with some inclusions of ultramafic rocks and norites. The groundmass is largely composed of quartz, plagioclase and some K-feldspar and whispy amphibole crystals. It forms a layer, 10-50 m thick between the SIC and the footwall gneisses and monzonites along much of the North Range of the Sudbury structure. Thin apophyses of this breccia extend up to 10 m farther into the footwall. It is also present along the South Range but is much less common (Grant and Bite 1984)

The Onaping Formation is also composed of breccias. It consists of four distinct units. (1) A basal zone (up to 300 m thick) of country-rock

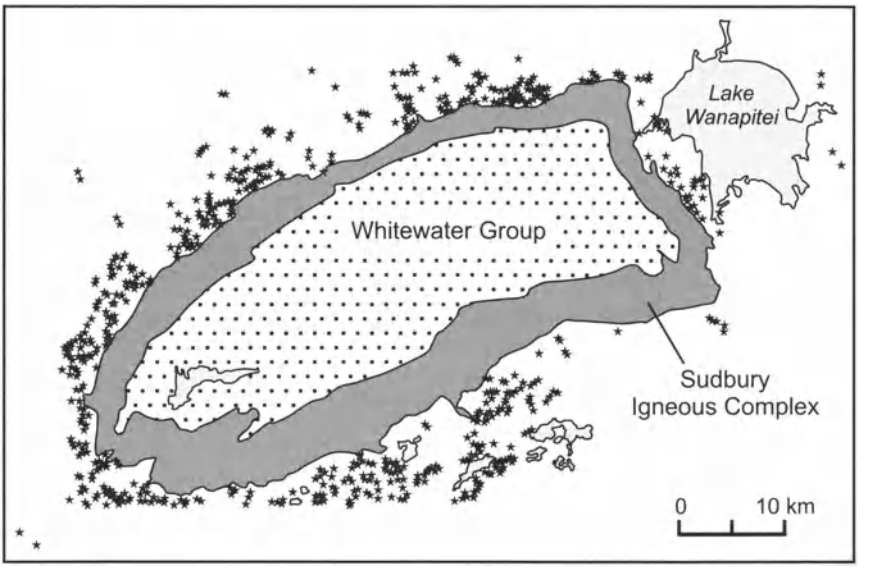


**Fig. 8.5.** Distribution of zones of Sudbury breccia (shown by stars) around the margin of the SIC. After Dressler (1984)

fragments set in an igneous matrix, that has been interpreted by Avermann (2000) as a melt breccia. (2) "Grey Onaping" (up to 500 m thick), composed of fragments of country rocks and recrystallized glassy material set in a matrix of glassy shards. This is equated with the suevite breccias that are associated with known impact structures. 3) "Green Onaping" (up to 70 m thick), which forms a thin layer that has been interpreted by Avermann (2000) as a collapsed fire ball that accomapanied the impact of a meteorite. (4) An upper zone of "Black Onaping" (up to 1000 m thick), that contains 1–3 wt% C and has been reworked or re-deposited in an aqueous environment.

The Sudbury Igneous Complex is situated between the Footwall Breccia and the Onaping Formation. The internal structure of the SIC is discussed below.

The Black Onaping Formation grades upwards into a slate (Onawatin slate, about 600 m thick) which, in turn, passes upwards into a unit composed of proximal turbidite flows (Chelmsford Formation, 850 m thick). The Onaping, Onawatin and Chelmsford formations are referred to as the Whitewater Group in some studies. The SIC and strata overlying it are exposed as a series of concentric, crudely elliptical rings which dip towards the center of the Complex and suggest that the structure is a basin (Fig. 8.3).

Card et al (1984) have drawn attention to a dominant linear gravity anomaly which extends 350 km from Eliot Lake eastward to Engelhardt (Fig. 8.2). The SIC straddles this feature and coincides with one of the three high-spots along it. Gupta et al (1984) analyzed the combined residual gravity and magnetic anomaly that marks the Sudbury region itself. They concluded that the broad +20 to +30 mGal anomaly could not be explained by the rocks of the SIC themselves and that a large mass of rock with a density similar to gabbro or gabbroic anorthosite (3.02±0.03 g/cc) underlay the complex at a depth of at least 5 km, extending well to the south of the southern limit of the complex. However a newer interpretation (see below) is at odds with this interpretation.

The seismic reflection data of Milkereit et al. (1992) that resulted from the 1990 Lithoprobe seismic transects across the Sudbury structure showed that the deep geometry of the Sudbury structure was markedly asymmetric. The seismic transect across the North Range indicated that the sediments and Onaping formation above the SIC, the units of the SIC itself and a dense unit immediately beneath the SIC (which projects up dip to coincide with the granulitic facies of the Levack gneiss complex) dip south at an average of 25° (Fig. 8.6). Reflections from the upper strata (sediments and

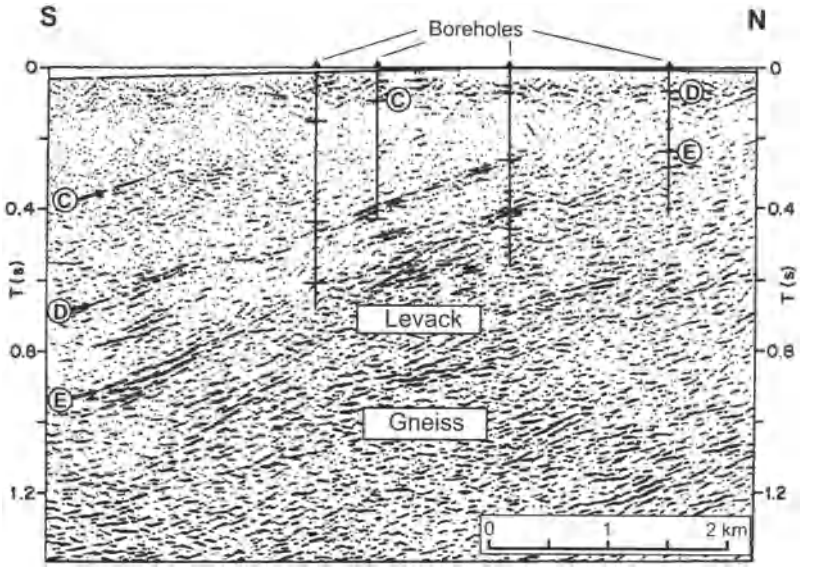


**Fig. 8.6.** Seismic profile through Sudbury North Range (after Milkereit et al. 1992). Position of the profile is shown in Fig. 8.15

Onaping formation) are interrupted by faults near the long axis of the Sudbury structure; the lower strata (norite and gneiss) can be traced with a continuous south dip south of the southern margin of the Sudbury. The base of the SIC is interpreted to be at a depth of 11–12 km at this point. In contrast, the seismic image of the South Range is dominated by a distinctive series of reflections with moderate south dip; these are interpreted as thrust faults or shear zones on which severe telescoping and imbrication of lithologic units, and considerable northwest-southeast shortening of the Sudbury structure have occurred (Fig. 8.7). This zone coincides at surface with the South Range Shear Zone, shown in Figs. 8.10 and 8.15. (Shanks and Schwerdtner 1991a). The seismic interpretation implies that the original diameter of the crater was of the order of 150-200 km.

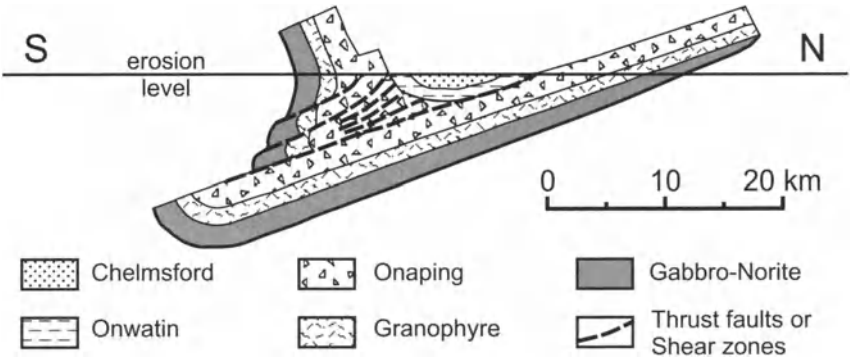


**Fig. 8.7.** North-South cross-section of the Sudbury structure as suggested by seismic data (after Shanks and Schwerdtner, 1991a)

The seismic data revealed no evidence of a large mafic-ultramafic body at a depth of 5-8 km. New gravity, density and seismic measurements allowed McGrath and Broome (1994) to develop a gravity model that accounted for the excess of mass present at Sudbury, without calling on a second layered intrusion hidden at depth, as had been required by previous models (Gupta et al. 1984). Magnetic susceptibility measurements on the same borehole material, together with the seismic constraints, enabled Hearst et al., (1994) to propose that the broad regional magnetic high which lies within and immediately northwest of the Sudbury Structure is produced by a strongly magnetic variant of the Levack Gneiss Complex, possibly the result of contact metamorphism against the SIC.

While the local gravity and magnetic fields in the vicinity of the SIC can be explained without Gupta et al.'s hidden intrusion, the most recent modeling provides no explanation for the regional gravity anomaly that extends west and east from the SIC (Fig. 8.2). It also provides no explanation for

the Temagami magnetic anomaly, that lies NE of Sudbury and resembles that at Sudbury (Fig. 8.8). Drilling to a depth of 2000 m has revealed a normal Precambrian sequence at Temagami. The explanation of both this and that at Sudbury, which show up so clearly in Fig. 8.8, remains unclear, although this author believes that they are likely the result of deeply buried intrusions belonging to the 2.45 Ga East Bull Lake-River Valley group (see Chap. 9).

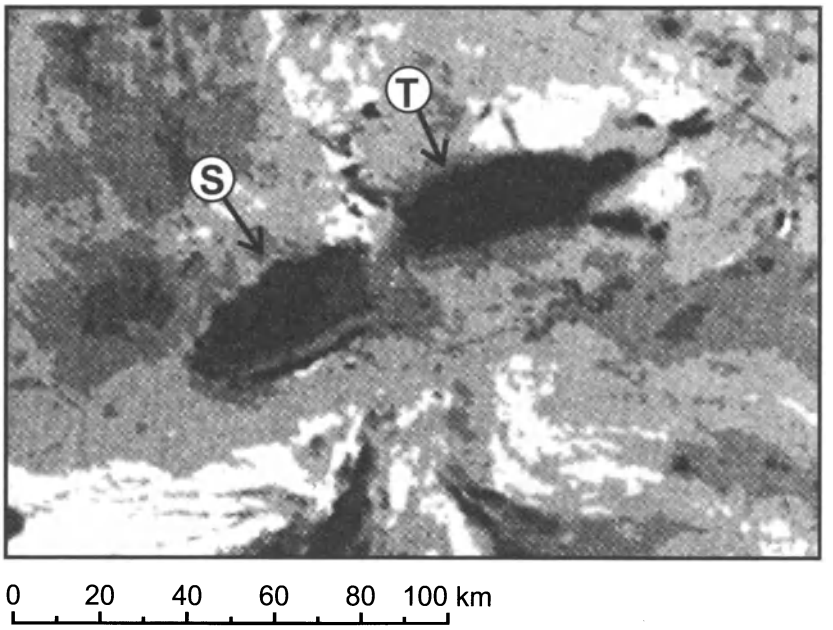


**Fig. 8.8.** Air-magnetic map of the Sudbury area showing the Sudbury (S) and Temagami (T) anomalies. After Card et al. (1984)

### 8.2.3 Evidence for Explosive Nature of the Sudbury Structure

Many aspects of the local geological setting suggest that an explosion of unusually large intensity gave rise to the Sudbury structure (see Pye et al. 1984 and studies, quoted below). The evidence includes:

1. The basinal shape of the structure as interpreted from surface and underground mapping and drilling, coupled with the seismic data from the Lithoprobe survey.

2. An upturned collar around the basin, as seen particularly in the Huronian rocks along the southern margin (Dressler 1984).
3. Shock metamorphic features, that include shatter cones and mineralogical evidence. Shatter cones occur up to 15 km away from the outer edge of the SIC (Fig. 8.9). When the orientation of the axes of the cones is adjusted for the rotation that is thought to have occurred after formation of the structure, they point towards the center of the presumed explosion. Minerals in many of the country rocks outside the SIC, and also in

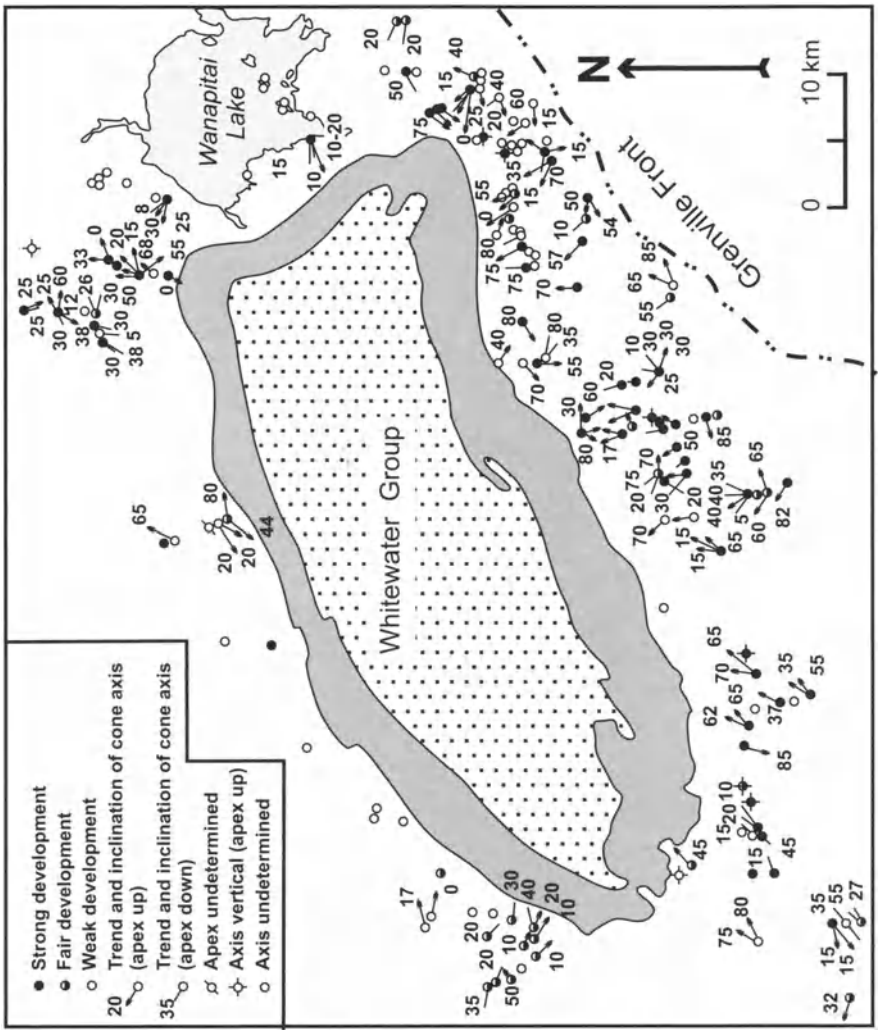


**Fig. 8.9.** Distribution of shatter cones and their orientation in Sudbury area (after Dressler 1984).

inclusions of the same rocks in the Onaping formation display textures indicating that they have been affected by shock of a magnitude up to 150 kb. This is far greater than could have resulted from a terrestrially induced explosion. Oriented quartz lamellae are a case in point. These lamellae show the same orientation with respect to the quartz c-axis as are shown by lamellae of thetamorphic glass in artificially shocked quartz. The lamellae in the Sudbury material are interpreted as marking the positions of similar glass which has since been recrystallized. The distribution of shocked quartz beyond the margin of the SIC is only slightly less than that of shatter cones (Fig. 8.10). Another example of minerals that can only be formed in an ultra high pressure environment, are the 6 micro-diamonds, similar in diameter to those from other impact sites, that were recovered from the Onaping formation by Masaiitis et al. (2000).

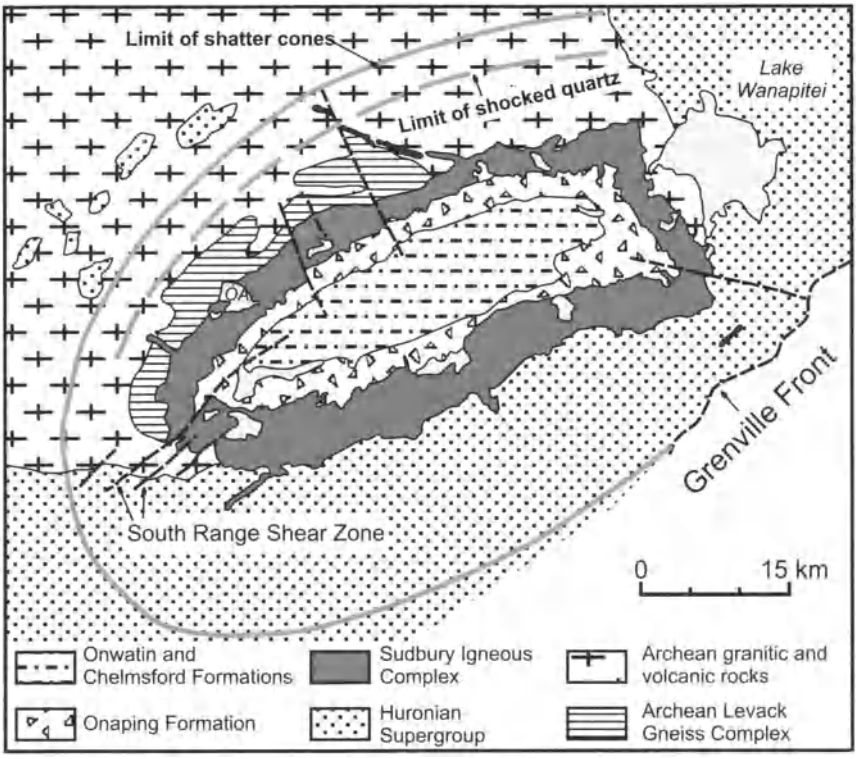


**Fig. 8.10.** Map showing limits for distribution of shatter cones and shocked quartz in the Sudbury area (after Grieve 1994)

4. The Sudbury Breccia, which has been compared with the pseudotachylite in the country rocks around the Vredefort and Ries impact structures (Dressler 1984).
5. The Footwall breccia beneath the Complex, mainly composed of fragments of crushed country rocks, that are interpreted as the debris lining the base of the impact crater.
6. The Onaping Formation, that, as discussed above, includes many components that are similar to those from other impact sites.

Most Sudbury geologists now accept the suggestion of Dietz (1964) that the cause of this explosion was the impact of a meteorite, although difficulties remain, as were summarized by Muir (1984).

## 8.3 Units of the Sudbury Igneous Complex

The Sudbury Igneous Complex includes the Main Mass, the Sublayer bodies and Offsets (Offset dikes). They are discussed in turn below.

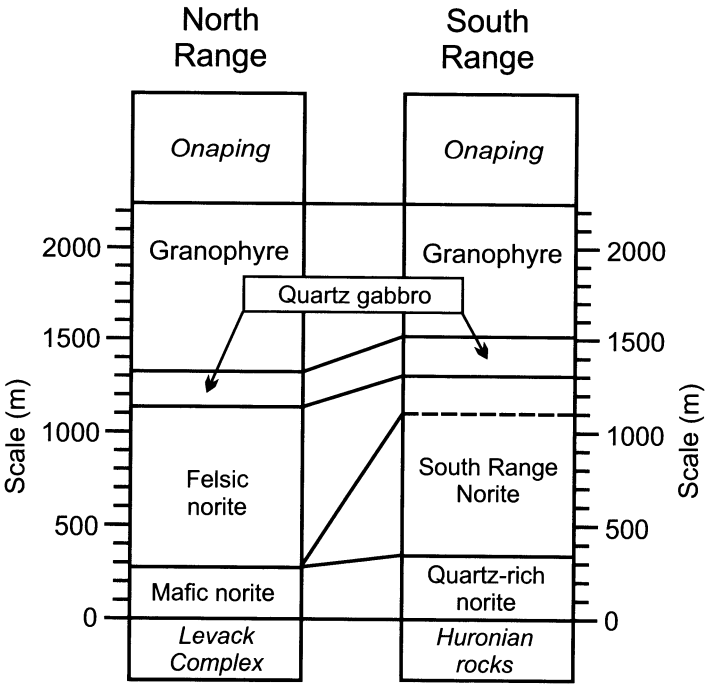


**Fig. 8.11.** Principal units within the Main Mass of the Sudbury Igneous Complex (after Naldrett and Hewins 1984)

### 8.3.1 Main Mass

The principal units of the Main Mass of the Complex are shown in Fig. 8.11. These comprise: (i) the marginal rocks (Quartz-rich Norite of the South Range and Mafic Norite of the North Range), (ii) the South Range Norite and Felsic Norite, developed in the North Range, (iii) the Quartz Gabbro, and (iv) the Granophyre, that includes the plagioclase-rich Granophyre. The modal composition of the rocks is shown in Fig. 8.12 along with variations of pyroxene composition in Figs. 8.13 and 8.14.

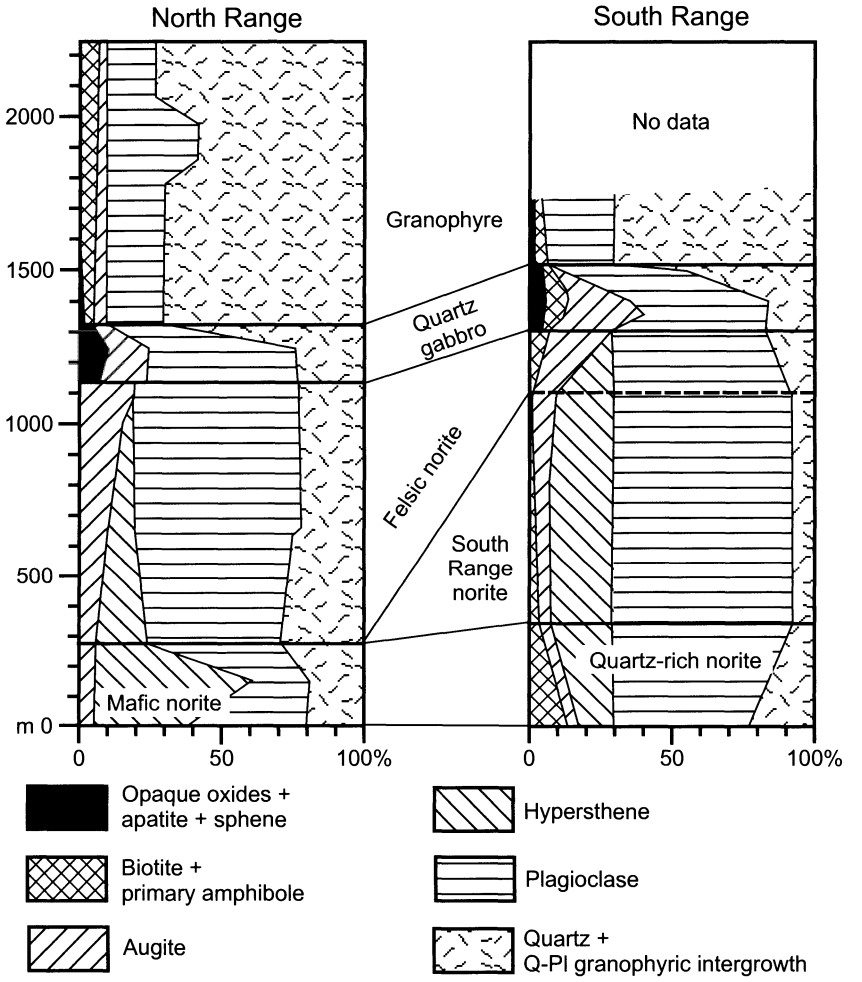


**Fig. 8.12.** Modal compositions of the Main Mass of the Sudbury Igneous Complex (generalized data). After Naldrett et al. (1970)

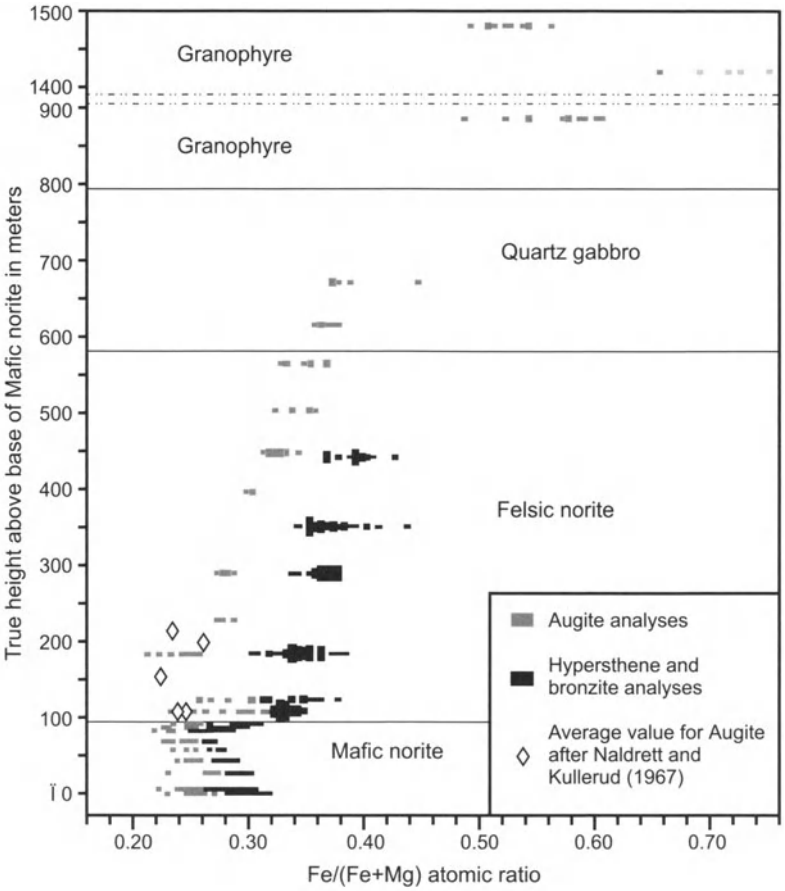


**Fig. 8.13.** Variation of pyroxene composition in the North Range sequence of the Main Mass of the Sudbury Igneous Complex (after Naldrett et al. 1970)

The marginal unit of the Main Mass on the South Range is the Quartz-rich Norite. In this unit, the quartz content (along with the $SiO_2$ content) increases progressively towards the contact over the outer 300 m (Fig. 8.12) (Naldrett et al., 1970). The increase in silica is unlikely to be due to contamination because the increase occurs as much where the footwall is composed of $SiO_2$-deficient greenstone as where it is composed of granite. This observation indicates that if contamination is involved, it is not in situ contamination. The increase in quartz is accompanied by an equally progressive decrease in the average Mg/(Mg+Fe) ratio of the pyroxenes (Fig. 8.14). This decrease is due to progressively more strongly zoned pyroxenes, within which Mg/(Mg+Fe) decreases towards the edges of grains while the cores retain a constant composition, thus giving a more Fe-rich

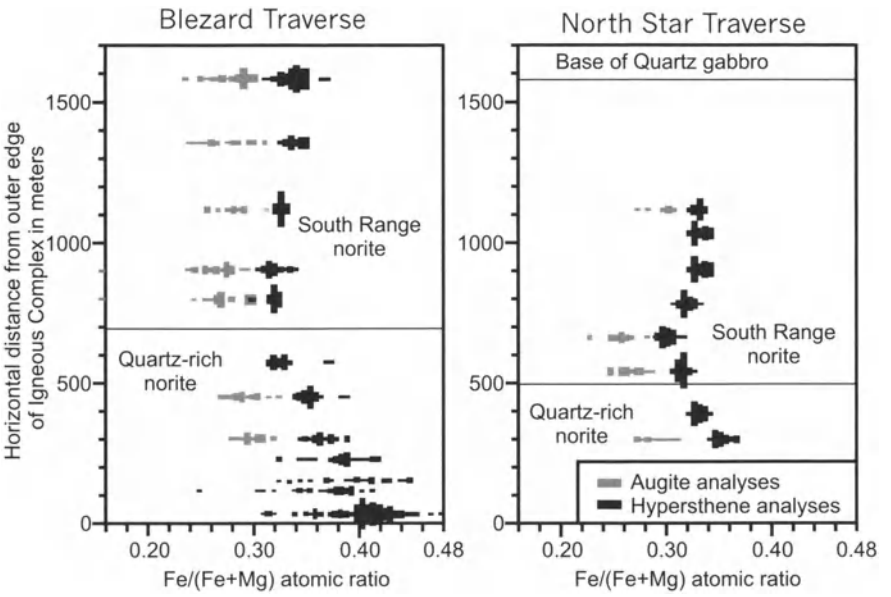


**Fig. 8.14.** Variations of pyroxene compositions in two sections of the South Range sequence of the Main Mass of the Sudbury Igneous Complex (after Naldrett et al., 1970)

average composition. These observations, coupled with a decrease in grain size towards the margins (Naldrett et al. 1970), indicate that the outer part of the Quartz-rich Norite is a non-cumulus rock that crystallized essentially in situ.

On the North Range, the marginal unit comprises the Mafic norite. This differs from the Quartz-rich norite in its much greater hypersthene content (30-50 mod%) (Fig. 8.12). The central part of the unit is poikilitc hypersthene cumulate in which the hypersthene chadacrysts are enclosed by plagioclase. This rock shows a gradation, both upward and downward into a hypersthene-plagioclase cumulate in which both minerals are of tabular shape.

On the South Range, the Quartz-rich norite grades inward and upward into South Range norite, while on the North Range, Mafic norite gives way to Felsic norite. Both South Range norite and Felsic norite are Pl-Opx-Cpx cumulates. They show cryptic variation in the Mg/(Mg+Fe) ratio of the pyroxenes (Figs. 8.13 and 8.14) and An content of plagioclase (Naldrett et al. 1970), with these variables decreasing upwards in a manner consistent with fractional crystallization. Quartz Gabbro overlies the norites in both North and South Ranges. Orthopyroxene disappears and titaniferous magnetite and apatite appear as cumulus phases in this rock. The cryptic varia-

tion characteristic of the underlying norites has been traced into the lower part of the Quartz Gabbro, but cannot be traced across it because of the intense hydrous alteration that has affected the upper part. The upper part of the Quartz Gabbro is characterized by a rapid increase in a granophyric intergrowth of plagioclase and quartz at the expense of cumulus plagioclase and pyroxene as the gabbro grades into the overlying Granophyre (Fig. 8.12). Most of the Granophyre is a uniform rock consisting of 75 modal percent granophyric intergrowth and 25 modal percent idiomorphic plagioclase plus clinopyroxene, although zones of plagioclase-rich granophyre containing up to 50 modal percent idiomorphic plagioclase are present.

According to descriptions by Coleman (1913), Burrows and Rickaby (1930), Moore (1930), Stevenson (1963) and Muir (1983), the Granophyre is overlain by Basal Onaping everywhere. Muir and Peredery (1985) observed a sharp contact between the two in the North Range.

### 8.3.2 Sublayer and its Inclusions

The Sublayer occurs discontinuously around the Complex (Fig. 8.15). Traditionally, it has been subdivided into those variants which occur close to the outer contact and those which occur as dykes that radiate outwards from the Complex and are known locally as "offsets". Lightfoot et al. (1997a) have shown (see Section 8.4.2 below) that the offsets comprise quartz diorite which is close to the Main Mass in its trace element content, and distinctly different to contact sublayer. In this chapter the term "Sublayer" is taken to refer only to what was formerly termed "Contact Sublayer".

The Sublayer bodies (up to 200-300 m thick) comprise of a suite of fine to medium-grained norites and gabbros that are distinguished from the Main Mass Felsic Norite and Quartz Gabbro by their lower quartz content in relation to pyroxene (Naldrett et al. 1972). Lightfoot et al. (1997a) noted that the texture and composition of the sublayer norites is quite variable, ranging from poikilitic to non-poikilitic norite and melanorite; contacts between different textural and compositional types are gradational. They concluded that many of the melanorites are best described as pods of poikilitic-textured norite; one melanorite pod that they studied at the Whistle mine (northeast corner of the Sudbury structure) grades from poikilitic texture on one side to hypidiomorphic granular on the other over a distance of 5 m. They subdivided the matrix of the Sublayer (i.e. excluding the melanorite pods) into (progressing from more evolved to less evolved)

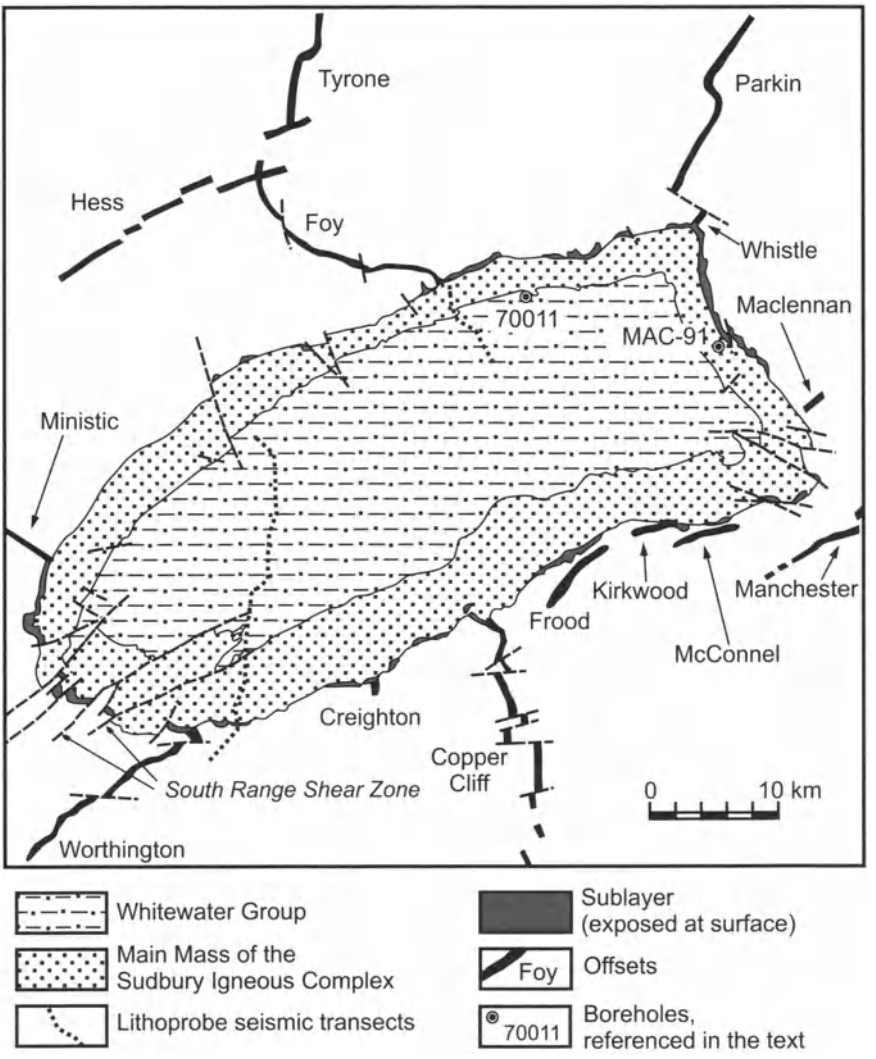


**Fig. 8.15.** Distribution of the Sublayer and Offsets in the Sudbury Igneous Complex (after Naldrett et al. 1984b, with additions from Lightfoot et al. 2001)

non-poikilitic leucocratic norites, orthopyroxene-rich non-poikilitic textured norite and two-pyroxene non-poikilitic textured norite.

Geological relationships between the Sublayer and the Main Mass give conflicting evidence as to the relative ages of the two units. Zones of marginal Quartz-rich Norite have been observed apparently included within Sublayer and zones of Sublayer have been observed enclosed in norite of the Main Mass of the Complex. Intrusive contacts are never marked by fine-grained chill zones, suggesting that they were nearly contemporane-

ous. On the North Range, the distinction between Main Mass and Sublayer is consistently clear, with the Sublayer having the finer grain-size and lower quartz content. This distinction is not necessarily the case on the South Range, where a number of researchers have commented on gradations between the two units (Slaught 1951; Cochrane 1984).

In some areas the Sublayer is characterized by inclusions. These can be divided into two groups, those of obviously local derivation, and those composed of mafic and ultramafic rocks, many of which do not outcrop in the immediate Sudbury area. The mafic-ultramafic inclusions are of particular interest here. Scribbins et al. (1984) described them as ranging from peridotite, through clino- and orthopyroxenites, to olivine gabbro and norite (Table 8.1). Most of the inclusions either display cataclastic or cumulus textures. Olivines range in composition from $Fo_{86}$ to $Fo_{72}$, with the Fo content decreasing as the plagioclase content increases (Fig. 8.16). Scribbins et al concluded that the inclusions were derived from layered intrusions that have fractionated at moderate depths in the crust.

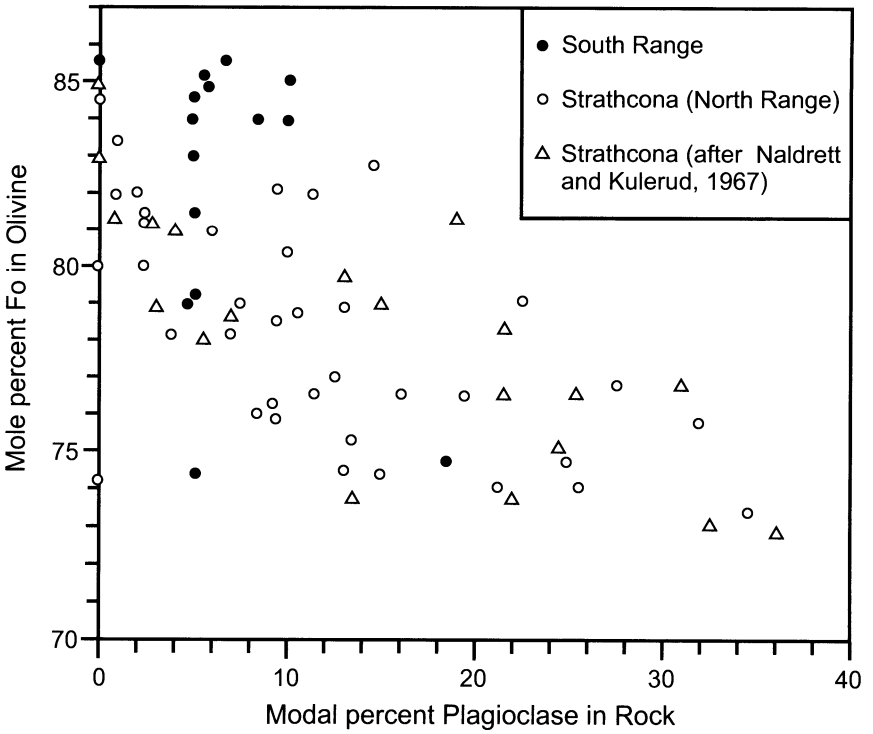


**Fig. 8.16.** Variation in Fo content of olivine versus the modal content of plagioclase for samples of mafic and ultramafic inclusions in the Sublayer (from Scribbins et al 1984)

**Table 8.1.** Petrography of mafic-ultramafic inclusions in the Sublayer (from Scribbins et al. 1984)

| Rock type | Minerals present | Approx. Mode % | Approximate grain size, and Mineral characteristics |
|---|---|---|---|
| Harzburgite | Olivine | 45–70 | Up to 2 mm (rarely to 6 mm). Anhedral, subequant; also as subrounded; resorbed grains 0.2 to 1 mm poikilitically enclosed within orthopyroxene and plagioclase |
| | Orthopyroxene | 15–50 | 1–3 mm. Tabular; coronas of orthopyroxene in places surround olivine enclosed in plagioclase |
| | Plagioclase | 5–10 | <0.5 mm. Interstitial; antithetic relationship between olivine size and plagioclase abundance |
| | Clinopyroxene | 0–5 | 0.5 to 1 mm. Ragged interstitial grains |
| Wehrlite | Olivine | 45-60 | Up to 10 mm. Large equant to elongate anhedral grains; also as spherical, resorbed grains 0.1 to 0.2 mm poikilitically enclosed within orthopyroxene and plagioclase |
| | Clinopyroxene | 30–50 | <3 mm. Smaller and more variable in size than olivine; simple twinning common to large grains |
| | Plagioclase | <10 | <0.5 mm. Interstitial |
| | Orthopyroxene | <5 | 0.2 to 0.4 mm. Generally poikilitically enclosed within plagioclase |
| Websterite | Clinopyroxene | 65–85 | 0.4 to 3 mm. Anhedral; generally cloudy owing to exsolution blebs |
| | Orthopyroxene | 10–25 | 0.1 to 3 mm. Anhedral with ragged edges except for subhedral to euhedral terminations within plagioclase |
| | Plagioclase | <10 | <0.5 mm. Interstitial |
| | Olivine | 0–10 | <0.4 mm. Resorbed, subrounded grains poikilitically enclosed within both pyroxenes |
| Melanorite | Orthopyroxene | 60–80 | 0.5 to 2 mm (rarely to 5 mm). Subhedral, generally tabular |
| | Plagioclase | 10–30 | Up to 2 mm. Interstitial, subhedral grains; also as laths subophitic to ophitically enclosed within orthopyroxene |
| | Clinopyroxene | <5 | <1 mm. Interstitial or intergrown with orthopyroxene |
| | Olivine | 0–10 | 0.1 to 2 mm. Subrounded 0.1 to 0.2 mm grains poikilitically enclosed within orthopyroxene and plagioclase |
| Augite melanorite | Orthopyroxene | 45–60 | 1.5 x 0.4 mm (tabular); 0.5 mm (prismatic). Common ragged appearance; often intergrown with clinopyroxene |
| | Plagioclase | 20–30 | <1.5 mm. Interstitial, anhedral grains; also as laths subophitically enclosed within orthopyroxene |
| | Clinopyroxene | 10–25 | Up to 1.5 mm. Ragged, anhedral grains intergrown with orthopyroxene |
| | Olivine | 0–5 | 0.05 to 0.2 mm. Resorbed grains poikilitically enclosed within plagioclase and orthopyroxene |

### 8.3.3 Offsets

Offsets are dyke-like bodies that were emplaced radial to, and in some cases concentric to the Main Mass of the SIC (Fig. 8.15). They extend up to 20 km from the Main Mass commonly with a width 70-100 m. Rocks forming the offsets generally have the composition of quartz diorite and are referred to as such. Grant and Bite (1984) recognize a number of variants of quartz diorite which form a continuum grading from hypersthene to biotite quartz diorite, a change that is attributed to varying degrees of contamination. Lightfoot et al. (1997a) describe the quartz diorite of the Parkin offset (this extends north from the northeast corner of the Sudbury structure) as a fine- to medium-grained, equigranular to inequigranular rock comprising 45–55% mafic minerals, 30–45% plagioclase, 5–15% quartz and trace amounts of granophyric intergrowth and opaques.

## 8.4 Geochemistry of the Sudbury Igneous Complex

Examples of major and trace element contents of the SIC rocks and overlying rocks of the Basal Onaping (from borehole 70011, located in the eastern part of the North Range) are given in Table 8.2[21]. In Fig. 8.17 variations of some geochemical parameters are shown through this section which intersected the whole sequence of the Sudbury Main Mass and Sublayer.

### 8.4.1 Major Elements

A selection of average and individual major element analyses of representative material from the Sudbury Igneous Complex are listed in Table 8.3.

**Main Mass.** Judging from field and petrographic criteria, the Quartz-rich Norite was close in composition to the SIC magma when it was emplaced along the South Range. The MgO/(MgO+FeOT) molecular ratio (henceforth referred to as MgNo) of 0.61 indicates that this is a reasonably primitive rock.

The SIC was emplaced in a near-surface environment in a continental setting, thus Naldrett (1984) argued that it is logical to compare its magma

[21] Analytical data for this Table and Figure 8.17 were provided by A. Deutsch and M. Ostermann (Munich University, Germany), to whom this author is very grateful.

composition with that of continental flood basalts. He pointed to the high $SiO_2$ and $K_2O$, low CaO and low $Na_2O/K_2O$ ratio of the Quartz-rich Norite

**Table 8.2.** Geochemical compositions of the SIC rocks and overlying rocks of the Basal Onaping (from borehole 70011, located in eastern part of the North Range). Analytical data by A. Deutsch and M. Ostermann (Munich University, Germany)

| Depth | 82 | 85 | 88 | 91 | 94 | 396 | 549 | 701 | 930 | 1006 |
|---|---|---|---|---|---|---|---|---|---|---|
| Rock | BO | BO | BO | Gr | Gr | Gr | Gr | Gr | Gr | Gr |
| MgNo | 0.52 | 0.50 | 0.39 | 0.44 | 0.28 | 0.30 | 0.30 | 0.31 | 0.34 | 0.31 |
| $SiO_2$ | 70.68 | 72.40 | 78.75 | 74.29 | 71.68 | 68.08 | 69.75 | 68.69 | 71.16 | 71.62 |
| $TiO_2$ | 0.19 | 0.45 | 0.41 | 0.57 | 0.73 | 1.00 | 0.93 | 0.97 | 0.86 | 0.83 |
| $Al_2O_3$ | 15.30 | 13.37 | 9.81 | 12.54 | 12.51 | 13.20 | 12.86 | 13.18 | 12.92 | 12.78 |
| FeOT | 2.26 | 2.97 | 2.64 | 2.53 | 4.94 | 6.55 | 4.54 | 6.74 | 4.02 | 4.67 |
| MnO | 0.03 | 0.03 | 0.03 | 0.03 | 0.07 | 0.08 | 0.06 | 0.08 | 0.07 | 0.07 |
| MgO | 1.16 | 1.39 | 0.79 | 0.93 | 0.93 | 1.31 | 0.93 | 1.47 | 1.00 | 1.01 |
| CaO | 2.67 | 1.63 | 2.74 | 1.63 | 2.19 | 2.38 | 3.08 | 1.36 | 3.13 | 1.71 |
| $Na_2O$ | 7.14 | 3.60 | 3.03 | 3.57 | 3.16 | 3.58 | 4.54 | 3.50 | 6.36 | 6.38 |
| $K_2O$ | 0.52 | 4.02 | 1.74 | 3.81 | 3.67 | 3.55 | 3.13 | 3.79 | 0.32 | 0.78 |
| $P_2O_5$ | 0.05 | 0.13 | 0.06 | 0.11 | 0.12 | 0.28 | 0.18 | 0.21 | 0.15 | 0.15 |
| S | 0.04 | 0.03 | 0.05 | 0.01 | 0.03 | 0.02 | 0.01 | 0.03 | 0.01 | 0.03 |
| Ni | 264 | 28 | 28 | 13 | 10 | 3 | 9 | 7 | 11 | 11 |
| Co | 35 | 34 | 41 | 70 | 42 | 45 | 34 | 56 | 37 | 44 |
| Cu | 8 | 10 | 7 | 3 | 7 | 14 | 10 | 4 | 13 | 10 |
| Cr | 49 | 48 | 46 | 29 | 33 | 22 | 21 | 33 | 18 | 39 |
| V | 31 | 67 | 25 | 34 | 53 | 134 | 36 | 52 | 24 | 18 |
| Rb | 16 | 113 | 46 | 91 | 94 | 96 | 86 | 164 | 14 | 38 |
| Sr | 620 | 319 | 459 | 210 | 224 | 170 | 152 | 150 | 202 | 144 |
| Ba | 321 | 2154 | 724 | 1382 | 1381 | 1105 | 868 | 1194 | 229 | 257 |
| Pb | 4 | 6 | 5 | 4 | 8 | 6 | 7 | 8 | 8 | 14 |
| Nb | 3 | 6 | 9 | 11 | 12 | 14 | 16 | 17 | 16 | 18 |
| Zr | 76 | 176 | 217 | 264 | 276 | 265 | 326 | 257 | 333 | 287 |
| La | 19.5 | 39.4 | 57.1 | 48.6 | | | | | | 57.5 |
| Ce | 33.6 | 79.8 | 113.1 | 100.5 | | | | | | 119.3 |
| Pr | 3.2 | 8.1 | 11.9 | 10.6 | | | | | | 11.5 |
| Nd | 10.3 | 27.4 | 40.4 | 36.7 | | | | | | 44.0 |
| Sm | 1.4 | 4.4 | 6.4 | 6.2 | | | | | | 8.2 |
| Eu | 1.1 | 1.3 | 1.0 | 1.3 | | | | | | 1.5 |
| Gd | 1.3 | 4.5 | 5.9 | 6.0 | | | | | | 7.1 |
| Tb | 0.13 | 0.45 | 0.73 | 0.70 | | | | | | 1.01 |
| Dy | 0.48 | 2.16 | 3.76 | 3.61 | | | | | | 5.62 |
| Ho | 0.08 | 0.40 | 0.69 | 0.72 | | | | | | 1.09 |
| Er | 0.26 | 1.11 | 1.94 | 2.06 | | | | | | 3.11 |
| Tm | 0.03 | 0.15 | 0.28 | 0.30 | | | | | | 0.48 |
| Yb | 0.30 | 1.01 | 1.84 | 2.01 | | | | | | 3.09 |
| Lu | 0.05 | 0.18 | 0.29 | 0.31 | | | | | | 0.48 |
| La/Sm | 13.92 | 8.96 | 8.92 | 7.83 | | | | | | 7.01 |
| Sm/Yb | 4.67 | 4.36 | 3.48 | 3.08 | | | | | | 2.65 |

**Table 8.2.** (cont.)

| Depth | 1311 | 1501 | 1539 | 1593 | 1631 | 1722 | 1731 | 1814 | 1821 | 1843 |
|---|---|---|---|---|---|---|---|---|---|---|
| Rock | Gr | QG | QG | QG | QG | QG | QG | QG | Nor | Nor |
| MgNo | 0.14 | 0.20 | 0.22 | 0.32 | 0.37 | 0.46 | 0.53 | 0.56 | 0.55 | 0.54 |
| $SiO_2$ | 71.45 | 69.89 | 65.15 | 58.74 | 56.28 | 57.17 | 56.66 | 59.07 | 59.81 | 60.40 |
| $TiO_2$ | 0.63 | 0.94 | 1.31 | 2.13 | 1.78 | 1.19 | 0.54 | 0.66 | 0.69 | 0.67 |
| $Al_2O_3$ | 12.60 | 13.08 | 13.35 | 13.70 | 14.64 | 14.69 | 16.03 | 16.49 | 16.27 | 16.33 |
| FeOT | 5.47 | 5.00 | 8.39 | 10.09 | 10.99 | 9.89 | 8.52 | 6.14 | 7.04 | 7.16 |
| MnO | 0.09 | 0.09 | 0.14 | 0.17 | 0.14 | 0.13 | 0.15 | 0.13 | 0.13 | 0.15 |
| MgO | 0.44 | 0.61 | 1.14 | 2.24 | 3.13 | 3.97 | 4.60 | 3.76 | 4.03 | 3.97 |
| CaO | 1.96 | 2.67 | 3.91 | 6.18 | 7.03 | 7.88 | 8.51 | 5.82 | 5.89 | 6.23 |
| $Na_2O$ | 3.34 | 6.07 | 3.69 | 3.72 | 3.25 | 3.42 | 3.50 | 7.38 | 4.20 | 3.26 |
| $K_2O$ | 3.90 | 1.47 | 2.63 | 2.27 | 2.15 | 1.53 | 1.40 | 0.40 | 1.84 | 1.66 |
| $P_2O_5$ | 0.12 | 0.17 | 0.30 | 0.75 | 0.61 | 0.12 | 0.08 | 0.14 | 0.10 | 0.17 |
| S | 0.02 | 0.01 | 0.03 | 0.02 | 0.05 | 0.07 | 0.05 | 0.02 | 0.01 | 0.02 |
| Ni | 3 | 13 | 9 | 6 | 15 | 11 | 14 | 20 | 18 | 13 |
| Co | 70 | 38 | 60 | 51 | 56 | 60 | 51 | 39 | 41 | 55 |
| Cu | 10 | 7 | 11 | 21 | 23 | 28 | 19 | 14 | 11 | 12 |
| Cr | 20 | 56 | 48 | 43 | 85 | 56 | 43 | 56 | 52 | 47 |
| V | 15 | 16 | 39 | 187 | 594 | 765 | 181 | 156 | 150 | 138 |
| Rb | 86 | 44 | 90 | 114 | 102 | 7 | 10 | 9 | 13 | 10 |
| Sr | 171 | 210 | 240 | 358 | 416 | 402 | 468 | 423 | 485 | 451 |
| Ba | 1048 | 456 | 966 |  | 923 | 465 | 465 | 234 | 832 | 559 |
| Pb | 9 | 10 | 15 | 6 | 7 | 8 | 9 | 13 | 10 | 12 |
| Nb | 13 | 17 | 15 | 13 | 7 | 5 | 6 | 8 | 9 | 8 |
| Zr | 344 | 269 | 225 | 173 | 137 | 125 | 123 | 151 | 147 | 138 |
| La | 61.7 | 42.2 | 61.7 | 38.0 | 31.6 | 22.0 | 22.9 | 27.9 | 26.4 | 30.6 |
| Ce | 124.7 | 90.8 | 131.2 | 86.5 | 72.3 | 46.7 | 49.2 | 58.5 | 56.6 | 62.3 |
| Pr | 13.6 | 9.8 | 14.8 | 9.4 | 8.3 | 5.4 | 5.2 | 6.5 | 5.9 | 7.1 |
| Nd | 49.5 | 36.2 | 55.9 | 36.6 | 32.7 | 20.4 | 19.3 | 24.3 | 21.8 | 26.9 |
| Sm | 8.9 | 6.7 | 10.4 | 6.9 | 6.3 | 4.1 | 3.6 | 4.5 | 4.0 | 4.9 |
| Eu | 1.5 | 1.5 | 2.4 | 1.6 | 1.7 | 1.1 | 1.0 | 1.3 | 1.2 | 1.2 |
| Gd | 8.0 | 6.1 | 9.6 | 6.2 | 6.5 | 4.6 | 3.6 | 4.6 | 4.1 | 5.0 |
| Tb | 1.11 | 0.82 | 1.26 | 0.83 | 0.80 | 0.64 | 0.45 | 0.69 | 0.48 | 0.60 |
| Dy | 6.01 | 4.77 | 6.38 | 4.63 | 4.01 | 3.16 | 2.56 | 3.37 | 2.58 | 3.31 |
| Ho | 1.22 | 0.96 | 1.26 | 0.89 | 0.77 | 0.63 | 0.51 | 0.66 | 0.52 | 0.64 |
| Er | 3.57 | 2.78 | 3.47 | 2.42 | 2.10 | 1.78 | 1.54 | 1.95 | 1.55 | 1.76 |
| Tm | 0.52 | 0.42 | 0.49 | 0.37 | 0.29 | 0.27 | 0.22 | 0.27 | 0.23 | 0.26 |
| Yb | 3.47 | 2.80 | 3.42 | 2.39 | 1.83 | 1.85 | 1.52 | 1.90 | 1.62 | 1.80 |
| Lu | 0.54 | 0.43 | 0.53 | 0.37 | 0.27 | 0.28 | 0.24 | 0.28 | 0.26 | 0.26 |
| La/Sm | 6.93 | 6.29 | 5.93 | 5.51 | 5.02 | 5.37 | 6.35 | 6.21 | 6.59 | 6.25 |
| Sm/Yb | 2.56 | 2.39 | 3.04 | 2.89 | 3.44 | 2.22 | 2.37 | 2.37 | 2.48 | 2.72 |

**Table 8.2.** (cont.)

| Depth | 1981 | 2012 | 2103 | 2217 | 2275 | 2280 | 2298 | 2317 | 2336 | 2352 |
|---|---|---|---|---|---|---|---|---|---|---|
| Rock | Nor | Nor | Nor | Nor | Sub | Sub | Sub | Sub | Sub | Sub |
| MgNo | 0.60 | 0.56 | 0.62 | 0.59 | 0.77 | 0.65 | 0.68 | 0.62 | 0.76 | 0.64 |
| $SiO_2$ | 60.04 | 61.20 | 58.92 | 60.28 | 57.26 | 54.74 | 52.22 | 54.04 | 53.10 | 54.58 |
| $TiO_2$ | 0.47 | 0.61 | 0.44 | 0.59 | 0.77 | 0.51 | 0.54 | 0.77 | 0.32 | 0.69 |
| $Al_2O_3$ | 16.51 | 16.02 | 17.63 | 16.26 | 10.02 | 16.14 | 9.59 | 16.18 | 3.63 | 13.80 |
| FeOT | 6.75 | 6.39 | 6.30 | 6.77 | 9.02 | 7.75 | 10.88 | 9.21 | 11.43 | 9.94 |
| MnO | 0.11 | 0.13 | 0.11 | 0.11 | 0.19 | 0.18 | 0.18 | 0.13 | 0.29 | 0.17 |
| MgO | 4.76 | 3.95 | 4.92 | 4.61 | 14.29 | 6.96 | 11.11 | 7.04 | 17.57 | 8.37 |
| CaO | 6.30 | 6.05 | 7.43 | 6.21 | 5.36 | 8.50 | 12.75 | 8.14 | 12.96 | 8.86 |
| $Na_2O$ | 3.07 | 4.14 | 2.92 | 3.32 | 2.05 | 3.75 | 2.14 | 3.26 | 0.60 | 2.45 |
| $K_2O$ | 1.81 | 1.33 | 1.23 | 1.70 | 0.93 | 1.40 | 0.51 | 1.04 | 0.06 | 0.94 |
| $P_2O_5$ | 0.19 | 0.17 | 0.09 | 0.14 | 0.13 | 0.07 | 0.07 | 0.18 | 0.04 | 0.18 |
| S | 0.03 | 0.02 | 0.05 | 0.04 | 0.13 | 0.24 | 1.29 | 0.16 | 0.09 | 0.12 |
| Ni | 17 | 22 | 22 | 29 | 153 | 159 | 468 | 193 | 269 | 181 |
| Co | 45 | 40 | 42 | 45 | 82 | 49 | 82 | 65 | 55 | 45 |
| Cu | 20 | 13 | 19 | 20 | 40 | 420 | 496 | 90 | 202 | 140 |
| Cr | 59 | 47 | 87 | 102 | 565 | 212 | 493 | 297 | 460 | 418 |
| V | 109 | 130 | 95 | 132 | 198 | 123 | 146 | 151 | 155 | 178 |
| Rb | 61 | 46 | 41 | 61 | 38 | 42 | 17 | 39 | 1 | 32 |
| Sr | 436 | 464 | 496 | 429 | 277 | 571 | 321 | 476 | 33 | 483 |
| Ba | 539 | 629 | 454 | 570 | 222 | 845 | 155 | 385 | 55 | 445 |
| Pb | 6 | 7 | 12 | 14 | 41 | 23 | 29 | 18 | 28 | |
| Nb | 6 | 8 | 5 | 7 | 4 | 4 | 3 | 4 | 1 | 2 |
| Zr | 126 | 156 | 101 | 108 | 69 | 75 | 71 | 96 | 38 | 89 |
| La | 28.1 | 26.5 | 24.1 | 25.8 | 15.2 | 14.3 | 15.5 | 23.8 | 11.2 | 21.1 |
| Ce | 59.5 | 56.3 | 43.2 | 54.3 | 32.3 | 30.5 | 38.1 | 50.6 | 27.1 | 49.2 |
| Pr | 6.7 | 6.3 | 4.7 | 6.0 | 3.5 | 3.2 | 4.9 | 5.7 | 3.6 | 6.1 |
| Nd | 25.4 | 23.5 | 16.9 | 22.0 | 13.7 | 11.4 | 21.5 | 21.9 | 15.5 | 24.9 |
| Sm | 4.6 | 4.4 | 3.1 | 4.1 | 2.8 | 2.2 | 4.8 | 3.8 | 3.6 | 5.3 |
| Eu | 1.1 | 1.1 | 1.1 | 1.1 | 0.7 | 0.8 | 1.2 | 1.2 | 0.7 | 1.3 |
| Gd | 4.7 | 4.7 | 3.4 | 4.7 | 3.1 | 2.6 | 4.0 | 3.7 | 3.5 | 4.9 |
| Tb | 0.54 | 0.64 | 0.39 | 0.64 | 0.46 | 0.31 | 0.59 | 0.45 | 0.50 | 0.61 |
| Dy | 2.93 | 2.88 | 2.13 | 2.94 | 2.21 | 1.48 | 3.22 | 2.34 | 2.58 | 3.29 |
| Ho | 0.58 | 0.60 | 0.44 | 0.59 | 0.46 | 0.31 | 0.60 | 0.45 | 0.51 | 0.64 |
| Er | 1.57 | 1.69 | 1.23 | 1.69 | 1.33 | 0.95 | 1.57 | 1.27 | 1.35 | 1.71 |
| Tm | 0.23 | 0.24 | 0.18 | 0.26 | 0.19 | 0.14 | 0.22 | 0.19 | 0.20 | 0.24 |
| Yb | 1.57 | 1.72 | 1.20 | 1.78 | 1.43 | 1.06 | 1.50 | 1.35 | 1.27 | 1.65 |
| Lu | 0.24 | 0.26 | 0.19 | 0.27 | 0.23 | 0.17 | 0.22 | 0.21 | 0.21 | 0.25 |
| La/Sm | 6.11 | 6.02 | 7.77 | 6.29 | 5.42 | 6.49 | 3.24 | 6.25 | 3.10 | 3.98 |
| Sm/Yb | 2.93 | 2.56 | 2.58 | 2.30 | 1.96 | 2.08 | 3.20 | 2.81 | 2.83 | 3.21 |

Depths in meters. Major elements and S in wt%, trace elements in ppm.
Rock type: *BO* Basal Onaping; *Gr* Granophyre; *QG* Quartz Gabbro; *Nor* Norites; *Sub* Sublayer rocks, including melanocratic fragments.
*MgNo* Molecular ratio MgO/(MgO+FeOT).

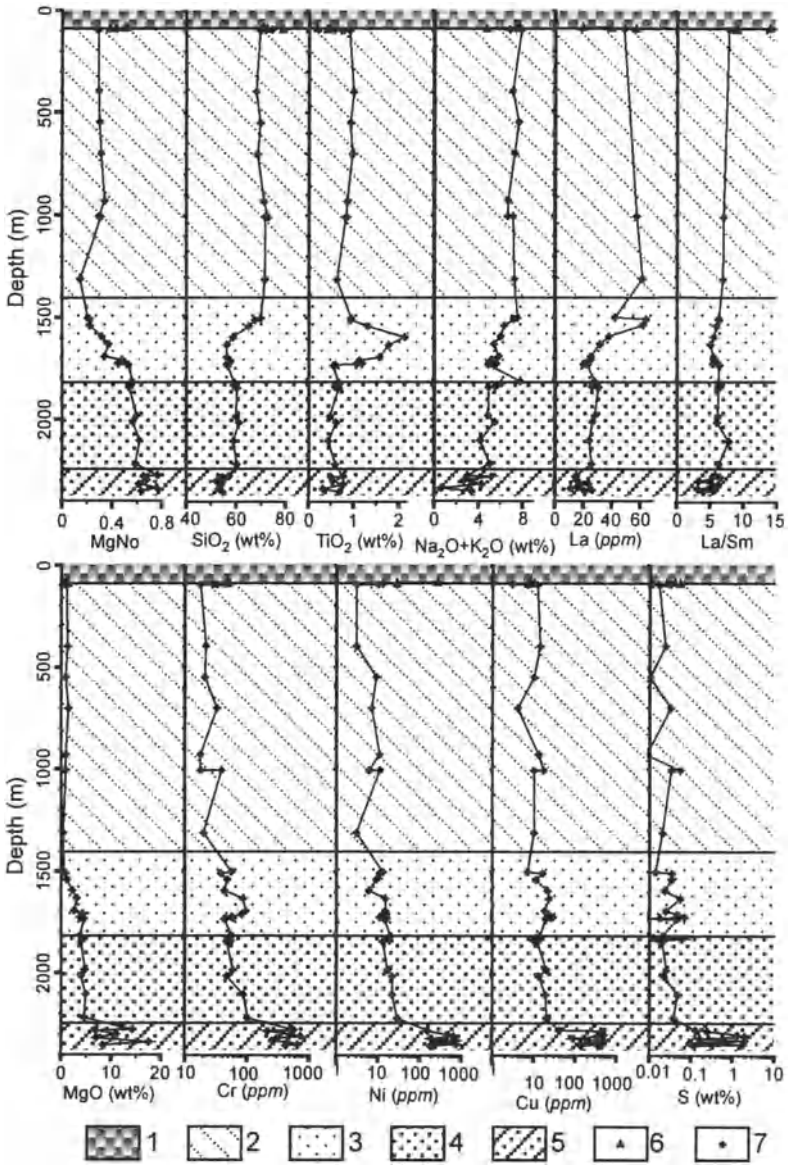


**Fig. 8.17.** Variations of some geochemical parameters through the lower part of Basal Onaping and the whole sequence of the Sudbury Main Mass and Sublayer intersected in borehole 70011 in the eastern part of the North Range. Analytical data by A. Deutsch and M. Ostermann (Munich University, Germany). Borehole location is shown in Fig. 8.15. 1 = Basal Onaping; 2 = Granophyre; 3 = Quartz Gabbro; 4 = Norites; 5 = Sublayer rocks, including melanocratic fragments; 6 = Analyzed Onaping samples; 7 = Analyzed SIC samples

when it is compared with Keweenawan and Columbia River flood basalts on the basis of MgNo, and showed that contamination of a relatively unfractionated Columbia River basalt with 50 percent of a 1:2 mixture respectively of Archean quartz monzonite and tonalitic gneiss gave rise to a major element composition similar to that of the Quartz-rich Norite. On the other hand, Grieve (1994) has shown, using least-squares mixing models, that the average composition of the SIC corresponds to a mix of Archean granite-greenstone terrain, with possibly a small component of Huronian cover rocks.

**Sublayer.** The texture and field relations of the constituent bodies of the Sublayer indicate that these bodies are also not cumulates but are rocks that have solidified essentially in situ. MgNos of samples of "Contact Sublayer" given by Rao et al (1983) range from 0.37 to 0.58 and average 0.48 for the North Range and 0.51 for the South Range. Comparison of the major element compositions of Sublayer with those of flood basalts indicates that the Sublayer is also enriched in $SiO_2$ and $K_2O$, and low in CaO and $Na_2O/K_2O$ ratio for a given degree of fractionation as indicated by the MgNo. These data therefore are also consistent with contamination by country rocks.

### 8.4.2 Trace Elements

**Main Mass.** Recent trace element studies of the SIC include those of Naldrett et al. (1986b), Chai and Eckstrand (1994, 1996) and Lightfoot et al. (1997a,b). Naldrett et al. (1986b) pointed out that, as with the major element data, the trace element data are explicable as the result of the contamination of flood basalt magma by a mix of country rocks exposed at the present erosion level of the SIC. Chai and Eckstrand (1994, 1996) documented a marked compositional break between the Quartz Gabbro and the overlying Granophyre, and argued that this implied derivation from two different magmas originating from different sources. They postulated that the norite and Quartz Gabbro were the product of a primary mantle melt that had become contaminated by Archean granulites typical of the lower crust, whereas the Granophyre was an upper crustal, impact melt.

However, Lightfoot et al. (1997a) pointed out that, with the exception of Sr, P, Eu and Ti (which are very dependent on addition or removal of plagioclase, apatite or Fe-Ti oxides) the Felsic Norite, Quartz Gabbro and Granophyre have extremely similar trace element patterns. This is brought out in the Sm vs. La plot of Fig. 8.18. Also, they drew attention to the similarity in Th/Zr ratios (0.04-0.05) between gabbro-noritic rocks of the

**Table 8.3.** Average and individual major element analyses of representative material from the Sudbury Igneous Complex (wt%)

| Rock Type | $SiO_2$ | $TiO_2$ | $Al_2O_3$ | FeOT | MnO | MgO | CaO | $Na_2O$ | $K_2O$ | $P_2O_5$ | LOI | Total | MgNo | $Na_2O/K_2O$ |
|---|---|---|---|---|---|---|---|---|---|---|---|---|---|---|
| 1 (Offset) | 50.70 | 1.56 | 16.30 | 11.40 | 0.17 | 4.91 | 7.92 | 2.76 | 1.66 | | | 97.38 | 0.43 | 1.66 |
| 2 (Offset) | 55.30 | 0.94 | 14.30 | 10.80 | 0.15 | 4.43 | 6.71 | 2.61 | 1.70 | | | 96.94 | 0.42 | 1.54 |
| 3 (Offset) | 61.50 | 0.73 | 14.90 | 6.84 | 0.11 | 3.82 | 4.70 | 3.15 | 2.60 | | | 98.35 | 0.50 | 1.21 |
| 4 (Q-r Norite) | 56.70 | 0.57 | 16.30 | 7.44 | 0.12 | 6.10 | 6.66 | | 1.40 | | | 95.29 | 0.59 | |
| 5 (Q-r Norite) | 57.00 | 1.34 | 16.40 | 7.33 | 0.13 | 6.40 | 7.28 | 2.41 | 1.55 | | | 99.84 | 0.61 | 1.55 |
| 6 (SR Norite) | 55.40 | 0.49 | 17.80 | 7.35 | 0.12 | 6.68 | 7.75 | 2.50 | 1.10 | | | 99.19 | 0.62 | 2.27 |
| 7 (F Norite) | 60.40 | 0.65 | 15.60 | 7.19 | 0.13 | 3.81 | 6.05 | 3.12 | 1.96 | | | 98.91 | 0.49 | 1.59 |
| 8 (Q Gabbro) | 58.80 | 1.62 | 13.50 | 10.50 | 0.14 | 2.66 | 5.48 | 3.13 | 2.13 | | | 97.96 | 0.31 | 1.47 |
| 9 (Granoph.) | 60.10 | 0.65 | 13.70 | 5.21 | 0.09 | 1.08 | 2.15 | 3.31 | 5.00 | | | 91.29 | 0.27 | 0.66 |
| 10 (Granoph.) | 69.89 | 0.80 | 12.67 | 4.97 | 0.08 | 1.02 | 2.25 | 4.17 | 2.78 | 0.17 | 1.04 | 99.84 | 0.27 | 1.50 |
| 11 (Q Gabbro) | 55.79 | 1.46 | 14.86 | 9.46 | 0.14 | 3.70 | 7.33 | 3.90 | 1.47 | 0.46 | 1.08 | 99.64 | 0.41 | 2.66 |
| 12 (Norites) | 57.79 | 0.60 | 15.53 | 7.64 | 0.13 | 5.75 | 6.45 | 3.22 | 1.42 | 0.15 | 1.31 | 99.99 | 0.57 | 2.26 |
| 13 (Sublayer) | 52.35 | 0.54 | 9.11 | 11.07 | 0.21 | 12.42 | 10.30 | 1.71 | 0.56 | 0.12 | 1.62 | 100.01 | 0.67 | 3.07 |
| 14 (A. w. SIC) | 64.37 | 0.84 | 13.32 | 6.52 | 0.11 | 3.07 | 4.31 | 3.79 | 2.18 | 0.20 | 1.14 | 99.84 | 0.46 | 1.74 |
| 15 (Av. SIC) | 64.19 | 0.75 | 14.89 | 5.57 | 0.08 | 2.90 | 4.10 | 3.35 | 2.96 | 0.23 | | 99.02 | 0.48 | 1.13 |
| 16 (Q-r Norite) | 57.00 | 1.34 | 16.40 | 7.33 | 0.13 | 6.40 | 7.28 | 2.41 | 1.55 | 0.16 | | 100.00 | 0.61 | 1.55 |

1 = Quartz-poor Offset, South Range (Grant and Bite 1984, Table 12.2, No. 4, average of 4); 2 = Typical Offset, South Range (Grant and Bite 1984, Table 12.2, No. 2, average of 14); 3 = Offset, North Range (Grant and Bite 1984, Table 12.2, No. 5, average of 17); 4 = Quartz-rich Norite (Grant and Bite 1984, Table 12.2, No. 6, average of 31); 5 = Quartz-rich Norite (Collins 1934, p.140, No. 92W); 6 = South Range Norite (Collins 1934, p. 140, No. 89W); 7 = Felsic Norite (Grant and Bite 1984, Table 12.2, No. 9, average of 31); 8 = Quartz Gabbro (Grant and Bite 1984, Table 12.2, No.10, average of 17); 9 = Granophyre (Collins 1934, p. 139, No. 56W);
10-14 = Average compositions for borehole 70011 intersection, North Range (Ariskin et al. 1999, Table 2): 10 = Granophyre (59.6 % of SIC intersection); 11 = Quartz Gabbro (13.7 % of SIC intersection); 12 = Norites (20.2 % of SIC intersection); 13 = Sublayer (6.5 % of SIC intersection); 14 = Average weighted SIC in the intersection; 15 = Average SIC (Collins 1934); 16 = Average Quartz-rich Norite (Naldrett and Hewins 1984).
*MgNo* Molecular ratio MgO/(MgO+FeOT)

SIC and the Granophyre which, they argue, would be an extraordinary coincidence if they had been contaminated by, or derived from different crustal reservoirs, as was proposed by Chai and Eckstrand (1994).

**Offset Quartz Diorite.** As mentioned above, although the offset quartz diorite has traditionally been regarded as Sublayer, it can be seen from Figs. 8.18 to 8.20 that the trace element concentrations are much closer to those of the Felsic Norite than the Sublayer. Lightfoot et al. (1997a) argued that this implies a close genetic relationship. On the other hand, they note that the Sr, Eu, P and Ti negative anomalies that characterize the Main Mass are either not present or are less pronounced in the offset quartz diorite, which implies that there was less fractionation of plagioclase, apatite and Fe-Ti oxides from the quartz diorite magma.

Lightfoot et al. (2001) and Lightfoot and Farrow (2002) emphasized the difference between the marginal (free of inclusions and nearly free of sulfide) and inclusion- and sulfide-rich variants of offset rocks. They pointed out that the marginal zone to the Worthington offset and their calculated average composition for the Main Mass are nearly identical in major and trace elements, with the exception of the chalcophile elements, and suggested that the marginal offset rock presents the initial composition of the SIC magma. They suggested that the inclusion- and sulfide-rich phase of the Offsets was introduced later, after sulfide immiscibility had occurred in the Main Mass magma. This idea is illustrated in Fig. 8.41 below, and is discussed further at end of this chapter.

Tuchscherer and Spray (2002) studied the longest of the offset dykes, the Foy offset, that extends for at least 30 km from the margin of the SIC.

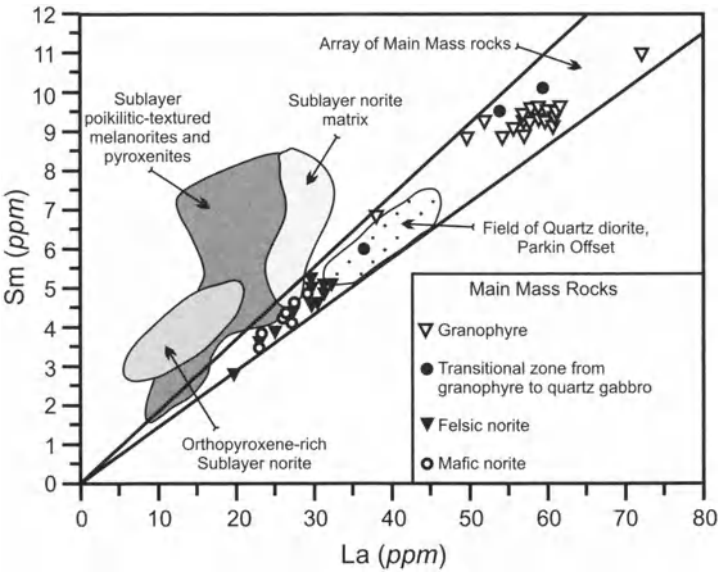


**Fig. 8.18.** Plot of Sm versus La for rocks of the Sudbury Igneous Complex. After Lightfoot et al. (1997a)

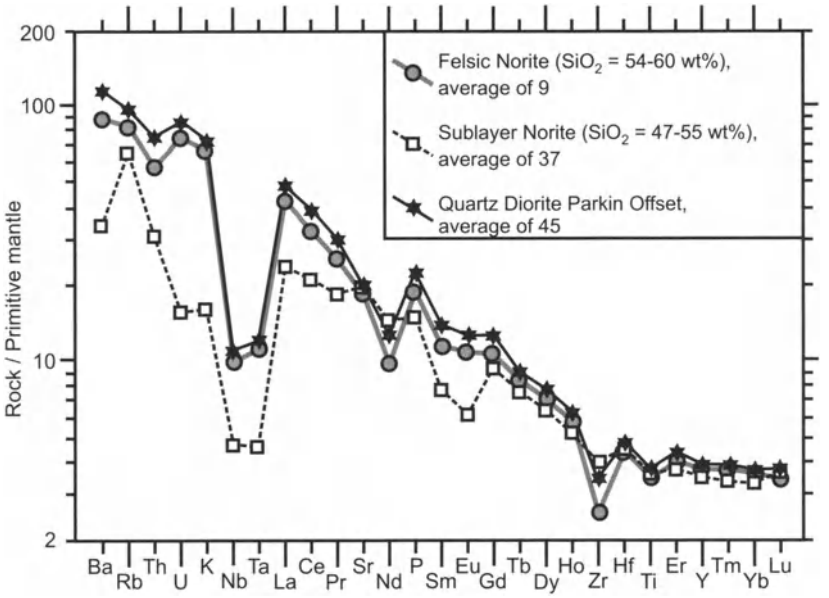


**Fig. 8.19.** Primitive mantle-normalized trace element data for average compositions of the Main Mass Felsic Norite, Sublayer Norite, and Quartz Diorite from Parkin Offset (primitive mantle after Sun and McDonough 1989). After Lightfoot et al. (1997b)

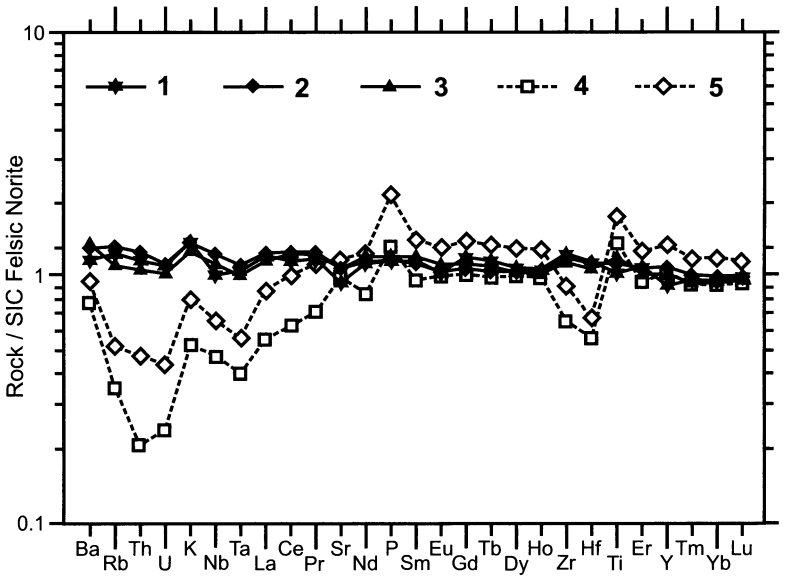


**Fig. 8.20.** Abundance patterns for selected incompatible elements in rocks normalized to the average composition of the Felsic Norite from the northeastern part of the SIC (after Lightfoot et al. 1997a). 1-3 = Offset rocks: 1 = Quartz diorite, Parkin Offset, average of 45; 2 = Quartz diorite, Whistle Offset, 1 sample; 3 = Leucocratic norite, Distal Whistle Embayment, average of 7; 4-5 = Sublayer norite matrix from Whistle Embayment: 4 = Rocks of >10% cumulus Opx, 6-9 wt% MgO, average of 37; 5 = Rocks of >10% cumulus Opx, 5-6 wt% MgO, average of 6

They also suggest that the dyke was emplaced very early during the development of the Sudbury structure before significant differentiation had occurred, and that chilled margins of the dyke are representative of the initial Sudbury magma. However, their field studies, along with those of Murphy and Spray (2002) on the Whistle-Parkin offset dyke indicate that the inclusion- and sulfide-enriched phase preceded the fine grained phase, albeit by only a very short time interval. It would seem that sulfide immiscibility occurred very early during development of the SIC.

**Sublayer**. The match between the relative proportions of trace elements in the Felsic Norite and Sublayer is much less close than between Felsic Norite and the other rock types discussed above (Figs. 8.18, 8.19, 8.20). The sublayer rocks are poorer in LREE and LILE but have similar HREE and HFSE to the Felsic Norite. Lightfoot et al. (1997a) argued that these differences cannot be explained by closed system fractional crystallization or partial melting . As seen in Fig. 8.21, Sublayer samples from a single

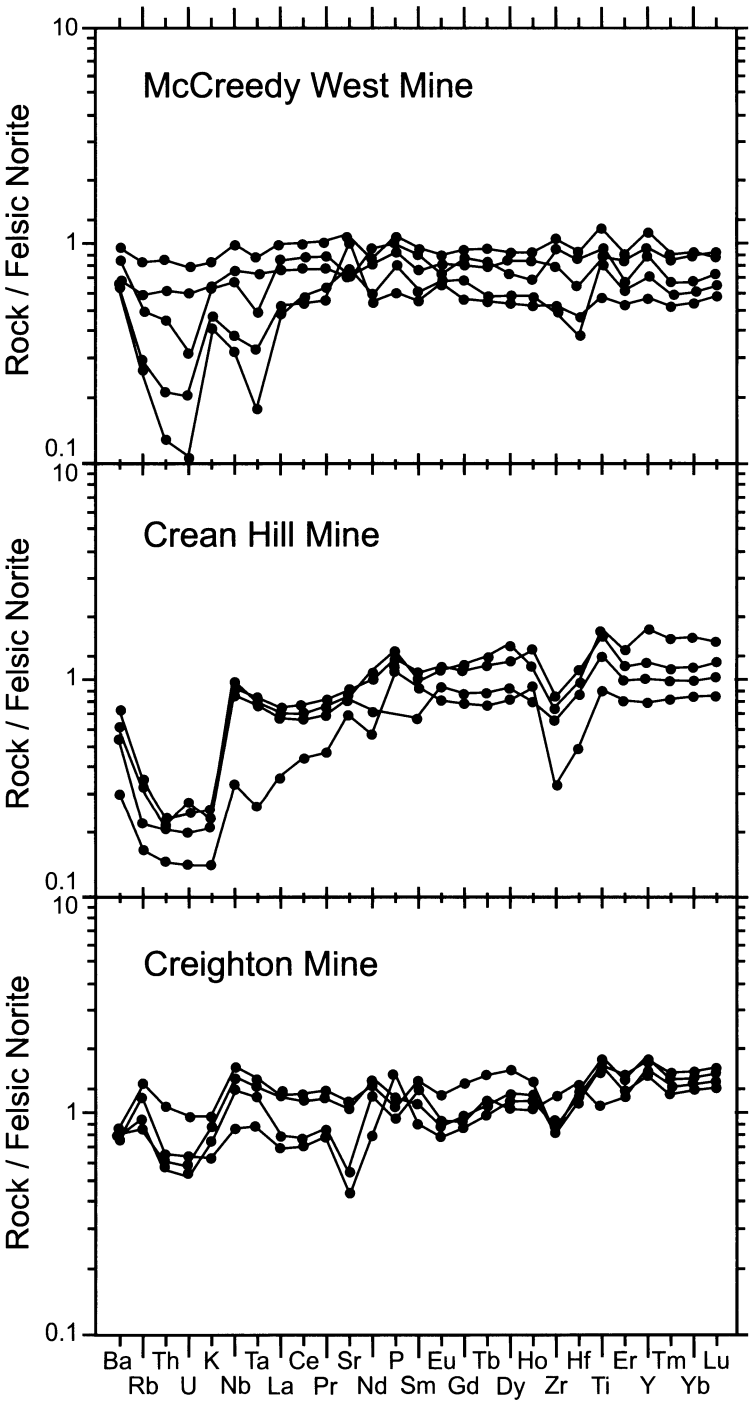
McCreedy West Mine
Crean Hill Mine
Creighton Mine
Rock / Felsic Norite
10
1
0.1
Ba Th K Ta Ce Sr P Eu Tb Ho Hf Er Tm Lu
Rb U Nb La Pr Nd Sm Gd Dy Zr Ti Y Yb

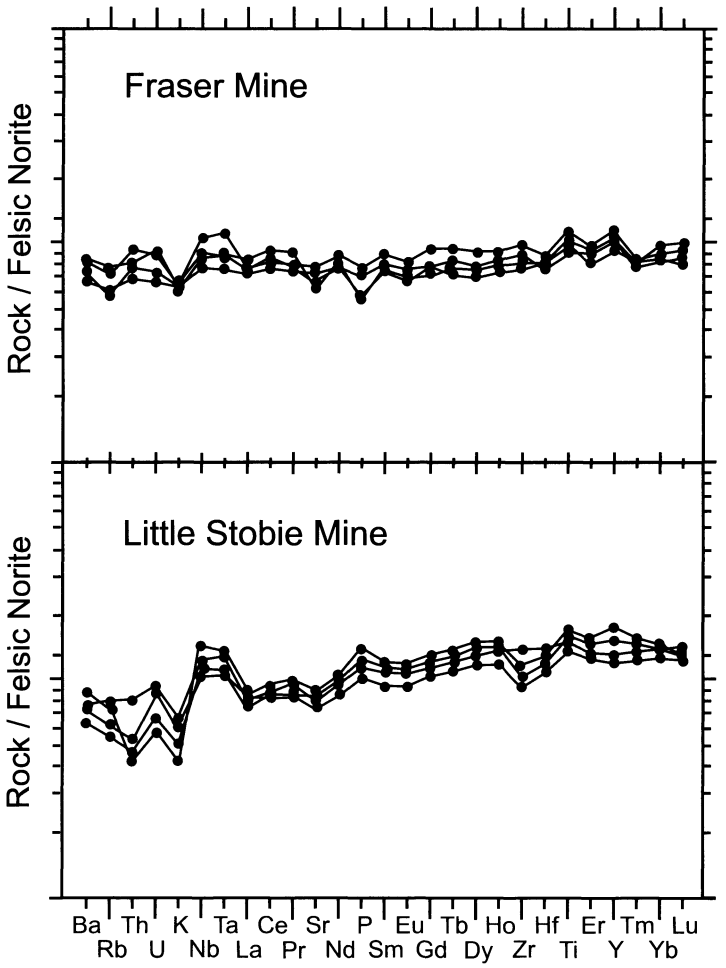


**Fig. 8.21.** Abundance patterns for selected incompatible elements in samples of Sublayer from different Sudbury localities normalized to the average composition of the Felsic Norite. After Lightfoot et al. (1997b)

embayment have similar compositions, but samples from different embayments have different compositions. It is likely that these differences are due to the provenance of the bulk of the Sublayer in each case being of very local derivation, a concept that is supported by the Nd and Sr isotopic data that are discussed below. These observations are also supported by the Sm vs. La plot of Fig. 8.18.

**Inclusions in the Sublayer.** Lightfoot at al.'s (1997b) trace element studies of the diabase inclusions in the Sublayer show that these are low in

LILE and LREE relative to Felsic Norite, but have similar HFSE and HREE. The melanorite pods and pyroxenite inclusions analyzed by them have trace element contents that indicate a general similarity with the Sublayer matrix in which they occur.

### 8.4.3 Isotopes

Krogh et al. (1984) showed from Pb-U radiometric dating of zircons and baddeleyite that the SIC has an age of 1.85 Ga. Using this as a model age, both Faggert et al. (1985) and Naldrett et al (1986) showed from studies of Nd-Sm and Sr-Rb isotopes that the both the Main Mass of the SIC and the Sublayer contain less radiogenic Nd and more radiogenic Sr than bulk earth (Fig. 8.22).

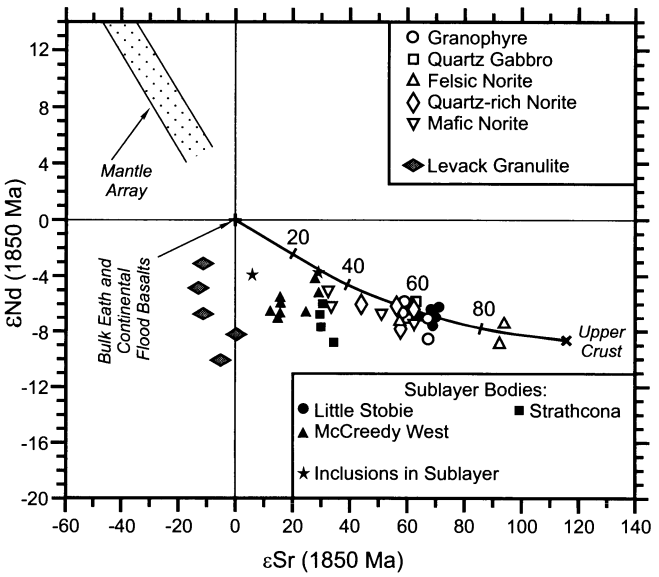


**Fig. 8.22.** εNd vs. εSr diagram for units of the Main Mass and samples of Mineralized Sublayer of the SIC, and Levack granulite gneiss. The measured values were recalculated to 1.85 Ga, the age of the Sudbury Igneous Complex (Krogh et al, 1984). Mixing curve calculated between bulk earth and the upper crust is shown. The upper crustal composition (at 1.85 Ga) was calculated using the data from McKulloch and Wasserburg (1978) and Taylor (1964). The Sr and Nd contents of the initial magma were assumed to be 400 and 15 ppm respectively. The tick marks on the mixing curve indicate the proportion of contaminant in the mixture. Note that the curvature of the mixing array on the diagram is controlled by the value of K, where $K = [(Sr/Nd)_{Magma}/(Sr/Nd)_{Contaminant}] = 2.2$. After Naldrett et al. (1986b)

Walker et al (1991) have shown that Re-Os isochrons for sulfide Sublayer ores from three mines, McCreedy West, Falconbridge and Strathcona, indicate that the Re-Os system remained closed since the time the ores crystallized at 1.85 Ga, or shortly thereafter. The isotopic compositions of Os contained within these ores at the time of crystallization was highly variable, with initial $^{187}Os/^{186}Os$ ratios ranging from 4.70±0.25 at McCreedy West, to 8.73±0.38 at Strathcona. Using estimated Os compositions and isotopic compositions of a hypothetical basaltic melt coupled with measurements of the Os abundance and isotopic composition in samples from the Levack gneiss complex, Walker et al (1991) calculated that the ancient crust had contributed 60-75% of the Os contained in the McCreedy West and Falconbridge ores, and probably nearly 100% of that contained in the Strathcona ores. Dickin et al. (1992) have pointed out that, given the uncertainties involved in assumptions about the Os content and isotopic composition of continental crust, the Os isotopic data are consistent with 100% of the Os at all three deposits being derived from sources that had been resident in the crust for several hundred million years. Morgan et al. (2002) used the very precise NITMS technique to study $^{186}Os/^{188}Os$ and $^{187}Os/^{188}Os$ ratios in samples from the McCreedy West, Strathcona and Falconbridge deposits. They concluded that the Re-Os systematics at Sudbury are clearly crustal, and can be explained as a binary mixture of Archean Superior and Huronian metasedimentary rocks, with the compositions for Strathcona, Falconbridge and McCreedy West requiring, respectively, 55%, 16% and 12% of the Superior-age component (Fig. 8.23). However, they found that ores with low $^{190}Pt/^{188}Os$ ratios at Falconbridge and McCreedy West (but not Strathcona) had $^{186}Os/^{188}Os$ ratios that were substantially superchondritic. They suggested that this could be due the admixture of a third component, most likely Archean or early Proterozoic mafic rocks with $^{190}Pt/^{188}Os \cong 1$, that were also sampled by the impact.

Corfu and Lightfoot (1997) have dated zircons and baddeleyite from inclusions of diabase, melanorite and pyroxenite from the Whistle mine. All dates correspond to the Sudbury age of 1.85 Ga, which links the origin of these rocks very closely with that of the SIC. In view of the importance of their findings, the nature of their samples requires comment. The diabase cuts across the contact between Sublayer and country rock at the northern end of the Whistle pit; in their article Corfu and Lightfoot suggest it could be a fragment of disrupted chilled-margin; however, many of the large bodies of diabase at the footwall of the SIC are disrupted and recrystallized, and occur in both igneous textured and metamorphic textured breccias and an alternative, and more likely (P.C. Lightfoot, personal communication, June 1998), interpretation is that they are samples of older

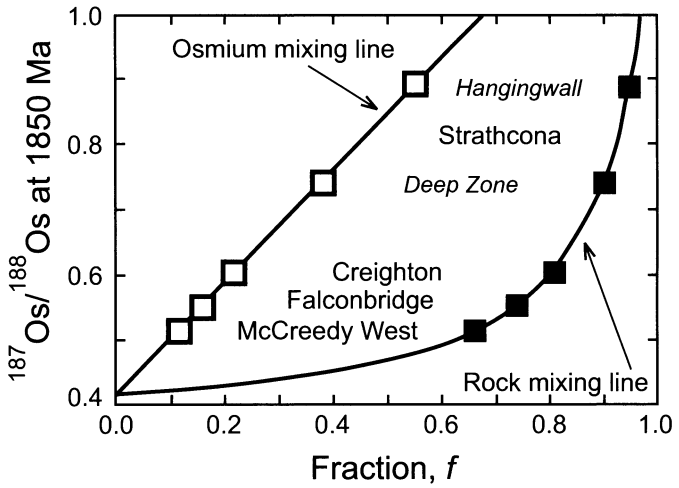


**Fig. 8.23.** Mixing model for $^{187}Os/^{188}Os$ in the Sudbury ores assuming an Archean end-member with 00.72 ppb Os and $(^{187}Os/^{188}Os)_{1850\ Ma} = 1.319$, and a Proterozoic end member with 0.108 ppb Os and $(^{187}Os/^{188}Os)_{1850Ma} = 0.416$. From Morgan et al. 2002 who used data for Creighton from Dickin et al. 1992

diabase for which the zircon age has been re-set by the impact. The melanorites are described as pods within a Sublayer matrix, without sharp margins and in one case gradational over 5 m into leuconorite; while this material is not typical of the inclusion suite described by Scribbins et al. (1984) (Table 8.1) P.C. Lightfoot has remarked to the author (personal communication, 1998) that inclusions of the type documented by Scribbins et al. are rare, and melanorites of the kind dated in the Corfu and Lightfoot study, which appear to belong to a spectrum of geochemically similar rocks, are the most common melanocratic inclusion type. In discussing their data, Corfu and Lightfoot (1997) concluded that the melanorite samples appear to have crystallized from magma in which the major elements indicated a much more magnesian bulk composition than any magma responsible for the Main Mass of the SIC, but in which the trace elements ratios were enriched in LREE and other incompatible elements to an extent inconsistent with their crystallization from primitive mantle melts.

Naldrett et al. (1986b) argued that the Nd-Sm and Sr-Rb isotope data presented in Fig. 8.22 are consistent with contamination of continental flood basalt by 40-70 percent of crustal material, pointing out that this interpretation was consistent with conclusions drawn from the trace element data. However, on the basis of similar data Faggert et al (1985), and subsequently Deutsch et al. (1989, 1990, 1992) proposed that the SIC was an impact melt with no component derived directly from the mantle.

The Levack gneisses, which have the mineralogy and texture of granulites, plot in the southwest quadrant of Fig. 8.22, which is also typically where lower crustal granulites plot. It is interesting to note that while the Sublayer samples from the South Range plot close to a mixing line between primitive mantle values and the average Huronian crust (Fig. 8.22), the North Range Sublayer samples plot well to the left of this line. Levack gneiss is not present on the South Range. Naldrett et al (1986b) concluded from this correspondence between local geology and isotopic composition that the Sublayer contains an appreciable contribution from the local country rocks.

## 8.5 Sulfide Ore Deposits

The nickel-copper ore deposits of the Sudbury camp can be divided into Marginal (Contact) North Range deposits, Marginal South Range deposits, Offset deposits, and a miscellaneous group. Some authors recognise copper-rich zones in the footwall as a separate type of deposit, although these can usually be linked to one or more of the contact deposits. Detailed descriptions of many of the deposits have been given by Naldrett and Kullerud (1967), Cowan (1968), Souch et al. (1969), Pattison (1979) and Farrow and Lightfoot (2002), and by a number of authors in both Pye et al. (1984) and Lightfoot and Naldrett (1994). Average chemical compositions of ores from some deposits are given in Table 8.4.

**Marginal (Contact) deposits.** The marginal deposits of the North Range occur principally along a 10 km stretch of the contact extending from the Hardy mine in the west to the Longvack ore body in the east (Fig. 8.3). They are shown with the outline of the different lenses projected onto a vertical longitudinal section in Fig. 8.24. It is seen that they are distributed in a "W"-shaped pattern. The eastern "V" of the "W" is defined by a pronounced embayment, the Strathcona embayment, but the control of the deposits defining the western "V" is less clear. Figs, 8.25 and 8.26 show a series of N-S vertical cross sections illustrating ore lenses at locations marked 1-8 in Fig. 8.24. In these deposits, the mineralization occurs primarily within brecciated country rocks (Footwall Breccia) at the basal contact of the SIC, and in fractures in country rock underlying the breccias, in all cases where this breccia is overlain by Sublayer. The Footwall Breccia consists of fragments of country rock, ultramafic inclusions, and rare norite in a quartzo-feldspathic matrix. It has been postulated that the

**Table 8.4.** Average chemical compositions of ores from some deposits of the Sudbury Camp

| Deposit and Ore Type | No | S | Ni | Cu | Pd | Pt | Rh | Ru | Ir | Os | Au | Pd/Pt |
|---|---|---|---|---|---|---|---|---|---|---|---|---|
| **North Range Marginal Deposits** | | | | | | | | | | | | |
| **Trillabelle** | | | | | | | | | | | | |
| Sublayer Ore | 83 | 7.94 | 0.56 | 0.31 | 78 | 82 | 16 | 17 | 5.8 | 4 | 128 | 0.95 |
| Footwall Ore | 38 | 13.29 | 0.90 | 0.70 | 121 | 126 | 16 | 26 | 6.8 | 4 | 22 | 0.96 |
| Massive Footwall Ore | 8 | 22.43 | 1.68 | 0.47 | 172 | 268 | 29 | 28 | 8.5 | 4 | 25 | 0.64 |
| **Onaping** | | | | | | | | | | | | |
| Sublayer Ore | 11 | 9.43 | 1.17 | 0.13 | 20 | 28 | 93 | 54 | 24.0 | 8 | 3 | 0.69 |
| Footwall Ore | 20 | 18.99 | 2.61 | 0.53 | 104 | 81 | 27 | 17 | 6.0 | 3 | 6 | 1.28 |
| **McCreedy West** | | | | | | | | | | | | |
| Sublayer Ore | 11 | 16.73 | 1.65 | 0.22 | 19 | 32 | 4 | 57 | 6.4 | 2 | 8 | 0.61 |
| Footwall Ore | 25 | 18.84 | 2.71 | 0.82 | 341 | 378 | 100 | 32 | 25.2 | 10 | 50 | 0.90 |
| Cu-rich Footwall Ore | 38 | 12.50 | 1.41 | 10.79 | 4 631 | 4 198 | 1 | 21 | 2.8 | 11 | 3 527 | 1.10 |
| Cu-rich Massive Footwall Ore | 31 | 26.68 | 2.31 | 22.41 | 7 830 | 7 210 | 1 | 22 | 1.3 | 15 | 3 558 | 1.09 |
| **Craig** | | | | | | | | | | | | |
| Sublayer Ore | 7 | 9.05 | 1.36 | 0.25 | 108 | 20 | 4 | 1 | 0.6 | 0 | 137 | 5.44 |
| Footwall Ore | 240 | 12.15 | 2.02 | 0.83 | 400 | 50 | 30 | 11 | 7.1 | 4 | 424 | 8.01 |
| **McCreedy East** | | | | | | | | | | | | |
| Sublayer Ore | 19 | 3.28 | 0.44 | 0.19 | 43 | 63 | 19 | 54 | 10.2 | 6 | 6 | 0.67 |
| Cu-rich Footwall Ore | 71 | 18.10 | 2.62 | 16.55 | 5 955 | 6 028 | 2 | 3 | 0.8 | 3 | 2 029 | 0.99 |
| **Fraser** | | | | | | | | | | | | |
| Sublayer Ore | 35 | 10.39 | 1.23 | 0.55 | 141 | 188 | 72 | 37 | 23.7 | 9 | 54 | 0.75 |
| Footwall Ore | 137 | 10.10 | 1.39 | 0.64 | 224 | 289 | 31 | 18 | 9.7 | 4 | 23 | 0.78 |
| **Strathcona** | | | | | | | | | | | | |
| Sublayer Ore | 10 | 18.24 | 1.44 | 0.12 | 49 | 49 | 29 | 24 | 14.2 | 10 | 7 | 0.99 |
| Footwall Ore | 34 | 24.41 | 2.41 | 1.86 | 707 | 370 | 10 | 6 | 3.1 | 2 | 38 | 1.91 |
| Cu-rich Footwall Ore | 72 | 23.05 | 2.01 | 19.08 | 5 021 | 5 408 | 0 | 12 | 0.4 | 9 | 967 | 0.93 |
| **Whistle** | | | | | | | | | | | | |
| Sublayer Ore | C | 27.30 | 2.48 | 0.27 | 176 | 188 | 146 | 38 | 42.5 | 19 | 18 | 0.94 |

**Table 8.4.** (cont.)

| Deposit and Ore Type | No | S | Ni | Cu | Pd | Pt | Rh | Ru | Ir | Os | Au | Pd/Pt |
|---|---|---|---|---|---|---|---|---|---|---|---|---|
| **East Range Marginal Deposits** | | | | | | | | | | | | |
| **Victor/Nickel Rim** | | | | | | | | | | | | |
| Sublayer Ore | 101 | 13.09 | 1.59 | 0.58 | 228 | 414 | 100 | 69 | 45.3 | 19 | 36 | 0.55 |
| Footwall Ore | 62 | 16.55 | 2.21 | 0.63 | 188 | 246 | 34 | 22 | 13.2 | 7 | 52 | 0.76 |
| Massive Footwall Ore | 29 | 21.65 | 2.96 | 0.28 | 241 | 299 | 44 | 23 | 13.8 | 7 | 15 | 0.81 |
| Cu-rich Footwall Ore | 119 | 10.04 | 1.47 | 10.91 | 3 532 | 4 975 | 1 | 12 | 0.5 | 60 | 820 | 0.71 |
| **South Range Marginal Deposits** | | | | | | | | | | | | |
| **Creighton** | | | | | | | | | | | | |
| Sublayer Ore | 90 | 6.58 | 1.18 | 1.11 | 308 | 496 | 100 | 65 | 43.3 | 16 | 185 | 0.62 |
| Massive Ore with Silicate Inclusions | 66 | 21.37 | 4.23 | 3.27 | 1 722 | 1 193 | 373 | 216 | 98.7 | 35 | 267 | 1.44 |
| Footwall Ore | 74 | 8.76 | 1.58 | 2.77 | 1 170 | 747 | 173 | 88 | 46.1 | 18 | 225 | 1.57 |
| Massive Footwall Ore | 21 | 26.85 | 4.99 | 5.49 | 1 572 | 1 281 | 398 | 176 | 99.2 | 34 | 111 | 1.23 |
| **Crean Hill** | | | | | | | | | | | | |
| Sublayer Ore | 18 | 9.28 | 1.21 | 1.41 | 676 | 1 104 | 104 | 44 | 25.9 | 13 | 246 | 0.61 |
| Massive Ore with Silicate Inclusions | 29 | 18.90 | 2.37 | 2.07 | 1 842 | 2 284 | 356 | 197 | 82.6 | 35 | 366 | 0.81 |
| Footwall Ore | 26 | 8.29 | 0.93 | 2.78 | 1 685 | 2 113 | 137 | 90 | 36.2 | 20 | 439 | 0.80 |
| Massive Footwall Ore | 14 | 26.79 | 2.45 | 2.69 | 2 205 | 1 339 | 270 | 111 | 46.8 | 19 | 227 | 1.65 |
| **Gertrude** | | | | | | | | | | | | |
| Sublayer Ore | 115 | 10.47 | 1.29 | 0.47 | 39 | 63 | 68 | 61 | 35.9 | 14 | 12 | 0.62 |
| **Lindsley** | | | | | | | | | | | | |
| Sublayer Ore | 184 | 9.82 | 1.02 | 0.92 | 457 | 520 | 87 | 47 | 27.8 | 12 | 147 | 0.88 |
| Footwall Ore | 74 | 26.83 | 1.82 | 4.47 | 6 099 | 2 488 | 255 | 59 | 32.0 | 14 | 498 | 2.45 |
| **South Range miscellaneous deposits** | | | | | | | | | | | | |
| **Falconbridge** | | | | | | | | | | | | |
| Massive Ore | 10 | 33.70 | 4.89 | 1.12 | 120 | 222 | 212 | 151 | 118 | 36 | 35 | 0.54 |
| Breccia Ore | 22 | 20.97 | 2.57 | 0.89 | 234 | 355 | 160 | 149 | 81 | 22 | 135 | 0.66 |
| Disseminated Ore | 1 | 2.32 | 0.36 | 0.62 | 85 | 545 | 18 | 37 | 19 | 9 | 80 | 0.16 |
| Hangingwall Disseminated Ore | 1 | 7.20 | 0.57 | 3.63 | 375 | 400 | 116 | 122 | 54 | 24 | 71 | 0.94 |

*No* Number of Samples; *C* Composite sample. S, Ni, and Cu in wt%; Pd, Pt, Rh, Ru, Os, Ir, and Au in mg/t (ppb)

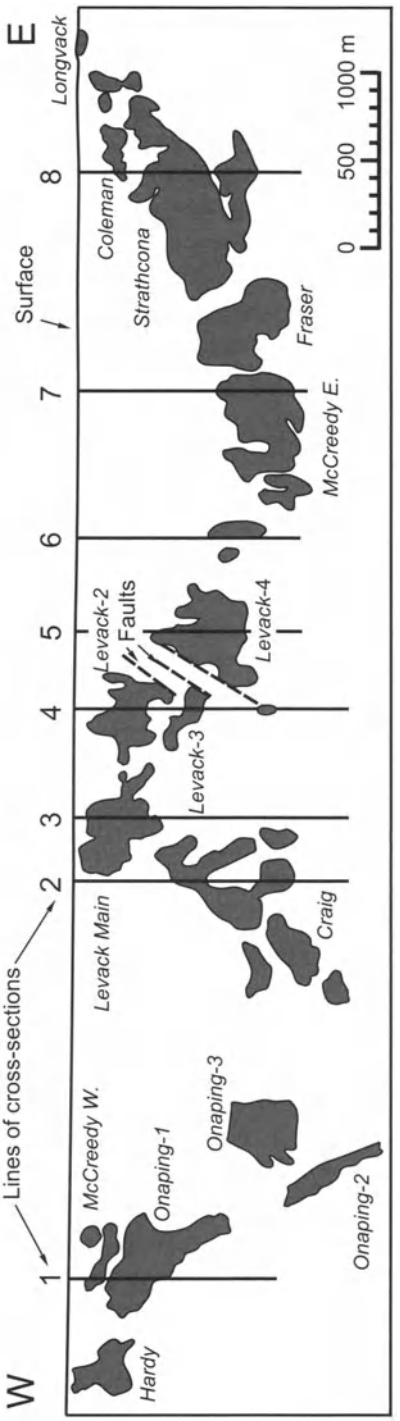


**Fig. 8.24.** Generalized longitudinal section (projection of ore bodies on vertical plane) through North Range deposits in the Onaping – McCreedy – Strathcona area (after Naldrett et al. 1994c). Positions of major mines are shown in Figure 8.3. Cross sections for lines from 1 to 4 are given in Fig. 8.25, for lines from 5 to 8 in Fig. 8.26

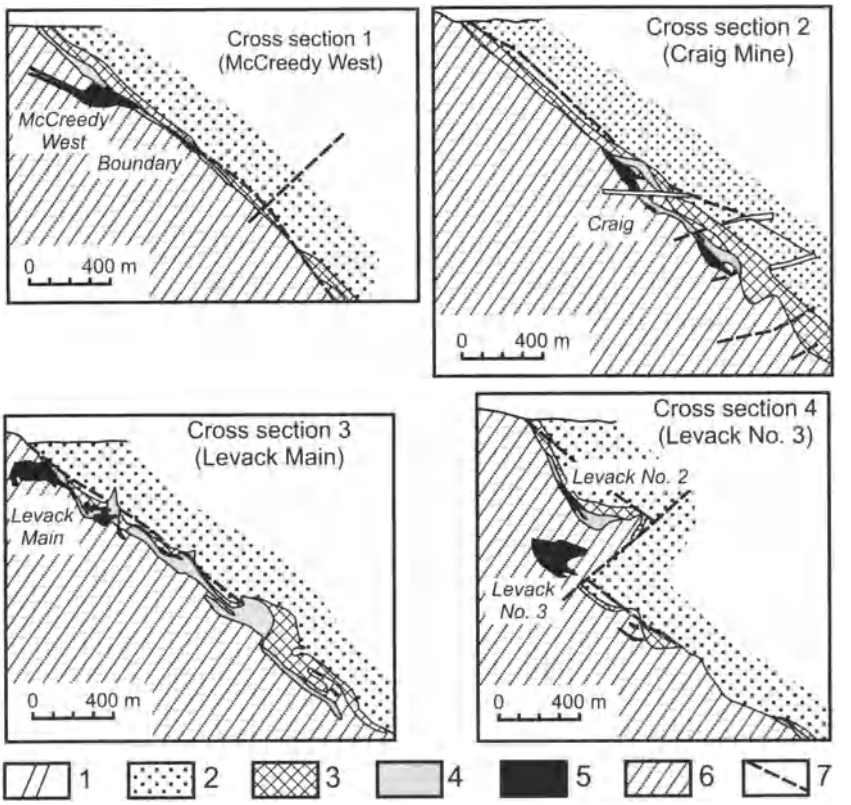


**Fig. 8.25.** North-south cross sections through North Range deposits for lines 1 to 4 in Fig. 8.24 (after Coats and Snajdr 1984). The locations of the cross-sections are shown in Figure 8.24. 1 = Diabase dikes; 2 = Felsic norite; 3 = Mafic norite and Sublayer; 4 = Footwall breccia; 5 = Sulfide ore; 6 = Country gneiss; 7 = Faults

breccia resulted from and lined the base of the impact crater, although post-ore brecciation can be demonstrated.

The Strathcona deposit (Fig. 8.27) is typical of the North Range marginal deposits. The sulfides occur (1) as fine and blebby disseminations and as massive stringers within the footwall breccias (Main Zone ore), (2) as stringers in the footwall fractures, and, (3) more rarely, as disseminations within overlying sublayer norite (Hangingwall ore). Cu-rich ore, consisting of nearly massive chalcopyrite enclosing a small percentage of pentlandite, is present 500 m into the footwall at the Strathcona mine (Abel et al. 1979; Abel 1981). This copper ore occurs in fractures within the footwall gneiss and particularly within veins of Sudbury breccia. At Strathcona and elsewhere (e.g. McCreedy East, Victor) it is also much richer in Pt, Pd and Au than the contact deposits.

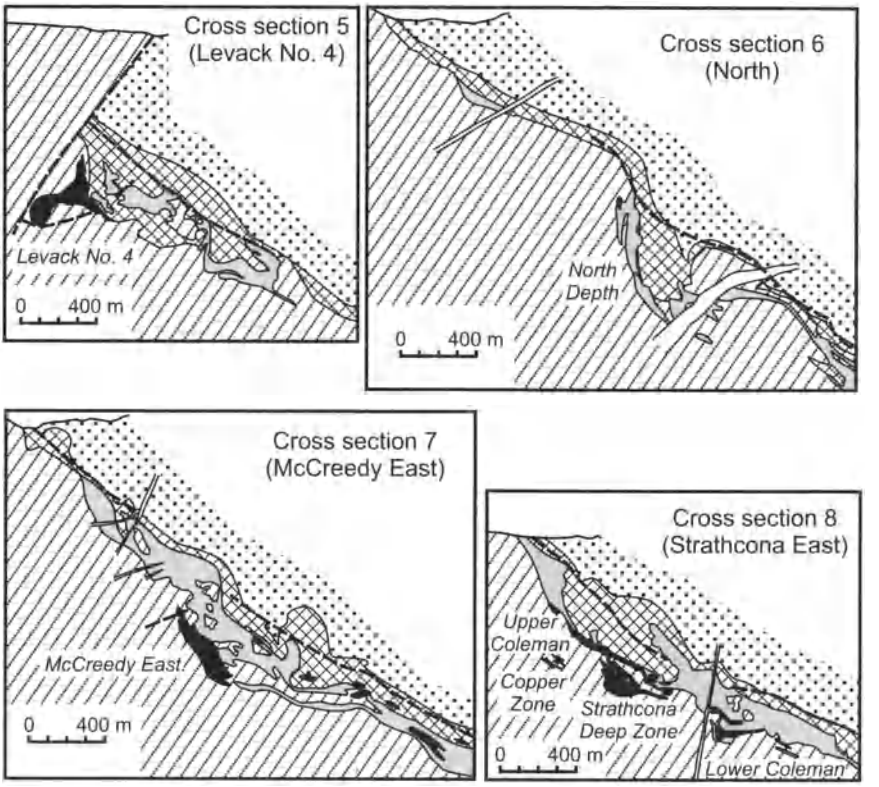


**Fig. 8.26.** North-south cross sections through North Range deposits for lines 5 to 8 in Fig. 8.24 (after Coats and Snajdr 1984). Legend is as for Fig. 8.25

The Murray mine (Fig. 8.28) is a typical example of a South Range contact deposit. The mineralization is generally zoned from massive ore at the footwall to disseminated sulfide ore toward the hangingwall. The massive ores rest directly on the footwall rocks and contain inclusions of footwall material as well as fragments of gabbro and peridotite. The host rock of the disseminated ores is Sublayer norite which is in sharp contact with the overlying Quartz-rich Norite of the Main Mass.

The Creighton mine (Fig. 8.29) is the largest of the South Range contact deposits and one of the longest-lived of the Sudbury mines. Production started in 1900 and to-date 280 million tones of ore have been produced (Farrow and Lightfoot, 2002). With mining operations extending to nearly 2,500 m, is also the deepest nickel mine in the world. The deposit is located along the keel of an embayment where a discontinuous offset dyke intersects the embayment. Farrow and Lightfoot (2002) point out that it contains many different styles of mineralization and suggest that in reality it is a "failed offset" deposit (see below).

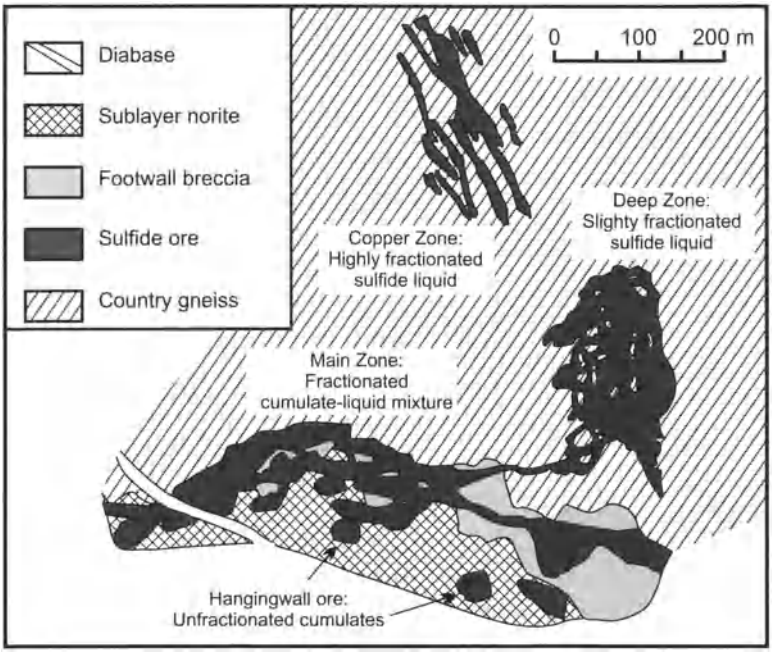


**Fig. 8.27.** 2625 ft (800 m) level plan of the Strathcona mine (from Naldrett et al. 1994)

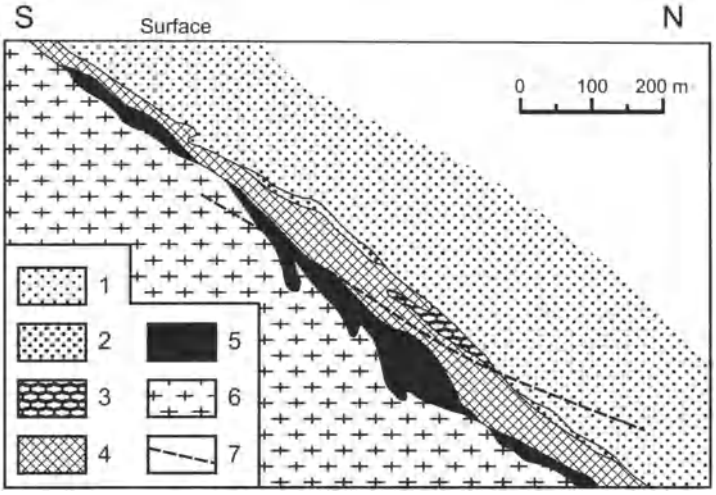


**Fig. 8.28.** Generalized section through the Murray mine, looking west (after Souch et al 1969). 1 = Quartz-rich Norite; 2-4 = Sublayer: 2 = Hosting ragged disseminated sulfide; 3 = Hosting interstitial sulfide; 4 = Hosting sulfide and mafic-ultramafic inclusions; 5 = Massive sulfide with fragments of country rocks and mafic-ultramafic inclusions; 6 = Country rocks; 7 = Shear

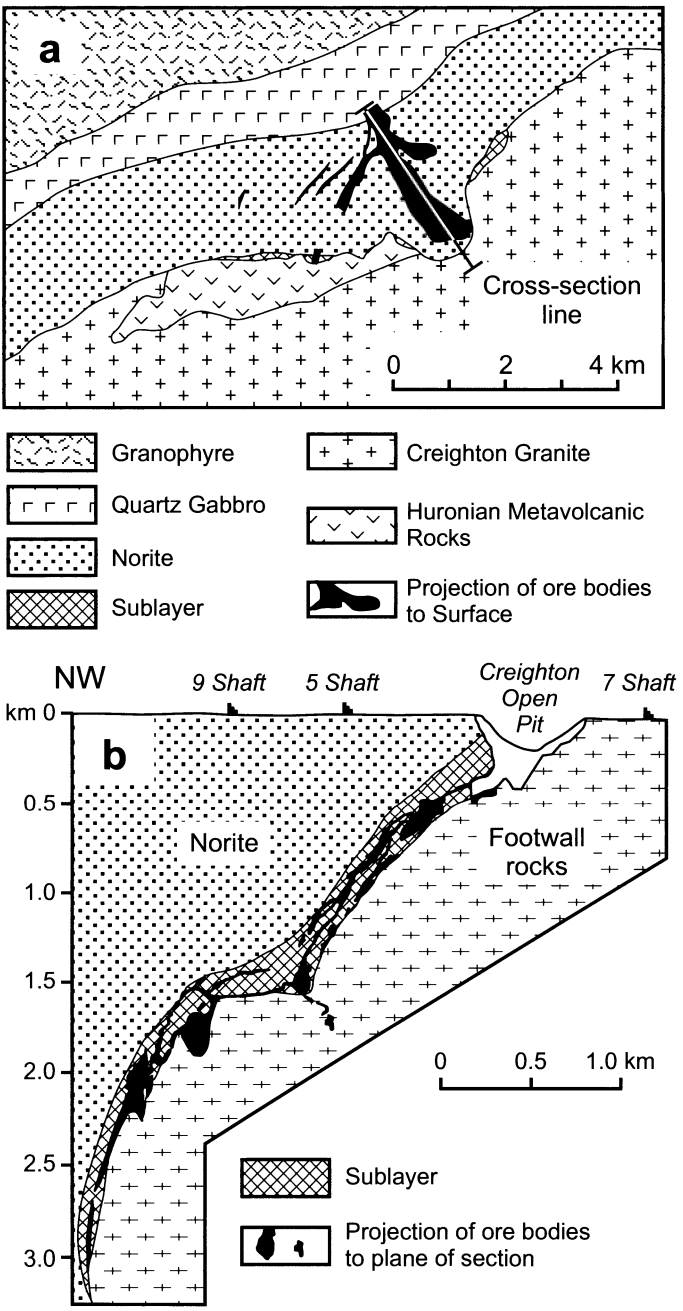


**Fig. 8.29.** Geological map of the Creighton area of the South Range (a), and north-south cross section of the Creighton deposit (b). After Farrow and Lightfoot (2002)

**Offset deposits.** The Offset deposits occur in the dyke-like offsets of quartz diorite that extend several kilometers away from the Complex into the footwall. The Copper Cliff offset is typical in many respects. Close to the SIC, it has the aspect of a funnel, both in plan (Fig. 8.30) and vertical section; it extends discontinuously at least 10 km away from the complex as a relatively narrow (50-150 m) dyke. Ore zones (Fig. 8.31) occur as steeply plunging, lens-like pods of massive and interstitial disseminated ore associated with high proportions of inclusions. The mineralized, inclusion-rich pods, appear to have been injected later than the quartz diorite that comprises the bulk of the offset (see below).

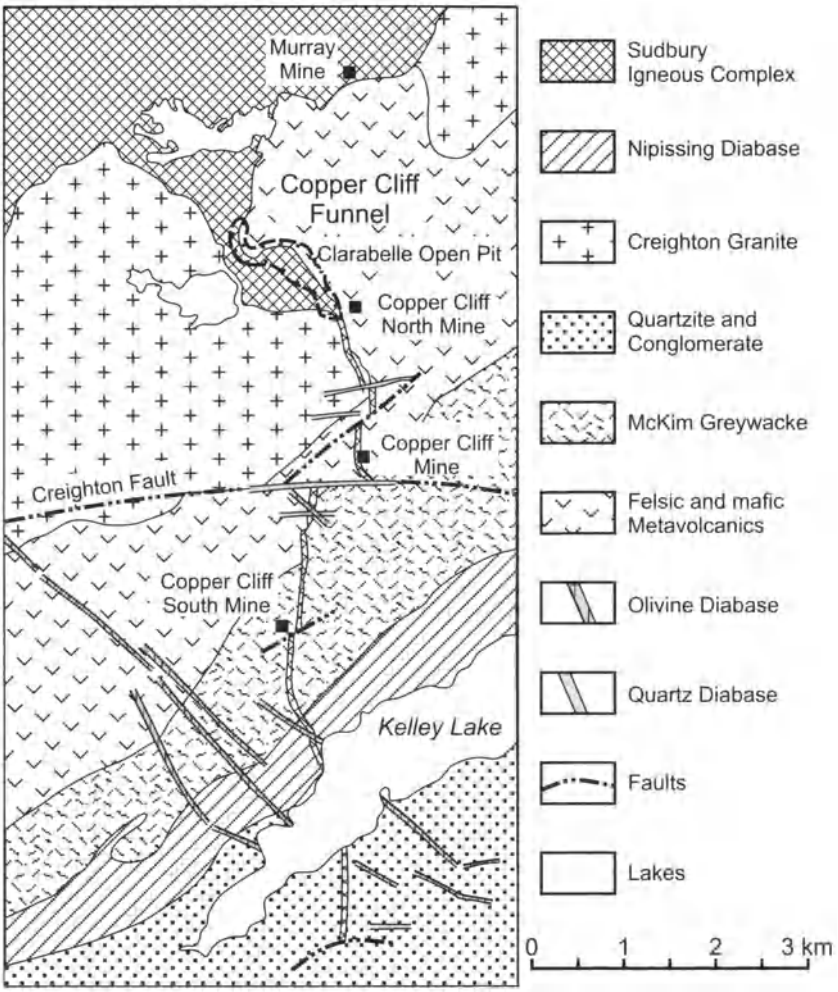


**Fig. 8.30.** Surface geology of the Copper Cliff offset (after Cochrane 1984)

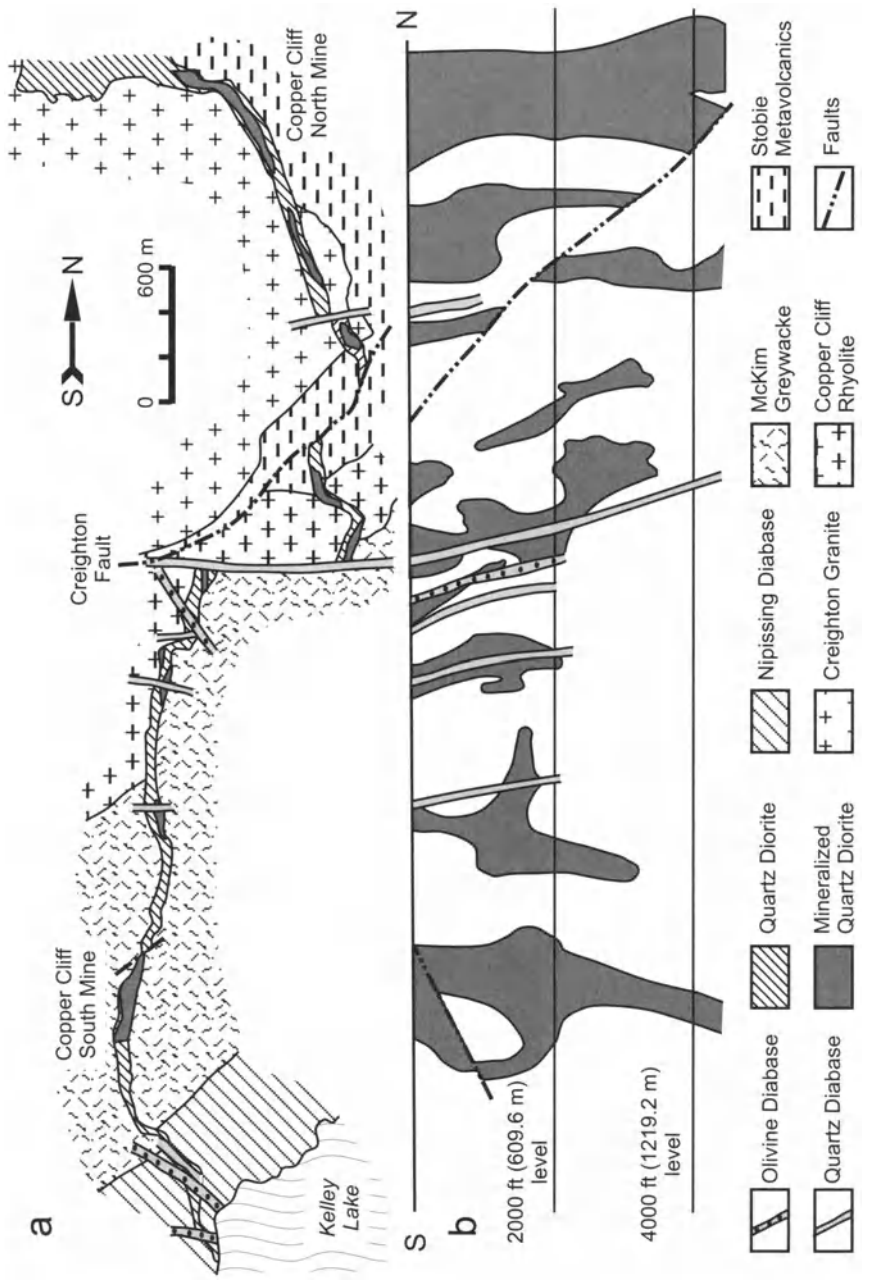


**Fig. 8.31.** Surface plan (a) and longitudinal section (b) showing the distribution of the ore bodies along the Copper Cliff offset. After Cochrane (1984)

The Frood Stobie, the largest offset deposit, is unusual in that it lies parallel and not radial with respect to the southern contact of the Irruptive. The offset resembles a dike with a maximal width of 275 m in surface plan and a downward-pointing wedge in cross section, and dips steeply to the north. Massive, inclusion-bearing sulfide ore is concentrated at the margins of the wedge and toward the base of the deposit, whereas the upper part of the orebody consists of disseminated sulfides in inclusion-bearing quartz diorite.

**Miscellaneous deposits.** The Falconbridge deposit belongs to the miscellaneous class, and is unusual in that it is localized along a fault that parallels the contact of the Complex. The fault forms the contact between rocks of the Complex and the Huronian country-rock greenstones over much of its length, although to the west it enters and dies out within the Complex and to the east it enters the greenstones. Naldrett et al. (1982) have shown that the deposit is poorer than many others in tenors of Cu, Pt, Pd and Au, and have suggested that a Cu-rich component of the original body has been removed by faulting.

## 8.6 Metal contents of different Ore Deposit Types

The average Ni, Cu, Pt and Pd contents in 100% sulfides for specific deposits representative of different ore environments at Sudbury are shown in Table 8.5. Data are from Farrow and Lightfoot (2002) and Naldrett et al. (1999). The data of the former are presumably weighted averages for the deposits (the authors do not specify how their values were derived) while the latter are simple averages of a large number (50 to >200) of representative samples. The Pt+Pd contents of 100% sulfides in North Range Contact deposits range from 0.7 to 3.0 g/t, but are higher in South Range Contact deposits (except the Gertrude deposit which is anomalously low) ranging from 4.1 to 5.3 g/t. Sulfides from the Offset deposits display very variable Pt+Pd contents from 1.2 to 29 g/t, but mostly over 12 g/t. Footwall Cu deposits are characterised by high Pt+Pd contents between 13 and 30 g/t. The ratio (Pt+Pd)/(Ni+Cu) (PGE in g/t, Ni and Cu in wt%) shows a similar, but more consistent trend than the total PGE content, with the ratio ranging from 0.03 to 0.25 in North Range Contact deposits, 0.27 to 0.82 in South Range Contact deposits (except for Gertrude), and 0.49 to 1.37 in Footwall Copper deposits (see the Appendix).

As discussed in Chap. 2, the high Pt+Pd (and high Cu) in Footwall Copper deposits is likely the result of their being the product of a fractionated

sulfide liquid that has escaped from fractionally crystallizing contact sulfides. The difference between the North and South Range Contact deposits is more difficult to account for. The sulfides of the South Range deposits are much richer in As than those of the North Range. This is supported (1) by unpublished data of the author which shows that the average As content of 30 samples from the Little Stobie South Range Contact Deposit is 139 ppm, while most massive sulfide samples from the McCreedy West Contact Ore contain less than 4 ppm, and (2) the prevalence of sperrylite ($PtAs_2$) as the main Pt mineral in South Range ores as contrasted with its absence in most deposits on the North Range. It is possible that the presence of As in the sulfide liquid scavenging metals from the SIC magma aided in the concentration of PGE.

**Table 8.5.** Metal Tenors of Sulfides from Different Sudbury Deposit, data from Farrow and Lightfoot (2002) and Naldrett et al. (1999)

| Deposit | Ni | Cu | Pt | Pd |
|---|---|---|---|---|
| **Offset Deposits** | | | | |
| Clarabelle [1] | 6.5 | 6.8 | 5.4 | 7.0 |
| Copper Cliff North [1] | 5.3 | 7.7 | 6.4 | 5.9 |
| Copper Cliff South [1] | 5.8 | 10.7 | 9.7 | 10.6 |
| Totten-Worthington [1] | 6.2 | 12.8 | 13.8 | 15.0 |
| Foy [1] | 3.2 | 2.6 | 0.6 | 0.6 |
| Stobie [1] | 3.4 | 3.5 | 1.7 | 1.6 |
| Frood [1] | 3.5 | 4.2 | 1.8 | 1.7 |
| **South Range Contact Deposits** | | | | |
| Creighton [1] | 5.3 | 7.1 | 2.0 | 2.2 |
| Little Stobie [1] | 5.9 | 3.8 | 2.3 | 3.0 |
| Crean Hill [1] | 5.3 | 6.1 | 2.6 | 2.7 |
| Gertrude [2] | 4.7 | 2.4 | 0.6 | 0.3 |
| Lindsley [2] | 4.0 | 3.9 | 2.2 | 1.9 |
| **North Range Contact Deposits** | | | | |
| McCreedy West [1] | 4.0 | 5.5 | 0.9 | 1.1 |
| Craig [2] | 6.1 | 3.3 | 1.6 | 1.4 |
| Strathcona-Coleman (main zone) [2] | 3.9 | 1.3 | 0.4 | 0.3 |
| **Footwall Copper-rich Ores** | | | | |
| Victor/Nickel Rim [2] | 5.7 | 38.3 | 18.8 | 11.3 |
| Strathcona Deep Copper Ore [2] | 3.5 | 28.8 | 6.5 | 6.9 |
| McCreedy East [2] | 8.7 | 30.3 | 13.9 | 12.7 |
| McCreedy West [2] | 4.5 | 29.4 | 13.9 | 14.7 |

[1] Data from Farrow and Lightfoot (2002). These data are presumably based on weighted averages for the deposits.

[2] Data from Naldrett et al. (1999). These data are based on simple averages of representative samples from the deposits

Ni, and Cu in wt%; Pt and Pd in g/t (ppm)

The reason for the variability in the Pt+Pd content of the Offset Deposits is not understood at the present time, although those rich in PGE are characterised by high Cu contents and those poorer in PGE by low Cu contents. Farrow and Lightfoot (2002) note that there is a sharp change in both the Cu and Pt+Pd contents of sulfides in the Copper Cliff Offset between those deposits north of the Creighton fault and those south of it. Rocks exposed south of the fault are thought to represent a much deeper erosion level than those exposed to the north. Farrow and Lightfoot suggest that it is possible that Offset Deposits show a vertical zoning with Cu, Pt and Pd increasing with depth. This being so, part of the variability in Cu, Pt and Pd in Offset deposits may be a function of the erosion level.

## 8.7 Ore mineralogy

Early mineralogical work at Sudbury has been summarized by Hawley and Stanton (1962) who contributed many of their own observations. These authors reported 32 metallic minerals as confirmed species. Subsequent mineralogical studies have involved investigations of the nature of the pyrrhotite (Cowan 1968), use of the microprobe in determining the ranges in composition of the major minerals, and studies of the platinum group minerals (PGM); (Cabri and Laflamme 1976; 1984).

Metallic minerals identified in the ores are summarized in Table 8.6. Details of their composition and occurrence are best obtained from key references that are cited in the table; space does not permit us to reproduce the data. Here, only some of the major groupings of minerals will be discussed, and relevant phase equilibria studies will be cited where appropriate.

**Fe-Ni-S Minerals.** These include pyrrhotite, pentlandite, and pyrite. Pyrrhotite is the principal host for all other sulfide minerals. Two distinct forms have been identified, ferromagnetic monoclinic pyrrhotite (more common) and diamagnetic hexagonal pyrrhotite (less common). The distribution of the 2 forms throughout the Strathcona Mine has been discussed by Cowan (1968). Where the monoclinic variety is the less common of the two, it may occur (Naldrett and Kullerud 1967): (1) rimming grains of hexagonal pyrrhotite; (2) spreading out away from fractures; (3) in association with pentlandite, often forming sheaths around exsolved pentlandite lamellae. Where the monoclinic variety is the more common, textures in many samples suggest that it is the result of the continued development of the textures just described in (1).

**Table 8.6.** Metallic minerals of the Sudbury ores*

| Mineral name | Formula | Notes | References |
|---|---|---|---|
| **Major minerals** | | | |
| Pyrrhotite Hexagonal | $Fe_{(1-x)}S$ | Distribution of hexagonal and monoclinic pyrrhotites studied intensively at Strathcona Mine | Cowan (1968)<br>Corlett (1972) |
| Pyrrhotite Monoclinic | $Fe_{(1-x)}S$ | | |
| Pentlandite | $(Fe,Ni)_9S_8$ | Ni content 33 to 35 wt%,<br>Co content 1 wt% | Hawley and Stanton (1962) |
| Chalcopyrite | $CuFeS_2$ | | Hawley and Stanton (1962) |
| Magnetite | $Fe_3O_4$ | Magnetite in the ores is low in $TiO_2$ | Hawley and Stanton (1962) |
| Pyrite | $FeS_2$ | 4 types: 1. Pink Nickelean<br>2. Early Resorbed<br>3. Exsolved<br>4. Hypogene Replacement | Naldrett and Kullerud (1967) |
| **Minor minerals** | | | |
| Cubanite | $CuFe_2S_3$ | Found particularly in the Frood- Stobie deposit and in Cu-zone at Strathcona. | Hawley and Stanton (1962)<br>Abel et a. (1979) |
| Galena | PbS | Found as small veins in fractures and as small flecks in pyrite. | Hawley and Stanton (1962) |
| Sphalerite | ZnS | Present with chalcopyrite as late veins and fault filling. | Hawley and Stanton (1962) |
| Millerite | NiS | Originally regarded as secondary. Hypogene mineral found in Footwall at Strathcona Mine. | |
| Niccolite | NiAs | Found at Worthington, Frood, and Garson in association with other arsenides | Hawley and Stanton (1962) |
| Gersdorffite | NiAsS | Occurs with chalcopyrite and as late stage veins. | |
| Cobaltite | CoAsS | | |

**Table 8.6.** (cont.)

| Mineral name | Formula | Notes | References |
|---|---|---|---|
| **Rare minerals** | | | |
| Gold | Au | Found in siliceous mineral zone at Frood Mine | Michener (1940)<br>Hawley and Stanton (1962) |
| Silver | Ag | Found near base of Frood Mine | Hawley and Stanton (1962) |
| Bismuth | Bi | Found associated with galena or with parkerite and bornite at Frood | Hawley and Stanton (1962) |
| Tetradymite | $Bi_2Te_2S$ | Commonly associated with veins of galena | Hawley and Stanton (1962) |
| Hessite | $Ag_2Te$ | Found at Frood Mine | Hawley and Stanton (1962) |
| Maucherite | $Ni_{11}As_8$ | Commonly occurs with niccolite and gersdorffite | Hawley and Stanton (1962) |
| Bornite | $Cu_5FeS_4$ | Observed in Cu-rich zones at Frood deposit and in terminations of veins in footwall Cu ores | Hawley and Stanton (1962) |
| Parkerite | $Ni_3Bi_2S_2$ | | Michener (1940) |
| Schapbachite | $AgBiS_2$ | Frood Mine-1 grain observed | Hawley and Stanton (1962) |
| Altaiite | PbTe | Found at Coleman, Frood, and Crean Hill Mines, often associated with PGM | Cabri and Laflamme (1974,1976) |
| Argentiferous Pentlandite | $Ag(Fe,Ni)_8S_8$ | Light pink, probably confused with bornite | Karpenkov et al. (1973)<br>Cabri and Laflamme (1976) |
| Breithauptite | $Ni_7(Bi,Sb,Te)_2S_8$ | | |
| Hauchecornite | | | |
| Mackinawite | (Fe,Ni)S | | |
| Wehrlite | $(BiPb)_{(1.05\text{-}1.28)}$<br>$(TeSb)_{(0.95\text{-}0.72)}$ | Associated with chalcopyrite - cubanite | Cabri and Laflamme (1976) |

**Table 8.6.** (cont.)

| Mineral name | Formula | Notes | References |
|---|---|---|---|
| **PGM (in relative order of abundance)** | | | |
| Michenerite | PdBiTe | Principal Pd mineral at Sudbury and occurs in most deposits | Cabri and Laflamme (1976)<br>Hawley and Berry (1958) |
| Moncheite | $PtTe_2$ | Observed at Creighton and McCreedy West | Cabri and Laflamme (1976) |
| Sperrylite | $PtAs_2$ | Most common Pt mineral of South Range | Hawley and Stanton (1967)<br>Cabri and Laflamme (1976) |
| Insizwaite | $PtBi_2$ | Found at Coleman Mine | |
| Sudburite | PdSb | Found at Copper Cliff South and Frood | Cabri and Laflamme (1976) |
| Froodite | $PdBi_2$ | Found at Frood, Vermilion, Creighton, McCreedy West, and Coleman | Hawley and Berry (1958)<br>Cabri and Laflamme (1976) |
| Kotulskite | PdTe | Found at McCreedy West and Creighton | Cabri and Laflamme (1976) |
| Niggliite | PtSn | Found at Coleman Mine | Cabri and Harris (1972) |
| Merenskeyite | $PdTe_2$ | Found at Creighton, Crean Hill, and McCreedy West | Cabri and Laflamme (1976) |
| Mertieite II | $Pd_8(Sb,As)_3$ | Found at Creighton Mine | Cabri and Laflamme (1976) |
| Unnamed | Pd(Bi,Sb,Te) | Found at Vermilion Mine | Cabri (1973)<br>Cabri and Laflamme (1976) |
| Unnamed | AgPdTe | Found at McCreedy West Mine | Cabri and Laflamme (1976) |
| Palladian melonite | $(Ni,Pd)(Te,Bi)_2$ | Found at Falconbridge, Strathcona, Crean Hill, and Creighton | Cabri and Laflamme (1976) |
| **Secondary minerals** | | | |
| Violarite | $FeNi_2S_4$ | Found in many ores subject to weathering | Hawley and Stanton (1962) |
| Marcasite | $FeS_2$ | Found as a replacement in cross-cutting seams and fractures | Hawley and Stanton (1962) |
| Vallerite | $(Fe,Cu,Ni)_2S_2$<br>$n(Mg,Al,Ca)(OH)_2$ | Found in chalcopyrite-rich samples | Hawley and Stanton (1962) |

*This Table was published in Naldrett (1985) originally. In 2002, at the request this author (AJN), the table was revised and added to by L.J. Cabri, to whom this author is very grateful

Pentlandite occurs as large (1 to 3 cm diameter) irregular masses, as smaller (<1 cm diameter) masses at triple junctions between pyrrhotite grains, as thin (<3 microns) rims around pyrrhotite grains, and as very fine (1 to 4 microns thick, 10 to 100 microns long) lamellae oriented parallel to the 0001 parting of pyrrhotite. Pyrite occurs as irregular, somewhat resorbed grains and as small (1 mm diameter) euhedral grains around the margins of pyrrhotite grains.

Naldrett and Kullerud (1967) discussed the crystallization of Fe-Ni sulfide ores of the bulk composition of those found at Sudbury in the light of phase relations in the Fe-Ni-S system. These authors pointed out that the $Fe_{(1-x)}S$-$Ni_{(1-x)}S$ monosulfide solid solution (mss) is continuous across the system from solidus temperatures to below 300°C. The bulk composition of Sudbury ore plots within and toward the sulfur-rich side of the mss (see Fig. 2.14b) as it occurs at 600°C. With cooling, the range in metal:sulfur ratios covered by the mss narrows (Naldrett et al. 1967) and ore compositions of the Sudbury-type will exsolve some pyrite. Pentlandite will not form until the *mss* breaks down and tie-lines joining the Ni-rich and Ni-poor variants resulting from the breakdown are replaced by those joining pyrite and pentlandite. Craig (1973) showed that this will happen between 200° and 250°C (see Fig. 2.15a). Thus, the formation of the second-most common mineral in the Sudbury ores, the mineral whose existence enables a reasonable Ni concentrate to be extracted from them and thus accounts for their economic viability, is a very low temperature phenomenon. Not all Ni exsolves as pentlandite; some remains in solid solution in pyrrhotite. Naldrett et al. (2000a) showed that the Ni content remaining in solid solution in pyrrhotite is a function of the metal:sulfur ratio of the pyrrhotite, varying from 0.15 wt% in pyrrhotite containing 63.2 wt % Fe to 0.64 wt% in pyrrhotite containing 59.8 wt % Fe. Corlett (1972) reported values of 0.1 to 1.2 wt% Ni in pyrrhotite from Sudbury. Furthermore, some pentlandite occurs as the fine flames discussed above. These are too fine to be separated by flotation, and hence are lost with the pyrrhotite tailings. Consequently, the low temperature cooling history of a Sudbury ore is most important with respect to the growth of coarse grains of pentlandite and hence to its milling characteristics.

**Cu-Fe-S Minerals.** These include chalcopyrite, cubanite, and rare amounts of bornite. Chalcopyrite is ubiquitous and accounts for by far the major part of the Cu in the Sudbury area. It forms irregular masses at boundaries of pyrrhotite grains and in association with exsolved pentlandite as well as threads cutting other sulfides and magnetite. Cubanite occurs in many deposits associated with chalcopyrite, but is particularly concentrated in the deeper parts of the Frood-Stobie deposit and in the Cu-Zone,

deep in the Footwall at the Strathcona deposit, where it comprises 18 % of the total sulfide (Abel et al. 1979). Where cubanite is present in minor amounts, it occurs as exsolution blades in chalcopyrite; where it makes up a greater proportion of the ore as at the Frood or Stratheona Mines, it is present in irregular masses, commonly enclosing pyrrhotite, in addition to the exsolution blades.

As seen in Fig. 2.16a, the Cu-Fe-S system is dominated by large areas of solid solution at temperatures just below the solidus. On cooling, these areas break down and, at Cu:Fe ratios of < 1, pyrite, pyrrhotite, and chalcopyrite are the usual products. Where the sulfur content is low, as often seems to be the case in fractionated, Cu-rich residual liquids, pyrite is absent and pyrrhotite, chalcopyrite, and cubanite form the stable assemblage.

Abel et al. (1979) described the exsolution of pentlandite lamellae along the edges of cubanite blades in chalcopyrite; this indicated that Ni dissolved in the Cu-rich solid solution that broke down to form the Cu minerals, so that phase relations in the Cu-Fe-S system provided only a rough guide to what may have happened in the more complex natural system of the ores.

Bomite occurs in only the most Cu-rich parts of ore deposits. Cabri and Laflamme (1976) believed that argentiferous pentlandite had been misidentified as bornite by many of the early investigators.

**Some Other Minerals.** Magnetite is a very common mineral, usually present in amounts ranging from 5 to 10 modal %, although some areas of some deposits have up to 25 modal % and zones of nearly massive magnetite have been reported. Sphalerite and galena occur in very minor amounts, particularly in Cu-rich zones of the main ores and as late, crosscutting veins. The arsenides, niccolite and maucherite, and sulfarsenides, gersdorffite and cobaltite, commonly occur together, but are largely restricted to the South Range ores (Hawley and Stanton 1962; Cabri and Laflamme 1976). This is consistent with the observation reported above that the As contents of the South Range deposits are a factor of 20 or more greater than those of the North Range. Compositional ranges for cobaltite and gersdorffite overlap, with Co in the two minerals ranging from 5 to 21 wt%, and Ni from 9 to 25 wt%.

**Platinum Group Minerals (PGM).** Cabri and Laflamme (1976) have identified or confirmed 13 PGM in the Sudbury ores. These are listed in Table 8.6 in the approximate order of their abundance. Cabri and Laflamme remarked that the South Range and Offset deposits are characterized by the presence of As-bearing minerals and the absence of Sn-bearing minerals, while Sn-bearing minerals are present and As-bearing

minerals are rare in deposits on the North Range. These authors also detected significant amounts of platinum group elements (PGE) in solid solution in the As-bearing minerals. Cobaltite contains from 1200 to 7600 ppm Pd, from < 400 to 1900 ppm Pt, and from < 500 to 15 000 ppm Rh; gersdorffite contains from 500 to 2000 ppm Pd, from < 400 to 2500 ppm Pt, and from < 500 to 30 000 ppm Rh; niccolite contains < 400 ppm of each of Pd, Pt, and Rh; and maucherite contains from < 800 to 1000 ppm Pd, and < 500 ppm of both Pt and Rh.

Cabri and Laflamme (1984) have found that 91 % of the Pt in a bulk concentrate could be accounted for by sperrylite, by-solid solution in the sulfarsenides, by moncheite and by platinian michenerite; in contrast, only 41 % of the Pd could be accounted for by michenerite, and by solid solution in arsenides or sulfarsenides, merenskyite, and palladian moncheite. It is generally believed that significant amounts of Pd can substitute in pentlandite. In the Noril'sk deposits pentlandite contains 67-98 % of the Pd; up to 200-1600 ppm Pd has been observed in pentlandite from Noril'sk (Sluzhenikin, Distler 1998; Distler at al. 1999). Even higher concentrations of Pd have been observed in pentlandites from the Stillwater deposit: Cabri and Laflamme (1974), reported 1.4 wt% Pd; Todd et al. (1982), reported 3.5 wt % Pd in pentlandite. Nevertheless, Cabri et al. (1983) were unable to detect even 1.8 ppm Pd in Sudbury pentlandite with a proton microprobe. Clearly, more work is required before the provenance of the PGE at Sudbury can be taken as completely solved.

## 8.8 Relationship of Ore Deposits to the Rocks of the Complex

Although, as outlined above, there is considerable variation in the characteristics of different ore deposits, there are a number of features common to all of them. These include:

1. Embayments or other irregularities at the base of the SIC. An increase in sulfide content is typically observed at the lower contact throughout the Complex, but it is where irregularities exist that the zone of sulfide thickens and increases in intensity sufficiently to form ore. On the North Range, the embayments are commonly associated with thickened zones of Footwall Breccia. Morrison (1984) has shown that the embayments characteristic of an individual deposit, or part of a deposit, actually constitute broad scale irregularities in the floor/walls of the SIC which he

terms "terraces". He attributes the terraces to the mechanics of crater excavation.

2. The presence of Sublayer. Sublayer tends to be most strongly developed within embayments. The spatial relationship of ore to Sublayer rocks is such that the sulfides constituting the ore bodies appear to have settled out of bodies of Sublayer. Sulfides also occur within Quartz-rich and Mafic norites, but ore bodies are invariably associated with Sublayer rocks, except where they have been moved from their original position by faulting.
3. Ultramafic inclusions within Sublayer host-rocks. Some Sublayer is mineralized, other varieties seem to be devoid of significant sulfide. There is little to distinguish mineralized from unmineralized Sublayer in so far as texture, mineralogy and chemical composition of the rocks are concerned, except for the obvious presence or absence of sulfides. All types of Sublayer contain inclusions, but both in the contact and the offset environments, the mineralization is associated primarily with Sublayer host-rocks that carry members of a suite of mafic and ultramafic inclusions that Scribbins et al. (1984) conclude are derived from one or more deep-seated layered intrusions.

## 8.9 Discussion of the Origin of the SIC and its Mineralization

### 8.9.1 Impact Events

As indicated above, Dietz (1964) was the first to suggest that the Sudbury structure was the impact scar of an extra-terrestrial projectile. Initially this suggestion was greeted by some scientists with skepticism. There is abundant evidence that an enormous explosion had occurred prior to consolidation of the SIC (see discussion in section 8.2.3). Shatter cones and shock metamorphic features, which are characteristic of impact structures, provide semi-quantitative evidence that the explosion created a greater shock wave than could have resulted from a volcanic explosion (estimates of the maximum shock pressure resulting from volcanism are in the range of 5-10 kb). Comparisons that have been made between the Sudbury Breccia and Onaping formation, and similar rock types associated with known impact structures give further strength to the impact hypothesis. Naldrett (1999a) commented that Masaiitis et al.'s (1999) "discovery of impact diamonds places yet another nail in the coffin of impact disbelivers!". The impact origin of the Sudbury structure can thus be taken as well established. It has

passed the test of 36 years of continued research and has grown stronger by the year.

The Lithoprobe transect (Milkereit et al. 1992) demonstrated that the Sudbury impact crater originally had a diameter of the order of 150-200 km. This led Grieve et al. (1991) to comment that the volume of impact melt likely to have formed during the generation of a crater of this magnitude was equal to or greater than the volume of the SIC, and to suggest that the whole of the SIC is an impact melt, with no primary mantle component. As has been discussed above, major and trace element and isotopic data are consistent with this interpretation, but do not require it. One of the problems is the average composition of the SIC.

Ariskin et al. (1999) modeled the crystallization of the SIC, using the computer program COMAGMAT-3.5 that had been developed with respect to other differentiated mafic bodies (see Ariskin and Barmina, 2000 for other examples of the use of this program). Their results (Fig. 8. 32) showed that calling upon either Collins's (1934) weighted average for the bulk composition of the SIC, or Naldrett and Hewins's (1984) Quartz-rich Norite as the initial composition of the SIC magma cannot account for the high proportion of granophyre to norite exposed at surface. On the other hand, a Quartz-rich Norite starting composition resulted in a model which gave a very close approximation to both the chemical variations and appearance and disappearance of phases in the lower, mafic portion of the SIC. Ariskin et al. (1999) concluded that the units of the SIC excluding the Granophyre, are likely to be the result of differentiation of a single magma. However, the cumulates that should have resulted from this differentiation do not correspond to the norite, quartz-rich gabbro and granophyre, in the proportions in which they are exposed. Ariskin et al. suggested two possible explanations for their results. The first was it might be possible that a larger body of mafic cumulates lies hidden somewhere within in the structure as Naldrett and Hewins (1984) had suggested earlier. The second is that it is possible that the superheat generated by the impact resulted in the incorporation of a large proportion of the overlying fall-back breccia into the upper part of the differentiating melt sheet. They suggested that, since the initial impact melt, and the breccias forming the roof of the SIC have been derived from the same target rocks, the continuity of all elements from norite through Quartz Gabbro into the Granophyre that they documented in their study, [author's note – and others have documented in other studies, e.g., Chai and Eckstrand 1994; Lightfoot et al. 1997a,b] is not incompatible with this late stage of assimilation of roof rocks.

Ivanov and Deutsch (1999) used a modified version of Amsden et al.'s (1980) SALE computer program for fluid flow (i) to construct a time dependent model for the formation of the transient crater, and thus show the

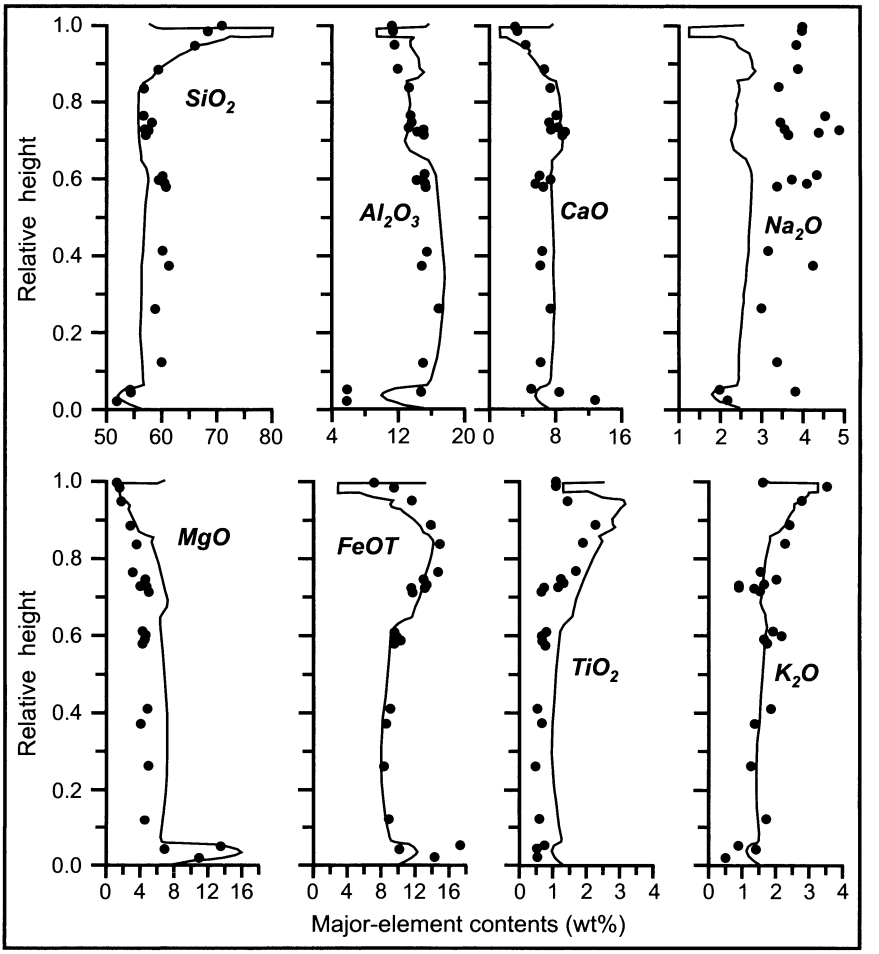


**Fig. 8.32**. Modeling of the differentiation of magma corresponding to Naldrett and Hewin's (1984) average composition of Sudbury Quartz-rich Norite. After Ariskin et al. (1999). Curves are the calculated composition assuming that the rocks are composed of 60 % cumulus minerals and 40 % trapped intercumulus liquid. Points are the analyzed compositions of the mafic part of the SIC sequence (thickness 823 m) intersected by borehole 70011 at the east end of the North Range (after Ostermann 1996)

progression in the distortion of layers in the target area and the position of isotherms close to and beneath the crater following impact, (ii) to model the maximum shock pressures experienced in the target area and (iii) to model the temperature evolution within and beneath the melt pool from $10^4$ to $10^7$ years after impact. Their modeling was applied to an impactor, 12.5 km diameter, traveling at 20 km/sec. They examined two models, one

in which standard rock mechanics were applied to the rocks of the target area and a second in which acoustic fluidization (Melosh, 1979) was called upon to decrease the internal friction of the target rocks. Accepting the assumptions behind the modeling, a number of points resulting from this work have major implications with respect our understanding of Sudbury geology. The first is that the transient crater reached a depth of 40-50 km (Fig. 8.33), but that the zone of impact melting did not extend this deep and would not have affected the sub-continental mantle (Fig. 8.34). Nevertheless, Ivanov and Deutsch's diagrams (Fig. 8.33) show that a substantial amount of lower crustal material could have been brought to surface (as the result of fluid flow and not merely as inclusions or impact melt). [This author's comment: it is likely that the granulites of the Levack complex, which so faithfully rim the northwestern part of the outer margin of the North Range of the SIC, were uplifted in this way]. Ivanov and Deutsch state that the amount to which the mantle would have been uplifted beneath the structure depends on which of their models is correct, being 20 km for the acoustically fluidised model, about 2 km for no contribution from acoustic fluidisation, and an intermediate amount if acoustic fluidisation occurred but was damped out by lithostatic load at depths approaching those of the mantle. Their work calls upon impact melting to be restricted to target rocks within a radius of about 15 km of the center of impact (i.e. beneath only the very central part of the final, 75–100 km-radius crater), but extending to a depth of 20–30 km beneath the surface. An important point raised by this study is the degree of superheat generated within the impact melt, and the length of time over which this would have persisted. According to Ivanov and Deutsch's estimates, the initial temperature of the impact melt would have been about 1727°C, and super-liquidus temperatures (>1177°C) would have persisted for 100,000–250,000 years after impact. Approximately 500,000 years would have been required for the whole of the impact sheet to cool to the solidus (997°C).

### 8.9.2 Development of the SIC and its Associated Mineralization

While the impact origin provides an answer for certain aspects of Sudbury geology, many problems remain.

#### *Structural considerations*

The original shape of the structure, and the extent to which it has been folded is open to question. Cowan et al (1999) found that measurements of remnant magnetic susceptibility showed that the Granophyre is character-

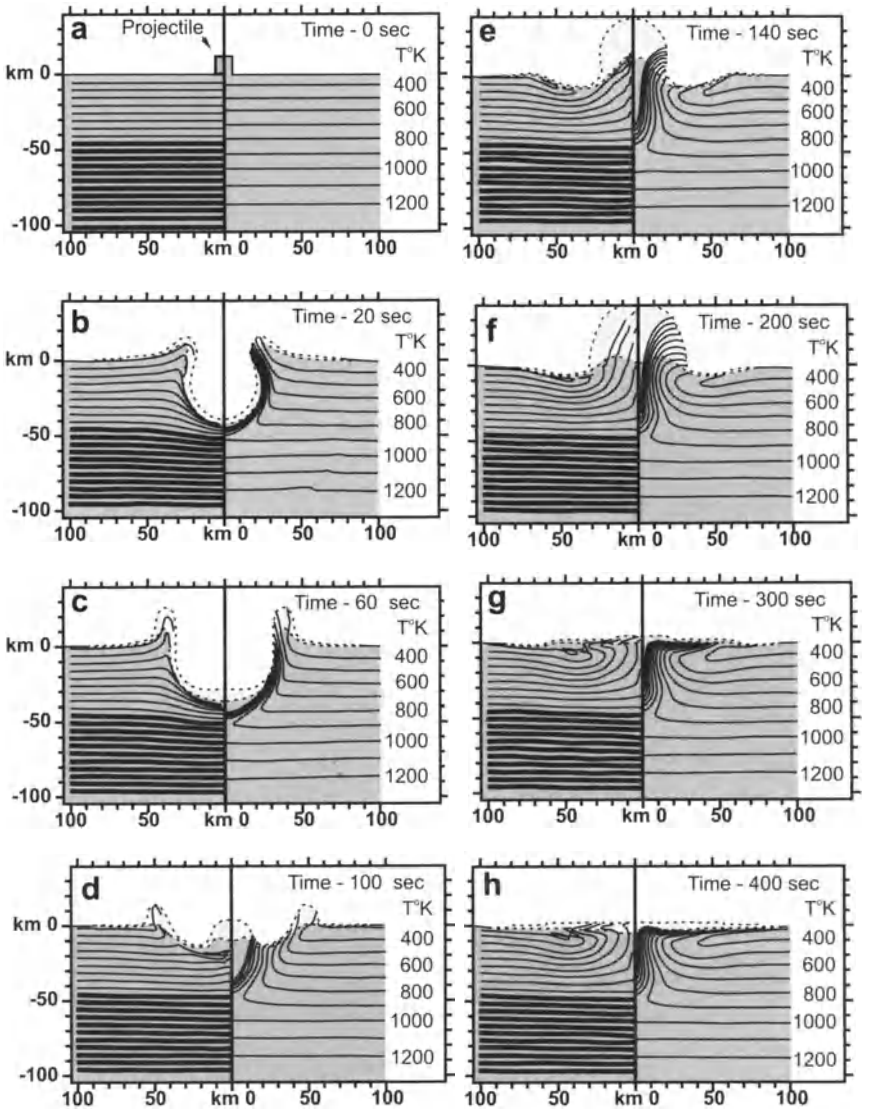


**Fig. 8.33.** Sequence of impact crater formation, simulated with the modified SALE hydrocode for the Sudbury event. A cylindrical projectile with height and diameter both equal 12.5 km is assumed to impact a granite surface at a velocity 20 km/sec. Selected frames correspond to 0, 20, 60, 100, 140, 200, 300, 350 and 400 sec after impact. Vertical (depth) and horizontal (radial distance) scales are in km. The axis of symmetry (zero radial distance) divides each frame in two halves. The left side shows the distortion and displacement of originally horizontal marked layers in the target area. Thick lines correspond to layers below 45 km (the estimated depth of the Moho). In the right half, the displacement and distor-

tion of the isotherms is shown. The variant used to construct this picture was computed for artificially decreased internal friction (Model 2 see text for further explanation). Isotherms from 300°K to 1200°K are shown. To outline the boundary of condensed matter, dark gray tone corresponds to a density above 2000 kg/m$^3$, and light gray tone marks cells with a density less than 2000 kg/m$^3$ but above 200 kg/m$^3$. Cells where the density is less than 200 kg/m$^3$ are left blank. Only the central part of the computational zone is shown. The computational boundaries are approximately 300 km from the point of impact. The assumed friction coefficient is 0.125. From Ivanov and Deutsch (1999)

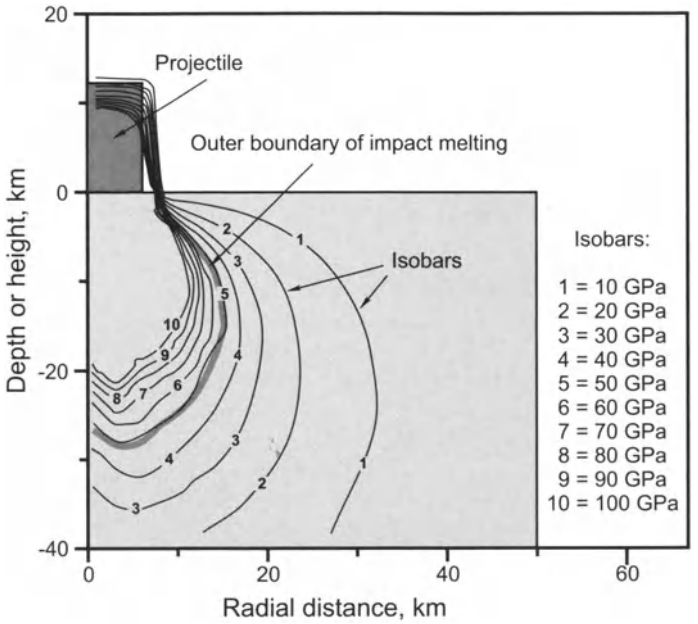


**Fig. 8.34.** Maximum shock pressure isobars overlapping the initial geometry of the target and the projectile. The 50 GPa isobar is close to the threshold of impact melting of the granite target. The maximal melt depth is close to 30 km, which is less than the mantle/crust boundary estimated at 45 km (see text). Zero radial distance is the axis of symmetry. From Ivanov and Deutsch (1999)

ized by a mineral lineation (which they interpreted as magmatic) that is orthogonal to the base of the SIC. Mineral fabrics in the norite and Quartz Gabbro are parallel to the synformal base of the SIC, with a magnetic lineation plunging towards the center of the structure. Their analysis suggested that the attitude in the norite and Quartz Gabbro is consistent with the gravitational strain experienced by crystals settling on an inclined wall. They made the point that the fabrics that they observed are not strained where the curvature of the body is greatest, indicating that folding is not

responsible for the curvature. They concluded that the SIC was emplaced as two separate events, a granophyre event and a norite-gabbro event, along a pre-folded structure which is essentially the present site of the SIC. Subsequently further compression, possibly during the waning post-SIC phases of the Penokean orogeny, gave rise to the South Range Shear Zone (Shanks and Schwerdtner 1991a, b). They remarked that the steep dips along the East Range cannot have resulted from folding; in their view this precluded an origin for the SIC involving in situ differentiation of a melt sheet. While the structural studies have shown that through-going strain related to folding does not appear to have developed in the rocks of the SIC, it is possible that some components of the present basinal structure owe their origin to flexural-slip folding (John Fedorowich, personal communication, 1998). For example, the steeply dipping East Range could possibly have been given its present orientation as a result of the 32 Ma Wanapitei impact, just to the east of the Sudbury basin, with uplift occurring along a series of co-planar reverse faults (e.g. the Waddell Lake fault system).

### *Towards a Genetic Model for the SIC*

Some of the greatest uncertainties remain in fitting the different phases of the SIC into a unified model. Particularly difficult are (i) the origin of the mafic and ultramafic inclusions in the Sublayer; are they derived in part from a pre-existing layered intrusion or did they form during cooling after impact? If the former is true, why do they have zircon and baddeleyite ages of 1.85Ga? If the latter is the case, how could dunites and pyroxenites have crystallized from a magma siliceous enough to give rise to the SIC? Another difficulty is the question of the Granophyre – as discussed above, Ariskin et al. (1999) showed that it is too abundant to be explained easily by fractionation of any reasonable estimate for the original magma composition. Chai and Eckstrand (1994) called upon the Granophyre to represent direct impact melt and the norite to be a mixture of primary basalt with this, but Lightfoot et al. (1997a) argued that the continuity in ratios of incompatible elements between norite and Granophyre implies a single, not a multiple magma source.

As discussed above, Re-Os isotopic systematics for a number of Sudbury deposits indicates that all of the Os in these deposits is likely crustal in origin. The work on the sulfide-bearing melanorite inclusions at Whistle (Hawkesworth et al. 1997), showed that these lie on a mixing line between a younger, low Re/Os end-member (the silicates of the inclusions) and an older (2.6 Ga), high Re/Os end-member (the sulfides). The sulfide component (which could itself be a well-homogenized mixture of two components) is undoubtedly crustal. Thus, it seems that the origin of the osmium

and, by implication, the ores, which one would have thought to have the best preserved evidence of a primary mantle contribution, is crustal. Much of the available isotopic evidence is starting to point to an exclusively crustal origin as the most reasonable explanation for the SIC.

Let us examine the Sudbury Structure from an exclusively crustal viewpoint. It is very rare for a terrestrial magma to intrude with sufficient superheat that 250,000 years will pass before the solidus is reached. Given Ivanov and Deutsch's (1999) demonstration that this was very possibly the case at Sudbury, a much greater degree of country-rock assimilation, particularly melting of the roof rocks but also of those forming the sides and base, is to be expected at Sudbury than is the case with other intrusions. It is suggested that a magma comprising cumulates represented by the South Range Norite+Felsic Norite+Quartz Gabbro represents the initial composition of the impact melt. Note that Chai and Eckstrand (1996), and Lightfoot et al. (1997a) calculated the average composition of the Main Mass of the SIC without including the South Range Norite in their calculations. This rock contains significantly lesser silica then the Felsic Norite which was the main component included by Chai and Eckstrand and Lightfoot et al. It is not easy to tell what rock type was predominant in the undeformed SIC, South Range Norite or Felsic Norite. If their volumes were equal, the average composition of the noritic layer would be significantly poorer in silica and denser than was included in the two foregoing sets of calculations. Given the depth to which Ivanov and Deutsch have indicated impact melting might have extended, the source for this melt would have included the relatively felsic Huronian strata, mafic early Huronian volcanic rocks and perhaps a layered intrusion(s) of the same age, along with Archean tonalites and possibly mafic to komatiitic Archaen greenstones.

It is reasonable to propose that ejecta from the crater contained a higher proportion of felsic Huronian strata and a lower proportion of the proposed Huronian mafic volcanics and related intrusion than the impact melt that remained in the crater. This being so, the roof rocks to the impact melt, which comprised the blanket formed by the fall-back of the ejecta, would have had a more felsic composition than the impact melt itself. As Ariskin et al. (1999) suggested, the hot impact breccias forming the roof would have been subjected to very considerable melting as a result of the superheat of the impact melt. Incorporation of the melted suevite into the upper part of the impact melt would have given it a lower density than the lower part.

Drawing on analogies with the Campbell and Turner's (1986) analogue and model studies applicable to inhomogeneous magma chambers, Naldrett (1999b) suggested that a compositionally stratified magma, such as

as that proposed at Sudbury, would have separated very quickly into two density stabilized layers, a lower density layer (= the Granophyre) overlying a higher density layer (= the norites) with an intervening boundary layer (Fig. 8.35). Both layers would have been convecting, but convecting separately. Heat from the cooling norite would have been convected up to the boundary layer, conducted across it and then convected up again through the granophyric layer where it would have augmented the melting of the roof rocks. Within the lower noritic layer, convection currents would have swept down the relatively cool margins of the basinal structure, and, once the solidus was reached and silicates began to crystallise, would have caused the downward and inward lineation that Cowan et al. (1999) have documented in this unit. The same would likely have occurred in the granophyric layer, but portions of the SIC in which the Granophyre was in contact with the walls are no longer preserved; the only border with which the Granophyre can be observed to be in contact is the roof. Once the granophyric layer reached its liquidus temperature, it is likely that crystallization occurred perpendicular to the isotherms, that is downward perpendicular to the roof. This crystallization would give rise to a fabric orthogonal to the roof, thus accounting for the observation of Cowan et al. (1999).

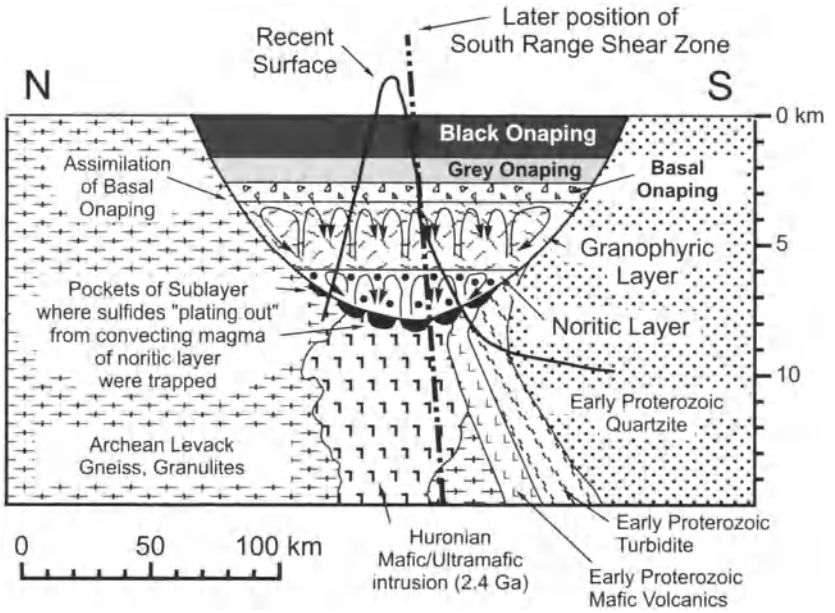


**Fig. 8.35.** Model of the Sudbury Igneous Complex after readjustments within the crater, and before complete consolidation of the Norite and Granophyre (adapted from Naldrett 1999a)

At first sight this model, which has much in common with that of Chai and Eckstrand (1996), would seem to be in conflict with the trace element data of Lightfoot et al. (1997a). However, the principal difference between the lower noritic and upper granophyric layers is that the former contains a higher proportion of postulated mafic material than the latter. The incompatible elements would have been derived largely from the felsic component incorporated in each, which would have been from essentially the same source and it is to be expected that ratios of incompatible elements in each will be similar. Lightfoot et al. (1977a) admit this possibility, and, in fact, Lightfoot et al. (2001) call upon a similar division into mafic and felsic layers of magma to explain variations in Ni and Cu in the SIC during its cooling and the separation of sulfides.

Lightfoot et al. (1997a) pointed out that a problem existed with respect to the Ni, Cu and S contents of the SIC if this is the result of melting of "average crust" This point is illustrated in Table 8.7. Average Felsic Norite contains 126 ppm Ni and 155 ppm Cu, not counting the Ni and Cu in the ores that should be back-calculated into any source magma. This is very much higher than the 25 ppm Ni and 30 ppm Cu which are characteristic of average crust. Even when a reasonable amount of granophyre is included with the norite, the Ni and Cu contents are still much higher than average crust. The model involving a lower layer of norite magma and upper zone of granophyre magma that has been proposed above, in which the noritic layer contains a much greater proportion of melted mafic/ultramafic rock than the granophyric layer, provides an answer to this dilemma.

The boundary layer between the two principal layers of magma proposed here would not only have been a zone of heat interchange. Diffusion of chemical constituents would also have been occurring across this layer. Watson and Jurewicz (1984) have shown that alkalis diffuse along chemical gradients much more quickly than $Al_2O_3$ or $SiO_2$, so that, given a higher alkali content in the granophyric than the norite layer, the upper part of the norite layer would have been subjected to a constant influx of alkalis from the overlying felsic layer. These would have been picked up by the convecting norite magma and would rapidly have become homogenised throughout that part of it which remained unsolidified.

Calling on the "norite" layer in Fig. 8.35 to be a well-homogenized mixture of felsic and mafic rocks in the target area also provides a clue, as Golightly (1994) suggested, to the formation of the high proportion of rich accumulations of sulfide ore at Sudbury. If the mafic rocks of the target area had contained sulfides, these would have dissolved in the impact melt. Subsequent felsification of the impact melt through the incorporation of material from the roof and walls, as discussed above, would have produced the right conditions for sulfide immiscibility (Li and Naldrett 1993; see

discussion in Chap. 2). The immiscibility might not have occurred immediately, but sulfides could well have become immiscible during cooling at a temperature that was still well above the liquidus of the hybrid magma. The high temperature would have facilitated rapid convection and efficient segregation of the immiscible sulfides (see below). Since the sulfides had developed from a magma that was a melt of Archean and early Proterozoic country rocks, they would have been characterized by very radiogenic Os.

### *Ni and Cu distribution in the SIC rocks*

Lightfoot et al. (2001) presented the most recent data on the distribution of Ni, Cu and PGE in the SIC. They showed that there is a steady decrease in Ni and Cu upward in the Mafic and Felsic Norite from values of 300–1000 ppm of each in the Mafic Norite through values of 100–300 ppm at the base of the Felsic Norite to about 15 ppm of each near the top of the Felsic Norite (Fig. 8.36). Variations in Cu/Zr (Fig. 8.37) and Ni/MgO indicate that the magma became sulfide saturated when it was precipitating rocks at or slightly below the base of the Main Mass norite (Note: it is difficult to be precise about the exact level because rocks at about this level have accumulated settling sulfides which obscure the chemical criteria for saturation). As mentioned above, Lightfoot et al. (2001) argued that the marginal Quartz Diorite of the Worthington offset is close in composition of the average magma responsible for the SIC, except for its chalcophile element content. The average Ni and Cu contents of this rock are 83 ppm Ni and 98 ppm Cu. The lowest commonly observed values is 50 ppm of both Ni and Cu, which is close to the calculated contents in the country rocks of the target area at Sudbury. The difference of 35 ppm in both Ni and Cu between the upper Felsic Norites (15 ppm) and the lowest values in the marginal offset Quartz Diorites (50 ppm) are assumed to have been stripped out of the Main Mass magma due to the segregation of sulfide. Lightfoot et al. (2001) state that this amount is more than ample to account for their estimate of these metals within the Sudbury ores. Using experimentally derived partition coefficients, and assuming an R factor of 1000, they calculated that the original SIC magma contained 210 ppm Ni and 109 ppm Cu at the time of the segregation of the contact (as opposed to the offset) deposits. They suggest that this elevated value, as compared to the Offset marginal rock, is due to the SIC magma separating into mafic and felsic layers after initial emplacement of the Offsets and before sulfide immiscibility was attained and sulfide segregation occurred. Ni and Cu within the whole intrusion then became concentrated in the mafic layer, increasing their concentrations dramatically.

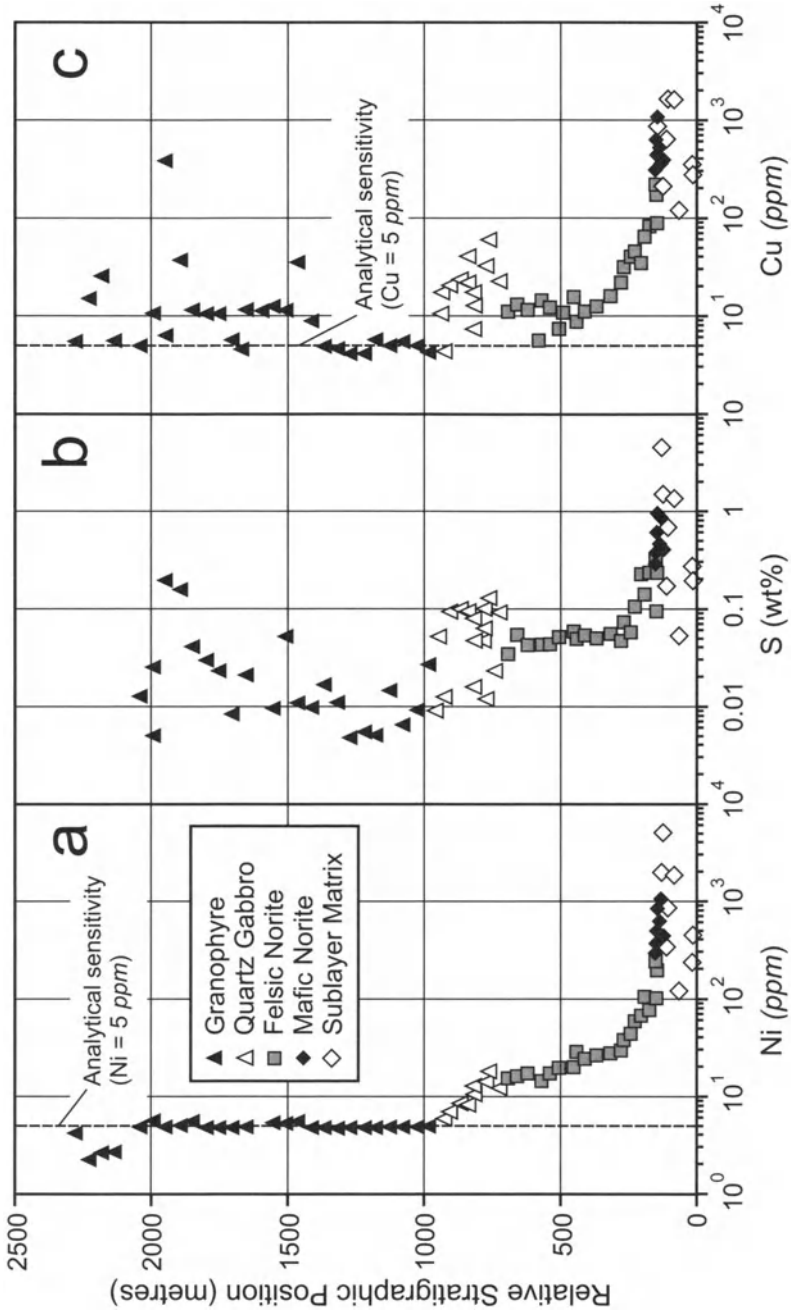


**Fig. 8.36.** Variations of Ni (a), S (b), and Cu (c) in borehole MAC-91 and surface outcrops of Granophyre in the East Range. The location of borehole MAC-91 is shown in Fig. 8.15. After Lightfoot et al. (2001)

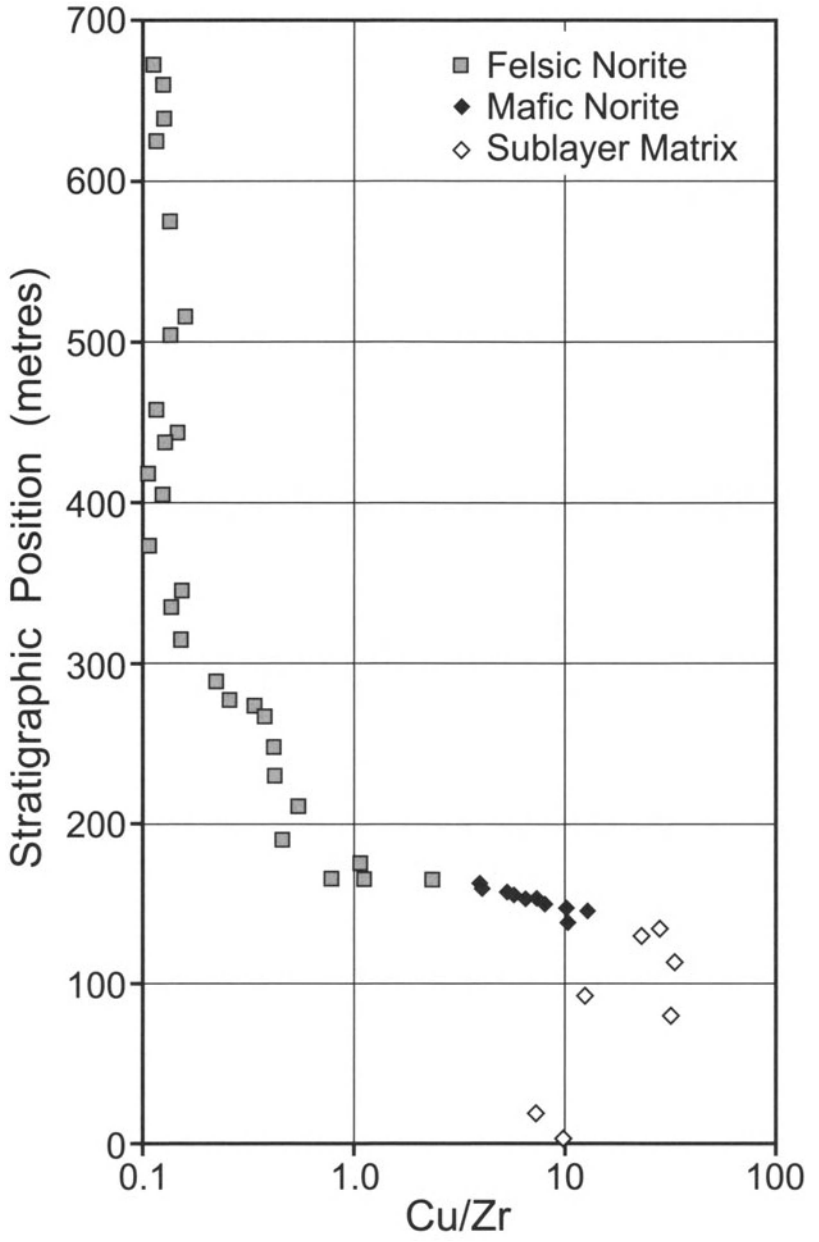


**Fig. 8.37.** Variations of Cu/Zr ratios in the SIC Felsic Norite, Mafic Norite, and Sublayer intersected in borehole MAC-91 in the East Range (the location of the borehole is shown in Fig. 8.15). After Lightfoot et al. (2001)

### *Origin of Inclusions in Sublayer*

If the scenario that the SIC is entirely an impact melt is correct and no primary mantle component is involved, how does one explain the 1.85 Ga age for the ultramafic inclusions obtained by Corfu and Lightfoot (1997)? As discussed above, trace element and isotopic data indicate that Sublayer from different parts of the Sudbury structure have a distinctly "local" signature, dissimilar both to each other and to the Main Mass of the SIC. It seems likely that these represent zones of local impact melt that did not become homogenized within the main body of the impact melt, but were protected by the embayments in which they formed. Incorporation of mafic/ultramafic rocks into the Sublayer melts may have resulted in local inhomogeneities, involving lenses of melt that were more mafic than the surrounding Sublayer magma. These could have crystallized to give rise to the melanocratic pods that were dated by Corfu and Lightfoot. The shattered remnants of this local material that were described by Scribbins et al. (1984) probably represent unmelted remnants of the mafic/ultramafic material. The sources of the mafic/ultramafic inclusions are probably in part ultramafic sills which have been intersected in drilling within the footwall of the North Range and in part the proposed Huronian mafic/ultramafic intrusion (Fig. 8.35).

### *Concentration of Ni-Cu Sulfides*

Souch, Podolsky et al. (1969) and Naldrett and Kullerud (1967) were amongst the first to emphasize the importance of the Sublayer as the key factor to the presence of sulfide concentrations along the footwall of the SIC. It was proposed (e.g. Naldrett and Kullerud 1969) that sulfides were introduced along with younger Sublayer magma that intruded along the basal contact. Since the appreciation that the SIC is most likely an impact melt with no primary mantle component, more thought has been given to the probability that sulfides settled from the Main Mass of the SIC in situ. Keays and Lightfoot (1999) and Lightfoot et al. (2001) have drawn attention to the progressive increase in Ni in units of the SIC from the Granophyre through the Quartz Gabbro into the Felsic and Mafic Norites (Fig, 8.36a), which loosely parallels the increase shown by S (Fig. 8.36b). Cu shows a similar but more scattered increase (Fig. 8.36c); Keays and Lightfoot (1999) attribute the scatter to hydrothermal remobilization of Cu.

Keays and Lightfoot (1999) also examined the Ni and Cu contents of the Felsic Norite, Mafic Norite and Sublayer as though the metals were held entirely in sulfide. Both metals show a progressive increase with depth in the Felsic Norite, but their plots show no convincing downward increase in

the Mafic Norite (Fig. 8.38). Attributing all of the Cu to sulfide is probably correct, but as Keays and Lightfoot remark, some of the Ni in their samples is held in mafic minerals, primarily pyroxene, so that attributing all of this Ni to the sulfide in the sample gives an overestimate of Ni in sulfide –

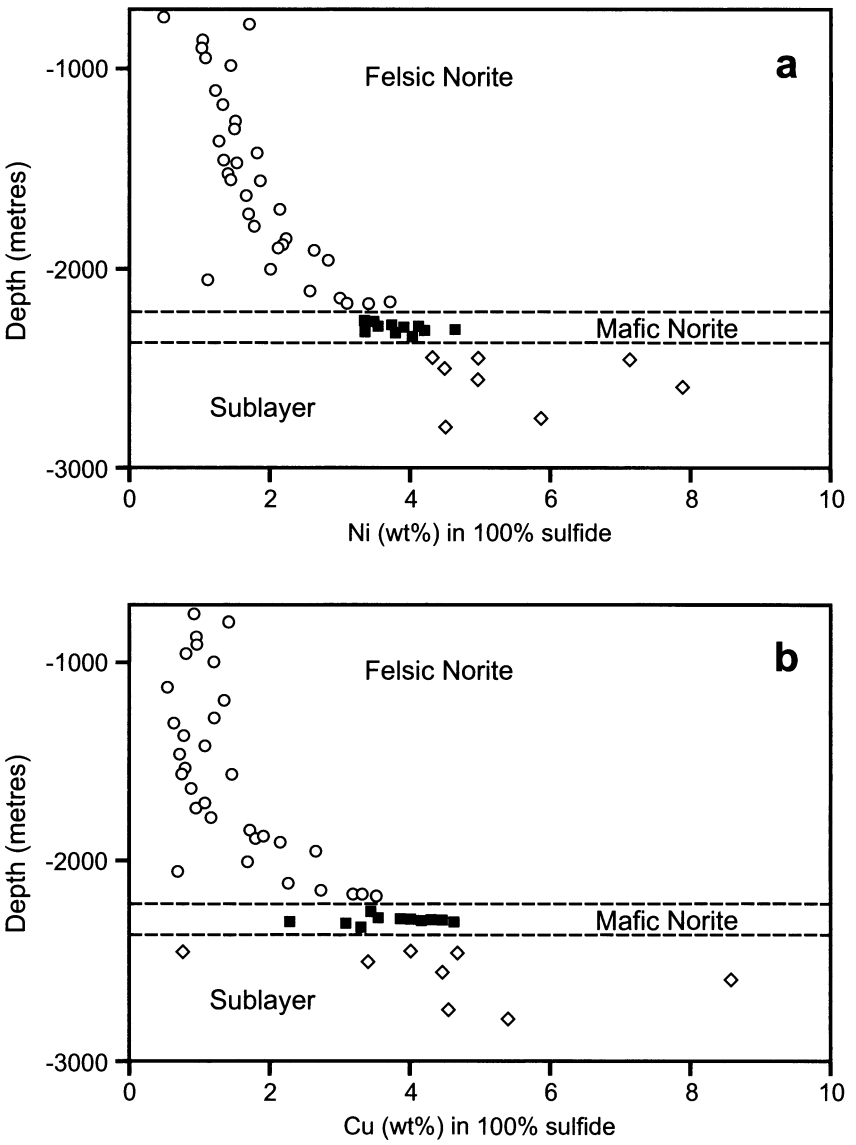


**Fig. 8.38.** Variation of Ni in 100% sulfides through Mafic Norite and Sublayer in two boreholes at Victor deposit (a, b) and one borehole at Trillabelle deposit (c). After Naldrett et al. (1999)

this effect will only be significant in sulfide poor samples. Keays and Lightfoot (1999) developed a model in which the segregation of sulfide during crystallization of the Felsic Norite resulted in depletion of the remaining magma in chalcophile metals, resulting in progressively later segregating sulfides forming from progressively more chalcophile-depleted magma, and thus containing lesser concentrations of these metals themselves.

As discussed above, the data of Lightfoot et al. (2001) indicate that Sublayer and Mafic Norite contain rather similar values of Ni and Cu (Fig. 8.36). Earlier Keays and Lightfoot (1999) noted that when their data are examined on the basis of Ni and Cu content in 100% sulfides, the Sublayer sulfides in the hole that they studied, MAC-91, contain an average of 5.8 wt% Ni in comparison with 4.1 wt% Ni in the Mafic Norite, suggesting that the Sublayer sulfides in the hole have a slightly higher Ni tenor than those in the Mafic Norite. However, the comprehensive data of Naldrett et al. (1999) for other areas do not support this. Fig, 8.39 shows the variation in Ni in 100% sulfides with depth in 2 drill holes at the Victor deposit and one drill hole in the Trillabelle deposit. Very little change is observed with depth in the Mafic Norite, and values in the underlying Sublayer are very similar to those in the Mafic Norite. Also shown are histograms showing the frequency distribution of Ni in 100% sulfides in all of the Sublayer samples collected from each locality (Fig. 8.40). It is seen that the maxima agree closely with the values in the adjacent Mafic Norite. It would seem that there is no progressive downward change in metal values throughout either the Mafic Norite or Sublayer, at least in the two localities where the availability of samples allows this to be examined. (Note: The use of Cu in making comparisons has been avoided, since the loss or gain of a Cu-rich liquid differentiate can greatly affect the Cu content of samples. As explained in Chap. 2, Ni is much less sensitive than Cu to variations brought about by differentiation.).

Table 8.8 gives average values for Ni, Cu, Pt, Pd and Rh in 100% sulfides for different ore types from some of the deposits studied by Naldrett et al. (1999). Despite the similarity between Mafic Norite and Sublayer, it is seen that in five (McCreedy West, Fraser, Strathcona, Victor and Creighton) of the six deposits where comparable data exist, the sulfides of footwall ore (Footwall Breccia ore in the North and East Range contact deposits, inclusion-bearing sulfide in the case of the South Range deposits) contains more Ni than overlying Sublayer ore. The sole exception is Crean Hill. The reason for this is not established. It could be due to Ni preferring the fractionated liquid during initial stages of crystallization of the sulfides in the Sublayer, and migrating, along with Cu, Pt, Pd and Au in the fractionated liquid into the footwall. If this were so, one would expect sulfides

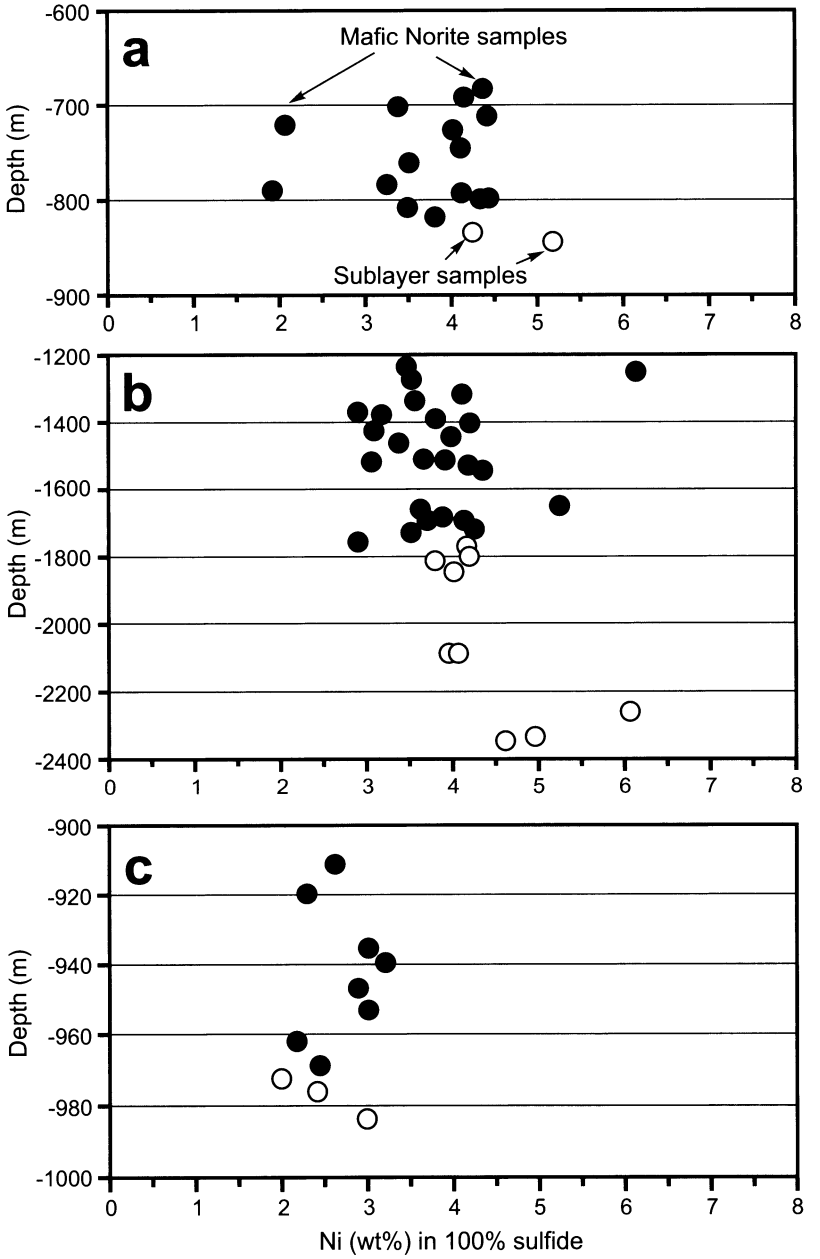


**Fig. 8.39.** Variation of Ni in 100% sulfides through Mafic Norite and Sublayer in two boreholes at Victor deposit (a, b) and one borehole at Trillabelle deposit (c). Data from Naldrett et al. (1999)

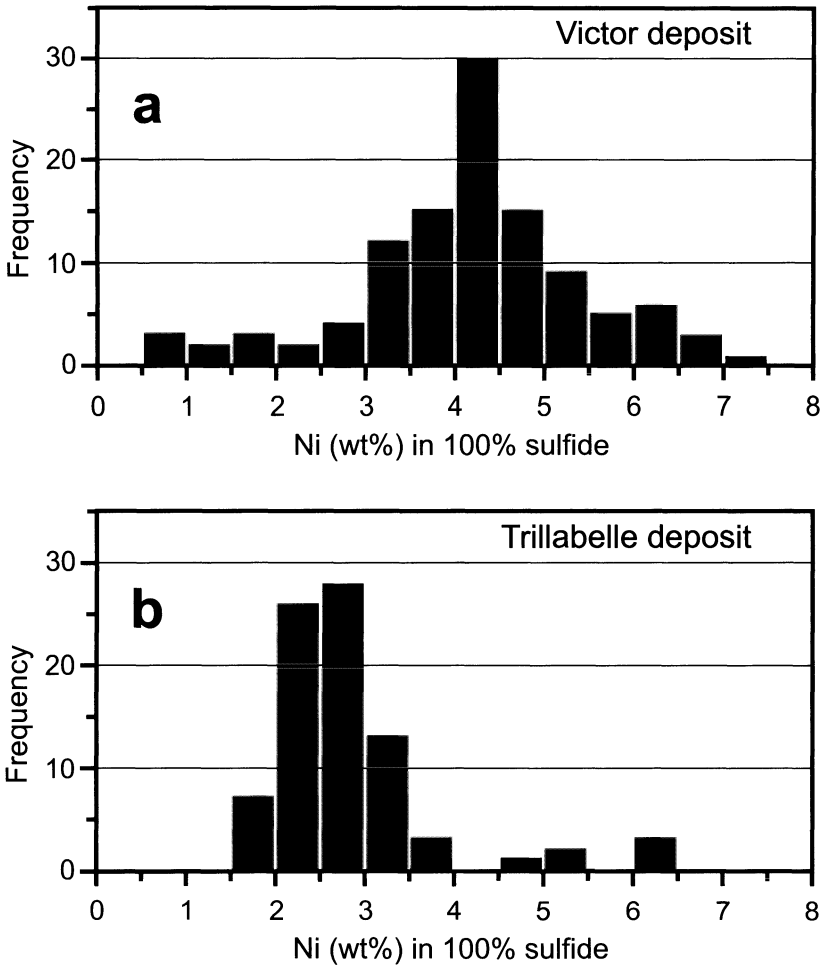


**Fig. 8.40.** Histograms showing the frequency distribution of Ni in 100% sulfides in all of the Sublayer samples collected from the Victor (a) and the Trillabelle (b) deposits. Data from Naldrett et al. (1999)

of the footwall ore to be poorer in Rh than those of the Sublayer. This is true of Fraser, Strathcona, and Victor, but not the case at McCreedy West, Creighton and Crean Hill. At the last 3 deposits, sulfides of a higher R factor gave rise to the footwall ores than the sulfides in the Sublayer ore. The most likely explanation is that sulfides present at the footwall segregated earlier from a magma that was less depleted in chalcophile metals than those in the overlying Sublayer and Mafic Norite. It has already been discussed that the Offset Deposits contain sulfides that are much richer in PGE than most contact deposits (Table 8.5), and that they probably segre-

gated from an even less depleted magma. Thus there seems to have been a continuum of sulfide segregation, (1) early segregation producing the richest sulfides, part of which were then injected into the Offsets, along with inclusion-bearing magma, (2) slightly later segregation giving rise to the majority of the sulfides that settled into the Footwall Breccia, (3) even later segregation that gave rise to sulfides in Sublayer and Mafic Norite and (4) continued segregation that is recorded in the steady upward depletion in chalcophile elements into and within the Felsic Norite.

**Table 8.8.** Average contents of Ni, Cu, Pt, Pd and Rh in different ore types from Sudbury Contact Deposits, recalculated for 100% sulfide (after the data of Naldrett et al. 1999)

| Deposit | Ore Type | No | Ni | Cu | Pt | Pd | Rh |
|---|---|---|---|---|---|---|---|
| **North Range** | | | | | | | |
| Trillabelle | Sublayer | 17 | 2.68 | 1.68 | 322 | 224 | 36 |
| McCreedy West | Sublayer | 11 | 3.82 | 0.51 | 131 | 47 | 61 |
| | Footwall Breccia | 25 | 5.14 | 2.44 | 788 | 873 | 175 |
| Craig | Footwall Breccia | 255 | 5.94 | 4.07 | 6 850 | 2 068 | 104 |
| McCreedy East | Sublayer | 8 | 5.27 | 2.21 | 629 | 436 | 141 |
| Fraser | Sublayer | 35 | 4.52 | 2.30 | 792 | 571 | 216 |
| | Footwall Breccia | 133 | 5.23 | 3.85 | 1 966 | 1 118 | 117 |
| Strathcona | Sublayer | 10 | 3.06 | 0.37 | 113 | 103 | 59 |
| | Footwall Breccia | 25 | 3.86 | 1.32 | 408 | 337 | 19 |
| **East Range** | | | | | | | |
| Victor | Sublayer | 120 | 4.35 | 3.24 | 943 | 519 | 229 |
| | Footwall Breccia | 63 | 5.07 | 1.94 | 683 | 461 | 75 |
| **South Range** | | | | | | | |
| Lindsley | Sublayer | 209 | 4.06 | 3.86 | 2 238 | 2 093 | 353 |
| Creighton | Sublayer | 89 | 6.57 | 7.28 | 3 685 | 1 994 | 571 |
| | Inclusion-rich ore | 68 | 7.39 | 5.89 | 2 274 | 3 261 | 632 |
| | Massive Sulfide | 21 | 6.82 | 7.32 | 1 749 | 2 093 | 538 |
| Crean Hill | Sublayer | 18 | 4.35 | 6.81 | 5 417 | 2 632 | 334 |
| | Inclusion-rich ore | 29 | 3.53 | 4.10 | 5 424 | 4 370 | 753 |
| | Massive Sulfide | 14 | 4.06 | 3.86 | 1 938 | 3 268 | 396 |
| Gertrude | Sublayer | 115 | 4.73 | 2.72 | 559 | 339 | 263 |

*No* Number of Samples. Ni, and Cu in wt%; Pd, Pt and Rh in mg/t (ppb)

From the foregoing discussion, it would seem that sulfides started to segregate relatively early during the cooling of the SIC, very likely before the Main Mass magma had reached its liquidus.

The analogue experiments of Kiersnowski (2000) demonstrated that convection speeds up the process of removal of immiscible sulfide from a body of magma. In many of her experiments, particles representing sulfide droplets showed essentially no tendency to settle over periods of a week or

more under static conditions, but were completely removed in a few days from convecting magma. Kiersnowski showed that as the convecting magma sweeps past a stagnant boundary layer that developed on the walls and floor of the tank in her experiments, particles adjacent to this layer become entrained within it. They then settled through the layer to concentrate near the lower contact of the tank. It is suggested here that these experiments may have application to Sudbury. Once droplets of immiscible sulfide developed in the convecting noritic layer, the droplets adjacent to the boundary layer became entrained within it. The stagnant layer would have been thicker within footwall embayments, and the sulfides would have settled to concentrate primarily in these structures.

## 8.10 Conclusions

In conclusion, based on the work discussed above, the following scenario is proposed for the development of the Sudbury structure:

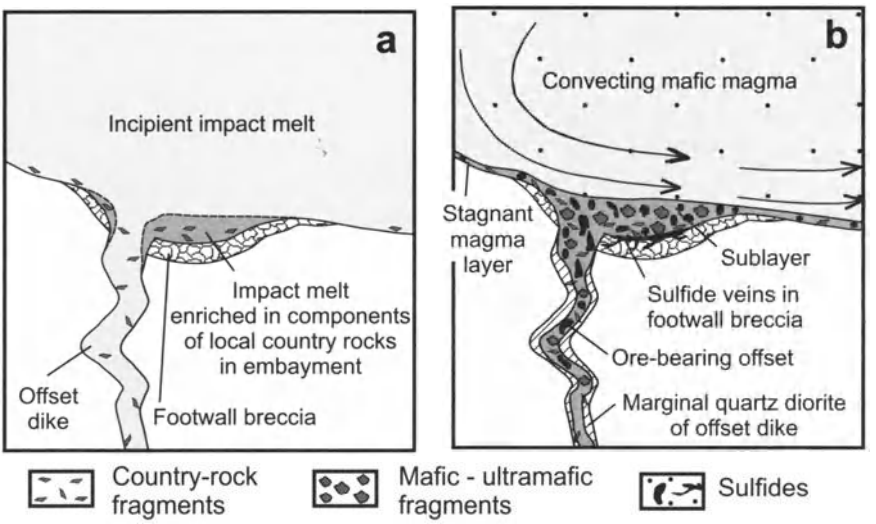


**Fig. 8.41.** Model for development of offset dikes and embayments in the footwall of the Sudbury Igneous Complex initially (a) and subsequently (b). Adapted from the model of Lightfoot et al. (2001, their Fig 12)

1. Prior to the Sudbury event, the area was underlain by Huronian sediments and underlying volcanic rocks which rested unconformably on Archean gneisses. These were cut by a mafic/ultramafic layered intru-

sion which was probably part of the 2.45 Ga mafic magmatism that is known to have accompanied the opening of the Huronian ocean.

2. The impact of a meteorite resulted in the excavation of a transient crater, 40 km deep, 60 km diameter. The impact also resulted in the formation of some of the Sudbury Breccia, ejection of country rocks in the target area, and melting of the target rocks, including a high proportion of the Huronian mafic/ultramafic intrusion, to form the "norite" layer. Pockets of molten rock filled embayments in the footwall (Fig. 8.41a). The embayments were also filled by fractured country rocks and acted as traps for fragments of the mafic/ultramafic intrusion that was present in the target area (Fig. 8.41a).
3. Rapid rebound at center of crater resulted in lower crustal high-grade gneisses of the Levack Complex being brought to surface beneath the melt rock filling the crater.
4. Part of the ejecta fell back into the crater to form a 2 km blanket over the melt rock. The Green Member of the Onaping Formation was the uppermost unit of this ejecta blanket.
5. The crater started to slump around the margins and the initial crater was enlarged in this way to a diameter of about 200 km. Other types of Sudbury Breccia formed at the contacts between structural blocks during this readjustment. Zones around the margin of the crater, where Sudbury Breccia is abundant, represent original zones of weakness along which slumping was particularly concentrated. Fall back breccia that had fallen outside the periphery of the crater was washed back into the crater during this phase of tectonic adjustment to give rise to the Black Member of the Onaping Formation. These units contain clasts of a black mudstone of unknown provenance.
6. The melt rock filling the crater was about 500° C above its liquidus temperature. This resulted in extensive melting of the wall rocks, in particular of the overlying Basal Member of the Onaping Formation. Mafic/ultramafic fragments within the embayments became melted at this stage, and acquired felsic components from the overlying impact melt to recrystallize as pods of melanorite.
7. The incorporation of material acquired as a result of melting of the roof rocks to the upper part of the SIC resulted in a strong chemical gradient developing within the impact melt, from a more felsic top to more mafic base. This compositional heterogeneity rapidly became stabilized as the impact melt separated into two layers, an upper "Granophyric" layer and a lower "Noritic" layer, both of which convected independently (Fig. 8.35). Continued melting of the breccias of the overlying Onaping Formation increased the felsic component in the Granophyric Layer.

8. As the impact sheet cooled, immiscible sulfides formed in the lower, "Noritic" layer, and were swept around in the rapidly convecting, low viscosity, superheated magma. They became entrained in a stagnant boundary layer lining the walls of the crater, concentrating particularly in embayments where the zones of stagnant magma were unusually thick and contained many country-rock fragments. Fragments of the Huronian mafic/ultramafic intrusion, that is hypothesized to have been present at depth in the area of the impact, also became concentrated and protected within these embayments (Fig. 8.41b). The sulfides soaked into Footwall Breccias at the base of the embayments and still later sulfides accumulated within the overlying Sublayer and Mafic Norite. The superheated environment existing in the SIC during this stage in its development provided the perfect conditions for sulfide settling and entrapment.
9. Magma from the stagnant layer was forced outward and downward along zones of weakness (i.e. zones of Sudbury Breccia) to form quartz diorite dykes or "offsets". Inclusion and sulfide-rich material that had developed within the embayments were driven out along with the rest of the magma, but became concentrated towards the centres of the dykes as a series of lenses which now form the pod-like ore zones within the offsets (Fig. 8.41b).
10. Since sulfide accumulation from the overlying convecting Main Mass norite was a progressive process, with the earliest sulfides settling from undepleted magma, and later sulfides settling from progressively more depleted magma, the earliest sulfides to settle out were the richest in chalcophile metals. The offsets developed at an early stage during the cooling of the SIC, and therefore contain sulfides that settled out early, so that these were richer than those that settled later. The latter form the bulk of the contact deposits.
11. With further cooling, the "Noritic" layer reached its liquidus temperature, and pyroxene followed very quickly by plagioclase started to crystallize. Since the walls were cooler than the central part of the layer, currents of magma swept down them (Fig. 8.35) giving rise to the lineated fabric documented by Cowan et al. (this volume). The upper "Granophyric" layer reached its liquidus at a later stage. The high viscosity of this very siliceous zone may have damped out convection after the temperature fell to a certain level and the fabric of the crystallizing minerals developed at right angles to the isotherms within the melt sheet (i.e. orthogonal to the roof).
12. Sulfides continued to segregate from the Felsic Norite as it crystallised, but, as Keays and Lightfoot (1999) proposed, the continued segregation of sulfide led to the remaining Felsic Norite magma becoming progres-

sively more depleted in chalcophile metals, giving rise to the upward decrease in the metal content of the sulfides (Fig. 8.38).

13. Some limited later mobility of the Sublayer would seem to be called for in view of conflicting age relationships that have been reported with respect to the Main Mass norites (Naldrett et al. 1984b).

I cannot finish this chapter without passing the comment that Sudbury differs in very many respects from other world-class accumulations of magmatic sulfides. Sudbury was used for so long as the archetype for these deposits, and yet it has turned out to be a very poor model to use. The superheat which appears to have existed for so long, and the formation of magma as the result of a process originating from above, rather than below, produced an unusual environment in which sulfides formed and accumulated in a manner quite different to the way in which deposits have developed elsewhere. It remains to be seen just how "unique" this unusual environment is. It is possible that it required not only the impact of a very large (10-15 km diameter) impactor, but also a special arrangement of rocks in the target area, comprising felsic rocks close to the surface and mafic/ultramafic rocks at depth.

# 9 Platinum group element (PGE) deposits

PGE accessible to mankind are derived from the earth's mantle, with possibly a component coming from the core. This chapter is concerned with (a) the distribution and behavior of PGE in the mantle and in magmas derived from the mantle, (b) the characteristics of deposits derived directly or indirectly from these magmas, and (c) the methods by which, and environments in which the PGE have been concentrated.

## 9.1 PGE in Mantle-derived Rocks and Mafic/Ultramafic Lavas

Crocket (2002) has summarized available data on the distribution of PGE, Ni and Cu in mantle-derived rocks and mafic/ultramafic lavas. Looking first at his averages for mantle rocks normalized against concentrations in C1 chondrite (Fig. 9.1), those that he classifies as orogenic lherzolites and harzburgites are from ultramafic bodies that have been repeatedly metamorphosed and possibly affected by metasomatism, which, he cautions, may have affected their PGE+Au contents. They have higher Pt and Au than other mantle rocks (ophiolites excepted), which may be due to the metasomatism that they have undergone. Most ophiolite samples are from convergent margins where the ophiolite is either from the wedge of mantle overlying the downgoing slab which again may have been affected by fluids rising from the down-going slab, or from a back-arc setting, which is also prone to metasomatism. The mantle nodules are from continental environments, and have been brought to surface relatively rapidly, mostly within eruptions of alkalic basalt. They probably provide the most reliable samples (albeit not totally reliable) of the sub-continental lithosphere; most PGE+Au concentrations in nodules are about 1/200 of that of C1 Chondrite.

Crocket's averages for igneous rocks that have been derived from the mantle are compared with average spinel lherzolite on a C1 chondrite-normalized basis in Fig. 9.2. All derivative melts are enriched in Cu by a factor of 3-8 over spinel lherzolite. Since Cu acts in an incompatible

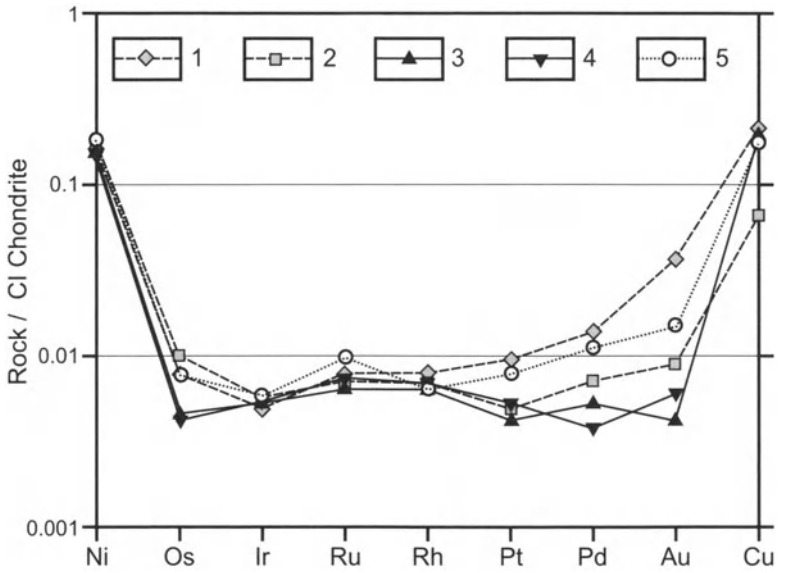


**Fig. 9.1.** Average contents of PGE, Au, Ni, and Cu (normalized to CI Chondrite) in rocks, representing mantle (from Crocket 2002). 1 = Orogenic Lherzolite; 2 = Orogenic Harzburgite; 3 = Spinel Lherzolite Nodules; 4 = Harzburgite Nodules; 5 = Ophiolite Harzburgite

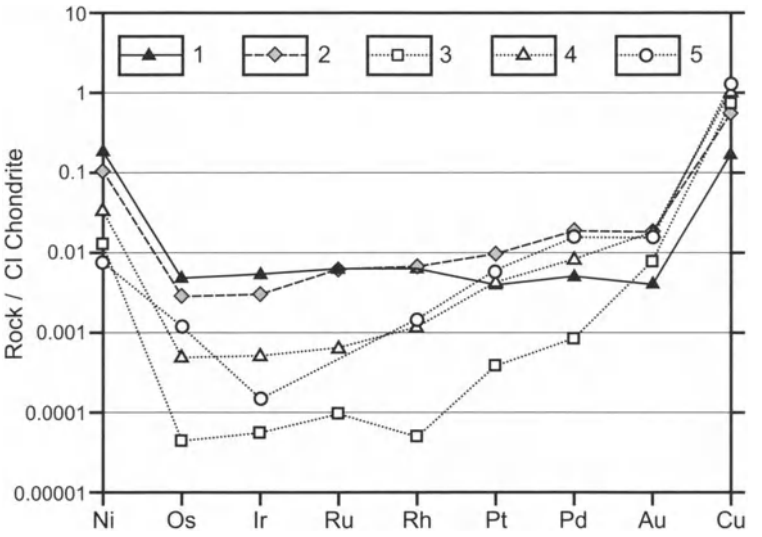


**Fig. 9.2.** Average contents of PGE, Au, Ni, and Cu (normalized to CI Chondite) in mantle-derived volcanic rocks in comparison to Spinel Lherzolite Mantle Nodules (from Crocket 2002). 1 = Spinel Lherzolite Nodules; 2 = Komatiites; 3 = MORB; 4 = OIB; 5 = Continental Flood Basalts

manner during partial melting once all sulfides have been removed from the source, this behavior is explicable so long as the degree of melting has been sufficient to remove all sulfides. As might be expected, komatiites, which represent the highest degree of partial melting of the magma types considered by Crocket, have profiles that are the closest to mantle profiles; they are enriched in Pd, Pt and Cu by a factor of about 4, contain similar amounts of Rh and Ru, and are slightly depleted in Ir and Os. The behavior of Rh, Ru, Ir and Os suggests that these metals act as though they are compatible in some phase or phases in the mantle residue and are thus retained in this residue. Ocean Island (OIB) and Continental Flood (CFB) basalts have similar profiles, except for differences in Ir, Os and Ni (no data is available for Ru in CFB's), which is probably partly due to differences in the extent of fractionation that they have undergone. Overall, their PGE+Au+Cu contents suggest that they are the result of sufficient partial melting of the mantle to remove all sulfide but that much Rh, Ru, Ir, Os and, of course Ni, is retained in the source. As is well known, MORB's are the major exception, containing only 1/10 of Pt and Pd, 1/100 of the Rh, Ru, Ir and Os, and 1/15 of the Ni of typical mantle material. Following many author's (Czamanske and Moore 1977; Keays and Scott 1976), Crocket (2002) attributes this to MORB having equilibrated with sulfide and the sulfide having stripped out those metals with high partition coefficients, but having affected those metals with lower coefficients (e.g. Cu) to a much lesser extent. This cannot be the complete answer, since Pt and Pd are depleted substantially less than Rh, Ru, Ir and Os, although experimental data indicate that the partition coefficients of most of the PGE (Ru is a possible exception) are comparable. Much of the PGE may have been stripped out by sulfide, but it would seem that the initial melt was already depleted in Rh, Ru, Ir and Os due to these metals having been retained in the source.

The North Atlantic Igneous Province (NAIP), shown in Fig. 9.3 is now one of the most intensively investigated (from the viewpoint of PGE) mafic/ultramafic provinces associated with continental break-up. Andersen et al. (2002) and Momme et al. (2003) provided some interesting insights into the PGE contents of the sources of the magmas contributing to this province, and of their subsequent behavior during the fractionation/mixing. The data set for PGE is particularly complete for lavas and intrusions from the East Coast of Greenland (lavas occur along a 400 km-long stretch of coast from Kangerlussuaq fjord in the south to Kangertittivaq in the north), offshore of this coast (results of Ocean Drilling Programme legs 152 and 163 which were located 300-500 km southwest of Kangerlussuaq)), and from Iceland; some of the results of this work are discussed below.

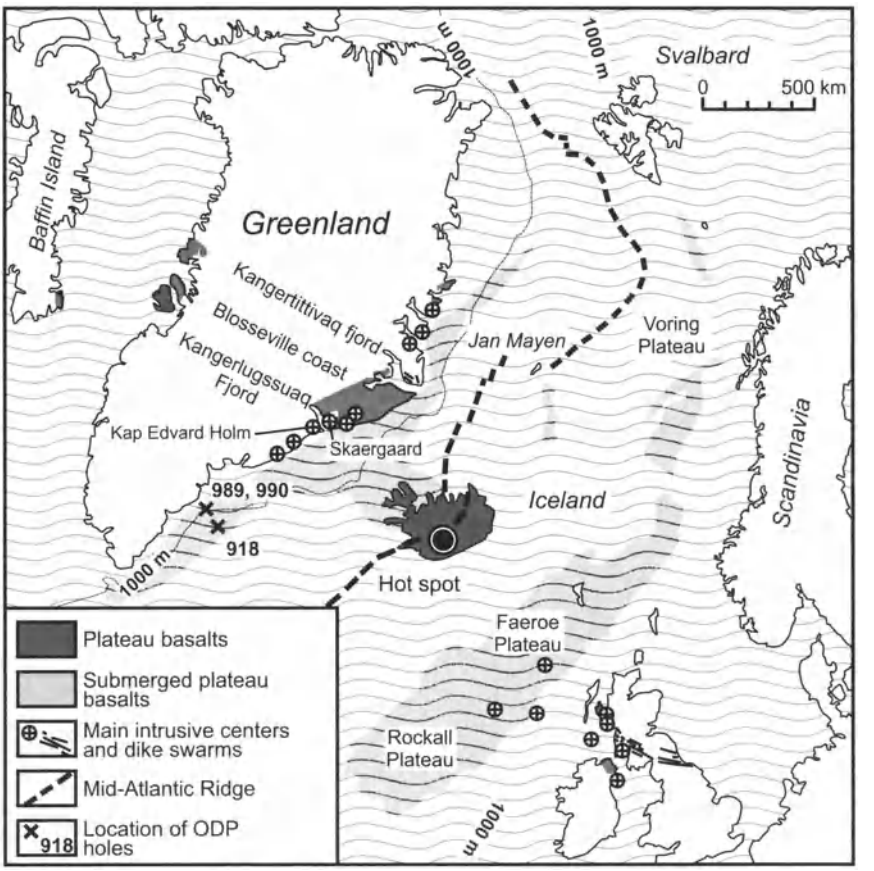


**Fig. 9.3.** Generalized map of the North Atlantic Igneous Province (from Andersen et al. 2002)

Andersen et al. (2002) noted that the behavior of Cu with respect to fractionation (as recorded by the MgO content of the magmas) of basaltic lava provides a guide as to whether a particular batch of magma was sulfide-saturated or unsaturated during fractionation. This is illustrated in Fig. 9.4a by variation in the Onshore basalts along the Greenland coast that were extruded contemporaneous with the breakup in this portion of the North Atlantic. In general, rocks with more than 12–13 wt% MgO (high-magnesium basalts and picrites) show a gentle increase in Cu with decreasing MgO, probably due to the Cu that was derived from the source being progressively less diluted by the incorporation (melting or entrainment) of additional olivine in the magma in progressively less magnesian lavas. At lower MgO contents than this, the basalts from Kangertittivaq and the Blosseville coast show a marked increase in Cu with decreasing

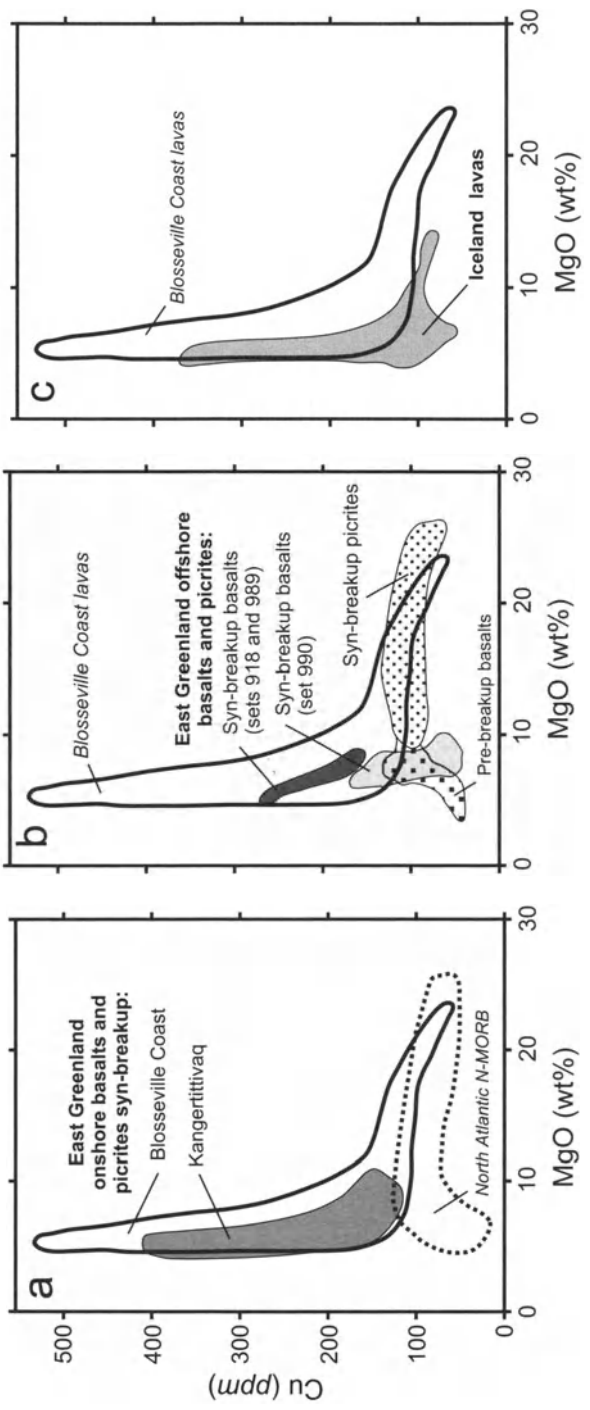


**Fig. 9.4.** Plot of Cu vs. MgO showing compositions of basaltic and picritic lavas of the North Atlantic Igneous Province. a. East Greenland onshore lavas syn-break. b. East Greenland offshore lavas. c. Iceland lavas. After Andersen et al. (2002)

MgO. This is due to the incompatible behavior of Cu, and thus its build up in the residual magma as olivine, pyroxene and plagioclase were removed. In contrast, Cu in the N-MORB decreases sharply with decreasing MgO due to the progressive removal of sulfide as fractionation proceeded (MORB are normally sulfide-saturated as discussed above). Andersen et al. also discuss data for pre-breakup basalts (the Lower Basalts). These comprise tholeiites and thin, interlayered picrites. The latter have higher PGE contents than the former, and their Os isotope systematics indicate that they were uncontaminated by continental crust. In contrast, the tholeiites display evidence of crustal contamination and sulfide saturation.

Considering offshore lavas, (Fig. 9.4b), the basalts that were erupted prior to break-up (and which thus would have been emplaced through continental crust) show a sulfide saturated trend analogous to N-MORB. They also display trace element concentrations supportive of crustal contamination (Andersen et al. 2002). The syn-breakup picrites show the normal picrite trend. When looked at from the viewpoint of Cu – MgO behavior, syn-breakup basalts fall into two groups; the basalts intersected in holes 918 and 989 show a classic sulfide-unsaturated fractionation trend while those from hole 990 show both sulfide-saturated and sulfide-unsaturated trends. These are discussed further below.

Basalts from Iceland are the youngest of those belonging to the NAIP. Andersen et al. (2002) have shown that they show both sulfide saturated and sulfide unsaturated fractionation trends (Fig. 9.4c).

Andersen et al.'s (2002) and Momme et al.'s (2003) data on the variations in the concentration of both Cu and the PGE with MgO content, along with their interpretation (augmented in part by the views of this author) of the cause of the variations are summarized in Table 9.1. Both Onshore and Offshore pre-breakup basalts display evidence of crustal contamination, sulfide-saturated fractionation and little correlation between PGE and MgO. Onshore syn-breakup basalts show increasing Cu and Pd with decreasing MgO, which Andersen et al. interpret to be the consequence of fractionation without the segregation of sulfide. Ir decreases with decreasing MgO, which indicates that it is being removed along with the fractionating phases. This behavior is often observed and is consistent with the observation made above that Rh, Ru, Ir and Os behave compatibly during mantle melting. Interestingly, Pt, which usually behaves in an incompatible manner similar to Pd, exhibits the same compatible behavior as Ir in these rocks (Andersen et al. do not address this problem).

Picrites and High-MgO basalts typically show variations that suggest that the degree of melting that gave rise to them (*i.e.* that was sufficient to produce a magma containing 12–13 wt% MgO) was also sufficient to dissolve all of the sulfide and thus take all of the Cu and PGE in the source

**Table 9.1.** Summary of conclusions derived from the variation of Cu (ppm) and PGE (ppb) with decreasing MgO in East Greenland and Icelandic lavas (after Andersen et al. 2002; and Momme et al. 2003; with added interpretations of the present author)

| | ECC | Cu | Pd | Pt | Ir | Summary | Interpretation |
|---|---|---|---|---|---|---|---|
| **East Greenland, onshore** | | | | | | | |
| Pre-breakup picrites | No | | | | | PGE are higher than in basalts (no quantitative data presented) | Sulfide unsaturated |
| Pre-breakup basalts | Yes | no data | 2 to 9 | 1 to 8 | 0.2 to 1.1 | No correlation of PGE with MgO, PGE show negative correlation with Zr | Sulfide saturated in part |
| Syn-breakup, low-Ti basalts | No | 100 to 245 | 10 to 24 | 10 to 2.5 | 1 to <0.05 | Cu & Pd increase, Pt & Ir decrease with decreasing MgO | Sulfide unsaturated |
| Syn-breakup, high-Ti basalts | No | 120 to 450 | 6 to 25 | 11 to 3 | 0.22 to <0.05 | Cu & Pd increase, Pt & Ir decrease with decreasing MgO | Sulfide unsaturated |
| **East Greenland, offshore** | | | | | | | |
| Pre-breakup | Yes | 120 to 35 | 0.52 to 5.91 | 0.39 to 5.55 | 0.10 to 0.39 | Cu decreases, PGE are uncorrelated with decreasing MgO | Sulfide saturated in part |
| Syn-breakup picrites and high-Mg basalts | No | 60 to 120 | 10 to 16 | 10 to 14 | 2.5 to 0.5 | Cu shows no systematic change, Pd and Pt increase, Ir decreases with decreasing MgO | Dilution of PGE by melting or entrainment of olivine |
| Syn-breakup basalts: Sets 918 and 989 | No | 160 to 280 | 17 to 2 | 14 to 3 | 0.4 to 0.1 | Cu increases and all PGE decrease with decreasing MgO | Mixing of low-Mg, high-Cu magma with high-Mg, low-Cu, high-PGE magma |
| Syn-breakup basalts: Set 990 | ? | 170 to 40 | no data | no data | no data | Cu decreases with decreasing MgO | |
| **Iceland** | | | | | | | |
| Hi Mg Tholeiites (10-14wt% MgO) | No | 74 to 124 | 17 to 3 | 7 to 3 | 0.32 to 0.12 | Cu increases, Pd, Pt and Ir decrease with decreasing MgO. Strong inverse correlation between Cu and PGE | Mixing of low-Mg, high-Cu magma with high-Mg, low-Cu, high-PGE magma |
| Olivine tholeiitic basalts (7-9wt% MgO) | No | 120 to 150 | 0.4 to 18.1 | 0.44 to 11.0 | 0.19 to 0.06 | Cu no change with decreasing MgO, Pd and Pt vary widely but show no correlation with MgO, Ir decreases with decreasing MgO | Magma developed immiscible sulfides and sulfides became inhomogeneously distributed as fractionation proceeded |
| Evolved basalts (4-7wt% MgO) | No | 155 to 39 | 2.14 to 0.19 | 2.23 to 0.31 | 0.04 to 0.08 | Cu decreases with decreasing MgO, Pt, Pd and Ir are low | Continuation of process affecting less evolved magma |

*ECC* evidence for crustal contamination

As discussed above, the Offshore syn-breakup basalts intersected in hole 990 follow a sulfide-saturated fractionation trend. In contrast, those from holes 918 and 989 and also the Hi-Mg tholeiites from Iceland show a trend of increasing Cu with decreasing MgO; this is consistent with sulfide-unsaturated fractionation. In contrast, considering now the behavior of PGE, all PGE decrease with decreasing MgO, which is not consistent with sulfide unsaturated fractionation. Both Andersen et al. (2002) and Momme et al (2003) conclude that the only explanation for the contrasting behavior of Cu and the PGE is that the compositional variations shown by these lavas are not the result of fractionation but are due to the mixing of two magmas from different sources, one a high MgO magma, poor in Cu and rich in PGE (they suggest a magma with 17 wt% MgO, 110 ppm Cu and 13 ppb Pd) and the other a lower MgO magma, rich in Cu and low in PGE (they suggest 6 wt% MgO, 280 ppm Cu and 2 ppb Pd). Momme et al. (2003) looked at possible sources for these two magma types in terms of Langmuir et al.'s (1992) triangular melting regime. They suggested that near the periphery of the triangular (in vertical section) melting zone beneath an oceanic ridge, relatively pristine, undepleted mantle is present and melts to give rise to a high Cu, low MgO magma. At the centre of the zone, directly beneath the ridge, within the principle column of the Iceland plume, the mantle has been depleted by previous removal of magma (but not all of the sulfide) and melts more extensively than at the periphery of the melting zone to give rise to a Cu-poor high MgO magma type. The picrites, along with their variations in Cu and PGE, are the consequence of the intermixing of varying proportions of these two types.

Other authors (e.g. Hamlyn and Keays 1985; Nielsen and Brooks 1995) have suggested that PGE-rich magmas are the result of the melting of mantle that had previously undergone a previous melting episode that had left some sulfide (and thus nearly all of the PGE) behind in the residue. The sulfide was then all taken into the melt, along with the PGE during the second phase of melting. Two-stage melting is also thought to be the way in which boninitic (high $SiO_2$, high MgO) magmas are produced. Hamlyn and Keays (1985) argued that the Bushveld magma is boninitic and attributed its PGE-rich nature to this process. There are thus two explanations for some magmas being unusually PGE-rich, derivation from a mantle plume and the product of two-stage melting. In the case of the NAIP, Andersen et al. (2002) argue that the majority of the PGE-rich lavas do not have a boninitic composition, and thus call upon a mantle plume source for one of the magmas involved.

## 9.2 Mechanisms for the Concentration of PGE

A number of different mechanisms are known to concentrate PGE. These include:

1. Fractionation of a sulfide magma. This mechanism occurs during the crystallization of a Ni-Cu sulfide liquid that has already been concentrated from mafic/ultramafic silicate magma. It results in sulfide ores that are rich in Cu, Pt, Pd, and Au and relatively poor in Rh, Ru, Ir, Os. These ores are found in close association with pyrrhotite-rich ores that are depleted in Cu, Pt, Pd and Au, and are thought to have resulted from the cooling and fractional crystallization of the sulfide liquid, with the separation of a fractionated component and its migration and concentration away from the early-crystallizing pyrrhotite-dominant component. Classic examples of this style of mineralization are found at Noril'sk and Sudbury. They have been described in the chapters (Chaps. 4 and 8) devoted to these deposits and will not be described further here.
2. The development of a very high R Factor environment during the crystallization of a layered intrusion. This gives rise to stratabound accumulations of sparsely (0.5–3 volume %) disseminated sulfides, the sulfides themselves having very high tenors of Ni, Cu and especially Pt, Pd, Rh, Ru, Ir, Os and Au. Deposits of this type include the Merensky and J-M reefs of the Bushveld and Stillwater complexes and the Main and Lower Sulfide Zones of the Great Dyke of Zimbabwe and are described below. The influence of the R-factor on the composition of sulfides equilibrating with a silicate magma is illustrated in Fig. 9.5.
3. The development of PGE-rich immiscible sulfides prior to or during emplacement into their present locations. This has given rise to weak marginal accumulations of sulfide in intrusions in northern Finland, the Kola Peninsula of Russia, and in Ontario, Canada near Sudbury and within the Coldwell Complex. The Platreef of the Bushveld Complex is likely also of this type. Typically the mineralized zones are characterized by inclusions of mafic/ultramafic cognate xenoliths and/or country rocks.
4. The delayed separation of sulfide during the crystallization of a layered intrusion. This mechanism gives rise to deposits that are relatively rich in Cu, Pt, Pd and Au, low in Ni, and probably (not enough data exists to be sure) low in Ru, Ir and Os. Examples of this style of mineralization occur in the Bushveld, Skaergaard and Sonju Lake intrusions and are described below. Another example is the Rincon del Tigre deposit of Eastern Brazil (Prendergast et al. 1998).

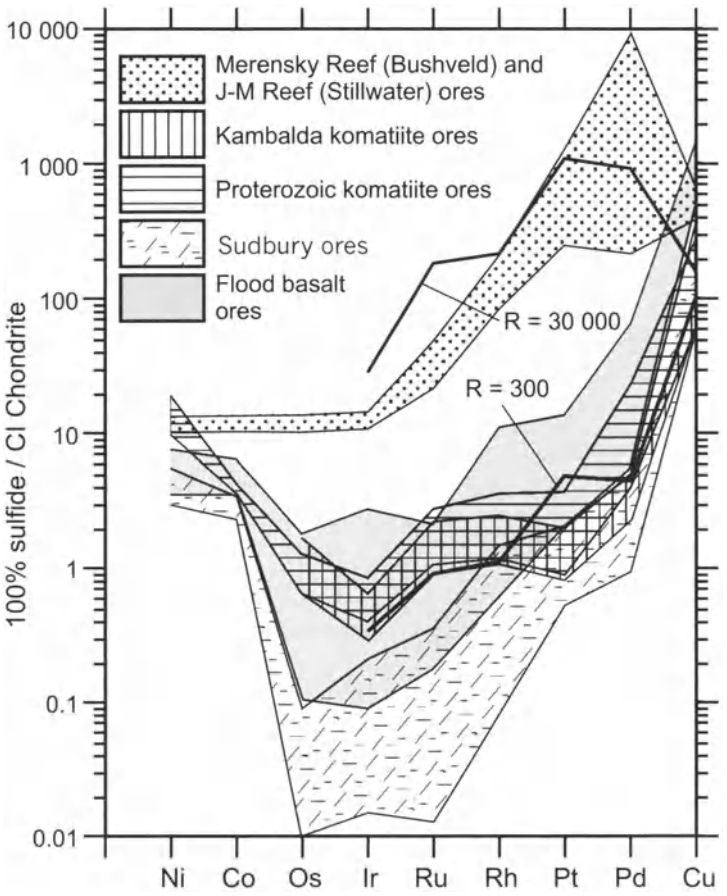


**Fig. 9.5.** Ranges of chondrite normalized average PGE concentrations in 100% sulfides of a number of important types of magmatic ores (from Naldrett 1989). The diagram illustrates that there is a large difference in PGE concentrations but relatively small difference in Ni, Cu and Co between sulfide-rich Ni-Cu ores and low-sulfide PGE-enriched ores. The effect of variation in magma/sulfide ratio (R) on the composition of sulfides segregating from a magma equivalent to Cawthorn and Davies's (1983) presumed magma responsible for the Lower Zone of the Bushveld Complex at R = 300 (lower heavy line and at R = 30000 (upper heavy line) is shown and it is seen that differences in the value of R of this order can go a long way towards accounting for the difference in PGE concentrations between the two types of deposit

5. Chromite crystallization without the development of sulfide immiscibility. Deposits formed in this way tend to be enriched in Ru, Ir and Os and relatively poor in Ni, Cu, Pt, Pd and Au. This style of deposit is beyond the scope of this book, which is devoted to magmatic sulfide de-

posits, but, for the sake of completeness, examples that occur in layered intrusions (in particular in the Stillwater Complex) are discussed briefly below. PGE concentrations are also found associated with chromite segregations in ultramafic rocks that occur in ophiolite successions. While examples of this association do not constitute significant in situ PGE resources, they give rise to important placer deposits in the Urals and elsewhere. In addition, mineralization that is also associated with chromite-enriched ultramafic rocks has been documented in a carbonatite-bearing alkaline-ultramafic intrusions in the Guli Complex in Northern Siberia (Malich 1999). The economic potential of this particular occurrence is still unknown.

6. The re-melting of a host intrusion and re-concentration of PGE. It is difficult to predict the metal proportions that will result from this mechanism, because of the few examples of this type of deposit that have been discovered to date. It is the opinion of this author that this deposit type will become an important resource in the future. One well-established deposit belonging to this type is that of North American Palladium at Lac des Iles, Ontario. This is discussed below.
7. Hydrothermal redistribution of PGE. Examples that are considered in this book are the low-sulfide ores of the Noril'sk area and the Duluth complex (Chap. 4) and the dunite pipes of the Bushveld Complex (this chapter). Other examples include the New Rambler mine in Wyoming, USA (McCallum et al. 1976), the Waterberg Deposit, Transvaal, South Africa (Distler et al. 2000), and the Coronation Hill deposit, Australia (Mernagh et al. 1994). The genesis of hydrothermal ores is not well understood as yet, but most appear to be the result of late-stage Cl-rich aqueous fluids concentrating PGE that occur dispersed in host intrusions. Typically, the metals tend to occur in very variable proportions in different deposits.
8. Secondary concentration of PGE associated with chromite schlieren in zoned dunite-pyroxenite intrusions. These intrusions, which are commonly referred to as "Alaskan" or "Ural- Alaskan" type are referred to here as Nizhny Tagil type after the major deposit in the Urals. Similar mineralization occurs in Koryakia, North-eastern Russia (Vidik at al. 1999) and in the Kondyor intrusion within the Siberian platform (Malich 1999). Pt is the principal PGE that is concentrated. Some in situ mining has occurred in this environment in the Urals (Soleviev Hills, see below), but their principal importance lies in the major Pt-rich placer deposits that result from erosion of these intrusions. Although the concentration of the PGE in this class of deposit has nothing to do with the development of magmatic sulfides, the protores are possibly an important future resource so a brief mention is made of them below.

9. Hydrothermally concentrated PGE (principally Pt) in black shales, often in association with Au. A classic example of this is the Sukhoi Log Au deposit in Siberia (Distler et al. 1996). This author has some concerns about how well some deposits of this style have been documented. It is difficult to obtain reliable analyses of PGE in an environment in which there are high concentrations of Au and native C, and some of the data reported in the literature is probably spurious. This style of deposit is far removed from the topic of this book, and is not discussed further.

## 9.3 Classification of PGE deposits based on Morphology and Composition

A "petro-tectonic" classification of PGE deposits was given in Chap. 1 in which the deposits were considered in terms of the composition of the magmas giving rise to PGE-bearing igneous complexes and the tectonic conditions of their origin. However several different kinds of deposits can be present in the same intrusion (e.g. the Bushveld Complex) and, on the other hand, deposits of similar style can be present in intrusions that have very different petrological and tectonic characteristics (e.g. compare the Volkovsky deposit in the Urals and the Bermuda deposit in the Coldwell Complex, Ontario with some deposits in the Bushveld Complex).

With this in mind, deposits are grouped on the basis of their morphology and composition in Table 9.2. The primary grouping is into those that are stratabound and those that are not. Within the stratabound group, one recognizes those that are predominantly stratiform, i.e. that define a particular stratigraphic horizon, and those that are merely confined to a stratigraphic interval. In turn, the deposits are subdivided into those with a predominantly sulfide association alone (small layers of chromite may also be present as in the Merensky Reef but the principal association of the PGE is with sulfide), and those in which the dominant association is a chromitite layer or alternatively a magnetitite layer. In the case of the chromitite and magnetitite associations, small amounts of sulfide may be present, and sulfide may have played a major role in concentrating the PGE.

The sulfide-related group can be further sub-divided into those associated with a "reef" (here defined as a mineralized rock-layer with a distinctive texture and/or mineralogy) and those that show no such association. The Merensky (Vermaak 1976; Viljoen and Hieber 1986; Viljoen 1999; Viljoen et al. 1986a, b; Naldrett et al. 1987, Kruger 1992, Cawthorn et al. 2002) and J-M (Bow et al. 1982, Barnes and Naldrett 1986, Raedke and Vian 1986, Zientek,et al. 2002) Reefs of the Bushveld and Stillwater Com-

plexes respectively, and the Ala-Penikka I and II, the Sompujarvi sulfide-associated deposit and the Paasivaara deposit of the Penikat intrusion (Halkoaho et al. 1990a; Halkoaho et al. 1990b; Huhtelin et al. 1990, Iljina et al. 1992), and the Rytikangas and Siika-Kama (SK) Reefs of the Portimo Complex (Iljina 1994; Alapieti and Lahtinen 2002) all occur within distinctive rock layers. In contrast, the Main and Lower Sulfide Zones of the Great Dyke of Zimbabwe occur in uniform bronzitite that has no obvious characteristics other than sulfide distinguishing the mineralized zones (Prendergast 1988, Prendergast and Keays 1989, Wilson and Tredoux 1990, Naldrett and Wilson 1990). The Platinova "Reefs" of the Skaergaard Intrusion occur within a unit known as the "Triple Group" but show no distinctive mineralogy or rock fabric, apart from the presence of the ore minerals (Andersen et al. 1998, 2002), and therefore constitute another example of a stratiform deposit lacking a "Reef" in the sense that "Reef" is defined in this chapter.

The chromitite-associated group include the deposits of the "Middle-" and "Upper Group" chromitites of the Bushveld Complex, particularly the UG-2 (von Gruenewaldt et al. 1986), the A and B chromitites of the Stillwater Complex (Page et al. 1985) and the Sompujarvi chromite association of the Penikat intrusion in Finland (Halkoaho et al. 1990b). The magnetitite-related group is a relatively newly recognized class; it includes mineralization in Upper Zone of the Bushveld Complex, the Volkovsky Ti-magnetite, apatite, Cu-sulfide deposits in the Platinum belt of the Central Urals and the Bermuda deposit in the Eastern Gabbro of the Coldwell Complex, Ontario (Barrie et al. 2002).

Exploration during the 1997-2001 "PGE exploration boom" has focused attention on deposits in marginal rocks (typically inclusion-bearing) to layered intrusions. These are generally irregular and cannot be described as stratiform, but they are stratabound in the sense that they occur in the marginal zones to mafic/ultramafic complexes. Examples include the marginal mineralization in the Portimo and Koillissima complexes in northern Finland (Iljina 1994), the East Bull Lake and River Valley intrusions respectively west and east of Sudbury (James et al. 2002), the Platreef of the Bushveld Complex (Buchanan and Rouse 1984) and the Marathon deposit in the Coldwell Complex, Ontario (Barrie et al. 2002).

The Robie Zone at Lac des Iles (Macdonald 1988; Brugmann et al. 1989; Watkinson et al. 2002) Ontario, and dunite pipes (Schiffries 1982) of the Bushveld Complex are examples of deposits associated with sulfides that are clearly discordant to strata. Chromitite veins and segregations forming a stockwork in recrystallised dunite provide a major control to lode Pt mineralization in the Nizhny Tagil, Ural-Alaskan type intrusion of

the Urals Platinum Belt (Ivanov 1997) and provide a further example of discordant mineralization.

**Table 9.2.** Classification of PGE deposits, based on morphology and mineral association of the ore bodies along with typical examples

| | | | |
|---|---|---|---|
| STRATABOUND | STRATIFORM | **Dominant Sulfide Association** | ***Associated with a "Reef"***[1]<br>Merensky Reef (Bushveld)<br>J-M Reef (Stillwater)[2]<br>Reefs in intrusions of Northern Finland |
| | | | ***Not Associated with a "Reef"***<br>Main and Lower Sulfide Zones (Great Dyke)<br>Platinova "Reefs" (Skaergaard)<br>Sonju Lake (Duluth) |
| | | **Dominant Chromitite Association** | UG-1, UG-2 (Bushveld)<br>"A" chromitite (Stillwater) |
| | | **Dominant Magnetitite (±apatite) Association** | Mineralization in Upper Zone of the Bushveld Complex<br>Bermuda deposit (Coldwell, Ontario) |
| | NOT STRATIFORM | **Dominant Sulfide Association** | River Valley, East Bull Lake (Sudbury area, Ontario)<br>Marginal Zones of Portimo and Koillissima Igneous Complexes (Northern Finland)<br>Platreef (Bushveld)<br>Marathon deposit (Coldwell, Ontario) |
| | | **Dominant Magnetitite (±apatite) Association** | Volkovsky deposit (Urals Platinum Belt, Russia) |
| **DISCORDANT TO STRATA** | | | Robie Zone (Lac des Iles)<br>Dunite Pipes (Bushveld)<br>Nizhny Tagil (Urals Platinum Belt, Russia) |

In this chapter a "Reef" is defined as a rock layer with a distinctive texture and mineralogy. In some areas (for example the Skaergaard and Kap Edvard Holm Intrusions) the term "Reef" is used to mean any horizon that contains PGE-enriched sulfide and/or sulfosalt minerals.

When examined in detail, the J-M Reef (Zientek et al. 2002) and, to a lesser extent, the Merensky Reef (Cawthorn et al. 2002) are not perfectly stratiform. However they are much more closely confined to stratigraphic horizons than the mineralization at the margins of the Finnish or Sudbury intrusions or the Platreef, which is why they are classified as stratiform here

The very large difference between typical Ni-Cu ores and those of interest primarily because of their PGE content that is brought out in Fig. 1.1 is also echoed in Fig. 9.5 in which PGE, Ni, Cu and Co data for different classes of magmatic sulfide deposit are expressed as average metal content in 100% sulfides and then chondrite normalized. Whereas there is relatively little spread in the Ni, Cu and Co contents of the sulfides from different deposits, the sulfides of the PGE-rich deposits are enriched by several orders of magnitude over those of the sulfide-rich Ni-Cu ores. A fundamental question relating to the origin of PGE-rich deposits is why is this so; in order to answer this, it is necessary to consider the geological setting of the different types of PGE-rich deposits found in layered intrusions. In the following section (9.4) the well layered intrusions that host the most important (mainly stratabound) deposits are reviewed. This is followed in section 9.5 by a discussion of non-stratabound deposits with special focus on that at Lac des Iles (Canada). A separate section (9.6) is devoted to the Urals Platinum Belt (Russia), where the deposits, unlike the other significant deposits, were formed in an active orogenic environment at the margin of an oceanic plate.

## 9.4 Deposits in layered intrusions

Three intrusions are host to the bulk of the worlds PGE deposits, the Bushveld and Stillwater Complexes and the Great Dyke ("The Big Three"). They are distinguished by containing a higher proportion of ultramafic to mafic rocks than many (but not all) other mafic/ultramafic intrusions, and all are characterized by orthopyroxene appearing on the liquidus before plagioclase. Of the three, the Bushveld is by far the most important with many mines in operation (Fig. 9.6), and other deposits scheduled to be developed. In the Stillwater Complex, the Stillwater mine has been in production since 1986, and the East Boulder mine started production in December 2002 (see Fig. 9.22). The Great Dyke is also in production, but the major development in the Hartley area (see Fig. 9.28 below), which operated from 1996-1999, has closed, and only two relatively small mines, the Mimosa mine, and the Ngezi mine in the southern part of the dyke are currently in production.

"The Big Three" PGE-bearing intrusions are described first, followed by the Munni-Munni intrusion (Western Australia), intrusive complexes in Finland, Ontario (Canada), Eastern Greenland, and the Sonju Lake intrusion of Duluth Complex (USA). Genetic models for ore deposition are discussed at end of this section.

### 9.4.1 Bushveld Complex

#### *Geology*

The Bushveld Complex (Fig. 9.6) is the largest known mafic/ultramafic intrusion, extending 450 km east-west and 250 km north-south. The country rocks consist mainly of quartzites, argillites and dolomites of the Transvaal Supergroup, in particular the Pretoria Group, although parts of the complex lie directly on Archean granitoids and greenstones.

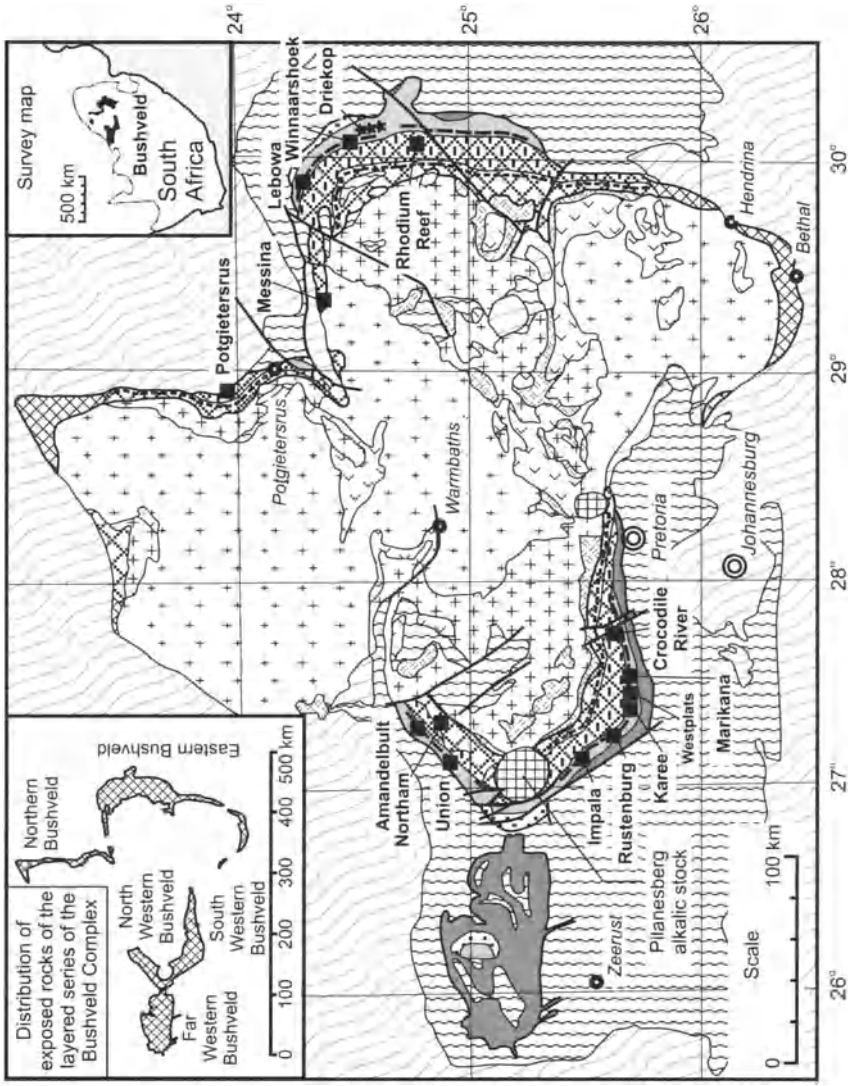

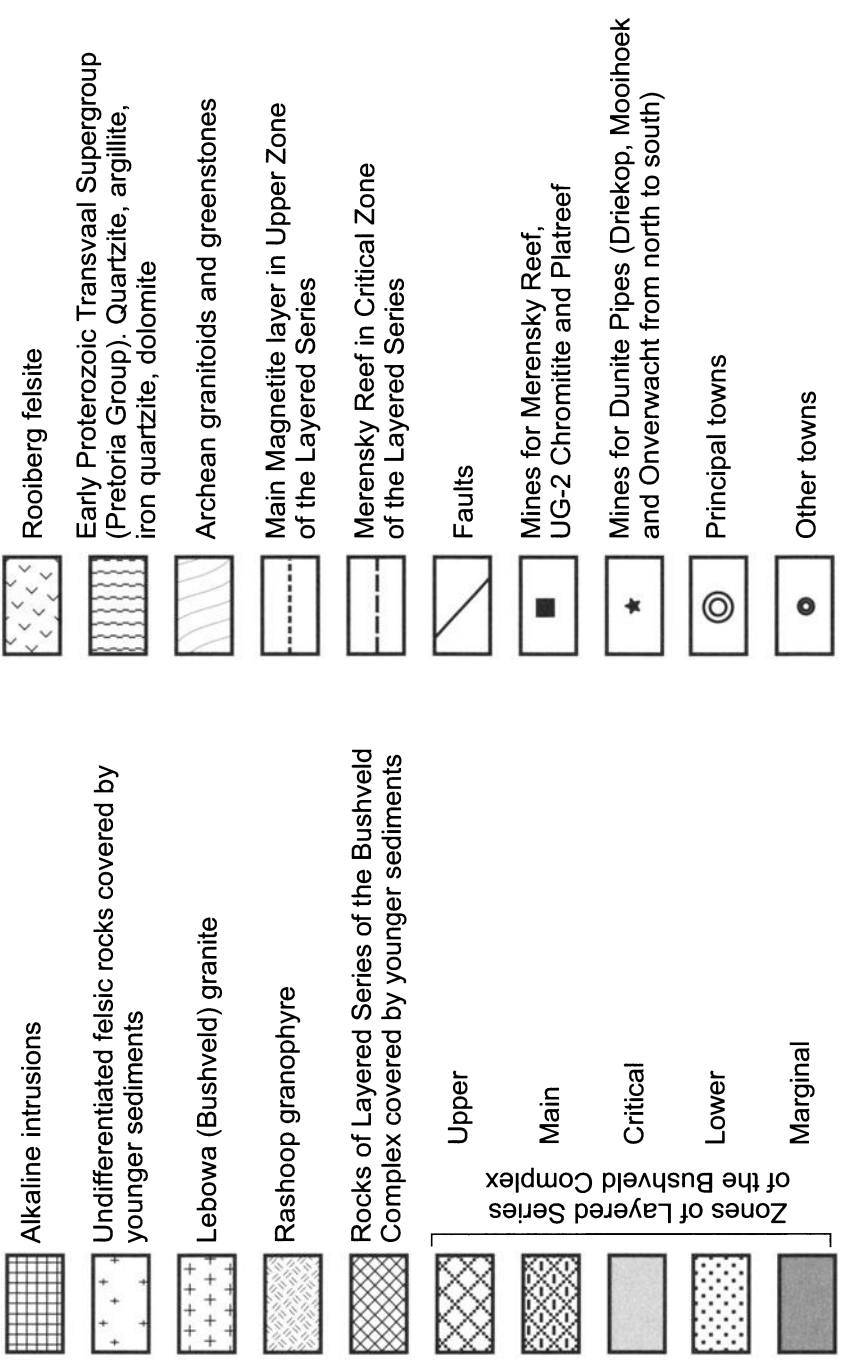


**Fig. 9.6.** Schematic geological map of the Bushveld Complex

While the Bushveld is known primarily for its layered mafic rocks, the Bushveld igneous event comprises four distinctive igneous suites. The first suite consists of early mafic sills (Cawthorn et al. (2002). These were followed by felsites belonging to the Rooiberg Group (2.06 Ga), which now form the roof to much of the layered igneous series and comprise the second suite. The felsites were followed by intrusion of the third suite, the layered mafic/ultramafic rocks (Rustenburg Layered Series = 2.06 Ga), along with accompanying dykes and sills. Repetitive major influxes of magma gave rise to the up to 10 km thick sequence of mafic/ultramafic rocks. Melting of roof rocks resulted in a series of granophyres which occur at intervals along the upper margin of the layered series. The final igneous suite belonging to the Bushveld igneous event is the Lebowa Granite Suite that was intruded into the center of the mafic/ultramafic rocks. Seismic and gravity data indicate that this has the form of a mushroom-like body with a central stock of granite pillowing out over the mafic rocks.

The layered series is preserved in four major structures. Three of these, the Eastern Bushveld, the Southeastern Bushveld and the Western Bushveld have the form of semi-circular basin-like lobes (Fig. 9.6). It is uncertain as to whether these lobes were closely interconnected at one time because intrusion of the Bushveld granite now obscures any interconnections that might have existed initially, but Cawthorn and Webb (2001) have suggested that they were originally contiguous. The Eastern and Western Bushveld lobes show a full development of rock types from the Marginal Zone through to the Upper Zone (see below) The Southeastern lobe lacks the lower two zones. The Western Bushveld lobe was effectively separated into two by the later intrusion of the Pilanesberg alkalic stock. Another structure (Far Western) lies west of the Pilanesberg. Here, except for one or two minor localities, only marginal rocks of the layered series are preserved – another fully-developed lobe could have existed in this area, but if so it has been mostly removed by erosion. The fifth structure, the Northern Limb is quite distinct from the other bodies. The stratigraphy has major differences to the others, and the intrusion cuts down through the lower part of the Pretoria system to reach underlying Archean rocks.

The stratigraphy of the Rustenburg Layered Series is divided into five zones (Fig. 9.7). The Marginal Zone (0–800 m thick) is formed of norite along with minor pyroxenite. The Lower Zone (800–1300 m thick) is composed mainly of bronzitites, harzburgites and dunites (Cameron 1978). It is overlain by the Critical Zone (1300–1800 m thick). The base of the Critical Zone is marked by the incoming of cumulus chromite. The zone is divided into two parts (Cameron 1980, 1982). The Lower Critical Zone consists primarily of bronzitites, chromitites and some harzburgites.

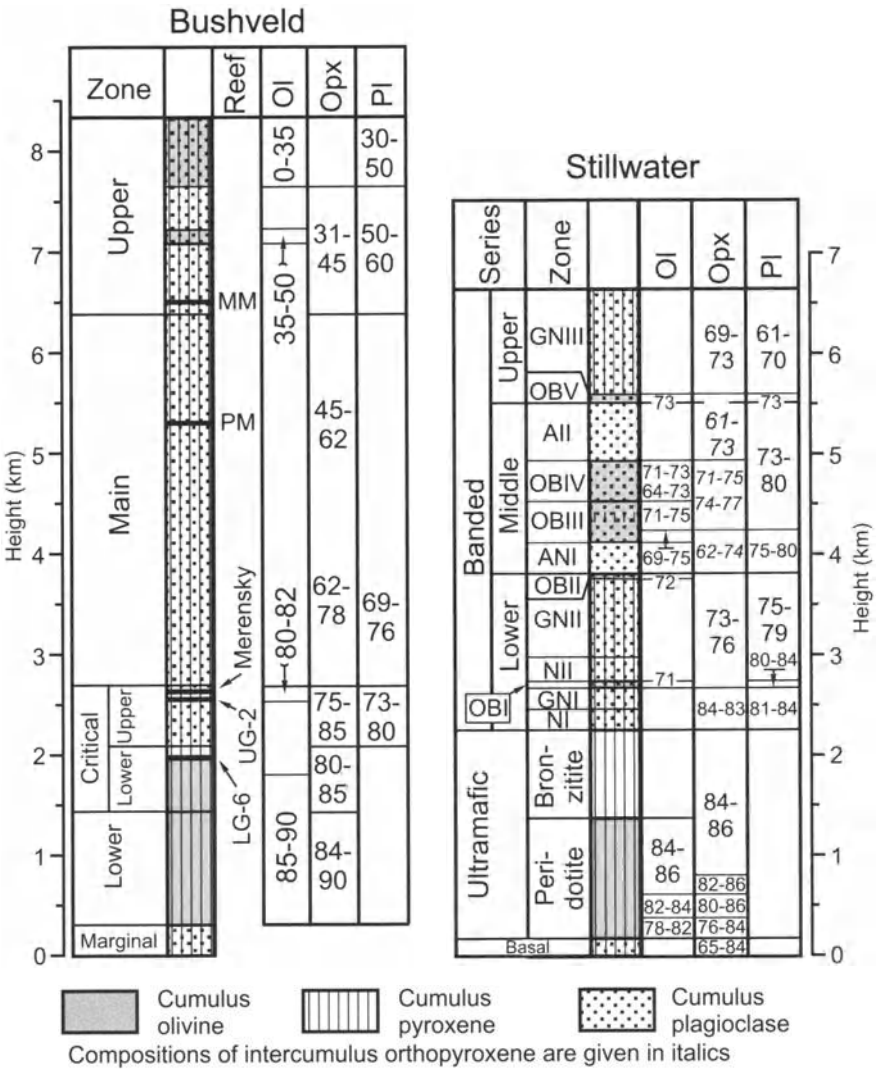


**Fig. 9.7.** Generalized succession of rock types in the Bushveld and Stillwater Complexes, showing variations of MgNo in orthopyroxene and olivine, and anorthite in plagioclase (after Naldrett et al. 1987)

The Upper Critical Zone is marked by the incoming of cumulus plagioclase and can itself be subdivided into two parts; (i) a lower part consisting of anorthosites, norites and minor bronzites, that occur in no systematic order, and define no classical cyclic units; and (ii) an upper part (starting with base of the UG-1 chromitite unit) which, in contrast, comprises units made up of a regular succession of rock types, consisting of some or all of chromitite, harzburgite, bronzitite, norite and anorthosite, in most cases in this order. The Critical Zone is overlain, in turn, by the norites, gabbros and anorthosites of the Main Zone (3000–3400 m thick), which are themselves capped by the ferrogabbros and ferrodiorites of the Upper Zone, 2000–2800 m thick (von Gruenewaldt 1973; Molyneaux 1974).

The different zones and units vary greatly in thickness throughout the Complex, and are absent in some areas. The lower zones vary in thickness due in part to their transgressive nature and appear to have had the most restricted development. In many places, the Critical Zone transgresses over a wider area of the Bushveld floor than the Lower Zone, and the Main Zone a still wider area. Von Gruenewaldt (1979) has attributed the transgression to the progressive addition of new magma as the Complex crystallized.

### *Geochemistry*

From a study of mafic/ultramafic sills intruding country rocks marginal to the Bushveld Complex, Sharpe and Irvine (1983) and Harmer and Sharpe (1985) recognized that two predominant magma types were involved, one of which, named "U-type" by Irvine and Sharpe (1986), was rich in MgO, $SiO_2$, and Cr and the other with a tholeiitic composition. The high MgO-$SiO_2$ magma has been termed boninitic and a two-stage melting process has been called upon to substantiate both its boninitic composition and high PGE content (Hamlyn and Keays 1985). However, Barnes and Maier (2002) pointed out that the trace element content of this magma type is consistent with a high MgO basalt that has undergone contamination in the upper crust. Sr, Nd and Pb isotopes support significant upper crustal contamination (Maier et al. 2000; Harmer et al. 1995). Barnes and Maier (2002) noted that the second (thoileiitic) magma type also has also undergone crustal contamination, albeit of lower crustal type. Their estimates of the compositions of the two Bushveld magmas are shown in Table 9.3. The high MgO magma composition is that of a magnesian basaltic andesite with an estimated 12.65 wt% MgO, 55.87 wt% $SiO_2$, 952 ppm Cr and 257 ppm Ni while the tholeiitic magma contains an estimated 7.26 wt% MgO, 50.58 wt% $SiO_2$, 314 ppm Cr, and 146 ppm Ni. The magnesian basaltic andesite is estimated to contain nearly 3 times as much sulfur and 1.5 to 2

times the concentration of PGE as the tholeiitic magma. The sequence of crystallization predicted to occur from the two magmas is very different. The basaltic andesite will crystallize olivine, orthopyroxene and then plagioclase+orthopyroxene. The tholeiitic magma will crystallize plagioclase followed by clinopyroxene, possibly preceded by minor olivine.

Barnes and Maier (2002) pointed out that rocks of the Lower Zone and Lower Critical Zone have a trace element and isotopic signature indicating that they have been derived from the MgO-rich liquid, and the Main Zone rocks a signature similar to that of the tholeiitic magma. The Upper Critical Zone, particularly in the vicinity of the PGE reefs, shows characteristics suggesting that these rocks crystallized from a mixture of the two magmas, with the proportion of tholeiitic magma in the mixture increasing progressively upward (see the variation in $Sr_i$ and Th/Hf ratios with height in Fig. 9.8).

Barnes and Maier (2002) compiled a wealth of data on the PGE content of rocks in the Lower, Critical and Main Zones of the Bushveld. Their data for Pt and Pd are shown projected onto a single stratigraphic section in Fig. 9.9. Lower Zone silicate rocks average 23 and 21 ppb Pt and Pd respectively, Lower Critical Zone silicate rocks 26 and 12 ppb, Upper Critical Zone silicate rocks 119 and 52 ppb and Main Zone silicate rocks 6 and 3 ppb Pt and Pd respectively. Barnes and Maier noted that there was no cumulus silicate or oxide mineral that could contain Pt and Pd, that the proportion of intercumulus liquid was generally between 5 and 15 wt%, that judging from the PGE content of the initial magmas the intercumulus liquid would have only been able to contribute 1–3 ppb of the contained Pt or Pd, and therefore concluded that during this crystallization interval the Bushveld magma must have been sulfide saturated and segregating cumulus sulfide along with the cumulus silicates. They used the Hf content of the rocks to calculate the amount of trapped liquid in each sample, and showed that the Lower Zone and Merensky Reef contain sufficient sulfide for the intercumulus liquid (and thus the magma giving rise to the these cumulates) to have been sulfide-saturated, but that the rocks of the Lower Critical Zone and much of the Upper Critical Zone contain too little sulfur. Barnes and Maier propose that rocks of the Upper Critical Zone have lost sulfur. Considering the Lower Zone silicate rocks, the sulfur content is 177 ppm, which corresponds roughly to 531 ppm sulfide. Assuming that all of the Cu, Pt and Pd was collected by this sulfide when it was liquid, the sulfide liquid would have contained 4.0 wt% Cu, 43 ppm Pt and 40 ppm Pd. A similar calculation for the Lower Critical Zone gives a sulfide liquid

containing 5.3 wt% Cu, 105 ppm Pt and 49 ppm Pd[22]. These are very high concentrations for magmatic sulfides in conventional Ni-Cu sulfide deposits (see the Appendix) but not as high as those in the Merensky Reef, which are 5.66 wt% Cu, 257 ppm Pt and 98 ppm Pd.

**Table 9.3.** Estimates of the Compositions of the Magmas Responsible for the Bushveld Complex (after Barnes and Maier 2002)

| | High Mg Magma | Tholeiitic Magma |
|---|---|---|
| $SiO_2$, wt % | 55.87 | 50.48 |
| $TiO_2$, wt % | 0.37 | 0.71 |
| $Al_2O_3$, wt % | 12.55 | 15.79 |
| FeO, wt % | 9.15 | 11.61 |
| MnO, wt % | 0.21 | 0.18 |
| MgO, wt % | 12.65 | 7.26 |
| CaO, wt % | 7.29 | 10.86 |
| $Na_2O$, wt % | 1.53 | 2.2 |
| $K_2O$, wt % | 0.77 | 0.16 |
| $P_2O_5$, wt % | 0.1 | 0.16 |
| S, ppm | 866 | 340 |
| Cr, ppm | 952 | 314 |
| Ni, ppm | 257 | 146 |
| Cu, ppm | 61 | 60 |
| Au, ppb | 3.05 | 2.91 |
| Pd, ppb | 11 | 9 |
| Pt, ppb | 18 | 14 |
| Rh, ppb | 1.1 | 0.6 |
| Ru, ppb | 2 | 1.5 |
| Ir, ppb | 0.32 | 0.18 |
| Os, ppb | 0.5 | <0.5 |
| Th/Hf | 1.9 | 0.47 |
| $^{87}Sr/^{86}Sr$* | 0.7032-0.7057 | 0.7059-0.7077 |
| εNd* | from -4.49 to –6.31 | from -4.92 to –6.74 |

*Initial isotopic ratios

[22] Note, we have not performed this simple calculation for the Upper Critical Zone rocks because of the possibility that they may have lost sulfur. Likewise, although they contain enough sulfur for Barnes and Maier's calculated intercumulus liquid to appear sulfur saturated, the Lower Critical Zone rocks may have lost some of their original sulfur, which would cause them to have a higher calculated tenor of their sulfides than would otherwise have been the case.

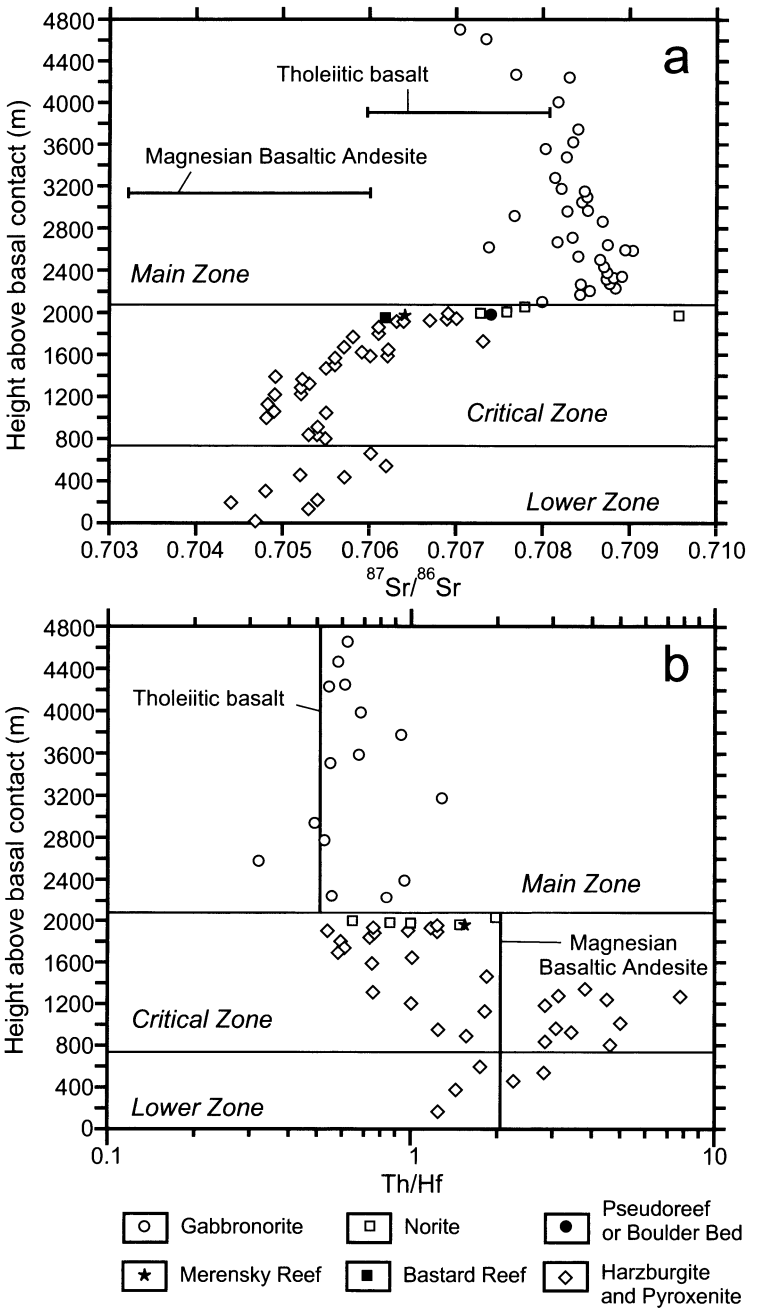


**Fig. 9.8.** Union stratigraphic section showing variations in initial Sr isotope composition (a) and Th/Hf ratios (a). After Barnes and Maier ( 2002)

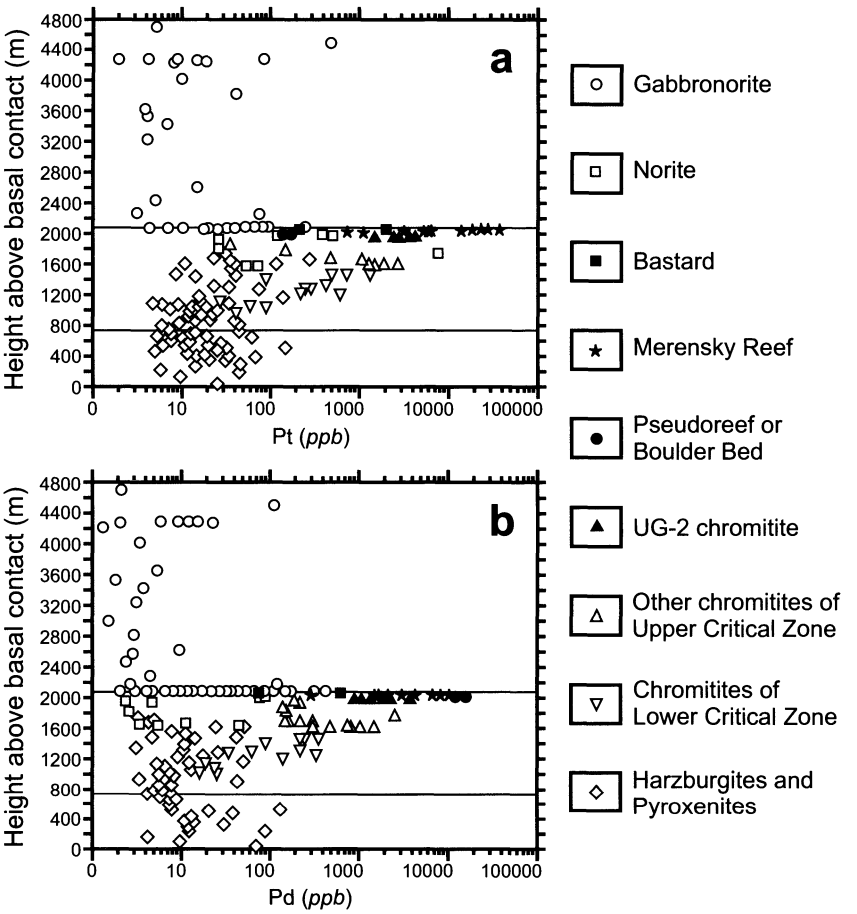


**Fig. 9.9.** Variations in (a) Pt and (a) Pd concentrations with stratigraphic height. All Western Limb and Eastern Limb data projected onto Union Section. After Barnes and Maier (2002)

## *Stratiform Mineralization: overview*

Stratiform deposits of the sulfide, chromitite, and magnetite associations are present in the Bushveld Complex. The most important of them: Merensky Reef and UG-2 chromitite occur in the Upper Critical Zone. As discussed above, this Zone is marked by the first appearance of cumulus plagioclase in the overall stratigraphy of the Bushveld Complex (Fig. 9.7), and also the first indication that a magma other than the high-MgO basaltic andesite is contributing to the formation of the cumulus rocks (see Fig. 9.8). The lower part of the Upper Critical Zone consists of pyroxenite,

norite and anorthosite layers that occur in no particular order, but in the upper part, starting at the base of the UG-1 chromitite, the layers are arranged in a series of clearly defined cyclic units comprising all or some of the following – chromitite, harzburgite, bronzitite, norite and anorthosite – in this order (Fig. 9.10). The Bastard cyclic unit, so-called because of its resemblance to the Merensky cyclic unit, but its comparative lack of PGE enrichment, is the uppermost of these units and is overlain by the much less regularly organized rocks of the Main Zone, which, except for the pyroxenite marker, lacks cyclic units.

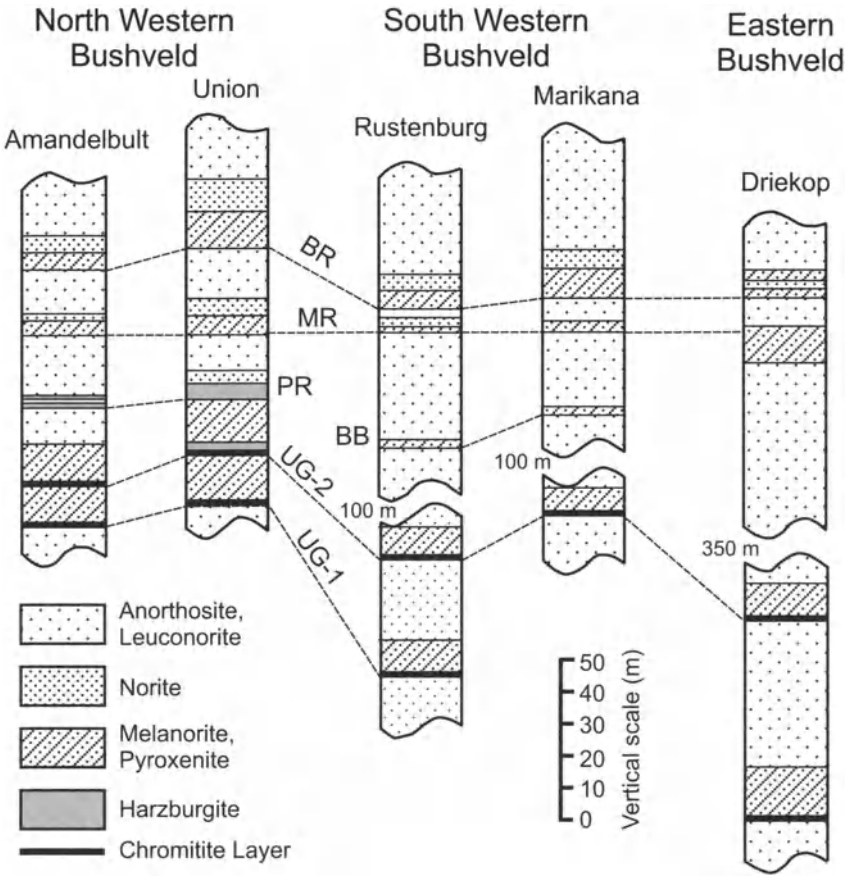


**Fig. 9.10.** Cyclic units forming the upper part of the Upper Critical Zone of the Bushveld Complex. After Naldrett (1981b) using data from Vermaak (1976), Gain (1980) and Farquhar (1985)

### *Stratiform Mineralization of sulfide association: Merensky Reef*

The cyclic unit with which the Merensky Reef is associated displays cryptic variation (Fig. 9.11) that is interpretable in terms of magma mixing but not of fractional crystallization alone (Naldrett et al. 1987). In the Merensky cyclic unit, Sr isotopic changes suggest that two magmas were contributing to the unit, with the more radiogenic magma contributing progressively more to rocks higher in the unit (Fig. 9.12). Naldrett et al. (1986) and Naldrett et al. (1987) have suggested that each cyclic unit in the upper part of the Critical Zone is initiated by a pulse of fresh high-MgO basaltic andesite magma entering the magma chamber. This is supported by the work of Lee and Butcher (1990) whose data show that the Bastard unit immediately overlying the Merensky is marked by an abrupt reversal to lower initial Sr ratios at its base, and then a similar progressive increase in initial Sr ratio to a value of about 0.708, which is maintained into the Main Zone (Fig. 9.12).

In detail, the Merensky Reef shows significant variations in different parts of the Bushveld Complex. In the Rustenburg area of the western Bushveld, the ore zone comprising the Merensky Reef is confined to a pegmatoid that occurs at the base of the Merensky cyclic unit (Fig. 9.13). PGE are concentrated in the vicinity of two chromite layers which occur at the top and bottom of the pegmatoid, and are particularly concentrated near the upper chromite layer. In the Union-Amandelbult area, the ore is also associated with chromite layers within pegmatoid, but here olivine is an important component of the pegmatoid, particularly towards its base. In the Marikana area, east of Rustenburg Mine, the pegmatoid is less common, occurring as isolated patches within porphyritic bronzitite, and the chromite layers are much wider apart. The upper chromite occurs approximately 50 cm below the contact of the bronzitite with the overlying anorthosite, whereas the lower chromite occurs at the base of the bronzitite (Fig. 9.13). The most important metal values are associated with the upper chromite layer. The Merensky Reef is also different in the vicinity of the Atok Mine near Jagdlust in the eastern section of the Complex. Here a pegmatoidal pyroxenite is present within bronzitite, but the chromite layers and PGE values occur above the pegmatoid, within overlying bronzitite (Fig. 9.13).

In the Rustenburg area the Merensky pegmatoid consists of coarse bronzite crystals (1 to 4 cm in length) enclosed in a matrix of plagioclase. Biotite, apatite and tremolite are common constituents. The lower bounding chromite layer varies from a few mm to a few cm in thickness. The upper chromite layer is only a few mm thick and is discontinuously developed in some areas. In many places some pegmatoid extends above the

upper chromite layer into the overlying bronzite. Elsewhere medium-grained, non-pegmatoidal bronzitite masses occur enclosed within the Reef pegmatoid.

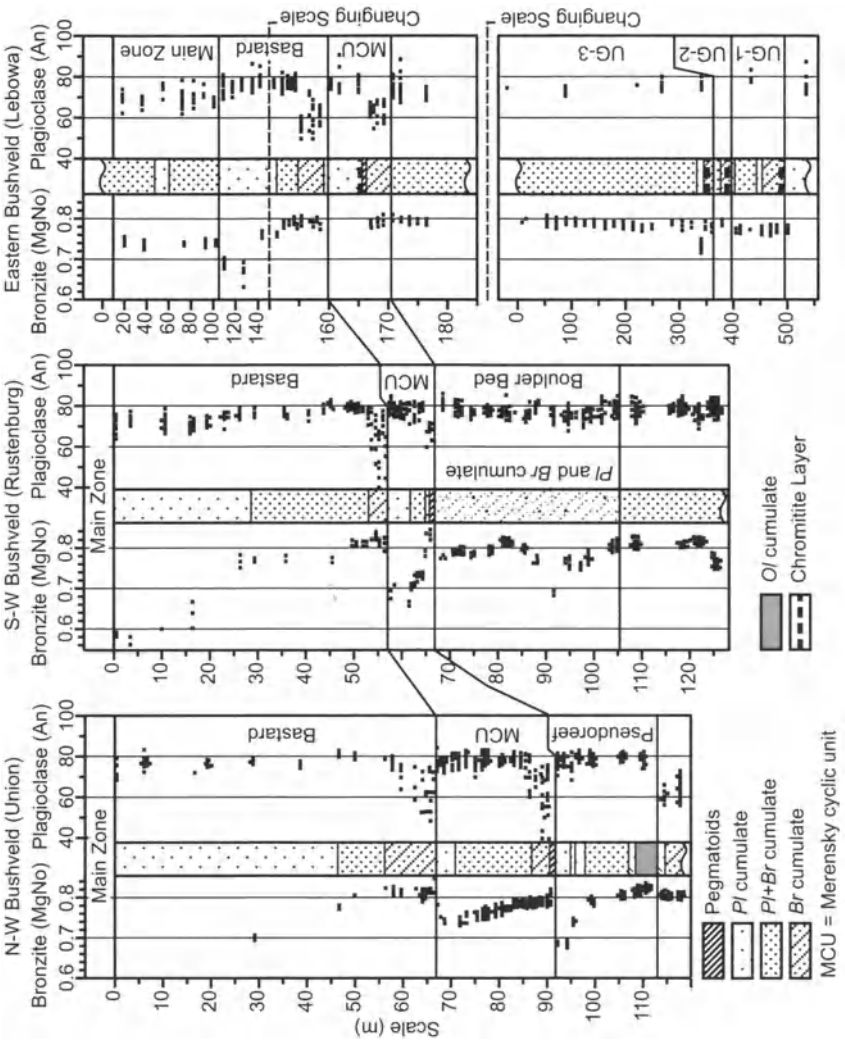


**Fig. 9.11.** Cryptic variations in orthopyroxene and plagioclase composition in cyclic units of the Bushveld Complex. After Naldrett 1989 (data for the Union and Rustenburg sections are adopted from Naldrett et al. 1986a, for the Lebowa section from Cameron 1988)

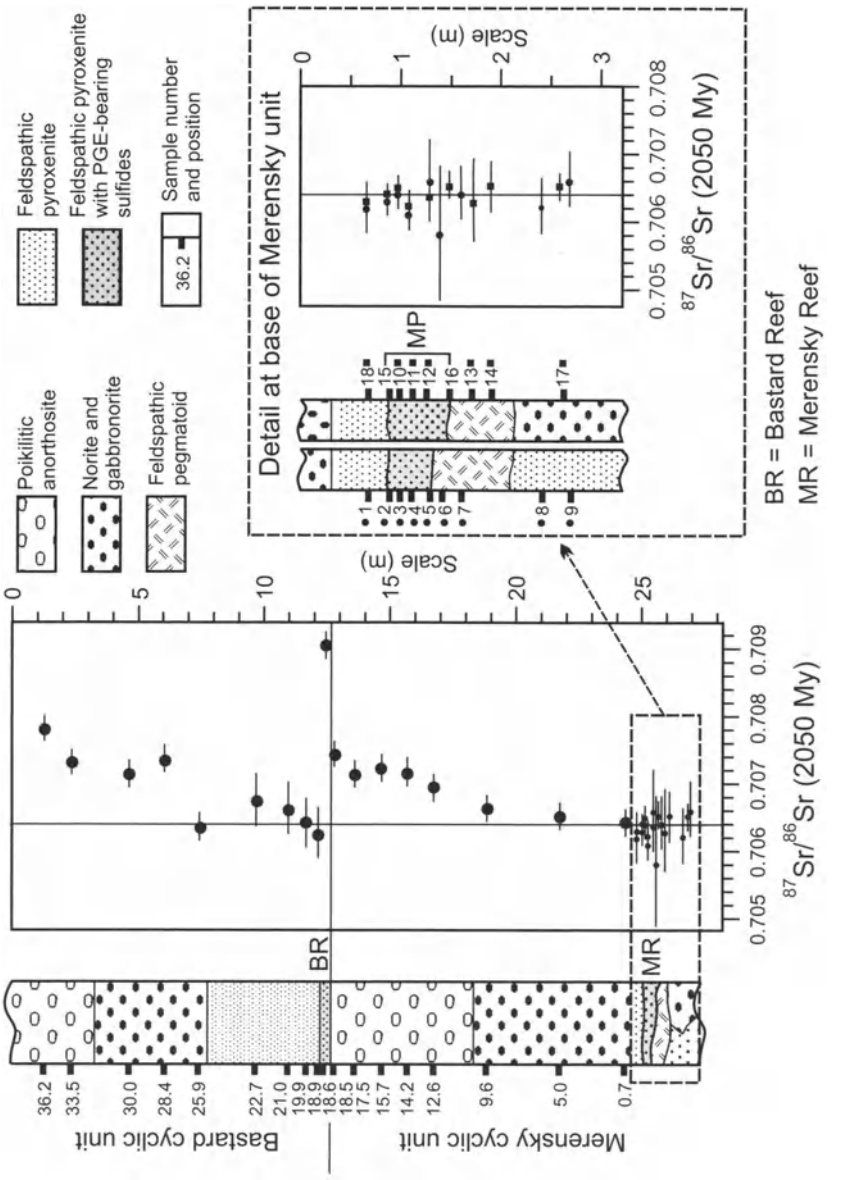


**Fig. 9.12.** Variations in Sr initial isotope ratios in the Bastard and Merensky cyclic units. After Lee and Butcher (1990)

Although the Reef is generally developed at the stratigraphic position shown in Fig. 9.11, in places it cuts down into the footwall rocks to reach a lower horizon (not always the same lower horizon) to form structures that are termed "potholes". Potholes are roughly circular to elliptical and their

sizes are very variable. Cawthorn et al. (2002) cited the average area of 950 potholes as being 55 $m^2$. Some are regional in extent and the deeper levels of the Union and Northam deposits lie 16 m deeper in the stratigraphy than "normal" Reef. The down-dip limit of this structure has not been delineated by mining yet, so the "pothole" extends at least 3 km down-dip.

The PGE contents in the Merensky Reef in different mines of the Bushveld are given in Table 9.4. Because the mining width varies from mine to mine, the data in the Table are given both for the mined width and for the best interval for each mine. Pd and Pt tenors (metal content in 100% sulfide) are of the order of 100 and 300 g/t respectively (see the Appendix) and the (Pt+Pd)/(Ni+Cu) ratio (PGE in g/t, Ni and Cu in wt%) is 16–19.

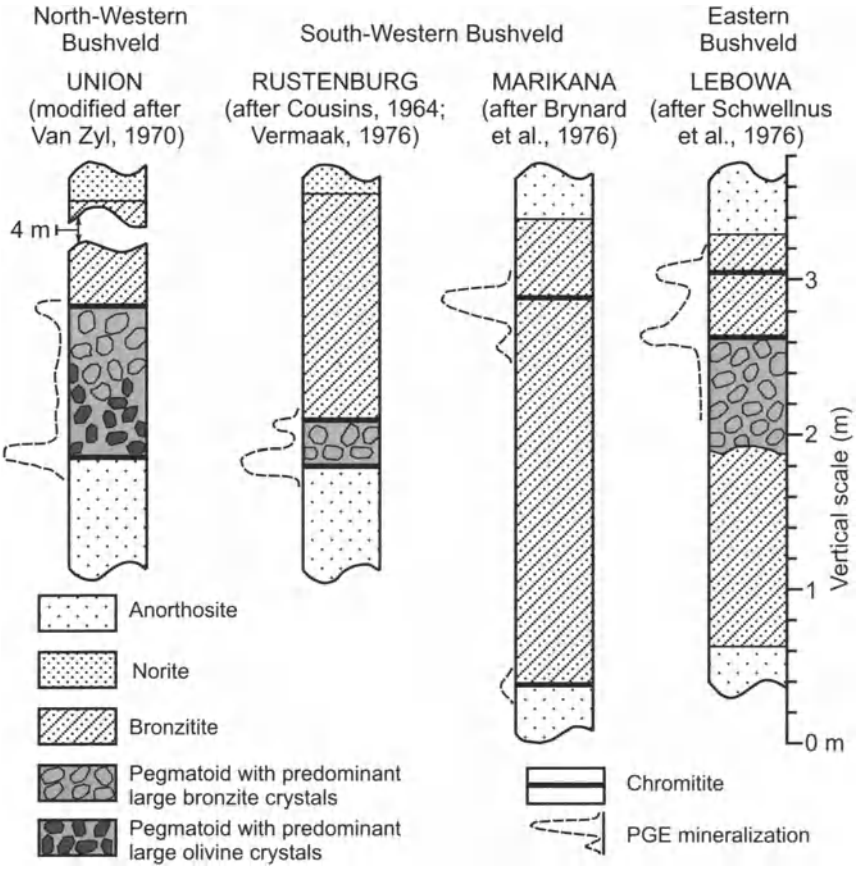


**Fig. 9.13.** The nature of the Merensky Reef at different locations within the Bushveld Complex (from Naldrett 1989)

**Table 9.4.** Average PGE grades associated with the Merensky Reef and UG-2 at different mines of the Bushveld Complex (after Cawthorn et al. 2002)

| | Total PGE grade (g/t) | | Individual PGE grades over mining width (g/t) | | | | | |
|---|---|---|---|---|---|---|---|---|
| | Over mining width | Over best interval | Pt | Pd | Rh | Ru | Ir | Os |
| **MERENSKY REEF** | | | | | | | | |
| **Western Limb** | | | | | | | | |
| Amandelbult | 6.7 | 7.9 | 3.89 | 1.88 | 0.27 | 0.47 | 0.10 | 0.07 |
| Union | 7.4 | 9.2 | 4.37 | 1.78 | 0.37 | 0.59 | 0.13 | 0.07 |
| Northam | 6.1 | | 3.72 | 1.59 | 0.18 | 0.43 | 0.08 | 0.12 |
| Impala | 4.9 | | 2.89 | 1.32 | 0.25 | 0.34 | 0.08 | 0.07 |
| Rustenburg | 6.9 | 8.5 | 4.07 | 1.86 | 0.28 | 0.55 | 0.09 | 0.06 |
| Western Plats | 5.6 | | 3.47 | 1.57 | 0.17 | 0.34 | 0.06 | 0.02 |
| **Eastern Limb** | | | | | | | | |
| Messina | 4.9 | | 2.35 | 2.01 | 0.15 | 0.25 | 0.10 | |
| Lebowa | 4.4 | 6.8 | 2.68 | 1.10 | 0.18 | 0.35 | 0.06 | 0.04 |
| Winnaarshoek | 5.9 | | 3.19 | 1.77 | 0.18 | 0.35 | 0.08 | |
| **UG-2 CHROMITITE** | | | | | | | | |
| **Western Limb** | | | | | | | | |
| Amandelbult | 5.1 | | 3.26 | 1.48 | 0.31 | | | |
| Union | 4.8 | | 2.98 | 1.44 | 0.43 | | | |
| Northam | 6.1 | | 3.29 | 1.28 | 0.61 | 0.61 | 0.12 | 1.83 |
| Impala | 5.2 | | 3.07 | 1.40 | 0.26 | 0.36 | 0.09 | 0.07 |
| Rustenburg | 6.1 | | 4.03 | 1.77 | 0.31 | | | |
| Kroondal | 5.8 | | | | | | | |
| Marikana | 4.6 | | | | | | | |
| Western Plats | 6.1 | | | | | | | |
| **Eastern Limb** | | | | | | | | |
| Messina | 6.1 | | | | | | | |
| Lebowa | 5.9 | | 3.78 | 1.89 | 0.24 | | | |
| Winnaarshoek | 7.1 | | | | | | | |

Note: Data are compiled from company annual reports, where available. However, these reports often quote average grade for the entire mine combining Merensky and UG-2 ore, and so Merensky grade is not given. In such cases, grade is taken from Hochrelter (2000). Variations in total PGE content occur in different reports. Some data are for metal produced, others are based on proven reserves, and yet others include resources. In some cases mine head grade is reported, in others it is in situ content. Some company reports quote assays for 4 or 5 PGE (which may exclude Ir and Os) and others include Au. The under-representation of the total PGE content due to such omission is less than 5%. Routine analyses for total PGE are by ICP-MS. The averaging of large numbers of analyses in this Table, and the monitoring of recoveries through the production of pure metal renders these data more reliable than analyses of single profiles by more precise techniques. The first column of figures is for the mined cut, which may include sections of lower grade ore in thin reef situations or cut-off grades of I.0 to 1.5 g/t for thick reef

### *Stratiform mineralization of chromite association*

The Chromitite horizons in the eastern and western lodes of the Bushveld Complex are divided into 3 groups (Fig. 9.14), the Lower Group comprising 8 distinct horizons (LG-1 to LG-6, LG-6A and LG-7), the Middle Group comprising up to 5 discrete horizons and the Upper Group comprising the UG-1, UG-2 (see Fig. 8.12.). No chromite occurs in the Lower Zone in these lobes. In contrast, 3 sequences of chromitite horizons occur in the Lower Zone of the Northern limb, a Lower Layer, and Upper Layer

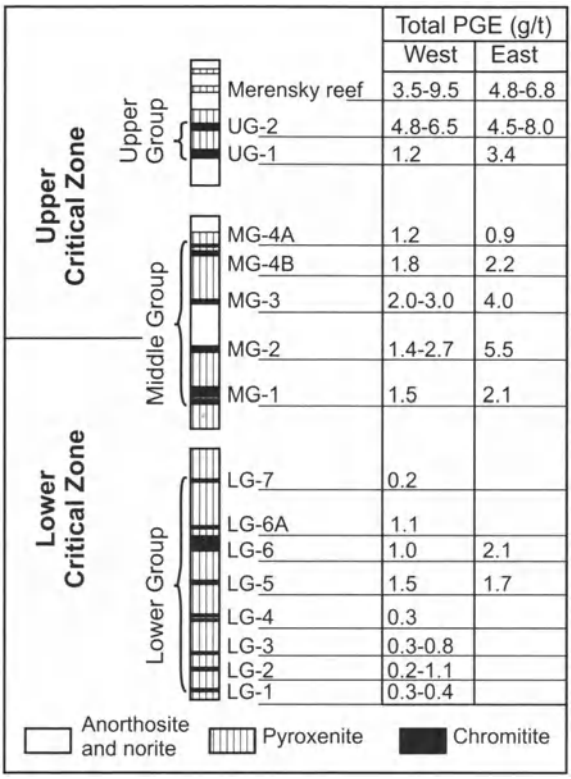


**Fig. 9.14.** Distribution of chromitite layers in a vertical section of Bushveld Complex along with the average PGE contents in chromitites of Western and Eastern Bushveld. Modified after Cawthorn et al. (2002)

comprising two separate layers, and, above this, a sequence of thin chromitite stringers (von Gruenewaldt et al. 1989). The Critical Zone of the northern limb, which is identified only south of the town of Potgietersrus (see section on Platreef below) contains one chromitite layer which von Gruenewaldt et al. compare with the UG-2.

Naldrett and von Gruenewaldt (1989) showed that all chromitites layers from the Bushveld (and Stillwater) Complex fall into two broad categories, those that formed above or close to the incoming of cumulus plagioclase, which tended to be PGE rich, have high (Pt+Pd)/(Ru+Ir+Os) ratios (2–5) and contain Fe-Ni-Cu sulfides, and those that formed below this level that tend to be PGE poor (< 1 ppm PGE), have (Pt+Pd)/(Ru+Ir+Os) <1and lack significant Fe-Ni-Cu sulfides (they may contain laurite). This is illustrated in Fig. 9.15, which is taken from their work, along with new data on the Great Dyke from Germann and Parry (1999) which shows that the generalizations derived from the Bushveld and Stillwater also apply to the Great Dyke. The Stillwater A chromitite appears to be an exception to the generalization, until it is appreciated that this unit occurs very close to and is

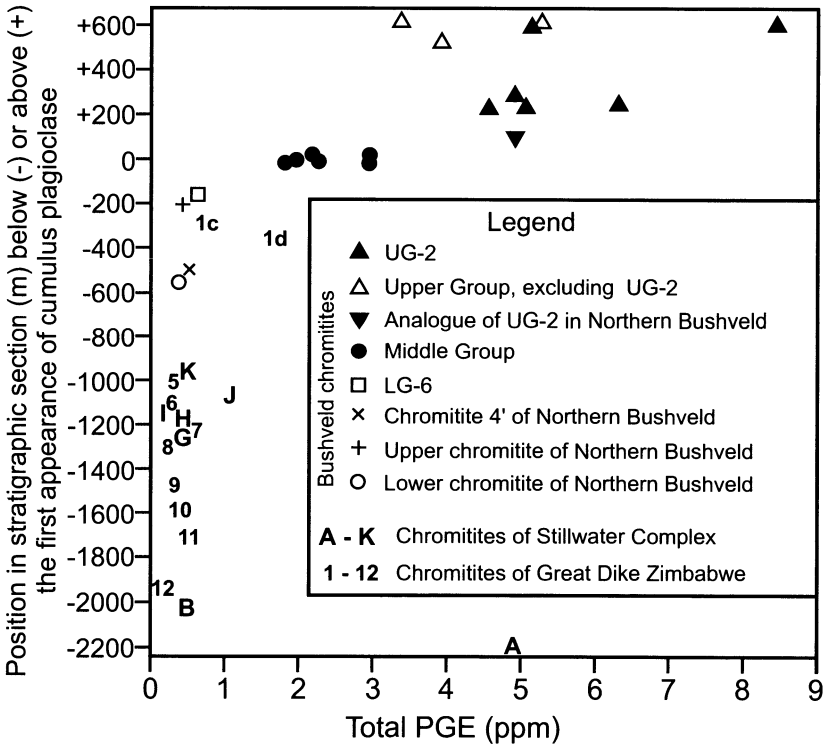


**Fig. 9.15.** Total PGE contents in chromitite layers through the stratigraphy of the Bushveld and Stillwater Complexes and the Great Dike of Zimbabwe. When Ir and/or Os contents were not determined each of of these elements was calculated as 0.25*Ru. After Naldrett and von Gruenewaldt (1989), with additional data from German and Parry (1999)

likely affected by the tendency for less primitive magma to be present near the margin of a large intrusion. The C1d chromitite of the Great Dyke is sulfide bearing, although it occurs several 100 m's below the incoming of cumulus plagioclase – this reflects the fact that the magma of the Great Dyke was closer to sulfide saturation during crystallization of ultramafic cumulates than was the magma responsible for either the Bushveld or Stillwater Complexes.

**UG-2.** The UG-2 chromitite horizon comprises the largest single known PGE resource in the world, even larger than the Merenasy Reef (see Table 1.1). The chromitite lies at the base of the UG-2 cyclic unit (Fig. 9.10), that varies in thickness from 15 to 400 m. Much of the following description is taken from Cawthorn et al (2002). The footwall to the chromitite is commonly a coarse, pegmatitic feldspathic pyroxenite. The main chromitite itself varies from 70 to 130 cm in the Western Bushveld. The layer consists of 60 to 90 modal percent chromite with interstitial plagioclase and orthopyroxene. The lower part of the layer has a granular texture, which becomes more poikilitic in the upper part. It is overlain by harzburgite or

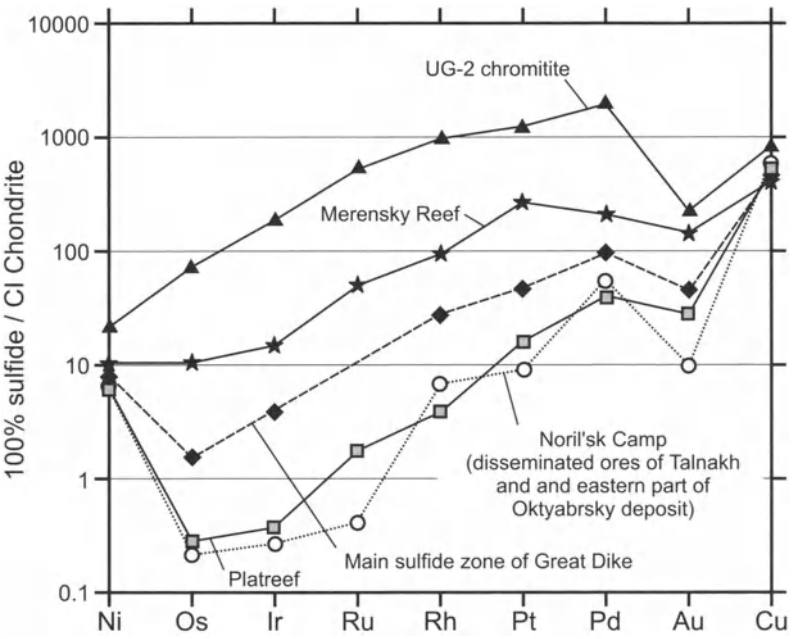


**Fig. 9.16.** Comparison of the chondrite normalized values of Ni, Cu and the noble metals in the average sulfides of some well-known deposits (data from Naldrett et al 1986 [Merensky Reef], Cabri and Naldrett 1984 [Platreef], Naldrett et al. 1987 [UG-2], Naldrett et al. 1996 [Noril'sk]; Naldrett and Wilson 1989 [Great Dyke])

feldspathic pyroxenite within which two to four, 1 mm to 12 cm-thick chromitite seams occur. Potholes also characterize the UG-2 horizon (Hahn and Ovendale 1994; Lomberg et al. 1999) and can be up to 50 m deep.

The average contents of PGE in the UG-2 at various mines of the Bushveld are compared with those for the Merensky Reef in Table 9.4. PGE contents over the mining width are quite similar in both horizons. The tenors of PGE in the sulfides of the UG-2 are compared with those of other deposits in Fig. 9.16, in which it is seen that the tenors are significantly higher than those of the Merensky Reef.

### *Stratiform mineralization of magnetite association*

**Late stage segregations of immiscible sulfides.** Von Gruenewaldt (1976) presented data for 3 samples (Table 9.5) from a layer of sparsely disseminated sulfide in anorthosite that occurs just below the Lower Magnetite layer 2 in the Bushveld complex.

**Table 9.5.** Sulfide Mineralization in the Bushveld Complex Upper Zone (whole-rock analyses of mineralized anorthosite below Lower Magnetite layer 2). From von Gruenewaldt (1976)

| Sample | S | Cu | Ni | Co% | Pt | Pd | Au | Pt+Pd |
|---|---|---|---|---|---|---|---|---|
| 1 | 2.23 | 1.10 | 0.18 | 0.02 | 0.76 | 0.76 | 0.40 | 1.52 |
| 2 | 2.30 | 0.92 | 0.17 | 0.02 | 0.83 | 0.96 | 0.47 | 1.79 |
| 3 | n.a. | 0.87 | 0.10 | n.a. | 0.61 | 0.99 | 0.54 | 1.60 |
| Average | 2.26 | 0.96 | 0.15 | 0.02 | 0.73 | 0.90 | 0.47 | 1.63 |

*n.a.* not analyzed. S, Cu, Ni and Co in wt%; PGE and Au in g/t (ppm)

As is to be expected in view of the fractionated nature of the magma from which they crystallized, the sulfides have high Cu/Ni ratios. The mineralization is, however, anomalous in having relatively high values of Pt, Pd and Au. This is due to the build up of incompatible noble metals during fractional crystallization. Fig. 9.17 illustrates this process for a magma containing an initial concentration of 20 ppb PGE. It is assumed that the magma undergoes perfect fractional crystallization and that periodically a new input of magma dilutes that already in the chamber so that the ratio of old to new magma is in a ratio of 2:1. Three scenarios are considered, the first assuming that 50% of magma crystallizes before new magma is introduced, the second assuming that 33 % crystallizes and the third that 25 % crystallizes before new magma is introduced. These assumptions are thought reasonable for large layered intrusions that are pos-

sibly acting as holding chambers for volcanism. It is seen that the build up in PGE in the magma chamber is substantial, particularly in the 50 % situation.

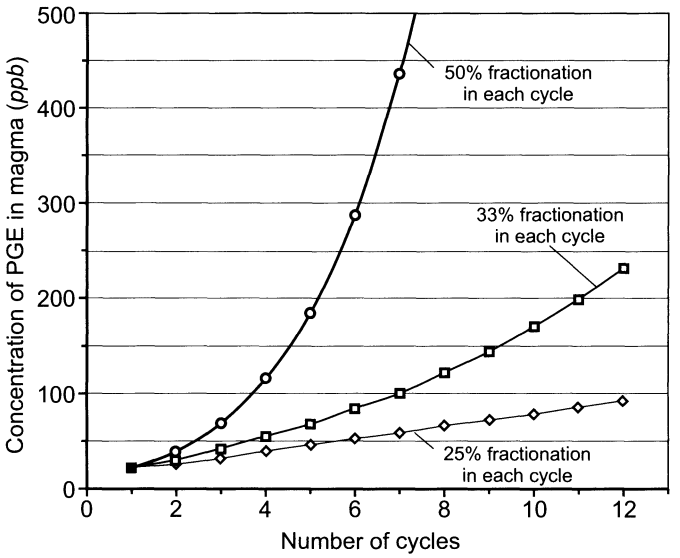


**Fig. 9.17.** Variation in PGE concentration with perfect fractional crystallization of a magma containing an initial concentration of 20 ppb total PGE, with repetitive inputs of fresh magma, assuming that the ratio of old to new magma is 2:1. The three scenarios shown consider the cases in which the magma in the chamber undergoes 50, 33 and 25 % crystallization each time before the new magma is introduced

While experience with actual deposits suggests that the noble and base metals of this association are unlikely to constitute ore in themselves, the occurrence of such sulfides in layers that are also enriched in Ti- and V-bearing magnetite along with apatite can result in the PGE's being an important by-product.

Examples of the latter association include the Volkovsky deposit in the Central Urals PGE belt (see discussion of Urals Platinum Belt below) and deposits in the Coldwell Complex of Northern Ontario.

### *Stratabound but non-Stratiform Deposits – The Platreef*

Mineralization in the Platreef is not strictly stratiform, but belongs to the stratabound category defined above. It lies within the Bushveld northern limb in which the geology is very different to that of the western and eastern lobes, so it is necessary to describe it here. Within the limb, a group of

mafic/ultramafic rocks that can be loosely equated with the Lower, Critical, Main and Upper Zones of the Bushveld Complex dip west at 30-40° where they pass beneath outcrops of Bushveld Lebowa granite and younger Proterozoic sediments of Waterberg group (Fig. 9.18). The length of the limb is approximately 110 km. In the south, the limb is terminated by the Zebediela fault, which brings the Bushveld rocks into sharp contact with Karoo-aged (Paleozoic-Mesozoic) sediments that lie south of the fault.

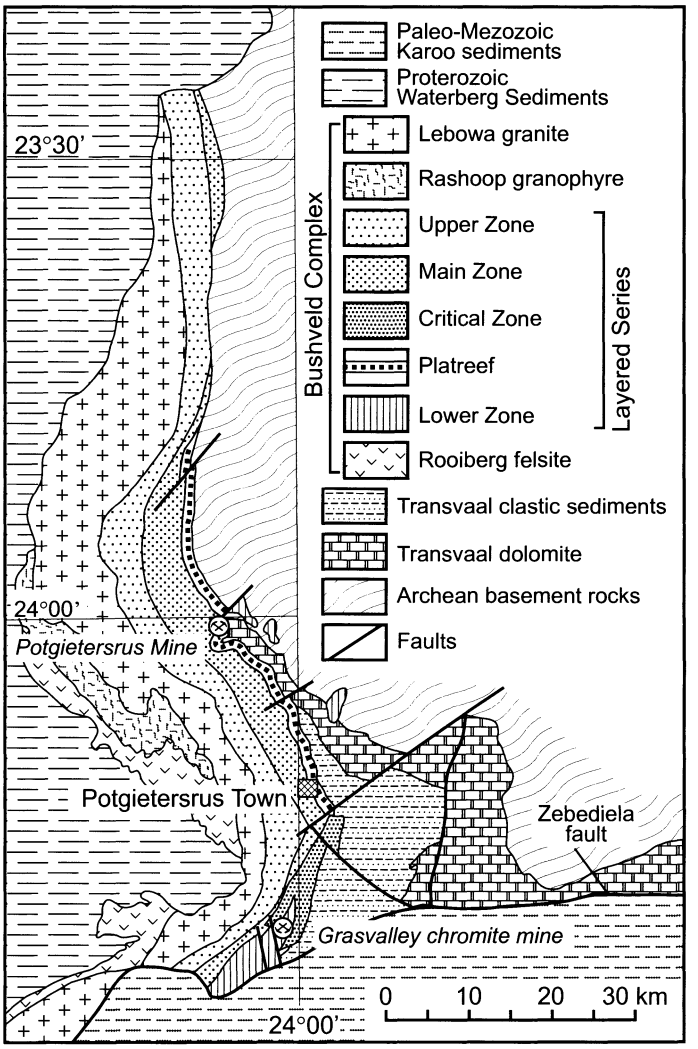


**Fig. 9.18.** Schematic geological map of the Northern Bushveld (after von Gruenewaldt 1989)

As shown in Fig. 8.15, at the southern end of the limb, rocks that have been equated with the Bushveld Lower Zone occur in contact with those equated with the Critical Zone. The Lower Zone rocks comprise harzburgite and orthopyroxenite. Harzburgite in this area is much more abundant than in Lower Zone rocks throughout much of the Bushveld. On the farms Volspruit, Zoetfeld, Rondeboschje and Grasvalley, chromite seams have been mined. The chromite has a Cr/Fe ratio of >2, which is unusually high in the context of the Bushveld. Rocks attributed to the Critical Zone overlie the Lower Zone unconformably. In this area, the Critical Zone (Fig. 9.19) consists of a lower, 20–30 m-thick layer of gabbro-norite, overlain by 70 m of orthopyroxenite and ortho+clinopyroxenite, both chromite-bearing, and then by a sequence of interlayered plagioclase-orthopyroxene ± clinopyroxene cumulates; these uppermost norites and gabbro-norites were termed Subzone 2 of the Critical Zone by Hulbert (1983), while the lower, more mafic rocks were termed Subzone 1. On the farm Grasvalley, a PGE-bearing chromitite occurs about 40 m above the base of the Critical Zone. Sulfide-containing intervals are found throughout the Critical Zone but, according to Hulbert, only 4 of these are significant. These are shown in Fig. 9.19. Contents of base and noble metals in those intervals are shown in Table 4.6.

At surface the Lower Zone is not present north of the farm Grasvalley, although Hulbert (1983) has suggested that it is present at depth. He concluded that introduction of early Critical Zone magma eroded ultramafic rocks of the Lower Zone in this area. It seems that the Critical Zone in the area south of Potgietersrus was emplaced as a series of highly energetic pulses of magma or magmatic mush, and that these eroded underlying material that had been deposited by earlier influxes of magma.

Little information is available about the Critical Zone in the vicinity of Potgietersrus. Farther north, in the area shown illustrated in Fig. 9.20, this part of the sequence is so changed that the name Critical Zone is not used, and the rocks in the equivalent part of the section are referred to as the Platreef, which takes on a distinctive layered character of its own. In the Sandsluit area, where the principal mining operations are centred at the present time (2004), the Platreef underlies a mottled anorthosite that is equated with the Main Zone. The upper part, which is referred to as C Reef, comprises an unmineralised pyroxenite (Fig. 9.21). This is underlain by a well-mineralised, coarse-grained pyroxenite with minor intercumulus plagioclase referred to as B Reef. Ortho- and clinopyroxene are normally present in equal proportions and virtually no olivine is present. This is underlain in turn by a very inhomogeneous (both texturally and compositionally) feldspathic pyroxenite, referred to as A Reef in which 1–3 cm diameter blebs of base metal sulfide (BMS) are common.

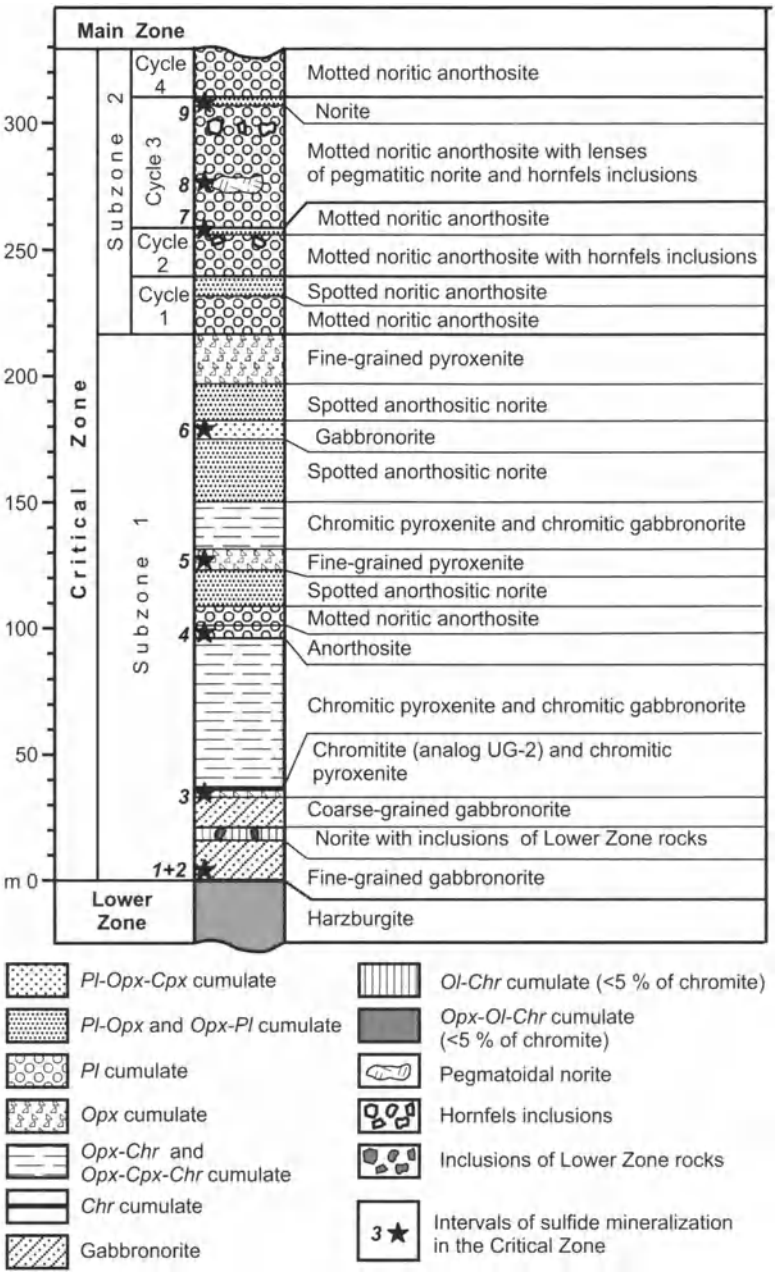


**Fig. 9.19.** Vertical section through the Critical Zone of the Northern Bushveld as it is developed south of Potgietersrus. Analytical data are given for the most significant intervals of sulfide mineralization in Table 9.6. Based on data from Hulbert (1983)

**Table 9.6.** The most significant contents of base and noble metals in intervals of sulfide mineralization (shown in Fig. 9.19). After Hulbert (1983)

| No | Rock | S | T | Ni | Cu | Pt | Pd | PGE + Au |
|---|---|---|---|---|---|---|---|---|
| 3 | Analogue of UG-2 chromitite | 1a | 1.35 | 0.19 | 0.05 | 1.92 | 0.99 | 3.38 |
| | | 1b | 1.65 | 0.27 | 0.19 | 1.06 | 0.90 | 2.15 |
| | | 1c | 1.06 | 0.14 | 0.12 | 0.94 | 0.45 | 1.56 |
| 6 | Gabbronorite | | | 0.09 | 0.05 | | | 0.90 |
| 8 | Pegmatoidal norite | 3a | 0.67 | 0.14 | 0.05 | 1.13 | 0.93 | 2.20 |
| | | 3b | 0.51 | 0.13 | 0.06 | 0.89 | 0.61 | 1.67 |
| | | 3c | 1.07 | 0.01 | 0.01 | | | <0.60 |
| | | 3d | 0.13 | 0.37 | 0.26 | | | 3.76 |
| 9 | Norite | 4a | 0.30 | 0.21 | 0.24 | | | 1.02 |
| | | 4b | 0.25 | 0.13 | 0.13 | | | 1.09 |

*No* Numbers of intervals; *S* Sample: *T* Thickness (m). Ni and Cu in wt%; PGE and Au in g/t

In the northern part of the reef, on the farms Drenthe and Zwartfontein, the Platreef is also overlain by a mottled anorthosite belonging to the Main Zone (Fig. 9.21). Well mineralized zones grading 1–2 g/t over 4–40 m, commonly associated with dolomite inclusions and resembling Platreef, occur as much as 100 m within the Main Zone in the northern part of the farm Drenthe (Mark Prefontaine, personal communication, March 2002). These are not found to the south. The designation into C, B and A reef is somewhat artificial in the Drenthe area. The C reef is defined as an impersistent, 1–2 m zone of unmineralized pyroxenite. This is underlain by a generally well-mineralized, pegmatitic pyroxenite, which constitutes the pyroxenitic B Reef. With increase in plagioclase, this may grade laterally, or downwards into feldspathic B Reef. Grain size decreases stratigraphically downward below the B reef, and mineralization also decreases; this part of the Platreef is referred to as A Reef. Commonly it becomes chilled and develops a trachytoidal texture adjacent to the footwall tonalite. Overall the texture of the Platreef in the Drenthe area is patchy, with large gradations in grain size. The more pegmatitic portions appear to be the result of crystallization in situ. A weakly developed lineation of pyroxene and plagioclase is observed, parallel to the 40° dip of the contact and aligned at right angles to the strike, suggestive that emplacement of the Platreef magma has been up-dip, from depth, rather than parallel to strike.

Throughout its development, the Platreef is highly contaminated. Inclusions of dolomite are always present, although they vary in amount, and are most prevalent and largest (up to 100 m in diameter) in areas where the footwall is dolomite. Smaller inclusions have been largely converted to calc-silicate rock. The calc-silicate xenoliths are typically mantled by up to

20 m of serpentinized pyroxenite containing serpentinized olivine and magnetite.

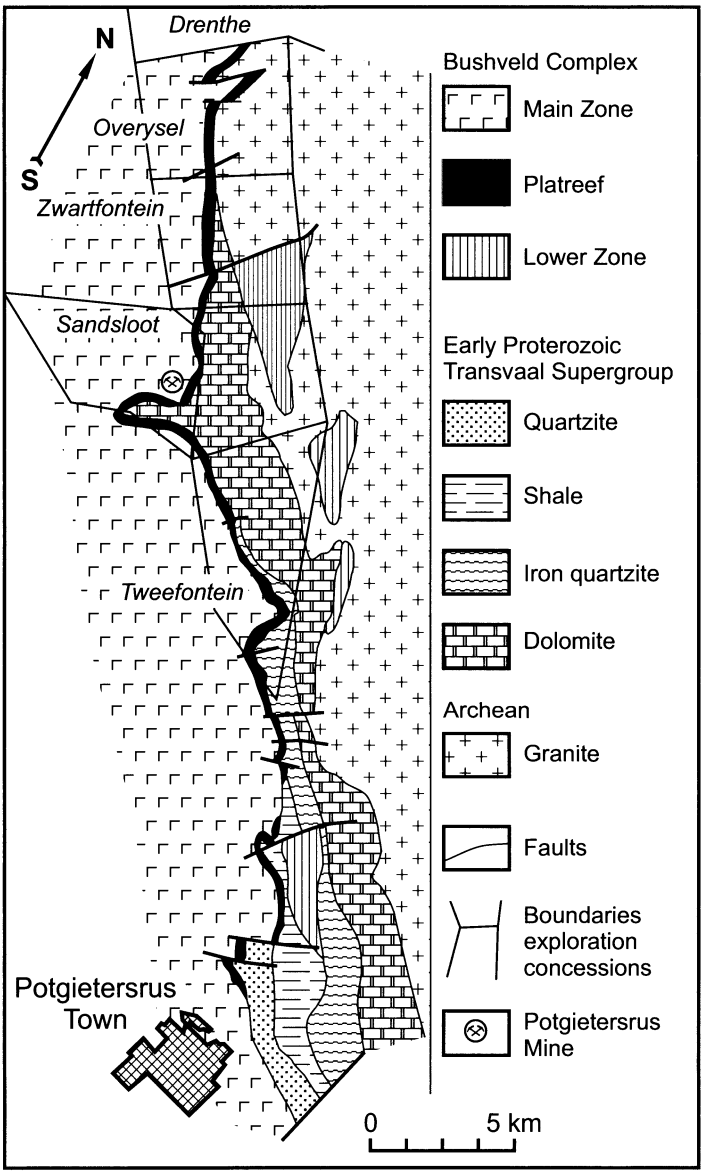


**Fig. 9.20.** Geological map showing the Platreef as it is developed north of Potgietersrus. Mining is in progress at the Potgietersrus open pit (Sandsloot area) and is being planned in the Overysel, Zwartfontein, and Tweefontein areas. Simplified after Cawthorn et al. (2002), who adopted this map from White (1994)

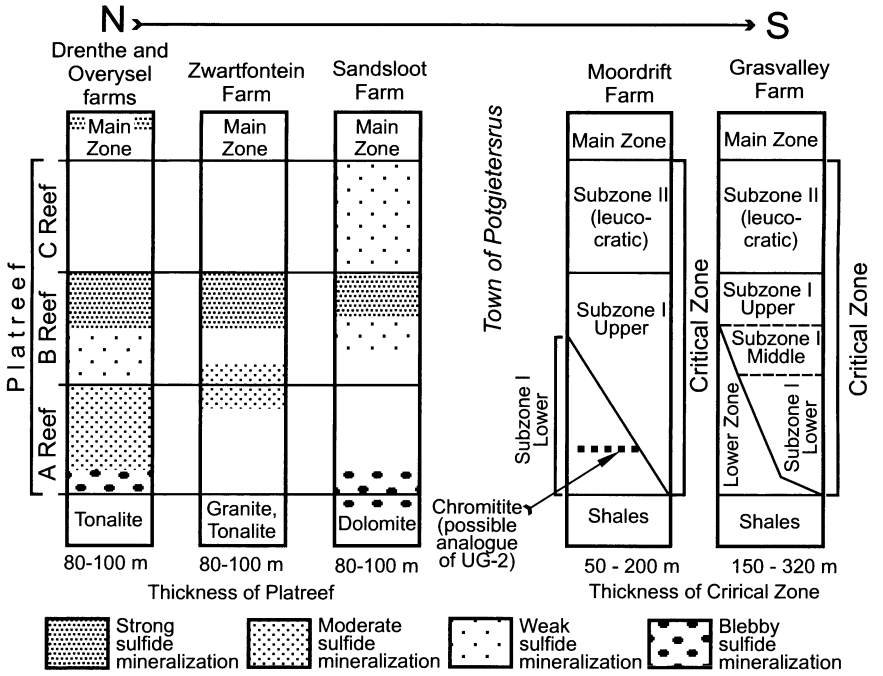


**Fig. 9.21.** Variations in stratigraphy of the Platreef from north to south along the Northern Limb of the Bushveld Complex

PGE distribution in the Platreef tends to be highly irregular (Fig. 9.21). In general the best mineralization occurs in the upper part of the B Reef, although coarse sulfides (in some cases almost massive) with good PGE values may occur towards the base of the A Reef. The C Reef is never strongly mineralized. Values cited in Table 1.1 for the Sandsluit mining operation are 0.41 wt% Ni, 0.20 wt% Cu, 1.77 ppm Pt, 2.01 ppm Pd and 0.11 ppm Rh. The PGE content in 100% sulfides and the (Pt+Pd)/(Ni+Cu) ratio are contrasted with those of sulfides in the UG-2, Merensky Reef, MSZ of the Great Dyke and typical Noril'sk mineralization in the Appendix. It is seen that the sulfides are less rich than those of stratiform reefs, and compare closely with typical Noril'sk sulfides.

### *Discordant Mineralization – Dunite Pipes*

The Bushveld Complex contains many cross-cutting igneous structures which are an integral part of the mafic/ultramafic igneous layered series, but which are not explicable in terms of straightforward igneous crystallization. These include vanadiferous magnetite pipes such as that at Kennedy's Vale, pegmatoidal pipes, and discordant replacement bodies in

which bronzitite, norite and particularly anorthosite layers are replaced by a pegmatoidal rock composed of bronzite and olivine (typically $\approx Fo_{70}$). Platiniferous dunite pipes are another example of these structures.

These pipes, along with their associated envelopes of olivine-bronzite-plagioclase pegmatoid occur in both the western and eastern sections of the Bushveld Complex. Mining and/or geological studies have been restricted to four pipes in the eastern section (Onverwacht, Mooihoek, Driekop and Maandagshoek) – see Fig. 9.6. The pipes have some of the highest PGE grades reported for the Complex. Wagner (1929) cited grades ranging up to 2,050 ppm total PGE. On the 65 ft-level of the Onverwacht pipe, the central 8-m-diameter core of the pipe averaged over 31 ppm Pt, and a 1-m shell surrounding this core graded between 15 and 30 ppm Pt. The average Pt grade for the mine was between 9 and 11 ppm, while that for the nearby Driekop pipe was 5 to 6 ppm.

The Onverwacht pipe (Wagner 1929; Cameron and Desborough 1964) is typical. A central 20-m-diameter zone of hortonolite dunite (olivine composition, $Fo_{22}$) tapers downwards and is encased within a 100-m-diameter zone of olivine dunite (olivine $Fo_{86\text{-}92}$ at the margin, $Fo_{80\text{-}84}$ near the core). The olivine dunite defines a pipe which is perpendicular to layering in the surrounding bronzitite. Patches of magnetite and ilmenite occur within the pipe; mining revealed the presence of numerous slabs of chromitite at the level at which the pipe transects the LG 6 chromite layer (Steelpoort seam) in the bronzitite. On the basis of textural studies and evidence such as the chromitite, Cameron and Desborough (1964) concluded that the pipe resulted from the replacement of bronzitite by hot aqueous solutions which leached $SiO_2$, $Al_2O_3$ and $Na_2O$ and introduced FeO, $TiO_2$, V and the PGE. Gain (1980) noted that the LG 6 chromitite layer dips markedly in towards a dunite pipe on the farm Maandagshoek, suggesting that simple volume-for-volume replacement is not a sufficient explanation of the emplacement of the pipes. Schiffries (1982) proposed a model in which Cl-rich brines had introduced Pt and other elements and removed Mg. Whereas the Mooihoek pipe is very similar to Onverwacht, the Driekoep pipe differs in that the dunite of the cores is less iron-rich, containing approximately 70 mole percent forsterite.

Similar Pt-bearing discordant structures have been reported from the Stillwater complex, but have not been described in the literature.

### 9.4.2 Stillwater Complex

#### *Geology and Geochemistry*

The Stillwater Complex (Fig. 9.22) is a differentiated, stratiform, mafic/ultramafic intrusive body of late Archean age (2.705±4 Ga; Premo et al. 1990). It was intruded shortly after the emplacement of a 2.73-2.79 Ga granitic batholith that is exposed in the Beartooth uplift of SW Montana (Wooden et al. 1991). The Stillwater outcrops for 48 km along the northern margin of the Beartooth mountains. In part, the complex has intruded mafic and ultramafic igneous rocks and clastic magnesium- and iron-enriched sediments, including iron formation, that are all older than 3.27 Ga and belong to the Wyoming Archean Province. The complex is only partly exposed, and its original size is unknown, although gravity data (Fig. 9.23) indicate that it extends 40 km northeast of the northern margin of the Beartooth Mountains. The dip of the igneous layering of the complex is steep to overturned. Intrusive contacts with the underlying Archean rocks are preserved in places, although the basal contact cuts across some of the stratigraphic units of the country rocks which implies that it may have been intruded along an unconformity or fault zone. The complex is cut by quartz monzonites that are dated at 2.700 Ga and mafic dykes of similar to younger age. Faulting and tilting of the complex occurred prior to the Middle Cambrian, from which time through to the Cretaceous 2,400–3000 m of marine and continental sediments were deposited with breaks during the Silurian and Permian. Volcanism began during Late Cretaceous time, and Laramide deformation was initiated. Deformation continued through to the early Eocene, accompanied by the emplacement of siliceous and intermediate sills, dykes and stocks. The Laramide deformation occurred in response to northward and southward thrusting along northwest-striking faults. The upper contact of the Stillwater complex is partly an unconformity with overlying Paleozoic sediments, partly a thrust contact along which the same sediments have been thrusted over the layered igneous rocks. As discussed below, by analogy with the Bushveld Complex, much of the upper part of the Stillwater complex is not exposed.

The layered igneous rocks of the Stillwater Complex are divided into three major series, the Basal, Ultramafic and Banded Series (Fig. 9.7). The Banded Series is further subdivided into the Lower, Middle and Upper Banded Series. Both series are subdivided into zones – the Ultramafic Series into the Peridotite Zone, within which all of the chromitite layers occur, and the overlying Bronzite Zone. The Banded Series is characterized by a sequence of zones of norite and gabbro, separated by zones in which

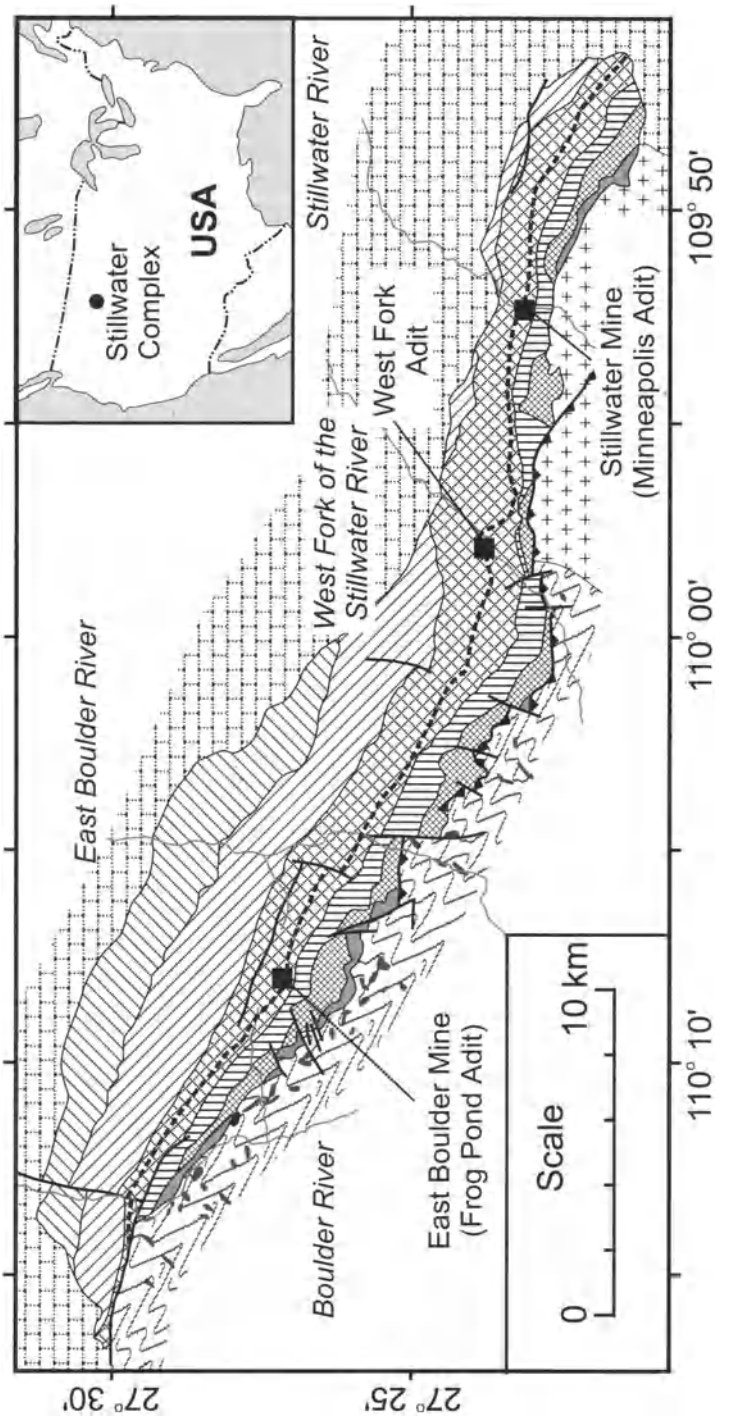
Stillwater Complex
USA
Stillwater River
West Fork of the Stillwater River
West Fork Adit
Stillwater Mine (Minneapolis Adit)
East Boulder River
Boulder River
East Boulder Mine (Frog Pond Adit)
Scale
0
10 km
109° 50'
110° 00'
110° 10'
27° 25'
27° 30'

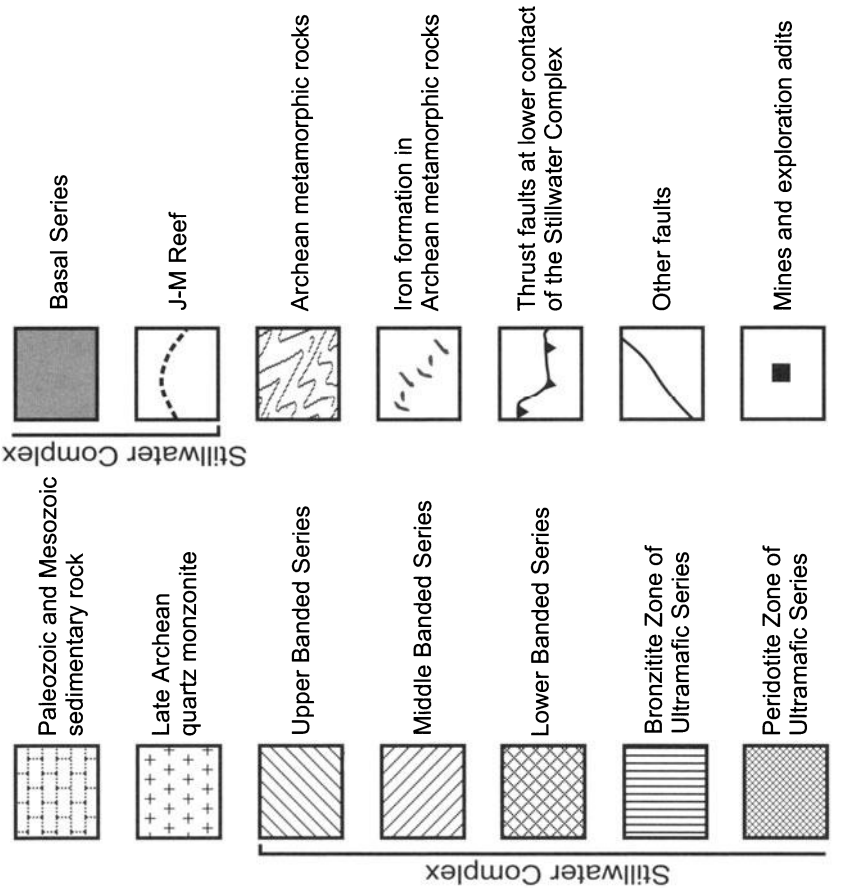


**Fig. 9.22.** Generalized geological map of the Stillwater complex drawn on the basis of maps and data presented in Czamanske and Zientek, eds (1985), and Zientek et al. (2002)

numerous cyclic units starting with olivine cumulates are present. The olivine-bearing packages of rocks are referred to as Olivine-bearing zone I, II, III etc. (OB-I, OB-II, OB-III etc.), and the intervening norite and gabbro zones as Norite Zone I, GabbroNorite Zone I etc. (N-I, GN-I etc). The cyclic units comprising the OB-1 Zone are illustrated in Fig. 9.24. As is seen, not all of these cyclic units are present throughout the complex. The principal mineralization comprises the J-M Reef. This occurs at the base of the sixth cyclic unit up from the base of OB-1, which is numbered 5b (because at the time the numbering was devised, one underlying cyclic unit had not been recognized!). The number of underlying cyclic units decreases from west to east and, at the Stillwater mine (Minneapolis adit) itself, much of

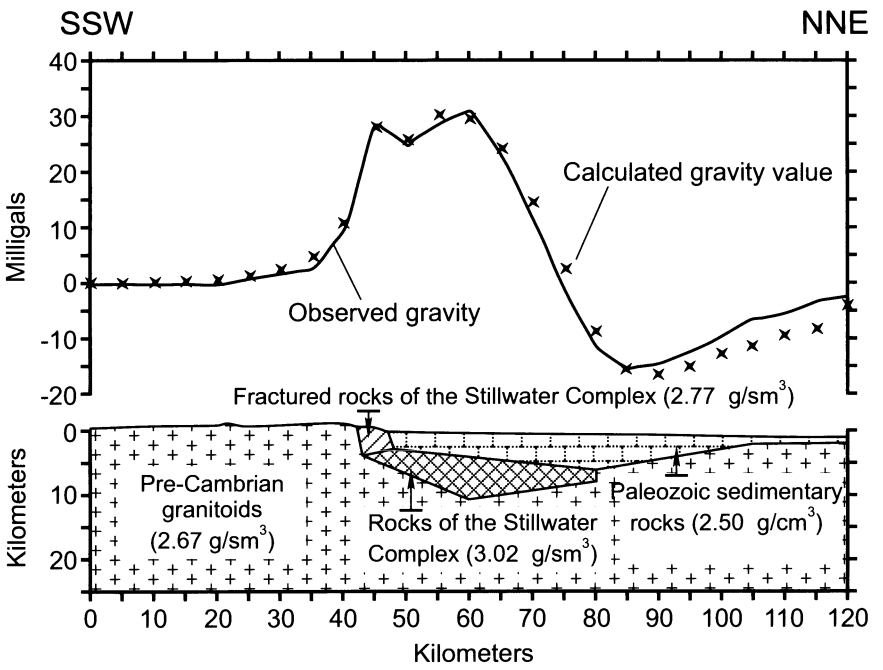


**Fig. 9.23.** Bouguer gravity profile and schematic geologic section oriented southwest-northeast across the Stillwater complex, showing the density determined for each unit. After Kleinkopf (1985)

the underlying stratigraphy is missing. It has been suggested (Turner 1985) that the base of the complex was uplifted in the Minneapolis adit area while crystallization was proceeding, and that magmatic erosion removed much of the lower part of OB-1, along with the underlying Gabbro Zone 1, so that cyclic unit 5b was deposited directly on Norite Zone 1.

Todd et al. (1982) concluded that changes in the sequence of appearance of cumulus phases from olivine followed by orthopyroxene to olivine followed by plagioclase in cyclic units adjacent to the J-M Reef horizon in the Stillwater complex required the addition of new magma of different, more aluminous composition at this stage in the development of the intrusion. The Sm-Nd and Re-Os studies of Lambert et al. (1989) on the J-M Reef have supported this interpretation, but their Os data (Fig. 9.25) require that a substantial component (up to 30 wt%) of the Os was derived from the crust. Crustal Os is also a component of the A and B chromitites near the base of the ultramafic series, and in the I chromitite in the centre of this series, but is not present in the G chromitite just below the I. This interplay of two magmas, one MgO-rich, and the other with a more tholeiitic (high-$Al_2O_3$) composition close to the level at which the princi-

pal PGE reefs occur is very analogous to the Bushveld Complex, and is thought significant from the point of view of the development of the reefs (see below). The Os isotope data would suggest that both magmas had interacted with the crust, just as is indicated for the magmas responsible for the Bushveld Complex.

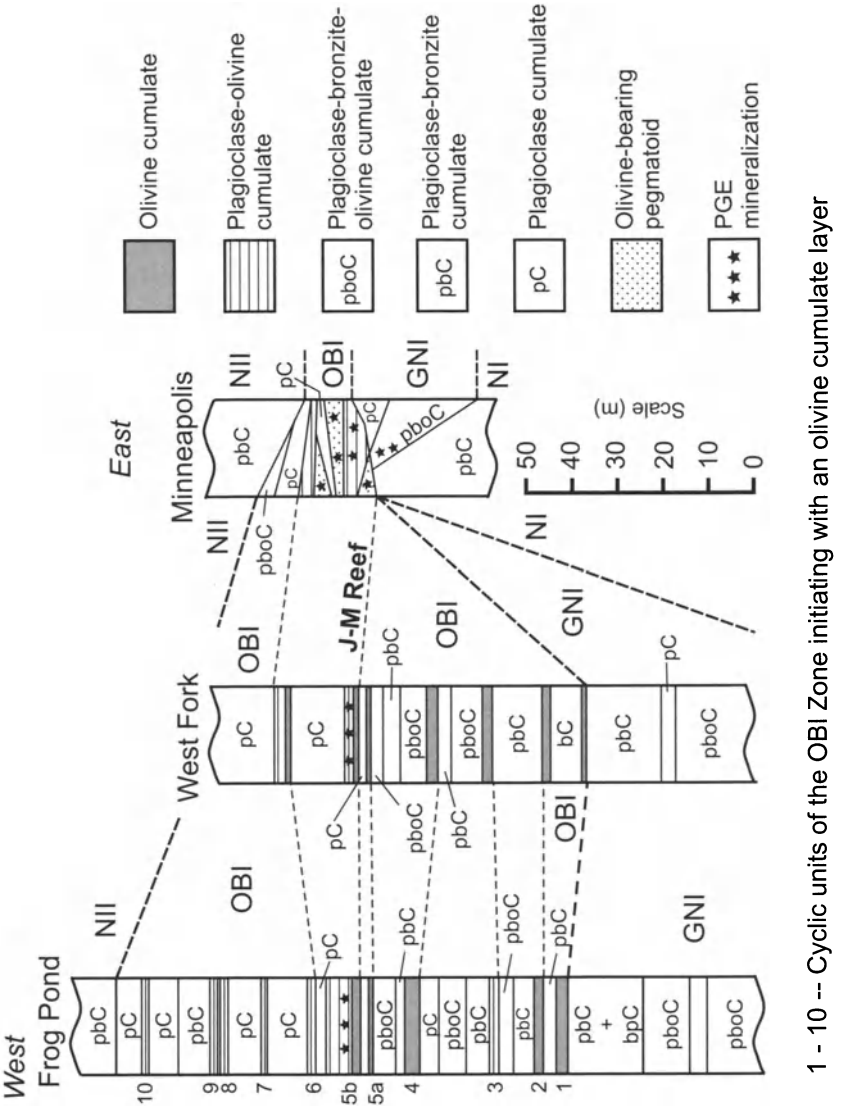


**Fig. 9.24.** Igneous stratigraphy of OBI Zone showing the cyclic units in the vicinity of the J-M Reef, in the Stillwater Complex. Modified after Naldrett et al. (1987); data from Todd et al. (1982), Leroy (1985) and Turner et al. (1985)

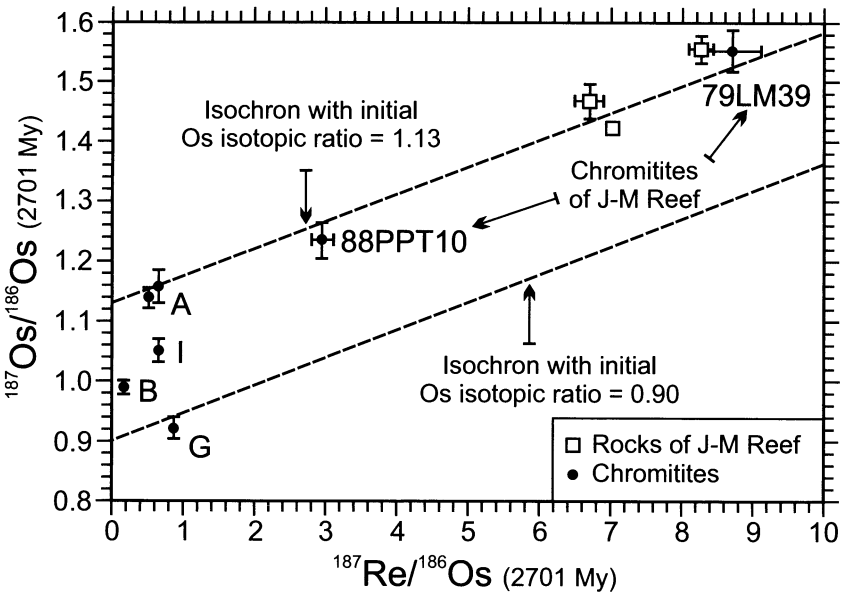


**Fig. 9.25.** Variation in $^{187}Os/^{186}Os$ initial ratios in chromitites and rocks of the J-M Reef of the Stillwater Complex. After Lambert et al. (1989)

Sulfide associated PGE mineralization in the Stillwater complex is of 4 types (Zientek,et al. 2002): (1) stratiform concentrations of disseminated, PGE-enriched sulfide minerals (J-M Reef); (2) sulfide and PGE mineralization concentrated at or below finer grained layers (the Picket Pin occurrence); (3) pegmatoidal lenses, pipes and other discordant mineralization (analogous to the dunite pipes of the Bushveld); and (4) magmatic sulfides concentrated near the base of the intrusion. Of these, the stratiform mineralization is the only type that is currently economic to mine, and is the only type discussed in detail here.

### *Stratiform mineralization: J-M Reef*

At present (2004) mining of the J-M Reef, which is the principal economically viable concentration of sulfide, is proceeding in two locations, one at the original Stillwater Mine in the valley of the Stillwater River, and the other at the East Boulder Mine, 22 km west along strike from the Stillwater Mine (Fig. 9.22). In the latter mine, mining operations are accessed via a 4.5 km adit which has been driven south through rocks stratigraphically higher than the Reef.

The J-M Reef occurs within a package of rocks referred to by mine geologists as the "Reef Package" (Corson et al. 2002). The mineralization itself is associated with pyrrhotite, chalcopyrite and pentlandite that form fine to coarse grained aggregates that are interstitial to silicates of the Reef Package. The sequence of layers within this package consists of varying thicknesses of troctolite, anorthosite, peridotite/dunite and norite, troctolite being the most abundant. The base of the package corresponds with the base of olivine-rich pegmatoidal rocks that contain coarse grained postcumulus pyroxenes. The top of the package cannot be defined on lithology alone, since it commonly cuts across lithologic contacts, but can always be recognized by a change in texture, where the pegmatoidal pyroxene, adcumulus rings of pyroxene around anhedral olivines and coarse grained interstitial pyroxene characteristic of the package give way to rounded cumulus olivine and fine to medium grained intercumulus pyroxene of the hangingwall. The top of the package is usually, but not invariably, coincident with the top of the PGE ore, because the grade and thickness of the mineralization is highly variable within the package itself. Horizons rich in PGE can be separated by PGE-poor zones within the package, and the mineralization can occur within any of the layers comprising the package, and, in places, in the noritic rocks beneath the olivine-rich layer that defines the base of the package (Fig. 9.26).

Very important from the point of view of economic mining are areas in which the mineralization extends up to 20 m below the base of the package to form thick, well-mineralized zones known as "ballrooms" (Fig. 9.27). These differ from the potholes of the Bushveld, which involve a displacement of the Merensky Reef itself to a lower stratigraphic level, in that all of the material constituting the ballrooms is well mineralized. Childs et al. (2002) noted that three types of ballroom structure have been identified at the Stillwater mine to-date. These are: (1) thickened zones of mineralization extending from the hangingwall down into lithologies of the footwall; (2) thickened mineralization within a thickened portion of the reef package itself; and (3) mineralization within footwall lithologies separate from that in the reef package. The first type is the most common. The textural relationships of sulfides constituting ballroom mineralization is generally similar to that in the typical reef package, although coarse sulfide clots with veinlets extending out from them for up to 5 cm are a particularly common occurrence when the ballroom mineralization is developed within the footwall gabbros and/or norites.

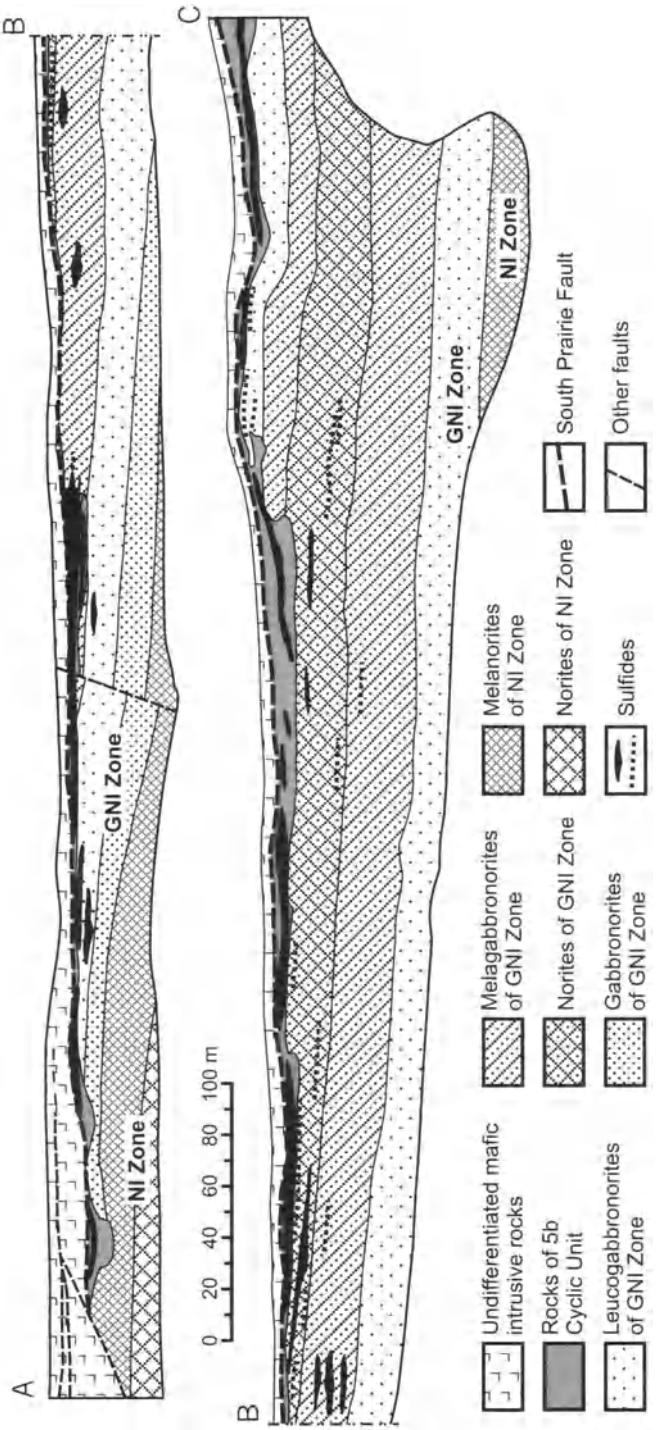


**Fig. 9.26.** Plan view of the 5700 W level of the Stillwater mine showing the angular discordance between the 05b cyclic unit and underlying rock of Gabbronorite Zone I (GNI) and Norite I (NI) and the distribution of PGE-enriched sulfide minerals. The western part of the plan is shown at the top (A to B) and the eastern part beneath (B to C). Stratigraphic tops are toward the top of the illustration. From Zientek et al. (2002), who used a compilation by D. Wolfgram and J. Holmgram (written communication 1988)

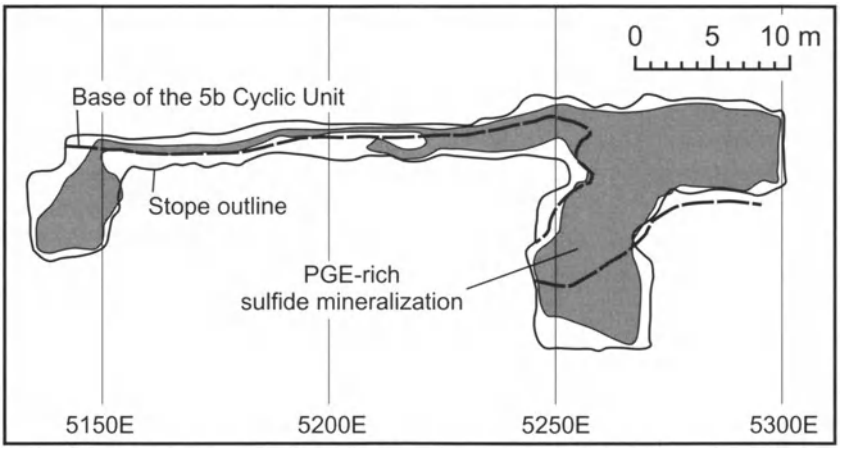


**Fig. 9.27.** Plan map of Floor 15 of the 52E 5280 slope, Stillwater mine, showing "ballroom"-style mineralization that extends into rocks underlying the olivine-bearing lithologies. Stratigraphic top is toward the top of the illustration. From Zientek et al. (2002)

Zientek (2002) has compiled the resources of (Pt+Pd) that are associated with the J-M Reef. These are reproduced here in Table 9.7. The Pd/Pt ratio is consistent at 3.27 throughout the Stillwater mine itself. The Pd and Pt tenors are extremely high, being 5410 and 1560 g/t respectively, with a (Pt+Pd)/(Ni+Cu) ratio (PGE in g/t, Ni and Cu in wt%) of 354 (see the Appendix).

**Table 9.7.** Resources of J-M Reef (Stillwater Complex). After Zientek et al. (2002)

| Mine | $10^6$ tonnes Mineralisation | ppm Pt+Pd |
|---|---|---|
| **Stillwater** | | |
| Proven Reserve | 2.44 | 25.7 |
| Probable Reserve | 17.74 | 24.3 |
| Mineralised Material | 19.66 | 24.7 |
| **East Boulder Mine** | | |
| Probable Reserve | 12.08 | 24.3 |
| Mineralised Material | 14.94 | 24.7 |
| **Entire Reef*** | 130 | 20 |

*Estimate based on 42 km strike length, 1.83 m width, 600 m depth and rock density of 2.87 g/cc

### 9.4.3 Great Dyke of Zimbabwe

#### *Geology*

The Great Dyke is a linear intrusion of mafic and ultramafic rocks that cuts across the Archean granites and greenstones of the Zimbabwe craton (Fig. 9.28). It is 550 km in length and from 4 to 11 km wide. Recent U-Pb age determinations on zircon indicate an emplacement age of 2.579±0.007 Ga (Armstrong and Wilson 2000). The general cross section of the Dyke is trumpet-like (Fig. 9.29) with layers dipping towards the center.

The intrusion consists of a series of narrow, contiguous magma chambers, each defined on the basis of structure, style and continuity of layering (Wilson and Prendergast, 2001). The North Chamber is subdivided into the Sebakwe, Darwendale and Musengezi subchambers, and the South Chamber into the Wedza and Selukwe subchambers. The stratigraphy comprises an upper mafic sequence of gabbro and norite and a lower ultramafic sequence of dunite, chromitite, harzburgite and pyroxenite. The thickest sequences are in the largest subchamber, which is the Darwendale (Fig. 9.30).

All subchambers are synclinal in transverse view with essentially the same lithological sequences exposed on both sides of the longitudinal axis. The plunge is to the south in the northern part of each subchamber and to the north in the southern part, so that the layers have the form of a series of stacked canoes. Wilson and Prendergast (2001) emphasize that the dominant aspect of the geology of the dyke is the cyclic layering. This differs in detail from subchamber to subchamber, but that shown in Fig. 9.30 for the Darwendale subchamber is typical. The cyclic units are interpreted to be the result of periodic influxes of fresh magma of one compositional type, a high magnesian basalt containing about 15 wt% MgO. A marginal border group has been identified in most subchambers. This consists of a series of layers close to the margins of the dyke that are almost parallel to the walls. The layers comprise gabbro, norite and pyroxenite; in some places the rocks show a strong crystal alignment perpendicular to the walls of the magma chamber. (Wilson 1982, Wilson and Prendergast 1989a). As seen in Fig. 9.30, the sequence of crystallization is (chromite), olivine, olivine + orthopyroxene, orthopyroxene, orthopyroxene + clinopyroxene, (olivine) + orthopyroxene + clinopyroxene + plagioclase, (orthopyroxene) + clinopyroxene + plagioclase. This sequence, along with the high proportion of ultramafic rocks, is indicative that the magma was of high magnesian type akin to the first magma introduced into both the Bushveld and Stillwater Complexes.

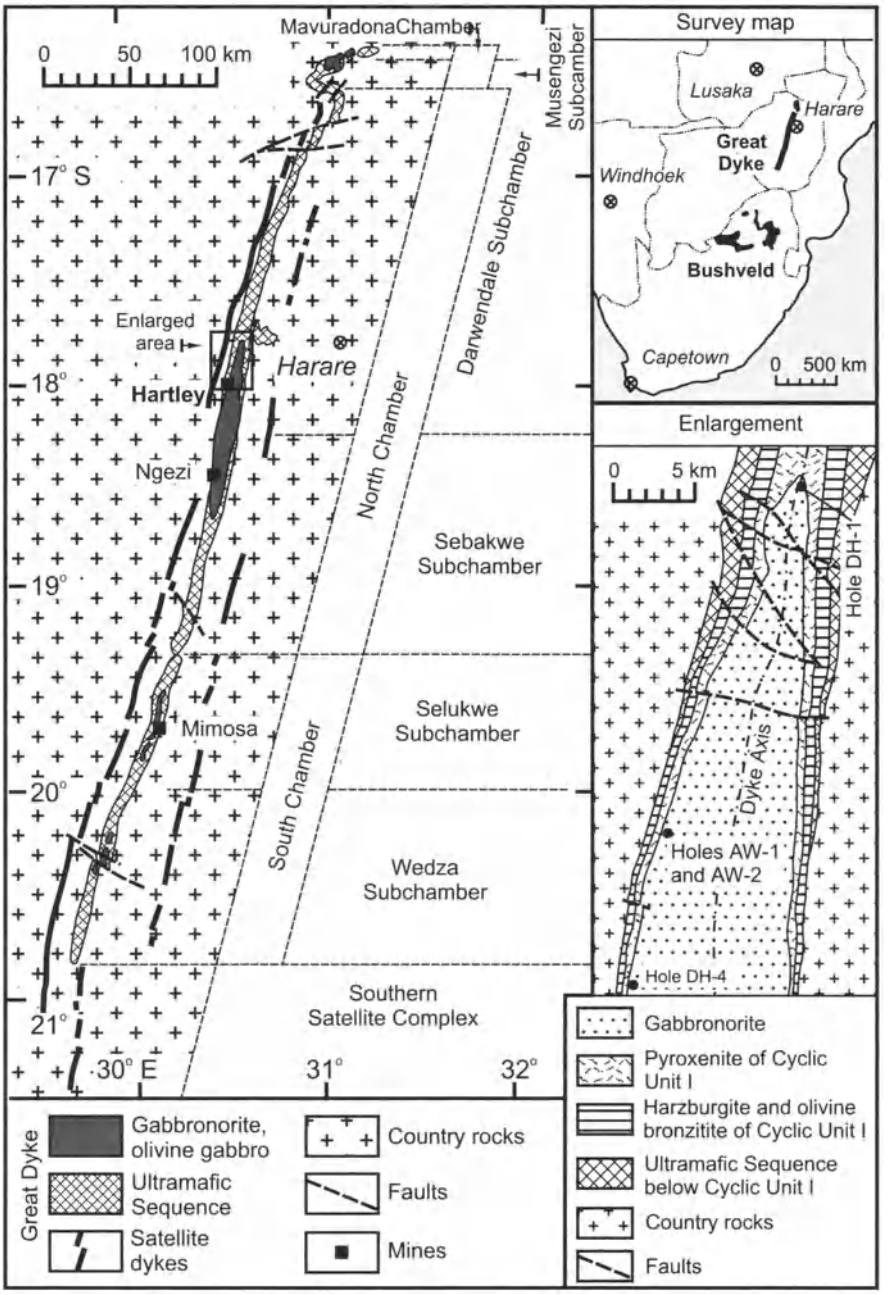


**Fig. 9.28.** Generalized geological map of Great Dyke of Zimbabwe with enlargement for southern part of the Darwendale Subchamber. After Wilson et al. (1989) and Wilson and Prendergast (2001)

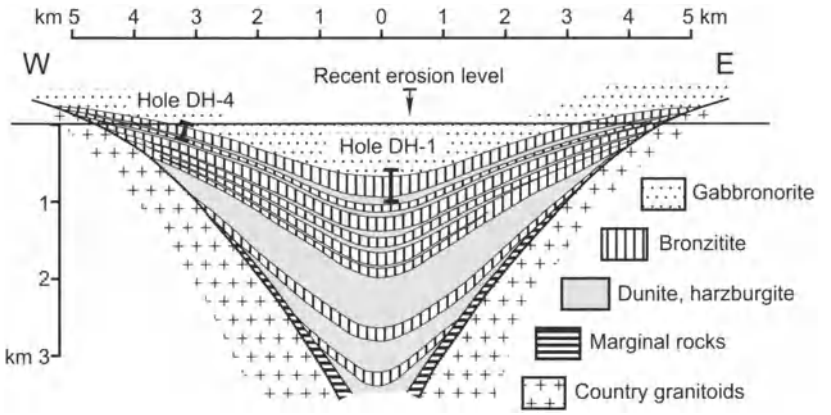


**Fig. 9.29.** Generalized east-west cross section of the Great Dyke in the southern part of the Darwendale subchamber. After Wilson and Prendergast (1989). Location of boreholes is shown in Figure 9.28

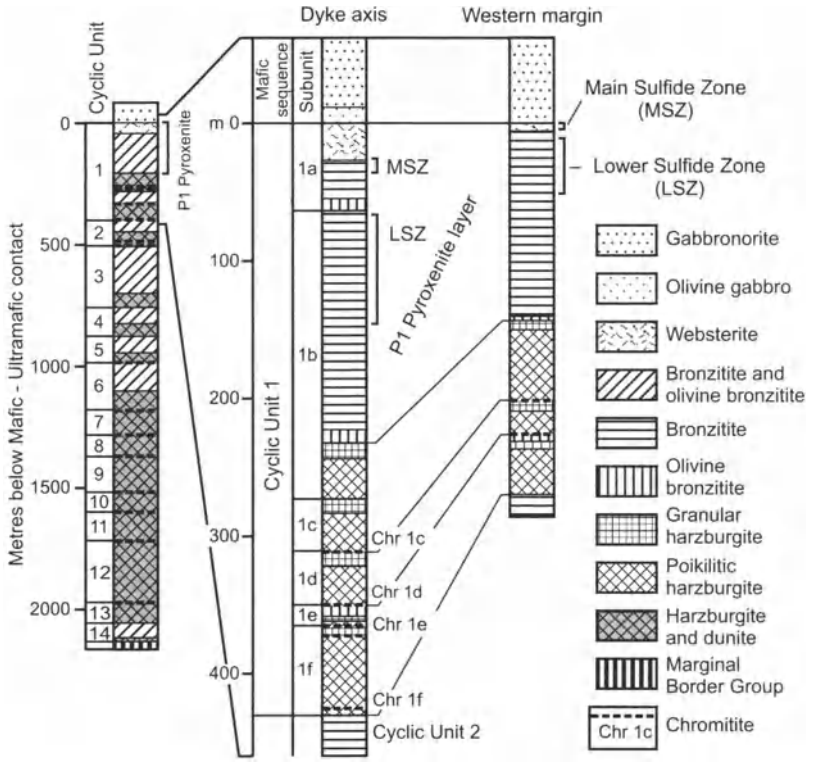


**Fig. 9.30.** Stratigraphy at the axis and western margin of the Great Dyke, in the southern part of the Darwendale subchamber. From Wilson and Prendergast (2001)

### *Mineralization*

The principal mineralized horizons in the dyke are the Main (MSZ) and Lower (LSZ) Sulfide Zones. These occur just below the horizon of gabbro and olivine gabbro (Fig. 9.30) which forms the cap to the intrusion, and which represents the first appearance of cumulus plagioclase. PGE also occur in significant (but not economic) amounts in the C1d chromitite (Fig. 9.30).

The MSZ and LSZ mineralized zones are situated within massive bronzitite and, in the case of the MSZ, partly within the overlying websterite, that are part of the uppermost cyclic unit (Fig. 9.30). The sulfides are developed interstitial to cumulus pyroxene, and the mineralized zones are not marked by textural or compositional changes in the rock, except for those associated with the sulfides. The orthopyroxenites hosting the sulfides consist of an interlocking network of 65-99 modal percent medium-grained granular orthopyroxene together with 1 to 30 modal percent post-cumulus clinopyroxene and plagioclase and up to 5 percent phlogopite, K-feldspar, micrographic intergrowths, spinel, rutile, apatite and zircon (Wilson and Prendergast 2002). Petrologically, the pyroxenites hosting the sulfides range from almost pure adcumulates at the axis and in the lower parts of the sequence to orthocumulates near the margins and in the upper parts. In general, calculation of the PGE content of the rock as though it were contained in sulfide indicates that values in 100% sulfide start to build up below the base of the sulfide zone and reach a maximum at the base (Fig. 9.31). Above the base the noble metal concentrations in the sulfides become lowered very rapidly over a few 10's of cm to a few m, with Ir and Pd declining most rapidly, followed by Pt and then Au. Both the MSZ and LSZ are present wherever the host horizon is present, but their thickness varies from 1 to 15 m in the case of the MSZ and 30 to 80 m in the case of the LSZ. Base metal sulfides comprise (in decreasing order of abundance) pyrrhotite, pentlandite, chalcopyrite and pyrite. Average Pt and Pd tenors (metal in 100% sulfide) over the PGE-rich part of the MSZ are fairly high (53 and 61 g/t), but distinctly lower than for the Merensky Reef (see the Appendix). The (Pt+Pd)/(Ni+Cu) ratio (PGE in g/t, Ni&Cu in wt%) is 9.

Very subtle changes in the Mg/(Mg+Fe) ratio of orthopyroxene have been observed over the section of the Great Dyke extending from 9 to 70 m below the gabbro cap. These have been documented in the published literature for the LSZ (Naldrett and Wilson 1990) and are known from unpublished data (Alan Wilson, personal communication, 1995) for the MSZ. Minima in the Mg/(Mg+Fe) ratio occur above the mineralized sections in each case, and then build up to reach maxima at the base of the next incoming sulfide zone. The Mg/(Mg+Fe) minima coincide with the cessation

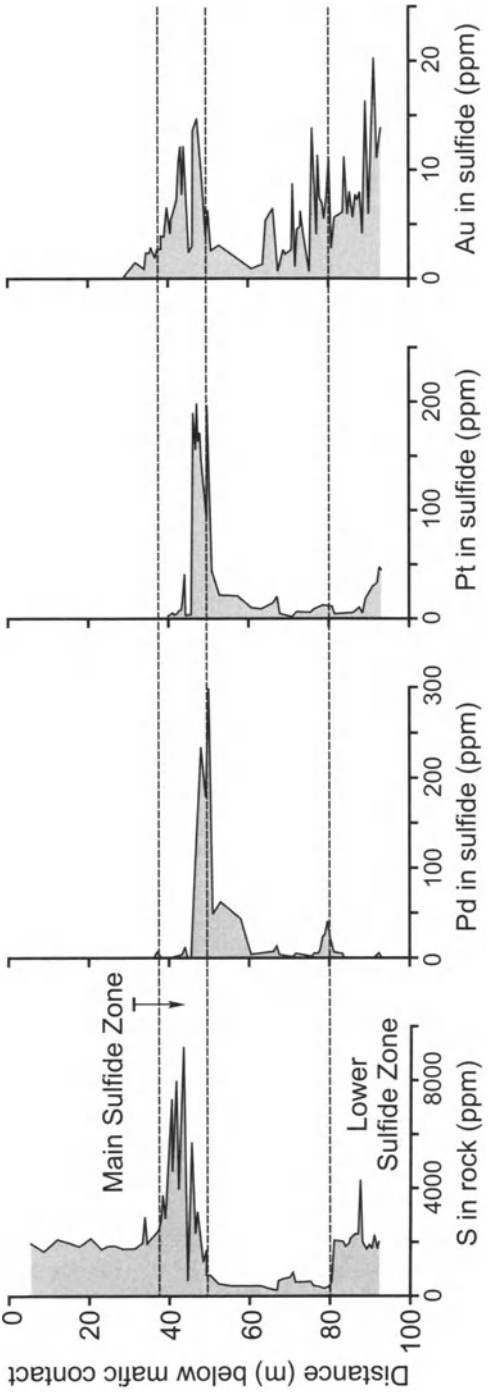


**Fig. 9.31.** Vertical variation in concentrations of S (in rock), Pd, Pt and Au (in 100% sulfide) in the Main and Lower Sulfide Zones of the Great Dyke based on data presented by Naldrett and Wilson (1991) for DH-1. The location of the hole is shown in Figure 9.28

of sulfide deposition and the subsequent increase in the ratio coincides with increase in the PGE tenor of sulfides upwards in the intrusion (Fig. 9.32).

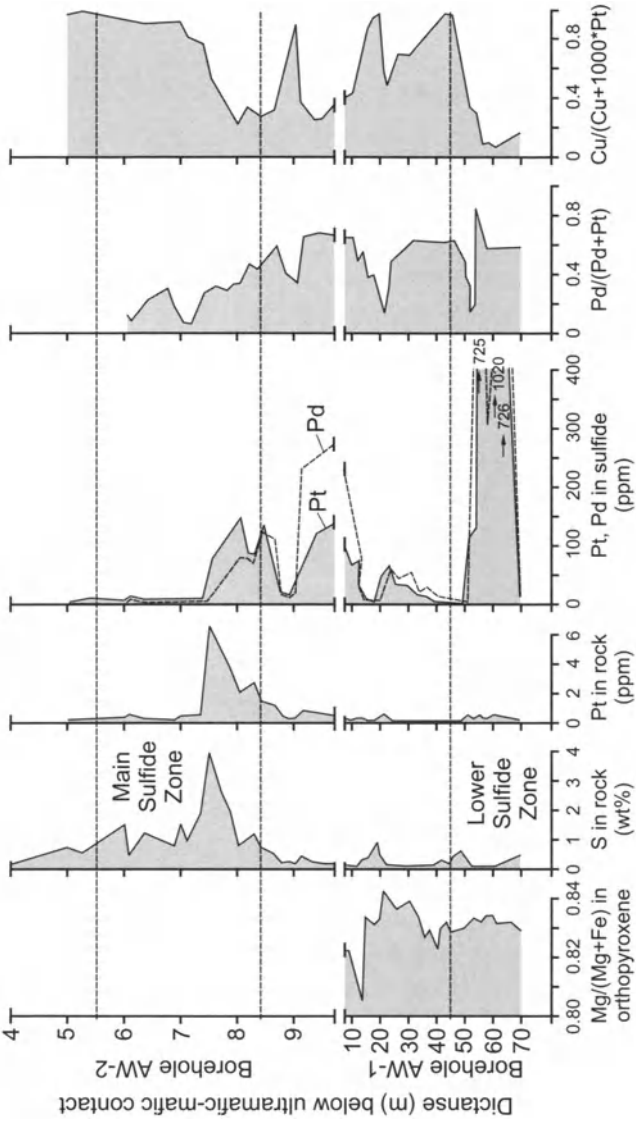


**Fig. 9.32**. Vertical variations in chalcophile elements and chalcophile element ratios through the Main Sulfide Zone (borehole AW-2) and Lower Sulfide Zone (borehole AW-1). Data on orthopyroxene compositions are also given for AW-1. After Wilson et al. (1989) and Naldrett and Wilson (1990). See Figure 9.28 for location of holes

Naldrett and Wilson (1990) pointed out that at the axis of the Dyke the PGE tenor of the sulfides of the ore zones is much higher than at the margin. The percentage increase from margin to axis of the maximum tenor of PGE in pure sulfides of the MSZ is given in Table 9.8. The increase is greatest for Ru, followed by Pd, Rh, Ir and Os together, then Pt and finally Au. Naldrett and Wilson ascribed the difference in tenor to a higher "R" factor at axis than margin, which was the consequence of the more rapid cooling at the margin.

**Table 9.8.** Percentage increase in noble metal tenor from margin to axis of the Great Dyke (values in ppm). After Naldrett and Wilson (1990)

| | Pt | Pd | Rh | Ru | Ir | Os | Au |
|---|---|---|---|---|---|---|---|
| Margin (maximum in DH-4 hole) | 94.90 | 97.60 | 8.90 | 6.40 | 3.36 | 0.99 | 14.20 |
| Axis (average in DH-1 hole) | 194.10 | 255.50 | 22.20 | 21.20 | 8.80 | 2.59 | 15.40 |
| Increase from margin to axis (%) | 105 | 162 | 150 | 230 | 163 | 163 | 8.3 |

### 9.4.4 Munni Munni Complex, Western Australia

This complex is a 2.925 Ga (Arndt 1992; Barnes and Hoatson 1994), boat-shaped, 25x9 km intrusion emplaced in Archean granitoids of the Western Pilbara craton of Western Australia. It has been described by Donaldson (1974), Hoatson (1986), Hoatson and Keays (1989) and Barnes et. al. (1990, 1991, 1992). A schematic cross section, after Barnes et al. (1990) is shown in Fig. 9.33. A keel of layered ultramafic rocks (wehrlite, clinopyroxenite) is overlain by a layer of porphyritic websterite (PWZ) which passes upwards into gabbroic rocks. The ultramafic layers thin to the west, but bulge down in one locality to join with the Cadgerina dyke, which is interpreted as a feeder to the complex that was active at the time of the formation of the PWZ. Barnes et al. (1992) noted that the upper part (upper 100 m) of the ultramafic series (UMS) and the whole of the PWZ are characterized by compositional variations suggestive of the mixing of a more primitive magma that was occupying the chamber and had given rise to the UMS, and a more fractionated magma that was injected subsequently and, after mixing with that resident in the chamber, gave rise to the overlying gabbros. A distinct compositional change, characterised by an abrupt decrease in the Cr content of clinopyroxene (the "Cr step"), occurs within the PWZ and, more than the change in cumulate rock, is thought to mark the beginning of a strong influence of the new magma. The analogies between

the postulated magmas involved at Munni Munni intrusion and Bushveld, Stillwater and Northern Finland are remarkable.

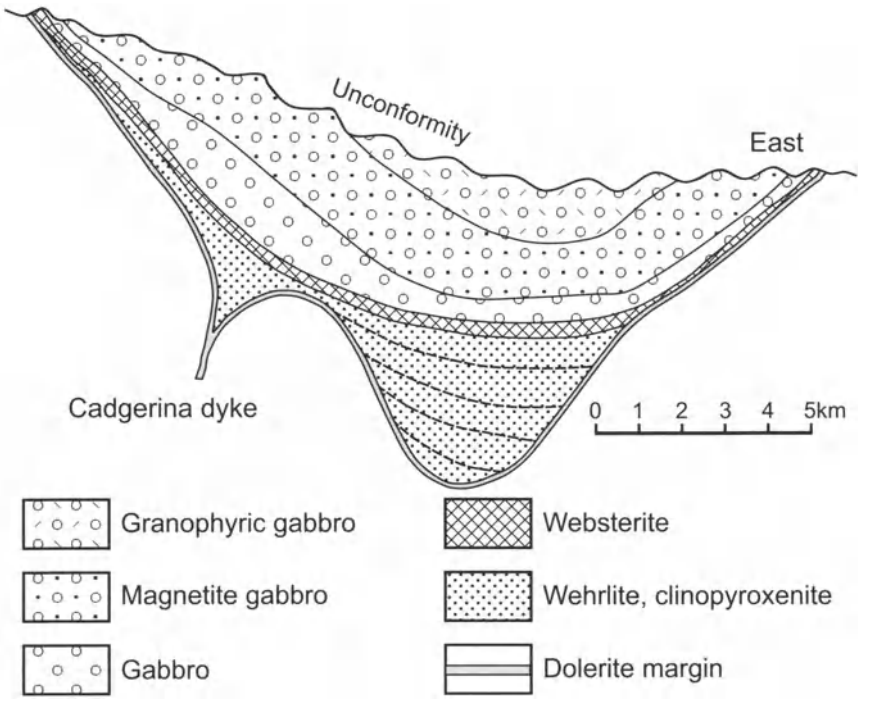


**Fig. 9.33.** Schematic cross-section through the Munni Munni Complex. After Barnes et al. (1990)

Barnes et al. (1992) show that the distribution of the sulfides within (and in some areas extending just above) the PWZ are characterized by two different extremes in terms of their vertical profiles of metal contents. In one type of profile (the coincident profile), peaks of maxima in PGE content coincide with maxima in sulfide content (as shown by the Cu content of the rock) and in the other the peaks in PGE content occur below the maxima in sulfide concentration. Both profile types are illustrated in the same holes in Fig. 9.34. While both profile types occur throughout the intrusion, the coincident profile is best developed on the flanks of the entry point of the Cadgerina dyke, the offset profile is best developed above it.

Barnes et al. (1992) drew attention to the close similarity between the behavior of the sulfides at Munni Munni and those in the MSZ and LSZ of the Great Dyke (see discussion in the section on genesis below).

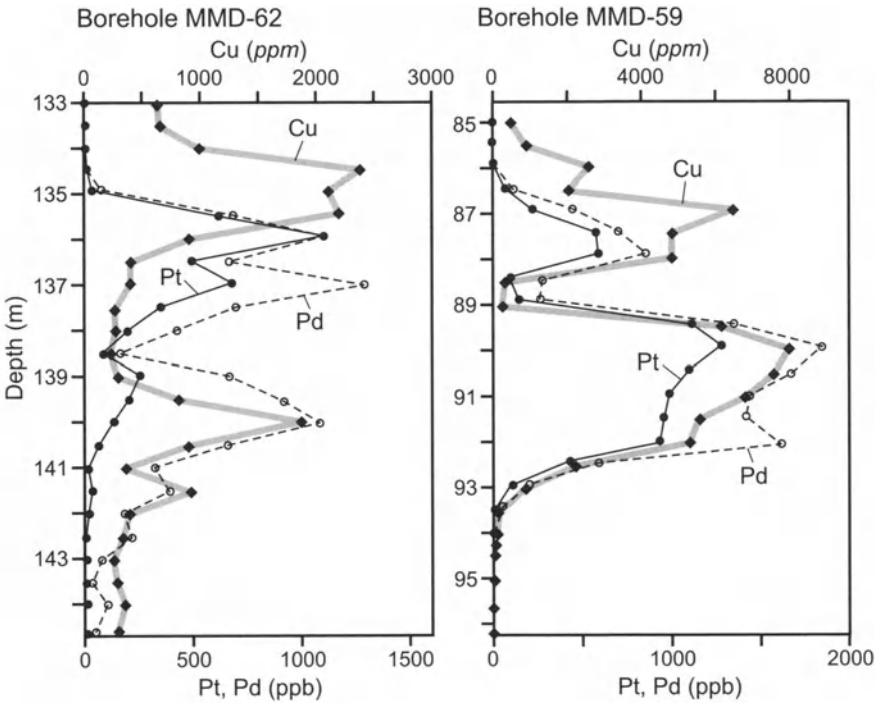


**Fig. 9.34.** Profiles through holes MMD 59 and MMD 62 showing "offset" sulfides overlying "coincident" sulfides (see text). The offset between the Cu and PGE distribution is particularly clear in MMD 62 (after Barnes et al., 1992: published with the permission of the Geological Society of Australia)

### 9.4.5 Layered intrusions of Northern Finland

At the beginning of the Proterozoic (2.50-2.45 Ga), rifting affected a large area of northern Finland and NW Russia (Kola Peninsular). Expressions of this rifting include the Pechenga-Imandra-Varzuga rift in the Kola Peninsular, the Central Lapland Greenstone belt, the Peraepohja schist belt and the Kuusamo schist belt in Finland and Northern Karelia, and Onega mulda in Central Karelia. (Fig. 9.35). Approximately 24 mafic/ultramafic intrusions accompanied this rifting. The discrete intrusions and fragments of disrupted intrusions include the Mt. Generalskaya, Monchegorsk, Pane (Russian name = Pansky) Tundra, Fedorova Tundra, and Imandra Complex intrusions associated with Imandra-Varzuga rift in the Kola Peninsular; the Kemi, Pennikat and Portimo-area intrusions associated with the Peraepohja belt in the southwestern part of northern Finland; and the Koillissima Igneous Complex (KIC) and Oulanka intrusion (Russian name =

Olanga) in the Kuusamo schist belt in the southeastern part of northern Finland and adjacent parts of Russia Karelia (Fig. 9.35).

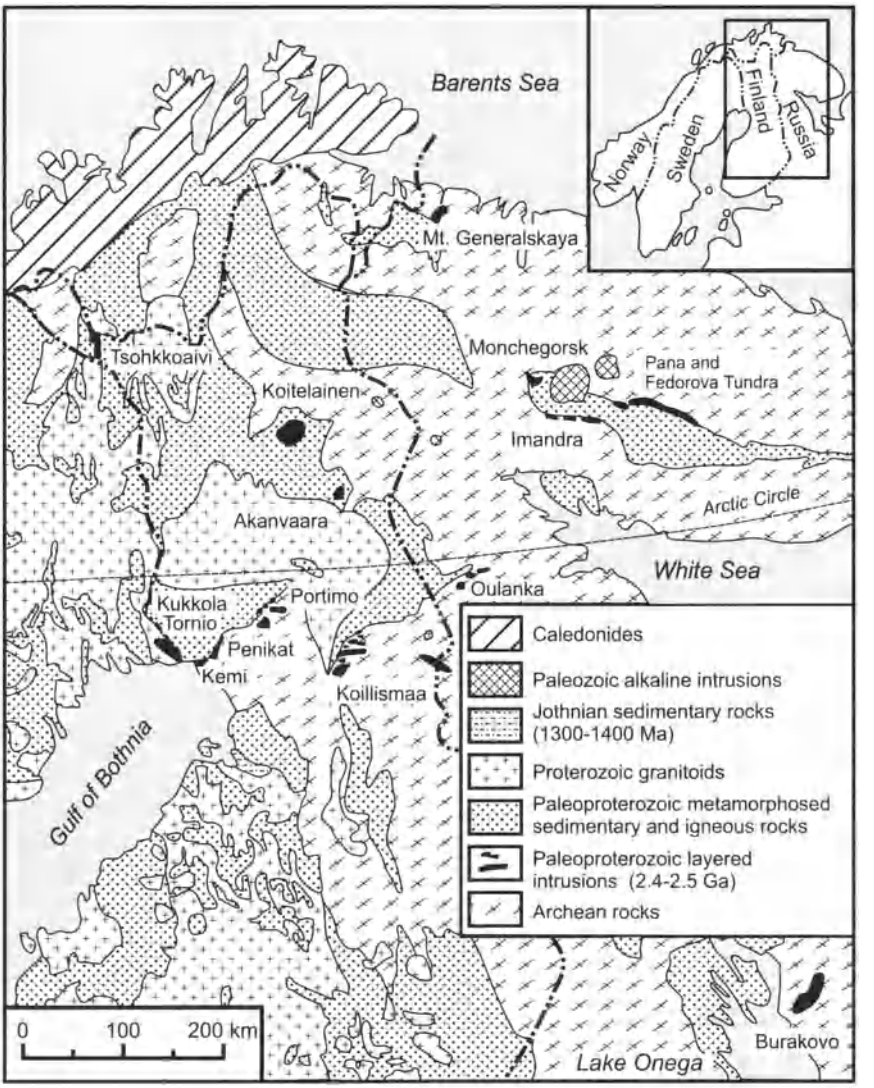


**Fig. 9.35.** Generalized geological map of the northeastern part of the Fennoscandian Shield showing the locations of the most important Paleoproterozpic layered intrusions (from Alapieti and Lahtinen 2002)

The oldest intrusions are those of the Kola Peninsular [Mt. Generalskaya – 2505–2493 Ma (Amelin et al., 1995; Bayanova et al., 1999); Monchegorsk – 2507–2500 Ma (Smolkin et al., 2001); Pansky (Pane) and Fe-

Fedorova Tundra – 2502–2491Ma (Balashov et al., 1993; Amelin et al., 1995)]. These were partly eroded before extrusion of Early Proterozoic volcanic rocks. The intrusions of Finland and Karelia were emplaced somewhat later, at 2449–2433 Ma [Huhma, (1986); Huhma et al., (1990); Balashov et al., (1993); Amelin et al., 1995)], at the same time as the chromite-bearing intrusions of the Imandra Compex of the Kola Peninsular [(2442–2437 Ma) Balashov et al., (1993); Amelin et al., (1995)]. These younger intrusions have thermally metamorphosed felsic volcanic rocks of the Pechenga- Varzuga rift zone. Mafic dykes contemporaneous with the layered intrusions have been documented. Amongst the oldest of these are norite and melanorite dykes of the Monchegorsk area [2496±14 to 2487±12 Ma (Smolkin et al., 2001)].

### *The Penikat Intrusion*

The Penikat intrusion is 23 km long and from 1.5 to 3.5 km wide (Fig. 9.36). Tectonic movements have resulted in it now consisting of 5 blocks, Sompujarvi, Kilkka, Yli-Penikka, Keski-Penikka and Ala-Penikka. Alapieti and Lahtinen (2002) recognized that the intrusion can be divided on the basis of mineralogy and cryptic variation (Fig. 9.37, column A) into a thin, 20-30 m-thick marginal series and 5 megacyclic units (MCU), each with an ultramafic cumulate at the base. The marginal series consists of highly contaminated gabbro, containing numerous partially melted country rock inclusions passing upward into bronzite-rich cumulates. MCU I consists of a bronzite-chromite orthocumulate with poikilitic augite and plagioclase, grading upward into gabbro as plagioclase and augite join as cumulus phases. MCU II and MCU III are similar, consisting of lherzolite cumulates grading both upward and downward into websterite, and passing upward into gabbronorites. A thin, frequently chromite-bearing plagioclase- bronzite orthocumulate, commonly associated with gabbroic pegmatoids, occurs at the contact between MCU III and the ultramafic cumulates of the overlying MCU IV. In places the uppermost cumulates of MCU III are missing and appear to have been eroded during emplacement of the overlying layer. MCU IV is the host to the bulk of the PGE mineralization, including the SJ Reef at the base, the AP I and II horizons 200-300 m above the SJ Reef and the PV Reef at the upper contact with MCU V. All of these Reefs occur at horizons in the magmatic stratigraphy at which new magma has been introduced. The SJ Reef is hosted by the plagioclase-bronzite orthocumulate at the contact between MCU III and MCU IV as mentioned above and comprises four principal types: (1) base-metal sulfide association, (2) chromite-association, (3) composite sulfide- and

chromite-association, and (4) silicate association (no visible sulfides or chromite).

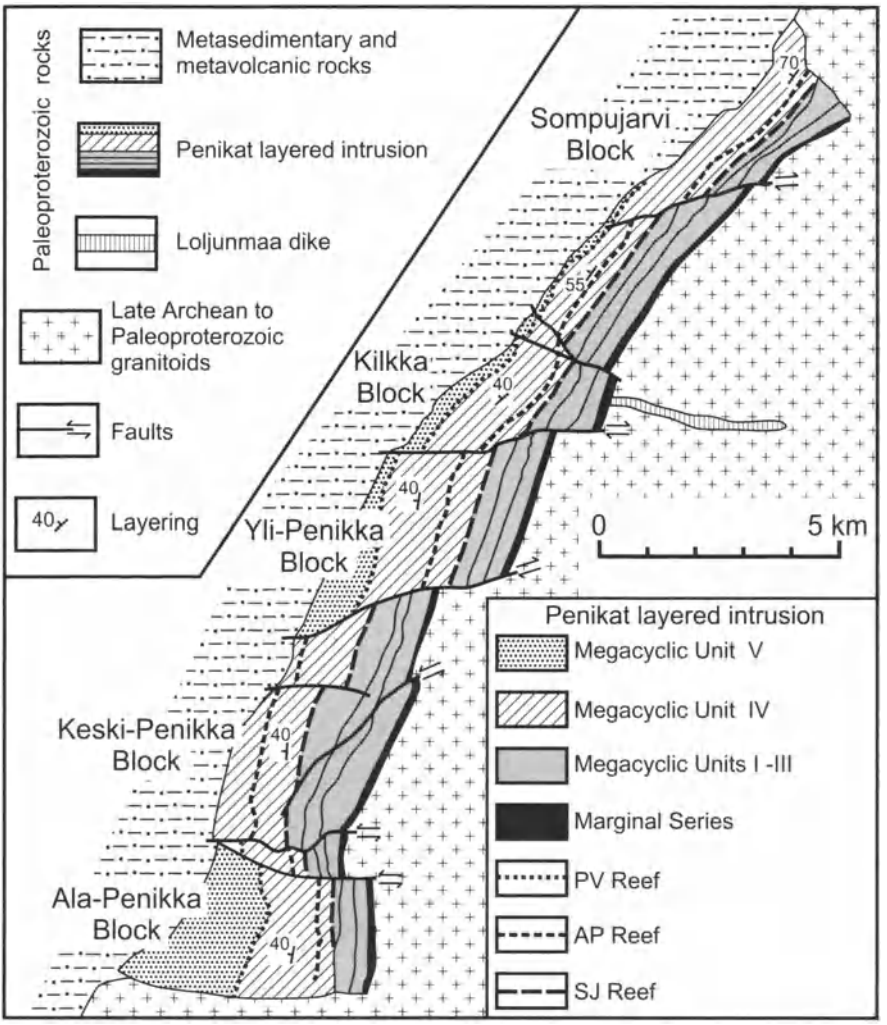


**Fig. 9.36.** Generalized geological map of the Penikat intrusion (after Alapieti and Lahtinen 1986)

The AP I and II Reefs occur in plagioclase-augite-bronzite adcumulates and in overlying plagioclase-bronzite mesocumulates. The best development of the PV Reef occurs in a plagioclase orthocumulate at the top of MCU IV. Ni, Cu, PGE and Au values of typical samples of all of these reefs are given in Table 9.9.

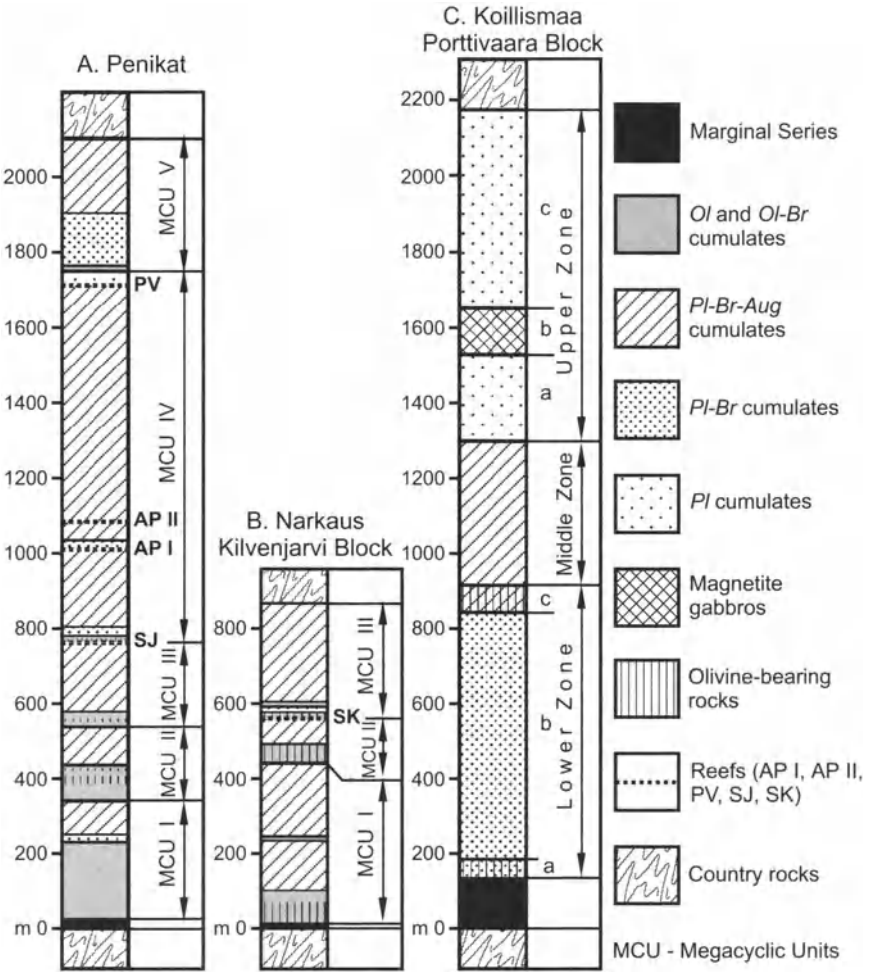


**Fig. 9.37.** Generalized stratigraphic sequences of the intrusions: Penikat (A), Narkaus, Kilvenjarvi Block (B), and Koillismaa, Porttivaara Block (C). After Alapieti and Lahtinen (2002)

### *Intrusions of the Portimo Area*

Ilijna (1994) has described the geology of the Portimo area and its mineralization. Much of the following is summarized from his work. Two major intrusions occur in the area which have again been tectonically disrupted into several blocks. These are the Suhanko-Konttijarvi Intrusion (the Suhanko and Konttijarvi blocks) and the Narkaus Intrusion (Lihalampi,

**Table 9.9.** Metal values in Reefs of the Penikat intrusion (after Alapieti and Lahtinen 2002)

| | NS | S | Ni | Cu | Pd | Pt | Rh | Ru | Ir | Os | Au |
|---|---|---|---|---|---|---|---|---|---|---|---|
| **SJ Reef** | | | | | | | | | | | |
| Chromite type | 6 | 0.03 | 0.08 | 0.04 | 156.60 | 51.07 | 5.53 | 0.48 | 1.19 | 0.35 | 1.14 |
| Sulfide type | 3 | 0.13 | 0.16 | 0.06 | 2.70 | 2.67 | 0.37 | 0.12 | 0.10 | 0.06 | 0.08 |
| **AP I Reef** | | | | | | | | | | | |
| Normal reef | 8 | 0.29 | 0.06 | 0.11 | 6.64 | 2.29 | 0.22 | 0.03 | 0.04 | 0.02 | 0.25 |
| Depression | 11 | 0.75 | 0.12 | 0.35 | 3.19 | 1.03 | 0.08 | 0.02 | 0.02 | 0.01 | 0.18 |
| **AP II Reef** | 3 | 0.35 | 0.06 | 0.20 | 11.37 | 3.40 | 0.22 | 0.04 | 0.06 | 0.03 | 0.61 |
| **PV Reef** | 7 | 0.79 | 0.24 | 0.25 | 2.32 | 3.91 | 0.09 | 0.11 | 0.08 | 0.05 | 0.27 |

*NS* Numbers of samples. S, Ni and Cu in wt%; PGE and Au in g/t (ppm)

Kilvenjarvi, Nutturalampi, Kuohunki and Sika-Kama blocks) (Fig. 9.38)[23]. The Kilvenjarvi block has the most complete stratigraphic succession preserved and this is compared (column B) with that of other intrusions in Fig. 9.37. All blocks of both intrusions are marked by a thin (generally 10–170 m) marginal series characterized by numerous inclusions of partially melted country rocks near the lower contact. The marginal series of the Suhanko-Kontijarvi intrusion differs from that at Narhaus in being thicker with the contaminated gabbro passing upward into well-layered pyroxenites and peridotites. The marginal rocks are overlain in all intrusions by a sequence of layered rocks. At Kilvenjarvi, where the thickest sequence is preserved, the layered rocks have been subdivided into three megacyclic units. MCU I consists of a lower unit of bronzite cumulate of which the lower 10 m contain cumulus chromite; this is overlain by gabbro norite as plagioclase and augite join orthopyroxene as cumulus phases. The ultramafic rocks of both MCU II and MCU III differ from those of MCU I in containing significant olivine. The lower 5 m of ultramafic cumulate of MCU II contain cumulus chromite, but chromite, although present, is less abundant in MCU III. The ultramafic cumulates of MCU II are overlain by gabbronorites. In MCU III, they are overlain by 25 m of plagioclase and plagioclase-bronzite cumulates before augite joins as a cumulus phase.

[23] This author suggests (see below) that the Narkaus and Suhanko-Konttijarvi intrusions are, in effect, a single intrusion, that has been disrupted by later deformation. The more primitive rocks (derived from the early injection of high-MgO magma) are only exposed as part of what is referred to as the Narkaus intrusion, but the rocks derived from the later injection of tholeiitic magma are more extensive and form not only the upper part of the Narkaus, but also the bulk of the Suhanko-Konttijarvi intrusion.

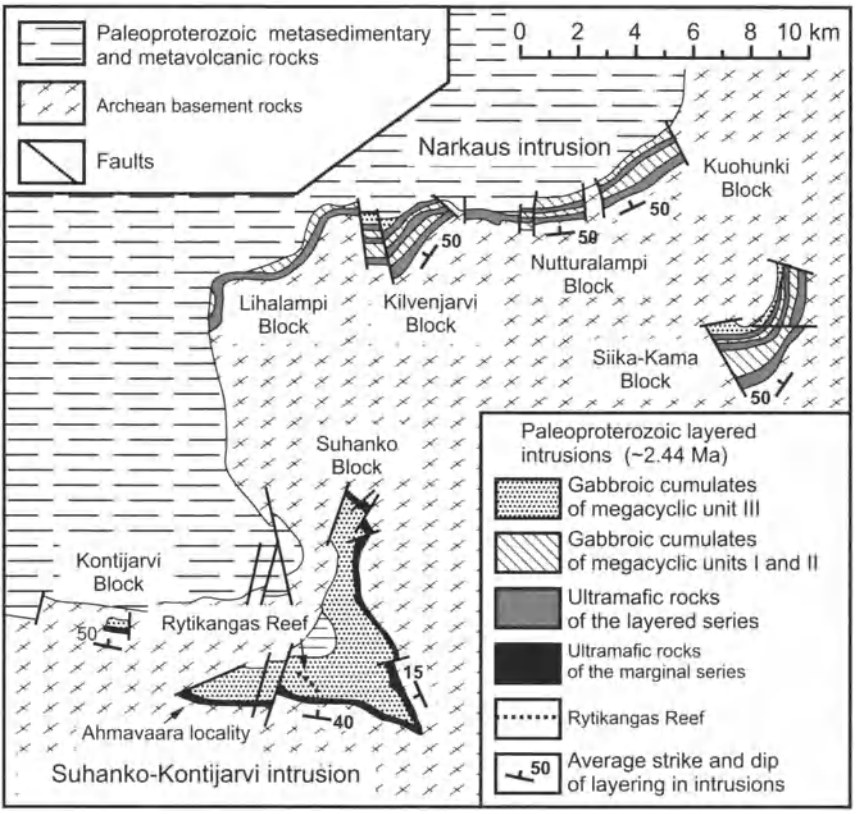


**Fig. 9.38**. Generalized geological map of the Portimo area showing the Suhanko-Kontijarvi and Narkaus intrusions. After Alapieti and Lahtinen (2002)

In 2000, an exploration syndicate was formed to explore for PGE in the intrusions of northern Finland. Shortly after they started their work, they obtained the most encouraging results from the Portimo area, and most of the subsequent exploration was focused in these intrusions. In consequence, of all of the intrusions in the general area, more is known about intrusions in the Portimo than those in other areas. The results of their project, released on the internet in July 2002, are shown in Table 9.10.

Five types of PGE deposit are associated with the Portimo intrusions. These are summarized in Table 9.11 and shown schematically in Fig. 9.39. They comprise disseminated sulfides in the marginal series, massive sulfides in the marginal series (rare and intermittent), the Portimo (= SK) Reef at the contact between MCU II and MCU III, the Rytikangas (= RV) Reef which is only found in the Suhanko-Kontijarvi intrusion, and PGE-rich veins filling fractures in the footwall of the complex. The marginal series sulfides constitute the most abundant PGE resource (see Table 9.10).

**Table 9.10.** Total resources of noble metals, (measured, indicated and inferred) of the Portimo area explored by Arctic Platinum Partnership (APP) at a cutoff 0.5 g/t (2PGE+Au), given on their Web-site in July 2002

| | Resources of ore (million t) | Grade | | | | | | Resources of Pt+Pd+Au [t] |
|---|---|---|---|---|---|---|---|---|
| | | Ni (wt%) | Cu (wt%) | Pt (g/t) | Pd (g/t) | Au (g/t) | Pt+Pd+ Au (g/t) | |
| Marginal Series of Konttijarvi block | 54.0 | 0.06 | 0.16 | 0.40 | 1.44 | 0.10 | 1.94 | 105 |
| Marginal Series of Suhanko block at Ahmaraara West | 99.8 | 0.09 | 0.22 | 0.23 | 1.10 | 0.14 | 1.47 | 147 |
| Marginal Series of Suhanko block at Ahmaraara East | 29.8 | 0.06 | 0.17 | 0.18 | 0.83 | 0.11 | 1.12 | 33 |
| SK Reef of Narhaus intrusion | 35.0 | 0.10 | 0.12 | 0.97 | 3.55 | 0.15 | 4.67 | 163 |
| Total | 218.6 | 0.08 | 0.18 | 0.38 | 1.54 | 0.13 | 2.05 | 448 |

**Table 9.11.** Summary of deposit types in intrusions of the Portimo area in Northern Finland

| Mineralization Type | Typical PGE grade | Relationship to Geology of host intrusion | Type of mineralization | Sulfide mineralogy |
|---|---|---|---|---|
| Disseminated sulfides in Marginal Series | Typically weakly anomalous to 2g/t but can reach 10g/t | Occurs below peridotite layers of marginal series in contaminated gabbro but can extend 30 m into basement | Disseminated sulfides interstitial to silicate grains – can occur in basement xenoliths | Po+Cp+Pn<br>Py is major constituent in basement gneiss |
| Massive sulfides in Marginal Series | PGE content generally from weakly anomalous to a few g/t. Higher grades occur in vicinity of ultramafic dykes in footwall, where host magma was high Cr-MgO type | Slab-like bodies ranging from 20 cm to 20 m in thickness. Vary from 30 m below contact to 20 m above it. Largest deposit is 2100 x 300–600 x 5–20 m | Massive sulfides with amphibole-plagioclase-quartz-chlorite-garnet gangue | Po+Cp+Pn |
| Portimo Reef = SK Reef (SJ Reef at Penikat) | Weakly anomalous to several 10's g/t | Typically occurs in orthocumulates at base of low Cr-MgO magma type. Gabbro-pegmatite veinlets containing 10's g/t Pt+Pd can occur 10's of m below level of reef. Reef can be laterally continuous with marginal series. Ranges in thickness from <1 m to several m | Sulfide poor mineralisation., often with no visible sulfide, and whole rock S content <1 wt% | Cp+Po+Pn with accessory millerite, bornite, violarite, sphalerite, galena-clausthalite and gersdorfite |

**Table 9.11.** (cont.)

| Mineralization Type | Typical PGE grade | Relationship to Geology of host intrusion | Type of mineralization | Sulfide mineralogy |
|---|---|---|---|---|
| Rytikangas Reef | PGE are irregularly distributed ranging from 20g/t in one location to nearly zero only 0.5 m away | Has typical thickness of 30-50 cm and occurs within low Cr-MgO magma, associated with poikilitic plagioclase and plagioclase orthopyroxene orthocumulates with augite oikocrysts | Low sulfide-type ore (about 0.1% sulfide) | Bornite+Cp and minor chalcocite, Po, Pn, millerite, sphalerite and galena-clausthalite |
| Offset Mineralization | Pt+Pd reach 100 g/t. This is richest mineralisation in the area | Comprise massive to semi-massive veins in footwall gneiss 20-100 m beneath base of intrusion. The veins are more massive close to the intrusion. Farther away from it sulfides are much less abundant although PGE grades are high | Pd/Pt ratio is much higher than in other deposits. Pd/Ir ratio is also extremely high | Cp and in some places chalcocite or bornite. Po and Pn are uncommon |

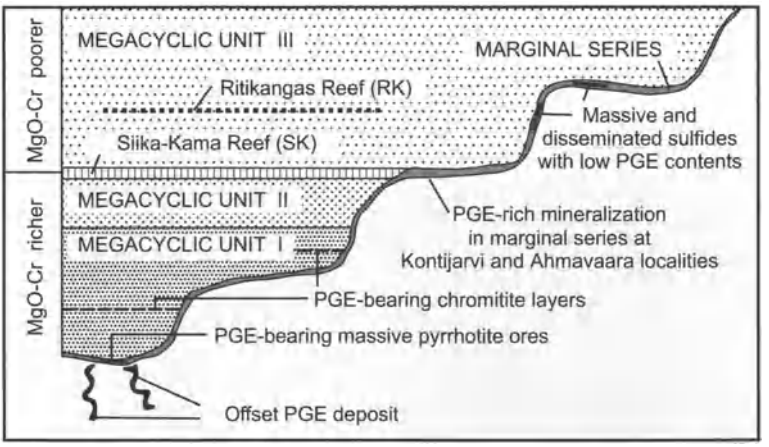


**Fig. 9.39.** Schematic illustration of the location of PGE deposits in the original structure of the Portimo Layered Complex. Modified after Ilijna (1994)

In the Portimo complex they are particularly rich in PGE in the Kontijarvi and Ahmavaara blocks where the SK Reef abuts the margin; published data for the Konttijarvi deposit indicate Pd and Pt tenors in 100% sulfides of 442 and 141 g/t respectively and a (Pt+Pd)/(Ni+Cu) ratio (PGE in g/t, Ni and Cu in wt%) of 18 (the Appendix). At Portimo, the SK Reef is in the equivalent stratigraphic position to the SJ Reef at Penikat, although at Portimo the host rock is usually a chlorite schist with no discernable preserved primary fabric. The offset deposits are rich in Cu and PGE but thus far have proved to be of limited extent. They occur up to several 100's of m in the footwall close, to where pyrrhotite-rich massive sulfides are present in the marginal series. They consist of two types, PGE accompanying chalcopyrite, and, slightly farther removed from the intrusions, PGE minerals with very little associated copper sulfide. It is thought that they are the result of a Cu-rich sulfide liquid, that is residual from the fractional crystallization of contact sulfides, leaking out away from the contact along fractures in the underlying footwall in an analogous manner to that proposed for the Cu-rich footwall ores at Sudbury. The low sulfide, more distal type, probably is the result of hydrothermal activity. PGE values are also found associated with chromitite horizons within the ultramafic cumulates of MCU I.

### *Intrusions of the Koillissima Layered Complex*

In the Koillissima area of the Kuusamo schist belt, mafic/ultramafic igneous activity was preceded in the western part by felsic (rhyolitic) volcanism and, in this area, the Koillissima Igneous Complex (KIC) spread out

between the rhyolites and the underlying Kuusamo Gneiss Complex (KGC) to form the KIC-West bodies (see below). In the process the rhyolites were largely melted and are now represented by granophyres. Uplift and erosion gave rise to a basal conglomerate (Unikumpu conglomerate) containing gneissic and rhyolitic (= granophyric), but no mafic/ultramafic boulders. This lies directly on the rhyolite. Subsequently, flood basalt volcanism covered a wide area of this area of Finland and is preserved, along with sedimentary rocks (now schistose) in basins overlying the locations formerly occupied by the rifts.

The KIC comprises 3 distinctive parts (Fig. 9.40a): (1) a series of thin (800-2500 m) bodies (KIC-West) which are interpreted as the disrupted remnants of a single differentiated lopolith (Fig. 9.40b), (2) a deeper, ultramafic-rich intrusion, the Narangavaara Complex (Fig. 9.40a), and (3) an apparently unexposed mafic/ultramafic body (referred to henceforth as the Connecting Intrusion) which has been referred to as a dyke-like connection between the lopolith and the Narangavaara body (Fig. 9.40a)[24].

KIC-West is thought originally to have been a single sheet-like lopolith that, as a result of north-south compression, has now been disrupted tectonically into a series of discrete blocks (Fig 9.40b). Three of these are major in size and comprise, from south to north, the Syote, Portivaara and Kuusjarvi-Lipeavaara blocks. The smaller blocks include the Phytis, Kaukua and Murtolampi bodies. Stratigraphic thicknesses of strata included within the blocks range from 800 to 2,500 m with the thickest section occurring within the Kuusijarvi-Lipeavaara block. This particular block has the form of a disrupted syncline, with strata dipping and topping south on the northern (Lipeavaara) limb and the reverse on the southern (Kuusjarvi) limb.

The mafic/ultramafic rocks of the KIC-West bodies are divided into two series, an upper Layered Series and a lower Marginal Series (Fig. 9.37, Column C). The Layered Series comprises 3 zones, a lower zone (maximum thickness 1 km) of olivine norite (PBOaC), a middle zone (max thickness 1.5 km) of gabbro-norite (PBAC) and an upper zone (750 m thick) of leucogabbro (PAC). Magnetite-rich gabbro occurs in a layer up to 200 m in thickness within the upper zone of the layered series – this hosts layers rich in V-rich magnetite, which has been mined at the Mustavaara mine. The Marginal Series varies between 50 and 250 m in thickness. The upper part commonly contains peridotite (ObpC) and pyroxenite (BpC) layers, but these give way downward to gabbro-norite and, within a few

[24] This author disagrees with the description "dyke-like". The geophysical expression of the body is not that of a dyke but of a significant concentration of mafic/ultramafic rock.

10's of m of the contact, to contaminated gabbro containing many partially digested gneissic inclusions.

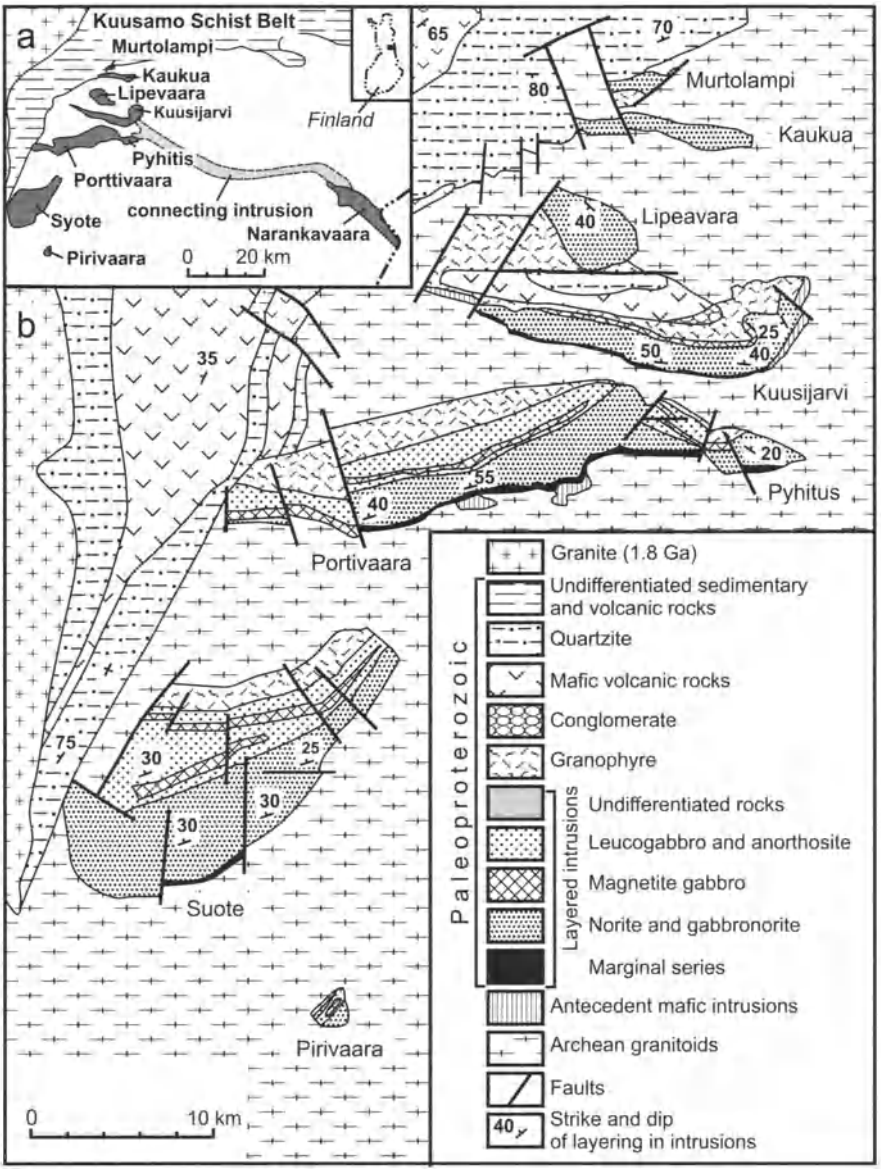


**Fig. 9.40. a**. Generalized geological map of the Koillismaa Layered Complex. **b**. Geological map of the Western part of the Koillismaa Complex. From Alapieti and Lahtinen (2002)

The Narankavaara intrusion has been much less studied than that exposed at KIC-West. Information available from outcrop, drill core and gravity and magnetic data indicate that it is dominantly ultramafic, with peridotite occurring along much of the southwestern margin and passing inward into pyroxenite. Gabbroic rocks are restricted to the northeastern margin, particularly at the western end. Thus far significant sulfide mineralization has not been reported at Narankavaara.

The only mineralization in the KIC that has been discovered to date is of a disseminated type in the marginal series rocks. This is very similar to that at Portimo, but grades are somewhat lower.

### *Magma Types in the Kemi-Portimo-Koillissima Intrusions*

As discussed above, the initial magma emplaced into the Bushveld, Stillwater and Great Dyke igneous complexes had a distinctive MgO, Cr- and $SiO_2$-rich composition (see analysis of Bushveld sample, Table 9.12 below). The consequence is that the first pyroxene to appear on the liquidus was orthopyroxene, and plagioclase and augite appeared relatively late in the crystallization sequence. In the case of the Bushveld and Stillwater complexes, repeated influxes of the initial magma type were followed by influxes of a more aluminous, tholeiitic magma. This mixed with that previously in the chamber to give rise to a gradual transition in the subsequent cumulates. It is within this transition zone that the most important concentrations of PGE occur.

**Table 9.12.** Some key elements in estimated magma compositions (estimates for the Finnish magma types are from Iljina 1994)

| | Bushveld Initial magma | Penikat and Portimo Initial magma | Penikat and Portimo Later magma | KIC-West (rough estimate) |
|---|---|---|---|---|
| $SiO_2$ (wt%) | 55.9 | 52 | <52 | ~50 |
| MgO (wt%) | 12.6 | 14.4 | 10.0 | ~8.0 |
| $TiO_2$ (wt% | 0.37 | 0.3-0.4 | 0.4-0.5 | 0.6-0.7 |
| $Al_2O_3$ (wt%) | 12.6 | 13.7 | 17.8 | ~16 |
| Cr (ppm) | 952 | 1500-2000 | 350-400 | 800-1000 |
| First Cumulus Pyroxene | Opx | Opx | Opx followed soon by Cpx | Opx followed by Cpx |

Table 9.12 is a summary (made with the assistance of Markku Ilijna – personal communication 2002) of some key elements distinguishing magmas involved in intrusions of the Kemi-Portimo-Koillissima area compared to the best estimate for the initial magma of the Bushveld Complex. At both Penikat and Portimo, the first magma to enter the system was characterized by relatively high $SiO_2$ and MgO, low $Al_2O_3$ and $TiO_2$, and very high Cr; orthopyroxene followed olivine in the crystallization sequence. The second magma type was somewhat lower in $SiO_2$, somewhat higher in $TiO_2$, significantly higher in $Al_2O_3$, and significantly lower in MgO and Cr; the crystallization sequence was orthopyroxene followed very closely by plagioclase, plagioclase+orthopyroxene+augite, and then plagioclase+augite. The contact between cumulates derived largely from the high MgO, Cr magma type and those derived from magma of more aluminous, tholeiitic composition is that between MCU III and MCU IV at Penikat and MCU III and MCU IV at Portimo. It is worth noting that these horizons are marked by significant PGE Reefs.

The magma responsible for the KIC-West intrusion was intermediate between these two types in terms of its Cr content, and somewhat higher in $TiO_2$, higher in $Al_2O_3$, and lower in $SiO_2$ and MgO than the high MgO magma at Portimo. The KIC-West magma is therefore closer in composition to the second (tholeiitic) magma-type at Portimo. At the same time, it should be appreciated that the Narankavara and Connecting Intrusion are also part of the KIC, so that perhaps in the Kuusamo schist belt, the cumulates from the high MgO, Cr magma type are preserved to the east, and the intrusions of KIC-West were formed from a mixture of a fractionated variant of the initial high-MgO magma and tholeiitic magma.

### 9.4.6 Intrusions of Sudbury area in Central Ontario, Canada

A series of intrusions occur along the southern edge of the Archean Superior Province in Ontario that are part of the magmatism that accompanied the opening of the Penokean (Southern) ocean in early Proterozoic time (Fig. 9.41). The Proterozoic Huronian Supergroup was deposited along the northern margin of this ocean. North of the line marking the margin of the rift (approximately the location of the Murray fault in Fig. 9.41), the Huronian is developed as a relatively thin cover on the Archean hinterland, but it thickens markedly southward into the rift and reaches a total thickness of 12 km. Mafic and felsic volcanic rocks occur at the base of the Huronian. The intrusions, which are grouped as the East Bull Lake Intrusive Suite, have been described most recently by James et al. (2002) from whom much of the following material has been taken. They include, from east to

east to west (Fig. 9.41), the River Valley [RV] (this lies largely in terrain that has been reworked during metamorphism of Grenville age [1.1–1.0 Ga]), Falconbridge [F], Wisner [W], Drury [D], Agnew Lake) [AL], May [M] and East Bull Lake [EBL] bodies. As shown in Figure 9.41, they range in age from 2.441 to 2.491 Ga. James et al. (2002) noted that the intrusions and their setting, which is related to a rifted continental margin, strongly resemble the similar-aged intrusions in Northern Finland.

The most complete stratigraphic succession is that of the Agnew Lake body, which is shown compared to that at East Bull Lake in Fig. 9.42. Important features of the intrusions are:

1. Footwall breccias which may or may not be present (they are absent at AL but well-developed at EBL).
2. The gabbronorite marginal series
3. An inclusion-bearing zone, metres to tens of metres thick, containing fragments of footwall rocks and cognate xenoliths ranging from pyroxenite to anorthosite, all in a gabbronorite±olivine matrix.
4. Plagioclase glomeroporphyritic leucogabbronorites underlying a zone of anorthosite.
5. Main series gabbronorites, which become strongly layered upward.
6. A zone of olivine gabbronorite that underlies the upper zone of both intrusions and is taken to indicate the introduction of a pulse of fresh, more primitive magma.
7. A 1 km-thick zone of gabbronorite, leucogabbro and minor ferrosyenite that is present at AL but absent at EBL.

The River Valley intrusion [RV] lies 150 km east of AL. Its stratigraphy is less well-documented, partly because it has been subject to Grenville metamorphism and deformation. It comprises (Fig. 9.42) a marginal zone, approximately 100 m thick, composed of gabbronorite containing cognate xenoliths (gabbronorite/pyroxenite) and rare footwall inclusions. It is overlain by olivine gabbronorite which passes up into gabbronorite and then a leucogabbronorite. As shown in Figure 9.42, a discordant, inclusion/autolith-bearing zone cuts across the layered rocks. Autoliths of marginal zone, olivine gabbronorite and gabbronorite, along with rare footwall rocks, occur in an olivine gabbronorite matrix which is more primitive than the marginal zone rocks.

Estimates of initial magma composition for the EBL-AL intrusions are that they were characterized by high $Al_2O_3$ (16–20 wt%), low $TiO_2$ (<0.5 wt%), low Cr (<250 ppm) and an MgO/MgO+FeO ratio of 0.54 to 0.60, which corresponds to an alumina-rich tholeiitic composition.

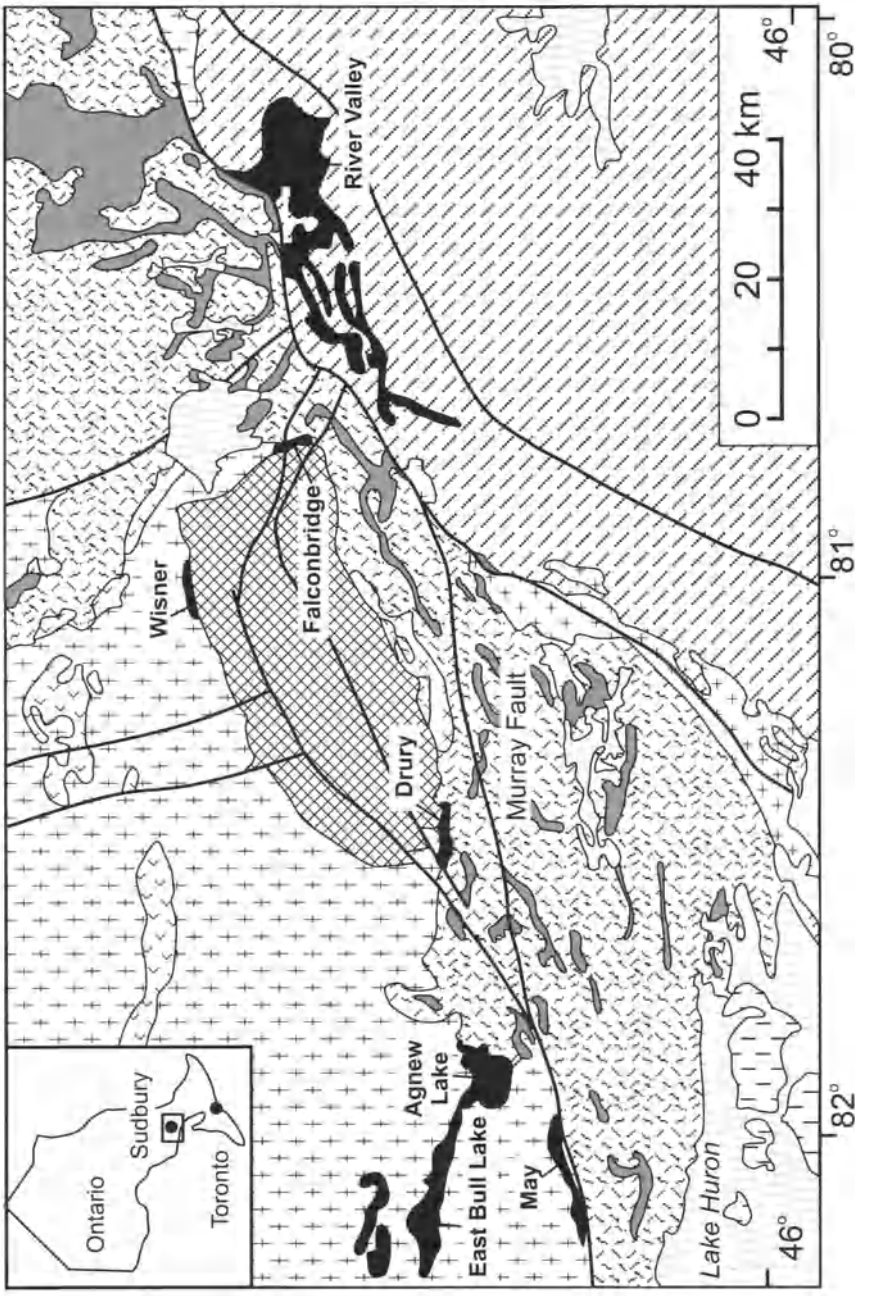
Ontario
Sudbury
Toronto
Wisner
Falconbridge
River Valley
Drury
Murray Fault
Agnew Lake
East Bull Lake
May
Lake Huron
0
20
40 km
46°
80°
81°
82°
46°

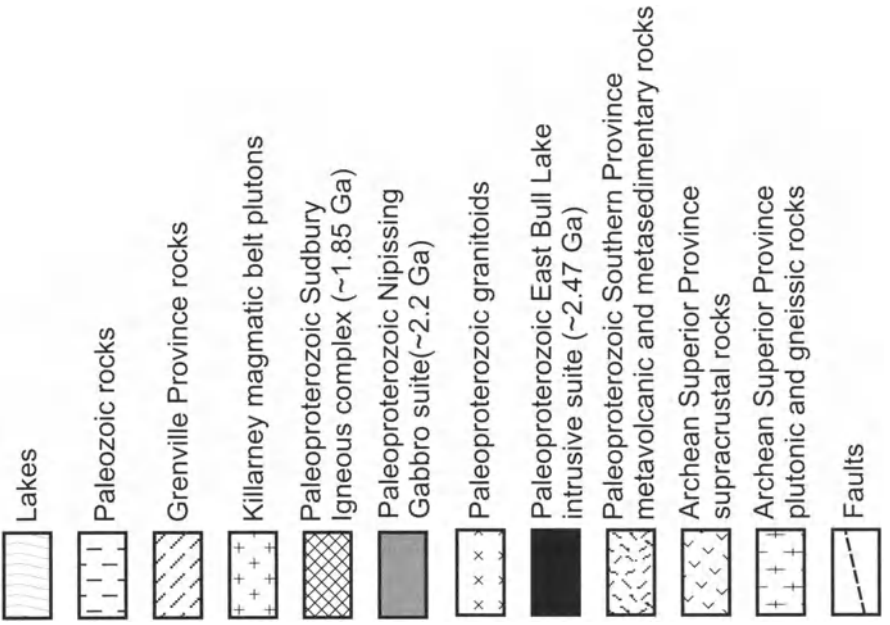


**Fig. 9.41.** Geological map of Sudbury area, showing the distribution of intrusions of the Paleoproterozoic East Bull Lake intrusive suite. After James et al. (2002)

Mineralization in both the RV and EBL-AL areas comprises PGE-rich sulfides disseminated within the matrix of inclusion-bearing breccia at the margins of the intrusions, and in a discordant autolith-bearing phase at RV. Figs. 9.43 and 9.44 illustrate schematically the mineralization at the Dana North Zone of the River Valley intrusion. The best mineralization occurs in a breccia containing primarily centimeter to decimeter-size melagabbro-gabbro xenoliths. Sulfide content varies from 1–5% and occurs as blebby to disseminated grains, coalescing in places to produce a net texture. Pyrrhotite and chalcopyrite constitute the principal base metal sulfides. The average Pd/Pt ratio is 2.95 and the Cu/Ni ratio is 4.8. As indicated in Table 9.13, grades are relatively low (1.423 ppm Pd+Pt+Au). The mineralization is of high PGE-type with a (Pt+Pd)/(Ni+Cu) (PGE in g/t, Ni and Cu in wt%) ratio of 11 (the Appendix). The problem of mining is compounded by the relatively steep dip (>45°), restricted thickness (<100 m) and intermittent nature of the mineralized zones, which implies a high stripping ratio.

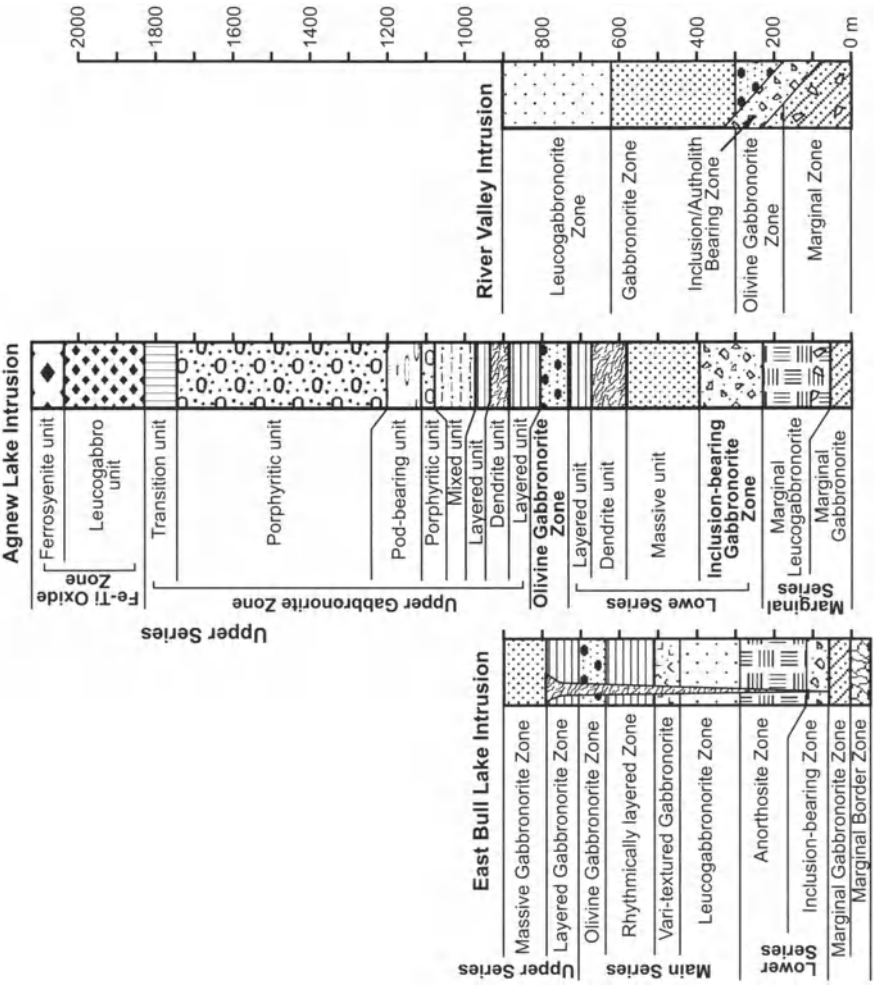


**Fig. 9.42.** Stratigraphy of the East Bull lake, Agnew Lake, and River Valley intrusions. After James et al. (2002), incorporating data from Vogel et al. (1999) and Hrominchuk (2000)

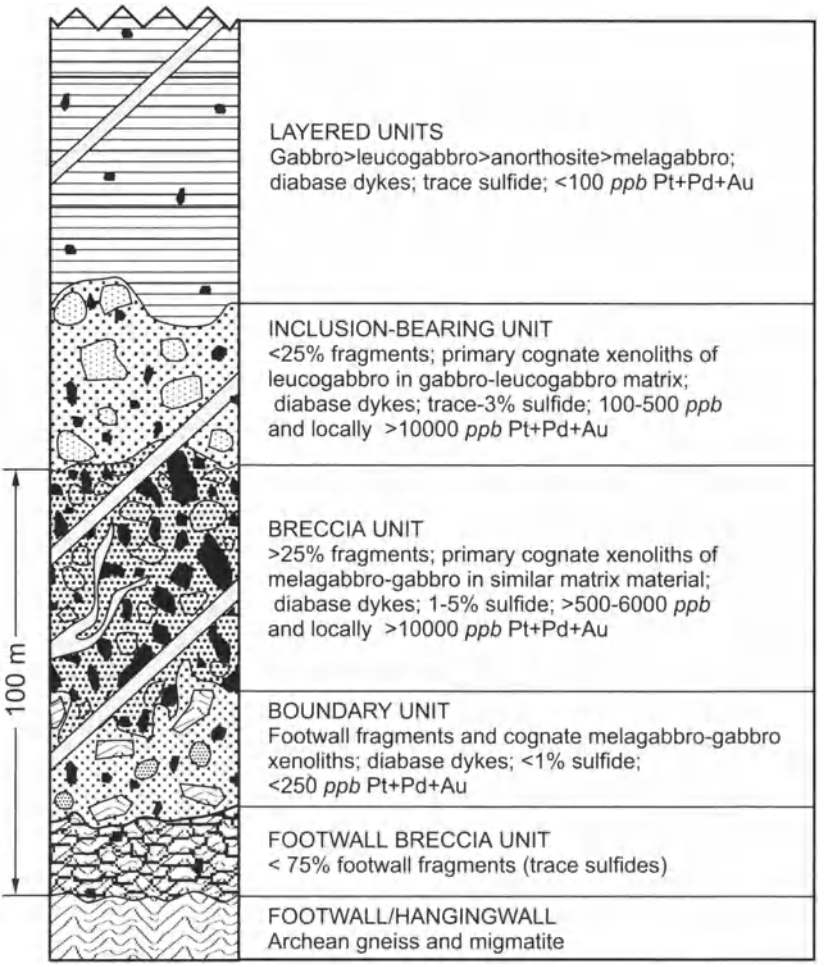


**Fig. 9.43.** Typical stratigraphy of the Dana North Ore Zone in the River Valley intrusion. After James et al. (2002), and incorporating unpublished data of Pacific North West Capital Corp. and Scott Joubin-Bevans

**Table 9.13.** Measured, Indicated and Inferred Resources at River Valley (taken from the Pacific North West Capital Corp. website, and reported as independent calculation by Derry, Michener, Booth and Wahl, mid-September 2002)

| | Ore resources (million t) | Grade | | | | |
|---|---|---|---|---|---|---|
| | | Ni (wt%) | Cu (wt%) | Pt (ppm) | Pd (ppm) | Au (ppm) |
| Measured and indicated | 18.053 | 0.021 | 0.100 | 0.344 | 1.016 | 0.063 |
| Inferred | 5.382 | 0.020 | 0.086 | 0.290 | 0.819 | 0.050 |

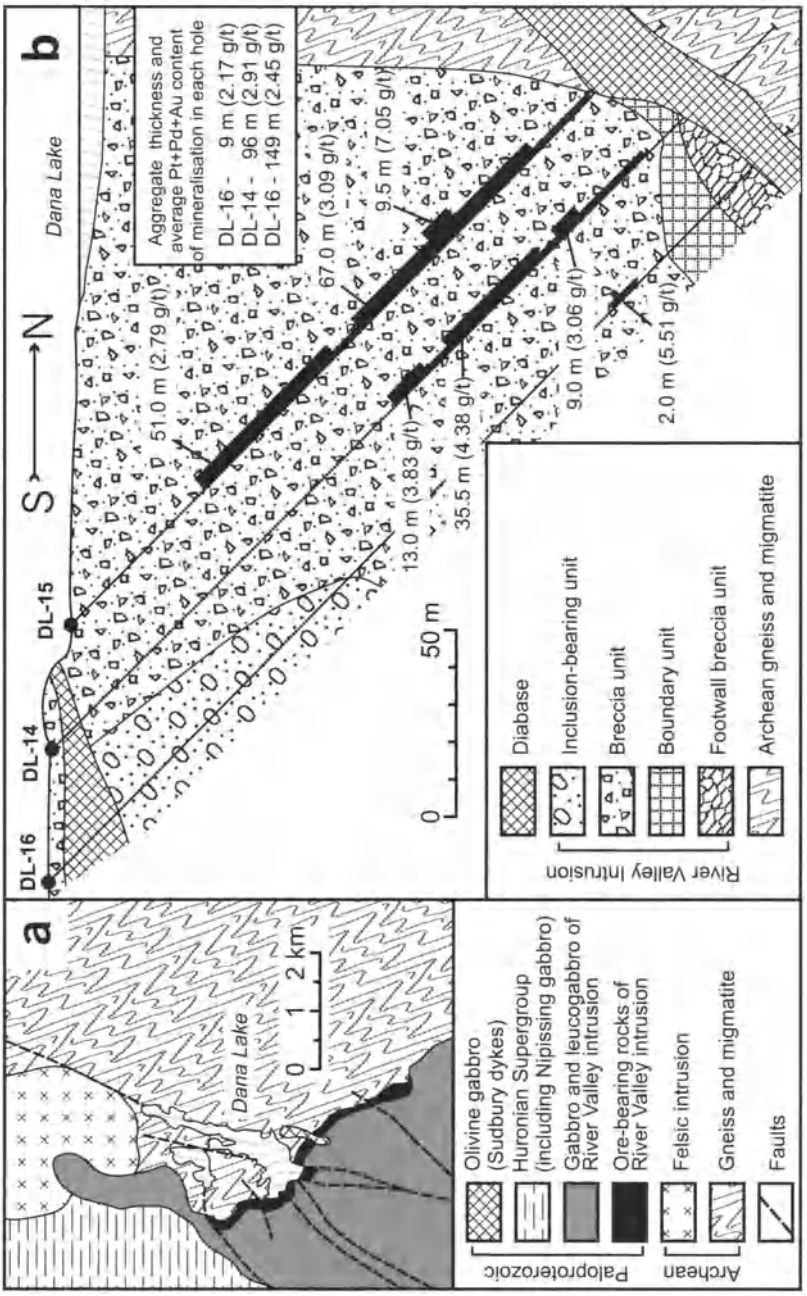


**Fig. 9.44.** Geological map (a) and east-west oriented geological section (b) through the Dana North Ore Zone in the River Valley intrusion. After James et al. (2002), incorporating unpublished data of Pacific North West Capital Corp. and Jobin-Bevans

### 9.4.7 Intrusions in East Greenland

About 12 large and several small mafic layered intrusions are exposed in Eastern Greenland at Kangerlugssuaq fjord (see Fig. 9.3). They relate to Tertiary plateau volcanism that accompanied the rifting accompanying the development of the North Atlantic. They fall into two age groups, 57–54 and 50–47 Ma (Andersen et al. 2002). Some of them host PGE mineralization, the most significant of which occurs in the Skaergaard and Kap Edvard Holm Intrusions.

#### *The Skaergaard Intrusion and the Platinova Reefs*

The Skaergaard intrusion (Fig. 9.45) in East Greenland formed at the time (55.7±0.03 Ma, Hirschmann et al. 1997) of the initial breakup of the North Atlantic. It is the type example of extreme magmatic diffentiation in

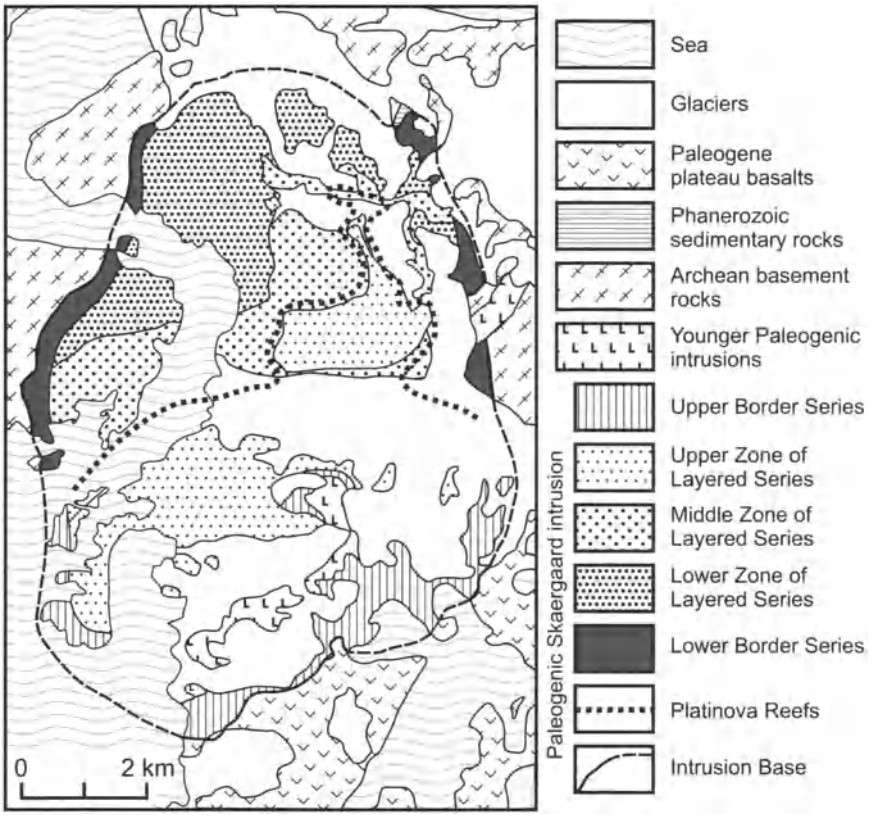


**Fig. 9.45.** Geological map of the Skaergaard Intrusion. After Andersen et al. (2002), incorporating data from McBirney (1989)

a closed magmatic system (Wager and Deer 1939; Wager and Brown 1968; McBirney 1989). Exploration for PGE was initiated by Platinova Resources Ltd. in 1987. This resulted in the discovery of what have come to be known as the Platinova Reefs in a distinctively rhythmically layered zone known as the Triple Group. The reefs have been traced around approximately 2/3 of the intrusion. Recent estimates of tonnage and grade are 280 m tones at 1.87 ppm Pd over a 4.7 m mining width with a 1ppm cut off and 91 m tonnes at 1.8 ppm Au (Andersen et al. 2002).

The initial magma of the Skaergaard evolved from a Ti-rich tholeiitic basaltic magma that was probably similar to the syn-breakup, high-Ti flood basalt magma characteristic of East Greenland (see above). The earliest exposed cumulates contain plagioclase ($An_{73}$) and olivine ($Fo_{74}$). The cumulates are extremely poor in Ni and Cr. These observations indicate that the magma had undergone substantial fractionation of olivine prior to emplacement.

Andersen et al. (2002) report that the Platinova Reefs occur in a sequence of rhythmically layered rocks (Triple Group) which are plagioclase-augite-titanomagnetite-ilmenite cumulates, with sporadic pigeonite and olivine. The Skaergaard intrusion crystallised both from the base up (LZ and MZ in Fig. 8.45) and from the top down (UZ in Fig. 8.45) and the Triple Group occurs essentially at the junction between the MZ and UZ, so that the horizon represented by this group comprises extremely fractionated cumulates. The reefs consist of possibly more than 10 distinct layers rich in PGE that are precisely concordant with the modal layering. The reefs are both concentrically and stratigraphically zoned with the highest Pt grades occurring at the centre of the lowermost layer, Pd dominating the lower parts of the succession and Au being concentrated towards the margins and in the upper layers. The PGE occur in discrete mineral grains associated with the first occurrence of Cu-Fe sulfides (bornite, digenite, chalcopyrite and minor idaite). Ni- and Fe-rich sulfides have not been observed, but the presence of abundant magnetite suggests that post-magmatic oxidation may have modified the sulfide assemblage. Andersen et al. indicate that the main characteristics of the reefs are:

1. They appear high in the succession, after magnetite has appeared on the liquidus.
2. Their PGE are very fractionated with only traces of Pt and almost no Rh, Ru, Ir and Os.
3. They are very rich in Au.
4. Peaks in Pt, Pd and Au are offset from one another.
5. They are associated with extremely Cu-rich sulfides.

The sulfides occur interstitial to the silicates of the host rocks and show every indication that they are magmatic. However, no magmatic reversals suggestive of the entry of and mixing with fresh magma, have been observed in the Skaergaard intrusion.

### *The Kap Edvard Holm Intrusion and the Willow Ridge Reef*

Platinova Resources Ltd also explored the Kap Edvard Holm intrusion and located the Willow Ridge Reef (Fig. 9.46). Much of the following description is taken from Andersen et al.'s (2002) summary of the work of others

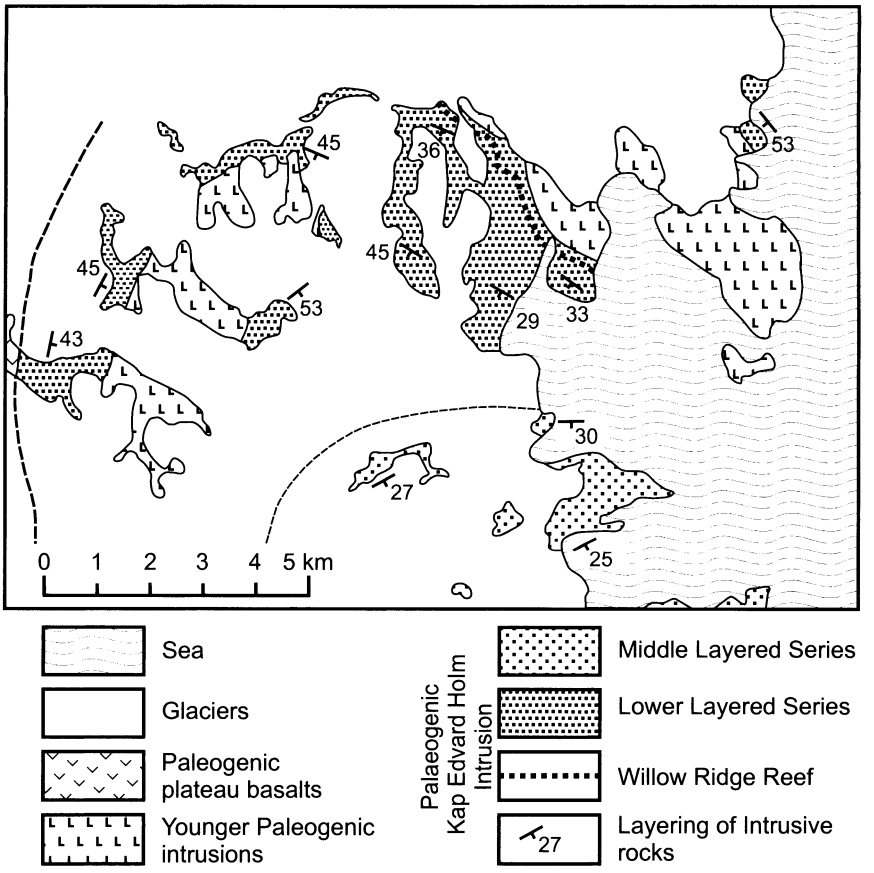


**Fig. 9.46.** Geological map of the northern part of the Kap Edvard Holm intrusion. After Andersen et al. (2002), incorporating data from Bernstein et al. (1992), Bird et al. (1995) and Arnason and Bird (2000)

(principally Tegener at al. 1998; Bird et al. 1995; and Arnason and Bird 2000). Unlike the Skaergaard, which crystallized with no influxes of fresh magma, the Kap Edvard Holm intrusion crystallized as an open system, and exhibits numerous reversals in cumulate succession, cryptic variation and intraplutonic quench zones. It covers 360 $km^2$ and comprises 7500 m of exposed stratigraphy that is divided into a Lower, Middle and Upper Layered Series (Wager and Brown 1968). The intrusion has been dated by the $^{40}Ar$-$^{39}Ar$ method at 47.3±0.3Ma (Tegener et al. 1998), and therefore belongs to the younger group of intrusions discussed above.

The Willow Ridge Reef is situated in a series of plagioclase-augite-olivine orthocumulates near the lowermost exposed level of the intrusion. The gabbros show compositional reversals in the vicinity of the reef. The reef is stratabound but Arnason and Bird (2000) report that it displays a stratification in the peak concentrations of Pd, Pt and Au which they liken to that displayed by the MSZ and LSZ in the Great Dyke and the mineralization at Munni Munni. Typically the Pd peak is lowermost, followed by Pt and then Au. Offsets in the peaks are of the order of 0.5–1 m. Average concentrations over a 3 m interval are reported as 250 ppb Pt, 40 ppb Pd and 50 ppb Au, with maximum concentrations in single samples reaching 5 ppm Pt and 8 ppm Au. The dominant PGM are Pt-alloys (probably isoferroplatinum), sperrylite, cooperite and moncheiite along with digenite, bornite and chalcopyrite. Arnason and Bird (2000) favor an origin as the result of sulfide immiscibility.

### 9.4.8 The Sonju Lake Intrusion, Duluth Complex

The Sonju Lake intrusion has been described by Miller and Ripley (1996) and Miller (1999) from which most of the following description has been taken. The intrusion is a 1200 m-thick tholeiitic layered mafic intrusion that is exposed in a 9 $km^2$ area near Finland, Minnesota and has been dated at 1.0961±0.0008 Ga. It is part of the Beaver Bay Complex, which is a suite of intrusions emplaced into the upper part of the Keweenawan North Shore volcanic group (see Chapter 4). The intrusion (Fig. 9.47) comprises a series of south-dipping layers which range upward from a marginal troctolite, through a thin layer of dunite and then a thick sequence of troctolites, gabbro, Fe-Ti oxide-gabbro, and apatite-bearing olivine diorite to an olivine monzodiorite. Miller (1999) reported that the sequence of cumulus phases and cryptic variation indicate that fractionation was continuous with no influxes of fresh magma. Preliminary isotopic data indicates limited contamination by the overlying Finland granite.

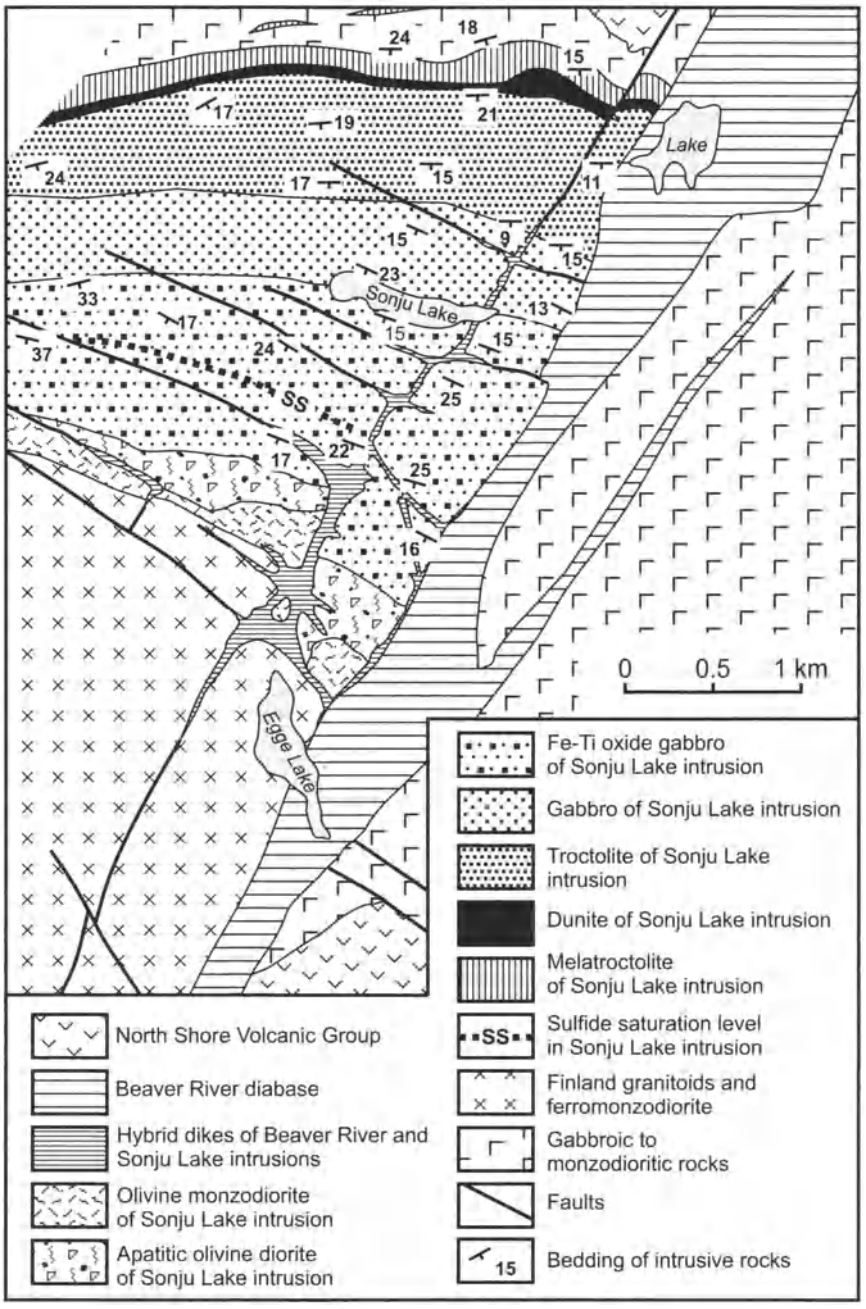


**Fig. 9.47.** Geological map of the Sonju Lake intrusion (after Miller et al. 1993)

Geochemical profiles, particularly that of Cu which increases abruptly from <100 ppm to >500 ppm through the intrusion indicate that initially it was sulfide undersaturated, and that saturation occurred at a specific level, 322 m above a level at which cumulus augite first appears in the stratigraphy and which is designated henceforth as maaa (this approach to defining stratigraphic levels was taken to eliminate irregularities resulting from the variable thickness of the marginal rocks and troctolites). By this stage Ni had been reduced to a very low level as a result of removal in fractionating olivine. Pd concentrations are generally between 0.5 and 3 ppb in the lower part of the intrusion, which is probably the result of Pd dissolved in trapped intercumulus liquid. Peak concentrations of Pd (100–320 ppb) occur within a 25 m thick interval just below the 322 maaa sulfide saturation level. For 50 m below this, Pd values increase from levels of 3 ppb or less to as much as 36 ppb. Pt generally follows Pd, showing a maximum coincident with the Pd peak, but there is also another Pt maximum about 90 m below the Pd peak. PGE levels above the PGE maxima are very low, attesting to the efficiency with which sulfides have scavenged the PGE and the absence of any subsequent influx of PGE-bearing magma.

### 9.4.9 Genetic Models for Deposits in Layered Intrusions

#### *Genetic Models for stratiform deposits not associated with chromitite layers*

Table 9.14 compares a number of aspects of the mineralization for most of the known intrusions in which deposits not associated with chromitite layers occur. It is apparent that orthocumulates are the host to many of the mineralized horizons. Very commonly, pegmatoidal rocks have been reported within or in the vicinity of these horizons. Another variable that correlates with the orthocumulate association is evidence either of reversals in the normal appearance of phases during fractional crystallization or in cryptic variation, that is suggestive of an influx of fresh magma at or close to the horizon in question.

The exceptions to this observation include the mineralization in the Sonju Lake, Skaergaard and Great Dyke mineralized zones, and the AP reefs in the Penikat intrusion. Miller and Andersen (2002) pointed out that the Skaergaard and Sonju Lake intrusions crystallized as closed systems, and that no fresh magma entered either body during crystallization. They remarked that in both bodies, sulfide saturation was reached late in the crystallization sequence, and proposed that this was the result of the build up of sulfur in the fractionating magma, perhaps aided by a release of pressure in the magma chamber. The mineralized zones in the Great Dyke

**Table 9.14.** A comparison of the aspects of stratiform PGE Mineralization not associated with chromitite layers

| Deposit | Type of cumulate related to mineralization | | | Chromite present | Significant BMS present | Pegmatoid in vicinity | Reversals in cryptic variation (and/or modal cyclicity) |
|---|---|---|---|---|---|---|---|
| | Ortho-cumulus | Meso-cumulus | Adcu-mulus | | | | |
| ***Bushveld*** | | | | | | | |
| Merensky Reef | Host | | Forms Base | Yes | Yes | Yes | Yes |
| ***Stillwater*** | | | | | | | |
| J-M Reef | Host | | | Rare | Yes | Yes | Yes |
| Picket Pin | Host | | Forms Cap | No | Yes | No | No |
| **Finnish Intrusions** | | | | | | | |
| ***Penikat*** | | | | | | | |
| S-J Reef | Host | Host | Forms Base | Yes | NU* | Yes | Yes |
| AP I and AP II Reefs | | Host | Host | No | Yes | No | No |
| PV Reef | Host | | | No | Yes | Yes | Yes |
| ***Portimo*** | | | | | | | |
| SK Reef | Host | | | No | Low | Yes | Yes |
| RK Reef | Host | | | No | No | Yes | No |
| ***Duluth Complex*** | | | | | | | |
| Sonju Lake | | Host | | No | Yes | No | No |
| ***East Greenland*** | | | | | | | |
| Skaergaard, Platinova Reefs | | Host | | No | No | No | No |
| Kap Edvard Holm, Willow Ridge Reef | Host | | | No | No | No | Yes |
| ***Great Dyke of Zimbabwe*** | | | | | | | |
| Main Sulfide Zone | | Host | | No | Yes | No | ES** |
| Lower Sulfide Zone | | Host | | No | Yes | No | ES** |

*NU = Not ubiquitous; **ES = Extremely subtle

occur in the middle of a sequence of pyroxenites. Extremely subtle reversals in the MgNo of pyroxenes crystallizing at this level have been documented (see discussion of the Great Dyke above), but these have nothing like the magnitude of reversals in other bodies.

It is this author's opinion that the widespread association of orthocumulates, pegmatoidal rocks and reversals both in crystallization sequence and in cryptic variation with stratiform PGE mineralization is not coincidental, but is the result of influxes of new magma causing sulfides to become immiscible and concentrate at or near the cumulate-magma interface. At the beginning of this chapter, it was pointed out that stratiform PGE deposits are characterized by much higher than normal PGE tenors in their sulfides than sulfide-rich Ni-Cu magmatic sulfide deposits, but that Ni and Cu were not unduly enriched, which leads to the high (Pt+Pd)/(Ni+Cu) (PGE in g/t, Ni and Cu in wt%) that is emphasized in Chap. 1 and illustrated in the Appendix. In Chap. 2, it was suggested that high magma/sulfide ratios can account for these differences. The work of Barnes and Maier (2002) has shown that cumulates in the Upper Critical Zone developed from a magma that was also precipitating sulfide and that these sulfides were relatively rich in PGE (see section on Bushveld above), containing about 40–100 ppm Pt and 40–50 ppm Pd. The sulfides of the Merensky Reef itself contain 400–600 ppm Pt+Pd, that is 3 to 4 times higher in PGE tenor than those in the enclosing cumulates. Some of the questions to be answered with respect to the origin of reefs such as the Merensky are, therefore, what caused sulfides to concentrate at a particular horizon, why do they have such high R Factors, why are they associated with orthocumulates, and why are they often associated with pegmatoids?

Campbell et al. (1983) pointed out that the density of a magma such as the Bushveld changes as it fractionally crystallizes. While olivine is on the liquidus, the density decreases, when olivine is replaced by bronzite, the density remains approximately constant, and once plagioclase joins bronzite in cotectic proportions (about 2 plagioclase to 1 bronzite), the density of the remaining magma increases. After a period of crystallizing plagioclase + bronzite, the density of the magma in the chamber will exceed that of the original magma. Prior to plagioclase becoming a liquidus phase, the momentum of any fresh influx of original magma will cause it to fountain into the old magma, before falling back to form a layer on the top of the pile of cumulates (Fig. 9.48a). However, once the magma in the chamber becomes significantly denser than the original magma, any influx of original magma into the chamber will rise as a turbulent plume, spreading out at the appropriate density level as a turbulently convecting layer (Figs. 9.48b, c). If sulfides had been present in the hybrid at this stage, the turbulent mixing and convection would have provided the ideal

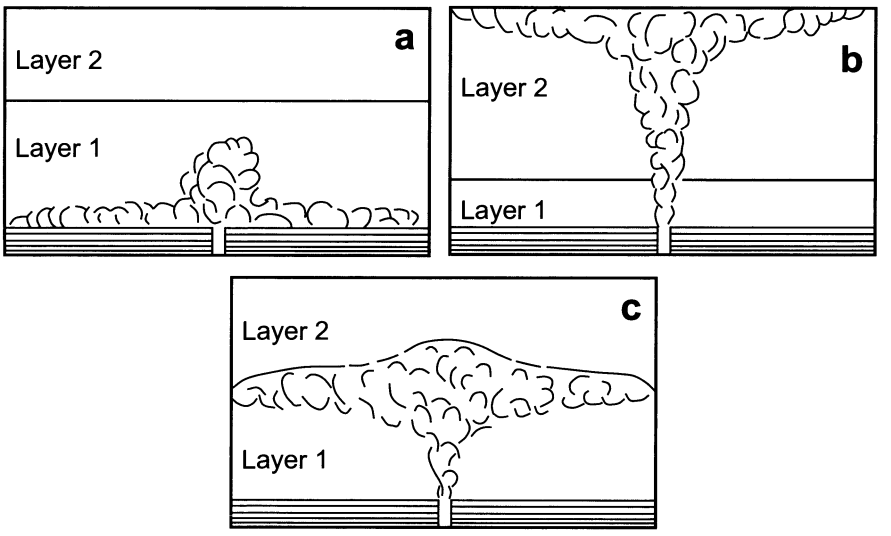


**Fig. 9.48.** The turbulent fountain (a) and plume (b) and (c) resulting from the injection of (a) denser and (b) and (c) less-dense primitive magma into residual magma in a magma chamber. In the case of (c), the primitive injection has a density intermediate between that of layer 1 and 2 in the chamber. After Campbell et al. (1983)

environment in which they could have developed a high R factor, and thus have become very enriched in PGE. Campbell et al. suggested that it is no coincidence that the Merensky and J-M Reefs occur about 400 m above where plagioclase has first entered as a cumulus phase in both the Bushveld and Stillwater intrusions.

Naldrett et al. (1987) pointed out that the mixing of a fresh input with cooler magma in the chamber would result in silicates crystallizing in the turbulent layer. They suggested that these would have remained in suspension while the layer remained turbulent, but as it cooled and the convection became lamina, they would have rapidly settled, along with the sulfides to form a sulfide-enriched orthocumulus layer at the cumulate-magma interface. As conditions changed and crystallization reverted to slow crystal growth at the top of the pile of cumulates, meso- and adcumulates would form again. This model is supported by the mineral variation documented throughout the Meresnky Cyclic Unit (Fig. 9.11). It accounts for the location of the sulfide concentration, their high R-factor sulfides and their association with orthocumulates.

Naldrett et al. (1987) also pointed out that any fluids released deeper in the cumulus pile as a result of the final solidification of interstitial magma would rise in an attempt to reach the interface between the top of the pile

of cumulates and the overlying magma. In doing this, the fluids would have had relatively little trouble diffusing along crystal boundaries and fractures in fully solidified cumulates. However, once they reached a partially solidified orthocumulus layer (orthocumulates, with their trapped liquid enriched in low melting point constituents, will remain liquid longer than adjacent meso- or adcumulates), they could only continue their ascent by dissolving in the intercumulus fluid and diffusing through it. The addition of fluids would cause additional fluxing of the layer and promote the development pegmatoidal recrystallization, thus accounting for the association with pegmatoid.

The case of the Platinova Reefs of the Skaergaard and the reef in the Sonju Lake intrusion cannot be explained in this way. In these two intrusions, which have had no influx of fresh magma, the PGE-bearing sulfide layers are likely the result of sulfur building up in the magma as silicates crystallized until saturation was achieved, perhaps aided by pressure release (Miller and Andersen 2002). In both cases the reefs occur at high levels in the intrusions following an extended period of fractional crystallization, which would have caused strong enrichment in the sulfide dissolved in the residual magma.

The Great Dyke of Zimbabwe presents a rather different situation: (i) the mineralization is in bronzitite and, in the case of the MSZ also partly in websterite, close to but just below the level at which cumulus plagioclase first appears; (ii) the mineralization defines a zone upwards across which the PGE tenor of the sulfides, and thus presumably of the magma with which it was equilibrating, drops abruptly but progressively.

As discussed above for the Skaergaard and Sonju Lake intrusions, simple crystallization of silicates in a fractionating magma will eventually cause sulfide saturation and give rise to weak disseminations of PGE-rich sulfides unrelated to cyclic units or the nature of the cumulus minerals. This mechanism, which is illustrated by the progression of a silicate magma from A to B in Fig. 9.49, is a likely explanation for the Lower Sulfide Zone of the Great Dyke. The progressive segregation of sulfide, as the magma moves down the sulfide saturation curve from B to C, can account for the upward depletion in PGE that is observed, with the different PGE becoming depleted in the order of their sulfide liquid-silicate magma partition coefficients (see below).

The above mechanism is unlikely to be the sole explanation for the Main Sulfide Zone of the Dyke because the amount of sulfide in the zone is greater than the cotectic proportions that would segregate from a magma moving down the saturation curve (1.5 to 3 wt%). As discussed above, the dyke is trumpet shaped in cross section, and originally it probably had

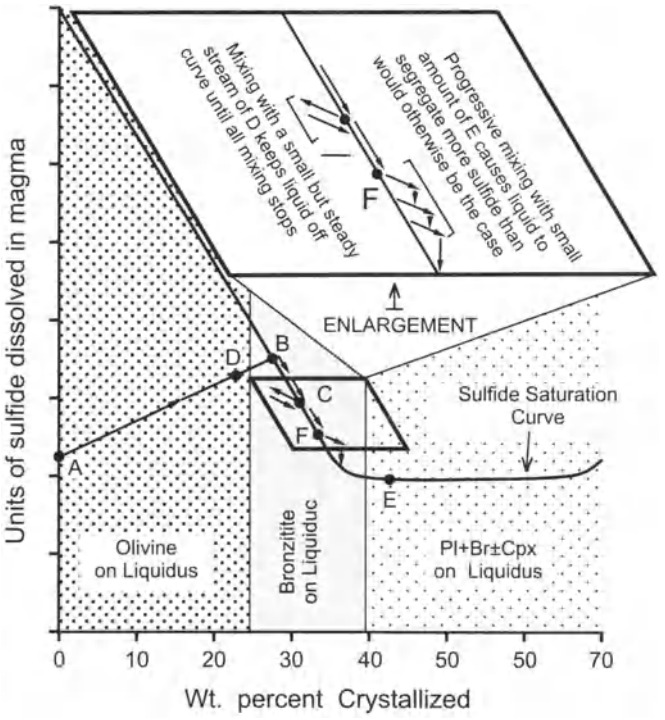


**Fig. 9.49.** Schematic diagram showing how the solubility of sulfide in the magma of the Great Dyke is likely to vary with fractional crystallization, and mixing with other more and less primitive magmas. This diagram is modified to reflect the more primitive nature of the Great Dyke from that developed for the Bushveld Complex by Naldrett and von Gruenewaldt (1989). After Naldrett (1989)

pronounced flared "wings" as shown in Fig. 9.50. Magma in the "wings" would have been more exposed to contamination and would also have lost heat more rapidly than that at the axis. Plagioclase therefore appeared on the liquidus slightly sooner in this region than in the body of the intrusion, and a gabbroic differentiate (which would be denser than a more primitive ultramafic magma) could have migrated down the top of the cumulate pile towards the axis. It could have become mixed with less-fractionated magma causing the composition of the mixture to become over saturated in sulfide, thus causing more than the cotectic proportion of sulfide to segregate.

Subsequent mixing with periodic inputs of fresh, primitive, PGE-rich magma took the resident magma back to the unsaturated side, halting sulfide segregation, and refreshing it. This accounts for the build-up in the Mg/(Mg+Fe) ratio of bronzite and PGE content of the magma above each sulfide zone.

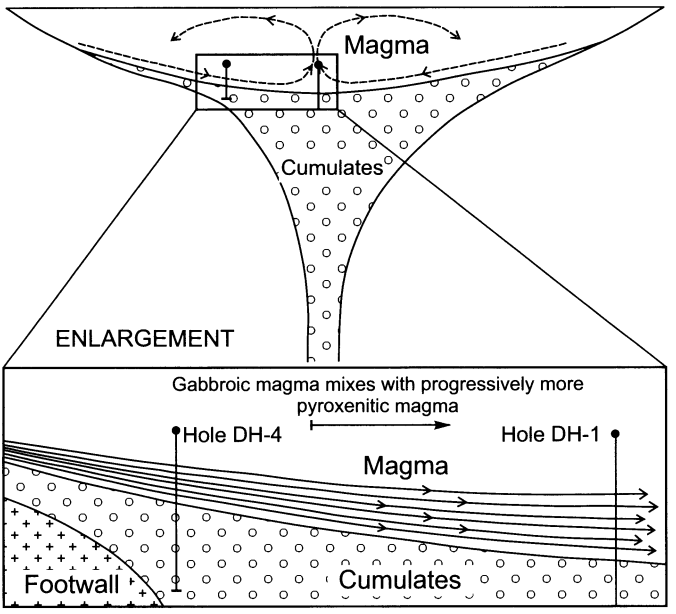


**Fig. 9.50.** Schematic cross-section through the Great Dyke showing the marginal "wings" within which cooling proceeded more rapidly than at the axis and from which more fractionated, "gabbroic" magma flowed towards the axis as shown, to become mixed with less-fractionated magma resident there and incorporated in convective overturn within the chamber

Turning to the second question, the systematic and smooth way in which Pd and Pt decrease upwards in the sulfides of a mineralized zone in the Great Dyke (Figs. 9.31 and 9.32) is very different to that observed in the Merensky Reef. This is illustrated in Fig. 9.51 which incorporates the data used by Naldrett and Wilson (1991) in constructing Figs. 9.31 and 9.32, but also uses new unpublished data that has been acquired since that time. The smooth, relatively rapid decrease in Pt in 100% sulfide across the LSZ zone while the percentage of sulfide in the rocks shows little change (Fig. 9.51b) is clearly illustrated in the figure. The behavior of Pt in 100% sulfides across the MSZ (Fig. 9.51c) is more complex. Sulfide saturation occurred at the stage shown by line (1), and Pt started to decrease. Then new magma entered the chamber at the stage illustrated by line (2) and the Pt content rose, up to the stage (line 3) at which saturation was again achieved, significant amounts of sulfide separated and the Pt in 100% sulfide decreased rapidly, but progressively upwards from this stage onward.

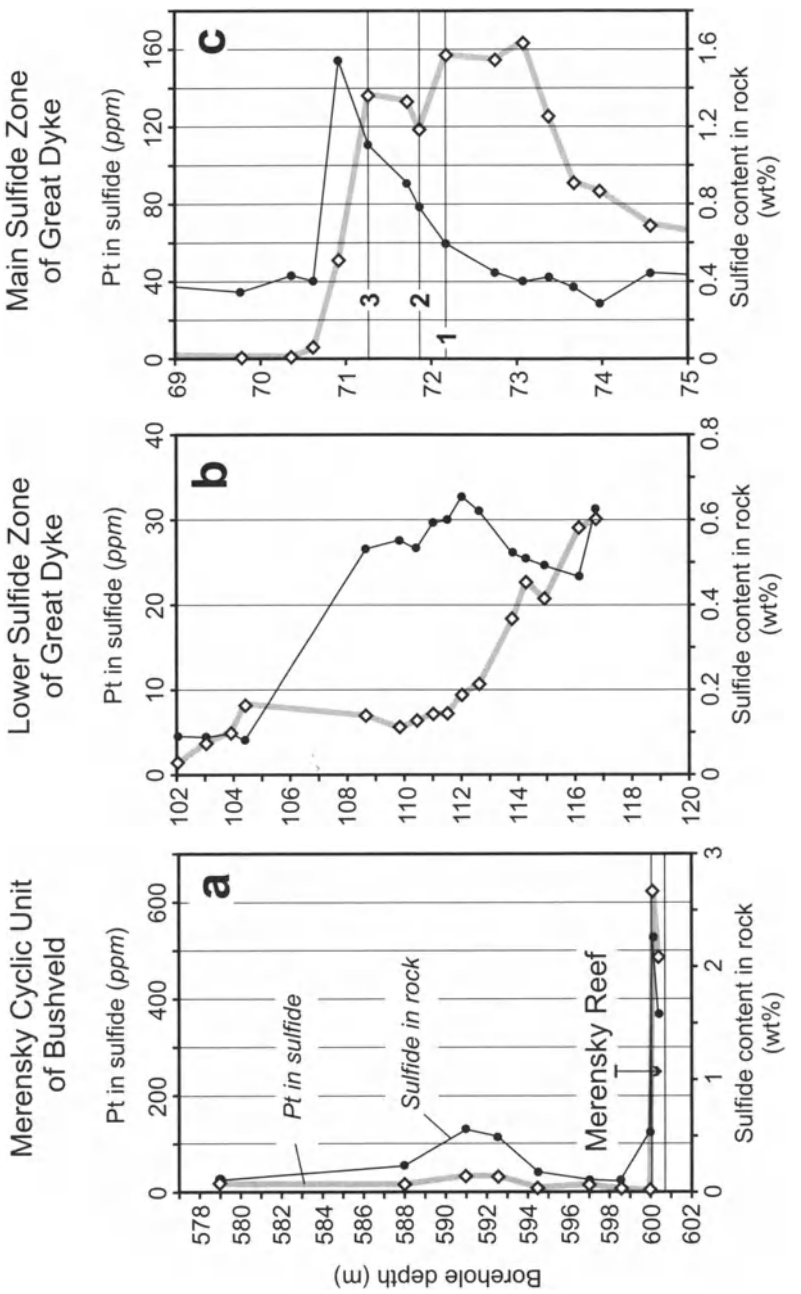


**Fig. 9.51.** Variations of total sulfide versus Pt contents in 100% sulfide of Merensky Cyclic Unit of Bushveld Complex (a), Lower (b) and Main (c) Sulfide Zones of Great Dike of Zimbabwe. After Naldrett and Wilson (1990) and unpublished data of the author. Lines 1, 2, and 3, shown in plot c are explained in text

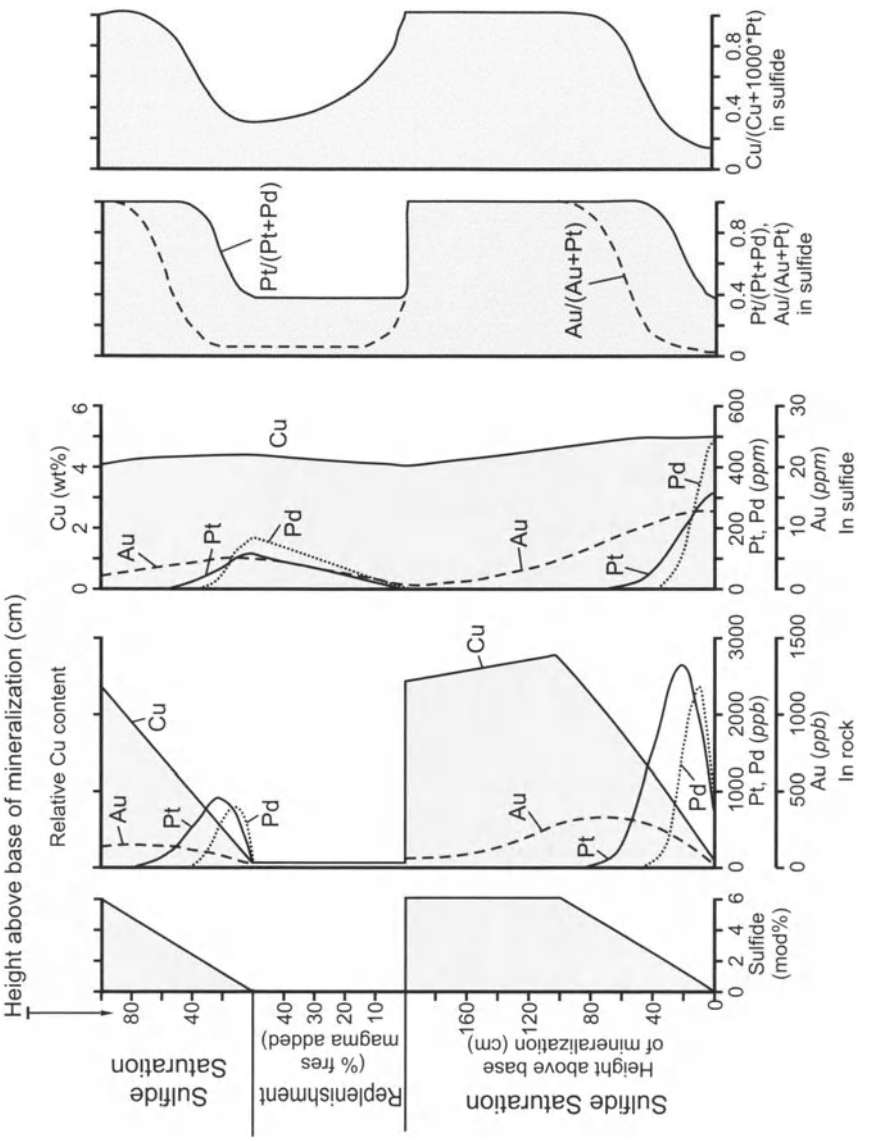


**Fig. 9.52.** Modeling of the variation in the concentrations and the ratios of Pd, Pt, Au and Cu in typical sulfide zones of the Great Dyke as a consequence of fractional segregation of sulfide. No data are available on the PGE content of the Great Dyke magma so typical values for continental flood basalt of 10 ppb Pt and 5 ppb Pd were assumed. Partition coefficients of $10^5$, $10^{4.5}$, $10^{3.5}$ and 250 were assumed for Pd, Pt, Au and Cu respectively. In order to facilitate comparison with the observed data, the sulfide concentration has been made to increase gradually from the base upwards. As described in the text, sulfide segregation is believed to have been halted as a consequence of the introduction of new magma. At this

stage the magma resident in the chamber was essentially devoid of PGE, as shown by the very low PGE content of sulfide segregating towards the top of each mineralized zone. As new magma (containing the original concentration of PGE) enters and mixes with that in the chamber, the PGE content of the resulting hybrid increases. Eventually crystallization of silicates (which is believed to occur while the new influx is occurring) brings the magma in the chamber back to the sulfide saturation curve, sulfides start to segregate and the whole process recommences, as shown at the top of the figure. The extent to which the magma in the chamber (and thus any sulfide to equilibrate with it) is enriched in PGE depends on the percentage of new magma that is introduced. From Naldrett and Wilson (1991)

The behavior illustrated in both of these diagrams is in strong contrast to that of the Merensky Reef (Fig. 9.51a). Here all of the sulfides in the Reef have a high Pt tenor (400–600 ppm) and, only a few mm above the thin chromite seam which defines the upper contact of the Reef, the Pt tenor falls to and remains at a value between 4 and 35 ppm. The behavior in the LSZ and MSZ of the Great Dyke is reminiscent. of the partitioning of elements into a phase that is continuously being removed from the magma, in this case sulfide. The case of the Merensky Reef suggests that the sulfides of the Reef underwent batch equilibration with magma at a high R factor, as is called for by Campbell et al's model already presented above.

The hypothesis for the Great Dyke can be tested by modeling the behavior of Pt, Pd and Cu for simple Rayleigh fractionation as has been done in Fig. 9.52. As can be seen by comparing Fig. 9.52 with Fig. 9.51, a reasonable match is obtained between observations and model. The values of the partition coefficients required for the modeling are $10^5$ for Pd, $10^{4.5}$ for Pt and $10^{3.5}$ for Au. Ru and Ir require partition coefficients slightly higher than those required by Pd. These partition coefficients are the same as those to account for the differences that Naldrett and Wilson (1991) noted in the tenor of each PGE between axis and margin (see Table 9.8 and related text).

Naldrett and Wilson's (1990) favored model of ore formation was that, initially, a column of magma of the order of 10's to 100's of meters high became saturated in sulfide, sulfides fractionally segregated from this and settled slowly through it to become mixed with bronzite cumulates on the chamber floor. Eventually, for reasons discussed above, the segregation ceased, by which stage the magma column had become extremely depleted in PGE. The data indicate that before the next mineralizing interval the magma overlying the cumulate pile became enriched in PGE again; because, as indicated above, this enrichment was accompanied by an increase in the MgNo of bronzite, Naldrett and Wilson proposed that it was due to its mixing with a fresh input of primitive, PGE-rich magma.

Barnes (1993) attempted similar modeling to that undertaken by Naldrett and Wilson (1990) and found that in the Munni Munni intrusion a constant value of D for the partitioning of PGE between sulfide and silicate melts was incapable of accounting for all of the observed variation. He concluded that the effective value of D must have varied by up to 1 order of magnitude, from locality to locality, and vertically at the same locality. He could find no evidence in the rocks to indicate changes in intensive variables that would have been required to cause such large fluctuations in D. He therefore concluded that the sulfides were actually saturated in, and crystallizing PGE phases as they were segregating. If this were true, and a PGE minerals were crystallizing from the sulfide liquid, it would lower the activity of the particular PGE in the sulfide liquid, which would cause more of that PGE to enter the liquid from the surrounding magma. Despite the lowering in PGE activity in the sulfide liquid itself, the effective concentration of the PGE in question in the mixture of sulfide liquid plus PGE mineral would have increased, giving the impression that the value of D was higher than it actually was.

### *Stratiform deposits associated with chromitite horizons*

**Chromitite-dominant deposits containing Fe-Cu-Ni sulfides.** Considering sulfide-bearing chromitite layers, Irvine (1975) pointed out that the mixing of two magmas, one mafic and Cr-rich and the other more felsic in composition could result in the hybrid falling in the field of chromite crystallization, with the result that chromite would be the sole liquidus phase, and a chromitite layer would form until the magma returned to a cotectic involving silicate phases in addition to chromite. It is argued above that magma mixing also promotes sulfide saturation, so that under circumstances in which one (or both) of the magmas was (were) close to sulfide saturation, sulfide would also segregate, thus explaining the association.

One aspect of UG-2 type deposits requires comment; this is the extremely high PGE tenors of the sulfides that is referred to above and is illustrated in Fig. 9.16. Naldrett and Lehman (1988) argued that when Fe-rich sulfides are trapped at high temperature in abundant chromitite, the non-stoichiometry of the chromite at high temperature (due to its magnetite component) results in Fe moving from the sulfide to the chromite during cooling to satisfy the requirement for stoichiometry at low temperature. They presented thermodynamic data to support their contention. The loss of Fe from the sulfide causes a rise in the $fS_2$ locally, with the result that S is lost to the surroundings. The resulting decrease in amount of sulfide causes a rise in the tenor of metals other than Fe in the sulfide. They sug-

gested that the high PGE tenors of sulfides associated with chromitites had resulted in this way.

**Chromitite-dominant, Fe-Cu-Ni sulfide-absent deposits.** These deposits are characterized by negative slopes on chondrite-normalized PGE plots, being enriched in Os, Ir and Ru (IPGE) and depleted in Pt, Pd and Au. This is illustrated in Fig. 9.53 which shows chondrite-normalized abundances of PGE in mineralized layers from the Stillwater complex. It is seen that the J-M Reef, which contains little or no chromite has the steepest positive slope, that sulfide-bearing chromitites have intermediate slopes, and that sulfide-free chromitites have negative slopes. The reason for the steep positive slopes in chromite-poor zones has been discussed above and is related to the presence of sulfide and the strong partitioning of Pt and Pd into this sulfide. The reason for chromite concentrating Os, Ir and Ru remains a matter for debate. Sattari et al. (2002) have shown that chromite does not concentrate Ir from a silicate melt, and that the presence of Ir in solid solution in chromite cannot account its concentration in sulfide-poor chromitites. Microscopic examination of chromitites from this environment shows the presence of laurite and Ir-Os alloys contained within chromite grains.

Mungall (2002) suggested that, because Ru, Ir and Os are present in a magma in the trivalent state, their solubilities will be strongly reduced by decreases in $fO_2$. Growth of chromite from a silicate melt consumes oxygen, with the result that a boundary layer with a lower than ambient $fO_2$ will surround each growing chromite grain. This zone of reduced $fO_2$ may be enough to promote supersaturation of the IPGE, which will nucleate to form micro-nuggets (in some cases invisible microscopically) that will become incorporated in the growing chromite crystals. The decrease in IPGE activity from the surrounding magma into the boundary layer will cause them to diffuse from the magma into the boundary layer, thus supplying a continuous feed to the growing chromite. Laurite growth cannot be explained in this way since decrease in $fO_2$ will inhibit the growth of a sulfide such as laurite, but if the boundary layer is eroded as the crystals gets washed by magmatic currents, laurite could nucleate and concentrate IPGE. Oscillation between a stagnant environment (favouring alloy micronugget development) and a dynamic environment (favouring laurite development) can explain the co-existence of both sets of minerals in a single grain. Recent experiments by Finnigan and Brenan (2004) have provided some confirmation of Mungall's suggestion. Finnigan and Brenan suspended beads of natural basalt containing small crystals of natural chromite at 1400° C and $fO_2$ = FMQ+4.3 using Pd or Pt/Rh alloy wires. Because the chromite crystals were out of equilibrium at the high $fO_2$ of the

experiments, they became converted at their margins to chromian magnetite, taking up $Fe^{3+}$ and yielding $Cr^{3+}$ to the immediately adjacent magma. This resulted in the zone of magma surrounding the chromite becoming reduced along with the deposition of very small PGE nuggets (the PGE being derived from the wires used to suspend the chromite crystals) on the surface of the chromite-chromian magnetite crystals. Finnigan and Brenan conclude that the nugget formation is apparently due to a decrease in the solubility of the PGE with decrease in $fO_2$ in the vicinity of the crystals.

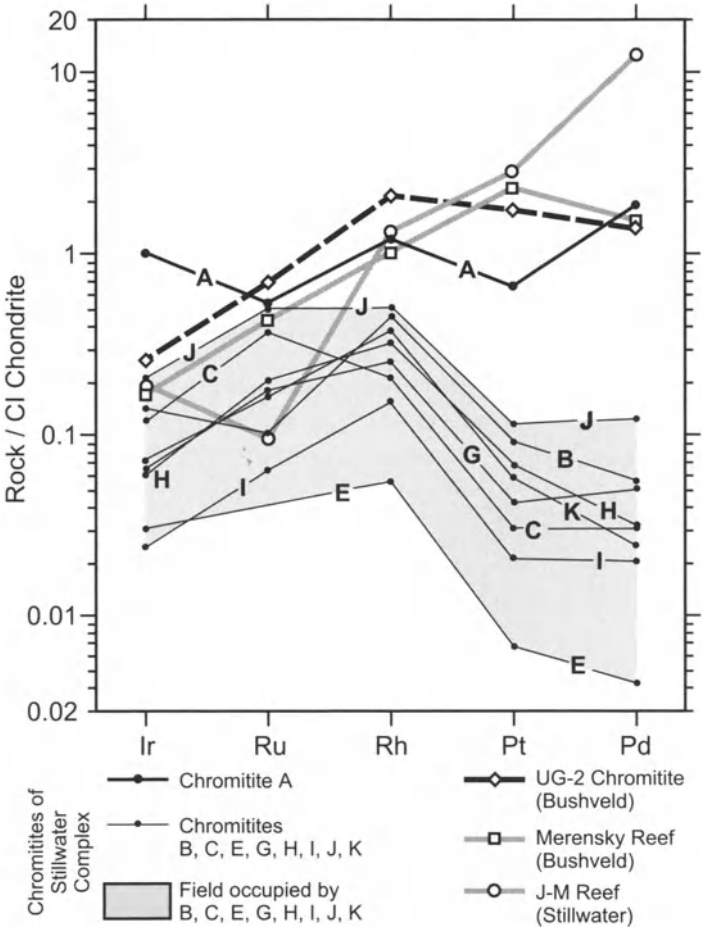


**Fig. 9.53.** Chondrite-normalized abundances of PGE in chromitite layers from Stillwater Complex in comparison to sulfide-bearing reefs (J-M and Merensky) and sulfide-bearing chromitite UG-2. Whole-rock contents from Table 1.1 are given for the J-M, Merensky Reefs and for the UG-2. Data for the Stillwater chromitites are from Page et al. (1985)

### *Model for Stratabound but not stratiform deposits in layered intrusion*

This section is devoted to considering how the marginal deposits found in the intrusions of Northern Finland and in those along the margin of the former Penokean ocean near Sudbury, Ontario might have formed. Alapieti and Lahtinen (2002) report that the tenors (concentrations in 100% sulfides) of marginal sulfides at Kontijarvi are 6.51 wt% Ni, 26.07 wt% Cu, 141 ppm Pt and 442 ppm Pd, with a (Pt+Pd)/(Ni+Cu) ratio (PGE in g/t, Ni and Cu in wt%) of 17.9 (see the Appendix). Calculation of the data of James et al. (2002) for the East Bull Lake and River Valley marginal mineralization, using estimates of sulfur concentrations based on their chondrite normalized plots of their Fig. 9, indicate that the tenors are also high, respectively 7.56 and 2.31 wt% Ni, 9.72 and 11.00 wt% Cu, 51 and 38 g/t Pt, 147 and 112 g/t Pd, both with (Pt+Pd)/(Ni+Cu) ratios of 11(the Appendix). These tenors and (Pt+Pd)/(Ni+Cu) ratios are significantly higher than those of massive to semi-massive Ni-Cu sulfide ores, indicating that something special has occurred in their formation.

The deposits are characterized by xenoliths of mafic igneous rocks, some of which have been derived very locally, and others of which are more mafic than the local in situ igneous rocks. It would seem likely that the sulfides have been introduced, along with the breccia, from a deeper source within the intrusion. In this author's opinion, it is significant that the richest marginal ore in the Portimo area occurs where the SK Reef abuts the marginal rocks. The SK Reef occurs at a horizon where high-MgO magma-derived cumulates give way upward to those derived from tholeiitic magma. It has been noted above that the mixing of these two magmas concentrated sulfides with a high R Factor, and so gave rise to the SK Reef. It is suggested here that some of the same high R Factor sulfides became entrained in early pulses of the hybrid magma that resulted from the intermixing of the high-MgO and later tholeiitic magmas, and that concentrated to form the SK Reef. This magma intruded farther than the restricted Narkaus intrusion in the Portimo area (see Fig. 9.38) to give rise to the marginal series of the Suhanko-Konttijarvi intrusion, thus accounting for the PGE-rich tenors of sulfides of the marginal deposits. Continued influx of tholeiitic magma gave rise to the upper part of the Narkaus intrusion and the bulk of the Suhanko-Konttijarvi intrusion. A similar explanation may account for the marginal rocks of East Bull Lake and River Valley. The stratigraphic level exposed in these intrusions is not as deep as that in the Portimo area, and it is possible that their deeper parts also formed from a high-MgO rather than a tholeiitic magma. Careful study of the cognate xenoliths may give some indication of what is hidden within them at depth.

## 9.5 Non-stratabound Deposits

### 9.5.1 Lac des Iles PGE-bearing Complex

#### *Geology*

The Lac des Iles complex lies within an Archean granite/granite gneiss terrain which belongs to the Wabigoon Subprovince in Northwest Ontario. Several mafic intrusions within the area appear to define the perimeter of a circle about 20 km in diameter, the center of which is occupied by hornblende and biotite tonalite rocks (Sutcliffe 1986). The Lac des Iles complex, which is the largest of the mafic bodies, consists of an ultramafic part centred on Lac des Iles itself and a gabbroic part to the south (Fig. 9.54). The ultramafic part has been further subdivided into northern (NUC) and southern (SUC) intrusive phases. Although age relationships are not well established by field evidence, it is believed that the different intrusive phases are coeval. Both the gabbroic and ultramafic parts contain PGE-bearing Ni-Cu sulfide mineralization, although only that within the Gabbroic Complex is of economic importance.

The hornblende and biotite tonalites belong to a group of late-stage felsic intrusions that have been recognised in NW Ontario (age approx. 2696 Ma) and that are referred to as sinucatoids. Where they are in contact with ultramafic and mafic rocks of the Lac des Iles complex, they form extensive reaction zones with a variable composition which is approximately that of hornblende diorite. It is likely that the sinucatoid magma was intruded when the Lac des Iles complex was still hot, perhaps partially molten, which accounts for the extensive reaction between the two.

**Ultramafic Complexes.** The SUC consists of a wehrlite and olivine-clinopyroxenite core, surrounded by websterite and gabbronorite. Petrographic and geochemical studies suggest that the NUC consists of at least 8 cyclic units which, if not beheaded, are composed of dunite and wehrlite to olivine-clinopyroxenite cumulates at the base, followed by clinopyroxenite and websterite, locally grading into gabbronorite. This indicates similar crystallization sequences in both ultramafic centers: olivine, olivine + clinopyroxene, clinopyroxene, clinopyroxene + orthopyroxene ± plagioclase.

The PGE-bearing sulfide mineralization in the NUC occurs at the top of cyclic units in websterite and orthopyroxenite cumulates. Sulfide bearing samples (up to 1 wt.% of sulfide) are enriched in Au, Pd, Pt and Cu relative to Ni, Ru, Ir, and Os with Pd/Ir ratios in the order of 250. Sulfide saturation was probably caused by the mixing of fractionated residual melt

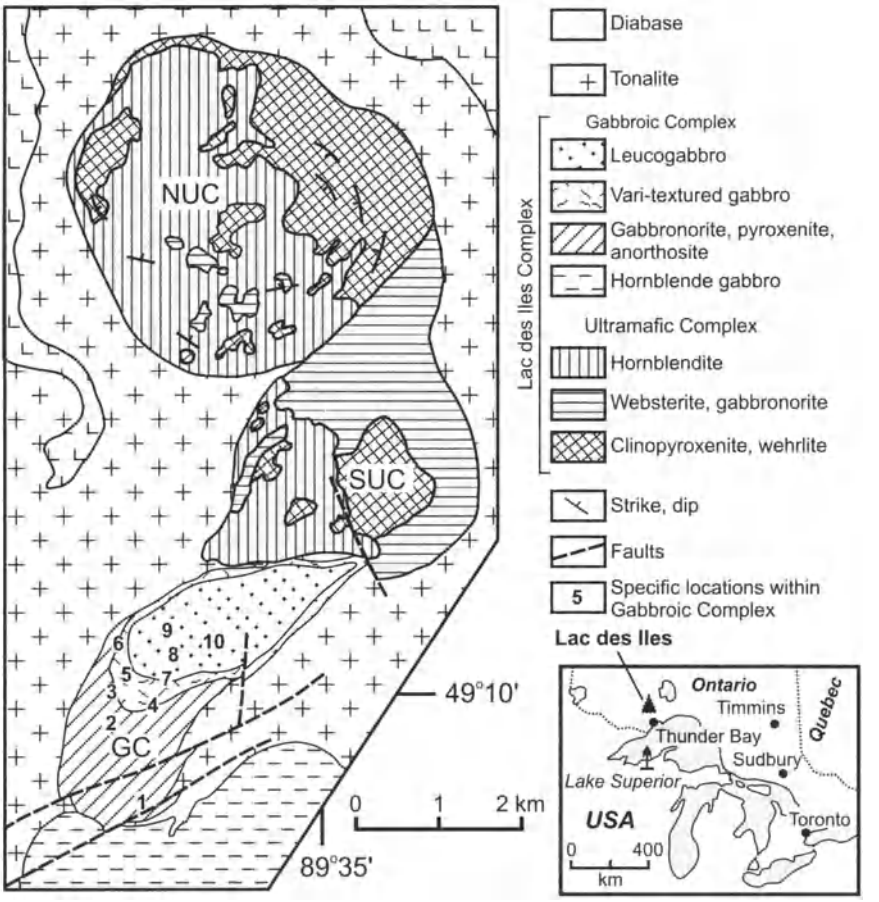


**Fig. 9.54.** Location and Geology of the Lac des Iles Complex (modified from Sutcliffe and Sweeney (1985). GC = gabbro complex; SUC = southern ultramafic complex; NUC = northern ultramafic complex. The Roby Zone is at location 5 in the Gabbroic Complex

with more primitive liquid, as the latter intruded the magma chamber. Sulfur-poor pyroxenite cumulates (S < 100 ppm) occurring at the center of cyclic units can contain elevated PGE concentrations which are characterized by low Pd/Ir ratios (9 to 40). The PGE enrichment can be explained by the segregation of very small amounts of a sulfide liquid from a silicate magma that became sulfide saturated during continuous crystallization. Because of the low PGE tenor of these sulfides, Ir contents in silicates, oxides or alloys contribute significantly to the whole rock concentrations and give rise to rather low Pd/Ir ratios.

**Gabbroic Complex.** The primary mineralogy of the Gabbroic Complex has been largely replaced by secondary alteration products and most information about it has been inferred from these products. The complex consists of a dominant clinopyroxene leucogabbro, although a number of distinctive phases, including magnetite-rich and hypersthene-bearing variants, have been recognized. A dark green, ultramafic sill or layer consisting of completely uralitized pyroxene and 5–25 % plagioclase occurs in sharp contact with the leucogabbro, parallel to the modal layering that has been tentatively identified within this gabbro.

The gabbro is cut by irregular zones composed of gabbro with a highly variable grain size and modal composition (vari-textured gabbro), and containing numerous fragments of cognate xenoliths representative of different phases of the gabbro. The inclusions have reacted with the enclosing vari-textured gabbro; in places their borders are sharp, in places they are gradational into vari-textured gabbro. The vari-textured gabbro itself grades into a pegmatoidal leucogabbro. It is cut by small (2-10cm thick, 1-3m in length) veins of gabbro pegmatoid and pegmatite, many of which contain sulfides. The largest zone of vari-textured gabbro lies in the west-central part of the Gabbroic Complex, mostly west of the pyroxenite sill, although it cuts through this in some places. Where this occurs, plastically deformed, inclusions of pyroxenite occur within the vari-textured gabbro.

### *Mineralization*

The economically most important ore metals are Pd, Pt and Au. The largest zone identified so far is the Robie Zone which occurs primarily within the vari-textured gabbro west of the pyroxenite layer. Based on noble metal abundances and the lithological association, Macdonald et al. (1989) distinguished 3 categories of mineralization:

1. Low grade mineralization (less than 1000 ppb PGE+Au) occurring in vari-textured gabbro breccias. Values occur primarily within the matrix, and tend to be lower in breccia with a high proportion of inclusions;
2. Mineralization with up to 15 ppm PGE+Au associated with the pyroxenitic layer;
3. High grade mineralization (up to 35 ppm PGE+Au) in gabbro pegmatite dikes.

Dunning (1979) and Cabri and Laflamme (1979) studied the PGE mineralogy. They observed Pt, Pd, Ni, Te, Bi, Sb, Ag and S-bearing minerals including vysotskite, braggite, kotulskite, isomerteite, merenskyite, sperrylite, moncheite, stillwaterite and palladoarsenide.

The most striking feature of the mineralization is its association with pegmatitic rocks. Many of the geological structures and textures are typical of granite pegmatites, namely miarolitic pods, asymmetric zoned patches, coarse-grained minerals, variable grain size and intensive alteration (Jahns and Bumham, 1969.)

Brugmann et al (1990) report results of a study of major, trace and Platinum-group elements at Lac des Iles. Some of their data on the Gabbroic Complex are present in Table 9.15. Comparison of their data on REE abundances in samples from the Roby Zone indicate a systematic increase from vari-textured gabbroic to pegmatoidal to pegmatitic rocks without significant change in the overall pattern of light REE enrichment (Fig. 9.55).

Noble metal contents in samples from the Gabbroic Complex are highly variable, ranging from 50 ppb total PGE in rocks not showing the varitexture to 15 ppm in mineralized samples from the Roby Zone. Brugmann et al. (1990) showed that good correlation factors exist between Pd and Pt, Pd and Ni, Pt and Ni, Pd and Au and Se and Pd, Se and Pt and Se and Ni, and between Cu and all of the preceding elements (Table 9.16) which indicates that sulfide phases are controlling the distribution of the Pt, Pd and Au. Correlation of all of the above elements with Ir and Os is distinctly poorer than it is between them. Furthermore, the Lac des Iles mineralization is remarkable in having extremely high ratios of Pd/Ir (= 4750 in comparison with 23 for the Merensky Reef) and Pd/Pt (= 11 in comparison with 0.51 for the Merensky Reef). Clearly the process responsible for concentrating the PGE has resulted in marked fractionation of the PGE with much more efficient concentration of Pd than of the other metals.

The progressive increase in REE concentrations that is referred to above is mirrored by the PGE content of the same rocks. Based on Brugmann et al.'s (1990) data, vari-textured gabbros from the Robie Zone contain an average of 1.97 ppm (Pt+Pd), those from pegmatoidal gabbro contain 3.98 ppm and those from pegmatite contain an average of 5.78 ppm (Pt+Pd). These figures contrast with an average of 0.062 ppm (Pt+Pd) in gabbros without vari-texture from outside the zone. The changes in PdI/r and Pd/Pt are also progressive and correlate with the increasing abundance of (Pt+Pd) in this succession of rock types. The variations in ratios are as follows: gabbro outside the Robie Zone Pd/Ir =119, Pd/Pt = 0.73; varitextured gabbro within the zone Pd/Ir = 3500, Pd/Pt = 4.4; pegmatoidal gabbro Pd/Ir = 2770, Pd/Pt = 8.98; pegmatite Pd/Ir = 8000, Pd/Pt = 12.9. Thus the process that accounts for the progressive increase in REE abundances in the succession of rock types also causes an increase in the abundance in Pd+Pt and the increases in Pd/Ir and Pd/Pt ratios.

**Table 9.15.** Major and trace element contents of samples from the gabbroic part of the Lac des Iles Complex (after Brugmann et al. 1989)

| Sample | LDI-03 | LDI-06 | LDI-08 | LDI-55 | LDI-57 | LDI-63 | 87-02 | 87-03 | 87-04 | 87-06 | 87-08 |
|---|---|---|---|---|---|---|---|---|---|---|---|
| Rock | Ga-No | Ga-No | Ga | Ma-Dy | Ga | Ga | Ga-No | Ga-No | Peg-Dy | Ga-No | Ga-Dy |
| Location | 3 | 8 | 9 | 5 | 10 | 2 | 5 | 5 | 5 | 5 | 7 |
| $SiO_2$ | 51.06 | 51.02 | 50.52 | 51.27 | 51.58 | 53.66 | 51.73 | 51.68 | 50.71 | 52.12 | 51.54 |
| $TiO_2$ | 0.09 | 0.27 | 0.19 | 0.29 | 0.16 | 0.15 | 0.12 | 0.23 | 0.20 | 0.13 | 0.09 |
| $Al_2O_3$ | 18.62 | 14.46 | 25.07 | 8.38 | 17.13 | 17.31 | 13.92 | 7.71 | 9.47 | 14.01 | 27.09 |
| FeO | 6.73 | 9.17 | 4.94 | 16.14 | 9.35 | 7.30 | 9.23 | 14.20 | 16.03 | 8.86 | 2.51 |
| MnO | 0.12 | 0.16 | 0.07 | 0.29 | 0.14 | 0.15 | 0.17 | 0.25 | 0.26 | 0.16 | 0.05 |
| MgO | 10.82 | 9.37 | 4.37 | 15.93 | 11.42 | 8.39 | 14.43 | 17.53 | 15.93 | 14.73 | 2.15 |
| CaO | 10.50 | 13.65 | 11.56 | 6.57 | 8.57 | 10.38 | 8.65 | 6.83 | 5.45 | 8.39 | 12.22 |
| $Na_2O$ | 1.63 | 1.76 | 2.93 | 0.51 | 1.47 | 2.45 | 1.31 | 1.00 | 1.28 | 1.34 | 3.66 |
| $K_2O$ | 0.41 | 0.11 | 0.32 | 0.17 | 0.16 | 0.19 | 0.12 | 0.09 | 0.08 | 0.22 | 0.67 |
| $P_2O_5$ | 0.01 | 0.02 | 0.03 | 0.02 | 0.02 | 0.02 | 0.02 | 0.02 | 0.02 | 0.02 | 0.02 |
| S | 0.02 | 0.01 | 0.00 | 0.44 | 0.00 | 0.00 | 0.29 | 0.45 | 0.56 | 0.02 | 0.00 |
| LOI | 2.40 | 0.50 | 1.80 | 3.10 | 0.80 | 1.00 | 0.70 | 0.70 | 0.50 | 1.50 | 1.30 |
| MgNo | 0.74 | 0.65 | 0.61 | 0.64 | 0.69 | 0.67 | 0.74 | 0.69 | 0.64 | 0.75 | 0.60 |
| Cr | 205 | 38 | 121 | 292 | | | 398 | 398 | 336 | 421 | 63 |
| Ni | 499 | 81 | 131 | 2082 | | | 2800 | 980 | 900 | 525 | 94 |
| Cu | | | | | | | 1450 | 1000 | 1250 | 237 | 69 |
| Co | 46 | 67 | 33 | 112 | | | 86 | | | | |
| V | 89 | 305 | 106 | | | | | | | | |
| Rb | 13 | 0 | 8 | 4 | 4 | 3 | | | | | |
| Sr | 192 | 170 | 357 | 42 | 207 | 294 | | | | | |
| Zr | 5 | 9 | 14 | 14 | 6 | 11 | | | | | |
| Y | 2 | 4 | 2 | 5 | 3 | 4 | | | | | |
| Sc | 24 | 74 | 16 | 48 | | | 33 | | | | |
| La | 0.7 | 0.81 | 2.1 | 1.32 | | | 1 | | | | |
| Ce | 1.4 | 1.9 | 4 | 2.8 | | | 2 | | | | |
| Sm | 0.14 | 0.47 | 0.31 | 0.54 | | | 0.2 | | | | |
| Eu | 0.21 | 0.24 | 0.24 | 0.24 | | | 0.2 | | | | |
| Yb | 0.22 | 0.58 | 0.19 | 0.68 | | | 0.3 | | | | |
| Lu | 0.05 | 0.08 | 0.03 | 0.13 | | | 0.05 | | | | |
| As | 0.08 | 0.05 | 0.20 | 0 | 0.11 | 0.11 | 17.50 | 1.28 | 1.34 | 3.066 | 0 |
| Se | 1.35 | 0.49 | 0.12 | 5.97 | 0.25 | 0.35 | 9.8 | 5.28 | 6.5 | 1.55 | 0.36 |
| Ir | 0.11 | 0.04 | 0.08 | 0.41 | 0.43 | 0.33 | 0.71 | 0.78 | 0.48 | 0.34 | 0.19 |
| Os | 1.1 | 0 | 0.4 | 0 | 1.6 | 1.5 | 0.9 | 0.5 | 1.2 | 2.1 | 0.7 |
| Ru | 3 | 7 | 12 | 16 | 15 | 9 | 23 | 8 | 80 | 5 | 12 |
| Pt | 109 | 29 | 35 | 372 | 38 | 42 | 510 | 316 | 263 | 105 | 14 |
| Pd | 1010 | 0 | 20 | 7200 | 0 | 85 | 6200 | 0 | 1800 | 0 | 0 |
| Au | 21 | 1.98 | 1.56 | 613 | 6.96 | 0.98 | 724 | 454 | 297 | 75.3 | 4.93 |

**Table 9.15.** (cont.)

| Sample | 87-09 | 87-10 | 87-14 | 87-15 | 85-31 | 85-52a | 86-118 | 86-125 | 86-203 | 86-211 |
|---|---|---|---|---|---|---|---|---|---|---|
| Rock | Ma-Dy | Ma-Dy | Peg-Dy | Ga | Peg-Ga | Peg-Dy | Peg-Ga | Ga-No | Ma-Dy | Ga |
| Location | 8 | 8 | 5 | 5 | 5 | 5 | 5 | 5 | 5 | 5 |
| $SiO_2$ | 50.07 | 49.97 | 51.41 | 50.30 | 52.32 | 50.33 | 52.34 | 52.50 | 49.19 | 50.05 |
| $TiO_2$ | 0.42 | 0.16 | 0.09 | 0.07 | 0.10 | 0.44 | 0.07 | 0.10 | 0.04 | 0.13 |
| $Al_2O_3$ | 10.51 | 15.04 | 12.17 | 15.97 | 11.65 | 16.12 | 12.21 | 15.86 | 23.00 | 19.37 |
| FeO | 10.11 | 9.54 | 9.85 | 7.58 | 9.55 | 10.23 | 11.46 | 8.45 | 6.06 | 6.93 |
| MnO | 0.20 | 0.18 | 0.18 | 0.13 | 0.14 | 0.19 | 0.19 | 0.21 | 0.12 | 0.09 |
| MgO | 16.55 | 11.33 | 17.85 | 15.56 | 12.90 | 8.11 | 15.71 | 11.69 | 8.35 | 7.84 |
| CaO | 10.62 | 11.75 | 6.60 | 7.99 | 11.96 | 10.54 | 7.24 | 7.61 | 8.08 | 12.04 |
| $Na_2O$ | 1.17 | 1.66 | 1.16 | 1.09 | 0.68 | 2.13 | 0.00 | 2.35 | 1.52 | 2.15 |
| $K_2O$ | 0.27 | 0.34 | 0.17 | 0.49 | 0.34 | 0.36 | 0.25 | 0.94 | 2.62 | 0.58 |
| $P_2O_5$ | 0.09 | 0.02 | 0.02 | 0.02 | 0.00 | 0.05 | 0.01 | 0.00 | 0.01 | 0.04 |
| S | 0.00 | 0.00 | 0.51 | 0.81 | 0.35 | 1.50 | 0.51 | 0.28 | 1.01 | 0.77 |
| LOI | 2.300 | 1.400 | 1.20 | 1.90 | 2.30 | 3.10 | 4.60 | 3.20 | 0.40 | 2.40 |
| MgNo | 0.74 | 0.68 | 0.76 | 0.79 | 0.71 | 0.59 | 0.71 | 0.71 | 0.71 | 0.67 |
| Cr | 2530 | 477 | 429 | 550 | | 148 | 350 | 229 | 247 | |
| Ni | 473 | 202 | 1700 | 3100 | 1602 | 2459 | 842 | 540 | 3070 | 1462 |
| Cu | 87 | 178 | 1990 | 3330 | 1484 | 3635 | 2216 | 516 | 3939 | 1933 |
| Co | 59 | | 109 | | 72 | 140 | 67 | 65 | 74 | 50 |
| V | | | | | 167 | 212 | 100 | 103 | 48 | 89 |
| Rb | | | 18 | | | | | | | |
| Sr | | | | | 172 | 217 | 69 | 182 | 177 | 200 |
| Zr | | | | | | | | | | |
| Y | | | | | 5 | 6 | 4 | 4 | 0 | 5 |
| Sc | 37 | | 36 | | 53 | 27 | 30 | 28 | 9 | 24 |
| La | 3.7 | | 0.8 | | 2.1 | 4.4 | 0.89 | 1.1 | 1.4 | |
| Ce | 8.1 | | 0 | | 4.4 | 8.7 | 1.9 | 2 | 2.3 | |
| Sm | 1.7 | | 0.2 | | 0.97 | 0.91 | 0.21 | 0.27 | 0.2 | |
| Eu | 0 | | 0 | | 0.29 | 0.32 | 0.15 | 0.19 | 0.14 | |
| Yb | 0.9 | | 0 | | 0.44 | 0.55 | 0.34 | 0.3 | 0.18 | |
| Lu | 0.1 | | 0 | | 0.07 | 0.09 | 0.05 | 0.05 | 0.04 | |
| As | 1.41 | 0.18 | 2.67 | 0.07 | 0.26 | 0 | 1..04 | 0.34 | 0 | 1..27 |
| Se | 0.35 | 0.49 | 13.2 | 27.9 | 4.9 | 13.3 | 3.9 | 1.4 | 13.2 | 6.48 |
| Ir | 0.34 | 1.06 | 0.6 | 1.79 | 1.82 | 0.93 | 0.27 | 0.15 | 0.62 | 0.67 |
| Os | 1.1 | 1.8 | 2 | 3.4 | 1.3 | 0 | 0 | 0 | 0 | 1.1 |
| Ru | 15 | 29 | 102 | 0 | 13 | 39 | 9 | 7 | 6 | 11 |
| Pt | 21 | 64 | 413 | 903 | 272 | 574 | 23 | 37 | 902 | 1110 |
| Pd | 55 | 170 | 5800 | 9600 | 1130 | 8500 | 26 | 21 | 12000 | 2400 |
| Au | 8.45 | 10.6 | 479 | 852 | 168 | 266 | 47 | 16.3 | 973 | 415 |

*Ga* gabbro; *Ga-No* gabbronorite; *Peg-Ga* pegmatoidal gabbro; *Ma-Dy* mafic dyke; *Peg-Dy* pegmatite dyke; *Ga-Dy* Gabbro dyke. Locations of the samples are shown in Fig. 9.54. Major elements, LOI, and S in wt%; PGE in ppb; other elements in ppm. Major-element data are normalized to 100% anhydrous

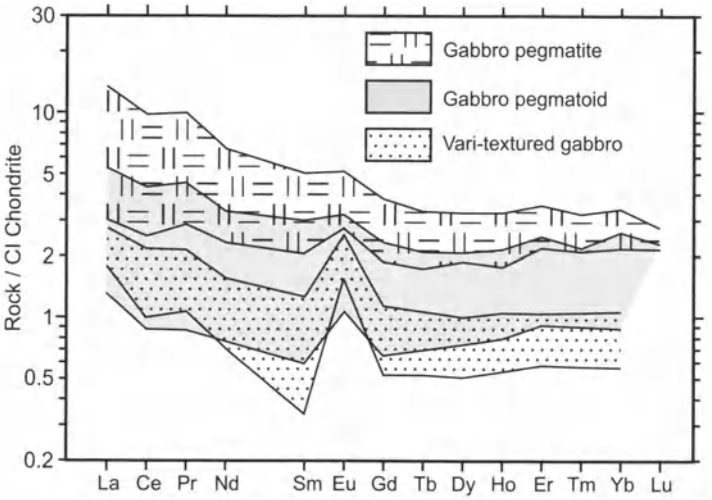


**Fig. 9.55.** Chondrite-normalized REE abundances in vari-textured gabbro, pegmatoidal gabbro and pegmatite from the Robie Zone (after Brugmann et al. 1990)

One aspect of the deposit that has only recently been recognized is a zone (the "no-see-em" zone) in which PGE are present as discrete PGE minerals with only a minimum of Fe-Ni-Cu- sulfides. This zone has only recently been discovered and little research work has been undertaken on it at the time of writing (January 2004).

### *Genesis of the Deposit*

The differences between the geological setting and the distribution of PGE in the gabbroic part of the Lac des Iles complex and other important PGE-rich mafic-ultramafic complexes (e.g. Bushveld and Stillwater) indicates that the genesis of the sulfide mineralization and the concentration of PGE at Lac des Iles is different to that responsible for the other deposits.

Macdonald et al. (1989) suggested that intensive fractional crystallization, which depleted Ir and Os, but enriched Pd, Pt and Au in the residual liquid led to the high Pd+Pt abundances and high Pd/Ir ratios. Concentration of the PGE by a supercritical fluid offers another possible explanation. It has been suggested on thermodynamic grounds that Pt and Au can be mobilized hydrothermally (Lydon 1987). Furthermore, the discordant PGE-rich pipes in the Bushveld Complex are evidence that Pt can be transported hydrothermally. Schiffries (1982), Stumpfl and Ballhaus (1986) and Boudreau et al. (1986) have proposed that hydrothermal fluids have played a major role in concentrating PGE in the sulfides of the

**Table 9.16.** Correlation factors for Cr, PGE and chalcophile elements of the gabbroic part of the Lac des lies Complex (after Brugmann et al. 1990)

| | Cr | Ni | Cu | Co | Ir | Os | Ru | Pt | Pd | Au | As | Se | S |
|---|---|---|---|---|---|---|---|---|---|---|---|---|---|
| Cr | 1.000 | 0.051 | 0.266 | 0.115 | 0.096 | 0.057 | 0.015 | 0.097 | 0.203 | 0.072 | 0.024 | 0.054 | 0.058 |
| Ni | | 1.000 | **0.868** | **0.663** | **0.593** | 0.503 | 0.205 | **0.816** | **0.931** | **0.908** | 0.531 | **0.864** | **0.687** |
| Cu | | | 1.000 | 0.582 | 0.432 | 0.548 | 0.173 | **0.761** | **0.865** | **0.731** | 0.058 | **0.814** | **0.884** |
| Co | | | | 1.000 | **0.399** | **0.791** | 0.384 | 0.303 | **0.686** | 0.455 | 0.434 | **0.740** | 0.608 |
| Ir | | | | | 1.000 | 0.335 | 0.194 | 0.330 | 0.399 | 0.478 | 0.048 | **0.653** | 0.444 |
| Os | | | | | | 1.000 | 0.352 | 0.344 | **0.683** | 0.375 | 0.143 | **0.669** | 0.297 |
| Ru | | | | | | | 1.000 | 0.156 | 0.209 | 0.230 | 0.118 | 0.522 | 0.270 |
| Pt | | | | | | | | 1.000 | **0.760** | **0.835** | 0.244 | **0.780** | **0.690** |
| Pd | | | | | | | | | 1.000 | **0.910** | 0.419 | **0.833** | 0.667 |
| Au | | | | | | | | | | 1.000 | 0.316 | **0.820** | 0.307 |
| As | | | | | | | | | | | 1.000 | 0.207 | 0.101 |
| Se | | | | | | | | | | | | 1.000 | **0.653** |
| S | | | | | | | | | | | | | 1.000 |

Numbers in bold refer to correlations which are significant at the 99% level

Merensky and J-M Reefs. The presence of pegmatitic textures and the extensive deuteric type alteration is evidence of a volatile-rich environment in the Roby Zone, which led to the suggestion that PGE were remobilized and concentrated by fluids (Watkinson and Dunning 1979; Talkington and Watkinson 1984; Sweeney and Edgar, 1987). However, in the southern part of the Roby Zone (C-Zone) the primary mineralogy is well preserved; nevertheless this zone exhibits all the characteristic features of the mineralization, in particular pegmatites with high grade mineralization. This would argue against a direct genetic relationship between PGE concentration and alteration processes.

Many aspects of the ore zone in the Roby Zone suggest localized remeltng of the original complex. These include:

1. The ubiquitous presence of breccia zones, in which melagabbro, gabbro, anorthositic gabbro and anorthositic segregations occur in a matrix which varies from mela- to anorthositic gabbro. All field aspects of this breccia indicate that it is an igneous breccia that involved at least partial melting of many of the lithologies characteristic of the gabbro.
2. Pyroxenitic layers or dykes which, outside the ore zone and in certain areas within it are cross cutting, but in other areas are cut by late stage pegmatites, and, on the scale of an outcrop, can be seen ranging from discrete layers or dykes to irregular blob-like masses to fragments in a gabbroic matrix.
3. A large number of pegmatites cut other rock types. Locally pegmatoids can be traced along strike undergoing a transition to pegmatites.
4. Cuspate contacts and interfingering phases of leucocratic to melanocratic gabbro, which suggest the presence of coeval liquid phases of differing composition.

McBimey (1987) suggested that if water comes into contact with overlying hot cumulates the transfer of water to the cumulates will cause them to melt partially. This zone of volatile-induced melting can progress upwards through the cumulate leaving behind a residue of more refractory unmelted material, plus material crystallizing from the secondary melt, as the more volatile-rich part of it proceeds upward. As McBimey pointed out, this process is analogous to zone refining in industry. The effect will also be the same as industrial zone refining, i.e. the removal of impurities from the material processed into the molten zone: in the case in point the partitioning of incompatible elements from the cumulates into the advancing zone of melting. These will be held in this zone and will become highly concentrated as more and more cumulate is processed.

Brugmann et al. (1990) noted that, so long as the partial melt is undersaturated in sulfur, sulfides in the cumulates will be dissolved in the melt. Au, Pd and Pt (PPGE) will thus be incompatible in the cumulates and will build up in the melt. Iridium, Os and Ru (IPGE) behave more compatibly than the PPGE in a sulfide-free environment and thus their concentrations will not build up nearly so rapidly in the melt. Thus in addition to concentrating Pt, Pd and Au in the melt phase, zone refining will also fractionate them from Ir, Os and Ru. Platinum is also somewhat less incompatible than Pd, so that Pd becomes more concentrated than Pt in the partial melt, causing the high Pd/Pt ratios. As more and more cumulate is processed, sulfur will build up in the melt and eventually reach sulfide saturation. Once this occurs, liquid or partially liquid sulfides will be left behind in the residue. Because of the high partitioning of PGE into sulfide liquid, these sulfides will retain most of the PGE, thus giving rise to a zone that is enriched in PGE. Brugmann et al. (1990) proposed that the Roby Zone at Lac des Iles originated in this way.

Zone refining in nature is unlikely to be the uniform, controlled process that it is in industry. On a local scale different areas are likely to be remelted to different degrees and the extraction of the partial melt is not likely to be uniform. It is suggested that the vari-textured gabbro, which forms the matrix of the ore zone, represents the residue of variable melting due to the zone refining process. Pegmatoids, pegmatites, plagioclase-rich gabbro segregations and dikes represent the product of zone refining. Zone refining will pass through a zone within a layered intrusion, cause a diminution in PGE concentration. It is only where sulfides remain behind that the PGE will be concentrated. It should be pointed out that any rocks within the zone of melting which contain pre-existing sulfide, such as for example the pyroxenitic dykes, will not lose their sulfides once the zone refining melt has become sulfide saturated; these sulfides will act as a sink for Pt, Pd, and Au and thus become very enriched in themselves.

The extensive reaction zones that have developed between the sinucatoidal felsic intrusions and the Lac des Iles complex, and the dating which suggests that within error the sinucatoids are coeval with the Lac des Iles complex, indicates that the felsic bodies could not only have acted as a source of aqueous fluid but could have done so when the Lac des Iles complex was still hot. Under these circumstances the water would have entered the mafic complex, fluxed the mafic cumulates, and given rise to a zone of partial melting that moved upward through the complex in the manner described above. This process is illustrated in Fig. 9.56. The zone of melting passed through the mafic cumulates, rising through them, scavenging PGE and concentrating and transporting them in the volatile-rich partial melt. As the melt zone rose to encounter the pyroxenite layer (sill?),

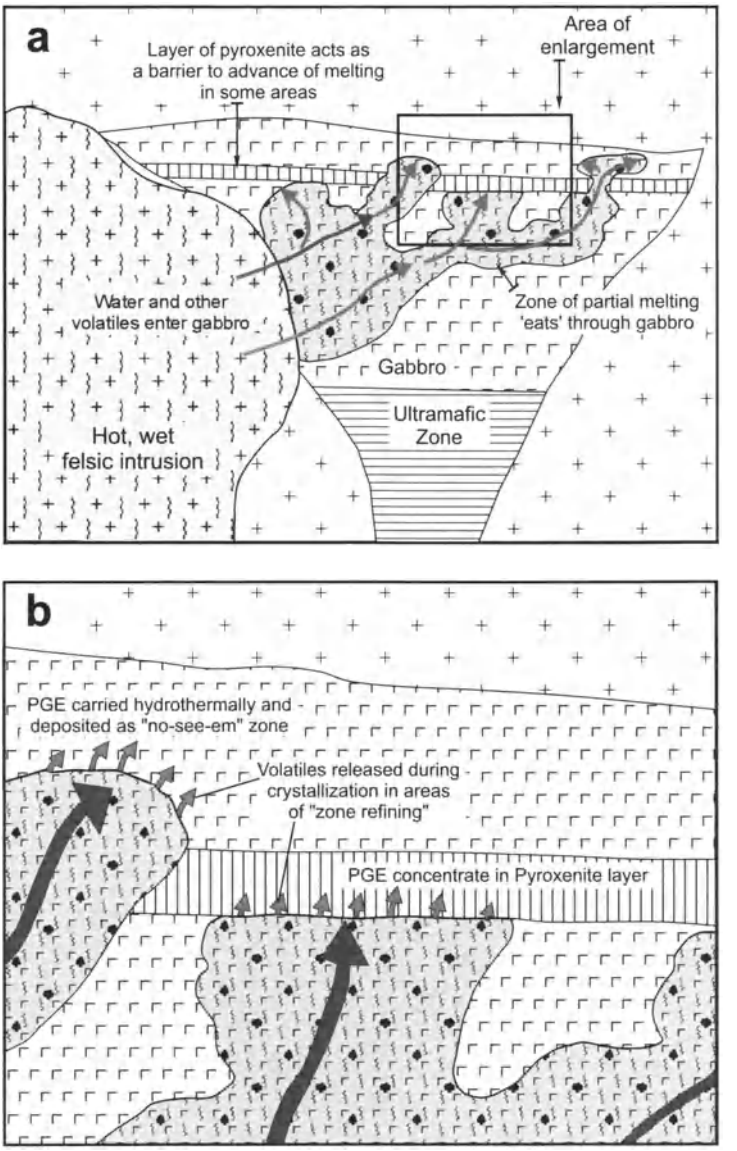


**Fig. 9.56.** (a) Schematic diagram illustrating a zone of partial melting moving through the Lac des Iles Gabbro Complex, concentrating PGE as a consequence of the process of "zone refining" that is discussed in the text, and becoming halted in part by the pyroxenite layer; (b) Enlargement of a portion of Figure a showing the zone of partial melting both failing to break through the pyroxenite layer with the deposition of PGE within this layer from volatiles, and, in other places, breaking through but becoming exhausted and releasing PGE-bearing volatiles which form the "no-see-em" ore zone

partial melting was largely halted, because of the higher temperature required to flux the more mafic cumulates. Except for a few places where it was able to break through, the partial melt became dammed beneath the layer, and started to crystallize (Fig. 9.56b). Immiscible sulfides separated from the crystallizing melt, and the PGE, which by this stage had become strongly concentrated in the melt, entered the sulfides. It is likely that fluids released as the melt crystallized penetrated upward into the pyroxenite, carrying PGE with them to give rise to PGE concentrations in the pyroxenite layer. In other areas, where the partial melt broke through the pyroxenite, it also cooled and crystallized, and PGE-bearing fluids continued farther, depositing the PGE as discrete PGM to form zones such as the "no-see-em" zone.

### 9.5.2 The Longwoods Igneous Complex, New Zealand

The Longwoods Igneous Complex (LIC) is a 32x12km fragment of a layered intrusion that is located at the southern tip of the South Island, New Zealand. The presence of platinum-group minerals (largely braggite and cooperite) in gold placer deposits exploited from 1897–1907 stimulated exploration in the Complex during the 1997–2001 PGE "boom". This brief description of the complex is included here because it is an example of mineralization derived from an intrusion emplaced in an island arc setting and marked by the characteristics of a calc-alkaline body. The complex is part of a largely Permian, discontinuous belt of volcanic, sedimentary and intrusive rocks that extend the length of the South Island (the "Brook Street terrane"). A fragment of the Gondwana craton lies to the west of this terrane and the Brook Street terrane is one of a series of terranes that have been accreted against the craton.

The LIC comprises the Pahia Layered Series (PLS) together with trondjhemite, marginal diorites and small granite intrusions (Cowden et al. 1990). The felsic intrusions are particularly abundant at the base of the PLS. The PLS is poorly exposed, but sparse outcrop and float show it to consist of phase and modally layered olivine gabbros, gabbro-norites and hornblende gabbros, together with minor peridotite, troctolite and anorthosite. A plot of olivine versus plagioclase composition (Fig. 9.57) proves the rocks of the PLS to have unusually An-rich plagioclase for a given Fo content of olivine, which supports its calc-alkaline affiliation. The LIC has been explored by a number of companies and PGE soil anomalies have been reported, but, to date, there have been no reports of horizons particularly enriched in PGE.

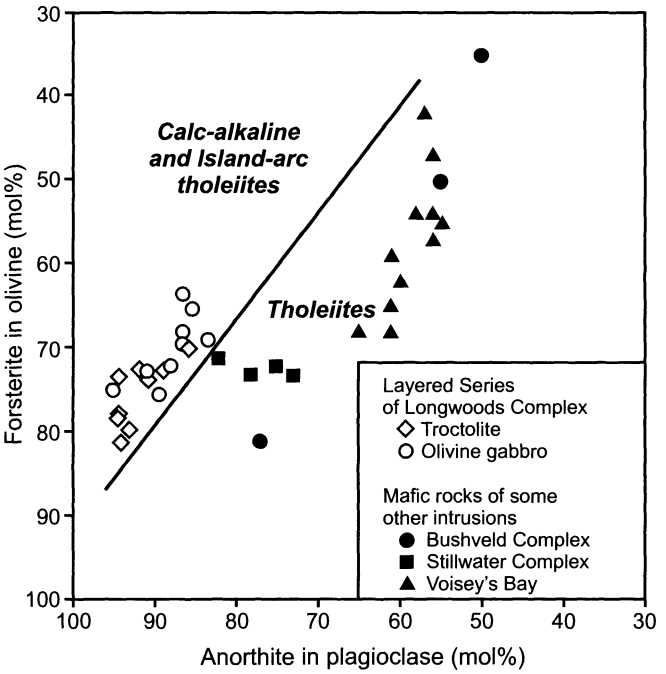


**Fig. 9.57.** A comparison of the forsterite content of olivine versus anorthite content of plagioclase for the Longwoods, Bushveld and Stillwater Igneous Complexes and the Voisey's Bay intrusion. The plot supports the calc-alkaline affinity of the Longwoods Complex

## 9.6 Deposits of the Urals Platinum Belt

The PGE deposits of the Urals Platinum Belt (UPB) were formed as a result of orogenic processes acting at the leading edge of an oceanic plate. The UPB is defined by a chain of complex intrusive massifs of dunite-gabbro-plagiogranite composition spread along the western margin of the Tagil mega-Synclinorium (Ivanov 1997). Both intrusions and their country rocks formed in an island arc environment (Ivanov 1997). The belt is orientated north-south, following the direction of the Urals folding; and can be traced for 920 km, from 64°40' to 55° 40' N (Fig. 9.58). The plutons are composed of several intrusive phases, principally dunite, gabbro, granitoids (plagiogranite, diorite, quartz diorite), syenite and diabase dikes (Ivanov 1997; Fershtater et al. 1999; Zoloev et al. 2001). Many age determinations exist, but the results are not in agreement because a range of methods have been used for their determination. It is generally agreed

(Kim Zoloev personal communication to Valeri Fedorenko, October 2001)[25] that the most probable ages of the intrusions are: dunite – late Ordovician; gabbros – late Ordovician to early Silurian; granitoids – late Silurian; syenites – late Silurian to early Devonian. The country rocks comprise Middle Ordovician to Lower Devonian sedimentary and volcanic rocks (see references in Ivanov 1997; Zoloev et al. 2001).

Zoloev et al. (2000) distinguished about 20 types of PGE mineralization in the Urals Platinum Belt. In this author's opinion, three of them are most interesting to the general reader, namely the Nizhny Tagil, Volkovsky, and Baron types and are discussed here.

### 9.6.1 Nizhny Tagil type Mineralization

#### *Nature and Origin of Intrusions*

The Nizhny Tagil type mineralization is the principal source of the Urals platinum placers that have operated since 1824. In addition, the source rocks to the Nizhny Tagil placers were the first such sources in the world to be discovered (found in 1892-1898).

The in situ mineralization is hosted by dunite-clinopyroxenite intrusions that are the first phase of the complex plutons comprising the UPB and that belong to a class of ultramafic body referred to as the Ural-Alaskan or Alaskan-type bodies. They are a unique class, and their origin is still contested. Johan (2002) presented the most recent synthesis of work on them and concluded that the following points (made by Taylor 1967) remain valid:

1. They exhibit a zonal structure with a dunite core surrounded successively by olivine-clinopyroxenite, biotite and hornblende clinopyroxenite, hornblendite and a monzonite-gabbro rim. Each ultramafic rock type has a uniform composition. Contacts between them are usually gradational, although conflicting age relationships exist in some bodies; giant blocks of olivine clinopyroxenite occur in dunite and wherlite in the Union Bay and Duke Island bodies. The relationship between the ultramafic rocks and gabbroic rocks is debated, with Russian workers (e.g. Ivanov et al. 1975) favoring a metasomatic origin for the gabbros of the Uralian bodies and western workers (e.g. Taylor 1967; Irvine 1963, 1974; Findlay 1969) favoring an igneous origin.

[25] All personal information, referenced in this Section was received by my colleague Valeri Fedorenko during his visit to the Urals in 2000-2001

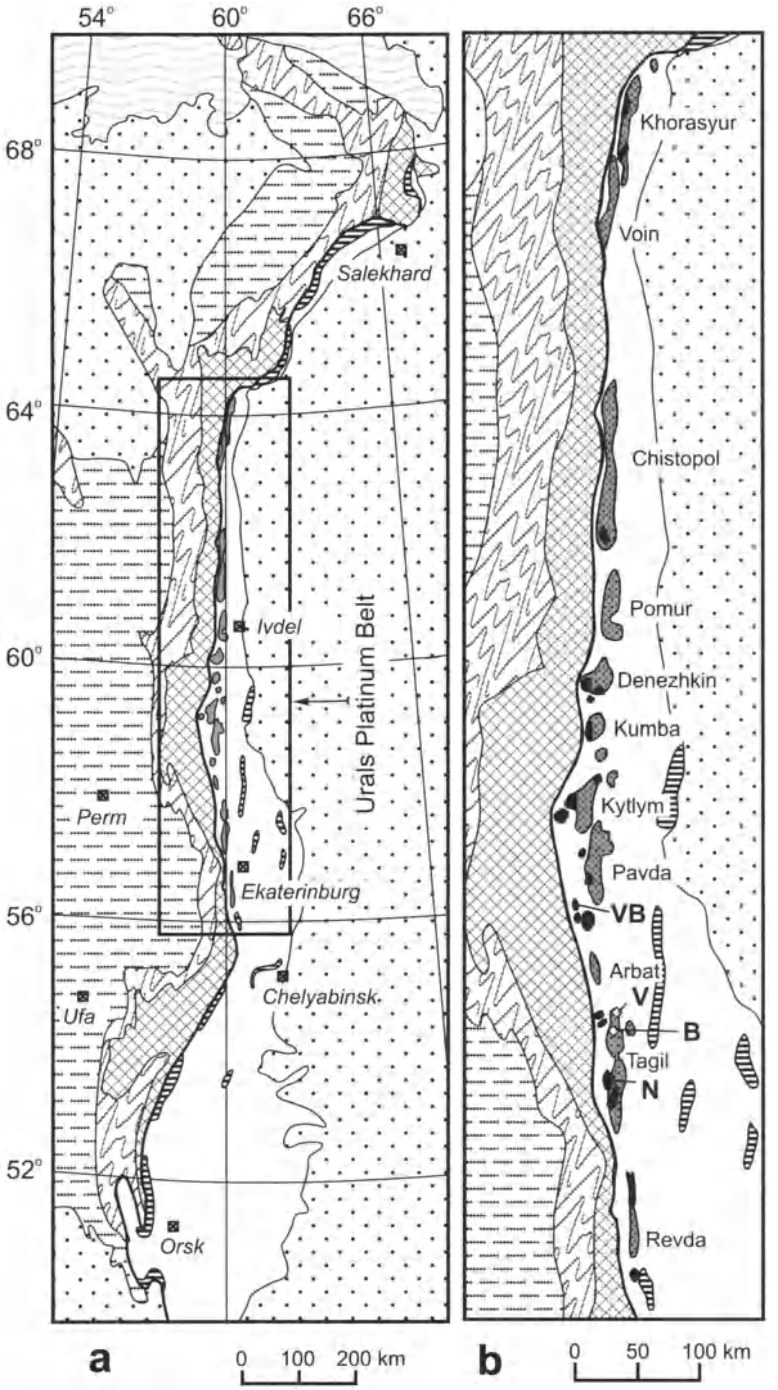
54°
60°
66°
68°
64°
60°
56°
52°
Salekhard
Ivdel
Urals Platinum Belt
Perm
Ekaterinburg
Chelyabinsk
Ufa
Orsk
a
0 100 200 km
Khorasyur
Voin
Chistopol
Pomur
Denezhkin
Kumba
Kytlym
Pavda
VB
Arbat
V
B
Tagil
N
Revda
b
0 50 100 km

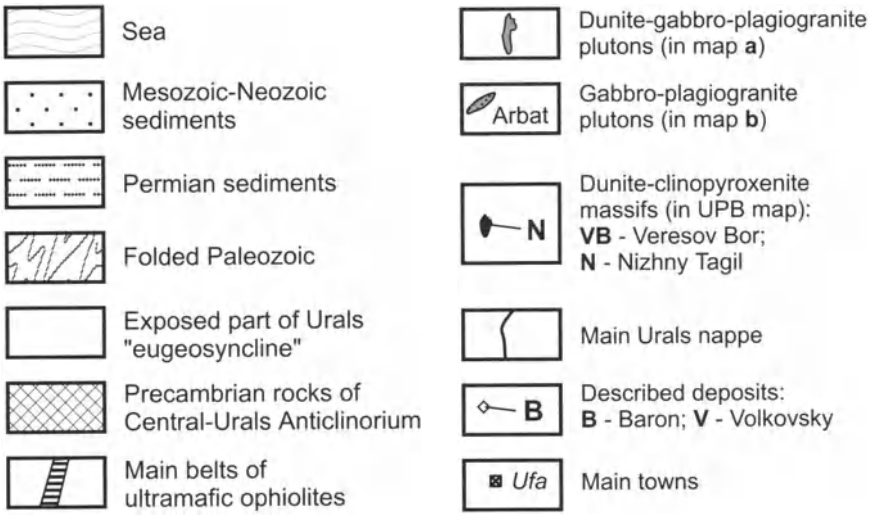


**Fig. 9.58. a.** Location of the Urals Platinum Belt (UPB) within the Urals fold belt; **b.** Distribution of main Intrusive Complexes of the UPB. After Ivanov (1997)

2. The ultramafic rocks are characterized by an absence of orthopyroxene and plagioclase, except in the hornblendite zone, in which a very calcium-rich plagioclase ($An_{90-98}$) occurs.
3. Olivines in the dunite cores are very magnesian ($Fo_{93}$) with the MgO/FeO ratio decreasing outward so that the olivine-clinopyroxenites contain olivine with $Fo_{75}$. Clinopyroxene varies from $Di_{99-70}$.
4. Chromite occurs exclusively in the dunite cores and magnetite and ilmenite are the only iron-bearing oxides in the clinopyroxenite and hornblendite.

There has been much debate as to the genetic relationships between the different component rock types of the bodies (Johan, 2002). It is generally accepted by western workers that the ultramafic rocks are related by fractional crystallization from a mafic magma of alkalic affinity (the activity of $SiO_2$ during crystallization remained very low, thus accounting for the absence of orthopyroxene in any of the rocks). Some workers believe that the gabbros are unrelated to the ultramafic rocks, but their common occurrence together is contrary to this interpretation. The tectonic setting of most of the known examples is that of an island arc (the intrusions of the Alden shield are exceptions). Johan favored Murray's (1972) suggestion that the bodies are feeder pipes to andesitic volcanism, that fractionation occurred within the pipes and at depth, and that olivine became concentrated at the

centres of pipes by flow differentiation. This model cannot be the sole answer, since it is difficult to conceive how the very well-preserved cross-bedding within olivine-rich rocks that was documented by Irvine (1974) could have occurred within material flowing up a pipe.

### *Mineralization*

There are 35 Ural-Alaskan type massifs in the Urals Platinum Belt, varying from 0.2x0.6 km to 6x14 km in size; typically they are lens-like in plan with a north-south elongation (Ivanov, 1997). The largest of these and the only one where mining of hard-rock Pt has been documented is the Nizhny Tagil massif. In this section, this author follows Zoloev at al.'s (2001) suggestion that this mineralization be referred to as "Nizhniy Tagil type".

The central parts of the Ural-Alaskan intrusions, as developed in the UPB, consist of dunite cores with peripheral shells of clinopyroxenite. Ivanov (1997) subdivided the dunite of the cores into protodunite and recrystallized dunite with quasi-dunite intermediate between the two. Protodunite is a fine-grained rock with uniformly distributed accessory chromite (0.6–1.0 mod%). Recrystallized dunite is subdivided on the basis of grain size into fine-, medium-, coarse-grained, and dunite-pegmatite (the last containing olivine crystals up to 5 cm across). Chromite is unevenly distributed, and forms segregations of variable morphology and size that control the Pt mineralization (see description of the Nizhny Tagil massif below). Ivanov (1997) concluded that the chromite segregations and Pt mineralization occurred at a late-magmatic stage accompanying recrystallization of the dunites. He suggested that Cr and Pt are concentrated towards the top of the dunite cores, in zones about 500 m thick. His suggestion concerning the late-post-magmatic origin of the Cr-Pt mineralization gains some support from the olivine compositions. The forsterite content of the olivine is typically 93–94 mol% in unrecrystallized dunite, but decreases to 88–90 mol% in mineralized areas (Volchenko 1999). The clinopyroxenite shells encasing the dunite cores represent, in Ivanov's opinion, contact-metasomatic rocks[26] formed at the contact of intrusive dunites with terrigenous-volcanic host rocks.

---

[26] There is a marked dichotomy between the viewpoint of Russian workers (e.g. Ivanov et al. 1975) who regard the gabbros rimming the ultramafic cores of the Ural intrusions as metasomatic, and western workers on the Alaskan intrusions (e.g. Taylor 1967; Irvine 1963, 1974; Findlay, 1969) who point to sharp contacts between the mafic and ultramafic rocks and, in some intrusions, blocks of gabbro within ultramafic rocks

As discussed above, the Nizhniy Tagil massif is the largest of the Ural-Alaskan type intrusions, extending 6x14 km (50.1 $km^2$) in plan; the shape is that of a harp-like body, plunging steeply to the east. The dunite core measures 5.5x10.5 km and is surrounded by an uneven shell of rock ranging from clinopyroxenite to wehrlite, 60-2000 m in width with a total area in plan of 18.3 $km^2$.

The core of the Nizhny Tagil massif consists primarily of protodunite (Fig. 9.59). Recrystallized dunite is restricted to a zone at the centre. Ring-like, arc-like and irregular zones containing chromite segregations occur in the outer parts of the recrystallized dunite. The chromite segregations themselves occur as veinlets, schlieren and networks of schlieren typically ranging from several millimeters to tens of centimeters in thickness, and several centimeters to several meters in length. Some chromite-rich bodies are larger. The ore body of the Gospodskaya mine is unique. It is a vertical column 5–7 m in diameter that was mined down to a depth of 180 m and continued below this level. Chromite segregations were elongated along the length of the column. The chromite content of the segregations is very variable, ranging from 15 to 100% (Ivanov, 1997). However the total volume of the segregations themselves amounts to less than than 0.01 % of the volume of dunite (Oleg Ivanov, personal communication, December 2000).

The most systematic information about the distribution of Pt in rock types of the Nizhniy Tagil massif is that of Ivanov (1996), who collected 361 samples (0.4–0.5 kg each) from different rocks of the massif. They were analyzed using a chemical-spectroscopic method (after pre-concentration) in the Tula laboratory of TsNIGRI. Two or three analyses were made of each sample and averaged. Averages for rock types are given in Table 9.16. Ivanov (1996) noted that the Pt concentration in silicate rocks does not normally exceed 200 mg/t. Pt concentrations in chromite segregations vary from 40 to 20,000 mg/t; more than half of them falling in the interval 500-10000 mg/t. However, 20,000 mg/t is not the highest concentration that has been reported from Nizhniy Tagil. Concentrations of up to 570 g/t are known in some areas, with individual samples from the Gospodskaya mine assaying up to 4.5 kg/t (Ivanov 1997).

Platinum occurs in the Nizhniy Tagil massif as tetraferroplatinum with subordinate isoferroplatinum The grain size of the tetraferroplatinum varies from 5x5 – 50x100 to 1000x2000 microns (two thirds of them are less than 100 microns). Grains of tetraferroplatinum themselves contain small (10x10–20 microns) grains of iridosmine and native Os. Microprobe analyses indicate a typical composition for the tetraferroplatinum (in wt%) of Pt = 76.4; Pd = 0.23; Ir = 2.8; Os = 0.25; Ru = 0.16; Rh = 0.46; Fe = 13.7; Cu = 2.1; Ni = 2.3 (Volchenko 1999).

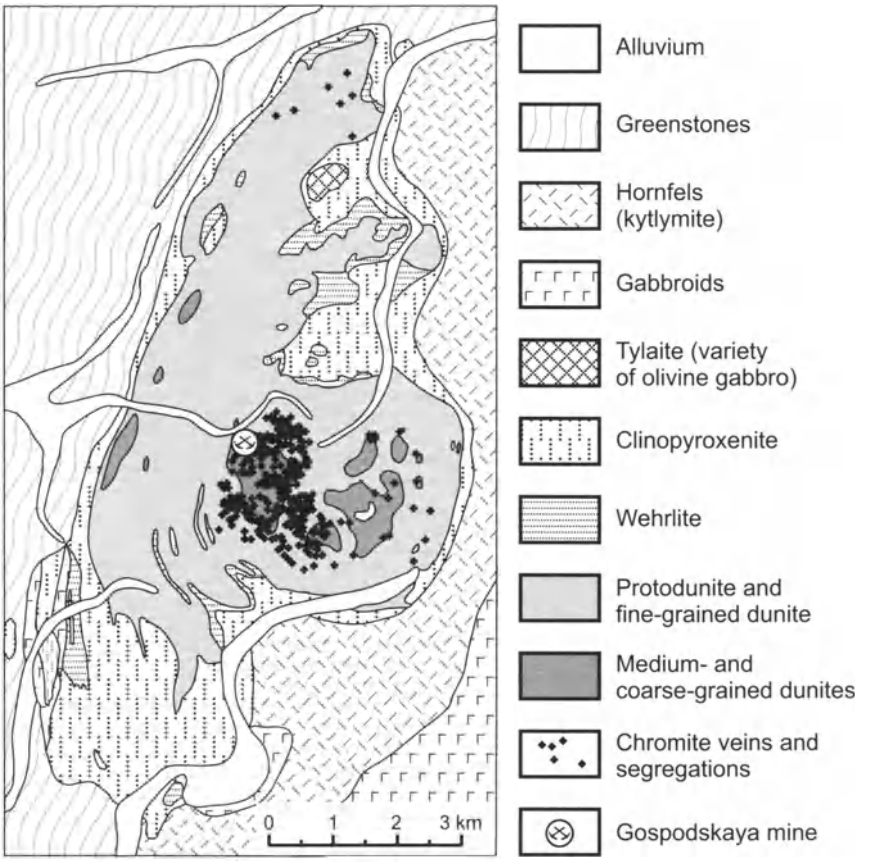


**Fig. 9.59.** Geological map of the Nizhny Tagil dunite-clinopyroxenite massif (after Ivanov 1997)

The economic significance of the Nizhny Tagil type mineralization lies mainly in the fact that it is source of the largest of the world's platinum placers. Hard rock Pt mining has only been documented in the Nizhny Tagil massif. Mining was conducted by the same prospectors who worked the placer deposits. From 1892 to end of 1940's more than 1600 chromite schlieren were discovered and mined by these prospectors. Total production from both the placers and hard-rock deposits of the Nizhniy Tagil area is estimated to be 160 t of Pt from the start of mining and dredging operations (Volchenko 1999).

So far the Nizhniy Tagil body appears to contain more Pt-bearing chromite schlieren than all of the other Ural-Alaskan type bodies of the UPB combined. This may be because Nizhniy Tagil is better exposed than the other bodies. More Pt has been recovered from the Is placer area than from

**Table 9.17.** Average contents of Pt and Pd (ppb) in silicate rocks and chromite segregations of the Nizhny Tagil dunite-clinopyroxenite massif (after Ivanov 1996)

| Rock | | No | Content (ppb) | | % of barren samples |
|---|---|---|---|---|---|
| | | | Pt | Pd | |
| Clino-pyroxenites | Magnetite | 4 | 23.5 | 0 | 0 |
| | Monomineralic | 5 | 11.0 | 0 | 0 |
| | Olivine | 1 | 7.5 | 0 | 0 |
| | Wehrlitic | 3 | 30.0 | 0 | 0 |
| Dunites | Protodunites | 28 | 41.9 | | 7.1 |
| | Fine-grained | 22 | 56.5 | 0 | 40.9 |
| | Medium-grained | 56 | 13.8 | | 73.2 |
| | Coarse-grained | 51 | 11.6 | | 80.4 |
| | Dunite-pegmatites | 9 | 73.2 | 0 | 55.5 |
| Chromite segregations | Microschlieren | 2 | 180 | 0 | 0 |
| | Small schlieren | 4 | 107 | 0 | 0 |
| | Schlieren | 168 | 3000 | 0 | 0 |
| | Massive | 5 | 2282 | 6 | 0 |
| | Veins in quasi-dunites | 3 | 7483 | 30 | 0 |

*No* Number of samples

that fed by Nizhniy Tagil. The Is placer lies 150 north of Nizniy Tagil in the drainage area of the Svetly Bor, Veresov Bor, and Kamenushka massifs (Leonid Desyatnichenko, personal communication, December 2000). The two largest platinum nuggets found so far in the world, with weights of 9620 g and 8395 g (the latter is on display at the Diamond exhibit at the Moscow Kremlin) came from the vicinity of the Veresov Bor massif (Igor Malakhov, Pavel Burmako, and Igor Savokhin, personal communication, June 2001).

The origin of the Nizhny Tagil-type mineralization is not clear. The PGE are clearly not in their initial positions. They appear to have been mobilized and re-precipiatated, as has the chromite. Questions that are unanswered include whether they were mobilized along with the chromitite or were mobilized later and introduced into chromite-rich zones; whether their co-precipitation with chromite was the result of chemical interaction with the surfaces of chromite grains, or whether it was the difference in physical properties of chromite-rich rock and chromite-poor rock that

caused the former to fracture and give rise to channels along which the PGE-bearing fluids could flow more easily.

### 9.6.2 Volkovsky and Baron type Deposits

Gabbro massifs belonging to the second type of Platinum Belt intrusion host the Pd-bearing Cu-Fe-V-Ti-P mineralization of Volkovsky type, and the Pd-Au-Pt mineralization of Baron type (only one significant deposit each of these two types is known to date in the UPB, Volkovsky and Baron respectively). Both occur in the northern part of Tagil pluton (Figs. 9.58 and 9.60), which is also referred to as the "Volkovsky gabbro massif" by some authors, e.g. Samonov and Pozhariskiy (1974).

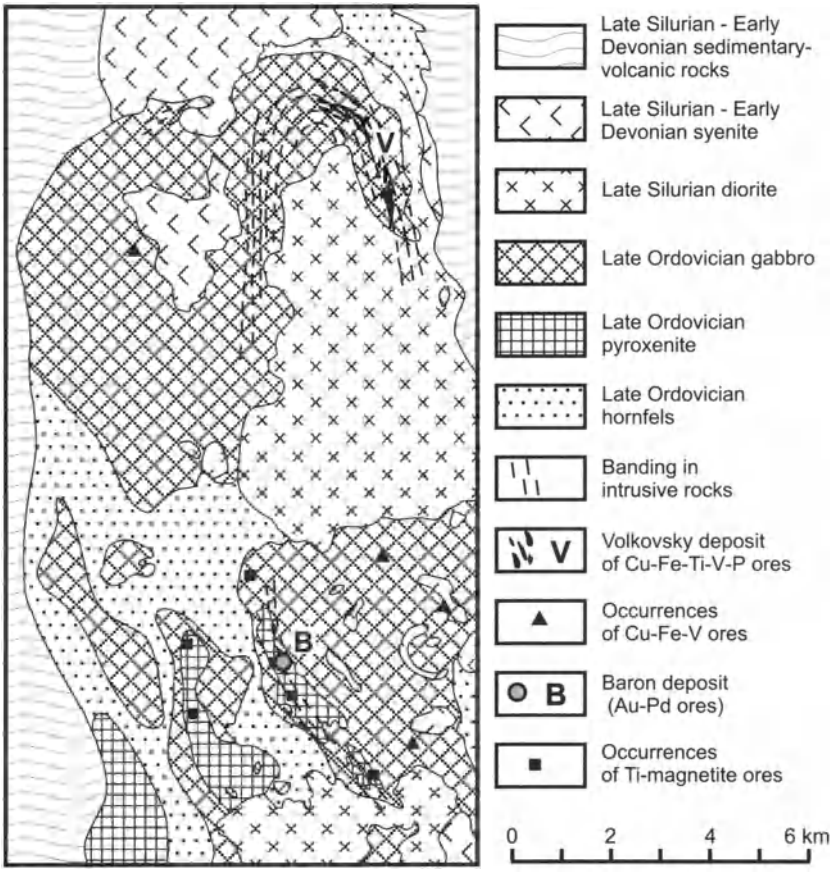


**Fig. 9.60.** Geological map of area of the Volkovsky and Baron deposits (after unpublished materials of the Urals Geological-Mapping Expedition)

### *Volkovsky Deposit*

This deposit is located in the northeastern part of the Volkovsky gabbro massif (Fig. 9.60). It was discovered in 1912 and since then has been explored and mined periodically in a series of small pits and underground workings. Restricted open-pit mining has continued to as recently as 2001. Comprehensive exploration of the deposit was undertaken in 1955-1960 by Timakhov and co-workers, whose results have been published by Samonov and Pozhariskiy (1974).

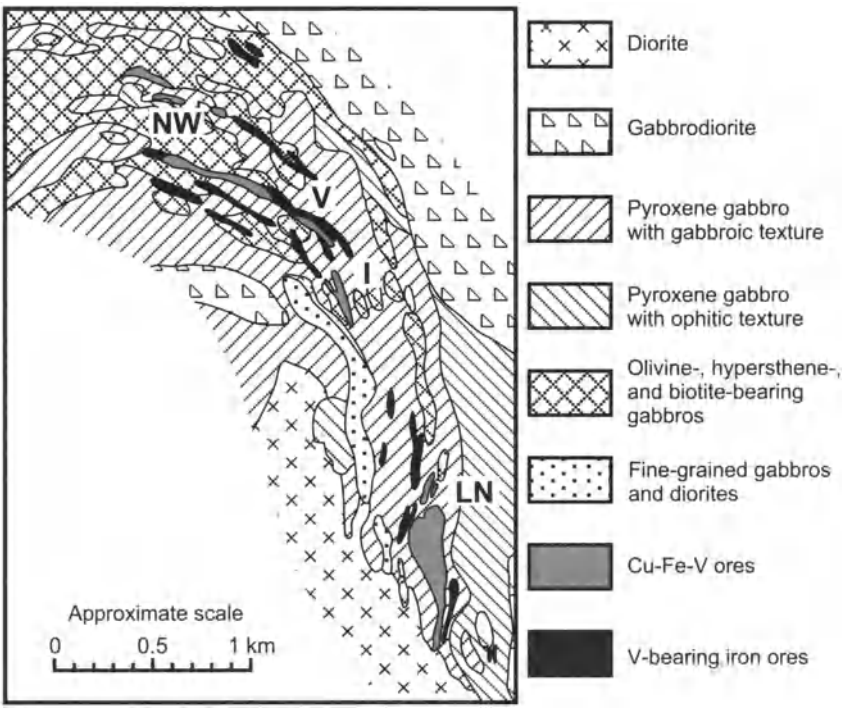


**Fig. 9.61.** Geological map of the Volkovsky deposit (after Timakhov et al. 1960), presented in the paper by Samonov and Pozhariskiy (1974). Sections of deposit: NW = North-Western, V = Volkovsky, I = Intermediate, LN = Lavrovo-Nikolaevsky

Copper provides the principal economic product and, thus far, $2x10^6$ tonnes of copper metal have been recovered. Fe, V, Ti, and P have been recovered as by-products, along with Au, Ag, Pd, Se and Te from some parts of the deposit. The ore minerals comprise bornite, chalcopyrite, vanadiferous titanomagnetite, and apatite. The mineralized zone, consisting of about 200 individual ore lenses is concordant with layering in the host intrusive rocks and has been traced over a distance of 3 km (Fig. 9.61)

with a thickness of several hundreds of meters (Fig. 9.62). Economic mineralization is impersistant and the deposit has been subdivided into 4 sections for the purpose of mining: North-Western, Volkovsky, Intermediate, and Lavrovo-Nikolaevsky (Fig. 9.62).

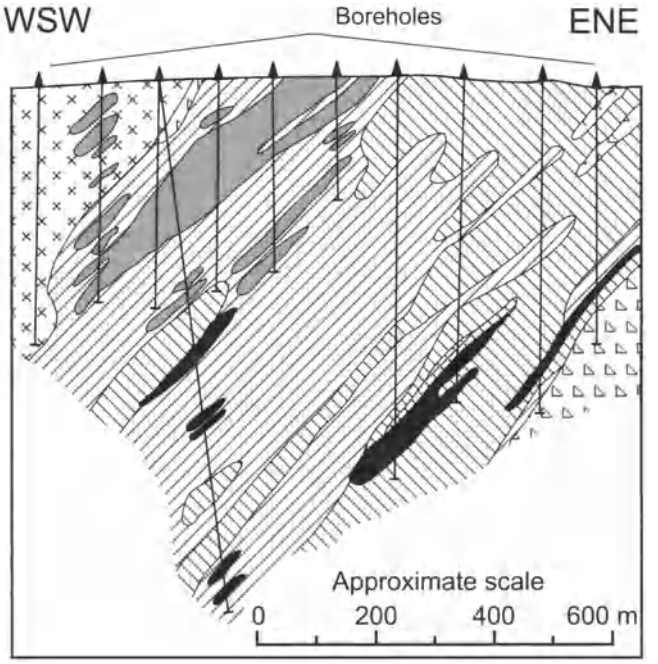


**Fig. 9.62.** Geological section of the Lavrovo-Nikolaevsky section of the Volkovsky deposit (after Timakhov et al. 1960), presented in the paper by Samonov and Pozhariskiy (1974). Legend is as for Figure 9.61

The ore zone and individual ore lenses dip 60° S in the North-Western section and 38° W in the Lavrovo-Nikolaevsky section (Samonov and Pozhariskiy 1974). The structure of the deposit is that of an over-turned anticline in cross-section, with the ore occurring on the hanging wall near the hinge of the anticline (Fig. 9.63). The majority of the ore lenses consist of both Cu-sulfide and Ti-magnetite-apatite mineralization. Less commonly, Cu-sulfide ores occur without associated magnetite and apatite. Despite their occurrence together, the Cu-sulfide mineralization is particularly enriched in the upper parts of the cross-section relative to the Ti-magnetite mineralization. The latter tends to occur in host rocks containing plagioclase of bytownite composition, in contrast to the former in which the plagioclase is usually a labradorite (Fig.9.63).

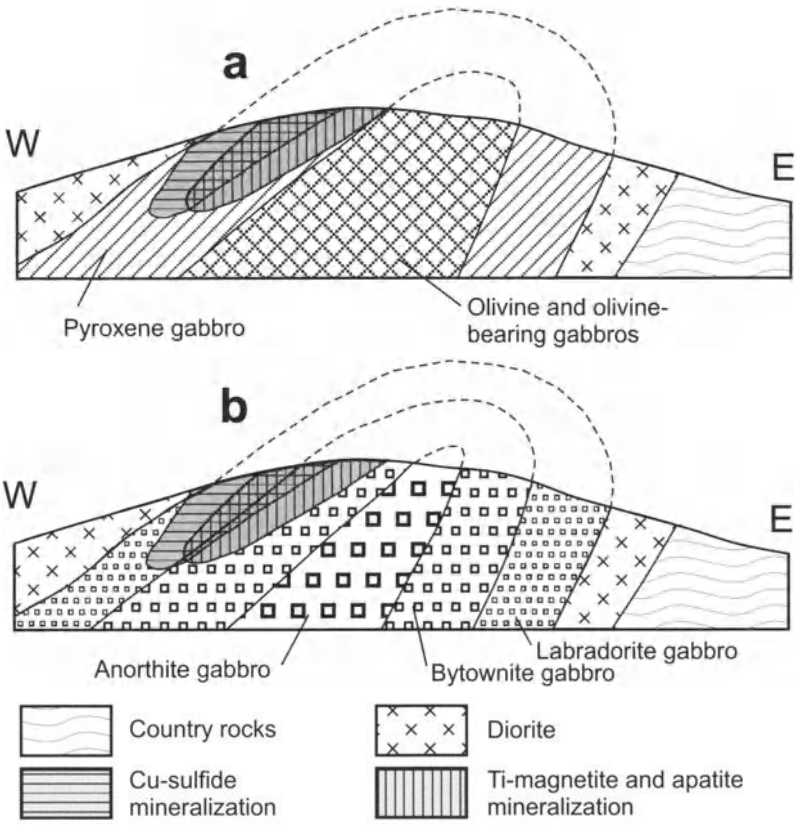


**Fig. 9.63.** Cross-section through the Volkovsky deposit (after Timakhov et al. 1960), presented in the paper by Samonov and Pozhariskiy (1974). Gabbroic rocks are subdivided on basis of their mafic index (a) and An content of plagioclase (b)

Cu-sulfide mineralization of the Volkovsky deposit is unevenly distributed and occurs as disseminations, bleb-like segregations, and more rarely as schlieren and veins of massive sulfides. The ore bodies are defined on the basis of a cut-off grade of 0.4 wt%. The average Cu content of the deposit is reported as 1.5 wt%.

A special investigation of the noble-metal mineralization in the ores was undertaken by the Urals Geological-Mapping Expedition (UGME) in 1987–1989 (Zoloev and Mardirosyan, unpublished manuscript 2000). The ore bodies as a whole grade 0.11–0.18 g/t Pd+Pt with a Pd/Pt ratio of about 50. The PGE follow the Cu sulfides and are more concentrated in the upper parts of the ore zones which grade from 0.3–1.0 to 5–10 g/t, depending on which particular ore section is being considered. Noble metals are concentrated mainly in bornite (Pd contents up to 22.65 g/t, Pt up to 0.34 g/t) and chalcopyrite (Pd up to 11.42 g/t, Pt up to 0.24g/t). Native Au (Pd-

bearing), merenskyite, kotulskite, keithconite, hessite, and a Pd-bearing telluride of Cu-Co are present in the deposit.

### *Baron type mineralization deposit*

In 1986 Alfred Mardirosyan investigated PGE mineralization in the Volkovsky gabbro massif to the south of the Volkovsky deposit. Some of his samples taken from the dump adjacent to an old pit related to the Baron Ti-magnetite deposit (see Fig. 9.60) showed high noble metal contents with Pd up to 33.15 g/t, Au up to 23.52 g/t, and Pt up to 0.5 g/t (analyses by Yuri Volchenko, Urals branch of Russian Academy of Science). The mineralized zone was stripped and trenched by UGME in 1995–1998 and then drilled by "Eurasia PGM Ltd" in 1999. Mineralization with a thickness of 1 to 10 meters was traced to a depth 50–70 m and for 60 m along strike. The ore zone has a steep to vertical dip. The average grade of the mineralization is Pd = 5 g/t, Au = 2 g/t, Pt = 0.5 g/t (Shalaginov 1999).

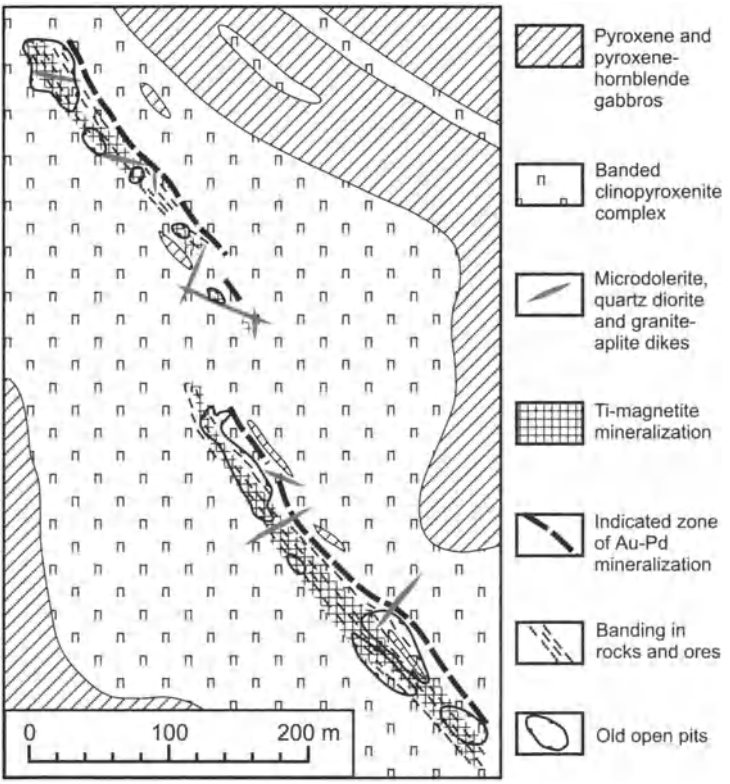


**Fig. 9.64.** Schematic geological map of the Baron deposit (after Zoloev at al. 2001)

The mineralization is located in a body of layered clinopyroxenite (3000x600 m) that occurs within the gabbro massif (Fig. 9.64). The clinopyroxenite hosting the mineralization varies from monomineralic to plagioclase- and olivine-bearing, with a grain size ranging from coarse to fine. Ti-magnetite mineralisation occurs adjacent to the Au-Pd mineralization (Fig. 9.64) and was mined in the late 19th or early 20th century. In the zone of Au-Pd mineralization the clinopyroxenite contains Ti-magnetite and apatite ranging from accessory amounts to more than 25 modal percent of each. The layered clinopyroxenite body complex contains bodies of breccia-like and pegmatoidal pyroxenite and pyroxene-plagioclase pegmatoid as well as sheet-like bodies of an unusual apatite olivinite (Figs. 9.65 and 9.66). The apatite olivinite contains ~60% Ol, 5 to 30 % apatite and 1 to 15 % titanomagnetite. $P_2O_5$ contents are ~8 wt% with 29-32 wt% $SiO_2$ and 24-26 wt% MgO (Table 9.18).

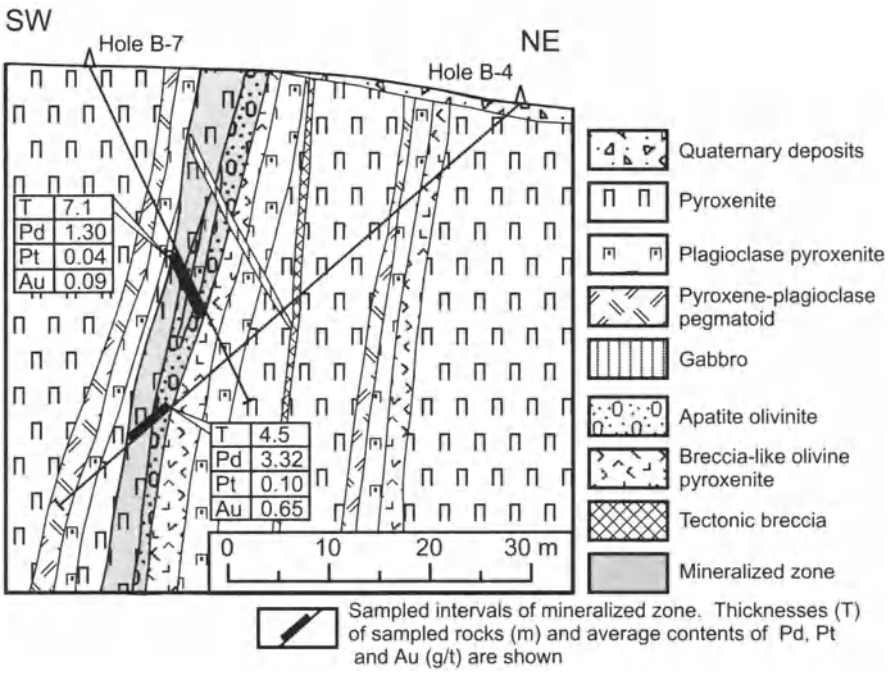


**Fig. 9.65.** Geological section through the Baron deposit (after Zoloev at al. 2001)

The Au-Pd mineralization is associated with the apatite olivinites and adjacent clinopyroxenite (Fig.9.65), although that in the olivinites is much the richer (see Table 9.18 and Fig. 9.66). The Au-Pd mineralization occurs along with sparse disseminated sulfide, comprising chalcopyrite, bornite,

chalcocite, carrolite and pyrite. Sulfide contents in the mineralized zone are typically 0.1-1 %, ranging up to 2-3 %; their grain size varies between 50 microns and 2 mm. The principal noble metal minerals are kotulskite, merenskyite, keithconite and native Au (sometimes containing Bi and Pd). These minerals are mainly associated with chalcopyrite (44 %) and bornite (33%) (Zoloev et al 2001).

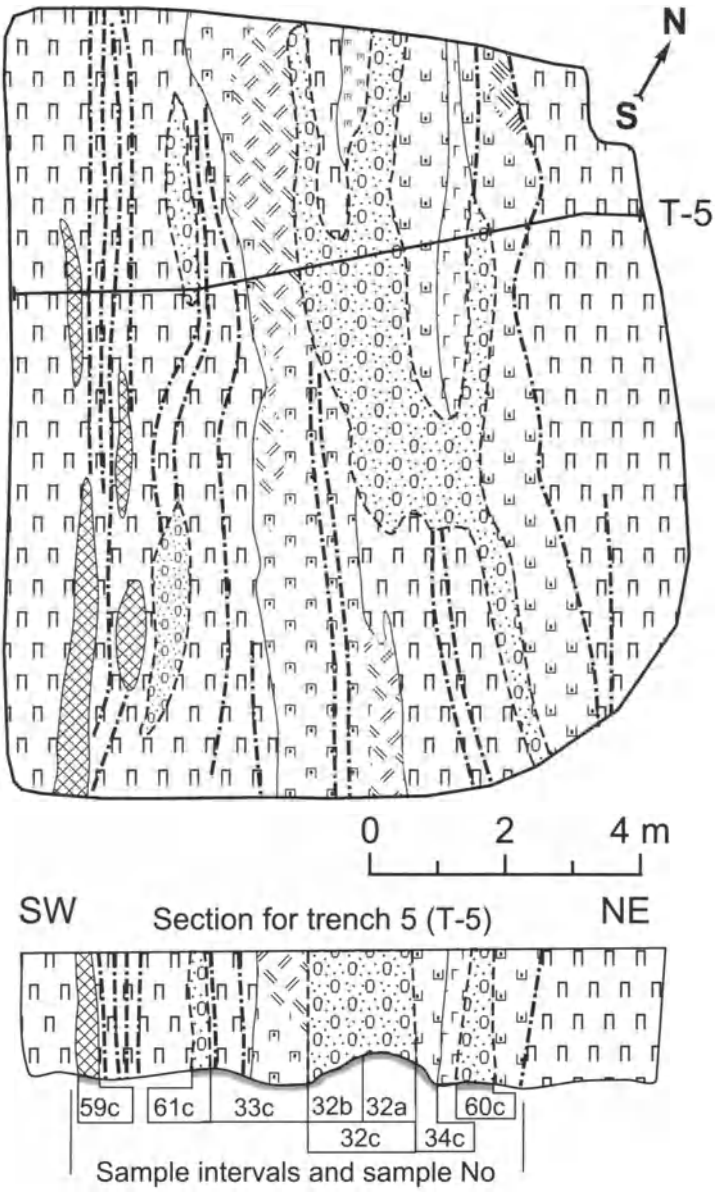

| S No | Metal content (g/t) | | | |
|---|---|---|---|---|
| | Pd | Pt | Au | Ag |
| 59c | 0.2 | <0.01 | 0.02 | |
| 61c | 7.2 | 0.11 | 0.8 | |
| 33c | 0.5 (2.0) | 0.09 | 0.02 | 0.10 |
| 32b | 15.5 | 0.17 | 1.8 | 3.6 |
| 32a | 29.9 (29.0) | 1.30 (0.13) | 9.2 (11.8) | 8.5 (8.0) |
| 32c | 18.4 (18.1) | 0.33 (0.16) | 2.2 (3.5) | 5.9 (4.2) |
| 34c | 0.2 | 0.04 | 0.04 | 0.23 |
| 60c | 6.1 (6.1) | 0.08 (0.14) | 0.6 (0.8) | 0.3 (0.3) |

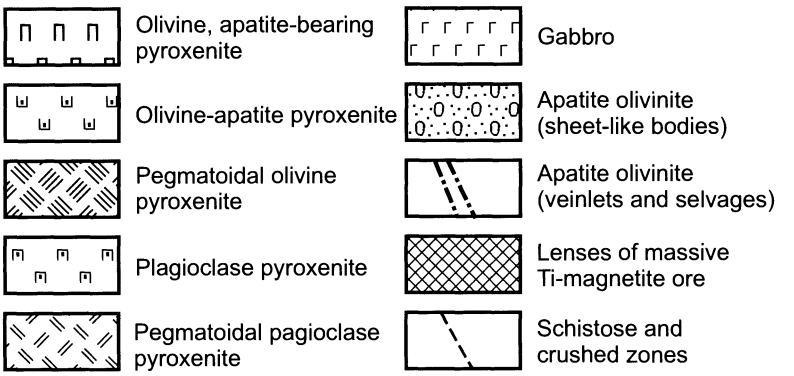


**Fig. 9.66.** Plan and geological section of the central part of the Baron deposit (after Zoloev at al., 2001)

The recent exploration has disclosed that there is a systematic change in noble metal concentration from the near-surface to the deeper part of the mineralized zone. Rich samples near surface contain Pd – 18.6 g/t, Au – 2.84 g/t, Pt – 0.4 g/t (average of 10 samples). At depths of 8-50 m the metal concentrations are: Pd – 5.23 g/t, Au – 0.6 g/t, Pt – 0.2 g/t (average of 13 core samples). As of December 2000, the inferred resources of the deposit were estimated to be 50 t PGE to a depth of 100 m (Zoloev and Mardirosyan, personal communication to Fedorenko, December 2000).

### *Genesis of Volkovsky type and Baron type mineralization*

The occurrence of both Volkovsky and Baron style mineralization with the second (gabbroic) phases of complex plutons, in association with titanomagnetite and apatite mineralisation, and with Cu sulfides leaves little doubt that they are related to each other with respect to their genesis. The Volkovsky mineralization occurs as sheet-like bodies that conform to the

**Table 9.18.** Chemical compositions of apatite olivinites of the Baron deposit (after Volchenko et al. 1998)

| | | | | |
|---|---|---|---|---|
| $SiO_2$ | 29.50 | 29.23 | 31.60 | 30.11 |
| $TiO_2$ | 0.09 | 0.04 | 0.05 | 0.06 |
| $Al_2O_3$ | 2.10 | 1.00 | 1.80 | 1.63 |
| $Fe_2O_3$ | 9.33 | 9.65 | 9.23 | 9.40 |
| FeO | 1.96 | 1.88 | 2.14 | 1.99 |
| MnO | 0.15 | 0.11 | 0.10 | 0.12 |
| MgO | 24.28 | 26.36 | 25.80 | 25.48 |
| CaO | 12.12 | 10.61 | 10.89 | 11.21 |
| $Na_2O$ | 0.07 | 0.11 | 0.18 | 0.12 |
| $K_2O$ | 0.04 | 0.02 | 0.05 | 0.04 |
| $P_2O_5$ | 8.20 | 7.89 | 7.82 | 7.97 |
| $Cr_2O_3$ | <0.01 | <0.01 | | |
| $V_2O_5$ | 0.02 | 0.02 | | 0.02 |
| LOI | 8.70 | 9.60 | 7.80 | 8.70 |
| Total | 98.38 | 98.18 | 98.00 | 98.19 |
| $H_2O+$ | 7.61 | 5.36 | 7.73 | 6.90 |
| S | 0.11 | 0.14 | | 0.13 |
| Cu | 1.68 | 1.50 | 0.51 | 1.23 |
| Ni | 0.009 | 0.007 | 0.009 | 0.008 |
| Co | 0.012 | 0.011 | | 0.012 |
| Zn | 0.008 | 0.009 | | 0.009 |
| Pt | 0.39 | 0.57 | 0.40 | 0.45 |
| Pd | 16.00 | 21.70 | 14.90 | 17.53 |
| Rh | 0.004 | 0.005 | <0.04 | 0.004 |
| Ir | <0.01 | <0.01 | | |
| Os | 0.016 | 0.014 | | 0.015 |
| Ru | 0.033 | 0.027 | | 0.030 |
| Au | 0.74 | 1.2 | 3.8 | 1.91 |
| Ag | 7.3 | 8.1 | 10 | 8.5 |

Major elements, LOI, S, and base metals in wt%; noble metals in g/t (ppm)

layering of their host intrusion. Thus far, the Baron mineralization appears to constitute a steeply dipping pipe within the plane of the layering of the host pyroxenites, although this may change as more is learned about the deposit as a result of further drilling. The Volkovsky deposit may have an origin similar to that of layers and dykes of nelsonite (apatite-ilmenite-magnetite) and of rocks transitional between nelsonite and silicate-apatite-ilmenite/magnetite layers within layered intrusions.

Recent reviews (see McLelland et al. 1994) on the origin of oxide-rich bodies transitional with nelsonites have considered three major origins, (1) extreme fractional crystallisation, (2) liquid immiscibility and (3) filter pressing. McLelland et al. (1994) proposed that the oxide-apatite gabbro norites of the Marcy Anorthosite are the result of the filter pressing of intercumulus liquid from partially crystalline anorthosite, although they indicate that the minimum $SiO_2$ content likely to originate in this way is 30 wt%. Naldrett (1999) expressed the view that nelsonites are connected to Fe- and P-enrichment resulting from fractional crystallization, although the bodies themselves are not necessarily extreme fractionates, concluding that the spatial association world-wide between nelsonites and the upper, fractionated parts of layered intrusions is just too close to be coincidental. A recently-reported important occurrence ($107x10^6$ tonnes grading 6.2 wt% $P_2O_5$, 8.4 wt% $TiO_2$) is that in the Sept Iles layered intrusion on the Gulf of St Lawrence in Quebec, Canada, (McCann et al. 1998). Here lenses of "nelsonite" (also containing olivine, pyroxene and minor plagioclase) are underlain by magnetitites and overlain by oxide- and apatite-rich gabbros which form the bulk of the deposit. Naldrett (1999) suggested that a solvus between a Fe-, Ti-, and P-rich silicate magma and a silicate bearing, Ti-, P-rich iron oxide liquid of the kind demonstrated experimentally by Philpotts (1967) exists in many natural systems. He proposed that once a silicate magma fractionates to the extent that it enters the range of composition and temperature/pressure/volatile partial pressure occupied by the solvus, a nelsonitic liquid will segregate. The silicate content of the nelsonitic liquid will depend on the temperature at which the magma composition intersects the solvus, which in turn will be related to volatile partial pressure – the higher the volatile partial pressure, the less the silicate content of the nelsonitic liquid. He emphasized that this was merely a suggestion and that proof of its viability would have to await future experimental work.

Given the uncertainty concerning the origin of accumulations of apatite + ilmenite/titaniferous magnetite, the reason for the association of Cu sulfides ± PGE with these accumulations is even more tenuous. It would seem that under certain conditions, an association of this kind does develop. The Baron deposit is evidence that PGE-bearing Cu sulfides, along with some apatite + titaniferous magnetite, can be distributed even more widely than the principal Volkovsky-type accumulations of apatite + titanomagnetite. However, the mechanism for this distribution remains obscure in the light of our inadequate knowledge about both the field relationships of the deposits and relevant physical-chemical data.

## 9.7 Summary

Most of the PDE deposit types discussed above are related to layered intrusions, although the types of intrusion vary from deposit type to deposit type. It is unlikely that all types would be found in any single intrusion. However, in order to provide a simplistic summary, most of the deposit types are included in Fig. 9.67 which shows a section through a hypothetical layered intrusion. This should figure be taken for what it is – a generalized picture of most deposit types that has been made in order to provide a simplistic summary of what has been discussed above.

Considering first, classic Bushveld-type layered intrusions, during crystallization of the deeper parts of the intrusion, where fresh inputs of magma occurred before sulfide saturation had been achieved, chromitites occur that are not enriched in Pt and Pd, but have concentrations of Os, Ir and Ru. The onset of sulfide saturation can give rise to deposits of sparsely disseminated sulfide such as the Lower Sulfide Zone of the Great Dyke. If one is close to the margin of an intrusion as would often be the case with a dyke-like body, particularly if it is trumpet-shaped in cross-section, a gabbroic differentiate may develop as a result of more rapid cooling at the margins, move down the walls of the intrusion and mix with less fractionated magma near the center of the body, causing sulfide segregation. Once plagioclase has appeared throughout the intrusion, introduction of fresh magma, particularly if it is from a different magma stem (i.e. high-$Al_2O_3$, tholeiite instead of high-MgO, Cr) may cause high R Factor sulfides to form and concentrate (with or without chromite) to form deposits such as the UG-2 or Merensky, J-M, SJ or SK Reefs.

If the surge of fresh magma develops immiscible sulfides as it mixes with old magma, and is also is more voluminous than can be contained within the footprint of the old chamber, the hybrid magma may continue laterally along the same structure beyond the limits of the old chamber to develop a new marginal zone. If some of the PGE-enriched sulfides are carried with this laterally-spreading hybrid magma, they can end up as concentrations within the marginal zone, giving rise to marginal deposits. The new marginal zone may form the base of a series of cyclic units derived from the new magma, as appears to have been the case with the igneous bodies of the Portimo area in Finland.

As the intrusion crystallizes, provided that it is unsaturated in sulfide, PGE levels may build up in the magma and, once sulfide immiscibility occurs, the resulting sulfides may be moderately rich in PGE (as has occurred in the vicinity of the magnetite layers in the Upper Zone of the Bushveld

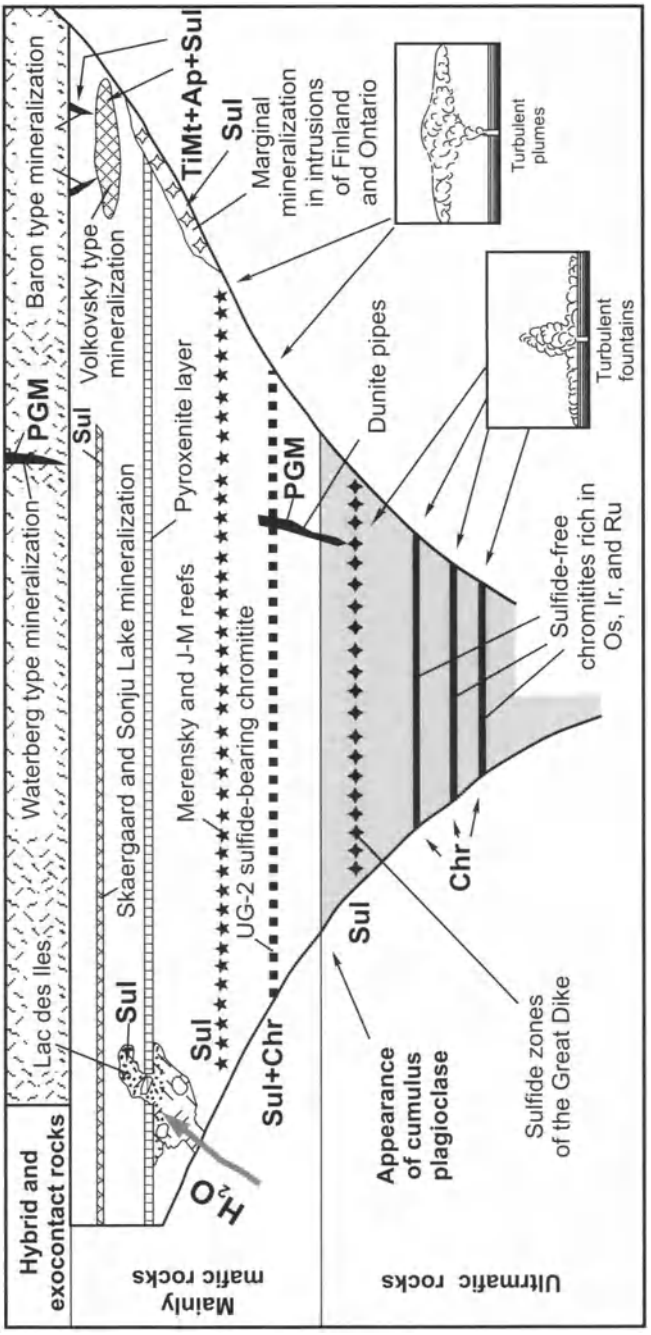


**Fig. 9.67.** Model cross-section through a hypothetical layered intrusion, showing different types of PGE deposits (adapted from Naldrett et al. (1990)

complex, or is the case for the Sonju Lake or Skaergaard intrusions). Alternatively, a layer enriched in titano-magnetite + apatite + Cu sulfides may develop, and PGE, particularly Pd, may be concentrated by the sulfides, as is the case in the Volkovsky deposit in the Central Urals, or in the Coldwell complex of NW Ontario. The Baron deposit is evidence that discordant zones significantly enriched in Cu sulfide and PGE can develop in the same environment as the Volkovsky-style magnetite-apatite layers.

Once the intrusion has crystallized, but while it is still hot, introduction of aqueous fluid can cause a zone of partial melting to pass through the gabbro cumulates, zone-refining them and giving rise to PGE concentrations associated with igneous breccia, as at Lac des Iles.

# 10 Summary and use of genetic concepts in exploration

The magmatic model for the formation of magmatic sulfide deposits carries with it concepts that have many implications for exploration - some simple, qualitative, and in common use and others not so simple, more quantitative, and not yet in common use. Examples of the application of these concepts form the subject of much of this chapter. PGE deposits have different characteristics, and bring with them different criteria for recognizing likely ore-bearing environments. In order to avoid confusion, Ni-Cu deposits are discussed first, followed by a discussion of PGE deposits.

## 10.1 Concepts used in Exploration for Ni-Cu Ores

### 10.1.1 Genetic Concepts and their use

Key aspects in the genesis of a magmatic sulfide ore deposit are:

1. That a magma develops that contains sufficient concentrations of Ni, Cu and PGE so that, if immiscible sulfides develop within it, these sulfides will become enriched in these metals.
2. That this magma becomes saturated in sulfide and segregates immiscible sulfide.
3. That these sulfides react with a sufficient amount of magma to concentrate chalcophile elements to an economic level.
4. That the sulfides are themselves concentrated in a restricted locality where their abundance is sufficient to constitute ore.

It is the objective of this chapter to draw both on information presented above and on new information with a view to determining what geological environments, magma types and intrusive bodies are most likely to these aspects.

The world's important deposits of Ni-Cu sulfides (as opposed to sulfide deposits of interest primarily because of their PGE content) occur almost

exclusively at the base of their associated igneous bodies, which implies that the magmas involved were saturated in sulfide, and carrying excess sulfide at the time of their final emplacement. It has been shown in Chap. 2 that as magmas ascend to environments of lower pressure, their ability to dissolve sulfide increases, so that even though they may leave their source regions saturated or nearly saturated in sulfide, they will become progressively less saturated during their ascent. The high PGE content (1–10 ppb Pt, Pd) of most basaltic magma other than MORB implies that these magmas are not sulfide saturated as they leave the mantle, and is further evidence that they have not become saturated during much of their ascent. Something has to happen to specific batches of magma prior to emplacement to cause sulfide saturation, if a significant magmatic deposit is to form.

The principal factors controlling the solubility of iron sulfide in a silicate melt are discussed in Chap. 2, where it is concluded that these are: (1) temperature, (2) pressure, (3) $FeO+TiO_2$ content of the melt, (4) oxidation state of the melt, (5) mafic versus felsic components in the melt.

With regard to (1), most melts are intruded or extruded close to their liquidus temperatures, so that on cooling, while their ability to dissolve FeS is reduced, they start to crystallize silicates. Any segregating sulfides will therefore be intermixed with cumulus silicates. Ni-Cu-dominant (as opposed to PGE-dominant) magmatic sulfide deposits need to be much richer in sulfide than will be produced by the co-precipitation of solid silicate and sulfide liquid in cotectic proportions. What is required is for some external factor to bring about the segregation of considerable sulfide in a magma without causing significant silicate crystallization.

As discussed in above, experimental studies indicate that the ability of a magma to dissolve sulfide increases with decreasing pressure. The data of Mavrogenes and O'Neil (1999) indicate that the effect of decreasing temperature during magma ascent is unlikely to overcome the effect of decreasing pressure.

The FeO or $TiO_2$ content of a magma (factor 3) will generally increase during the early to intermediate stages of fractionation, increasing its ability to dissolve sulfide, but this an intensive property of the magma and is not something that can be imposed externally to affect its closeness to sulfide saturation.

Oxidation (factor 4) is capably of causing sulfide precipitation without necessarily causing silicates to form; to this author's knowledge, the only situation where this might have played a role is that of the Platreef of the Bushveld Complex, where the Bushveld magma has ingested a large amount of limestone from adjacent country rocks (Buchanan and Rouse

1984). However, this is a deposit of rather weakly disseminated sulfide, important primarily for its PGE content.

With regard to factor 5, Irvine (1975) pointed out that the addition of silica to a mafic magma depresses its capacity to dissolve sulfide. Li and Naldrett (1993) used functions relating the composition of a silicate melt to the activity of FeO within the melt to calculate the depression in the solubility of sulfur in mafic magma that results when it becomes contaminated with felsic material. Their results supported Irvine's suggestion. Thus, felsification of a mafic/ultramafic magma can result in the segregation of immiscible sulfide.

In this book, the following points have emerged as important in the genesis of many of the world's major Ni-Cu sulfide deposits:

1. The formation of a magmatic sulfide deposit requires the concentration of large amounts of sulfide in one location without the concurrent crystallization of abundant silicates. As emphasized above, this does not occur as part of the normal, closed-system, evolution of basaltic or komatiitic magma, during which the sulfides tend to be distributed in cotectic proportions as sparse (generally less than 1%) blebs within cumulus silicates. Where evidence is available as to the cause of sulfide immiscibility, interaction with crustal rocks is the primary cause. Interaction has resulted in: (i) the addition of (a) sulfur from an external source; for example sulfide at Kambalda (Chap. 3), Duluth (Chap. 4), Voisey's Bay (Chap. 6), Pechenga (Chap. 5), and (b) possibly anhydrite at Noril'sk (Chap. 4); And (ii) the contamination of basalt or komatiite by a crustal melt; for example Kambalda (Chap. 3), Noril'sk (Chap. 4) and Sudbury (Chap. 8).
2. The resulting sulfides must then be concentrated in restricted localities so that the deposit is of economic grade. The geological environments in which this has occurred include: at Kambalda (Chap 3), thermal erosion channels that have developed beneath the main flow axes of lava rivers; at Noril'sk (Chap. 4), conduits feeding extrusive magmatism; at Jinchuan (Chap. 7) in the funnel-shaped, ultramafic feeders to a large mafic intrusion of which the gabbroic part has been removed by erosion; and at Voisey's Bay within a feeder linking a lower reaction chamber with an overlying intrusion, and along the line of entry of this feeder to the intrusion (Chap. 6). Sudbury is the exception in that sulfide concentrations are at the base of the magma chamber and no dynamic control appears to have been exerted from flowing magma. Naldrett (2003) suggested that the very complete settling that occurred at Sudbury is because of the extended period of superheat that existed within the Igneous Complex. The sulfides along the northwestern margin of the Duluth

Complex (Chap. 4) are an example of what normally occurs if the mixture of magma plus sulfide is not subjected to the hydrodynamic forces operating during magma flow; the result is a cloud of weakly disseminated sulfide (<5%) that is too low in grade to be economic.

3. The sulfides must also have had the opportunity to react with sufficient magma in order to be able to scavenge adequate quantities of Ni, Cu and PGE (i.e. they must have achieved a sufficiently large N or R factor). In Chap. 4 it is argued that at Noril'sk flow of later magma through the magma conduits, subsequent to the initial emplacement of the sulfides, has enriched these in chalcophile metals. The extent and efficiency with which this process has operated varies from deposit to deposit, with the greatest enrichment having occurred at Noril'sk-1 and the least enrichment within the Kharaelakh intrusion. The Kambalda camp provides another example: there are marked differences in the Ni tenor of sulfides in two adjacent lava channels in the Juan deposit at Kambalda (Chap. 3), which is well explained as the result of different volumes of lava having flowed along the two channels. Similarly, the ores at Voisey's Bay have been upgraded through interaction with magma passing along the feeder channel linking the lower (reaction) and upper chambers.

The application of these conclusions in exploration is clear. Thus, feeder conduits to intrusions, and the entry zones of feeders to the intrusions themselves are more attractive targets than the other embayment structures at the base of intrusions.

The presence of sulfur in country rocks is a definite plus in evaluating any igneous body as an exploration prospect. Sulfur as pyrite is particularly attractive, since this mineral breaks down thermally at temperatures above 800°C with the release of sulfur (Ripley 1981, 1986). This could occur in the metamorphic aureole of a mafic intrusion, thus obviating the necessity for wholesale assimilation of country rock. Gypsum and anhydrite (the sulfur-bearing minerals of evaporites) require reduction before the sulfur is available to form immiscible iron sulfide; the potential of a mafic magma for reduction is limited, so that a nearby source of a reductant, such as coal, is a likely requirement in this environment. It must be admitted that the precise mechanism by which the addition of country rock sulfur to a body of magma remains enigmatic. In many cases (e.g. Voisey's Bay, Duluth) the trace element evidence does not support the bulk assimilation of enough country rock to account for the amount of sulfur added. Where the country rock contains pyrite, the sulfur fugacity induced by the thermal breakdown of this mineral is sufficient to cause diffusion of sulfur against the thermal gradient into the intrusion, but where the sulfide is pyrrhotite this is less likely to be true. Ripley (1986) has proposed that a sulfur-

bearing fluid is generated in the country rocks and that this transports sulfur into the intrusion. In many deposits, the isotopic composition of the sulfur provides strong evidence that external sulfur has been involved.

Felsification by reaction with country rocks is another important factor. Although, as discussed in previous chapters, the presence of external sulfur in igneous rocks can be demonstrated by sulfur isotopic analysis (provided the potential source rocks are Proterozoic or younger), the influence of felsification is more difficult to establish. The presence of partially digested gneiss, or inclusions with reaction rims of hercynite and/or cordierite are indicative of reaction. Also, Naldrett and Lightfoot (1994) showed that a positive correlation of La/Sm ratio with $SiO_2$ content is a useful indicator of reaction at Noril'sk and in the Keweenawan volcanics of the Black Bay Peninsular, Lake Superior. However, reaction with country rocks is evident in many intrusions, and the role that reaction played in the development of sulfide immiscibility can only be inferred, not proved. Nevertheless, evidence of reaction with the country rocks is undoubtedly a favorable omen when evaluating an intrusion as a potential exploration target.

### 10.1.2 Empirical Concepts and their use

Concepts and axioms in active use by all exploration geologists include:

1. The almost universal association of Ni-Cu deposits with mafic and ultramafic rocks, which can commonly be located by airborne magnetic surveys.
2. The relationship of ore to the basal intrusive contact. This initially empirical observation is one of the principle arguments in favor of a magmatic model that incorporates the gravitational settling of dense sulfide liquid. The model has been established so well that it has become customary to establish the stratigraphic base of an igneous body and concentrate most exploration along this zone. It should not be forgotten, however, that it is shown in Chap. 4 that significant resources of PGE-rich Ni-Cu sulfide occur at the TOP of the mineralized Noril'sk intrusions.
3. The relationship of deposits to certain petro-tectonic settings. This aspect is discussed in detail in the following section.
4. Recognition of favorable and unfavorable mafic and ultramafic environments. Naldrett (1973) pointed out that, because they lacked significant associated Ni-Cu sulfide bodies, certain types of mafic and ultramafic bodies appear to be unfavorable hosts. These consisted of (1)

Alpine ultramafic bodies, including both cumulate and metamorphic-textured portions of ophiolite complexes, (2) Alaskan-type ultramafic bodies, (3) those mafic and ultramafic rocks associated with alkalic intrusive complexes and kimberlite pipes and dykes. The belief that the metamorphic-textured harzburgites, lherzolites, and dunites of ophiolite complexes represent portions of the mantle led, on the basis of genetic ideas, to the conclusion that significant concentrations of magmatic sulfides are unlikely to have had the chance to form within these rocks. The rarity of deposits within Alaskan-type rocks, or in the cumulate portions of ophiolite complexes remains, however, enigmatic from a genetic point of view. Arndt and Lesher (in press) have suggested that the high volatile content of alkalic magmas imparts a lower density to them than the density of tholeiitic magmas, so that they ascend rapidly to surface without "ponding" en route. This, in turn, means that they have little opportunity to react with crustal rocks.

### 10.1.3 Tectonic Setting of the Deposits

One of the most important approaches to exploration is to recognize the geological settings that host known deposits. With the exception of those at Sudbury, all important nickel deposits appear to be related to various degrees of crustal rifting. In most cases, the rifting has permitted magma to ascend rapidly into supracrustal rocks. Either en route, or at its final destination, the magma has reacted with these rocks, becoming contaminated and developing immiscible sulfides. Some different styles of rifting and important magmatic sulfide deposits associated with them are shown in Fig. 10.1.

#### *Deposits developed at incipient rifting*

The Great Dyke of Zimbabwe of Late Archean age (2.58 Ga) is an example of an intrusion in this setting (Fig. 10.1a). It is an elongate layered intrusion (16 km (max) x 550 km) comprising three distinct subchambers with underlying feeder systems that is located within a linear fracture zone. The principal fracture is flanked by satellite fractures within which dykes composed of magma of similar age and composition to that filling the main fracture have intruded. As described in Chap. 9 the main intrusion is host to important disseminated PGE mineralization.

In this author's opinion, another example is that of the Proterozoic Voisey's Bay deposit. As discussed above, the Voisey's Bay mineralization is located within a feeder dyke that links the Reid Brook intrusion

(Western Subchamber) with the Eastern Deeps intrusion, and also along the intersection of this feeder with the base of the latter intrusion. Detailed drilling during the exploration of the deposit (Evans-Lamswood 2000) has shown that except close to the Eastern Deeps intrusion, this dyke has a sub-vertical orientation and trends east-west. There is a strong indication that east-west-trending structures have exerted a strong control on the intrusions at Voisey's Bay (for example the northern wall of the Eastern Deeps intrusion), and on the dykes linking them (the main mineralized feeder is not the only dyke of Voisey's Bay troctolite that has been recognized in the vicinity of the deposit, but all such dykes show the same trend). As seen on the regional map of north central Labrador (Fig. 10.2), a series of east-west fractures have been eroded and give rise to prominent fjords in this area. While the latest reactivation of the fractures is likely related to the recent opening of Baffin Bay, the fractures probably represent long-lived zones of weakness. The Voisey's Bay deposit itself lies on the projection of the Abloviak shear zone, which separates the Proterozoic Churchill Province to the west from the Archean Nain province to the east (Fig. 6.1). However, Ryan (2000) has argued that the actual boundary between these two provinces lies farther to the east, and that there may be no major structure along the projected trend of the Abloviak shear. The significance of Nain-Churchill boundary to the mineralized system is therefore uncertain, particularly since the intrusions comprising the system show no relationship to it. As pointed out above, these intrusions show a marked relationship to the east-west structures, and it is thought that early east-west zones of tension exerted an important control on their emplacement.

### *Deposits developed in mature intracontinental rift structures*

One characteristic example of this group of deposits (Fig. 10.1b) is the Duluth complex of Late Proterozoic age that has intruded the northwest margin of the Midcontinent rift system, close to the triple junction. As discussed in Chap. 4, it has exploited step-like normal faults that mark this margin and has come into contact with sulfide-bearing iron formation and overlying shales, gaining sulfur from them and developing immiscible sulfides. These sulfides occur in zones that are spread out along much of the northwestern contact of the intrusion and constitute one of the largest known concentrations of sulfide mineralization. The sulfides themselves are of high Ni, Cu and PGE tenor but are not sufficiently concentrated to constitute ore.

The Crystal Lake - Mt Mollie intrusion occurs close to the Duluth complex within the Lake Superior Rift System. To the east it has the form of a

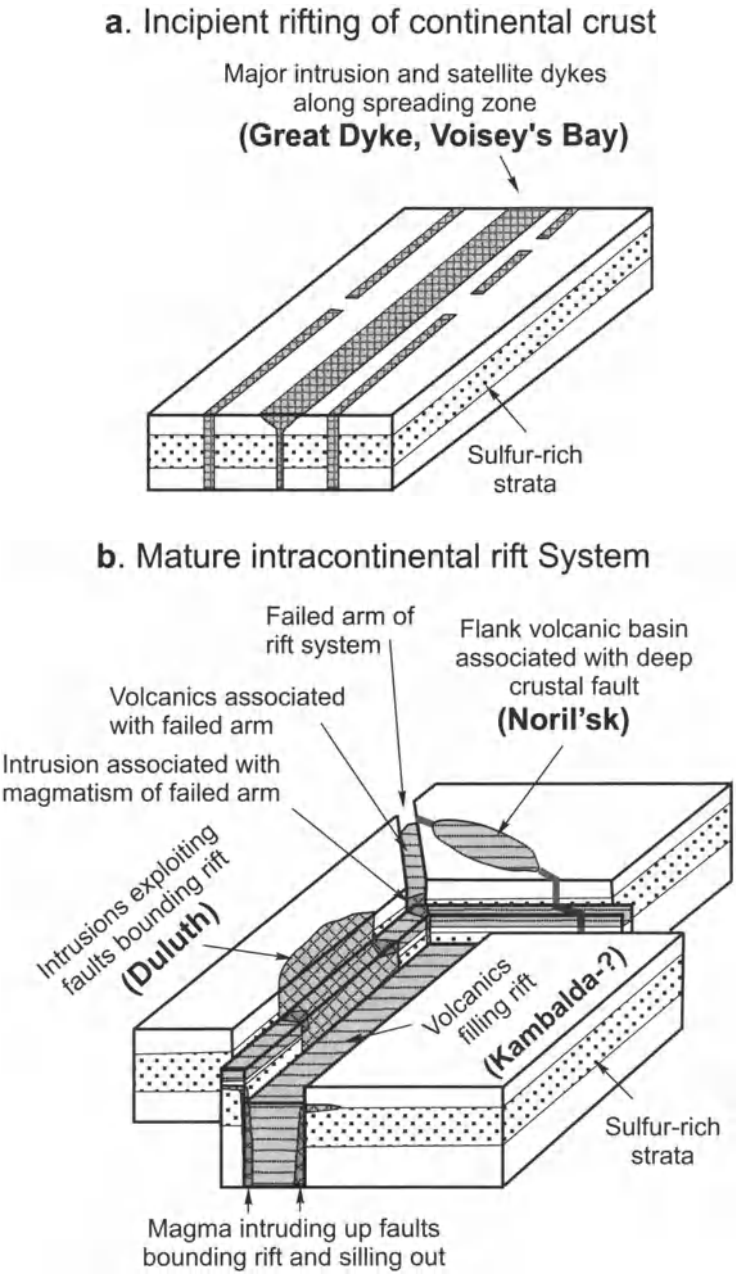
a. Incipient rifting of continental crust
Major intrusion and satellite dykes
along spreading zone
(Great Dyke, Voisey's Bay)
Sulfur-rich
strata
b. Mature intracontinental rift System
Failed arm of
rift system
Flank volcanic basin
associated with deep
crustal fault
(Noril'sk)
Volcanics associated
with failed arm
Intrusion associated with
magmatism of failed arm
Intrusions exploiting
faults bounding rift
(Duluth)
Volcanics
filling rift
(Kambalda-?)
Sulfur-rich
strata
Magma intruding up faults
bounding rift and silling out

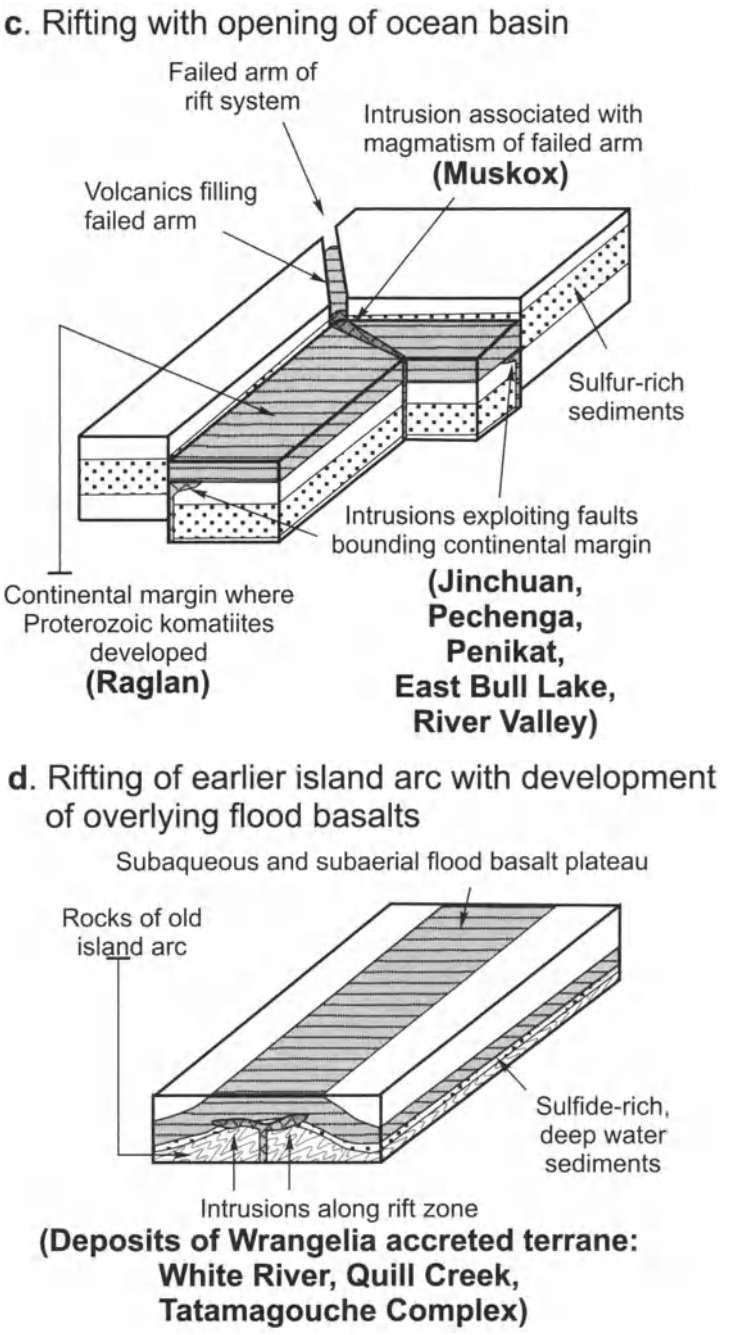


**Fig. 10.1.** Rifting styles, related igneous activity, and examples of associated Ni-Cu and PGE deposits

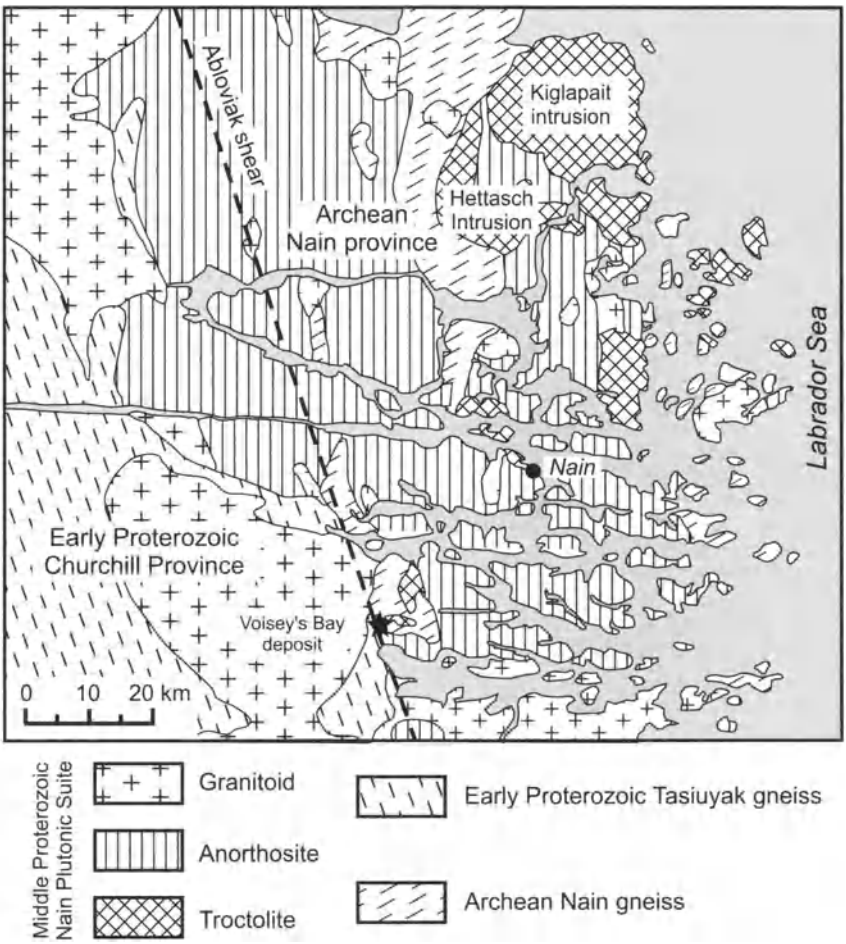


**Fig. 10.2.** Regional geology of East Central Labrador, showing intrusions of the Nain Plutonic Suite and the fjords that have developed over what are believed to be long-lived zones of weakness

dyke (Mt Mollie dyke) which trends east-west and thus, to the west it cuts into the northeast-trending margin of the rift system. As it does so, it develops a floor and is transformed into an intrusion with the form of two fingers splayed apart from each other (Crystal Lake intrusion). A weak accumulation of high-tenor sulfides occurs within one of the fingers. The sulfides are of such high tenor that if one or more rich zones of similar sulfides occur within the body, they would constitute a very attractive exploration target.

Lake Superior itself marks the location of the thickest development of volcanic rocks within the Midcontinent rift and the zone within which the

trend of the rift changes from northeast in the west to southeast in the east. The third arm of this rift would thus be expected to extend to the north, away from the other two arms, in this region. Traditionally, the shallow sills of the Nipigon plate are thought to mark this arm. However, it is possible that initially the Coldwell complex, which is one of the earliest (1108 Ma) intrusions of the Midcontinent rift, marks the location of the initial triple junction, and that the junction shifted westward to the southern margin of the Nipigon plate shortly after intrusion of this body (see Fig. 4.44). A linear belt of alkalic ring complexes extends for 200 km north northeast from the Coldwell complex, and this belt may mark the zone of weakness. The Coldwell complex consists of three intrusive phases, an early tholeiitic, relatively extensive, layered intrusion succeeded by two, more localized alkalic intrusions. The early tholeiitic intrusion hosts several zones of PGE-enriched sulfide, including an intermittent layer of Volkovsky-type apatite-magnetite-chalcopyrite mineralization enriched in Pd (the Skipper Lake and some of the deposits on the Marathon property, see Table 1.3).

The most important deposits belonging to this tectonic setting are, of course, those at Noril'sk. As discussed in Chap. 4, the deposits occur within a volcanic basin that developed on the flank of the rift system along the Noril'sk-Kharaelakh fault that cuts between two arms of the triple junction. The deposits themselves are at least 60 km from the major faults bounding the rift system.

The Archean komatiitic lavas that are hosts to mineralization appear to have formed in rift zones that have developed within pre-existing Archean crust, and thus can also be regarded as belonging to the tectonic setting of an intracontinental rift.

### *Deposits developed during rifting with opening of an ocean basin*

Deposits related to this kind of rifting usually exploit faults bounding continental margins (Fig. 10.1c). The Jinchuan deposit, Gansu Province, China is the most important deposit belonging to this setting. The deposit occurs within an elongate lens of ultramafic rock (see Chap. 7). This occupies a fault that is believed to have formed part of a system of half grabens that bordered a Proterozoic ocean. The ocean opened and subsequently closed with the formation of a fold belt that lies to the south of Jinchuan. Geochemical data indicate that the sulfide-bearing ultramafic rocks were originally part of a gabbroic/ultramafic complex of which the upper, gabbroic portion has been removed by erosion.

Another group of deposits belonging to this setting are those developed within the Pechenga-Varzuga rift zone of the Kola Peninsular, Russia. The most important deposits are those at Pechenga (see Chap. 5). A number of cross faults, essentially perpendicular to the rift resulted in a graben developing on the northern side of the main rift zone. A large thickness of volcanics and sediments, comprising four cycles of volcanism and intervening sedimentation, developed within the graben. Intrusions feeding the fourth volcanic episode spread out within the underlying sulfide-bearing sediments, and developed magmatic sulfides. The main Pechenga-Varzuga rift developed into an ocean that then closed from the south. This has resulted in a sequence of calc-alkaline rocks becoming crumpled and thrusted against the tholeiitic lavas that are preserved in the graben on the northern side of the rift.

A further example is a series of 2.4 Ga mafic/ultramafic complexes that are located along a suture which extends from the Kemi area at the northern end of the Gulf of Bothnia east-northeast into Russia (see Chap. 9). Archean rocks lie south of the suture with folded Proterozoic rocks to the north. The intrusions intrude both the Archean and Proterozoic rocks, with apparent feeder dykes cutting up through the Archean basement to connect with intrusions that are spread out within the overlying Proterozoic sediments. The suture is thought to be part of a rift that was associated with the opening of an ocean to the north of the existing Archean rocks, with the Proterozoic rocks representing sediments developing along the margin of the Archean continent. The intrusions are marked by basal zones of breccia containing PGE-enriched sulfides and overlying sulfide "reefs" (see Chap. 9).

A very similar situation is present south of the Archean Superior Province in the Sault Saint Marie – Sudbury region of Ontario, Canada. Here 2.4 Ga Huronian sediments overlie the Archean rocks and thicken to the south into the former "Huronian ocean". This ocean developed along what is now the southern margin of the Superior Province, and subsequently closed during the 1.8–1.9 Ga Penokean orogeny. A series of 2.4 Ga mafic/ultramafic intrusions developed close to the principal faults defining the margin of the Huronian ocean, spreading out within the Proterozoic sediments. Several of the intrusions (River Valley, East Bull lake) are currently (2004) being explored, and have been found to contain basal breccia zones with weak disseminations of PGE-rich sulfide (see Chap. 9).

The Muskox intrusion is an example of a major intrusion that occurs within fractures related to the failed arm of a triple junction. The triple junction is part of the rift system that gave rise to the Late Proterozoic Poseidon ocean that was located at the present position of the northern shore of continental Canada (Fig. 10.3). The stress field that gave rise to the

failed arm is represented by the fractures that control the huge Mackenzie dyke swarm, and also provided the structure that was filled by the Muskox intrusion. The intrusion is exposed at the current surface as a dyke which opens out to the north into a funnel-shaped layered intrusion. The intrusion plunges north beneath a series of flood basalts, the Copper Mine basalts. No economic sulfide concentrations have yet been discovered within the Muskox intrusion, although substantial amounts of low Ni-tenor sulfides (1-2 wt% Ni in 100% sulfide) have been discovered in marginal rocks close to where the feeder dyke opens out into the funnel. Veins of Cu-rich sulfide extend outward into the country rocks from these marginal sulfides, and carry high concentrations of PGE. However, to date these veins have not proved to be sufficiently voluminous to constitute ore.

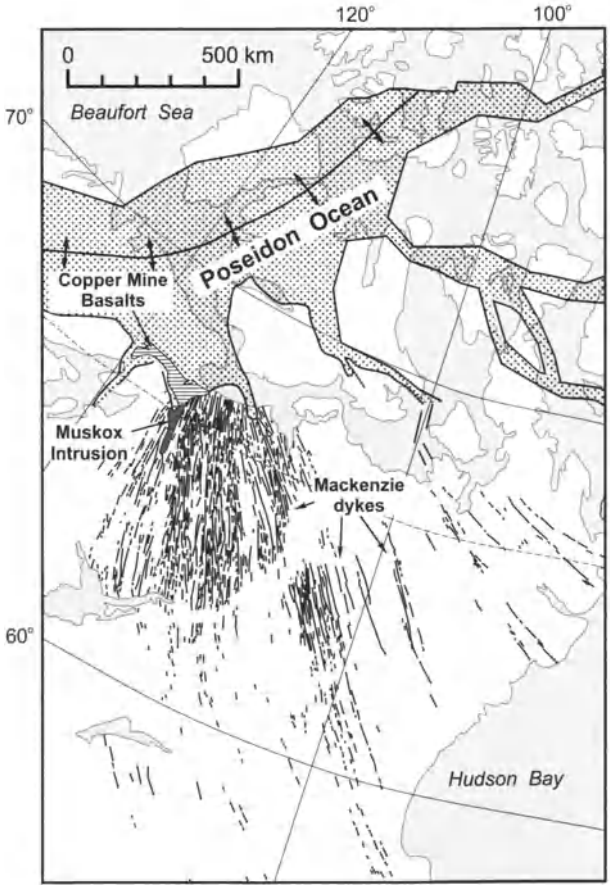


**Fig. 10.3.** Igneous events related to the failed arm associated with the opening of the Poseidon ocean. The Mackenzie dyke swarm developed at this time, as did the Copper mine basalts and the Muskox intrusion

### *Deposits developed during rifting of a pre-existing island arc*

This is an unusual setting in that it is an intra-oceanic environment. Only one example is known to this author, that of the Wrangelia accreted terrane that extends from Alaska, through the Yukon Territory of Canada into northern British Columbia. The deposits occurring within it have not proved to be economically important to-date, but they are included here because of their unique setting. Hulbert (1997) showed that an island arc became covered with sulfide-bearing, deep-sea sediments, and was then rifted (Fig. 10.4). The rifting gave rise to the development of an overlying series of sub-aerial and submarine flood basalts. Intrusions feeding the basalts interacted with sulfur in the sediments and developed immiscible sulfides (Hulbert, 1997).

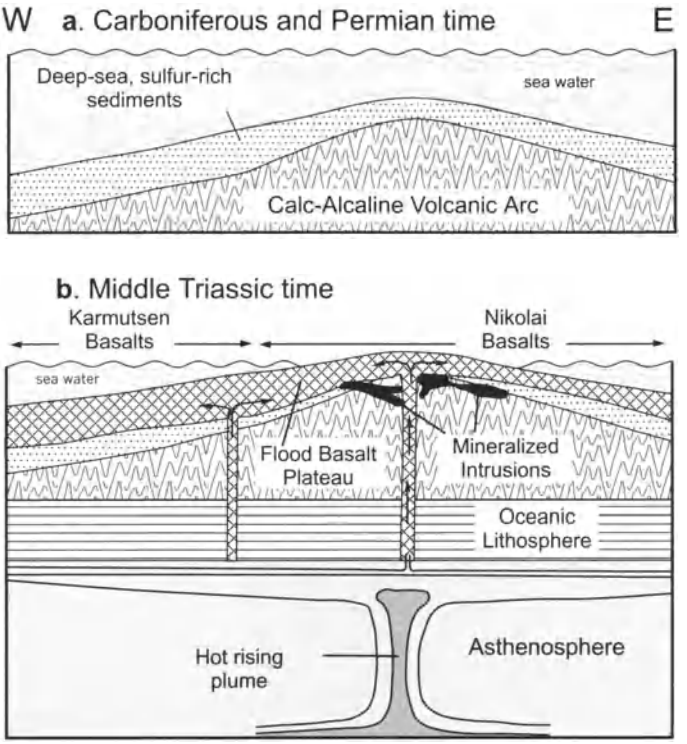


**Fig. 10.4.** Model for Ni-Cu mineralization in the Wrangelia accreted terrane (after Hulbert, 1997). A calc-alkaline volcanic arc became covered by sulfide-bearing deep sea sediments and was then uplifted and rifted by a mantle plume. This also gave rise to flood-basalt volcanism. Sulfide immiscibility developed in the flood basalt magma once it encountered the sulfide-rich sediments, and Ni-Cu sulfide mineralization accumulated where the magma silled out en route to the sea floor (or to surface – some of the flood basalts are subaerial)

### 10.1.4 Methods for Determining whether a given Igneous Body has developed Immiscible Sulfide

When faced with the task of evaluating a mafic or ultramafic body as an exploration target, one of the first questions that an exploration geologist must attempt to answer is whether the magma, or a portion of the magma, responsible for the body was ever saturated in sulfur. The question is raised because of:

1. The demonstration that many important deposits result from sulfur assimilation should lead the geologist to investigate whether the magma could have come into contact with sulfide or sulfate deposits during its ascent from its source.
2. The experimental demonstration that oxidation or felsification may result in the "salting-out" of immiscible sulfides should lead to an investigation of whether there is evidence that either of these processes was active throughout, or within a particular portion of the body that is being considered.

Any of the above aspects might lead to the conclusion that a mafic or ultramafic body had had a reasonable chance of sulfide saturation in its magma, but will not answer with any certainty the question of whether it actually became saturated. A number of approaches have been made recently to answer this question. At first sight it would seem logical that the best method of recognizing a sulfide-saturated magma would be to determine the sulfur contents of rocks thought to be representative of the initial magma of the igneous body, and then to compare these with the experimentally-based estimates of the saturation level expected in magmas of similar composition. This approach was attempted by the author on a series of spinifex-textured lavas from the Abitibi greenstone belt, but was unsuccessful because of the extreme mobility of the sulfides during metamorphism, even under the zeolite-facies metamorphism that occurred in the Munro Township area, Ontario. Sulfur may also be lost as a result of oxidation in the case of sub-aerial lavas (Naldrett and Goodwin 1977). It is concluded that the best approach is to monitor the composition of the silicates of the lava or intrusion, as discussed in the following sections.

#### *Quantitative modeling of sulfide segregation based on bulk rock geochemistry*

The quantitative understanding of how metals partition between sulfide and silicate melts has reached a stage where modeling their behavior can

assist in exploration by identifying favorable districts, and by distinguishing favorable from less favorable bodies of mafic or ultramafic rock and, in special circumstances, favorable from less favorable zones within a given body of rock (Naldrett et al. 1984a). It can also provide an estimate of the nickel tenor of the ore that might be discovered within a given intrusion.

The basic premise in attempting to determine whether a particular body of rock has crystallized from a magma from which molten sulfide has previously segregated or not is straightforward; because chalcophile elements partition strongly into sulfide in preference to silicate melts and minerals, magmas from which sulfide has segregated are depleted in these elements. The magnitude of the depletion depends on the degree to which the particular element partitions into the sulfide as well as on the amount and manner in which sulfide was segregated.

In principle, the elements with the highest values of the partition coefficients are the most sensitive indicators of sulfide segregation. In practice, it is found that Ni is the most useful indicator, not only because of its high partition coefficient, but also because it is normally present in readily detectable quantities (unlike Pt) and is relatively immobile during alteration (unlike Cu). Accordingly the examples that are discussed in this section deal with Ni.

**Types of Sulfide Segregation.** Sulfide may react with and segregate from a magma in a number of ways, of which batch equilibration and fractional segregation can be regarded as two end-members.

In ***batch equilibration***, a significant proportion of the internal dissolved sulfide becomes immiscible or there is a significant addition of external sulfur which induces this immiscibility. The critical feature of this process is that immiscible sulfides form and equilibrate with the silicate melt at one time. Sulfide becomes immiscible throughout the magma, forming droplets which equilibrate with the silicate liquid, settle and accumulate, after which the magma begins to crystallize olivine. Sulfide saturation may occur in only a small portion of the magma, in which case the process is called ***"localized batch equilibration."*** Obviously, the degree of depletion of Ni (or other chalcophile element) in a given mass of magma that has equilibrated with a batch of sulfide is related to the relative masses of the magma and sulfide (i.e. to the value of the magma/sulfide ratio or "R" as defined in Chap. 2). If the proportion of sulfide is very small, it removes very little Ni from the silicate magma and the Ni content of this magma is much the same as it was before liquation and equilibration with the sulfide. On the other hand, if the proportion of sulfide is large, a great deal of the

available Ni is removed, lowering its concentration in the silicate magma appreciably.

The concentration of Ni in a typical basaltic magma which initially contained 300 ppm but has undergone batch equilibration with sulfide is shown in Fig. 10.5. It can be seen that the Ni depletion is almost negligible where the R value is high, but increases rapidly once the value drops below about 1000. As a first approximation, an R value of 1000 or less is required for batch equilibration to produce conspicuous Ni depletion in basaltic magma.

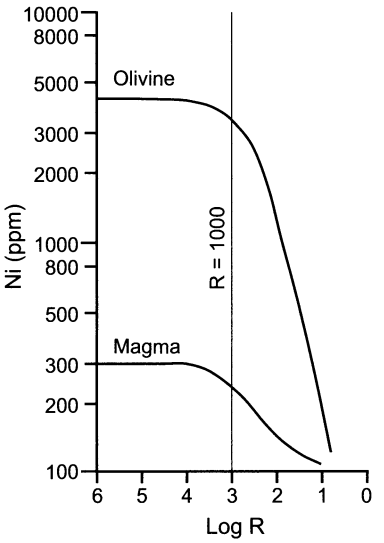


**Fig. 10.5.** Variation in the Ni content of primitive basaltic magma and olivine in equilibrium with the magma resulting from batch equilibration with sulfide as a function of the magma:sulfide ratio (R). Values of $D_{Ni}^{sul/magma} = 275$, $D_{Ni}^{olivine/magma} = 7.23$

In ***fractional segregation***, very small amounts of sulfide continuously become immiscible, equilibrate with the silicate magma, and then settle or are removed in some other way so that further effective communication with the magma is precluded. The typical situation in which fractional segregation would occur would be during the fractional crystallization of a sulfide-saturated silicate magma as depicted schematically in Fig. 10.6b. Because the silicate melt contains the maximum possible amount of sulfide in solution, crystallization of even a small amount of olivine (or other sulfur-free minerals) increases the sulfide concentration in the remaining liquid, and thereby, in most cases, forces some of the dissolved sulfide out of solution.

The variation in concentration of elements in a magma undergoing simultaneous fractional crystallization of olivine and fractional segregation of sulfide can be calculated using the Rayleigh Fractionation law. Obviously, a critical factor is the relative proportion of sulfide to olivine being removed. In most cases this proportion appears to be in the range of 1:50 to 1:400 (Naldrett et al. 1984a).

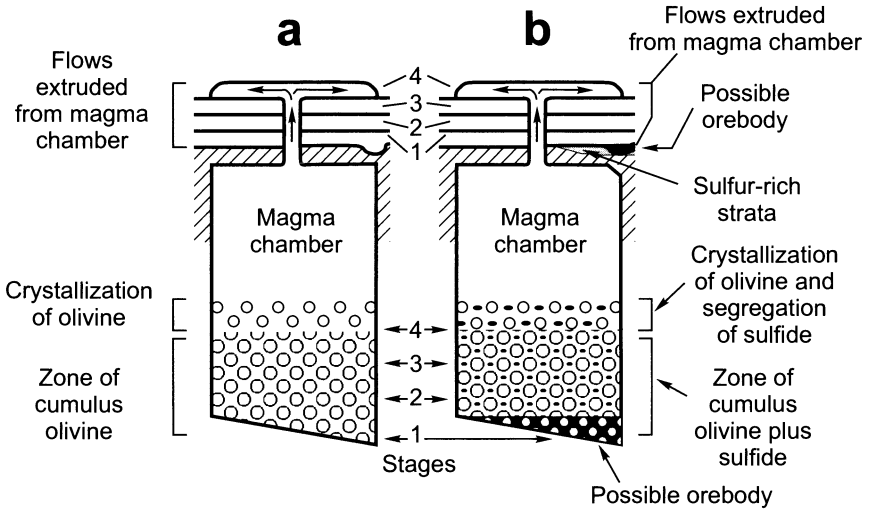


**Fig. 10.6.** Fractional crystallization of olivine and fractional segregation of sulfide from a cooling komatiitic magma. (a) Sulfide unsaturated case. (b) Sulfide saturated case. Note that the magma is assumed to erupt periodically to give rise to a series of komatiitic flows of successively lower MgO content. After Naldrett et al. (1984a)

The compositional trends of silicate magmas derived by the fractionation of a komatiitic starting liquid which initially contained 1750 ppm Ni and 32 wt% MgO are plotted in Fig. 10.7a for sulfide-unsaturated and a series of sulfide-saturated conditions. Although Mg is not incorporated into sulfide, it partitions strongly into olivine, and fractional crystallization of olivine depletes the magma in Mg as well as Ni. For this reason the MgO concentration is commonly used as an index of fractionation for mafic and ultramafic rocks. It can be seen from Fig. 10.7a that there is a major difference in the co-variance of Ni and MgO between the sulfide-saturated and unsaturated cases.

**Examples of the Application of Theoretical Models in Nature.** Nickel sulfide deposits occur associated with flows and intrusions of the komatiite magma suite in Western Australia, Zimbabwe, and Canada. Not all areas

of komatiitic volcanism appear to have associated deposits and it is important to develop criteria for distinguishing sequences of komatiites with high nickel potential from those with low potential.

Accumulations of komatiitic lavas are characterized by cyclical variations in composition such that the flows in each cycle become less magnesian upwards. It has been shown (Naldrett and Smith 1981; Arndt and Nisbet 1982) that the intra-cycle variation is due to low-pressure fractional crystallization of olivine as illustrated in Fig. 10.6a. As olivine crystallizes and accumulates at the base of the shallow crustal magma chamber, the magma becomes less magnesian and is tapped off from time to time to extrude on the surface as lava flows. Phenocryst-free, spinifex-textured samples in the volcanic succession provide a guide to the composition of the magma in the chamber as it fractionates. A komatiite magma that gives rise to magmatic sulfide deposits must be sulfide saturated as in Fig. 10.6b.

**Barren Komatiite.** The compositions of spinifex-textured komatiites and basaltic komatiites from apparently unmineralized komatiite sequences in greenstone belts in Canada, Australia, Zimbabwe, and Finland are shown in Fig. 10.7b, together with the fractional segregation model curves of Fig. 10.7a. The analyses define a reasonably coherent trend which agrees well with the unsaturated trend calculated for the model parent komatiite composition. The agreement between the trends is important because it implies that the computer-based model curves may be used as a standard against which to compare "liquid equivalent" komatiites in general.

**Komatiites of Kambalda, Western Australia.** The deposits of the Kambalda camp, described in Chap. 3, are typical of Ni-sulfide ores of the komatiite association. The numerous small but high-grade deposits occur mainly at the base of a sequence of komatiite flows from which the sulfides are believed to have settled. The sequence averages 500 m in thickness and becomes progressively less magnesian upwards. Lesher et al (1981) analyzed a series of spinifex-textured samples from the Kambalda sequence and compared these to the model fractionation curves of Duke (1979). Their data for Kambalda is compared in Fig. 10.7c with the model curves of Fig. 10.7a. The Ni depletion is quite apparent by comparison, for example, with the barren komatiites of Fig. 10.7b.

**Komatiites of Scotia, Western Australia.** The Scotia deposit is located about 120 km north-northwest of Kambalda and has been described by Stolz and Nesbitt (1981) as a typical example of the komatiite ore association. Their analyses of spinifex-textured rocks are plotted in Fig. 10.7d. The resulting pattern is very similar to the Kambalda data: the rocks are

significantly depleted in Ni in comparison with the barren komatiites and the model sulfide-unsaturated trend.

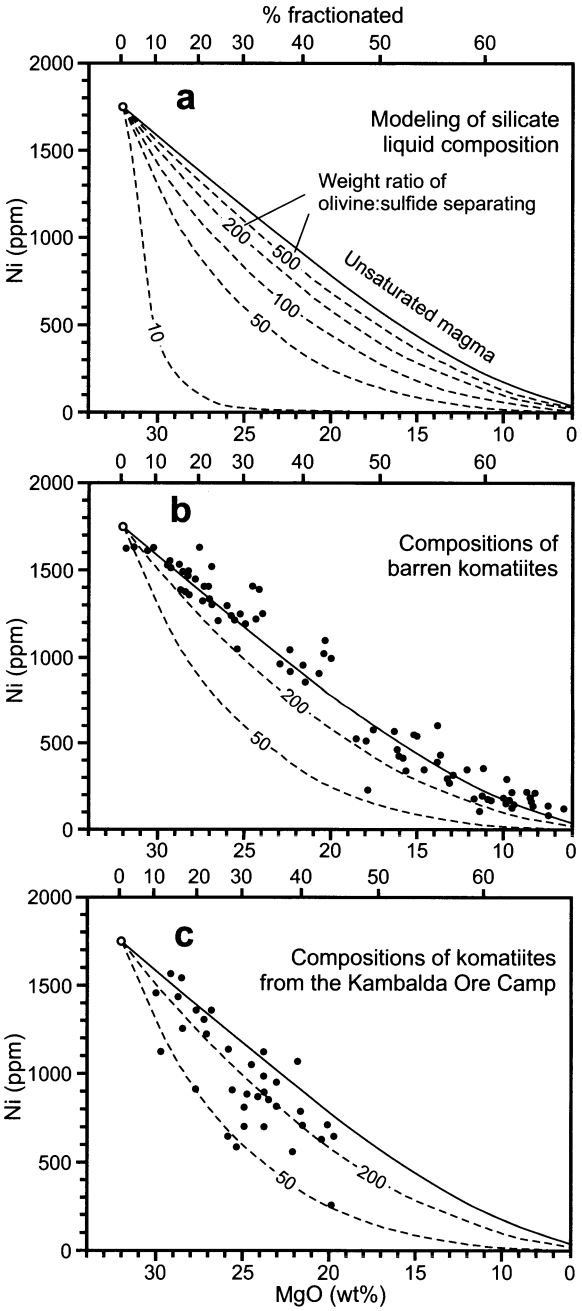

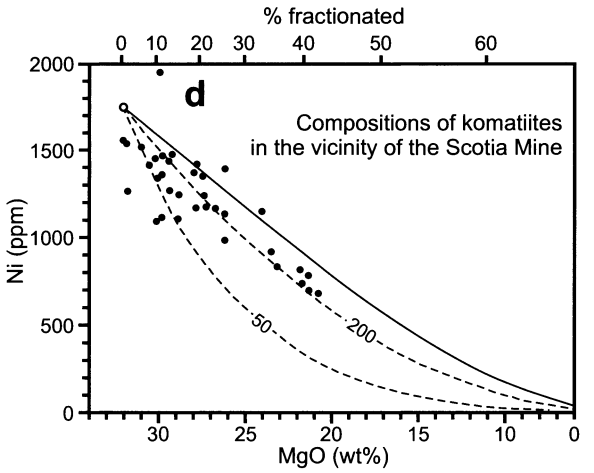


**Fig. 10.7.** Bulk compositions of spinifex-textured komatiites from different regions of the world in comparison to model curves of komatiitic magma fractionation on plots Ni vs. MgO (modified after Naldrett et al. 1984a). (**a**) Computer simulation of the fractionation of a komatiitic magma containing 32 wt % MgO as a consequence of the separation of olivine (unsaturated) or a mixture of different proportions of olivine + sulfide. The numbers indicate the weight ratio of olivine:sulfide separating (modified after Duke and Naldrett 1978). (**b**) Compositions of "barren" spinifex-textured komatiites from greenstone belts Wiluna-Norseman, Western Australia; Belingwe, Zimbabwe; Abitibi, Canada; Barberton, South Africa; and Finland (after Naldrett et al. 1984a). (**c**, **d**) Composition of spinifex-textured komatiitic peridotites from ore-bearing areas of Western Australia: (**c**) from Kambalda (data by Lesher et al 1981); (**d**) from vicinity of the Scotia mine (data from Stolz and Nesbitt 1981)

### *Quantitative modeling of sulfide segregation based on olivine composition*

Bulk rock samples which can provide reliable estimates of liquid composition at various stages during the crystallization of mafic/ultramafic intrusions, are rare in nature. However, some information can be obtained from the composition of cumulus minerals, particularly olivine. Since nickel is present as a trace constituent in magmas, its behavior during crystallization of solid phases tends to follow Henry's law, and its concentration in silicates provides a guide to the concentration in the magma. The same is not true for major constituents such as magnesium and iron, but Roeder and Emslie (1970) have shown that in the case of olivine crystallizing from basaltic magma the ratio $(FeO/MgO)^{olivine}/(FeO/MgO)^{magma}$ is constant with a value of 0.3. Thus the Fo content of olivine, subject to certain reservations,

indicates the FeO/MgO ratio of the magma from which it crystallized. The reservations include the effect to which the initial composition of the olivine has been modified by interaction with trapped intercumulus silicate liquid, and adjacent cumulus phases such as chromite or sulfide liquid.

This section is concerned with the use of olivine in mafic/ultramafic intrusions as an indicator of processes which have affected the intrusions, particularly whether the magmas forming the intrusions have become saturated in sulfide at any stage during their emplacement or subsequent crystallization. The importance of this aspect in evaluating any specific intrusion as a host for magmatic sulfide ore is self-evident.

Magmas that have come directly from the mantle without undergoing fractionation or oxidation (primary magmas) will have MgO/FeO ratios and Ni contents that generally are in equilibrium with the residual olivine remaining in their source regions. Mantle source regions, unless they are particularly Fe-rich, typically contain olivine with 89-94 mole percent forsterite and 3000–5000 ppm Ni. In general, as fractional crystallization of primary or primitive magma proceeds, the MgO and Ni contents and MgO/FeO of the magma, and of the olivine crystallizing from it, will decrease.

Perfect fractional crystallization (segregation) occurs if crystals or droplets of immiscible liquid are removed from a magma as soon as they form – this gives rise to the maximum change in the composition of the remaining magma. In many natural examples, some magma will remain trapped between accumulating crystal phases – this has two results (1) the fractional crystallization of the main body of magma is less extreme than that due to perfect fractional crystallization and (2) the trapped liquid reacts with early forming phases, modifying their compositions.

In some cases, a liquid that is out of equilibrium with the cumulus phases percolates through the cumulus pile, perhaps because it is denser than the trapped intercumulus liquid (Tait et al., 1984), reacting and modifying the composition of the cumulates. A variant of this process is discussed below, in which olivine becomes enveloped by a sulfide liquid with which it is initially out of equilibrium, but with which it reacts. Olivines in close proximity to significant (>10%) amounts of sulfide may have had their Ni contents modified in this way, and should be avoided in attempts to interpret the initial composition of the magma.

**Approach to modeling.** Crystallization of magma is clearly not a simple process. Since this section is concerned with identifying magmatic systems in which chalcophile depletion, due to reaction with sulfide liquid, has occurred, we have chosen to model perfect fractional crystallization of silicates, since this will produce the maximum compositional change. If the

observed change is greater than this, then one must look to other factors such as reaction with sulfide.

A numerical approach has been taken in the modeling. A very small fraction (generally 0.1 wt%) of magma has been removed as olivine, olivine + plagioclase, olivine + plagioclase + clinopyroxene, olivine + sulfide, or olivine + plagioclase + sulfide, and the composition of the magma remaining after the subtraction has been recalculated. The proportions of the silicate phases that have been removed at each step were based on the cumulus mineralogy of the igneous bodies that were being modeled.

In the case of the modeling of olivine from the Voisey's Bay environment (see papers by Naldrett et al. 1996b; Li and Naldrett 1999; Li et al. 2000 for descriptions), the Roeder and Emslie (1970) relationship was applied to the most primitive olivine from the suite to calculate the FeO/MgO ratio of the initial magma. An appropriate FeO content (11 wt%) was then assumed for the magma, on the basis of available analyses of chilled margins which, coupled with the FeO/MgO ratio gave an MgO content for the magma of 7.4 wt%. The partition coefficient for Ni was obtained from the MgO content of the magma, using literature data (Arndt 1977, Duke 1979, Snyder and Carmichael 1992) to obtain a linear variation between a value of 3 at 28 wt% MgO to 9 at 2 wt% MgO. This was then used to calculate the Ni content of olivine, assuming that the initial liquid contained 350 ppm Ni. Clinopyroxene was assumed to have the same FeO/MgO ratio as coexisting olivine (this is not strictly correct, but the error introduced in the curves in this way is insignificant). The partition coefficient (Ni in clinopyroxene)/(Ni in magma) was assumed to be 1; again, there are wide ranges given for these coefficients in the literature (see Kennedy et al. 1993), and the above values are only approximate – they are relatively unimportant in this study, since most of our modeling involves the fractionation of olivine, plagioclase and sulfide liquid.

In situations in which the segregation of liquid sulfide was also modeled, the partition coefficient between sulfide liquid and magma was assumed to be 500 (Peach and Mathez 1993). The Ni content of the sulfide was calculated by applying this coefficient to the Ni content of the magma. The Fe content of the sulfide was calculated assuming that the (Fe+Ni) content of the sulfide liquid was 60 wt%, which is a typical value for sulfide liquids in mafic igneous magmas (see Naldrett et al. 2000a). The Fe removed as sulfide was subtracted as FeO from the FeO content of the magma, along with the FeO involved in the silicate phases removed at each step.

Typical curves resulting from our modeling are shown, superimposed on the data of Simkin and Smith (1970) in Fig. 10.8. At first sight, it would appear strange that the fractionation of, for example, olivine + clinopyrox-

ene + plagioclase depletes the magma in Ni more rapidly than the fractionation of olivine alone. However, if one considers the amount of fractionation involved (the markers on each of the curves in Fig. 10.8 represent 10 wt% fractional crystallization of the magma), it becomes clear that the steepness of the curves is a function of the balance between the lowering of the nickel content and the change in the FeO/MgO ratio of the magma that results from the removal of different combinations of cumulus phases. Variations on the modeling illustrated in Fig. 10.8 are discussed with respect to specific areas below.

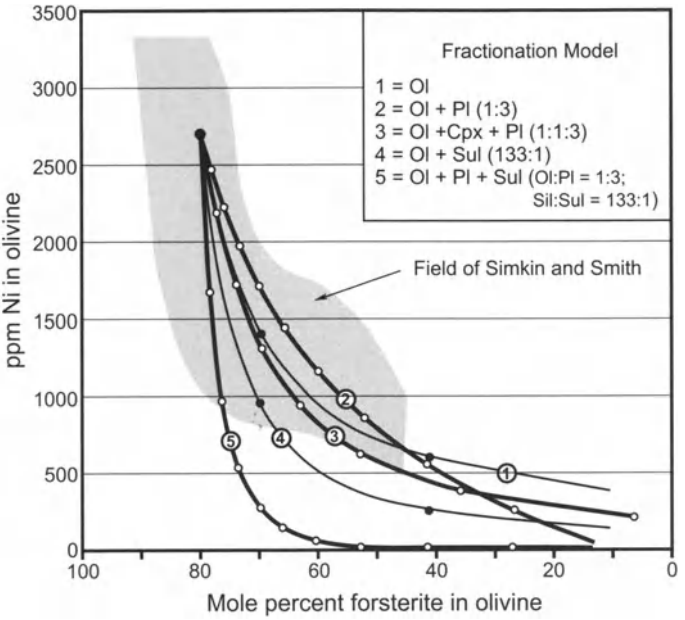


**Fig. 10.8.** Curves showing the relationship between the Ni and Fo content of olivine resulting from the perfect fractionation of a magma containing 7.4 wt% MgO, 11 wt% FeO and 350 ppm Ni. Points on the curves correspond to intervals representing 10 percent fractional crystallization of the original liquid. The curves are superimposed on Simkin and Smith's (1970) compositional field

**Modeling of Voisey's Bay Olivines.** The Voisey's Bay deposit is described in Chap. 6, where a model is presented for its development. Picritic magma rose from the mantle and, during its ascent, reacted with mid-crustal rocks, developing a mid-crustal trace element and isotopic signature. The magma then rose farther to intrude sulfide- and graphite-bearing pelitic/psamitic Tasiuyak paragneiss, where it formed a lower intrusive chamber (Reid Brook chamber). Fractionation and reaction with country gneisses occurred at this level, peridotitic and melatroctolitic (olivine + in-

tercumulus plagioclase) cumulates accumulated, an additional trace element signature related to the enclosing gneiss was imposed on the magma, and sulfides segregated, depleting the magma in chalcophile elements. A second wave of fresh magma entered the system, forcing the depleted magma, along with its contained sulfides, up a 1.5 km-long dyke-like conduit to spread out as a higher level intrusion (Eastern Deeps chamber). Continued flow of the fresh, undepleted magma up the conduit, into the upper chamber, upgraded sulfides that had lodged in the conduit and at its entry line at the base of the higher level intrusion. It also disrupted cumulates within the lower intrusion, giving rise to the peridotitic and melatroctolitic inclusions, found in the magmatic breccia of the conduit and upper chamber. These provide a record of this early phase of crystallization. The bulk of the troctolite that has resulted from the second wave of magma is a plagioclase-olivine cumulate (plagioclase:olivine = 3:1).

Plots of Ni in olivine versus Fo in olivine are given in Fig. 10.9. Figure 10.9a shows data for rocks formed from the first wave of magma crystallization along with two model curves. The first of these models olivine crystallization alone for olivines $>Fo_{65}$ and olivine + plagioclase (1 olivine:3 plagioclase) for olivines $<Fo_{65}$. The second curve models olivine + sulfide fractionation in a proportion of 133 parts olivine:1 part sulfide[27]. A third curve splits away from the first at $Fo_{65}$. The vertical part of this curve shows the decrease in the Ni content of olivine crystallizing from magma from which 1% sulfide containing 4.2 wt% Ni has been removed. The sloping part of the third curve is a model curve for olivines forming from a magma that is crystallizing olivine and plagioclase together, in a ratio of 3 plagioclase to 1 olivine, but from which sulfide is being segregated in the ratio of 133 parts olivine+plagioclase : 1 part sulfide.

It is seen from Fig. 10.9a that olivine compositions from the ultramafic inclusions correspond well with the model line representing olivine fractionation alone. Olivines from leucotroctolite, olivine gabbro and feeder olivine gabbro, (these contain $<Fo_{65}$) lie along the model curve representing the fractionation of olivine + plagioclase along with sulfide (curve 3). The onset of sulfide saturation in the magma along with the segregation of

[27] This ratio has been chosen because it is the ratio to be expected in the cumulus phases separating from a mafic magma that is sulfide saturated, but for which the solubility of sulfide is not changing as a result of compositional changes in the magma and from which sulfide segregates solely in response to the diminution in the mass of magma as silicate minerals (in this case olivine) are removed from it. This is the simplest assumption to make, given that we don't have the data to model changes in sulfide solubility with composition more precisely.

1 wt% sulfide containing 4.2 wt% Ni accounts well for the abrupt drop in the Ni content of olivine that occurs at about $Fo_{65}$.

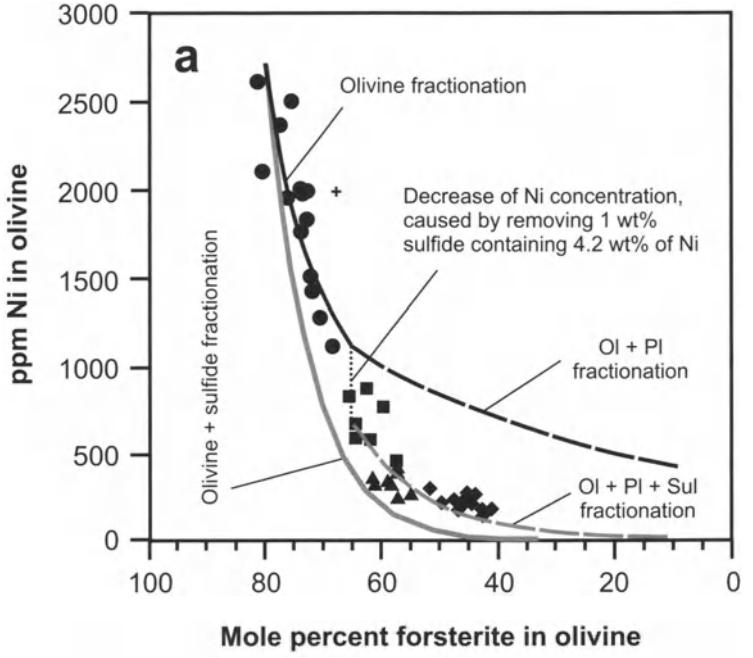


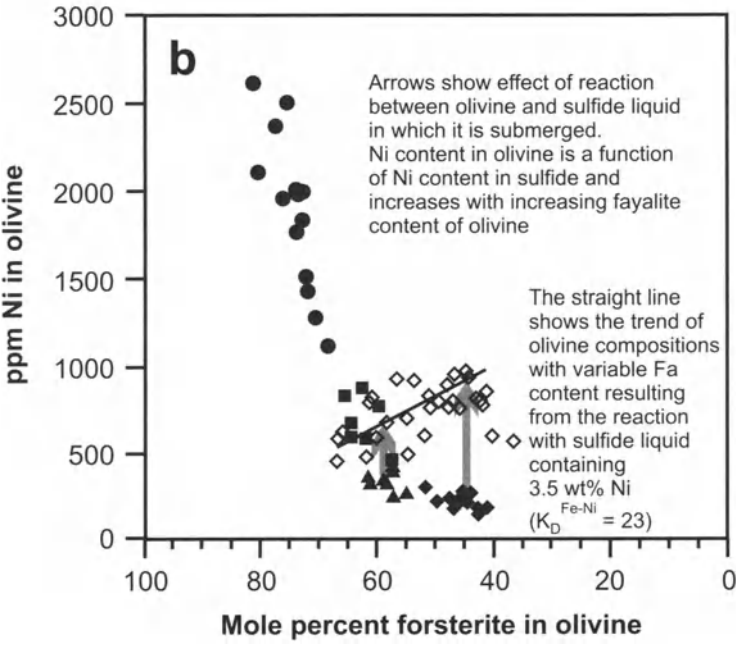

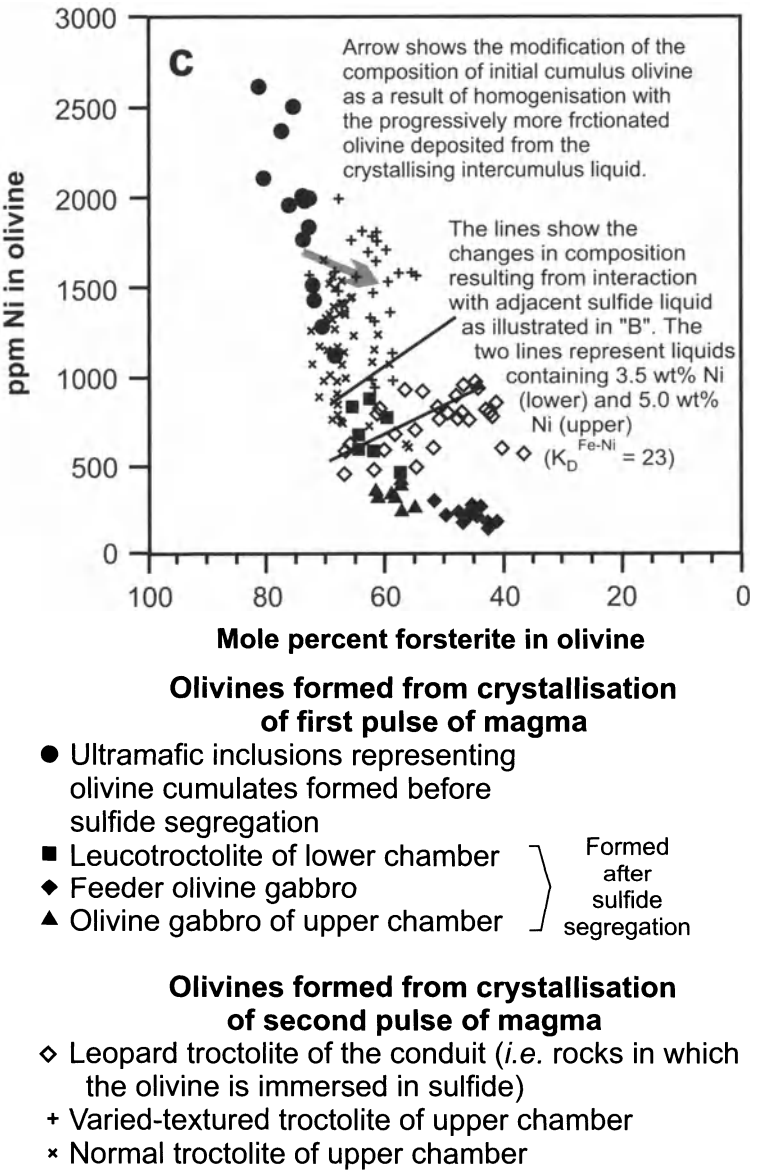


**Fig. 10.9.** Plots of Ni in olivine versus forsterite in olivine from the Voisey's Bay igneous complex and modeling of olivine compositions (olivine compositions from Li and Naldrett 1999). (**a**) Data for rocks formed from first pulse of magma; (**b**) The same data together with data for leopard troctolite; (**c**) All data for Voisey's Bay

As shown, the above model provides a good fit for the crystallization of the first magma pulse, but, as seen in Figs. 10.9b, c, the Leopard Troctolite, Normal Troctolite and Varied-textured Troctolite samples are much more scattered. Part of the answer to this scatter lies in considering the Leopard Troctolite samples. This is a rock type comprising olivine and plagioclase in a matrix of >20% sulfide that occurs in the conduit linking the lower and upper intrusions. As seen in Fig. 10.9b, the Ni content increases with decreasing Fo content of the olivine. Li and Naldrett (1999) discuss this behavior and argue that it is due to re-equilibration of Ni and Fe between olivine and sulfide of the kind shown in reaction (10.1) below:

$$NiO^{olivine} + FeS^{sulfide} = FeO^{olivine} + NiS^{sulfide} \qquad (10.1)$$

The Ni:Fe ratio in the sulfide will then be related to that in the olivine by a constant, $K_D$, as shown below, assuming that the activity coefficients of NiO and FeO in olivine and NiS and FeS in sulfide liquid are constant over the compositional ranges under consideration:

$$(NiS/FeS)^{sulfide} = (K_D{}^{sulfide/olivine})^* (NiO/FeO)^{olivine} \qquad (10.i)$$

Li and Naldrett showed that the trend of the Leopard Troctolite data are explicable as the result of reaction of olivines with initial compositions similar to those from the Leucotroctolite, Olivine Gabbro and Feeder Olivine Gabbro with sulfides containing 3.5 wt% Ni (many of the sulfides in the conduit have this Ni content) where $K_D{}^{sulfide/olivine} = 23$ (this is a very reasonable value to expect to have applied in the Voisey's Bay environment – Brenan and Caciagli 2000). The reaction has a significant effect on the Ni and Fe contents of the olivine when the amount of Ni in the sulfide that lies within a distance comparable to that achievable by diffusion at high temperature approaches or is greater than the amount of Ni in the adjacent olivine. The magnitude of this distance is not fully understood. It certainly seems to be of the order of 1 cm (i.e. we observe a modification in the compositions of olivines that lie up to 1 cm away from masses of sulfide >1 cm diameter), but it could be greater than this.

If the sulfide liquid interacting with olivine contained 5 wt% Ni, the olivine compositions would correspond to the line marked 5 wt% in Fig. 10.9c. Higher Ni contents in the sulfide liquid would result in even more Ni-rich, re-equilibrated olivine compositions. The Varied-textured Troctolite at Voisey's Bay contains localized concentrations of sulfide containing up to 8 wt% Ni, and Ni contents in olivines from this rock are very high – up to 2000 ppm (see Fig. 10.9c). It is reasonable to account for much of the scatter shown by olivines from this environment as a result of the re-equilibration of olivine with sulfide, and the consequent upgrading of the olivine in Ni.

Barnes (1986) emphasized the effect that the crystallization of intercumulus liquid can have on the composition of cumulus olivine and pyroxene. Li and Naldrett (1999) discuss this aspect with respect to their Voisey's Bay data and show that in cumulates containing 30–50 percent trapped liquid, and olivine and plagioclase in a ratio of 1:3, a decrease in the Fo content of the original cumulus olivine of 10–15 mole% Fo is to be expected, along with a less dramatic fall in the Ni content. The arrow in Fig. 10.9c indicates the magnitude of this effect. Rocks containing more olivine and less trapped liquid will be less affected by this reaction, which accounts for the lesser scatter in the olivine data for the peridotitic and melatroctolitic inclusions.

**Modeling of the South Voisey's Bay (Pants Lake).** As described in Chap. 6, a series of "olivine gabbro" (the principle cumulus phases are olivine and plagioclase) intrusions, occur within Proterozoic pelitic/psamitic and quartzo-feldspathic orthogneisses 80 km south of the Voisey's Bay area. The intrusions comprise a younger, northern set of sheet-like bodies and an older southern, much thicker body. The mineralization was explored by Donner Minerals Ltd. and joint venture partners in 1996, and by Donner and partners in conjunction with Teck Corporation in 1997 and 1998. Part of the exploration approach involved the analysis of olivine compositions from many samples, and I am very grateful to Harvey Keats, President, Donner Minerals Ltd., for permission to include these data in this book (Fig. 10.10).

Since inclusions of very primitive material were not present in the drill holes sampled in the study, and given the great similarity between the igneous rocks of the Pants Lake sheets and those at Voisey's Bay, it has been decided to use model curves developed for Voisey's Bay to examine the Pants Lake intrusions.

It is seen from Fig. 10.10 that the Pants Lake samples describe a trend well below the curve modeling olivine fractionation followed, for olivines $<Fo_{65}$, by olivine + plagioclase fractionation (1 olivine : 3 plagioclase). On the other hand fractionation of the same silicate minerals plus sulfide in a ratio of 1 part sulfide to 133 parts silicate reproduces the trend of the data very well. It is concluded that unlike Voisey's Bay, the Pants Lake magmas responsible for the bodies that have been sampled to-date became sulfide-saturated at an early stage and segregated sulfides throughout much of their fractionation. This has resulted in strong chalcophile depletion of the magma, with the result that any sulfides that have formed have generally had low Ni contents. Furthermore, at Pants Lake there is little evidence, in the sheets investigated so far, of a second surge of undepleted magma such

as that which is believed to have upgraded the tenor of the sulfides at Voisey's Bay.

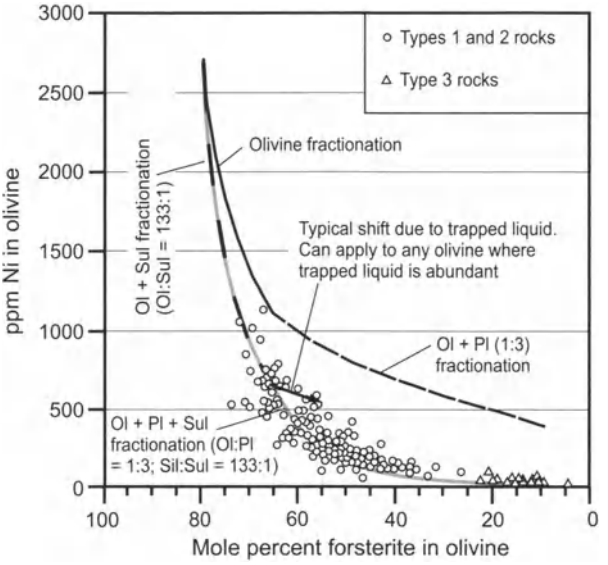


**Fig. 10.10.** Ni versus forsterite variation in olivines from the Pants Lake intrusions, along with model curves

If one takes a value of 2.75 wt% Ni in 100% sulfide as a minimum for a deposit to be economic, given the partition coefficients used in our modeling, this translates into a magma crystallizing olivine with 500 ppm Ni or more (Fig. 10.11). Thus one would predict that sulfides with adequate tenor are only likely to occur associated with those sheets that contain olivine with Fo<60 mole percent at Pants Lake.

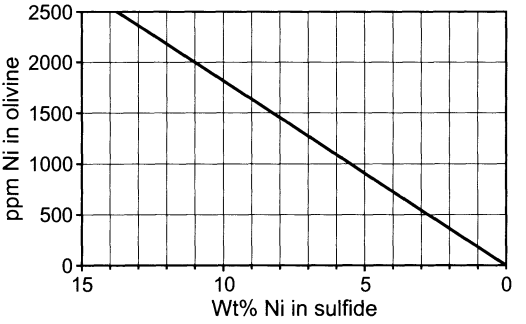


**Fig. 10.11.** Relationship between Ni in olivine and Ni in sulfide for olivine and sulfide in equilibrium with the same silicate magma. $D_{Ni}^{Sul/Ol} = 55$

**Modeling of the Moxie and Katahdin intrusions, Maine, USA**. Thompson and Naldrett (1984) studied the Ni content of olivines in the Moxie and Katahdin intrusions in the Appalachian mountains of northern Maine. Both are synorogenic, Devonian-age intrusions emplaced during the Acadian orogeny into Siluro-Devonian sedimentary rocks. They contain uneconomic Ni sulfide deposits that are interesting from a genetic point of view.

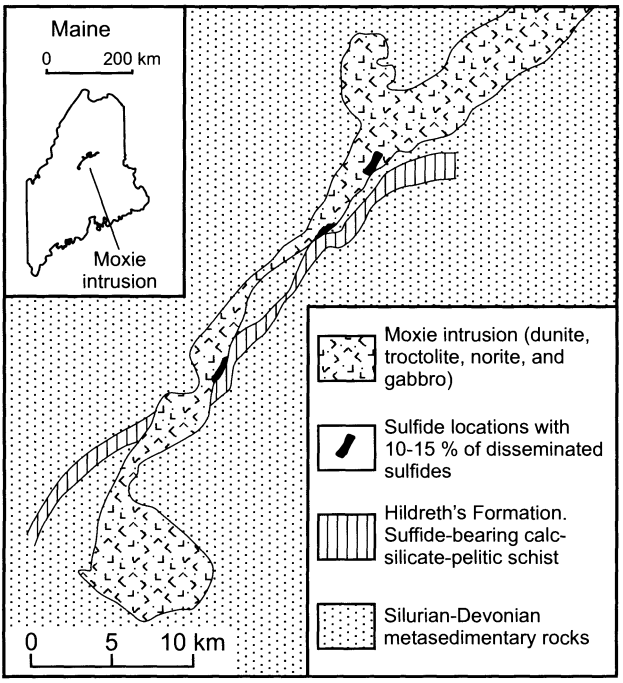


**Fig. 10.12.** Schematic map, demonstrating locations of sulfide showings in the Moxie intrusion (after Thompson and Naldrett 1984)

The Moxie body is a 70 km long, 2-8 km wide intrusion elongated in a southwest-northeast direction. It is composed of rocks ranging from dunite and peridotite to olivine gabbro, and shows the characteristic, rather chaotic layering of a synorogenic intrusion. The magma appears to have moved as it was fractionating, so that more primitive, olivine cumulates occur to the southwest and more fractionated, olivine-plagioclase and plagioclase cumulates occur to the northeast. Disseminated sulfides are ubiquitous in the rocks of the western part of the intrusion and three small sulfide showings (containing 10-50 % of sulfide) have been discovered in the western and central parts, where the basal contact approaches a sulfide-rich formation within the country rocks, the Hildreth's Formation (Fig. 10.12).

The sulfur isotope compositions ($\delta^{34}S$ –8 to –23‰) and S/Se ratios (10,000–40,000) of the sulfides of these showings leaves little doubt that much of the sulfur was derived from the Hildreth's Formation ($\delta^{34}S$ = –26‰; and S/Se = 27,000 to 50,000).

The Katahdin intrusion occurs as a small 4.5 by 1.5 km stock 15 km south of the Moxie intrusion. It consists of olivine gabbro and the similarity in rock types, rock chemistry and age indicates that the stock has been formed by a magma that was very similar to that responsible for the Moxie body. The only outcrop is in the south where a deposit of in excess of 200 million tonnes of nearly massive magmatic sulfides occurs within the gabbro. The tenor of these sulfides is 0.2 wt% Ni, 0.1 wt% Cu, and 0.17 wt% Co. Their isotopic compositions ($\delta^{34}S$ –11 to –22‰) and S/Se ratios (23,000 to 33,000) indicate that a high proportion of country-rock sulfur has been incorporated in the deposit.

Thompson and Naldrett (1984) focused their study on olivine and olivine-plagioclase cumulates in the southwestern half of the Moxie intrusion, particularly in the vicinity of the three sulfide showings referred to above, and on the Katahdin body.

Olivines at Moxie-Katahdin (Fig. 10.13) are more forsteritic than those at Voisey's Bay (Fig. 10.9), and it was necessary to choose a starting composition with a much higher MgO/FeO ratio (9 wt% FeO, 12 wt% MgO, 350 ppm Ni) for the purposes of modeling. The model curves are superimposed on the data in Fig. 10.13. Because of the complicated, relatively unmapped nature of the layering, it has not been possible to select an arbitrary value of Fo at which to replace olivine fractionation by olivine + plagioclase fractionation, and in Fig. 10.13 all curves have been calculated originating at the initial composition. They model different possible scenarios in which, following the modal mineralogy of the rocks, olivine and plagioclase crystallize in a ratio of 1:1. Some Moxie samples fall on or close to the olivine and olivine +plagioclase curves (curves 1 and 2), but others fall well below them. As Thompson and Naldrett (1984) pointed out, the olivines from Katahdin are much poorer in Ni, and fall close to curves corresponding to the fractionation of olivine + sulfide. Many of the Moxie data in Fig. 10.13 fall along or just to the right of the 133:1 silicate + sulfide model curve; the displacement due to trapped liquid shift, that was discussed above and is illustrated in Fig. 10.9a, applies equally in the case of the Moxie data and can account for some samples plotting to the right of the curve. In contrast, the Katahdin data describe no trend, and could be the result of the late stage addition of country rock sulfide to a magma that had fractionated along one of the other curves, olivine, olivine + plagioclase or olivine + plagioclase + sulfide.

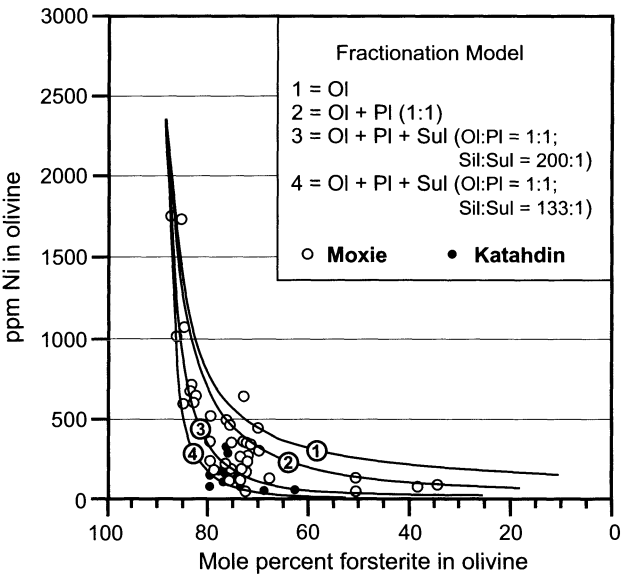


**Fig. 10.13.** Data for olivines from the Moxie and Katahdin intrusions, along with model curves (olivine compositions from Thompson and Naldrett 1984)

**Modeling of the Insizwa and Tabankulu intrusions, South Africa.** A series of Karoo-age intrusions, the Insizwa, Ingeli, Tonti and Tabankulu bodies, that are described in Chap. 4, occur south and west of Kokstad in South Africa. In contrast to much of the Karoo magmatism in this area, these bodies contain much more olivine, and an argument has developed between those who maintain that the primary magma was magnesian basalt (Cawthorn 1980) and those who believe that they are of typical, low-magnesian Karoo basalt, enriched in MgO as the result of olivine accumulation (Lightfoot and Naldrett 1984b; Lightfoot et al. 1984). Of these bodies, the Tabankulu intrusion has been described by Lightfoot and Naldrett (1984a) and the Insizwa intrusion by Lightfoot et al. (1984). Both studies paid considerable attention to the variation in olivine composition, and are the source of the data discussed here. The Insizwa intrusion has the form of a sheet, several 100's of m thick, while the Tabankulu body has that of an elongate trough developed above a feeder conduit. Both bodies have a basal layer of olivine gabbro, overlain by picrite (50 m thick in the case of the Waterfall Gorge section at Insizwa, 200 m thick at the northern end of the Tabankulu trough), and then by repetitively layered gabbros and olivine gabbros at Insizwa and troctolites and olivine gabbros at Tabankulu. Discontinuities in mineral compositions indicate that both bodies developed as a result of the repetitive introduction of magma.

Lightfoot et al. (1984) and Naldrett et al. (1984a) compared the olivines at both Insizwa and Tabankulu to the field occupied by Simkin and Smith's (1970) data and concluded that the Ni-poor olivines of both bodies indicated that the magma had reacted with sulfide before intruding to the level covered by the sampling. The location of these hypothetical sulfides has been the subject of several exploration projects, that were not successful.

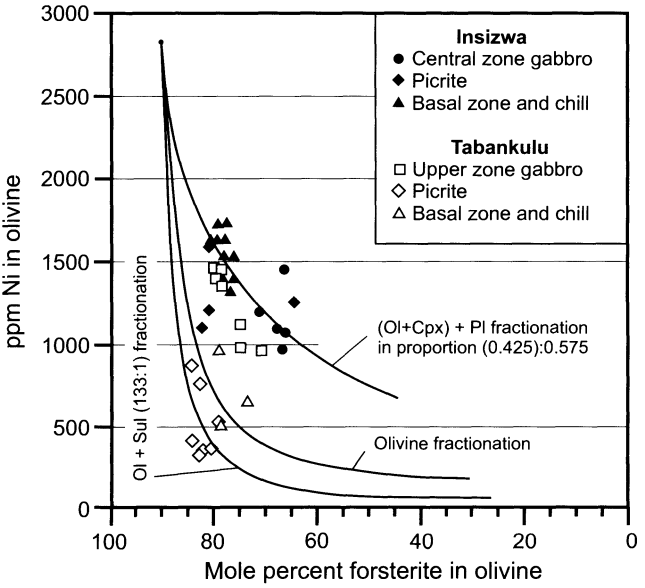


**Fig. 10.14.** Data for olivines from the Insizwa and Tabankulu picrites and olivine gabbros along with model curves (olivine compositions from Lightfoot and Naldrett 1984a; Lightfoot et al. 1984)

Model curves are projected onto the data from Insizwa and Tabankulu in Fig. 10.14. In developing the curves and at the same time maintaining a reasonable FeO content of 9 wt%, the composition of the more primitive olivines required us to choose an initial magma containing 14 wt% MgO and 450 ppm Ni. It is seen that the fractionation of olivine alone rapidly depletes the magma (and thus olivines in Ni) and that all of the Insizwa rocks plot above this line. The Insizwa gabbros describe a trend which can be modeled by fractionating 3.5 wt% olivine (this reduces the Fo content from 90 to 89.3 mole percent and the Ni in the liquid from 450 to 367 ppm), followed by fractionation of olivine + clinopyroxene (ratio 1:1) plus plagioclase (ratio 0.425 (Ol+Cpx) : 0.575 Pl). These ratios correspond to the average cumulus mineralogy.

Much of the Tabankulu basal gabbro and picrite falls below the olivine fractionation line, but can be modeled reasonably well on the basis of the fractionation of olivine + sulfide in a ratio of 133:1. The segregation of a slightly higher proportion of sulfide, or the bulk equilibration with sulfide as was suggested at Voisey's Bay or Katahdin, would produce an even closer match for the data.

**Concluding Statement.** It has been shown that, using reasonable estimates of partition coefficients, and reasonable starting compositions for the magma, model curves of Ni versus Fo based on Rayleigh-type fractionation of olivine, plagioclase and pyroxene in the proportions observed in the cumulus mineralogy ± sulfide can account for the variations observed at many of the locations for which data are available. One lesson emerges from this analysis which is that the comparison of observational data with the field defined by Simkin and Smith (1970) is not a satisfactory method of identifying chalcophile depletion. Fractionation of olivine, or olivine + plagioclase can result in a very sharp decrease in Ni with Fo, as is shown in Figs. 10.9 and 10.13. The Insizwa magma has not necessarily reacted with sulfide, although it seems very likely that the Tabankulu magma has. In using the Ni versus forsterite technique, it is necessary to observe the cumulus mineralogy of an intrusion, and any clues as to the previous crystallization history that is not preserved in visible cumulates (for example the inclusions at Voisey's Bay), arrive at reasonable estimates for initial magma composition (results are not highly sensitive to this) and derive curves that represent the most likely crystallization history. In this study highly detailed models in which each influx of new magma is taken into account have not been attempted – better models may be developed in the future, but modeling of this kind is always constrained by the accuracy of the partition coefficients. As discussed above, a linear correlation between MgO and $D_{Ni}^{Olivine/Magma}$, has been used and the effects on the coefficient that are know to occur as a result of variations in $fO_2$ (Snyder and Carmichael 1992; Gaetani and Grove 1997) have been ignored, because of the difficulty in defining oxygen fugacity in the intrusions considered here. Likewise, a constant sulfide/magma coefficient of 500 for Ni has been used, despite evidence (Brenan and Caciagli 2000) that the value is likely to vary with both $fO_2$ and the NiS-content of the sulfide. These decisions have been made for the purpose of opening up discussion of the method by presenting preliminary attempts at modeling without waiting for further experimental data. Where reasonable estimates of the initial magma composition are available (such is the case at Noril'sk), Ghiorso and Sacks (1995) "MELTS" programme (JAVA version 1.1.1, 2001, provided online by M.S. Ghiorso) can be used to predict variations in magma composi-

tion. This allows the use of more refined, composition related, estimates of the required partition coefficients as they become available (see, for example, Li at al. 2003a).

### 10.1.5 Use of Cu/Zr Ratios in volcanic rocks and layered intrusions

It has been argued in Chaps. 4 and 6 that both Cu and Zr are incompatible elements during the early stages in the fractional crystallization of sulfide-unsaturated mafic/ultramafic magmas, and thus both increase in concentration as fractionation proceeds, with the Cu/Zr ratio remaining constant. Once sulfide saturation occurs, Cu is no longer incompatible, and is removed progressively with the progressive segregation of sulfide. Lightfoot et al. (1994), who were the first to emphasize the importance of Cu/Zr ratios, pointed out that Noril'sk basalts that were known **not** to have reacted with sulfide (Tuklonsky, Upper Morongovsky and Mokulaevsky ) had Cu/Zr ratios between 1 and 3, while those that were known to have reacted (Lower-Middle Nadezhdinsky, Upper Nadezhdinsky and Lower Morongovsky ) had ratios <1 (Fig. 10.15a).

Since in cumulate rocks incompatible elements are contributed by the magma that has become trapped interstitially between cumulus grains, the Cu/Zr ratio of any sample of cumulate will reflect the ratio in the magma that gave rise to the cumulate just as effectively as a sample of volcanic rock. It has been shown above that the olivines of both the northern, sheet-like bodies and the southern intrusion at Pants Lake (see Chapter 6) follow a trend indicative of chalcophile depletion. The Cu/Zr ratios of these cumulus rocks are shown in Fig. 10.15b. All values for the northern intrusions, except for mineralized samples have Cu/Zr ratios of less than 1, as do most values from the southern body, which is consistent with the conclusion that the magmas of both bodies have reacted with significant amounts of sulfide. Li and Naldrett (1999) showed that there is a correlation between Ni-depletion shown by olivine and the Cu/Zr ratios of the rocks hosting the olivine in the Voisey's Bay deposit, as discussed in Chap. 6 (see Fig. 6.17). Thus, there is a mounting body of evidence that Cu/Zr ratios are a very useful indicator of rocks that have formed from magma that has interacted with sulfide liquid and have become chalcophile-depleted. The critical value of Cu/Zr = 1 as that separating magmas that have and have not reacted with sulfide may vary from environment to environment, depending on the initial contents of Zr and Cu; it is just coincidence that the value is the same at Noril'sk and in the Voisey's Bay area. It is also obvious that Cu can be ratioed against other

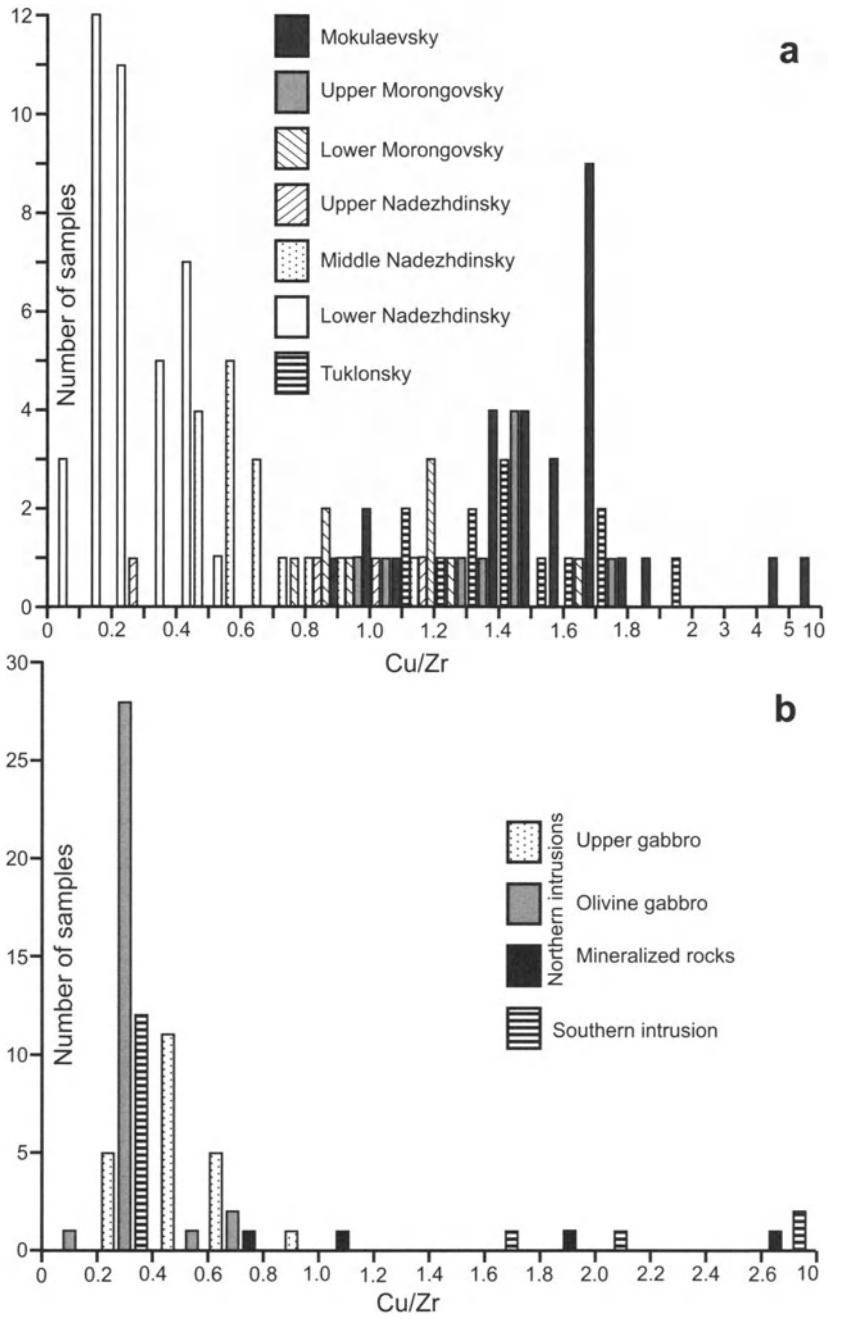


**Fig. 10.15.** Cu/Zr ratios in (**a**) basalts from the Noril'sk area and (**b**) in intrusive rocks from the Pants Lake area, Labrador. Data for (a) from Lightfoot et al. (1994) and for (b) from MacDonald (1999)

incompatible elements such as Y or Yb – all that is required is that the element remains incompatible until a late stage in the crystallization.

### 10.1.6 Use of the Noril'sk model in selecting other regions for Exploration

The model presented for the origin of the Noril'sk ores in Chap. 4 has general applications to areas of flood basalt, and an example is given below.

#### *Key metallogenic features of the Noril'sk Region*

In this author's opinion key metallogenic features of the Noril'sk region include:

1. A "hot spot" (see discussion in Chap. 4 relating to the existence of a plume) in the mantle giving rise to vast amounts of flood basalt.
2. Continental-scale rifting following "hot spot" development.
3. Major faults, penetrating to the mantle, activated or reactivated during rifting, and serving as the conduits for volcanic eruptions and magma intrusions.
4. Crustal contamination of some of the magma.
5. Chalcophile element depletion of contaminated magma; this is probably most easily (cheaply and unambiguously) recognized in terms of Ni depletion (that is low Ni values decoupled from MgNo and therefore not due to magmatic differentiation and thus probably due to sulfide segregation). At Noril'sk, the clearest indication of chalcophile depletion is observed within certain volcanic suites penecontemporaneous with the ore-bearing intrusions.
6. The trapping of sulfides in feeder channels, and the exposure of these sulfides to later magma using the same channels, leading to an upgrading of the trapped sulfides.
7. The presence of sulfate-bearing evaporites throughout the Paleozoic from the Cambrian to the Devonian, coupled with overlying coal measures.

#### *Recognition of Crustal Contamination*

A good simple indication, but not conclusive proof of crustal contamination is to plot La/Sm against $SiO_2$ – both should increase with increasing contamination by continental crust. La/Sm is plotted against $SiO_2$ for the Noril'sk volcanics above the Gudchikhinsky in Fig. 10.16a. The jump from the uncontaminated Tuklonsky to the contaminated Lower-Middle

Nadezhdinsky is very clear, as is the decrease in contamination through the Upper Nadezhdinsky and Lower Morongovsky to the Upper Morongovsky and Mokulaevsky.

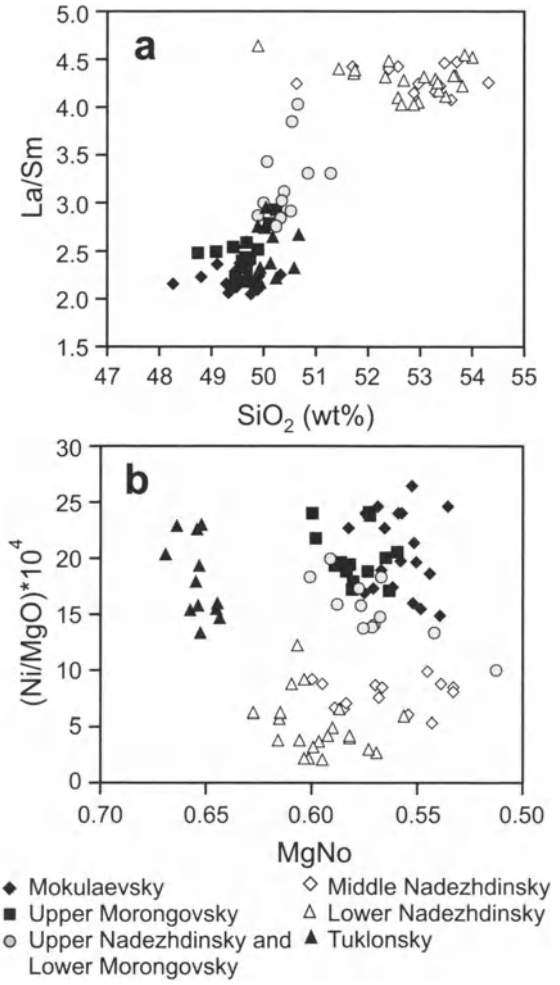


**Fig. 10.16.** Plot illustrating the relationship between (**a**) La/Sm vs. $SiO_2$ and (**b**) (Ni/MgO)*$10^4$ vs. MgO for basalts of the Tuklonsky, Nadezhdinsky, Morongovsky and Mokulaevsky Suites from the Noril'sk region (data from Lightfoot et al. 1990). MgNo was calculated here as molecular ratio MgO/[MgO+(0.85*FeOT)]

Other trace element and isotope ratio plots are also useful, as has been discussed in Chaps. 4, 5, 6, 8 and 9 of this book, but they involve analytical work that is not commonly performed during exploration.

### *Recognition of Chalcophile Element Depletion*

It is suggested above that Ni depletion is the most reliable (and most economically determined) index of chalcophile element depletion. The reason for choosing Ni is that it substitutes in silicate structures, and is therefore less mobile than Cu, Pt and Pd which are normally associated with sulfide in a rock. A convenient way of looking at Ni variation in a series of lavas is to plot Ni/MgO against MgNo. MgNo is the molecular MgO/(MgO+x*FeOT) ratio of a rock, where x is a number between 0.85 and 1.0, and is used to account for that proportion of total FeO existing as $Fe_2O_3$. MgNo decreases as differentiation proceeds. Ni decreases more rapidly with differentiation than MgO, since Ni is removed from a mafic magma and concentrated in early forming mafic minerals such as olivine to a greater degree than MgO. The sharpness of the decrease in Ni with decreasing MgNo is reduced by plotting Ni/MgO against MgNo rather than Ni alone. This has been done in Fig. 10.16b which shows the same rocks from Noril'sk as are shown in Fig. 10.16a. It is those samples that are most contaminated, i.e. those from the Lower-Middle Nadezhdinsky unit, that are most Ni-depleted. Depletion, as indicated on this plot, decreases through the Upper Nadezhdinsky and Lower Morongovsky to the Upper Morongovsky and Mokulaevsky basalts.

While, as discussed above, Ni-depletion can serve as a guide to magma that has interacted with sulfide, it may not be possible to detect it in the intrusions that are hosts to ore consisting of sulfides with a very high tenor of chalcophile elements. This is apparent from the observation, reported in Chap. 4, that the Talnakh intrusion contains olivine with a normal Ni content, and that it is the poorly mineralized Lower Talnakh intrusion that contain olivines that are recognizably depleted in Ni. This illustrates the point that while chalcophile element depletion is very important as a regional guide to localities where sulfides have formed from mafic magma, on the local scale, when one has to select individual targets within a region for exploration, Ni-depletion has to be used carefully, with an understanding of the geological evolution of the region as a whole. It is not a simple formula for pin-pointing the best targets. At Noril'sk, for example, localized use of Ni-depletion would have pin-pointed the Lower Talnakh-type intrusions, which are distinctly less desirable than others as exploration targets.

### *A Case Example of the Selection of a Region for Exploration*

The great areas of continental flood basalt activity throughout the world include, in addition to the Siberian platform, those of the Karoo (Southern

Africa), Deccan (India), Parana (South America) and Lake Superior (North America). Of these, the Lake Superior region stands out in having significant quantities of associated Cu-Ni sulfide (Listerud and Meineke 1977). As described in Chap. 4, Lake Superior lies on the trend of the Midcontinent Gravity High, which extends from Oklahoma northeast to the lake where it turns southeast to become lost beneath the Michigan basin. It is marked by a series of aeromagnetic anomalies suggestive that mafic rocks underlie much of the structure. This has been confirmed by boreholes that have penetrated the Paleozoic cover to reach the Precambrian (Fig. 4.44). The Lake Superior region itself is thought to include the triple junction associated with the rift structure, which accounts for the change in the trend of the structure. As discussed above, the vicinity of the Coldwell intrusive complex and also of the Lake Nipigon region, which extends northward from Lake Superior, may represent the failed arms of this triple junction.

The geology of the Lake Superior region is shown in Figs. 4.45, 4.46 and 4.48. The North Shore volcanics and their equivalent, the Osler group, dip gently and young to the south on the north side of the structure. The Bayfield group, Jacobsville sandstone and Oronto group sediments occur on the south side and dip northward. These sediments overlie the Portage Lake lavas which comprise a younger sequence of volcanics than the Osler to the north. Lake Superior itself consists of a central graben, defined by major faults and hinge lines, within which Archean crust has been thinned to less than 1/4 of its previous thickness, and over 26 km of volcanics and sediments have accumulated. The north arm of the system is thought to be centered on Lake Nipigon as has been discussed above. The Sibley sediments, which are located in a graben controlled by a series of north-south faults, have been intruded by diabase sills, sheets and dykes (Sutcliffe 1987). The sills stand up as mesas dominating the topography of the area. To the south, the sills dip beneath the Osler volcanics.

Lightfoot et al (1991) reported on the geochemistry of the Osler. They divide it into a series of 3 units, the Lower, Central and Upper units. The lower parts of both the Central and Upper units show signs of crustal contamination (Fig. 10.17a). Uncontaminated magma appears to have contained about 49-50 wt% $SiO_2$ and had a La/Sm ratio of about 3. These values increase to 54 wt% $SiO_2$ and La/Sm = 6 at the base of the Central unit and to 55 wt% $SiO_2$ and La/Sm = 4.5 at the base of the Upper unit.

A plot of Ni/MgO vs MgNo (Fig. 10.17b) shows that samples from near the base of the Central and Upper units are distinctly depleted in Ni. The most Ni-poor rocks in the Upper cycle also have the lowest MgNos, indicating that differentiation played a role in decreasing the Ni in these, although the amount of Ni depletion is so great that differentiation alone is an insufficient explanation. The MgNo throughout the Central unit is con-

stant, indicating that the observed Ni depletion is not related to differentiation. Interaction with sulfide that has segregated from the magma as a result of crustal contamination thus appears to be important, particularly in rocks from the lower part of the Central unit, but also in those from the lower part of the Upper unit.

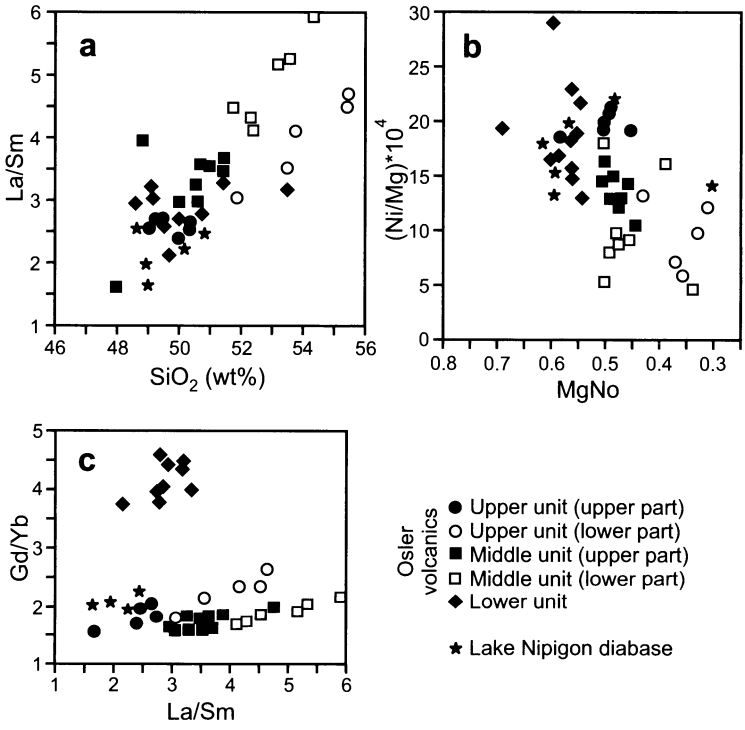


**Fig. 10.17.** Plots of (**a**) La/Sm vs. $SiO_2$, (**b**) (Ni/MgO)*$10^4$ vs. MgNo and (**c**) Gd/Yb vs. La/Sm for the Osler volcanics. Data from Lightfoot et al (1991)

If one looks at the plot of Gd/Yb vs La/Sm shown in Fig. 10.17c, one sees that the Nipigon diabase sills resemble the upper part of the upper volcanic unit. Any chalcophile elements that have been removed from the contaminated magma that extruded to form the lavas at the base of the Upper unit might therefore have been inherited by magma that intruded to form the Nipigon sills. These sills are part of the Logan sills of the Lake Superior region, which are not noted for their Ni sulfides. Analogies with Noril'sk, however, suggest many marked similarities.

The Lake Superior area has the correct regional tectonic setting (triple junction and associated rifting), has a widespread development of basalt, and some of the basalts show evidence of chalcophile element depletion.

What then is missing from the equation in the Lake Superior area that so far has precluded a "Giant", Noril'sk-type deposit being found there?

One obvious point is the lack of recognition of major faults of trans-crustal magnitude, that have served as the locus for ore-bearing magma. Listerud and Meineke (1977), estimated that deposits along the western margin of the Duluth Complex contain $>4x10^9$ tonnes of ore averaging 0.66 wt % Cu, 0.2 wt% Ni. However these sulfides are thought to be the result (Mainwaring and Naldrett 1977; Ripley 1986) of near-surface assimilation or absorption of rock sulfur from supra-crustal rocks, by fractionated, probably partially crystalline magma, close to the present site of the deposits. Close control of magmatism by deep faults may be prerequisite for the focussing of mineralization of this kind. A second difference is the failure (so far) to distinguish in the Lake Superior area a "network" of feeder conduits for the Keweenawan lavas within sulfur-bearing country rocks. The closest analogy to the "Main Bodies" of the intrusions at Noril'sk, is the Crystal Lake gabbro (see Chap. 4). It should be noted that the Noril'sk mineralized intrusions occur at the very center of the volcanic basin, and have been brought to surface by a structural arch. Perhaps similar deposits lie many kilometers beneath Lake Superior.

## 10.2 Exploration for PGE in Layered Intrusions: Concepts and Methods

The main differences between PGE-rich magmatic sulfide ores and typical Ni-Cu ores include:

1. The former tend to occur as relatively weak disseminations of sulfide within silicate rocks and chromitites, rather than as massive concentrations.
2. Many deposits occur at specific, clearly defined horizons within layered intrusions, with no particular association with the base.
3. They often show an association with chromite, either occurring as very sparse sulfides within massive chromitite, or within strata which also contain small amounts of chromite, in contrast to chromite-free strata above and below the mineralized horizons.
4. The Merensky Reef and Upper Group chromitites of the Bushveld Complex, the J-M Reef of the Stillwater Complex and the mineralized horizons of the Penikat and Portimo intrusions occur closely associated with plagioclase-bearing rocks, within a few 100 m above the first appearance of cumulus plagioclase in their respective layered intrusions.

The Main Sulfide Zone of the Great Dyke of Zimbabwe is an exception to this rule. In general, chromitite layers that occur at horizons below the incoming of cumulus plagioclase in layered intrusions are much lower in PGE, and have a much lower (Pt+Pd)/(Ru+Ir+Os) ratio than those that occur above, although the A chromitite of the Stillwater and the 1d Chromitite of the Great Dyke are exceptions.

5. In both the Bushveld and Stillwater Complexes, isotope ratios, and cryptic variation and the sequence of appearance and disappearance of cumulus phases in cyclic units, in igneous strata close to those carrying PGE mineralization suggest that the interaction of two magmas was involved in the crystallization of these units. In the Bushveld, Stillwater and Pennikat and Portimo of Finland intrusions it has been shown that the first magma was marked by having high concentrations of MgO, $SiO_2$, and Cr and a low content of $Al_2O_3$, while the second magma was tholeiitic in type.
6. The presence of hydrous minerals, high Cl/F ratios in apatite, high Cl in biotite, fluid inclusions, graphite and pegmatoidal recrystallization suggest that the Merensky and J-M Reefs concentrated volatiles more than their surrounding rocks.

Throughout this book, variation in magma/sulfide ratio (R Factor) has been proposed as the explanation for differences in the tenors of chalcophile metals in the sulfides of magmatic sulfide deposits. PGE deposits are particularly clear examples of the role of R Factor in controlling the tenor of sulfides. Since a very small amount of sulfide with a very high tenor of PGE is sufficient to produce a deposit, the removal of this sulfide, while affecting the PGE content of the magma, may not result in significant Ni and Cu depletion in the magma. This rules out some of the exploration criteria described above for exploring for Ni-Cu ores (Ni versus MgO in volcanics, Ni content of olivine and Cu/Zr ratios). It is possible that depletion of PGE in silicates could be used in the same way as Ni, but as a much more sensitive indicator in view of their much higher partition coefficients. However, at the present time, the analytical problem of detecting PGE at the ppb or sub-ppb level in silicate grains remains insoluble, and other approaches are necessary.

It is shown in Chap. 9 that Campbell et al.'s (1983) model of magma mixing in a turbulent plume can account for sulfide immiscibility, the achievement of a high magma/sulfide ratio, the characteristics of both the J-M and Merensky Reefs, including their high volatile contents, and the association of PGE-rich sulfides with chromite (in the Merensky Reef). This model requires plagioclase to have started to crystallize within a layered intrusion, and thus would direct attention to that part of the cumulus

pile just above which plagioclase-bearing rocks first occur. This would have been successful in directing exploration towards the UG-2, Merensky and J-M Reefs, and much of the mineralization in the Penikat and Portimo intrusions, but it would not have drawn attention to the Lower and Main Sulfide Zones of the Great Dyke or mineralization in the Skaergaard or Sonju Lake intrusions.

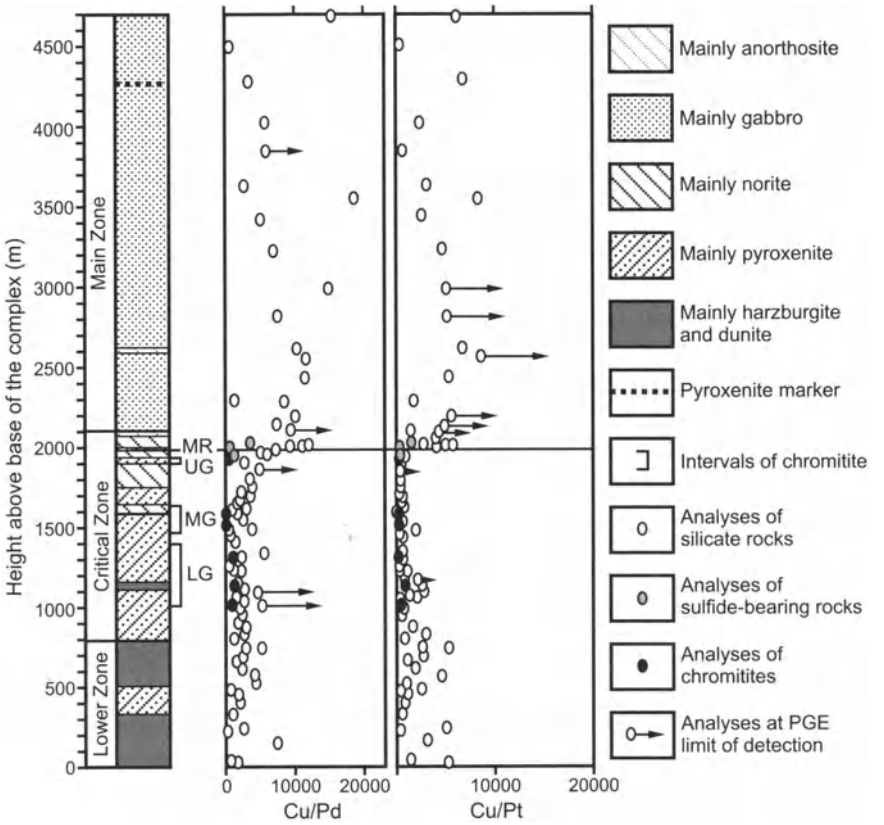


**Fig. 10.18.** Cu/Pd and Cu/Pt ratios in the Lower, Critical, and Main Zones at Union section, Bushveld Complex (from Maier et al. 1996)

There is a growing body of evidence that bulk analyses of rocks, using existing analytical techniques, can serve to draw attention to mineralized horizons. This is discussed below with respect to the Bushveld and Fox River intrusions.

### 10.2.1 Use of Cu/Pd and Cu/Pt ratios in bulk rock compositions (example of the Bushveld Complex)

Maier et al. (1996) and Li et al. (2001b) have studied variations of Cu/Pd and Cu/Pt ratios through the stratigraphy of the Bushveld Complex (Fig. 10.18). The principal behind using this ratio is that while Pt, Pd and Cu all partition into a sulfide phase once it develops, Pt and Pd do so much more strongly than Cu, because of their much higher partition coefficients. The result is that their concentrations in the magma decrease more rapidly than Cu, with a resulting increase in the Cu/Pd and Cu/Pt ratios. If the location of the UG-2 and Merensky Reefs in the Bushveld stratigraphy were unknown, the sharp increase in both ratios would have focused attention on this particular portion of the stratigraphic succession (Fig. 10.18).

### 10.2.2 Use of variation of PGE contents in bulk rock compositions and calculated PGE tenors in sulfides (example of the Fox River Sill)

#### *Geology of the Fox River Sill*

The Fox River Sill occurs within the Fox River Belt, which, along with the Thompson Belt, forms the northwestern margin of the Superior Province in Manitoba, Canada (Fig. 10.19). The Fox River belt borders the northern edge of the Superior Province for about 300 km (approximately half of the belt lies beneath Paleozoic cover rocks, although geophysical data attest to its presence) and is part of the Circum-Superior Boundary Zone (Baragar and Scoates 1981). The belt is a 15–20 km-wide, north facing homoclinal, supracrustal sequence comprising sedimentary and volcanic rocks, as well as mafic/ultramafic differentiated intrusions of Early Proterozoic age. Volcanic rocks comprise about 40 percent of the rocks of the belt. They form two sequences referred to as the Lower and Upper Volcanic formations separated by the Middle Sedimentary formation which is a sequence of fine-grained, quartz-rich terrigenous rocks. The Fox River sill, which is 275 km long, has intruded the Middle Sedimentary formation. The Upper Volcanic Formation, lying above the sill, consists of a lower zone of layered, differentiated flow units and komatiitic basalt flows, a middle zone of pillowed olivine clinopyroxenite and massive and layered komatiitic basalt flows and an upper zone of massive and pillowed basalt. It is interpreted to represent magma flushed out of the Fox River Sill chamber at different stages in its development.

The rocks of the Fox River Belt are similar lithologically to Proterozoic supracrustal rocks of the Thompson Nickel Belt. These latter rocks, known

as the Opswagan Group, contain abundant ultramafic rocks, some of which host nickel sulfide ore deposits (see Chap. 3). Initially, the Fox River Belt and Opswagan Group rocks were believed to be of the same age. However, Heeman et al. (1986) have shown that the Fox River Sill and a group of dykes known as the Molson dykes, that occur within the Superior Province, have the same age (1.883 Ga). Molson dykes have been documented cutting Opswagan Group rocks; thus the Opswagan group is considered to be older than the Fox River Belt rocks.

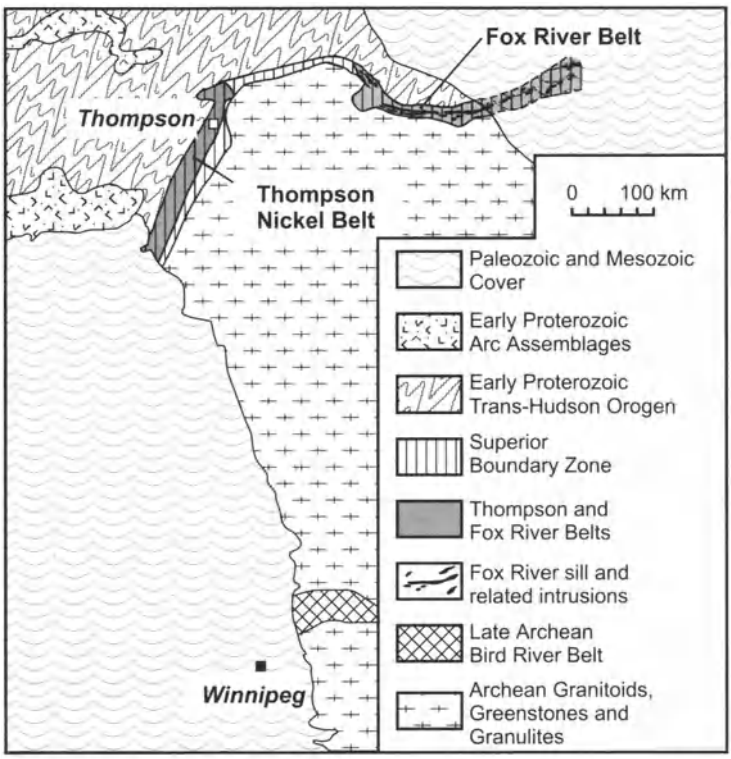


**Fig. 10.19.** Generalized geological map showing locations of the Thompson and Fox River Belts at the margin of the Superior Province in Manitoba, Canada. (from Peck et al. 2002)

This following discussion is based on the study by Naldrett et al. (1994b) on PGE variation in samples collected from holes drilled by BP Resources at the western extremity of the sill. In this area, as seen in Fig. 10.20, the sill consists of the Marginal Series, the Main Layered Series (comprising the Lower and Upper Central Layered Zones) and the Hybrid Roof Series.

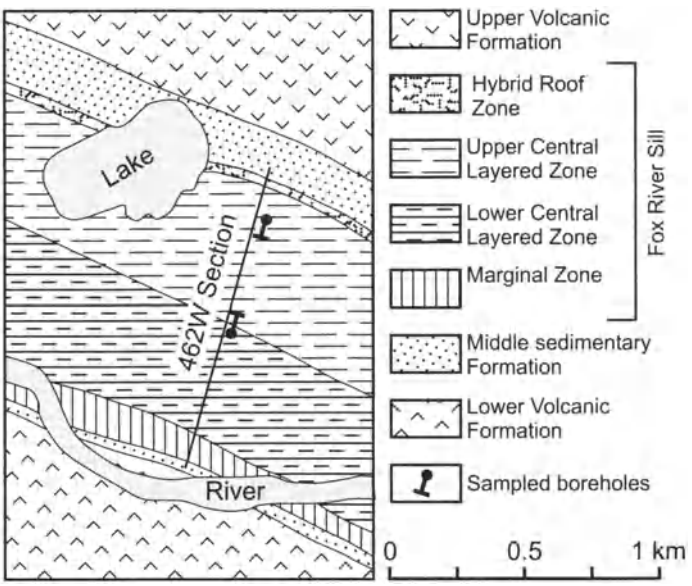


**Fig. 10.20.** Geologic map illustrating the units of the Fox River sill (after Scoates and Eckstrand 1986) and the section line (462 W) on which the holes sampled by Naldrett et al. (1994b) were drilled

The Lower Central Layered Zone (LCLZ) is approximately 900 m thick and consists of a simple succession of cyclic units, each of which comprises a lower, relatively thick olivine cumulate layer and an overlying, relatively thin clinopyroxene cumulate layer. The Upper Central Layered Zone, or UCLZ, consists of 1000 m of layered dunite, peridotite, pyroxenite and gabbro forming cyclic units. Layers range from <1 m up to several 10's of m in thickness.

The stratigraphic sequence that was studied by Naldrett et al. (1994b) comprises a 610 m vertical section extending from the top of the LCLZ to over half way up the UCLZ. This portion can be considered as consisting of 4 intervals, which are referred to as "regimes" in Fig. 10.21. Each regime is distinctive with regard to its crystallization.

Regime 1 extends from 0 to 125 m and overlies the dunite of the LCLZ. It consists of alternating layers of peridotite and olivine pyroxenite. Regime 2 (125–245 m) is characterized by the appearance of plagioclase cumulates. Regime 3 (245–380 m) is marked by much thicker layering, many layers exceeding 10 m. Classic cyclic units are absent and the stratigraphy is complicated by an intrusion of ilmenite gabbro. Regime 4 starts at 380 m; it is characterized by a series of cyclic units which pass from peridotite (or olivine pyroxenite) at the base, through olivine pyroxenite to gabbro at the top.

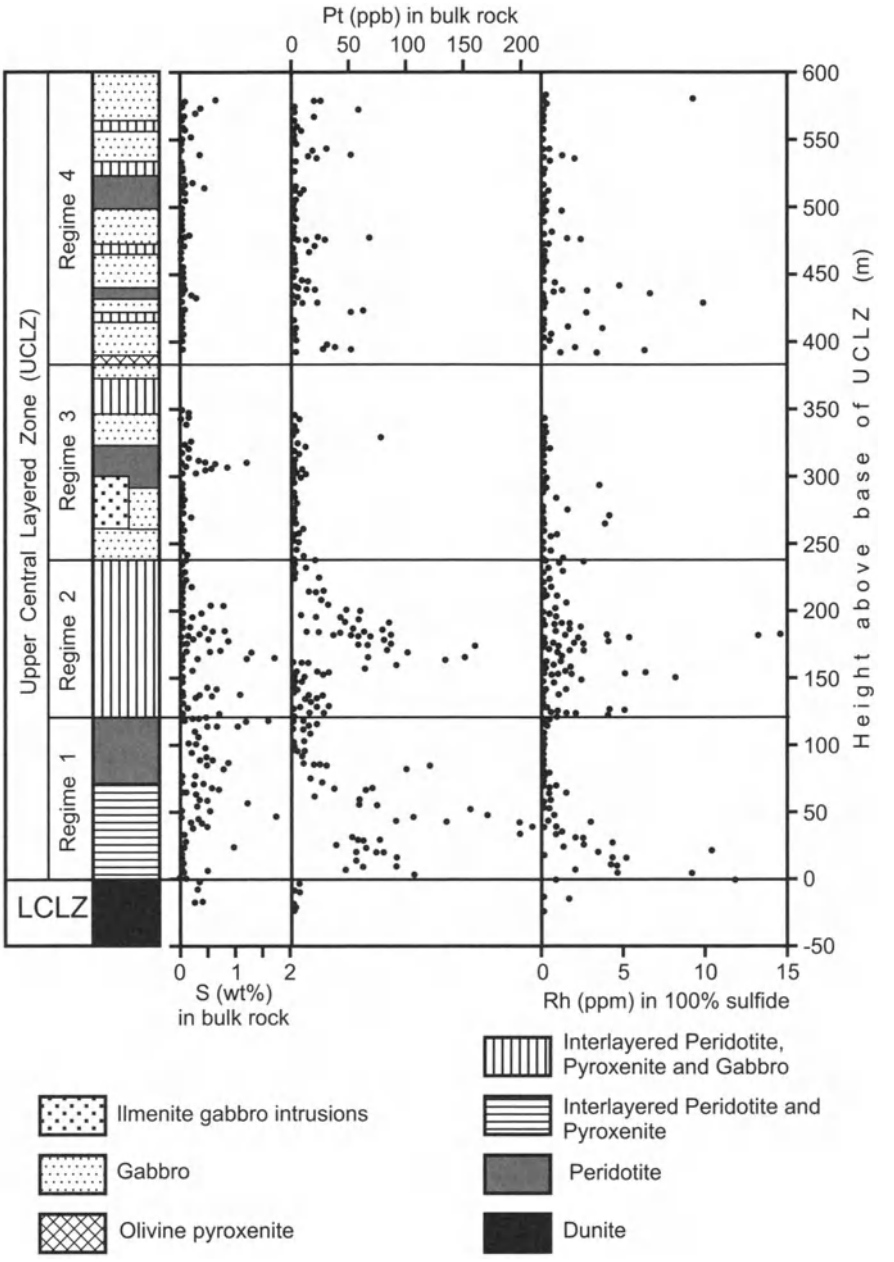


**Fig. 10.21.** Variation in wt% S, ppb Pt in bulk rock and ppb Rh in 100% sulfide from -16 to 590 m above the base of the UCLZ in the Fox River Sill. From Naldrett et al. (1994b)

### *Distribution of Sulfide Mineralization and PGE in vertical section of the sill*

The distribution of sulfide zones is illustrated in the plot of wt% sulfur against height in Fig. 10.21. The dunite at the top of the LCLZ is characterized by 0.2–0.4 wt% S. This drops sharply at the base of regime 1 of the UCLZ, at 0 m, before rising to 0.3–0.5 wt% 37 m above the base, and remaining at or above this concentration in the majority of samples to 89 m. Above this and extending up to 205 m, background levels of sulfur occur separated by several short intervals within which sulfur contents reach 1 wt% and more. Above 205 m and extending to 438 m, the S of nearly all the samples is below 0.1 wt%, except for a restricted horizon at about 310 m. Above the 438 m level, within regime 4, several short intervals with 0.2 to 0.6 wt% S are present. These are associated with rocks that occur at or close to the bases of the cyclic units that constitute this regime.

Figure 10.22 is an enlargement of the lower 280 m of Fig. 10.21. The upper part of the LCLZ is marked by generally very low PGE, both in bulk rock and when recalculated on the basis of metal content in 100% sulfide, illustrated here by Pt and Rh. Cu is at or near the detection limit of 10 ppm in bulk rock, while Ni is between 2000 and 3000 ppm, so that the Cu/(Cu+Ni) ratios are very low.

The base of regime 1 of the UCLZ, above the 0 m level, is marked by sulfur contents of about 1/4 of the values of the LCLZ, but by very much higher levels of Pt, Pd and Rh in bulk rock and in 100% sulfides. Cu increases abruptly by a factor of 10–30 at the base of the UCLZ, and Ni decreases equally abruptly by a factor of 3–4, so that there is a very sharp rise in the Cu/(Cu+Ni) ratio.

A decrease in all PGE when calculated as concentrations in 100% sulfides begins at 37 m above the base of the UCLZ. This is associated with a pronounced increase in the sulfur content of the rock and characterizes the PGE-rich zone occurring between 37 and 89 m. The PGE levels in sulfides decrease rapidly from 37 m to 47 m, and then undergo three oscillations, but continue decreasing overall to reach very low concentrations at 89 m. They remain at these concentrations to 120 m where sulfides disappear from the profile. The Cu/(Cu+Ni) ratio shows a similar decrease, with matching oscillations, also reaching a very low value at 89 m and remaining low to 120 m.

At the base of regime 2, at 125m, PGE concentrations in 100% sulfides start to increase rapidly over the sulfide absent interval to 137 m, where another increase in the sulfide content of the rock is associated with the almost complete elimination of PGE from the immediately overlying rocks. With the abrupt decrease in sulfide content at 144 m, the PGE con-

centrations in 100% sulfides increase again over the following sulfide-absent interval to 160 m.

Significant amounts of sulfide reappear in the rocks at 160 m and remain to 205 m, but, despite this, PGE levels in both sulfides and bulk rock remain relatively high. In general, the PGE content of the sulfides is not nearly as sensitive to sulfide removal over this interval as it is elsewhere in the profile. Another difference is that while between the base of the UCLZ and 120 m, the Cu/(Cu+Ni) ratios parallel the behaviour of PGE closely, between 120 and 200 m the Cu/(Cu+Ni) ratios appear decoupled from the PGE.

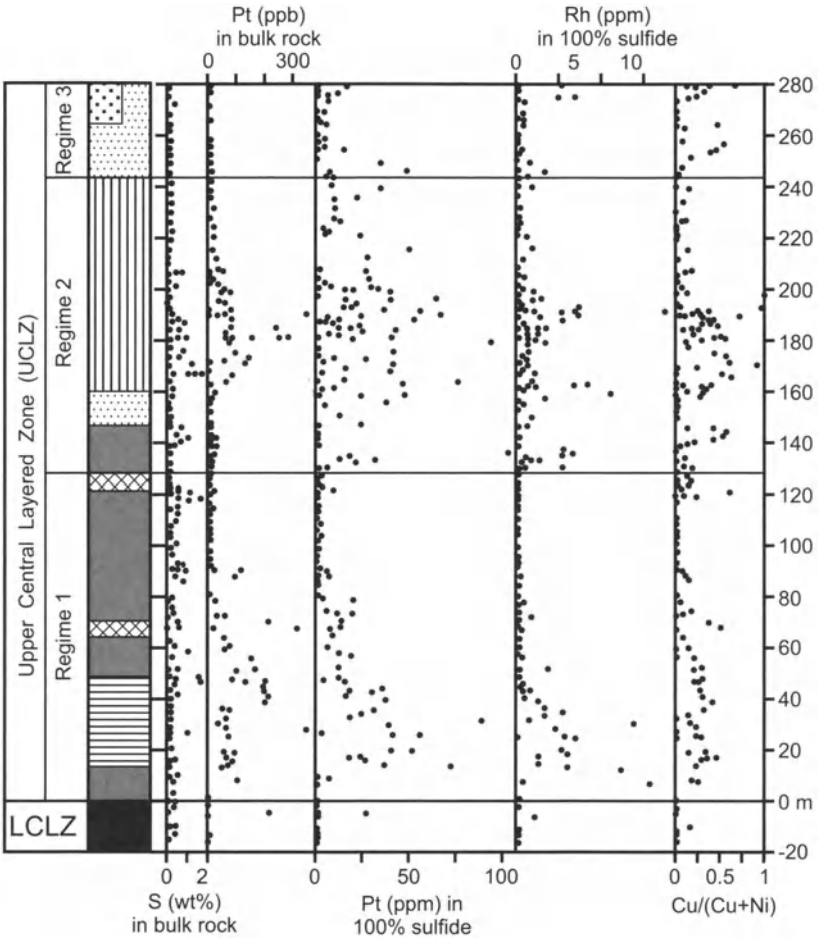


**Fig. 10.22.** Variation in wt% S, ppb Pt in bulk rock, ppb Pt and Rh in 100% sulfides, and Cu/(Cu+Ni) ratios from -16 to 280 m above the base of the UCLZ in the Fox River Sill. See Figure 10.21 for legend. From Naldrett et al. (1994b)

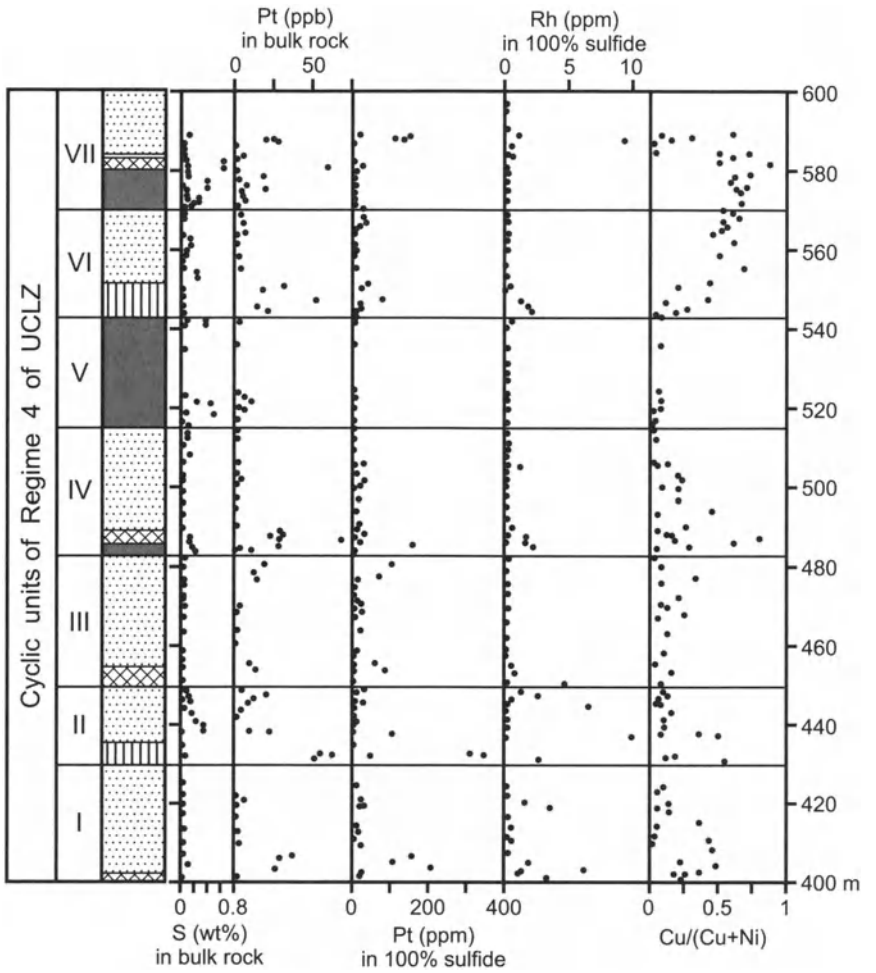


**Fig. 10.23.** Variation in wt% S, ppb Pt in bulk rock, ppb Pt and Rh in 100% sulfides, and Cu/(Cu+Ni) ratios from 400 to 590 m above the base of the UCLZ in the Fox River Sill. See Figure 10.21 for legend. From Naldrett et al. (1994b)

The section between 400 and 590 m, belonging to Regime 4, is shown in Fig. 10.23. It consists of 7 cyclic units. Most range from peridotite or olivine pyroxenite at the base to gabbro at the top. In contrast to the preceding regimes, sulfides occur at or near the base of many units, and in units II, IV and VI the PGE level in 100% sulfides decrease relatively systematically upward in each unit. No sulfides are associated with unit III, which passes directly from peridotite to gabbro; across this both the PGE levels and the Cu/(Cu+Ni) ratio increase.

### *Interpretation of PGE and Cu variation*

Interpretation of the behavior of these metals can be accomplished on the basis of certain initial premises. These are:

1. That Pt, Pd, Rh and Cu are essentially incompatible in the common rock-forming minerals, except for sulfide.
2. That Ni is compatible in both olivine and sulfide and weakly compatible in pyroxene.
3. That the sulfides represent stratigraphic marker horizons, and have not diffused through the cumulus pile, or been changed in composition subsequently.

The very low Pt, Pd, Rh and Cu contents of the LCLZ samples, coupled with their relatively high sulfide content, indicates that this sulfide has formed from magma that has become depleted in chalcophile elements through reaction with sulfide. In contrast, the absence of appreciable sulfide in the UCLZ magma indicates that it was unsaturated with sulfide when it was emplaced. Chalcophile elements such as Pt, Pd, Rh and Cu are high, indicating that it is unlikely that it ever reacted with sulfide. The jump in the sulfide content to over 1 wt% above the 37 m level suggests that this is the stage at which sulfide saturation was achieved and the magma started to become depleted in PGE; this accounts for the trends of decreasing PGE in 100% sulfide from this point upwards. The Cu/(Cu+Ni) ratio increases sharply at 37 m, reflecting the additional Cu added to the rock by the incoming of cumulus sulfides, but above this starts to decrease, due to Cu being removed from the magma more rapidly than Ni and this being reflected in the Cu content of the sulfides. The three coincident oscillations in PGE levels and Cu/(Cu+Ni) ratio that I have pointed out are present between 40 and 89 m are interpreted as the consequence of influxes of new magma refreshing the levels of these elements in the zone of crystallization.

Despite the presence of significant sulfide, the rocks between 89 and 125 m are very low in PGE and Cu, indicating the extent to which the magma responsible for these particular rocks had become chalcophile element-depleted, and the fact that during the crystallization of this interval, no fresh influxes of magma entered the zone of crystallization.

Above 125 m, PGE build up progressively over zones with little sulfide, and drop abruptly with the appearance of cumulus sulfides, reflecting the periodic inflow of new magma, followed after an interval of crystallization, by sulfide saturation and segregation. This behavior continues to the 160 m level, but, above this, the PGE levels in sulfides remain fairly high

to 205 m, despite the presence of significant sulfide; over this interval the PGE level in 100% sulfides is not nearly as sensitive to sulfide removal as it was in regime 1. Also, as I have mentioned previously, the Cu/(Cu+Ni) ratio shows only a slight variation as a result of fractionation due to sulfide segregation. These observations, coupled with the rapid alternations in layering which are present, are interpreted as the result of very frequent mixing with fresh magma which has influenced crystallization in the magma chamber during this period.

Despite there being some horizons with appreciable sulfide, regime 3 is characterized by very low levels of Pt, Pd and Rh throughout. It would seem that it was a period of stabilization in the magma chamber, during which new magma was not introduced.

In regime 4, the increase in sulfide in bulk rock present at or near the base of units II, IV, and VI, together with the coincident increase in the PGE level in 100% sulfides, suggests that these are classic cyclic units that were initiated by inputs of fresh magma that also partially replenished the PGE levels within the magma chamber.

Figure 10.24 has been modified after that by Li et al. (2001a) (shown in Chap. 2 as Fig. 2.5) for the purpose of explaning the variation in S content of a magma such as that responsible for the Fox River Sill as it undergoes fractional crystallization. Note that compositions lying above and to the right of the curve will be saturated in sulfide, those lying below and to the left will be unsaturated. A primitive magma such as that represented by point A, on undergoing fractional crystallization, will move along the path A–B. An influx of fresh magma of composition A that mixes with the fractionated magma in the chamber before this has reached B will pull the bulk composition back towards A, initiating a new cyclic unit. No sulfides will be present in the rocks forming during these early stages, except for the small amount segregating from any trapped intercumulus liquid as this crystallizes, because the magma is unsaturated with sulfide. Eventually, during the crystallization of a cyclic unit, the composition of the magma will reach B, sulfides will start to segregate and will be part of the cumulate assemblage, together with olivine and/or pyroxene, as the magma moves down the curve towards C. The initial sulfides will be rich in PGE, but will become progressively less rich as their fractional segregation lowers the PGE concentration in the magma. Introduction of fresh magma of composition A and its mixing with that in the chamber with the composition E will do a number of things: firstly it will pull the composition of this off the sulfide saturation curve into the undersaturated region, possibly to reach a composition represented by point (D), secondly it will, at the same time, replenish the PGE concentrations in the magma chamber to some

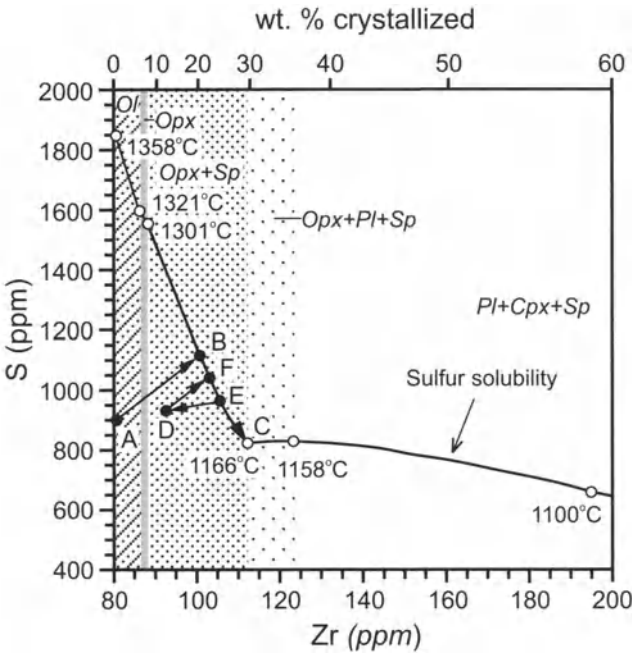


**Fig. 10.24.** Schematic diagram, modified after Li et al. (2001a), and similar to that of Fig. 2.5, showing the variation in the solubility of sulfide in a magma such as that responsible for the Fox River Sill

degree, and thirdly it will initiate another cyclic unit. Continued crystallization of magma D will lead to the magma rejoining the sulfide saturation curve at a point such as (F), PGE-enriched sulfides will start to segregate again, and the cycle will continue. Numerous cycles of this type can develop. Note that during this stage, sulfide saturation and the development of PGE-enriched zones will develop **during** the crystallization of a cyclic unit, **not** at its base; mineralization will not therefore be associated with the base of the unit. This stage accounts for many of the characteristics of the mineralization in regime 1 of the UCLZ.

If one accepts the hypothesis, proposed in Chap. 9, that magma mixing will induce sulfide saturation for magmas that have entered the field of plagioclase stability, the sulfide and PGE concentrations at the base of cyclic units in the upper part of the UCLZ (regime 4) are to be expected.

### *Summary and discussion of relevance to exploration*

In summary, four distinct regimes of crystallization have been identified within the UCLZ. The lowermost, regime 1, is marked by relatively closed system crystallization, the attainment of sulfide saturation during this crys-

tallization, and strong fractionation of PGE from this stage on into the segregating sulfide. Regime 2 appears to have been characterized by largely open system crystallization, with frequent replenishment of magma, which obscures trends due to fractionation. Regime 3 corresponds to the stabilization of the magmatic system during which no fresh magma entered the chamber. In Regime 4 the magma crystallized as a series of classic cyclic units.

The study of the Fox River Sill indicates that the validity of using trace levels of PGE, outside the limits of mineralization, to indicate the proximity of this mineralization depends on how the intrusion in question has behaved. In the Fox River Sill, the contrast between the high levels of Pt (about 40,000 ppb) and Rh (about 5000 ppb) in 100% sulfides below the mineralization in regime 1 and the low values (<1000 ppb for Pt; < 200 ppb for Rh) above is clear and of practical application. Analyses of these two zones would inevitably guide one to the mineralized zone that lies between them (anywhere between 37m and 89 m) where sulfides might be concentrated. A contrast of this kind is not seen in what is interpreted as the open system environment of regime 2.

In regime 4, the precipitation of sulfides commonly coincides with the influx of new, PGE-rich magma into the zone of crystallization, and the initiation of cyclic units. The result is that PGE depletion starts as soon as the magma in the chamber is replenished in these elements, so that little or no "warning" of replenishment is recorded in cumulates that have formed before sulfides start segregating.

In the general application of this approach in exploration, it is very important to understand the nature of the crystallization that occurred at different levels in an intrusion including: (i) was the magma acting as an essentially open system, with an almost constant inflow of fresh magma, or was it crystallizing in a more closed environment with only intermittent inflow? (ii) was the magma in a composition range in which the sulfur content built up in the magma as silicates crystallized and thus sulfide saturation was reached, or did saturation occur immediately as a result of the mixing of fresh magma with that already in the chamber? In this second case the sulfides could be expected to occur near the base of a cyclic unit and little "build up" in PGE would recorded in the rocks below the level of a mineralized horizon. These questions can be answered from a relatively straightforward study of an intrusion, the nature of its layering, and the chemical variation in major and trace elements.

# Appendix

## Concentrations of Ni, Cu and Noble metals in 100% sulfides, for different types of ore deposits

Ni and Cu in wt%; Noble metals in ppb (mg/t)

For the ratio (Pt+Pd)/(Ni+Cu) PGE in ppm (g/t); Ni,Cu in wt%

R = References for data used: 1 = Naldrett, Unpublished Data; 2 = Barnes and Naldrett (1987); 3 = Green and Naldrett (1981); 4 = Cowden et al. (1986); 5 = Good and Naldrett (1993); 6 = Bleeker (1990); 7 = Hauck et al. (1997); 8 = Lightfoot et al (1983); 9 = Brugmann et al. (2000); 10 = Chai and Naldrett (1992); 12 = Barnes and Naldrett (1985); 13 = Naldrett (1989); 14 = Brugmann et al. (1989); 15 = Alapieti and Lahtinen (2002); 16 = Published independent resource estimate of Derry, Michener, Booth and Wahl, September 2002, with estimate of sulfide content and Rh, Ir and Ru data from Figure 9 of James et al. (2002); 17 = interpolated from Fig. 9 of James et al. (2002)

| | Ni | Cu | Pd | Pt | Rh | Ir | Os | Ru | Au | (Pt+Pd)/(Ni+Cu) | R |
|---|---|---|---|---|---|---|---|---|---|---|---|
| **Archean Komatiite Magmatism** | | | | | | | | | | | |
| ***Ontario, Canada*** | | | | | | | | | | | |
| Alexo | 6.42 | 0.43 | 2 909 | 1 112 | 157 | 38 | 57 | 309 | 284 | 0.59 | 2 |
| Dundonald prospect | 31.83 | 0.49 | 4 942 | 4 623 | 685 | 459 | 519 | 2 208 | 1 230 | 0.30 | 2 |
| Hart prospect | 3.57 | 0.11 | 568 | 233 | 76 | 43 | 51 | 167 | 70 | 0.22 | 2 |
| Texmont Mine | 25.22 | 1.05 | 3 185 | 1 832 | 405 | 344 | 562 | 1 943 | 883 | 0.19 | 2 |
| Langmuir Mines 1 and 2 | 12.33 | 0.49 | 1 146 | 609 | 189 | 195 | 325 | 607 | 91 | 0.14 | 3 |
| ***Zimbabwe*** | | | | | | | | | | | |
| Epoch mine | | | | | | | | | | | |
| *Disseminated ore* | 30.12 | 1.69 | 9 200 | 4 174 | 1 162 | 451 | 497 | 3 126 | 706 | 0.42 | 1 |
| *Massive and rich disseminated ores* | 20.73 | 0.32 | 1 239 | 562 | 1 460 | 583 | 637 | 4 911 | 146 | 0.09 | 1 |
| Shangani Mine | | | | | | | | | | | |
| *Disseminated ore* | 19.79 | 1.40 | 6 087 | 2 545 | 635 | 205 | 260 | 1 505 | 340 | 0.41 | 1 |
| *Massive ore* | 13.18 | 0.76 | 2 441 | 712 | 699 | 102 | 98 | 1 078 | 34 | 0.23 | 1 |
| Trojan Mine | | | | | | | | | | | |
| *Disseminated ore* | 16.32 | 1.43 | 2 688 | 1 617 | 368 | 224 | 243 | 1 149 | 169 | 0.24 | 1 |
| *Massive ore* | 10.76 | 1.06 | 2 262 | 881 | 357 | 149 | 160 | 1 092 | 182 | 0.27 | 1 |
| Perseverance | 2.97 | 1.20 | 1 818 | 594 | 183 | 27 | 15 | 109 | 86 | 0.58 | 1 |
| ***Kambalda, Australia*** | | | | | | | | | | | |
| Fisher | 14.71 | 0.91 | 1 916 | 1 588 | 297 | 207 | 472 | 847 | 5 413 | 0.22 | 4 |
| Juan | 13.02 | 0.87 | 1 750 | 1 666 | 295 | 225 | 512 | 961 | 529 | 0.25 | 4 |
| Durkin | 17.82 | 1.33 | 3 004 | 2 033 | 485 | 332 | 772 | 1 492 | 674 | 0.26 | 4 |

| | Ni | Cu | Pd | Pt | Rh | Ir | Os | Ru | Au | (Pt+Pd)/(Ni+Cu) | R |
|---|---|---|---|---|---|---|---|---|---|---|---|
| Lunnon | 12.71 | 1.00 | 1 884 | 1 553 | 245 | 190 | 417 | 675 | 4 453 | 0.25 | 4 |
| Ken | 13.60 | 1.20 | 2 071 | 1 200 | 299 | 209 | 479 | 874 | 439 | 0.22 | 4 |
| Jan | 17.48 | 1.29 | 3 500 | 1 597 | 424 | 244 | 542 | 1 116 | 506 | 0.27 | 4 |
| Hunt | 10.43 | 0.80 | 1 262 | 1 297 | 196 | 181 | 330 | 765 | 4 461 | 0.23 | 4 |
| McMahon | 11.37 | 0.88 | 1 520 | 756 | 256 | 210 | 386 | 849 | 338 | 0.19 | 4 |
| Carnelia Hill | 18.84 | 1.15 | 3 155 | 1 466 | 438 | 411 | 752 | 1 382 | 307 | 0.23 | 4 |
| **Proterozoic Komatiite Magmatism** | | | | | | | | | | | |
| ***Raglan*** | | | | | | | | | | | |
| Donaldson West | 14.98 | 3.34 | 11 521 | 3 304 | 895 | 385 | 435 | 2 409 | 377 | 0.81 | 1 |
| Katinik | 10.32 | 2.83 | 6 653 | 3 238 | 581 | 209 | 315 | 1 191 | 212 | 0.75 | 1 |
| ***Thompson Nickel Belt*** | | | | | | | | | | | |
| Pipe | 3.95 | 0.16 | 117 | 52 | 34 | 54 | 105 | 214 | 58 | 0.04 | 1 |
| Bucko | 25.76 | 3.38 | 6 922 | 2 354 | 491 | 433 | 819 | 1 275 | 278 | 0.32 | 5 |
| Thompson | 8.65 | 0.40 | 1 853 | 346 | 159 | 113 | 144 | 248 | 147 | 0.24 | 6 |
| Manibridge | 10.00 | 0.75 | 2 600 | 950 | 260 | | | | 240 | 0.33 | 13 |
| **Flood Basalt Magmatism** | | | | | | | | | | | |
| ***Talnakh Ore Junction*** | | | | | | | | | | | |
| Kharaelakh | | | | | | | | | | | |
| *Disseminated ore* | 4.35 | 10.02 | 19 190 | 5 211 | 307 | 38 | 42 | 62 | 1 944 | 1.70 | 1 |
| *Massive ore* | 3.84 | 4.82 | 8 097 | 1 801 | 464 | 38 | 23 | 54 | 125 | 1.14 | 1 |
| *Oktyabrsky Cu-rich ore* | 2.82 | 22.02 | 44 426 | 9 202 | 149 | 16 | 12 | 4 | 3 055 | 2.16 | 1 |
| *Upper Copper Ore* | 3.58 | 16.94 | 35 504 | 3 407 | 143 | 8 | 24 | 14 | 12 201 | 1.90 | 1 |

| | Ni | Cu | Pd | Pt | Rh | Ir | Os | Ru | Au | (Pt+Pd)/(Ni+Cu) | R |
|---|---|---|---|---|---|---|---|---|---|---|---|
| Eastern Kharaelakh | | | | | | | | | | | |
| *Disseminated ore* | 5.86 | 11.83 | 31 253 | 7 726 | 1 075 | 86 | 68 | 185 | 1 760 | 2.20 | 1 |
| *Massive ore* | 4.89 | 11.09 | 14 501 | 2 371 | 663 | 30 | 19 | 36 | 606 | 1.06 | 1 |
| Talnakh | | | | | | | | | | | |
| *Disseminated ore* | 5.68 | 8.86 | 25 269 | 8 130 | 1 358 | 145 | 101 | 302 | 1 292 | 2.30 | 1 |
| *Massive ore* | 5.54 | 4.72 | 9 616 | 2 387 | 1 483 | 153 | 83 | 307 | 126 | 1.17 | 1 |
| ***Noril'sk Ore Junction*** | | | | | | | | | | | |
| Noril'sk-1 | | | | | | | | | | | |
| *Disseminated ore* | 8.36 | 14.08 | 67 262 | 39 916 | 2 991 | 518 | 302 | 1 077 | 5 529 | 4.78 | 1 |
| *Massive ore* | 6.85 | 4.77 | 24 621 | 9 417 | 6 357 | 747 | 283 | 1 157 | 692 | 2.93 | 1 |
| Noril'sk-2 | | | | | | | | | | | |
| *Disseminated ore* | 5.90 | 7.46 | 45 097 | 15 177 | 4 809 | 450 | 352 | 741 | 1 195 | 4.51 | 1 |
| Mt. Chernaya | | | | | | | | | | | |
| *Disseminated ore* | 9.85 | 12.87 | 71 274 | 29 760 | 4 918 | 461 | 293 | 855 | 11 601 | 4.45 | 1 |
| ***Duluth Complex*** | | | | | | | | | | | |
| Babbit | | | | | | | | | | | |
| *Disseminated ore* | 3.95 | 17.46 | 3 704 | 5 042 | 133 | 46 | 47 | 130 | 1 034 | 0.41 | 1 |
| Dunka Road | | | | | | | | | | | |
| *Disseminated ore* | 7.64 | 20.79 | 29 949 | 18 580 | | 382 | 212 | | 3 012 | 1.71 | 1 |
| *Massive ore* | 1.24 | 2.08 | 1 464 | 31 | | | | | 50 | 0.45 | 1 |
| Birch Lake | | | | | | | | | | | |
| *PGE-rich, low sulfide ore* | 25.61 | 15.76 | 494 457 | 544 099 | | 16 548 | 11 229 | | 15 957 | 25.10 | 7 |

| | Ni | Cu | Pd | Pt | Rh | Ir | Os | Ru | Au | (Pt+Pd)/(Ni+Cu) | R |
|---|---|---|---|---|---|---|---|---|---|---|---|
| ***Crystal Lake Gabbro, Ontario*** | | | | | | | | | | | |
| Great Lakes Nickel | | | | | | | | | | | |
| *Disseminated ore* | 4.23 | 8.03 | 16 614 | 4 215 | 458 | 57 | 96 | 282 | 1 945 | 1.70 | 1 |
| ***Karoo, South Africa*** | | | | | | | | | | | |
| Insizwa, Waterfall Gorge | | | | | | | | | | | |
| *Disseminated mineralization* | 5.91 | 6.42 | 6 334 | 2 639 | 266 | 355 | 186 | 420 | 2 199 | 0.73 | 8 |
| **Sudbury** | | | | | | | | | | | |
| ***South Range*** | | | | | | | | | | | |
| Creighton | | | | | | | | | | | |
| *Sublayer and inclusion sulfide* | 6.95 | 6.03 | 2 268 | 2 490 | 598 | 213 | 77 | 370 | 799 | 0.37 | 1 |
| *Massive Footwall ore* | 6.86 | 7.55 | 2 162 | 1 762 | 547 | 136 | 46 | 242 | 153 | 0.27 | 1 |
| Crean Hill | | | | | | | | | | | |
| *Sublayer and inclusion sulfide* | 4.79 | 4.74 | 3 313 | 4 521 | 599 | 142 | 63 | 310 | 830 | 0.82 | 1 |
| *Massive Footwall ore* | 3.48 | 3.81 | 3 125 | 1 897 | 382 | 66 | 27 | 158 | 321 | 0.69 | 1 |
| Gertrude | | | | | | | | | | | |
| *Sublayer* | 4.67 | 1.70 | 143 | 229 | 249 | 131 | 52 | 221 | 43 | 0.06 | 1 |
| Lindsley | | | | | | | | | | | |
| *Sublayer* | 3.93 | 3.56 | 1 764 | 2 007 | 335 | 107 | 46 | 180 | 566 | 0.50 | 1 |
| *Masive Footwall ore* | 2.56 | 6.30 | 8 594 | 3 506 | 359 | 45 | 20 | 83 | 702 | 1.37 | 1 |

| | Ni | Cu | Pd | Pt | Rh | Ir | Os | Ru | Au | (Pt+Pd)/(Ni+Cu) | R |
|---|---|---|---|---|---|---|---|---|---|---|---|
| ***North Range*** | | | | | | | | | | | |
| Trillabelle | | | | | | | | | | | |
| *Sublayer* | 2.72 | 1.48 | 376 | 396 | 77 | 28 | 21 | 81 | 618 | 0.18 | 1 |
| *Masive Footwall ore* | 2.87 | 0.80 | 295 | 459 | 50 | 15 | 7 | 48 | 44 | 0.21 | 1 |
| Onaping | | | | | | | | | | | |
| *Sublayer* | 4.74 | 0.54 | 79 | 114 | 377 | 97 | 34 | 218 | 14 | 0.04 | 1 |
| *Footwall ore* | 5.22 | 1.07 | 208 | 162 | 54 | 12 | 5 | 33 | 13 | 0.06 | 1 |
| McCreedy West | | | | | | | | | | | |
| *Sublayer* | 3.79 | 0.51 | 44 | 72 | 9 | 15 | 4 | 131 | 19 | 0.03 | 1 |
| *Cu-rich footwall ore* | 3.52 | 29.71 | 11 695 | 10 667 | 3 | 5 | 26 | 46 | 7 490 | 0.67 | 1 |
| Craig | | | | | | | | | | | |
| *Sublayer* | 5.71 | 1.04 | 454 | 83 | 15 | 3 | 2 | 6 | 573 | 0.08 | 1 |
| *Footwall ore* | 6.25 | 2.57 | 1 239 | 155 | 92 | 22 | 13 | 35 | 1 315 | 0.16 | 1 |
| McCreedy East | | | | | | | | | | | |
| *Sublayer* | 5.10 | 2.17 | 492 | 731 | 218 | 118 | 66 | 622 | 75 | 0.17 | 1 |
| *Cu-rich footwall ore* | 4.94 | 31.18 | 11 219 | 11 357 | 3 | 1 | 5 | 5 | 3 823 | 0.63 | 1 |
| Fraser | | | | | | | | | | | |
| *Sublayer* | 4.51 | 2.02 | 514 | 688 | 264 | 87 | 33 | 134 | 196 | 0.18 | 1 |
| *Footwall ore* | 5.21 | 2.41 | 840 | 1 083 | 117 | 37 | 17 | 69 | 85 | 0.25 | 1 |
| Strathcona | | | | | | | | | | | |
| *Sublayer* | 3.04 | 0.26 | 103 | 104 | 61 | 30 | 20 | 51 | 15 | 0.06 | 1 |
| *Cu-rich footwall ore* | 3.05 | 28.98 | 7 625 | 8 212 | 1 | 1 | 13 | 18 | 1 468 | 0.49 | 1 |
| Whistle | | | | | | | | | | | |
| *Sublayer* | 3.49 | 0.38 | 247 | 264 | 205 | 60 | 27 | 53 | 26 | 0.13 | 1 |

| | Ni | Cu | Pd | Pt | Rh | Ir | Os | Ru | Au | (Pt+Pd)/(Ni+Cu) | R |
|---|---|---|---|---|---|---|---|---|---|---|---|
| ***East Range*** | | | | | | | | | | | |
| Victor/Nickel Rim | | | | | | | | | | | |
| *Sublayer* | 4.61 | 1.69 | 663 | 1 202 | 289 | 132 | 56 | 201 | 106 | 0.30 | 1 |
| *Masive Footwall ore* | 5.21 | 0.50 | 424 | 525 | 77 | 24 | 12 | 40 | 26 | 0.17 | 1 |
| *Cu-rich footwall ore* | 4.78 | 35.58 | 11 518 | 16 224 | 3 | 2 | 196 | 39 | 2 674 | 0.69 | 1 |
| **Other areas** | | | | | | | | | | | |
| ***Pechenga*** | | | | | | | | | | | |
| Kaula | 10.24 | 7.31 | 495 | 349 | 45 | 34 | 54 | 101 | 294 | 0.05 | 9 |
| Pilgujarvi | 12.53 | 3.54 | 962 | 563 | 62 | 65 | 122 | 118 | 489 | 0.09 | 9 |
| Kotselvaara | 13.64 | 9.54 | 2 154 | 1 607 | 38 | 22 | 10 | 8 | 48 | 0.16 | 9 |
| Ortoavi | 13.56 | 5.16 | 2 500 | 2 328 | 48 | 25 | 11 | 7 | 165 | 0.26 | 9 |
| Kammikivi | 12.35 | 3.80 | 2 142 | 1 385 | 43 | 28 | 16 | 14 | 230 | 0.22 | 9 |
| ***Voisey's Bay*** | | | | | | | | | | | |
| Varied-textured Troctolite | 5.40 | 3.07 | 354 | 404 | 19 | 6 | 7 | 46 | 451 | 0.09 | 1 |
| Leopard Troctolite | 3.61 | 2.21 | 218 | 198 | 12 | 3 | 7 | 28 | 211 | 0.07 | 1 |
| Basal Breccia Sequence | 4.09 | 2.73 | 339 | 326 | 14 | 5 | 9 | 55 | 310 | 0.10 | 1 |
| Massive sulfide | 3.71 | 1.87 | 180 | 94 | 11 | 3 | 7 | 20 | 72 | 0.05 | 1 |
| ***Jinchuan*** | | | | | | | | | | | |
| Ore Body No 24 | 9.35 | 6.83 | 2 019 | 3 811 | 87 | 186 | 172 | 205 | 1 804 | 0.36 | 10 |
| Ore Body No 1 | 9.97 | 6.90 | 1 472 | 6 147 | 109 | 181 | 178 | 200 | 1 049 | 0.45 | 10 |
| Ore Body No 2 | 8.25 | 4.76 | 299 | 235 | 28 | 41 | 38 | 41 | 125 | 0.04 | 10 |

| | Ni | Cu | Pd | Pt | Rh | Ir | Os | Ru | Au | (Pt+Pd)/(Ni+Cu) | R |
|---|---|---|---|---|---|---|---|---|---|---|---|
| **PGE deposits** | | | | | | | | | | | |
| ***Bushveld*** | | | | | | | | | | | |
| Merensky Reef | | | | | | | | | | | |
| *Impala* | 16.06 | 5.66 | 97 894 | 257 513 | 14 035 | 5 516 | 4 958 | 33 236 | 29 466 | 16.36 | 11 |
| *Rustenburg* | 17.63 | 4.72 | 106 377 | 307 089 | 16 831 | 6 719 | 4 723 | 28 873 | 28 474 | 18.50 | 11 |
| UG-2 | | | | | | | | | | | |
| *Mandagshoek* | 14.68 | 10.91 | 1 391 715 | 1 490 580 | 220 545 | 133 087 | 0 | 492 424 | 32 321 | 112.63 | 11 |
| Platreef (Drenthe) | | | | | | | | | | | |
| *Upper Zone* | 5.06 | 5.80 | 14 603 | 8 437 | 324 | 88 | 111 | 577 | 2 750 | 2.12 | 1 |
| *Lower Zone* | 7.78 | 6.11 | 32 490 | 29 031 | 1 455 | 370 | 266 | 2 337 | 6 857 | 4.43 | 1 |
| ***Stillwater*** | | | | | | | | | | | |
| J-M Reef, | | | | | | | | | | | |
| Minneapolis Adit | 13.20 | 6.49 | 5 410 000 | 1 560 000 | 48 000 | 6 000 | 7 000 | 16 000 | 200 000 | 353.99 | 12 |
| ***Great Dyke*** | | | | | | | | | | | |
| Main Sulfide Zone, | | | | | | | | | | | |
| Hartley | 6.55 | 5.89 | 60 649 | 52 641 | 6 262 | 2 290 | 818 | 5 366 | 7 794 | 9.11 | 1 |
| ***Lac des Iles*** | | | | | | | | | | | |
| Robie Zone | 10.51 | 11.84 | 259 527 | 28 032 | 0 | 55 | 111 | 960 | 24 300 | 12.87 | 14 |
| ***Portimo Area, Finland*** | | | | | | | | | | | |
| Kontttijarvi | 6.52 | 26.07 | 442 120 | 141 218 | 9 994 | 2 064 | 978 | 1 521 | 26 071 | 17.90 | 15 |
| SK Reef | 6.04 | 27.16 | 752 693 | 214 904 | 24 901 | 4 905 | 2 415 | 3 547 | 25 656 | 29.14 | 15 |
| ***Sudbury Area, Canada*** | | | | | | | | | | | |
| River Valley | 2.31 | 11.00 | 111 760 | 37 840 | 6 347 | 922 | | 2 358 | 6 930 | 11.24 | 16 |
| East Bull Lake | 7.56 | 9.72 | 147 150 | 51 050 | 13 000 | 810 | | 1 035 | 9 424 | 11.47 | 17 |

# References


Abel MK (1981) The Structure of the Strathcona Mine Copper Zone. Bull Can Inst Min-Metall 14: 89–97

Abel MK, Buchan R, Coats CJA, Penstone ME (1979) Copper mineralization in the footwall complex Strathcona mine Sudbury Ontario. Can Min 17: 275–286

Abraham KP, Davies MW, Richardson FD (1960) Sulfide capacities of silicate melts pt. I. J. Iron and Steel Inst 196: 309-312

Abzalov MZ, Both RA (1997) The Pechenga Ni-Cu deposits Russia: data on PGE and Au distribution and sulphur isotope compositions. Mineralogy and Petrology 61: 119–143

Absalov MZ, Both RA, Brewer TS (1995) Geochemistry and sulfur isotope characteristics of the sulfidic black shales from the Pechenga Group Kola Peninsula Russia: Implications for genesis of the sulfide mineralisation. *In* Geology of the eastern Finmark-western Kola Peninsula region (eds D Roberts, O Nordgulen). Proc. of the 1st International Barents Symposium Geology and Minerals of the Barents Region Norske Geologiske Undersokelse Spec. Pub. No 7 pp 357–369

Alapieti TT, Lahtinen JJ (1986) Stratigraphy petrology and platinm-group element mineralization of the early Proterozoic Penikat layered intrusion northern Finland. Econ Geol 81: 1126-1136

Alapieti TT, Lahtinen JJ (2002) Platinum-Group Element Mineralization in Layered intrusions of Northern Finland and the Kola Peninsula Russia. *In* The Geology Geochemistry Mineralogy and Mineral Beneficiation of Platinum-Group Elements (ed LJ Cabri) Ottawa Ontario. Can Inst Min Met Spec Vol 54 pp. 507–546

Albino GV, (1984) Petrology geochemistry and mineralization of the Boundary ultramafic complex. Quebec Canada. Unpublished M Sc thesis Colorado State University 220 pp

Amelin YuV, Heaman LM, Semenov VS (1995) U-Pb geochronology of layered mafic intrusions in the eastern Baltic Shield: implications for the timing and duration of Paleoproterozoic continental rifting. Prec Res 75: 31–46

Amelin YuV, Li C, Naldrett AJ (1999) Geochronology of the Voisey's Bay complex Labrador Canada by precise U-Pb dating of co-existing baddeleyite zircon and apatite. Lithos 47: 33–51

Amelin YuV, Li C, Valeyev O, Naldrett AJ (2000) Nd-Pb-Sr isotope systematics of crustal assimilation in the Voisey's Bay and Mushuau intrusions Labrador Canada. Econ Geol 94: 815–830

Amsden AA, Ruppel H,M Hirt CW (1980) SALE: A simplified ALE computer program for fluid flow at all speeds. Los Alamos New Mexico Los Alamos National Laboratory Report LA-8095 101 p

Andersen JCO, Power MR Momme P (2002) Platinum-Group Elements in the Paleogene North Atlantic Igneous Province. *In* The Geology Geochemistry Min-

eralogy and Mineral Beneficiation of Platinum-Group Elements (ed LJ Cabri) Ottawa Ontario. Can Inst Min Met Spec Vol 54 pp 637–667

Anderson DL (1994) The sub-lithospheric mantle as the source of continental flood basalts; the case against the continental lithosphere and plume head reservoirs. Earth Planet Sci Let 123: 269–280

Archibald NJ, Bettenay LF, Binns RA, Groves DI, Gunthorpe RJ (1978) The evolution of Archean greenstone terrains Eastern Goldfields province Western Australia. Prec Res 6: 89-91

Ariskin AA, Barmina GS (2000) Modeling phase equilibria at crystallization of basalt magmas. Nauka MAIK "Nauka/Interperiodika" Moscow, 363 p (in Russian)

Ariskin AA, Deutsch A, Ostermann M (1999) Sudbury Igneous Complex: Simulating phase equilibria and in situ differentiation for two proposed parental magmas. *In* Large meteorite impacts and planetary evolution II (eds BO Dressler, VL Sharpton) Geol Soc Amer Spec Pap 339, pp 373–388

Armstrong R, Wilson AH (2000) A SHRIMP U-Pb study of zircons from the layered sequence if the Great Dyke Zimbabwe and a granitoid anataectic dyke. Earth Planet Sci Let 180: 1–12

Arnason JG, and Bird DK (2000) A gold and platinum mineralized layer in gabbros of the Kap Edvard Holm Complex: Field petrologic and geochemical relations. Econ Geol 95: 945–970

Arndt NT (1977) Partitioning of nickel between olivine and ultrabasic and basic komatiite liquids. Carnegie Inst. Washington Yearbook vol 76, pp 553–557

Arndt NT, Genner GA (1986) Crustally contaminated komatiites from Kambalda Western Australia. Chem Geol 56: 229-256

Arndt NT, Lesher CM (1992) Fractionation of REEs by olivine and the origin of Kambalda komatiites Western Australia. Geochim Cosmochim Acta 56: 4191–4204

Arndt NT, Nesbitt RW (1982) Geochemistry of Munro Township basalts. *In* Komatiites (eds. N.T. Arndt and E.G. Nisbet). Allen and Unwinm London, pp 309-330

Arndt NT, Nisbet EG, eds (1982) Komatiites. Allen and Unwin, London, 526 p

Arndt NT, Naldrett AJ, Pyke DR (1977) Komatiitic and iron-rich tholeiitic lavas of Munro Twp. northeast Ontario. J Petrol 18: 319-369

Arndt NT, Czamanske GK, Walker RJ, Chauvel C, Fedorenko VA (2003) Geochemistry and origin of the intrusive hosts of the Noril'sk-Talnakh Cu-Ni-PGE sulfide deposits. Econ Geol 98: 495–516

Avermann ME (1999) The green member of the Onaping formation the collapsed fireball layer of the Sudbury impact structure Ontario Canada. *In* Large meteorite impacts and planetary evolution II (eds BO Dressler, VL Sharpton) Geol Soc Amer Spec Pap 339, pp 323–330

Bacuta GC, Lipin BR, Gibbs AK, Kay RW (1987) Platinum-group element abundances in chromite deposits of the Acoje ophiolite block Zimbales ophiolite complex Philippines. Abstract Geo-platinum 87 Symposium Open University UK, pp 381–382

Balashov YA, Bayanova TB, Mitrofanov FP (1993) Isotope data on the age and genesic of layered basic-ultrabasic intrusions in the Kola Peninsula and northern Karelia northeastern Baltic Shield. Prec Res 64: 197–205

Ballhaus CG (1999) A liquid miscibility gap in the system Fe-Ni-Cu-S? Abstract 24 Geol Assoc – Can Mineral Assoc. Can Joint Annual Meeting 1999, pp 5–6

Ballhaus CG, Stumpfl EF (1986) Sulfide and platinum mineralization in the Merensky Reef: evidence from hydreous silicates and fluid inclusions. Contr Mineral Petrol 94: 193–204.

Baragar WRA, Scoates RFJ (1981) The Circum-Superior belt: a Proterozoic plate margin? *In* Precambrian Plate Tectonics (ed A Kroner). Elsevier, Amsterdam, pp 297–330

Barker DS (1983) Igneous Rocks. Prentice-Hall Inc. Englewood Cliff, New Jersey, pp 132–133

Barker WW (1983) The Fe-Ni-S system (CoCu). CSIRO Aust. FP Report 26, 23 p

Barnes SJ (1993) Partitioning of the platinum group elements and gold between silicate and sulfide magma in the Munni Munni Complex Western Australia. Geochim Cosmochim Acta 57: 1277–1290

Barnes SJ, Barnes S-J (1990) A new interpretation of the Katinniq nickel deposit Ungava northern Quebec. Econ Geol 85: 1269–1272

Barnes SJ, Hoatson DM (1994) The Munni Munni Complex Western Australia: stratigraphy structure and petrogenesis. J Petrol 35: 715–751

Barnes SJ, Tang ZL (1999) Chrome spinels from the Jinchuan Ni-Cu sulfide deposit Gansu province People's Republic of China. Econ Geol 94: 343–356

Barnes SJ, Coats CJA, Naldrett AJ (1982) Petrogenesis of a Proterozoic Nickel Sulfide - Komatiite Association: the Katiniq Sill Ungava Quebec. Econ Geol 77: 413-429

Barnes SJ, Gole MJ, Hill RET (1988a) The Agnew nickel deposit Western Australia: Part I. Structure and stratigraphy. Econ Geol 83: 524–536

Barnes SJ, Gole MJ and Hill RET (1988b) The Agnew nickel deposit Western Australia: Part II. Sulfide geochemistry with emphasis on the Platinum-group elements. Econ Geol 83: 537–550

Barnes SJ, McIntyre JR, Nisbet BW, Williams CR (1990) Platinum-group Element mineralisation in the Munni Munni Complex Western Australia. Mineralogy and Petrology 42: 141–164

Barnes SJ, Hoatson DM, McIntyre JR (1991) The Munni Munni Complex. *In* Mafic-Ultramafic Complexes of Western Australia (eds SJ Barnes, and RET Hill). Geol Soc Austr WA Division. Perth Excursion Guide Book 3, pp 77–96

Barnes SJ, Keays RR, Reid R, Hoatson DM (1992) Distribution of sulfides and PGE within the porphyritic websterite zone of the Munni Munni Complex Western Australia. Austr J Earth Sci 39: 289–302

Barnes S-J (1985) The petrography and geochemistry of komatiite flows from the Abitibi greenstone belt Canada and a model for their formation. Lithos 18: 241–270

Barnes S-J, Maier WD (2002) Platinum-Group Element Distributions in the Rustenberg Layered Suite of the Bushveld Complex South Africa. *In* The Geology Geochemistry Mineralogy and Mineral Beneficiation of Platinum-Group

Elements (ed LJ Cabri). Ottawa Ontario. Can Inst Min Met Spec Vol 54, pp 431–458

Barnes S-J, Naldrett AJ (1986) Variations in platinum-group element concentrations in the Alexo mine komatiite Abitibi greenstone belt northen Ontario. Geol Mag 123: 515–524

Barnes S-J, Naldrett AJ (1987) Fractionation of the Platinum-Group Elements and Gold in Some Komatiites of the Abitibi Greenstone Belt Northen Ontario. Econ Geol 82: 165–183

Barnes S-J, Picard CP (1993) The behavior of platinum-group elements during partial melting crystal fractionation and sulphide segregation: An example from the Cape Smith fold belt northern Quebec. Geochim Cosmochim Acta 57: 79–87

Barnes S-J, Makovicky E, Makovicky M, Rose-Hansen J, Karup-Moller S (1997) Partition coefficients for Ni Cu Pd Pt Rh and Ir between monosulfide solid solution and sulfide liquid and the formation of compositionally zoned Ni-Cu sulfide bodies by fractional crystallization of sulfide liquid. Can J Earth Sci 34: 366–374

Barrett FM, Binns RA, Groves DI, Marston RJ, McQueen KG (1977) Structural history and metamorphic modification of Archean volcanic type nickel deposits Yilgarn Block Western Australia. Econ Geol 72: 1195-1224

Barrie CT, Naldrett AJ (1988) The geology and tectonic setting of the Montcalm Gabbroic Complex and Ni-Cu deposit Western Abitibi Subprovince. Ontario Canada. Proc. of the 5th Magmatic Sulfides Conference Harare Zimbabwe, Spec Pub Inst Min Met, pp151–164

Barrie CT, MacTavish AD, Walford PC, Chataway R, Middaugh R (2002) Contact-type and Magnetitite Reef-type Pd-Cu Mineralization in Ferroan Olivine Gabbros of the Coldwell Complex Ontario. *In* The Geology Geochemistry Mineralogy and Mineral Beneficiation of Platinum-Group Elements (ed LJ Cabri). Ottawa Ontario. Can Inst Min Me. Spec Vol 54, pp 321–337

Barton PB Jr (1973) Solid solutions in system Cu-Fe-S Part I. The Cu-S and Cu Fe-S join. Econ Geol 68: 455-465

Batanova VG, Astrakhantzev OV (1992) Tectonic position and genesis of zonal mafic-ultramafic plutons in the north of the Olyutor zone. Geotektonika No 2: 87–103 (in Russian)

Bavington OA (1979) Interflow sedimentary rocks from the Kambalda ultramafic sequence: Their geochemistry metamorphism and genesis. Unpub PhD thesis Australian National University

Bavington OA (1981) The nature of sulfidic metasediments at Kambalda and their broad relationship with associated ultramafic rocks and nickel ores. Econ Geol 76: 1606–1628

Bayanova TB, Smolkin VF, Levkovich NV, Ryungenen GI (1999) U-Pb age of rocks from the Mt. Generalskaya layered intrusion Kola peninsula. Geokhimiya No 1: 3–13 (in Russian)

Bell CK (1966) Churchill-Superior boundary in northeastern Manitoba. Geol Surv Can Paper 66-1, pp 133–136

Bell CK (1971) Boundary geology upper Nelson River area Manitoba and northwestern Ontario. *In* Geoscience studies in Manitoba (ed AC Turnock). Geol Assoc Can Spec Pap 9, pp 11–39

Bell PM, England JW, and Kullerud G (1964) Pentlandite: Pressure effect on breakdown. Carnegie Inst. Wash. Yr. Book 63, pp 206-207

Bezmen NI (1997) Influence of $fO_2$ on the solubility of Pd and Pt in hydrous silicate melts. Abstract in supplement to Eos Trans AGU vol 78 No. 46, p F781

Bezmen NI, Asif M, Brugmann GE, Romanenko IM, Naldrett AJ (1994) Distribution of Pd Rh Ru Ir Os and Au between sulfide and silicate melts. Geochim Cosmochim Acta 58: 1251–1260

Billington LG (1984) Geological review of the Agnew nickel deposit Western Australia. *In* `Sulfide Deposits in Mafic and Ultramafic Rocks' (eds DL Buchanan, MJ Jones). Spec Pub Inst Min Met, pp 43-54

Bird DK, Arnason JG, Brandriss ME, Nevle RJ, Radford G, Bernstein S, Gannicott RA, Kelemen PB (1995) A gold-bearing horizon in the Kap Edvaard Holm Complex East Ggeenland. Econ Geol 90: 1288–1300

Bleeker W (1989a) Litho- structural map of the Thompson Open Pit Thompson Nickel Belt Manitoba scale 1: 200 000 with accompanying map description. Geol Surv Can Open File 2089

Bleeker W (1989b) New structural-metamorphic constraints on Early Proterozoic oblique collision along the Thompson Nickel Belt northern Manitoba Canada. *In* The Early Proterozoic Trans-Hudson Orogen of North America (eds JF Lawry, MR Staufferads) Geol Assoc Can Spec Pap 37, pp 57–74

Bleeker W (1990) Evolution of the Thompson nickel belt and its nickel deposits. Manitoba Canada. Unpublished PhD thesis University of New Brunswick, Fredericton, New Brunswick, 356 p

Bleeker W, Macek JJ (1988) Thompson Nickel Belt Project: Pipe Pit Mine. Report of Field Activities 1988, Manitoba Energy and Mines, pp 111–115

Bog S, Rosenqvist T (1958) A thermodynamic study of the iron sulfide-oxide melts. *In* Meddelebse Nr 12 fra Metallurgisk Komite, Trondheim Norway

Boctor NZ, Yoder HS Jr (1983) Partitioning of nickel between silicate and iron sulfide melts. Carnegie Inst. Washington Yr. Book 82, pp 275-277

Boerner DE, and Milkreit B (1999) Structural evolution of the Sudbury impact structure in the light of seismic reflection data. *In* (BO Dressler, VL Sharpton eds) "Large meteorite impacts and planetary evolution II" Geol Soc Amer Spe. Pub 339, pp 419-429

Bonnichsen W (1970) Geologic map of the Allen Babbitt Babbitt NE Babbitt SE and Babbitt SW 7 1/2 minute quadrangles. Minnesota Geol Surv Open File Maps

Bonnichsen W (1972) Southern part of the Duluth complex. *In* Geology of Minnesota (eds PK Sims, GB Morey). A centennial volume: St. Paul Minnesota Geol Surv, pp 361–387

Borisov A, Palme H (1997) Experimental determination of the solubility of platinum in silicate melts. Geochim Cosmochim Acta 61: 4349–4351

Borisov A, Palme H, Spettel B (1994) Solubility of Pd in silicate melts: Implications for core formation in the Earth. Geochim Cosmochim Acta 58: 705–716

Boudreau AE, Mathez EA, McCallum IS (1986) Halogen geochemistry of the Stillwater and Bushveld complexes: Evidence for transport of the platinum group elements by Cl-rich fluids: J Petrol 27: 967–986

Bowring SA, Erwin DH, Jin YG, Martin MW, Davidek K, Wang W (1998) The age of the Permian-Triassic boundary at Meishan southern China. Science 280: 1039–1045

Boyd R, Mathiesen CO (1979) The nickel mineralization of the Rana mafic intrusion Nordland Norway. Can Min 17: 287-298

Brenan JM, Caciagli NC (2000) Fe-Ni exchange between olivine and sulfide liquid: Implications for oxygen barometry in sulfide-saturated magmas. Geochim Cosmochim Acta 64: 307–320

Brugmann GE, Naldrett AJ, Macdonald AJ (1989) Magma mixing and constitutional zone refining in the Lac des Iles complex Ontario: genesis of platinum-group element mineralization. Econ Geol 84: 1557–1573

Brugmann GE, Naldrett AJ, Duke JM (1990) The Platinum-Group Element Distribution in the Dumont Sill Quebec. Implications for the formation of Ni-Sulfide Mineralization. Mineralogy and Petrology 40: 97–119

Brugmann GE, Naldrett AJ, Asif M, Lightfoot PC, Gorbachev NS, Fedorenko VA (1993) Siderophile and chalcophile metals as tracers of the evolution of the Siberian trap in the Noril'sk region Russia. Geochim Cosmochim Acta 57: 2001–2018

Brugmann GE, Hanski EJ, Naldrett AJ, Smolkin VF (2000) Sulfide segregation in ferropicrites from the Pechenga complex Kola peninsula Russia. J Petrol 41: 1721–1742

Bruynzyl D (1957) A petrographic study of the Waterfall Gorge profile at Insizwa. Annals Univ Stellenbosch 33, pp 434-535

Buchanan DL, Nolan J (1979) Solubility of sulfur and sulfide immiscibilty in synthetic tholeiitic melts and their relevance to Bushveld-complex rocks. Can Min 17: 483-494

Buchanan DL, Rouse JE (1984) Role of contamination in the precipitation of sulphides in the Platreef of the Bushveld Complex. *In* Sulfide Deposits in Mafic and Ultramafic Rocks (eds DL Buchanan, MJ Jones). Spec Pub Inst Min Met, pp 141-146

Buchanan DL, Nolan J, Wilkinson N, de Villiers JPR (1983) An experimental investigation of sulfur solubility as a function of temperatures in synthetic silicate melts. Geol Soc S Africa Spec Pub 7, pp 383–391

Burnham OM, Lesher CM, Keays RR (1999) Geochemistry and Petrogenesis of Mafic-Ultramafic Complexes and Associated Basalts in the Raglan Block Chapter 16 *In* Komatiitic Peridotite-Hosted Ni-Cu-(PGE) Deposits of the Raglan Area Cape Smith Belt New Quebec (ed CM Lesher). Guidebook Series vol 2. Mineral Exploration Research Centre Laurentian University, Sudbury, pp 159–173

Burrows AJ, Rickaby HC (1930) Sudbury Basin Area. Ontario Dept of Mines Annual Report for 1929 vol 38 part 3, 55 p

Burt DRL, Sheppy NR (1975) Mount Keith nickel sulfide deposit. *In*_Econ Geol of Australia and Papua New Guinea I. Metals (ed C.L. Knight). Australasian Inst Min Metal Mon 5, pp 159-168

Cabri LJ (1973) New Data on Phase relations in the Cu-Fe-S System. Econ Geol 68: 443-454

Cabri LJ, Laflamme JHG (1974) Rhodium Platinum and gold alloys from the Stillwater complex. Can Min 12: 399–403

Cabri LJ, Laflamme JHG (1976) The mineralogy of the platinum-group elements from some Cu-Ni deposits in the Sudbury area Ontario. Econ Geol 71: 1159–1195

Cabri LJ, Laflamme JHG (1979) Mineralogy of Samples from the Lac des Iles Area Ontario. CANMET Report 79-27, 20 p

Cabri LJ, Laflamme JHG (1984) Mineralogy and distribution of platinum-group elements in mill products from Sudbury. *In*: Applied Mineralogy (eds W Park, DM Hausen, R Hagni). Proc 2nd International Congress on Applied Mineralogy in the Mineral Industries. The Mineral Soc AIME, pp 911–922

Cabri LJ, Naldrett AJ (1984) The nature of the distribution and concentration of platinum-group elements in various geological environments. Proc 27th Internat Geol Congress, 10 Mineralogy, pp 17-46

Cabri LJ, Blank H, El Goresy A, Laflamme JHG, Nobiling R, Sizgoric MB, Trascel K (1983) Quantitative Proton Microprobe Analyses of Major Sulfides in Ore Deposits of the Sudbury Area. Geol Assoc Can – Mineral Assoc Can.Annual Meeting Programme with Abstracts.

Cameron EN (1978) The lower zone of the eastern Bushveld complex in the Olifants river trough. J Petrol 19: 437-462

Cameron EN (1980) Evolution of the Lower Critical Zone Central Sector eastern Bushveld Complex and its chromite deposits. Econ Geol 75: 845-871

Cameron EN (1982) The Upper Critical Zone of the eastern Bushveld Complex – precursor to the Merensky Reef. Econ Geol 77: 1307-1327

Cameron EN, Desborough G.A. (1964) Origin of certain magnetite-bearing pegmatites in the eastern part of the Bushveld Complex South Africa. Econ Geol 59: 197–225

Cameron G.H. (1988) A geochemical investigation into the origin of the Upper Critical Zone of the Eastern Bushveld Complex South Africa. Unpub MSc Thesis Univ of Toronto

Campbell IH, Barnes SJ (1984) Partition coefficients for platinum and palladium between immiscible sulfide and silicate liquids. Can Min 22: 151–160

Campbell IH, Griffiths RW (1990) Implications of mantle plume structure for the evolution of flood basalts. Earth Planet Sci Let 99: 79–93

Campbell IH, Naldrett AJ (1979) The influence of silicate: sulfide ratios on the geochemistry of magmatic sulfides. Econ Geol 74: 1503-1505

Campbell IH, Turner JS (1986) The role of convection in the formation of platinum and chromitite deposits in layered intrustions. *In* Short Course on Silicate Melts (ed CM Scarfe) Mineral Assoc Canada 12, pp 236–278

Campbell IH, Naldrett AJ, Roeder PL (1979) Nickel activity in silicate liquids: Some preliminary results. Can Min 17: 495-506

Campbell IH, Naldrett AJ, Barnes SJ (1983) A model for the origin of the platinum-rich sulfide horizons in the Bushveld and Stillwater Complexes. J Petrol 24: 133-165

Card KD, Gupta VK, McGrath PH, Grant FS (1984) The Sudbury Structure: Its Regional Geological and Geophysical Setting. *In* The Geology and Ore deposits of the Sudbury Structure. (eds EG Pye, AJ Naldrett, PE Giblin). Ontario Geol Surv Spec Vol 1, pp 25–44

Cawthorn RG (1980) High-MgO Karoo tholeiite and the formation of Ni-Cu mineralization in the Insizwa intrusion. Transkei South African J of Sci 76: 467–470

Cawthorn RG (2002) The role of magma mixing in the genesis of PGE mineralisation in the Bushveld Complex. Thermodynamic calculations and new interpretations – a discussion. Econ Geol 97: 663–666

Cawthorn RG, Davies G (1983) Experimental data at 3 Kbars pressure on parental magma to the Bushveld Complex. Contrib Min Petrol 83: 128-135

Cawthorn RG, Webb SJ (2001) Connectivity between the western and eastern limbs of the Bushveld Complex. Tectonophysics 330: 195–209

Cawthorn RG, Merkle RK, Viljoen MJ (2002) Platinum-Group Element Deposits in the Bushveld Complex South Africa. *In* The Geology Geochemistry Mineralogy and Mineral Beneficiation of Platinum-Group Elements (ed LJ Cabri). Ottawa Ontario. Can Inst Min Met.Spec Vol 54, pp 389–429

Celmer RS (1987) The distribution of minor elements in nickel matte smelting. Unpub PhD Theis Univer of Toronto, 341 p

Chai G, Eckstrand OR (1994) Origin of the Sudbury Igneous Complex Ontario – differentiation of two separate magmas. Geol Surv Can Paper 93-17, pp 219–230

Chai G, Eckstrand OR (1996) Rare Earth Element characteristics of the Sudbury Igneous Complex and its country rocks: New constraints on genesis. Chem Geol 102: 303–325

Chai G, Naldrett AJ (1992a) Petrology and geochemistry of the Jinchuan ultramafic intrusion: Cumulate of a high-Mg basaltic magma. J Petrol 33: 1–27

Chai G, Naldrett AJ (1992b) PGE mineralization of the Jinchuan Ni-Cu sulfide deposit NW China. Econ Geol 87: 1475–1495

Chalokwu CI, Grant NK (1987) Reequilibration of olivine with trapped liquid in the Duluth complex Minnesota. Geology 15: 71–74

Chang YA, Hsieh K-C (1986) Thermochemical description of the ternary iron-nickel-sulfur system in Nickel Metallurgy: volume 1. Extraction and Refining of Nickel (eds E Ozberk, SW Marcuson). Proc of the 25th Annual Conference of Metallurgists Can Inst Min Met, pp 248–277

Chauvel C, Dupre , Jenner GA (1985) The Sm-Nd age of Kambalda volcanics is 500 Ma too old! Earth Planet Sci Lett 74: 314-324

Childs JF Evans JR Wood KY Koski MS, Evans JD (2002) Some preliminary descriptive aspects of ballroom mineralisation at the Stillwater Palladium-Platinum mine Stillwater Mining Company Nye Montana. *In* Extended Abstracts 9th Internat Platinum Symposium (ed A Boudreau), pp 91–92

Chuang Y-Y, Hsieh K-C, Chang YA (1985) Thermodynamics and phase relationships of transition metal sulfur systems: Part V. A re-evaluation of the Fe-S system using an associated solution model for the liquid phase. Metall Trans 16B: 277–285

Clark T, Naldrett AJ (1972) The distribution of Fe and Ni between synthetic olivine and sulfide at 900°C. Econ Geol 67: 939–952

Coats CJA, Brummer JJ (1971) Geology of the Manibridge nickel deposit Wabowden Manitoba. *In* Geoscience studies in Manitoba (ed AC Turnock). Geol Assoc Can Spec Pap 9, pp 155–165

Coats CJA, Snajdr P (1984) Ore Deposits of the North Range Onaping-Levack Area Sudbury. *In*: The Geology and Ore Deposits of the Sudbury Structure (eds EG Pye, AJ Naldrett, PE.Giblin). Ontario Geol Surv Spec Vol 1, pp 327-346

Coats CJA, Quirke TT Jr, Bell CK, Cranstone DA, Campbell FHA (1972) Geology and mineral deposits of the Flin Flon Lynn Lake and Thompson areas Manitoba and the Churchill-Superior form of the Western Precambrian shield: Internat Geol Cong 24th Montreal 1982 Guidebook, Field Excursions A31-C31, pp 1-96

Cochrane LB (1984) Ore deposits of the Copper Cliff Offset. *In* The Geology and Ore Deposits of the Sudbury Structure (eds EG Pye, AJ Naldrett, PE Giblin) Ontario Geol Surv Spec Vol 1, pp 97–138

Cogulu EH (1990) Mineralogical and petrological studies of the Crystal Lake intrusion Thunder Bay Ontario. Geol Surv Can Open File Report 2277, 67 p

Coleman AP (1913) The nikel industry with special reference to the Sudbury region Ontario. Canada Dept of Mines, Mines Branch No 170, 206 p

Collins WH (1934) Life history of the Sudbury nickel irruptive (i). Roy Soc Can Trans sec IV28, pp 123–177

Compston W, Williams IS, Campbell IH, Gresham JJ (1986) Zircon xenocrysts from the Kambalda volcanics: age constraints and direct evidence for older continental crust below the Kambalda-Norseman greenstones. Earth Planet Sci Let 76: 299–311

Connolly JWD, Haughton DR (1972) The volume of sulfur in glass of basaltic composition formed under conditions of low oxidation potential. Amer Mineral 57: 1515-1517

Corfu F, Lightfoot PC (1997) U-Pb geochronology of the Sublayer environment Sudbury Igneous Complex Ontario. Econ Geol 91: 1263–1269

Corlett M (1971) Minor element variation in pyrrhotite from Falconbridge mine; an aid in geological interpretation. Geol Assoc Can – Mineral Assoc Can joint Annual Meeting. Abstracts of papers, pp 15–16

Corson SR, Childs JF, Dahy JP, Keith DW, Koski MS, LeRoy LW (2002) The Reef Package Stratigraphy that contains the J-M Platinum-Palladium Reef of the Stillwater Complex Montana. *In* Extended Abstracts 9th Internat. Platinum Symposium (ed A Boudreau), pp 101–102

Courtillot V, Besse J, Vandamme D, Montigny R, Jaeger JJ, and Capetta H (1986) Deccan flood basalts at the Cretaceous/Tertiary boundary? Earth Planet Sci Let 80: 361–374

Courtillot V, Feraud G, Maluski H, Vandamme D, Moreau MG, Besse J (1988) Deccan flood basalts and the Cretaceous/Tertiary boundary. Nature 333: 843–846

Cowan EJ, Riller U, Schwerdtner WM (1999) Emplacement geometry of the Sudbury Igneous Complex: Structural examination of a proposed impact melt sheet. *In* Large meteorite impacts and planetary evolution II (eds BO Dressler, VL Sharpton) Geol Soc Amer Spec Pap 339, pp 399–418

Cowan JC (1968) The Geology of the Strathcona ore deposit district Ontario. Can. Inst Min Met Bull 61, pp 38–54

Cowden A, Donaldson MJ, Naldrett AJ, Campbell IH (1986) Platinum-group elements in the komatiite-hosted Fe-Ni-Cu sulfide deposits at Kambalda Western Australia. Econ Geol 81: 1226-1235

Cowden A, Ruddock R, Reay A, Nicolson P, Waterman P, and Banks MJ (1990) Platinum mineralisation potential of the Longwood Igneous Complex New Zealand. Mineralogy and Petrology 42, No 1-4, pp 181–195

Cox KG, Bell JD, Pankhurst RJ (1979) The interpretation of Igneous Rocks. Allen and Unwin, London, 450 p

Craig JR (1971) Violarite stability relations. Amer Mineral 56: 1303–1311

Craig JR (1973) Pentlandite-pyrrhotite and other low – temperature relations in the Fe-Ni-S systems. Amer J Sci 273-A: 496-510

Craig JR, Kullerud G (1969) Phase relations in the Cu-Fe-Ni-S system and their application to magmatic ore deposits. Econ Geol Monograph vol 4, pp 344–358

Craig JR, Naldrett AJ (1967) Minimum melting of nickel ferrous pyrrhotite ores. Ann Rep Dir of Geophys Lab Carnegie Inst of Washington, Year Book vol 66, pp 417–419

Craig JR, Scott SD (1974) Sulfide phase equilibria. Mineral Soc Amer Short Course Notes vol 1 (ed PH Ribbe). Sulfide Mineralogy CS1–CS110

Cranstone DA, Turek A (1976) Geological and geochronological relationships of the Thompson Nickel Belt Manitoba. Can J Earth Sci 13: 1058–1069

Crocket JH (2002) Platinum-Group Element Geochemistry of Mafic and Ultramafic Rocks. *In* The Geology Geochemistry Mineralogy and Mineral Beneficiation of Platinum-Group Elements (ed L.J. Cabri). Ottawa Ontario. Can Inst Min Met Special Vol 54, pp 177–210

Crocket JH, Fleet ME, Stone WE (1992) Experimental partitioning of osmium iridium and gold between basalt melt and sulfide liquid at 1300°C. Austr J Earth Sci 39: 427–432

Czamanske GK, Moore JG (1977) Composition and phase chemistry of sulfide globules in basalt from the mid-Atlantic Ridge rift valley near 37° N Lat. Geol Soc Amer Bull 88, pp 587–599

Czamanske GK, Zientek ML, eds (1985) The Stillwater Complex Montana: Geology and Guide. Montana Bureau of Mines and Geology Spec Pub 92, 396 p

Czamanske GK, Kunilov VYe, Zientek ML, Cabri L J, Likhachev AP, Calk LC, Oscarson RL (1992) A proton-microprobe study of magmatic sulfide ores from the Noril'sk-Talnakh district Siberia. Can Min 30: 249–287

Czamanske GK, Zen'ko TE, Fedorenko VA, Calk LC, Budahn JR, Bullock JH Jr, Fries TL, King B-SW, Siems DF (1995) Petrographic and geochemical characterisation of ore-bearing intrusions of the Noril'sk type Siberia: with discussion of their origin. Resource Geology Special Issue 18, pp 1–48

Czamanske GK, Gurevich AB, Fedorenko VA, Simonov O (1998) Demise of the Siberian plume: paleogeographic and paleotectonic reconstruction from the prevolcanic and volcanic records North-Central Siberia. Internat Geol Rev 40: 95–115

Czamanske GK, Wooden JL, Walker RJ, Fedorenko VA, Simonov ON, Budahn JR, Siems DF (2000) Geochemical isotopic and SHRIMP age data for Precambrian basement rocks Permian volcanic rocks and sedimentary host rocks of the ore-bearing intrusions Noril'sk-Talnak district Siberian Russia. Internat Geol Rev 42: 895–297

DePaolo DJ (1985) Isotopic processes in mafic magma chambers: I. The Kiglapait intrusion Labrador. J Petrol 26: 925–951

Deutsch A, Lakomy R, and Buhl D (1989) Strontium and neodymium characteristics of a heterolithic breccia in the basement of the Sudbury impact structure Canada. Earth Planet Sci Let 93: 359–370

Deutsch A, Brockmeyer JM, Buhl D (1990) Sudbury again: New and old isotope data (Abstract). Lunar and Planetary Science vol 21, pp 282–283

Deutsch A, Buhl D, Brockmeyer P, Lakomy R, Flucks M (1992) Isotope systematics support the impact origin. Volume of abstracts Internat Conference on Large Meteorite Impacts and Planetary Evolution. Lunar and Planetary Inst Contribution No 790, pp 21–22

De Waal SA, Xu ZH Li C, Mouri H (2003) Emplacement of dense viscous crystal mushes Jinchuan Ultramafic Intrusion western China. Can Min (in press)

De Witt MJ, Hart RA, Hart RJ (1987) The Jamestown Ophiolite Complex Barberton mountain belt: A section through the 3.5Ga oceanic crust. J African Earth Sci 6: 681–730

Dickin AP, Richardson JM, Crockett JH, McNutt RH, Peredery WV (1992) Osmium isotope evidence for a crustal origin of platinum group elements in the Sudbury nikel ore Ontario Canada. Geochim Cosmochim Acta 56: 3531–3537

Dietz RS (1964) Sudbury structure as an astrobleme. J Geol 72: 412–434

Dillon-Leitch H.H, Watkinson DH, Coats CJA (1986) Distribution of Platinum-Group Elements in the Donaldson West Deposit Cape Smith Belt Quebec. Econ Geol 81: 1147–1158

Distler VV, Kunilov VE, eds (1994) Geology and Ore Deposits of the Noril'sk Region. VII Internat Platinum Symposium Guidebook, Moskovskiy Contact, Moscow, 67 p

Distler VV, Filimonova AA, Grokhovskaya TL, and Laputina IP (1989 Platinum metals in nickel-copper ores of the Pechenga ore field. Geologiya rudnykh mestorozhdeniy 31, No 6: 3–17 (in Russian)

Distler VV, Mitrofanov GL, Nemerov VK, Kovalenker VA, Mokhov AV, Semeykina L.K, Yudovskaya MA (1996) Styles of platinum metals occurrence and the genesis of PGE mineralization in the Sukhoy Log gold deposit. Geologiya rudnykh mestorozhdeniy 38, No 6: 467–484 (in Russian)

Distler VV, Sluzhenikin SF, Cabri LJ, Krivolutzkaya NA, Turovtzev DM, Golovanova TA, Mokhov AV, Knayf VV, Oleshkevich OI (1999) Platinum ores of the Noril'sk layered intrusions: interrelation of magmatic and fluid concentration of noble metals. Geologiya rudnykh mestorozhdeniy 41, No 3: 241–265 (in Russian)

Distler VV, Yudovskaya MA, Prokofev VA, Sluzhenikin SF, Mokhov AV, Mun YaB (2000) Hydrothermal platinum mineralization of the Waterberg deposit (Transvaal Republic of South Africa). Geologiya rudnykh mestorozhdeniy 42, No 4: 263–376 (in Russian)

Donaldson MJ (1974) Petrology of the Munni Munni Complex Roebourne Western Australia. J Geol Soc Austr 21: 1–16

Doyle CD, Naldrett AJ (1986) Ideal mixing of divalent cations in mafic magma and its effect on the solution of ferrous oxide. Geochim Cosmochim Acta 50: 435-443

Dressler BO (1984) The effects of the Sudbury event and the intrusion of the Sudbury Igneous Complex on the Footwall of the Sudbury structure. *In* The Geology and Ore Deposits of the Sudbury Structure (eds EG Pye, AJ Naldrett, P Giblin) Ontario Geol Surv Special Vol No.1, pp 97–138

Du Toit AL (1920) The geology of Pondoland and portions of the Alfred and Umzimkulu Counties Natal. South Africa Geol Surv Explanation Sheet 28 (Pondoland)

Duke JM (1979) Computer simulation of the fractionation of olivine and sulfide from mafic and ultramafic magmas. Can Min. 17: 507–514

Duke JM (1986) The Dumont nickel deposit: a genetic model for disseminated magmatic sulphide deposits of komatiitic affinity. *In* Metallogeny of Basic and Ultrabasic Rocks (eds MJ Gallagher, RA Ixer, CR Neary, HM Prichard) Spec Pub.Inst Min Met London. pp 151-160.

Duke JM, Naldrett AJ (1978) A numerical model of the fractionation of olivine and molten sulfide from komatiite magma. Earth Planetary Science Letters 39: 255–266

Duncan RA, Hooper PR, Rehacek J, Marsh JS, Duncan R (1997) The timing and duration of the Karoo igneous event southern Gondvana. J Geophy Research 102, No B8: 18127–18138

Dunning GR (1979) The geology and platinum group element mineralization of the Roby Zone Lac des Iles complex northwestern Ontario. MSc Thesis, Ottawa Ontario, 129 p

Dyuzhikov OA, Fedorenko VA, Nesterovsky VS, Demidovich VI (1976) New North-Kharaelakh camp and perspective of its Nickel mineralization. Doklady Akademii Nauk 229, No 5: 1184–1187 (in Russian)

Duzhikov OA, Distler VV, Strunin BM, Mkrtychyan AK, Sherman ML, Sluzhenikin SF, Lurje AM (1992) Geology and Metallogeny of Sulfide Deposits of Noril'sk Region USSR. (English translation of 1988 Russian edition). Soc of Econ Geol Spec Pub No 1, 242 p

Eales HV (1980) Contrasted trace element variations in two Karoo cumulus complexes. Chem Geol 29: 39–48

Ebel D, Naldrett AJ (1996) Experimental fractional crystallisation of Cu- and Ni-bearing Fe-sulfide liquids. Econ Geol 91: 607–621

Ebel D, Naldrett AJ (1997) Crystallisation of sulfide liquids and the interpretation of ore composition. *In* Proc. of IGCP Project 336 conference "Intraplate Magmatism and related Mineralisation" Can J Earth Sci 34 No 4: 352–365

Eckstrand OR (1975) The Dumont serpentinite: A model for control of opaque nickel ferrous mineral assemblages by alteration reactions in ultramafic rocks. Econ Geol 70: 183–201

Eckstrand OR, Cogulu EH (1989) The role of sulfur contamination in magmatic Cu-Ni-PGE mineralisation in the Crystal Lake intrusion Thunder Bay area Ontario (abs). Geol Soc Finland Bull vol 61, pp 6–7

Eckstrand OR, Grinenko LN, Krouse HR, Paktunc AD, Schwann PL, Scoates RFJ (1989) Preliminary data on sulfur isotopes and Se/S ratios and the source of Sulfur in magmatic Sulfides from the Fox River Sill Molson Dykes and Thompson nickel deposits northern Manitoba. *In* Current Research part C Geol Surv Can Paper 89-1C, pp 235–242

Edwards AM, Silk MH (1987) Platinum in South Africa. Spec Pub Council of Mineral Technology vol 12, 55p

Emslie RF, Hamilton MA, Theriault RJ (1994) Petrogenesis of a mid-Proterozoic anorthsite-mangerite-charnockite-granite (AMGC) complex: Isotopic evidence for the Nain Plutonic Suite. J Geol 102: 539–558

Evans-Lamswood DM, Butt DP, Jackson RS, Lee DV, Muggridge MG, Wheeler RI, Wilton DHC (2000) Physical controls associated with the distribution of sulphides in the Voisey's Bay Ni-Cu-Co deposit Labrador. Econ Geol 95: 749–770

Faggart BE, Basu AB, Tatsumoto M (1985) Origin of the Sudbury Complex by meteorite impact: Neodymium isotopic evidence. Science 230: 436–439

Farnetani CG, Richards MA (1994) Numerical investigations of the mantle plume initiation model for flood basalt events. J Geophys Research 99 (B7): 13813–13833

Farquhar J (1985) The Geology of Western Platinum Mine. *In* Bushveld excursion. Some Ore Deposits in Southern Africa; Excursion Guidebook (eds E Vermaak, G von Gruenwaldt). Third Internat Platinum Symposium, Geol Soc of South Africa, pp 16–19

Farrow CEG, Lightfoot PC (2002) Sudbury PGE Revisited: Toward an Integrated Model. *In* The Geology Geochemistry Mineralogy and Mineral Benefication of Platinum-Group Elements (ed LJ Cabri). Ottawa Ontario, Can Inst Min. Met Special Vol 54, pp 273–297

Fedorenko VA (1979) Paleotectonics of Late Paleozoic - Early Mesozoic volcanism of the Noril'sk region and paleotectonic control of the Nickel-bearing intrusions. *In* Geology and Mineralization of the Taymyr-Severnaya Zemlya folding area. NIIGA, Leningrad, pp 16–23 (in Russian)

Fedorenko VA (1981) Petrochemical series of extrusive rocks of the Noril'sk region. Soviet Geology and Geophysics 22, No 6: 66–74

Fedorenko VA (1994) Evolution of magmatism as reflected in the volcanic sequence of the Noril'sk region. Proc of the Sudbury-Noril'sk symposium. Ontario Geol Surv Spec Pub 5, pp 171–184

Fedorenko VA, Lightfoot PC, Naldrett AJ, Czamanske GK, Hawkesworth CJ, Wooden JL, Ebel DS (1996) Petrogenesis of the flood-basalt sequence at Noril'sk North Central Siberia. Internat Geol Rev 38: 99–135

Fedorova ZhN, Sinyakova EF (1993) Experimental investigation of physiochemical conditions of pentlandite generation. Geologiya i geofizika 34: 84–92 (in Russian)

Ferreira Filho CF, Naldrett AJ, Asif M (1995) Distribution of Platinum Group Elements in the Niquelandia Layered Mafic Ultramafic Intrusion Brazil. Can Min 33: 165–184

Fershtater GB, Bea F, Pushkarev EV, Garuti G, Montero P, Zakkarini F (1999) New data on the geochemistry of the Urals Platinum Belt: contributions to understanding of petrogenesis. Geokhimiya No 4: 352–370 (in Russian)

Fincham CJB, Richardson FD (1954) The behaviour of sulfur in silicate and aluminate melts. Proc of the Royal Society A223, pp 40–62

Findlay DC (1969) Origin of the Tulameen ultramafic-gabbro complex southern British Columbia. Can J Earth Sci 6: 399–425

Finnigan CS, Brenan JM (2004) Experimental evidence for the formation of PGE alloy inclusions in chromite by local reduction. Abstract Volume of Abstracts Geol Assoc Can / Mineral Assoc Can Joint Annual Meeting May 12-14 2004, St Catherines Ontario Canada

Fisher D (1979) The petrology of the Mt. Edwards nickel sulfide deposit Widgiemooltha Western Australia. Unpublished PhD thesis, Univ of Toronto, 320 p

Fleet ME, MacRae ND (1983) Partition of Ni between olivine and sulfide and its application to Ni-Cu sulfide deposits. Contr Mineral Petrol 83: 75–81

Fleet ME, MacRae ND (1987) Partition of Ni between olivine and sulfide: the effect of temperature, $fO_2$ and $fS_2$. Contr Mineral Petrol 95: 336–342

Fleet ME, Pan Y (1994) Fractional crystallisation of anhydrous sulfide liquid in the system Fe-Ni-S with application to magmatic sulfide deposits. Geochim Cosmochim Acta 58: 3369–3377

Fleet ME, Stone WE (1990) Nickeliferous sulfides in xenoliths olivine megacrysts and basaltic glass. Contr Mineral Petrol 105: 629–636

Fleet ME, Stone WE, Crocket JH (1991) Partitioning of palladium iridium and platinum between sulfide liquid and basalt melt: Effects of melt composition concentration and oxygen fugacity. Geochim Cosmochim Acta 55: 2545–2554

Fleet ME, Chryssoulis SL, Stone WE, Weisener CG (1993) Partitioning of platinum-group elements and Au in the Fe-Ni-Cu-S system: experiments on the fractional crystallisation of sulfide melt. Contr Mineral Petrol 115: 36–44

Fletcher TA (1987) Nickel-copper and precious metal mineralisation in the Caledonian mafic and ultramafic intrusions of north-east Scotland (abs). *In* Geoplatinum 87 (eds HM Pritchard, PJ Potts, JFW Bowles, SJ Cribb). Elsevier, p. 163

Foose M, Wieblen P (1986) The Physical and Petrologic Setting and Textural and Compositional Characteristics of Sulfides from the South Kawishiwi Intrusion Duluth Complex Minnesota USA. *In* Geology and Metallogeny of Copper Deposits (eds GH Freidrich, AD Genkin, AJ Naldrett, JD Ridge, RH Sillitoe, FM Vokes), Springer-Verlag Heidelberg Berlin, pp 8–24

Fraser HS (1985) The Great Thompson Nickel Discovery. Inco Limited, Manitoba, 388 p

Frost KM, Groves DI (1989) Ocellar units at Kambalda: evidence for sediment assimilation by komatiite lavas. *In* Magmatic Sulphides - The Zimbabwe Volume (eds MD Prendergast, and MJ Jones) Spec Pub Inst Min Met, London, pp 207–214

Fudali RF (1965) Oxygen fugacities of basaltic and andesitic magmas. Geochim Cosmochim Acta 29: 1063–1075

Gaetani GA, Grove TL (1997) Partitioning of moderately siderophile elements among olivine sulfide melt and silicate melt: Constraints on core formation in the Earth and Mars. Geochim Cosmochim Acta 61: 1829–1846

Gain SB (1980) The geology and PGE distribution in the Upper Group chromatite layers at Maandagshoek 254 K.T. eastern Bushveld Complex. Inst Geol Research on the Bushveld Research Report 22, 24 p

Gansser A, Dietrich VJ, Cameron WE (1979) Paleogene komatiites from Gorgona Island. Nature 278: 545–546

Genkin AD, Distler VV, Gladyshev GD, Filimonova AA, Evstigneeva TL, Kovalenker VA, Laputina IP, Smirnov AB, Grokhovskaya TL (1981) Sulfide nickel-copper ores of the Noril'sk deposits. Nauka, Moscow, 234 p (in Russian)

German K, Schmidt F (1999) Platinum-group element concentrations in chromitities of the Great Dyke Zimbabwe, Bundesanstalt fur Geowissenschaften und Rohstoffe (BGR), Hannover. Berichte zur Lagerstatten-und Rohstofforschung vol 34, 68p

Ghiorso MS, Sack RO (1995) Chemical mass transfer in magmatic processes. IV. A revised and internally consistent thermodynamic model for the interpolation and extrapolation of liquidus-solidus equilibria in magmatic systems at elevated temperatures and pressure. Contr Mineral Petrol 119: 197–212

Gibb RA (1968) A geological interpretation of the Bouguer anomalies adjacent to the Churchill - Superior boundary in northern Manitoba. Can J Earth Sci 5: 439–453

Gillies SL (1993) Physical Volcanology of the Katinniq Peridotite Complex and associated Fe-Ni-Cu-(PGE) mineralization Cape Smith Belt Northern Quebec. Unpublished MSc thesis, University of Alabama, 146 p

Giovenazzo D (1991) Geologie et caracteristiques geochemique des mineralisations Ni-Cu-EPG de la region de Delta ceinture de Cape-Smith Nouveau Quebec. Unpubl. PhD thesis, Universite du Quebec a Chicoutimi

Giovenazzo D, Picard C, Guha J (1989) Tectonic setting of Ni-Cu-PGE deposits in the central part of the Cape Smith Belt. Geoscience Canada 16, No 3: 134–136

Godlevsky MN (1959a) Towards a question on the genesis of sulfide nickel-copper deposits in the Siberian platform. Geologiya rudnykh mestorozhdeniy No 2: 17–30 (in Russian)

Godlevsky MN (1959b) Traps and ore-bearing intrusions of the Noril'sk region. Gosgeoltekhizdat Moscow, 68 p (in Russian)

Godlevsky MN, Grinenko LN (1963) Some data on sulfur isotope compositions from sulfides of the Noril'sk deposits. Geokhimiya No 1: 35–40 (in Russian)

Gole MJ, Hill RET, Barnes SJ (1986) Komatiite Flows and Lava Lakes - Environments for Formation of Spinifex and Adcumulate Textures. Volume of Abstracts Internat Volcanological Congress New Zealand

GolightlyJP (1994) The Sudbury Igneous Complex as an impact melt Evolution and ore genesis. *In* Proc. of the Sudbury-Noril'sk Symposium (eds PC Lightfoot, AJ Naldrett) Ontario Geol Surv Spec Vol 5, pp 105–118

Good DJ, Naldrett AJ (1993) Geology and distribution of platinum-group elements Bucko lake Intrusion Thompson belt Manitoba. Can Min 31: 45–60

Gorbachev NS, Grinenko LN (1973) Sulfur isotope compositions from sulfides and sulfates of the Oktyabrsky nickel-copper deposit (Noril'sk region) and some aspects of their genesis. Geokhimiya No 8: 1127–1136 (in Russian)

Gorbunov GI (1968) Geology and genesis of sulfide nickel-copper deposits at Pechenga. Nedra Moscow, 352 p (in Russian)

Gorbunov GI, Zagorodny VG, Robonen WI (1985a) Main features of the geological history of the Baltic Shield and the epochs of ore formation. Geol Surv Finland Bull vol 333. pp 17–41

Gorbunov GI, Yakovlev YuN, Goncharov YuV, Gorelov VA, Tel'nov VA (1985b) The nickel areas of the Kola peninsula. Geol Surv Finland Bull vol 333, pp 42–122

Gorbunov GI, Korchagin AU. Mednikov AI (1989) About mineralization in picrites. Doklady Akademii Nauk 103: 1205–1208 (in Russian)

Gorbunov GI, Astafev YuA, Goncharov YuV, Korchagin AU, Neradovsky YuN, Smolkin VF, Sokolov SV, Sharov NV, Yakovlev YuN (1999) Pechenga nickel-copper deposits. GEOS, Moscow, 236 p (in Russian)

Grant RW, Bite A (1984) Sudbury quartz diorite offset dikes: *In* The Geology and Ore Deposits of the Sudbury Structure (eds EG Pye, AJ Naldrett, PE Giblin). Ontario Geol Surv Spec Vol l, pp 275–301

Graterol M, ,Naldrett AJ (1971) Mineralogy of the Marbridge No.3 and No.4 deposits with some comments on low temperature equilibration in the Fe-Ni-S sytem. Econ Geol 66: 886–900

Green AG, Cumming GL, Cedarwell D (1979) Extension of the Superior Churchill boundary zone into southern Canada. Can J Earth Sci 16: 1691–1701

Green AG, Hajnal Z, Weber W (1985) An evolutionary model of the western Churchill Province and western margin of the Superior Province in Canada and the north-central United States. Tectonophysics 116: 281–322

Green AH, Naldrett AJ (1981) Volcanic peridotite-associated nickel sulfide deposits of the Abitibi belt Canada with special reference to those in Langmuir Township, Ontario, Canada. Econ Geol 76: 1503–1523

Green AH, Dupras N (1999) Exploration Model for Komatiitic Peridotite-Hosted Ni-Cu-(PGE) Mineralization in the Raglan Belt Chapter 20. *In* Komatiitic Peridotite-Hosted Ni-Cu-(PGE) Deposits of the Raglan Area Cape Smith Belt New Quebec (ed CM Lesher). Guidebook Series vol 2 Mineral Exploration Research Centre, Laurentian University, Sudbury, pp 191–199

Green JC, Phinney WC, Weiblen PW (1966) Gabbro Lake Quadrangle Lake County. Minnesota Geol Surv Miscellaneous Map M2

Gresham JJ (1986) Depositional Environments of Volcanic Peridotite-Associated Nickel Sulphide Deposits with Special Reference to the Kambalda Dome. *In* Geology and Metallogeny of Copper Deposits (eds GH Freidrich, AD Genkin, AJ Naldrett, JD Ridge, RH Sillitoe, FM Vokes) Springer-Verlag, Heidelberg, Berlin, pp 63–90

Gresham JJ, Loftus-Hills GD (1981) The Geology of the Kambalda Nickel Field Western Australia. Econ Geol 76: 1373–1416

Grieve RAF (1994) An impact model of the Sudbury Structure. *In* Proc. of the Sudbury-Noril'sk Symposium (eds PC Lightfoot, AJ Naldrett). Ontario Geol Surv Spec Vol 5, pp 119–132

Grieve RAE, Stoffler D, Deutsch A (1991) The Sudbury structure controversial or misunderstood? J Geophys Research 96: 22753–22764

Griffiths RW, Campbell IH (1991) Interaction of mantle plume heads with the Earth's surface and onset of small-scale convection. J Geophys Research 96: 18295–18310

Grinenko LN (1985a) Sources of sulfur of the nickeliferous and barren gabbrodolerite intrusions of the northwest Siberian platform. Internat Geol Rev 27: 695–708

Grinenko LN (1985b) Sulfur sources of nickel-bearing and barren gabbrodolerite intrusions in the north-west part of the Siberian platform. Geologiya rudnykh mestorozhdeniy No 1: 3–15 (in Russian)

Grinenko LN, Smolkin VF (1991) Sulfur isotope compositions and contents in ferropicrites and gabbro-wehrlites of the Pechenga zone. Geokhimia No 9: 1250–1261 (in Russian)

Grinenko LN, Grinenko VA, Lyakhnitzkaya IV (1967) Sulfur isotope composition in sulfides of nickel-copper deposits of the Kola peninsular. Geologiya rudnykh mestorozhdeniy No 4: 3–17 (in Russian)

Grout FF (1918) The lopotholith; an igneous form exemplified by the Duluth Gabbro. Amer J Science 4th series, 46: 516–522

Groves DI, Lesher CM (1982) Regional Geology and Nickel deposits of the Norseman-Wiluna belt Western Australia. Univ Western Australia Geological Dept Ext Service Publication 7

Groves DI, Lesher CM, Gee RD (1984) Tectonic setting of the sulphide nickel deposits of the Western Australia Shield. *In* Sulfide Dposits in Mafic and Ultramafic Rocks (eds DL Buchanan, and MJ Jones). Spec Pub Inst Min Met, pp 1–13

Gupta VK, Grant FS, Card KD (1984) Gravity and Magnetic Characteristics of the Sudbury Structure. *In* The Geology and Ore Deposits of the Sudbury Structure

(eds EG Pye, AJ Naldrett, PE Giblin). Ontario Geol Surv Spec Vol 1, pp 381–410

Hahn UF, Ovendale B (1994) UG2 chromitite layer potholes at Wildebeestfontein north mine Impala Platinum Limited. Proc 15th CMMI Congress, South African Inst Min Met, pp 195–200

Halkoaho TAA, Alapieti TT, Lahtinen JJ, Lerssi JM (1990) The Ala-Penikka PGE Reef in the Penikat layered intrusion northern Finland. Mineralogy and Petrology 42: 23–38

Hall AL (1932) The Bushveld Igneous Complex of the central Transvaal. South Africa Geol Surv Memoir vol 28, 560 p

Halls HC (1978)The late Precambrian central North American rift system – a survey of recent geological and geophysical investigations. *In* Tectonics and Geophysics of Continental Rifts (eds IB Ramberg, E-R Newmann). NATO Advanced Study Inst Series C vol 37, pp 111–123

Hamilton MA (1994) Review of isotopic data for the Nain Plutonic Suite. *In* Anorthositic Grantoid and Related Rocks of the Nain Plutonic Suite. Field Excursion Guide to the Nain Area August 4-10 1994 Internat Geol Correlation Programme Projects 290 and 315, pp 15–19

Hamlyn PR, Keays RR (1985) Precious metals in magnesian low-Ti lavas: Implications for metallogenesis and sulfur saturation in primary magmas. Geochim Cosmochim Acta 49: 1797–1811

Hanski EJ (1992) Petrology of the Pechenga ferropicrites and cogenetic Ni-bearing gabbro-wehrlite intrusions Kola Peninsula Russia. Geol Surv of Finland Bull, 367 p

Hanski EJ, Smolkin VF (1989) Pechenga ferropicrites and other Early Proterozoic picrites in the eastern part of the Baltic Schield. Prec Res vol 45, No 1-3, pp 63–82

Hanski EJ, Smolkin VF (1990) Thick layered ferropicritic flows in the Pechenga area and their relation to associated Ni-Cu deposits. Volcanological Congress 3-8 September 1990, Mainz (FRG), Abstracts

Hanski EJ, Smolkin VF (1995) Iron- and lREE-enriched mantle source for early Proterozoic intraplate magmatism as exemplified by the Pechenga ferropicrites Kola Peninsula Russia. Lithos 34: 107–125

Harmer RE, Sharpe MR (1985) Field relations and Sr isotope systematics of the marginal rocks of the eastern Bushveld Complex. Econ Geol 80: 813–837

Harmer RE, Auret JM, Eglington BM (1995) Lead isotope variations within the Bushveld Complex Southern Africa; a reconnaissance study. J African Earth Sci 21: 595–606

Hauck SA, Severson M, Zanko LM, Barnes S-J, Morton P, Alminas H, Foord EE, Dahlberg H (1997) An overview of the geology and oxide sulfide and platinum-group element mineralisation along the western and northern contacts of the Duluth Complex. Geol Soc Amer Spec Pap 312: 137-186

Haughton DR, Roeder PL, Skinner BJ (1974) Solubility of sulfur in mafic magmas. Econ Geol 69: 451–467

Hawkesworth CJ, Lightfoot PC, Fedorenko VA, Blake S, Naldrett AJ, Doherty W, Gorbachev NS (1995) Magma differentiation and mineralization in the Siberian continental flood basalts. Lithos 34: 61–88

Hawkesworth CJ, Cohen AS, Cooper M, Lightfoot PC, Burnham OM (1997) Significant differences in the ore forming processes Sudbury and Noril'sk Constraints from Os isitopes. Trans Amer Geophy. Union vol 78, p. F 809

Hawley JE (1965) Upside-down zoning at Frood Sudbury Ontario. Econ Geol 60: 529–575

Hawley JE, Stanton RL (1962) The facts the ores their minerals metals and distribution in the Sudbury Ores: Their Mineralogy and Their Origin. Can Min 7: 30–145

Heaman LM, Machado N, Krogh TE, Weber W (1986) Precise U-Pb zircon ages for the Molson dyke swarm and the Fox River Sill: Constraints for early Proterozoic crustal evolution in northeastern Manitoba Canada. Contr Mineral Petrol 94: 82–89

Hearst RB, Morris WA, Thomas MD (1994) Magnetic interpretation along the Sudbury structure LITHOPROBE transect. *In* Proc. of the Sudbury Noril'sk Symposium (eds PC Lightfoot, AJ Naldrett). Ontario Geol Surv Spec Pub 5, pp 33–44

Hill RET (1984) Experimental study of phase relations at 600°C in a portion of the Fe-Ni-Cu-S system and its application to natural sulphide assemblages. *In* Sulfide Deposits in Mafic and Ultramafic Rocks (eds DL Buchanan, MJ Jones). Spec Pub Inst Min Metall, pp 14–21

Hill RET, Gole MJ, Barnes SJ (1989) Olivine adcumulates in the Norseman-Wiluna greenstone belt Western Australia: implications for the volcanolgy of komatiites. *In* Magmatic Sulfides - The Zimbabwe Volume (eds MD Prendergast, MJ Jones). Spec Pub Inst Min Metall London, pp 189–206

Hill RET, Barnes SJ, Gole MJ, Dowling SE (1990 Physical volcanolgy of komatiites Excursion Guide Book No 1, Geol Soc Austr. (WA Division), East Perth Western Australia

Hill RET, Barnes SJ, Gole MJ, Dowling SE (1995) The volcanolgy of komatiites as deduced from field relationships in the Norseman-Wiluna greenstone belt Western Australia. Lithos 34: 159–188

Hiller JE, Probsthain K (1956) Thermischa un rontgenographiache Untersuchungen an Kupferkres: Zeitschrift fur Kristallog 108, pp 108–129

Hilty DC, Crafts W (1952) Liquidus surface of the Fe-S-O system. J Metals 4: 1307–1312

Hoatson DM (19860 Geology of the Munni Munni layered intrusion 1:20 000 scale map and explanatory notes. Bureau of Mineral Resources Geology and Geophysics Canberra Australia

Hoatson DM, Keays RR (1989) Formation of platiniferous sulfide horizons by crystal fractionation and magma mixing in the Munni Munni layered intrusion West Pilbara Block Western Australia. Econ Geol 84: 1775–1804

Hochrelter R (2000) Platinum Producers. Barnard Jacobs and Mellet, Johannesburg, 140 p

Hoffman EL, Naldrett AJ, Alcock RA, Hancock RGV (1979) The noble metal content of ore in the Levack West and Little Stobie mines Ontario. Can Min 17: 437–452

Hoffman PF (1985) Is the Cape Smith Belt (northern Quebec) a klippe? Can J Earth Sci 22: 1361–1369

Holzheid A, Palme H, Chakroborty S (1997) The activities of NiO, CoO and FeO in silicate melts. Chem Geol 139: 451–461

Hsieh KC, Chang YA, Zhong T (1982) The Fe-Ni-S system above 700°C. Bull Alloy Phase Diagrams 3, pp 165–172

Huang W-L, Williams RJ (1980) Melting relations of portions of the system Fe-S-Si-O to 32 kb with implication to the nature of the mantle core boundary (abstract). Lunar and Planet Sc XI Lunar and Planetary Inst, Houston, pp 486–488

Huhma H (1986) Sm-Nd, U-Pb and Pb-Pb isotopic evidence for the origin of the Early Proterozoic Svecokarelian crust in Finland. Geol Surv Finland Bull 337, 48 p

Huhma H, Clift RA, Perttunen V, Sakko M (1990) Sm-Nd and Pb isotopic stuty of mafic rocks associated with early Proterozoic continental rifting: The Perapohia schist belt in Northern Finland. Contr Mineral Petrol 104: 369–379

Huhma H, Smolkin VF, Hanski EJ, Fedotov ZhA (1996) Sm-Nd isotope study of the Nyasyukka dyke complex in the northern Pechenga area Kola Peninsula Russia. Program and Abstracts IGCP Project 336 Symposium in Rovaniemi Finland August 21-23 1996. University of Turku Publication 33, pp 57–58

Hulbert LJ (1983) A petrological investigation of the Rustenburg layered suite and associated mineralisation south of Potgietersrus. Unpublished PhD thesis, University of Pretoria, 511 p

Hulbert LJ (1997) Geology and Metallogeny of the Kluane mafic-ultramafic belt Yukon Territory Canada: Eastern Wrangelia – a new Ni-Cu-PGE metallogenic terrane. Geol Surv Can Bull 506, 265 p

Huppert HE, Sparks RSJ (1985a) Cooling and contamination of mafic and ultramafic magmas during ascent through continental crust. Earth Planet Sci Let 74: 371–386

Huppert HE, Sparks RSJ (1985b) Komatiites I: Eruption and flow. J Petrol 26: 694–725

Iljina M (1994) The Portimo Layered Igneous Complex – With Emphasis on Diverse Sulphide and Platinum-Group Element Deposits. Department of Geology University of Oulu Finland PhD thesises, University of Oulu Finland Acta Universitatis Ouluensis Series A Scientiae Rerum Naturalium 258, 158 p

Irvine TN (1963) Origin of the ultramafic complex at Duke Island southeastern Alaska. Int Miner Assoc Symposium on Layered Intrusions Washington, Amer Mineral Spec Pap No 1, pp 36–45

Irvine TN (1974) Petrology of the Duke Island ultramafic complex southeastern Alaska. Geol Soc Amer Memoir 138, 240 p

Irvine TN (1975) Crystallization sequences of the Muskox intrusion and other layered intrusions – II. Origin of chromitite layers and similar deposits of other magmatic ores. Geochim Cosmochim Acta 39: 991–1020

Irvine TN (1977) Origin of chromite layers in the Muskox intrusion and other stratiform intrusions: a new interpretation. Geology 5: 273–277

Irvine TN (1982 Terminology for layered intrusions. J Petrol 23: 127–162

Irvine TN, Kushiro I (1976) Partitioning of Ni and Mg between olivin and silicate liquids. Carnegie Inst Washington Year Book vol 75, pp 668–675

Irvine TN, Sharpe MR (1986) Magma mixing and the origin of stratiform oxide ore zones in the Bushveld and Stillwater Complexes. *In* Metallogeny of basic and ultrabasic rocks (eds MG Gallagher, RA Ixer, CR Neary, HM Prichard), Inst Min Metall London, pp 183–198

Ivanov BA, Deutsch A (1999) Sudbury impact event: Cratering mechanism and thermal history. *In* Large meteorite impacts and planetary evolution II (eds BO Dressler, VL Sharpton). Geol Soc Amer Spec Pap No 339, pp 389–398

Ivanov MK, Ivanova TK, Tarasov AV, Shatkov VA (1971 Peculiarities of the geology and mineralization of differentiated intrusions of the Noril'sk ore junction (Noril'sk-1 Noril'sk-2 and Mt. Chernaya deposits). *In* Petrology and mineralization of the Talnakh and Noril'sk differentiated intrusions (Trydy NIIGA vol 167), Leningrad, pp 197–305 (in Russian)

Ivanov OK (1996) Platinum mineralization of the Nizhniy Tagil concentric zoned pyroxenite-dunite massif. Izvestiya vysshikh uchebnykh zavedeniy Gorny zhurnal No 3-4, pp 63–71 (in Russian)

Ivanov OK (1997) Concentric zoned pyroxenite-dunite massifs of Urals (Mineralogy petrology genesis). Urals university, Ekaterinburg, 488 p (in Russian)

Ivanov SN, Perfiliev AS, Efimov AA, Smirnov GA, Necheukhin VM, Fershtater GB (1975) Fundamental features in the structure and evolution of the Urals. Amer J Science 275-A: 107–130

Jahns RH, Bumham CW (1969) Experimental studies of pegmatite genesis: I. A model for derivation and crystallization of granitic pegmatites. Econ Geol 64: 843–864

James RS, Dressler BO (1992) Nature and significance of the Levack Gneiss Complex – footwall rocks of the North and East Ranges of the Sudbury Igneous Complex. Can Min 30: 487

James RS, Jobin-Bevans S, Easton RM, Wood P, Hrominchuk JL, Keays RR, Peck DC (2002) Platinum-Group Element Mineralization in Paleoproterozoic Basic Intrusions in Central and Northeastern Ontario Canada. *In* The Geology Geochemistry Mineralogy and Mineral Beneficiation of Platinum-Group Elements (ed LJ Cabri). Ottawa Ontario, Can Inst Min Met Spec Vol 54, pp 339–365

Jensen ML (1967) Sulfur isotopes and mineral genesis. *In* Geochemistry of Hydrothermal Ore Deposits (ed HL Barnes). New York, Holy Reinhart Winston, pp 143–165

Jia EF (1986) Geological Characteristics of the Jinchuan Cu-Ni sulfide deposit in Gansu province. Mineral Deposits vol 4, pp 27–37 (in Chinese)

Johan Z (2002) Alaskan-type Complexes and Their Platinum-Group Element Mineralization. *In* The Geology Geochemistry Mineralogy and Mineral Beneficiation of Platinum-Group Elements (ed LJ Cabri). Ottawa Ontario, Can Inst Min Met Spec Vol 54, pp 669–719

Jones JH, Drake MJ (1986) Geochemical constraints on core formation in the earth. Nature 332: 221–228

Kamo SL, Czamanske GK, Amelin YuV, Fedorenko VA, Trofimov VR (2000) U-Pb zircon and baddeleyite and U-Th-Pb perovskite ages for Siberian flood volcanism Maymecha-Kotuy area Siberia. J Conference Abstracts 2000 vol 5 No 2, p 569

Kamo SL, Czamanske GK, Krogh TE (1996) A minimum U-Pb age for Siberian flood-basalt volcanism. Geochim Cosmochim Acta 60: 3505–3511

Karup-Moller S, Makovicky E (1995) The phase system Fe-Ni-S at 725°C. Neues Jahrbuch fur Mineralogie Monatshefte, pp 1–10

Keays RR, Crocket JH (1970) A study of precious metals in the Sudbury Nickel Irruptive ores. Econ Geol 65: 438–450

Keays RR, Davison RM (1976) Palladium Iridium and Gold in the ores and host rocks of nickel sulfide deposits in Western Australia. Econ Geol 71: 1214–1228

Keays RR, Lightfoot PC (1999 The role of meteorite impact source rocks protores and mafic magmas in the genesis of the Sudbury Ni-Cu-PGE Sulfide ore deposits. *In* Dynamic Processes in Magmatic Ore Deposits and Their Application in Mineral Exploration (eds RR Keays, CM Lesher, PC Lightfoot, CE Farrow). Geol Assoc Can Short Course Notes 13, pp 329–366

Keays RR, Scott RB (1976) Precious metals in ocean-rige basalts: Implications for basalts as source rocks for gold mineralization. Econ Geol 71: 705–720

Kennedy AK Lofgren GE, Wasserburg GJ (1993) An equilibrium study of trace element partitioning between olivine orthopyroxene and melt in chondrules: equilibrium values and kinetic effects. Earth Planet Sci Let 115: 177–195

Kerr A (1999) Mafic rocks of the Pants Lake Intrusion and related Ni-Cu-Co mineralization in north-central Labrador. Newfoundland Department of Mines and Energy Geol Surv Branch Report 99-1, pp 215–255

Kerr A (2003) Nickeliferous gabbroic intrusions of the Pants Lake area Labrador Canada: Implications for the development of magmatic sulfides in mafic systems. Amer J Science 303: 221–258

Kerr A, Ryan B (2000) Threading the eye of the needle: Lessons from the search for another Voisey's Bay in Northern Labrador. Econ Geol 95: 725–748

Kharitonov LYa, ed (1958) Geology of the USSR vol XXXII Murmansk province, GNTI, Moscow, 714 p (in Russian)

Kiersnowski D (2000) Experimental determination of the behaviour of sulfide droplets in convecting magmas. Unpublished MSc thesis, University of Toronto, 250 p

King RW, Anderson DL (1995) An alternative mechanism of flood basalt formation. Earth Planetary Science Letters 136: 269–279

Kleinkopf MD (1985) Regional gravity and magnetic anomalies of the Stillwater Complex area. *In* The Stillwater Complex Montana: Geology and Guide (eds GK Czamanske, M L Zientek). Spec Pub 92 Montana Bureau of Mines and Geology, pp 33–38

Kornev TYa, Ekhanin AG (1997) Standard of the Kingash basalt-komatiitic complex (Estern Sayan). Standards of magmatic complexes of Siberia, MPR, Novosibirsk, 89 p (in Russian)

Kornik LJ (1969) An aeromagnetic study of the Moak Lake-Setting Lake structure in northern Manitoba. Can J Earth Sci 6: 373–381

Kornik LJ, MacLaren AS (1966) Aeromagnetic study of the Churchill-Superior boundary in northern Manitoba. Can J Earth Sci 3: 547–557

Korovyakov IA, Nelyubin AE, Raykova ZA, Khortova LK (1963) Origin of the Noril'sk trap intrusions hosting sulfide Ni-Cu ores. Gosgeoltekhizdat, Moscow, 102 p (in Russian)

Kress V (1997) Thermochemistry of sulfide liquids. 1. The system O-S-Fe at 1 bar. Contr Mineral Petrol 127: 176–186

Krogh TE, Davis DW, ,Corfu F (1984) Precise U-Pb Zircon and Baddeleyite Ages for the Sudbury Area. *In* The Geology and Ore Deposits of the Sudbury Structure (eds EG Pye, AJ Naldrett, PE Giblin). Ontario Geol Surv Spec Vol 1, pp 431–447

Kullerud G (1963) Thermal stability of pentlandite. Can Min 7: 353–366

Kullerud G (1967) Sulfide studies in Researches in Geochemistry 2. John Wiley and Sons, New York

Kullerud G, Yoder HS (1959) Pyrite stability relations in the Fe-S system. Econ Geol 54: 533–572

Kullerud G, Yund RA (1962) The Ni-S system and related minerals. J Petrology 3: 126–175

Kullerud G, Yund RA, Moh G (1969) Phase relations in the Fe-Ni-S Cu-Fe-S and Cu-Ni-S systems. Econ Geol Monograph 4, pp 323–343

Kunilov VE (1994) Geology of the Noril'sk region: The history of the discovery Prospecting Exploration and mining of the Noril'sk deposit. *In* Proc. of the Sudbury-Noril'sk symposium (eds PC Lightfoot, AJ Naldrett). Ontario Geol Surv Spec Pub 5, pp 203–216

Lambert DD, Morgan JW, Walker RJ, Shirey SB, Carlson RW, Zientek ML, Koski MS (1989) Re-Os, Sm-Nd and Rb-Sr isotope systematics of the Stillwater Complex Montana: Evidence for the origin of platinum-group element deposits in mafic layered intrusions. Science 244: 1169–1174

Lambert DD, Foster JG, Frick LR, Li C, and Naldrett AJ (1999). Re-Os isotopic systematics of the Voisey's Bay Ni-Cu-Co magmatic ore system Labrador Canada. Lithos 47: 69–88

Lambert DD, Frick LR, Foster JG, Li C, Naldrett AJ (2000) Re-Os Isotopic Systematics of the Voisey's Bay Ni-Cu-Co Magmatic Sulfide System Labrador Canada: II. Implications for Parental Magma Chemistry Ore Genesis and Metal Redistribution. Econ Geol 95: 867–888

Langmuir CH, Klein EM, and Plank T (1992) Petrological systematics of mid-ocean ridge basalts: constraints on melt generation beneath ocean ridges. *In*: Morgan JP, Blackman DK, Sinton JM (eds) Mantle Flow and Melt Generation at Mid-Ocean Ridges. Geophysical Monograph vol 71, pp. 183–275

Latypov RM (2002) Phase equilibria constraints on relations of ore-bearing intrusions with flood basalts in the Noril'sk region Russia. Contr Mineral Petrol 143: 438–449

Lee CA, (1996) A review of mineralisation in the Bushveld Complex and some other layered intrusions. *In* Layered Intrusions (ed RG Cawthorn), Elsevier, Amsterdam, pp 103–145

Lee CA, Butcher AR (1990) Cyclicity in the Sr isotope stratigraphy through the Merensky and Bastard Reef unbits Atok section eastern Bushveld Complex. Econ Geol 85: p 883–891

Lenz JG, Conard RS, Warner (1978) The liquidus surface and tie-lines in the iron-nickel-sulfur-system between 1473 and 1673°K. Metallurgical Trans B 9B, pp 459–462

Leroy LW (1985) Tractolite-Anorthosite Zone l and the J-M Reef: Frog Pond Adit to the Graham Creek Area. *In* Stillwater Complex (eds GK Czamanske, ML Zientek). Montana Bureau of Mines and Geology Spec Pub 92, pp 325–333

Lesher CM (1983) Localization and genesis of komatiite-associated Fe-Ni-Cu sulfide mineralization at Kambalda Western Australia. Unpub PhD thesis, Univ of Western Australia, 318 p

Lesher CM (1990) Komatiite-associated nickel sulfide deposits. *In* Ore Deposition Associated with Magmas (eds JA Whitney, AJ Naldrett). Reviews in Econ Geol No 4, Soc of Economic Geologists, pp 45–102

Lesher CM, ed (1999 Komatiitic Peridotite-Hosted Ni-Cu-(PGE) Deposits of the Raglan Area Cape Smith Belt New Québec. Guidebook Series vol 2, Mineral Exploration Research Centre Laurentian University, Sudbury, 212 p

Lesher CM, Arndt NT (1995) REE and Nd Isotope geochemistry peotrogenesis and volcanic eveolution of contaminated komatiites at Kambalda Western Australia. Lithos 34: 127–157

Lesher CM, Burnham OM (1999) Mass balance and mixing in dynamic ore-forming magmatic systems. *In* Dynamic processes in magmatic ore deposits and their application in mineral exploration (eds. RR Keays, CM Lesher, PC Lightfoot, CEG Farrow), Geol Assoc Can Short Course Notes 13, p. 413–449

Lesher CM, Groves DI (1984) Geochemical and Mineralogical criteria for the identification of mineralized komatiites in Archean Greenstone Belts of Australia. *In* Petrology: Igneous and Metamorphic rocks, Proc 27th Internat Geological Congress Moscow, Vol 9. VNU Science Press, Utrecht, pp 283–302

Lesher CM, Groves DI (1986) Controls on the Formation of Komatiite-Associated Nickel-Copper Sulfide Deposits. *In* Geology and Metallogeny of Copper Deposits (eds GH Freidrich, AD Genkin, AJ Naldrett, JD Ridge, RH Sillitoe, FM Vokes). Springer-Verlag, Heidelberg-Berlin, pp 43–62

Lesher CM, Ripley EM (1992) Stable isotope geochemistry of Proterozoic komatiitic peridotite-associated Fe-Ni-Cu sulfide deposits Raglan block Cape Smith belt New Quebec. Geol Soc Amer Annual Meeting Abstracts with Programs vol 24 No 7, p A62

Lesher CM, Stone WE (1996) Exploration geochemistry of komatiites. *In* Igneous Trace Element Geochemistry: Applications for Massive Sulphide Exploration (ed D. Wyman). Geol Assoc Can Short Course Notes vol 12, pp 153–204

Lesher CM, Lee RF, Groves DI, Bickle MJ, Donaldson MJ (1981) Geochemistry of comatiites at Kambalda: I. Chalcophile element depletion – A consequence of sulfide liquid separation from komatiitic magmas. Econ Geol 76: 1714–1728

Lesher CM, Arndt NT, Groves DI (1984) Genesis of komatiite-associated nickel sulfide deposits at Kambalda Western Australia; a distal volcanic model. *In* Sulfide deposits in mafic and ultramafic rocks (eds DL Buchanan, MJ Jones), Inst Min Met London, pp 70–80

Lesher CM, Burnham OM, Keays RR, Barnes SJ, Hulbert L (1999a) Geochemical determination of barren and mineralised komatiites in dynamic ore-forming magmatic systems. *In* Dynamic Processes in Magmatic Ore Deposits and their Application in Mineral Exploration (eds R Reid, C Keays, M Lesher, PC Lightfoot, CEG Farrow). Geol Assoc Can Short Course Notes vol 13, pp 451–477

Lesher CM, Thibert F, Gillies SL, Stilson CM, Thacker JL, Williams DA (1999b) Lithology and Physical Volcanology of Komatiitic Peridotite-Gabbro Complexes in the Raglan Block Chapter 4. *In* Komatiitic Peridotite-Hosted Ni-Cu-(PGE) Deposits of the Raglan Area Cape Smith Belt New Quebec (ed CM Lesher), Guidebook Series vol 2, Mineral Exploration Research Centre Laurentian University, Sudbury, pp 43–60

Li C, Naldrett AJ (1993) Sulfide capacity of magma: a quantitative model and its application to the formation of sulfide ores at Sudbury Ontario. Econ Geol 88: 1253–1260

Li C, Naldrett AJ (1999) Geology and petrology of the Voisey's Bay intrusion: reaction of olivine with sulfide and silicate liquids. Lithos 47: 1–31

Li C, Naldrett AJ (2000) Melting reactions of gneissic inclusions with enclosing magma at Voisey's Bay: Implications with respect to ore genesis. Econ Geol 95: 801–814

Li C, Naldrett AJ, Coats CJ, Johannessen P (1992) Platinum palladium gold and copper-rich stringers at Strathcona Mine Sudbury: Their enrichment by fractionation of a sulfide liquid. Econ Geol 87: 1584–1596

Li C, Naldrett AJ, Rucklidge JC, ‚Kilius LR (1993) Partitioning of platinum group elements and gold in sulfides and its application to the ore zonation of the Strathcona mine Sudbury Ontario. Can Min 30: 523–531

Li C, Barnes S-J, Makovicky E, Rose-Hansen J, Makovicky M (1996a) Partitioning of Ni Cu Ir Rh Pt and Pd between monosulfide solid solution and sulfide liquid: Effects of composition and temperature. Geochim Cosmochim Acta 60: 1231–1238

Li C, Naldrett AJ, Krstic S (1996b) The Voisey's Bay Ni-Cu-Co deposit: Crustal contamination and petrological variation. Geol Soc Amer Abstracts with Programs vol 28 No 7, p A92

Li C, Lightfoot PC, Amelin Y, Naldrett AJ (2000) Contrasting petrological and geochemical relationships in the Voisey's Bay and Mushuau intrusions Labrador Canada: Implications for ore genesis. Econ Geol 95: 771–800

Li C, Maier WD, de Waal SA (2001a) The role of magma mixing in the genesis of PGE mineralisation in the Bushveld Complex: Thermodynamic calculations and new interpretations. Econ. Geol. 96: 653–662

Li C, Maier WD, de Waal SA (2001b) Magmatic Ni-Cu versus PGE deposits: Contrasting genetic controls and exploration implications. South African J Geol 104: 309–318

Li C, Ripley EM, and Naldrett AJ (2003a) Compositional variations of olivine and sulfur isotopes in the Noril'sk and Talnakh intrusion Siberia: Implications for ore-forming processes in dynamic magma conduits. Econ Geol 98: 69–86

Li C, Xu Z, deWaal SA, Ripley EM, and Maier WD (2003b) Compositional variations of olivine from the Jinchuan Ni–Cu sulfide deposit western China: implications for ore genesis. Mineralium Deposita

Lightfoot PC (1982) The geology of the Tabankulu section of the Insizwa Complex Transkei. Unpub MSc thesis, Univ Toronto, 247 p

Lightfoot PC (1997) Geological and Geochemical relationships in the Reid Brook intrusive complex Labrador: Implications for the origin of the voisey's Bay magmatic Ni-Cu-Co ores. Supplement to EOS Transactions Amer Geophys Union 78 No 46, p F810

Lightfoot PC, Farrow CEG (2002) Geology geochemistry and mineralogy of the Worthington offset dyke: A genetic model for offset dyke mineralization in the Sudbury Igneous Complex. Econ Geol 97: 1419–1446

Lightfoot PC, Hawkesworth CJ (1997) Flood basalts and Ni Cu and PGE mineralisation: comparative geochemistry of the Noril'sk (Siberian traps) and West Greenland sequences. *In* Large Igneous Provinces: Continental Oceanic and Planetary Flood Volcanism Geophysical Monograph vol 100, pp 357–380

Lightfoot PC, Naldrett AJ (1984a) The geology of the Tabankulu section of the Insizwa complex Transkei Southern Africa. Transactions Geol Soc South Africa vol 86 pt 3, pp 169–187

Lightfoot PC, Naldrett AJ (1984b) Chemical variation of the Insizwa Complex Transkei and the nature of the parent magma. Can Min 22: 111–123

Lightfoot PC, and Naldrett AJ, eds (1994) Proc of the Sudbury-Noril'sk Symposium, Ontario Geol Surv Spec Vol 5, 423 p

Lightfoot PC and Naldrett AJ (1999) Geological and geochemical relationships in the Voisey's Bay intrusion Nain Plutonic Suite Labrador Canada. *In* Dynamic processes in magmatic ore deposits and their application in mineral exploration (eds RR Keays, CM Lesher, PC Lightfoot, CEG Farrow), Geol Assoc Can Short Course Notes vol 13, pt 9, pp1–31

Lightfoot PC, Naldrett AJ, Hawkesworth CJ (1984) The geology and geochemistry of the Waterfall Gorge section of the Insizwa complex with particular reference to the origin of nickel sulfide deposits. Econ Geol 79: 1857–1879

Lightfoot PC, Naldrett AJ, Gorbachev NS, Doherty W, Fedorenko VA (1990) Geochemistry of the Siberian Trap of the Noril'sk area USSR with implications for the relative contributions of crust and mantle to flood basalt magmatism. Contr Mineral Petrol 104: 631–644

Lightfoot PC, Sutcliffe RH, Doherty W (1991) Crustal contamination identified in the Keweenawan Osler group tholeiites Ontario: A trace element perspective. J Geol 99: 739–760

Lightfoot PC, Hawkesworth CJ, Hergt J. Naldrett AJ, Gorbachev NS, Fedorenko VA, Doherty W (1993) Remobilisation of continental lithosphere by mantle plumes: Major trace element and Sr- Nd- and Pb-isotope evidence for picritic and tholeiitic lavas of the Nori'sk district Siberian trap Russia. Contr Mineral Petrol 114: 171–188

Lightfoot PC, Naldrett AJ, Gorbachev NS, Fedorenko VA, Hawkesworth CJ, and Doherty W (1994) Chemostratigraphy of Siberian Trap lavas Noril'sk district Russia: Implications and source of flood basalt magmas and their associated Ni-Cu mineralization. *In* Proc of the Sudbury-Noril'sk symposium (eds PC Lightfoot, AJ Naldrett). Ontario Geol Surv Spec Pub 5, pp 283–312

Lightfoot PC, Keays R.R. Morrison GG, Bite A, Farrell KP (1997a) Geologic and geochemical relationships between the Contact Sublayer Inclusions and the Main Mass of the Sudbury Ingeous Complex: A case study of the Whistle Mine Embayment. Econ Geol 92: 647–673

Lightfoot PC, Doherty W, Farrell KP, Keays RR, Pekeski D, ,Moore M (1997b) Geochemistry of the Main Mass Sublayer Offsets and Inclusions from the Sudbury Ingeous Complex Ontario. Mineral Deposit Study No 5959, Ontario Geol Surv

Lightfoot PC, Keays RR, Doherty W (2001) Chemical Evolution and Origin of Nikel Sulfide Mineralization in the Sudbury Ingeous Complex Ontario Canada. Econ Geol 96: 1855–1875

Likhachev AP (1965) Role of leucocratic gabbro in the generation of the Noril'sk differentiated intrusions. Izv Akad Nauk SSSR Geol Series No 10: 75–88 (in Russian)

Likhachev AP (1978) About conditions of generation of ore-bearing and barren mafic-ultramafic magmas. Doklady Akademii Nauk 338: 447–450 (in Russian)

Likhachev AP (1994) Ore-bearing intrusions of the Noril'sk region. *In* Proc of the Sudbury-Noril'sk symposium (ed PC Lightfoot, AJ Naldrett). Ontario Geol Surv Spec Pub 5, pp 185–202

Listerud WH, Meineke DG (1977) Mineral resources of a portion of the Duluth Complex and adjacent rocks in St Louis and Lake counties northeastern Minnesota. Minnesota Dept of Natural Resources Division of Minerals, Minerals Exploration Section, Report 93

Lomberg KG, Martin ES, Patterson MA, Venter JE (1999) The morphology of potholes in the UG2 Cromitite layer and Merensky Reef (pothole reef facies) at Union Section Rustenburg Platinum Mines. South African J Geol 102: 209–220

Luck J-M, Allegre CJ (1982) The study of molybdenitesw through the $^{187}Re$-$^{187}Os$ chronometer. Earth Planet Sci Let 61: 291–296

Lydon JW (1987) Potential for hydrothermal platinum deposits. Can Mining J March, pp 24–25

Macdonald AJ, Brugmann GE, Naldrett AJ (1989) Coeval felsic mafic and ultramafic magmas: Magma mixing during formation of PGE-rich Ni-Cu sulfides at Lac des lies Ontario Canada. *In* Magmatic sulfides – the Zimbabwe volume (eds MD Prendergast, MJ Jones ). Inst of Mining and Metal London, pp 139–150

MacDonald H (1999) Petrology of mafic intrusions, Pants Lake area, Labrador. Unpublished MSc thesis, University of Toronto

Machado N, Heaman L, Krogh TE, Weber W (1987) U-Pb geochronology program: Thompson Belt Northern Superior Province. Report of field activities 1987, Manitoba Energy and Mines

Mackovicky M, Mackovicky E, Rose-Hansen J (1986) Experimental studies on the solubility and distribution of platinum group elements in base-metal sulfides in platinum deposits. *In* Metallogeny of basic and ultrabasic rocks (eds MJ Gallagher, RA Ixer, CR Neary, HM Prichard). Inst Min Met Spec Pub, pp 415–426

MacLean WH (1969) Liquidus phase relations in the FeS-FeO-$Fe_3O$-$SiO_2$ systems and their application in geology. Econ Geol 64: 865–884

Mahoney J, Coffey MJ, eds (1997) Large igneous provinces: continental oceanic and planetary flood volcanism. Amer Geophys Union, Geophysics Monograph 100, 438 p

Maier WD, Barnes S-J, De Klerk WJ, Teigler B, Mitchell AA (1996) Cu/Pd and Cu/Pt ratios of silicate rocks in the Bushveld Complex: Implications for PGE exploration. Econ Geol 91: 1151–1158

Maier WD, Arndt NT, Curl E (2000) Progressive crustal contamination of the Bushveld Complex; Evidence from Nd isotopic analyses of the cumulus rocks. Contr Mineral Petrol 140: 328–343

Mainwaring PR (1968) The sulfide assemblage of the Great Lakes Nickel intrusion. Unpublished BSc thesis, Univ of Western Ontario

Mainwaring PR, Naldrett AJ (1977) Country-rock assimilation and the genesis of Cu-Ni sulfides in the Waterhen intrusion Duluth Complex Minnesota. Econ Geol 72: 1269–1284

Malich KN (1999) Platinum-group elements in clinopyroxenite-dunite massifs of the East Siberia (geochemistry mineralogy and genesis). Sankt-Peterburgskaya kartograficheskaya fabrika VSEGEI, St. Petersburg, 296 p (in Russian)

Marsh JS, Eales HV (1984) The chemistry and petrogenesis of igneous rocks of the Karoo central area southern Africa. *In* Petrogenesis of the Volcanic Rocks of the Karoo Province (ed AJ Erlank). Spec Pub Geol Soc S Afr vol 13, pp 27–68

Marston RJ, Kay BD (1980) The distribution petrology and genesis of nickel ores at the Juan complex Kambalda Western Australia. Econ Geol 75: 546–565

Marston RJ, Groves DI, Hudson DR, Ross JR (1981) Nickel sulfide deposits in Western Australia. A review. Econ Geol 69: 1330–1363

Martineau MP (1989) Empirically derived controls on Cu-Ni mineralisation: A comparison between fertile and barren gabbros in the Duluth complex Minne-

sota USA. *In* Magmatic Sulfides – The Zimbabwe Volume (eds M. Prendergast, MJ Jones). Spec Pub Inst Mining and Metallurgy London, pp 117–138

Masaitis VL (1983) Permian and Triassic volcanism in Siberia: problems of dinamic reconstruction. Zapiski VMO pt CXII issue 4, pp 412–425 (in Russian)

Masaitis VL, Shafranovsky GI, Grieve RAF, Langenhorst F, Peredery WV, Therriault AM, Balmasov EL, Fedorova IG (1999) Impact diamonds in the suevitic breccias of the black member of the Onaping formation Sudbury structure Ontario Canada. *In* Large meteorite impacts and planetary evolution II (eds BO Dressler, VL Sharpton). Geol Soc Amer Spec Pap No 339, pp 317–322

Maske S (1966) The petrography of the Ingeli mountain range. Univ Stellenbosch Annals series A 41 No 1, 109 p

Maslov GD (1963) Tectonics of the Igarka-Noril'sk region and mineralizing structures. *In* Tectonics of Siberia vol 2, Nedra, Novosibirsk, pp 336-350 (in Russian)

Mathez EA (1976) Sulfur solubility and magmatic sulfides in submarine basalt glass. J Geophys Research 81: 4269–4276

Mathez EA (1990) Vapour associated with mafic magma and controls on its composition. I*n* Ore deposition associated with magmas (eds JA Whitney, AJ Naldrett). Reviews in Econ Geol vol 4, pp 21–31

Matlock WF, Watowich SN (1980) Geology and sulfide mineralization of the Duluth Compex –Virginia formation contact Minnamax deposit Minnesota (abs). Geol Soc Amer Abstracts with Programs, pp 477–478

Mavrogenes JA, O'Neill HSC (1999) The relative effects of pressure temperature and oxygen fugacity on the solubility of sulfide in mafic magmas. Geochim Cosmochim Acta 63: 1173–1180

McBirney AR (1987) Constitutional zone refining of layered intrusions. *In* Origin of igneous layering (ed I. Parsons). Nato ASI Series C vol 196, pp 437–452

McBirney AR (1989a) Geological map of the Skaergaard Intrusion East Greenland 1:200000. University of Oregon Eugene

McBirney AR (1989b) The Scaergaard layered series: i. Structure and average composition. J Petrol 30: 363–397

McCallum ME, Loucks RR, Carlson RR, Cooley EF, Doerge TA (1976) Platinum metals associated with hydrothermal copper ores of the New Rambler mine Medicine Bow Mountains Wyoming. Econ Geol 71: 1429–1450

McCann AJ, Trzcienski WE Jr, Birkett TC (1998) The Soquem Sept-Iles Fe-Ti-P deposit. Abstract volume Geol Assoc Can – Mineral Assoc Can Annual Meeting Quebec, p. A-121

McClelland J, Ashwal Z, Moore L (1994) Composition and petrogenesis of oxide-apatite-rich gabbronorites associated with Proterozoic anorthosite massifs: examples from the Adirindack Mountains New York. Contr Mineral Petrol 116: 225–238

McGrath PH, Broome HJ (1994) A gravity model for the Sudbury structure. I*n* Proc of the Sudbury Noril'sk Symposium (eds PC Lightfoot, AJ Naldrett). Ontario Geol Surv Spec Pub 5, pp 21–33

McNaughton NJ, Frost KM, Groves DI (1988) Ground melting and ocellar komatiites: a lead isotopic study at Kambalda Western Australia. Geol Mag 125: 285–295

McQueen KG (1981) Volcanic-associated nickel deposits from around the Widgiemooltha dome Western Australia. Econ Geol 76: 1417–1443

McRae ND, Reeve EJ (1968) Differentiation sequence of the Great Lakes Nickel intrusion. Abstracts 14th Annual Inst of Lake Superior Geology, Superior, Wisconsin, p 28

Melezhik VA, Sturt BF (1994) General geology and evolutionary history of the Early Proterozoic Polmak - Pasvik - Pechenga/Imandra - Varsuga - Ust'Ponoy Greenstone Belt in the northeastern Baltic Shield. Earth Science Reviews vol 36, pp 205–241

Melezhik VA, Hudson-Edwards KA, Green AN, Grinenko LN (1994) Pechenga area Russia – Part 2: nickel-copper deposits and related rocks. Trans Instn Mining Metall (Section B: Applied Earth Sci) vol 103, pp B87–162

Melezhik VA, Sturt BA, Ramsay DM, Nilsson L-P, Balashov YuA (1995) The early Proterozoic Pasvik-Pechenga Greenstone Belt: 1:200000 geological map stratigraphic correlation and revision in stratigraphic nomenclature. Nor Geol Unders. Geology of the Eastern Finnmark – Western Kola Peninsula region, Spec Pub 7, pp 81–91

Melosh HJ (1979) Acoustic fluidization: A new geologic process? J Geophys Research 84: 7513–7520

Melosh HJ, Ivanov BA (1999) Impact crater collapse. Annual Reviews in Earth and Planetary Science vol 27, pp 385–415

Mernagh TP, Heinrich CA, Leckie JF et al. 1994. Chemistry of low-temperature hydrothermal gold platinum and palladium (± uranium) mineralisation of Coronation Hill Northern Territory Australia. Econ Geol 89: 1053-1073

Merwin HE, Lombard RH (1937) The system Cu-Fe-S. Econ Geol 32: 203–284

Milkereit B, Green A, Berrer E, Boerner D, Broome J, Cosec M, Cowan J, Davidson A, Dressler B, Fueten F, Grieve R, James R, Kraus B, McGrath P, Meyer W, Moon W, Morris W, Morrison G, Naldrett A, Peredery W, Rousell D, Salisbury M, Schwerdtner W, Snajdr P, Thomas M, Watts A (1992) Geometry of the Sudbury Structure from High Resolution Seismic Reflection Profiling. Geology 20: 807–811

Miller JD Jr (1999) Geochemical evaluation of platinum group element (PGE) mineralisation in the Sonju Lake Intrusion Finland Minnesota. Minnesota Geol Surv Information Circular 44, 32 p

Miller JD Jr, Andersen JCO (2002) Attributes of Skaergaard-type reefs. *In* Extended Abstracts 9th Internat Platinum Symposium (ed A Boudreau), pp 305–308

Miller JD Jr, Chandler VW (1999) Bedrock geologic map of the central Duluth Complex and western part of the Beaver Bay Complex Lake and St. Louis Counties Minnesota. Minnesota Geol Surv Miscellaneous map series M-101, 1:100000 scale

Miller JD Jr, and Ripley EM (1996) Layered intrusions of the Duluth Complex Minnesota USA. *In* Layered Intrusions (ed RG Cawthorn), Elsevier, pp 257–301

Miller JD Jr, Green JC Chandler VW, Boerboom TJ (1993) Geologic map of the Finland and Doyle Lake quadrangles Lake County Minnesota. Minnesota Geol. Surv Miscellaneous Map series M-72, scale 1:24000

Mungall JE, Andrews DRA, Cabri LJ, Sylvester PJ, Tubrett M (submitted) Partioning of Cu Ni Au and Platinum-group elements between monosulfide solid solution and sulfide melt under controlled oxygen and sulfur fugacities. Geochim Cosmochim Acta

Mintz NV, Glaznev VN, Konilov AN, Kunina NM, Nikitichev AP, Raevsky AB, Sedykh YuP, Stupak VM, Fonarev VI (1996) Early Pre-Cambrian of the north-eastern part of the Baltic shield: paleogeodynamics, construction and evolution of the continental crust. Nauchny mir, Moscow, 287 p (in Russian)

Misra KC, and Fleet ME (1973) The chemical compositions of synthetic and natural pentlandite assemblages. Econ Geol 68: 518–539

Misra KC, Fleet ME (1974) Chemical composition and stability of violarite. Econ Geol 69: 391–403

Mitchell RH, Platt RG (1994) Aspects of the geology of the Coldwell alkaline complex. Field trip A2, Geol Assoc Can – Mineral Asso. Can Joint Annual Meeting, Waterloo Ontario, 36 p

Molyneaux TG (1974) A geological investigation of the Bushveld Complex in Sekhukhunelan and apart of the Steelpoort Valley. Geol Soc South Africa Trans 77: 329–338

Momme P, Oskarsson N, Keays RR (2003) Platinum-group elements in the Icelandic rift system: Melting processes and mantle sources beneath Iceland. Chem Geol 196: 209–234

Moore ES (1930) Geological Structure of the Southwest Portion of the Sudbury Basin. Transactions of the Can Inst Min Met vol 33, pp 292–302

Morgan JW, Walker RJ, Horan MF, Beary ES, Naldrett AJ (2002) $^{190}$Pt-$^{186}$Os and $^{187}$Re-$^{187}$Os systematics of the Sudbury Igneous Complex Ontario. Geochim Cosmochim Acta 66: 273–290

Morrison GG (1984) Morphological features of the Sudbury Structure in relation to impact origin. *In* The Geology and Ore Deposits of the Sudbury Structure (eds EG Pye, AJ Naldrett, PE Giblin). Ontario Geol Surv Spec Vol 1, pp 513–520

Morse SA (1961) The Kiglapait layered intrusion Labrador. Geol Soc Amer Memoir 112, p 204

Morse SA (1979a) Kiglapait geochemistry I: Systematics sampling and density. J Petrol 20: 555–590

Morse SA (1979b) Kiglapait geochemistry II: Petrography. J Petrol 20: 591–624

Morse SA (1980) Kiglapait mineralogy II: Fe-Ti oxide minerals and the activities of oxygen and silica. J Petrol 21: 685–719

Morse SA (1981a) Kiglapait geochemistry III: Potassium and rubidium. Geochim Cosmochim Acta 45: 163–180

Morse SA (1981b) Kiglapait geochemistry IV: The major elements. Geochim Cosmochim Acta 45: 461–479

Morse SA (1982) Kiglapait geochemistry V: Strontium. Geochim Cosmochim 46: 223–234

Muir TL (1983) Geology of the Morgan Lake-Nelson Area District of Sudbury. Ontario Geol Surv Open File Report 5426, 203 p

Muir TL (1984) The Sudbury Structure; Considerations fnd Models for an Endogenic Origin. *In* The Geology and Ore Deposits of the Sudbury Structure (eds EG Pye, AJ Naldrett, PE Giblin). Ontario Geol Surv Spec Vol .1, pp 449–490

Muir TL, Peredery WV (1984) The Onaping Formation. *In* The Geology and Ore Deposits of the Sudbury Structure (eds EG Pye, AJ Naldrett, PE Giblin). Ontario Geol Surv Spec Vol .1, pp 139–210

Mukaiyama H and Izawa E (1970) Phase relations in the Cu-Fe-S system: The copper-deficient part. *In* Volcanism and Ore Genesis (ed T Tatsumi), Univ Tokyo Press, pp 339–355

Mungall J (2002) A model for the co-precipitation of platinum-group minerals with chromite from silicate melts. *In* Extended Abstracts 9th Internat Platinum Symposium (ed A Boudreau), pp 321–324

Mungall JE, Keast T (2003) Cu-Ni-PGE mineralization at the Expo-Ungava and Mesamax deposits, New Quebec. Quebec Exploration 2003, Quebec, November, pp 24-27

Murphy AJ, Spray JG (2002) Geology mineralisation and emplacement of the Whistle-Parkin offset dyke Sudbury. Econ Geol 97: 1399–1418

Murray CG (1972) Zoned ultramafic complexes of the Alaskan type: Feeder pipes of andesitic volcanoes. Geol Soc Amer Memoir vol 132, pp 313–335

Nagamori M, Kameda M (1965) Equilibria between Fe-S-O system melts and CO-$CO_2$-$SO_2$ gas mixtures at 1200°C. Transactions of the Japan Inst of Metallurgy vol 6, pp 21–30

Naldrett AJ (1964) Ultrabasic rocks of the Porcupine and related nickel deposits. Unpub PhD thesis, Queen's University Canada, 264 p

Naldrett AJ, (1969) A portion of the Fe-S-O and its application to sulfide ore magmas. J Petrology 10: 171-201

Naldrett AJ (1973) Nickel sulfide deposits – Their classification and genesis with special emphasis on deposits of volcanic association. Trans Can Inst Mining Metallurgy 76, pp 183–201

Naldrett AJ (1981a) Nickel sulfide deposits: Classification Composition and Genesis. Econ Geol 75 ann vol, pp 628–685

Naldrett AJ (1981b) Pt group element deposits. *In* Platinum Group Elements: Mineralogy Geology Geochemistry (ed LC Cabri). Can Inst Mining Metallurgy Spec Vol 23, pp 197–232

Naldrett AJ (1984) Summary Discussion and Synthesis. *In* The Geology and Ore Deposits of the Sudbury Structure (eds EG Pye, AJ Naldrett, PE Giblin). Ontario Geol Surv Spec Vol 1, pp 533–570

Naldrett AJ (1989) Magmatic sulfide deposits. Oxford - New York, Oxford Univ Press, 196 p

Naldrett AJ (1992) A model for the Ni-Cu-PGE ores of the Noril'sk region and its application to other areas of flood basalt. Econ Geol 87: 1945–1962

Naldrett AJ (1999a) Summary: Development of ideas on Sudbury geology 1992-1998. *In* Large meteorite impacts and planetary evolution II (eds BO Dressler, VL Sharpton), Geol Soc Amer Spec Pap 339, pp 431–442

Naldrett AJ (1999b) World class Ni-Cu-PGE Deposits: Key factors in their genesis. Mineralium Deposita 34: 227–240

Naldrett AJ (2000) Evidence for sulfide and Fe-Ti-P-rich liquid immiscibility in the Duluth Complex Minnesota: comments on the paper by Ripley et al. SEG Newsletter No 36, p 5

Naldrett AJ (2003) From impact to riches: evolution of geological understanding as seen at Sudbury Canada. GSA today 13, No 2: 4–9

Naldrett AJ, Cabri LJ (1976) Ultramafic and related mafic rocks: Their classification and genesis with special reference to the concentration of nickel sulfides and platinum-group elements. Econ Geol 71: 1131–1158

Naldrett AJ, Duke JM (1980) Platinum metals in magmatic sulfide ores. Science 208: 1417–1428

Naldrett AJ and Gasparrini EL (1971) Archean nickel sulfide deposits in Canada: their classification geological setting and genesis with some suggestions as to exploration. Geol Soc Austr Spec Pub 3, pp 201–226

Naldrett AJ, Goodwin AM (1977) Volcanic rocks of the Blake River group Abitibi greenstone belt Ontario and their sulfur content. Can J Earth Sci 14: 539–550

Naldrett AJ, Hewins RH (1984) The main mass of the Sudbury Igneous Complex. *In* The Geology and Ore Deposits of the Sudbury Structure (eds EG Pye, AJ Naldrett, PE Giblin), Ontario Geol Surv Spec Vol 1, pp 235–251

Naldrett AJ, Kullerud G (1967) A study of the Strathcona mine and its bearing on the origin of the nickel-copper ores of the Sudbury district Ontario. J Petrology 8: 453–531

Naldrett AJ, Lehmann J (1988) Spinel non-stoichiometry as the explanation for Ni- Cu- and PGE-enriched sulphides in chromitites. *In* Geoplatinum '87 (eds H. Prichard, P Potts, J Bowles, S Cribb). Elsevier, London, pp 93–110

Naldrett AJ, Lightfoot PC (1994) The Ni-Cu-PGE ores of the Noril'sk region Siberia: A model for giant magmatic sulfide deposits associated with flood basalts. *In* Proc of Symposium on Giant Ore Deposits, Queen's University May 1992, Soc of Econ Geol Spec Pub 2, pp 81–123

Naldrett AJ, Mason GD (1968) Contrasting Archean ultramafic igneous bodies in Dundonald and Clergue townships Ontario. Can J Earth Sci 5: 111–143

Naldrett AJ, Pessaran A (1992) Compositional variation in the Sudbury ores and prediction of the proximity of footwall copper-PGE ore bodies. *In* Geoscience Research Programme Summary of Research 1991-1992 (ed VC Milne), Ontario Geol Surv Miscellaneous Paper 159, pp 49–64

Naldrett AJ, Richardson SW (1967) Effect of water on the melting of pyrrhotite-magnetite assemblages. Annual Report of the Director of the Geophysical Laboratory Carnegie Inst of Washington, Year Book vol 66, pp 429–431

Naldrett AJ, Smith IEM (1981) Mafic and ultramafic volcanism during the Archean. *In* Basaltic volcanism in the terrestrial planets. Basaltic volcanism study project, Pergamon Press In, New York, pp 5–28

Naldrett AJ, Turner AR (1977) The geology and petrogenesis of a greenstone belt and related nickel sulfide mineralization at Yakabindi Western Australia, Prec Res vol 5, pp 43–103

Naldrett AJ, von Gruenewaldt G (1989) The association of the PGE with chromitite in layered intrusions and ophiolite complexes. Econ Geol 84: 180–187

Naldrett AJ, Wilson AH (1990) Horizontal and vertical variations in noble metals in the Great Dyke of Zimbabwe: A model for the origin of the PGE mineralization by fractional segregation. Chem Geol 88: 279–300

Naldrett AJ Craig JR, Kullerud G (1967) The central portion of the Fe-Ni-S system and its bearing on pentlandite solution in iron-nickel sulfide ores. Econ Geol 62: 826–847

Naldrett AJ, Bray JG, Gasparrini EL, Podolsky T, Rucklidge JC (1970) Cryptic variation and the petrology of the Sudbury Nickel Irruptive. Econ Geol 65: 122–155

Naldrett AJ, Greenman L, Hewins RH (1972) The main Irruptive and the sublayer at Sudbury Ontario. Internat Geological Congress 24th Montreal Proc section 4, pp 206–214

Naldrett AJ, Hoffman EL, Green AH, Chou CL, Naldrett SR, Alcock RA (1979) The composition of Ni-sulfide ores with particular reference to their content of PGE and Au. Can Min 17, Pt. 2: 403–415

Naldrett AJ, Innes DG, Sowa J, Gorton M (1982) Compositional variation within and between 5 Subury ore deposits. Econ Geol 77: 1519–1534

Naldrett AJ, Duke JM, Lightfoot PC, Thompson JFH (1984a) Quantitative Modelling of the segregation of magmatic sulfides: an exploration guide. Bull Can Inst Min Metall 77: 46–57

Naldrett AJ, Hewins RH, Dressler BO, Rao BV (1984b) The contact sublayer of the Sudbury Igneous Complex. *In* The Geology and Ore Deposits of the Sudbury Structure (eds EG Pye, AJ Naldrett, PE Giblin), Ontario Geol Surv Spec Vol 1, pp 253–274

Naldrett AJ, Gasparrini EC, Barnes SJ, von Gruenewaldt G, Sharpe MR (1986a) The upper critical zone of the Bushveld Complex and a model for the origin of Merensky-type ores. Econ Geol 81: 1105–1118

Naldrett AJ, Rao BV, Evensen NM (1986b) Contamination at Sudbury and its role in ore formation. *In* Metallogeny of Basic and Ultrabasic Rocks (eds MJ Gallagher, RA Ixer, CR Neary, HM Pritchard), Spec Pub Inst Min Met, London, 75–92

Naldrett AJ, Cameron G, von Gruenewaldt G, Sharpe MR (1987) The formation of stratiform PGE deposits in layered intrusions. *In* Origins of Igneous Layering (ed I Parsons). NATO Advanced Sc Inst Series, Series C, vol 196, pp 313–397, Reidel Dudrecht

Naldrett AJ, Lightfoot PC, Fedorenko VA Gorbachev NS, Doherty W (1992) Geology and geochemistry of intrusions and flood basalts of the Noril'sk region

USSR with implications for the origin of the Ni-Cu ores. Econ Geol 87: 975–1004

Naldrett AJ, Asif M, Gorbachev NS, Kunilov VE, Stehkin AI, Fedorenko VA, Lightfoot PC (1994a) The composition of the Ni-Cu ores of the Noril'sk region. *In* Proc. of the Sudbury Noril'sk Symposium (eds PC Lightfoot, AJ Naldrett), Ontario Geol Surv Spec Pub 5, pp 357–372

Naldrett AJ, Asif M, Scoates RFJ, Eckstrand OR, Schwann PL (1994b) Platinum-Group Elements in the Fox River Sill Manitoba Canada: Implications with respect to influxes of fresh magma and exploration for PGE deposits. Trans Inst Min Met vol 103, pp 10–21

Naldrett AJ, Pessaran A, Asif M, and Li C (1994c) Compositional variation in the Sudbury ores and prediction of the proximity of footwall copper-PGE ore bodies. *In* Proc. of the Sudbury Noril'sk Symposium (eds PC Lightfoot, AJ Naldrett), Ontario Geol Surv Spec Pub 5, pp 133–146

Naldrett AJ, Fedorenko VA, Lightfoot PC, Kunilov VE, Gorbachev NS, Doherty W, Johan J (1995) Ni-Cu-PGE deposits of the Noril'sk region Siberia: Their formation in conduits for flood basalt volcanism. Trans Inst Min Met vol 104, pp B18–B36

Naldrett AJ, Fedorenko VA, Asif M, Lin S, Kunilov VE, Stekhin AI, Lightfoot PC, Gorbachev NS, (1996a) Controls on the composition of Ni-Cu sulfide deposits as illustrated by those at Noril'sk Siberia. Econ Geol 91: 751–773

Naldrett AJ, Keats H, Sparkes K, Moore R, (1996b) Geology of the Voisey's Bay Ni-Cu-Co deposit Labrador Canada. Exploration and Mining Geology J 5: 169–179

Naldrett AJ, Li C, Krstic S, (1997) The Voisey's Bay Ni-Cu-Co deposit Labrador Canada: Implications for exploration elsewhere. *In* Mineral Deposits: Research and Exploration Where do they meet? (ed H Papunen). Proc of the fourth biennial SGA meeting Turku Finland August 1997, Balkema Rotterdam, pp 7–8

Naldrett AJ, Ebel DS, Asif M, Morrison G, and Moore C (1997) Fractional crystallisation of sulfide melts as illustrated at Noril'sk and Sudbury. European J Mineralogy 9: 365–377

Naldrett AJ, Asif M, Schandl E, Searcy T, Morrison G, Binney P, Moore C (1999) PGE in the Sudbury Ores: Significance with respect to the origin of different ore zones and the exploration for footwall ore bodies. Econ Geol 94: 185–210

Naldrett AJ, Asif M, Krstic S, Li C (2000a.) The composition of ore at the Voisey's Bay Ni-Cu sulfide deposit with special reference to platinum-group elements. Econ Geol 95: 845–866

Naldrett AJ, Singh J, Krstic S and Li C (2000b) The mineralogy of the Voisey's Bay Ni-Cu-Co deposit Northern Labrador Canada: Influence of oxidation state on textures and mineral compositions. Econ Geol 95: No. 4 889–900

Negrutza VZ (1984) Early Proterozoic stages of evolution of the eastern part of the Baltic shield. Nedra, Leningrad, 270 p (in Russian)

Nesbitt RW (1971) Skeletal crystal forms in the ultramafic rocks of the Yilgarn block Western Australia: Evidence for an Archean ultramafic liquid. Geol Soc Austr Spec Pub 3, pp 331–350

Nielsen TFD, Brooks CK (1995) Precious metals in magmas of East Greenland: Factors important to the mineralization in the Skaergaard intrusion. Econ Geol 90: 1911–1917

Ostermann M (1996) Die Geochemic der Impaktschemelzecke (Sudbury Igneous Complex) im Multiring-Becken Sudbury. PhD thesis. Munster, 168 p

Page NJ, Zientek ML, Czamanske GK, Foose MP (1985) Sulfide mineralization in the Stillwater Complex and underlying rocks. *In* Stillwater Complex (eds GK Czamanske, ML Zientek). Montana Bureau of Mines and Geology Spec Pub 92, pp 93–96

Papunen H, Gorbunov GI, eds (1985). Nickel-copper deposits of the Baltic Shield and Scandinavian Caledonides. Geol Surv Finland Bull 333, 394 p

Papushis BI (1952) On the problem of differentiation of ultramafic and mafic intrusions from Pechenga *In* Ultramafic and mafic intrusions and sulfide nickel-copper deposits of Pechenga. AN SSSR, Leningrad, pp 17–35 (in Russian)

Parrish RR(1989) U-Pb geochronology of the Cape Smith Belt and Sugluk block northern Quebec. Geoscience Canada 16, No 3: 126–130

Paterson HL, Donaldson MJ, Smith RN, Lenard MF, Gresham JJ, Boyack DJ, and Keays RR (1984) Nickeliferous sediments and sediment-associated nickel ores at Kambalda Western Australia. *In* Sulfide deposits in mafic and ultramafic rocks (eds DL Buchanan, MJ Jones). Inst Min Met, London, pp 81–94

Pattison EF (1979) The Sudbury sub-layer: Its characteristics and relationships with the main mass of the Sudbury Irruptive. Can Min 17, pt 2: 257–274

Peach CL, Mathez EA (1993) Sulfide melt-silicate melt distribution coefficients for nickel and iron and implications for the distribution of other chalcophile elements. Geochim Cosmochim Acta 57: 3013–3021

Peach CL, Mathez EA, Keays RR (1990) Sulfide melt-silicate melt distribution coefficience for noble metals and other chalcophile elements as deduced from MORB: Implications for partial melting. Geochim Cosmochim Acta 54: 3379–3389

Peach CL, Mathez EA, Keays RR, Reeves SJ (1994) Experimentally determined sulfide melt-silicate melt partition coefficients for Ir and Pd. Chem Geol 117: 361–377

Peck DC, Scoates RFJ, Theyer P, Desharnais G, Hulbert LJ, Huminicki MAE (2002) Stratiform and Contact-type PGE-Cu-Ni Mineralization in the Fox River Sill and the Bird River Belt Manitoba. *In* The Geology Geochemistry Mineralogy and Mineral Beneficiation of Platinum-Group Elements (ed LJ Cabri). Ottawa Ontario, Can Inst Min Met Spec Vol 54, pp 367–387

Peredery WV and Geological Staff (1982) Geology and nickel sulfide deposits of the Thompson belt Manitoba; in Precambrian Sulfide deposits. HS Robinson memorial volume (eds RW Hutchinson, CD Spence, J M Franklin). Geol Assoc Can Spec Pap 25, pp 165–209

Peregoedova AV, Fedorova ZhN, Sinyakova EF (1995) Physiochemical conditions of the pentlandite formation in Cu-bearing sulfide paragenesis (according to experimental data). Russian Geology and Geophysics 36: 91-98

Philpotts AR (1967) Origin of certain iron-titanium oxide and apatite rocks. Econ Geol 62: 303–315

Phinney WC (1970) Chemical relations between Keewanawan lavas and the Duluth complex Minnesota. Geol Soc Amer Bull 81, pp 2487–2496

Phinney WC (1972) Northwestern part of the Duluth complex. *In* Geology of Minnesota (eds PD Sims, GB Morey). A centennial volume, St Paul, Minnesota, Geol Surv, pp 335–345

Picard C, Lamothe D, Piboule M, Oliver R (1990) Magmatic and tectonic evolution of a Proterozoic basin system: the Cape Smith Thrust-Fold Belt (New-Quebec). Prec Res 47, pp 223–249

Platt JP, Allchurch PD and Rutland RWR (1978) Archean tectonics in the Agnew supracrustal belt Western Austrlia. Prec Res 7, pp 3–30

Pozhilenko VI, Smolkin VF, Sharov NV (1997) Seismogeological models of the crust of the Lapland-Pechenga region. *In* Seismogeological model of the lithosphere of North Europe: Lapland-Pechenga region (ed NV Sharov). Kolsky nauchny tsentr RAN, Apatity, pp 181–208 (in Russian)

Predovsky AA, Zhangurov AA, Fedotov ZhA (1971) Evolution of the composition of mafic-ultramafic rocks and its role in generation of nickel-copper mineralization at Pechenga. *In* Problems of magmatism of the Baltic shield. Nauka, Leningrad, pp 166–175 (in Russian)

Predovsky AA, Fedotov ZhA, Akhmedov AM (1974) Geochemistry of the Pechenga complex (metamorphosed sediments and volcanics). Nauka, Leningrad, 139 p. (in Russian)

Premo WR Helz RT Zientek ML, Langston RB (1990) U-Pb and Sm-Nd ages for the Stillwater Complex and its associated sills and dikes, Beartooth Mountains Montana. Identification of a parent magma? Geology 18: 1065–1068

Prendergast MD, Bennett M, and Henicke O (1998) Platinum in the Rincon del Tigre Complex eastern Bolivia. Transactions Inst Min Met 107: B39–47

Pye E, Naldrett AJ, Giblin P, eds (1984) The Geology and Ore Deposits of the Sudbury Structure. Ontario Geol Sur. Spec Vol 1, 603 p

Pyke DR, Naldrett AJ, Eckstrand OR (1973) Archean ultramafic flows in Munro Township Ontario. Geol Soc Amer Bull 84, pp 955–978

Rad'ko VA (1991) Model of dynamic differentiation of intrusive traps in the northwestern Siberian platform. Soviet Geology and Geophysics 32, No 11: 15-20

Rajamani V, Naldrett AJ (1978) Partitioning of Fe Co Ni and Cu between sulfide liquid and basaltic melts and the composition of Ni-Cu sulfide deposits. Econ Geol 73: 82–93

Rao BV, Ripley EM (1983) Petrochemical studies of the Dunka Road Cu-Ni deposit. Econ Geol 78: 1222–1238

Rao BV, Naldrett AJ, Evensen NM, Dressler BO (1983) Grant 146. Contamination and genesis of the Sudbury Ores. *In* Geoscience Research Programme Summary of Research 1982–1983. Ontario Geol Surv Miscellaneous Paper 113, pp 139–152

Reeve EJ (1969) Petrology and Mineralogy of a gabbroic intrusion in Pardee township near Port Arthur Ontario. Unpublished MSc thesis, University of Wisconsin

Rempel GG (1994) Regional geophysics at Noril'sk. *In* Proc of the Sudbury-Noril'sk symposium. Ontario Geol Surv Spec Pub 5, pp 147–160

Richards MA, Duncan RA, Courtillot VE (1989) Flood basalt and hotspot tracks: Plume heads and tails. Science 246: 103–107

Ripley EM (1981) Sulfur isotopic abundances of the Dunka Road Cu-Ni deposit Duluth Complex Minnesota. Econ Geol 76: 619–620

Ripley EM (1986) Applications of stable isotope studies to problems of magmatic sulfide ore genesis with special reference to the Duluth Complex Minnesota. *In* Geology and Metallogeny of Copper Deposits (eds GH Friedrich, AD Genkin, AJ Naldrett, JD Ridge, RH Sillitoe, FM Vokes). Soc for Geology Applied to Ore Deposits Spec Pub 4. Springer-Verlag, Berlin-Heidelberg p, pp 25–42

Ripley EM, Li C, Sarker A (2003) Sulfur and oxygen isotopic geochemistry of the Jinchuan Ni-Cu sulfide deposit Western China [abstract]. Geol Assoc Can – Mineral Assoc Can –Soc of Economic Geologists meeting, Vancouver BC, May 2003. Volume of abstracts

Ripley EM, Park Y-R, Li C, Naldrett AJ (1999) Sulfur and oxygen isotopic evidence of country rock contamination in the Voisey's Bay Ni-Cu-Co deposit Labrador Canada. Lithos 47: 53–68

Ripley EM, Park Y-R, Li C, Naldrett AJ (2000) Oxygen isotopic study of the Voisey's Bay Ni-Cu-Co deposit Labrador Canada. Econ Geol 95: 831–844

Roeder PL (1974) Activity of iron and olivine solubility in basaltic liquids. Earth Planetary Science Letters 23: 397–410

Roeder PL, Emslie RF (1970) Olivine-liquid equilibrium. Contr Mineral Petrol 29: 275–289

Rosenqvist T (1954) A thermodynamic study of the iron cobalt and nickel sulfides. J. Iron and Steel Inst 176: 37–57

Ross JR, Hopkins GMF (1975) The nickel sulfide deposits of Kambalda Western Australia. *In* Econ Geol Austr and Papua - New Guinea (ed C Knight). Austr Inst Min Metall Monograph 51, Metals, pp 100–121

Ross JR, Travis GA (1981) The nickel sulfide deposits in western Australia in global perspective. Econ Geol 76: 1291–1329

Ryabov VV (1982) About the concentration of chromium and platinum group elements at the roof of the layered Noril'sk-type intrusions. Doklady Akademii Nauk 266: 466–469 (in Russian)

Ryabov VV, Shevko AYa, Gora MP (2000) Magmatic formations of the Noril'sk region. Vol 1. Petrology of traps. Nonparel, Novosibirsk, 408 p (in Russian)

Ryan B (1990) Geological Map of the Nain Plutonic Suite and surrounding rocks (Nain-Nutak NTS 14SW). Newfoundland Department of Mines and Energy Geol Surv Branch, Map 90-44, scale 1:500000

Ryan B (1996) Commentary of the location of the Nain-Churchill boundary in the Nain area. Newfoundland Department of Natural Resources Geol Surv Report 96-1, pp 109–129

Ryan B (2000) The Nain-Churchill Boundary and the Nain Plutonic Suite: A Regional Perspectiva on the Geological Setting of the Voisey's Bay Ni-Cu-Co Deposit. Econ Geol 95: 703–724

Ryan B, Phillips E, Shwetz J, Machado G (1998) A tale of more than ten plutons [Geology of the region between Okak Bay and Staghorn Lake Labrador (parts of NTS maps 14e/2 7 8)]. Newfoundland Department of Mines and Energy, Geol Surv Branch, Report 98-1, pp 143–171

Ryan B, Wardle RJ, Gower CF, Nunn GAG (1995) Nickel-Copper sulphide mineralisation in Labrador: The Voisey Bay discovery and its exploration implications.*In* Current Research Report 95-1 Geol Surv, Department of Natural Resources. Government of Newfoundland and Labrador, pp 177–204

Ryzhenko B, Kennedy GC (1973) The effect of pressure on the eutectic in the system Fe-FeS. Amer J Sc 273: 803–810

Sage RP (1991) Alkalic rock carnonatite and kimberlite complexes of Ontario Superior Province. *In* Geology of Ontario (eds PC Thurston, HR Williams, RH Sutcliffe, GM Stott). Ontario Geol Surv Spec Vol 4, pp 683–709

Samonov IZ, Pozharisky IF (1974) Copper deposits. *In* Ore deposits of the USSR, vol 2. Nedra, Moscow, pp 99–168 (in Russian)

Sattari P, Brenan JM, Horn I, McDonough WF (2002) Experimental constraints on the sulfide- and chromite-silicate melt partitioning behaviour of rhenium and the platinum-group elements. Econ Geol 97: 385–398

Schiffries CM (1982) The petrogenesis of a platiniferous dunite pipe in the Bushveld Complex: Infiltration metasomatism by a chloride solution. Econ Geol 77: 1439–1453

Schlegel H, Schiller A (1952) Die Schmelzund Kristallisations gleischgeinwichte in System Cu-Fe-S und ihre Bedentung fur Kupfergewinnung. Freiberg Forsch Sec Be No 2, pp 1–32

Schmulian ML (1984) Windarra nickel deposits Western Australia. *In* Sulfide deposits in mafic and ultramafic rocks (eds DL Buchanan, MJ Jones), Inst Mining Metallurgy Spec Pub, pp 95–102

Scholtz DL (1936) The magmatic nickeliferous ore deposits of East Griqualand and Pondoland. Transactions of the Geol Soc South Africa vol 39, pp 81–210

Scholtz DL (1952) Fourth bi-annual report on the Insizwa mine. Unpub company report, Nickel Corp of Africa Ltd, 9 p

Scoates RFJ, Eckstrand OR (1986) Platinum-group elements in the upper central layered zone of the Fox River Sill northeastern Manitoba. Econ Geol 81: 1137–1148

Scoates JS, Mitchell JN (2000) The evolution of troctolitic and high Al basaltic magmas in Proterozoic anorthosite plutonic suites and implications for the Voisey's Bay massive Ni-Cu sulfide deposit. Econ Geol 95: 677–702

Scott SD, Naldrett AJ, Gasparrini E (1974) Regular solution model for the $Fe_{1-X}S$ – $Ni_{1-}XS$ (mss) solid solution (Abstract). Internat Mineral Assoc. 9th General Meeting, Berlin and Regensburg, p. 172

Scott DJ, St-Onge MR, Lucas SB, Helmstaedt H (1989) The 1998 Ma Purtuniq ophiolite: imbricated and metamorphosed oceanic crust in the Cape Smith thrust belt northern Quebec. Geoscience Canada vol 16, No 3, pp 144–147

Scribbins B, Rae DR, Naldrett AJ (1984) Mafic and ultramafic inclusions in the Sublayer of the Sudbury Igneous Complex. Can Min 22, pt. 1: 67–75

Seccombe PK, Groves DI, Binns RA, Smith JW (1977) A sulfur isotope study to test a genetic model for Fe-Ni sulfide mineralization at Mt. Windarra Western Australia. *In* Stable isotopes in Earth Sciences. New Zealand Department of Scientific and Industrial Research Bull 220, pp 187–202

Segnor AMC, Natal'in BA, Burtman VS (1993) Evolution of the Altaid tectonic collage and Paleozoic crustal growth in Eurasia. Nature 364: 299–307

Severson MJ (1988) Geology and structure of a portion of the Partridge River intrusion. A progress report. (Technical Report NRRI/GMIN-TR-88-08) Natural Resources Research Inst University of Minnesota, Duluth, 78 p

Severson MJ (1991) Geology mineralisation and geostatistics of the Minnamax/Babbitt Cu-Ni deposit (Local Boy area) Minnesota Part I: Geology. (Technical Report NRRI/TR-91/13a) Natural Resources Research Inst University of Minnesota, Duluth, 96 p

Severson MJ (1994) Igneous stratigraphy of the South Kawishiwi Intrusion Duluth Complex northeastern Minnesota. Natural Resources Research Inst Univ Minn, Duluth, Technical Report NRRI/TR-93/94, 210p

Severson MJ, Hauck S (1990) Geology geochemistry and stratigraphy of a portion of the Partridge River intrusion. A progress report. (Technical Report NRRI/GMIN-TR-89-11) Natural Resources Research Inst University of Minnesota, Duluth, 230 p

Shalaginov VV, ed (1999) State geological map of Russian Federation scale 1:200000. Second edition. Middle Urals Series. Sheet O-40-XVIII. Explanation note. Ministerstvo prirodnykh resursov RF. Ekaterinburg, 100 p (in Russian)

Shanks WS, Schwerdtner WM (1991a) Grude quantitative estimates of the original northwest-southeast dimension of the Sudbury Structure south-central Canadian Shield. Can J Earth Sci 28: 1677–1686

Shanks WS, Schwerdtner WM (1991b) Structural analisis of hte central and southwestern Sudbury Structure Southern Province Canadian Shield. Can J Earth Sci 28: 411–430

Sharma RC, Chang YA (1980) Thermodynamics and phase relationships of transition metal-sulfur systems, part IV: Thermodynamic properties of the Ni-S liquid phase and the calculation of the Ni-S diagram. Metallurgical Trans B vol 11B, pp 139–146

Sharp WE (1969) Melting curves of sphalerite galena and pyrrhotite and the decomposition of pyrite between 30 and 60 kilobars. J Geophys Research 74: 1645–1652

Sharpe MR (1982) Noble metals in the marginal rocks of the Bushveld Complex. Econ Geol 77: 1286–1295

Sharpe MR, Irvine TN (1983) Melting relations of two Bushveld chilled margin rocks and implications for the origin of chromitite. Carnegie Inst of Washington Year Book vol 82, p- 295–300

Shima H, Naldrett AJ (1975) Solubility of sulfur in an ultramafic melt and the relevance of the system Fe-S-O. Econ Geol 70: 960–967

Shimazaki H, MacLean WH (1976) An experimental study on the partition of zinc and lead between silicate and sulfide liquids. Mineralium Deposita II, pp 125–132

Shirey SB, Barnes S-J (1994) Re-Os and Sm-Nd isotopic constraints on basaltic volcanism and magmatic sulphide formation in the Cape Smith fold belt Quebec. Mineral Magazine vol 58A, pp 835–836

Shirey SB, Barnes S-J (1995) Os-Nd isotope systematics of ultramafic-mafic magmatism: Cape Smith foldbelt and midcontinent rift system. *In* Proc of Internat Symposium on Petrology and Metallogeny of Volcanic and Intrusive Rocks of the Midcontinent Rift System (IGCP Project 336: Petrology and Metallogeny of Intraplate Mafic and Ultramafic Magmatism). University of Minnesota at Duluth Continuing Education and Extension, Duluth, pp 175–176

Simkin T, Smith JV (1970) Minor element distribution in olivine. J Geol 78: 304–325

Simonov ON, Lul'ko VA, Amosov YuN, Salov VM (1994) Geological structure of the Noril'sk region. *In* Proc. of the Sudbury-Noril'sk symposium. Ontario Geol Surv Spec Pub 5, pp 161–170

Skufin PK, Fedotov ZhA (1989) Picritic globular lavas in the sequence of the early Pre-Cambrian volcanics of the Pechenga srtucture. Doklady Akademii Nauk 305: 956–962 (in Russian)

Slaught WH (1951) A petrographic study of the Copper Cliff offset in the Sudbury District. Unpub MSc Thesis, McGill University

Sluzhenikin SF (2000) Low-sulfide platinum mineralization in differentiated mafic-ultramafic intrusions of the Noril'sk region. Abstracts of candidate thesis. IGEM RAN, Moscow, 26 p (in Russian)

Sluzhenikin SF, Distler VV (1998) Disseminated ores of the Talnakh ore junction as sources of platinum metals. *In* Large and giant deposits of rare and noble metals. Sankt-Peterburgsky gorny institut, St. Petersburg, pp 247–256 (in Russian)

Sluzhenikin SF, Distler VV, Duzhikov OA, Kravtsov VF, Kunilov VE, Laputina IP, Turovtsev DM (1994) Low-sulfide platinum mineralization in the Noril'sk differentiated intrusions. Geologiya rudnykh mestorozhdeniy 36: 195-217 (in Russian)

Smith RL, Wilton DHC, Sparkes K, Dunning GR (1999) Magmatic Ni-Cu-Co sulfide mineralization in the Pants Lake intrusion South Voisey's Bay project Labrador. Geol Assoc Can – Mineral Assoc Can Annual Meeting, Sudbury Ontario Programme with abstracts vol 24, p A119

Smith RL, Wilton DHC, Connelly JN, Sparkes K (2001) Geology geochemistry and sulfide mineralization of the basal gabbro subdivision of the Pants Lake intrusion Labrador. St John's Newfoundland Geol Assoc Can, Annual Meeting Programme with abstracts vol 26, p A141

Smolkin VF, 1977. Petrology of the Pilgujarvi ore-bearing intrusion (Pechenga). VINITI No 2114-77 Kolsky filial AN SSSR Apatity 261 p. (in Russian).

Smolkin VF (1992) Komatiitic and picritic magmatism of Early Pre-Cambrian in Baltic shield. Nauka, St Petersburg, 278 p (in Russian)

Smolkin VF (1993) The Kola (Pechenga-Varzuga) rift system. *In* Magmatism and metalogeny of rift systems of eastern part of the Baltic Shield (chief ed AD Tsheglov). Nedra, St Petersburg, pp 24–63 (in Russian)

Smolkin VF (1997) Magmatism of the Early Proterozoic (2.51.7 Ga) paleorift system north-west of the Baltic shield. Petrologiya 5: 394-411 (in Russian)

Smolkin VF, Abzalov MZ (1990) Rodingites and serpentine veins from the Pilgujarvi ore-bearing gabbro-wehrlitic massif (Pechenga). Geologiya rudnykh mestorozhdeniy No 5: 70–79 (in Russian)

Smolkin VF, Bayanova TB (1999) Origination and age of gabbro from the Zhdanov Ni-Cu deposit (Pechenga). *In* Riftogenesis magmatism and metallogeny in Pre-Cambrian; Correlation of Fennoscandian geological complexes. Proc of Internat conference. Korelsky NTs RAN, Petrozavodck, pp 147–148 (in Russian)

Smolkin VF, Dain AD (1985) Gabbro-wehrlitic formation of the Karelian-aged Imandra-Varzuga zone. Sovetskaya geologiya No 12: 94–105 (in Russian)

Smolkin VF, Mitrofanov FP, Avedisyan AA, Balashov YuA, Balagansky VV, Borisov AE, Borisova VV, Voloshina ZM, Kozlova NE, Kravtsov NA, Negrutsa VZ, Mokrousov VA, Petrov VP, Radchenko AT, Skufin PK, Fedotov ZhA (1995a) Magmatism sedimentation and geodynamics of the Pechenga paleorift structure. Kolsky nauchny tsentr RAN, Apatity, 256 p (in Russian)

Smolkin VF, Skuf'in PK, Mokrousov VA (1995b) Stratigraphic position geochemistry and genesis of volcanic associations of the Early Proterozoic Pechenga area. Nor geol unders Geology of the Eastern Finnmark - Western Kola Peninsula region. Spec Pub 7, pp 93–110

Smolkin VF, Bayanova TB, Mitrofanov FP et al (2001) Mantle-plume magmatism in Early Proterozoic (2.5 Ga) of Kola peninsula. Abstracts of XVI Symposium on isotope geochemistry in memory of Academician AP Vinogradov at 20-23 November 2001. Moscow, pp 230–231 (in Russian)

Snyder DA, Carmichael ISE (1992) Olivine-liquid equilibria and chemical activities of Fe NiO $Fe_2O_3$ and MgO in natural basaltic melts. Geochim Cosmochim Acta 56: 303–318

Souch BE, Podolsky T and Geological Staff of the International Nickel Co Canada Ltd (1969) The sulfide ores of Sudbury: Their particular relation to a distinctive inclusion-bearing facies of the Nickel Irruptive. Econ Geol Monograph 4, pp 252–261

Stekhin AI (1994) Mineralogical and Geochemical Characteristics of the Cu-Ni ores of the Oktyabr'sky and Talnakh deposits. *In* Proc of the Sudbury Noril'sk Symposium (eds PC Lightfoot, AJ Naldrett), Ontario Geol Surv Spec Pub 5, pp 217–230

Stevenson JS (1963) The upper contact phase of the Sudbury micropegmatite. Can Min 7: 413–419

Stolz GW, Nesbitt RW (1981) The Komatiite Nickel Sulfide Association at Scotia: A petrochemical investigation of the ore environment. Econ Geol 76: 1480–1502

Stone KE, Masterton EE (1998) Kambalda nickel deposits. *In* Geology of Australian and Papua New Guinea Mineral Deposits (eds BD Berkman, DH Mackenzie) The Australasian Inst Min Met. Melbourne, pp 365–374

Stone WE, Crocket JH, Fleet ME (1990) Partitioning of palladium, iridium, platinum and gold between sulfide liquid and basalt melt at 1200°C. Geochim Cosmochim Acta 54: pp 2341–2344

St-Onge MR, Lucas SB (1990) Evolution of the Cape Smith Belt: Early Proterozoic continental underthrusting ophiolite subduction and thick-skinned folding. Geol Assoc Can Spec Pap 37, pp 313–352

St-Onge MR, Lucas SB (1993) Controls on the regional distribution of iron-nickel-copper-platinum-group element mineralization in the eastern Cape Smith Belt Quebec. Can J Earth Sci 31: 206–218

Stratten T (1986) Environmental and stratigraphic setting of the Karoo basin and its mineral deposits. *In* Mineral deposits of Southern Africa (eds CR Anhaeusser, S Maske), vol II, pp 1863–1873

Streckeisen (1976) To each plutonic rock its proper name. Earth-Sci Revol 12: 1–33

Sugaki A, Kitakaze A (1998) High form Pentlandite and its thermal stability. Amer Mineral 83: 133–140

Sun SS, McDonough WF (1989) Chemical and isotopic systematics of ocean basalts: Implications of mantle composition and processes. *In* Magmatism of the Ocean Basins (eds AD Saunders, MJ Norry). Geol Soc of London 42, pp 313–345

Sun XS (1986) The discovery of Pt enrichment parts and existing status of Pt and Pd in Mining Area of Jinchuan sulfide Ni-Cu deposit. Geology and Prospecting 12, pp 36–39

Sutcliffe RH (1986) Regional geology of the Lac des Iles area District of Thunder Bay. *In* Summary of field work and other activities 1986 (eds PC Thurston, RB Barlow, OL White, AC Colvine). Ontario Geol Surv Miscellaneous Paper 132, pp 70–75

Sutcliffe RH (1987) Petrology of middle Proterozoic diabases and picrites from Lake Nipigon Canada. Contr Mineral Petrol 96: 201–211

Sutcliffe RH, Sweeny JM (1985) Geology of the Lac des Iles Complex District of Thunder Bay. *In* Summary of field work and other activities 1985 (eds J Wood, RB Barlow, OL White, AC Colvine) Ontario Geol Surv Miscellaneous Paper 126, pp 47–53

Sweeny JM, Edgar AD (1987) The geochemistry origin and economic potential of platinum group element bearing rocks of the Lac des Iles Complex northwestern Ontario. *In* Geoscience Research Grant Program Summary of Research 1986-1987 (e. VG Milne). Ontario Geol Surv Miscellaneous Paper 136, pp 140–152

Tait S, Huppert HE, Sparks RSJ (1984) The role of compositional convection in the formation of adcumulate rocks. Lithos 1: 139–146

Talkington RW, Watkinson DH (1984) Trends in the distribution of the precious metals in the Lac des Iles Complex northwestern Ontario. Can Min 22: 125–136

Tang ZL (1990) Mineralization model of the Jinchuan sulfide Cu-Ni deposit. Modern Geology 4: 55–64 (in Chinese)

Tang ZL (1993) Genetic models of the Jinchuan nickel-copper deposit. *In* Mineral Deposit Modelling (eds RV Kirkham, WD Sinclair, RI Thorpe, JM Duke). Geol Assoc Can Spec Pap 40, pp 389–401

Tang ZL, Yang J, Xu S, Tao X and Li WY, (1992) Sm–Nd dating of the Jinchuan ultramafic rock body Gansu China. China Science Bull. 37 p.1988–1991 (in Chinese).

Tang ZL, Li WY (1995) The metallogenetic model and geological contrast on the Jinchuan platinum-bearing Ni-Cu sulfide deposit. Geol. Publishing House Beijing (in Chinese)

Taylor HP Jr (1967) The zoned ultramafic complexes of southeastern Alaska. *In* Ultramafic and Related Rocks (ed PJ Wyllie), John Wylie and Sons Inc, New York, pp 27–121

Tegner C, Duncan RA, Bernstein S, Brooks CK, Bird DK, Storey M (1998) $^{40}Ar/^{39}Ar$ geochronology of Tertiary mafic intrusions along the East Greenland rifted margin: Relation to flood basalts and the Iceland hotspot track. Earth Planet Sci Let 156: 75-88

Theyer P (1980) Stratigraphic Setting of Selected Ultramafic Bodies in the Superior and Churchill Provinces and certain Aspects of Nickel-Copper Deposits in the Thompson Nickel Belt (ed P Theyer). Manitoba Energy and Mines Mineral resource division. Econ Geol Division ER79-2, 71 p

Thibert F (1993) Petrogenese du filon-couche differencie Romeo 1 situe dans la cienture plissee-faillee du Cap Smith Nouveau-Quebec. MSc These, Universite de Montreal, 145 p

Thompson JFH, Naldrett AJ (1984) Sulfide-silicate reactions as a guide to Ni-Cu-Co mineralization in central Main *In* Sulfide deposits in mafic and ultramafic rocks (eds DL Buchanan, MJ Jones). Inst Mining Metall Spec Pub, pp 103–113

Todd SG, Keith DW, Le Roy LW, Schissel DJ, Mann EL, Irvine TN (1982) The J-M Platinum-Palladium Reef of the Stillwater Complex Montana. 1. Stratigraphy and Petrology. Econ Geol 77: 1454–1480

Torgashin AS (1994) Geology of the massive and copper ores of the western part of the Oktyabr'sky deposit. *In* Proc. of the Sudbury-Noril'sk symposium (eds PC Lightfoot, AJ Naldrett). Ontario Geol Surv Spec Pub 5, pp 231-241

Tuchscherer MG, Spray JG (2002) Geology mineralization and emplacement of the Foy offset dyke Sudbury Impact Structure. Econ Geol 97: 1377–1397

Turner AR, Wolfgram D, Barnes SJ (1985) Geology of the Stillwater County Sector of the J-M Reef including the Minneapolis adit. *In* Stillwater Complex (eds GC Czamanske, M.L. Zientek). Montana Bureau of Mines and Geology Spec Pub 92, pp 210–230

Turner JS, Huppert HE, Sparks RSJ (1986) Komatiites II: Experimental and theoretical investigations of post-emplacement cooling and crystallization. J Petrol 27: 397–438

Urvantsev NN (1972) Some problems of generation of the ore-bearing intrusions and ores at Noril'sk. *In* Nickel-copper ores of the Talnakh ore junction. NIIGA, Leningrad, pp 100–105 (in Russian)

Usselman TM (1975) Experimental approach to the state of the core: Part I. The liquidus relations of the Fe-rich portion of the Fe-Ni-S system from 30-100 Kbars. Amer J of Science 275: 278–290

Van Kranendonk M (1996) Tectonic evolution of the Paleo-proterozoic Torngat orogen: Evidence from pressure-temperature-time deformation paths in the North River map area. Tectonics 15: 843–869

Vermaak CF (1995) The Platinum-group Metals: A global perspective. Mintek Randburg South Africa, p 247

Vermaak CF (1976) The Merensky reef – Thoughts on its environment and genesis. Econ Geol 71: 1270–1298.

Vidik SV, Tolstykh ND, Sidorov EG (1999) Hard-rock platinum mineralization in rocks of the Galmoenan massif. *In* Urals summer mineralogical scool-99. Ekaterinburg, pp 145–152 (in Russian)

Viljoen MJ, Viljoen RP (1969) Evidence of the existence of a mobile extrusive peridotitic lava from the Komati formation of the Onverwacht group. *In* Geol Soc of South Africa Spec Pub 2, pp 87–113

Vogel DC, Keays RR, James RS, Reeves SJ (1999) The geochemistry and petrogenesis of the Agnew Intrusion Canada: A product of S-undersaturated high-Al low-Ti tholeitic magmas. J Petrol 40: 423–450

Volchenko YuA (1999 Platinum mineralization of the Nizhniy Tagil massif (original showings and placers). Excursion guidebook. Uralskaya Gosudarstvennaya gorno-geologicheskaya akademiya. Ekaterinburg, 27 p (in Russian)

Volchenko YuA, Zoloev KK, Koroteev VA, Mardirosyan AN, Neustroeva II (1998) New and perspective types of Urals platinum-metal mineralization. *In* Geology and metallogeny of Urals vol 1. UGSE, Ekaterinburg, pp 238–255 (in Russian)

Von Gruenewaldt G (1973) The main and upper zones of the Bushveld complex in the Roossenekal area Eastern Transvaal. Geol Soc South Africa Transactions 76, pp 207–227

Von Gruenewaldt G (1976) Sulphides in the upper zone of the Eastern Bushveld Complex. Econ Geol 71: 1324–1336

Von Gruenewaldt G (1979) A review of some recent concepts of the Bushveld Complex with particular reference to sulfide mineralization. Can. Min 17, No 2: 233–256

Von Gruenewaldt G, Hulbert LJ, Naldrett AJ (1989) Contrasting platinum-group element concentration patterns in cumulates of the Bushveld Complex. Mineralium Deposita 24: 219–229

Von Groenewald PB, Painter MGM, Roberts FI, McCabe M, Fox A (2000) East Yilgarn Geoscience Database 1:100000 Geology Menzies to Norseman – an explanatory note. West Australian Geol Surv. Perth Austr Report 78, 53 pp plus 1 CD

Wager LR, Brown GM (1968) Layered Igneous Roscks. Oliver and Boyd, Edinburgh and London, 588 p.

Wager LR, ,Deer WA (1939) Geological investigations in East Greenland. Part III. The petrology of the Skaergaard Intrusion Kangerdlugssuaq East Greenland. Meddeleser om Gronlan 105, No 4, 352 p (re-issue 1962)

Wager RE, Podolsky T, Alcock RA, Weiblen PW, Phinney WC (1969) A comparison of the Cu-Ni deposits of the Sudbury and Duluth basins. Amer Inst Mining Engineers 52nd Annual Meeting Minnesota Section. 30th Annual Mining Symposium Proc, pp 95–96

Wagner PA (1929) The platinum deposits and mines of South Africa. C Struik (Pty) Ltd, Capetown, 356 p

Walker RJ, Morgan JW, Naldrett AJ, Li C, and Fassett JD (1991) Re-Os Isotopic systematics of Ni-Cu Sulfide Ores Sudbury Igneous Complex Ontario: Evidence for a major crustal component. Earth Planet Sci Let 105: 416–429

Walker RJ, Morgan JW, Horan MF, Czamanske GK, Krogstad EJ, Fedorenko VA, Kunilov VE (1994) Re-Os isotopic evidence for an enriched-mantle plume source for the Noril'sk-type ore-bearing intrusions Siberia. Geochim Cosmochim Acta 58: 4179–4197

Walker RJ, Morgan JW, Hanski EJ, Smolkin VF (1997) Re-Os Systematics of Early Proterozoic ferropicrites Pechenga complex NW Russia: evidence for ancient $^{187}$Os - enriched plumes. Geochim Cosmochim Acta 61: 3145–3160

Watkinson DH, Dunning G (1979) Geology and the platinum group mineralization, Lac des lies complex northwestern Ontario. Can Min 17: 453–462

Watson EB, Jurewicz SR (1984) Behaviour of alkalies during diffusive interaction of granitic xenoliths with basaltic magma. J Geol 92: 121-0131

Watts T, Osmond R (1999) 3D Geophysical Model of the Raglan Belt Chapter 19. *In* Komatiitic Peridotite-Hosted Ni-Cu-(PGE) Deposits of the Raglan Area Cape Smith Belt New Quebec (ed CM Lesher). Guidebook Series vol 2. Mineral Explor Research Centre Laurentian University, Sudbury, pp 185–190

Weber W, Scoates RFJ (1978) Archean and Proterozoic metamorphism in the northwestern Superior province and along the Churchill - Superior boundary Manitoba. *In* Metamorphism in the Canadian Shield. Geol Surv Can. paper 78-10, pp 5–16

Weiblen PW, Morey GB (1975) The Duluth complex – a Petrographic and tectonic summary. 36th Ann Minn Mining Symp. Dept of Conferences and Continuing Education Univ of Minnesota, pp 72–95

Weiblen PW, Morey GB (1980) A summary of the stratigraphy petrology and structure of the Duluth complex. Amer J of Science 280-A: 88–133

Weis D, Morse SA (1993) Disparate U-Pb systematics of mafics and plagioclase in the Kiglapait intrusion Labrador. EOS 43, p. 623

Wendlandt RF (1982) Sulfur saturation of basalt and andesite melts at high pressures and temperatures. Amer Mineral 67: 877–885

Wendlandt RF, Huebner JS (1979) Melting relations of portions of the system Fe-S-O at high pressure and applications to the compositions of the earth's core (Abstract). Lunar Planetary Sc. X Lunar and Planetary Inst, pp 1329–1331

White JA (1994) The Potgietersrus project: Geology and exploration history. Proc 15th CMMI Congress. South African Inst Min Met, pp 173–182

Whitney J, and Naldrett AJ, eds (1990) Ore deposits associated withmagmas. Soc of Econ Geol Reviews in Econ Geol vol 4, 250 p

Wilson AH (1982) The geology of the great "Dyke" Zimbabwe: The ultramafic rocks. J Petrol 42: 109–124

Wilson AH, Prendergast MD (1989) The Great Dyke of Zimbabwe – I: Tectonic setting stratigraphy petrology structure emplacement and cristallisation. *In* Magmatic Sulphides – The Zimbabwe Volume (eds MD Prendergast, MJ Jones). Inst Min Met, London, pp 1-=20

Wilson AH, Prendergast MD (2001) Platinum-group element mineralisation in the Great Dyke Zimbabwe and its relationship to magma evolution and magma chamber structure. South African J Geol 104: 319–342

Wilson AH, Naldrett AJ, Tredoux M (1989) Distribution and controls of platinum group element and base element mineralization in the Darwendale subchamber of the Great Dyke Zimbabwe. Geology 17: 649–652

Woodall R, Travis GA (1969) The Kambalda nickel deposits Western Australia. Commonwealth Mining and Metallurgical Congress 9th. Public Pap 26, 17 p

Wooden JL, Czamanske GK, Zientek ML (1991) A lead isotopic study of the Stillwater Complex Montana; constraints on crustal contamination and source regions. Contr Mineral Petrol 107: 80–93

Wooden JL, Czamanske GK, Fedorenko VA, Arndt NT, Chauvel C, Bouse RM, King B-SW, Knight RJ, Siems DF (1993 Isotopic and trace element constraints on mantle and crustal contributions to characterization of Siberian continental flood basalts Noril'sk area Siberia. Geochim Cosmochim Acta 57: 3677–3704

Wu J, Milkereit B, Boerner D (1994) Timing constraints on deformation history of the Sudbury Impact Structure. Can J Earth Sci 31: 1654–1660

Yakovlev YuN, Yakovleva AK, Neradovsky YuN, Osokin AS, Balabonin NL, Dokuchaeva VS, Orsoev DA, Distler VV, Filimonova AA (1981) Mineralogy of the sulfide nickel-copper deposits of Kola peninsula. Leningrad, 352 p (in Russian)

Yang XZ (1989) Platinoid and gold geochemistry in the Jinchuan Ni-Cu sulfide deposit Gansu province China. Bull Xi'an Inst Geol Mineral Research Chinese Academy of Geol Sciences 26, pp 57–68 (in Chinese)

Yund RA, Kullerud G (1966) Thermal stability of assemblages in the Cu-Fe-S system. J Petrol 7: 454–488

Zagorodny VG, Mirskaya DD, Suslova SN (1964) Geology of the Pechenga sedimentary-volcanic series. Nauka, Moscow, 208 p (in Russian)

Zak S, Makarov VN, Proskuryakov VV, Kochnev-Pervukhov VI, Zaskind ES, Batashev EV (1982) Geology, magmatism and mineralization of the Pechenga ore field. Nedra, Leningrad, 112 p (in Russian)

Zen'ko TE (1983) Mechanism of formation of the Noril'sk ore-bearing intrusions. Izv Akad Nauk SSSR Geol Series No 11: 21–39 (in Russian)

Zen'ko TE (1986) Regularities of localization and construction of intrusions of the western part of the Talnakh region. TsNIGRI, Iss 209, pp 21–28 (in Russian)

Zen'ko TE (1994) Quantitative genetic-geological models of Noril'sk-type ore fields and deposits. Rudy i metally No 3-5: 57–72 (in Russian)

Zenko TE, Czamanske GK (1994a) Tectonic controls on ore-bearing intrusions of the Talnakh ore junction: Position morphology and ore distribution. Intern Geol Rev 36: 1033–1057

Zen'ko TE, Czamanske GK (1994b) Physical and petrologic aspects of the intrusions of the Noril'sk-Talnakh ore junctions Siberia. *In* Proc. of the Sudbury-Noril'sk symposium (eds P. Lightfoot, AJ Naldrett). Ontario Geol Surv Spec Pub 5, pp 263–282

Zhou MF Yang ZX Song XY Keays RR, Lesher CM (2002) Magmatic Ni-Cu-(PGE) sulfide deposits in China. In: Cabri LJ (ed) The geology geochemistry mineralogy and mineral beneficiation of the platinum-group elements. Can Inst Min Metall Petrol Spec Vol 54, pp 619–636

Zientek ML, Likhachev AP, Kunilov VE, Barnes S-J, Meier AL, Carlson RR, Briggs PH, Fries TL, Adrian BM (1994) Cumulus processes and the composition of magmatic ore deposits: Examples from the Talnakh district Russia. *In* Proc. of the Sudbury-Noril'sk Symposium (eds PC Lightfoot, A.J Naldrett). Ontario Geol Surv Spec Pub 5, pp 373–392

Zientek ML, Cooper RW, Corson SR, Geraghty EP (2002) Platinum-Group Element Mineralization in the Stillwater Complex Montana. *In* The Geology Geochemistry Mineralogy and Mineral Beneficiation of Platinum-Group Elements (ed LJ Cabri) Ottawa Ontario. Can Inst Min Met Spec Vol 54, pp 459–481

Zoloev KK, Volchenko YuA, Koroteev VA, Malakhov IA, Mardirosyan AN, Khrypov VN (2001) Platinum-metal mineralization in the Urals geological complexes. UGSE, Ekaterinburg ,199 p (in Russian)

Zolotukhin VV (1964) Main regularities of prototectonics and aspects of origin of ore-bearing trap intrusions. Nauka, Moscow, 192 p (in Russian)

Zolotukhin VV (1991) Sulfide Ni-Cu formation and its place among endogenic ore formations as an indicator of ore genesis. Geologiya i geofizika No 4: 27–36 (in Russian)

Zolotukhin VV (1997) Basic pegmatoids of the Noril'sk ore-bearing intrusions and the problem of genesis of the PGE-Ni-Cu mineralization of the Noril'sk type. SO RAN NITs OIFFM, Novosibirsk, 89 p (in Russian)

Zolotukhin VV, Ryabov VV, Vasil'ev YuR, Shatkov VA (1975) Petrology of the Talnakh ore-bearing differentiated intrusion. Nauka, Novosibirsk, 432 p (in Russian)

Zotov IA (1979) Genesis of trap intrusions and metamorphic formations of the Talnakh. Nauka, Moscow, 156 p (in Russian)

Zotov IA (1980) About role of transmagmatic fluids in genesis of magmatogenic ore deposits. Sovetskaya geologiya No 1: 45–57 (in Russian)

Zurbrigg HF (1963a) Thompson Mine Geology. Can Inst Min Met Transactions 66, pp 227–236

Zurbrigg HF (1963b) Thompson Mine geology. Can Inst Mining Metallurgy Bull 56, pp 451–460

# Index

Erratum

We would like to acknowledge the Queen`s Printer for Ontario for granting their permission to reprint the figures on pp. 206, 207, 209, 407, 410, 413, 414, 415, 416, 421, 435, 442, 443, 444, 445 and 447, all previously published in Ontario Geological Survey.